1-1-2014

Experimental And Theoretical Studies Of Binding Interactions In Divalent Transition Metal Cation-N-Donor Ligand Complexes: Structures, Sequential Bond Dissociation Energies, Mechanisms And Energetics Of Collision-Induced Dissociation

Holliness Nose
Wayne State University,

EXPERIMENTAL AND THEORETICAL STUDIES OF BINDING INTERACTIONS IN DIVALENT TRANSITION METAL CATION-*N*-DONOR LIGAND COMPLEXES: STRUCTURES, SEQUENTIAL BOND DISSOCIATION ENERGIES, MECHANISMS AND ENERGETICS OF COLLISION-INDUCED DISSOCIATION

by

HOLLINESS NOSE

DISSERTATION

Submitted to the Graduate School

of Wayne State University,

Detroit, Michigan

in partial fulfillment of the requirements

for the degree of

DOCTOR OF PHILOSOPHY

2014

MAJOR: CHEMISTRY (Inorganic)

Approved By:

Advisor	Date

DEDICATION

To my best friend and soul mate, Dr. P. M. Dikirr, and our Son, Lemaiyan. None of this work would have been possible without your love, advice, and support.

ACKNOWLEDGEMENTS

Many people have contributed to the work in this thesis and my development in Graduate School in a variety of ways. First of all, I would like to thank the department of Chemistry, Wayne State University (WSU) for admitting me and giving me the opportunity to further my studies in the United States of America. I am particularly grateful to my research advisor, Professor M. T. Rodgers, for accepting me into her research group even though I had no background in Mass Spectrometry research. She gave me consistent scientific guidance, personal and career assistance, encouragement, and advice. Throughout, I have admired and appreciated her deep commitment to her students and their education. All these aspects made my study in WSU an invaluable experience and will continue to play an important role in my future career. Special thanks to Dr. D. E. Benson and Dr. A. Matthews for their assistance in my early stages of research at WSU. I would also like to thank my committee members: Professor Gavin Reid, Professor Christine Chow, and Professor Claudio Verani for serving on my committee, providing support, making suggestions regarding my research project and for their time. I also wish to thank many other faculty and staff members in chemistry department for their teaching and service throughout my stay in WSU. In addition, I am very grateful to Professor P. B. Armentrout for his many thoughtful discussions. Funding provided by WSU (Thomas C. Rumble Fellowship), the department of chemistry teaching program, summer dissertation Fellowship, and the National Science Foundation are gratefully acknowledged. In addition, Computer time and technical support provided by WSU Department of Computer and Information Technology is appreciatively acknowledged.

I would also like to thank all members, past and present, of Professor M. T. Rodgers research group for sharing their knowledge and time with me during the course of my research work. I am also indebted to Professor H. B. Schlegel and his graduate students for their enthusiastic computational support. Dr. Cliff Frieler is as well acknowledged for his technical support. I am also thankful to Professor Claudio Verani, Professor Peter Andreana and their graduate students for allowing me to synthesize my metal complexes in their laboratories. Also, I am very grateful to Nestor Ocampo for always "lending an ear." I would also like to thank the graduate students in this department for their valuable experiences, helpful support and friendship during my graduate study. I know later in life I will always be able to smile from thinking about the things they have done.

Special thanks are due to my mother, Elizabeth, my siblings, and all close relatives for their unwavering love and support. The creativity that my mum cultivated within me has paid off every step in my life. I have been blessed with some of the best friends in the world. Mrs. Miriam Cherogony opened my door to higher education. Mrs. Mwangola, Laura, Julius, Marlene, Joyce and Patience are a great people to spend a weekend with, reminding me what is really important in life. I hope Aunt Pauline Mazrui will be my doula once more. Thanks to Kit and Tony Ilardi for always making me feel at home away from home during holidays. Your "life lessons" and common sense attitude continue to guide and inspire me.

Finally, and most importantly, I thank my husband, Dr. P. M. Dikirr and Son, Lemaiyan for enduring all the loneliness in the world while I was studying abroad. The best is yet to come.

TABLE OF CONTENTS

LIST OF TABLES

LIST OF FIGURES

CHAPTER 1

INTRODUCTION AND DISSERTATION OVERVIEW

1.1 Introduction

1.1.1 Transition Metal Cations

Transition metals such as iron, cobalt, nickel, copper, and zinc are essential trace elements that occur in nature.[1] Iron occurs primarily as a metal oxide whereas cobalt, nickel, copper, and zinc occur primarily as sulfides and arsenides and are recovered from their alloys by well known methods.[2] Their physical properties are largely derived from their electronic structure. Many first-row transition metals are of key importance in biology, especially iron, copper, and zinc.[3,4] Their levels vary considerably among organisms and different components of organisms.[5,6] Nickel is essential for most microorganisms and is used by plants.[7] Zinc and its derivatives are present in some biological molecules of outstanding interest such as phospholipase C and bovine lens leucine amino peptidase.[8,9] The use of cobalt by higher organisms depends upon it being incorporated into a special cofactor (cobalamin) by microorganisms.[10] Transition metals combine with organic compounds or biological molecules to form strong stable or weak reactive complexes and perform a wide range of specific functions.[11] Coordination of zinc to specific histidine and cysteine residues as found in zinc fingers enables a protein to recognize and bind to precise sequences of DNA base pairs and plays a crucial role in transferring information from the gene.[10] Copper cations (Cu^{+}/Cu^{2+}) are involved in oxidation-reduction reactions in biological compounds.[12,13] Specifically; copper has been known to destabilize nucleic acids by binding to the bases.[14] Cobalt macrocycle complexes that are cofactors in many enzymes (cobalamins) catalyze radical-based rearrangements, methyl group transfers, and

dehalogenation reactions.[10] Active sites based on iron catalyze a great variety of redox reactions ranging from electron transfer to oxygenation, as well as acid-base reactions that include reversible oxygen binding.[15,16] Thus, transition metal cations play important roles in biochemical transformations that depend on their intrinsic nature and the local environment.

Deficiencies of essential transition metal cations may lead to diseases such as anemia for lack of iron and Menkes disease for lack of copper.[17] When their concentration exceeds natural levels, essential transition metal cations become toxic to cells and may cause diseases such as thalassaemia (iron) or Wilson's disease (copper).[18] However, chelating agents can be provided to reduce the free concentrations of the metals thereby preventing or limiting damage. For example, to avoid iron overload and effects resulting from it, drugs such as desferrioxamine are given to chelate the iron and facilitate its excretion.[4]

1.1.2 *N*-Donor Ligands

N-donor ligands such as pyridine (Pyr), 2,2′-bipyridine (Bpy) and 1,10-phenanthroline (Phen) have been widely employed to construct transition metal cation-*N*-donor ligand complexes because of their ability to form stable structures and to coordinate with various transition metal cations.[19-21] The *N*-donor ligands (Pyr, Bpy, Phen) exhibit unique features that enable them to play different roles in chemical, physical, or biochemical processes that occur in nature.[22,23] *N*-Donor ligands are able to bind transition metals through the nitrogen and form strong metal-ligand interactions. Pyr binds to transition metal cations via a single nitrogen donor atom, whereas Bpy and Phen use both nitrogen atoms forming a chelate complex. Chelate complexes tend to be more stable than the corresponding complexes containing monodentate ligands as a result of entropy effects. The chelate effect is of great importance because most chemical or biochemical transition metal

cation binding sites involve chelating ligands.[24] *N*-Donor ligands are capable of producing very stable species in solution and the gas-phase due to π back-bonding from the metal to the aromatic amine.[25] *N*-Donor ligands have a planar π system that enables them to interact with biological systems or to form supramolecular architectures through van der Waals interactions.[26,27] Phen is a very rigid moiety that provides a high degree of preorganization, whereas the Bpy ligand takes advantage of the flexibility of its central C–C bond that enables it to rotate freely. *N*-Donor ligands can be functionalized leaving the aromaticity and planarity of the rings intact and thus provides additional potential interaction sites. These characteristics enable *N*-donor ligands to be useful in a wide variety of areas such as catalysis, supramolecular chemistry, sensing, and structural support.[28-31]

The functional groups of *N*-donor ligands such as Pyr, Bpy, and Phen resemble many ligands found in chemical and biochemical systems. The ligands in the chemical or biochemical processes may be simple anions such as cyanide, small molecules such as ammonia, larger molecules such as histidine or even macromolecules, such as proteins. The donor groups that are either chemically hard or soft confer a particular affinity for specific metal cations. The *N*-donor groups of Pyr, Bpy, and Phen provide hard nitrogen donor atoms that have the ability to coordinate borderline acid metal cations such as Fe^{2+}, Co^{2+}, Ni^{2+}, and Cu^{2+}. In contrast, zinc generally forms stable complexes with softer donors. Thus, it is not surprising that zinc is usually found coordinated to histidine and cysteine residues in proteins. Histidine, which has an imidazole ring with two coordination sites, the ε–N atom (more common) and the *δ*–N atom, is an important ligand for iron, copper, and zinc.[15] Transition metal cations are also bound in proteins by special organic *N*-donor ligands such as porphyrins and pterin-dithiolenes. For example, iron binds to the porphyrin group in

hemoglobin, whereas cobalt coordinates to the corrin ligand in cobalamin.[10] Thus, the *N*-donor ligands of interest in this thesis study (Pyr, Bpy, and Phen) and their interactions with transition metal cations can serve as model compounds in understanding the binding strength in chemical and biochemical processes.

1.1.3 Transition Metal Cation-*N*-Donor Ligand Complexes

The transition metal cation-*N*-donor ligand complexes examined in this study are examples of coordination compounds that are formed through binding of one or several ligands to a single central metal cation. The number of electron pairs arising from the ligand *N*-donor atoms to which the metal cation is directly bonded depends on the size of the central cation, the nature of the *N*-donor ligands, and steric interactions between the transition metal cation and the *N*-donor ligands.[22,23] For the transition metal cations involved in this study, i.e., Fe^{2+}, Co^{2+}, Ni^{2+}, Cu^{2+}, and Zn^{2+}, the number of *N*-donor ligands bound to the central cation vary from one to six. Depending on the nature of the *N*-donor ligands, mono-, bis-, tris-, tetra-, penta-, or hexa- coordinated complexes result. The properties of transition metals, particularly valence electronic configuration, ionization potential, and ionic radii, and those of the *N*-donor ligands, such as their dipole moments and polarizabilities, underlie the intrinsic binding interactions in the transition metal cation-*N*-donor ligand complexes.[12,13] The thermodynamics of formation and stability of the transition metal *N*-donor ligand complexes reveal insights into the nature of the metal-ligand bonding and contribute to an understanding of the ways in which the ligand structure and electronic properties of the metal relates to the strength of binding[19-21] Therefore, the properties of the transition metals and those of the *N*-donor ligands and the stability of the metal complexes allow complexes with particular properties to be designed to suit particular applications.

1.2 Applications of Transition Metal Cation-*N*-Donor Ligand Complexes

1.2.1 Catalysis Applications

Transition metal complexes such as $[CuPhen]X_2$ and $[CuPhen_2]X_2$, where X = Cl^-, Br^-, and SCN^- have been known to catalyze the decomposition of hydrogen peroxide.[32-34] The catalytic effect of these complexes has been associated with their electronic and molecular structure.[35-38] In these complexes, the Phen ligand has been found to act as an inhibitor, while the Cu^{2+} acts as a promoter of hydrogen peroxide formation. Transition metals such as iron, cobalt, nickel, and copper have desirable properties such as variable oxidation states, partially occupied d orbitals, variable ionic radii, and ionization energies that strongly influence the chemical properties of a transition metal complex.[39-41] The *N*-donor ligands, Pyr, Bpy, and Phen, have unique characteristics such as the number of donor atoms available for binding, the molecular polarizability, and dipole moment that influences the chemical behavior of a transition metal complex.[42-45] Metal-ligand interactions define the structure of transition metal complexes by maintaining the stability of molecular systems, and therefore have a profound impact on their chemical properties and reactivity, and hence underlie their chemical behavior.[10] Steric interactions are also important in determining the geometry and strength of binding of a transition metal complex. These features make the transition metal cation-*N*-donor ligand complexes examined in this work suitable as catalysts. The coordination of *N*-donor ligand (s) to a transition metal cation may lead to distortion from ideal geometries and hence destabilization of the coordinated complex. The result involves changes in bond distances and bond angles of the atoms in the coordinated geometries relative to the free ligand or deviation from ideal geometries predicted by the valence shell electron pair repulsion model. The implication is that the number and nature of

the *N*-donor ligands or the electronic properties of transition metal cations can be used to enforce particular coordination geometry, and hence tune the stability and reactivity of a transition metal complex. The Phen and Bpy ligands are sterically constrained, and hence can be used to cause strain or destabilize the starting materials and thus find use in catalysis.

The $M^{2+}(N\text{-}L)_x$ complexes where M^{2+} = Fe^{2+}, Co^{2+}, Ni^{2+}, Cu^{2+}, and Zn^{2+}, *N*-*L* = Phen or Bpy, and x = 1–3 can be utilized as catalysts. The tris-complexes can be used in ligand substitution catalytic reactions as the ligands are less strongly bound to the metal cation and can be easily substituted. The geometric structures of the mono- and bis-complexes feature a vacant site around the metal center that can allow substrate binding at the exposed position. The π-electronic charge density of the *N*-*L* ligand moiety can be utilized as a light absorber for solar fuel applications.[46] The *N*-*L* ligands can be derivatized in the peripheral region with special functional groups that carry out important transformations such as asymmetric catalysis.[47] In addition, divalent transition metal cations are earth abundant and affordable metal cations, easy to handle on a large scale and often lack the problems of water sensitivity and dimerization exhibited by most main group Lewis acids.[48-50] All these factors emphasize the importance of identifying the late first-row divalent transition metal cation-*N*-donor ligand complexes as potential catalysts that can be used to replace the most expensive complexes of precious metals such as rhodium, iridium, and ruthenium that have been in use for a long time.[51-55]

1.2.2 Metallo-supramolecular Applications

The formation of well-defined structures by self-assembly is the central theme of supramolecular chemistry.[56,57] The basic concept lays in the use of noncovalent interactions such as van der waals forces, hydrogen bonding, and ionic or metal coordinative interactions

that are usually weaker than covalent bonds. Supramolecular chemistry has become one of the most fascinating fields because synthesis of large molecules by traditional covalent chemistry is time consuming and expensive.[58] Nature utilizes a wide range of different noncovalent interactions for the construction of large supramolecular architectures.[59,60] For example, self-recognition of the complementary base pairs by hydrogen-bonding leads to self-assembly of the double helix in DNA.[61] Moreover, noncovalent interactions are reversible, whereas covalent bonds are usually irreversible or only reversible under harsher conditions.[62] *N*-donor ligands (*N*-*L*) such as Pyr, Bpy, and Phen have the ability to act as complexation agents for several transition metal cations including: Fe^{2+}, Co^{2+}, Ni^{2+}, Cu^{2+}, and Zn^{2+}.[63] This complexation behavior can be utilized in supramolecular chemistry for the construction of metal complexes and metal containing architectures with applications that range from gas sensing to solar energy conversion.[64-66] The stability of the transition metal cation-*N*-donor ligand complex is a fundamental requirement for such applications. In this respect, the use of Pyr, Bpy or Phen as chelating ligands is highly promising, because these molecules are known to form highly stable complexes with interesting physical properties with transition-metal cations.[19-23] The transition metal cation-*N*-donor ligand complexes are easily synthesized and their substituted forms are accessible in good yields thereby increasing their usefulness in areas such as catalysis.[67-70] These metal complexes have very interesting photochemical properties which, for example, make them suitable for applications in solar energy conversion.[71] The variability of transition metal cations (Fe^{2+}, Co^{2+}, Ni^{2+}, Cu^{2+}, and Zn^{2+}) offers an additional advantage in that the chemical and physical properties of a material can be changed without synthetic expenditure by simply altering the metal cation. Furthermore, transition metal cation-*N*-donor ligand complexes allow the reversible

formation and cleavage of the coordinative bond by external stimuli, e.g., redox processes or the addition of competing ligands.[72,73] Research has shifted from analytical purposes such as complexing of metal cations to the creation of new smart supramolecular materials such as organic light emitting devices or solar cells. However, fundamental details regarding the transition metal cation-*N*-donor ligand complexes such as the $M^{2+}(N\text{-}L)_x$ complexes investigated here that can be used as cores in building supramolecules is lacking. The current studies of $M^{2+}(N\text{-}L)_x$ complexes will provide geometric information responsible for their specific structure as well as information on the strength of interactions responsible for the binding in these complexes. The information gained from this study will increase the viability of the $M^{2+}(N\text{-}L)_x$ complexes in use as cores or peripherals in constructing well defined supramolecules.

1.2.3 Electron- and Proton-Transfer Applications

Electron- and proton-transfer processes are of great importance to life.[74] Photosynthesis is an excellent example of a biological process involving electron and proton transfer in which metal complexes are exploited to absorb light, separate electric charge, shuttle protons around, and ultimately convert solar energy into biologically useful chemical energy.[75-77] The flow of electrons along electron-transport chains in metalloenzymes such as hydrogenases found in almost all bacteria and archaea is coupled to chemical processes such as proton transfer.[78-81] Electron- and proton-transfer between proteins and DNA also plays an important role in biochemical processes such as replication, transcription, and DNA repair.[82-84] The general operation and construction of a fuel cell that converts fuel such as hydrogen, methane, or methanol, by reaction with oxygen into electrical energy involves both proton and electron transfer.[85-87]

The main objective behind studying transition metal cation-*N*-donor ligand complexes is to understand their fragmentation pathways and the energetics involved in electron- and proton transfer processes. The knowledge derived from this study can be applied to potential practical applications like solar energy conversion and light-driven information processing,[88] DNA and RNA cleavage,[89,90] and luminescent materials.[91-93] These applications result because of the ability of transition metal complexes to be involved in ligand-to-metal charge transfer (LMCT) and/or metal-to-ligand charge transfer (MLCT) depending on the nature of the metal center and the ligands. For example, electrons can be introduced into DNA by intercalating special metal complexes such as Cu^{2+}(2,2′-bipyridine)$_2$ along the chain of DNA base pairs. Incorporation of this complex results in the destruction of DNA through the motion of radicals, and may play a crucial role in the processes of mutagenesis and carcinogenesis.[94-96] The intense color of transition metal cation-*N*-donor ligand complexes that arises from d-d transitions or charge transfer processes such as MLCT and LMCT can be utilized in the development of photo luminescent materials such as LED devices.[97-99]

Electronic structure methods such as B3LYP can be used to understand electron- and proton-transfer mechanisms in model compounds such as those studied in this thesis. By mapping the potential energy surfaces for electron- and proton-transfer processes in model complexes, the geometries and relative energies of the reactants, intermediates, transition states, and products along the reaction pathway can be predicted. It is also possible to tune the ground and excited state properties in a more predictable manner by using an appropriate metal cation. This information will be helpful to scientists seeking to understand electron- and proton-transfer mechanisms in small metal complexes involving Phen and Bpy ligands.

Such mechanistic information can also be utilized to design more efficient chemical processes or for the exploration of techniques designed to confirm the proposed reaction mechanism.

1.3 Dissertation Overview

This dissertation involves a series of experiments that have been designed to probe the influence of the electronic structure of the metal cation, the nature and number of ligands, as well as the effects of chelation and steric interactions on the geometry and binding strength of metal cation-ligand complexes. Because of the widespread importance and applications of the transition metal cation-*N*-donor ligand complexes it is desirable to better understand and quantitatively characterize metal cation-ligand interactions in the late first-row divalent transition metal cations (M^{2+}) and *N*-donor ligands (*N*-*L*). The experimental studies make use of energy-resolved collision-induced dissociation (CID) techniques that are carried out in a custom built guided ion beam tandem mass spectrometer (GIBMS) to probe the structures, energetics, and fragmentation behavior of the complexes of interest. Electronic structure theory calculations including several density functional theory methods are employed to determine stable low-energy structures of the $M^{2+}(N\text{-}L)_x$ complexes and the relevant species associated with their CID behavior. The five late first-row transition metal cations in their +2 oxidation states, Fe^{2+}, Co^{2+}, Ni^{2+}, Cu^{2+}, and Zn^{2+}, are included in this work. The *N*-donor ligands investigated here include Pyr, a monodentate ligand, and two bidentate ligands, Bpy, and Phen. The structures of these complexes are investigated theoretically, while the CID behavior is examined experimentally. The energetics of binding, and the mechanisms and energetics of electron transfer and proton transfer charge fission pathways are extracted theoretically while experimental studies are only limited to electron

transfer process. By studying these complexes where the electron configuration of the metal cation is systematically varied from $Fe^{2+}(d^6)$, to $Co^{2+}(d^7)$, to $Ni^{2+}(d^8)$, to $Cu^{2+}(d^9)$, to $Zn^{2+}(d^{10})$, periodic trends in the nature of the binding are elucidated. Ligand field effects are examined by comparing the behavior of the complexes among three related *N*-donor ligands and by varying the extent of ligation. Complexes with one to three Bpy or Phen ligands are investigated theoretically, while experimental studies are limited to the bis and tris-ligated complexes, i.e., those that can be readily generated by electrospray ionization (ESI). Theoretical studies of the complexes involving one to six Pyr ligands are also included in this work for comparative purposes, but are not investigated experimentally here. The periodic trends in these complexes are then compared with the analogous complexes involving the monovalent first-row transition metal cations, Co^+, Ni^+, Cu^+, and Zn^+ previously investigated.[100- 104] These comparisons allow the effects of the charge and electronic structure of the metal cation on the structures and strength of binding to be further elucidated.

1.4 References

(1) Guy, R. H.; Hostynek, J. J.; Hinz, R. S.; Lorence, C. R. *Metals and the Skin: Topical Effects and Systematic Absorption.* Marcel Dekker, Inc. New York. **1999**, pp. 121–408.

(2) Shriver, D. F.; Atkins, P. W.; Overton, T. L.; Rourke, J. P.; Weller, M. T.; Armstrong, F. A. *Inorganic Chemistry* (4th ed). W. H. Freeman and Company, New York. **2006**, pp. 433–437.

(3) Frieden, A. *A Survey of the Essential Biochemical Elements, Biochemistry of the Essential Ultratrace Elements.* Plenum Press. **1984**, pp. 1–15.

(4) Stephen, J. L.; Berg, J. M. *Principles of Bioinorganic Chemistry*. University Science Books, Mill Valley, California. **1994**, pp. 103–136.

(5) Theophanides, T. *Can. J. Spectrosc*. **1981**, *26*, 165.

(6) Williams, R. J. *Coord. Chem. Rev*. **1990**, *100*, 573.

(7) Sigel, A.; Sigel, H.; Sigel, R. K. O. *Nickel and its Surprising Impact in Nature*. Chichester, West Sussex, England. **2007**, pp. 654–720.

(8) Huogh, E.; Hansen, L. K.; Birknens, B.; Jynge, K.; Hansen S.; Hardvick, A.; Little, C.; Dodson, E.; Derewende, Z. *Nature*. **1989**, *338*, 357.

(9) Burley, S. K.; David, P. R.; Sweet, R. M.; Taylor, A.; Lipscomb, W. N. *J. Mol. Biol*. **1992**, *124*, 113.

(10) Frausto da silva, J. J. R.; Williams, R. J. P. *The Biological Chemistry of the Elements: The Inorganic Chemistry of Life* (2nd ed). Oxford University Press, Oxford. **2001**, pp. 320–325.

(11) Stryer, L. *Biochemistry*. W. H. Freeman Co., New York. **1995**, pp. 145–438.

(12) Aust, S. D.; Morehouse, L. A.; Thomas, C. J. *Free Radic. Biol. Med.* **1985**, *1*, 3.

(13) May, P. M.; Williams, D. R. *Metal Ions in Biological Systems*. Sigel, H. (ed). Marcel Dekker, New York. **1981**, pp. 283.

(14) Kagawa, T. F.; Geierstanger, B. H.; Wang, A. H. J.; Shing Ho, P. *J. Biol. Chem*. **1991**, *266*, 20175.

(15) Kiley, P. J.; Beinert, H. *Curr. Opin. Chem. Biol*. **2003**, *6*, 182.

(16) Anastassopoulou, J.; Anifantakis, B.; Anifantakis, Z. A.; Dovas, A.; Theophanides, T. *Bioinorganic Chem*. **2000**, *79*, 327.

(17) Sigel, H. *Metal Ions in Biological Systems: Inorganic Drugs in Deficiency and Disease*. Marcel Dekker, New York. **1982**, pp. 125–171.

(18) Theophanides, T.; Anastassopoulou, J. *Crit. Rev. Oncology and Haematology*. **2002**, *42*, 57.

(19) va Albada, G. A.; Mohamadou, A.; Mutikainen, I.; Turpeinen, U.; Reedijk, J. *Eur. J. Inorg. Chem*. **2004**, 3733.

(20) Dell'Amico, D. B.; Calderazzo, F.; Curiardi, M.; Labella, L.; Marchetti, F. *Inorg. Chem.* **2004**, *43*, 5459.

(21) Constable, E. C. *Adv. Inorg. Chem*. **1989**, *34*, 1.

(22) Zhang, D. P.; Tian, N. C.; Zhang, X. M. *Acta Crystallogr*. **2010**, *E66*, m614.

(23) Constable, E. C. *Metals and Ligand Reactivity*. Ellis Horwood Limited, England. **1990**, pp. 23–79.

(24) Hancock, R. D. *J. Chem. Educ*. 1992, *8*, 619.

(25) Sigel, H. *Inorg. Chem*. **1980**, *19*, 1413.

(26) Wejnen, J. G.; Koudijs, A.; Engbersen, J. F. J. *J. Org. Chem*. **1992**, *57*, 7258.

(27) Engbersen, J. F. J.; Koudijs, A.; van der Plas, H. C. *J. Org. Chem*. **1990**, *55*, 3647.

(28) Schoffers, E. *Eur. J. Org. Chem*. **2003**, *7*, 1145.

(29) Armaroli, N. *Chem. Soc. Rev*. **2001**, *30*, 113.

(30) Gray, H. B.; Malmstrom, B. G.; Williams, R. J. P. *J. Biol. Inorg. Chem*. **2000**, *5*, 551.

(31) Hogue, C. *Chem. Eng. News*. **2005**, *83*, 67.

(32) Craciunescu, D.; Fruma, A.; Ghirvu, C. *Inorg. Chim. Acta.* **1970**, *4*, 305.

(33) Anderson, V.; Taylor, J. *J. Am. Chem. Soc.* **1921**, *45*, 605.

(34) Sigel, H.; Flierl, C.; Griesser, R. *J. Am. Chem. Soc*. **1969**, *91*, 1061.

(35) Bohnson, A.; Robertson, V. *J. Am. Chem. Soc.* **1923**, *45*, 2512.

(36) Bohnson, A.; Robertson, V. *J. Am. Chem. Soc.* **1925**, *47*, 1299.

(37) Bail, V. S.; Baxendal, S. P. *Trans. Faraday Soc.* **1951**, *47*, 662.

(38) Walton, J. I.; Filson, J. *J. Am. Chem. Soc.* **1932**, *54*, 3226.

(39) Segal, M. G.; Sykes, A. G. *J. Am. Chem. Soc.* **1978**, *100*, 4585.

(40) Mashiko, T.; Reed, C. A.; Haller, K. J.; Kastner, M. E.; Scheidt, W. R. *J. Am. Chem. Soc.* **1981**, *103*, 5758.

(41) Mauk, A. G.; Scott, R. A.; Gray, H. B. *J. Am. Chem. Soc.* **1980**, *102*, 4360.

(42) Chen, X. M.; Liu, G. J. *Chem. Eur. J.* **2002**, *8*, 4811.

(43) Collman, J. P.; Buckingham, D. A. *J. Am. Chem. Soc.* **1963**, *85*, 3039.

(44) Fischler, I.; Wagner, R.; Koerner von Gustorf, E. *J. Organomet. Chem.* **1976,** *112*, 1557.

(45) Dumas, H.; Levisalles, J.; Rudler, H. *J. Organomet. Chem.* **1980**, *187*, 405.

(46) Hamilton, R. J.; Bergens, S. H. *J. Am. Chem. Soc.* **2008**, *130*, 11979.

(47) Schoffers, E. *Eur. J. Org. Chem.* **2003**, 1145.

(48) Gladysz, J. A.; Boone, B. J. *Angew. Chem., Int. Ed. Engl.* **1997**, *36*, 551.

(49) Hollis, T. K.; Odenkirk. W.; Robinson, N. P.; Whelan, J.; Bosnich, B. *Tetrahedron* **1993**, *49*, 54150.

(50) Davenport, A. J.; Fawcett, J.; Lad, L.; Russell, R. R. *Chem. Commun*. **1997**, 2347–2348.

(51) Hull, J. F.; Balcells, D.; Blakemore, J. D.; Incarvito, C. D.; Eisenstein, O.; Brudvig, G. W.; Crabtree, R. H. *J. Am. Chem. Soc.* **2009**, *131*, 8730.

(52) Cheng, H. Y.; Hao, J. M.; Wang, H. J.; Xi, C. Y.; Meng, X. C.; Cai, S. X.; Zhao, F. Y. *J. Mol. Catal. A* **2007**, *278*, 6.

(53) Concepcion, J. J.; Jurss, J. W.; Brennaman, M. K.; Hoertz, P. G.; Patrocinio, A. O. T.; Iha, N. Y. M.; Templeton, J. L.; Meyer, T. J. *Acc. Chem. Res*. **2009**, *42*, 1954.

(54) Martins, J. E. D.; Wills, M. *Tetrahedron* **2009**, *65*, 5782.

(55) Gnanamgari, D.; Moores, A.; Rajaseelan, E.; Crabtree, R. H. *Organometallics* **2007**, *26*, 1226.

(56) Constable, E. C.; Cargill, A. M. W.; Tochter, D. A. *Supramolecular Chemistry*. NATO AS1 Ser. Ser. C. **1992**, *371*, 219.

(57) Lehn, J. M. *Comprehensive Supramolecular Chemistry*. VCH, Weinheim, Germany. **1996**, pp. 1–595.

(58) Hofmeier, H.; Schubert, U. S. *Chem. Commun*. **2005**, 2423.

(59) Philp, D.; Stoddart, F. J. *Angew. Chem.* **1996**, *108*, 1242.

(60) Philp, D.; Stoddart, F. J. *Angew. Chem., Int. Ed*. **1996**, *35*, 1154.

(61) Lodish, H.; Berk, A.; Zipursky, S. L.; Matsudaira, P.; Baltimore, D.; Darnell, J. *Molecular Cell Biology* (4th ed). W. H. Freeman and Company, New York. **2000**, pp. 2–25.

(62) Schubert, U. S. *Tailored Polymers and Applications*. Yagci, M. K.; Muyken, O.; Ito, K.; Wnek, G (ed). VSP Publishers, Utrecht. **2000**, pp. 63–85.

(63) Schubert, U. S.; Eschbaumer, C. *Angew Chem. Int. Ed.* **2002**, *41*, 2892.

(64) Murray, L. J.; Dinca, M.; Long, J. *Chem. Soc. Rev*. **2009**, *38*, 1294.

(65) Hermes, S.; Schroter, M.; Schmid, R.; Khodeir, L.; Muhler, M.; Tissler, A.; Fisher, R. W.; Fischer, R. A. *Angew. Chem., Int. Ed*. **2005**, *44*, 6237.

(66) Stoddart, J. F. *Chem. Br*. **1991**, 714.

(67) Gillard, R. D.; Hill, R. E.; Maskill, R. J. *J. Chem. Soc. A* **1970**, *9*, 1447.

(68) Hunt, H. R., Jr. *J. Chem. Ed*. **1977**, *54*, 710.

(69) Farruseng, D.; Aguado, S.; Pinel, C. *Angew. Chem.; Int. Ed.* **2009**, *48*, 7502.

(70) Lei, Z. Q.; Han, X. G.; Hu, Y. L.; Wang, R. M.; Wang, Y. P. *J. Appl. Polym. Sci*. **2000**, *75*, 1068.

(71) Kalyanasundaram, K. *Coord. Chem. Rev*. **1982**, *46*, 159.

(72) Gohy, J. F.; Lohmeijer, B. G. G.; Schubert, U. S. *Macromol. Rapid Commun*. **2002**, *23*, 555.

(73) Andres, P. R.; Schubert, U. S. *Adv. Mater*. **2004**, *16*, 1043.

(74) Ferreira, K. N.; Iverson, T. M.; Maghlaoui, K.; Barber, J.; Iwata, S. *Science* **2004**, *303*, 1831.

(75) Wang, X. F.; Koyama, Y.; Kitao, O.; Wada, Y.; Sasaki, S.; Tamiaki, H.; Zhou, H. S. *Biosens. Bioelectron*. **2010**, *25*, 1970.

(76) Kramer, I. J.; Sargent, E. H. *ACS Nano*. **2011**, *5*, 8506.

(77) Li, L.; Duan, L.; Xu, Y.; Gorlov, M.; Hagfeldt, A.; Sun, L. *Chem. Commun*. **2010**, 46, 7307.

(78) Peters, J. W.; Lanzilotta, W. N.; Lemon, B. J.; Seefeldt, L. C. *Science*, **1998**, *282*, 1853.

(79) Nicolet, Y.; Piras, C.; Legrand, P.; Hatchikian, C. E.; Fontecilla-Camps, J. C. *Structure*, **1999**, *7*, 13.

(80) Pierik, A. J.; Hulstein, M.; Hagen, W. R.; Albracht, S. P. J. *Eur. J. Biochem.* **1998**, *258*, 572.

(81) Chen, Z. J.; Lemon, B. J.; Huang, S.; Swartz, D. J.; Peters. J. W.; Bagley, K. A. *Biochemistry*, **2002**, *41*, 2036.

(82) Tronche, C.; Goodman, B. K.; Greenberg, M. M. *Chem. Biol*. **1998**, *5*, 263.

(83) Steenken, S. *Biol. Chem*. **1997**, *378*, 1293.

(84) Fialko, N. S.; Lakhno, V. D. *Phys. Lett. A* **2000**, *278*, 108.

(85) Chang, Y. J.; Chow, T. J. *Tetrahedron* **2009**, *65*, 4726.

(86) Gust, D.; Moore, T. A.; Moore, A. L. *Acc. Chem. Res*. **2009**, *42*, 1890.

(87) McConnell, I.; Li, G. H.; Brudvig, G. W. *Chem. Biol*. **2010**, *17*, 434.

(88) Nazeeruddin, M. K.; Pechy, P.; Renouard, T.; Zakeeruddin, S. M.; Humpry-Baker, R.; Comte, P.; Liska, P.; Cevey, L.; Costa, E.; Shklover, V.; Spiccia, L.; Deacon, G. B.; Bignozzi, C. A.; Gratzel, M. *J. Am. Chem. Soc.* **2001**, *123*, 1613.

(89) Razskazovskii, Y.; Swarts, S. G.; Falcone, J. M.; Taylor, G.; Sevilla, M. D. *J. Phys. Chem. B* **1997**, *101*, 1460.

(90) Ly, D.; Sanii, L.; Schuster, G. B. *J. Am. Chem. Soc*. **1999**, *121*, 9400.

(91) Shinar, J.; Shinar, R. *J. Phys. D. Appl. Phys.* **2008**, *41*, 133001.

(92) Tang, C. W.; Vanslyke, S. A. *Appl. Phys. Lett.* **1987**, *51*, 913.

(93) Dunbar, A. D. F.; Brittle, S.; Richardson, T. H.; Hutchinson, J.; Hunter, C. A. *J. Phys. Chem. B.* **2010**, *114*, 11697.

(94) Fink, H. W.; Schonenberger, C. *Nature*. **1999**, *398*, 407.

(95) Nunez, M.; Hall, D. B.; Barton, J. K. *Chem. Biol*. **1999**, *6*, 85.

(96) An, Y.; Tong, M.; Ji. L.; Mao, Z. *Dalton Trans*. **2006**, *17*, 2066.

(97) Harris, C.; Kamat, P. V. *ACS Nano*. **2009**, *3*, 682.

(98) Dimitrijevic, N. M.; Poluektov, O. G.; Saponjic, Z. V.; Rajh, T. *J. Phys. Chem. B* **2006**, *110*, 25392.

(99) Asryan, L. V. *J. Nanophotonics* **2009**, *3*, 0131601.

(100) Rannulu, N. S.; Rodgers, M. T. *J. Phys. Chem. A* **2007**, *111*, 3465.

(101) Rannulu, N. S. Doctoral dissertation, Wayne State University. 2008, pp. 1–383.

(102) Rannulu, N. S.; Rodgers, M. T. *J. Phys. Chem. A* **2009**, *113*, 4534.

(103) Rannulu, N. S.; Rodgers, M. T. *J. Phys. Chem. A* **2012**, *116*, 1319.

(104) Rodgers, M. T.; Stanley, J. R.; Amunugama, R. *J. Am. Chem. Soc*. **2000**, *122*, 10969.

CHAPTER 2

EXPERIMENTAL AND THEORETICAL METHODS

2.1 Experimental Procedures

2.1.1 Synthesis of Metal Complexes

All chemicals were procured from commercial sources and used as received without further purification. The synthesis of $[M(N\text{-}L)_x](PF_6)_2$, where x = 1–3, M = Fe, Co, Ni, Cu, and Zn, and *N-L* = 2,2′-bipyridine (Bpy), 1,10-phenanthroline (Phen), or pyridine (Pyr) was carried out by adapting literature procedures[1,2] using $(NH_4)_2Fe(SO_4)_2$, $CoCl_2$, $Ni(NO_3)_2$, $Cu(NO_3)_2$, and $Zn(NO_3)_2$ salts, respectively. Briefly, the $[M(N\text{-}L)_x](PF_6)_2$ complexes are obtained by reacting an aqueous solution of the metal salt with a methanolic solution of the Bpy or Phen ligand stoichiometrically depending on the number of *N-L* ligands to be complexed to the M^{2+} cation. For instance, the $[M(N\text{-}L)_3](PF_6)_2$ complexes are obtained by reacting 3.0 equivalents of the *N-L* ligand with 1.0 equivalent of the metal salt. After 15 minutes of reflux, a methanolic solution of NH_4PF_6 is added to facilitate precipitation of the $[M(Phen)_x](PF_6)_2$ salt, which is isolated by filtration.

2.2 Overview of Guided Ion Beam Mass Spectrometer

A schematic diagram of the home-built guided ion beam tandem mass spectrometer (GIBMS) in which experiments were performed is shown in Figure 2.1. The vacuum system comprises six regions that are individually pumped: (1) the electrospray ionization (ESI) source/ion funnel hexapole collision cell interface, (2) the first differentially pumped region, (3) the second differentially pumped region, (4) the magnetic sector flight tube and third differentially pumped region, (5) the reaction chamber, and (6) the detector chamber. All regions are pumped by diffusion pumps with integral water baffles except the ESI source/ion

funnel/hexapole collision cell interface, which is pumped by a roots blower. A detailed explanation of each region of the GIBMS is given below.

2.2.1 Electrospray Ionization Source/Ion Funnel/Hexapole Ion Guide/Collision Cell Interface

2.2.1.1 Electrospray Ionization Source

Ions are generated in an ESI source[3,4] similar in design to that developed by Moision et al.[5] A schematic overview of the ESI source/ion funnel/hexapole ion guide collision cell interface (ESI/IF/6P) is shown in Figure 2.2. Solutions containing the ions of interest at concentrations of ~0.01–0.1 mM are prepared using a 1:1 (v/v) mixture of water and acetonitrile. A syringe pump (Harvard Apparatus, PHD 22/2000) is used to introduce the ions into the ESI needle at a rate of 1.0 μL/min. The ESI needle is made of 35 gauge stainless steel (SS) tubing (Small Parts) biased at ~1.7–2.0 kV provided by a high voltage dc power supply (Glassman, model EQ5R240). The XYZ translation stage (Line Tool Co, model A RH-1/2″ travel) is used to mount the entire needle assembly and allows for fine-tuning of the location of the needle relative to the entrance limiting orifice (ELO). Using a fiber optic illuminator (Cole-Parmer, WU-41723-00) and a light pipe (Cole-Parmer, EW-41720-75), the ESI spray emanating from the needle is visualized, monitored with a CCTV camera (Panasonic, WV-BP330), and displayed on a CCTV monitor (Videology, 40 VM9). A 4″ long SS capillary, 0.030″ ID and 0.063″ OD (McMaster-Carr) that is held within a capillary tubing holder (CTH) introduces the droplets emanating from the ESI needle into the vacuum region. The 0.375″ OD CTH is reamed out to an ID of 0.067″ for easy insertion of the 0.063″ OD SS capillary. The CTH is electrically isolated from the SS capillary using PEEK thermoplastic material. The ELO covers the entrance of the CTH, and reduces the

orifice to 0.009″. The ELO serves to throttle the gas load into the vacuum, such that the diameter of the ELO is directly correlated with the pressure in the source interface region. The SS capillary is biased at 20–50 V provided by a dc power supply (BK Precision, model 1623 A) and heated to ~90–200 °C using heating tape (Omega, HTC-030) and a temperature controller (Staco, 3PN1010). The capillary temperature is monitored using a thermocouple (MDC, TC PWR K). A digital multi-meter connected to the thermocouple provides the temperature readout.

2.2.1.2 Radio Frequency Ion Funnel

The ESI source is interfaced to a radio frequency (rf) ion funnel, similar in design to that developed by Smith and co-workers.[6,7] The ion funnel consists of 88 electrically isolated ring electrodes (or plates) with decreasing inner diameters (from 1.000″ to 0.094″) in the direction of the exit. Each electrode is separated by a 0.020″ thick Teflon sheet. A linear dc gradient is applied across the ion funnel by applying a dc voltage to the first and last plates of the ion funnel with a resistor chain connecting all intervening plates. Adjacent electrodes receive equal and opposite phases of an rf signal with peak-to-peak voltage in the range between 10 and 30 V, and is operated at a frequency in the range between 0.6 and 1.2 MHz. This oscillating field on the plates focuses ions radially to the center of the ion funnel. A 0.25″ diameter metal disc, Jet disrupter (JD) located ~1.0″ from the entrance of the ion funnel prevents large droplets from the spray from depositing downstream on the hexapole ion guide. The JD is biased at 15–25 V. A dc-only hexapole injection lens (HIL) with a 0.140″ ID follows the last plate of the ion funnel to prevent ions that have entered the hexapole from diffusing back upstream toward the ion funnel. The HIL is biased at a voltage that lies between the voltage on the final ion funnel plate and the hexapole dc voltage, which

is typically held at ground potential. The circuit board that provides the dc and rf signals to the ring electrodes was designed using an internet vendor (www.ExpressPCB.com). The circuit board provides both rf and dc outputs, such that it requires only one electrical connection per plate. Surface-mount resistors (200 kOhm, 1/8 Watt, size 1206, Allied Electronics) and capacitors (0.01 μF, 100 V, size 1206, Allied Electronics) are used on the circuit board. Two dc voltages, (DC^+, on the entrance lens, DC^-, on the exit lens) are applied across the ion funnel to define the linear voltage gradient. Normal operating conditions for the ion funnel are DC^+ = ~25 V and DC^- = ~5 V. A home-built dc voltage divider that consists of a 75 V dc linear regulated power supply (Acopian Technical, model B75GT05) and a four-channel circuit provides four dc voltages for DC^+, DC^-, JD, and HIL, respectively. The rf signal is applied to the ion funnel using a 20 MHz sweep function generator (B&K Precision, model 4040A), and is amplified with an rf amplifier (Electronics and Innovation, model 240L). The signal from the amplifier is split into equal and opposite phases with a 100–Ohm trifilar wound ferrite toroids (Amidon Inc. FR-290-77) wrapped with 14-gauge magnet wire. The ion funnel facilitates efficient transfer of ions from the high pressure (10^{-2} Torr) source region to the low pressure (10^{-5} Torr) region of the mass spectrometer.

2.2.1.3 Radio Frequency Hexapole Ion Guide/Collision Cell

Ions exits the ion funnel (IF) and enter an rf hexapole ion guide (6P) that traps them radially. In this region, the ions are thermalized by collisions with the background gases. The hexapole ion guide consists of six 0.125″ diameter x 6.0″ long SS rods (Small parts), equally spaced on a 0.375″ BC. The rf signal is applied to the rods using a simple rf generator described by Jones et al.[8,9] and is normally operated at a frequency of 5.5 MHz with a peak to peak voltage (V_{pp}) of 200–300 V. The dc voltage of the 6P is maintained at 0 V; therefore,

the ions pass through the hexapole region primarily by diffusion. The collision cell/ligand exchange cell aligns the 6P with respect to the IF. Gases such as argon, helium, and nitrogen can be added to the collision cell to facilitate thermalization of the ions. Other gases can be introduced into collision cell to react with the ions produced by the ESI through ligand exchange or condensation processes. The ESI source region of the instrument is pumped by a 300 L/s roots blower (Model EH1200; Edwards High Vacuum, Sussex, UK). The hexapole ion guide crosses two vacuum regions, the ESI source vacuum interface region and the differential region. The pressure in the source region is ~5–8 x 10^{-5} Torr during operation. These pressures ensure sufficient collisions in the hexapole ion guide for thermalization.

2.2.2 Differential Focusing Stage

Ions emanating from the source region are extracted by a series of lenses including the aperture lens (DL3), the differential aperture (DA), and the deflectors in the differential focusing stage (DFS). Lens voltages in this region are typically kept below 300 V in order to avoid energetic collisions with the background air that might internally excite the ions. The DFS lenses have an open design to maximize gas conductance, which reduces the probability of energetic collisions in this region. The pressure in the differential region is maintained at ~5–8 x 10^{-5} Torr (uncorrected for ion gauge sensitivity to background gases) during operation of the ESI source by a 2000 L s^{-1} diffusion pump with integral water cooled baffles (Edwards Diffstak MK2 250/2000P). Differential pumping of the following region is maintained by a 5.0 mm diameter exit aperture.

2.2.3 Ion Beam Formation

The ions exiting the DFS are handled by focusing stage 1 (FS1), which is designed to shape and steer the beam and accelerate it to the voltage used for momentum analysis. The

ions are extracted from the first differential region and collimated by a double aperture immersion lens, focused by an einzel lens, and then accelerated to the momentum analysis potential. An electrostatic quadrupole doublet lens converts the beam from cylindrical symmetry to a ribbon shape appropriate for momentum analysis. The quadrupole doublets focus the beam onto the entrance slit of the momentum analyzer. A gate valve mounted on the flight tube of the analyzer (and biased at the mass analysis potential during operation) allows isolation of the source end of the instrument for cleaning the source region without venting the entire instrument. The magnetic momentum analyzer consists of a magnetic sector (Nuclide Corporation) with a 30.5 cm radius ion flight path and a 90° defection angle. The entrance and exit slit widths are 1 mm. The analysis potential is typically 2800 V. Under these conditions, the momentum analyzer serves as a mass filter providing a mass range from 1 to 1500 Da, with a mass resolution of approximately 500 (m/Δm fwhm) for ions with an initial energy spread of less than 1 eV ($E/\Delta E$ fwhm). After passing through the exit slit of the momentum analyzer, the ion beam is reconverted to cylindrical symmetry by a second electrostatic quadrupole doublet lens and focused by an einzel lens in focusing stage 2 (FS2). A set of horizontal and vertical deflectors allows centering of the beam onto a 2 mm aperture, the entrance to the reaction region vacuum chamber. This aperture also serves to separate vacuum regions for differential pumping. The pressure in the flight tube and FS2 region is maintained by a 300 L s^{-1} diffusion pump with integral water baffles (Edwards Diffstak MK2 100/300P). The ions enter an exponential retarder, which is 9.8 cm long and consists of 33 evenly spaced plates. The retarder plate potentials are determined by internally connected resistors that establish an exponentially decreasing field.[10] The last three plates are connected and their voltage controlled externally. These final plates act as

the first lens in a four element lens sequence focusing stage 3 (FS3) that focuses and injects the ions into the octopole ion beam guide.

2.2.4 Reaction Region

The reaction region is the heart of the GIBMS instrument, comprising an octopole ion guide surrounded by a gas reaction cell. The octopole ion guide comprises eight rods of 3.2 mm x 27.9 cm long, equally spaced on a 11.7 mm diameter circle. Opposing phases of the rf potential are applied to alternate rods, which provides a radial effective potential well for highly efficient collection of ionic products.[11] The rf is generated using a high voltage rf generator described by Jones et. al.[9] The peak-to-peak amplitude of the rf potential is typically 300 V, which provides a trapping well of 2.83 V.[12] The dc potential of the octopole (and surrounding gas cell) is also controlled in order to vary the kinetic energy of the ions using a bipolar operation power supply (Kepco BOP 100–M).

The octopole passes through a gas reaction cell located midway along its length. The gas cell consists of 51 mm long x 51 mm diameter central body with smaller extension tubes, 32 mm long x 17 mm diameter, extending from each end of the gas cell along the octopole rods, and designed to limit gas conductance from the cell.[13] Two SS tubes emanating perpendicularly from the gas reaction cell are electrically isolated from ground via glass to metal seals and are used to introduce the collision gas and measure pressure in the reaction cell. The gas pressure introduced to the cell is controlled by a leak valve (Granville Phillips 203) and measured using a capacitance manometer (MKS Baratron 690A). Assuming a trapezoidal pressure profile,[13] the effective cell length is estimated to be 8.3 cm with a 10% uncertainty. To ensure that secondary collisions are improbable, gas cell pressures in the range of 0.025 to 0.02 mTorr are used for cross section measurements. Xe is used as the

collision gas in all of the collision-induced dissociation (CID) studies performed because it is heavy and polarizable, and therefore leads to more efficient kinetic to internal energy transfer.[14-16] During operation, a pressure difference ratio of approximately 70:1 can be maintained between the reaction cell and the reaction region vacuum chamber, which is continuously pumped by a 2000 L s^{-1} diffusion pump with water cooled baffles (Edwards Diffstak MK2 250/2000P). The background signals arising from collisions that occur outside of the reaction cell are measured by diverting the gas flow from the reaction cell directly to the reaction region vacuum chamber using remotely controlled electropneumatic valves mounted on the gas inlet lines. In this configuration, the background pressure in the reaction chamber is the same as when the gas is flowing to the reaction cell. The effective length for background reactions is approximately twice as long as the reaction cell path length, resulting in a measured foreground/background ion intensity of nearly 40:1.

2.2.5 Quadrupole Mass Spectrometer and Ion Detector

After collision with Xe gas, all product ions and remaining reactant ions drift to the end of the octopole ion guide, where they are extracted from the octopole and injected into a quadrupole mass filter by a series of five lenses of cylindrical symmetry in focusing stage 4 (FS4). The quadrupole mass filter (Extrel, ¾″ Tri-filter Quadrupole Mass Filter, 150 QC RF/DC Power Supply) has rods that are 19 mm diameter x 22.9 cm long. The quadrupole rods consist of three segments, pre-rods, center-rods, and post-rods. The pre- and post-rods work as ion guides and are shorted to receive a single dc voltage. The center-rods work as a mass filter and are controlled by a 150 QC power supply. The 880 kHz rf voltage generated by 150 QC power supply provides a mass range of 1–1000 Da. The quadrupole is generally operated at a fairly low mass resolution in order to achieve maximum transmission of ions.

Ions emanating from the quadrupole mass filter are then focused by a series of three lenses of cylindrical symmetry in the detector focusing stage. Ions are detected using a secondary electron scintillation detector of the Daly type,[17] operated at an ion target potential of 28 kV. The detector, combined with pulse counting electronics, provides high counting efficiency and low mass discrimination. The scintillation photons are detected using a photomultiplier tube (Hamamatsu R329SEL). The output pulses of the photomultiplier are directly discriminated from noise using a constant fraction discriminator (Canberra model 2126) and counted using a dual counter timer (Canberra model 2071A) for digital data acquisition. A linear ratemeter (EG&G Ortec model 661) is used for visual display during tuning of the ion beam. The counting response of the ion detection system is linear up to ~2 x 10^7 s^{-1}, and the counting noise background is typically less than 10 s^{-1}, providing a dynamic range in excess of 6 orders of magnitude.

2.2.6 Data Acquisition System

A computer equipped with a Pentium 133 MHz processor is used to control the GIBMS. A commercial GPIB interface board with 12-bit resolution (Keithley PCI-488) and a custom digital I/O board provide the hardware control functions. The Canberra dual counter timer 2071A (used in ion detection) and a Kepco BOP 100–IM power supply (used to control the dc voltage applied to the reaction region) are controlled by the GPIB board. The Kepco BOP has two modes with high (0 to ±100 eV) and low (0 to ±10 eV) ranges, such that the 12-bit resolution of the GPIB results in a minimum energy step size of 0.002 eV below 10 eV and 0.024 eV above 10 eV. A 16-bit optically isolated DAC contained in the custom digital I/O board is used to set the m/z of the quadrupole mass filter with a minimum step size of 0.0153 Da. The electropneumatic valves that direct the neutral reactant gas to the

collision gas cell or reaction chamber are controlled by two digital outputs connected to solid-state relays and contained in the custom digital I/O board. The custom digital I/O board is interfaced to the Baratron through an SCSI cable such that the pressure output is read digitally. The gas flow rates in the source and interaction regions, and all other lens potentials in the instrument do not vary with the ion interaction energy and are therefore not automated. Collision gas flow rates are controlled manually with leak valves (Granville Philips, model 203). The custom-built voltage dividers powered by standard dc power supplies provide the lens potentials.

The GIBMS instrument is controlled by two 32-bit multithreaded graphical user interface programs namely, MSCAN and EMP (energy, mass, and pressure). These two programs are written using Compaq Vision FORTRAN 6.1 A with lower level device interfaces written in C and are used to acquire data during experiments. The MSCAN program allows the quadrupole mass filter to be scanned at fixed octopole interaction energy and records the intensity of detected ions as a function of the mass-to-charge ratio. The EMP program allows the octopole interaction energy to be scanned and records the intensity of the specified reactant and product ions as a function of this energy. Each program has a real-time graphical display and I/O windows, a control panel, and a color and symbol palette. The control panel requires user input for instrument control and set up of a desired experiment, reports details and progress of the current experiment, and allows changes to be made in the graphical display window during data acquisition.

2.2.7 General Procedures

Ion intensities are converted to absolute cross sections using Beer's law. The experimental total reaction cross section, σ_{tot}, is determined by the relation,

$$I_R = \left(I_R + \sum I_P \right) e^{-\sigma_{tot} nL} \tag{2.1}$$

where I_R and I_P are the measured transmitted intensities of the reactant and product ions, respectively, n is the gas density, and L is the effective collision gas cell length. Individual product cross sections are calculated using the following formula

$$\sigma_p = \sigma_{tot} \left(I_p \Big/ \sum I_P \right) \tag{2.2}$$

Equations 2.1 and 2.2 presume that sum of the transmitted reactant and product ions are equal to the incident ion intensity, that is, $I_0 = I_R + \sum I_P$. Due to the 4π collection characteristics of the octopole, this is valid as long as all significant channels are monitored. Absolute uncertainties in the cross sections are estimated to be ±20%, and are derived largely from errors in the pressure measurements and the effective length of the interaction region. Relative uncertainties are approximately ±5%.

Ion kinetic energies in the laboratory frame, E_{lab}, are converted to energies in the center-of-mass frame, E_{cm}, using the formula, $E_{cm} = E_{lab} m/(m+M)$, where M and m are the masses of the ionic and neutral reactants, respectively. Because the reactant ions are doubly charged, the laboratory energies, $E_{lab} = 2V_{lab}$, where V_{lab} is the applied voltage in the octopole region. All energies reported in this study are in the center-of-mass frame unless otherwise noted. The absolute zero and distribution of ion kinetic energies are determined using the octopole ion guide as a retarding potential analyzer as previously described.[13] The potential difference between the ESI capillary and the interaction region, (that is, the dc voltage of the octopole) establishes the nominal laboratory ion kinetic energy. The octopole ion guide also serves as a highly efficient retarding energy analyzer. The ion beam intensity, I_0, is monitored as the dc voltage of the octopole is swept through the ion energy zero, producing a

retardation curve such as that shown in Figure 2.3. This figure shows the ion intensity of the $Zn^{2+}(Phen)_3$ complex as a function of the laboratory kinetic energy. The trapping characteristics of the octopole prevent dispersion of low energy ions due to space charge. Further, because reactions take place in the same region as the energy analysis, there is no ambiguity in the interaction determination due to contact potential differences. For the ESI source, the experimental primary ion kinetic energy distribution, as determined by the retarding energy analysis, is nearly Gaussian. A Gaussian curve fitted to the experimental distribution from the retarding energy analysis of Figure 2.3 is shown in Figure 2.4, where the ion beam energy distribution was obtained by taking the derivative with respect to energy of the retarding energy analysis curve. The solid line is a Gaussian curve fitted to the data points. The apparent full width at half-maximum (fwhm) from the retardation curve adequately describes the width of the Gaussian fit. For most experiments performed here, the distribution of ion kinetic energies is nearly Gaussian with a fwhm typically between 0.2 and 0.4 eV (lab). The uncertainty in the absolute energy scale is ±0.10 eV (lab).

Previous studies have demonstrated that the effect of multiple collisions can significantly influence the shape of CID cross sections even when the pressure of the reactant neutral is low.[18] Because the presence and magnitude of these pressure effects are difficult to predict, pressure-dependent studies have been performed for all cross sections examined in this study. Data free from pressure effects is obtained by extrapolating to zero reactant pressure, as described previously.[18] Thus, results reported in these studies are due to single bimolecular encounters.

2.2.8 Thermochemical Analysis.

The threshold regions of the measured CID cross sections are modeled using an empirical threshold law, equation 2.3,

$$\sigma(E) = \sigma_0 \sum_i g_i \left(E + E_i - E_0\right)^n / E \qquad (2.3)$$

where σ_0 is an energy independent scaling factor, E is the relative translational energy of the reactants, E_0 is the threshold for reaction of the ground electronic and ro-vibrational state, and n is an adjustable parameter that is inversely correlated with the efficiency of kinetic to internal energy transfer.[12] The summation is over the ro-vibrational states of the reactant ions, i where E_i are the excitation energies, and g_i the populations of those states $\left(\sum g_i = 1\right)$. The relative reactivity of all ro-vibrational states, as reflected by σ_0 and n, is assumed to be equivalent. The Beyer-Swinehart algorithm[19,20] is used to evaluate the density of the ro-vibrational states and the relative populations, g_i, are calculated for a Maxwell Boltzmann distribution at 298 K, the internal temperature of the reactant ions.

An important consideration in the analysis of threshold energies is whether dissociation occurs within the ~10^{-4} s it takes for the complex to pass from the collision cell to the quadrupole mass filter. If the lifetime of the activated complex exceeds this time frame, the apparent thresholds are shifted to higher energies, resulting in a kinetic shift. Therefore, the CID cross sections are analyzed by incorporating Rice-Ramsperger-Kassel-Marcus (RRKM) statistical theories into equation 2.3, resulting in equation 2.4, as described in detail elsewhere.[21,22]

$$\sigma(E) = \frac{n\sigma_0}{E} \sum_i g_i \int_0^{E+E_i-E_0} \left[1 - e^{-k\left(E+E_i-\Delta E\right)\tau}\right] \left(\Delta E\right)^{n-1} d\left(\Delta E\right) \qquad (2.4)$$

Most of the parameters are the same as in equation 2.3, τ is the experimental time available for dissociation, and k is the unimolecular dissociation rate constant. The term ΔE is the energy that remains in translation after the collision between the reactants. Thus, $E - \Delta E$ is the energy transferred to the internal modes of the dissociating ion by this collision at a relative translational energy E. The internal energy of the energized molecule after the collision is therefore, $E + E_i - \Delta E$. The unimolecular dissociation rate constant, k is defined in the usual manner by the RRKM theory.

Several systems investigated here result in multiple dissociation pathways occurring in parallel and competing with each other. To properly account for competitive effects and extract accurate threshold energies from the experimental data, the statistical model of equation 2.4 is modified to incorporate the competition between the various dissociation pathways as shown in equation 2.5 and described in detail previously.[23]

$$\sigma_j\left(E\right) = \frac{n\sigma_{0,j}}{E}\sum_i g_i \int_0^{E+E_i-E_{0,j}} \frac{k_j\left(E^*\right)}{k_{tot}\left(E^*\right)}\left[1 - e^{-k_{tot}\left(E^*\right)\tau}\right]\left(\Delta E\right)^{n-1} d\left(\Delta E\right) \qquad (2.5)$$

Again, most of the parameters are the same as in equations 2.3 and 2.4. E^* is the internal energy of the energized molecule after collision, $E^* = E + E_i - \Delta E$. The indices j refer to a particular product channel. $\sigma_{0,j}$ is an energy independent scaling factor for product channel j, $E_{0,j}$ is the threshold energy for CID of the ground electronic and rovibrational state of the reactant ion at 0 K for channel j. The term $k_j\left(E^*\right)$ is the unimolecular rate constant for dissociation of the energized molecule a long channel j, and its summation over all channels

yields the total unimolecular rate constant, $k_{tot}\left(E^*\right)$. The rate coefficients $k_j\left(E^*\right)$ necessary for competitive modeling and $k_{tot}\left(E^*\right)$ are defined by RRKM theory as described in detail elsewhere.[21,22] Incorporation of lifetime and competitive effects into equations 2.3–2.5 requires sets of ro-vibrational frequencies appropriate for the energized molecules and the transition states (TSs) leading to dissociation. For dissociation reactions limited by loose TSs, most frequencies used to describe the TS are those of the products with the transitional frequencies treated as rotors, an approach that corresponds to a phase space limit (PSL), as described in detail elsewhere.[22,23] For dissociation reactions that involve tight TSs, the frequencies are determined by the rate-limiting (highest energy) TS along the reaction pathway. In all cases, the molecular parameters of the reactant and rate-limiting TSs are taken from theoretical results. The calculated vibrational frequencies (pre-scaled by 0.9804) are increased and decreased by 10% in order to bring calculated frequencies into agreement with experimentally determined frequencies.[24,25] The corresponding change in the average vibrational energy is taken to be an estimate of one standard deviation of the uncertainty in vibrational energy and is included in the uncertainties listed with the threshold values.

Equations 2.3–2.5 are convoluted with the kinetic and internal energy distributions of the reactants and a nonlinear least-squares analysis of the data is performed to give optimized values for the parameters $\sigma_{0,j}$, n, $E_{0,j}$, and $E_{0,j}\left(\mathrm{TTS}\right)$ or $E_{0,j}\left(\mathrm{PSL}\right)$. Uncertainties in $E_{0,j}$ and $E_{0,j}\left(\mathrm{TTS}\right)$ or $E_{0,j}\left(\mathrm{PSL}\right)$ are determined from the range of threshold values determined from different data sets, 10% variations associated with the vibrational frequencies, and the error in the absolute energy scale, ±0.1 eV (lab). For analyses that include the RRKM lifetime analysis, the uncertainties in the reported $E_{0,j}\left(\mathrm{TTS}\right)$ or $E_{0,j}\left(\mathrm{PSL}\right)$ values also include

the effects of increasing and decreasing the time assumed available for dissociation by a factor of 2. For loose TSs, the $E_{0,j}(\mathrm{PSL})$ values determined here by analysis with equations 2.3–2.5 can be equated to 0 K bond dissociation energies (BDEs) because these CID processes are simple noncovalent bond cleavage reactions.[26,27] The threshold energies for the activated dissociation pathways of the complexes determined by analysis with equations 2.3–2.5, $E_{0,j}(\mathrm{TTS})$, correspond to activation energies (AEs) at 0 K.[12,28,29] The accuracy of the thermochemistry obtained by the modeling procedures described here have been verified for many systems by comparing values derived from other experimental techniques and to ab initio calculations.[30]

2.3 Overview of Solarix 7 T FTMS Hybrid Mass Spectrometer

All Fourier transform ion cyclotron resonance mass spectrometry (FT-ICR MS) experiments were performed on the 7.0 Tesla (T) Bruker Solarix^{TM} FTMS Hybrid Mass Spectrometer (Bruker Daltonik GmbH, Bremen, Germany). FT-ICR mass spectrometers function according to the effect of a magnetic field upon a moving ion.[31,32] An ion of charge q, and mass m travelling along a linear path with an initial velocity v_o will experience a magnetic Lorentz force, $F = qv_oxB_o$, that is perpendicular to both the direction of the ion velocity and magnetic field B_o upon interaction with a fixed magnetic field.[33,31] As a result, a moving ion will have a circular path in the plane perpendicular to the magnetic field, gyrating with a cyclotron frequency given by, $w_c = qxB_o/m$, Figure 2.5. The cyclotron frequency is inversely proportional to the mass-to-charge ratio; this value is measured in the FT-ICR mass spectrometer in order to determine the mass value m of the ion. Because frequency can be measured with high precision, mass measurements in FT-ICR can have high resolution.[34]

A schematic diagram of the Solarix 7 T FTMS Hybrid mass spectrometer is illustrated in Figure 2.6. This instrument incorporates five major sections; the atmospheric pressure ionization (API) or matrix-assisted laser desorption ionization (MALDI) source, the quadrupole-hexapole (Qh) interface, the ion transfer optics, the detector, and the electronics required for data acquisition and processing in the Fourier transform mode. Six differential pumping stages maintained by four turbo-molecular pumps (TP1–TP4) and two mechanical roughing pumps allow the introduction of ions at atmospheric pressure while providing the ultrahigh vacuum of $\leq 10^{-9}$ mbar necessary to operate the analyzer (Bruker Daltonik GmbH, Bremen, Germany).

2.3.1 Electrospray Ionization Source

Ions are introduced into the FT-ICR mass spectrometer from either a MALDI source under vacuum or an API source such as ESI, which is used exclusively in this thesis. Solutions containing the ions of interest at concentrations of ~0.1μM are prepared using a 1:1 (v/v) mixture of acetonitrile and water. The ESI flow rate was set at 120 μL/h and nitrogen nebulizing gas was operated at 2.0 bar. A voltage ranging from –500 V to –1100 V was applied to the entrance of the mass spectrometer to generate the positive ionization mode electrospray. Positively charged droplets were separated from the solvent using a nebulizer and a counter-flow of drying gas in the atmospheric pressure spray chamber. Ions pass through a capillary heated to ~180°C into the first vacuum region at ~3.0 mbar.

2.3.2 Quadrupole–Hexapole Interface

The ions are passed orthogonally through a dual ion funnel, which focuses the ion beam by means of DC and RF voltages. The ions are guided through a hexapole–quadrupole–hexapole region prior to ion focusing and entry to the ICR cell. The

ions are decelerated before entering the first hexapole where they can be stored for a defined amount of time (~300–500 ms), or simply passed through onto the mass selective quadrupole.[35] In the mass selective quadrupole, it is possible to define an m/z window, whereby only those ions whose m/z lies within the given window are allowed to pass through onto the hexapole collision cell. The second hexapole can be operated as a focusing region or a collision cell, where ions are stored for a given amount of time (~0.5–1.0 s), and if desired, the conditions within the collision cell can be changed in order to induce fragmentation of the ions stored within the cell after colliding with an inert gas such as helium or argon of a higher pressure (10^{-3} mbar). Ions are then pulsed out of the collision cell and focused using a series of optical lenses and accelerated through the magnetic field into the ICR cell.

2.3.3 The Infinity Cell

The infinity cell, which is the heart of the FT-ICR mass spectrometer, is located at the center of the superconducting magnet. The cell is composed of three sets of "wall plates" (electrodes) used for trapping, excitation, and detection (see Figure 2.7). Ions enter the cell and experience the strong magnetic field, which traps them in the radial direction and induces cyclotron motion. Although the ions are radially confined, they can still move freely along the magnetic field lines and easily escape along the axis of the magnetic field or ICR cell. To prevent the radially trapped ions from escaping along the axis of the ICR cell, a small voltage ~0.5–1.5 V is applied to the trapping plates. This confines the ions within the cell, where they could theoretically be stored indefinitely.[33] The trapped ions can be excited by application of a spatially uniform rf electric field that oscillates at or near their cyclotron frequency. Ions with the same cyclotron frequency as the applied rf frequency sweep (chirp)

absorb power from the field, which accelerates ions coherently to a larger and thus detectable orbital radius.[32] Once the coherent ions are excited to a sufficiently large radius they induce a charge (image current) on the two opposing detection plates.[36] The detection process is repeated for the entire m/z range of interest by scanning the range of radio frequencies appropriate for exciting ions that are trapped within the ICR cell. The image current or transient is the time-domain signal that results from the digital conversion of an analog signal corresponding to all of the detected frequencies and their respective amplitudes.[37] To obtain frequency-domain data, the mathematical algorithm of fast Fourier transform (FFT) is applied by Solarix control software (version 1.5.0) in broadband mode with 25 k data points summed over 10-18 scans to convert the time-domain signal to a frequency-domain signal, and the frequency data are converted to m/z values and displayed in a mass spectrum of ion abundance versus m/z.[31]

2.3.4 General Procedures

All FT-ICR MS experiments were performed using a Bruker Solarix^{TM} FTMS Hybrid Mass Spectrometer equipped with a 7 T superconducting magnet and an infinity cell. Ions that are left over from previous experiments are quenched or purged within 25 ms by application of a voltage of reverse polarity to the trapping plates, such that ions are accelerated out of the ICR cell, and hence are no longer trapped. The ions generated by the ESI source are accumulated in the first hexapole for 0.05–0.1 s and transferred to the quadrupole for mass selection. The mass selected ions, $M^{2+}(N\text{-}L)_2$ reactant ions are then transferred to the second hexapole (collision cell) and accumulated for 5–20 s (mass selected using a 1 Da isolation window for MS/MS experiments) prior to being transferred into the ICR cell through ion transfer optics, where in-cell isolation of monoisotopically clean

$M^{2+}(N\text{-}L)_2$ reactant ions along with subsequent MS/MS experiments takes place. The mass selected ions are accumulated using a continuous accumulation of selected ions (CASI) technology equipped in the Solarix FT-ICR MS. As the ions are continuously generated by the source, they are continuously accumulated in the collision cell, building up their population thereby increasing the sensitivity needed for subsequent MS/MS experiments. The monoisotopically clean $M^{2+}(N\text{-}L)_2$ ion was isolated using a stored waveform inverse Fourier transformed (SWIFT) excitation pulse by adjusting the notch width to 5 Da inside the infinity cell. A series of notched SWIFT pulses are applied to resonantly eject all ions whose resonance frequencies fall within the frequency range of the pulse while injecting only those precursor ions whose resonance frequencies fall within the limits of the notch. This allows selective injection and accumulation of the ions of interest and continuous ejection of the unwanted ions. By application of SWIFT pulses, a significant improvement in S/N ratio, resolution, and sensitivity for the $M^{2+}(N\text{-}L)_2$ ions was observed. Fragmentation of $M^{2+}(N\text{-}L)_2$ reactant ions was carried out using sustained off-resonance irradiation (SORI) CID, and is discussed in more detail in the next section. The condition for SORI-CID was as follows: the pressure for the Argon reservoir was set to 12 mbar and the pulse length was 100–250 ms, the frequency offset was set to −1500 Hz with SORI power varying from 1.5–2%; the final pumping delay before excitation/detection was 3 s. During detection, the pressure in the ICR cell was 10^{-8} mbar. All experimental parameters were controlled using software and hardware incorporated into the Bruker Solarix^{TM} (Bruker Daltonik GmbH, Bremen, Germany) data acquisition system. All mass spectra were acquired with Solarix control software (version 1.5.0) in broadband mode with 256 k data points summed over 10–18 scans. Frequencies corresponding to m/z 50–1500 summed over 10–18 scans were displayed

using the Bruker Solarix^{TM} data analysis software version 4.0. Data analysis was carried out both manually and automatically using Data Analysis software version 4.0 (Bruker Daltonik GmbH, Bremen, Germany).

2.3.5 Tandem Mass Spectrometry (MS/MS)

FT-ICR mass spectrometer can be used to perform tandem mass spectrometric measurements.[38- 41] In this dissertation, tandem mass spectrometry (MS/MS) is used to isolate the desired precursor ion from a mixture of ions followed by activation and dissociation into products through collision with an inert gas, argon. The resulting product ions are then mass analyzed in the ICR cell providing accurate mass measurements. Different modes of activation of the precursor ions can be employed in the FT-ICR mass spectrometer such as CID, also known as CAD, (collisionally activated dissociation),[42] SORI-CID,[43] infrared multiple photon dissociation (IRMPD),[44] and electron capture dissociation (ECD).[45] In an FT-ICR instrument, CID can take place in the source region, collision cell, or in the ICR cell (in the case of SORI-CID). In the experiments performed in this thesis, SORI-CID activation is employed. In SORI-CID, the selected precursor is periodically excited and de-excited by applying, in the presence of argon, a low-amplitude radio frequency pulse slightly off resonance (−1500 Hz) compared to the cyclotron frequency of the selected ion.[46] During this process, the ions undergo multiple collisions with the argon gas. In each collision event, a portion of the kinetic energy of the ions is converted into internal energy leading to dissociation when a sufficient amount of internal energy is obtained. In this way, the internal energy of the excited ions can be modulated, thereby enabling the study of the lowest energy fragmentation pathways.

2.4 Computational Details

2.4.1 Geometry Optimizations and Frequency Analyses

To determine geometries, molecular parameters needed for the thermochemical analysis of experimental data (i.e., vibrational frequencies and rotational constants), and energetics for the reactant transition metal complexes and their CID products used in this study, density functional theory (DFT) calculations are performed using the Gaussian 09 suites of programs.[47] Geometry optimizations and frequency analyses are performed using several DFT methods including the BHandHLYP, B3LYP, and M06 functionals using the 6-31G* basis set. In all cases, the default methods are used such that for closed-shell systems a spin restricted model is employed, whereas for open-shell systems a spin-unrestricted model is employed. The B3LYP method has been extensively used and shown to reliably predict energetics for most monovalent transition-metal-containing systems.[48] The BHandHLYP functional is also examined as its overall performance for treating the spin multiplicity of transition-metal-containing systems has recently been shown to be better than that of B3LYP.[49] The M06 functional has also been shown to be reasonably accurate and affordable for computations of transition metal systems.[50] Vibrational frequencies and rotational constants used in the modeling procedures are extracted from these calculations. Zero-point energies (ZPE) are calculated for the reactants, TSs, intermediates, and products associated with the CID of the transition metal cation-*N*-donor ligand complexes using the computed frequencies scaled by factors of 0.9804, 0.9472, and 0.9940 for the geometries determined using the B3LYP, BHandHLYP, and M06 functionals, respectively.[51-53]

2.4.2 Single Point Energy Calculations

Single point energies are calculated using the BHandHLYP, B3LYP, and M06 levels of theory with an extended basis set, 6-311+G(2d,2p), to increase the accuracy of the energetics determined. ZPE corrections are included in the calculated BDEs and AEs to provide theoretical estimates for these quantities for the various processes investigated. Basis set superposition error (BSSE) corrections are also calculated and subtracted from the computed BDEs in the full counterpoise approximation.[54,55] Comparison of the experimental energies to theoretical values for the various possible geometries of the complexes facilitates proper interpretation of the experimental data and also allows the accuracy of the theories employed to be quantitatively assessed.

2.4.3 Reaction Pathway Modeling

The $M^{2+}(N\text{-}L)_x$ complexes, where M^{2+} = Fe^{2+}, Co^{2+}, Ni^{2+}, Cu^{2+}, and Zn^{2+}, *N-L* = Bpy or Phen, and x = 2–3 result in multiple dissociation pathways (reactions 2.6–2.9) occurring in parallel and competing with each other. Reaction 2.6, simple CID, results in the loss of an intact *N-L* ligand. Reaction 2.7, electron transfer Coulomb fission (ETCF), results in the production of $M^{+}(N\text{-}L)$ and $[N\text{-}L]^{+}$ ions corresponding to reduction of M^{2+} to M^{+} and oxidation of [*N-L*] ligand to a radical cation, $[N\text{-}L]^{+}$, respectively. Reaction 2.8, proton transfer Coulomb fission (PTCF), results in the formation of the $[M(N\text{-}L\text{–}H)]^{+}$ and $[N\text{-}L\text{+}H]^{+}$ product ions, corresponding to the transfer of a proton from $M^{2+}(N\text{-}L)$ to the other [*N-L*] ligand facilitating charge fission dissociation. Reaction 2.9, dehydrogenation results in loss of hydrogen through an activated dissociation process.

$$M^{2+}(N\text{-}L)_x + Xe \rightarrow M^{2+}(N\text{-}L)_{x-1} + [N\text{-}L] + Xe \quad (2.6)$$

$$M^{2+}(N\text{-}L)_x + Xe \rightarrow [M(N\text{-}L\text{–}H)_{x-1}]^{+} + [N\text{-}L\text{+}H]^{+} + Xe \quad (2.7)$$

$$M^{2+}(N\text{-}L)_x + Xe \rightarrow M^{+}(N\text{-}L)_{x-1} + [N\text{-}L]^{+} + Xe \quad (2.8)$$

$$M^{2+}(N\text{-}L)_x + Xe \rightarrow [M(N\text{-}L)\text{–}H_2]^{2+} + H_2 + Xe \quad (2.9)$$

The simple noncovalent bond cleavage observed in these systems, reactions 2.6, allows the second and third sequential BDEs to be determined using a loose PSL TS model. This model requires molecular parameters for the reactant complex and CID products to be determined. The PTCF, ETCF, and dehydrogenation processes, reactions 2.7 through 2.9, respectively, exhibit barriers in excess of the endothermicity of dissociation, and thus analysis of the CID cross sections for these pathways allows the AEs for these pathways to be determined. However, molecular parameters for the rate-limiting TS are needed. Thus, these reaction pathways are mapped to characterize the rate-limiting TSs along the dissociation pathways by performing relaxed potential energy scans and TS calculations.

2.4.4 Transition State Calculations

Transition states are located using the synchronous transit-guided quasi-Newton (STQN) methods as implemented in Gaussian 09.[47] STQN methods use three different functions for the TS calculation. The first function utilizes an initial guess structure only for the TS calculation. The second function, QST2, uses the reactant and the product for the TS calculation.[56] The third function, QST3, makes use of three molecule specifications; the reactant, products, and an initial guess for the TS calculation.[57] The QST2 function was successfully used to generate a guess structure for the TS of the metal complexes in this study based upon the geometries of reactants and products. For some systems it was necessary to use the QST3 function and an initial guess structure for the TS. The initial guess structures are located by performing a PES scan, whereby a series of geometry optimizations are performed on structures related by an assumed reaction coordinate to

identify the elementary steps. The scan was performed by progressively increasing the interatomic distances in 20, 40 or 60 steps of 0.01, 0.10 or 0.15 Å, respectively. For the ETCF processes, the interatomic distance scanned is the M^{2+}–N bond length, whereas for PTCF process, the C–H, N–H, and M^{2+}–H bonds are also scanned. In each case, the highest energy structure on the PES scan is taken as the starting geometry (initial guess structure) for the TS search. Transition state and intermediate structures occurring along the PESs are further optimized at the B3LYP/6-31G* level of theory, each TS is confirmed to have a single imaginary frequency, whereas each intermediate is conformed to be vibrationally stable. All TSs are examined using an intrinsic reaction coordinate (IRC) calculation, which determines the reaction pathways leading to and from the TS. Each calculation starts at the saddle point and follows the path in both directions from TS, optimizing the geometry at each point. In this way, an IRC calculation connects two minima on the PES by a path that passes through the TS connecting them. The local minima for the products are found using an unconstrained geometry optimization.

2.4.5 Calculation of Dipole Moments and Molecular Polarizabilities

The dipole moments and isotropic molecular polarizabilities of Pyr, *trans*-Bpy, *cis*-Bpy, and Phen are 2.31, 0.0, 3.04, 3.31 D and 9.27, 19.92, 19.67, 23.78 $Å^3$, respectively, and have been reported previously.[48]

2.4.6 Thermal Corrections

To allow comparison to literature values and commonly employed experimental conditions, the 0 K measured and calculated BDEs and AEs determined here are converted to 298 K bond enthalpies, activation enthalpies, and free energies. The conversions are calculated using standard formulae (assuming harmonic oscillator and rigid rotor models)

and the vibrational and rotational constants determined for the B3LYP/6-31G* optimized geometries.[51-53] Uncertainties in the enthalpic and entropic corrections are determined by ±10% variation in the molecular constants.

2.5 References

(1) Gillard, R. D.; Hill, R. E.; Maskill, R. J. *J. Chem. Soc. (A)*. **1970**, *9*, 1447.

(2) Hunt, H. R. *J. Chem. Ed*. **1977**, *54*, 710.

(3) Chen, Y.; Rodgers, M. T. *J. Am. Chem. Soc.* **2012**, *134*, 2313.

(4) Chen, Y.; Rodgers, M. T. *J. Am. Chem. Soc*. **2012**, *134*, 5863.

(5) Moision, R. M.; Armentrout, P. B. *J. Am. Soc. Mass Spectrom.* **2007**, *18*, 1124.

(6) Shaffer, S. A.; Prior, D. C.; Anderson, G. A.; Udseth, H. R.; Smith, R. D. *Anal. Chem.* **1998**, *70*, 4111.

(7) Shaffer, S. A.; Tolmachev, A.; Prior, D. C.; Anderson, G. A.; Udseth, H. R.; Smith, R. D. *Anal. Chem.* **1999**, *71*, 2957.

(8) Jones, R. M.; Anderson, S. L. *Rev. Sci. Instrum.* **2000**, *71*, 4335.

(9) Jones, R. M.; Gerlich, D.; Anderson, S. L. *Rev. Sci. Instrum.* **1997**, *68*, 3357.

(10) Vestal, M. L.; Blakly, C. R.; Ryan, P. B.; Futrell, J. H. *Rev. Sci. Instrum.* **1976**, *47*, 15.

(11) Teloy, E.; Gerlich, D. *Chem. Phys*. **1974**, *4*, 417.

(12) Muntean, F.; Armentrout, P. B. *J. Phys. Chem.* **2001**, *115*, 1213.

(13) Ervin, K. M.; Armentrout, P. B. *J. Chem. Phys*. **1985**, *83*, 166.

(14) Rodgers, M. T.; Armentrout, P. B. *J. Am. Chem. Soc*. **2002**, *124*, 2678.

(15) Aristov, N.; Armentrout, P. B. *J. Phys. Chem.* **1986**, *90*, 5135.

(16) Hales, D. A.; Armentrout, P. B. *J. Cluster Sci*. **1990**, *1*, 127.

(17) Daly, N. R. *Rev. Sci. Instrum.* **1959**, *31*, 264.

(18) Dalleska, N. F.; Honma, K.; Sunderlin, L. S.; Armentrout, P. B. *J. Am. Chem. Soc.* **1994**, *116*, 3519.

(19) Stein, S. E.; Rabinovitch, B. S. *J. Chem. Phys.* **1973**, *58*, 2438.

(20) Stein, S. E.; Rabinovitch, B. S. *Chem. Phys. Lett.* **1977**, *49*, 183.

(21) Khan, F. A.; Clemmer, D. E.; Schultz, R. H.; Armentrout, P. B. *J. Phys. Chem.* **1993**, *97*, 7978.

(22) Rodgers, M. T.; Ervin, K.M.; Armentrout, P. B. *J. Chem. Phys.* **1997**, *106*, 4499.

(23) Rodgers, M. T.; Armentrout, P. B. *J. Chem. Phys.* **1998**, *109*, 1787.

(24) Pople, J. A.; Schlegel, H. B.; Krishnan, R.; Defrees, D. J.; Binkley, J. S.; Frisch, M. J.; Whiteside, R. A.; Hout, R. F.; Hehre, W. J. *Int. J. Quantum Chem. Symp*. **1981**, *15*, 269.

(25) Defrees, D. J.; Mclean, A. D. *J. Chem. Phys.* **1985**, *82*, 333.

(26) Dalleska, N. F.; Honma, K.; Armentrout, P. B. *J. Am. Chem. Soc*. **1993**, *115*, 12125.

(27) Armentrout, P. B.; Simons, J. *J. Am. Chem. Soc*. **1992**, *114*, 8627.

(28) Muntean, F.; Armentrout, P. B. *J. Phys. Chem. B* **2002**, *106*, 8117.

(29) Muntean, F.; Armentrout, P. B. *J. Phys. Chem. A* **2003**, *107*, 7413.

(30) Rodgers, M. T.; Armentrout, P. B. *Mass Spectrom Rev*. **2000**, *19*, 215.

(31) Marshall, A. G. *Acc. Chem. Res.* **1985**, *18*, 316.

(32) Comisarow, M. B.; Marshall, A. G. *Chem. Phys. Lett*. **1974**, *25*, 282.

(33) Marshall, A. G.; Hendrickson, C.; Jackson, G. S. *Mass Spectrom. Rev*. **1998**, *17*, 1.

(34) Shi, S. D. H.; Hendrickson, C. L.; Marshall, A. G. *Proc. Natl. Acad. Sci. U. S. A.* **1998**, *95*, 11532.

(35) Taban, I. M.; McDonell, L. A.; Rompp, A.; Cerjak, I.; Heeren, R. M. A. *Int. J. Mass Spectrom.* **2005**, *244*, 135.

(36) Comisarow, M. B. *Hyperfine Interact*. **1993**, *81*, 171.

(37) Amster, I. J. *J. Mass Spectrom.* **1996**, *31*, 1325.

(38) Haddon, W. F.; McLafferty, F. W. *J. Am. Chem. Soc*. **1968**, *90*, 4745.

(39) Buchanan, M. V.; Hettich, R. L. *Anal. Chem*. **1993**, *65*, 245A.

(40) Marshall, A. G.; Grosshans, P. B. *Anal. Chem.* **1991**, *63*, 215A.

(41) Wilkins, C.; Chowdury, A. K. *Mass Spectrom. Rev*. **1989**, *8*, 67.

(42) Cody, R.; Burnier, R.; Cassady, C.; Freiser, B. S. *Anal. Chem.* **1982**, *54*, 2225.

(43) Gauthier, J. W.; Trautman, T. R.; Jacobson, D. B. *Anal. Chim. Acta.* **1991**, *246*, 211.

(44) Little, D. P.; Speir, J. P.; Senko, M. W.; O'Connor, P. B.; McLafferty, F. W. *Anal. Chem*. **1994**, *66*, 2809.

(45) Zubarev, R. A.; Kelleher, N. L.; McLafferty, F. W. *J. Am. Chem. Soc.* **1998**, *120*, 3265.

(46) Mirgorodskaya, E.; O'Connor, P. B.; Costello, C. E. *J. Am. Soc. Mass Spectrom.* **2002**, *13*, 318.

(47) Frisch, M. J.; Trucks, G. W.; Schlegel, H. B.; Scuseria, G. E.; Robb, M. A.; Cheeseman, J. R.; Scalmani, G.; Barone, V.; Mennucci, B.; Petersson, G. A.; Nakatsuji, H.; Caricato, M.; Li, X.; Hratchian, H. P.; Izmaylov, A. F.; Bloino, J.; Zheng, G.; Sonnenberg, J. L.; Hada, M.; Ehara, M.; Toyota, K.; Fukuda, R.; Hasegawa, J.; Ishida, M.; Nakajima, T.; Honda, Y.; Kitao, O.; Nakai, H.; Vreven, T.; Montgomery, Jr., J. A.; Peralta, J. E.; Ogliaro, F.; Bearpark, M.; Heyd, J. J.; Brothers, E.; Kudin, K. N.; Staroverov, V. N.; Kobayashi, R.; Normand, J.; Raghavachari, K.; Rendell, A.; Burant, J. C.; Iyengar, S. S.; Tomasi, J.; Cossi, M.; Rega, N.;

Millam, N. J.; Klene, M.; Knox, J. E.; Cross, J. B.; Bakken, V.; Adamo, C.; Jaramillo, J.; Gomperts, R.; Stratmann, R. E.; Yazyev, O.; Austin, A. J.; Cammi, R.; Pomelli, C.; Ochterski, J. W.; Martin, R. L.; Morokuma, K.; Zakrzewski, V. G.; Voth, G. A.; Salvador, P.; Dannenberg, J. J.; Dapprich, S.; Daniels, A. D.; Farkas, Ö.; Foresman, J. B.; Ortiz, J. V.; Cioslowski, J.; Fox, D. J. Gaussian, Inc., Wallingford CT, 2009.

(48) Rannulu, N. S.; Rodgers, M. T. *J. Phys. Chem. A* **2007**, *111*, 3465.

(49) Meng, L.; Hu, A.; Pang, R.; Lin, Z. *J. Phys. Chem. A.* **2012**, *116*, 7177.

(50) Zhao, Y.; Truhlar, D. G. *Theor. Chem. Account.* **2008**, *120*, 215.

(51) Becke, A. D. *J. Chem. Phys*. **1993**, *98*, 5648.

(52) Lee, C.; Yang, W.; Parr, R. G. *Phys. Rev. B.* **1988**, *37*, 785.

(53) Foresman, J. B.; Frisch, A. E. *Exploring Chemistry with Electronic Structure Methods*, 2nd Ed, Gaussian, Pittsburgh, PA, **1996**, pp. 64.

(54) Boys, S. F.; Bernardi, R. *Mol. Phys*. **1970**, *19*, 553.

(55) van Duijneveldt, F. B.; van Duijneveldt de Rijdt, J. G. C. M.; van Lenthe, J. H. *Chem. Rev*. **1994**, *94*, 1873.

(56) Peng, C.; Schlegel, H. B. *Isr. J. Chem.* **1993**, *33*, 449.

(57) Peng, C.; Ayala, P. Y.; Schlegel, H. B.; Frisch, M. J. *J. Comput. Chem.* **1996**, *17*, 49.

2.6 Figure Captions and Figures

Figure 2.1. Schematic diagram of the guided ion beam tandem mass spectrometer.

Figure 2.2. Schematic diagram of the electrospray ionization source/ion funnel/hexapole ion guide/collision cell interface.

Figure 2.3. Retarding potential analysis of the $Zn^{2+}(Phen)_3$ ion beam as a function of the laboratory ion kinetic energy.

Figure 2.4. Kinetic energy distribution of the $Zn^{2+}(Phen)_3$ complex ion beam.

Figure 2.5. Schematic diagram displaying the forces on a positively charged ion trapped in a uniform magnetic field. The red solid line represents an ion travelling along a linear path with an initial velocity, v_o. The magnetic field (X) is shown directed into the plane of the paper. The blue solid line represents the circular trajectory induced in the ion by the magnetic field. The black dotted line represents the Lorentz force (adapted from Bruker Solarix^{TM} User Manual Revision 2.0).

Figure 2.6. Schematic diagram of the Bruker Solarix^{TM} FT-MS Hybrid mass spectrometer used for this study (adapted from the Bruker Solarix^{TM} Users Manual, Revision 2.0).

Figure 2.7. The Infinity ICR cell geometry composed of three set of electrodes for trapping, excitation, and detection of ions. The inset shows a picture of the Infinity cell (adapted from the Bruker Solarix^{TM} Users Manual, Revision 2.0).

Figure 2.1.

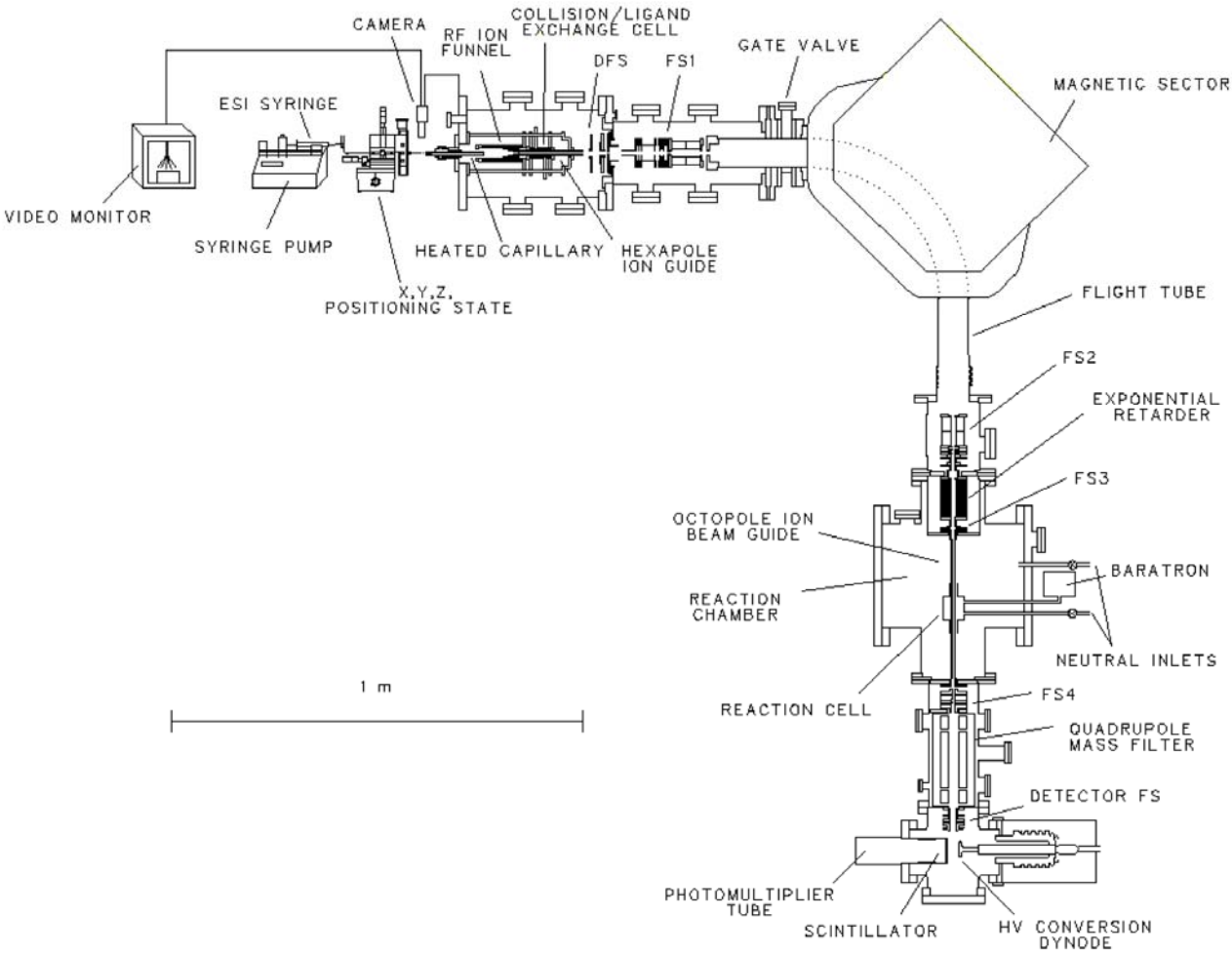
CAMERA
RF ION FUNNEL
COLLISION/LIGAND EXCHANGE CELL
DFS
FS1
GATE VALVE
MAGNETIC SECTOR
ESI SYRINGE
VIDEO MONITOR
SYRINGE PUMP
HEATED CAPILLARY
HEXAPOLE ION GUIDE
X,Y,Z, POSITIONING STATE
FLIGHT TUBE
FS2
EXPONENTIAL RETARDER
FS3
OCTOPOLE ION BEAM GUIDE
BARATRON
REACTION CHAMBER
NEUTRAL INLETS
1 m
REACTION CELL
FS4
QUADRUPOLE MASS FILTER
DETECTOR FS
PHOTOMULTIPLIER TUBE
SCINTILLATOR
HV CONVERSION DYNODE

Figure 2.2.

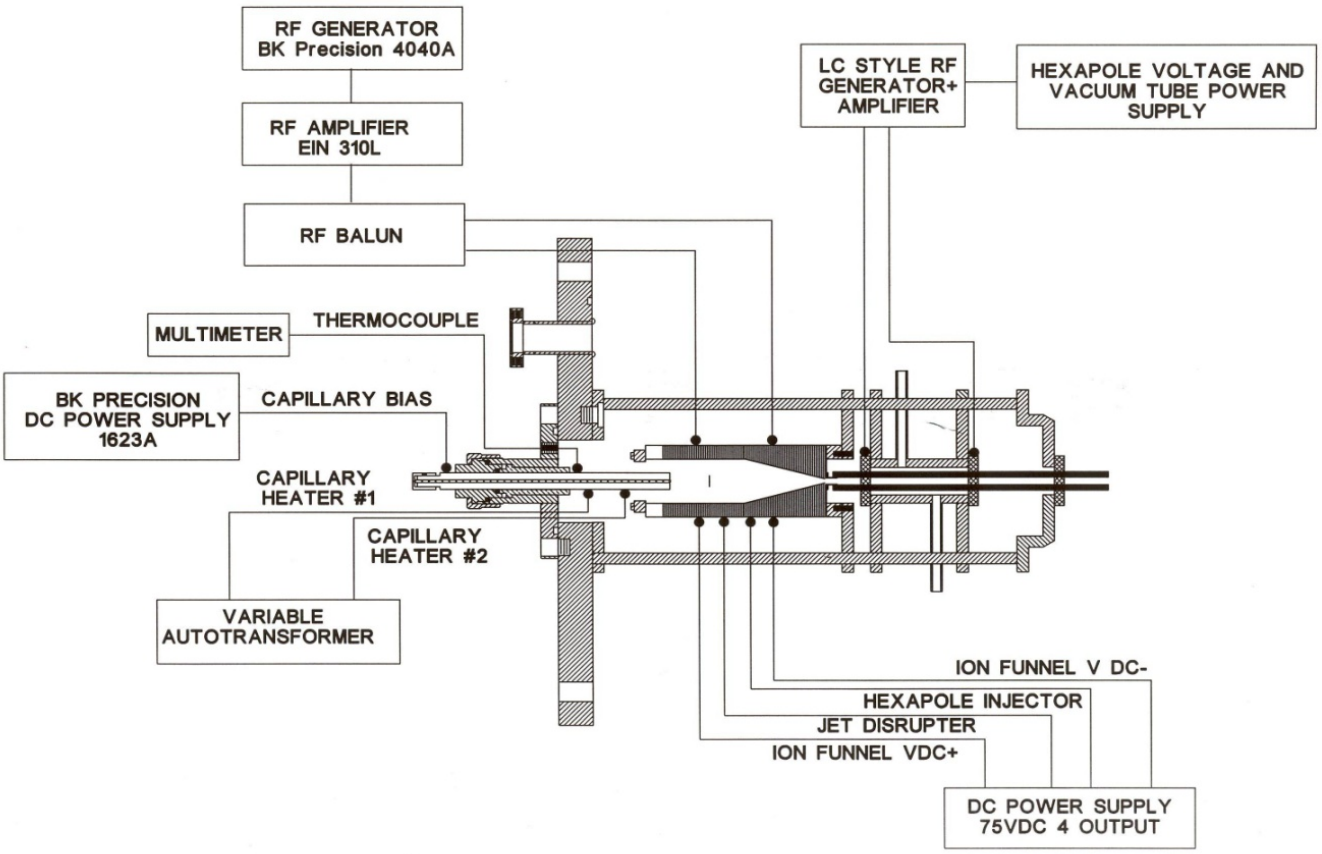
RF GENERATOR
BK Precision 4040A
RF AMPLIFIER
EIN 310L
RF BALUN
LC STYLE RF
GENERATOR+
AMPLIFIER
HEXAPOLE VOLTAGE AND
VACUUM TUBE POWER
SUPPLY
MULTIMETER
THERMOCOUPLE
BK PRECISION
DC POWER SUPPLY
1623A
CAPILLARY BIAS
CAPILLARY
HEATER #1
CAPILLARY
HEATER #2
VARIABLE
AUTOTRANSFORMER
ION FUNNEL V DC-
HEXAPOLE INJECTOR
JET DISRUPTER
ION FUNNEL VDC+
DC POWER SUPPLY
75VDC 4 OUTPUT

Figure 2.3.

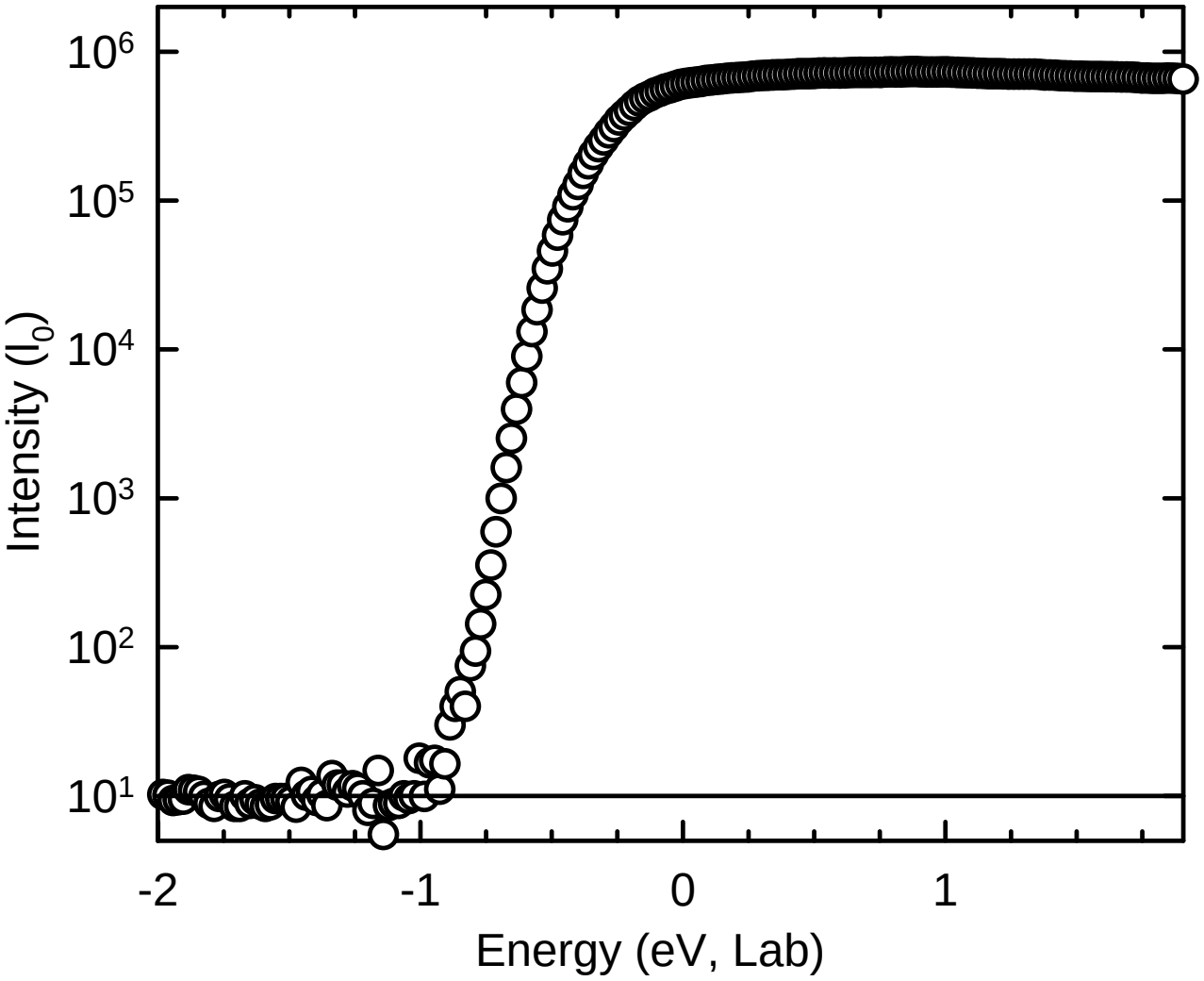

Figure 2.4.

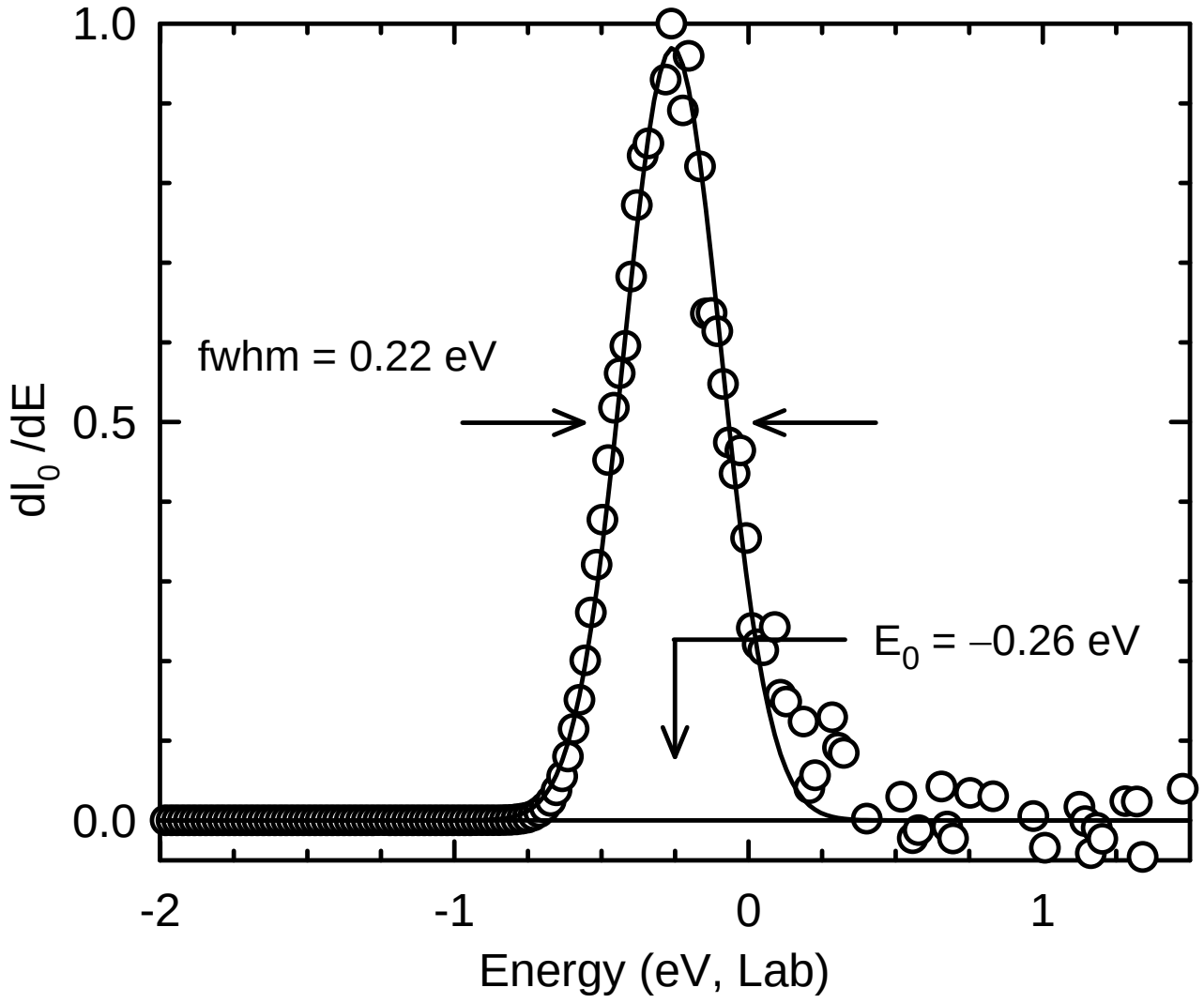

Figure 2.5.

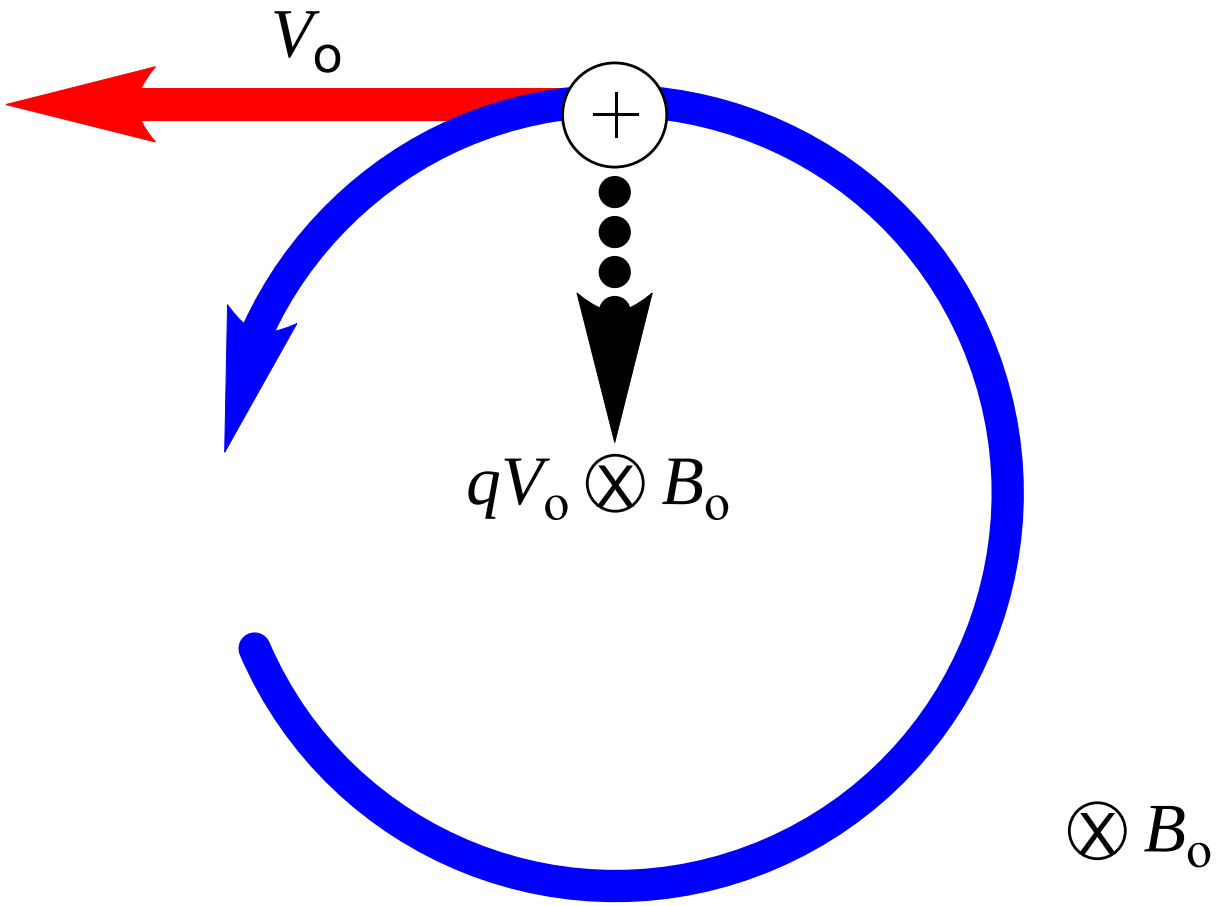

Figure 2.6.

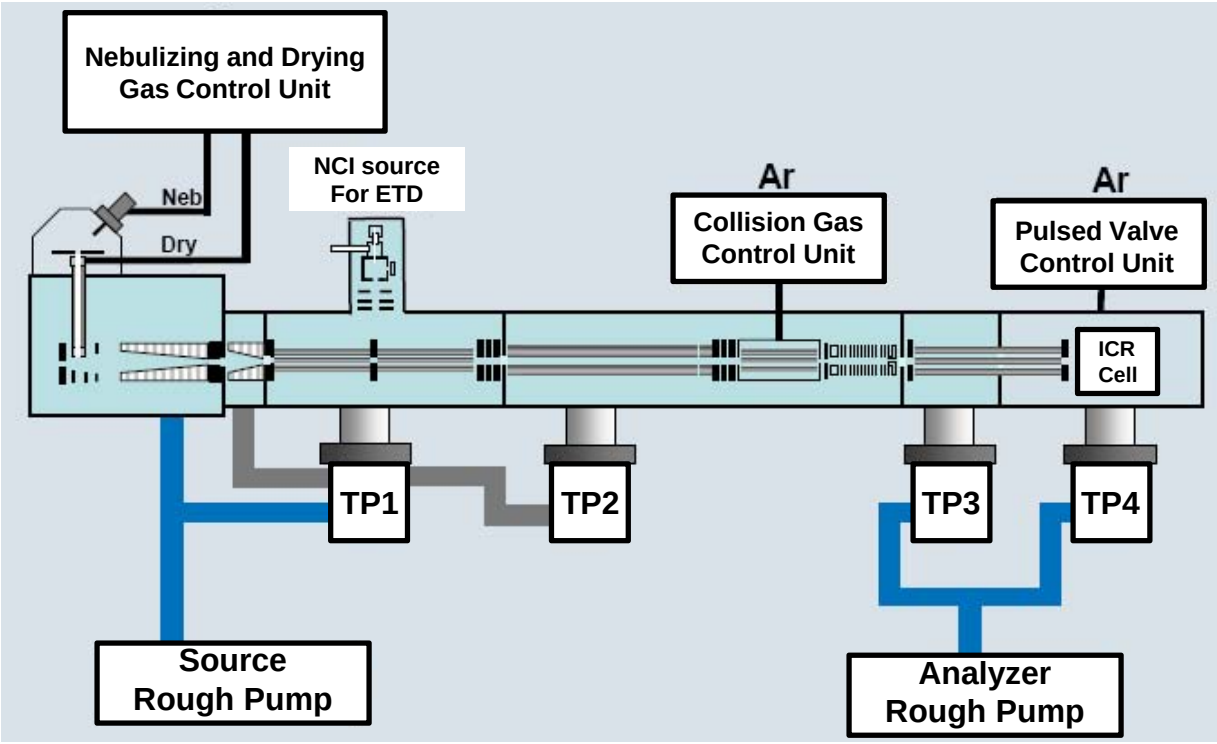
Nebulizing and Drying Gas Control Unit
Neb
Dry
NCI source For ETD
Ar
Collision Gas Control Unit
Ar
Pulsed Valve Control Unit
ICR Cell
TP1
TP2
TP3
TP4
Source Rough Pump
Analyzer Rough Pump

Figure 2.7.

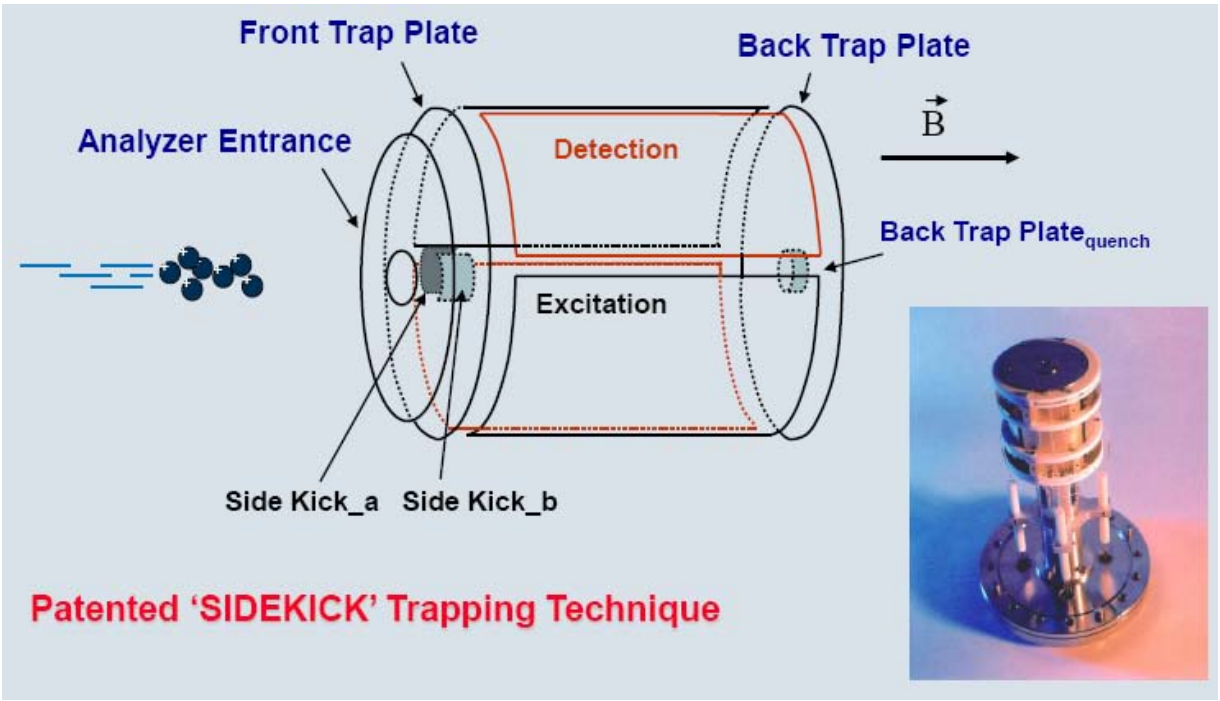
Front Trap Plate
Back Trap Plate
Analyzer Entrance
Detection
B
Back Trap Plate quench
Excitation
Side Kick_a
Side Kick_b
Patented 'SIDEKICK' Trapping Technique

CHAPTER 3

ENERGY-RESOLVED COLLISION-INDUCED DISSOCIATION STUDIES OF 1,10-PHENANTHROLINE COMPLEXES OF THE LATE FIRST-ROW DIVALENT TRANSITION METAL CATIONS: DETERMINATION OF THE THIRD SEQUENTIAL BINDING ENERGIES

Reprinted (adapted) with permission from the Journal of Physical Chemistry A, 2013, 117 (20), 4316-4330.

3.1 Introduction

Transition metal coordination complexes (TMCCs) are a very diverse and important class of molecules due to the variation in electronic and geometric structures they exhibit as a function of the local chemical environment. TMCCs can be sterically and electronically tuned by appropriate choice of the metal center and by manipulating the type, structure, and number of ligands.[1,2] Bulky ligands exert steric effects on the metal center and may influence catalytic activity by changing the geometry of the complex and controlling accessibility to the metal center. 1,10-Phenanthroline (Phen) is a bulky ligand and a strong chelator to a variety of transition metals.[3-6] Therefore, transition metal–Phen complexes have become attractive templates as Lewis acid binding sites and catalysts.[7-10] Substituted Phen ligands have found widespread use in asymmetric catalysis.[11-13] The rigidity of the Phen core helps stabilize favorable TMCCs and translates their chiral information with greater fidelity during catalysis. TMCCs exhibit advantages over main group Lewis acid catalysts. Their occupied d orbitals, which main group Lewis acids do not possess, offer unique electronic properties and a greater number of possible geometries to influence the binding and activation of molecules.[14] TMCCs also often lack the problems of water sensitivity and potential for dimerization exhibited by aluminum and boron catalysts.[15,16] In

addition, many TMCCs are easy to handle on any scale. A systematic understanding of the influence of the metal center and ligands on the properties of a TMCC can be used to improve its performance as a catalyst.

1,10-Phenanthroline has been widely studied in solution.[17-21] Irving and coworkers measured binding constants of the complexed forms of Phen and derivatives of Phen in solution using spectrophotometric techniques. Although the thermodynamic information obtained from their studies is reliable, the measured binding constants are influenced by both the solvent, and the counterions. The gas phase provides an ideal environment for examining the intrinsic binding in the absence of solvent effects and counterions. The ability to produce both coordinatively saturated and unsaturated complexes in the gas phase also allows the binding interactions to be examined as a function of the extent of ligation.

In this study, we characterize the structures and binding energies of divalent transition metal cation–Phen complexes. In particular, we elucidate the influence of the electronic structure of the transition metal cation on the geometric structure and strength of binding by systematically varying the metal cation from $Fe^{2+}(d^6)$ to $Co^{2+}(d^7)$ to $Ni^{2+}(d^8)$ to $Cu^{2+}(d^9)$ to $Zn^{2+}(d^{10})$. Previous work in our laboratory focused on the coordination behavior of singly charged transition metal cations with Phen ligands to examine how the electronic structure of the metal cation and chelation interactions influence the geometry and strength of binding.[22-25] In this work, studies of the analogous complexes in their +2 oxidation state allow the influence of the charge/oxidation state of the metal cation on the binding interactions to also be elucidated. The interactions between Phen and the five late first-row divalent transition metal cations are examined by measuring the kinetic energy dependence of their collision-induced dissociation (CID) behavior and performing complementary

electronic structure theory calculations. Complexes with one to three Phen ligands are investigated theoretically, while experimental studies presented here are limited to the tris-complexes, $M^{2+}(Phen)_3$. The energy resolved CID processes are analyzed using methods developed previously.[26] The analysis explicitly includes the effects of the internal and translational energy distributions of the reactants, multiple ion-neutral collisions, and their lifetimes for dissociation. We derive the third sequential bond dissociation energies (BDEs) of five $M^{2+}(Phen)_3$ complexes, and compare these results to values obtained from density functional theory calculations performed here. Periodic trends in the structures and BDEs of these complexes are examined and compared to the analogous Phen complexes to the monovalent first-row transition metal cations, Co^+, Ni^+, Cu^+, and Zn^+ previously investigated.[22-25]

3.2 Collision-Induced Dissociation Experiments

Cross sections for CID of five $M^{2+}(Phen)_3$ complexes with Xe, where M^{2+} = Fe^{2+}, Co^{2+}, Ni^{2+}, Cu^{2+}, and Zn^{2+} were measured using a guided ion beam tandem mass spectrometer (GIBMS) that has been described in detail in Chapter 2. The $M^{2+}(Phen)_3$ complexes were generated using an electrospray ionization (ESI) source that has been described in detail in Chapter 2. HPLC grade acetonitrile and deionized water were used to prepare solutions containing concentrations of ~0.01 to 0.1 mM $[M(Phen)_3](PF_6)_2$ in a 1:1 (v/v) acetonitrile-water mixture. Thermochemical analyses of the experimental results are explicitly discussed in Chapter 2.

3.3 Theoretical Calculations

Theoretical calculations were performed for the $M^{2+}(Phen)_x$ complexes, where $M^{2+} = Fe^{2+}$, Co^{2+}, Ni^{2+}, Cu^{2+}, and Zn^{2+}, and x = 1–3, using the Gaussian 09 suites of programs.[27] The relative energies of all possible spin states of the $M^{2+}(Phen)_x$ complexes were carefully evaluated to determine the spin state of the ground-state species. In this work, the following spin states were examined: singlet, triplet, and quintet for $Fe^{2+}(Phen)_x$; doublet and quartet for $Co^{2+}(Phen)_x$; singlet and triplet for $Ni^{2+}(Phen)_x$; doublet for $Cu^{2+}(Phen)_x$; and singlet for $Zn^{2+}(Phen)_x$ complexes. Further details of the theoretical calculations are given in Chapter 2. The B3LYP scaled vibrational frequencies and rotational constants for the ground-state structures of the Phen and the $M^{2+}(Phen)_x$ complexes are listed in Tables A.1 and A.2 of Appendix A.

3.4 Experimental Results

3.4.1 Cross Sections for Collision-Induced Dissociation

Experimental cross sections were obtained for the interaction of Xe with five $M^{2+}(Phen)_3$ complexes, where $M^{2+} = Fe^{2+}$, Co^{2+}, Ni^{2+}, Cu^{2+}, and Zn^{2+}. Figure 3.1 shows the data for the $M^{2+}(Phen)_3$ complexes. For all five $M^{2+}(Phen)_3$ complexes, simple CID resulting in loss of an intact Phen ligand, reaction 3.1, is observed as the dominant dissociation pathway over the entire range of collision energies examined, typically 0 to > 11 eV.

$$M^{2+}(Phen)_x + Xe \rightarrow M^{2+}(Phen)_{x-1} + Phen + Xe \qquad (3.1)$$

The apparent threshold for the $M^{2+}(Phen)_2$ CID product shifts to lower energies from Fe^{2+} to Co^{2+}, increases for Ni^{2+}, but then decreases again from Ni^{2+} to Cu^{2+} to Zn^{2+} as the d electron occupation of the metal cation increases from d^6 to d^{10} across this series. The magnitudes of the CID cross sections generally follow the reverse trend. Sequential dissociation of the

$M^{2+}(Phen)_2$ primary CID product is observed at elevated energies. Simple CID, reaction 3.1, resulting in the loss of a second Phen ligand is observed as a very minor sequential dissociation pathway only for the $Fe^{2+}(Phen)_3$ and $Zn^{2+}(Phen)_3$ complexes. Proton transfer Coulomb fission (PTCF), reaction 3.2, and electron transfer Coulomb fission (ETCF), reaction 3.3, are also observed as very minor sequential reaction pathways for all five of the $M^{2+}(Phen)_3$ complexes.

$$M^{2+}(Phen)_2 \rightarrow [M(Phen\text{-}H)]^+ + [Phen+H]^+ \quad (3.2)$$

$$M^{2+}(Phen)_2 \rightarrow M^+(Phen) + Phen^+ \quad (3.3)$$

Because the experiments were intentionally performed under low-resolution conditions to optimize sensitivity of the threshold determination, severe overlap of the $Phen^+$ and $[Phen+H]^+$ as well as the $[M(Phen\text{-}H)]^+$ and $M^+(Phen)$ sequential products is observed. Thus, only the species with the larger m/z of each pair were monitored, $[Phen+H]^+$ and $M^+(Phen)$. In all cases, PTCF is favored over ETCF as indicated by the larger cross section and lower apparent threshold of the $[Phen+H]^+$ products as compared to the $M^+(Phen)$ products. The simple CID, PTCF, and ETCF pathways resulting from the $M^{2+}(Phen)_2$ primary CID product will be investigated in detail in a follow up to this study, where the CID of the $M^{2+}(Phen)_2$ complexes formed directly in the ESI process will be examined.

3.4.2 Threshold Analysis

The model of equation 2.3 was used to analyze the thresholds for CID reactions 3.1 of five $M^{2+}(Phen)_3$ complexes. The results of these analyses are provided in Table 3.1 and the results for the $M^{2+}(Phen)_3$ complexes are shown in Figure 3.2. In all cases, even after zero-pressure extrapolation, small low-energy features were observed in the CID cross sections suggesting that a small population (~3–4%) of vibrationally or electronically excited ions are

present. Therefore, the model of equation 2.3 was used to analyze both raw zero-pressure extrapolated data and data obtained after subtraction of the low-energy feature. The low-energy feature can be reproduced nicely by shifting the threshold energy down by ~0.6 to 0.7 eV, retaining the same value of *n* as determined from fits to the dominant feature, and reducing σ_0 by a factor of ~25 to 35 depending on the system. The model for the low-energy feature was then subtracted from the data and the remaining cross section re-analyzed to yield the analysis after subtraction of the low-energy feature. The modeling parameters for these analyses are given in Table 3.1. The difference in the thresholds for the two analyses are 0.23 eV for the complex to Co^{2+}, 0.14 eV for Ni^{2+}, 0.31 eV for Cu^{2+}, 0. 37 eV for Zn^{2+}, 0.18 eV for the singlet ground state of $Fe^{2+}(Phen)_3$, and 0.15 eV for the quintet excited state of $Fe^{2+}(Phen)_3$. Figure 3.2 shows analyses before and after subtraction of the low-energy features. As can be seen in the figure, the cross sections are reproduced by equation 2.3 over a large range of energies (> 6 eV) and over four orders of magnitude. Previous work has shown that this model provides the most accurate assessment of the kinetic shifts for simple CID processes of electrostatically bound metal ligand complexes.[22-24] Table 3.1 also includes the kinetic shifts observed from the difference in thresholds obtained with and without the inclusion of lifetime effects. The Fe^{2+}, Co^{2+}, and Ni^{2+} complexes exhibit similar kinetic shifts, which are significantly larger than those of the Cu^{2+} and Zn^{2+} complexes. Similarly, the binding in the Fe^{2+}, Co^{2+}, and Ni^{2+} complexes is stronger than in the Cu^{2+} and Zn^{2+} complexes. Because the total number of vibrations, 195, and heavy atoms, 43, and hence the number of low-frequency vibrations remains the same for all five $M^{2+}(Phen)_3$ complexes, the kinetic shifts should directly correlate with the density of states at threshold, which depends on the measured BDE, consistent with the results determined here. The large number of

modes available to the $M^{2+}(Phen)_3$ complexes over which the internal energy can be randomized also results in relatively large *n* values, ~1.7 ± 0.1 for these systems.

The entropy of activation, $\Delta S^{\dagger}$, describes the looseness of the TS and is a reflection of the size and complexity of the system. It is largely determined by the molecular parameters used to model the energized molecule and the TS, but also depends on the threshold energy. Listed in Table 3.1, $\Delta S^{\dagger}$(PSL) values at 1000 K vary between 66.5 and 154.4 J mol^{-1} K^{-1} and are directly correlated with the measured BDEs for these complexes. The relatively large entropies of activation determined for these systems are the result of the weak noncovalent binding of the third Phen ligand and conformational relaxation of the $M^{2+}(Phen)_2$ product resulting from the reduction in steric crowding upon dissociation.

3.5 Theoretical Results

Ground-state structures of the $M^{2+}(Phen)_x$ complexes, where M^{2+} = Fe^{2+}, Co^{2+}, Ni^{2+}, Cu^{2+}, and Zn^{2+} and *x* = 1–3, were calculated using the Gaussian 09[27] suites of programs as described in section 3.3. Detailed information of the theoretical calculations is given in Chapter 2. The ground electronic spin states of the $M^{2+}(Phen)_x$ complexes to Co^{2+}, Ni^{2+}, Cu^{2+}, and Zn^{2+} were found to be quartet, triplet, doublet, and singlet, respectively for all values of *x* = 1–3. For the $Fe^{2+}(Phen)$ and $Fe^{2+}(Phen)_2$ complexes, the ground electronic spin states were found to be quintet. The ground state spin multiplicity of the $Fe^{2+}(Phen)_3$ complex was predicted to be low- spin singlet when the B3LYP functional was employed, whereas BHandHLYP and M06 predict the ground state to be high-spin quintet. Relative energies of the $M^{2+}(Phen)_x$ complexes, where *x* = 1–3 computed for the various possible spin states of each metal cation are summarized in Table 3.2.

The sequential BDEs calculated for all five of the $M^{2+}(Phen)_x$ complexes determined at the B3LYP, BHandHLYP, and M06 levels of theory using a 6-311+G(2d,2p) basis set using the B3LYP/6-31G*, BHandHLYP/6-31G*, and M06/6-31G* optimized geometries including independent ZPE and BSSE corrections are listed in Table 3.3 and Table A.3 of Appendix A. Table 3.4 lists the enthalpic and entropic corrections needed to convert the 0 K BDEs to 298 K bond enthalpies and free energies. The B3LYP functional was found to deliver results that are most consistent with values measured for the third sequential binding energies. Therefore, except as noted, the following discussion is based on the B3LYP results. The B3LYP/6-31G* optimized geometries of the $M^{2+}(Phen)_x$ complexes are shown in Figure 3.3. Relevant structural details of the B3LYP/6-31G*, BHandHLYP/6-31G*, and M06/6-31G* optimized structures for each of these species are listed in Table 3.5 and Tables A.4–A.5 of Appendix A. Cartesian coordinates of the B3LYP/6-31G* optimized geometries of the ground-state structures of the neutral Phen ligand and $M^{2+}(Phen)_x$ complexes are shown in Table A.6 of the Appendix A. In the ground-state structures, the metal cation binds to the Phen ligand(s) through the lone pairs of both nitrogen atoms, in agreement with previous results obtained for the analogous singly charged complexes.[22-25] Theoretical details regarding the geometry, dipole moment, and isotropic molecular polarizability of the Phen ligand have been reported previously.[22] The calculated dipole moment and isotropic molecular polarizability of Phen are 3.31 D and 23.78 $Å^3$, respectively, relatively large values as a result of the extended π network of this planar and rigid molecule.

3.5.1 $M^{2+}(Phen)_x$ Complexes, $M^{2+} = Fe^{2+}$, Co^{2+}, Ni^{2+}, and Zn^{2+}

The B3LYP/6-31G* ground-state structures of the $M^{2+}(Phen)_x$ complexes where M^{2+} = Fe^{2+}, Co^{2+}, Ni^{2+}, and Zn^{2+} are shown in Figure 3.3. The structures of the $Cu^{2+}(Phen)_x$

complexes are sufficiently different from those to the other metal cations that these complexes are discussed independently in the next section. In the monocomplexes, M^{2+}(Phen), the metal cation binds to the lone pairs of both nitrogen atoms of the Phen ligand, resulting in a bent geometry of the N donor atoms around the metal cation as a result of the structural rigidity of the Phen ligand. The two M^{2+}–N bond lengths are equal and decrease from Fe^{2+} (1.967 Å) to Co^{2+} (1.934 Å) to Ni^{2+} (1.892 Å), and then slightly increase again for Zn^{2+} (1.913 Å). The decrease in the bond lengths from Fe^{2+} to Co^{2+} to Ni^{2+} closely matches the decrease in the radii of these metal cations: 0.76, 0.74, and 0.73 Å, respectively. Zn^{2+} deviates from this simple trend as its radius, 0.72 Å is the smallest.[28-29] The ∠NM^{2+}N bond angles decrease from Fe^{2+} (90.9°) to Co^{2+} (89.9°), and then increase from Ni^{2+}(91.6°) to Zn^{2+}(94.6°), nearly parallel in behavior to the variations in the M^{2+}–N bond lengths. The ∠NCCN dihedral angles are 0.0° for all of the monocomplexes as found for the free Phen ligand.

In the bis-complexes, the metal cation binds to all four nitrogen atoms of the two Phen ligands in a distorted tetrahedral coordination geometry. The structural rigidity of the Phen ligands prevents the ideal tetrahedral coordination geometry from being achieved. The two Phen ligands are nearly perpendicular to one another, with ∠NM^{2+}NC dihedral angles of ~81.2°. The four M^{2+}–N bond lengths are equal and decrease from Fe^{2+} (2.062 Å) to Co^{2+} (2.024 Å) to Ni^{2+} (2.003 Å), and then slightly increase for Zn^{2+} (2.023Å), parallel to that found for the monocomplexes. The intraligand ∠NM^{2+}N bond angles vary between 83.0° and 84.6°, while the interligand ∠NM^{2+}N bond angles vary between 123.2° and 124.1°. The ∠NCCN dihedral angles in all of the bis complexes are ~0.0° as found for the free Phen ligand and M^{2+}(Phen) complexes.

In the tris-complexes, all six nitrogen atoms of the three Phen ligands are coordinated to the metal cation in a distorted octahedral arrangement. The six M^{2+}–N bond lengths are equal and decrease from Fe^{2+} (2.204 Å) to Co^{2+} (2.163 Å) to Ni^{2+} (2.117 Å), and then slightly increase for Zn^{2+} (2.193 Å) when comparing the quintet state of $Fe^{2+}(Phen)_3$, again parallel to that found for the mono- and bis-complexes. However, the spin change to singlet results in shorter Fe^{2+}–N bond lengths of 2.006 Å in the ground-state $Fe^{2+}(Phen)_3$ complex. The intraligand ∠NM^{2+}N bond angles are ~78.0°, significantly smaller than the octahedral value of 90.0°. The interligand ∠NM^{2+}N bond angles for the N atoms cis to each other are ~95.0°, whereas for the trans N atoms, these angles are ~169.0°. These deviations from perfect octahedral coordination are again the result of the structural rigidity of the Phen ligands. The individual Phen ligands are nearly planar, with average ∠NCCN dihedral angles of 1.3° for two of the Phen ligands, and 1.8° for the third Phen ligand. The dihedral angle between any two Phen ligands varies between 57.1° and 60.6°. In all cases, the M^{2+}–N bond lengths increase with increasing ligation as shown in Figures 3.3 and 3.4, as a result of the decreasing electrostatic attraction between the metal cation and the Phen ligands, and increasing ligand–ligand repulsive interactions. Only $Fe^{2+}(Phen)_3$ deviates from these trends as a result of the spin cross over from quintet to singlet upon binding of the third ligand. As the bond lengths increase, the intraligand ∠NM^{2+}N bond angles decrease.

3.5.2 $Cu^{2+}(Phen)_x$ Complexes

As found for the $M^{2+}(Phen)_x$ complexes to Fe^{2+}, Co^{2+}, Ni^{2+}, and Zn^{2+}, the Phen ligands bind to Cu^{2+} via the lone pairs of both nitrogen atoms, leading to similar bent, distorted tetrahedral, and distorted octahedral geometries for the mono-, bis-, and tris-complexes to Cu^{2+}, respectively, as shown in Figure 3.3. In the $Cu^{2+}(Phen)$ complex, the

Cu^{2+}–N bond distances are 1.884 Å and the ∠NCu^{2+}N bond angle is 91.2°. In the $Cu^{2+}(Phen)_2$ complex, the Cu^{2+}–N bond lengths increase to 1.986 Å. The bond angles between Cu^{2+} and the N atoms differ slightly, with intraligand ∠NCu^{2+}N angles of 84.4° and interligand ∠NCu^{2+}N bond angles of 103.8° and 149.2°. The individual Phen ligands are almost planar with average ∠NCCN dihedral angles of 0.9°. The planes of the two Phen ligands are twisted relative to each other with ∠NM^{2+}NC dihedral angles of 49.0°. In contrast, the other $M^{2+}(Phen)_2$ complexes exhibit much larger ∠NM^{2+}NC dihedral angles of 81.2°. The tris-complex is tetragonally elongated such that the Cu^{2+}–N bond distances of the four equatorial nitrogen atoms are 2.055 Å, while the Cu^{2+}–N bond distances are 2.397 Å for the axial nitrogen atoms. The relevant intra- and interligand ∠NCu^{2+}N bond angles that define the distorted octahedral geometry (and their degeneracies) are 75.8°(2), and 81.2°, and 91.3°(3), 94.3°(4), 99.1°(2), and 170.4°(3), respectively. The distortions from the idealized tetrahedral and octahedral geometries of the bis- and tris-complexes are more severe for the $Cu^{2+}(Phen)_x$ complexes, than for the other metal cations. Similar to the other $M^{2+}(Phen)_x$ complexes, as the number of Phen ligands increases, the Cu^{2+}–N bond lengths increase due to decreasing electrostatic attractions and increasing ligand–ligand repulsive interactions as shown in Figures 3.3 and 3.4. As the Cu^{2+}–N bond lengths increase, the intraligand ∠NCu^{2+}N bond angles decrease, while the trans interligand bond angles increase to minimize ligand repulsive interactions.

3.6 Discussion

3.6.1 Metal-Ligand Bonding Interactions of the $M^{2+}(Phen)_3$ Complexes

The metal-ligand bonding interactions in the $M^{2+}(Phen)_3$ complexes involve the metal 3d orbitals, the σ lone pairs on the N atoms, and the delocalized π-systems of the Phen

ligands. The principal bonding mechanisms feature electron donation from the lone-pairs of the N atoms to the metal with a synergic back-bonding contribution from the occupied metal d_π orbitals to vacant π^* orbitals of the Phen ligands. The metal 3d orbitals, transforming as d_π (d_{xy}, d_{xz}, d_{yz}) and $d_{\sigma*}$ (d_{z^2} and $d_{x^2-y^2}$) orbitals are split through interaction with the Phen ligand orbitals of similar symmetry. The magnitude of the energy difference between the d_π and $d_{\sigma*}$ set depends on the nature and number of the ligands bound to the metal center. When the ligand field splitting is small the electrons form a high-spin complex, where all of the unpaired spins are aligned as prescribed for the free metal cation by Hund's rule, to minimize electron–electron repulsion. When the ligand field splitting becomes large enough that the energy gained by dropping from the $d_{\sigma*}$ to the d_π level is sufficient to overcome the electron pairing energy, a low-spin complex results. Therefore, the ground-state spin of the $M^{2+}(Phen)_3$ complexes is determined by a balance between Hund's rule of maximum multiplicity, which favors high-spin states, and metal–ligand bonding, which favors low spin states. On this basis the principal bonding interactions that occur between the metal 3d orbitals and the ligand π orbitals find the ground electronic spin states of the $M^{2+}(Phen)_x$ complexes to Co^{2+}, Ni^{2+}, Cu^{2+}, and Zn^{2+} to be high spin quartet, triplet, doublet, and singlet, respectively, when the B3LYP, BHandHLYP, and M06 functionals are employed. For the $Fe^{2+}(Phen)$ and $Fe^{2+}(Phen)_2$ complexes, the ground electronic spin states were found to be high spin quintet. In contrast, the ground state spin multiplicity of the $Fe^{2+}(Phen)_3$ complex was predicted to be low-spin singlet when the B3LYP functional was employed, whereas BHandHLYP and M06 predicted the ground state to be high-spin quintet. The tendency of different density functionals to predict different ground electronic spin states for the

$Fe^{2+}(Phen)_3$ complex is consistent with other recent theoretical calculations of related iron-containing compounds with spin states that lie close in energy.[30-31]

Previous studies have shown that spin crossover or spin transitions are involved in most complexes involving the Fe^{2+} ion.[32] These studies show that for the Fe^{2+} d^6 configuration in an octahedral field, there is a value for the ligand field strength beyond which the ground state of the Fe^{2+} ion changes from a quintet to singlet state. Hence, a spin crossover or spin transition can be expected to be induced when the ligand field strength about the Fe^{2+} ion is in the vicinity of this critical value such that minor external perturbations can tip the scales in favor of one or the other for the ground states.[33,34] For example, studies of Fe^{2+} complexes using Mossbauer spectroscopy indicate that quintet–singlet transitions of ground-state Fe^{2+} are temperature dependent.[35-38] Other studies have shown that the ligand structure can influence the symmetry of the Fe^{2+} ion environment causing spin transition.[17-21] Extensive data exist establishing that nearly all six-coordinate Fe^{2+} complexes of the type $Fe^{2+}(Phen)_3$ have diamagnetic ground states.[39] In the current studies, the progressive addition of Phen ligands to the Fe^{2+} center effects spin pairing in the Fe^{2+} ion upon coordination of the third Phen ligand according to B3LYP results. This is a clear indication that the ligand structure is influencing the symmetry of the Fe^{2+} ion environment causing a spin transition. The quintet and singlet states of the $Fe^{2+}(Phen)_x$ complexes possess four and zero unpaired electrons, respectively. In the $Fe^{2+}(Phen)$ and $Fe^{2+}(Phen)_2$ ions, the degenerate 3d levels split into three lower d_π and two higher energy d_{σ^*} orbitals, but the electrons are not spin-paired as the energy separation is insufficient to overcome the necessary inter-electron repulsions. Under the stronger field splitting provided by three Phen ligands, the six electrons become spin-paired, so that a diamagnetic

$Fe^{2+}(Phen)_3$ complex results. That the BHandHLYP and M06 functionals suggest a paramagnetic $M^{2+}(Phen)_3$ complex is due to the functionals overstabilizing the quintet state by about 97.1 and 38.4 kJ/mol over the singlet state, respectively. The small difference in energy computed between the quintet and the singlet states of $Fe^{2+}(Phen)_3$, ~2.5 kJ/mol using the B3LYP functional, indicate that the two states may co-exist at room temperature.

To establish which electronic spin states of the $Fe^{2+}(Phen)_3$ complex are accessed in the experiments, the TCID experimental data for the $Fe^{2+}(Phen)_3$ system is analyzed twice, once assuming that the threshold arises from dissociation of the singlet ground state, and the other assuming that the threshold describes dissociation from the quintet excited state. The BDE extracted assuming that the precursor $Fe^{2+}(Phen)_3$ complex is in the singlet ground state is 236.5 ± 17.0 kJ/mol, whereas the value extracted assuming that the threshold is influenced by the presence of a reasonable population of the quintet excited state is 210.7 ± 11.1 kJ/mol, the latter corresponding to a diabatic BDE for this system. As compared to the B3LYP values calculated for dissociation from the singlet ground state and quintet excited states of $Fe^{2+}(Phen)_3$, 215.0 and 212.5 kJ/mol, respectively, these analyses suggest that quintet excited state is indeed accessed in the experiments and shifts the threshold to lower values. These results are indeed consistent with the B3LYP results that indicate that ~37% of the ions should exist in the quintet excited state, whereas ~63% of the ions would exist in the singlet ground state at room temperature. Thus, the threshold should be determined by the dissociation behavior of the quintet excited state as it provides the lowest energy pathway to dissociation. Hence, the computed B3LYP BDEs and the TCID experimental results for the $Fe^{2+}(Phen)_3$ complex suggest that the singlet ground state and the excited quintet state of Fe^{2+}

are both accessed in the experiments, and that the threshold energy we measure for the third sequential binding energy of $Fe^{2+}(Phen)_3$ is more likely the diabatic value.

3.6.2 Trends in the BDEs of the $M^{2+}(Phen)_3$ Complexes

The measured BDEs of the $M^{2+}(Phen)_3$ complexes, where M^{2+} = Fe^{2+}, Co^{2+}, Ni^{2+}, Cu^{2+}, and Zn^{2+} are illustrated in Figure 3.5 and summarized in Table 3.3 and Table A.3 of Appendix A along with the corresponding theoretical BDEs calculated at the B3LYP/6-311+G(2d,2p), BHandHLYP/6-311+G(2d,2p), and M06/6-311+G(2d,2p) levels of theory. The measured BDEs are reported as the average values obtained from threshold analyses of the raw zero-pressure extrapolated data and analyses after subtraction of the low-energy feature, Table 3.1. At first glance, the stability of $M^{2+}(Phen)_3$ complexes should be dominated by electrostatic interactions, the strength of binding depending on the ionic radii, second ionization energies of the metal, and the M^{2+}–N bond lengths. However, the nature of the Phen ligands also contributes. The measured BDEs of the $M^{2+}(Phen)_3$ complexes follow the order $Cu^{2+} < Zn^{2+} < Co^{2+} < Fe^{2+} < Ni^{2+}$ as shown in Figure 3.5. The size of the metal cation decreases as the d orbital occupation increases: 0.76 Å, 0.74 Å, 0.73 Å, 0.72 Å, and 0.72 Å for Fe^{2+}, Co^{2+}, Ni^{2+}, Cu^{2+} and Zn^{2+}, respectively. Roughly parallel to the trend is the ionic radii of the metal cations; the M^{2+}–N bond lengths decrease from Fe^{2+}(2.204 Å) to Co^{2+}(2.163 Å) to Ni^{2+}(2.117 Å), and then increase for Zn^{2+}(2.193 Å) when comparing the quintet states. However, the spin change that the $Fe^{2+}(Phen)_3$ complex undergoes enables the ligands to approach the metal ion more closely resulting in a decrease in the M^{2+}–N bond lengths to 2.006 Å for $Fe^{2+}(Phen)_3$ in its singlet ground state. The structural variation observed in the $Cu^{2+}(Phen)_3$ complex resulting in two different Cu^{2+}–N bond lengths (2.055 and 2.397 Å) as compared to the $M^{2+}(Phen)_3$ complexes to Fe^{2+}, Co^{2+}, Ni^{2+}, and Zn^{2+} is due

to Jahn–Teller effects by which the $Cu^{2+}(Phen)_3$ complex shows pronounced distortions leading to much weaker binding of the third Phen ligand. Although the difference in size between the metal cations is not that significant, the effective nuclear charge increases across the period and therefore the binding interactions between the Phen ligands and M^{2+} cation is expected to increase across the period from Fe^{2+} to Zn^{2+}. The steric interactions between the bulky Phen ligands also lead to a lower binding energy, but this effect should be approximately independent of the identity of the metal cation. The weak BDEs of the $M^{2+}(Phen)_3$ complexes also confirm that the binding is noncovalent in nature. This is supported by the fact that in all the $M^{2+}(Phen)_3$ complexes, the most prominent fragmentation channel is the loss of an intact Phen ligand. The energy required to break a typical C–C covalent bond is > 400 kJ/mol,[40] which is much greater than the BDEs of the $M^{2+}(Phen)_3$ complexes determined here, which are < 240 kJ/mol for all five metal cations.

3.6.3 Comparison with Solution Phase

The third sequential binding energies determined here provide a measure of the intrinsic stability of the $M^{2+}(Phen)_3$ complexes in the gas phase, and are found to follow the order $Cu^{2+} < Zn^{2+} < Co^{2+} < {}^5Fe^{2+} < Ni^{2+} < {}^1Fe^{2+}$ (see Table 3.3 and Figure 3.5). Binding constants for the stepwise coordination of M^{2+} cations with Phen in aqueous solution at 298 K and an ionic strength μ = 0.1 have been reported.[41] The values for log k_3 of the $M^{2+}(Phen)_3$ complexes in aqueous solution provide a quantitative measure of the stability of these complexes in solution and similar to that found here follow the order $Cu^{2+}(5.02) < Zn^{2+}(5.1) < Co^{2+}(6.28) < Ni^{2+}(7.9) < Fe^{2+}(10.3)$. While a highly quantitative comparison is not possible without considering solvent and counterion effects, the parallel stability order

observed in the gas phase and in solution phase indicates that gas phase measurements can provide insight into solution phase relative stabilities in favorable cases.

3.6.4 Comparison between Experiment and Theory

Theoretical BDEs of the $M^{2+}(Phen)_3$ complexes derived from the B3LYP, BHandHLYP, and M06 levels of theory roughly parallel the measured BDEs, but differ in absolute magnitude, Figure 3.5. The measured third sequential BDEs for all five $M^{2+}(Phen)_3$ complexes exhibit very good agreement with B3LYP theory. The mean absolute deviation (MAD) between B3LYP theory and experiment is 13.7 ± 6.7 kJ/mol for all five complexes when values for the singlet ground-state $Fe^{2+}(Phen)_3$ complex are used. The BDE of the singlet ground-state $Fe^{2+}(Phen)_3$ is 236.5 ± 17.0 kJ/mol, whereas the diabatic BDE of the excited-state $Fe^{2+}(Phen)_3$ is 210.7 ± 11.1 kJ/mol. The diabatic BDEs agree better with the B3LYP results. When values for the quintet excited-state of the $Fe^{2+}(Phen)_3$ complex are used the MAD reduces to 9.7 ± 6.7 kJ/mol. The measured third sequential BDEs for the Phen complexes to Co^{2+}, Cu^{2+}, Zn^{2+} and Fe^{2+} (in its singlet state) also exhibit very good agreement with BHandHLYP theory, whereas the value calculated for the complex to Ni^{2+} and the quintet state of $Fe^{2+}(Phen)_3$ differ markedly from the measured BDEs. The MAD between BHandHLYP theory and experiment for all the five complexes is 22.3 ± 25.1 kJ/mol when the values for the singlet state of $Fe^{2+}(Phen)_3$ are used, but reduces to 11.2 ± 3.4 kJ/mol when Ni^{2+} is not included. The MAD between BHandHLYP and experiment increases to 43.2 ± 45.7 kJ/mol when the values for the quintet state of $Fe^{2+}(Phen)_3$ are used. This implies that the singlet state of $Fe^{2+}(Phen)_3$ agrees much better with BHandHLYP than the quintet state of $Fe^{2+}(Phen)_3$ as well. The third sequential BDEs computed using M06 theory are systematically higher than BDEs obtained using the B3LYP and BHandHLYP

theories by 42.5 ± 23.3 and 33.9 ± 33.6 kJ/mol, respectively. The larger binding energies found with M06 theory are consistent with the shorter M^{2+}–N bond lengths in the optimized geometries as compared to those for structures computed at the B3LYP and BHandHLYP levels of theory. The agreement between M06 theory and the measured BDEs for all of the complexes is very poor. M06 theory systematically overestimates the measured BDEs by 56.2 ± 22.3 kJ/mol when the singlet $Fe^{2+}(Phen)_3$ complex is used in the comparison. When the quintet state of $Fe^{2+}(Phen)_3$ is considered, the MAD increases to 68.6 ± 22.1 kJ/mol. Again, the BDE computed for the complex to Ni^{2+} and quintet state of $Fe^{2+}(Phen)_3$ exhibit the largest deviations from the measured values. The MAD between M06 theory and the TCID measured values reduces to 47.6 ± 13.1 kJ/mol when Ni^{2+} and the quintet state of the $Fe^{2+}(Phen)_3$ complex are not included. The average experimental uncertainty (AEU) in the measured BDEs is 13.3 ± 2.6 kJ/mol when the singlet $Fe^{2+}(Phen)_3$ complex is considered. The AEU values decrease to 12.1 ± 1.9 kJ/mol if the quintet state $Fe^{2+}(Phen)_3$ complex is used. The AEU values are only slightly different than the MAD for B3LYP theory, but significantly smaller than the MADs for BHandHLYP and M06 theories. Thus, B3LYP theory provides the best description of the binding of the third ligand in the $M^{2+}(Phen)_3$ complexes.

3.6.5 Trends in the Sequential and Total BDEs of the $M^{2+}(Phen)_x$ Complexes

Trends in the B3LYP/6-311+G(2d,2p) sequential and total binding energies of the $M^{2+}(Phen)_x$ complexes are illustrated in Figure 3.6 and summarized in Table 3.3. As illustrated in Figure 3.6 parts a and b, the strength of binding of the Phen ligands to the M^{2+} cations falls off rapidly with increasing ligation. The binding of the first Phen ligand is very strong, and varies between 1018.3 and 1259.1 kJ/mol across these systems. The four N

donor electrons of the Phen ligand stabilize the M^{2+} center greatly through electrostatic interactions. Hybridization of the M^{2+} cation also plays a major role in enhancing the binding energy of the first Phen ligand. Because the d_σ orbitals in all of the M^{2+}(Phen) complexes are occupied, greater repulsion between the metal cations and the ligand occurs. 4s-3d_σ hybridization removes electron density along the metal-ligand bonding axis exposing the ligand to greater charge, and allowing the ligand to approach the metal cation more closely (the M^{2+}–N bond distances vary between 1.884 and 1.967Å), and results in very strong binding of the first Phen ligand. The M^{2+}(Phen) complexes are still electron deficient, and therefore binding of the second Phen ligand is still very strong. The strength of binding of the second Phen ligand varies between 511.8 and 545.2 kJ/mol, ~40–50% as strong as binding of the first ligand. The weaker binding in the bis-complexes is the result of three effects, the decline in the effective positive charge retained by M^{2+} upon binding to the first ligand via two M^{2+}–N dative interactions, repulsive interactions between the second Phen ligand and the occupied sd hybridized orbital, and the repulsive interactions between the electron density of the first and second ligands. Binding of the second Phen overcomes much of the electron deficiency such that the M^{2+}–N bond lengths increase by ~0.1 Å and vary between 1.986 Å and 2.062 Å. Binding of the third Phen ligand is much weaker, and varies between 149.1 and 233.2 kJ/mol, ~14–20% as strong as binding to the first ligand, and the M^{2+}–N bond lengths again increase and vary between 2.006 to 2.397 Å. The even weaker binding in the tris-complexes is again the result of three effects, the continued decline in the effective positive charge retained by M^{2+} upon binding to the first and second ligands via four M^{2+}–N dative interactions, repulsive interactions between the third Phen ligand and the

occupied sd hybridized orbital, and the repulsive interactions between the electron density of the three Phen ligands.

With each Phen ligand bound to the M^{2+} metal center, the electrostatic contributions to the binding decrease because the effective charge retained by the metal cation decreases as more electrons are added to the metal center. Similarly, ligand-ligand repulsive interactions between the Phen ligands increase upon sequential ligation, leading to weaker binding. These effects act in concert to lengthen the M^{2+}–N bond lengths with increasing ligation. Notably, the variation in the BDEs of the first ligand to all five metal cations is largest, 240.8 kJ/mol. This large variation directly reflects the differences in stabilization the metal cations achieve via sd hybridization, which increases with increasing d orbital occupation. The second sequential BDEs exhibit the least variation, 33.4 kJ/mol, primarily because sd hybridization effects diminish greatly as binding of the second Phen ligand produces much greater repulsion with the occupied sd hybrid orbital. The variation in the third sequential BDEs is intermediate, 84.1 kJ/mol. The larger variation in the BDEs across the tris-complexes arises because of spin crossover in the Fe^{2+} system, and slight Jahn–Teller effects in the Co^{2+} and significant Jahn–Teller effects in the Cu^{2+} systems.

The evolution in the nature of the binding in the $M^{2+}(Phen)_x$ complexes as a function of ligation is clearly seen in the dissociation behavior of these complexes. In all of the $M^{2+}(Phen)_3$ complexes, the most prominent fragmentation channel is the loss of an intact Phen ligand. The measured BDEs of the $M^{2+}(Phen)_3$ complexes are all < 240 kJ/mol, weaker than a typical C–C covalent bond, > 400 kJ/mol.[40] Thus, their CID behavior indicates that the nature of the binding of the third ligand in the $M^{2+}(Phen)_3$ complexes is predominantly noncovalent. In comparison with the $M^{2+}(Phen)_3$ complexes, the BDEs calculated for the

$M^{2+}(Phen)_2$ complexes are > 400 kJ/mol, implying that the binding of the second Phen ligand is more covalent in nature. As a result, the CID behavior of the $M^{2+}(Phen)_2$ complexes is much richer and provides an opportunity to probe the metal-to-ligand and ligand-to-metal charge transfer behavior in much greater detail. The BDEs of the $M^{2+}(Phen)$ complexes are calculated to be > 1000 kJ/mol suggesting that covalent interactions dominate the binding. However, the high electron deficiency of these complexes makes these complexes too reactive to generate in sufficient intensity to enable direct studies of their CID behavior.

3.6.6 Periodic Trends in the Sequential BDEs of the $M^{2+}(Phen)_x$ Complexes

Periodic trends in the BDEs of the mono-complexes are shown in Figure 3.6, parts a, and b. The M^{2+}–Phen BDEs follow the order: $Fe^{2+} < Co^{2+} < Zn^{2+} < Ni^{2+} < Cu^{2+}$. This trend is explained by the relative sizes of the metal cations, which have ionic radii of 0.76, 0.74, 0.73, 0.72, and 0.72 Å for Fe^{2+}, Co^{2+}, Ni^{2+}, Cu^{2+} and Zn^{2+}, respectively.[28,29] The variation in metal cation radii roughly parallels the M^{2+}–N bond lengths, which decrease from Fe^{2+} to Cu^{2+} as the d-orbital occupation increases. This trend is also inversely correlated with the second ionization energies (IEs) of the metal: 16.19, 17.08, 18.17, and 20.29 eV for Fe, Co, Ni, and Cu, respectively.[42] The ionic radii, M^{2+}–N bond lengths, and the second IEs serve as guides to the magnitude of the electrostatic interactions involved in these complexes, and determines how closely the Phen ligand can approach the metal center. Considering the M^{2+}–N bond lengths, ionic radii, and second IEs, the trend in the BDEs, $Cu^{2+}(Phen) > Zn^{2+}(Phen)$ is reasonable. However, no simple correlation exists because Zn has a higher second IE (17.96 eV) than Fe (16.19 eV) and Co (17.08 eV), but Zn^{2+} has a smaller ionic radius than Fe^{2+}, Co^{2+} and Ni^{2+}. The second sequential BDEs, $(Phen)M^{2+}$–Phen increase in the order: $Fe^{2+} < Cu^{2+} < Co^{2+} < Zn^{2+} < Ni^{2+}$. The stability order has changed immensely for $Cu^{2+}(Phen)_2$ due

to increased ligand-ligand repulsion as two Phen ligands position themselves around the very small Cu^{2+} cation adopting a geometry close to a square planar to minimize repulsion with the occupied sd hybrid orbital, and also suggesting that Jahn–Teller effects are beginning to take effect in the bis-complexes. Overall, the sequential BDEs of the $M^{2+}(Phen)_2$ complexes remain closely related to the minor structural differences found for these complexes. The third sequential BDEs, $(Phen)_2M^{2+}$–Phen, follow the order: $Cu^{2+} < Zn^{2+} < Co^{2+} < Fe^{2+} < Ni^{2+}$. The trend in the third sequential BDEs differs from that observed for binding of the first and second ligands. The relative BDEs vary primarily because the Cu^{2+} complexes shift from being the most strongly bound when $x = 1$ to the least strongly bound when $x = 3$. This anomaly in the BDEs is a consequence of Jahn–Teller effects, by which the $Cu^{2+}(Phen)_3$ complex exhibits pronounced tetragonal distortions leading to a weaker third sequential BDE. Changes in the trends in the BDEs calculated for the Co^{2+} complex due to Jahn-Teller distortions are slight. Fe^{2+} on the other hand exhibits the weakest binding energy among the monocomplexes, while the tris-complex exhibits a much stronger binding energy. As the extent of ligation increases, the order of stabilities changes drastically with the $Fe^{2+}(Phen)_3$ becoming more stable. This anomalous stability of the $Fe^{2+}(Phen)_3$ complex arises due to the formation of a low-spin complex. Under the stronger field-splitting provided by the three Phen ligands, the electrons become spin paired, so that a more stable diamagnetic complex results. This results in the $d_{\sigma*}$ orbitals being empty, and hence less repulsion with the third Phen ligand, and increasing the third sequential BDE of the $Fe^{2+}(Phen)_3$ complex.

3.6.7 Periodic Trends in the Total BDEs of the $M^{2+}(Phen)_x$ Complexes

The trends in the total binding energies of the $M^{2+}(Phen)_x$ complexes as a function of the number of Phen ligands interacting with the M^{2+} cation are shown in Figure 3.6, parts c

and d. The total binding energy obviously increases as the number of Phen ligands increases. The binding energy of the first Phen ligand varies between 1018.3 to 1259.1 kJ/mol. The total binding energies for the bis- and tris-complexes are ~1.5 and ~1.7 times as strong as those for the monocomplexes, respectively. The total binding energies increase sharply from $x = 1$ to $x = 2$, and less dramatically from $x = 2$ to $x = 3$. The trends in the total binding energies for the five metal complexes roughly parallel each other. The total energy of binding follows the order: $Cu^{2+} > Ni^{2+} > Zn^{2+} > Co^{2+} > Fe^{2+}$. This trend can be explained by the three most important factors that control the strength of binding in these $M^{2+}(Phen)_x$ complexes, i.e., sd hybridization of the metal cation, Jahn–Teller effects, and ligand–ligand repulsion. sd Hybridization plays a key role when binding the first ligand to the M^{2+} cation. When binding the second Phen ligand, stabilization from sd hybridization is lost, while Jahn–Teller effects become pronounced for the $Cu^{2+}(Phen)_2$ complex as the ligands attempt to mimimize repulsion with the occupied sd hybridized orbital by reducing the $\angle NM^{2+}NC$ dihedral angles between the Phen ligands. Upon binding of the third ligand, Jahn–Teller effects become the dominant factor, strongly influencing the structure and binding in the $Cu^{2+}(Phen)_3$ complex. The effects of the spin change of the $Fe^{2+}(Phen)_x$ systems upon binding of the third Phen ligand helps to provide additional stabilization to the tris-complex, but the lesser stabilization achieved from sd hybridization of the $x = 1$ complex leads to Fe^{2+} exhibiting the weakest total binding energy among the tris-complexes.

3.6.8 Comparison of the BDEs of $M^{2+}(Phen)_x$ and $M^{+}(Phen)_x$

The sequential BDEs of the $M^{2+}(Phen)_x$ complexes, where $x = 1–3$, are compared to those of the analogous $M^{+}(Phen)_x$ complexes in Figure 3.7, part a.[22-25] As can be seen in the figure, the sequential BDEs decrease monotonically as the number of ligands increases from

one to three for the complexes to both the M^{2+} and M^{+} cations. The rapid decrease in the sequential BDEs for both the $M^{2+}(Phen)_x$ and $M^{+}(Phen)_x$ complexes arises because the electrostatic contributions to the binding decrease rapidly upon sequential ligation because each Phen ligand provides two N donor interactions such that the charge retained by the metal cation decreases rapidly. In both cases, an increase in M^{n+}–N bond distances as the size of the complex increases is observed. For example, the Zn^{+}–N bond lengths of the $Zn^{+}(Phen)_x$ complexes increase from 2.057 to 2.010 to 2.191 Å, whereas Zn^{2+}–N bond lengths of the $Zn^{2+}(Phen)_x$ increase from 1.913 to 2.023, to 2.193 Å as *x* increases from 1 to 3, respectively. In contrast, the BDEs decrease from 362.2 to 223.7 to 82.6 kJ/mol for the $Zn^{+}(Phen)_x$ complexes, whereas those of the $Zn^{2+}(Phen)_x$ decreases from 1120.2, to 539.0 to 161.0 kJ/mol as *x* increases from 1 to 3, respectively. The difference in the Zn^{n+}–N bond distances is greater in the mono- complexes, and decreases as the number of ligands increases. Ligand-ligand repulsion also contributes to the sequential decrease in BDEs. The BDEs are larger for the M^{2+} complexes as compared to the analogous M^{+} complexes. The ratio between the BDEs of the doubly charged to the singly charged complexes decreases as the number of ligand increases, and is roughly 2.95:1 for the mono-, 2.46:1 for the bis-, and 1.70:1 for the tris-complexes. In spite of these large differences in the binding energies, the structural differences between the analogous $M^{2+}(Phen)_x$ and $M^{+}(Phen)_x$ complexes are very nominal. For example, the difference between the bond lengths found in $Zn^{+}(Phen)_x$ compared to their analogous $Zn^{2+}(Phen)_x$ complexes is quite small except for the mono-complexes. The differences in the BDEs of these complexes are largely the result of electrostatics, i.e., the ion-dipole and ion-induced dipole interactions are twice as strong for the M^{2+} complexes as those to M^{+} when the M^{n+}–N bond lengths are preserved. However,

the M^{2+} cations are smaller than the M^{+} cations, and hence the binding interactions with the Phen ligand are more than twice as strong because the Phen ligand can approach the M^{2+} cation more closely. The difference in BDEs between the analogous doubly and singly charged complexes becomes narrower as the number of ligands increases as illustrated in Figure 3.7, part b. Thus, it is clear that additional ligands are required to stabilize the M^{2+} cations to a point where the energies become comparable to those of the complexes to the M^{+} cations.

The trends in the sequential BDEs of these $M^{n+}(Phen)_x$ complexes can be understood in terms of several competing factors including electrostatic interactions, metal-ligand hybridization, and ligand-ligand repulsion. The metal-ligand bonding interactions in the $M^{2+}(Phen)_x$ and $M^{+}(Phen)_x$ complexes are similar. The $Co^{2+}(d^7)$, $Ni^{2+}(d^8)$, $Co^{+}(d^8)$, $Cu^{2+}(d^9)$, and $Ni^{+}(d^9)$ cations are partially occupied. The $Zn^{2+}(d^{10})$ is isoelectronic with the $Cu^{+}(d^{10})$ cation, which is fully occupied, whereas the $Zn^{+}(4s^{1}3d^{10})$ cation has an extra electron in its s orbital. When these cations form bonds with Phen ligands π-back donation is expected to increase from Co^{2+} to Zn^{2+} and further from Co^{+} to Zn^{+} across the period. Most favorable π-back donation arises when there is a filled d orbital because the metal cation overlaps better with the π* orbital of the planar π network of Phen. Because the d_{σ^*} orbitals in all of the $M^{n+}(Phen)_x$ complexes are occupied, greater repulsion between the metal cation and the ligands is expected. Even more repulsion is expected for the $Zn^{+}(Phen)_x$ complexes because the s orbital is occupied. In the $M^{n+}(Phen)$ mono-complexes, 4s-3d hybridization effectively removes electron density from the metal-ligand axis by placing the electron density in a hybridized orbital that is perpendicular to the bonding axis for all of the metal cations except Zn^{+}. This results in a higher BDE for all of the monocomplexes. The enhancements in

binding increase across the period with increasing orbital occupation. In the case of Zn^+(Phen), sp polarization plays a similar role as sd hybridization and removes electron density from the metal–ligand axis by placing the electron density in a hybridized orbital oriented 180° away from the bonding axis. However, sp polarization produces less stabilization than sd hybridization as the orbitals lie higher in energy. The decline in the effective positive charge and repulsive interactions between electron densities further diminish the BDEs. Hence the differences in the binding patterns observed in the $M^{n+}(Phen)_x$ complexes are dominated by the charge. Figure 3.8 shows the trends in the third sequential BDEs for the Phen complexes of M^{2+} and M^+. The binding in the d^8, d^9, and d^{10} complexes is roughly parallel for the M^{2+} and M^+ complexes. However, the $Cu^+(Phen)_3$ complex is actually calculated to be unbound at room temperature. This is supported by the Gibbs free energy at 298 K (–56.7 kJ/mol) for the loss of Phen from the $Cu^+(Phen)_3$ complex, suggesting that dissociation would be spontaneous. Appreciable ion beams of any of the $M^+(Phen)_3$ complexes were not obtained because their internal energies at room temperature exceed the BDEs.[22-25] However, our ability to generate intense ion beams of $Cu^{2+}(Phen)_3$ and the other $M^{2+}(Phen)_3$ complexes, and measure their CID behavior clearly establishes that these species are bound, and loss of a single Phen ligand from these complexes is endothermic.

3.7 Conclusions

The kinetic energy dependences of the CID of the tris-ligated complexes of the late first-row divalent transition metal cations to Phen, $M^{2+}(Phen)_3$, with Xe are examined in a guided ion beam tandem mass spectrometer. The dominant dissociation pathway for all complexes is loss of an intact Phen ligand. The thresholds for these processes are determined

after consideration of the effects of the internal energy distribution of the reactant $M^{2+}(Phen)_3$ complexes,[43] multiple collisions with Xe,[44] and lifetime effects.[26,45-46]Sequential BDEs of the $M^{2+}(Phen)_x$ complexes are determined at the B3LYP/6-311+G(2d,2p)//B3LYP/6-31G*, BHandHLYP/6-311+G(2d,2p)//BHandHLYP/6-31G*, and M06/6-311+G(2d,2p)//M06/6-31G* levels of theory. The computed sequential BDEs are highly parallel, but differ in absolute magnitude. BDEs computed using the M06 functional are the strongest, BHandHLYP values are intermediate, whereas B3LYP produces the weakest BDEs. Very good agreement between the B3LYP theoretically calculated and TCID experimentally determined BDEs is found, suggesting that the B3LYP functional is capable of accurately describing the binding in the tris-complexes. The present results suggest that the bonding in the $M^{2+}(Phen)_x$ complexes is dominantly electrostatic. Comparison of the $M^{2+}(Phen)_x$ to the analogous $M^{+}(Phen)_x$ complexes indicates that the charge (or oxidation state) of the metal cation is the dominant contributing factor to the differences in the strength of binding among these complexes. The strength of binding is also found to depend on the electron configuration of the metal cation, however differences in the strength of binding are much smaller for cations of the same charge.

3.8 References

(1) Costello, J. F.; Davies, S. G.; McNally, D. *J. Chem. Soc., Perkin Trans. 2* **1999**, 465.

(2) Noyori, R.; Takaya, H. *Acc. Chem. Res.* **1990**, *23*, 345.

(3) Brandt, W. W.; Dwyer, F. P.; Gyarfas, E. C. *Chem. Rev.* **1954**, *54*, 959.

(4) Summers, L. A. *Adv. Heterocyclic Chem.* **1978**, *22*, 1.

(5) Holyer, R. H.; Hubbard, C. D.; Kettle, S. F. A.; Wilkins, R. G. *Inorg. Chem.* **1965**, *4*, 929.

(6) Graham, B. *Six-Membered Heterocyclic Nitrogen Compounds with Three Condensed Rings*. Wiley-Interscience, New York. **1958**, pp. 386.

(7) Keipert, S. J.; Knobler, C. B.; Cram, D. J. *Tetrahedron* **1987**, *43*, 4861.

(8) Chandler, C. J.; Deady, L. W.; Reiss, J. A. *J. Heterocyclic Chem.* **1986**, *23*, 1327.

(9) Gladiali, S.; Chelucci, G.; Soccolini, F.; Delogu, G.; Chessa, G. *J. Organomet. Chem.* **1989**, *370*, 285.

(10) Gladiali, S.; Pinna, L.; Delogu, G.; De Martin, S.; Zassinovich, G.; Mestroni, G. *Tetrahedron Asymmetry* **1990**, *1*, 635.

(11) Schoffers, E. *Eur. J. Org. Chem.* **2003**, *7*, 1145.

(12) Chelluci, G.; Thummel, R. P. *Chem. Rev.* **2002**, *102*, 3129.

(13) Puglisi, A.; Benaglia, M.; Annunziata, R.; Bologna, A. *Tetrahedron Lett*. **2003**, *44*, 2947.

(14) Gladysz, J. A.; Boone, B. J. *Angew. Chem., Int. Ed. Engl.* **1997**, *36*, 551.

(15) Hollis, T. K.; Odenkirk, W.; Robinson, N. P.; Whelan, J.; Bosnich, B. *Tetrahedron* **1993**, *49*, 5415.

(16) Davenport, A. J.; Fawcett, J.; Lad, L.; Russell, R. R. *Chem. Commun*. **1997**, 2347.

(17) Irving, H.; Mellor, D. H. *J. Chem. Soc.* **1962**, 5222.

(18) Irving, H.; Mellor, D. H. *J. Chem. Soc.* **1962**, 5237.

(19) McBryde, W. A. E.; Brisbin, D. A.; Irving, H. *J. Chem. Soc.* **1962**, 5245.

(20) Irving, H. M.; Williams, R. J. P. *J. Chem. Soc.* **1953**, 3192.

(21) Irving, H. M.; Cabell, M. J.; Mellor, D. H. *J. Chem. Soc.* **1953**, 3417.

(22) Rannulu, N. S.; Rodgers, M. T. *J. Phys. Chem. A* **2007**, *111*, 3465.

(23) Rannulu N. S.; Rodgers, M. T. *J. Phys. Chem. A* **2012**, *116*, 1319.

(24) Rannulu, N. S.; Rodgers, M. T. *J. Phys. Chem. A* **2009**, *113*, 4534.

(25) Rannulu, N. S. Doctoral dissertation, Wayne State University. **2008**, pp. 283.

(26) Rodgers, M. T.; Ervin, K. M.; Armentrout, P. B. *J. Chem. Phys.* **1997**, *106*, 4499.

(27) Frisch, M. J.; Trucks, G. W.; Schlegel, H. B.; Scuseria, G. E.; Robb, M. A.; Cheeseman, J. R.; Scalmani, G.; Barone, V.; Mennucci, B.; Petersson, G. A.; Nakatsuji, H.; Caricato, M.; Li, X.; Hratchian, H. P.; Izmaylov, A. F.; Bloino, J.; Zheng, G.; Sonnenberg, J. L.; Hada, M.; Ehara, M.; Toyota, K.; Fukuda, R.; Hasegawa, J.; Ishida, M.; Nakajima, T.; Honda, Y.; Kitao, O.; Nakai, H.; Vreven, T.; Montgomery, J. A, Jr.; Peralta, J. E.; Ogliaro, F.; Bearpark, M.; Heyd, J. J.; Brothers, E.; Kudin, K. N.; Staroverov, V. N.; Kobayashi, R.; Normand, J.; Raghavachari, K.; Rendell, A.; Burant, J. C.; Iyengar, S. S.; Tomasi, J.; Cossi, M.; Rega, N.; Millam, J. M.; Klene, M.; Knox, J. E.; Cross, J. B.; Bakken, V.; Adamo, C.; Jaramillo, J.; Gomperts, R.; Stratmann, R. E.; Yazyev, O.; Austin, A. J.; Cammi, R.; Pomelli, C.; Ochterski, J. W.; Martin, R. L.; Morokuma, K.; Zakrzewski, V. G.; Voth, G. A.; Salvador, P.; Dannenberg, J. J.; Dapprich, S.; Daniels, A. D.; Farkas, O.; Foresman, J. B.; Ortiz, J. V.; Cioslowski, J.; Fox, D. J. Gaussian, Inc., Wallingford, CT, 2009.

(28) Shannon, R. D. *Acta Crystallogr*. **1976**, *A32*, 751.

(29) Jia, Y. Q. *J. Solid Sate Chem.* **1991**, *95*, 184.

(30) Reiher, M. *Inorg. Chem*. **2002**, *41*, 6928.

(31) Swart, M. *J. Chem. Theory Comput*. **2008**, *4*, 2057.

(32) Tanabe, Y.; Sugano, S. *J. Phys. Soc. Japan.* **1954**, *9*, 753.

(33) Fisher, D. C.; Drickamer, H. G. *J. Chem. Phys*. **1971**, *54*, 4825.

(34) Bargerum, C. B.; Drickamer, H. G. *J. Chem. Phys.* **1971**, *55*, 3471.

(35) Goodwin, H. A.; Sylva, R. N. *Aust. J. Chem*. **1968**, *21*, 83.

(36) Harris, C. M.; Kokot, S.; Patil, H. R. H.; Sinn, E.; Wong, H. *Aus. J. Chem*. **1972**, *25*, 1631.

(37) Konig, E.; Ritter, G.; Spiering, H.; Kremer, S.; Madeja, K.; Rosenkranz, A. *J. Chem. Phys*. **1972**, *56*, 3139.

(38) Reiff, W. M.; Long, G. J. *Inorg. Chem*. **1974**, *13*, 2150.

(39) Collins, R. L.; Pettit, R.; Baker, W. A. *J. Inorg. Nucl. Chem.* **1966**, *28*, 1001.

(40) Carey, F. A.; Giuliano, R. M. *Organic Chemistry* (8th ed). McGraw-Hill, New York. **2011**, pp. 165.

(41) *NIST Critical Stability Constants of Metal Complexes*, Version 8, National Institute of Standards and Technology. Washington, D.C. **2004**.

(42) Sansonetti, J. E.; Martin, W. C.; Young, S. L. *Handbook of Basic Atomic Spectroscopic Data*. *J. Phys. Chem. Ref. Data.* **2005**, *34*, 1559. *NIST Physical Data Web Site <http://www.nist.gov/pml/data/handbook/index.cfm >* (December **2012**).

(43) Ervin, K. M.; Armentrout, P. B. *J. Chem. Phys*. **1985**, *83*, 166.

(44) Daleska, N. F.; Honma, K.; Sunderlin, L. S.; Armentrout, P. B. *J. Am. Chem. Soc*. **1994**, *116*, 3519.

(45) Khan, F. A.; Clemmer, D. E.; Schultz, R. H.; Armentrout, P. B. *J. Phys. Chem*. **1993**, *97*, 7978.

(46) Loh, S. K.; Hales, D. A.; Lian, L.; Armentrout, P. B. *J. Chem. Phys*. **1989**, *90*, 5466.

Table 3.1. Modeling Parameters of Equation 2.3, Threshold Dissociation Energies at 0 K, and Entropies of Activation at 1000 K of $M^{2+}(Phen)_3$ Complexes[a]

M^{2+}	σ_0[b]	n[b]	E_0[c]	E_0(PSL)[b]	Kinetic Shift	$\Delta S^{\dagger}$(PSL)[b]
			(eV)	(eV)	(eV)	(J mol^{-1} K^{-1})
Fe^{2+}	35.6 (11.2)	2.1 (0.1)	4.84 (0.31)	2.36 (0.12)	2.48	154.4 (4.3)
	72.4 (24.4)	*1.8 (0.2)*	*5.72 (0.30)*	*2.54 (0.13)*	*3.18*	*154.1 (4.3)*
	47.3 (11.0)	**2.0 (0.1)**	**5.03 (0.25)**	**2.11 (0.11)**	**2.92**	**90.8 (4.4)**
	103.5 (42.9)	***1.6 (0.2)***	***5.62 (0.28)***	***2.26 (0.12)***	***3.36***	***90.5 (4.4)***
Co^{2+}	59.5 (11.1)	1.9 (0.1)	4.48 (0.11)	2.00 (0.08)	2.48	94.0 (4.4)
	174.4 (12.2)	*1.3 (0.1)*	*5.36 (0.11)*	*2.23 (0.11)*	*3.13*	*93.5 (4.4)*
Ni^{2+}	53.8 (3.0)	1.9 (0.1)	4.96 (0.10)	2.14 (0.09)	2.82	98.4 (4.4)
	108.4 (8.1)	*1.5 (0.1)*	*5.52 (0.10)*	*2.28 (0.10)*	*3.24*	*98.1 (4.4)*
Cu^{2+}	30.4 (4.3)	2.3 (0.1)	3.02 (0.12)	1.50 (0.06)	1.52	67.3 (4.4)
	166.6 (25.5)	*1.2 (0.1)*	*3.99 (0.12)*	*1.81 (0.08)*	*2.18*	*66.5 (4.4)*
Zn^{2+}	54.9 (19.8)	2.0 (0.2)	3.17 (0.29)	1.58 (0.10)	1.59	77.6 (4.4)
	280.6 (88.8)	*1.0 (0.2)*	*4.34 (0.25)*	*1.95 (0.11)*	*2.39*	*76.7 (4.4)*

[a] Uncertainties are listed in parentheses. Analyses of raw zero-pressure extrapolated data are shown in standard font, while analyses of zero-pressure extrapolated data after subtraction of the low-energy feature are shown in italicized font. Analyses of the singlet state of the $Fe^{2+}(Phen)_3$ complex are shown in standard font, while that of the quintet state are shown in boldface. [b] Average values for loose PSL transition state. [c] No RRKM analysis.

Table 3.2. Relative Energies between the various Spin States of a Given $M^{2+}(Phen)_x$ Complex in their Ground-State Conformations where M^{2+} = Fe^{2+}, Co^{2+}, and Ni^{2+} at 0 K in kJ/mol.

Complex	Multiplicity	B3LYP[a]	BHandHLYP[b]	M06[c]
Fe^{2+}	5	0.0	0.0	0.0
	3	241.3	263.6	260.2
	1	378.4	404.4	408.5
$Fe^{2+}(Phen)$	5	0.0	0.0	0.0
	3	71.1	104.3	95.2
	1	196.7	235.3	203.1
$Fe^{2+}(Phen)_2$	5	0.0	0.0	0.0
	3	49.9	105.8	92.9
	1	216.6	252.2	241.2
$Fe^{2+}(Phen)_3$	5	2.5	0.0	0.0
	3	49.9	106.2	92.9
	1	0.0	97.1	38.4
Co^{2+}	4	0.0	0.0	0.0
	2	252.6	273.5	304.6
$Co^{2+}(Phen)$	4	0.0	0.0	0.0
	2	45.6	110.2	28.4
$Co^{2+}(Phen)_2$	4	0.0	0.0	0.0
	2	50.5	110.2	24.0
$Co^{2+}(Phen)_3$	4	0.0	0.0	0.0
	2	25.9	94.6	10.9
Ni^{2+}	3	0.0	0.0	0.0
	1	297.0	317.3	234.6
$Ni^{2+}(Phen)$	3	0.0	0.0	0.0
	1	44.4	128.0	26.1
$Ni^{2+}(Phen)_2$	3	0.0	0.0	0.0
	1	24.6	107.4	65.7
$Ni^{2+}(Phen)_3$	3	0.0	0.0	0.0
	1	124.3	201.2	110.2

[a]Calculated at the B3LYP/6-311+G(2d,2p)//B3LYP/6-31G* level of theory including ZPE corrections with frequencies scaled by 0.9804. [b]Calculated at the BHandHLYP/6-311+G(2d,2p)//BHandHLYP/6-31G* level of theory including ZPE corrections with frequencies scaled by 0.9472. [c]Calculated at the M06/6-311+G(2d,2p)//M06/6-31G* level of theory including ZPE corrections with frequencies scaled by 0.9940.

Table 3.3. Measured and Calculated Sequential and Total Enthalpies of Binding of $M^{2+}(Phen)_x$ Complexes at 0 K in kJ/mol

		Theory		
		B3LYP[b]		
Complex	TCID[a]	D_0	$D_{0,BSSE}$[e]	total[e]
$Fe^{2+}(Phen)$	–	1021.2	1018.3	1018.3
$Fe^{2+}(Phen)_2$	–	515.6	511.8	1530.1
$Fe^{2+}(Phen)_3$	236.5 (17.0)	223.0	215.0	1745.1
$Fe^{2+}(Phen)_3$	**210.7 (11.1)**	**220.5**	**212.5**	**1742.6**
$Co^{2+}(Phen)$	–	1084.4	1080.9	1080.9
$Co^{2+}(Phen)_2$	–	549.8	545.2	1626.1
$Co^{2+}(Phen)_3$	203.8 (12.3)	200.1	193.6	1819.7
$Ni^{2+}(Phen)$	–	1157.9	1154.4	1154.4
$Ni^{2+}(Phen)_2$	–	542.1	537.5	1691.9
$Ni^{2+}(Phen)_3$	213.2 (12.8)	240.3	233.2	1925.1
$Cu^{2+}(Phen)$	–	1262.8	1259.1	1259.1
$Cu^{2+}(Phen)_2$	–	518.9	514.0	1773.1
$Cu^{2+}(Phen)_3$	159.6 (9.9)	156.0	149.1	1922.2
$Zn^{2+}(Phen)$	–	1126.3	1123.3	1123.3
$Zn^{2+}(Phen)_2$	–	544.7	540.4	1663.7
$Zn^{2+}(Phen)_3$	170.1 (14.3)	171.0	163.9	1827.6
AEU/MAD[f]	13.3 (2.6)		13.7 (6.7)	
AEU/MAD[g]	**12.1 (1.9)**		**9.7 (6.7)**	

[a]Average values from fits to raw data and data after subtraction of the low-energy feature, Table 3.1. Average values for the singlet state of $Fe^{2+}(Phen)_3$ complex are shown in standard font, while those of the quintet state of $Fe^{2+}(Phen)_3$ are shown in boldface. [b]Calculated at the B3LYP/6-311+G(2d,2p)//B3LYP/6-31G* level of theory including ZPE corrections with frequencies scaled by 0.9804. [e]Also includes BSSE corrections. [f]AEU/MAD values using the singlet state of $Fe^{2+}(Phen)_3$ in the analysis. [g]AEU/MAD values using the quintet state of $Fe^{2+}(Phen)_3$ in the analysis.

Table 3.4. Enthalpies and Free Energies of Binding of $M^{2+}(Phen)_x$ Complexes at 0 and 298 K in kJ/mol.[a]

Complex	ΔH_0	ΔH_{298}-ΔH_0[b]	ΔH_{298}	$T\Delta S_{298}$[b]	ΔG_{298}
$Fe^{2+}(Phen)$	–	2.4 (0.3)	–	33.5 (0.5)	–
$Fe^{2+}(Phen)_2$	–	–1.3 (0.9)	–	51.6 (1.6)	–
$Fe^{2+}(Phen)_3$	236.5 (17.0)	–2.3 (0.7)	234.2 (17.0)	55.2 (1.4)	179.0 (17.1)
$Fe^{2+}(Phen)_3$	**210.7 (11.1)**	**–2.3 (0.7)**	**208.4 (11.1)**	**55.2 (1.4)**	**153.2 (11.2)**
$Co^{2+}(Phen)$	–	2.6 (0.3)	–	36.3 (0.4)	–
$Co^{2+}(Phen)_2$	–	–0.2 (0.9)	–	54.7 (1.5)	–
$Co^{2+}(Phen)_3$	203.8 (12.3)	–2.4 (0.6)	201.4 (12.3)	56.1 (1.4)	145.3 (12.4)
$Ni^{2+}(Phen)$	–	2.6 (0.3)	–	36.5 (0.4)	–
$Ni^{2+}(Phen)_2$	–	–0.4 (0.9)	–	53.7 (1.5)	–
$Ni^{2+}(Phen)_3$	213.2 (12.8)	–2.2 (0.7)	211.0 (12.8)	57.3 (1.4)	153.7 (12.9)
$Cu^{2+}(Phen)$	–	1.6 (0.3)	–	33.4 (0.5)	–
$Cu^{2+}(Phen)_2$	–	0.5 (0.8)	–	56.9 (1.4)	–
$Cu^{2+}(Phen)_3$	159.6 (9.9)	–3.6 (0.9)	156.0 (9.9)	50.2 (1.8)	105.8 (10.1)
$Zn^{2+}(Phen)$	–	2.6 (0.3)	–	36.6 (0.4)	–
$Zn^{2+}(Phen)_2$	–	–1.0 (0.9)	–	52.8 (1.6)	–
$Zn^{2+}(Phen)_3$	170.1 (14.3)	–3.4 (0.7)	166.5 (14.3)	52.1 (1.6)	114.4 (14.4)

[a]Uncertainties are listed in parentheses. Values of singlet ground-state $Fe^{2+}(Phen)_3$ are shown in standard font, while those of quintet excited-state $Fe^{2+}(Phen)_3$ are shown in boldface. [b]Values from calculations at the B3LYP/6-311+G(2d,2p) level of theory using B3LYP/6-31G* optimized geometries with frequencies scaled by 0.9804.

Table 3.4. (continued) Enthalpies and Free Energies of Binding of $M^{2+}(Phen)_x$ Complexes at 0 and 298 K in kJ/mol.[a]

Complex	ΔH_0[b]	ΔH_{298}-ΔH_0[b]	ΔH_{298}[b]	$T\Delta S_{298}$[b]	ΔG_{298}[b]
$Fe^{2+}(Phen)$	1018.3	2.4 (0.3)	1020.7	33.5 (0.5)	987.2
$Fe^{2+}(Phen)_2$	511.8	–1.3 (0.9)	510.5	51.6 (1.6)	458.9
$Fe^{2+}(Phen)_3$	215.0	–2.3 (0.7)	212.7	55.2 (1.4)	157.5
$Fe^{2+}(Phen)_3$	**212.5**	**–2.3 (0.7)**	**210.2**	**55.2 (1.4)**	**155.0**
$Co^{2+}(Phen)$	1080.9	2.6 (0.3)	1083.5	36.3 (0.4)	1047.2
$Co^{2+}(Phen)_2$	545.2	–0.2 (0.9)	545.0	54.7 (1.5)	490.3
$Co^{2+}(Phen)_3$	193.6	–2.4 (0.6)	191.2	56.1 (1.4)	135.1
$Ni^{2+}(Phen)$	1154.4	2.6 (0.3)	1157.0	36.5 (0.4)	1120.5
$Ni^{2+}(Phen)_2$	537.5	–0.4 (0.9)	537.1	53.7 (1.5)	483.4
$Ni^{2+}(Phen)_3$	233.2	–2.2 (0.7)	231.0	57.3 (1.4)	173.7
$Cu^{2+}(Phen)$	1259.1	1.6 (0.3)	1260.7	33.4 (0.5)	1227.3
$Cu^{2+}(Phen)_2$	514.0	0.5 (0.8)	514.5	56.9 (1.4)	457.6
$Cu^{2+}(Phen)_3$	149.1	–3.6 (0.9)	145.5	50.2 (1.8)	95.3
$Zn^{2+}(Phen)$	1123.3	2.6 (0.3)	1125.9	36.6 (0.4)	1089.3
$Zn^{2+}(Phen)_2$	540.4	–1.0 (0.9)	539.4	52.8 (1.6)	486.6
$Zn^{2+}(Phen)_3$	163.9	–3.4 (0.7)	160.5	52.1 (1.6)	108.4

[a]Uncertainties are listed in parentheses. Values of singlet ground-state $Fe^{2+}(Phen)_3$ are shown in standard font, while those of quintet excited-state $Fe^{2+}(Phen)_3$ are shown in boldface. [b]Values from calculations at the B3LYP/6-311+G(2d,2p) level of theory using B3LYP/6-31G* optimized geometries with frequencies scaled by 0.9804.

Table 3.5. Geometrical Parameters of the B3LYP/6-31G* Ground-State Structures of the Neutral Phen Ligand and $M^{2+}(Phen)_x$ Complexes[a]

Complex	M^{2+}–N	∠NCCN	∠NM^{2+}NC	∠NM^{2+}N[b]	∠NM^{2+}N[c]
Phen	–	0.0	–	–	–
$Fe^{2+}(Phen)$	1.967	0.0	–	90.9	–
$Fe^{2+}(Phen)_2$	2.062	0.0	81.1	83.0	124.1
$Fe^{2+}(Phen)_3$	2.006	1.3	60.4	82.1	89.1 (3), 94.5 (6), 175.3 (3)
$Fe^{2+}(Phen)_3$	**2.204**	**1.3 (2) 1.8**	**57.0**	**76.4**	**91.4, 94.2 (4), 96.3 (4), 167.1, 169.6 (2)**
$Co^{2+}(Phen)$	1.934	0.0	–	89.9	–
$Co^{2+}(Phen)_2$	2.024	0.0	81.2	84.2	123.4
$Co^{2+}(Phen)_3$	2.163	1.2	61.1	77.6	89.5 (3), 96.7 (6), 172.1 (3)
$Ni^{2+}(Phen)$	1.892	0.0	–	91.6	–
$Ni^{2+}(Phen)_2$	2.003	0.0	82.1	83.3	124.0
$Ni^{2+}(Phen)_3$	2.117	1.5 (2) 1.3	59.3	79.3	90.7 (3), 95.2 (6), 172.3 (3)
$Cu^{2+}(Phen)$	1.884	0.0	–	91.2	–
$Cu^{2+}(Phen)_2$	1.986	0.9	49.0	84.4	103.8 (2), 149.2 (2)
$Cu^{2+}(Phen)_3$	2.055 (4) 2.397 (2)	2.3 (2) 0.4	56.9	75.8 (2), 81.2	91.3 (3), 94.3 (4), 99.1 (2), 170.4 (3)
$Zn^{2+}(Phen)$	1.913	0.0	–	94.6	–
$Zn^{2+}(Phen)_2$	2.023	0.0	81.1	84.6	123.2
$Zn^{2+}(Phen)_3$	2.193	1.7	56.9	76.8	94.8 (9), 168.4 (3)

[a]Average values are given for similar bond distances or angles; degeneracies are listed in parentheses for values that differ sufficiently such that more than one value is needed to describe the bond angle or bond distance. Geometrical parameters for the singlet ground state of $Fe^{2+}(Phen)_3$ are shown in standard font, while those for quintet excited state are shown in boldface. All bond angles (∠) are given in degrees (°) and M^{2+}–N bond lengths in angstroms (Å). [b] intraligand angles. [c] interligand angles.

3.10 Figure Captions and Figures

Figure 3.1. Cross sections for collision-induced dissociation of the $M^{2+}(Phen)_3$ complexes, where M^{2+} = Fe^{2+}, Co^{2+}, Ni^{2+}, Cu^{2+}, and Zn^{2+} with Xe as a function of kinetic energy in the center-of-mass frame (lower *x*-axis) and laboratory frame (upper *x*-axis). Data are shown for a Xe pressure of ~0.2 mTorr.

Figure 3.2. Zero-pressure-extrapolated cross sections for collision-induced dissociation of the $M^{2+}(Phen)_3$ complexes, where M^{2+} = Fe^{2+}, Co^{2+}, Ni^{2+}, Cu^{2+}, and Zn^{2+} with Xe in the threshold region as a function of kinetic energy in the center-of-mass frame (lower *x*-axis) and laboratory frame (upper *x*-axis). Parts a, c, e, g, and i show raw zero-pressure extrapolated data and composite fits to the low and high energy regions of the CID cross sections, whereas parts b, d, f, h, and j show data and fits obtained after subtraction of the low-energy feature. Solid lines show the best fits to the data using equation 2.3 convoluted over the kinetic and internal energy distributions of the reactants. Dotted lines show the model cross sections in the absence of experimental kinetic energy broadening for reactants with an internal energy corresponding to 0 K.

Figure 3.3. B3LYP/6-31G* optimized geometries of $M^{2+}(Phen)_x$ complexes, where M^{2+} = Fe^{2+}, Co^{2+}, Ni^{2+}, Cu^{2+}, and Zn^{2+}, and x = 1–3.

Figure 3.4. Variation in the average M^{2+}–N bond distances in B3LYP/6-31G* optimized $M^{2+}(Phen)_x$ complexes where x = 1–3 as a function of the metal cation, M^{2+}, where M^{2+} = Fe^{2+}, Co^{2+}, Ni^{2+}, Cu^{2+}, and Zn^{2+}. For the $Fe^{2+}(Phen)_3$ complex values for the singlet state are plotted as closed symbols, while the open symbols represent M^{2+}–N bond lengths obtained from the quintet state of the $Fe^{2+}(Phen)_3$ complex. The ionic radii of the bare metal cation; M^{2+} are also shown. Ionic radii of M^{2+} are taken from Refs 28 and 29.

Figure 3.5. Comparison of theoretical and TCID measured $(Phen)_2M^{2+}$–Phen BDEs at 0 K (in kJ/mol), where M^{2+} = Fe^{2+}, Co^{2+}, Ni^{2+}, Cu^{2+}, and Zn^{2+}. Closed symbols represent dissociation from the ground-state reactant complex to ground-state products. For the $Fe^{2+}(Phen)_3$ complex, values for the singlet state are plotted as closed symbols, while open symbols represent BDEs obtained from dissociation of the quintet state of the $Fe^{2+}(Phen)_3$ complex. Theoretical BDEs determined at the B3LYP, BHandHLYP, and M06 levels of theory using the 6-311+G(2d,2p) basis set including ZPE and BSSE corrections. All values are taken from Table 3.3.

Figure 3.6. $(Phen)_{x-1}M^{2+}$–Phen BDEs where M^{2+} = Fe^{2+}, Co^{2+}, Ni^{2+}, Cu^{2+}, and Zn^{2+} as a function of the number of Phen ligands (x) and the metal cation, M^{2+}, parts a and b, respectively. Total energy of binding of $M^{2+}(Phen)_x$ complexes as a function of the number of Phen ligands (x) and the metal cation, M^{2+}, parts c and d, respectively. Theoretical BDEs at 0 K (in kJ/mol) determined at the B3LYP/6-311+G(2d,2p) level of theory including ZPE and BSSE corrections. All values are taken from Table 3.3.

Figure 3.7. Comparison of B3LYP/6-311+G(2d,2p) calculated BDEs of the $M^{n+}(Phen)_x$ complexes as a function of the number of Phen ligands (*x*) and charge (*n*+), parts a and b, respectively. Values for M^{2+} are taken from Table 3.3 and include ZPE and BSSE corrections. Values for M^+ are taken from references 22–25.

Figure 3.8. Periodic trends in the TCID measured and calculated $(Phen)_2M^{n+}$–Phen BDEs at 0 K (in kJ/mol), where M = Fe, Co, Ni, Cu, and Zn and *n* = 1 and 2. Closed symbols represent dissociation from the ground-state reactant complex to ground-state products. For the $Fe^{2+}(Phen)_3$ complex, values for the singlet state are plotted as closed symbols, while the open symbols represent BDEs obtained from dissociation of the quintet state of the $Fe^{2+}(Phen)_3$ complex. Calculated values determined at the B3LYP/6-311+G(2d,2p) level of theory including ZPE and BSSE corrections. Values for M^{2+} are taken from Table 3.3. Values for M^+ are taken from references 22–25.

Figure 3.1.

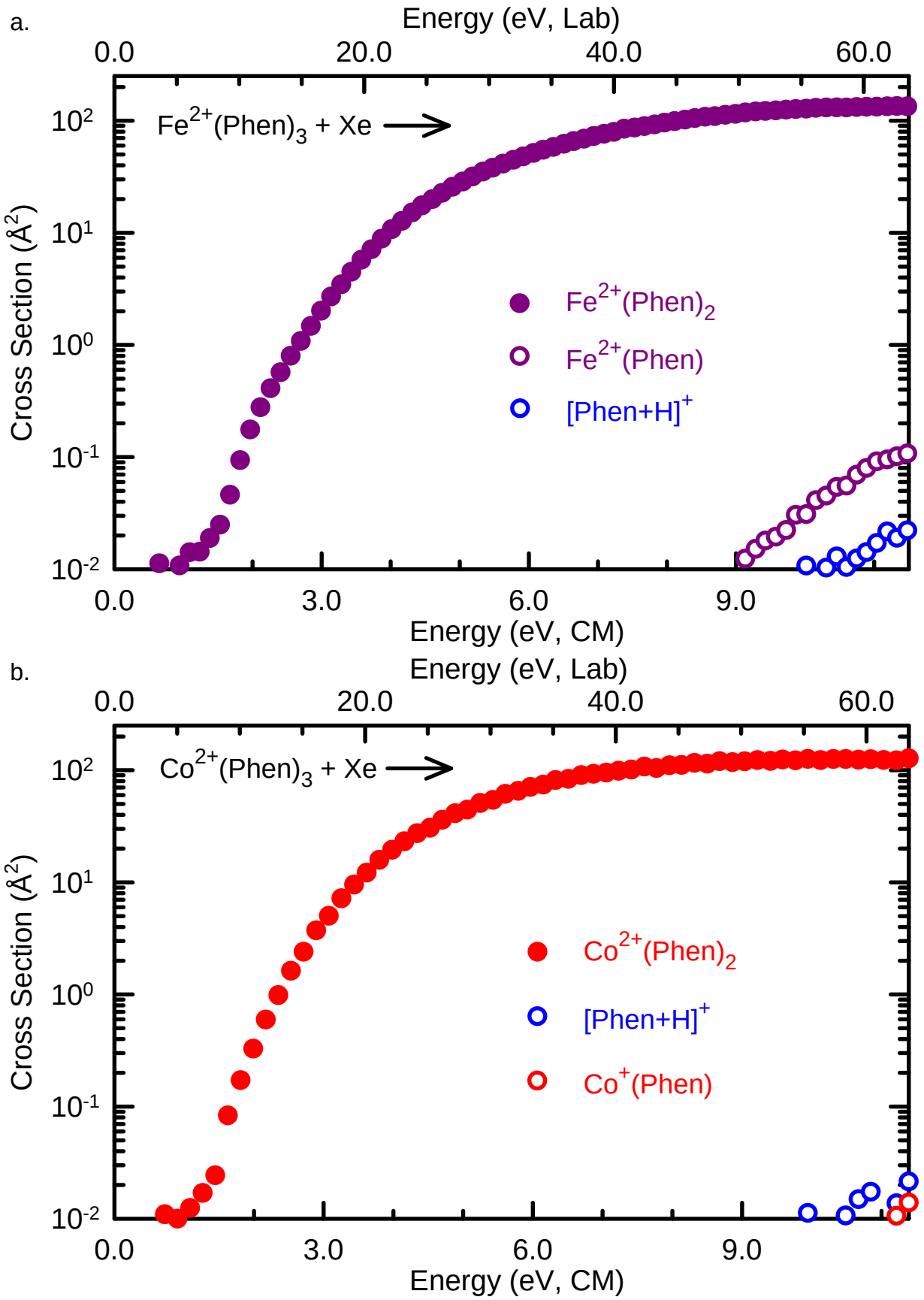
a.
Energy (eV, Lab)
0.0
20.0
40.0
60.0
$Fe^{2+}(Phen)_3 + Xe$
Cross Section (Å^2)
10^2
10^1
10^0
10^{-1}
10^{-2}
$Fe^{2+}(Phen)_2$
$Fe^{2+}(Phen)$
$[Phen+H]^+$
0.0
3.0
6.0
9.0
Energy (eV, CM)
b.
Energy (eV, Lab)
0.0
20.0
40.0
60.0
$Co^{2+}(Phen)_3 + Xe$
Cross Section (Å^2)
10^2
10^1
10^0
10^{-1}
10^{-2}
$Co^{2+}(Phen)_2$
$[Phen+H]^+$
$Co^+(Phen)$
0.0
3.0
6.0
9.0
Energy (eV, CM)

Figure 3.1.

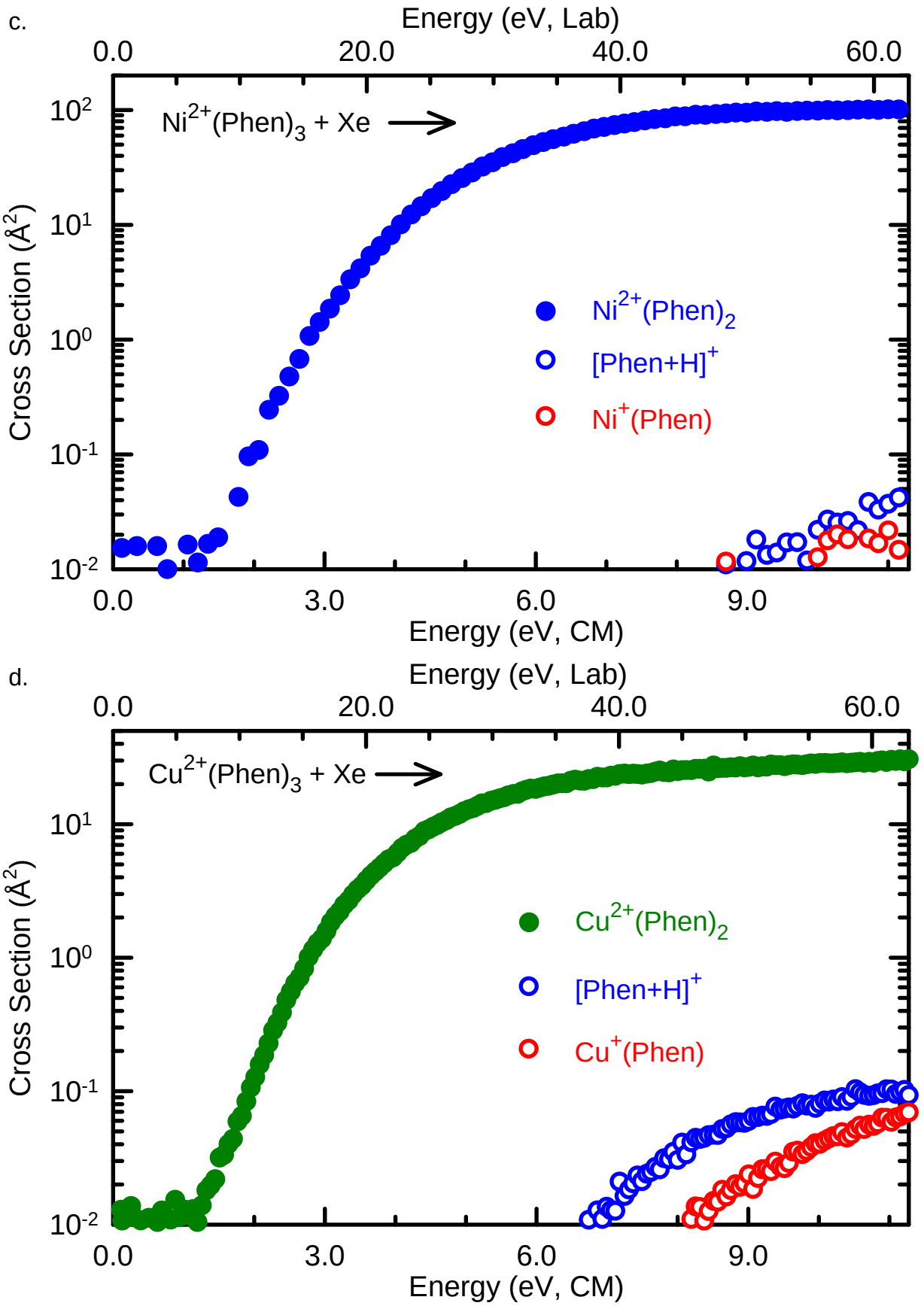
c.
Energy (eV, Lab)
0.0
20.0
40.0
60.0
$Ni^{2+}(Phen)_3$ + Xe
Cross Section (Å^2)
10^2
10^1
10^0
10^{-1}
10^{-2}
$Ni^{2+}(Phen)_2$
$[Phen+H]^+$
$Ni^+(Phen)$
0.0
3.0
6.0
9.0
Energy (eV, CM)
d.
Energy (eV, Lab)
0.0
20.0
40.0
60.0
$Cu^{2+}(Phen)_3$ + Xe
Cross Section (Å^2)
10^1
10^0
10^{-1}
10^{-2}
$Cu^{2+}(Phen)_2$
$[Phen+H]^+$
$Cu^+(Phen)$
0.0
3.0
6.0
9.0
Energy (eV, CM)

Figure 3.1.

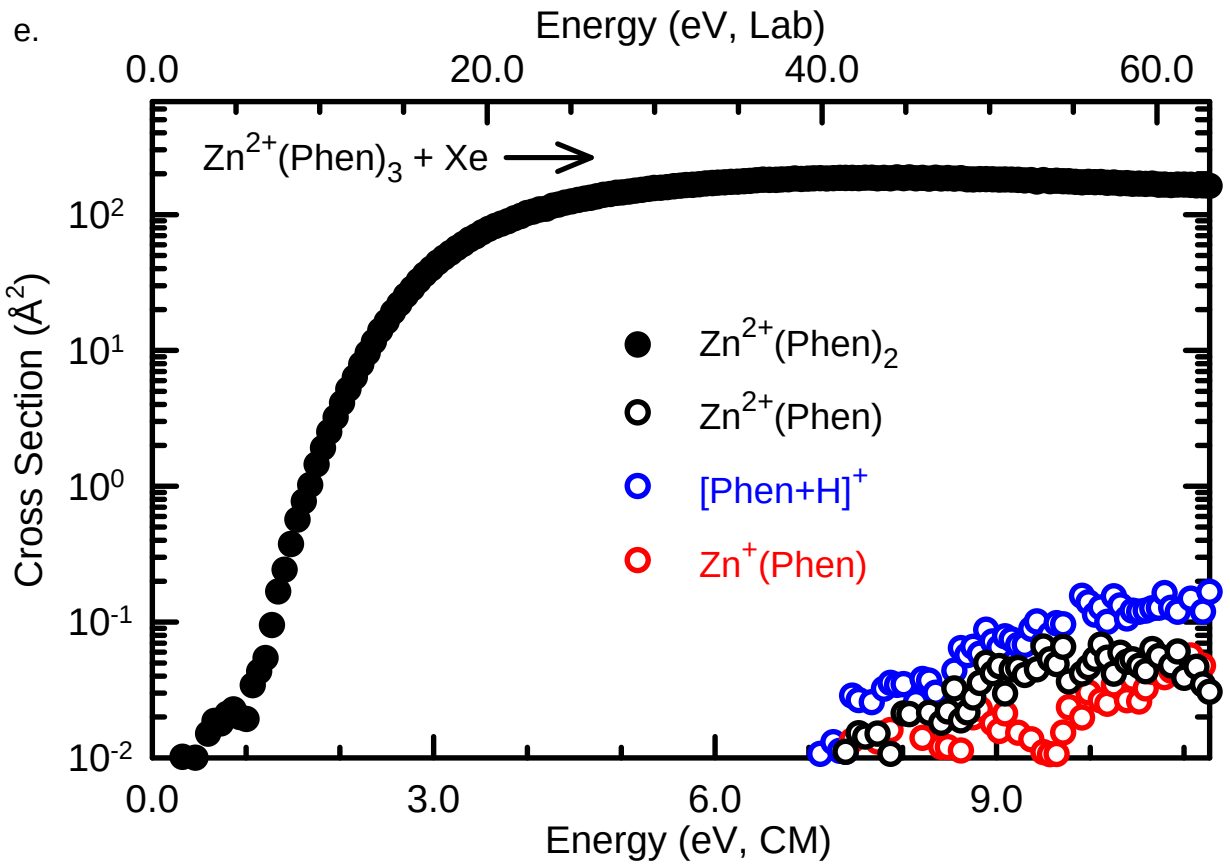
e.
Energy (eV, Lab)
0.0
20.0
40.0
60.0
Zn2+(Phen)3 + Xe
Cross Section (Å2)
10^2
10^1
10^0
10^-1
10^-2
Zn2+(Phen)2
Zn2+(Phen)
[Phen+H]+
Zn+(Phen)
0.0
3.0
6.0
9.0
Energy (eV, CM)

Figure 3.2.

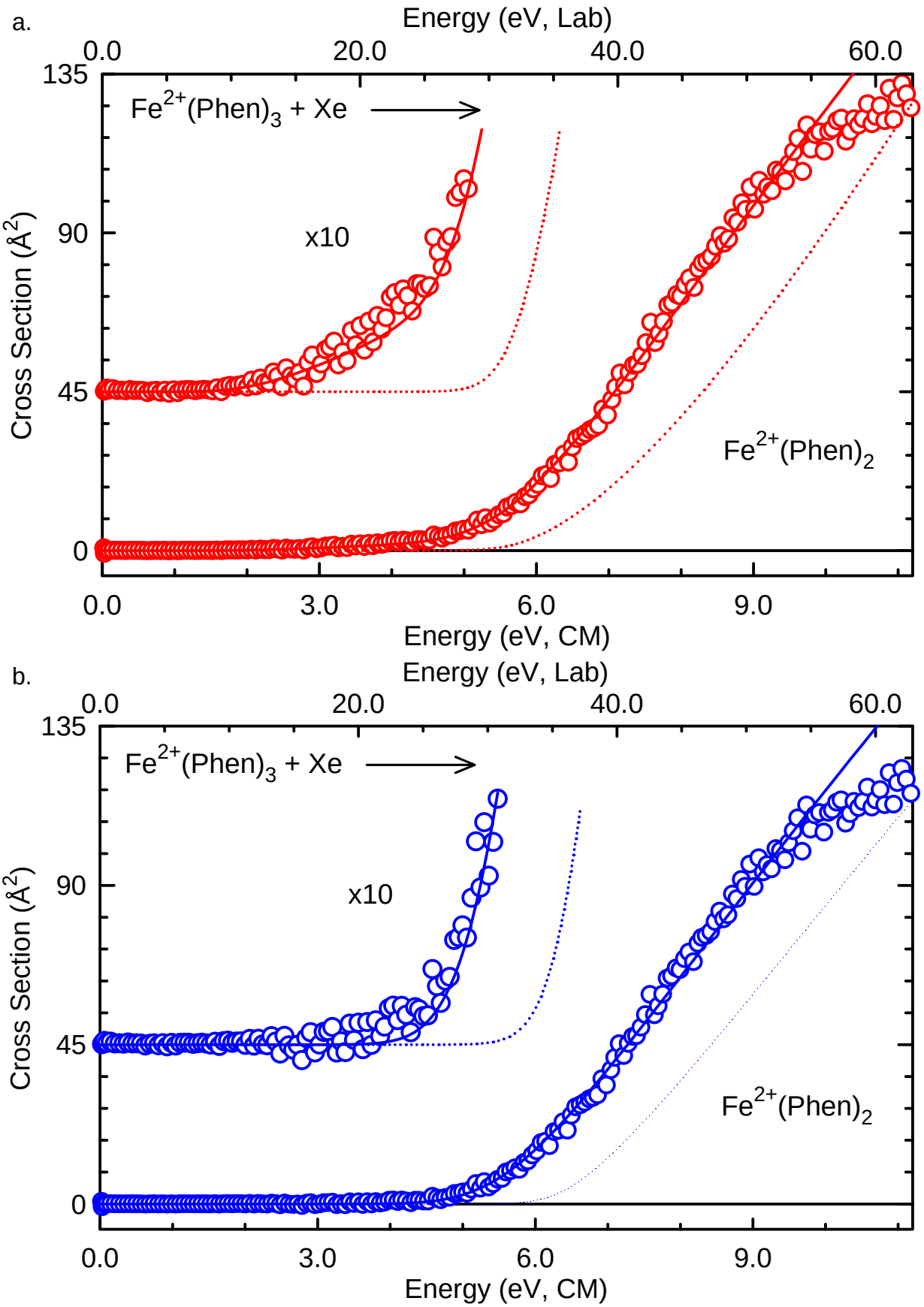
a.
Energy (eV, Lab)
0.0
20.0
40.0
60.0
135
90
45
0
Cross Section (Å^2)
Fe^{2+}(Phen)$_3$ + Xe
x10
Fe^{2+}(Phen)$_2$
0.0
3.0
6.0
9.0
Energy (eV, CM)
b.
Energy (eV, Lab)
0.0
20.0
40.0
60.0
135
90
45
0
Cross Section (Å^2)
Fe^{2+}(Phen)$_3$ + Xe
x10
Fe^{2+}(Phen)$_2$
0.0
3.0
6.0
9.0
Energy (eV, CM)

Figure 3.2.

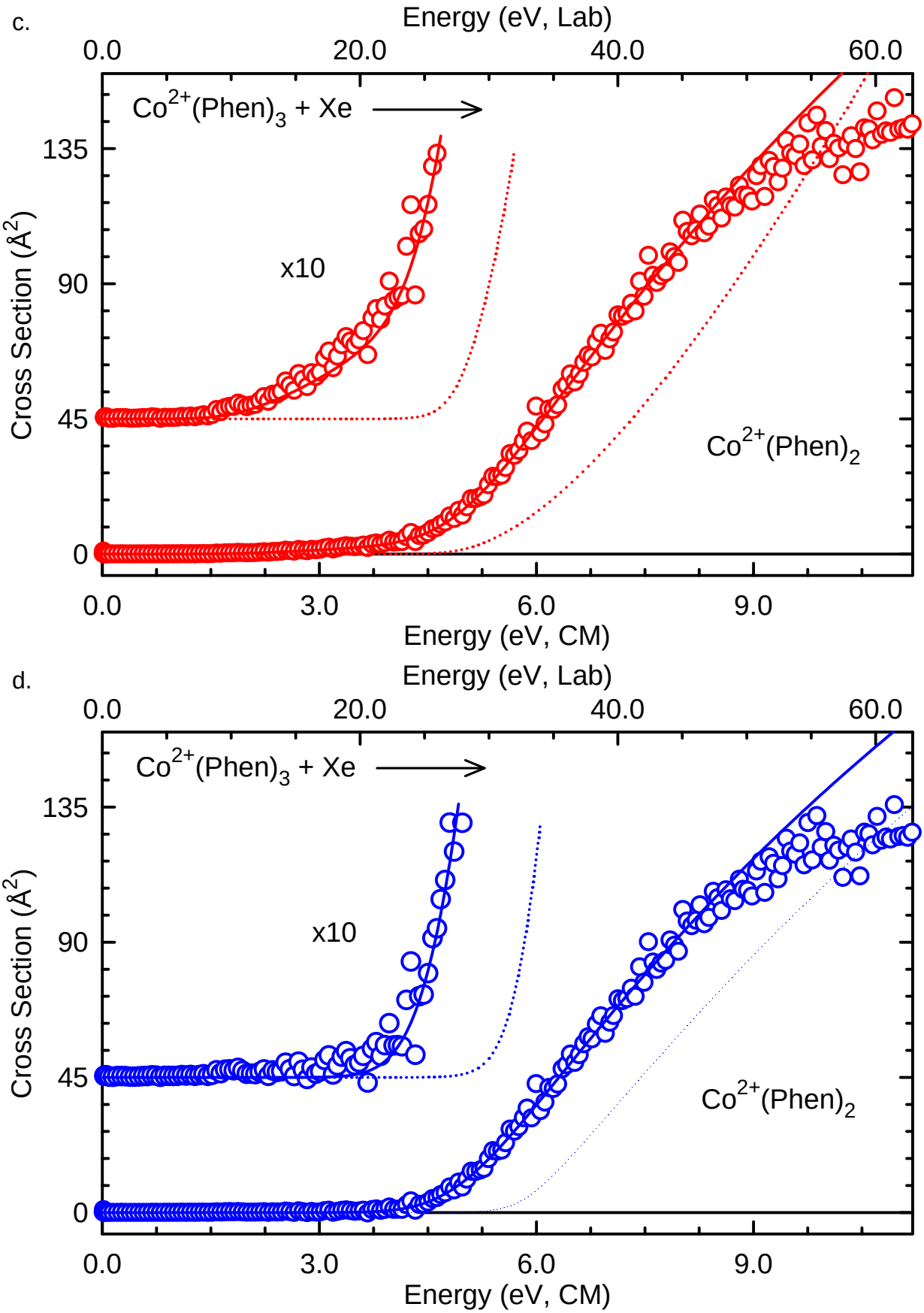
c.
Energy (eV, Lab)
0.0
20.0
40.0
60.0
Co2+(Phen)3 + Xe
135
90
45
0
Cross Section (Å2)
x10
Co2+(Phen)2
0.0
3.0
6.0
9.0
Energy (eV, CM)
d.
Energy (eV, Lab)
0.0
20.0
40.0
60.0
Co2+(Phen)3 + Xe
135
90
45
0
Cross Section (Å2)
x10
Co2+(Phen)2
0.0
3.0
6.0
9.0
Energy (eV, CM)

Figure 3.2.

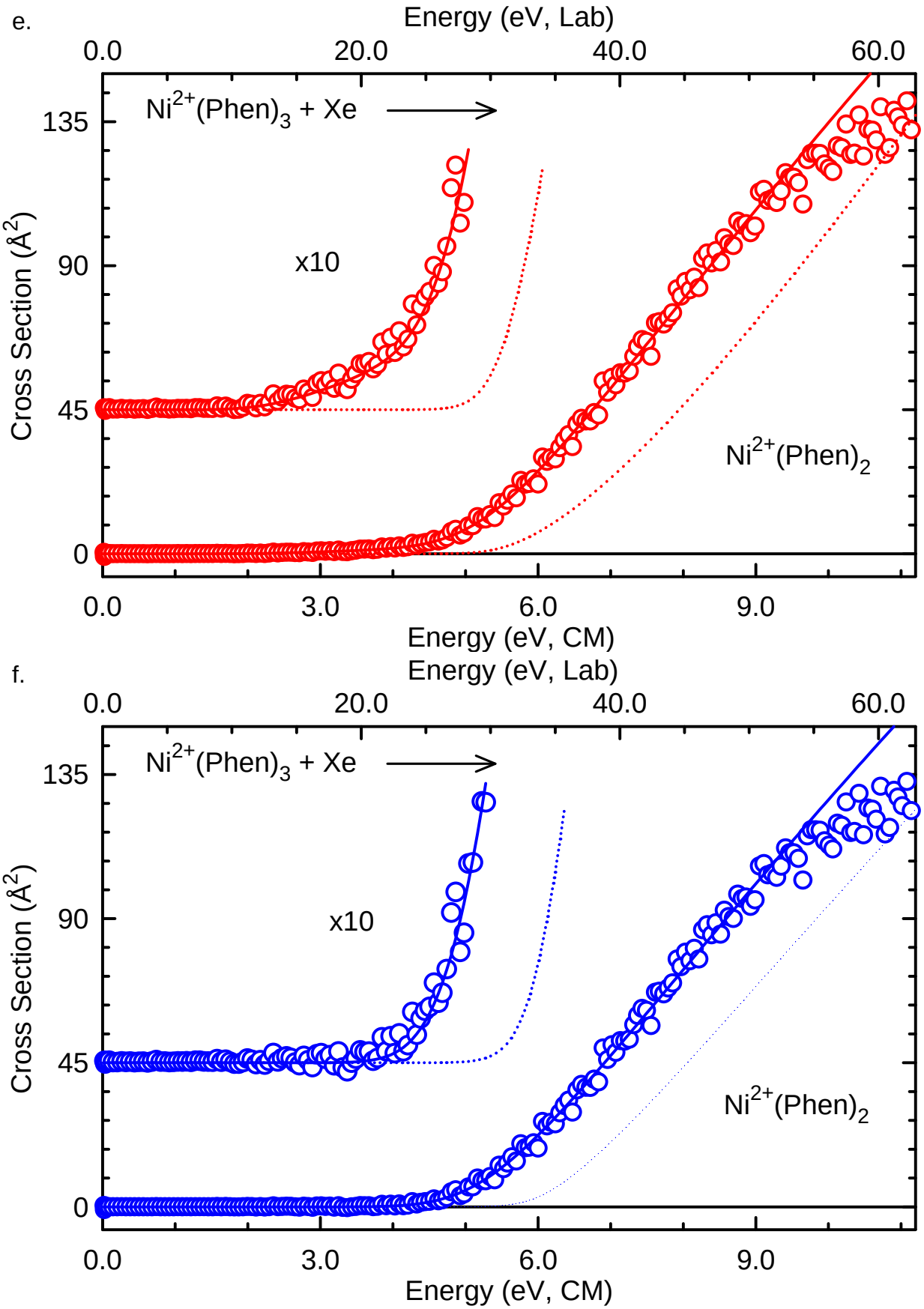
e.
Energy (eV, Lab)
0.0
20.0
40.0
60.0
Ni2+(Phen)3 + Xe
135
90
45
0
Cross Section (Å2)
x10
Ni2+(Phen)2
0.0
3.0
6.0
9.0
Energy (eV, CM)
f.
Energy (eV, Lab)
0.0
20.0
40.0
60.0
Ni2+(Phen)3 + Xe
135
90
45
0
Cross Section (Å2)
x10
Ni2+(Phen)2
0.0
3.0
6.0
9.0
Energy (eV, CM)

Figure 3.2.

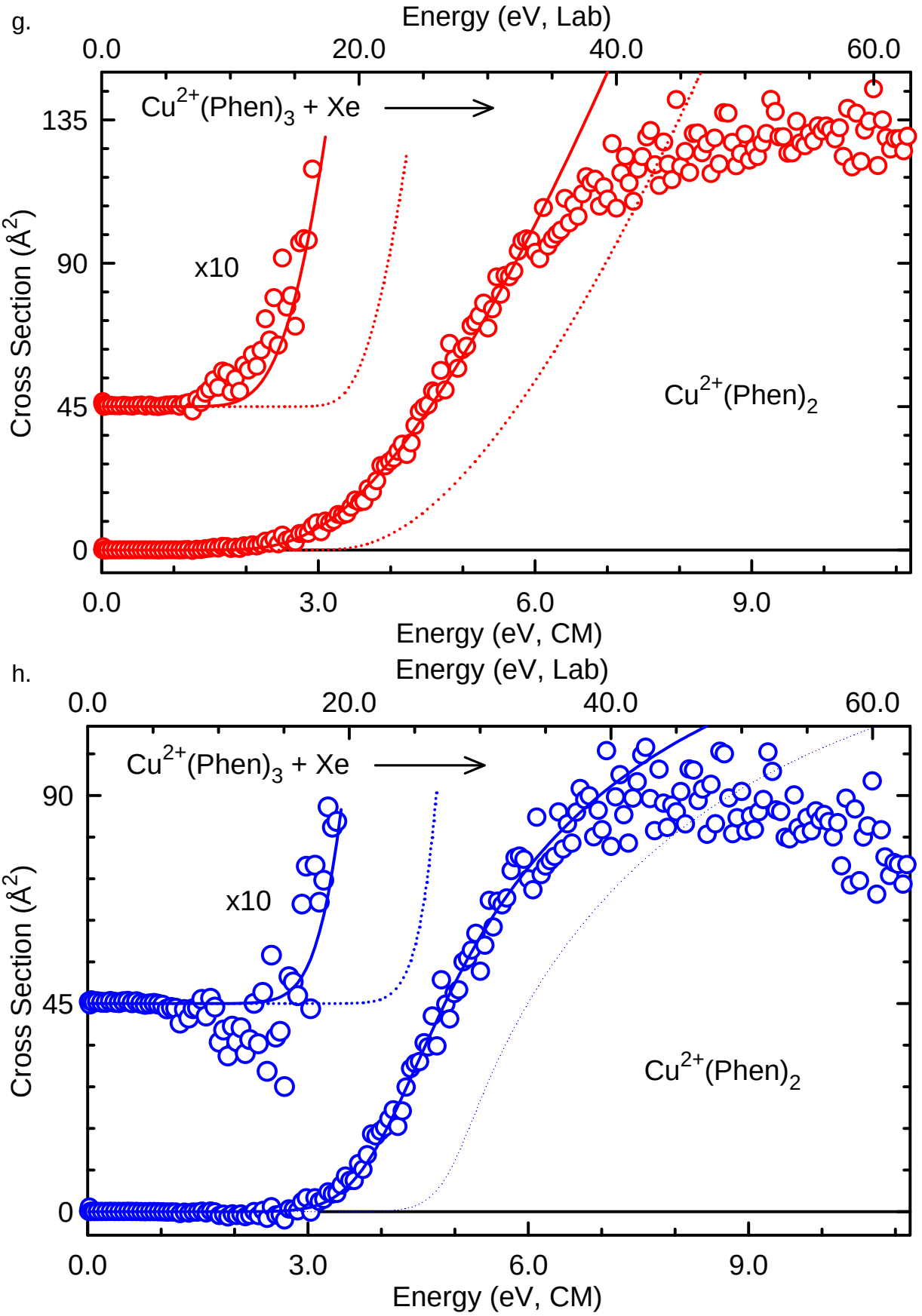
g.
Energy (eV, Lab)
0.0
20.0
40.0
60.0
Cu2+(Phen)3 + Xe
135
90
45
0
Cross Section (Å2)
x10
Cu2+(Phen)2
0.0
3.0
6.0
9.0
Energy (eV, CM)
h.
Energy (eV, Lab)
0.0
20.0
40.0
60.0
Cu2+(Phen)3 + Xe
90
45
0
Cross Section (Å2)
x10
Cu2+(Phen)2
0.0
3.0
6.0
9.0
Energy (eV, CM)

Figure 3.2.

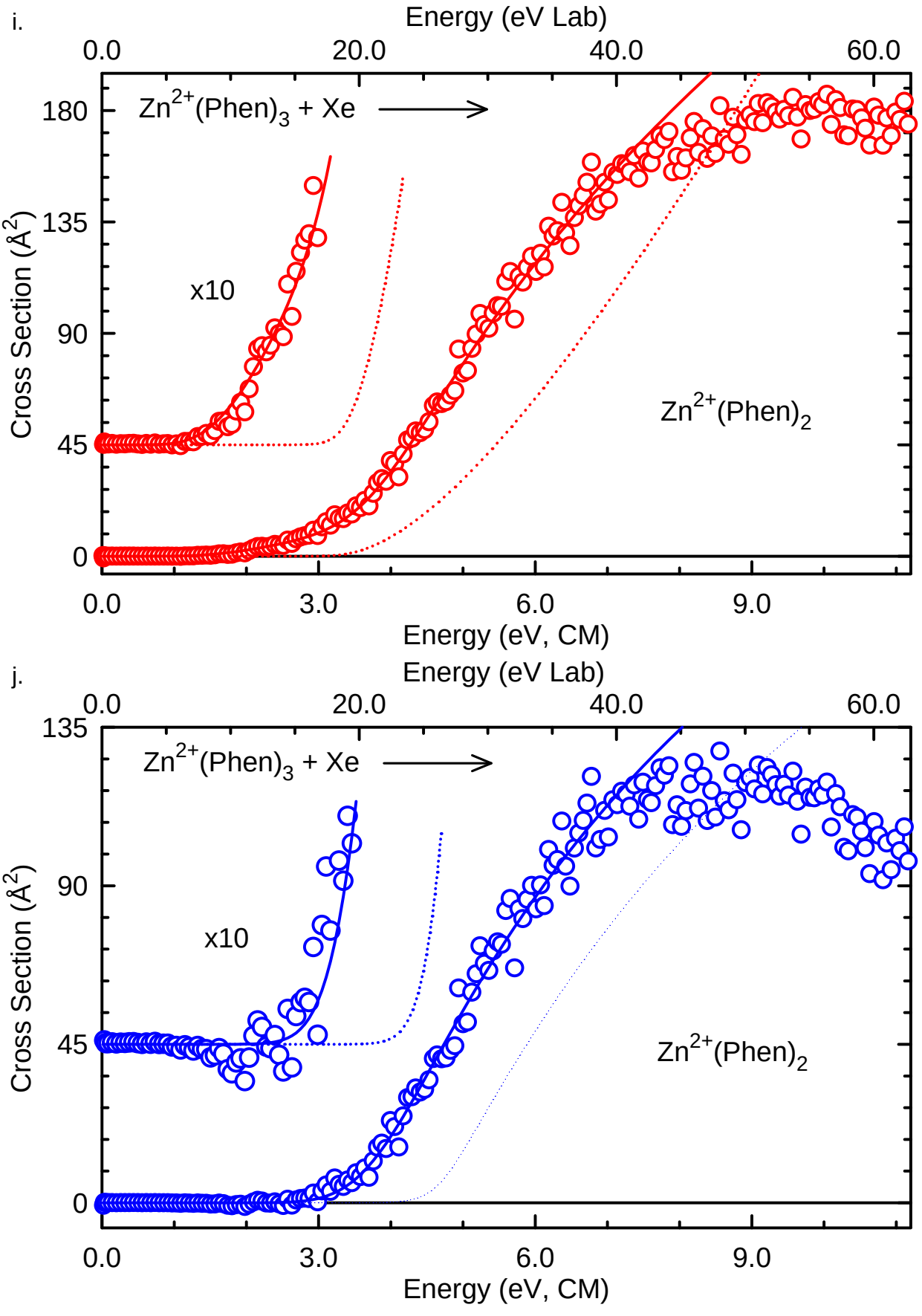
i.
Energy (eV Lab)
0.0
20.0
40.0
60.0
180
135
90
45
0
Zn2+(Phen)3 + Xe
x10
Zn2+(Phen)2
Cross Section (Å2)
0.0
3.0
6.0
9.0
Energy (eV, CM)
j.
Energy (eV Lab)
0.0
20.0
40.0
60.0
135
90
45
0
Zn2+(Phen)3 + Xe
x10
Zn2+(Phen)2
Cross Section (Å2)
0.0
3.0
6.0
9.0
Energy (eV, CM)

Figure 3.3.

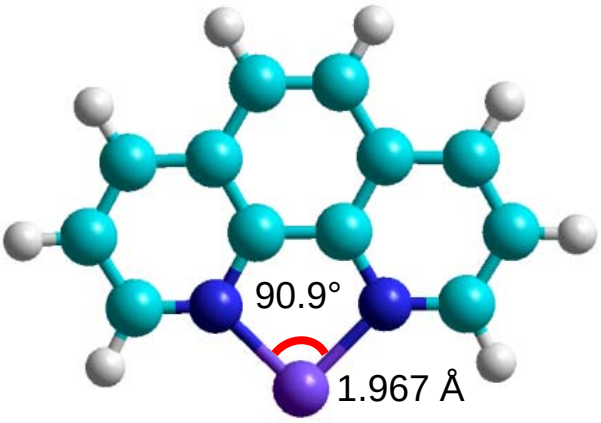

Fe^{2+}(Phen)

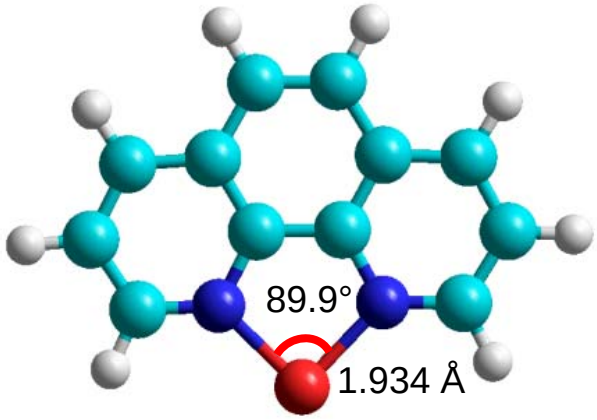

Co^{2+}(Phen)

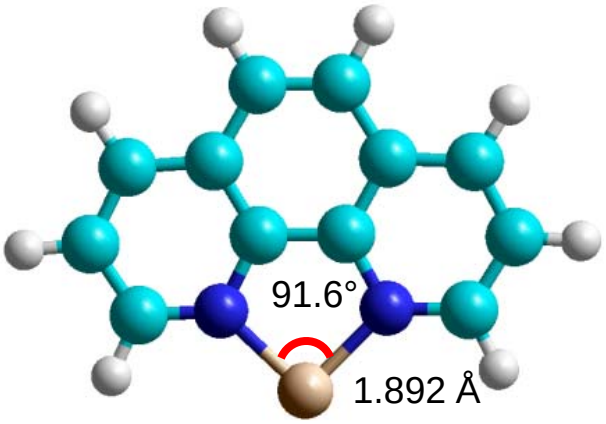

Ni^{2+}(Phen)

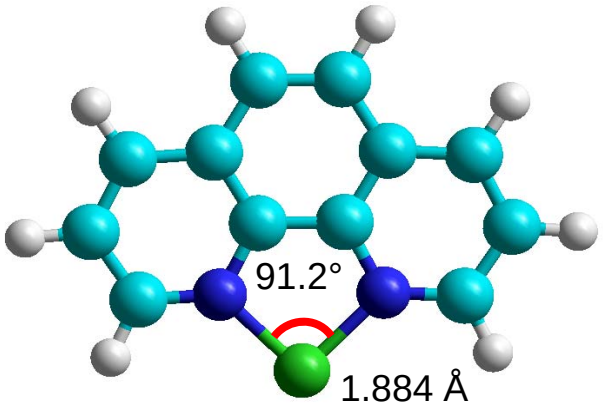

Cu^{2+}(Phen)

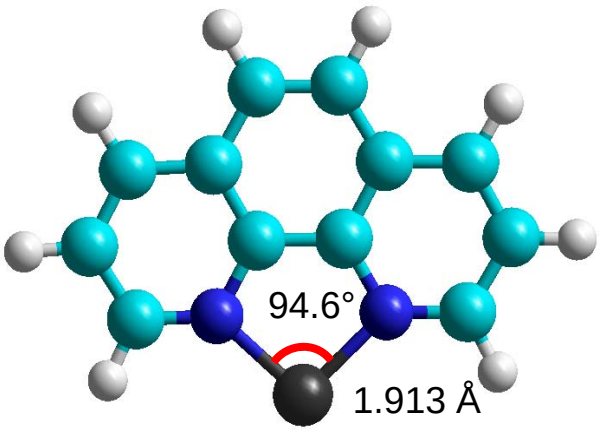

Zn^{2+}(Phen)

Figure 3.3.

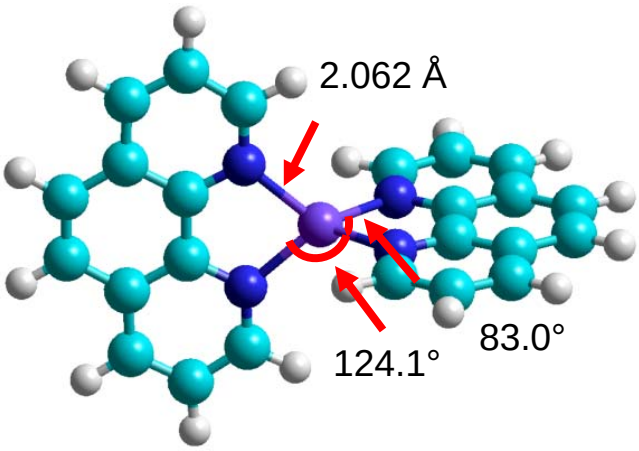

$Fe^{2+}(Phen)_2$

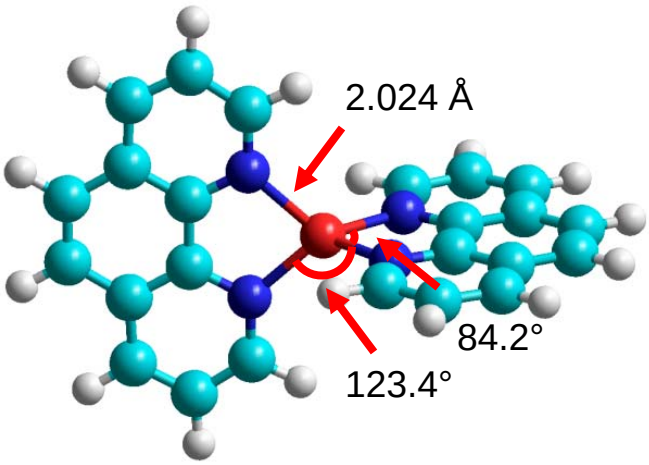

$Co^{2+}(Phen)_2$

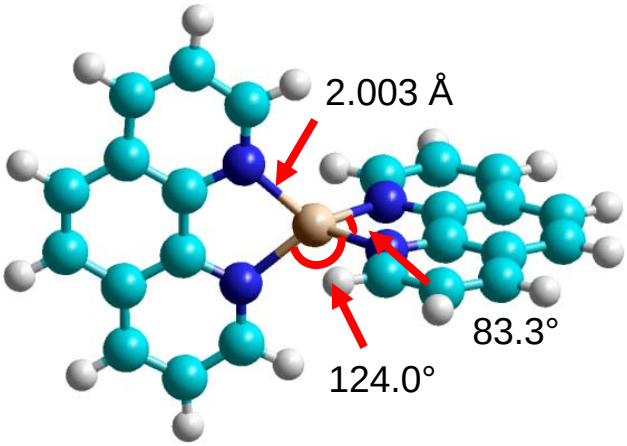

$Ni^{2+}(Phen)_2$

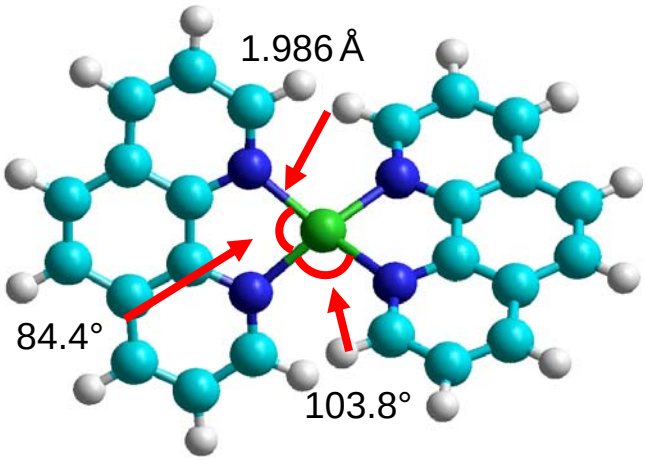

$Cu^{2+}(Phen)_2$

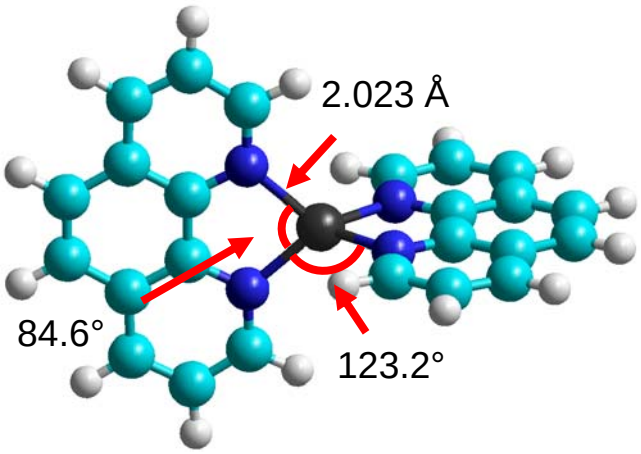

$Zn^{2+}(Phen)_2$

Figure 3.3.

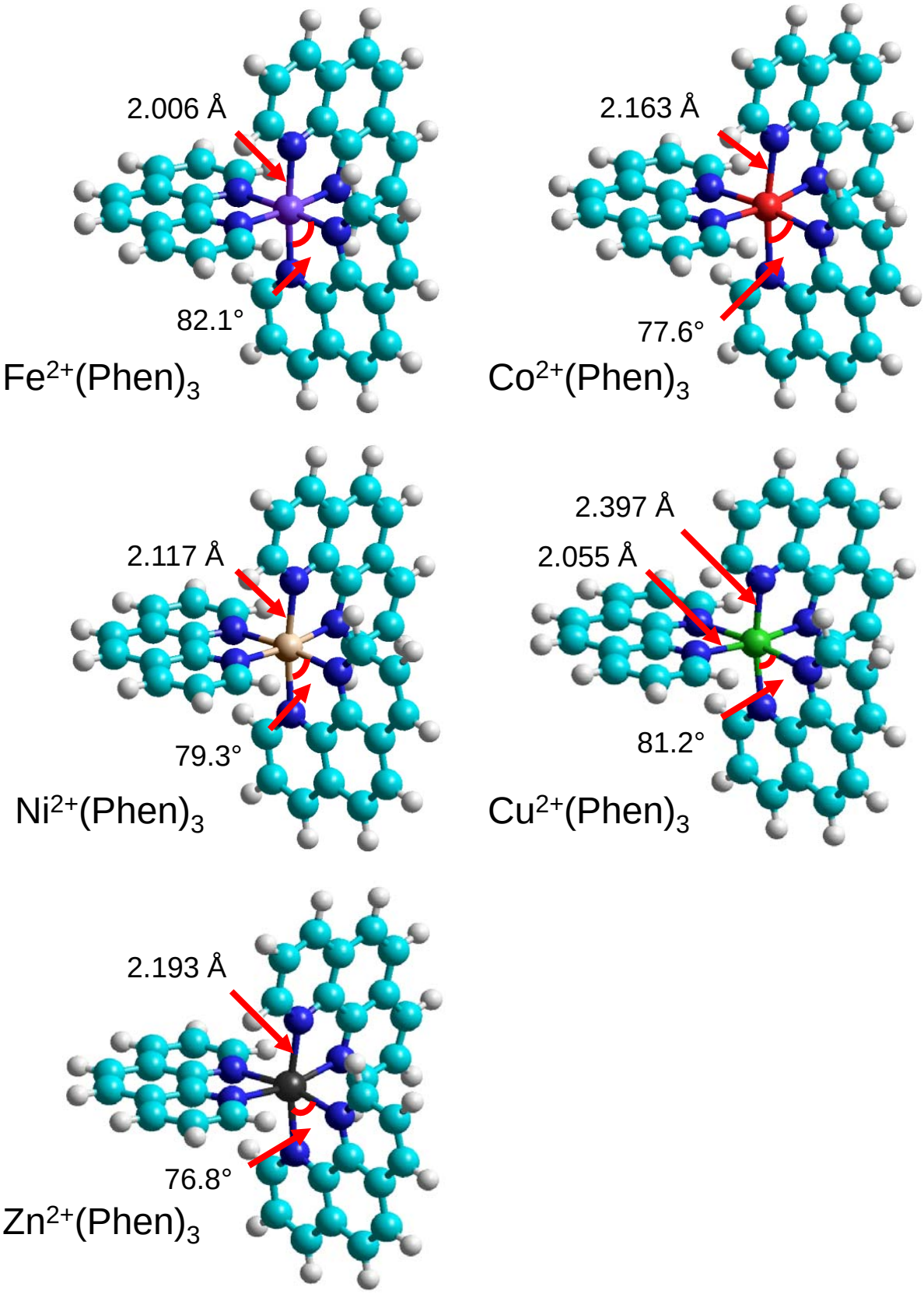
2.006 Å
82.1°
$Fe^{2+}(Phen)_3$
2.163 Å
77.6°
$Co^{2+}(Phen)_3$
2.117 Å
79.3°
$Ni^{2+}(Phen)_3$
2.397 Å
2.055 Å
81.2°
$Cu^{2+}(Phen)_3$
2.193 Å
76.8°
$Zn^{2+}(Phen)_3$

Figure 3.4.

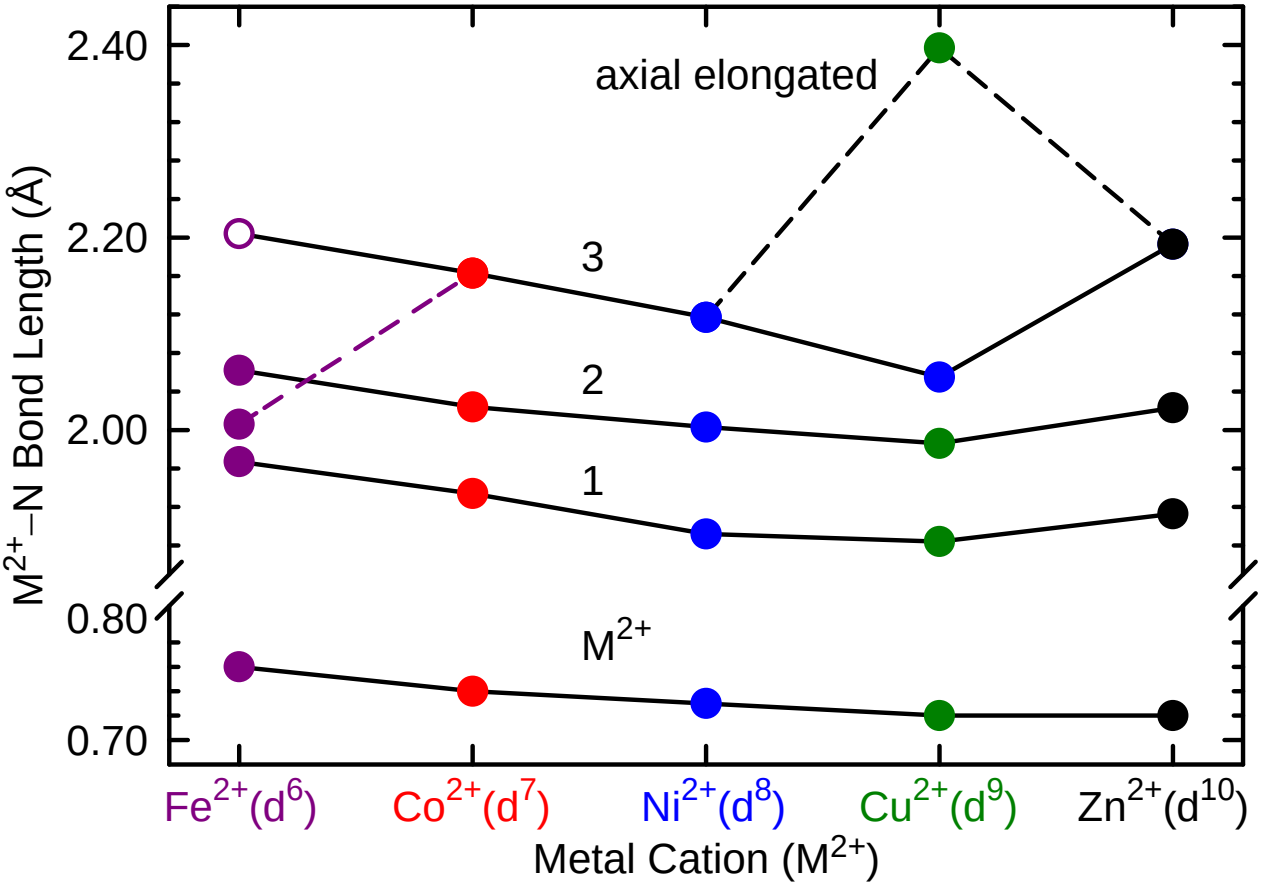
2.40
2.20
2.00
0.80
0.70
axial elongated
3
2
1
M2+
M2+–N Bond Length (Å)
Fe2+(d6)
Co2+(d7)
Ni2+(d8)
Cu2+(d9)
Zn2+(d10)
Metal Cation (M2+)

Figure 3.5.

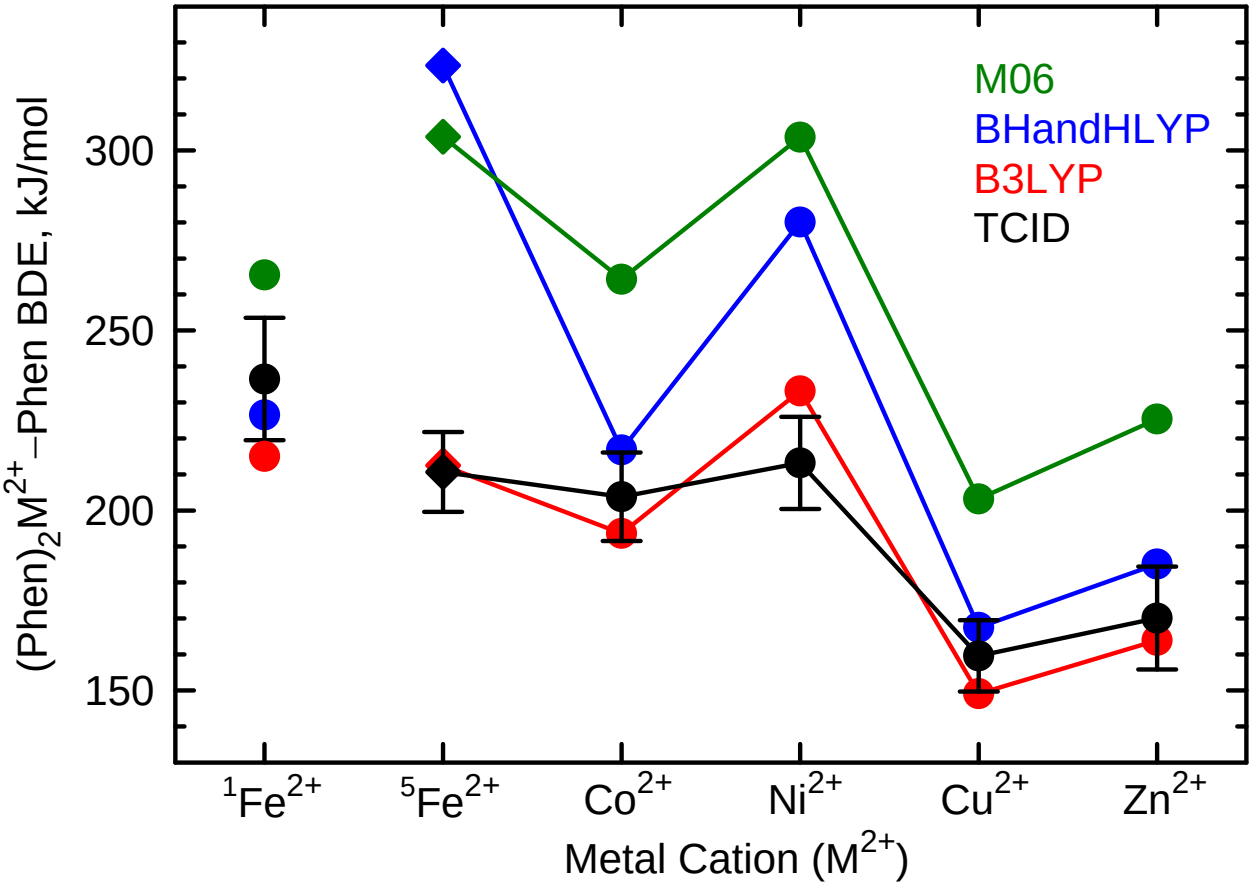
M06
BHandHLYP
B3LYP
TCID
(Phen)2M2+–Phen BDE, kJ/mol
300
250
200
150
1Fe2+
5Fe2+
Co2+
Ni2+
Cu2+
Zn2+
Metal Cation (M2+)

Figure 3.6.

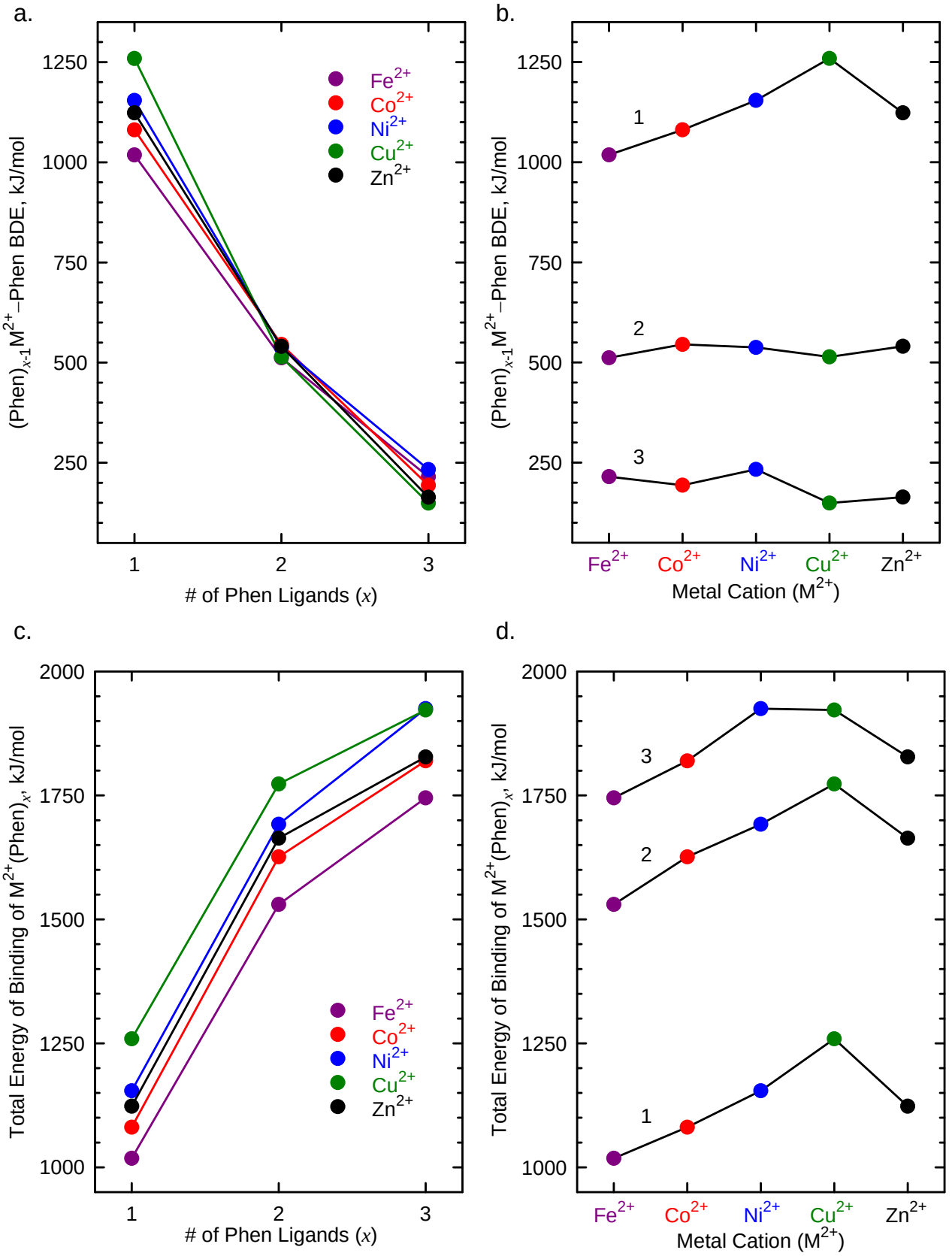
a.
b.
c.
d.
(Phen)x-1M2+–Phen BDE, kJ/mol
# of Phen Ligands (x)
Metal Cation (M2+)
Total Energy of Binding of M2+(Phen)x, kJ/mol
Fe2+
Co2+
Ni2+
Cu2+
Zn2+
1
2
3
1250
1000
750
500
250
2000
1750
1500
1250
1000

Figure 3.7.

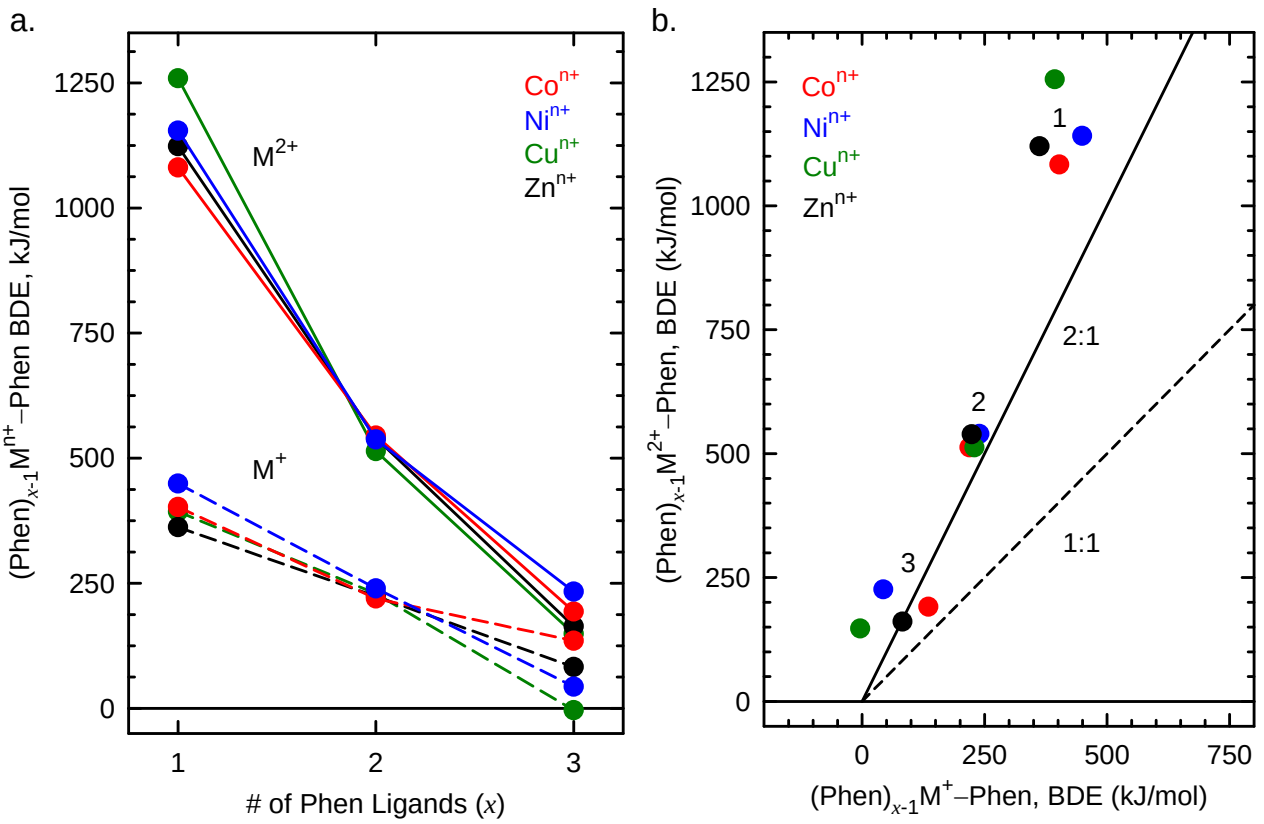
a.
1250
1000
750
500
250
0
1
2
3
# of Phen Ligands (x)
(Phen)x-1Mn+–Phen BDE, kJ/mol
M2+
M+
Con+
Nin+
Cun+
Znn+
b.
1250
1000
750
500
250
0
0
250
500
750
(Phen)x-1M+–Phen, BDE (kJ/mol)
(Phen)x-1M2+–Phen, BDE (kJ/mol)
Con+
Nin+
Cun+
Znn+
1
2
3
2:1
1:1

Figure 3.8.

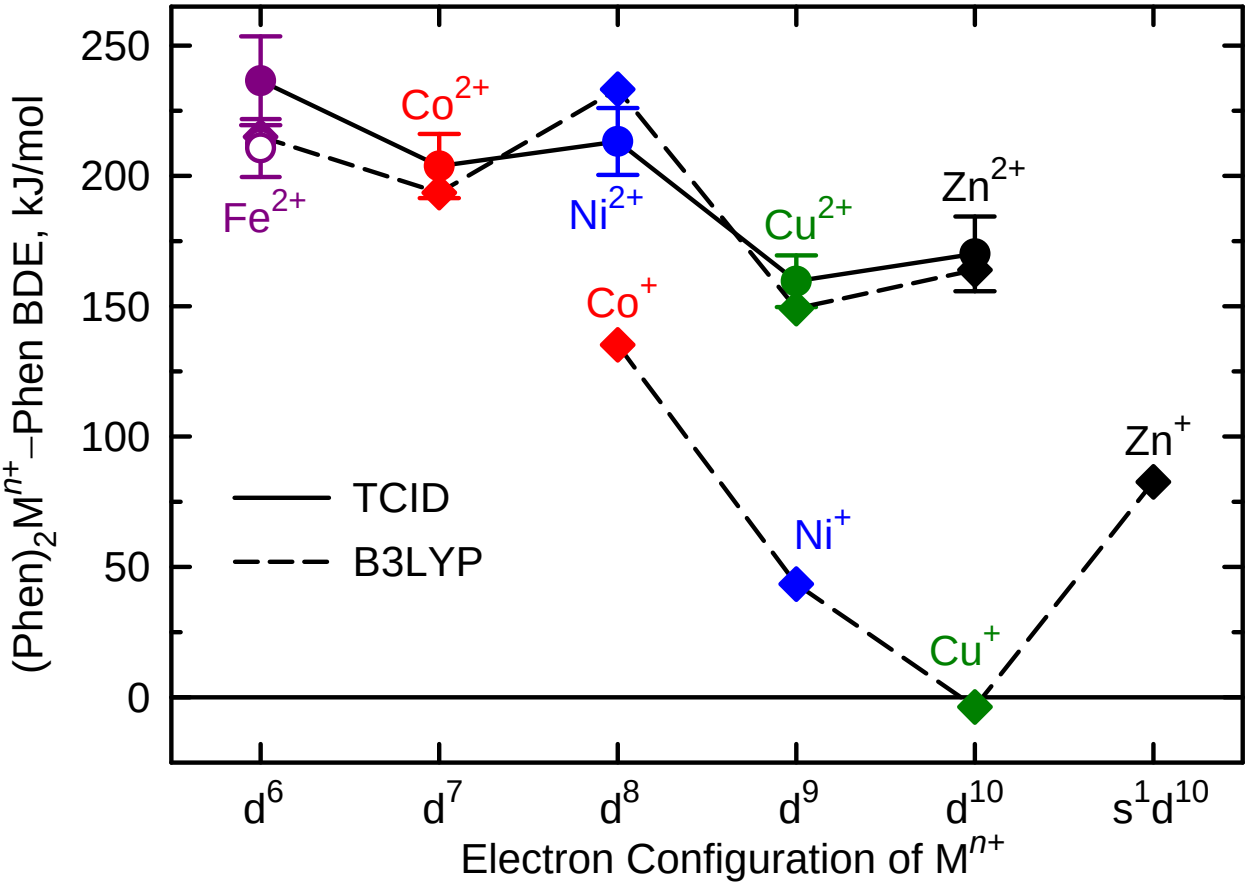
250
200
150
100
50
0
(Phen)2Mn+–Phen BDE, kJ/mol
Fe2+
Co2+
Ni2+
Cu2+
Zn2+
Co+
Ni+
Cu+
Zn+
TCID
B3LYP
d6
d7
d8
d9
d10
s1d10
Electron Configuration of Mn+

CHAPTER 4

ENERGY-RESOLVED COLLISION-INDUCED DISSOCIATION STUDIES OF 2,2′-BIPYRIDINE COMPLEXES OF THE LATE FIRST-ROW DIVALENT TRANSITION METAL CATIONS: DETERMINATION OF THE THIRD SEQUENTIAL BINDING ENERGIES

4.1 Introduction

The chemistry of a transition metal complex can be understood on the basis of its electronic structure and how this influences its strength of binding to a ligand system. Properties of transition-metal cations such as ionic size, variable oxidation state, ionization energy, and electronic structure strongly influence the chemical properties of a transition metal complex. Both biological systems as well as inorganic and bioinorganic chemists have exploited the properties of transition-metal ions to facilitate specific binding to ligands, and in some cases, by controlling the redox potentials of the resulting transition metal complex to their advantage.[1-3] Characteristics of the ligand such as the nature and number of donor atoms available for binding, the molecular polarizability, and dipole moment also influence the chemical behavior of a transition metal complex. In addition, steric interactions are important in determining the geometry and strength of binding of a transition-metal complex. Thus, derivatization of ligands has been widely used by synthetic chemists to fine-tune the electronic properties of a transition metal complex. The ability of metal ions to bind to several ligands in a single complex has implications for synthesis in that metal ions may also be used to assemble polynuclear structures, control the structures of reacting ligands, and under appropriate conditions activate ligands towards reaction.[4-7] Metal–ligand interactions

define the structure of complexes by maintaining the stability of molecular systems, and therefore have a profound impact on their chemical properties and reactivity, and hence underlie their chemical behavior. The unique and tunable features of transition-metal complexes have led to their use in studies relating to DNA cleavage[8-12] in the hope of developing artificial nucleases.[13-17] Systematic studies of the stable structures and bond dissociation energies (BDEs) of families of related transition metal complexes, such as performed in the current study, and examinations of the structural and energetic trends among these systems provide information that can be used to gain insight into the roles that the transition-metal cations and ligands play in determining their stability and reactive pathways. By elucidating the coordination geometries and the energetics of their dissociation pathways as a function of the electronic structure of the metal cations and extent of ligation, the data can be used to rationally design new catalysts, provide greater insight into biological processes, and provide detailed information on how to optimize the synthesis of supramolecular materials. For example, the metal-ion selectivity can be tuned by favoring or disfavoring specific coordination geometries through manipulation of the geometry of ligands and may lead to transition-metal compounds with predictable and interesting properties, that is, electrochemical or spectroscopic properties due to the stabilization or destabilization of ground states.[18-20] The 2,2′-bipyridine ligand (Bpy), has often been used to construct transition metal complexes because of its ability to coordinate with various metals.[21-23] Bpy has been widely studied in solution. Irving and co-workers measured binding constants of the complexed forms of Bpy and derivatives of Bpy in solution using spectrophotometric techniques.[24-28] Although the thermodynamic information obtained from their studies is reliable, the measured binding constants are influenced by both the

solvent and the counterions. The gas phase provides an ideal environment for examining the intrinsic binding in the absence of solvent effects and counter ions. The ability to produce both coordinatively saturated and unsaturated complexes in the gas phase also allows the binding interactions to be examined as a function of the extent of ligation.

In the present study, the interactions between Bpy ligands and five late first-row divalent transition-metal cations, Fe^{2+}, Co^{2+}, Ni^{2+}, Cu^{2+}, and Zn^{2+}, are examined by measuring the kinetic-energy dependence of their collision-induced dissociation (CID) behavior and performing complementary electronic structure theory calculations. $M^{2+}(Bpy)_x$ complexes with one to three Bpy ligands are investigated theoretically, whereas experimental studies are limited to the tris complexes, $M^{2+}(Bpy)_3$ complexes. The energy-resolved CID processes are analyzed using methods developed previously.[29] The analysis explicitly includes the effects of the internal and translational energy distributions of the reactants, multiple ion-neutral collisions, and the lifetimes for dissociation. We derive the third-sequential BDEs of five $M^{2+}(Bpy)_3$ complexes, and compare these results to values obtained from density functional theory calculations performed herein. Periodic trends in the structures and BDEs of these complexes are examined and compared with the analogous complexes to 1,10-Phenanthroline (Phen).[30] Comparisons are also made to the analogous Bpy complexes to the late first-row monovalent transition-metal cations, Co^+, Ni^+, Cu^+, and Zn^+, previously investigated.[31-34]

4.2 Collision-Induced Dissociation Experiments

Cross sections for CID of five $M^{2+}(Bpy)_3$ complexes with Xe, where M^{2+} = Fe^{2+}, Co^{2+}, Ni^{2+}, Cu^{2+}, and Zn^{2+}, were measured using a guided-ion-beam tandem mass spectrometer (GIBMS) that has been described in detail in Chapter 2. The $M^{2+}(Bpy)_3$

complexes were generated by electrospray ionization (ESI) as described in detail in Chapter 2. HPLC-grade acetonitrile and deionized water were used to prepare solutions containing concentrations of approximately 0.01 to 0.1 mM $[M(Bpy)_3](PF_6)_2$ in a 1:1 (v/v) acetonitrile/water mixture. Thermochemical analyses of the experimental results are explicitly discussed in Chapter 2.

4.3 Theoretical Calculations

Theoretical calculations were performed for the $M^{2+}(Bpy)_x$ complexes, where M^{2+} = Fe^{2+}, Co^{2+}, Ni^{2+}, Cu^{2+}, and Zn^{2+} and x = 1–3 using the Gaussian 09 suites of programs.[35] The relative energies of all possible spin states of the $M^{2+}(Bpy)_x$ complexes were carefully evaluated to determine the spin state of the ground-state species. In this study, the following spin states were examined: singlet, triplet, and quintet for $Fe^{2+}(Bpy)_x$; doublet and quartet for $Co^{2+}(Bpy)_x$; singlet and triplet for $Ni^{2+}(Bpy)_x$; doublet for $Cu^{2+}(Bpy)_x$ and singlet for $Zn^{2+}(Bpy)_x$ complexes. Further details of the theoretical calculations are given in Chapter 2. The B3LYP scaled vibrational frequencies and rotational constants for the ground-state structures of the Bpy ligand and the $M^{2+}(Bpy)_x$ complexes are listed in Tables B.1 and B.2 of Appendix B.

4.4 Experimental Results

4.4.1 Cross Sections for Collision-Induced Dissociation

Experimental cross sections were obtained for the interaction of Xe with five $M^{2+}(Bpy)_3$ complexes, where M^{2+} = Fe^{2+}, Co^{2+}, Ni^{2+}, Cu^{2+}, and Zn^{2+}. Data for the $M^{2+}(Bpy)_3$ complexes are shown in Figure 4.1. The primary and most favorable process observed for all the $M^{2+}(Bpy)_3$ complexes over the range of collision energies range examined, typically 0–12 eV, is the loss of a single intact Bpy ligand in the CID reaction 4.1.

$$M^{2+}(Bpy)_x + Xe \rightarrow M^{2+}(Bpy)_{x-1} + Bpy + Xe \quad (4.1)$$

The apparent threshold for the $M^{2+}(Bpy)_2$ product cross section shifts to lower energies from Fe^{2+} to Co^{2+}, increases for Ni^{2+}, but then decreases again from Ni^{2+} to Cu^{2+} to Zn^{2+} as the d electron occupation of the metal cation increases from d^6 to d^{10} across this series. The magnitudes of the CID cross sections generally follow the reverse trend. Sequential dissociation of the $M^{2+}(Bpy)_2$ primary CID product is observed at elevated energies. Loss of a second intact Bpy ligand is observed only for the Fe^{2+}, Co^{2+}, and Ni^{2+} complexes. Proton transfer Coulomb fission (PTCF), reaction 4.2, and electron transfer Coulomb fission (ETCF), reaction 4.3, are also observed as very minor sequential reaction pathways for all of the $M^{2+}(Bpy)_3$ complexes.

$$M^{2+}(Bpy)_2 \rightarrow [M(Bpy\text{-}H)]^+ + [Bpy+H]^+ \quad (4.2)$$

$$M^{2+}(Bpy)_2 \rightarrow M^+(Bpy) + Bpy^+ \quad (4.3)$$

Because the experiments were intentionally performed under low-mass-resolution conditions to optimize sensitivity of the threshold determination for the primary CID pathway, severe overlap of the Bpy^+ and $[Bpy+H]^+$ as well as the $[M(Bpy\text{-}H)]^+$ and $M^+(Bpy)$ sequential products was observed. Thus, only the species with the larger m/z of each pair were monitored here, $[Bpy+H]^+$ and $M^+(Bpy)$. In all cases, PTCF is favored over ETCF as indicated by the larger cross section and lower apparent threshold of the $[Bpy+H]^+$ products as compared to the $M^+(Bpy)$ products. The dissociation pathways resulting from sequential fragmentation of the $M^{2+}(Bpy)_2$ primary CID product will be investigated in detail in a follow up to this study, in which the CID of the $M^{2+}(Bpy)_2$ complexes formed directly in the ESI process will be examined. Sequential loss of HCN from the Bpy^+ product is also

observed at elevated energies for the Fe^{2+}, Co^{2+}, Ni^{2+}, and Cu^{2+} complexes, whereas loss of C_5H_5N from $M^{2+}(Bpy)_2$ was observed only for the Fe^{2+} complex.

4.4.2 Threshold Analysis

The model of equation 2.3 was used to analyze the thresholds for CID reactions 4.1 of five $M^{2+}(Bpy)_3$ complexes, as described in Chapter 2. The results of these analyses are provided in Table 4.1 and the results for the $M^{2+}(Bpy)_3$ complexes are shown in Figure 4.2. In all cases, even after zero-pressure extrapolation, small low-energy features were observed in the CID cross sections, which suggest that, a small population (~3–4%) of vibrationally or electronically excited ions are present. Therefore, the model of equation 2.3 was used to analyze both raw zero-pressure extrapolated data, and data obtained after subtraction of the low-energy feature. The low-energy feature can be reproduced nicely by shifting the threshold energy down by approximately 0.5 to 0.7 eV, retaining the same value of *n* as determined from fits to the dominant feature, and reducing σ_0 (an energy-independent scaling factor) by a factor of approximately 25 to 35 depending on the system. The model for the low-energy feature was then subtracted from the data and the remaining cross section re-analyzed to yield the analysis after subtraction of the low-energy feature. The modeling parameters for these analyses are given in Table 4.1. The difference in the thresholds for the two analyses are 0.27 eV for the complex to Co^{2+}, 0.20 eV for Ni^{2+}, 0.18 eV for Cu^{2+}, 0.13 eV for Zn^{2+}, 0.47 eV for the singlet ground-state of $Fe^{2+}(Bpy)_3$, and 0.31 eV for the quintet excited state of $Fe^{2+}(Bpy)_3$. Figure 4.2 show the analyses before and after subtraction of the low-energy feature. The cross sections are reproduced by equation 2.3 over a large range of energies (> 5 eV) and over three orders of magnitude. Previous study has shown that this model provides the most accurate assessment of the kinetic shifts for CID processes of

electrostatically bound ion-molecule complexes.[29-34] Kinetic shifts, corresponding to the difference in thresholds obtained with and without the inclusion of lifetime effects are also listed in Table 4.1. The Fe^{2+}, Co^{2+}, and Ni^{2+} complexes exhibit kinetic shifts that are significantly larger than those for the Cu^{2+} and Zn^{2+} complexes. Because the total number of vibrations, 177, and heavy atoms, 37, and hence the number of low-frequency vibrations remains the same for all five $M^{2+}(Bpy)_3$ complexes, the kinetic shifts should directly correlate with the density of states at threshold, which depends on the measured BDE, consistent with the results determined here. However, analyses based on singlet ground state $Fe^{2+}(Bpy)_3$ and quintet excited state $Fe^{2+}(Bpy)_3$ complexes exhibit very different kinetic shifts, which lead to a large difference in the threshold energies extracted. The singlet state exhibits tighter binding, and therefore the metal–ligand frequencies are larger such that its density of states is lower, leading to a faster dissociation rate, a smaller kinetic shift, and therefore a higher threshold. The entropy of activation, $\Delta S^{\dagger}$, describes the looseness of the transition state (TS) and also reflects the complexity of the system. Listed in Table 4.1 are $\Delta S^{\dagger}$(PSL) values at 1000 K, which vary between 75.3 and 168.4 J mol^{-1} K^{-1}, and are directly correlated with the measured BDEs for these complexes.

4.5 Theoretical Results

Stable structures of the $M^{2+}(Bpy)_x$ complexes, where M^{2+} = Fe^{2+}, Co^{2+}, Ni^{2+}, Cu^{2+}, and Zn^{2+}, and x = 1–3, were calculated using the Gaussian 09 suites of programs[35] as described in section 4.3. Detailed information of the theoretical calculations is given in Chapter 2. The ground electronic spin states of the $M^{2+}(Bpy)_x$ complexes to Co^{2+}, Ni^{2+}, Cu^{2+}, and Zn^{2+} were found to be quartet, triplet, doublet and singlet, respectively. For the $Fe^{2+}(Bpy)$ and $Fe^{2+}(Bpy)_2$ complexes, the ground electronic spin states were found to be

quintet. The ground-state spin multiplicity of the $Fe^{2+}(Bpy)_3$ complex was predicted to be low-spin singlet when the B3LYP functional was employed, whereas BHandHLYP and M06 predict the ground-state to be high-spin quintet. Relative energies of the $M^{2+}(Bpy)_x$ complexes, in which $x = 1–3$, computed for the various possible spin states of each metal cation are summarized in Table 4.2.

Theoretical sequential BDEs for all of the $M^{2+}(Bpy)_x$ complexes determined at B3LYP, BHandHLYP, and M06 levels of theory with a 6-311+G(2d,2p) basis set using the B3LYP/6-31G*, BHandHLYP/6-31G* and M06/6-31G* optimized geometries including independent zero-point energy (ZPE) and basis set superposition error (BSSE) corrections are summarized in Table 4.3 and Table B.3 of Appendix B. Table 4.4 lists the enthalpic and entropic corrections to convert the 0 K BDEs to 298 K bond enthalpies and free energies. The B3LYP functional was found to deliver results that were most consistent with values measured for the third sequential binding energies. Therefore, except as noted, the following discussion is based on the B3LYP results. The B3LYP/6-31G* optimized ground-state geometries of the $M^{2+}(Bpy)_x$ complexes are shown in Figure 4.3. Geometrical parameters of the $M^{2+}(Bpy)_x$ complexes optimized at the B3LYP/6-31G*, BHandHLYP/6-31G*, and M06/6-31G*levels of theory are given in Table 4.5 and Tables B.4–B.5 of Appendix B. Cartesian coordinates of the B3LYP/6-31G* optimized geometries of the *cis* and *trans* conformers of the neutral Bpy ligand and the ground state structures of the $M^{2+}(Bpy)_x$ complexes are shown in Table B.6 of Appendix B. Detailed geometries, dipole moments, and isotropic molecular polarizabilities for the neutral Bpy ligand have been reported previously.[31] The ground-state *trans*-Bpy conformer is planar, whereas the aromatic rings of the excited *cis*-Bpy conformer, which lies 24.5 kJ/mol higher in energy, are twisted by 35.1°

relative to each other. The *trans*-Bpy conformer exhibits no net dipole moment because the local dipole moments cancel as a result of the symmetry of this ligand. In contrast, the local dipoles reinforce to produce a large dipole moment in the *cis*-conformer, 3.04 D. The *trans*-Bpy conformer has a slightly larger isotropic molecular polarizability of 19.92 $Å^3$ relative to that of *cis*-Bpy, 19.67 $Å^3$. Upon binding to M^{2+}, Bpy adopts a *cis* conformation via rotation about the central C–C bond.

4.5.1 $M^{2+}(Bpy)_x$ Complexes, $M^{2+} = Fe^{2+}$, Co^{2+}, Ni^{2+}, and Zn^{2+} and $x = 1–3$

The $Cu^{2+}(Bpy)_x$ complexes behave sufficiently different from the other metal cations that these complexes are discussed independently in the next section. The ground-state structures of the $M^{2+}(Bpy)_x$ complexes, where $M^{2+} = Fe^{2+}$, Co^{2+}, Ni^{2+}, and Zn^{2+} and $x = 1–3$, optimized at the B3LYP/6-31G* level of theory are shown in Figure 4.3. The coordination geometry of the M^{2+} cation in the $M^{2+}(Bpy)$ complexes is bent, as the two nitrogen atoms of the Bpy ligand are constrained by the central C–C bond. The two M^{2+}–N bond lengths are equal and decrease from Fe^{2+} (1.964 Å) to Co^{2+} (1.931 Å) to Ni^{2+} (1.882 Å), and then slightly increase for Zn^{2+} (1.907 Å). The decreases in the bond lengths from Fe^{2+} to Co^{2+} to Ni^{2+} closely match the decreases in the ionic radii of these metal cations: 0.76 Å, 0.74 Å, and 0.73 Å, respectively. Zn^{2+} deviates from this simple trend as its radius, 0.72 Å is the smallest, yet the Zn^{2+}–N bond lengths are larger than the Ni^{2+}–N bond lengths.[36,37] The $\angle NM^{2+}N$ bond angles decrease from Fe^{2+} (89.3°) to Co^{2+} (87.6°), and then increase from Ni^{2+} (90.2°) to Zn^{2+} (93.6°), nearly parallel in behavior to the M^{2+}–N bond lengths. The $\angle NCCN$ dihedral angles in all five $M^{2+}(Bpy)$ complexes are 0.0°, versus 35.1° for the free *cis*-Bpy ligand. The planar conformation of the Bpy ligand induced by coordination to the metal cation enables the strongest binding, which easily overcomes the steric repulsions of the N2, N2′ nitrogen lone

pairs and C6–H6, C6′–H6′ *ortho*-hydrogen atoms responsible for the nonplanar geometry of the free *cis*-Bpy ligand.

In the $M^{2+}(Bpy)_2$ complexes, the metal cation exhibits a distorted-tetrahedral coordination of the four nitrogen atoms. The four M^{2+}–N bond lengths are equal and decrease from Fe^{2+} (2.053 Å) to Co^{2+} (2.013 Å) to Ni^{2+} (1.987 Å), and then slightly increase for Zn^{2+} (2.013 Å), parallel to that found for the mono complexes. The intraligand ∠NM^{2+}N bond angles decrease relative to that in the mono-complexes, and vary between 81.8° and 83.6°, while the interligand ∠NM^{2+}N bond angles vary between 123.8° and 124.9°. The aromatic rings of each Bpy ligand lie in the same plane in all of the bis complexes, such that the ∠NCCN dihedral angles are 0.0°. The two Bpy ligands are nearly perpendicular to each other such that the ∠NM^{2+}NC dihedral angles between the planes of the two Bpy ligands are approximately 84.2°.

The coordination geometry around the metal cation in the $M^{2+}(Bpy)_3$ complexes is distorted-octahedral, with the metal chelated through the lone pairs of all six nitrogen atoms. The six M^{2+}–N bond lengths are equal and decrease from Fe^{2+} (2.196 Å) to Co^{2+} (2.157 Å) to Ni^{2+} (2.112 Å), and then slightly increase for Zn^{2+} (2.187 Å), again parallel to that found for the mono and bis complexes. The intraligand ∠NM^{2+}N bond angles again decrease relative to that in the mono and bis complexes, and are approximately 76.4°, and significantly smaller than the octahedral value of 90.0°. The interligand ∠NM^{2+}N bond angles between the Bpy ligands *cis* to each other are approximately 93.9°, whereas for the *trans* ligands, these angles are approximately 170.2°. These deviations from perfect octahedral coordination are again the result of the constrained geometry of the Bpy ligands. The aromatic rings in the individual Bpy ligands are slightly distorted, with average ∠NCCN dihedral angles of 7.1°

for two of the Bpy ligands, and 10.2° for the third Bpy ligand. The ∠NM^{2+}NC dihedral angles between any two Bpy ligands vary between 61.1° and 65.7°.

In almost all cases, the M^{2+}–N bond lengths increase with increasing ligation, as shown in Figures 4.3 and 4.4, as a result of the decreasing electrostatic attraction between the metal cation and the Bpy ligands and increasing ligand-ligand repulsive interactions. This trend is maintained for Fe^{2+}(Bpy)$_3$ in its quintet state; only Fe^{2+}(Bpy)$_3$ in its singlet state deviates from these trends, and exhibits Fe^{2+}–N bond lengths that are shorter than those of Fe^{2+}(Bpy)$_2$ as a result of the spin crossover from a quintet to singlet state upon binding of the third Bpy ligand. The decrease in the intraligand ∠NM^{2+}N bond angles is largely due to the increase in the M^{2+}–N bond lengths with increasing ligation.

4.5.2 Cu^{2+}(Bpy)$_x$, x = 1–3 Complexes

As found for the M^{2+}(Bpy)$_x$ complexes with Fe^{2+}, Co^{2+}, Ni^{2+}, and Zn^{2+}, the Bpy ligands bind to Cu^{2+} through the lone pairs of the nitrogen atoms leading to similar bent, distorted-tetrahedral, and distorted-octahedral geometries for the mono, bis, and tris complexes, respectively, as shown in Figure 4.3. In the Cu^{2+}(Bpy) complex, the Cu^{2+}–N bond distances are 1.870 Å and the ∠NCu^{2+}N bond angle is 89.7°. The aromatic rings of the Bpy ligand lie in the plane as indicated by the ∠NCCN dihedral angle of 0.0°. In the Cu^{2+}(Bpy)$_2$ complex, the Cu^{2+}–N bond lengths increase to 1.973 Å. The bond angles between Cu^{2+} and the N atoms differ slightly, with intraligand ∠NCu^{2+}N angles of 83.3° and interligand ∠NCu^{2+}N bond angles of 105.3° and 148.6°, whereas the latter two are equal for the complexes to the other four metal cations. The two pyridyl rings in each Bpy ligand are twisted about the central C–C bond as indicated by the ∠NCCN dihedral angle of 5.8°. The planes of the two Bpy ligands are twisted relative to each other with ∠NM^{2+}NC dihedral

angles of 55.9°. In contrast, the other $M^{2+}(Bpy)_2$ complexes exhibit much larger ∠NM^{2+}NC dihedral angles of 84.2°. The tris complex is tetragonally elongated such that the Cu^{2+}–N bond lengths of the four equatorial nitrogen atoms are 2.050 Å, whereas the Cu^{2+}–N bond distances are 2.390 Å for the axial nitrogen atoms. The relevant intra- and interligand ∠NCu^{2+}N bond angles and their degeneracies that define the distorted-octahedral geometry are 76.6(3), 91.6(3), 95.0(4), 99.0(2), and 169.4(3)°, respectively. The aromatic rings of the Bpy ligands are twisted relative to each other with average ∠NCCN dihedral angles of 0.2 and 16.3°, respectively. The distortions from the idealized tetrahedral and octahedral geometries of the bis and tris complexes are more severe for the $Cu^{2+}(Bpy)_x$ complexes than for the other metal cations because Jahn–Teller effects exert a pronounced influence on the geometry of these complexes. Similar to the other $M^{2+}(Bpy)_x$ complexes, as the number of Bpy ligands increases, the Cu^{2+}–N bond lengths increase owing to decreasing electrostatic attractions and increasing ligand–ligand repulsive interactions as shown in Figures 4.3 and 4.4. As the Cu^{2+}–N bond lengths increase, the intraligand ∠NCu^{2+}N bond angles decrease, whereas the *trans* interligand bond angles increase to minimize ligand–ligand repulsive interactions.

The $M^{2+}(Bpy)_x$ complexes exhibit M^{2+}–N bond lengths that are highly parallel to, but slightly shorter by ≤ 0.01 Å than those in the analogous $M^{2+}(Phen)_x$ complexes previously examined.[30] This suggests that the M^{2+}–N bond lengths of $M^{2+}(Phen)_x$ and $M^{2+}(Bpy)_x$ complexes are most closely linked to the rigidity and flexibility of the ligand framework, respectively. 1,10-Phenanthroline is extremely rigid and theoretical calculations suggest that the two nitrogen-donor atoms are highly constrained by the extended π network of the aromatic ligand. Phen thus exhibits a nearly fixed distance between the two coordinating

nitrogen-donor atoms. Due to the flexibility inferred by the single C–C bond linking the two pyridyl rings of the Bpy ligand, the rings bend upon complexation allowing both nitrogen-donor atoms to achieve a more optimal binding orientation about the metal cation, and resulting in slightly shorter M^{2+}–N bond distances. The flexibility of the Bpy ligand also becomes important with increasing ligation as seen by the larger deviations from planarity with increasing ligation.

4.6 Discussion

4.6.1 Metal-Ligand Bonding Interactions of the $M^{2+}(Bpy)_3$ Complexes

When three Bpy ligands interact with the M^{2+} cation, the lone pairs of electrons on the six nitrogen atoms donate their electron densities to the approximately sp^3d^2 hybridized orbitals of the M^{2+} cation and form six comparatively strong σ bonds. The occupied orbitals of M^{2+} having the appropriate symmetry donate electron density to the unoccupied π^* orbitals of the Bpy ligands. Both binding interactions act synergistically to produce relatively strong binding of Bpy ligands to M^{2+}. The metal–ligand binding interactions of the $M^{2+}(Bpy)_3$ complexes are very similar to those observed in $M^{2+}(Phen)_3$ complexes.[30] The spin state in the tris complexes is established by the balance between the orbital energy necessary to occupy all of the 3d levels (measured by the strength of the ligand field) and the increased interelectronic repulsion involved in spin pairing. Hence, the metal–ligand bonding interactions that occur between the metal 3d and ligand orbitals produce ground electronic spin states of the $M^{2+}(Bpy)_x$ complexes to Co^{2+}, Ni^{2+}, Cu^{2+}, and Zn^{2+} of quartet, triplet, doublet and singlet, respectively, when the B3LYP, BHandHLYP, and M06 functionals are employed. For the $Fe^{2+}(Bpy)$ and $Fe^{2+}(Bpy)_2$ complexes, the ground electronic spin states are found to be quintet. In contrast, the ground state spin multiplicity of the $Fe^{2+}(Bpy)_3$ complex

is predicted to be low-spin singlet when the B3LYP functional is employed, whereas BHandHLYP and M06 predict the ground state to be high-spin quintet. Similar behavior was found for the analogous $M^{2+}(Phen)_x$ complexes.[30] That the BHandHLYP and M06 functionals suggest a quintet $M^{2+}(Bpy)_3$ complex is due to the functionals over-stabilizing the high spin quintet state by approximately 94.9 and 30.9 kJ/mol over the singlet state, respectively (Table 4.3 and Table B.3 of Appendix B). The small difference in energy computed between the quintet and the singlet states of $Fe^{2+}(Bpy)_3$ when using the B3LYP functional, approximately 5.9 kJ/mol, indicate that the two states may co-exist at room temperature. Because B3LYP predicts a singlet ground state, while BHandHLYP and M06 predict a quintet ground state for the $Fe^{2+}(Bpy)_3$ complex, the threshold collision-induced dissociation (TCID) experimental data was analyzed in two different ways, one assuming that the threshold arises from dissociation of the singlet ground state, and the other assuming that the threshold describes dissociation from the quintet excited state. The BDE extracted assuming that the precursor $Fe^{2+}(Bpy)_3$ complex is in the singlet ground state is 248.1 ± 15.7 kJ/mol, whereas the value extracted assuming that the threshold is influenced by the presence of a reasonable population of the quintet excited state is 214.8 ± 10.4 kJ/mol, the latter corresponding to a diabatic BDE for this system. When compared to the B3LYP values calculated for dissociation from the singlet ground and quintet excited states of $Fe^{2+}(Bpy)_3$, 218.4 and 212.5 kJ/mol, respectively, these analyses suggest that quintet excited state is indeed accessed in the experiments and shifts the threshold to lower values. These results are consistent with the B3LYP results, which suggest that ~9.2% of the ions should exist in the quintet excited state, whereas approximately 90.8% of the ions would exist in the singlet ground state in a Maxwell-Boltzman distribution at room temperature. Thus, the threshold

should be determined by the dissociation behavior of the quintet excited state as it provides the lowest-energy pathway to dissociation. Theory suggests that both states could be present in the experiments, but comparison of the measured and calculated binding energies is clearly most consistent with the threshold corresponding to the quintet state. Similar findings were observed for the $Fe^{2+}(Phen)_3$ complex, which is not surprising as the Phen and Bpy ligands are both strong σ-donors and weak π acceptors.

4.6.2 Trends in the BDEs of the $M^{2+}(Bpy)_3$ Complexes

The measured BDEs of the $M^{2+}(Bpy)_3$ complexes, where M^{2+} = Fe^{2+}, Co^{2+}, Ni^{2+}, Cu^{2+}, and Zn^{2+} are illustrated in Figure 4.5 and summarized in Table 4.3 along with the corresponding theoretical BDEs calculated at the B3LYP/6-311+G(2d,2p), BHandHLYP/6-311+G(2d,2p), and M06/6-311+G(2d,2p) levels of theory. The measured BDEs are reported as the average values obtained from threshold analyses of the raw zero-pressure extrapolated data and analyses after subtraction of the low-energy feature, Table 4.1. As can be seen in Figure 4.5, the measured BDEs of the $M^{2+}(Bpy)_3$ complexes follow the order, $Cu^{2+} < Zn^{2+} < Co^{2+} < Ni^{2+} < {}^5Fe^{2+}$. The magnitudes of the BDEs indicate that the binding interactions between the $M^{2+}(Bpy)_x$ complexes and the third Bpy ligand are noncovalent in nature. The energy required to break a typical C–C covalent bond is > 400 kJ/mol,[38] much greater than the third-sequential BDEs of the $M^{2+}(Bpy)_3$ complexes determined here, which are < 350 kJ/mol for all five metal cations. The trends in the BDEs can be explained in terms of valence orbital occupations. Since $M^{2+}(Bpy)_3$ complexes are pseudo-octahedral complexes, the d orbitals are approximately split into three t_{2g} nonbonding and two e_g antibonding orbitals. Thus, the quintet state of Fe^{2+}, quartet state of Co^{2+}, and triplet state of Ni^{2+} all have an e_g^2 occupation with different numbers of t_{2g} electrons. Hence, to first order, their BDEs should

be the same, as observed. Upon the addition of one and two more electrons leading to doublet Cu^{2+} and singlet Zn^{2+}, the valence-electron configurations become e_g^3 and e_g^4, respectively. Hence the third-sequential binding energies should decrease as the occupation of the antibonding e_g orbitals increases from Ni^{2+} to Cu^{2+} to Zn^{2+} as observed. Apparently the Jahn–Teller distortions of Co^{2+} and Cu^{2+} are sufficient to weaken these bond energies further, although perhaps this is mainly because of the stability of the $M^{2+}(Bpy)_2$ complex.

Nearly parallel behavior was also found for the $M^{2+}(Phen)_3$ complexes.[30] The measured BDEs of the $M^{2+}(Phen)_3$ complexes follow the order, $Cu^{2+} < Zn^{2+} < Co^{2+} < {}^5Fe^{2+} < Ni^{2+}$ (see Figure 4.5). As can be seen in the Figure 4.5, the binding strength of the $M^{2+}(Phen)_3$ complexes slightly exceeds that of the $M^{2+}(Bpy)_3$ complexes, by 8.8 kJ/mol. The rigidity of the extensively delocalized Phen ligand should give its complexes high thermodynamic stability as compared to its less preorganized analogue Bpy. However, the flexibility of the single C–C bond linking the two aromatic pyridyl rings of the Bpy ligand allows it to rotate and/or bend the pyridyl rings, such that the effect of the higher level of preorganization of the Phen ligand is nearly compensated for by the greater ability of the Bpy ligand to optimize to its geometry for binding. Upon complexation to one Bpy ligand, the ∠NCCN dihedral angle changes from 180° in the free Bpy ligand to 0.0° in the mono complexes. Steric repulsions of the C6-H6, C6′-H6′ *ortho*-hydrogen atoms lead to slight destabilization in the Bpy complex accounting for the small energy difference between the Phen and Bpy mono complexes. With increasing ligation the flexibility of the Bpy ligand becomes increasingly important as seen by the larger deviations from planarity. The ∠NCCN dihedral angles increase from 0.0° in the mono complexes to as much as 10.0° in the tris-ligated Bpy complexes. The distortions from planarity help reduce steric and electronic repulsions

between the *ortho*-hydrogen atoms. The dipole moments and polarizabilities of the Bpy and Phen ligands also contribute to the electrostatic component of their M^{2+} complexes. The perfect coplanar arrangement of *cis*-Bpy (observed in the mono-complexes) with a ∠NCCN dihedral angle of 0.0° is calculated to have a much higher dipole moment, 3.24 D, relative to that computed for free *cis*-Bpy, where the pyridyl rings are twisted by approximately 35.1° and exhibits a dipole moment and polarizability of 3.04 D and 19.67 $Å^3$, respectively. The dipole moment and polarizability of the Phen ligand are slightly larger, 3.31 D and 23.78 $Å^3$, respectively. These small differences in the magnitude of the dipole moment and polarizability should lead to slightly enhanced ion–dipole and ion-induced dipole attractions between Phen and the metal ion. However, the flexibility of the Bpy ligand allows the metal ion to approach the ligand slightly more closely such that the shorter M^{2+}–N bond distances lead to an increase in strength of these electrostatic attractions, and thus roughly cancel the effects of the slightly larger dipole moment and polarizability of Phen. Upon dissociation, the Bpy ligand relaxes to its ground-state *trans* conformation producing a more stable free ligand such that less energy (~24.5 kJ/mol) is required for dissociation and is the main source of the difference in the BDEs of the tris complexes of Phen and Bpy with Co^{2+}, Ni^{2+}, Cu^{2+}, and Zn^{2+}. However, for the $^5Fe^{2+}$ complexes, the Bpy and Phen ligands exhibit the opposite behavior as portrayed by both the TCID measured and theoretically determined third-sequential BDEs. The TCID-measured third-sequential BDEs for $^5Fe^{2+}(Bpy)_3$ are 4.1 kJ/mol higher than those for $^5Fe^{2+}(Phen)_3$. B3LYP theory predicts BDEs of $^5Fe^{2+}(Phen)_3$ = $^5Fe^{2+}(Bpy)_3$, whereas BHandHLYP and M06 theories predict that $^5Fe^{2+}(Phen)_3 > {}^5Fe^{2+}(Bpy)_3$ by approximately 6.3 kJ/mol. These results suggest that the theoretical methods used to

determine the BDEs may not perform as well for Fe^{2+} as for the other M^{2+} cations examined here.

4.6.3 Comparison with Solution Phase

Binding constants for the stepwise coordination of M^{2+} cations with Bpy in aqueous solutions at 298 K and an ionic strength μ = 0.1 M have been reported.[24] The log k_3 values increase in the order Cu^{2+} (3.4) < Zn^{2+} (3.8) < Co^{2+} (4.8) < Ni^{2+} (6.2) < Fe^{2+} (9.5), and provides a measure of the stability of the tris complexes in solution. The CID reactions 4.1 observed in the gas phase mimic that in solution in that these reactions involve the loss of a single Bpy ligand, and represent the intrinsic stability of the $M^{2+}(Bpy)_3$ complexes. As summarized in Table 4.3, the BDEs for the loss of Bpy from $M^{2+}(Bpy)_3$, and thus the intrinsic stabilities of the $M^{2+}(Bpy)_3$ complexes, follow the order Cu^{2+} < Zn^{2+} < Co^{2+} < Ni^{2+} < $^5Fe^{2+}$. The agreement in the stability order observed in the gas phase and in solution indicates that solution-phase relative stabilities can be reproduced in the gas phase in the absence of solvent effects and counterions in favorable cases, that is, in which the order of intrinsic stabilities are not altered by solvation or the counterions. In the gas phase, the difference in the third-sequential BDEs of the complexes to Phen and Bpy differ only slightly (< 20 kJ/mol),[30] while in solution the stability constants exhibit much larger differences. The larger difference in stability in solution arises from differential stabilization of the Phen versus Bpy ligands in aqueous solution as a result of the large difference in the dipole moments of the free ligands, 3.31 D versus 0 D, whereas the $M^{2+}(N\text{-L})_3$ complexes should exhibit very similar free energies of solvation.

4.6.4 Comparison between Experiment and Theory

Theoretical BDEs of the $M^{2+}(Bpy)_3$ complexes derived from the B3LYP, BHandHLYP, and M06 levels of theory nearly parallel the measured BDEs, but differ in absolute magnitude, (Figure 4.5). The measured third sequential BDEs for all five $M^{2+}(Bpy)_3$ complexes exhibit very good agreement with B3LYP theory. The BDE of the $^{1}Fe^{2+}(Bpy)_3$ is 248.1 ± 15.7 kJ/mol, whereas the diabatic BDE of the $^{5}Fe^{2+}(Bpy)_3$ is 214.8 ± 10.4 kJ/mol. The diabatic BDEs agree better with the B3LYP results. The average experimental uncertainty (AEU), 9.9 ± 1.8 kJ/mol, differs only slightly from the mean absolute deviation (MAD) for B3LYP theory, 8.4 ± 8.1 kJ/mol (Table 4.3). The measured third sequential BDEs for the Bpy complexes with $^{1}Fe^{2+}$, Co^{2+}, Cu^{2+}, and Zn^{2+} exhibit good agreement with BHandHLYP theory, whereas the values calculated for the complexes to Ni^{2+} and $^{5}Fe^{2+}$ differ markedly from the measured BDEs. The AEU is significantly smaller than the MAD for BHandHLYP theory, 44.3 ± 39.4 kJ/mol. The third-sequential BDEs computed using M06 theory are systematically higher than BDEs obtained using the B3LYP and BHandHLYP theories. The larger binding energies found with M06 theory are consistent with the shorter M^{2+}–N bond lengths found in the optimized geometries as compared to those for structures computed at the B3LYP and BHandHLYP levels of theory. The agreement between M06 theory and the measured BDEs for all of the complexes is very poor except for the $^{1}Fe^{2+}(Bpy)_3$ complex. The MAD for M06 theory, 65.1 ± 13.5 kJ/mol, is significantly larger than the AEU. Therefore, B3LYP theory provides the best description of the binding of the third ligand in the $M^{2+}(Bpy)_3$ complexes.

The agreement between theory and experiment is roughly parallel for the $M^{2+}(Bpy)_3$ and $M^{2+}(Phen)_3$ complexes as illustrated in Figure 4.5. In both cases, B3LYP produces third-

sequential BDEs that are smaller and more consistent with the TCID measured values. The diabatic BDE of the complex to $^5Fe^{2+}$ exhibits better agreement with B3LYP results as compared to the $^1Fe^{2+}$ for both the $Fe^{2+}(Phen)_3$ and $Fe^{2+}(Bpy)_3$ complexes. For both the $M^{2+}(Phen)_3$ and $M^{2+}(Bpy)_3$ complexes, BHandHLYP produces BDEs that are intermediate between B3LYP and M06, which exhibit good agreement with TCID values for all M^{2+} except Ni^{2+} and $^5Fe^{2+}$. M06 theory systematically overestimates the third-sequential BDEs in both the $M^{2+}(Phen)_3$ and $M^{2+}(Bpy)_3$ complexes. These results suggest that the M06 level of theory has difficulties accurately describing the strength of binding in the $M^{2+}(Phen)_3$ and $M^{2+}(Bpy)_3$ complexes.

4.6.5 Trends in the Sequential and Total BDEs of the $M^{2+}(Bpy)_x$ Complexes

The theoretical $(Bpy)_{x-1}M^{2+}$–Bpy BDEs determined here follow the order $M^{2+}(Bpy) > M^{2+}(Bpy)_2 > M^{2+}(Bpy)_3$ (see Figure 4.6). Significant changes in terms of the M^{2+}–N bond lengths are observed as the numbers of ligands increases. The enhanced binding found in the $M^{2+}(Bpy)$ complexes arises from 4s-3d$_\sigma$ hybridization, which allows the Bpy ligand to approach the metal cation more closely as the electron density along the metal–ligand bonding axis is removed to an orbital perpendicular to the bonding axis. This results in enhanced binding of the first Bpy ligand as illustrated by their short M^{2+}–N bond lengths, which vary between 1.870 and 1.964 Å. Binding of the second Bpy ligand leads to an increase in M^{2+}–N bond lengths by approximately 0.1 Å such that these bond lengths vary between 1.973 and 2.053 Å. Upon binding of the third Bpy ligand, the M^{2+}–N bond lengths increase further and range from 2.050 to 2.390 Å. These results clearly indicate that the electrostatic contributions to the binding decrease as the number of ligands increase because the effective charge retained by the metal cation decreases as more electrons are added to the

metal center, which leads to weaker binding of the second and third ligands. Furthermore, the effects of 4s-3d$_\sigma$ hybridization are lost upon binding of additional ligands as a result of repulsive interactions between the occupied sd-hybrid orbital and the second and third Bpy ligands. Similarly, ligand–ligand repulsive interactions between the Bpy ligands increase upon sequential ligation. Thus, the $M^{2+}(Bpy)_3$ complexes experience the weakest electrostatic attractions and the most steric repulsion leading to significantly weaker binding.

The variation in the BDEs of the first ligand to all five metal cations is largest, 263.9 kJ/mol. The second-sequential BDEs exhibit the least variation, 29.2 kJ/mol, while the variation in the third-sequential BDEs are intermediate, 87.4 kJ/mol. The larger variation in the $M^{2+}(Bpy)$ complexes directly reflects the differences in stabilization these metal cations achieve via sd hybridization, which increases with increasing d-orbital occupation. The relatively small variation in the binding of the second ligand in the $M^{2+}(Bpy)_2$ complexes is a result of diminished sd hybridization effects as binding of the second Bpy ligand produces much greater repulsion with the occupied sd hybrid orbital as well as introducing ligand–ligand repulsion. The intermediate variations in the BDEs across the $M^{2+}(Bpy)_3$ complexes arise because of the varying valence-orbital occupation that leads to the slight Jahn–Teller effects in the complex to Co^{2+}, significant Jahn–Teller effects in the Cu^{2+} complexes, and the spin cross over in the Fe^{2+} complex.

The $M^{2+}(Bpy)$ complexes display BDEs that are significantly greater than twice that of a typical C–C bond > 400 kJ/mol.[38] The higher BDEs of the $M^{2+}(Bpy)$ complexes suggest that very strong electrostatic interactions dominate the binding. However, the high electron deficiency of these complexes makes them too reactive to generate in sufficient intensity to enable studies of their CID behavior. In comparison to $M^{2+}(Bpy)$, the binding in the

$M^{2+}(Bpy)_2$ complexes is also strongly electrostatic in nature, but significantly weaker than in the $M^{2+}(Bpy)$ complexes. As a result, their CID behavior provides an opportunity to probe the metal-to-ligand and ligand-to-metal charge transfer behavior in much greater detail. The nature of the binding of the third ligand is predominantly noncovalent, consistent with the fact that the only primary CID channel observed for the $M^{2+}(Bpy)_3$ complexes is the loss of an intact Bpy ligand.

Analogous behavior was also observed for the $M^{2+}(Phen)_3$ complexes.[30] The trends in the sequential BDEs follow the order: $M^{2+}(Phen) > M^{2+}(Phen)_2 > M^{2+}(Phen)_3$ (see Figure 4.6). The ratios of the $M^{2+}(Phen)_x$ to $M^{2+}(Bpy)_x$ theoretical BDEs to the first, second, and third ligands are approximately 1.02, 1.00, and 1.03, respectively. TCID experiments suggest a similar ratio of approximately 1.03 between the $M^{2+}(Phen)_3$ to $M^{2+}(Bpy)_3$ complexes. The slightly weaker binding to the Bpy ligands is largely the result of relaxation of Bpy from a *cis* to a *trans* conformation upon dissociation. The $M^{2+}(Bpy)_x$ complexes exhibit bond lengths that are slightly shorter than those of the $M^{2+}(Phen)_x$ complexes. The ratio of the M^{2+}–N distances for the $M^{2+}(Phen)_x$ complexes as compared to $M^{2+}(Bpy)_x$ for the binding of the first, second, and third ligands are constant, and ±1.01. Because of its flexible central C–C bond, the pyridyl rings bend toward the metal cation and lead to a slight decrease in the bite angle and shortening of the M^{2+}–N bond distances, and thus enhanced binding to the M^{2+} cations. The flexible central C–C bond also enables the pyridyl rings to twist to minimize ligand–ligand repulsive interactions that increase with sequential ligation. However, the rigid conjugated π system of Phen constrains this ligand to a planar geometry with a nearly constant bite angle. The dipole moments of free *cis*-Bpy with an ∠NCCN dihedral angle of 35.1°, and *cis*-Bpy and Phen with ∠NCCN dihedral angles of 0.0°, are

3.04, 3.24, and 3.31 D, respectively. Thus, the ion-dipole interactions to Phen ligands should be slightly stronger than to Bpy ligands when the M^{2+}–N bond lengths are equal. The calculated molecular polarizabilities of *cis*-Bpy and Phen are 19.67 $Å^3$ and 23.78 $Å^3$, respectively. The polarizability determines the strength of the ion-induced dipole attraction, which makes an important contribution to the overall binding energy. Thus, the ion-induced dipole interactions should be slightly larger for the $M^{2+}(Phen)_x$ complexes than the $M^{2+}(Bpy)_x$ complexes when the M^{2+}–N bond lengths are equal. However, the flexibility of Bpy enables greater distortion of the ligand, and thus slightly shorter M^{2+}–N bond distances, such that these effects roughly cancel producing binding interactions that are approximately of equal strength. The slightly weaker BDEs of the Bpy complexes are largely the result of relaxation of the *cis* conformation of Bpy in the complexes to the *trans* conformation of the free Bpy ligand, which provides 24.5 kJ/mol stabilization, almost exactly equal to the differences in the BDEs to Phen and Bpy. The minor changes in relative binding energies observed for the bis and tris complexes to Fe^{2+} are likely related to tendency toward low-spin complexes for d^6 metal ions, and the small differences in the strengths of their ligand fields.

4.6.6 Periodic Trends in the Sequential BDEs of the $M^{2+}(Bpy)_x$ Complexes

Periodic trends in the theoretical BDEs of the $M^{2+}(Bpy)_x$ complexes are shown in Figure 4.6. The M^{2+}(Bpy) BDEs follow the order $Fe^{2+} < Co^{2+} < Zn^{2+} < Ni^{2+} < Cu^{2+}$. These results indicate that the M^{2+}(Bpy) BDEs increase across the period except for Zn^{2+}(Bpy). These results suggest that the electrostatic interactions responsible for the binding in the M^{2+}(Bpy) complexes are greatly influenced by the ionic radii of the metal cation. The ionic radii of the M^{2+} cations decrease from 0.76 Å to 0.74 Å to 0.73 Å to 0.72 Å and 0.72 Å for Fe^{2+}, Co^{2+}, Ni^{2+}, Cu^{2+}, and Zn^{2+}, respectively. As the cations become smaller in size, they

interact with the Bpy ligands more strongly owing to the electrostatic component of the binding, and lead to higher BDEs. The enhancement in binding energy with decreases in the ionic radii are illustrated by the short M^{2+}–N bond lengths that vary between 1.870 Å (Cu^{2+}) and 1.964 Å (Fe^{2+}), and are very consistent with the order of stability in the M^{2+}(Bpy) complexes. By considering the M^{2+}–N bond lengths and ionic radii, the trend in the BDEs, Cu^{2+}(Bpy) > Zn^{2+}(Bpy) is reasonable. However, no simple correlation exists across the entire series because Zn^{2+} has a smaller ionic radius than Fe^{2+}, Co^{2+}, and Ni^{2+}. The second-sequential BDEs increase in the order $Cu^{2+} < Fe^{2+} < Ni^{2+} < Zn^{2+} < Co^{2+}$, whereas the third-sequential BDEs follow the order $Cu^{2+} < Zn^{2+} < Co^{2+} < Fe^{2+} < Ni^{2+}$. Clearly, as the extent of ligation increases, the stability order in the series changes, especially for the Cu^{2+} and Fe^{2+} complexes. These results suggest that factors other than electrostatic interactions play significant roles in determining the strength of binding of the $M^{2+}(Bpy)_x$ complexes. The spin change from high-spin quintet to low-spin singlet in the $Fe^{2+}(Bpy)_x$ complexes as the extent of ligation increases lead to its increase in relative stability. The low-spin singlet configuration of Fe^{2+} (t_{2g}^6 e_g^0) allows for a better approach of the Bpy ligands as compared to the high spin quintet configuration of Fe^{2+} (t_{2g}^4 e_g^2) where the occupied e_g orbital is antibonding. This argument is further supported by the significantly shorter Fe^{2+}–N distances in the low spin singlet $Fe^{2+}(Bpy)_3$ complex (1.998 Å) relative to the high-spin quintet $Fe^{2+}(Bpy)_3$ complex (2.196 Å). Changes in the relative stability order observed for the Cu^{2+} complexes are influenced by Jahn–Teller effects, which are quite significant in Cu^{2+} (d^9) complexes leading to weaker binding. In addition to the small size of the Cu^{2+} cation, $Cu^{2+}(Bpy)_2$ adopts a geometry closer to square planar to minimize repulsion with the occupied sd-hybrid orbital. Consequently, $Cu^{2+}(Bpy)_3$ exists preferentially in a tetragonally

distorted octahedral arrangement with four equivalent relatively shorter M^{2+}–N bonds and two much longer axial bonds. This arrangement makes it easier to lose one of the tetragonally elongated ligands.

Parallel behavior was observed for the $M^{2+}(Phen)_x$ complexes, in which significant changes in the relative stability order were observed again mainly for the Cu^{2+} and Fe^{2+} complexes.[30] For both the Phen and Bpy complexes, the change in valence-electron configuration of the Fe^{2+} is the direct cause of this enhancement in relative stability that occurs with upon binding of the third ligand. With both ligands, the bis and tris complexes of Cu^{2+} were found to be tetragonally distorted due to Jahn–Teller effects. For similar reasons, the tris complex of Cu^{2+} exhibits weaker binding to both Phen and Bpy ligands.

4.6.7 Comparison of the BDEs of $M^{2+}(N\text{-}L)_x$ and $M^{+}(N\text{-}L)_x$, *N*-*L* = Bpy or Phen

As expected, the $M^{2+}(Bpy)_x$ complexes exhibit much larger BDEs as compared to the analogous $M^{+}(Bpy)_x$ complexes as illustrated in Figure 4.7. Very similar trends were observed for the sequential BDEs of Phen ligands to M^{2+} and M^{+} (data not shown).[30-34] The higher charge of the dication enforces stronger electrostatic bonding. The absolute differences in the BDEs between the analogous M^{2+} and M^{+} complexes become narrower as the number of ligands increases. Thus, more ligands are required to stabilize the M^{2+} cations as compared to M^{+} to a point where the energies become comparable.

Trends in the third-sequential BDEs for the Bpy and Phen complexes with M^{2+} and M^{+} are illustrated in Figure 4.8. The binding in the M^{2+} and M^{+} complexes is again roughly parallel for the Bpy and Phen complexes. As expected the BDEs of the Phen complexes are slightly greater than those of the Bpy complexes except for the bis and tris complexes of Fe^{2+}. Although stable structures for the $Cu^{+}(Bpy)_3$ and $Cu^{+}(Phen)_3$ complexes were found,

they are calculated to be less stable than the $Cu^+(Bpy)_2$ + Bpy dissociation products as indicated by the negative BDE plotted for the $Cu^+(Bpy)_3$ and $Cu^+(Phen)_3$complexes in the figures. Indeed, the Gibbs free energies at 298 K for the loss of a single Phen and Bpy ligand from these complexes, –56.7 and –105.6 kJ/mol, respectively, suggest that dissociation would be spontaneous. Appreciable ion beams of any of the $M^+(N\text{-}L)_3$ complexes could not be generated because their internal energies at room temperature exceed the BDEs.[31-34] However, our ability to generate intense ion beams of $Cu^{2+}(Bpy)_3$ and the other $M^{2+}(Bpy)_3$ complexes examined here, and measure their CID behavior, clearly establish that these species are bound and that loss of a single Bpy ligand from these complexes is endothermic.

4.7 Conclusions

The kinetic-energy dependences of the CID of five $M^{2+}(Bpy)_3$ complexes with Xe is examined in a guided-ion beam mass spectrometer. The dominant dissociation process observed for all five $M^{2+}(Bpy)_3$ complexes is loss of a single intact neutral Bpy ligand. The threshold energies for this process at 0 K are determined after consideration of the effects of the reactant internal energy, multiple collisions with Xe, and lifetime effects.[29,39] The experimental results were compared with density functional theory calculations performed at B3LYP/6-311+G(2d,2p)//B3LYP/6-31G*, BHandHLYP/6-311+G(2d,2p)//BHandHLYP/6-31G* and M06/6-311+G(2d,2p)//M06/6-31G* levels of theory. The calculated sequential BDEs are highly parallel, but differ in absolute magnitude. BDEs computed using the M06 functional are the strongest, BHandHLYP values are intermediate, whereas B3LYP produces the weakest BDEs. B3LYP theory was found to provide results that are most consistent with experimental results, which suggests that the B3LYP functional is capable of accurately describing the binding in the tris complexes. Comparison between the $M^{2+}(Phen)_x$ and

$M^{2+}(Bpy)_x$ complexes indicates that Phen complexes exhibit slightly greater BDEs than Bpy complexes for the M^{2+} cations examined here except Fe^{2+}, which exhibits a modest variation resulting from the tendency towards low spin d^6 metal complexes and the slightly stronger ligand field provided by Phen. The flexibility of the Bpy ligand plays a significant role in that it enhances its binding interactions with the M^{2+} cations, leading to BDEs for its complexes that approach those of the analogous Phen complexes, where the difference in the strength of binding is largely the result of relaxation of Bpy upon dissociation, and thus requiring less energy (~24.5 kJ/mol) to dissociate. Comparison of the $M^{2+}(Bpy)_x$ complexes to the analogous $M^{+}(Bpy)_x$ complexes show that the charge on the cation is the major contributing factor to the differences in binding found for these complexes. The strength of binding is also found to depend on the valence-electron configuration of the metal cation. However, differences in the strength of binding are much smaller for cations of the same charge. Thus, these results suggest that the bonding in the Phen and Bpy complexes is dominantly electrostatic with the d-orbital occupation playing a secondary role in determining the strength of interaction.

4.8 References

(1) Segal, M.G.; Sykes, A. G. *J. Am. Chem. Soc.* **1978**, *100*, 4585.

(2) Mashiko, T.; Reed, C. A.; Haller, K. J.; Kastner, M. E.; Scheidt, W. R. *J. Am. Chem. Soc.* **1981**, *103*, 5758.

(3) Mauk, A. G.; Scott, R. A.; Gray, H. B. *J. Am. Chem. Soc.* **1980**, *102*, 4360.

(4) Chen, X. M.; Liu, G. J. *Chem. Eur. J.* **2002**, *8*, 4811.

(5) Collman, J. P.; Buckingham, D. A. *J. Am. Chem. Soc.* **1963**, *85*, 3039.

(6) Fischler, I.; Wagner, R.; Koerner von Gustorf, E. *J. Organomet. Chem.* **1976,** *112*, 1557.

(7) Dumas, H.; Levisalles, J.; Rudler, H. *J. Organomet. Chem.* **1980**, *187*, 405.

(8) Morrow, J. R.; Trogler, W. C. *Inorg. Chem.* **1989**, *28*, 2330.

(9) Kövér, E.; Kramer, R. *Chem. Ber*. **1994**, *127*, 2151.

(10) Liu, S.; Hamilton, A. D. *Tetrahedron Lett*. **1997**, *38*, 1107.

(11) Livieri, M.; Mancin, F.; Saielli, G.; Chin, J. Tonellato, U. *Chem.-Eur. J*. **2007**, *13*, 2246.

(12) Fan, Y. B.; Gao, Y. Q. *J. Am. Chem. Soc*. **2007**, *129*, 905.

(13) Jiang, Q.; Xiao, N.; Shi, P. F.; Zhu, Y. G.; Guo, Z. *Coord. Chem. Rev.* **2007**, *251*, 1951.

(14) Mancin, F.; Scrimin, P.; Tecillab, P.; Tonellato, U. *Chem. Commun*. **2005**, 2540.

(15) Suh, J. *Acc. Chem. Res*. **2003**, *36*, 562.

(16) Williams, N. H.; Takasaki, B.; Wall, M.; Chin, J. *Acc. Chem. Res.* **1999**, *32*, 485.

(17) Asadi, M.; Safaei, E.; Ranjbar, B.; Hasani, L. *New J. Chem.* **2004**, *28*, 1227.

(18) Williams, R. J. P. *Eur. J. Biochem*. **1995**, *234*, 363.

(19) Comba, P. *Coord. Chem. Rev*. **2000**, *200–202*, 217.

(20) Larsson, S. *J. Biol. Inorg. Chem*. **2000**, *5*, 560.

(21) van Albada, G. A.; Mohamadou, A.; Mutikainen, I.; Turpeinen, U.; Reedijk, J. *Eur. J. Inorg. Chem.* **2004**, *18*, 3733.

(22) Dell'Amico, D. B.; Calderazzo, F.; Curiardi, M.; Labella, L.; Marchetti, F. *Inorg. Chem*. **2004**, *43*, 5459.

(23) Constable, E. C. *Adv. Inorg. Chem*. **1989**, *34*, 1.

(24) Irving, H.; Mellor, D. H. *J. Chem. Soc.* **1962**, 5222.

(25) Irving, H.; Mellor, D. H. *J. Chem. Soc.* **1962**, 5237.

(26) McBryde, W. A. E.; Brisbin, D. A.; Irving, H. *J. Chem. Soc.* **1962**, 5245.

(27) Irving, H. M.; Williams, R. J. P. *J. Chem. Soc.* **1953**, 3192.

(28) Irving, H. M.; Cabell, M. J.; Mellor, D. H. *J. Chem. Soc.* **1953**, 3417.

(29) Rodgers, M. T.; Ervin, K. M.; Armentrout, P. B. *J. Chem. Phys.* **1997**, *106*, 4499.

(30) Nose, H.; Chen, Y.; Rodgers, M. T. *J. Phys. Chem. A* **2013**, 117, 4316.

(31) Rannulu, N. S.; Rodgers, M. T. *J. Phys. Chem. A* **2007**, *111*, 3465.

(32) Rannulu, N. S.; Rodgers, M. T. *J. Phys. Chem. A* **2012**, *116*, 1319.

(33) Rannulu, N. S.; Rodgers, M. T. *J. Phys. Chem. A* **2009**, *113*, 4534.

(34) Rannulu, N. S. Doctoral dissertation, Wayne State University, **2008**, pp. 134.

(35) Frisch, M. J.; Trucks, G. W.; Schlegel, H. B.; Scuseria, G. E.; Robb, M. A.; Cheeseman, J. R.; Scalmani, G.; Barone, V.; Mennucci, B.; Petersson, G. A.; Nakatsuji, H.; Caricato, M.; Li, X.; Hratchian, H. P.; Izmaylov, A. F.; Bloino, J.; Zheng, G.; Sonnenberg, J. L.; Hada, M.; Ehara, M.; Toyota, K.; Fukuda, R.; Hasegawa, J.; Ishida, M.; Nakajima, T.; Honda, Y.; Kitao, O.; Nakai, H.; Vreven, T.; Montgomery, J. A, Jr.; Peralta, J. E.; Ogliaro, F.; Bearpark, M.; Heyd, J. J.; Brothers, E.; Kudin, K. N.; Staroverov, V. N.; Kobayashi, R.; Normand, J.; Rendell, A.; Burant, J. C.; Iyengar, S. S.; Tomasi, J.; Rega, N.; Millam, J. M.; Klene, M.; Cross, J. B.; Bakken, V.; Adamo, C.; Jaramillo, J.; Gomperts, R.; Stratmann, R. E.; Yazyev, O.; Cammi, R.; Pomelli, C.; Ochterski, J. W.; Martin, R. L.; Morokuma, K.; Zakrzewski, V. G.; Salvador, P.; Dannenberg, J. J.; Dapprich, S.; Daniels, A. D.; Farkas, O.; Foresman, J. B.; Ortiz, J. V.; Cioslowski, J.; Fox, D. J. Gaussian, Inc., Wallingford, CT, 2009.

(36) Shannon, R. D. *Acta Crystallogr*. **1976**, *A32*, 751.

(37) Jia, Y. Q. *J. Solid State Chem.* **1991**, *95*, 184.

(38) Carey, F. A.; Giuliano, R. M. *Organic Chemistry* (8th ed). McGraw-Hill, New York. **2011**, pp. 165.

(39) Loh, S.; Hales, D. A.; Lian, L.; Armentrout, P. B. *J. Chem. Phys*. **1989**, *90*, 5466.

Table 4.1. Modeling Parameters of Equation 2.3, Threshold Dissociation Energies at 0 K, and Entropies of Activation at 1000 K of $M^{2+}(Bpy)_3$ Complexes[a]

M^{2+}	σ_0[b]	n[b]	E_0[c]	E_0(PSL)[b]	Kinetic Shift	$\Delta S^{\dagger}$(PSL)[b]
			(eV)	(eV)	(eV)	(J mol^{-1} K^{-1})
Fe^{2+}	55.7 (13.2)	2.0 (0.1)	4.24 (0.22)	2.34 (0.11)	1.90	168.4 (4.3)
	275.9 (49.7)	*1.0 (0.1)*	*5.47 (0.24)*	*2.81 (0.12)*	*2.66*	*167.6 (4.2)*
Fe^{2+}	**84.3 (19.5)**	**1.8 (0.1)**	**4.49 (0.21)**	**2.07 (0.10)**	**2.42**	**92.5 (4.4)**
	309.0 (59.5)	***1.0 (0.1)***	***5.56 (0.26)***	***2.38 (0.11)***	***3.18***	***91.9 (4.4)***
Co^{2+}	58.0 (5.1)	2.0 (0.1)	3.57 (0.11)	1.86 (0.07)	1.71	102.0 (4.4)
	194.9 (31.3)	*1.3 (0.1)*	*4.42 (0.12)*	*2.13 (0.09)*	*2.29*	*101.4 (4.4)*
Ni^{2+}	67.2 (4.6)	1.9 (0.1)	4.15 (0.10)	2.03 (0.08)	2.12	100.6 (4.4)
	171.4 (13.5)	*1.4 (0.1)*	*4.82 (0.10)*	*2.23 (0.09)*	*2.59*	*100.1 (4.4)*
Cu^{2+}	116.4 (9.4)	1.8 (0.1)	2.66 (0.09)	1.47 (0.05)	1.19	75.8 (4.4)
	250.3 (18.7)	*1.2 (0.1)*	*3.12 (0.10)*	*1.65 (0.06)*	*1.47*	*75.3 (4.4)*
Zn^{2+}	150.9 (41.3)	1.6 (0.2)	2.99 (0.09)	1.61 (0.04)	1.38	85.1 (4.5)
	248.3 (18.6)	*1.2 (0.1)*	*3.29 (0.09)*	*1.74 (0.07)*	*1.55*	*84.8 (4.4)*

[a] Uncertainties are listed in parentheses. Analyses of raw zero-pressure extrapolated data are shown in standard font; analyses of zero-pressure extrapolated data after subtraction of the low-energy feature are shown in italicized font. Analyses of the singlet state of the $Fe^{2+}(Bpy)_3$ complex are shown in standard font; those of the quintet state are shown in boldface. [b] Average values for loose PSL transition state. [c] No RRKM analysis.

Table 4.2. Relative Energies of the Various Spin States of a $M^{2+}(Bpy)_x$ Complexes in their Ground State Conformations, where $M^{2+} = Fe^{2+}$, Co^{2+}, and Ni^{2+} at 0 K in kJ/mol.

Complex	Multiplicity	B3LYP[a]	BHandHLYP[b]	M06[c]
Fe^{2+}	5	0.0	0.0	0.0
	3	241.3	263.6	260.2
	1	378.4	404.4	408.5
$Fe^{2+}(Bpy)$	5	0.0	0.0	0.0
	3	41.5	101.5	82.1
	1	126.6	233.7	192.3
$Fe^{2+}(Bpy)_2$	5	0.0	0.0	0.0
	3	41.5	99.7	71.4
	1	259.4	235.7	231.5
$Fe^{2+}(Bpy)_3$	5	5.9	0.0	0.0
	3	52.6	105.7	68.8
	1	0.0	94.9	30.9
Co^{2+}	4	0.0	0.0	0.0
	2	252.6	273.5	304.6
$Co^{2+}(Bpy)$	4	0.0	0.0	0.0
	2	46.1	102.1	18.5
$Co^{2+}(Bpy)_2$	4	0.0	0.0	0.0
	2	43.1	103.5	15.9
$Co^{2+}(Bpy)_3$	4	0.0	0.0	0.0
	2	24.0	94.1	7.7
Ni^{2+}	3	0.0	0.0	0.0
	1	297.0	317.3	234.6
$Ni^{2+}(Bpy)$	3	0.0	0.0	0.0
	1	31.1	117.6	11.7
$Ni^{2+}(Bpy)_2$	3	0.0	0.0	0.0
	1	50.1	106.2	35.1
$Ni^{2+}(Bpy)_3$	3	0.0	0.0	0.0
	1	122.6	200.3	104.6

[a]Calculated at the B3LYP/6-311+G(2d,2p)//B3LYP/6-31G* level of theory including ZPE corrections with frequencies scaled by 0.9804. [b]Calculated at the BHandHLYP/6-311+G(2d,2p)//BHandHLYP/6-31G* level of theory including ZPE corrections with frequencies scaled by 0.9472. [c]Calculated at the M06/6-311+G(2d,2p)//M06/6-31G* level of theory including ZPE corrections with frequencies scaled by 0.9940.

Table 4.3. Measured and Calculated Sequential and Total Enthalpies of Binding of $M^{2+}(Bpy)_x$ Complexes at 0 K in kJ/mol

		Theory		
		B3LYP[b]		
Complex	TCID[a]	D_0	$D_{0,BSSE}$[e]	total[e]
$Fe^{2+}(Bpy)$	–	987.2	983.9	983.9
$Fe^{2+}(Bpy)_2$	–	530.8	526.6	1510.5
$Fe^{2+}(Bpy)_3$	248.1 (15.7)	224.5	218.4	1728.9
$Fe^{2+}(Bpy)_3$	**214.8 (10.4)**	**218.6**	**212.5**	**1723.0**
$Co^{2+}(Bpy)$	–	1072.1	1067.1	1067.1
$Co^{2+}(Bpy)_2$	–	546.2	541.7	1608.8
$Co^{2+}(Bpy)_3$	192.4 (11.2)	194.1	187.3	1796.1
$Ni^{2+}(Bpy)$	–	1145.8	1142.4	1142.4
$Ni^{2+}(Bpy)_2$	–	539.7	534.1	1676.5
$Ni^{2+}(Bpy)_3$	205.4(11.9)	234.0	226.9	1903.4
$Cu^{2+}(Bpy)$	–	1252.4	1247.8	1247.8
$Cu^{2+}(Bpy)_2$	–	517.9	512.5	1760.3
$Cu^{2+}(Bpy)_3$	150.3 (8.1)	146.3	139.5	1899.8
$Zn^{2+}(Bpy)$	–	1109.4	1106.4	1106.4
$Zn^{2+}(Bpy)_2$	–	545.3	540.9	1647.3
$Zn^{2+}(Bpy)_3$	161.3 (7.9)	166.2	159.2	1806.5
AEU/MAD[f]	11.0 (3.2)		13.8 (11.6)	
AEU/MAD[g]	**9.9 (1.8)**		**8.4 (8.1)**	

[a]Average values from fits to raw data and data after subtraction of the low-energy feature, Table 4.1. Average values for the singlet state of $Fe^{2+}(Bpy)_3$ complex are shown in standard font, while those of the quintet state of $Fe^{2+}(Bpy)_3$ are shown in boldface. [b]Calculated at the B3LYP/6-311+G(2d,2p)//B3LYP/6-31G* level of theory including ZPE corrections with frequencies scaled by 0.9804. [e]Also includes BSSE corrections. [f]AEU/MAD values using the singlet state of $Fe^{2+}(Bpy)_3$ in the analysis. [g]AEU/MAD values using the quintet state of $Fe^{2+}(Bpy)_3$ in the analysis.

Table 4.4. Enthalpies and Free Energies of Binding of $M^{2+}(Bpy)_x$ Complexes at 0 and 298 K in kJ/mol.[a]

Complex	ΔH_0	ΔH_{298}-ΔH_0[b]	ΔH_{298}	$T\Delta S_{298}$[b]	ΔG_{298}
$Fe^{2+}(Bpy)$	–	2.4 (0.3)	–	33.6 (0.4)	–
$Fe^{2+}(Bpy)_2$	–	–1.2 (0.7)	–	50.9 (1.4)	–
$Fe^{2+}(Bpy)_3$	248.1 (15.7)	–2.2 (0.5)	245.9 (15.7)	55.7 (1.3)	190.2 (15.8)
$Fe^{2+}(Bpy)_3$	**214.8 (10.4)**	**–2.2 (0.5)**	**212.6 (10.4)**	**55.7 (1.3)**	**156.9 (10.5)**
$Co^{2+}(Bpy)$	–	2.7 (0.3)	–	36.7 (0.4)	–
$Co^{2+}(Bpy)_2$	–	0.1 (0.7)	–	56.1 (1.3)	–
$Co^{2+}(Bpy)_3$	192.4 (11.2)	–1.9 (0.5)	190.5 (11.2)	57.8 (1.3)	132.7 (11.3)
$Ni^{2+}(Bpy)$	–	2.8 (0.3)	–	36.9 (0.4)	–
$Ni^{2+}(Bpy)_2$	–	0.1 (0.7)	–	53.7 (1.3)	–
$Ni^{2+}(Bpy)_3$	205.4 (11.9)	–2.1 (0.5)	203.3 (11.9)	57.9 (1.3)	145.4 (12.0)
$Cu^{2+}(Bpy)$	–	2.6 (0.3)	–	34.8 (0.4)	–
$Cu^{2+}(Bpy)_2$	–	–0.1 (0.7)	–	56.5 (1.2)	–
$Cu^{2+}(Bpy)_3$	150.3 (8.1)	–3.1 (0.7)	147.2 (8.1)	50.7 (1.5)	96.5 (8.3)
$Zn^{2+}(Bpy)$	–	2.7 (0.3)	–	36.6 (0.4)	–
$Zn^{2+}(Bpy)_2$	–	–0.9 (0.7)	–	52.9 (1.4)	–
$Zn^{2+}(Bpy)_3$	161.3 (7.9)	–2.8 (0.5)	158.5 (7.9)	53.8 (1.4)	104.7 (8.0)

[a]Uncertainties are listed in parentheses. Values for the singlet ground-state $Fe^{2+}(Bpy)_3$ are shown in standard font; those for the quintet excited state are shown in boldface. [b]Values from calculations at the B3LYP/6-311+G(2d,2p) level of theory using B3LYP/6-31G* optimized geometries with frequencies scaled by 0.9804.

Table 4.4. (continued) Enthalpies and Free Energies of Binding of $M^{2+}(Bpy)_x$ Complexes at 0 and 298 K in kJ/mol.[a]

Complex	ΔH_0[b]	ΔH_{298}-ΔH_0[b]	ΔH_{298}[b]	$T\Delta S_{298}$[b]	ΔG_{298}[b]
$Fe^{2+}(Bpy)$	983.9	2.4 (0.3)	986.3	33.6 (0.4)	952.7
$Fe^{2+}(Bpy)_2$	526.6	–1.2 (0.7)	525.4	50.9 (1.4)	474.5
$Fe^{2+}(Bpy)_3$	218.4	–2.2 (0.5)	216.2	55.7 (1.3)	160.5
$Fe^{2+}(Bpy)_3$	**212.5**	**–2.2 (0.5)**	**210.3**	**55.7 (1.3)**	**154.6**
$Co^{2+}(Bpy)$	1067.1	2.7 (0.3)	1069.8	36.7 (0.4)	1033.1
$Co^{2+}(Bpy)_2$	541.7	0.1 (0.7)	541.8	56.1 (1.3)	485.7
$Co^{2+}(Bpy)_3$	187.3	–1.9 (0.5)	185.4	57.8 (1.3)	127.6
$Ni^{2+}(Bpy)$	1142.4	2.8 (0.3)	1145.2	36.9 (0.4)	1108.3
$Ni^{2+}(Bpy)_2$	534.1	0.1 (0.7)	534.1	53.7 (1.3)	480.4
$Ni^{2+}(Bpy)_3$	226.9	–2.1 (0.5)	224.8	57.9 (1.3)	166.9
$Cu^{2+}(Bpy)$	1247.8	2.6 (0.3)	1250.4	34.8 (0.4)	1215.6
$Cu^{2+}(Bpy)_2$	512.5	–0.1 (0.7)	512.5	56.5 (1.2)	456.0
$Cu^{2+}(Bpy)_3$	139.5	–3.1 (0.7)	136.4	50.7 (1.5)	85.7
$Zn^{2+}(Bpy)$	1106.4	2.7 (0.3)	1109.1	36.6 (0.4)	1072.5
$Zn^{2+}(Bpy)_2$	540.9	–0.9 (0.7)	540.0	52.9 (1.4)	487.1
$Zn^{2+}(Bpy)_3$	159.2	–2.8 (0.5)	156.4	53.8 (1.4)	102.6

[a]Uncertainties are listed in parentheses. Values for the singlet ground-state $Fe^{2+}(Bpy)_3$ are shown in standard font; those for the quintet excited state are shown in boldface. [b]Values from calculations at the B3LYP/6-311+G(2d,2p) level of theory using B3LYP/6-31G* optimized geometries with frequencies scaled by 0.9804.

Table 4.5. Geometrical Parameters of the B3LYP/6-31G* *cis* and *trans* Conformers of the Neutral Bpy Ligand and Ground-State Structures of the $M^{2+}(Bpy)_x$ Complexes[a]

Complex	M^{2+}–N	∠NCCN	∠NM^{2+}NC	∠NM^{2+}N[b]	∠NM^{2+}N[c]
trans-Bpy	–	180.0	–	–	–
cis-Bpy	–	35.1	–	–	–
$Fe^{2+}(Bpy)$	1.964	0.0	–	89.3	–
$Fe^{2+}(Bpy)_2$	2.053	0.0	83.7	81.8	124.9
$Fe^{2+}(Bpy)_3$	1.998	4.0	65.0	81.1	88.2 (3), 95.5 (6), 175.2 (3)
$Fe^{2+}(Bpy)_3$	**2.196**	**7.1, 10.1 (2)**	**65.7**	**75.4**	**92.3 (3), 96.6 (6), 168.7 (3)**
$Co^{2+}(Bpy)$	1.931	0.0	–	87.6	–
$Co^{2+}(Bpy)_2$	2.013	0.0	84.0	83.0	124.1
$Co^{2+}(Bpy)_3$	2.157	6.5	61.1	76.4	88.8 (3), 97.6 (6), 171.8 (3)
$Ni^{2+}(Bpy)$	1.882	0.0	–	90.2	–
$Ni^{2+}(Bpy)_2$	1.987	0.0	85.2	82.2	124.6
$Ni^{2+}(Bpy)_3$	2.112	7.6	65.5	78.1	90.1 (3), 96.2 (6), 172.0 (3)
$Cu^{2+}(Bpy)$	1.870	0.0	–	89.7	–
$Cu^{2+}(Bpy)_2$	1.973	5.8	55.9	83.3	105.3 (2), 148.6 (2)
$Cu^{2+}(Bpy)_3$	2.050 (4), 2.390 (2)	0.2, 16.3 (2)	64.5	76.6	91.6 (3), 95.0 (4), 99.0 (2), 169.4 (3)
$Zn^{2+}(Bpy)$	1.907	0.0	–	93.6	–
$Zn^{2+}(Bpy)_2$	2.013	0.1	83.7	83.6	123.8
$Zn^{2+}(Bpy)_3$	2.187	10.2	64.0	75.8	93.5 (3), 95.9 (6), 168.1 (3)

[a] Average values are given for similar bond distances or angles; degeneracies are listed in parentheses for values that differ sufficiently such that more than one value is needed to describe the bond angle or bond length. Geometrical parameters for the singlet ground-state of $Fe^{2+}(Bpy)_3$ are shown in standard font, while those for quintet excited state are shown in boldface. All bond angles (∠) are given in degrees (°) and M^{2+}–N bond lengths in angstroms (Å). [b] Intraligand angles. [c] Interligand angles.

4.10 Figure Captions and Figures

Figure 4.1. Cross sections for collision-induced dissociation of the $M^{2+}(Bpy)_3$ complexes, where M^{2+} = Fe^{2+}, Co^{2+}, Ni^{2+}, Cu^{2+}, and Zn^{2+} with Xe as a function of kinetic energy in the center-of-mass frame (lower *x*-axis) and laboratory frame (upper *x*-axis). Data are shown for a Xe pressure of approximately 0.2 mTorr.

Figure 4.2. Zero-pressure-extrapolated cross sections for collision-induced dissociation of the $M^{2+}(Bpy)_3$ complexes, where M^{2+} = Fe^{2+}, Co^{2+}, Ni^{2+},Cu^{2+}, and Zn^{2+}, with Xe in the threshold region as a function of kinetic energy in the center-of-mass frame (lower *x*-axis) and laboratory frame (upper *x*-axis). Parts a, c, e, g, and i show raw zero-pressure extrapolated data and composite fits to the low and high energy regions of the CID cross sections, whereas parts b, d, f, h, and j show data and fits obtained after subtraction of the low-energy feature. Solid lines show the best fits to the data using equation 2.3 convoluted over the kinetic and internal energy distributions of the reactants. Dotted lines show the model cross sections in the absence of experimental kinetic energy broadening for reactants with an internal energy corresponding to 0 K.

Figure 4.3. B3LYP/6-31G* optimized geometries of $M^{2+}(Bpy)_x$ complexes, where M^{2+} = Fe^{2+}, Co^{2+}, Ni^{2+},Cu^{2+}, and Zn^{2+} and x = 1–3.

Figure 4.4. Variation in the average M^{2+}–N bond distances in B3LYP/6-31G* optimized $M^{2+}(Bpy)_x$ complexes where x = 1–3 as a function of the metal cation, M^{2+}, where M^{2+} = Fe^{2+}, Co^{2+}, Ni^{2+}, Cu^{2+}, and Zn^{2+}. For the $Fe^{2+}(Bpy)_3$ complex values for the singlet state are plotted as closed symbols, while the open symbols represent M^{2+}–N bond lengths obtained from the quintet state of the $Fe^{2+}(Bpy)_3$ complex. The ionic radii of the bare metal cation; M^{2+} are also shown. Ionic radii of M^{2+} are taken from Refs 36 and 37.

Figure 4.5. Comparison of theoretical and TCID measured $(N\text{-L})_2M^{2+}$–*N*-L BDEs at 0 K (in kJ/mol), where M^{2+} = Fe^{2+}, Co^{2+}, Ni^{2+}, Cu^{2+}, and Zn^{2+} and *N*-L = Bpy and Phen. Closed symbols represent BDEs of Bpy complexes, whereas open symbols represent BDEs of the Phen complexes. Circles represent dissociation from the ground-state reactant complex to ground-state products. For the Fe^{2+} complexes, values for the quintet excited state are also plotted as diamonds. Theoretical BDEs determined at the B3LYP, BHandHLYP, and M06 levels of theory using the 6-311+G(2d,2p) basis set including ZPE and BSSE corrections. Values for Bpy are taken from Table 4.3. Values for Phen are taken from reference 30.

Figure 4.6. Theoretical $(N\text{-}L)_{x\text{-}1}M^{2+}$–*N-L* BDEs at 0 K (in kJ/mol), in which M^{2+} = Fe^{2+}, Co^{2+}, Ni^{2+}, Cu^{2+}, and Zn^{2+} and *N*-L = Bpy and Phen, as a function of the metal cation determined at the B3LYP/6-311+G(2d,2p) level of theory including ZPE and BSSE corrections. Values for Bpy are taken from Table 4.3. Values for Phen are taken from reference 30.

Figure 4.7. Theoretical $(Bpy)_{x-1}M^{n+}$–Bpy BDEs as a function of the number of Bpy ligands (x) at 0 K (in kJ/mol) determined at B3LYP/6-311+G(2d,2p) level of theory including ZPE and BSSE corrections. Filled symbols represent M^{2+} complexes, whereas open symbols represent M^{+} complexes. Values for M^{2+} are taken from Table 4.3. Values for M^{+} are taken from references 31–34.

Figure 4.8. Periodic trends in the $(N\text{-}L)_2M^{n+}$–N-L BDEs at 0 K (in kJ/mol), in which M = Fe, Co, Ni, Cu, and Zn, n = 1 and 2, and N-L = Bpy and Phen. Circles represent TCID-measured BDEs for the M^{2+} complexes, whereas triangles represent values calculated at the B3LYP/6-311+G(2d,2p) level of theory including ZPE and BSSE corrections for the M^{+} complexes. Values for the Bpy complexes are shown as closed symbols, whereas values for the Phen complexes are shown as open symbols. Values for Bpy are taken from Table 4.3. Values for Phen are taken from reference 30. Values for M^{+} values are taken from references 31–34.

Figure 4.1.

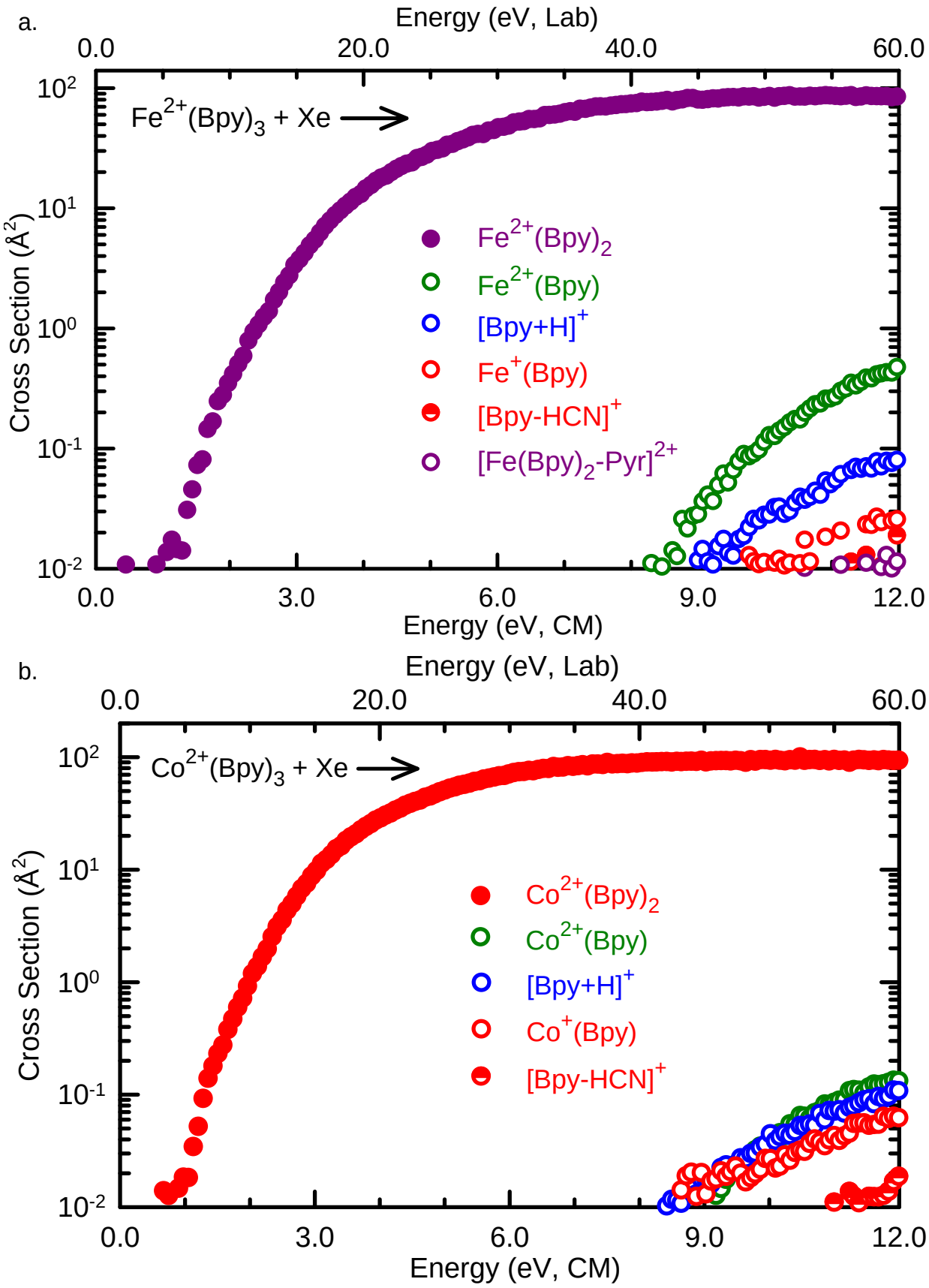
a.
Energy (eV, Lab)
0.0
20.0
40.0
60.0
10^2
10^1
10^0
10^{-1}
10^{-2}
Cross Section (Å^2)
$Fe^{2+}(Bpy)_3$ + Xe
$Fe^{2+}(Bpy)_2$
$Fe^{2+}(Bpy)$
$[Bpy+H]^+$
$Fe^+(Bpy)$
$[Bpy-HCN]^+$
$[Fe(Bpy)_2\text{-}Pyr]^{2+}$
0.0
3.0
6.0
9.0
12.0
Energy (eV, CM)
b.
Energy (eV, Lab)
0.0
20.0
40.0
60.0
10^2
10^1
10^0
10^{-1}
10^{-2}
Cross Section (Å^2)
$Co^{2+}(Bpy)_3$ + Xe
$Co^{2+}(Bpy)_2$
$Co^{2+}(Bpy)$
$[Bpy+H]^+$
$Co^+(Bpy)$
$[Bpy-HCN]^+$
0.0
3.0
6.0
9.0
12.0
Energy (eV, CM)

Figure 4.1.

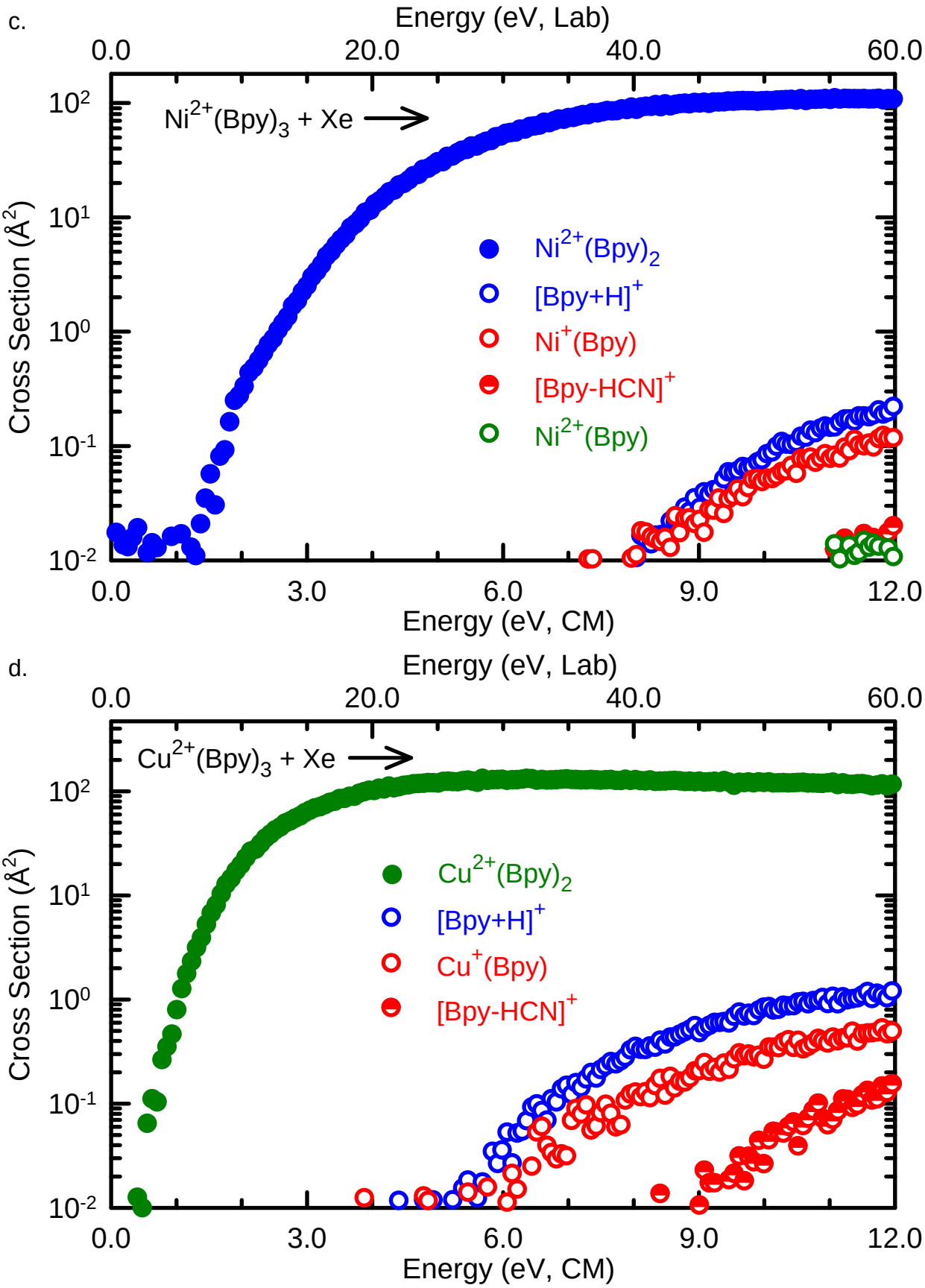
c.
Energy (eV, Lab)
0.0
20.0
40.0
60.0
$Ni^{2+}(Bpy)_3$ + Xe
Cross Section (Å^2)
10^2
10^1
10^0
10^{-1}
10^{-2}
$Ni^{2+}(Bpy)_2$
$[Bpy+H]^+$
$Ni^+(Bpy)$
$[Bpy-HCN]^+$
$Ni^{2+}(Bpy)$
0.0
3.0
6.0
9.0
12.0
Energy (eV, CM)
d.
Energy (eV, Lab)
0.0
20.0
40.0
60.0
$Cu^{2+}(Bpy)_3$ + Xe
Cross Section (Å^2)
10^2
10^1
10^0
10^{-1}
10^{-2}
$Cu^{2+}(Bpy)_2$
$[Bpy+H]^+$
$Cu^+(Bpy)$
$[Bpy-HCN]^+$
0.0
3.0
6.0
9.0
12.0
Energy (eV, CM)

Figure 4.1.

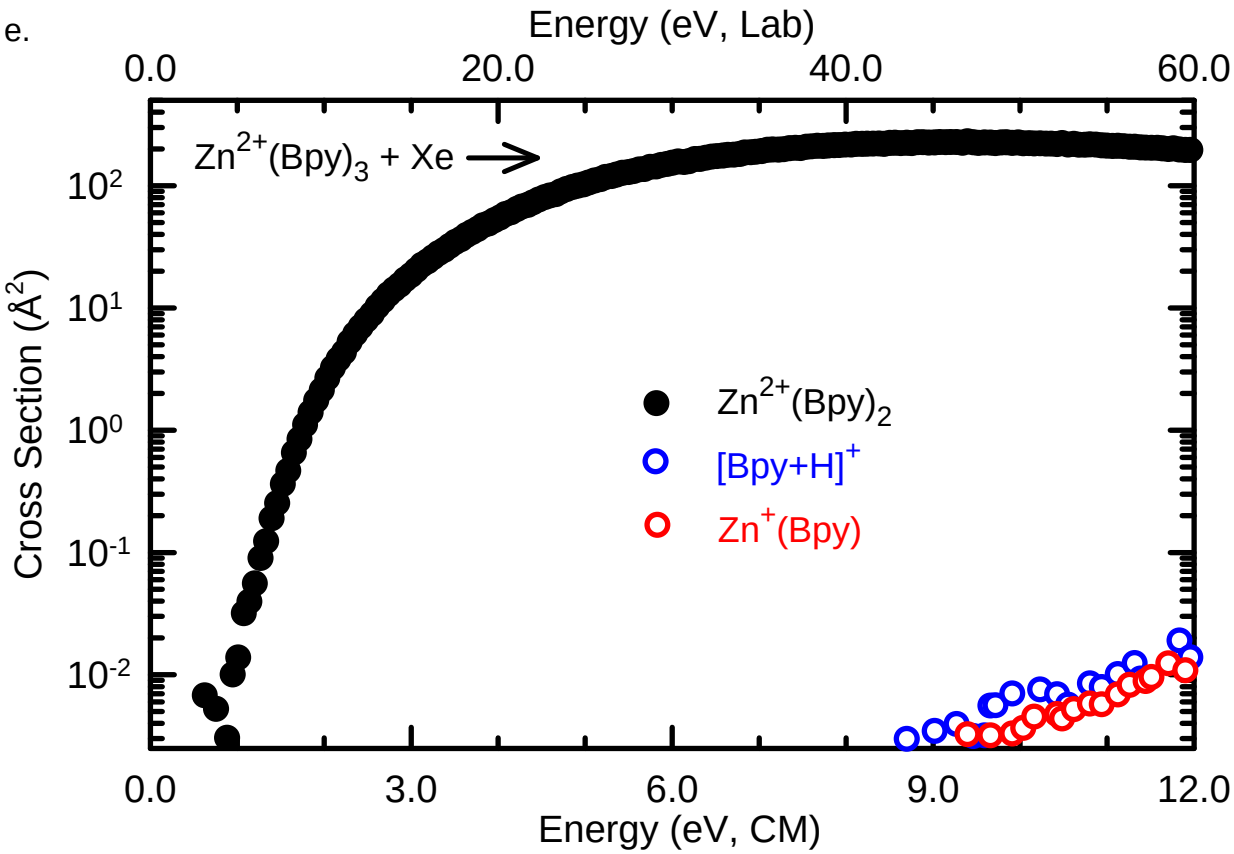
e.
Energy (eV, Lab)
0.0
20.0
40.0
60.0
Zn2+(Bpy)3 + Xe
Cross Section (Å2)
10^2
10^1
10^0
10^-1
10^-2
Zn2+(Bpy)2
[Bpy+H]+
Zn+(Bpy)
0.0
3.0
6.0
9.0
12.0
Energy (eV, CM)

Figure 4.2.

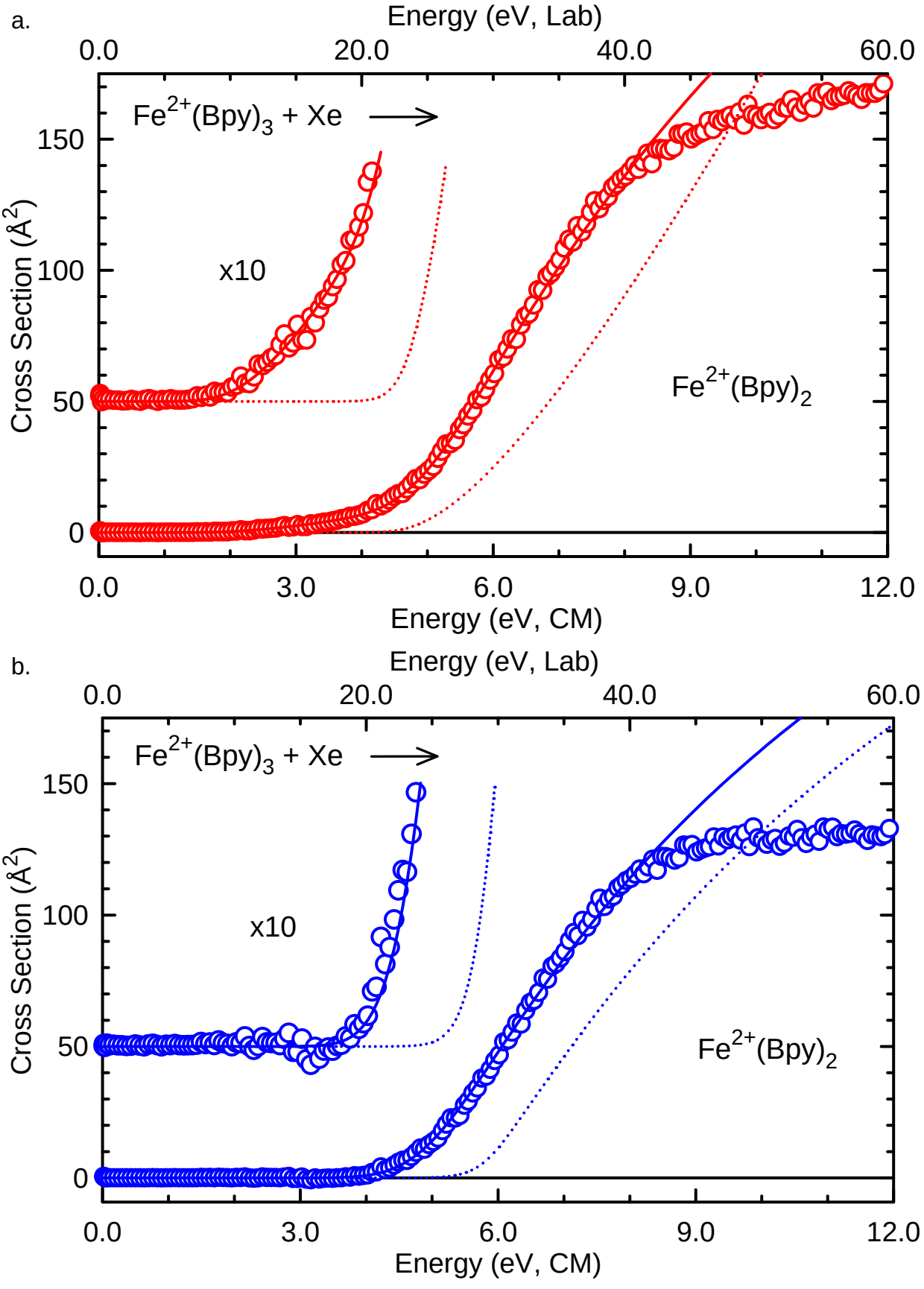
a.
Energy (eV, Lab)
0.0
20.0
40.0
60.0
$Fe^{2+}(Bpy)_3$ + Xe
150
100
50
0
Cross Section (Å^2)
x10
$Fe^{2+}(Bpy)_2$
0.0
3.0
6.0
9.0
12.0
Energy (eV, CM)
b.
Energy (eV, Lab)
0.0
20.0
40.0
60.0
$Fe^{2+}(Bpy)_3$ + Xe
150
100
50
0
Cross Section (Å^2)
x10
$Fe^{2+}(Bpy)_2$
0.0
3.0
6.0
9.0
12.0
Energy (eV, CM)

Figure 4.2.

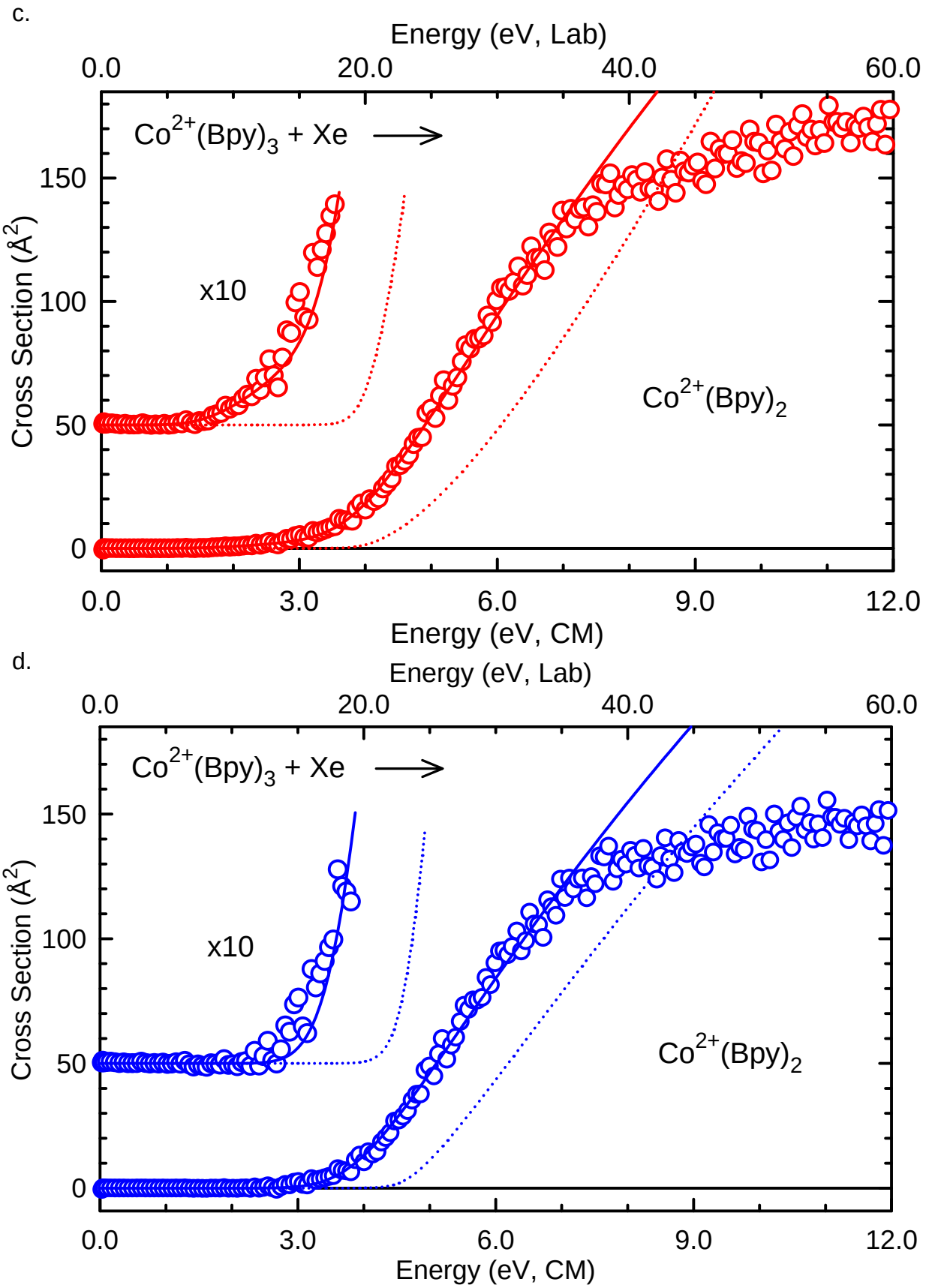
c.
Energy (eV, Lab)
0.0
20.0
40.0
60.0
$Co^{2+}(Bpy)_3$ + Xe
x10
$Co^{2+}(Bpy)_2$
Cross Section (Å^2)
150
100
50
0
0.0
3.0
6.0
9.0
12.0
Energy (eV, CM)
d.
Energy (eV, Lab)
0.0
20.0
40.0
60.0
$Co^{2+}(Bpy)_3$ + Xe
x10
$Co^{2+}(Bpy)_2$
Cross Section (Å^2)
150
100
50
0
0.0
3.0
6.0
9.0
12.0
Energy (eV, CM)

Figure 4.2.

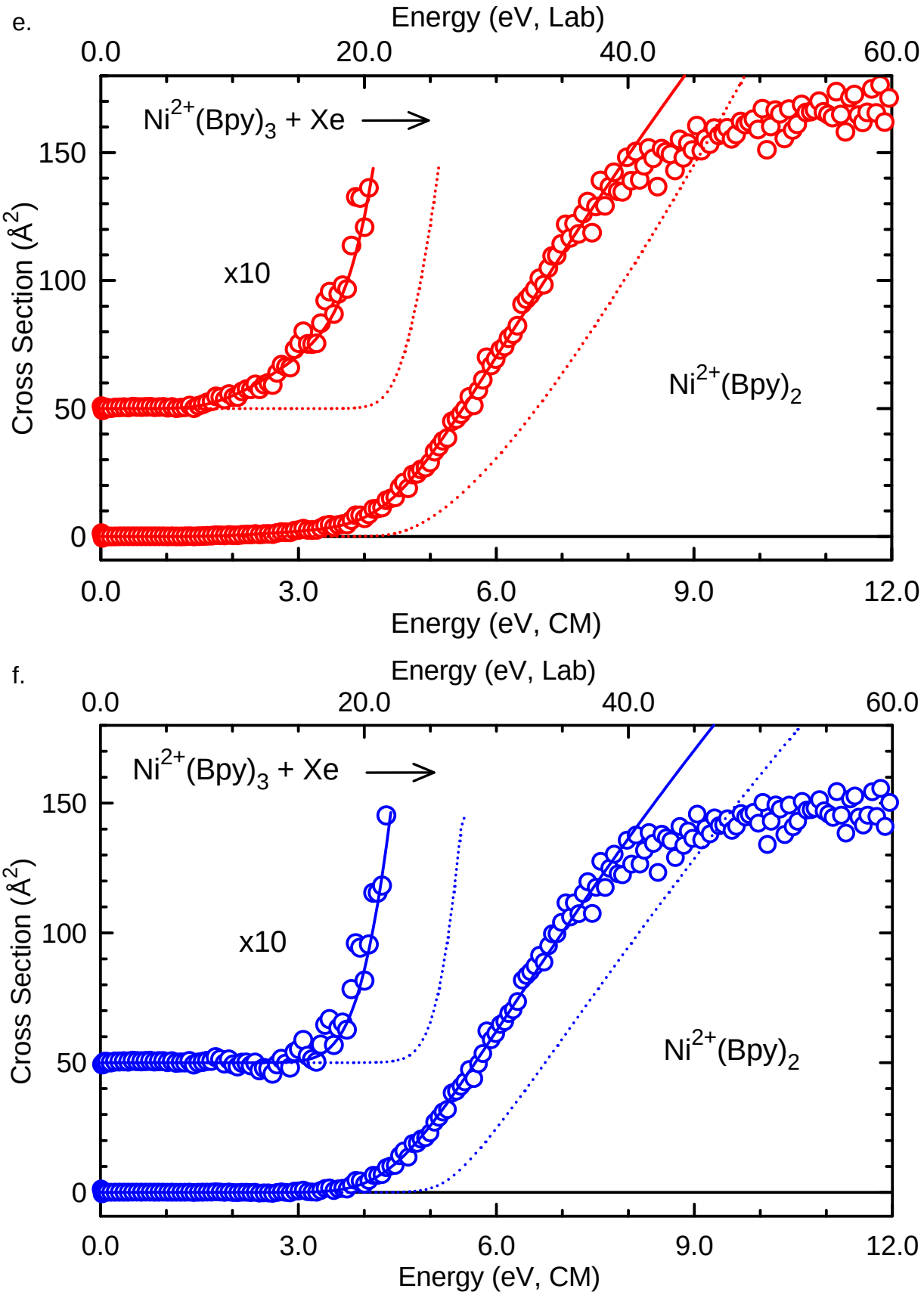
e.
Energy (eV, Lab)
0.0
20.0
40.0
60.0
Ni2+(Bpy)3 + Xe
150
100
50
0
Cross Section (Å2)
x10
Ni2+(Bpy)2
0.0
3.0
6.0
9.0
12.0
Energy (eV, CM)
f.
Energy (eV, Lab)
0.0
20.0
40.0
60.0
Ni2+(Bpy)3 + Xe
150
100
50
0
Cross Section (Å2)
x10
Ni2+(Bpy)2
0.0
3.0
6.0
9.0
12.0
Energy (eV, CM)

Figure 4.2.

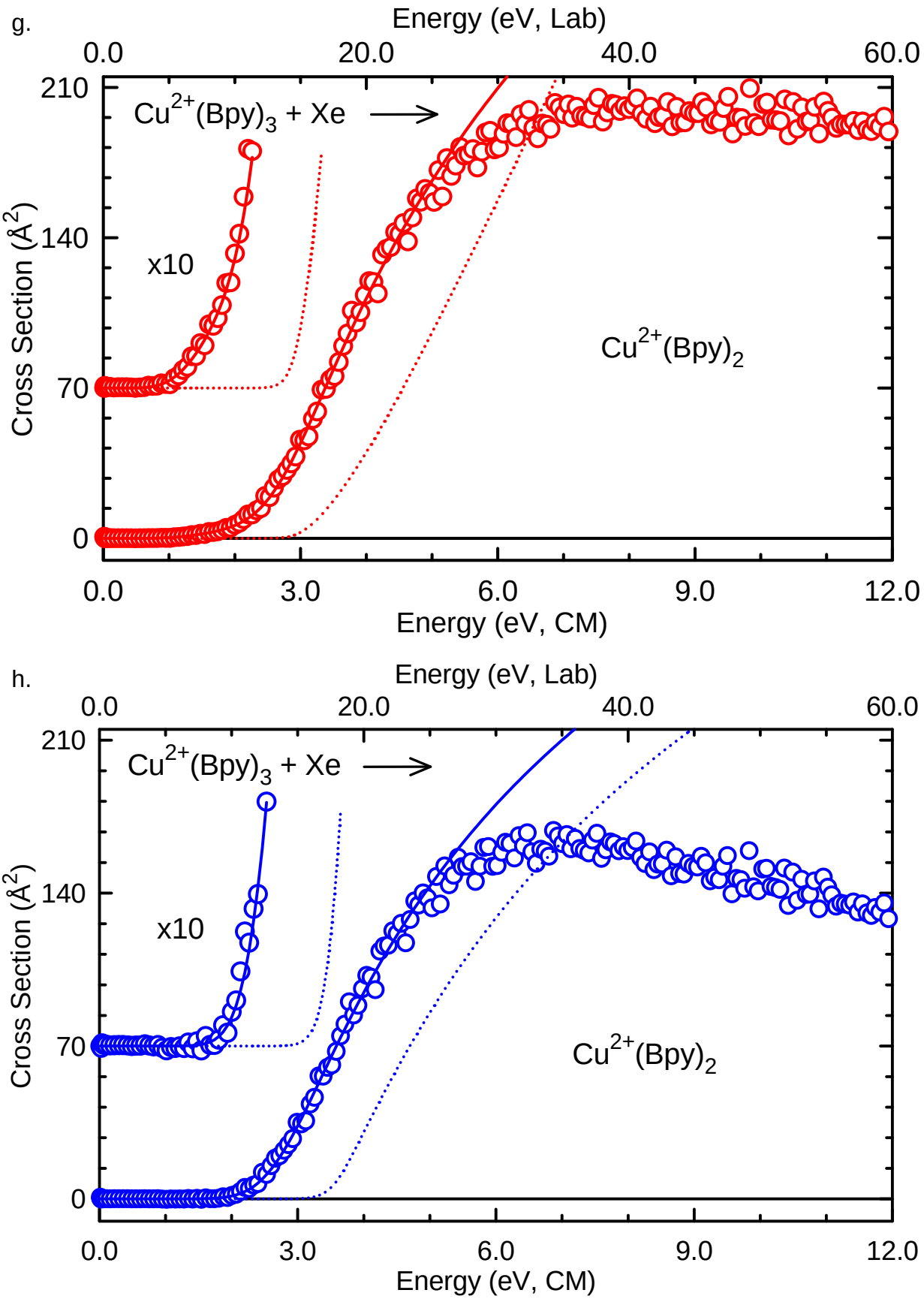
g.
Energy (eV, Lab)
0.0
20.0
40.0
60.0
210
140
70
0
Cross Section (Å^2)
Cu^{2+}(Bpy)$_3$ + Xe
x10
Cu^{2+}(Bpy)$_2$
0.0
3.0
6.0
9.0
12.0
Energy (eV, CM)
h.
Energy (eV, Lab)
0.0
20.0
40.0
60.0
210
140
70
0
Cross Section (Å^2)
Cu^{2+}(Bpy)$_3$ + Xe
x10
Cu^{2+}(Bpy)$_2$
0.0
3.0
6.0
9.0
12.0
Energy (eV, CM)

Figure 4.2.

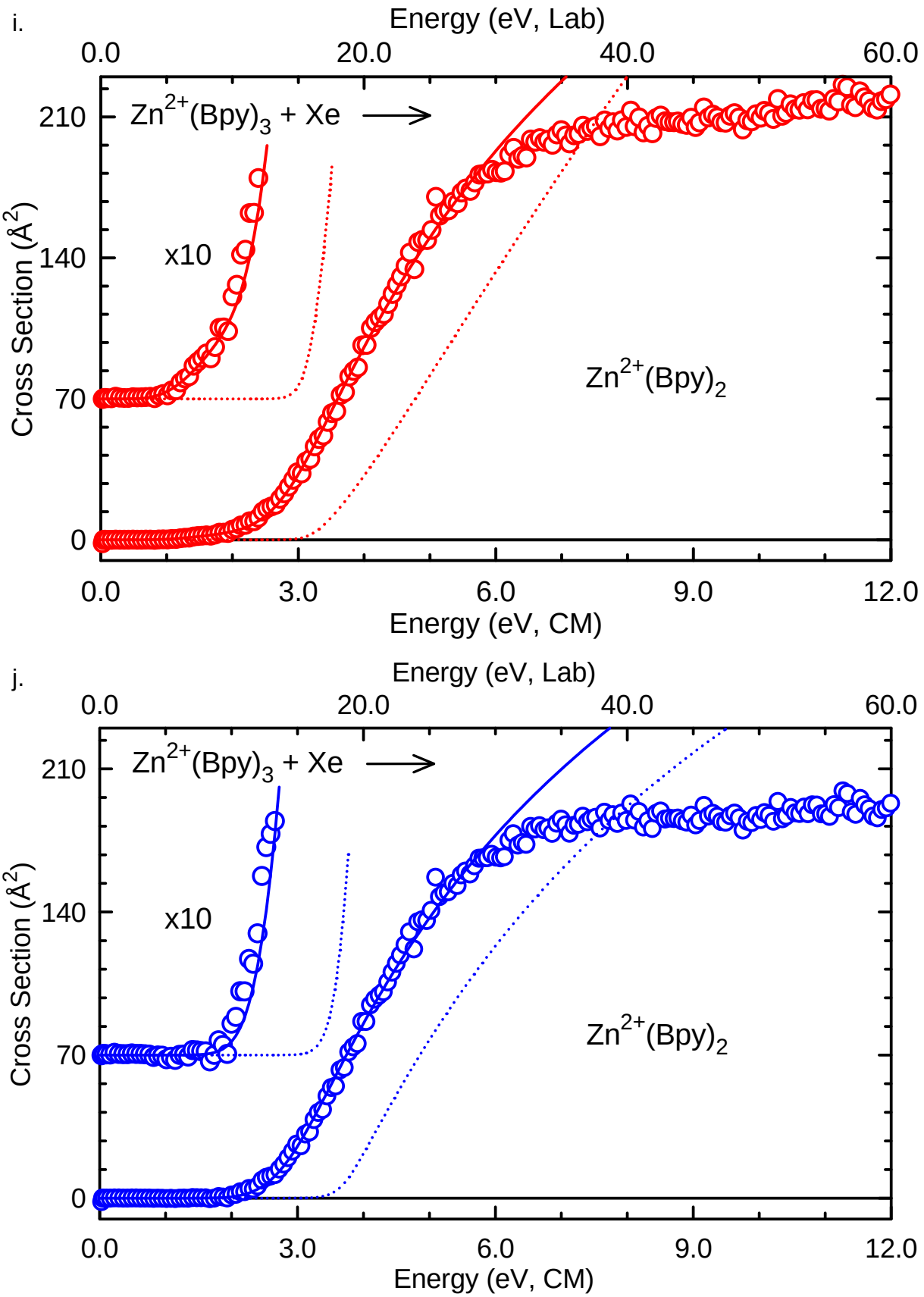
i.
Energy (eV, Lab)
0.0
20.0
40.0
60.0
210
140
70
0
Cross Section (Å^2)
$Zn^{2+}(Bpy)_3$ + Xe
x10
$Zn^{2+}(Bpy)_2$
0.0
3.0
6.0
9.0
12.0
Energy (eV, CM)
j.
Energy (eV, Lab)
0.0
20.0
40.0
60.0
210
140
70
0
Cross Section (Å^2)
$Zn^{2+}(Bpy)_3$ + Xe
x10
$Zn^{2+}(Bpy)_2$
0.0
3.0
6.0
9.0
12.0
Energy (eV, CM)

Figure 4.3.

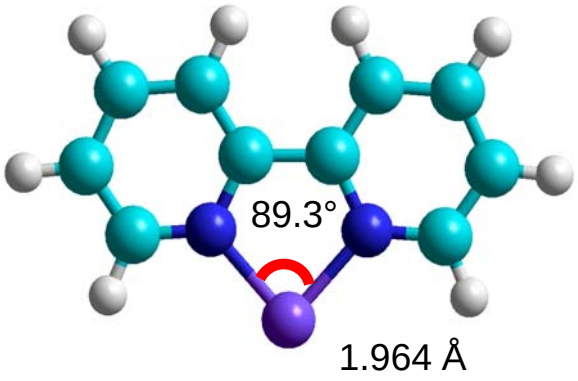

Fe^{2+}(Bpy)

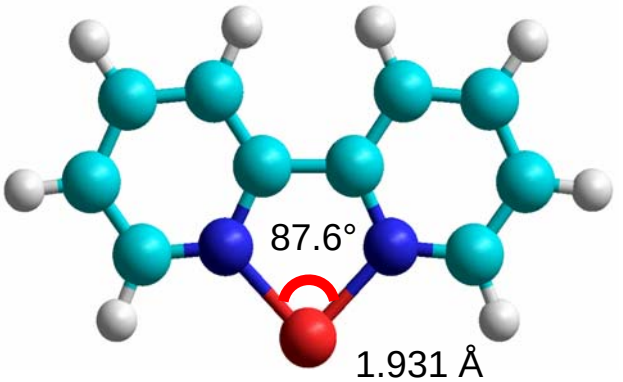

Co^{2+}(Bpy)

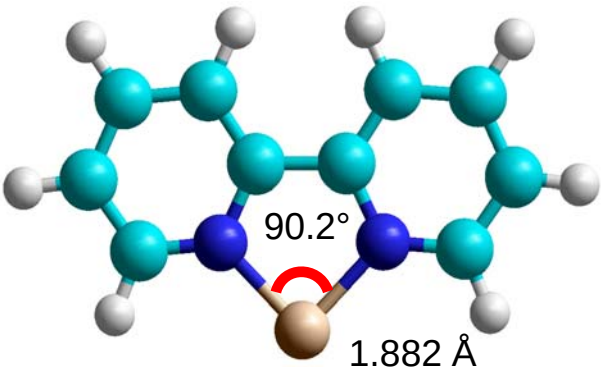

Ni^{2+}(Bpy)

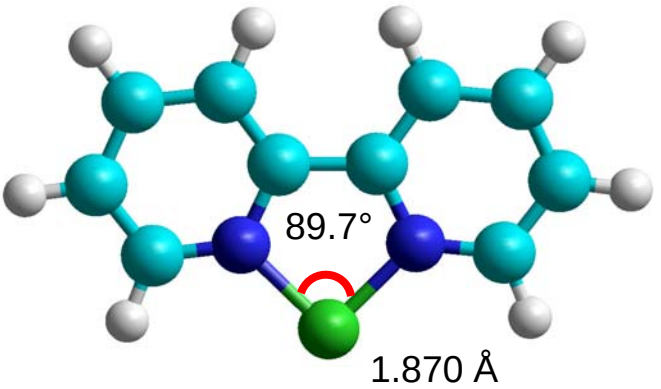

Cu^{2+}(Bpy)

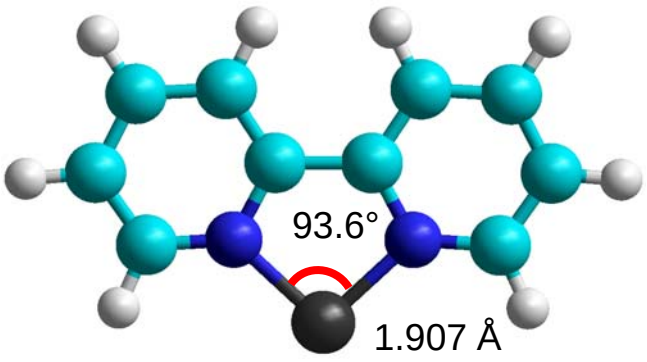

Zn^{2+}(Bpy)

Figure 4.3.

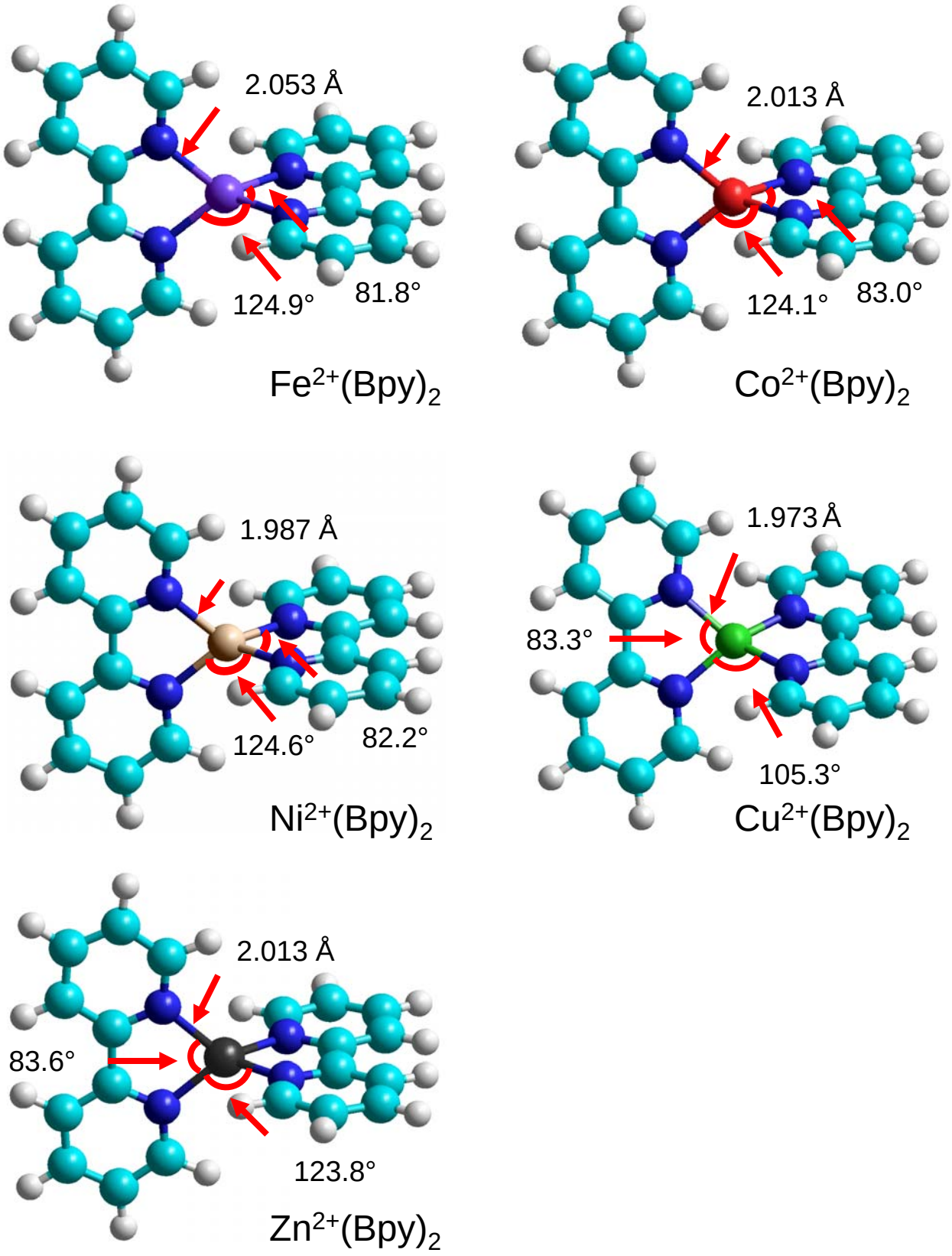
2.053 Å
124.9°
81.8°
$Fe^{2+}(Bpy)_2$
2.013 Å
124.1°
83.0°
$Co^{2+}(Bpy)_2$
1.987 Å
124.6°
82.2°
$Ni^{2+}(Bpy)_2$
1.973 Å
83.3°
105.3°
$Cu^{2+}(Bpy)_2$
2.013 Å
83.6°
123.8°
$Zn^{2+}(Bpy)_2$

Figure 4.3.

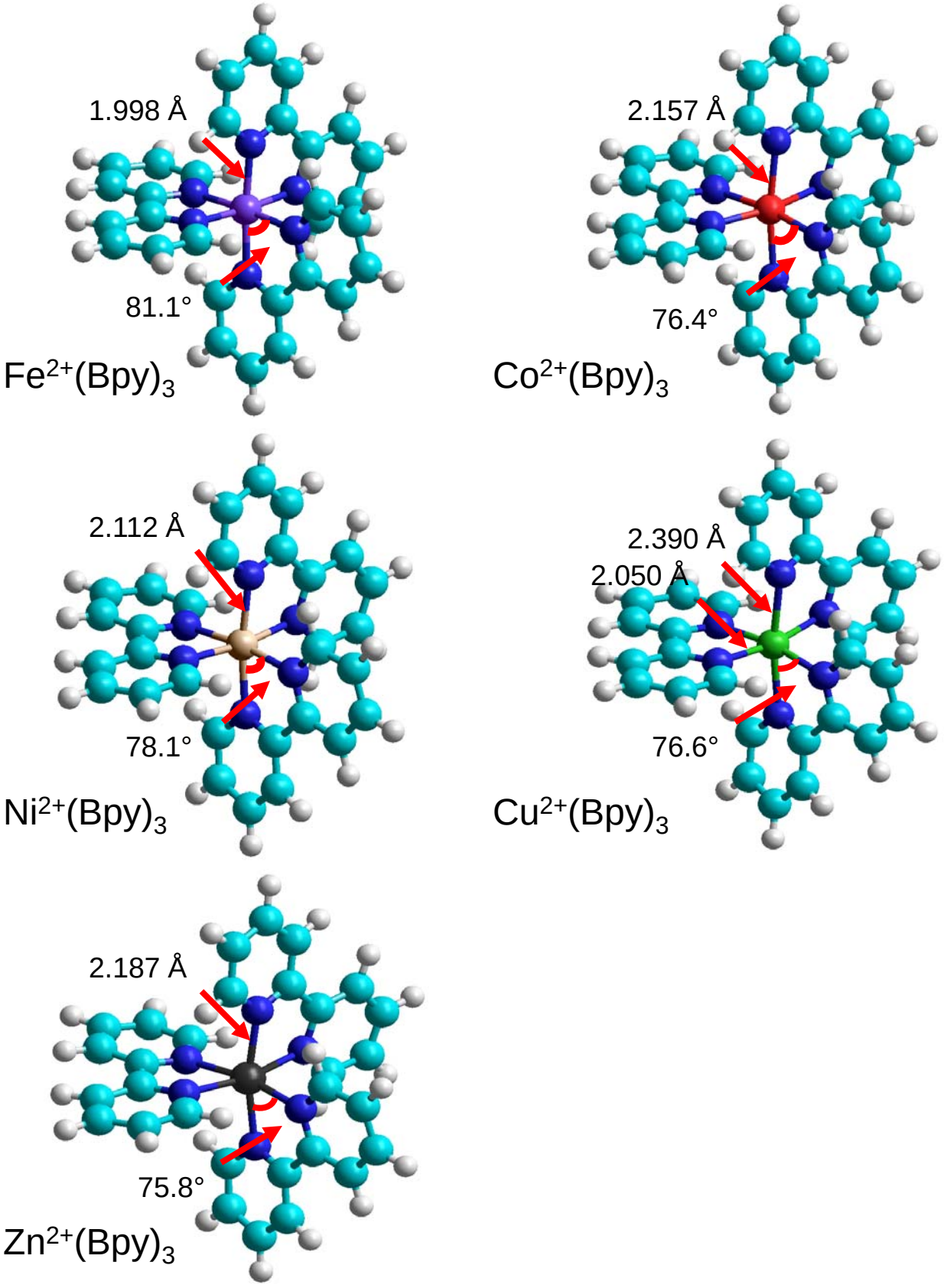
1.998 Å
81.1°
Fe2+(Bpy)3
2.157 Å
76.4°
Co2+(Bpy)3
2.112 Å
78.1°
Ni2+(Bpy)3
2.390 Å
2.050 Å
76.6°
Cu2+(Bpy)3
2.187 Å
75.8°
Zn2+(Bpy)3

Figure 4.4.

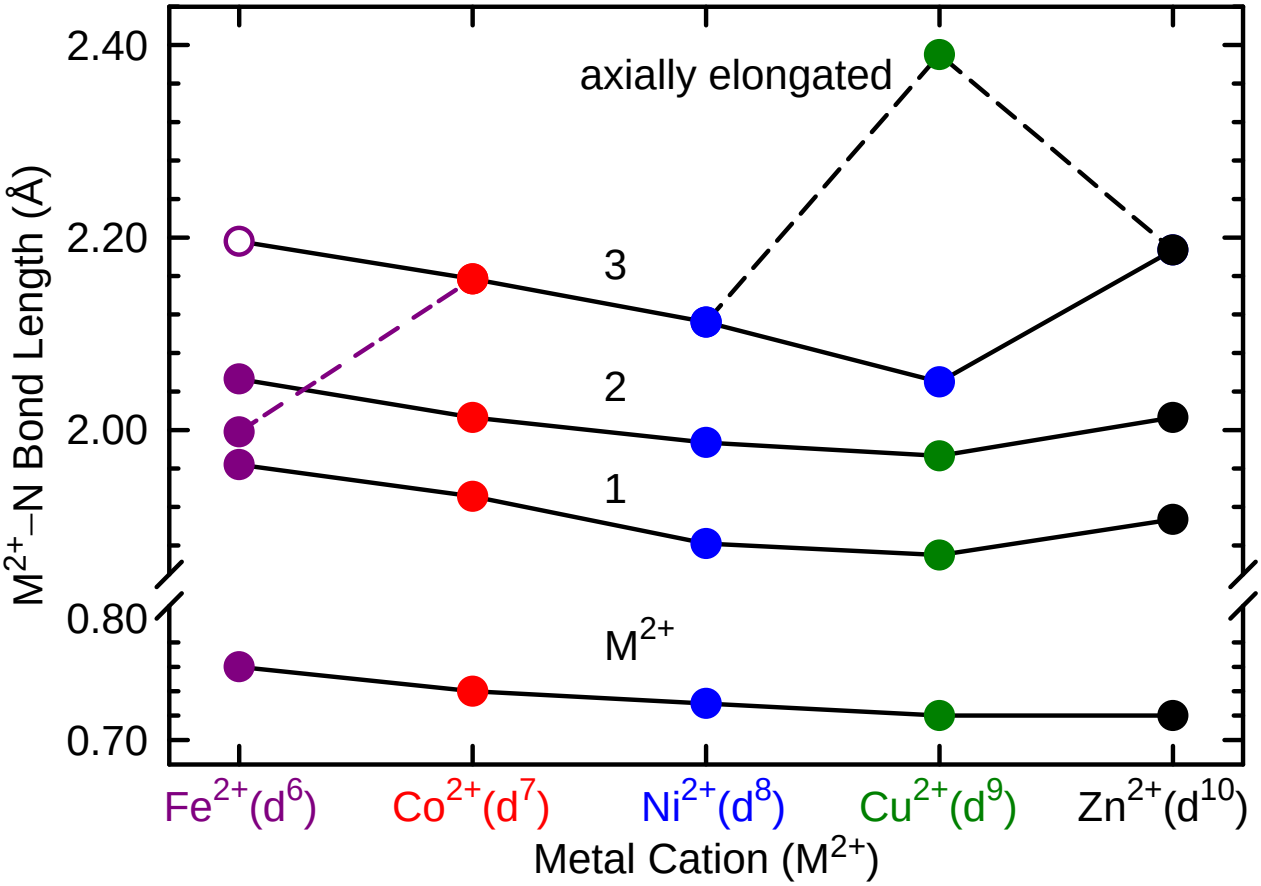
2.40
2.20
2.00
0.80
0.70
M2+–N Bond Length (Å)
axially elongated
3
2
1
M2+
Fe2+(d6)
Co2+(d7)
Ni2+(d8)
Cu2+(d9)
Zn2+(d10)
Metal Cation (M2+)

Figure 4.5.

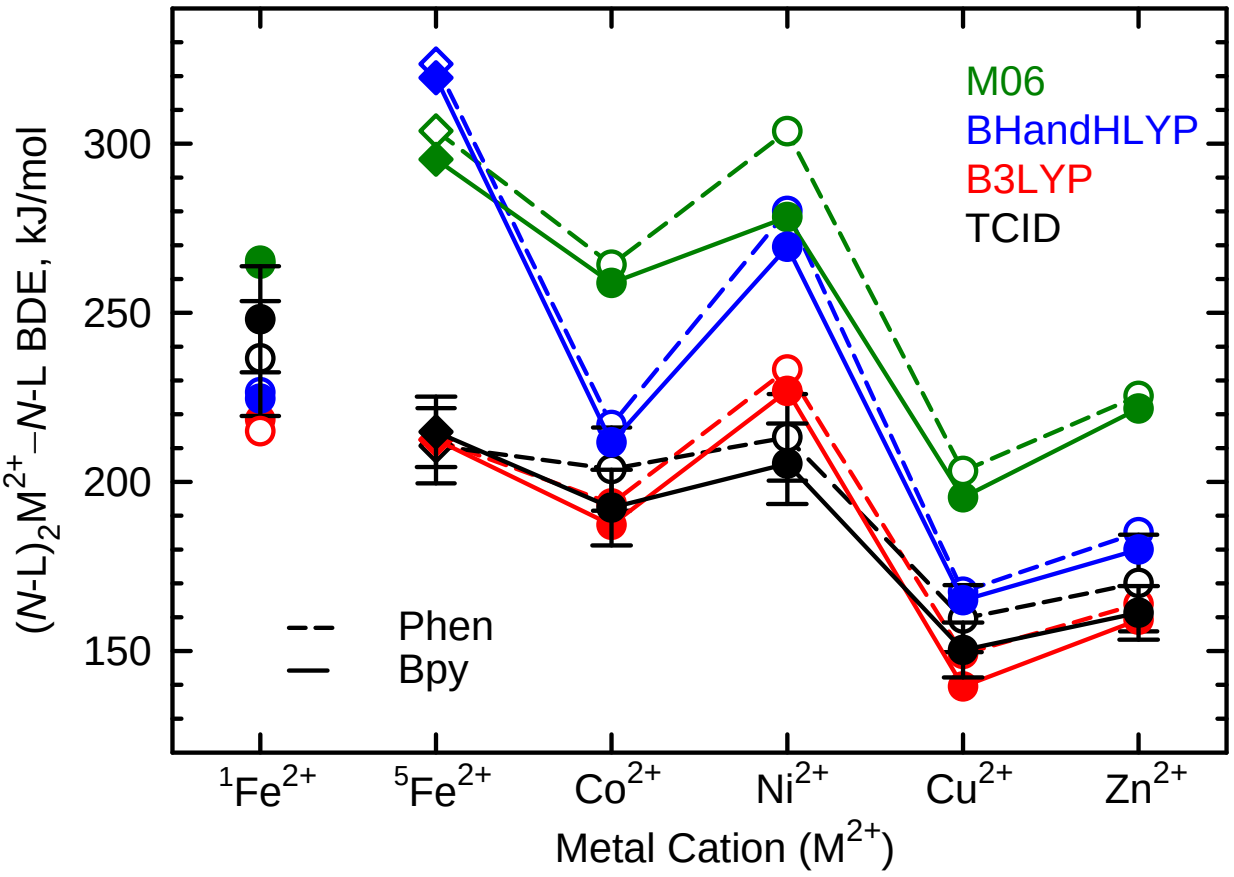
M06
BHandHLYP
B3LYP
TCID
Phen
Bpy
(N-L)2M2+–N-L BDE, kJ/mol
300
250
200
150
1Fe2+
5Fe2+
Co2+
Ni2+
Cu2+
Zn2+
Metal Cation (M2+)

Figure 4.6.

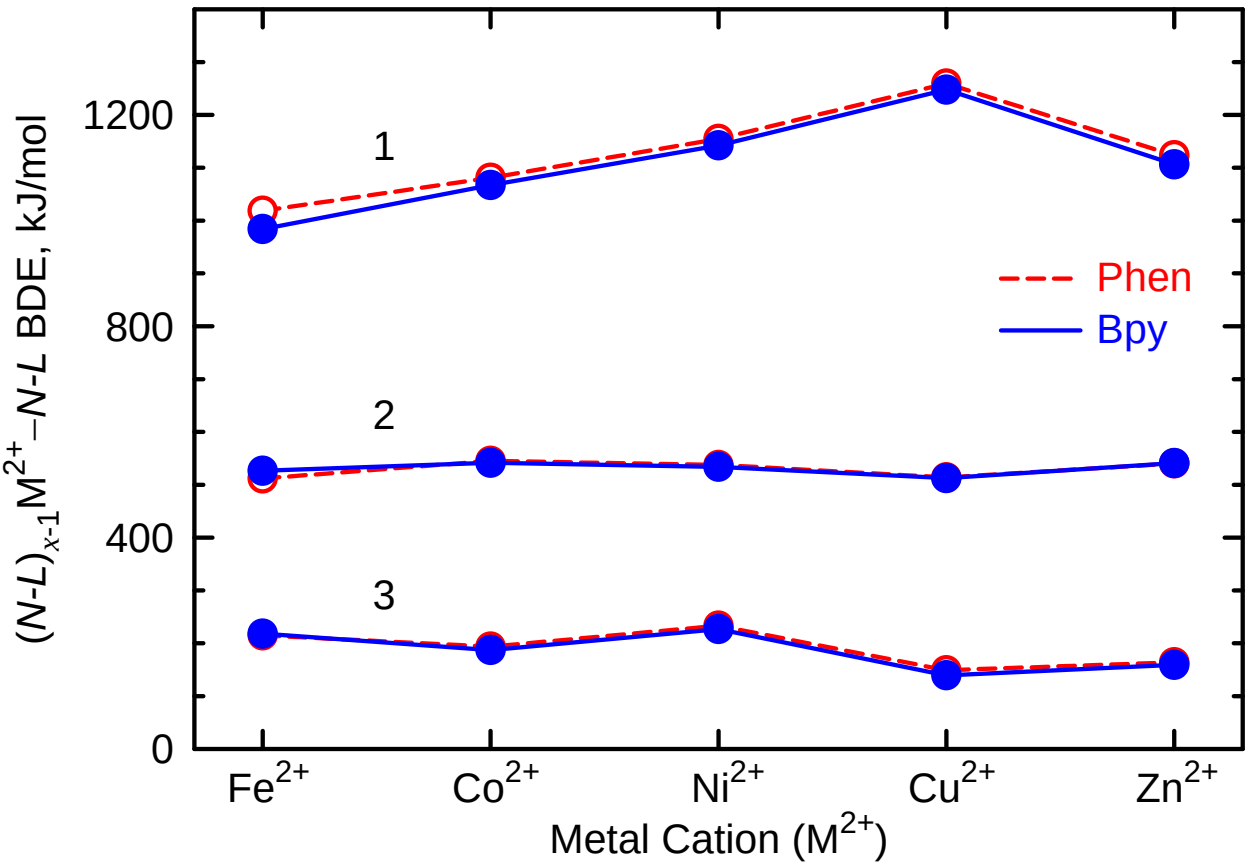
1200
800
400
0
1
2
3
Phen
Bpy
$(N\text{-}L)_{x\text{-}1}M^{2+}$–$N$-$L$ BDE, kJ/mol
Fe^{2+}
Co^{2+}
Ni^{2+}
Cu^{2+}
Zn^{2+}
Metal Cation (M^{2+})

Figure 4.7.

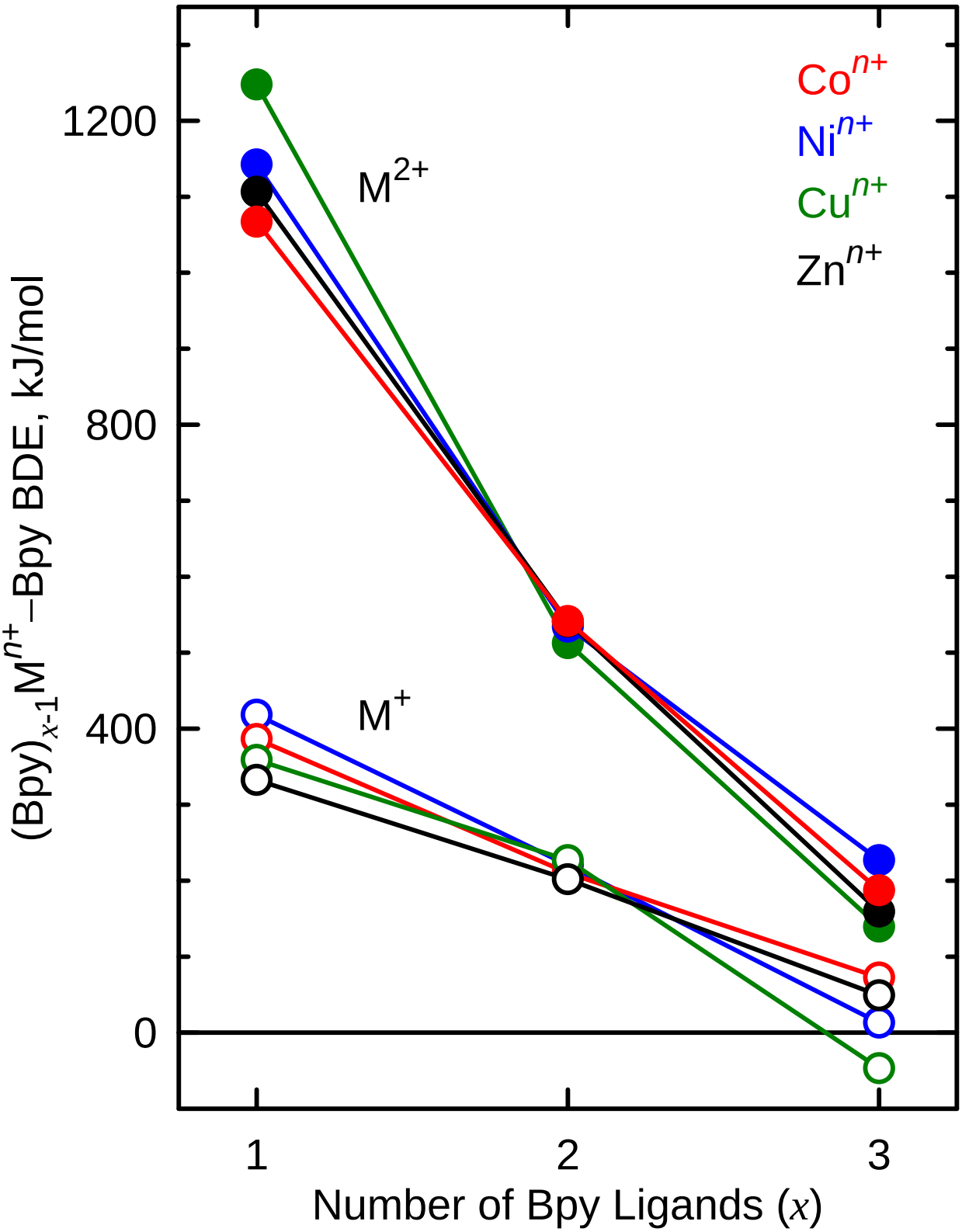
1200
800
400
0
1
2
3
Number of Bpy Ligands (x)
(Bpy)x-1Mn+–Bpy BDE, kJ/mol
M2+
M+
Con+
Nin+
Cun+
Znn+

Figure 4.8.

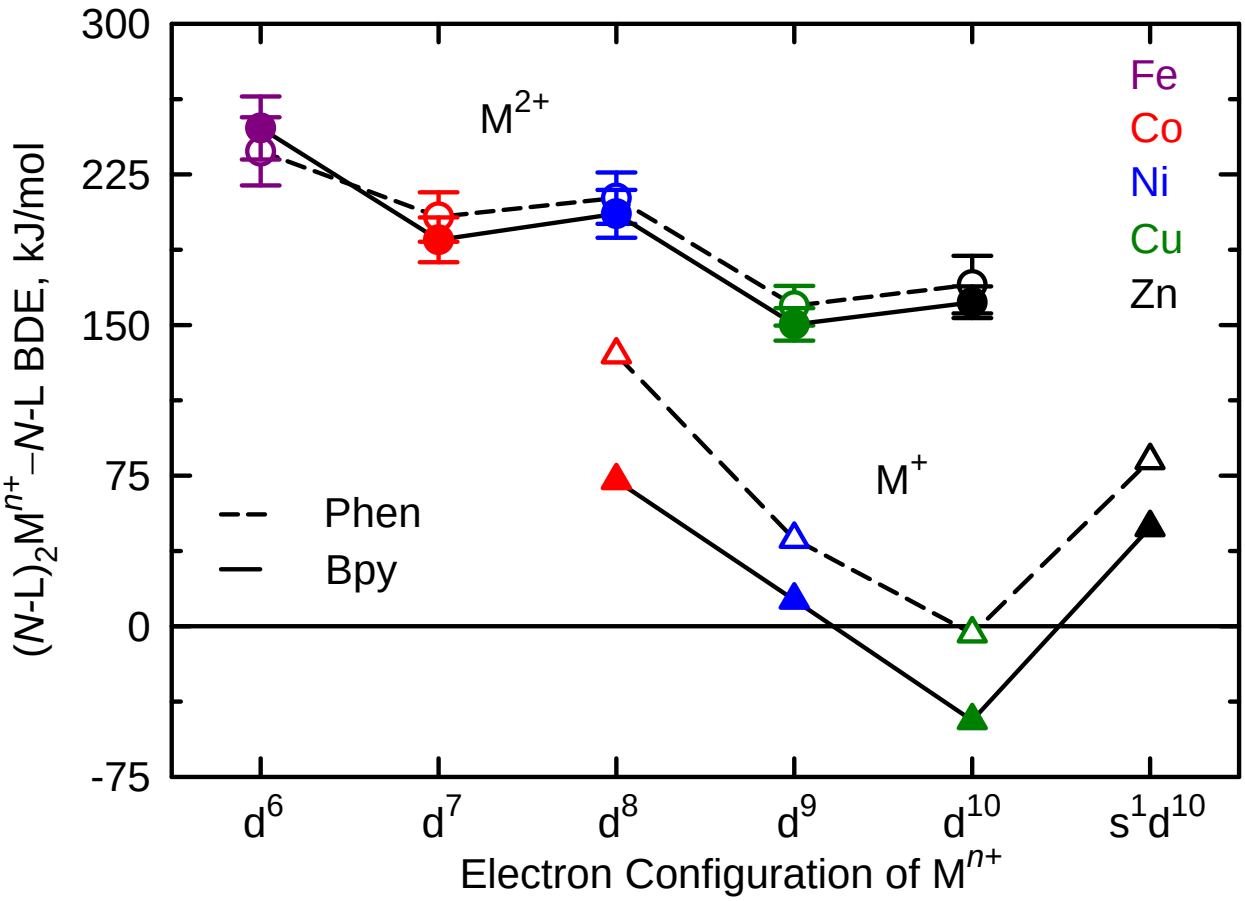
300
225
150
75
0
-75
(N-L)2Mn+–N-L BDE, kJ/mol
M2+
M+
Fe
Co
Ni
Cu
Zn
Phen
Bpy
d6
d7
d8
d9
d10
s1d10
Electron Configuration of Mn+

CHAPTER 5

INFLUENCE OF THE d ORBITAL OCCUPATION ON THE STRUCTURES AND SEQUENTIAL BINDING ENERGIES OF PYRIDINE TO THE LATE FIRST-ROW DIVALENT TRANSITION METAL CATIONS: A DFT STUDY

5.1 Introduction

Nitrogen-donor ligands are featured prominently as organic building blocks in many transition metal complexes.[1] In particular, the pyridine (Pyr) ligand has been widely used in the industrial synthesis of herbicides and catalysts.[2,3] The ability of the pyridyl moieties of polypyridyl ligands to chelate with transition metals can be used in the design and synthesis of supramolecular complexes.[4] The design, synthesis, and characterization of supramolecular complexes have become very active areas in coordination chemistry due to the novel topologies, fascinating structural diversities, and special chemical and physical properties of supramolecular complexes as well as their potential applications in electrical conductivity, host-guest chemistry, catalysis, and luminescent materials.[5,6] The design of supramolecular complexes depends heavily on understanding and exploiting the nature and geometric arrangement of the contacts between the supramolecular building blocks.[7] Transition metal cations such as Fe^{2+}, Co^{2+}, Ni^{2+}, Cu^{2+}, and Zn^{2+} have the potential to bind more than one Pyr ligand from simple mono- to hexa-coordinated, are readily available, and exhibit redox properties. Coordinated metal cations can also play bridging roles, hence these transition metal cations are favorable for creating a variety of metallo-supramolecular complexes. Pyr is an interesting ligand because it possesses a wealth of orbitals that can be used for bonding with metal cations. The nitrogen lone pair can donate electron density to

the metal cation forming strong metal-ligand electrostatic interactions that generally dominates the binding. The π-orbitals of the Pyr ligand can also act as electron donors, whereas the delocalized π* antibonding orbitals can act as acceptors of electron density. The Pyr ligand can also utilize hydrogen-bonding and aromatic π–π stacking for coordination.[8] The Pyr ligand can also be derivatized to increase its usefulness in building supramolecules. In the process of derivatization, other important functional groups can be incorporated depending on the use of the final product(s). For example, derivatized forms of Pyr have been used to build drug molecules as the aromatic rings and their interactions are crucial for activity.[9,10] The ability to take advantage of all of these interactions makes Pyr a particularly good building block for the construction of supramolecular structures. The combination of transition metal cations with Pyr and Pyr-based ligands can be used to tune the properties of the resulting supramolecular structures extending their utility to photoluminescent materials with potential applications based on charge transfer transitions.[11,12] A gas phase study of metal cation-Pyr complexes provides an ideal environment for examining the intrinsic binding in the absence of the effects of solvent and counterions. The ability to produce both coordinatively saturated and unsaturated complexes in the gas phase allows the binding interactions to be examined as a function of the extent of ligation. The chemical insight gained regarding the relationship between structure and binding can be used to further elucidate the principles that guide related molecular self-assemblies.

In this study, we investigate Pyr complexes of the late first-row divalent transition metal cations to better understand the structure and bonding in this class of transition metal coordination complexes. We characterize the structures and sequential binding energies of Pyr for the entire first coordination sphere to five first-row divalent transition metal cations.

We explore the periodic trends in the geometric structure and strength of binding by systematically varying the d electron occupation from $Fe^{2+}(d^6)$ to $Co^{2+}(d^7)$ to $Ni^{2+}(d^8)$ to $Cu^{2+}(d^9)$ to $Zn^{2+}(d^{10})$. To further assess the effects of the d-orbital occupation on the structures and sequential BDEs, the structures of $Ca^{2+}(Pyr)_x$ complexes are compared to those of the $M^{2+}(Pyr)_x$ complexes to Fe^{2+}, Co^{2+}, Ni^{2+}, Cu^{2+}, and Zn^{2+}. To understand how the charge/oxidation state of the metal cation influences the binding interactions, we compare the structures and BDEs determined here to those for the analogous Pyr complexes to the first-row monovalent transition metal cations, Co^+, Ni^+, Cu^+, and Zn^+ previously investigated.[13–17] Comparisons are also made to the analogous $M^{2+}(water)_x$,[18,19] $M^{2+}(imidazole)_x$,[20] $M^{2+}(2,2'\text{-bipyridine})_x$, and $M^{2+}(1,10\text{-phenanthroline})_x$ complexes previously investigated.[21,22]

5.2 Theoretical Calculations

Theoretical calculations were performed for the $M^{2+}(Pyr)_x$ complexes, where $M^{2+} = Fe^{2+}$, Co^{2+}, Ni^{2+}, Cu^{2+}, and Zn^{2+}, and x = 1–6, using the Gaussian 09 suite of programs.[23] The relative energies of all possible spin states of the $M^{2+}(Pyr)_x$ complexes were carefully evaluated to determine the spin state of the ground-state species. In this work, the following spin states were examined: singlet, triplet, and quintet for $Fe^{2+}(Pyr)_x$; doublet and quartet for $Co^{2+}(Pyr)_x$; singlet and triplet for $Ni^{2+}(Pyr)_x$; doublet for $Cu^{2+}(Pyr)_x$; and singlet for $Zn^{2+}(Pyr)_x$ complexes. Further details of the theoretical calculations are given in Chapter 2.

5.3 Theoretical Results

5.3.1 Structures

Theoretical structures of the $M^{2+}(Pyr)_x$ complexes, where $M^{2+} = Fe^{2+}$, Co^{2+}, Ni^{2+}, Cu^{2+}, Zn^{2+}, and Ca^{2+} and x = 1–6 were calculated using the Gaussian 09 suites of programs[23] as described in section 5.2. The B3LYP scaled vibrational frequencies and rotational constants for the ground-state structures of Pyr and the $M^{2+}(Pyr)_x$ complexes are listed in Tables C.1 and C.2 of Appendix C. The ground electronic spin states of the $M^{2+}(Pyr)_x$ complexes to Fe^{2+}, Co^{2+}, Ni^{2+}, Cu^{2+}, Zn^{2+}, and Ca^{2+} were found to be the same as that of the bare metal cation, quintet, quartet, triplet, doublet, singlet, and singlet, respectively, for all values of x. Relative energies of the $M^{2+}(Pyr)_x$ complexes computed for the various possible spin states of the Fe^{2+}, Co^{2+}, and Ni^{2+} are summarized in Table 5.1. In all cases, spin contamination of the $M^{2+}(Pyr)_x$ complexes was eliminated in the geometry and wave-function optimization procedures. The B3LYP/6-31G* ground-state structures of the $M^{2+}(Pyr)_x$ complexes are shown in Figure 5.1. Ground-state structures of the $M^{2+}(Pyr)_x$ complexes to the transition metal cations at the BHandHLYP/6-31G* and M06/6-31G* levels of theory are highly parallel to those found using B3LYP/6-31G* theory. Relevant structural details of the B3LYP/6-31G*, BHandHLYP/6-31G*, and M06/6-31G* optimized structures for the $M^{2+}(Pyr)_x$ complexes are listed in Table 5.2 and Table C.3 of Appendix C. Cartesian coordinates of the B3LYP/6-31G* optimized geometries of the ground-state structures of the neutral Pyr ligand and $M^{2+}(Pyr)_x$ complexes are shown in Table C.4 of Appendix C.

In the $M^{2+}(Pyr)_x$ complexes, the M^{2+} cation binds to the nitrogen lone pair(s) regardless of the identity of the metal cation or the level of theory employed, in agreement

with previous results obtained for the analogous $M^+(Pyr)_x$ complexes.[13-17] Because experimental structures and sequential BDEs for the $M^{2+}(Pyr)_x$ complexes have not been reported, we are unable to assess which of the three computational methods most accurately describes the geometries and binding in these complexes. However, parallel studies of the $M^{2+}(Phen)_x$ and $M^{2+}(Bpy)_x$ complexes suggest that B3LYP performs the best.[21,22] Therefore, the following discussion focuses on the B3LYP results, and summarizes similarities and differences found using the BHandHLYP and M06 theoretical methods. The $M^{2+}(Pyr)_x$ complexes adopt coordination geometries that closely approach the ideal geometries predicted by the valence shell electron pair repulsion (VSEPR) model.[24]

5.3.1.1 $M^{2+}(Pyr)$

All $M^{2+}(Pyr)$ complexes adopt a linear coordination geometry with M^{2+}–N bond lengths that vary with the identity of the metal cation. The M^{2+}–N bond length in the $Ca^{2+}(Pyr)$ complex is much longer than those in the $M^{2+}(Pyr)$ complexes to the transition metal cations. For the B3LYP/6-31G* optimized structures, the M^{2+}–N bond lengths decrease from Ca^{2+}(2.377 Å) to Fe^{2+}(1.939 Å) to Co^{2+}(1.854 Å) to Ni^{2+}(1.848 Å) to Cu^{2+}(1.844 Å), and then slightly increase for Zn^{2+}(1.870 Å). Parallel behavior is found for the BHandHLYP and M06 structures of the transition metal complexes. For the transition metal complexes, trends across all three levels of theory are very similar with M06 bond lengths generally being the shortest, BHandHLYP the longest, and B3LYP intermediate.

5.3.1.2 $M^{2+}(Pyr)_2$

In all $M^{2+}(Pyr)_2$ complexes, the Pyr ligands take on a linear coordination geometry with an $\angle NM^{2+}N$ bond angle of ~180.0° regardless of the identity of the metal cation. The Pyr ligands are twisted such that the planes of the Pyr rings are roughly perpendicular to each

other to minimize ligand-ligand repulsive interactions. In all cases, the two M^{2+}–N bond lengths are equal and ~0.05 Å longer than those of the analogous M^{2+}(Pyr) complexes. The M^{2+}–N bond lengths in the $Ca^{2+}(Pyr)_2$ complex are again much longer than in the $M^{2+}(Pyr)_2$ complexes to the transition metal cations. For the B3LYP/6-31G* optimized structures, the M^{2+}–N bond lengths decrease from Ca^{2+} (2.422 Å) to Fe^{2+} (1.953 Å) to Co^{2+} (1.908 Å) to Ni^{2+} (1.896 Å) to Cu^{2+} (1.877 Å), and increase slightly for Zn^{2+} (1.884 Å), parallel to that found for the M^{2+}(Pyr) complexes. Parallel behavior is found for the BHandHLYP and M06 structures of the transition metal complexes. Trends across these three levels of theory are fairly systematic with M06 bond lengths generally being the shortest, BHandHLYP the longest, and B3LYP intermediate.

5.3.1.3 $M^{2+}(Pyr)_3$

The $M^{2+}(Pyr)_3$ complexes to Ca^{2+}, Fe^{2+}, Co^{2+}, and Zn^{2+} adopt a trigonal planar coordination geometry, where the $\angle NM^{2+}N$ bond angles are ~120.0° and the three M^{2+}–N bond distances are essentially equal. However, in the complexes to Ni^{2+} and Cu^{2+}, the metal cation adopts a T-shaped coordination geometry with two different M^{2+}–N bond lengths and $\angle NM^{2+}N$ bond angles. The Pyr ligands are twisted relative to each other by ~76.1° in the trigonal planar structures, and by ~67.1° and 82.6° in the T-shaped structures to minimize ligand-ligand repulsive interactions. The M^{2+}–N bond lengths predicted by B3LYP/6-31G* theory decrease from Ca^{2+} (2.455 Å) to Fe^{2+} (2.019 Å) to Co^{2+} (1.969 Å) to Ni^{2+} (1.940, 1.945 (2) Å) to Cu^{2+} (1.910 (2), 1.929 Å), and increase for Zn^{2+} (1.958 Å), as found for the M^{2+}(Pyr) and $M^{2+}(Pyr)_2$ complexes. Parallel behavior is found for the BHandHLYP and M06 structures of the transition metal complexes. Again M06 predicts the shortest M^{2+}–N bond lengths, BHandHLYP the longest, and B3LYP intermediate.

5.3.1.4 $M^{2+}(Pyr)_4$

The $M^{2+}(Pyr)_4$ complexes to Fe^{2+}, Co^{2+}, Ni^{2+}, Cu^{2+}, and Zn^{2+} adopt a distorted tetrahedral coordination geometry, whereas $Ca^{2+}(Pyr)_4$ adopts an almost perfect tetrahedral coordination geometry. In all cases, the four M^{2+}–N bond lengths are equal. The distorted tetrahedral geometries result in different $\angle NM^{2+}N$ bond angles such that two similar, comparatively smaller and four larger angles are found for the transition metal complexes, whereas $Ca^{2+}(Pyr)_4$ exhibits equal $\angle NM^{2+}N$ bond angles of 109.5°. The $Cu^{2+}(Pyr)_4$ complex exhibits more significant distortion from an ideal tetrahedral coordination geometry as shown by the larger $\angle NCu^{2+}N$ bond angles of 97.2° and 141.9°, and displays a coordination geometry closer to square planar. The Pyr ligands are twisted relative to each other by ~64.4° in $M^{2+}(Pyr)_4$ complexes to Ca^{2+}, Fe^{2+}, Co^{2+}, Ni^{2+}, and Zn^{2+}, and by ~63.7° and 91.5° in the $Cu^{2+}(Pyr)_4$ complex to reduce ligand-ligand repulsive interactions. The M^{2+}–N bond lengths determined using B3LYP/6-31G* again decrease from Ca^{2+} (2.490 Å) to Fe^{2+} (2.079 Å) to Co^{2+} (2.028 Å) to Ni^{2+} (2.013 Å) to Cu^{2+} (2.004 Å), and then slightly increase for Zn^{2+} (2.032 Å). Analogous behavior is also found for the BHandHLYP and M06 structures of the transition metal complexes. In general, M06 predicts the shortest bond lengths, BHandHLYP the longest, and B3LYP intermediate.

5.3.1.5 $M^{2+}(Pyr)_5$

The $M^{2+}(Pyr)_5$ complexes to Fe^{2+}, Co^{2+}, and Zn^{2+} adopt a trigonal bipyramidal coordination geometry. Axial elongation is observed such that the three equatorial ligands exhibit comparatively shorter M^{2+}–N bond lengths than the two axial ligands. In contrast, the $Ca^{2+}(Pyr)_5$, $Ni^{2+}(Pyr)_5$, and $Cu^{2+}(Pyr)_5$ complexes adopt a square pyramidal coordination geometry with four nitrogen donor atoms in the equatorial plane and one coordinated

nitrogen donor atom in the apical position. The Pyr ligands are twisted relative to each other by ~57.1° and 69.1° in the trigonal bipyramidal and square pyramidal coordination geometries, respectively, to minimize ligand-ligand repulsive interactions. The M^{2+}–N bond lengths determined at the B3LYP/6-31G* level of theory decrease from Ca^{2+} (2.523, 2.553 Å) to Fe^{2+} (2.161, 2.229 Å) to Co^{2+}(2.090, 2.211 Å) to Ni^{2+} (2.061, 2.117 Å), and slightly increase for Cu^{2+} (2.065, 2.277 Å) and Zn^{2+}(2.098, 2.241 Å). Nearly parallel behavior is found for the BHandHLYP and M06 structures of the transition metal complexes. Trends across all three levels of theory are generally systematic such that the M06 bond lengths are the shortest, BHandHLYP the longest, and B3LYP intermediate.

5.3.1.6 $M^{2+}(Pyr)_6$

All of the $M^{2+}(Pyr)_6$ complexes adopt distorted octahedral coordination geometries. The six M^{2+}–N bond lengths are equal in all of the $M^{2+}(Pyr)_6$ complexes except for $Cu^{2+}(Pyr)_6$, which undergoes Jahn-Teller distortion resulting in four short Cu^{2+}–N equatorial bonds and two long Cu^{2+}–N axial bonds. In all cases, the $\angle NM^{2+}N$ bond angles are ~89.9° and 179.8°. The Pyr ligands are twisted relative to each other by ~49.5° in the $M^{2+}(Pyr)_6$ complexes to Ca^{2+}, Fe^{2+}, Co^{2+}, Ni^{2+}, and Zn^{2+} and by ~55.6° in the $Cu^{2+}(Pyr)_6$ complex to minimize ligand-ligand repulsive interactions. The M^{2+}–N bond lengths determined using B3LYP/6-31G* theory decrease from Ca^{2+} (2.603 Å) to Fe^{2+} (2.302 Å) to Co^{2+} (2.267 Å) to Ni^{2+} (2.220 Å) to Cu^{2+} (2.027 Å), and increase for Zn^{2+} (2.279 Å) when comparing the equatorial Cu^{2+}–N bond lengths. Jahn-Teller distortion in the $Cu^{2+}(Pyr)_6$ complex results in significant lengthening of the Cu^{2+}–N axial bonds, by 1.147 Å. The BHandHLYP and M06 levels of theory find similar trends in the M^{2+}–N bond lengths of the transition metal

complexes. Again, M06 bond lengths are generally the shortest, BHandHLYP the longest, and B3LYP intermediate.

5.3.2 Sequential BDEs

The sequential BDEs for the $M^{2+}(Pyr)_x$ complexes, where M^{2+} = Fe^{2+}, Co^{2+}, Ni^{2+}, Cu^{2+}, and Zn^{2+} and x = 1–6 were calculated as described in Section 5.2 and Chapter 2, are listed in Table 5.3 and Table C.5 of Appendix C, and plotted as a function of the number of Pyr ligands bound, x, in Figure 5.2. Table 5.4 and Table C.6 of Appendix C lists the enthalpic and entropic corrections needed to convert the 0 K BDEs to 298 K bond enthalpies and free energies. As can be seen in Figure 5.2, the sequential BDEs calculated using the 6-311+G(2d,2p) basis set fall off monotonically with increasing ligation for all five transition metal cations regardless of which theory is employed. Binding of the first Pyr ligand is quite strong, and exceeds 620 kJ/mol for all five transition metal cations at the B3LYP level of theory. Binding of additional Pyr ligands becomes progressively weaker such that binding of the second Pyr ligand is ~60% as strong as binding of the first Pyr ligand at the B3LYP level of theory. The second sequential BDEs are still quite strong, and vary between ~400–500 kJ/mol at the B3LYP level of theory, and thus are comparable to or stronger than a typical C–C bond (~400 kJ/mol). The strength of binding continues to fall off such that binding of the third, fourth, fifth, and sixth Pyr ligands is ~38%, 24%, 10%, and 6.3% as strong as binding of the first Pyr ligand (B3LYP theory). The third, fourth, fifth, and sixth sequential BDEs are all weaker than a typical C–C bond and vary between ~240–320 kJ/mol, ~150–190 kJ/mol, ~40–90 kJ/mol, and ~30–55 kJ/mol, respectively. Trends in the sequential BDEs computed using the M06 and BHandHLYP functionals are highly parallel.

To illustrate the importance of d orbital effects on the binding, the sequential BDEs of the $M^{2+}(Pyr)_x$ complexes calculated using the 6-31G* basis set are compared to values obtained using the 6-311+G(2d,2p) basis set in Figure 5.3. As can be seen in the figure, the computed binding energy of the first Pyr ligand is significantly weaker than determined using the extended 6-311+G(2d,2p) basis set for all five metal cations. In contrast, the computed sequential BDEs for binding of additional Pyr ligands using the 6-31G* basis set are relatively parallel to and only moderately exceed the values determined using the 6-311+G(2d,2p) basis set. These results clearly establish the importance of the additional diffuse and polarization functions for computing accurate BDEs, especially for binding of the first ligand where sd hybridization effects are expected to be very important to the binding. Analogous comparisons for the BHandHLYP and M06 functionals are highly parallel to that found for the B3LYP functional.

5.4 Discussion

5.4.1 Nature of the Binding in $M^{2+}(Pyr)_x$ Complexes

Both electrostatic interactions and charge transfer are important contributors to the binding in the $M^{2+}(Pyr)_x$ complexes. As discussed above, the M^{2+} cations bind to the nitrogen lone pairs enabling very strong ion-dipole and ion-induced dipole interactions as the M^{2+}–N bonds are oriented along the dipoles of the Pyr ligands. The dominant charge transfer interactions involve ligand-to-metal σ donation of the nitrogen lone pairs of the Pyr ligands to the unoccupied valence shell orbitals (s, p, and d_σ) of the metal cation forming strong dative M^{2+}–N bonds. The binding is also enhanced by metal-to-ligand charge transfer via π backdonation from the occupied d_π orbitals of the metal cation to the unoccupied π* orbitals of the Pyr ligand. π Backdonation is quite favorable as Pyr is a strong π acceptor, and

increases as the occupation of the d_π orbitals of the metal cation increases. Additional ligand-to-metal charge transfer via π donation from the occupied orbitals of the Pyr ligands to unoccupied d_π orbitals of the metal cation is also possible, however these interactions are not very significant for the $M^{2+}(Pyr)_x$ complexes because Pyr is a weak π donor.

The nature of the metal-ligand interactions that underlie the $M^{2+}(Pyr)_x$ complexes can be evaluated using natural bond orbital (NBO) analysis. The calculated natural orbital populations and the NBO charges of the $M^{2+}(Pyr)_x$ complexes at B3LYP/6-31G* and B3LYP/6-311+G(2d,2p) levels of theory are summarized in Table 5.5, parts a and b, respectively. The natural valence electronic configuration for the M^{2+} cation, constrained to the 4s, 3d, 4p, 4d, and 5p atomic orbitals may be represented by the $4s^n3d^m4p^j4d^k5p^l$ formula, where n = 0.13–0.70, m = 6.00–10.00, j = 0.01–0.37, k = 0.01–0.07, and l = 0.00–0.01, for all $M^{2+}(Pyr)_x$ complexes as shown in Table 5.5, part a. Based on the above results, one can conclude that the M^{2+} cation coordination with nitrogen atoms is mainly on 4s, 3d, and 4p orbitals (the electron number of other orbits is so small that can be omitted). Compared to the valence electronic configuration of the bare M^{2+} cations, $4s^03d^6$, $4s^03d^7$, $4s^03d^8$, $4s^03d^9$, and $4s^03d^{10}$ for Fe^{2+}, Co^{2+}, Ni^{2+}, Cu^{2+}, and Zn^{2+}, respectively, the results also suggest that electron transfer from lone pair orbitals of nitrogen to different orbitals of M^{2+} cations occurs in all the $M^{2+}(Pyr)_x$ complexes. In the $M^{2+}(Pyr)_x$ complexes, charge is also transferred from the metal orbitals to the Pyr ligand orbitals. The extent of π-back bonding in the $M^{2+}(Pyr)_x$ complexes may be estimated by the amount of charge (q) transferred from the M^{2+} cation to the nitrogen and these are summarized in Table 5.5, part b. The charge on the M^{2+} cation and *N*-donor atom changes with basis sets presumably due to variation of the hybrid functional. As can be seen in Table 5.5b, the net charge on the free metal cation, $q_{M^{2+}}$ is positive two at

B3LYP/6-31G* and B3LYP/ 6-311+G(2d,2p) levels of theory. In the $M^{2+}(Pyr)_x$ complexes, the magnitude of $q_{M^{2+}}$ decreases being accompanied by decreasing negative net charge on the nitrogen atom, q_N = –0.668 to –0.570 at B3LYP/6-31G* level of theory, that agrees well with expectations based on electrostatic interactions. This also implies that there is significant charge transfer from the nitrogen atom to the M^{2+} cation that causes the M^{2+} cation to lose charge of 2.000 and to retain a small amount of charge of ~0.853 to 1.482 at B3LYP/6-31G*, which takes place mainly through nitrogen free electron pairs with dative bonding. The charges of the M^{2+} cations are found to be decreased in the $M^{2+}(Pyr)_x$ complexes for x = 1–4, whereas the charges in the $M^{2+}(Pyr)_5$ and $M^{2+}(Pyr)_6$ are found to be increased compared to that of the free metal cation, $q_{M^{2+}}$ at B3LYP/6-311+G(2d,2p), suggesting a larger metal–nitrogen charge polarization. This indicates that binding of the 5th and 6th Pyr ligands involves greater metal to ligand charge transfer than ligand to metal charge transfer. It is also worth noting that the nitrogen donor atom total charges slightly decrease or slightly increase during complexation. The increase in donor charge, q_N from –0.281 at B3LYP/6-311+G(2d,2p) in free nitrogen atom to ~0.034 to 0.294 during complexation suggests a back-donation from metal to ligand. The more positive charges on the nitrogen atoms also suggests that electrons move from many atoms in the Pyr ligand to metal during complexation due to hyperconjugation, suggesting that delocalization occurs. Therefore, the orbital mixings are responsible for the nature of the donor-acceptor bonds in the $M^{2+}(Pyr)_x$ complexes.

5.4.2 Influence of the d-Orbital Occupation on the Structures of $M^{2+}(Pyr)_x$

The structures of the $M^{2+}(Pyr)_x$ complexes to Fe^{2+}, Co^{2+}, Ni^{2+}, Cu^{2+}, and Zn^{2+} are similar to those of the analogous $Ca^{2+}(Pyr)_x$ complexes and are predominantly determined by minimizing ligand-ligand repulsive interactions as predicted by the VSEPR model.[24] However, the Ca^{2+}–N and M^{2+}–N bond distances differ markedly in the $M^{2+}(Pyr)_x$ complexes. For the $M^{2+}(Pyr)$ complexes, the M^{2+}–N bond distances decrease from Ca^{2+}(2.377 Å) to Fe^{2+}(1.939 Å) to Co^{2+}(1.854 Å) to Ni^{2+}(1.848 Å) to Cu^{2+}(1.844 Å), and then slightly increase for Zn^{2+}(1.870 Å). A decrease in the M^{2+}–N bond distance from Ca^{2+} to Cu^{2+} is expected on the basis of the sizes of these cations, and consequently, stronger electrostatic contributions to the binding. The trend in the M^{2+}–N bond lengths of the $M^{2+}(Pyr)$ complexes is predominantly determined by the ionic radii of the bare metal cations: 1.04 (Ca^{2+}), 0.76 (Fe^{2+}), 0.74 (Co^{2+}), 0.73 (Ni^{2+}), and 0.72 Å (Cu^{2+}). Zn^{2+} deviates from this simple trend as its radius, 0.72 Å is the same as that of Cu^{2+}, yet the M^{2+}–N bond length increases from Cu^{2+} to Zn^{2+}.[25] However, the difference between the ionic radius of the bare M^{2+} cation and the M^{2+}–N bond length (Δ_r) is much larger (~1.3 Å) for $Ca^{2+}(Pyr)$ as compared to the $M^{2+}(Pyr)$ complexes to the transition metal cations (~1.1 Å). Δ_r is smaller for the transition metal cations as a result of sd hybridization, which the transition metal cations undergo to reduce Pauli repulsion between the metal cation and the Pyr ligand. As shown in Table 5.5, the reduced positive charge retained on the metal cation and negative charge on the nitrogen atom(s) of the Pyr ligands provides strong evidence for significant charge transfer from the lone pair of the Pyr ligand to the M^{2+} cation. In addition, the increased populations of both the 4s and 3d orbitals of the metal cation upon binding of a Pyr ligand indicate that sd hybridization is indeed occurring. Such sd hybridization increases

favorable electrostatic contributions as well as orbital overlap between the Pyr ligand orbitals and the empty sd hybridized orbital of the M^{2+} cation leading to a decrease in M^{2+}–N bond lengths. The effects of sd hybridization increase from Fe^{2+} to Cu^{2+} as the d electron occupation increases, consistent with the decrease in the M^{2+}–N bond distances from Fe^{2+} to Cu^{2+}. The M^{2+}–N bond lengths for the $M^{2+}(Pyr)_2$ complexes decrease from Ca^{2+} to Fe^{2+} to Co^{2+} to Ni^{2+} to Cu^{2+} and increase slightly for Zn^{2+}, parallel to that found for the $M^{2+}(Pyr)$ complexes. For the $Ca^{2+}(Pyr)_2$ complex, $\Delta_r \sim 1.4$ Å whereas $\Delta_r \sim 1.2$ Å for the $M^{2+}(Pyr)_2$ complexes to the transition metal cations indicating that sd hybridization is still effective. Relatively parallel behavior is found for the larger complexes. However, the differences in the Δ_r values for the $Ca^{2+}(Pyr)_x$ versus the $M^{2+}(Pyr)_x$ complexes diminish as *x* increases and become roughly equal for the $Ca^{2+}(Pyr)_6$ and $M^{2+}(Pyr)_6$ complexes, suggesting that the effects of sd hybridization diminish as *x* increases because the additional Pyr ligands interact repulsively with the occupied sd hybridized orbital.

Jahn-Teller effects also influence the geometries of several of the $M^{2+}(Pyr)_x$ complexes, leading to structural distortions that remove orbital degeneracies and lower the symmetry and overall molecular energy of the complex.[26,27] Jahn-Teller effects lead to a T-shaped and a highly distorted tetrahedral coordination geometry for the $Cu^{2+}(Pyr)_3$ and $Cu^{2+}(Pyr)_4$ complexes, respectively. Cu^{2+} is subject to significant Jahn-Teller distortion because its d^9 electron configuration results in orbital degeneracy for the orbitals that point directly at the Pyr ligands in both complexes. Structural distortions that lead to a T–shaped geometry for the $Ni^{2+}(Pyr)_3$ complex are unrelated to Jahn-Teller effects because Ni^{2+} d^8 high spin is nondegenerate under the trigonal planar ligand field. Spin contamination is also ruled out as a cause for the distortion as is eliminated during the geometry and wave function

optimization procedures of the theoretical calculations for all of the $M^{2+}(Pyr)_x$ complexes. However, high spin d^8 Ni^{2+} is degenerate in the trigonal bipyramidal ligand field, and thus is subject to weak Jahn-Teller distortion leading to $Ni^{2+}(Pyr)_5$ adopting a low symmetry square pyramidal geometry. It is possible that loss of sd hybridization effects and ligand-ligand repulsion lead to distortions in the $Cu^{2+}(Pyr)_5$ complex as Cu^{2+} d^9 is nondegenerate in the trigonal bipyramidal ligand field, and therefore should not be subject to Jahn-Teller distortion. The d^9 electron configuration of Cu^{2+} is degenerate in the octahedral ligand field and is therefore subject to significant Jahn-Teller distortion, which leads to elongation of the M^{2+}–N bonds of the degenerate orbitals that directly interact with the Pyr ligands (axial elongation).

5.4.3 Trends in the Sequential BDEs

Trends in the sequential binding energies of the $M^{2+}(Pyr)_x$ complexes are illustrated in Figures 5.2 and 5.3. As can be seen in the Figure 5.2, the strength of binding of the Pyr ligands to the M^{2+} cations determined using 6-311+G(2d,2p) basis set falls off monotonically with increasing ligation for all five metal cations regardless of which theory is employed. The factors that contribute to the decrease in the sequential BDEs of $M^{2+}(Pyr)_x$ complexes include, attractive electrostatic interactions; charge transfer from the Pyr ligands to the metal cation; electronic orbital effects including ion core polarization, sd hybridization, and Jahn-Teller distortion; metal cation-ligand repulsion; and ligand-ligand repulsion. Because electrostatic interactions and charge transfer are both important contributors to the bonding in the $M^{2+}(Pyr)_x$ complexes, binding of the first ligand is quite strong, > 620 kJ/mol for all five cations at the B3LYP/6-311+G(2d,2p) level of theory. Binding of the second Pyr ligand is still quite strong at B3LYP/6-311+G(2d,2p) level of theory, and thus comparable to or

stronger than a typical C–C bond (~400 kJ/mol). In contrast, the first and second sequential BDEs of $M^{2+}(Pyr)_x$ complexes determined at B3LYP/6-31G* do not decrease monotonically with increasing number of Pyr ligands, Figure 5.3. This indicates that the first sequential BDE is more sensitive to the basis set used suggesting that 6-31G* basis set is insufficiently describing the d orbitals in the $M^{2+}(Pyr)$ complexes leading to lower binding energies compared to those of the $M^{2+}(Pyr)_2$ complexes. The electrostatic and charge transfer contributions to the binding of the third, fourth, fifth, and sixth ligands decrease upon sequential ligation for both basis sets because the effective charge retained by the metal cation decreases, and the M^{2+}–N bond distances increase as shown in Figure 5.1. In addition to the decrease in effective charge with ligation, an equally important cause of the decrease in the sequential BDEs with ligation is the loss of sd hybridization. Such sd hybridization removes electron density along the metal-ligand bonding axis, exposing the ligand to greater nuclear charge, allowing the first ligand to approach the metal cation more closely, and resulting in very strong binding of the first Pyr ligand. As the number of ligands increases, sd hybridization becomes much less efficient at reducing the metal cation-ligand repulsion, leading to weaker BDEs because the additional Pyr ligands are forced to interact repulsively with the occupied sd hybridized orbital of the M^{2+} cation. The increase in ligand-ligand repulsive interactions with each successive Pyr ligand bound also contributes to the fall off in the strength of binding with increasing ligation.

5.4.4 Influence of d Orbital Occupation on the Sequential BDEs of $M^{2+}(Pyr)_x$

Periodic trends in the sequential binding energies of the $M^{2+}(Pyr)_x$ complexes calculated at the B3LYP, BHandHLYP, and M06 levels of theory using 6-311+G(2d,2p) basis set are illustrated in Figure 5.4. The first sequential BDEs of the $M^{2+}(Pyr)$ complexes

determined using B3LYP/6-311+G(2d,2p) theory range between 620 and 920 kJ/mol, and increase from Fe^{2+} to Co^{2+} to Ni^{2+} to Cu^{2+} and decrease at Zn^{2+}. Because electrostatic interactions are major contributors to the binding in the M^{2+}(Pyr) complexes, the bonding is expected to increase from Fe^{2+} to Co^{2+} to Ni^{2+} to Cu^{2+} in accord with the decreasing ionic radii of the metal cations, as observed. The trend in the BDEs, Cu^{2+}(Pyr) > Zn^{2+}(Pyr) is reasonable as both cations have similar ionic radii, but Zn^{2+}(Pyr) encounters greater Pauli repulsion because its sd hybridized orbital is doubly occupied. Also obvious in the periodic trend of the M^{2+}(Pyr) complexes is the significant role that sd hybridization plays. Such sd hybridization increases favorable electrostatic contributions as well as orbital overlap between the ligand orbitals and the empty sd hybridized orbitals, thus facilitating ligand-to-metal charge transfer, and is also consistent with the increase in the BDEs from Fe^{2+} to Cu^{2+}. In comparison to B3LYP, BHandHLYP and M06 produce a roughly parallel trend with the difference in magnitude of the BDEs between the theories being as large as 170 kJ/mol. The second sequential BDEs of the $M^{2+}(Pyr)_2$ complexes range between 390–500 kJ/mol and exhibit small even-odd oscillations in magnitude from Fe^{2+} to Co^{2+} to Ni^{2+} to Cu^{2+} to Zn^{2+} as determined using B3LYP theory. The BDEs for Fe^{2+}, Co^{2+}, Ni^{2+}, and Cu^{2+} are of similar magnitude, whereas Zn^{2+} exhibits a much larger BDE, balancing its weaker binding of the first Pyr ligand. Compared to B3LYP, trends observed for BHandHLYP and M06 are again very roughly parallel with the difference in magnitude being < 70 kJ/mol between the theories. The third sequential BDEs of the $M^{2+}(Pyr)_3$ complexes range between 240–320 kJ/mol and increase from Fe^{2+} to Co^{2+}, and then decrease from Co^{2+} to Ni^{2+} to Cu^{2+} to Zn^{2+} as determined using B3LYP theory. The increase in the BDEs from Fe^{2+} to Co^{2+} arises from the increases in electrostatic interactions associated with the shorter M^{2+}–N bond lengths,

whereas the cause of the trends for the later metal cations is not obvious. Compared to B3LYP, the trends observed for BHandHLYP and M06 differ somewhat, but the difference in the magnitude of the BDEs among these three theories is much smaller than found for mono- and bis-complexes, ~50 kJ/mol for the tris-complexes. For the $M^{2+}(Pyr)_4$ complexes, the fourth sequential BDEs range from 140–200 kJ/mol as determined using B3LYP theory, and increase from Fe^{2+} to Co^{2+}, decrease for Ni^{2+} and Cu^{2+}, and increase again at Zn^{2+}, concomitant with the increase in electrostatic interactions across this period despite the minor difference (~2.8 kJ/mol) between Co^{2+} and Ni^{2+}. Jahn-Teller effects also contribute to the weak binding in the Cu^{2+} complex. Compared to B3LYP, the trends for BHandHLYP and M06 are relatively parallel, and the magnitudes of the BDEs again exhibit only modest differences, < 45 kJ/mol. The fifth sequential BDEs of the $M^{2+}(Pyr)_5$ complexes range between 40–90 kJ/mol (B3LYP) and increase from Fe^{2+} to Co^{2+} to Ni^{2+}, and then decrease for Cu^{2+} and Zn^{2+}. Again, the increase in BDEs of Fe^{2+}, Co^{2+}, and Ni^{2+} agree with the increase in electrostatic interactions across this series, whereas the effects of Jahn Teller distortion lead to a lower BDE for the Cu^{2+} complex relative to Fe^{2+}, Co^{2+}, and Ni^{2+}. The lower BDE for Zn^{2+} is attributed to an increase in Pauli electron-electron repulsion because its d_{z^2} orbital is doubly occupied. The B3LYP trend is highly parallel to BHandHLYP and M06 for all complexes except Co^{2+}, and the difference in magnitude across these three theories is again small and < 45 kJ/mol. The sixth sequential BDEs of the $M^{2+}(Pyr)_6$ complexes determined using B3LYP theory range from 30–55 kJ/mol and increase from Fe^{2+} to Co^{2+}, and then decrease from Co^{2+} to Zn^{2+}. The variation in BDEs in these five metal cations is small implying that the ligand-ligand repulsive interactions impose similar effects on the complexes to all five metal cations. For Fe^{2+} and Co^{2+}, the electrostatic component

seems to be the dominant contributor to the difference in their BDEs. Again, Jahn-Teller effect leads to a lower BDE for the Cu^{2+} complex, whereas Pauli electron-electron repulsion contributes to the low BDE for the Zn^{2+} complex. The trends across these three theories are relatively parallel for all the five metal cations. The difference in the magnitude of the BDEs between the three theories is again small, and < 45 kJ/mol for all five metal cations.

5.4.5 Influence of Charge on the Structures and Sequential BDEs of $M^{n+}(Pyr)_x$

The sequential BDEs of the $M^{2+}(Pyr)_x$ complexes are compared to those of the analogous $M^{+}(Pyr)_x$ complexes in Figure 5.5. As can be seen in the figure, the BDEs of the $M^{2+}(Pyr)_x$ complexes decrease monotonically as the extent of ligation increases. The BDEs are much larger, but the trend is similar to that observed for the $Zn^{+}(Pyr)_x$ complexes. In contrast, the trend in the BDEs differs from that observed for the $M^{+}(Pyr)_x$ complexes to Co^{+}, Ni^{+}, and Cu^{+}. In these latter complexes, the BDEs of the first and second Pyr ligands are quite strong, but decrease only slightly from the first to the second Pyr ligand. A sharp decrease in the BDEs occurs for binding of the third Pyr ligand, whereas a fairly small decrease in the BDEs is observed from the third to the fourth Pyr ligand. Periodic trends in the sequential BDEs of the $M^{2+}(Pyr)_x$ complexes roughly parallel those of the $M^{+}(Pyr)_x$ complexes, but differ in absolute magnitude as illustrated in Figure 5.5. For the mono-complexes, the BDEs increase from Co^{n+} to Ni^{n+} to Cu^{n+}, and then fall off from Cu^{n+} to Zn^{n+}. The $M^{n+}(Pyr)$ BDEs are inversely correlated with the ionic radii of the metal cation and directly correlated with the magnitude of the stabilization gained via sd hybridization, which increases with the d orbital occupation from Fe^{n+} to Cu^{n+}. As the extent of ligation increases, periodic trends in the BDEs remain similar with minor differences due to the s orbital occupation of the complexes to Zn^{+}.

As expected, the M^{2+} cations bind more strongly to the Pyr ligands than the analogous M^{+} cations due to stronger electrostatic interactions as a result of larger charge and smaller size of the metal cation (see Figures 5.5 and 5.6). The ratio between the BDEs of the M^{2+} to the M^{+} complexes is roughly 3.05:1 for the mono-, 2.41:1 for the bis-, 3.81:1 for the tris-, and 3.80:1 for the tetrakis-complexes. Inspite of these large differences in the binding energies resulting from charge effects, the differences in the geometries (i.e., the bond lengths and bond angles) for the analogous complexes are very minor. The M^{n+}–N bond lengths vary by < 0.1 Å, whereas the bond angles vary by < 5.0°. The highly parallel structures found for M^{2+} an M^{+} indicate that the structures are primarily determined by minimizing ligand-ligand repulsive interactions as previously discussed. However, the optimized ground-state geometries of several complexes do differ. For example, the d^{10} $Cu^{+}(Pyr)_3$ complex favors the high-symmetry trigonal planar coordination geometry, whereas the corresponding d^{9} $Cu^{2+}(Pyr)_3$ complex favors the low-symmetry T-shaped coordination geometry. This difference is related to the d-orbital occupation of the metal cation and how the d orbitals hybridize upon ligand binding. For this reason, comparison between the $M^{n+}(Pyr)_x$ complexes with the same electronic configurations, i.e., $Co^{+}(d^{8})$ vs Ni^{2+} (d^{8}), Ni^{+} (d^{9}) vs Cu^{2+} (d^{9}), and Cu^{+} (d^{10}) vs Zn^{2+} (d^{10}), do not show significant differences in their coordination geometries. As the number of Pyr ligands increases, the BDEs of the analogous $M^{2+}(Pyr)_x$ and $M^{+}(Pyr)_x$ complexes become closer as illustrated in Figure 5.6, indicating that one to two more Pyr ligands are required to stabilize the M^{2+} cations to a point where the sequential binding energies become comparable to those of the complexes to the M^{+} cations.

5.4.6 Comparison to $M^{2+}(Phen)_x$ and $M^{2+}(Bpy)_x$ Complexes

5.4.6.1 Ground Electronic Spin States

The ground electronic spin states of the $M^{2+}(Pyr)_x$ complexes to the Fe^{2+}, Co^{2+}, Ni^{2+}, Cu^{2+}, and Zn^{2+} were found to be quintet, quartet, triplet, doublet, and singlet, respectively for values of x = 1–6 when the B3LYP, BHandHLYP, and M06 methods are employed. These results suggest that Pyr is not a strong enough field ligand to induce spin changes upon sequential ligation. Similar results were found for the $M^{2+}(Phen)_x$ and $M^{2+}(Bpy)_x$ complexes to Co^{2+}, Ni^{2+}, Cu^{2+}, and Zn^{2+}, which bind in a bidentate fashion for values of x = 1–3, when the B3LYP, BHandHLYP and M06 theoretical methods were employed.[21,22] In contrast, addition of the third Phen or Bpy ligand to Fe^{2+} results in a change of spin state from quintet to singlet as determined using the B3LYP method, suggesting that Phen and Bpy are sufficiently strong field ligands capable of inducing spin change. However, the BHandHLYP and M06 methods suggest that no spin change occurs for the tris-complexes of Fe^{2+} to Phen and Bpy indicating that the theoretical methods used are incapable of properly describing the binding in these complexes.[28] The fact that no spin state change is found for the $Fe^{2+}(Pyr)_x$ complexes at all levels of theory is consistent with the weaker ligand field effects of Pyr as compared to the Phen and Bpy ligands.

5.4.6.2 Structures

Although the Pyr ligand is a building block of the Phen and Bpy ligands, and binds to metal cations in a similar fashion, modest differences in the binding geometries exist.[21,22] When an M^{2+} cation binds to two *N*-donor atoms as in the $M^{2+}(Pyr)_2$ complexes, the $\angle NM^{2+}N$ bond angles are ~180.0°, orienting the Pyr ligands as far from each other as possible to minimize ligand-ligand repulsive interactions, and maximize stabilization via sd

hybridization. Although both, the Phen and Bpy ligands bind via two *N*-donor interactions, these ligands are geometrically constrained and bind to M^{2+} with $\angle NM^{2+}N$ bond angles of 87.6–94.6°, and hence are unable to take full advantage of sd hybridization. The M^{2+}–N bond lengths increase in the order Pyr < Bpy < Phen for complexes with two *N*-donor interactions. With four and six *N*-donor interactions with the M^{2+} center, the interligand $\angle NM^{2+}N$ bond angles of the Bpy and Phen complexes closely approach those of the Pyr complexes. But because of the constrained geometries of the Bpy and Phen ligands, the intraligand $\angle NM^{2+}N$ bond angles hinder these complexes from achieving perfect tetrahedral or octahedral coordination geometries, whereas the Pyr ligands allow near optimal orientations of the *N*-donor atoms around the metal center resulting in complexes that exhibit almost perfect tetrahedral or octahedral coordination geometries. With four and six *N*-donor interactions with the M^{2+} center, the M^{2+}–N bond lengths increase in the order Bpy < Phen < Pyr, suggesting that the monodentate Pyr ligand experiences more ligand-ligand repulsion as compared to the bidentate Bpy and Phen ligands. The slightly shorter M^{2+}–N bond lengths of the $M^{2+}(Bpy)_x$ complexes as compared to the $M^{2+}(Phen)_x$ complexes are enabled by the flexibility of the central C–C bond that allows Bpy to form slightly more compact structures.

5.4.6.3 Energetics of Binding

As can be seen in Figure 5.7, the sequential BDEs of Pyr, Bpy, and Phen to the M^{2+} cations fall off rapidly with increasing ligation. The more rapid decrease in the sequential BDEs for the bidentate Phen and Bpy ligands arises because the electrostatic contributions to the binding decrease more rapidly upon sequential ligation as the chelating ligands provide two *N*-donor interactions such that the charge retained by M^{2+} decreases more rapidly than for the complexes to the monodentate Pyr ligand. The BDEs of the $M^{2+}(Pyr)_x$ complexes are

smaller as compared to those of the analogous $M^{2+}(Bpy)_x$ and $M^{2+}(Phen)_x$ complexes because Pyr is a monodentate ligand, whereas the Bpy and Phen ligands bind in a bidentate fashion. Comparisons based on the number of *N*-donor interactions rather than the number of ligands provides additional insight. With two *N*-donor interactions, the $M^{2+}(Phen)$ and $M^{2+}(Bpy)$ complexes exhibit slightly weaker binding energies as compared to the sum of the first and second sequential BDEs of $M^{2+}(Pyr)_x$ (see Figure 5.7, open circles). However, with four *N*-donor interactions, the $M^{2+}(Phen)_2$ and $M^{2+}(Bpy)_2$ complexes exhibit stronger second sequential binding energies as compared to the sum of the third and fourth sequential BDEs of $M^{2+}(Pyr)_x$. Similarly, with six *N*-donor interactions, $M^{2+}(Phen)_3$ and $M^{2+}(Bpy)_3$ exhibit slightly stronger third sequential binding energies as compared to the sum of the fifth and sixth sequential BDEs of $M^{2+}(Pyr)_x$. A similar trend is found for the total binding energies. As can be seen in Figure 5.8, for all five metal cations the total binding energy of the $M^{n+}(Pyr)_2$ complex is greater than the BDEs of the $M^{n+}(Bpy)$ or $M^{n+}(Phen)$ complexes with two *N*-donor interactions. However, as the number of *N*-donor interactions increases to four and six, the total binding energies of the bidentate complexes become greater than the analogous $M^{2+}(Pyr)_4$ and $M^{2+}(Pyr)_6$ complexes. This change in the trends in the sequential and total binding energies as the number of *N*-donor interactions increases is due to the constrained geometries of the bidentate ligands, Bpy and Phen, which do not allow optimum orientation of the intraligand *N*-donor atoms. Therefore, the $M^{n+}(Bpy)$ and $M^{n+}(Phen)$ complexes are unable to take full advantage of sd-hybridization, resulting in less favorable binding. With four and six *N*-donor interactions, the trend changes suggesting that the monodentate Pyr complex experiences more ligand-ligand repulsion as compared to the bidentate, $M^{n+}(Bpy)_x$ and $M^{n+}(Phen)_x$ complexes.

5.4.6.4 Chelation Effects

As can be seen in Figure 5.8, the differences ($-T\Delta S$) between the total enthalpies (ΔH) and total free energies (ΔG) of binding increase with increasing number of *N*-donor interactions regardless of the charge or identity of the metal cation. The charge of the cation does not significantly impact the magnitude of the $T\Delta S$ (entropy term), largely because it is primarily associated with loss of translational degrees of freedom upon binding. However, higher charge enables binding to more ligands and thus a greater overall chelate effect. As a result, the $M^{2+}(Pyr)_x$ complexes exhibit much larger differences in the total enthalpies and free energies of binding than the analogous $M^{2+}(Bpy)_x$ and $M^{2+}(Phen)_x$ complexes with the same number of *N*-donor interactions. Thus, higher levels of coordination can be achieved with the chelating ligands as the entropic cost of binding approaches and even exceeds the enthalpy of binding for the fifth and sixth Pyr ligands, whereas the binding energies of the third Phen and Bpy ligands are still quite large, ~139–320 kJ/mol. In solution, entropic effects will easily overcome the differences in the total enthalpies such that the free energies of binding will greatly favor the chelating ligands, Bpy and Phen, over the monodentate ligand, Pyr.

5.4.6.5 Charge Transfer

From previous studies of the $M^{2+}(Phen)_x$ and $M^{2+}(Bpy)_x$ complexes, where x = 1–3,[21,22] it was determined that the minimum number of ligands at which dissociative charge transfer is competitive with neutral ligand loss occurs at $x = 2$. For these complexes, the BDEs calculated for the mono-complexes exceed > 900 kJ/mol, suggesting that very strong electrostatic interactions dominate the binding. However, the high electron deficiency of the mono complexes makes them too reactive to generate in sufficient intensity to enable studies

of their CID behavior. In comparison, the BDEs of the bis-complexes vary between 500–600 kJ/mol, and competition between charge transfer and neutral ligand loss is observed. In contrast, the BDEs of the tris-complexes are < 320 kJ/mol and only neutral ligand loss is observed. An obvious question then is, at and below which critical value (x_{crit}) would an $M^{2+}(Pyr)_x$ complex dissociate not solely by simple ligand loss, but also experience electron transfer Coulomb fission (ETCF) or proton transfer Coulomb fission (PTCF), or both processes. The B3LYP computed BDEs of the $M^{2+}(Pyr)$ complexes are quiet strong and exceed 620 kJ/mol. The second sequential BDEs of the $M^{2+}(Pyr)_2$ complexes are still quite strong, and vary between 400–500 kJ/mol at the B3LYP and thus are comparable to or stronger than a typical C–C bond (~400 kJ/mol). The third sequential BDEs of the $M^{2+}(Pyr)_3$ complexes are < 350 kJ/mol, much weaker than a typical C–C bond, and closely approach those of the tris- Phen/Bpy complexes. The fourth, fifth, and sixth sequential BDEs of the $M^{2+}(Pyr)_x$ complexes continue to fall off and are < 215 kJ/mol for all M^{2+}. Trends in the sequential BDEs computed using the M06 and BHandHLYP functionals are highly parallel. Because the computed BDEs of the $M^{2+}(Pyr)$ and $M^{2+}(Pyr)_2$ complexes exceed 400 kJ/mol significant charge transfer interactions should dominate the binding, and therefore dissociation through Coulombic repulsions is likely to occur. Based on the comparison to the $M^{2+}(Phen)_x$ and $M^{2+}(Bpy)_x$ complexes, and the computed sequential BDEs of the $M^{2+}(Pyr)_x$ complexes, an $x_{crit} = 2$ is also expected. Thus, the enthalpies and free energies of the binding of the $M^{2+}(Pyr)_x$ complexes computed in this study suggest that experimental studies can be performed for $M^{2+}(Pyr)_x$ complexes where x = 2–4, but are not feasible for x = 1, 5, and 6. The $M^{2+}(Pyr)$ complexes are expected to be very reactive due to the high electron deficiency and are likely to undergo spontaneous charge fission and thus may not be generated in

sufficient intensity to enable CID studies. Although stable structures for the $M^{2+}(Pyr)_5$ and $M^{2+}(Pyr)_6$ complexes were found, they are calculated to be less stable than their dissociation products as indicated by the negative free energies of binding, or bind so weakly that at room temperature the internal energy of the complexes would exceed the binding energy such that sufficient intensities of these complexes are unlikely to be generated.

5.4.7 Comparison to Other $M^{2+}(Ligand)_x$ Complexes

Among the divalent transition metal cations examined here, sequential binding energies to other monodentate ligands have only been reported for the Fe^{2+} and Zn^{2+} complexes to water (W)[18,19] and the Zn^{2+} complexes to imidazole (Imid).[20] The sequential binding energies of these complexes are compared to the analogous complexes to Pyr examined here in Figure 5.9. As can be seen in the figure, the sequential BDEs of these complexes also decrease monotonically as the number of ligands increases. The first and second sequential BDEs of the $M^{2+}(Pyr)_x$ and $M^{2+}(Imid)_x$ complexes are much stronger than those of the $M^{2+}(W)_x$ complexes. However, the fall off in the BDEs is much more rapid for Pyr and Imid than W such that the differences in the third sequential BDEs to those ligands are much smaller. A cross over occurs between x = 3 and 4 such that the fourth, fifth, and sixth sequential BDEs of the $M^{2+}(W)$ complexes exceed those of $M^{2+}(Pyr)_x$ and $M^{2+}(Imid)_x$ complexes. The strength of binding of Imid is very parallel to, but slightly stronger than that of Pyr. The slight increase in BDEs from Pyr to Imid is understandable on the basis of the polarizabilities and dipole moments of these ligands (9.51 $Å^3$ and 2.20 D for Pyr versus 7.17 $Å^3$ and 3.67 D for Imid).[29] Thus, the effect of the 28% decrease in the polarizability nearly cancels the 50% increase in the dipole moment. Because Pyr and Imid are bigger ligands than W, ligand-ligand repulsions are more important in weakening of the sequential

BDEs. Hence, the sequential BDEs of the $M^{2+}(Pyr)_x$ and $M^{2+}(Imid)_x$ complexes fall off more rapidly than those for the analogous $M^{2+}(W)_x$ complexes. However, the total binding energies of the $M^{2+}(Pyr)_x$ complexes are stronger as compared to those of the analogous $M^{2+}(W)_x$ complexes. Consequently, the total binding energies of the $M^{2+}(Imid)_x$ complexes can also be expected to be stronger than for the analogous $M^{2+}(W)_x$ complexes. Thus, strong field ligands such as Pyr and Imid exert their influence most effectively for binding of the first few ligands.

5.5 Conclusions

In the ground-state structures of the $M^{2+}(Pyr)_x$ complexes, the Pyr ligands bind in a fashion consistent with the simple VSEPR model, where very minor distortions from the idealized geometries are correlated with the structure of the Pyr ligand, and more significant distortions with the valence electron configuration of the metal cation. Although the $M^{2+}(Pyr)_x$ complexes to the transition metal cations and the $Ca^{2+}(Pyr)_x$ complexes exhibit similar geometries, differences in the M^{2+}–N bond lengths between analogous structures illustrate the effects of sd hybridization and π-back donation on the binding. The absolute sequential binding energies for all of the $M^{2+}(Pyr)_x$ complexes examined at all three levels of theory vary both with the metal cation (due to electronic structure effects) and the level of theory employed. However, the overall trends for all five metal cations at all three levels of theory examined are relatively parallel. Comparison of the $M^{2+}(Pyr)_x$ to the analogous $M^{+}(Pyr)_x$ complexes indicates that the charge of the metal cation is the dominant contributing factor to the differences in the strength of binding among these complexes. The strength of binding is also found to depend on the valence electronic configuration of the metal cation. Differences in sequential and total binding energies based on the number of *N*-donor

interactions between the $M^{n+}(Pyr)_x$, $M^{n+}(Bpy)_x$, and $M^{n+}(Phen)_x$ complexes depict the interplay between the flexibility of the Pyr ligand that allows Pyr to take full advantage of sd hybridization, the geometric constraints of the Bpy and Phen ligands, ligand-ligand repulsive interactions, and chelation effects. The differences in the BDEs of the $M^{2+}(W)_x$, $M^{2+}(Imid)_x$, and $M^{2+}(Pyr)_x$ indicate that the larger ligands (Pyr and Imid) experience more ligand-ligand repulsion as compared to the smaller W ligand, and hence their BDEs weaken much more rapidly with increasing ligation. However, the total BDEs of the $M^{2+}(Pyr)_x$ and $M^{2+}(Imid)_x$ complexes still exceed those of the analogous $M^{2+}(W)_x$ complexes, indicating that the effects of strong field ligands are most important for binding of the first few ligands.

5.6 References

(1) Khlobystov, A. N.; Blake, A. J.; Champness, N. R.; Lemenovskii, D. A.; Majouga, A. G.; Zyk, N. V.; Schrödér, M. *Coord. Chem. Rev.* **2001**, *222*, 155.

(2) Yue-gen, Z.; Fan-lei, K. *Nongyao* **2012**, *51*, 717.

(3) Hassan, J.; Penalva, V.; Lavenot, L.; Gozzi, C.; Lemaire, M. *Tetrahedron* **1998**, *54*, 13793.

(4) Doshi, A.; Sundararaman, A.; Venkatasubbaiah, K.; Zakharov, L. N.; Rheingold, A. L.; Myahkostupov, M.; Piotrowiak, P.; Jakle F. *Organomet*. **2012**, *31*, 1546.

(5) Schubert, U. S.; Eschbaumer, C. *Angew. Chem. Int. Ed.* **2002**, *41*, 2892.

(6) Amouri, H.; Desmarets, C.; Moussa, J. *Chem. Rev*. **2012**, *112*, 2015.

(7) Zaman, M. B.; Smith, M. D.; Ciurtin, D. M.; Loye, H. C. *Inorg. Chem.* **2002**, *41*, 4895.

(8) Chen, C. Y.; Zeng, J. Y.; Lee, H. M. *Inorg. Chim. Acta* **2007**, *360*, 21.

(9) Schurr, A.; West, C. A.; Rigor, B. M. *Brain Res.* **1991**, *568*, 199.

(10) Henry, G. D. *Tetrahedron* **2004**, *60*, 6043.

(11) Allendorf, M. D.; Bauer, C. A.; Bhakta, R. K.; Houk, R. J. T. *Chem. Soc. Rev*. **2009**, *38*, 1330.

(12) Zhao, B.; Chen, X. Y.; Cheng, P.; Liao, D. Z.; Yan, S. P.; Jiang, Z. H. *J. Am. Chem. Soc.* **2004**, *126*, 15394.

(13) Rannulu, N. S.; Rodgers, M. T. *J. Phys. Chem. A* **2007**, *111*, 3465.

(14) Rannulu, N. S.; Rodgers, M. T. *J. Phys. Chem. A* **2009**, *113*, 4534.

(15) Rannulu, N. S.; Rodgers, M. T. *J. Phys. Chem. A* **2012**, *116*, 1319.

(16) Rannulu, N. S. Doctoral dissertation, Wayne State University. **2008**, pp. 383.

(17) Rodgers, M. T.; Stanley, J. R.; Amunugama, R. *J. Am. Chem. Soc*. **2000**, *122*, 10969.

(18) Hoftstetter, T. E.; Armentrout, P. B. *J. Phys. Chem. A* **2013**, *117*, 1110.

(19) Cooper, T. E.; Carl, D. R.; Armentrout, P. B. *J. Phys. Chem. A* **2009**, *113*, 13727.

(20) Peschke, M.; Blades, A. T.; Kebarle, P. *J. Am. Chem. Soc.* **2000**, *122*, 1492.

(21) Nose, H.; Rodgers, M. T. *ChemPlusChem*. **2013**, *78*, 1109.

(22) Nose, H.; Chen, Y.; Rodgers, M. T. *J. Phys. Chem. A* **2013**, *117*, 4316.

(23) Frisch, M. J.; Trucks, G. W.; Schlegel, H. B.; Scuseria, G. E.; Robb, M. A.; Cheeseman, J. R.; Scalmani, G.; Barone, V.; Mennucci, B.; Petersson, G. A.; Nakatsuji, H.; Caricato, M.; Li, X.; Hratchian, H. P.; Izmaylov, A. F.; Zheng, G.; Sonnenberg, J. L.; Hada, M.; Ehara, M.; Toyota, K.; Fukuda, R.; Hasegawa, J.; Ishida, M.; Nakajima, T.; Honda, Y.; Kitao, O.; Nakai, H.; Vreven, T.; Montgomery, J. A, Jr.; Ogliaro, F.; Bearpark, M.; Heyd, J. J.; Brothers, E.; Kudin, K. N.; Staroverov, V. N.; Kobayashi, R.; Raghavachari, K.; Rendell, A.; Burant, J. C.; Iyengar, S. S.; Tomasi, J.; Cossi, M.; Rega, N.; Millam, J. M.; Klene, M.; Knox, J. E.;

Bakken, V.; Adamo, C.; Jaramillo, J.; Gomperts, R.; Stratmann, R. E.; Yazyev, O.; Austin, A. J.; Cammi, R.; Pomelli, C.; Ochterski, J. W.; Martin, R. L.; Morokuma, K.; Voth, G. A.; Salvador, P.; Dannenberg, J. J.; Dapprich, S.; Daniels, A. D.; Farkas, O.; Foresman, J. B.; Ortiz, J. V.; Cioslowski, J.; Fox, D. J. Gaussian, Inc., Wallingford, CT, 2009.

(24) McKenna, A. G.; McKenna, J. F. *J. Chem. Educ.* **1984**, *61*, 771.

(25) Shannon, R. D. *Acta Crystallogr*. **1976**, *A32*, 751.

(26) Jahn, H. A.; Teller, E. *Proc. R. Soc. London*. **1937**, *A161*, 220.

(27) Bersuker, I. B. *Chem. Rev.* **2001**, *101*, 1067.

(28) Swart, M. *J. Chem. Theory Comput.* **2008**, *4*, 2057.

(29) Miller, K. J. *J. Am. Chem. Soc.* **1990**, *112*, 8533.

Table 5.1. Relative Energies of the Various Spin States of $M^{2+}(Pyr)_x$ Complexes in Their Ground-State Conformations at 0 K in kJ/mol.

Complex	Multiplicity	B3LYP[a]	BHandHLYP[b]	M06[c]
Fe^{2+}	5	0.0	0.0	0.0
	3	241.3	263.6	260.2
	1	378.4	404.4	408.5
$Fe^{2+}(Pyr)$	5	0.0	0.0	0.0
	3	101.5	158.1	112.5
	1	242.4	297.3	257.0
$Fe^{2+}(Pyr)_2$	5	0.0	0.0	0.0
	3	131.4	168.7	145.4
	1	263.3	304.2	283.7
$Fe^{2+}(Pyr)_3$	5	0.0	0.0	0.0
	3	122.6	143.2	134.4
	1	188.5	269.4	212.5
$Fe^{2+}(Pyr)_4$	5	0.0	0.0	0.0
	3	81.4	142.2	137.3
	1	244.6	342.5	307.4
$Fe^{2+}(Pyr)_5$	5	0.0	0.0	0.0
	3	44.0	101.0	61.6
	1	89.2	170.0	131.5
$Fe^{2+}(Pyr)_6$	5	0.0	0.0	0.0
	3	70.1	127.3	119.7
	1	85.9	170.1	117.4

Table 5.1. (continued) Relative Energies of the Various Spin States of $M^{2+}(Pyr)_x$ Complexes in Their Ground-State Conformations at 0 K in kJ/mol.

Complex	Multiplicity	B3LYP[a]	BHandHLYP[b]	M06[c]
Co^{2+}	4	0.0	0.0	0.0
	2	252.6	273.5	304.6
$Co^{2+}(Pyr)$	4	0.0	0.0	0.0
	2	66.9	87.7	62.5
$Co^{2+}(Pyr)_2$	4	0.0	0.0	0.0
	2	37.3	100.6	117.2
$Co^{2+}(Pyr)_3$	4	0.0	0.0	0.0
	2	71.6	135.6	74.2
$Co^{2+}(Pyr)_4$	4	0.0	0.0	0.0
	2	48.1	132.4	187.7
$Co^{2+}(Pyr)_5$	4	0.0	0.0	0.0
	2	6.8	152.4	14.3
$Co^{2+}(Pyr)_6$	4	0.0	0.0	0.0
	2	78.3	170.2	103.3
Ni^{2+}	3	0.0	0.0	0.0
	1	297.0	317.3	234.6
$Ni^{2+}(Pyr)$	3	0.0	0.0	0.0
	1	98.9	163.4	105.7
$Ni^{2+}(Pyr)_2$	3	0.0	0.0	0.0
	1	77.7	145.2	62.4
$Ni^{2+}(Pyr)_3$	3	0.0	0.0	0.0
	1	19.9	105.6	19.1
$Ni^{2+}(Pyr)_4$	3	0.0	0.0	0.0
	1	13.5	44.8	76.7
$Ni^{2+}(Pyr)_5$	3	0.0	0.0	0.0
	1	26.3	122.6	20.8
$Ni^{2+}(Pyr)_6$	3	0.0	0.0	0.0
	1	19.6	129.6	46.2

[a]Calculated at the B3LYP/6-311+G(2d,2p)//B3LYP/6-31G* level of theory including ZPE corrections with frequencies scaled by 0.9804. [b]Calculated at the BHandHLYP/6-311+G(2d,2p)//BHandHLYP/6-31G* level of theory including ZPE corrections with frequencies scaled by 0.9472. [c]Calculated at the M06/6-311+G(2d,2p)//M06/6-31G* level of theory including ZPE corrections with frequencies scaled by 0.9940.

Table 5.2a. Select Geometrical Parameters of the B3LYP/6-31G* Ground-State Structures of the $M^{2+}(Pyr)_x$ Complexes.[a]

Complex	M^{2+}–N	∠NM^{2+}N
$Fe^{2+}(Pyr)$	1.939	
$Fe^{2+}(Pyr)_2$	1.953	179.9
$Fe^{2+}(Pyr)_3$	2.019	120.0
$Fe^{2+}(Pyr)_4$	2.079	108.7 (2), 111.1 (4)
$Fe^{2+}(Pyr)_5$	2.161 (3), 2.229 (2)	86.5 (2), 90.2 (2), 94.7 (2), 111.1 (2), 137.7, 170.7
$Fe^{2+}(Pyr)_6$	2.302	89.3 (6), 90.7 (6), 179.1 (3)
$Co^{2+}(Pyr)$	1.854	
$Co^{2+}(Pyr)_2$	1.908	179.1
$Co^{2+}(Pyr)_3$	1.969	120.0
$Co^{2+}(Pyr)_4$	2.028	105.3 (2), 111.6 (4)
$Co^{2+}(Pyr)_5$	2.090 (3), 2.211 (2)	86.2 (2), 92.0 (4), 117.5 (2), 125.1, 176.3
$Co^{2+}(Pyr)_6$	2.267	84.5 (6), 95.0 (6), 179.1 (3)
$Ni^{2+}(Pyr)$	1.848	
$Ni^{2+}(Pyr)_2$	1.896	180.0
$Ni^{2+}(Pyr)_3$	1.940, 1.945 (2)	106.5 (2), 147.1
$Ni^{2+}(Pyr)_4$	2.013	103.7 (4), 134.1 (2)
$Ni^{2+}(Pyr)_5$	2.061, 2.117 (4)	86.5 (2), 89.6 (2), 100.8 (4), 158.5 (2)
$Ni^{2+}(Pyr)_6$	2.220	89.8 (5), 90.1 (7), 179.8 (3)
$Cu^{2+}(Pyr)$	1.844	
$Cu^{2+}(Pyr)_2$	1.877	180.0
$Cu^{2+}(Pyr)_3$	1.910 (2), 1.929	104.8 (2), 150.5
$Cu^{2+}(Pyr)_4$	2.004	92.8, 97.2 (3), 141.9 (2)
$Cu^{2+}(Pyr)_5$	2.065, 2.277 (4)	86.6 (2), 90.2 (2), 96.4 (2), 104.5 (2), 159.1 (2)
$Cu^{2+}(Pyr)_6$	2.027 (4), 3.174 (2)	89.5 (6), 90.5 (6), 179.0 (3)
$Zn^{2+}(Pyr)$	1.870	
$Zn^{2+}(Pyr)_2$	1.884	180.0
$Zn^{2+}(Pyr)_3$	1.958	120.0
$Zn^{2+}(Pyr)_4$	2.032	105.8 (2), 111.4 (4)
$Zn^{2+}(Pyr)_5$	2.098 (3), 2.241 (2)	87.9 (3), 92.1 (3), 118.8, 120.6 (2), 177.6
$Zn^{2+}(Pyr)_6$	2.279	89.9, 90.0 (11), 179.9 (3)

Table 5.2b. Select Geometrical Parameters of the B3LYP/6-31G* Ground-State Structures of the $Ca^{2+}(Pyr)_x$ Complexes.[a]

Complex	M^{2+}–N	$\angle NM^{2+}N$
$Ca^{2+}(Pyr)$	2.377	
$Ca^{2+}(Pyr)_2$	2.422	180.0
$Ca^{2+}(Pyr)_3$	2.455	120.0
$Ca^{2+}(Pyr)_4$	2.490	109.5
$Ca^{2+}(Pyr)_5$	2.553 (4), 2.525	87.9 (4), 99.2 (2), 103.3 (2), 157.4 (2)
$Ca^{2+}(Pyr)_6$	2.603	90.0 (12), 180.0 (3)

[a]The spin states of the $Fe^{2+}(Pyr)_x$, $Co^{2+}(Pyr)_x$, $Ni^{2+}(Pyr)_x$, $Cu^{2+}(Pyr)_x$, $Zn^{2+}(Pyr)_x$, and $Ca^{2+}(Pyr)_x$ complexes are quintet, quartet, triplet, doublet, singlet, and singlet, respectively, for all values of *x*. Average values are given for similar bond distances or angles; degeneracies are listed in parentheses for values that differ significantly such that more than one value is needed to describe the bond angle or bond distance. Bond angles ($\angle$) are given in degrees (°) and M^{2+}–N bond lengths in angstroms (Å).

Table 5.3. Sequential and Total BDEs of Ground-State $M^{2+}(Pyr)_x$ Complexes at 0 K in kJ/mol.[a]

		B3LYP Theory					
		6-31G*//6-31G*			6-311+G(2d,2p)// 6-31G*		
Complex	Spin	D_0	$D_{0,BSSE}$[b]	Total[b]	D_0	$D_{0,BSSE}$[b]	Total[b]
$Fe^{2+}(Pyr)$	5	343.8	343.1	343.1	621.8	621.1	621.1
$Fe^{2+}(Pyr)_2$	5	487.2	484.6	827.7	424.9	422.3	1043.4
$Fe^{2+}(Pyr)_3$	5	322.5	319.9	1147.6	302.4	299.9	1343.3
$Fe^{2+}(Pyr)_4$	5	203.8	199.4	1347.0	170.3	165.9	1509.2
$Fe^{2+}(Pyr)_5$	5	87.2	83.4	1430.4	68.1	64.3	1573.5
$Fe^{2+}(Pyr)_6$	5	62.5	58.4	1488.8	57.3	53.2	1626.7
$Co^{2+}(Pyr)$	4	323.8	321.9	321.9	663.9	661.9	661.9
$Co^{2+}(Pyr)_2$	4	454.0	450.5	772.4	403.1	399.6	1061.5
$Co^{2+}(Pyr)_3$	4	374.0	370.0	1142.4	324.3	320.2	1381.7
$Co^{2+}(Pyr)_4$	4	227.2	224.0	1366.4	196.1	192.9	1574.6
$Co^{2+}(Pyr)_5$	4	127.2	123.2	1489.6	85.5	81.6	1656.2
$Co^{2+}(Pyr)_6$	4	71.2	66.9	1556.5	59.0	54.7	1710.9
$Ni^{2+}(Pyr)$	3	351.3	349.3	349.3	752.8	750.8	750.8
$Ni^{2+}(Pyr)_2$	3	473.4	470.3	819.6	443.4	440.3	1191.1
$Ni^{2+}(Pyr)_3$	3	330.1	327.2	1146.8	274.7	271.8	1462.9
$Ni^{2+}(Pyr)_4$	3	209.0	205.3	1352.1	193.7	190.1	1653.0
$Ni^{2+}(Pyr)_5$	3	106.9	102.9	1455.0	95.4	91.4	1744.4
$Ni^{2+}(Pyr)_6$	3	53.4	48.5	1503.5	50.1	45.1	1789.5
$Cu^{2+}(Pyr)$	2	318.4	316.4	316.4	918.9	916.8	916.8
$Cu^{2+}(Pyr)_2$	2	496.5	493.0	809.4	398.8	395.3	1312.1
$Cu^{2+}(Pyr)_3$	2	326.6	312.6	1122.0	266.8	252.8	1564.9
$Cu^{2+}(Pyr)_4$	2	186.4	182.7	1304.7	151.3	147.5	1712.4
$Cu^{2+}(Pyr)_5$	2	89.2	89.2	1393.9	65.4	65.4	1777.8
$Cu^{2+}(Pyr)_6$	2	46.7	43.7	1437.6	44.8	41.8	1819.6
$Zn^{2+}(Pyr)$	1	183.9	182.3	182.3	740.9	739.3	739.3
$Zn^{2+}(Pyr)_2$	1	528.6	525.1	707.4	496.4	493.0	1232.3
$Zn^{2+}(Pyr)_3$	1	289.3	286.8	994.2	246.6	244.1	1476.4
$Zn^{2+}(Pyr)_4$	1	202.2	198.6	1192.8	172.5	168.8	1645.2
$Zn^{2+}(Pyr)_5$	1	57.5	53.0	1245.8	45.4	41.0	1686.2
$Zn^{2+}(Pyr)_6$	1	37.5	32.3	1278.1	36.1	30.9	1717.1

[a]Calculated at the B3LYP/6-31G* and the B3LYP/6-311+G(2d,2p) level of theory using B3LYP/6-31G* including ZPE corrections with frequencies scaled by 0.9804. [b]Also includes BSSE corrections.

Table 5.4. Enthalpies and Free Energies of Binding of $M^{2+}(Pyr)_x$ Complexes at 298 K in kJ/mol.[a]

Complex	ΔH_{298}-ΔH_0[b]	ΔH_{298}[b]	$\sum \Delta H_{298}$[b]	$T\Delta S_{298}$[b]	ΔG_{298}[b]	$\sum \Delta G_{298}$[b]
$Fe^{2+}(Pyr)$	1.2 (0.5)	622.3	622.3	29.0 (1.5)	593.3	593.3
$Fe^{2+}(Pyr)_2$	–1.7 (1.8)	420.6	1042.9	42.0 (4.9)	378.6	971.9
$Fe^{2+}(Pyr)_3$	–1.7 (2.1)	298.2	1341.1	45.0 (4.3)	253.2	1225.1
$Fe^{2+}(Pyr)_4$	–1.2 (1.6)	164.7	1505.8	54.1 (3.9)	110.6	1335.7
$Fe^{2+}(Pyr)_5$	–2.0 (1.9)	62.3	1568.1	51.4 (4.6)	10.9	1346.6
$Fe^{2+}(Pyr)_6$	–2.3 (1.9)	50.8	1618.9	50.1 (4.3)	0.7	1347.3
$Co^{2+}(Pyr)$	1.4 (0.5)	663.3	663.3	31.2 (1.4)	632.1	632.1
$Co^{2+}(Pyr)_2$	–2.1 (2.8)	397.5	1060.8	39.4 (5.1)	358.1	990.2
$Co^{2+}(Pyr)_3$	–1.3 (1.8)	318.9	1379.7	47.9 (4.2)	271.0	1261.2
$Co^{2+}(Pyr)_4$	–0.9 (1.5)	192.0	1571.7	54.3 (3.8)	137.7	1398.9
$Co^{2+}(Pyr)_5$	–1.3 (1.6)	80.3	1652.0	53.9 (4.2)	26.4	1425.3
$Co^{2+}(Pyr)_6$	–2.6 (1.4)	52.1	1704.1	51.1 (3.7)	1.0	1426.3
$Ni^{2+}(Pyr)$	1.9 (0.4)	752.7	752.7	31.8 (1.3)	720.9	720.9
$Ni^{2+}(Pyr)_2$	–2.2 (1.8)	438.1	1190.8	42.0 (5.0)	396.1	1117.0
$Ni^{2+}(Pyr)_3$	–1.1 (1.8)	270.7	1461.5	49.2 (4.1)	221.5	1338.5
$Ni^{2+}(Pyr)_4$	–1.3 (1.7)	188.8	1650.3	51.4 (4.2)	137.4	1475.9
$Ni^{2+}(Pyr)_5$	–0.9 (1.4)	90.5	1740.9	56.2 (4)	34.3	1510.2
$Ni^{2+}(Pyr)_6$	–2.1 (1.9)	43.0	1783.8	49.9 (4.3)	–6.9	–
$Cu^{2+}(Pyr)$	1.1 (0.5)	917.9	917.9	29.6 (1.4)	888.3	888.3
$Cu^{2+}(Pyr)_2$	–1.3 (1.7)	394.0	1311.9	44.0 (4.6)	350.0	1238.3
$Cu^{2+}(Pyr)_3$	–0.7 (1.6)	252.1	1564.0	50.6 (3.9)	201.6	1439.9
$Cu^{2+}(Pyr)_4$	–1.2 (1.7)	146.3	1710.3	50.5 (4.2)	95.8	1535.7
$Cu^{2+}(Pyr)_5$	–1.9 (1.9)	63.5	1773.8	52.1 (4.0)	11.4	1547.1
$Cu^{2+}(Pyr)_6$	–3.3 (2.7)	38.5	1812.3	41.4 (5.3)	–2.9	–
$Zn^{2+}(Pyr)$	1.5 (0.5)	740.8	740.8	31.7 (1.3)	709.1	709.1
$Zn^{2+}(Pyr)_2$	–1.2 (1.6)	491.8	1232.6	44.8 (4.6)	447.0	1156.1
$Zn^{2+}(Pyr)_3$	–1.9 (2.0)	242.2	1474.8	44.9 (4.6)	197.3	1353.4
$Zn^{2+}(Pyr)_4$	–1.6 (1.8)	167.2	1642.0	50.9 (4.2)	116.3	1469.7
$Zn^{2+}(Pyr)_5$	–2.1 (1.9)	38.9	1680.9	49.0 (4.7)	–10.1	–
$Zn^{2+}(Pyr)_6$	–2.5 (1.9)	28.4	1709.3	51.5 (4.3)	–23.1	–

[a]Uncertainties are listed in parentheses. [b]Values from calculations at the B3LYP/6-311+G(2d,2p) level of theory using B3LYP/6-31G* optimized geometries with frequencies scaled by 0.9804.

Table 5.5a. The Natural Valence Electron Configurations for $M^{2+}(Pyr)_x$ Complexes.

	B3LYP Theory						
	6-31G*			6311+G(2d,2p)			
Complex	4s	3d	4p	4s	3d	4p	4d
Fe^{2+}	0.00	6.00		0.00	6.00		
$Fe^{2+}(Pyr)$	0.22	6.10	0.01	0.16	6.21	0.01	0.01
$Fe^{2+}(Pyr)_2$	0.36	6.03	0.06	0.31	6.12	0.08	0.01
$Fe^{2+}(Pyr)_3$	0.29	6.12	0.15	0.26	6.23	0.18	0.01
$Fe^{2+}(Pyr)_4$	0.28	6.11	0.24	0.25	6.24	0.30	0.02
$Fe^{2+}(Pyr)_5$	0.28	6.09	0.26	0.23	6.24	0.32	0.04
$Fe^{2+}(Pyr)_6$	0.26	6.08	0.29	0.21	6.25	0.34	0.07
Co^{2+}	0.00	7.00		0.00	7.00		
$Co^{2+}(Pyr)$	0.21	7.23	0.02	0.13	7.51	0.01	
$Co^{2+}(Pyr)_2$	0.36	7.03	0.08	0.27	7.21	0.08	0.01
$Co^{2+}(Pyr)_3$	0.30	7.16	0.18	0.26	7.31	0.19	0.01
$Co^{2+}(Pyr)_4$	0.29	7.14	0.28	0.26	7.31	0.31	0.02
$Co^{2+}(Pyr)_5$	0.28	7.13	0.29	0.24	7.31	0.33	0.04
$Co^{2+}(Pyr)_6$	0.26	7.10	0.30	0.22	7.27	0.35	0.05
Ni^{2+}	0.00	8.00		0.00	8.00		
$Ni^{2+}(Pyr)$	0.19	8.21	0.02	0.14	8.34	0.01	
$Ni^{2+}(Pyr)_2$	0.70	8.22	0.06	0.28	8.19	0.09	
$Ni^{2+}(Pyr)_3$	0.37	8.15	0.18	0.31	8.33	0.19	0.01
$Ni^{2+}(Pyr)_4$	0.31	8.13	0.30	0.27	8.31	0.32	0.02
$Ni^{2+}(Pyr)_5$	0.29	8.14	0.30	0.24	8.34	0.34	0.03
$Ni^{2+}(Pyr)_6$	0.26	8.14	0.31	0.23	8.35	0.36	0.05

Table 5.5a. (continued) The Natural Valence Electron Configurations for $M^{2+}(Pyr)_x$ Complexes.

	B3LYP Theory								
	6-31G*				6311+G(2d,2p)				
Complex	4s	3d	4p	5p	4s	3d	4p	4d	5p
Cu^{2+}	0.00	9.00			0.00	9.00			
$Cu^{2+}(Pyr)$	0.20	9.40	0.02		0.19	9.84	0.01		
$Cu^{2+}(Pyr)_2$	0.61	9.20	0.06		0.30	9.43	0.08		
$Cu^{2+}(Pyr)_3$	0.40	9.17	0.18		0.34	9.35	0.19	0.01	
$Cu^{2+}(Pyr)_4$	0.36	9.15	0.28		0.30	9.33	0.30	0.02	
$Cu^{2+}(Pyr)_5$	0.32	9.15	0.32		0.27	9.33	0.35	0.03	
$Cu^{2+}(Pyr)_6$	0.34	9.17	0.27		0.28	9.35	0.31	0.02	
Zn^{2+}	0.00	10.0			0.00	10.00			
$Zn^{2+}(Pyr)$	0.44	9.94	0.03		0.38	9.98	0.03		
$Zn^{2+}(Pyr)_2$	0.57	9.87	0.09		0.49	9.94	0.10		
$Zn^{2+}(Pyr)_3$	0.45	9.90	0.25		0.40	9.96	0.26	0.01	
$Zn^{2+}(Pyr)_4$	0.39	9.90	0.37		0.34	9.97	0.38	0.02	
$Zn^{2+}(Pyr)_5$	0.36	9.92	0.34	0.01	0.33	9.98	0.36	0.02	
$Zn^{2+}(Pyr)_6$	0.34	9.95	0.33	0.01	0.32	9.99	0.36	0.02	0.01

Table 5.5b. Natural Bond Orbital Charges for $M^{2+}(Pyr)_x$ Complexes.

	B3LYP Theory			
	6-31G*		6311+G(2d,2p)	
Complex	$q_{M^{2+}}$	q_N	$q_{M^{2+}}$	q_N
Pyr		–0.406		–0.281
Fe^{2+}	2.000		2.000	
$Fe^{2+}(Pyr)$	1.482	–0.662	1.250	0.132
$Fe^{2+}(Pyr)_2$	1.278	–0.668	0.896	0.054
$Fe^{2+}(Pyr)_3$	1.181	–0.651	1.002	0.038
$Fe^{2+}(Pyr)_4$	1.177	–0.624	0.609	0.114
$Fe^{2+}(Pyr)_5$	1.193	–0.588	3.482	–0.173
$Fe^{2+}(Pyr)_6$	1.192	–0.570	2.549	–0.067
Co^{2+}	2.000		2.000	
$Co^{2+}(Pyr)$	1.370	–0.640	1.068	0.029
$Co^{2+}(Pyr)_2$	1.215	–0.635	0.577	0.068
$Co^{2+}(Pyr)_3$	1.069	–0.627	0.889	0.034
$Co^{2+}(Pyr)_4$	1.053	–0.600	0.856	0.093
$Co^{2+}(Pyr)_5$	1.057	–0.562	4.108	–0.273
$Co^{2+}(Pyr)_6$	1.070	–0.547	3.431	–0.334
Ni^{2+}	2.000		2.000	
$Ni^{2+}(Pyr)$	1.397	–0.653	1.148	0.126
$Ni^{2+}(Pyr)_2$	0.776	–0.581	0.274	0.119
$Ni^{2+}(Pyr)_3$	1.008	–0.616	0.510	0.127
$Ni^{2+}(Pyr)_4$	0.992	–0.586	1.021	0.071
$Ni^{2+}(Pyr)_5$	1.011	–0.550	2.865	–0.244
$Ni^{2+}(Pyr)_6$	1.036	–0.539	4.288	–0.474

Table 5.5b. (continued) Natural Bond Orbital Charges for $M^{2+}(Pyr)_x$ Complexes.

	B3LYP Theory			
	6-31G*		6311+G(2d,2p)	
Complex	$q_{M^{2+}}$	q_N	$q_{M^{2+}}$	q_N
Cu^{2+}	2.000		2.000	
$Cu^{2+}(Pyr)$	1.224	–0.633	0.710	0.073
$Cu^{2+}(Pyr)_2$	0.853	–0.594	0.217	0.223
$Cu^{2+}(Pyr)_3$	0.917	–0.587	0.404	0.208
$Cu^{2+}(Pyr)_4$	0.854	–0.560	0.170	0.294
$Cu^{2+}(Pyr)_5$	0.910	–0.533	2.282	0.001
$Cu^{2+}(Pyr)_6$	0.901	–0.518	4.058	–0.063
Zn^{2+}	2.000		2.000	
$Zn^{2+}(Pyr)$	1.362	–0.640	1.135	0.133
$Zn^{2+}(Pyr)_2$	1.090	–0.630	0.088	0.223
$Zn^{2+}(Pyr)_3$	1.004	–0.606	0.734	0.046
$Zn^{2+}(Pyr)_4$	0.966	–0.581	1.589	–0.067
$Zn^{2+}(Pyr)_5$	1.004	–0.541	3.698	–0.433
$Zn^{2+}(Pyr)_6$	1.038	–0.530	5.043	–0.820

5.8 Figure Captions and Figures

Figure 5.1. B3LYP/6-31G* optimized geometries of $M^{2+}(Pyr)_x$ complexes, where M^{2+} = Fe^{2+}, Co^{2+}, Ni^{2+}, Cu^{2+}, Zn^{2+}, and Ca^{2+}, and x = 1–6 parts a–f, respectively.

Figure 5.2. Theoretical $(Pyr)_{x-1}M^{2+}$–Pyr BDEs at 0 K (in kJ/mol), where M^{2+} = Fe^{2+}, Co^{2+}, Ni^{2+}, Cu^{2+}, and Zn^{2+} as a function of the number of Pyr ligands (x) and the metal cation determined at the B3LYP/6-311+G(2d,2p)//B3LYP/6-31G*, BHandHLYP/6-311+G(2d,2p)//BHandHLYP/6-31G*, and M06/6-311+G(2d,2p)//M06/6-31G* levels of theory including ZPE and BSSE corrections. All values are taken from Tables 5.3 and C.5.

Figure 5.3. Theoretical $(Pyr)_{x-1}M^{2+}$–Pyr BDEs at 0 K (in kJ/mol), where M^{2+} = Fe^{2+}, Co^{2+}, Ni^{2+}, Cu^{2+}, and Zn^{2+} as a function of the number of Pyr ligands (x) and the metal cation determined at the B3LYP level of theory using 6-311+G(2d,2p) and 6-31G* basis sets. All values include ZPE and BSSE corrections and taken from Table 5.3.

Figure 5.4. Theoretical $(Pyr)_{x-1}M^{2+}$–Pyr BDEs at 0 K (in kJ/mol) where M^{2+} = Fe^{2+}, Co^{2+}, Ni^{2+}, Cu^{2+}, and Zn^{2+} as a function of the metal cation and the number of Pyr ligands, x, determined at the B3LYP/6-311+G(2d,2p)//B3LYP/6-31G*, BHandHLYP/6-311+G(2d,2p)//BHandHLYP/6-31G*, and M06/6-311+G(2d,2p)//M06/6-31G* levels of theory including ZPE and BSSE corrections. All values are taken from Tables 5.3 and C.5.

Figure 5.5. Comparison of B3LYP/6-311+G(2d,2p)//B3LYP/6-31G* BDEs of the $M^{n+}(Pyr)_x$ complexes as a function of the number of Pyr ligands (x), metal cation (M^{n+}), and charge (n+). Values for M^{2+} complexes are taken from Table 5.3. Values for M^{+} complexes are taken from references 13–16.

Figure 5.6. Comparison of B3LYP/6-311+G(2d,2p)//B3LYP/6-31G* BDEs of the $M^{2+}(Pyr)_x$ versus $M^{+}(Pyr)_x$ complexes as a function of the number of Pyr ligands (x) and charge. Values for M^{2+} complexes are taken from Table 5.3. Values for M^{+} complexes are taken from references 13–16.

Figure 5.7. Theoretical $(N\text{-}L)_{x-1}M^{2+}$–$N\text{-}L$ BDEs in kJ/mol, where M^{2+}= Fe^{2+} and Cu^{2+} and $N\text{-}L$ = Pyr, Bpy, and Phen plotted versus the number of N-donor interactions. Open circles represent the sum of the first and second, third and fourth, and fifth and sixth binding energies of the $M^{2+}(Pyr)_x$ complexes. Values for $M^{2+}(Pyr)_x$ are taken from Table 5.4. Values for the Bpy and Phen complexes are taken from references 21–22. All values are at 298 K.

Figure 5.8. Trends in the total enthalpies and free energies of binding of the $M^{n+}(N\text{-}L)_x$ complexes as a function of the number of *N*-donor interactions at 298 K (in kJ/mol), where n = 1–2, *N*-*L* = Pyr, Bpy, and Phen, and M = Fe, Co, Ni, Cu, and Zn, parts a–e, respectively. Energies are determined from calculations at B3LYP/6-311+G (2d,2p) level of theory including ZPE and BSSE corrections. Values for Pyr are taken from Table 5.4. Values for the Bpy and Phen complexes are taken from references 21–22. Values for M^+ complexes are taken from references 13–16. All values are at 298 K. Values for Bpy and Phen for x = 2, 4, and 6 are shown slightly offset to facilitate comparisons.

Figure 5.9. Theoretical $(Ligand)_{x-1}M^{2+}$–Ligand BDEs in kJ/mol, where M^{2+}= Fe^{2+} and Zn^{2+} and Ligand = Pyr, Imid, and W plotted versus the number of ligands (x). Values for $M^{2+}(Pyr)_x$ are taken from Table 5.4. Values for the W and Imid complexes are taken from references 18–20. All values are at 298 K.

Figure 5.1a.

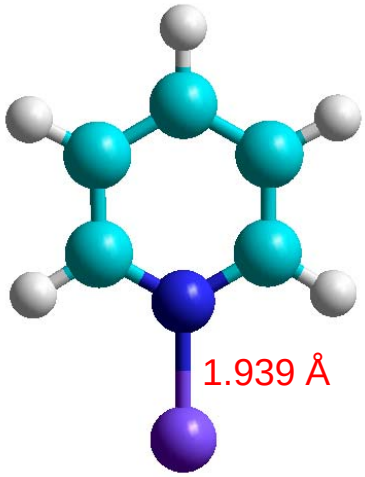

Fe^{2+}(Pyr)

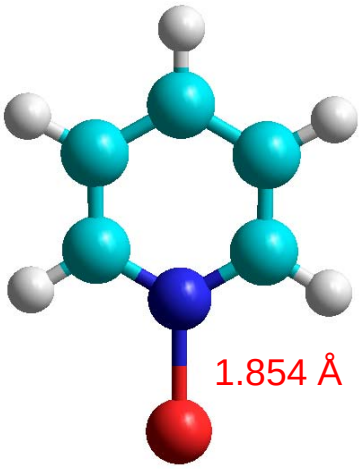

Co^{2+}(Pyr)

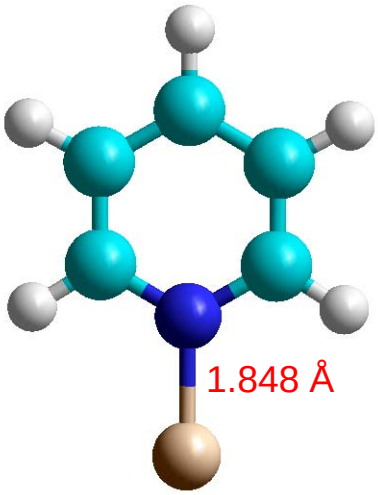

Ni^{2+}(Pyr)

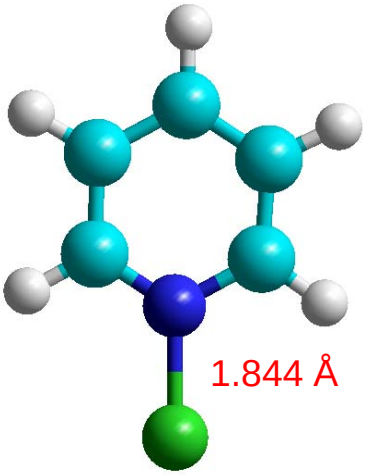

Cu^{2+}(Pyr)

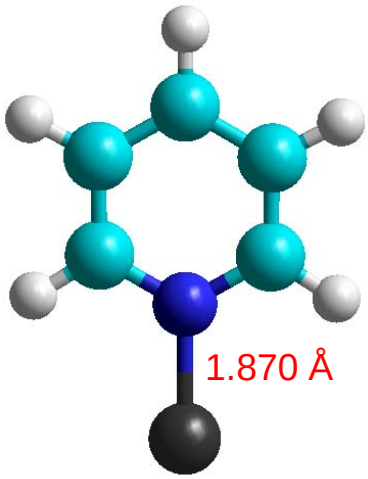

Zn^{2+}(Pyr)

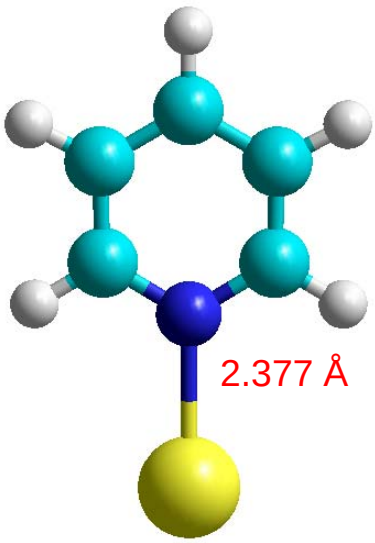

Ca^{2+}(Pyr)

Figure 5.1b.

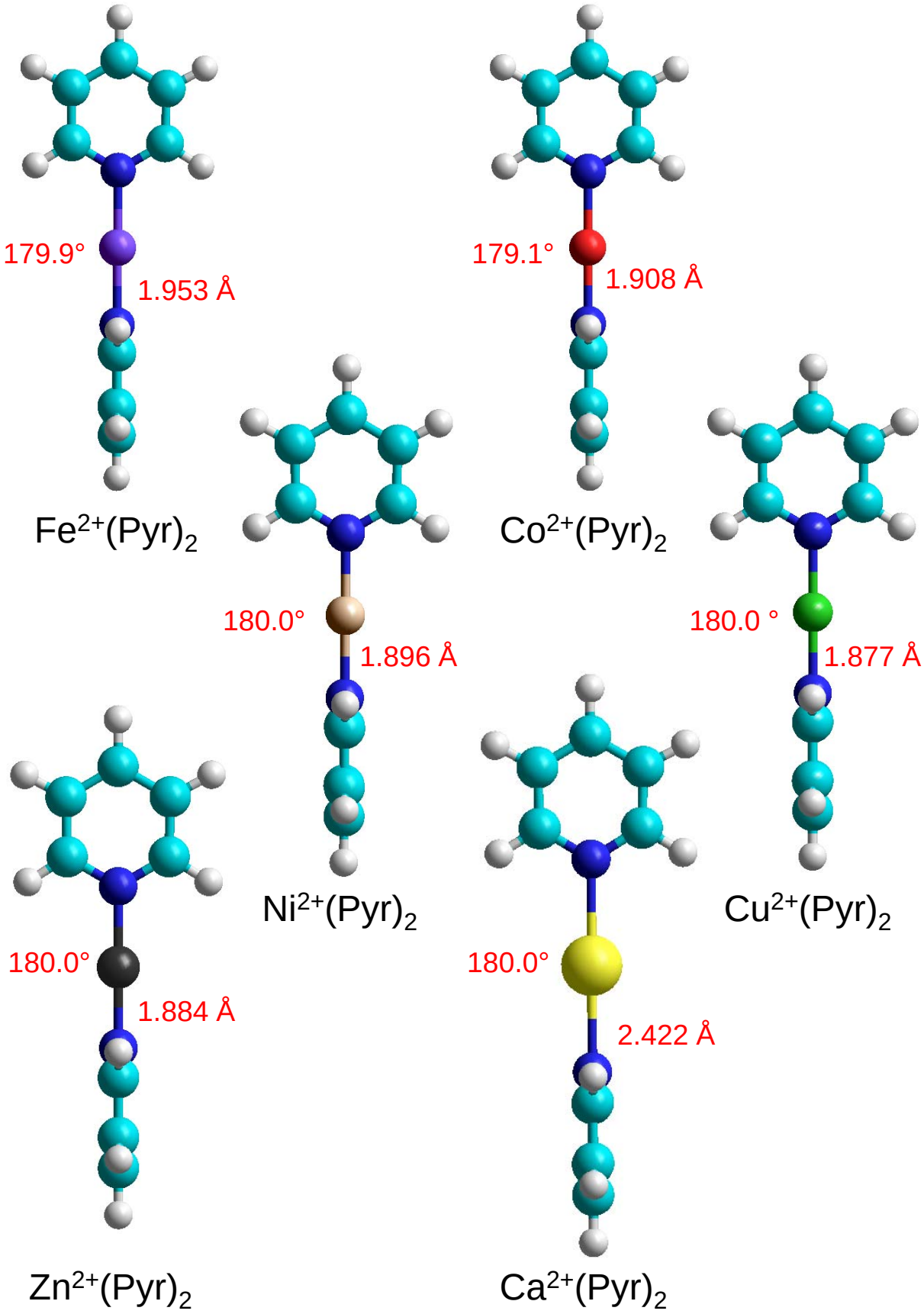
179.9°
1.953 Å
$Fe^{2+}(Pyr)_2$
179.1°
1.908 Å
$Co^{2+}(Pyr)_2$
180.0°
1.896 Å
$Ni^{2+}(Pyr)_2$
180.0 °
1.877 Å
$Cu^{2+}(Pyr)_2$
180.0°
1.884 Å
$Zn^{2+}(Pyr)_2$
180.0°
2.422 Å
$Ca^{2+}(Pyr)_2$

Figure 5.1c.

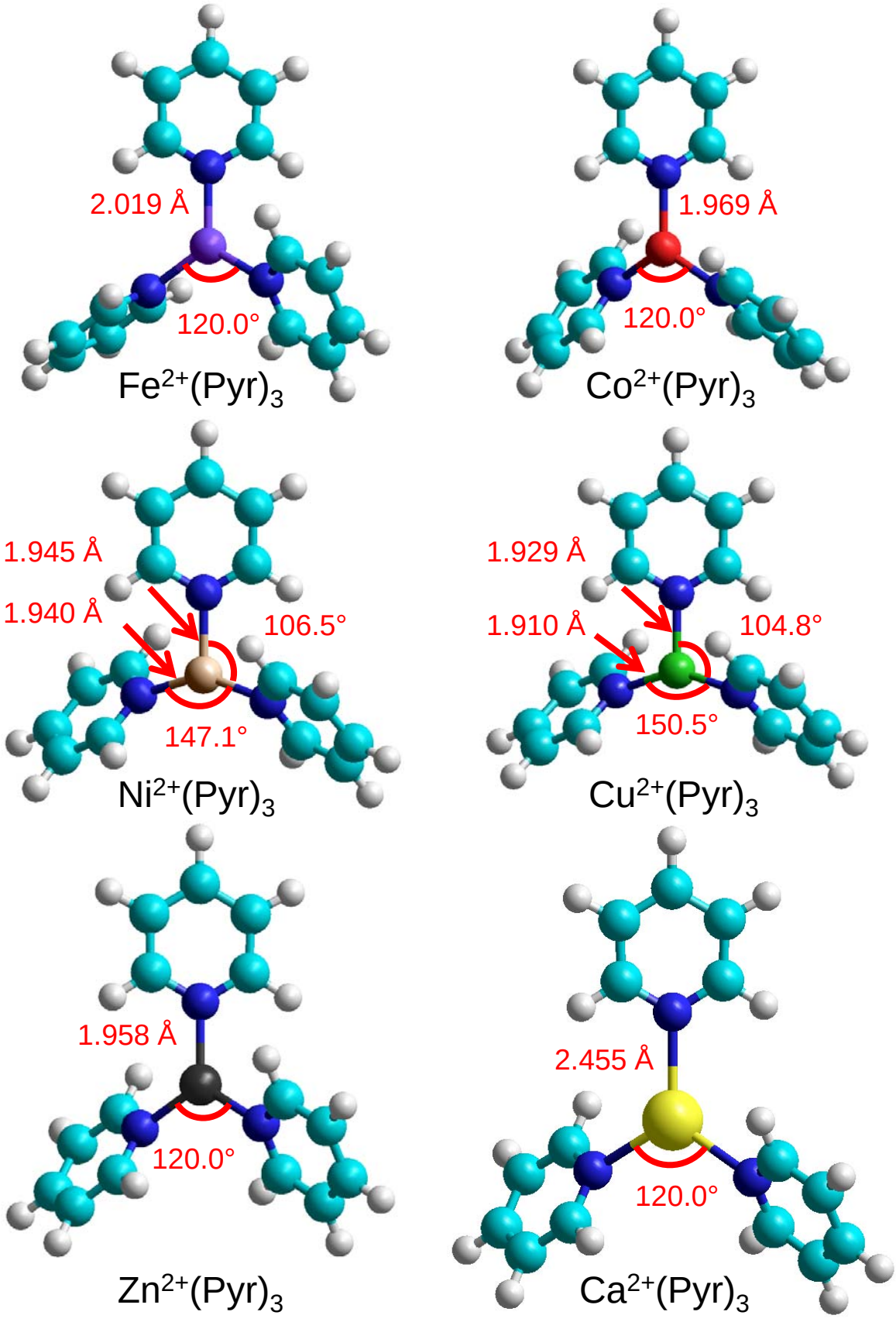
2.019 Å
120.0°
Fe2+(Pyr)3
1.969 Å
120.0°
Co2+(Pyr)3
1.945 Å
1.940 Å
106.5°
147.1°
Ni2+(Pyr)3
1.929 Å
1.910 Å
104.8°
150.5°
Cu2+(Pyr)3
1.958 Å
120.0°
Zn2+(Pyr)3
2.455 Å
120.0°
Ca2+(Pyr)3

Figure 5.1d.

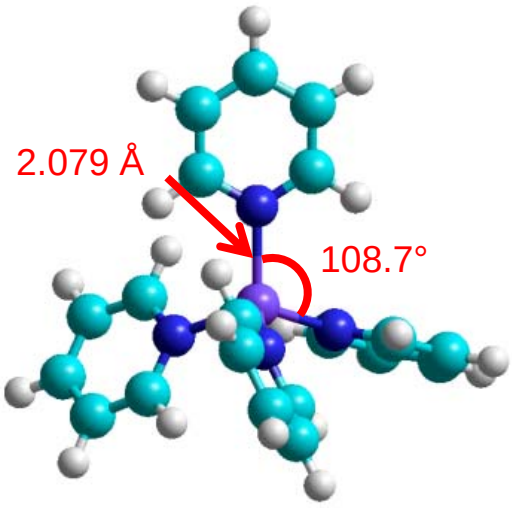

$Fe^{2+}(Pyr)_4$

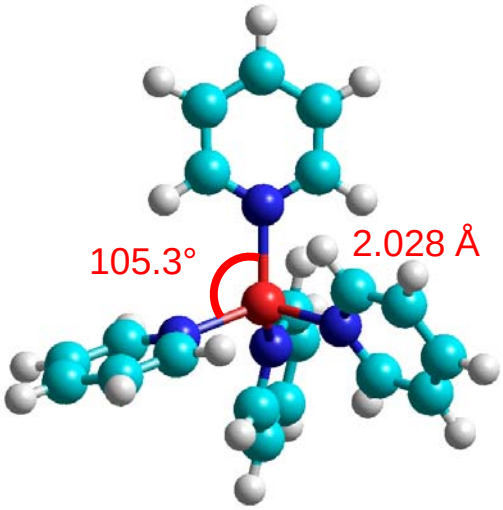

$Co^{2+}(Pyr)_4$

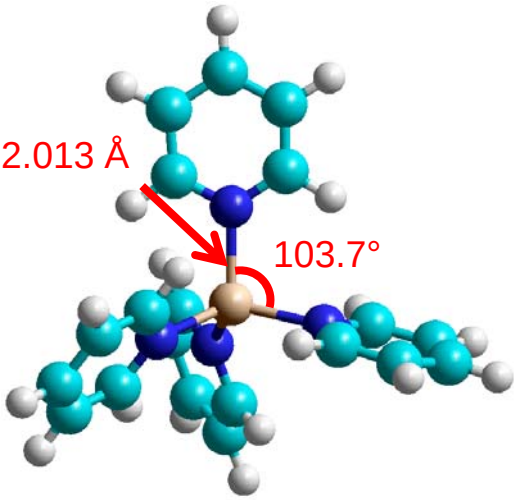

$Ni^{2+}(Pyr)_4$

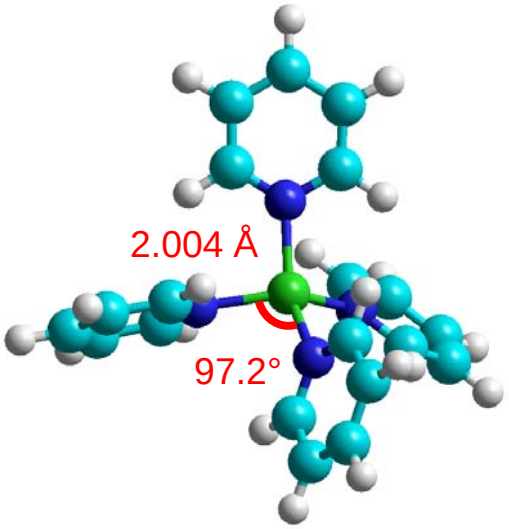

$Cu^{2+}(Pyr)_4$

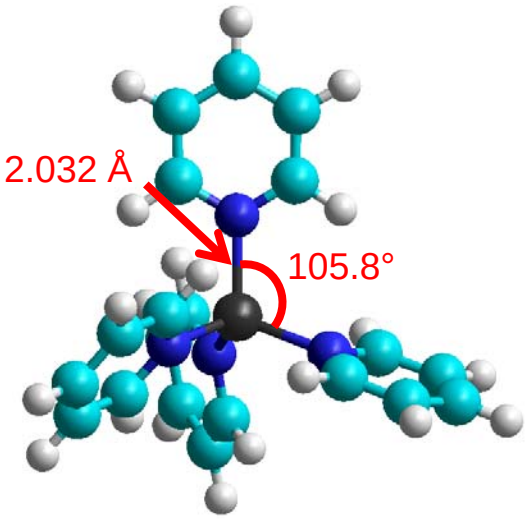

$Zn^{2+}(Pyr)_4$

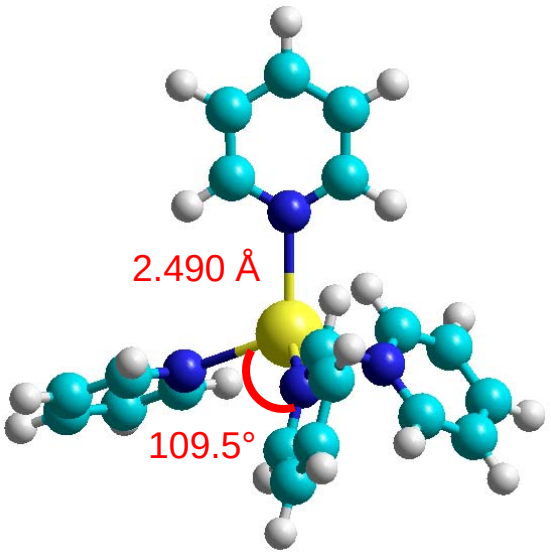

$Ca^{2+}(Pyr)_4$

Figure 5.1e.

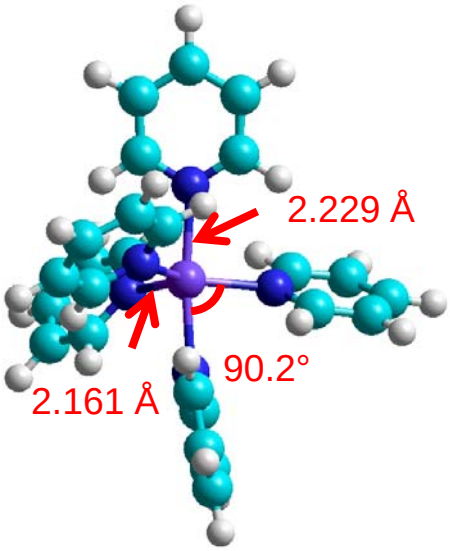

$Fe^{2+}(Pyr)_5$

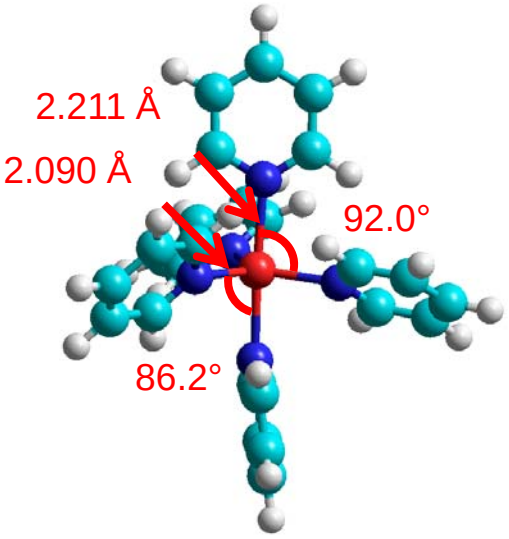

$Co^{2+}(Pyr)_5$

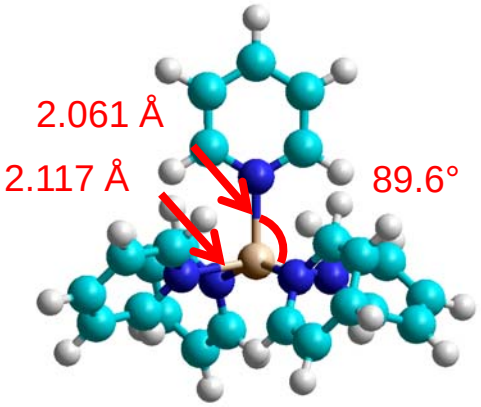

$Ni^{2+}(Pyr)_5$

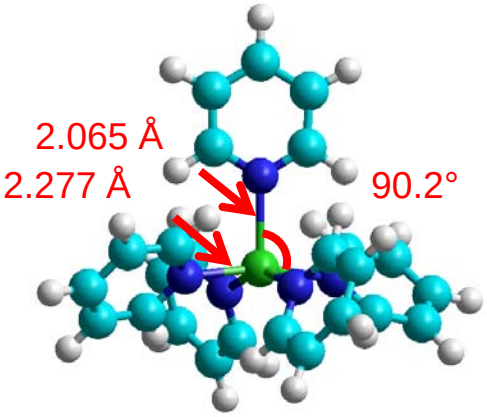

$Cu^{2+}(Pyr)_5$

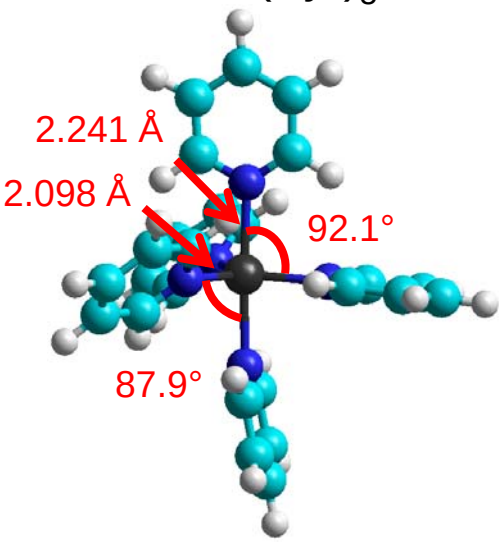

$Zn^{2+}(Pyr)_5$

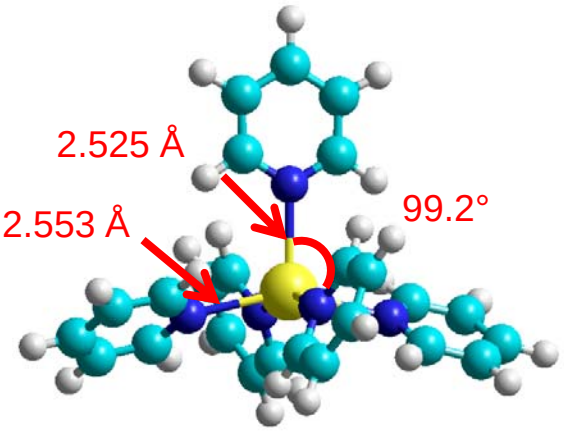

$Ca^{2+}(Pyr)_5$

Figure 5.1f.

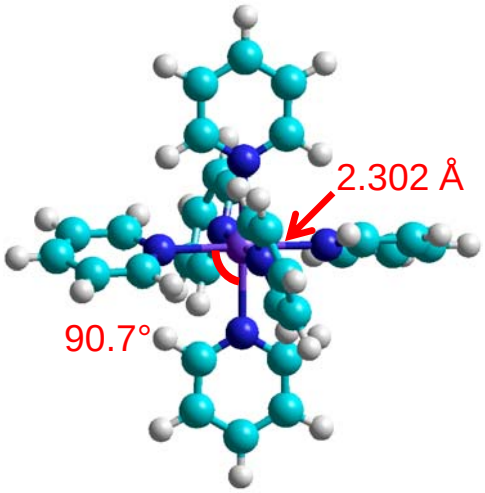

$Fe^{2+}(Pyr)_6$

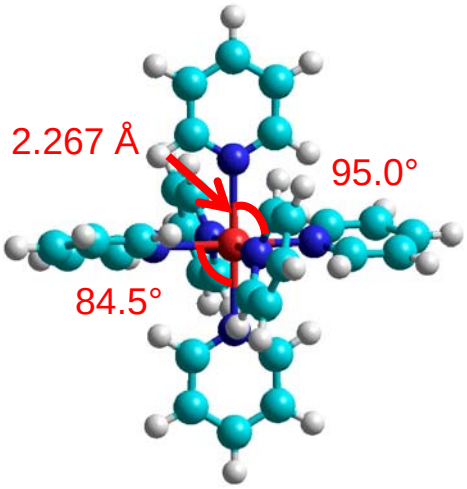

$Co^{2+}(Pyr)_6$

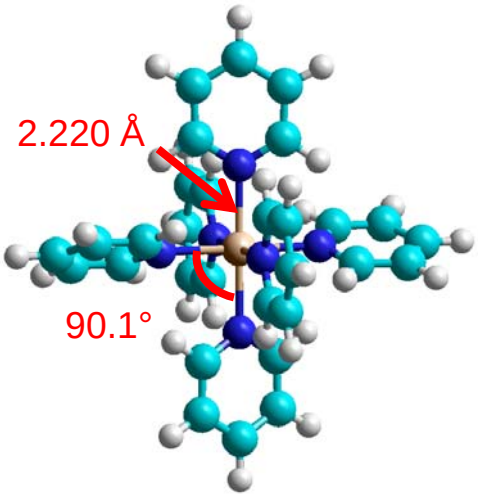

$Ni^{2+}(Pyr)_6$

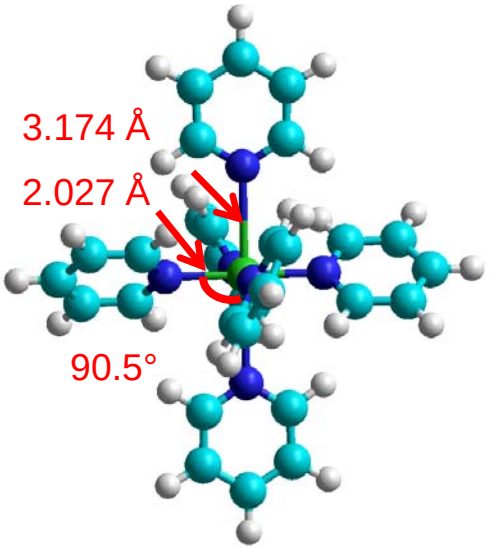

$Cu^{2+}(Pyr)_6$

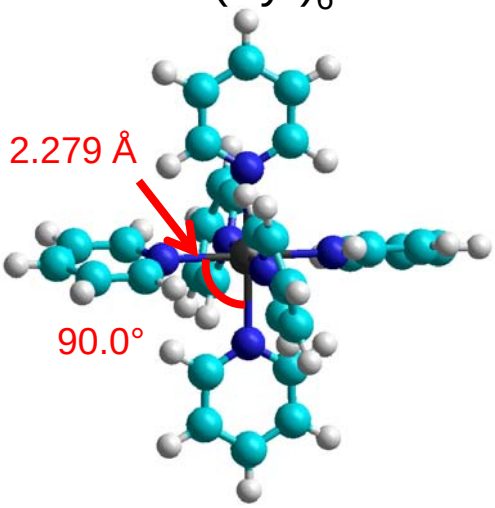

$Zn^{2+}(Pyr)_6$

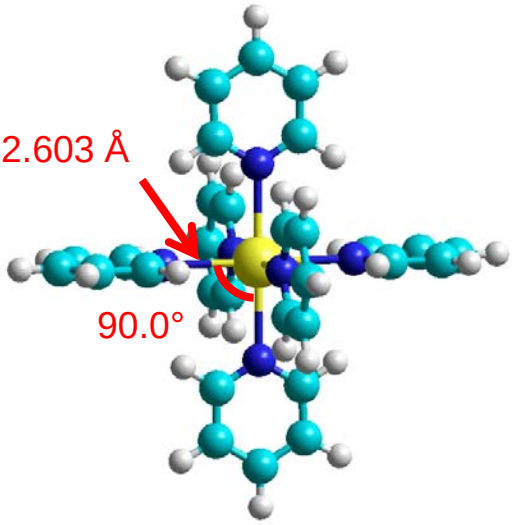

$Ca^{2+}(Pyr)_6$

Figure 5.2.

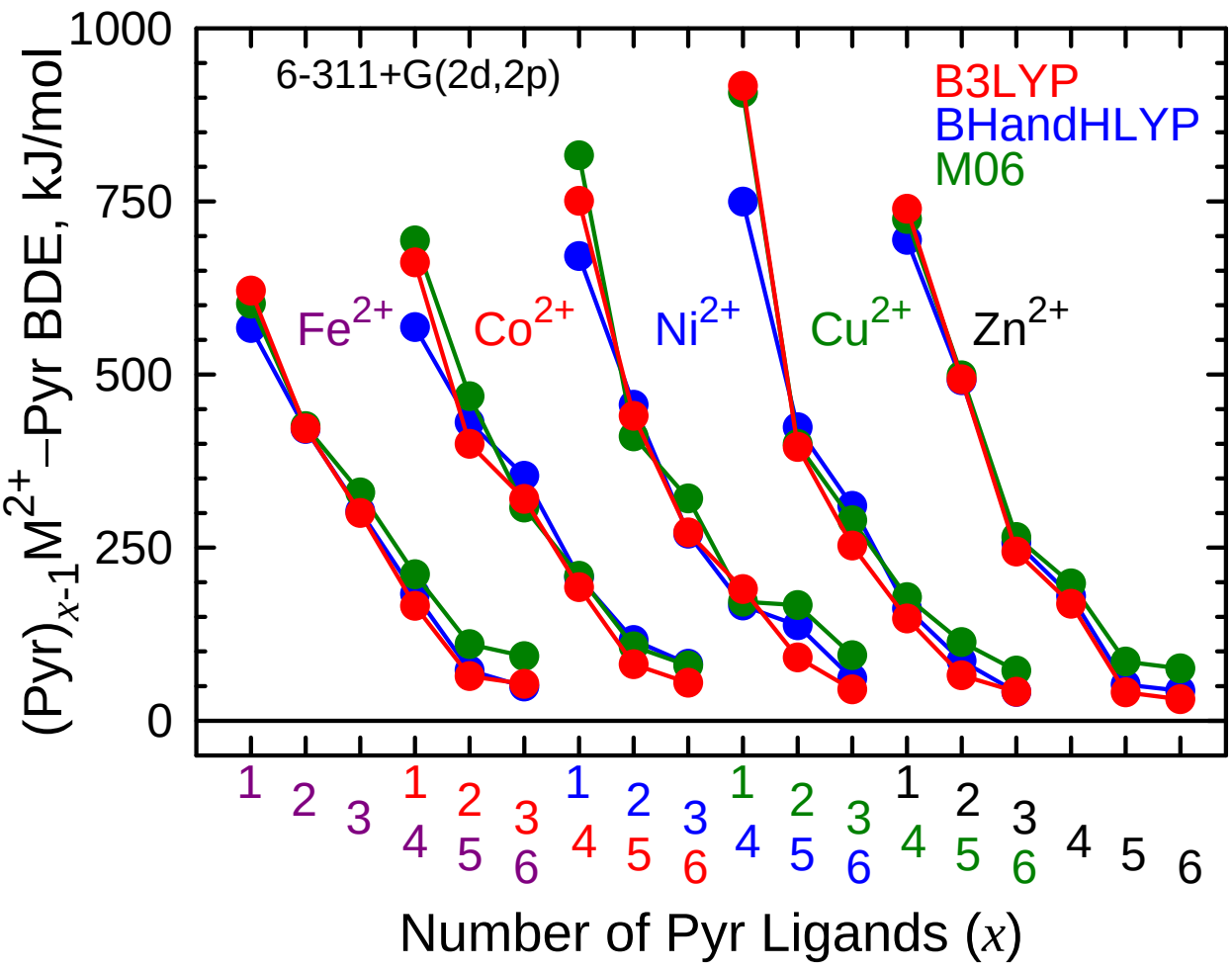
6-311+G(2d,2p)
B3LYP
BHandHLYP
M06
Fe2+
Co2+
Ni2+
Cu2+
Zn2+
(Pyr)x-1M2+–Pyr BDE, kJ/mol
1000
750
500
250
0
Number of Pyr Ligands (x)

Figure 5.3.

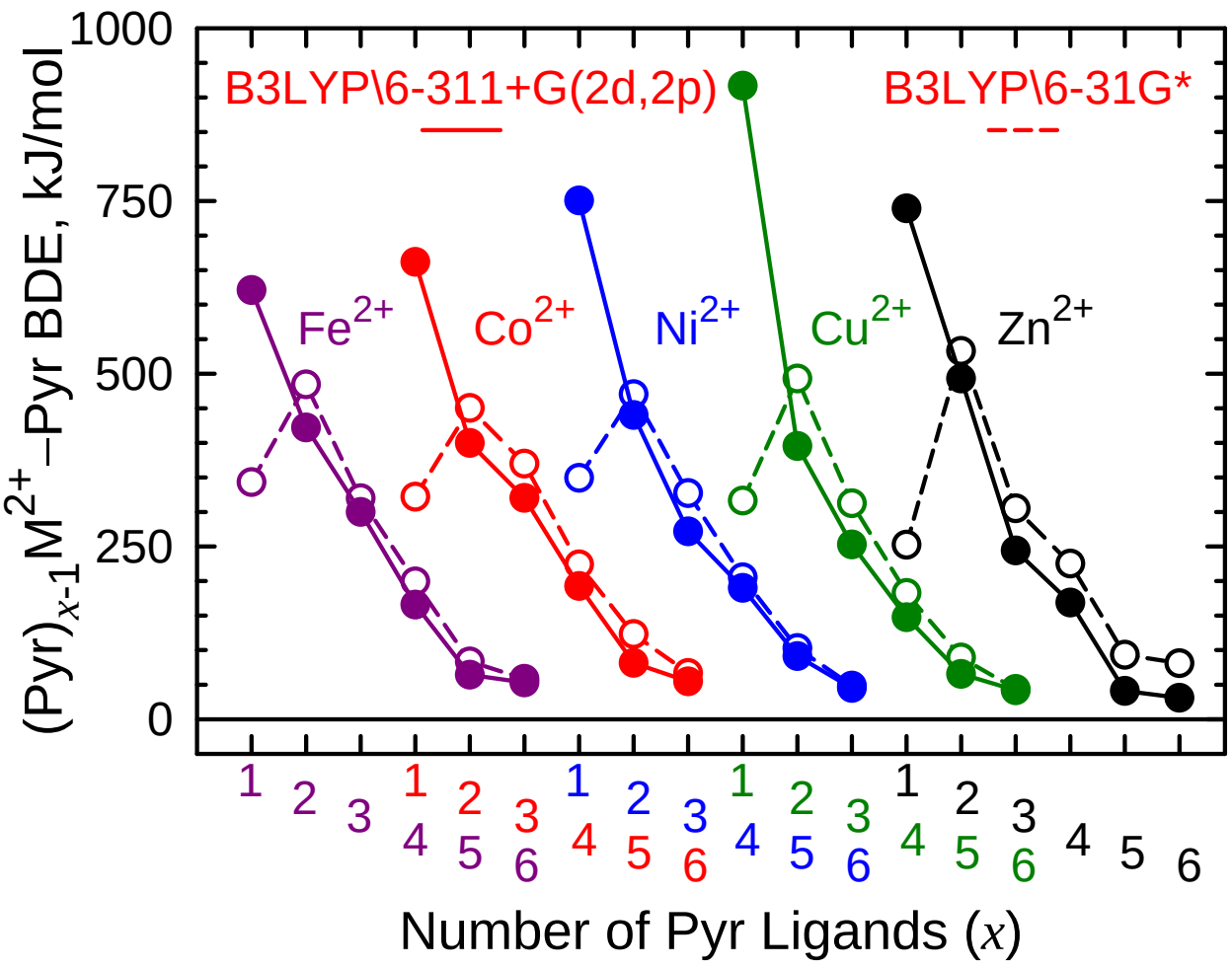
B3LYP\6-311+G(2d,2p)
B3LYP\6-31G*
Fe2+
Co2+
Ni2+
Cu2+
Zn2+
(Pyr)x-1M2+–Pyr BDE, kJ/mol
1000
750
500
250
0
Number of Pyr Ligands (x)

Figure 5.4.

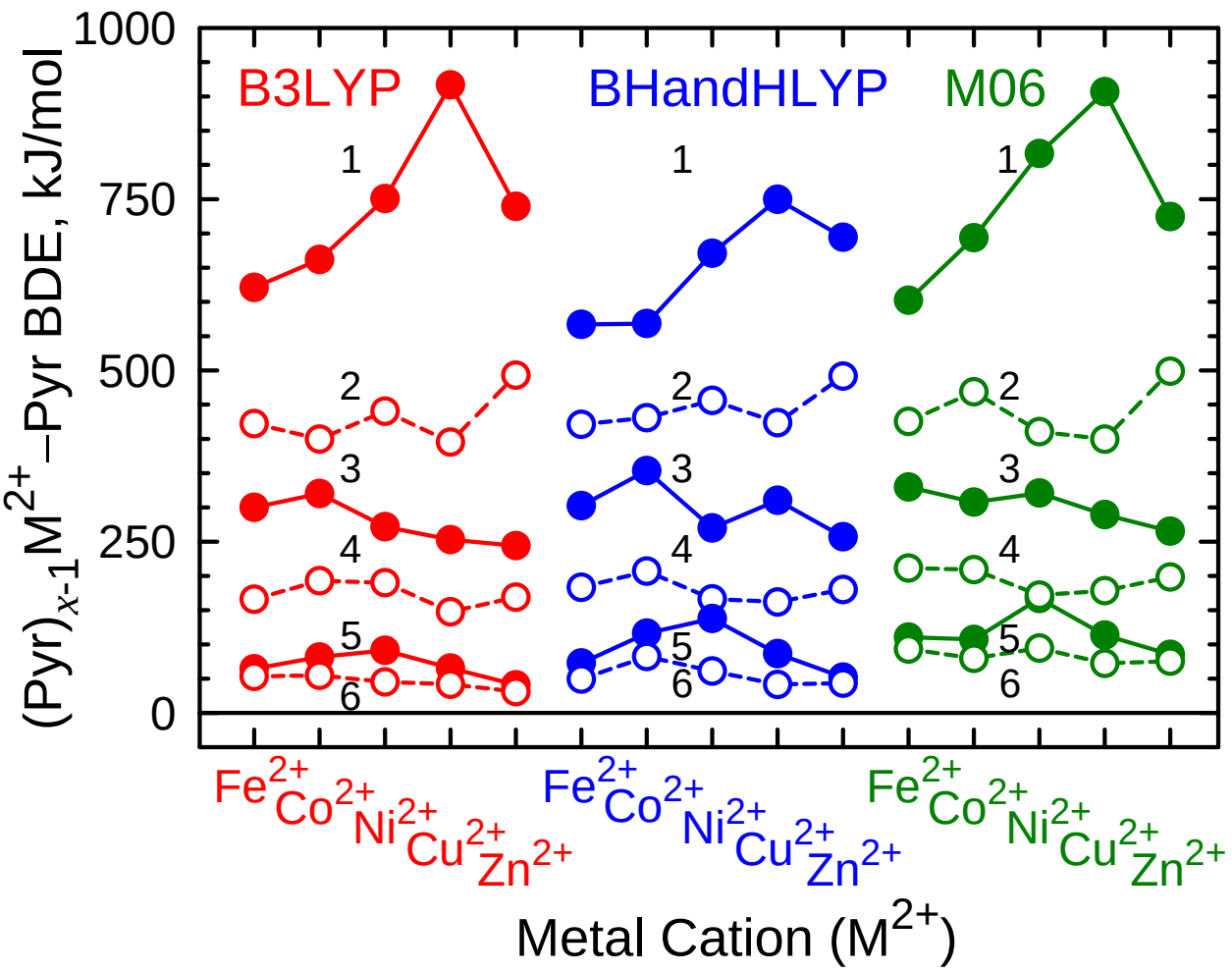
B3LYP
BHandHLYP
M06
1
2
3
4
5
6
1000
750
500
250
0
(Pyr)x-1M2+–Pyr BDE, kJ/mol
Fe2+ Co2+ Ni2+ Cu2+ Zn2+
Metal Cation (M2+)

Figure 5.5.

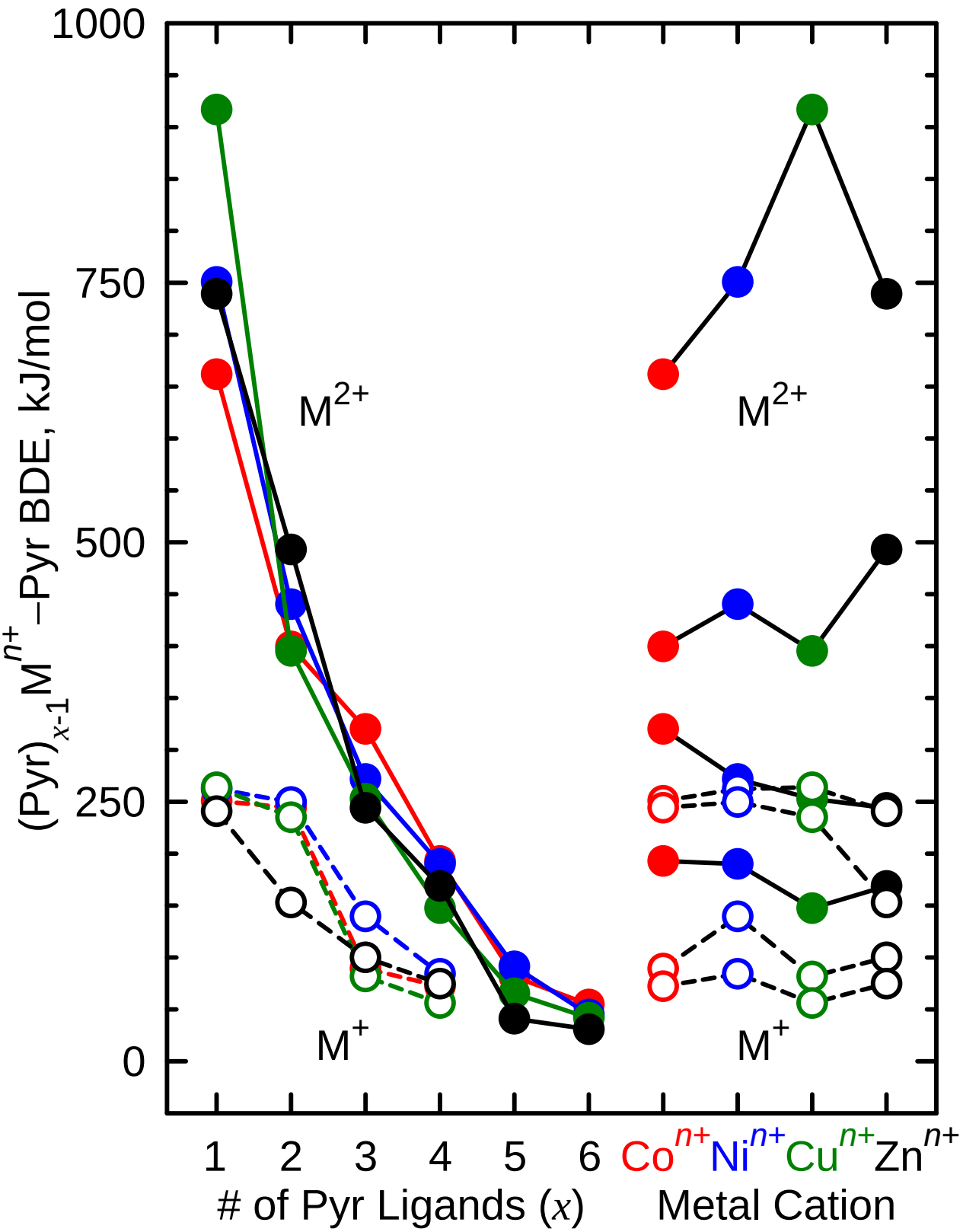
1000
750
500
250
0
(Pyr)$_{x-1}$M^{n+}–Pyr BDE, kJ/mol
M^{2+}
M^{2+}
M^{+}
M^{+}
1
2
3
4
5
6
# of Pyr Ligands (x)
Co^{n+} Ni^{n+} Cu^{n+} Zn^{n+}
Metal Cation

Figure 5.6.

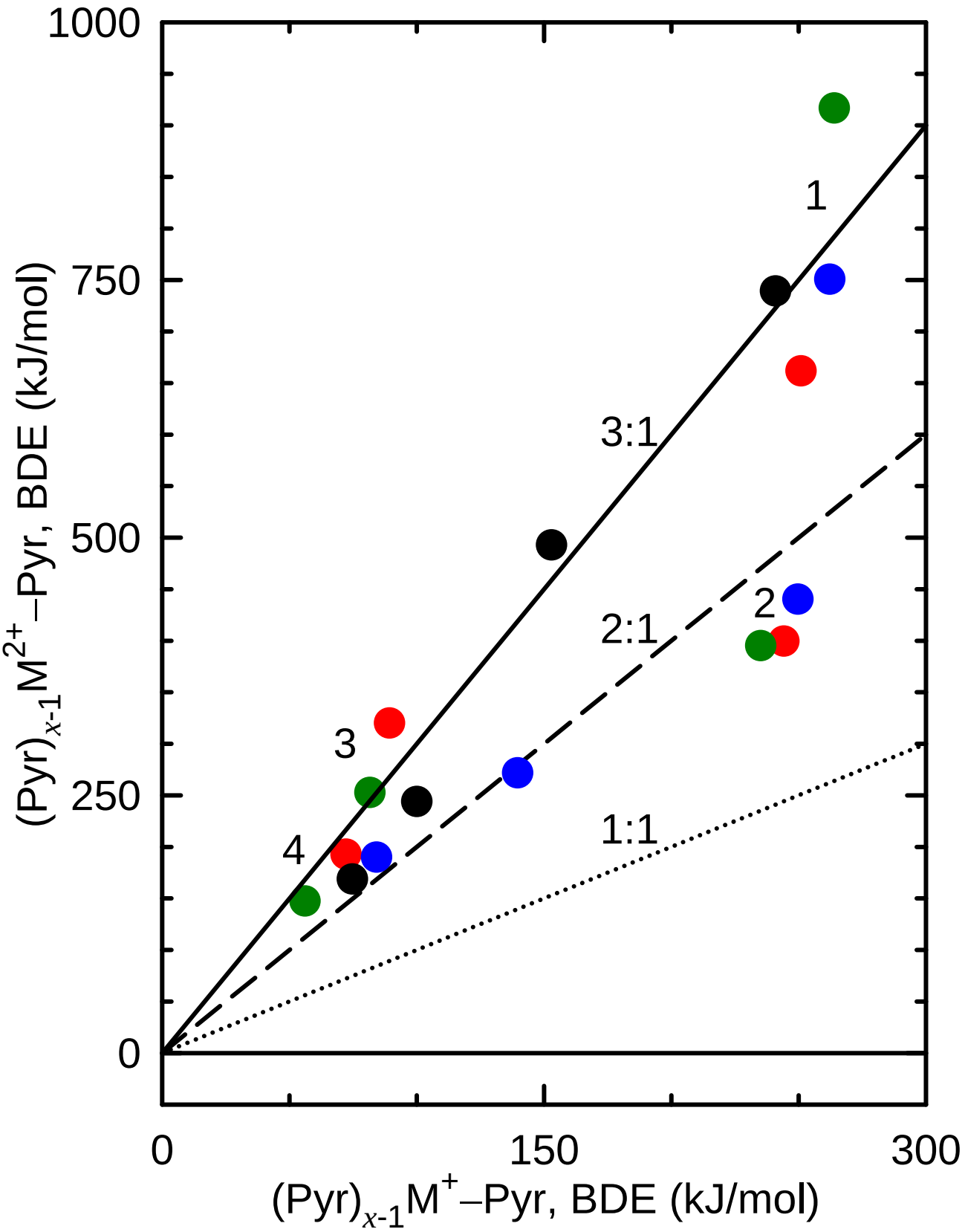
1000
750
500
250
0
0
150
300
(Pyr)x-1M2+–Pyr, BDE (kJ/mol)
(Pyr)x-1M+–Pyr, BDE (kJ/mol)
1
3:1
2
2:1
3
4
1:1

Figure 5.7.

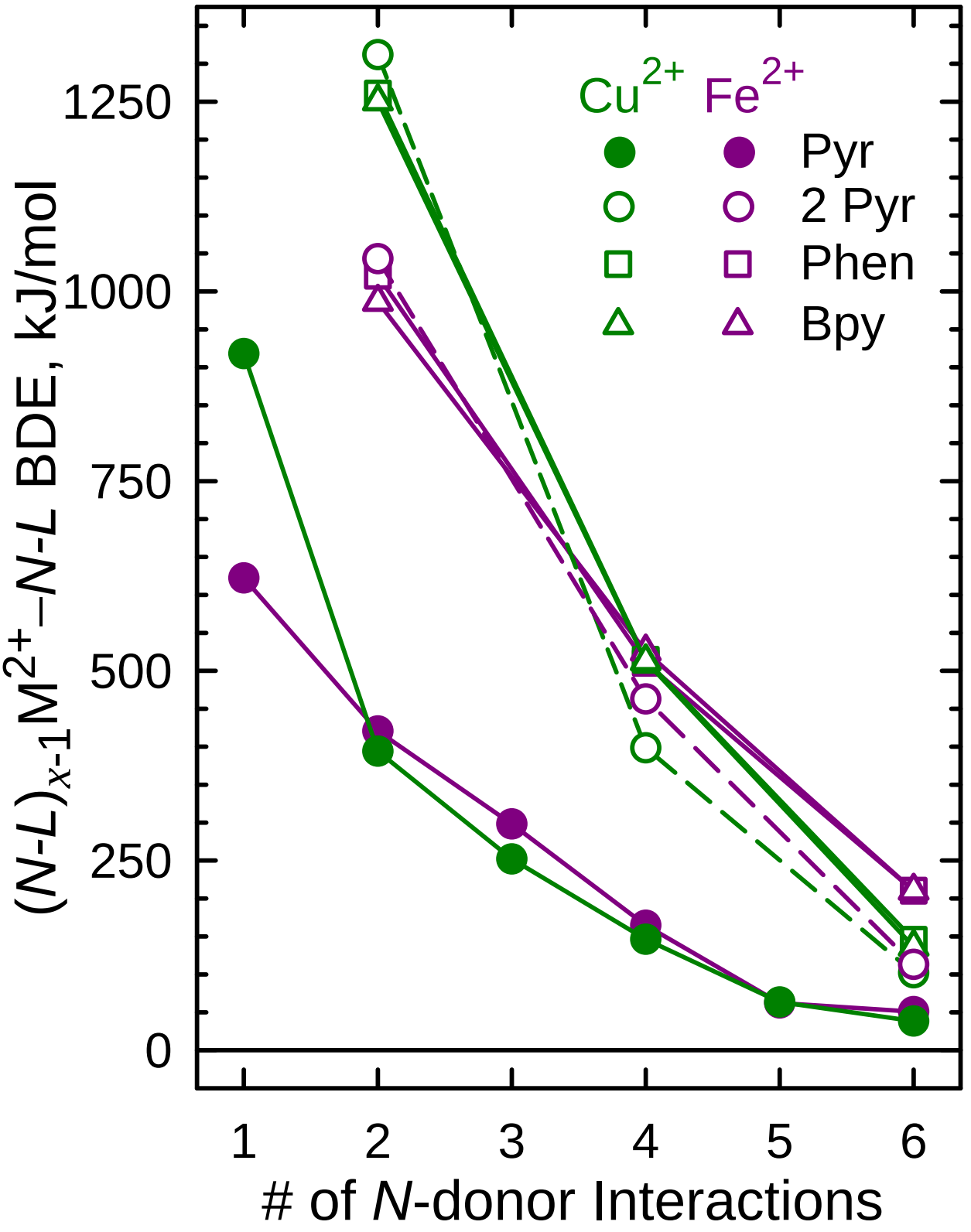
Cu2+ Fe2+
Pyr
2 Pyr
Phen
Bpy
(N-L)x-1M2+–N-L BDE, kJ/mol
1250
1000
750
500
250
0
1
2
3
4
5
6
# of N-donor Interactions

Figure 5.8a.

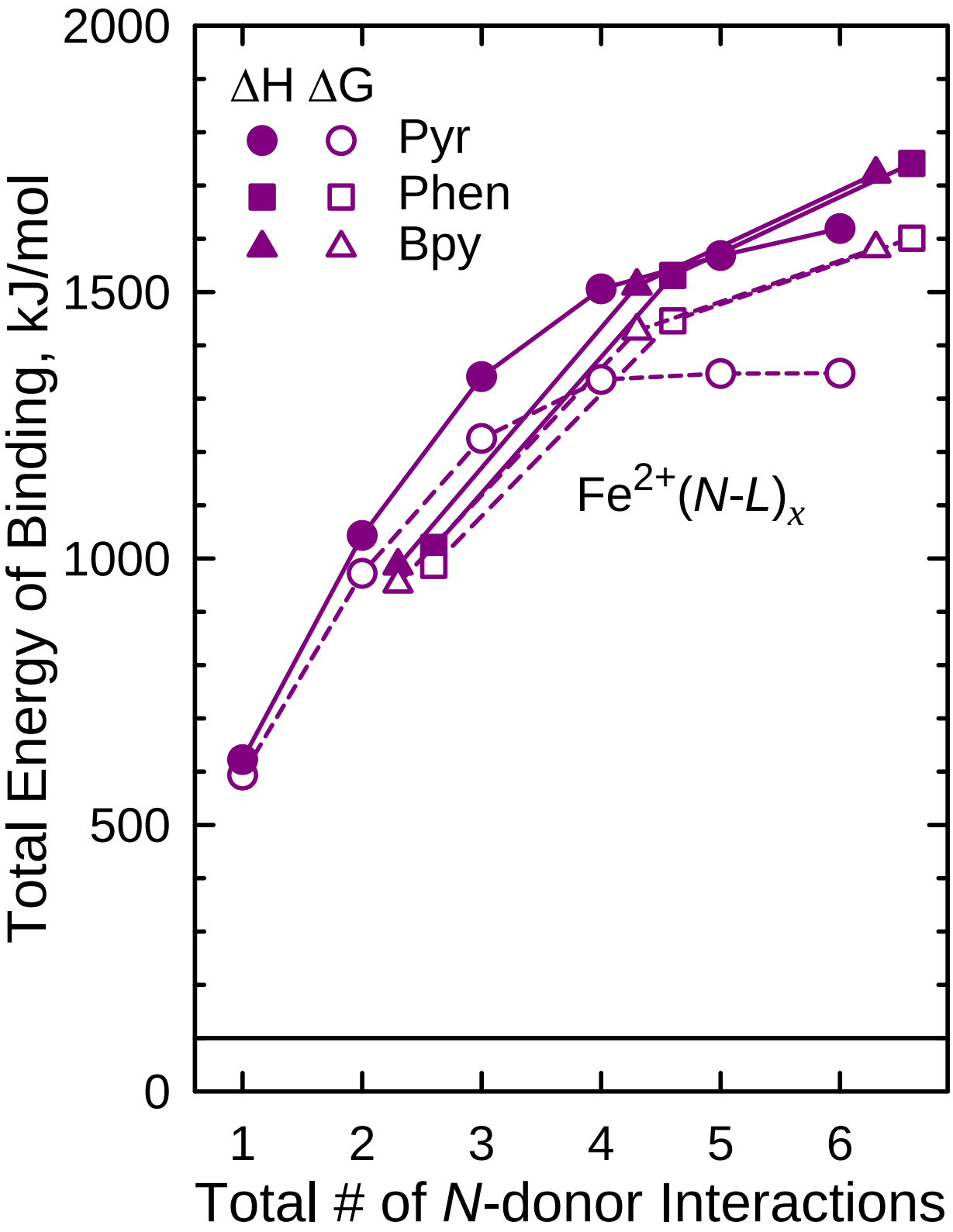
2000
1500
1000
500
0
ΔH ΔG
Pyr
Phen
Bpy
Fe2+(N-L)x
Total Energy of Binding, kJ/mol
1
2
3
4
5
6
Total # of N-donor Interactions

Figure 5.8b.

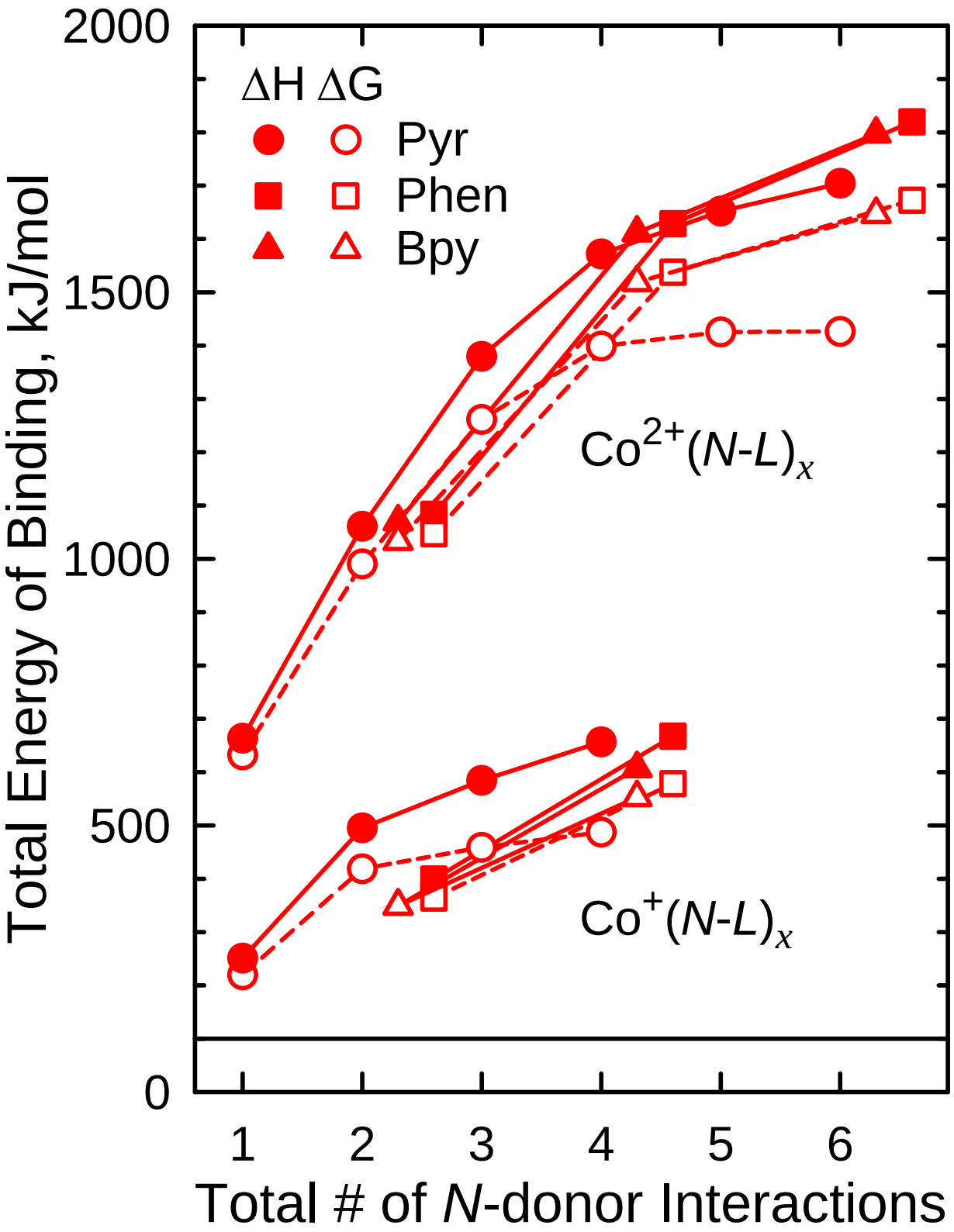
ΔH ΔG
Pyr
Phen
Bpy
Co2+(N-L)x
Co+(N-L)x
Total Energy of Binding, kJ/mol
2000
1500
1000
500
0
1
2
3
4
5
6
Total # of N-donor Interactions

Figure 5.8c.

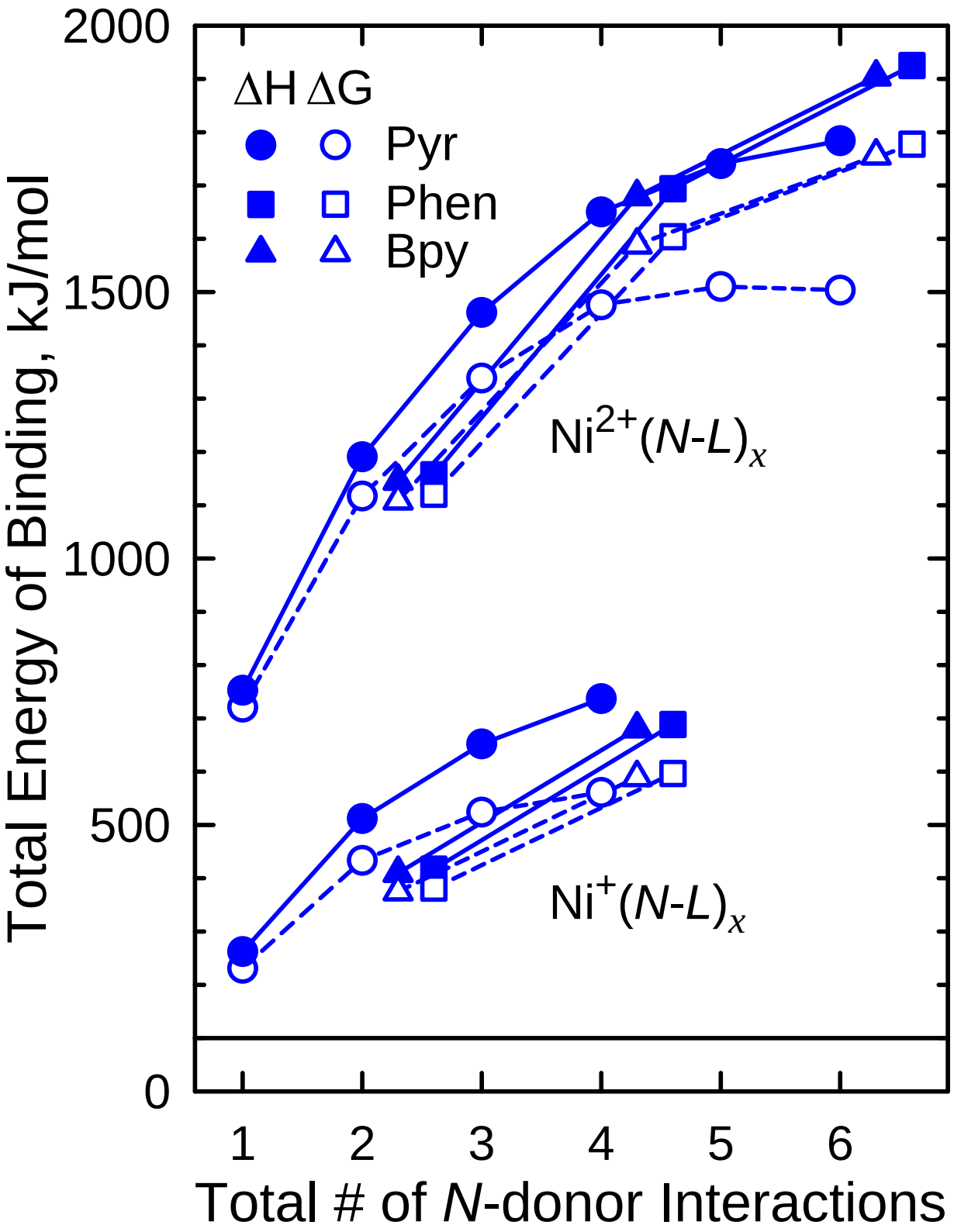
2000
1500
1000
500
0
ΔH ΔG
Pyr
Phen
Bpy
Ni2+(N-L)x
Ni+(N-L)x
Total Energy of Binding, kJ/mol
1
2
3
4
5
6
Total # of N-donor Interactions

Figure 5.8d.

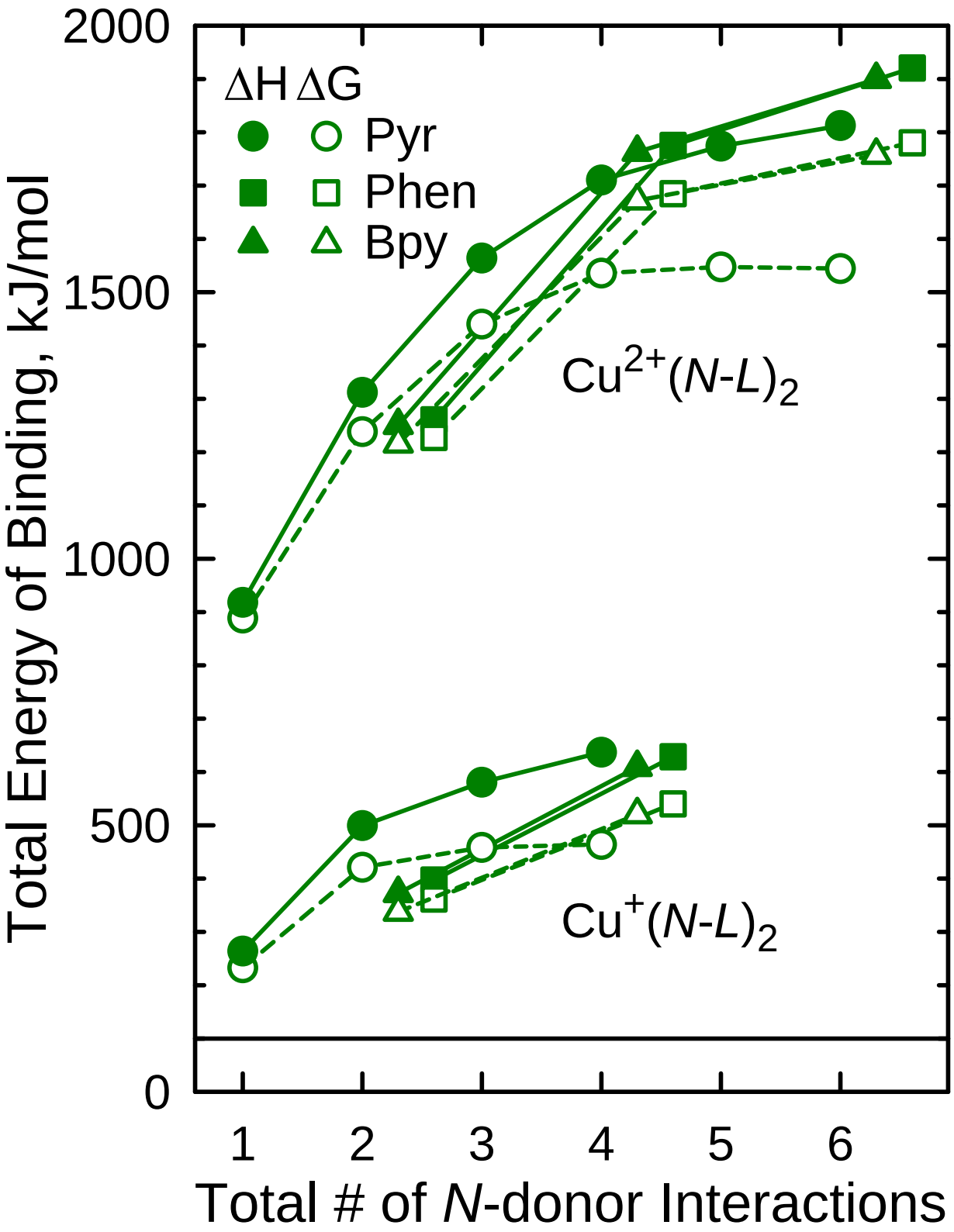
2000
1500
1000
500
0
ΔH ΔG
Pyr
Phen
Bpy
Cu2+(N-L)2
Cu+(N-L)2
Total Energy of Binding, kJ/mol
1
2
3
4
5
6
Total # of N-donor Interactions

Figure 5.8e.

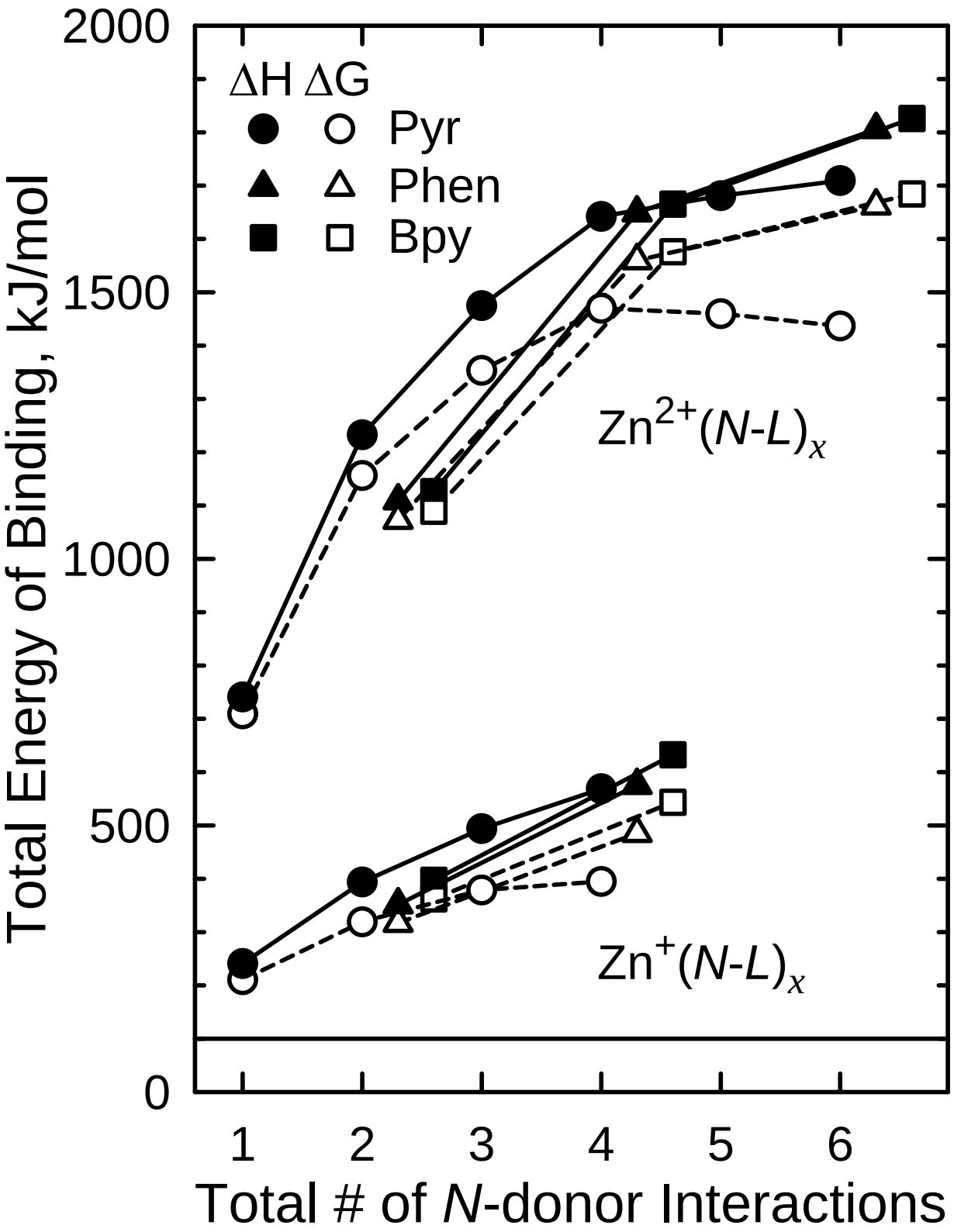
2000
1500
1000
500
0
ΔH ΔG
Pyr
Phen
Bpy
Zn2+(N-L)x
Zn+(N-L)x
Total Energy of Binding, kJ/mol
1
2
3
4
5
6
Total # of N-donor Interactions

Figure 5.9.

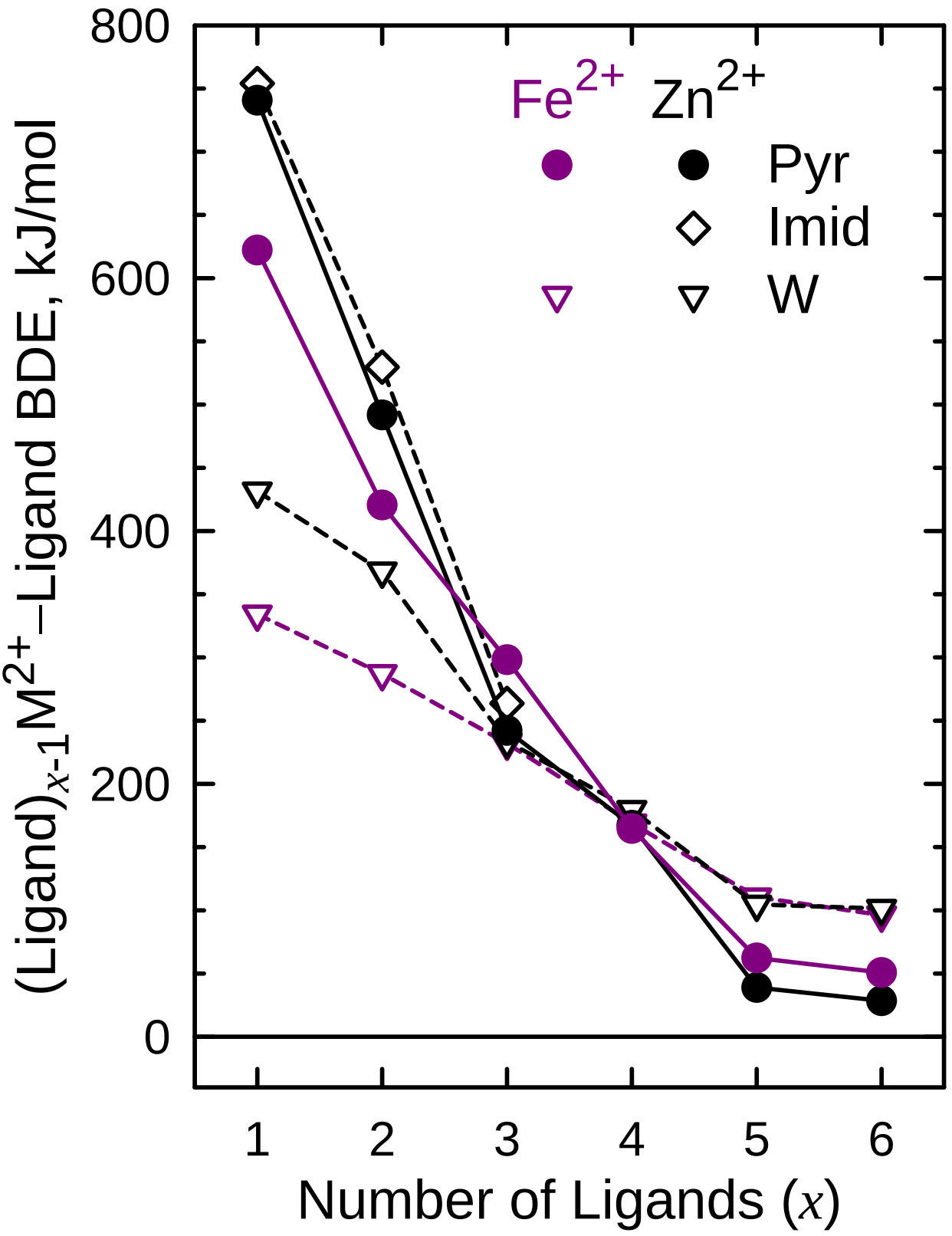
800
600
400
200
0
1
2
3
4
5
6
Number of Ligands (x)
(Ligand)x-1M2+–Ligand BDE, kJ/mol
Fe2+
Zn2+
Pyr
Imid
W

CHAPTER 6

GENERAL CONCLUSIONS AND FUTURE DIRECTIONS

6.1 General Conclusions

Energy-resolved collision-induced dissociation (CID) studies carried out in a custom-built guided ion beam tandem mass spectrometer (GIBMS) have been used to probe the structures, energetics of binding, and fragmentation behavior of a series of transition metal-ligand complexes. These experimental studies are supported and enhanced by complementary electronic structure theory calculations using several theoretical methods including B3LYP, BHandHLYP, and M06 functionals to determine the stable low-energy structures of the transition metal-ligand complexes and the relevant species associated with their CID behavior. These studies probe the effects of the electronic structure of the metal cation on the structures and binding energies by including the five late first-row transition metals cation in their +2 oxidations states, $Fe^{2+}(d^6)$, $Co^{2+}(d^7)$, $Ni^{2+}(d^8)$, $Cu^{2+}(d^9)$, and $Zn^{2+}(d^{10})$. The *N-L* donor ligands investigated include pyridine (Pyr), a monodentate ligand, and two bidentate ligands, 2,2'-bipyridine (Bpy) and 1,10-phenanthroline (Phen). Complexes with one to six Pyr ligands and one to three Bpy or Phen ligands are included in this work. The series of inter-related studies carried out in this dissertation are designed to probe the influence of the electronic structure of the metal cation, the nature and number of *N-L* donor ligands, as well as the effects of chelation and extent of ligation on the geometry and binding strength of these transition metal cation-ligand complexes, which are relevant to catalysis, metallo-supramolecular chemistry and electron and proton transfer processes.

The geometric structures of $M^{2+}(N\text{-}L)_x$ where $M^{2+} = Fe^{2+}$, Co^{2+}, Ni^{2+}, Cu^{2+}, and Zn^{2+}, *N-L* = Pyr, Bpy, and Phen, and x = 1–6 for Pyr and x = 1–3 for Bpy and Phen complexes are

determined at B3LYP, BHandHLYP, and M06 levels of theory using the 6-31G* basis set. Sequential BDEs are determined at B3LYP, BHandHLYP, and M06 levels of theory with 6-311+G(2d,2p) basis set using the B3LYP/6-31G*, BHandHLYP/6-31G*, and M06/6-31G* optimized geometries, respectively. In all of the $M^{2+}(N\text{-}L)_x$ complexes, the binding is dominated by σ donation from the nitrogen lone pair(s) to the M^{2+} cations regardless of the level of theory employed. The binding is also enhanced by π-backdonation from occupied d_π orbitals of the M^{2+} cations to the unoccupied π^* orbitals of the *N-L* ligands. Π-backdonation from the *N-L* ligands to M^{2+} is also found to enhance the binding, but its contribution to the binding is not very significant. The ground-state geometries of all the $M^{2+}(N\text{-}L)_x$ complexes show that the *N-L* ligands bind in a fashion consistent with the simple valence shell electron pair repulsion model, where minor distortions from the idealized geometries are correlated with the structure of the *N-L* ligands and more significant distortions with the valence electron configuration of the metal cation.

In almost all cases, the M^{2+}–N bond lengths of $M^{2+}(N\text{-}L)_x$ complexes increase with increasing ligation as a result of the decreasing electrostatic attraction between the M^{2+} cation and the *N-L* ligands and increasing ligand-ligand repulsive interactions. This trend is an exception to Phen and Bpy complexes of Fe^{2+} whereby singlet state tris-complexes exhibit shorter Fe^{2+}–N bond lengths than those of quintet state bis-complexes as a result of the spin crossover from a quintet to singlet state upon binding of the third *N-L* ligand. The $M^{2+}(Bpy)_x$ complexes exhibit M^{2+}–N bond lengths that are highly parallel to, but slightly shorter by ≤ 0.01 Å than those of in the analogous $M^{2+}(Phen)_x$ complexes suggesting that these M^{2+}–N bond lengths are closely linked to the rigidity and flexibility of the ligand framework. Because Phen is extremely rigid, the two nitrogen-donor atoms are highly constrained by the

extended π network of the aromatic ligand, and therefore exhibit a nearly fixed distance between the two coordinating nitrogen-donor atoms. Due to the flexibility inferred by the single C–C bond linking the two pyridyl rings of the Bpy ligand, the rings bend upon complexation allowing both nitrogen-donor atoms to achieve a more optimal binding orientation about the metal cation, and resulting in slightly shorter M^{2+}–N bond lengths.

Comparison between the $M^{2+}(Pyr)_x$ complexes to the transition metal cations and the $Ca^{2+}(Pyr)_x$ complexes show that the differences in the M^{2+}–N bond lengths between analogous structures are a result of the effects of sd hybridization and π-backdonation on the binding. Hybridization of the 4s and 3dσ orbitals exhibits a very strong preference for ligation at 180.0° such that chelating ligands, i.e., Bpy and Phen are under strong geometric constraints. The constrained geometries of these ligands do not allow the two *N*-donor atoms to bind to these metal cations with the ideal ∠NM^{2+}N bond angle of 180.0°. Therefore, these ligands do not take full advantage of sd hybridization. However, the constrained ligand geometries lead to stronger binding interactions when the metal cations bind to two and three chelating ligands because of the chelation interactions and reduced ligand-ligand repulsion. As a result, the M^{2+}–N bond lengths increase in the order Pyr < Bpy < Phen for complexes with two *N*-donor interactions. With four and six *N*-donor interactions with the M^{2+} center, the M^{2+}–N bond lengths increase in the order Bpy < Phen < Pyr, suggesting that the monodentate Pyr ligand experiences more ligand-ligand repulsion as compared to the bidentate Bpy and Phen ligands.

The sequential BDEs of the $M^{2+}(Phen)_x$ complexes determined at the B3LYP, BHandHLYP, and M06 levels of theory are relatively parallel, but differ in absolute magnitude. BDEs computed using the M06 functional are the strongest, BHandHLYP values

are intermediate, whereas B3LYP produces the weakest BDEs. Similar results are found for the $M^{2+}(Bpy)_x$ complexes. In contrast, the absolute sequential binding energies for all of the $M^{2+}(Pyr)_x$ complexes examined at all the three levels of theory do not follow a similar trend like the $M^{2+}(Phen)_x$ and $M^{2+}(Bpy)_x$ complexes. However, the overall trends for all five metal cations at the three levels of theory examined are relatively parallel. The sequential BDEs of the $M^{2+}(N\text{-}L)_x$ complexes are observed to decrease monotonically with increasing ligation for all five metal cations regardless of which theory is employed. The sd hybridization of the M^{2+} cation plays a major role in enhancing the binding energy of the first *N-L* ligand. The decline in effective charge retained by the M^{2+} cation upon binding of *N-L* ligand (s), Pauli repulsion between the valence electrons of the metal cation and those donated by *N-L* ligands, and ligand-ligand repulsive interactions which increase with each successive *N-L* ligand bound also contribute to the fall off in the strength of binding with increasing ligation. Periodic trends indicate that the binding in all of the $M^{2+}(N\text{-}L)_x$ complexes is dominated by the electronic structure of the metal cation and to a lesser extent by the nature of the *N-L* ligand.

In all cases, binding in the Phen complexes is slightly stronger than that for the Bpy complexes for the M^{2+} cations examined. An exception is found for Fe^{2+} complexes whereby the measured third-sequential BDEs for $^5Fe^{2+}(Bpy)_3$ are 4.1 kJ/mol higher than those for $^5Fe^{2+}(Phen)_3$. This variation results from the tendency of Fe^{2+} complexes towards low spin d^6 metal complexes and slightly stronger ligand field provided by Phen. The flexibility of the Bpy ligand plays a significant role in that it enhances its binding interactions with the M^{2+} cations, leading to BDEs for its complexes that approach those of the analogous Phen complexes, where the difference in the strength of binding is largely the result of relaxation

of Bpy upon dissociation, and thus requiring less energy (~24.5 kJ/mol) to dissociate. Differences in sequential and total binding energies based on the number of *N*-donor interactions between the Pyr, Bpy, and Phen complexes depict the interplay between the flexibility of the Pyr ligand that allows Pyr to take full advantage of sd hybridization, the geometric constraints of the Bpy and Phen ligands, ligand-ligand repulsive interactions, and chelation effects. Comparison of the sequential BDEs of the $M^{2+}(N\text{-}L)_x$ to the analogous $M^{+}(N\text{-}L)_x$ complexes indicates that the charge (or oxidation state) of the metal cation is the dominant factor contributing to the differences in the strength of binding among these complexes. The strength of binding is also found to depend on the electron configuration of the metal cation; however differences in the strength of binding are much smaller for cations of the same charge.

The kinetic energy dependent cross sections for the interaction of M^{2+} cations with Phen and Bpy ligands are determined by collision-induced dissociation using a guided ion beam tandem mass spectrometer. The M^{2+} cations examined in these studies include: Fe^{2+}, Co^{2+}, Ni^{2+}, Cu^{2+}, and Zn^{2+}. CID experiments of $M^{2+}(Phen)_3$ and $M^{2+}(Bpy)_3$ experiments were intentionally performed under low-resolution conditions to optimize sensitivity of the threshold determination for the primary CID pathway. The kinetic energy dependences of the CID of $M^{2+}(Phen)_3$ complexes reveal that the dominant dissociation pathway for all complexes is the loss of an intact Phen ligand. Sequential dissociation of the $M^{2+}(Phen)_2$ primary CID product is observed at elevated energies. Activated dissociation pathways corresponding to electron transfer Coulomb fission (ETCF) and proton transfer Coulomb fission (PTCF) are also observed as very minor sequential dissociation pathway at higher energies. The $M^{2+}(Bpy)_3$ complexes exhibit similar behavior. Thus, the CID behavior of

both $M^{2+}(Phen)_3$ and $M^{2+}(Bpy)_3$ complexes indicates that the nature of the binding of the third ligand in these complexes is predominantly noncovalent. Comparison between TCID measured values and theoretical values determined at B3LYP, BHandHLYP, and M06 show very good agreement between B3LYP and TCID, suggesting that B3LYP functional is capable of accurately describing the third sequential BDEs of the $M^{2+}(Phen)_x$ and $M^{2+}(Bpy)_x$ complexes.

6.2 Future Directions

In the future, CID experimental studies on $M^{2+}(Pyr)_x$ complexes need to be performed. Theoretical calculations determining the geometric structures and sequential BDEs of these complexes have been examined in this thesis. Enthalpies and free energies of the binding of the $M^{2+}(Pyr)_x$ complexes computed in this thesis suggest that the experimental studies can be performed for $M^{2+}(Pyr)_x$ complexes where x = 2–4, but are not feasible for x = 1, 5, and 6. In the future, theoretical and experimental study of the influence of other metal cations, higher oxidation states, and substituted forms of *N*-*L* donor ligands need to be determined. Such studies will allow assessment of new metals, substituent effects, and further determination of the influence of charge on the geometric structures and binding energies. The strength of metal-ligand interactions is found to depend upon a number of properties of the metals and *N*-*L* donor ligands. Ionic radii, ionization energies, oxidation states, and valence electronic configuration strongly influence the binding interaction. The nature and number of *N*-*L* donor atoms available for binding, and the molecular polarizability and dipole moment also influence the binding interaction. Metal-ligand interactions define the structure of transition metal complexes by maintaining the stability of molecular system, and therefore have a profound impact on their physical and chemical properties and hence

underlie their functionality. Geometric structures and binding energies of transition metal complexes involving Pyr, Bpy, and Phen have been studied[1-8] and continue to be of interest to our group. Thus, comparison between the results from current and future work via complimentary studies of higher oxidation states, substituted *N-L* donor ligands, and other metal cations that enable the geometric structures and binding energies to be tuned should establish the most favorable complexes for use in catalysis and metallo-supramolecular applications.

6.3 References

(1) Rodgers, M. T.; Stanley, J. R.; Amunugama, R. *J. Am. Chem. Soc*. **2000**, *122*, 10969.

(2) Rannulu, N. S.; Rodgers, M. T. *J. Phys. Chem. A* **2007**, *111*, 3465.

(3) Rannulu, N. S. Doctoral dissertation, Wayne State University. 2008, pp.393.

(4) Rannulu, N. S.; Rodgers, M. T. *J. Phys. Chem. A* **2009**, *113*, 4534.

(5) Rannulu, N. S.; Rodgers, M. T. *J. Phys. Chem. A* **2012**, *116*, 1319.

(6) Nose, H.; Chen, Y.; Rodgers, M. T. *J. Phys. Chem. A* **2013**, 117, 4316.

(7) Nose, H.; Rodgers, M. T. *ChemPlusChem* **2013**, 78, 1109.

(8) Nose, H.; Rodgers, M. T. *J. Phys. Chem. A* **2014**, under review.

APPENDIX A

Table A.1. Vibrational Frequencies and Average Vibrational Energies at 298 K.

Species	E_{vib} (eV)[a]	Vibrational frequencies (cm^{-1})[b]
Phen	0.22 (0.03)	98, 108, 233, 235, 238, 402, 405, 434, 457, 497, 509, 550, 554, 603, 618, 702, 725, 739, 763, 801, 833, 844, 852, 879, 943, 946, 955, 971, 975, 1032, 1044, 1076, 1098, 1144, 1154, 1206, 1215, 1229, 1279, 1309, 1332, 1364, 1400, 1430, 1436, 1465, 1515, 1520, 1572, 1616, 1629, 1639, 3099(2), 3115, 3123(2), 3133, 3150(2)
Fe^{2+}(Phen)	0.26 (0.03)	71, 137, 142, 229, 239, 244, 280, 293, 399, 424, 437, 467, 500, 507, 522, 558, 598, 658, 701, 724, 729, 762, 784, 819, 858, 873, 904, 958, 962, 991, 1015, 1018, 1023, 1078, 1104, 1105, 1165, 1174, 1214, 1225, 1228, 1261, 1324, 1335, 1342, 1411, 1417, 1440, 1454, 1503, 1529, 1580, 1594, 1600, 1631, 3157, 3158, 3159, 3164(2), 3169, 3183(2)
Co^{2+}(Phen)	0.26 (0.03)	79, 143, 147, 231, 247, 266, 267, 295, 402, 427, 440, 472, 503, 506, 522, 559, 600, 657, 702, 723, 737, 765, 784, 819, 857, 876, 908, 961, 964, 991, 1015, 1018, 1025, 1076, 1101, 1107, 1164, 1173, 1219, 1226, 1228, 1255, 1328, 1335, 1349, 1416, 1423, 1441, 1454, 1500, 1529, 1578, 1588, 1597, 1629, 3157, 3158, 3159, 3164(2), 3169, 3182(2)
Ni^{2+}(Phen)	0.26 (0.03)	81, 144, 152, 231, 247, 276, 281, 298, 402, 425, 442, 475, 502, 505(2), 561, 587, 660, 693, 723, 733, 737, 781, 814, 853, 880, 916, 957, 960, 990, 1014, 1017, 1023, 1073, 1099, 1107, 1166, 1173, 1220, 1227, 1229, 1255, 1323, 1338, 1353, 1417, 1426, 1440, 1456, 1499, 1524, 1574, 1584, 1593, 1630, 3157, 3159(2), 3165(2), 3169, 3182(2)
Cu^{2+}(Phen)	0.27 (0.03)	72, 142, 146, 215, 227, 267, 271, 273, 300, 425, 432, 444, 478, 497, 504, 510, 562, 656, 681, 721, 727, 745, 759, 799, 834, 880, 915, 948, 950, 973, 1009, 1014, 1020, 1071, 1096, 1116, 1164, 1172, 1223, 1224, 1231, 1257, 1332, 1343, 1351, 1416, 1429, 1437, 1457, 1497, 1518, 1574, 1592, 1595, 1632, 3156, 3158(2), 3161(2), 3168, 3180(2)
Zn^{2+}(Phen)	0.26 (0.03)	80, 138, 154, 232, 244, 245, 288, 308, 398, 430, 439, 468, 496, 507, 515, 562, 595, 658, 699, 724, 731, 748, 785, 817, 860, 873, 912, 963, 967, 992, 1017, 1019, 1022, 1081, 1105, 1106, 1167, 1174, 1214, 1225, 1230, 1265, 1333, 1335, 1346, 1411, 1419, 1442, 1453, 1504, 1527, 1583, 1596, 1603, 1630, 3157, 3159, 3160, 3169, 3175 (2), 3185(2)

Table A.1. (continued) Vibrational Frequencies and Average Vibrational Energies at 298 K.

Species	E_{vib} (eV)[a]	Vibrational frequencies (cm^{-1})[b]
$Fe^{2+}(Phen)_2$	0.56 (0.06)	18, 26, 26, 75(2), 124, 138, 140, 141(2), 232(2), 237(2), 248, 249, 267, 282, 291, 407(2), 425, 435(3), 475(2), 508(2), 510(2), 538, 539, 556, 558, 606, 607, 651(2), 719(2), 724(2), 730, 731, 781(2), 792, 794, 821, 822, 857(2), 869, 871, 904(2), 955(2), 958(2), 984(2), 1005(2), 1009(2), 1033(2), 1070(2), 1099(2), 1111, 1112, 1160(2), 1169(2), 1218, 1220, 1224, 1225, 1232(2), 1267(2), 1331, 1333, 1335(2) 1349, 1351, 1423, 1424, 1426 (2), 1440(2), 1463(2), 1508(2), 1536, 1537, 1594(2), 1603(2), 1613(2), 1638, 1639, 3151(2), 3152(4), 1349, 1351, 1423, 1424, 1426(2), 1440(2), 1463(2), 1508(2), 1536, 1537, 1594(2), 1603(2), 1613(2), 1638, 1639, 3151(2), 3152(4), 3155, 3156(3), 3164(2), 3180 (4)
$Co^{2+}(Phen)_2$	0.56 (0.06)	18, 28, 28, 77(2), 126, 139, 146(3), 231(2), 248, 251(2), 254, 287(2), 309, 404, 411, 427, 437(2), 438, 477(2), 508(2), 509(2), 539, 540, 557, 559, 604, 608, 651(2), 717(2), 724(2), 733, 735, 780(2), 793, 795, 821, 822, 856(2), 871, 873, 907(2), 953(2), 955(2), 984(2), 1004(2), 1008(2), 1033(2), 1069, 1070, 1099(2), 1113, 1114, 1161(2), 1169(2), 1219, 1220, 1225, 1226, 1233(2), 1267(2), 1335(2), 1337(2), 1350, 1351, 1426(2),1427, 1428, 1440(2), 1464(2), 1508(2), 1537, 1538, 1597(2), 1604(2), 1614(2), 1639(2), 3151(2), 3154(4), 3157(4), 3164(2), 3180(4)
$Ni^{2+}(Phen)_2$	0.55 (0.06)	14, 33, 33, 88(2), 135, 146, 147, 166(2), 232(2), 251, 253, 263(2), 284, 294, 326, 408, 411, 429, 439, 445(2), 486(2), 507(2), 516(2), 539, 540, 558, 560, 604, 606, 655(2), 718(2), 723(2), 739(2), 781(2), 795, 798, 823, 824, 856(2), 873(2), 911(2), 953(2), 956(2), 983(2), 1004(2), 1008(2), 1034(2), 1067, 1068, 1097(2), 1114, 1116, 1161(2),1168(2), 1221, 1222, 1227, 1229, 1233(2),1264(2), 1338(2), 1341(2), 1351, 1353, 1426(2), 1435(2), 1441(2), 1466(2), 1506(2), 1537, 1538, 1597(2), 1603(2), 1614(2), 1639(2), 3152(2), 3154(4), 3157(4), 3164(2), 3180(4)

Table A.1. (continued) Vibrational Frequencies and Average Vibrational Energies at 298 K.

Species	E_{vib} (eV)[a]	Vibrational frequencies (cm^{-1})[b]
$Cu^{2+}(Phen)_2$	0.55 (0.06)	27, 39, 39, 90(2), 140, 141, 145, 159, 168, 196, 233, 238, 251, 261, 273, 281, 299, 318, 409, 415, 430, 435, 440, 445, 480, 488, 507, 508, 511, 513, 539, 543, 560(2), 603, 607, 648, 653, 719, 720, 722, 723, 738, 741, 781, 783, 792, 794, 822, 825, 856, 857, 874, 875, 907, 913, 954, 957, 961, 964, 984(2), 1004, 1005, 1008(2), 1033, 1034, 1067, 1069, 1096, 1098, 1115, 1118, 1160, 1161, 1168(2), 1222, 1223, 1226, 1229, 1233, 1235, 1263, 1266, 1339(2), 1341, 1342, 1350, 1354, 1426(2), 1435(2), 1440, 1442, 1465, 1467, 1507(2), 1537, 1538, 1597(2), 1603, 1604, 1613, 1614, 1639(2), 3153(2), 3156(4), 3160(2), 3162(2), 3165(2), 3180(4)
$Zn^{2+}(Phen)_2$	0.55 (0.06)	24, 27(2), 81(2), 129, 141, 147, 151, 152, 222(2), 233(2), 250, 256, 279, 294, 301, 406, 412, 428, 434, 441(2), 478(2), 509(2), 511(2), 543, 544, 559, 560, 607, 610, 652(2), 724(2), 725(2), 733, 735, 782(2), 804, 806, 829, 831, 859(2), 872, 873, 909(2), 958(2), 961(2), 985(2), 1006(2), 1010(2), 1035(2), 1072, 1073, 1101(2), 1115, 1117, 1162(2), 1169(2), 1220(2), 1227, 1229, 1235(2), 1270(2), 1335(2), 1340(2), 1353, 1355, 1426(2), 1430(2), 1442(2), 1464, 1465, 1509(2), 1538, 1540, 1600(2), 1606(2), 1616(2), 1639(2), 3151(2), 3155(4), 3159(4), 3164(2), 3180(4)
$Fe^{2+}(Phen)_3$	0.82 (0.09)	27, 28, 44(2), 45(2), 85, 86, 93, 142, 164, 165(2), 166, 175, 176, 200(2), 230(2), 234, 280(2), 288, 289, 290, 306, 348, 361, 362, 427(3), 430, 431, 439, 458, 465(2), 490(2), 493, 509, 510(2), 530, 532(2), 541(2), 544, 557(3), 614(2), 619, 643(2), 644, 716, 718(2), 723(3), 731, 732, 737, 777(2), 778(2), 779, 780, 813, 814, 816, 852(2), 853, 872(2), 875, 908(3), 942, 943, 945, 946, 947, 950, 978(2), 979, 993(3), 997, 998(2), 1034, 1037, 1038, 1065, 1066(2), 1096(2), 1098, 1110(2), 1116, 1157(2), 1158, 1165(3), 1219, 1220(2), 1221, 1223, 1226, 1233(2), 1234, 1263, 1265, 1267, 1323(2), 1324, 1336, 1337(2), 1351, 1353, 1354, 1425, 1427(2), 1435, 1436(2), 1439(2), 1440, 1465, 1467(2), 1509, 1510(2), 1533, 1534(2), 1593, 1597(2), 1602(3), 1615(2), 1616, 1643(2), 1644, 3147, 3148(2), 3153(4), 3154(2), 3161(3), 3168, 3169(6), 3180(2), 3181, 3182(3)

Table A.1. (continued) Vibrational Frequencies and Average Vibrational Energies at 298 K.

Species	E_{vib} (eV)[a]	Vibrational frequencies (cm^{-1})[b]
$Fe^{2+}(Phen)_3$	*0.87 (0.09)*	*19, 21, 27, 30, 31, 34, 77(2), 79, 107, 109, 110, 134, 137, 142, 150, 152, 161, 206, 218, 226, 232, 233, 234, 249, 254, 256, 273, 277, 280, 407, 410, 411, 417, 419, 420, 437, 440, 449, 472, 473, 476, 507, 508(2), 509, 510(2), 542, 543, 545, 554, 555(2), 606(2), 608, 634, 639, 640, 719, 722(2), 723(3) 724, 725, 728, 779, 780, 781, 793(2), 802, 817, 818, 822, 855, 856, 857, 862, 864, 868, 894, 895, 897, 950, 951, 954, 956, 957, 959, 979(2), 980, 995, 996, 998, 1000, 1001, 1002, 1033, 1035, 1037, 1064(3), 1093, 1094, 1096, 1108, 1110, 1112, 1155, 1156(2), 1165, 1166(2), 1217, 1218(2), 1221, 1223, 1224, 1232, 1233, 1234, 1268(2), 1270, 1324, 1325, 1326, 1337(2), 1338, 1351, 1352, 1353, 1419(2), 1421, 1428, 1429(2), 1437, 1438(2), 1462, 1465, 1467, 1510, 1511(2), 1532, 1535, 1539, 1591, 1593(2), 1605, 1607, 1608, 1617(2), 1619, 1639, 1640, 1641, 3146(3), 3148, 3149(4), 3150, 3152(2), 3153(3), 3154, 3160(3), 3174(3), 3175(3)*
$Co^{2+}(Phen)_3$	0.87 (0.09)	21, 23, 31(2), 35, 35, 79, 80, 81, 108, 110, 116, 139, 142, 142, 158(2), 159, 188, 226, 228, 233, 234, 235, 253, 254, 264, 279, 283, 285, 409(2), 417, 418(2), 421, 438, 442, 443, 474, 475, 477, 508(2), 509(2), 510(2), 542(2), 544, 555(3) 605(2), 609, 637, 638, 639, 721, 722(2), 723(3), 724(2), 727, 779, 780(2), 794(2), 795, 818(2), 819, 855(2), 856, 864(2), 865, 896(2), 899, 952(2), 954, 955, 956, 958, 979(2), 980, 997(3), 1001(3), 1033, 1036(2), 1063, 1064(2), 1093(2), 1095, 1109(2), 1112, 1156(3), 1165(3), 1218(2), 1219, 1222, 1223, 1226, 1233(2), 1234, 1268, 1269, 1271, 1326(2), 1327, 1339(3), 1352, 1353, 1355, 1422(2), 1423, 1429, 1430(2), 1438(2), 1439, 1465(2), 1466, 1510, 1511(2), 1535(3), 1593, 1595(2), 1607(2), 1608, 1618, 1619(2), 1640(3), 3146(3), 3149(2), 3150(4), 3153, 3154(5), 3159(2), 3160, 3174(3), 3175(3)

Table A.1. (continued) Vibrational Frequencies and Average Vibrational Energies at 298 K.

Species	E_{vib} (eV)[a]	Vibrational frequencies (cm^{-1})[b]
$Ni^{2+}(Phen)_3$	0.86 (0.09)	23, 24, 35, 36, 36, 38, 81, 82, 85, 117, 118, 122, 144, 147, 148, 160, 168, 169, 232(2), 234, 236, 239, 241, 259(2), 265, 283, 291, 292, 411, 412, 417, 420(2), 422, 441, 444, 445, 476, 477, 480, 509(3), 510, 511(2), 542(2), 544, 556(3), 606(2), 608, 638, 639, 640, 721(3), 723(2), 724(3), 730, 780(2), 781, 794(2), 795, 818(2), 819, 855(2), 856, 865(2), 867, 898(2), 901, 952(2), 955(2), 956, 959, 979, 980(2), 997(3), 1001(3), 1033, 1036(2), 1064(3), 1093, 1094, 1095, 1110, 1111, 1114, 1156, 1157(2), 1165(2), 1166, 1218, 1219, 1220, 1223, 1224, 1227, 1233, 1234, 1235, 1267, 1268, 1270, 1327, 1328(2), 1339(2), 1340, 1353, 1354, 1355, 1424(2), 1425, 1429, 1430(2), 1438(2), 1439, 1466, 1467(2), 1511(3), 1536(3), 1594, 1596, 1597, 1608(3), 1619(2), 1620, 1640(2), 1641, 3146(3), 3150(5), 3151, 3157, 3158(3), 3159(2), 3160(3), 3175(6)
$Cu^{2+}(Phen)_3$	0.87 (0.09)	17, 21, 23, 31, 33, 35, 75, 76, 79, 82, 96, 113, 125, 126, 129, 149, 155, 159, 175, 231, 232, 235, 238, 238, 255, 259, 266, 271, 278, 296, 407, 409, 412, 416, 419, 424, 439, 442, 444, 471(2), 482, 507, 508(3), 510, 511, 541, 546, 548, 554(2), 557, 603, 606, 609, 635, 638, 642, 717, 718, 721, 723, 725, 726(2), 728, 732, 779, 780(2), 791, 805(2), 818, 822, 823, 854, 857(2), 861, 862, 869, 894, 897, 903, 952, 955, 957, 958, 959, 962, 979(2), 980, 997, 998(2), 1001, 1002(2), 1032, 1035, 1036, 1062, 1063, 1066, 1093, 1094, 1096, 1109, 1111, 1114, 1155, 1156, 1158, 1165(2), 1166, 1217(2), 1220, 1221, 1223, 1227, 1233(2), 1234, 1266, 1271, 1273, 1324, 1325, 1332, 1337(2), 1341, 1354, 1356, 1358, 1414(2), 1429(2), 1431, 1432, 1438(2), 1439, 1464(2), 1468, 1510, 1511(2), 1535(2), 1538, 1590, 1592, 1598, 1608, 1609(2), 1619, 1620, 1621, 1639(2), 1640, 3132(2), 3145(2), 3148, 3149, 3150(3), 3152(2), 3159(2), 3161, 3162, 3163, 3166(2), 3172(2), 3177(2), 3178(2)

Table A.1. (continued) Vibrational Frequencies and Average Vibrational Energies at 298 K.

Species	E_{vib} (eV)[a]	Vibrational frequencies (cm^{-1})[b]
$Zn^{2+}(Phen)_3$	0.87 (0.08)	19, 21, 28, 29, 31, 33, 79(2), 80, 88, 89, 116, 134, 138, 139, 149, 155, 156, 160, 182, 186, 233(2), 236, 251, 252, 254, 280, 281, 282, 407, 408, 411, 417(2), 421, 438, 442, 443, 471, 472, 476, 508(3), 509, 510(2), 546, 547, 549, 555, 556(2), 607(2), 609, 637(2), 640, 721, 722, 723(2), 724, 728(4), 780(2), 781, 807(2), 808, 825, 826, 827, 857(2), 858, 863(2), 865, 894, 895, 898, 957(2), 959, 960, 961, 963, 980(3), 998(2), 999, 1002(3), 1034, 1036(2), 1065(3), 1093, 1094, 1095, 1110(2), 1113, 1156(3), 1165(3), 1217, 1218(2), 1223, 1224, 1227, 1234(2), 1235, 1268, 1269, 1272, 1327(3), 1340, 1341(2), 1354, 1355, 1357, 1419, 1420(2), 1431, 1432(2), 1438, 1439(2), 1466(2), 1467, 1511(3), 1536, 1537(2), 1593, 1595, 1596, 1609(2), 1610, 1620, 1621(2), 1639, 1640(2), 3146(3), 3149(6), 3153(6), 3159(2), 3160, 3174(2), 3175(4)

[a]Uncertainties listed in parentheses are determined as described in the text. [b]Vibrational frequencies scaled by 0.9804 obtained from vibrational analyses of the B3LYP/6-31G* geometry optimized structures. Degeneracies are indicated in parentheses. [c]Vibrational frequencies and average vibrational energies for singlet state $Fe^{2+}(Phen)_3$ are shown in standard font, while those for quintet state are shown in italics.

Table A.2. Rotational Constants (in cm^{-1}) of $M^{2+}(Phen)_x$, where x = 1–3 and the corresponding PSL Transition States for Dissociation of $M^{2+}(Phen)_3$.

Complex	Energized Molecule		Transition State		
	1-D[a]	2-D[b]	1-D[c]	2-D[c]	2-D[d]
$Fe^{2+}(Phen)$	0.025	0.014	–	–	–
$Fe^{2+}(Phen)_2$	0.010	0.003	–	–	–
$Fe^{2+}(Phen)_3$	0.003	0.003	0.010, 0.054	0.003, 0.017	0.0004
$Co^{2+}(Phen)$	0.024	0.014	–	–	–
$Co^{2+}(Phen)_2$	0.010	0.004	–	–	–
$Co^{2+}(Phen)_3$	0.003	0.003	0.010, 0.054	0.004, 0.017	0.0004
$Ni^{2+}(Phen)$	0.025	0.015	–	–	–
$Ni^{2+}(Phen)_2$	0.010	0.004	–	–	–
$Ni^{2+}(Phen)_3$	0.003	0.003	0.010, 0.054	0.004, 0.017	0.0004
$Cu^{2+}(Phen)$	0.024	0.015	–	–	–
$Cu^{2+}(Phen)_2$	0.010	0.004	–	–	–
$Cu^{2+}(Phen)_3$	0.003	0.003	0.010, 0.054	0.004, 0.017	0.0003
$Zn^{2+}(Phen)$	0.024	0.014	–	–	–
$Zn^{2+}(Phen)_2$	0.010	0.004	–	–	–
$Zn^{2+}(Phen)_3$	0.003	0.003	0.010, 0.054	0.004, 0.017	0.0004

[a]Active external. [b]Inactive external. [c]Rotational constants of the PSL TS treated as free internal rotors. [d]Two-dimensional rotational constant of the PSL TS at threshold, treated variationally and statistically.

Table A.3. Measured and Calculated Sequential and Total Enthalpies of Binding of $M^{2+}(Phen)_x$ Complexes at 0 K in kJ/mol

		Theory					
		BHandHLP[c]			M06[d]		
Complex	TCID[a]	D_0	$D_{0,BSSE}$[e]	total[e]	D_0	$D_{0,BSSE}$[e]	total[e]
$Fe^{2+}(Phen)$	–	939.6	936.4	936.4	991.7	988.3	988.3
$Fe^{2+}(Phen)_2$	–	547.0	543.0	1479.4	572.8	567.9	1556.2
$Fe^{2+}(Phen)_3$	236.5 (17.0)	234.1	226.5	1705.9	275.8	265.4	1821.6
$Fe^{2+}(Phen)_3$	**210.7 (11.1)**	**331.2**	**323.6**	**1803.0**	**314.2**	**303.8**	**1860.0**
$Co^{2+}(Phen)$	–	1015.0	1011.6	1011.6	1085.4	1081.3	1081.3
$Co^{2+}(Phen)_2$	–	557.7	553.3	1564.9	573.1	567.0	1648.3
$Co^{2+}(Phen)_3$	203.8 (12.3)	223.3	216.8	1781.7	272.3	264.2	1912.5
$Ni^{2+}(Phen)$	–	1079.0	1076.1	1076.1	1202.0	1197.2	1197.2
$Ni^{2+}(Phen)_2$	–	523.7	519.1	1595.2	556.4	551.2	1748.4
$Ni^{2+}(Phen)_3$	213.2 (12.8)	287.0	280.1	1875.3	312.6	303.7	2052.1
$Cu^{2+}(Phen)$	–	1154.3	1151.3	1151.3	1256.4	1252.6	1252.6
$Cu^{2+}(Phen)_2$	–	546.3	540.9	1692.2	544.1	538.4	1791.0
$Cu^{2+}(Phen)_3$	159.6 (9.9)	174.5	167.5	1859.7	211.6	203.2	1994.2
$Zn^{2+}(Phen)$	–	1084.2	1081.2	1081.2	1114.2	1111.1	1111.1
$Zn^{2+}(Phen)_2$	–	555.7	551.4	1632.6	561.1	556.0	1667.1
$Zn^{2+}(Phen)_3$	170.1 (14.3)	192.2	185.1	1817.7	233.4	225.4	1892.5
AEU/MAD[f]	13.3 (2.6)		22.3 (25.1)			56.2 (22.3)	
AEU/MAD[g]	**12.1 (1.9)**		**43.2 (45.7)**			**68.6 (22.1)**	

[a]Average values from fits to raw data and data after subtraction of the low-energy feature, Table 3.1. Average values for the singlet state of $Fe^{2+}(Phen)_3$ complex are shown in standard font, while those of the quintet state of $Fe^{2+}(Phen)_3$ are shown in boldface. [c]Calculated at the BHandHLYP/6-311+G(2d,2p)//BHandHLYP/6-31G* level of theory including ZPE corrections with frequencies scaled by 0.9472. [d]Calculated at the M06/6-311+G(2d,2p)//M06/6-31G* level of theory including ZPE corrections with frequencies scaled by 0.9940. [e]Also includes BSSE corrections. [f]AEU/MAD values using the singlet state of $Fe^{2+}(Phen)_3$ in the analysis. [g]AEU/MAD values using the quintet state of $Fe^{2+}(Phen)_3$ in the analysis.

Table A.4. Geometrical Parameters of the BHandHLYP/6-31G* Ground-State Structures of the Neutral Phen Ligand and $M^{2+}(Phen)_x$ Complexes[a]

Complex	M^{2+}–N	∠NCCN	∠NM^{2+}NC	∠$NM^{2+}N^b$	∠$NM^{2+}N^c$
Phen	–	0.0	–	–	–
Fe^{2+}(Phen)	1.987	0.0	–	88.8	–
$Fe^{2+}(Phen)_2$	2.076	0.0	81.2	82.2	124.6
$Fe^{2+}(Phen)_3$	2.042	1.2	60.1	81.2	89.3 (3), 94.9 (6), 174.5 (3)
$Fe^{2+}(Phen)_3$	**2.213**	**1.2, 1.6 (2)**	**57.3**	**75.9**	**92.6 (2), 95.3 (5), 97.0 (2), 167.7 (2), 169.6**
Co^{2+}(Phen)	1.956	0.0	–	88.3	–
$Co^{2+}(Phen)_2$	2.044	1.3	81.2	83.4	104.7 (2), 149.5 (2)
$Co^{2+}(Phen)_3$	2.174	1.3 (2), 1.4	60.9	76.9	89.9 (3), 96.9 (6), 171.4 (3)
Ni^{2+}(Phen)	1.908	0.0	–	90.9	–
$Ni^{2+}(Phen)_2$	2.018	0.0	82.0	82.7	124.3
$Ni^{2+}(Phen)_3$	2.130	1.5	59.8	78.5	91.5 (3), 95.3 (6), 171.2 (3)
Cu^{2+}(Phen)	1.886	0.0	–	91.0	–
$Cu^{2+}(Phen)_2$	1.994	1.1 (2)	49.3	83.8	104.2 (2), 149.7 (2)
$Cu^{2+}(Phen)_3$	2.073 (4) 2.339 (2)	0.6, 2.1 (2)	57.1	76.0 (2), 80.3	91.8 (3), 94.7 (4), 98.0 (2), 170.1 (3)
Zn^{2+}(Phen)	1.912	0.0	–	93.5	–
$Zn^{2+}(Phen)_2$	2.021	0.0	81.2	84.2	123.4
$Zn^{2+}(Phen)_3$	2.181	1.7	56.6	76.8	94.8 (9), 168.3 (3)

[a] Average values are given for similar bond distances or angles; degeneracies are listed in parentheses for values that differ sufficiently such that more than one value is needed to describe the bond angle or bond distance. Geometrical parameters for the singlet ground state of $Fe^{2+}(Phen)_3$ are shown in normal font while those for quintet excited quintet state are shown in bold. All bond angles (∠) are given in degrees (°) and M^{2+}–N bond lengths in angstroms (Å). [b] intraligand angles. [c] interligand angles.

Table A.5. Geometrical Parameters of the M06/6-31G* Ground-State Structures of the Neutral Phen Ligand and $M^{2+}(Phen)_x$ Complexes[a]

Complex	M^{2+}–N	∠NCCN	∠NM^{2+}NC	∠NM^{2+}N[b]	∠NM^{2+}N[c]
Phen	–	0.0	–	–	–
Fe^{2+}(Phen)	1.971	0.0	–	88.1	–
$Fe^{2+}(Phen)_2$	2.048	0.0	81.2	82.8	124.2 (4)
$Fe^{2+}(Phen)_3$	1.982	0.6 (2), 1.0	58.2	82.9	89.4 (3), 93.9 (6), 175.5 (3)
$Fe^{2+}(Phen)_3$	**2.164**	**0.4, 1.2 (2)**	**57.2**	**77.7**	**92.8 (4), 95.7 (5), 169.7 (3)**
Co^{2+}(Phen)	1.926	0.0	–	89.6	–
$Co^{2+}(Phen)_2$	2.007	1.3	81.2	84.3	109.1 (2), 140.7 (2)
$Co^{2+}(Phen)_3$	2.132	0.7, 1.2 (2)	60.8	78.7	90.8 (2), 94.9 (7), 171.1 (3)
Ni^{2+}(Phen)	1.906	0.0	–	90.7	–
$Ni^{2+}(Phen)_2$	1.985	0.0	82.2	83.5	123.8 (4)
$Ni^{2+}(Phen)_3$	2.089	1.1 (3)	59.6	80.2	90.7 (3), 94.7 (6), 172.9 (3)
Cu^{2+}(Phen)	1.869	0.0	–	89.0	–
$Cu^{2+}(Phen)_2$	1.970	1.0	49.2	84.8	103.3 (2), 149.3 (2)
$Cu^{2+}(Phen)_3$	2.028 (4) 2.336 (2)	0.1, 1.9 (2)	57.3	78.9	91.1 (4), 94.0 (3), 99.5 (2), 171.2 (3)
Zn^{2+}(Phen)	1.905	0.0	–	94.3	–
$Zn^{2+}(Phen)_2$	2.002	0.0	80.9	85.2	122.8
$Zn^{2+}(Phen)_3$	2.155	0.9, 1.2 (2)	56.7	78.0	94.3 (9), 169.1 (3)

[a] Average values are given for similar bond distances or angles; degeneracies are listed in parentheses for values that differ sufficiently such that more than one value is needed to describe the bond angle or bond distance. Geometrical parameters for the singlet ground state of $Fe^{2+}(Phen)_3$ are shown in standard font, while those for quintet excited state are shown in boldface. All bond angles (∠) are given in degrees (°) and M^{2+}–N bond lengths in angstroms (Å). [b] intraligand angles. [c] interligand angles.

Table A.6. Cartesian Coordinates of the B3LYP/6-31G* Optimized Geometries of the Ground State Structures of the Neutral Phen Ligand and the $M^{2+}(Phen)_x$ Complexes.[a]

	Phen				Fe^{2+}(Phen)		
	x	y	z		x	y	z
C	0.000000	0.000000	0.000000	C	0.263795	-3.493814	0.000000
C	0.000000	0.000000	1.378694	C	1.481408	-2.834210	0.000000
C	1.230324	0.000000	2.073152	C	1.530033	-1.417756	0.000000
C	2.427170	0.000075	1.299634	C	0.298274	-0.720715	0.000000
N	2.414973	0.000047	-0.053665	N	-0.904859	-1.401383	0.000000
C	1.243317	-0.000053	-0.666561	C	-0.917938	-2.745202	0.000000
C	1.295806	-0.000128	3.506346	C	2.760610	-0.682229	0.000000
C	3.711274	0.000076	1.990126	C	0.298274	0.720715	0.000000
C	3.725943	-0.000106	3.415098	C	1.530033	1.417756	0.000000
C	2.494221	-0.000125	4.150759	C	2.760610	0.682229	0.000000
C	4.983703	-0.000100	4.058539	C	1.481408	2.834210	0.000000
H	5.027305	-0.000237	5.145247	H	2.409786	3.398987	0.000000
C	6.133850	0.000079	3.298306	C	0.263795	3.493814	0.000000
C	6.004328	0.000251	1.893538	C	-0.917938	2.745202	0.000000
N	4.846964	0.000188	1.254069	N	-0.904859	1.401383	0.000000
H	0.364299	-0.000228	4.067355	H	3.695714	-1.233691	0.000000
H	-0.925589	0.000000	-0.567741	H	0.206954	-4.576996	0.000000
H	-0.930611	0.000040	1.941545	H	2.409786	-3.398987	0.000000
H	1.272667	-0.000125	-1.756111	H	-1.888722	-3.231371	0.000000
H	2.539859	-0.000266	5.237201	H	3.695714	1.233691	0.000000
H	7.117864	0.000089	3.757394	H	0.206954	4.576996	0.000000
H	6.897083	0.000394	1.268260	H	-1.888722	3.231371	0.000000
				Fe^{2+}	-2.285541	0.000000	0.000000

Table A.6. (continued) Cartesian Coordinates of the B3LYP/6-31G* Optimized Geometries of the Ground State Structures of the $M^{2+}(Phen)_x$ Complexes.[a]

Co^{2+}(Phen)				Ni^{2+}(Phen)			
	x	y	z		x	y	z
C	-0.020148	0.000000	0.008354	C	-0.008856	0.000000	0.003943
C	0.001891	0.000000	1.395399	C	0.003201	0.000000	1.392122
C	1.237835	0.000000	2.090279	C	1.233520	0.000000	2.094267
C	2.414044	0.000000	1.309562	C	2.412880	0.000000	1.318165
N	2.373640	0.000000	-0.068238	N	2.380662	0.000000	-0.060508
C	1.186407	0.000000	-0.700396	C	1.201168	0.000000	-0.701915
C	1.349258	0.000000	3.520856	C	1.346843	0.000000	3.525405
C	3.695924	0.000000	1.948000	C	3.689759	0.000000	1.954112
C	3.781479	0.000000	3.357137	C	3.780896	0.000000	3.362983
C	2.572574	0.000000	4.130126	C	2.570398	0.000000	4.134794
C	5.080731	0.000000	3.924907	C	5.082557	0.000000	3.921887
H	5.193418	0.000000	5.005818	H	5.204327	0.000000	5.001786
C	6.201039	0.000000	3.106806	C	6.197756	0.000000	3.095136
C	6.039761	0.000000	1.716809	C	6.032081	0.000000	1.704113
N	4.819919	0.000000	1.150127	N	4.809518	0.000000	1.149179
H	0.440086	0.000000	4.114141	H	0.438002	0.000000	4.119211
H	-0.956133	0.000000	-0.539883	H	-0.941639	0.000000	-0.549978
H	-0.928701	0.000000	1.956707	H	-0.932056	0.000000	1.945571
H	1.199658	0.000000	-1.786044	H	1.219929	0.000000	-1.787466
H	2.646835	0.000000	5.213209	H	2.644044	0.000000	5.217926
H	7.202527	0.000000	3.523524	H	7.201852	0.000000	3.505874
H	6.898257	0.000000	1.052134	H	6.887178	0.000000	1.035098
Co^{2+}	4.206722	0.000000	-0.683721	Ni^{2+}	4.182999	0.000000	-0.636090

Table A.6. (continued) Cartesian Coordinates of the B3LYP/6-31G* Optimized Geometries of the Ground State Structures of the $M^{2+}(Phen)_x$ Complexes.[a]

Cu^{2+}(Phen)				Zn^{2+}(Phen)			
	x	y	z		x	y	z
C	0.000000	0.000000	0.000000	C	-0.044225	0.000000	0.012389
C	0.000000	0.000000	1.385827	C	0.002038	0.000000	1.395980
C	1.226172	0.000000	2.098301	C	1.247917	0.000000	2.073684
C	2.408033	0.000000	1.330159	C	2.419585	0.000000	1.282409
N	2.383749	0.000000	-0.040926	N	2.342891	0.000000	-0.094315
C	1.218194	0.000000	-0.698971	C	1.152674	0.000000	-0.713483
C	1.344036	0.000000	3.529976	C	1.359056	0.000000	3.503168
C	3.683106	0.000000	1.965207	C	3.714257	0.000000	1.927218
C	3.782104	0.000000	3.371279	C	3.788651	0.000000	3.339092
C	2.568442	0.000000	4.139789	C	2.580788	0.000000	4.111649
C	5.089510	0.000000	3.920649	C	5.080179	0.000000	3.925139
H	5.220801	0.000000	4.999449	H	5.173066	0.000000	5.007839
C	6.195568	0.000000	3.085692	C	6.212325	0.000000	3.128453
C	6.019471	0.000000	1.692297	C	6.070530	0.000000	1.735847
N	4.792029	0.000000	1.158514	N	4.859257	0.000000	1.158957
H	0.436317	0.000000	4.125684	H	0.448626	0.000000	4.094479
H	-0.925991	0.000000	-0.565355	H	-0.987818	0.000000	-0.522618
H	-0.940116	0.000000	1.931014	H	-0.918052	0.000000	1.974168
H	1.246410	0.000000	-1.784650	H	1.156548	0.000000	-1.798245
H	2.639892	0.000000	5.223172	H	2.657382	0.000000	5.194546
H	7.204696	0.000000	3.484120	H	7.207838	0.000000	3.559215
H	6.868976	0.000000	1.015659	H	6.933968	0.000000	1.079189
Cu^{2+}	4.175620	0.000000	-0.621274	Zn^{2+}	4.179541	0.000000	-0.629146

Table A.6. (continued) Cartesian Coordinates of the B3LYP/6-31G* Optimized Geometries of the Ground State Structures of the $M^{2+}(Phen)_x$ Complexes.[a]

$Fe^{2+}(Phen)_2$				$Fe^{2+}(Phen)_2$			
	x	y	z		x	y	z
C	-2.701993	2.456213	2.456538	H	6.149137	-0.871712	0.871823
C	-3.927022	2.003063	2.003329	H	2.631479	-3.221302	3.221746
C	-3.982566	1.003453	1.003581	H	4.850246	-2.407978	2.408290
C	-2.752466	0.508827	0.508884	H	0.554364	-2.249485	2.249716
N	-1.544802	0.965824	0.965907	H	6.149134	0.871759	-0.871822
C	-1.529634	1.911666	1.911890	H	2.631465	3.221321	-3.221758
C	-5.213746	0.482048	0.482121	H	0.554354	2.249489	-2.249735
C	-2.752464	-0.508848	-0.508895	Fe^{2+}	0.000000	0.000000	-0.000010
C	-3.982562	-1.003484	-1.003588				
C	-5.213744	-0.482088	-0.482124				
C	-3.927013	-2.003093	-2.003336				
H	-4.850235	-2.408015	-2.408294				
C	-2.701982	-2.456234	-2.456550				
C	-1.529626	-1.911678	-1.911906				
N	-1.544798	-0.965836	-0.965923				
H	-6.149137	0.871712	0.871823				
H	-2.631479	3.221302	3.221746				
H	-4.850246	2.407978	2.408289				
H	-0.554364	2.249485	2.249715				
H	-6.149133	-0.871760	-0.871823				
H	-2.631465	-3.221321	-3.221758				
H	-0.554354	-2.249489	-2.249735				
C	2.701993	-2.456213	2.456538				
C	3.927022	-2.003063	2.003329				
C	3.982566	-1.003453	1.003582				
C	2.752466	-0.508827	0.508884				
N	1.544802	-0.965824	0.965907				
C	1.529634	-1.911666	1.911891				
C	5.213746	-0.482048	0.482121				
C	2.752464	0.508848	-0.508895				
C	3.982562	1.003484	-1.003588				
C	5.213744	0.482088	-0.482124				
C	3.927013	2.003093	-2.003336				
H	4.850235	2.408015	-2.408294				
C	2.701982	2.456233	-2.456550				
C	1.529626	1.911678	-1.911906				
N	1.544798	0.965835	-0.965923				

Table A.6. (continued) Cartesian Coordinates of the B3LYP/6-31G* Optimized Geometries of the Ground State Structures of the $M^{2+}(Phen)_x$ Complexes.[a]

$Co^{2+}(Phen)_2$				$Co^{2+}(Phen)_2$			
	x	y	z		x	y	z
C	0.146051	1.195067	0.139693	H	7.346576	1.207579	-6.050923
C	0.130752	0.974737	1.504651	H	6.776872	4.311868	-2.369952
C	1.293220	0.493190	2.152801	H	7.424573	3.252934	-4.538335
C	2.431828	0.259020	1.348772	H	5.431996	3.001343	-0.731572
N	2.435096	0.480727	-0.001500	H	6.597715	-1.108761	-6.434555
C	1.321025	0.935673	-0.583098	H	4.011906	-4.241115	-3.786411
C	1.366320	0.236824	3.563484	H	3.508226	-2.947031	-1.717085
C	3.642720	-0.230190	1.950321	Co^{2+}	4.247640	0.025178	-0.778114
C	3.686691	-0.474095	3.341832				
C	2.515198	-0.227496	4.134225				
C	4.905629	-0.955139	3.876719				
H	4.982757	-1.155829	4.941624				
C	5.987277	-1.165714	3.041503				
C	5.856452	-0.897036	1.670018				
N	4.719885	-0.442290	1.133541				
H	0.485466	0.420326	4.171016				
H	-0.730573	1.563595	-0.381445				
H	-0.766825	1.168131	2.085342				
H	1.360232	1.099880	-1.655791				
H	2.560790	-0.418425	5.201998				
H	6.932351	-1.533634	3.425349				
H	6.690106	-1.053481	0.991992				
C	6.482482	3.295484	-2.606945				
C	6.838537	2.705290	-3.805604				
C	6.437164	1.376513	-4.082320				
C	5.676534	0.711644	-3.093827				
N	5.330149	1.306077	-1.911005				
C	5.724925	2.562014	-1.680443				
C	6.761797	0.686845	-5.298898				
C	5.239473	-0.639760	-3.317726				
C	5.573477	-1.294893	-4.524775				
C	6.347235	-0.595455	-5.511273				
C	5.115634	-2.624172	-4.688226				
H	5.350045	-3.164519	-5.601092				
C	4.374745	-3.224122	-3.686711				
C	4.088155	-2.499938	-2.518935				
N	4.505427	-1.243801	-2.333494				

Table A.6. (continued) Cartesian Coordinates of the B3LYP/6-31G* Optimized Geometries of the Ground State Structures of the $M^{2+}(Phen)_x$ Complexes.[a]

$Ni^{2+}(Phen)_2$				$Ni^{2+}(Phen)_2$			
	x	y	z		x	y	z
C	-0.007107	0.000136	-0.025481	H	7.005083	1.231190	-6.249384
C	-0.017556	0.000107	1.358427	H	5.397517	4.534140	-3.052850
C	1.206653	0.000037	2.069283	H	6.404116	3.430274	-5.053542
C	2.390084	0.000011	1.300953	H	4.471613	3.125341	-1.216138
N	2.392670	0.000002	-0.064324	H	7.004143	-1.231151	-6.249863
C	1.221061	0.000050	-0.706989	H	5.393988	-4.534116	-3.054646
C	1.311837	0.000009	3.502149	H	4.469313	-3.125324	-1.217309
C	3.666819	-0.000026	1.947651	Ni^{2+}	4.256105	0.000008	-0.798955
C	3.747618	-0.000066	3.356305				
C	2.530240	-0.000056	4.119281				
C	5.045018	-0.000123	3.922652				
H	5.162437	-0.000188	5.002696				
C	6.154537	-0.000130	3.095441				
C	5.977299	-0.000036	1.702088				
N	4.765972	0.000003	1.137827				
H	0.399307	0.000028	4.090354				
H	-0.930535	0.000221	-0.593978				
H	-0.957759	0.000164	1.902763				
H	1.255611	0.000058	-1.792374				
H	2.595923	-0.000086	5.202970				
H	7.159204	-0.000201	3.503550				
H	6.831843	-0.000025	1.032007				
C	5.437186	3.453482	-3.133544				
C	5.994208	2.837488	-4.240608				
C	6.029874	1.424169	-4.313341				
C	5.480658	0.715606	-3.223796				
N	4.932632	1.330196	-2.134802				
C	4.913644	2.665770	-2.095150				
C	6.583255	0.682912	-5.412636				
C	5.480121	-0.715580	-3.224069				
C	6.028799	-1.424139	-4.313889				
C	6.582732	-0.682876	-5.412903				
C	5.992046	-2.837459	-4.241709				
H	6.401455	-3.430240	-5.054897				
C	5.434539	-3.453457	-3.134892				
C	4.911679	-2.665749	-2.096151				
N	4.931674	-1.330174	-2.135291				

Table A.6. (continued) Cartesian Coordinates of the B3LYP/6-31G* Optimized Geometries of the Ground State Structures of the $M^{2+}(Phen)_x$ Complexes.[a]

$Cu^{2+}(Phen)_2$				$Cu^{2+}(Phen)_2$			
	x	y	z		x	y	z
C	0.213515	-1.186279	0.052721	N	4.503397	-1.238921	-2.326901
C	0.169839	-0.972096	1.419076	H	7.403833	1.156207	-6.019209
C	1.319553	-0.492365	2.090124	H	6.801434	4.258295	-2.318160
C	2.468422	-0.258304	1.303695	H	7.472763	3.219575	-4.487993
N	2.507693	-0.490809	-0.040228	H	5.473305	2.920549	-0.683981
C	1.406331	-0.939573	-0.646857	H	6.651281	-1.157164	-6.400796
C	1.382307	-0.233230	3.501729	H	4.020884	-4.258953	-3.728061
C	3.658646	0.258059	1.907348	H	3.487033	-2.921037	-1.691148
C	3.702863	0.492214	3.298883				
C	2.526849	0.233174	4.082215				
C	4.923529	0.971940	3.830038				
H	5.009665	1.165450	4.895548				
C	6.000155	1.186028	2.987572				
C	5.859901	0.939232	1.611888				
N	4.719776	0.490470	1.081686				
H	0.497953	-0.418091	4.103716				
H	-0.655347	-1.544966	-0.488025				
H	-0.740745	-1.165536	1.979072				
H	1.470116	-1.104172	-1.717709				
H	2.563609	0.418107	5.151370				
H	6.949764	1.544709	3.369113				
H	6.686223	1.103756	0.927778				
Cu^{2+}	4.279145	-0.000228	-0.791212				
C	6.518908	3.239976	-2.561447				
C	6.886353	2.661487	-3.763534				
C	6.490073	1.334144	-4.052367				
C	5.726992	0.666102	-3.070222				
N	5.385759	1.238346	-1.879482				
C	5.770348	2.493506	-1.636495				
C	6.813614	0.640461	-5.268014				
C	5.262567	-0.666778	-3.305717				
C	5.604169	-1.334921	-4.501574				
C	6.393890	-0.641341	-5.480839				
C	5.136965	-2.662257	-4.650578				
H	5.375033	-3.220421	-5.551664				
C	4.384126	-3.240642	-3.643909				
C	4.080093	-2.494076	-2.493562				

Table A.6. (continued) Cartesian Coordinates of the B3LYP/6-31G* Optimized Geometries of the Ground State Structures of the $M^{2+}(Phen)_x$ Complexes.[a]

$Zn^{2+}(Phen)_2$				$Zn^{2+}(Phen)_2$			
	x	y	z		x	y	z
C	0.146382	1.197236	0.135320	H	7.342289	1.207892	-6.043430
C	0.134329	0.975644	1.500105	H	6.775285	4.314794	-2.368856
C	1.297563	0.493675	2.145562	H	7.420491	3.250538	-4.535634
C	2.435571	0.259769	1.339175	H	5.430548	3.006860	-0.727427
N	2.433363	0.483061	-0.008416	H	6.594318	-1.109144	-6.426622
C	1.319862	0.938282	-0.589319	H	4.011995	-4.244054	-3.784505
C	1.370330	0.237091	3.556090	H	3.505803	-2.952580	-1.713476
C	3.648133	-0.230858	1.941550	Zn^{2+}	4.247639	0.025179	-0.778115
C	3.689860	-0.474514	3.334004				
C	2.518691	-0.227698	4.126570				
C	4.907111	-0.956002	3.871119				
H	4.981613	-1.156174	4.936303				
C	5.990578	-1.167851	3.038589				
C	5.862129	-0.899604	1.667181				
N	4.726458	-0.444580	1.130746				
H	0.489356	0.420963	4.163330				
H	-0.731310	1.566198	-0.383673				
H	-0.761889	1.168508	2.083058				
H	1.358035	1.103005	-1.661714				
H	2.564590	-0.418996	5.194261				
H	6.934584	-1.536224	3.424575				
H	6.696169	-1.056570	0.990157				
C	6.480133	3.298117	-2.603555				
C	6.834733	2.704933	-3.801169				
C	6.432723	1.376266	-4.075129				
C	5.671996	0.712775	-3.084618				
N	5.328779	1.311101	-1.905604				
C	5.723066	2.566584	-1.675695				
C	6.757720	0.686739	-5.291536				
C	5.234853	-0.640971	-3.308568				
C	5.570408	-1.294713	-4.516898				
C	6.343812	-0.595417	-5.503584				
C	5.114381	-2.623860	-4.682516				
H	5.350339	-3.162158	-5.596188				
C	4.373461	-3.226787	-3.682814				
C	4.085497	-2.504548	-2.514627				
N	4.501954	-1.248867	-2.329186				

Table A.6. (continued) Cartesian Coordinates of the B3LYP/6-31G* Optimized Geometries of the Ground State Structures of the $M^{2+}(Phen)_x$ Complexes.[a]

$Fe^{2+}(Phen)_3$				$Fe^{2+}(Phen)_3$			
	x	y	z		x	y	z
C	-0.032843	0.047698	-0.003649	H	7.736857	-5.377065	-2.140516
C	-0.041723	0.051365	1.377299	H	3.123693	-5.188391	-0.716847
C	1.184396	0.042461	2.079681	H	5.390338	-5.968463	-1.430290
C	2.378270	0.031820	1.314100	H	2.693695	-2.735630	-0.537185
N	2.377242	0.019085	-0.049214	H	9.434478	-3.654697	-2.621591
C	1.200617	0.031115	-0.676563	H	9.416422	1.172845	-2.430754
C	1.261053	0.038535	3.512841	H	7.100101	1.693672	-1.658483
C	3.651970	0.030233	1.989278	C	4.610391	4.514122	-0.464761
C	3.692415	0.017526	3.407188	C	4.198241	4.958662	-1.705677
C	2.464956	0.022042	4.150641	C	3.855797	4.017023	-2.702127
C	4.963527	0.003039	4.024056	C	3.955444	2.642565	-2.366831
H	5.033712	-0.009157	5.108169	N	4.372769	2.212866	-1.142153
C	6.102783	0.003988	3.242139	C	4.683360	3.131201	-0.226576
C	5.966589	0.027045	1.844867	C	3.423479	4.396331	-4.017165
N	4.783432	0.044715	1.228622	C	3.606521	1.647238	-3.349491
H	0.336070	0.045656	4.081680	C	3.190711	2.055807	-4.642694
H	-0.955696	0.056118	-0.573532	C	3.108270	3.455045	-4.950503
H	-0.977575	0.061073	1.928887	C	2.871397	1.044057	-5.575870
H	1.233485	0.025826	-1.761909	H	2.551576	1.319034	-6.577120
H	2.514951	0.014445	5.235332	C	2.969732	-0.283422	-5.204989
H	7.092054	-0.009229	3.686479	C	3.380457	-0.594239	-3.898829
H	6.843595	0.033691	1.204635	N	3.686612	0.334300	-2.991120
C	3.915612	-4.481968	-0.940933	H	3.355228	5.453521	-4.255709
C	5.168942	-4.909149	-1.333994	H	4.878077	5.209872	0.323127
C	6.176183	-3.957293	-1.613594	H	4.133781	6.020826	-1.924317
C	5.839010	-2.587438	-1.470161	H	5.005693	2.756850	0.740435
N	4.594154	-2.177042	-1.097843	H	2.786167	3.749676	-5.944764
C	3.670899	-3.102172	-0.837245	H	2.733550	-1.082218	-5.899559
C	7.498846	-4.322978	-2.033731	H	3.461559	-1.627967	-3.576811
C	6.840425	-1.579659	-1.728211	Fe^{2+}	4.399706	0.014170	-0.936397
C	8.134213	-1.976052	-2.152013				
C	8.437283	-3.371230	-2.298459				
C	9.077476	-0.954683	-2.408450				
H	10.078815	-1.219355	-2.736657				
C	8.715566	0.367510	-2.239411				
C	7.412188	0.663931	-1.805964				
N	6.499012	-0.272500	-1.550023				

Table A.6. (continued) Cartesian Coordinates of the B3LYP/6-31G* Optimized Geometries of the Ground State Structures of the $M^{2+}(Phen)_x$ Complexes.[a]

$Co^{2+}(Phen)_3$				$Co^{2+}(Phen)_3$			
	x	y	z		x	y	z
C	-0.007799	0.172682	-0.019882	H	7.709236	-5.328868	-2.041066
C	-0.014851	0.128697	1.360740	H	3.120585	-5.122854	-0.522869
C	1.210248	0.056247	2.061792	H	5.374644	-5.917108	-1.260027
C	2.400957	0.033180	1.293146	H	2.682006	-2.670464	-0.403937
N	2.396808	0.065794	-0.068339	H	9.377365	-3.608267	-2.616802
C	1.223499	0.137521	-0.696443	H	9.294337	1.228851	-2.599740
C	1.293165	0.002838	3.493888	H	6.989136	1.743978	-1.795812
C	3.676579	-0.027283	1.959779	C	4.503531	4.486360	-0.419364
C	3.724288	-0.081784	3.375505	C	4.124180	4.932587	-1.670594
C	2.499628	-0.067399	4.124197	C	3.833494	3.993752	-2.686385
C	4.999664	-0.142585	3.981150	C	3.947861	2.619886	-2.356563
H	5.079704	-0.186171	5.063756	N	4.333519	2.190525	-1.122981
C	6.130746	-0.142812	3.187658	C	4.596831	3.103219	-0.188494
C	5.983639	-0.078133	1.791425	C	3.438487	4.370543	-4.014052
N	4.797915	-0.019168	1.187129	C	3.653474	1.622338	-3.353263
H	0.371644	0.018631	4.068092	C	3.273019	2.027316	-4.657365
H	-0.930943	0.230095	-0.586341	C	3.173569	3.426770	-4.961186
H	-0.950178	0.149726	1.913018	C	3.005557	1.010407	-5.601803
H	1.258620	0.164013	-1.781353	H	2.712450	1.278878	-6.612906
H	2.553010	-0.109183	5.207982	C	3.120504	-0.314195	-5.226537
H	7.123548	-0.188750	3.621985	C	3.495719	-0.618548	-3.906774
H	6.855913	-0.072749	1.144861	N	3.751561	0.313617	-2.990041
C	3.904518	-4.420689	-0.785224	H	3.357244	5.427109	-4.251269
C	5.150980	-4.856157	-1.191677	H	4.731911	5.181622	0.381171
C	6.145578	-3.908612	-1.523672	H	4.047208	5.995354	-1.882531
C	5.802134	-2.537482	-1.415718	H	4.897380	2.724929	0.783855
N	4.566672	-2.118890	-1.023827	H	2.879141	3.720424	-5.964316
C	3.654145	-3.039548	-0.716281	H	2.923748	-1.117530	-5.928212
C	7.462458	-4.274274	-1.962696	H	3.588646	-1.651321	-3.584546
C	6.782686	-1.531742	-1.736456	Co^{2+}	4.379923	0.034554	-0.936439
C	8.071103	-1.925948	-2.176926				
C	8.385086	-3.322831	-2.280495				
C	8.992052	-0.901385	-2.492661				
H	9.989602	-1.161822	-2.835271				
C	8.611414	0.420210	-2.362892				
C	7.313525	0.714200	-1.911146				
N	6.421982	-0.225697	-1.599177				

Table A.6. (continued) Cartesian Coordinates of the B3LYP/6-31G* Optimized Geometries of the Ground State Structures of the $M^{2+}(Phen)_x$ Complexes.[a]

$Ni^{2+}(Phen)_3$				$Ni^{2+}(Phen)_3$			
	x	y	z		x	y	z
C	0.282854	0.024666	-0.134137	H	8.252918	-4.990306	-1.922202
C	0.215392	-0.038935	1.244150	H	3.594030	-5.030959	-0.604126
C	1.410408	-0.055009	1.998540	H	5.909974	-5.706717	-1.263648
C	2.632314	-0.000749	1.282913	H	3.044506	-2.604113	-0.430919
N	2.688609	0.050410	-0.076402	H	9.865665	-3.179445	-2.359111
C	1.543329	0.065983	-0.755405	H	9.561846	1.648216	-2.155983
C	1.436462	-0.125404	3.432117	H	7.202516	2.027459	-1.445992
C	3.879055	-0.004087	2.002317	C	4.637069	4.536442	-0.169321
C	3.871849	-0.079873	3.417311	C	4.295020	4.997556	-1.425810
C	2.617470	-0.141213	4.112672	C	4.074852	4.071483	-2.470488
C	5.123795	-0.087352	4.073220	C	4.217284	2.695912	-2.161247
H	5.163350	-0.145874	5.157345	N	4.567111	2.251667	-0.922667
C	6.283273	-0.019350	3.325465	C	4.765079	3.151899	0.038763
C	6.189239	0.060947	1.925060	C	3.722786	4.460280	-3.806763
N	5.026982	0.072413	1.274668	C	3.992451	1.709362	-3.184835
H	0.492418	-0.168510	3.967044	C	3.651276	2.125008	-4.495882
H	-0.615411	0.039723	-0.741865	C	3.523998	3.526361	-4.779806
H	-0.743645	-0.076796	1.753217	C	3.447722	1.116074	-5.464407
H	1.623177	0.109226	-1.836932	H	3.186504	1.391246	-6.482419
H	2.627138	-0.198139	5.197045	C	3.582522	-0.210281	-5.102968
H	7.259425	-0.023564	3.798255	C	3.915570	-0.525564	-3.774056
H	7.084506	0.121214	1.314252	N	4.113311	0.398952	-2.835694
C	4.358215	-4.288784	-0.808133	H	3.619508	5.517975	-4.029912
C	5.638416	-4.658771	-1.172184	H	4.810965	5.221022	0.653792
C	6.604543	-3.659670	-1.428866	H	4.193573	6.061844	-1.619021
C	6.196693	-2.309473	-1.291793	H	5.040125	2.763061	1.014050
N	4.929623	-1.954727	-0.942719	H	3.261595	3.830280	-5.788747
C	4.044863	-2.922004	-0.707209	H	3.432933	-1.008115	-5.822336
C	7.954860	-3.951178	-1.819343	H	4.021784	-1.559848	-3.462313
C	7.143131	-1.251792	-1.531795	Ni^{2+}	4.672283	0.142012	-0.811439
C	8.467285	-1.571939	-1.922129				
C	8.847309	-2.949322	-2.060442				
C	9.354170	-0.495876	-2.152179				
H	10.378054	-0.696825	-2.454828				
C	8.906586	0.800474	-1.987389				
C	7.576272	1.018522	-1.588560				
N	6.714156	0.029130	-1.362031				

Table A.6. (continued) Cartesian Coordinates of the B3LYP/6-31G* Optimized Geometries of the Ground State Structures of the $M^{2+}(Phen)_x$ Complexes.[a]

$Cu^{2+}(Phen)_3$				$Cu^{2+}(Phen)_3$			
	x	y	z		x	y	z
C	-0.000078	-0.000318	0.000260	H	8.275020	-5.002661	-2.053788
C	0.000067	-0.000540	1.380659	H	3.668468	-4.889778	-0.643332
C	1.230257	-0.000361	2.077978	H	5.950558	-5.625045	-1.361318
C	2.419241	0.006684	1.302725	H	3.202189	-2.445269	-0.439228
N	2.408813	-0.007507	-0.053986	H	9.964578	-3.263382	-2.503926
C	1.234560	-0.008060	-0.675739	H	9.920921	1.558142	-2.214488
C	1.311545	-0.016523	3.510125	H	7.598137	2.048189	-1.439367
C	3.699824	0.015234	1.972913	C	4.653289	4.476883	-0.124173
C	3.742812	-0.017237	3.392280	C	4.306246	4.947677	-1.376022
C	2.518635	-0.031773	4.140905	C	4.077147	4.028598	-2.425311
C	5.011513	-0.030541	4.013292	C	4.219420	2.653348	-2.123370
H	5.076461	-0.058814	5.097424	N	4.563783	2.199453	-0.887198
C	6.153332	-0.008708	3.236770	C	4.771083	3.090857	0.079930
C	6.021127	0.037700	1.840848	C	3.714988	4.417851	-3.759225
N	4.838948	0.056149	1.223325	C	4.002227	1.671292	-3.146896
H	0.389460	-0.023217	4.083830	C	3.646125	2.082531	-4.453339
H	-0.926657	-0.001161	-0.563833	C	3.508724	3.484466	-4.732065
H	-0.932416	-0.003552	1.938180	C	3.443290	1.068660	-5.417239
H	1.263859	-0.019962	-1.762718	H	3.169272	1.337467	-6.433539
H	2.575553	-0.052687	5.225065	C	3.596745	-0.255390	-5.053165
H	7.141398	-0.021850	3.683651	C	3.952569	-0.566761	-3.729148
H	6.896273	0.066566	1.200247	N	4.149156	0.363978	-2.797486
C	4.450627	-4.169305	-0.856165	H	3.608072	5.475562	-3.980264
C	5.711524	-4.570966	-1.251126	H	4.835215	5.155641	0.701919
C	6.704219	-3.601088	-1.514363	H	4.207875	6.013598	-1.561346
C	6.354126	-2.233801	-1.354536	H	5.040156	2.696634	1.053845
N	5.097235	-1.855874	-0.982285	H	3.235536	3.789356	-5.737775
C	4.184435	-2.797047	-0.736795	H	3.448790	-1.056714	-5.768866
C	8.030896	-3.951355	-1.934470	H	4.081183	-1.598206	-3.419489
C	7.351165	-1.214889	-1.593168	Cu^{2+}	4.674796	0.142869	-0.817473
C	8.650432	-1.600583	-2.014994				
C	8.963941	-2.990454	-2.181961				
C	9.591475	-0.570344	-2.244472				
H	10.596160	-0.824593	-2.570554				
C	9.222313	0.745163	-2.047864				
C	7.912208	1.021791	-1.613720				
N	7.002097	0.080231	-1.388843				

Table A.6. (continued) Cartesian Coordinates of the B3LYP/6-31G* Optimized Geometries of the Ground State Structures of the $M^{2+}(Phen)_x$ Complexes.[a]

$Zn^{2+}(Phen)_3$				$Zn^{2+}(Phen)_3$			
	x	y	z		x	y	z
C	0.224548	-0.091092	-0.087496	H	8.336873	-5.031760	-2.012130
C	0.155186	-0.111216	1.291709	H	3.666254	-5.112714	-0.770162
C	1.347230	-0.079056	2.050490	H	5.995031	-5.760635	-1.414396
C	2.572780	-0.022948	1.339072	H	3.108465	-2.689850	-0.541567
N	2.629613	-0.017001	-0.019345	H	9.963314	-3.212759	-2.366381
C	1.487192	-0.045538	-0.702925	H	9.688421	1.599914	-2.023082
C	1.359711	-0.106378	3.485383	H	7.317917	1.976012	-1.342768
C	3.815941	0.019869	2.071422	C	4.794073	4.601070	-0.259100
C	3.792411	-0.021189	3.488784	C	4.409099	5.053001	-1.506261
C	2.534042	-0.084055	4.176080	C	4.116977	4.120214	-2.527415
C	5.035396	0.004344	4.161168	C	4.235870	2.743638	-2.207980
H	5.059071	-0.028299	5.246874	N	4.629422	2.311191	-0.980553
C	6.205427	0.069301	3.429832	C	4.892553	3.216342	-0.040161
C	6.126956	0.118303	2.027574	C	3.716272	4.510280	-3.849205
N	4.973132	0.100085	1.362975	C	3.937212	1.753046	-3.215700
H	0.410986	-0.150232	4.011866	C	3.551507	2.174120	-4.513807
H	-0.671737	-0.113492	-0.697868	C	3.449265	3.575894	-4.804344
H	-0.804093	-0.152225	1.800120	C	3.279573	1.169265	-5.470099
H	1.572103	-0.033967	-1.785363	H	2.982991	1.451970	-6.476327
H	2.536092	-0.111164	5.261641	C	3.394783	-0.160361	-5.114200
H	7.174491	0.087350	3.916567	C	3.774873	-0.480064	-3.799497
H	7.028902	0.178472	1.425757	N	4.033536	0.440830	-2.873263
C	4.430357	-4.362577	-0.942683	H	3.632508	5.569153	-4.074926
C	5.717503	-4.716755	-1.297470	H	5.022189	5.291561	0.545600
C	6.685443	-3.708908	-1.509814	H	4.327637	6.116761	-1.711583
C	6.273682	-2.362388	-1.341054	H	5.196971	2.830766	0.928334
N	4.999950	-2.025305	-1.007310	H	3.150906	3.878441	-5.803658
C	4.113814	-2.999749	-0.810888	H	3.195586	-0.954240	-5.825841
C	8.041124	-3.994757	-1.884305	H	3.869725	-1.516274	-3.488707
C	7.230769	-1.298309	-1.528871	Zn^{2+}	4.680641	0.129872	-0.805210
C	8.560679	-1.616450	-1.904868				
C	8.940103	-2.989554	-2.079322				
C	9.460544	-0.541656	-2.085990				
H	10.487729	-0.744300	-2.376177				
C	9.023009	0.753675	-1.890825				
C	7.687880	0.968670	-1.508326				
N	6.814525	-0.019934	-1.326278				

[a]Standard Orientation, Å.

APPENDIX B

Table B.1. Vibrational Frequencies and Average Vibrational Energies at 298 K.

Species	E_{vib} (eV)[a]	Vibrational frequencies (cm^{-1})[b]
trans-Bpy	0.20 (0.02)	57, 95, 162, 224, 327, 404, 411, 438, 441, 561, 616, 622, 659, 745, 746, 763, 771, 825, 904, 913, 958, 963, 993, 995, 996(2), 1039, 1053, 1075, 1100, 1104, 1158(2), 1268, 1273, 1309, 1314, 1325, 1436, 1462, 1476, 1499, 1585, 1604, 1614, 1615, 3106, 3107, 3130(2), 3151(2), 3180(2)
cis-Bpy	0.21 (0.02)	57, 90, 127, 247, 316, 368, 409, 411, 491, 557, 610, 626, 657, 746, 748, 759, 769, 816, 891, 896, 957, 961, 985, 985, 988, 989, 1038, 1059, 1083, 1101, 1114, 1161, 1168, 1271, 1284, 1285, 1317, 1321, 1439, 1448, 1485, 1496, 1591, 1601, 1611, 1612, 3105, 3106, 3128, 3129, 3144, 3148, 3153, 3155
Fe^{2+}(Bpy)	0.25 (0.02)	56, 76, 139, 205, 227, 250, 280, 380, 390, 407, 428, 446, 531, 641, 661, 674, 711, 723, 750, 772, 786, 887, 899, 972, 975, 1006, 1025(2), 1029, 1036, 1067, 1070, 1119, 1135, 1185, 1199, 1267, 1279, 1301, 1318, 1329, 1441, 1460, 1472, 1499, 1576, 1581, 1599, 1612, 3162(2), 3168, 3169, 3183, 3184, 3186, 3201
Co^{2+}(Bpy)	0.24 (0.02)	71, 84, 149, 195, 228, 267, 289, 378, 391, 408, 433, 457, 526, 641, 661, 677, 708, 714, 755, 770, 781, 888, 897, 969, 973, 1012, 1025, 1028, 1031, 1036, 1064, 1070, 1118, 1134, 1184, 1194, 1270, 1280, 1301, 1327, 1329, 1441, 1461, 1472, 1499, 1575, 1580, 1601, 1612, 3159(2), 3168, 3169, 3179, 3183, 3184, 3192
Ni^{2+}(Bpy)	0.24 (0.02)	72, 82, 149, 196, 231, 285, 300, 383, 394, 407, 429, 458, 525, 639, 668, 682, 703, 706, 752, 769, 780, 888, 892, 972, 975, 1013, 1025, 1028, 1030, 1036, 1062, 1068, 1118, 1136, 1184, 1194, 1270, 1280, 1302, 1328, 1331, 1440, 1462, 1471, 1498, 1569, 1575, 1594, 1608, 3161(2), 3167, 3168, 3179, 3183, 3184, 3191
Cu^{2+}(Bpy)	0.24 (0.02)	71, 79, 141, 193, 232, 274, 301, 382, 391, 405, 427, 460, 525, 637, 663, 683, 689, 695, 750, 754, 774, 861, 883, 965, 969, 1018, 1023, 1025, 1026, 1042, 1063, 1072, 1119, 1132, 1182, 1191, 1269, 1280, 1303, 1325, 1335, 1440, 1459, 1470, 1501, 1578, 1579, 1594, 1602, 3155, 3156, 3166, 3167, 3176, 3182, 3182, 3186

Table B.1. (continued) Vibrational Frequencies and Average Vibrational Energies at 298 K.

Species	E_{vib} (eV)[a]	Vibrational frequencies (cm^{-1})[b]
$Zn^{2+}(Bpy)$	0.24 (0.02)	56, 84, 152, 207, 229, 267, 288, 384, 388, 410, 433, 447, 529, 641, 664, 676, 708, 712, 750, 775, 783, 887, 905, 976, 979, 1014, 1027, 1028, 1031, 1034, 1067, 1072, 1123, 1136, 1185, 1199, 1255, 1287, 1302, 1325, 1330, 1442, 1463, 1473, 1495, 1579, 1584, 1598, 1613, 3167, 3168, 3176(2), 3185, 3186, 3187, 3203
$Fe^{2+}(Bpy)_2$	0.53 (0.05)	14, 31, 31, 59, 62, 76(2), 127, 134, 134, 201, 224, 228, 229, 241, 241, 280, 357, 379, 399, 400, 416, 416, 437, 437, 455, 455, 544(2), 645(2), 649(2), 660, 668, 729(2), 736, 737, 761(2), 770(2), 802, 804, 889, 890, 901(2), 967(2), 969(2), 1012(2), 1016(2), 1020(2), 1024(2), 1039(2), 1070(2), 1078(2), 1118(2), 1131(2), 1179(2), 1193, 1194, 1278, 1283(3), 1300, 1302, 1322(2), 1328(2), 1445(2), 1459(2), 1484(2), 1502, 1504, 1586(2), 1593(2), 1612, 1613, 1624(2), 3153(4), 3165(2), 3166(2), 3179(2), 3182(2), 3183(2), 3195(2)
$Co^{2+}(Bpy)_2$	0.52 (0.05)	12, 34, 34, 56, 75, 76(2), 128, 140(2), 204, 227(2), 235, 255(2), 322, 360, 380, 391, 408, 417(2), 437(2), 458(2), 543, 545, 646(2), 6492), 662, 669, 727(2), 735, 738, 762(2), 769(2), 802, 804, 890(2), 899(2), 965, 966, 967(2), 1015, 1016(3), 1019(2), 1030(2), 1039(2), 1069, 1070, 1078(2), 1118, 1119, 1131(2), 1178(2), 1192(2), 1278, 1281, 1283(2), 1301(2), 1326(2), 1328(2), 1446(2), 1461(2), 1484(2), 1506(2), 1587(2), 1594(2), 1614(2), 1626(2), 3155(4), 3165(2), 3166(2), 3179(2), 3182(2), 3183(2), 3192(2)
$Ni^{2+}(Bpy)_2$	0.51 (0.05)	10, 42, 42, 76, 78, 85, 85, 131, 171(2), 199, 233, 235, 241, 285, 285, 339, 362, 380, 400, 407, 422, 422, 444(2), 489(2), 544, 545, 648, 648, 652(2), 664, 670, 731(2), 739, 740, 765(2), 771(2), 803, 806, 893(2), 899(2), 966(2), 967(2), 1016(2), 1019(4), 1031, 1033, 1039(2), 1067, 1068, 1079(2), 1118(2), 1131(2), 1178(2), 1189(2), 1278, 1283, 1287(2), 1302(2), 1328(2), 1335(2), 1447(2), 1462(2), 1484(2), 1509(2), 1587, 1588, 1594(2), 1614(2), 1625(2), 3154(3), 3155, 3165(2), 3166(2), 3177(2), 3182(2), 3183(2), 3188(2)

Table B.1. (continued) Vibrational Frequencies and Average Vibrational Energies at 298 K.

Species	E_{vib} (eV)[a]	Vibrational frequencies (cm^{-1})[b]
$Cu^{2+}(Bpy)_2$	0.52 (0.05)	30, 32, 46, 75, 85, 95, 111, 137, 138, 166, 192, 196, 235, 236, 254, 291, 330, 364, 368, 405, 415, 418, 419, 439, 444, 464, 474, 545, 550, 643, 648(2), 650, 666, 667, 728, 730, 738, 740, 765, 766, 771, 773, 801, 803, 895, 899, 901, 905, 969, 970, 976(2), 1016(2), 1017, 1020(3), 1031, 1036, 1037, 1038, 1067, 1068, 1078, 1080, 1118, 1119, 1130, 1133, 1178(2), 1189(2), 1279, 1284, 1285, 1288, 1303(2), 1327, 1328, 1333, 1334, 1447(2), 1461, 1463, 1484, 1485, 1507, 1508, 1587, 1588, 1593, 1595, 1614(2), 1625(2), 3160(2), 3161, 3162, 3166(2), 3167(2), 3177(2), 3182(2), 3183(2), 3187, 3188
$Zn^{2+}(Bpy)_2$	0.52 (0.05)	19, 33, 33, 64, 78, 81(2), 130, 146(2), 206, 227(2), 230, 234, 236, 304, 363, 376, 399, 409, 419(2), 441(2), 459, 460, 547, 548, 646(2), 651(2), 664, 668, 735(2), 740, 742, 763(2), 772(2), 812, 814, 894, 895, 904(2), 970(2), 972(2), 1017(2), 1019(2), 1021(2), 1031, 1034, 1041(2), 1070, 1071, 1080(2), 1121, 1122, 1133(2), 1179(2), 1193(2), 1280, 1283, 1287(2), 1302, 1303, 1327, 1328, 1331(2), 1447, 1448, 1462(2), 1488(2), 1505(2), 1588, 1589, 1596(2), 1615(2), 1628(2), 3158(4), 3165(2), 3166(2), 3180(2), 3182(2), 3183(2), 3195(2)
$Fe^{2+}(Bpy)_3$	0.77 (0.08)	34, 35, 36, 37, 38, 59, 82, 84, 92, 113, 115, 125, 144, 166(2), 179, 200, 201, 228, 229, 252, 269(2), 277, 353, 361(2), 364, 370, 371, 424, 425, 433, 435(2), 452, 454, 469(2), 488, 489, 492, 547(2), 551, 634, 635, 636, 651(2), 652, 656(2), 659, 727, 730(2), 739(2), 742, 767, 768(2), 769, 770(2), 794(2), 795, 885(2), 887, 894(2), 898, 962(2), 963(2), 965, 966, 1004(3), 1008(3), 1011, 1013(2), 1017, 1018, 1029, 1039, 1043(2), 1073(2), 1074, 1078, 1079, 1080, 1118(3), 1133(2), 1134, 1175(2), 1176, 1186, 1187(2), 1276(2), 1278(2), 1280, 1285, 1298, 1299, 1300, 1323(2), 1324(2), 1325, 1326, 1444, 1447(2), 1459(2), 1460, 1483, 1488, 1489, 1502, 1503, 1504, 1585(3), 1593(2), 1594, 1621(3), 1625, 1628(2), 3160(2), 3161, 3162(3), 3170, 3171(2), 3173(3), 3176(2), 3177, 3185(2), 3186, 3188, 3189(2), 3190(2), 3191

Table B.1. (continued) Vibrational Frequencies and Average Vibrational Energies at 298 K.

Species	E_{vib} (eV)[a]	Vibrational frequencies (cm^{-1})[b]
$Fe^{2+}(Bpy)_3$	**0.82 (0.07)**	**21, 23, 24, 27, 30, 45, 61, 77(2), 80, 81, 87, 107, 109, 119, 129, 135, 149, 184, 190, 210, 214, 233, 236, 238, 246, 256, 345, 346, 348, 403, 407, 412, 413, 414, 416, 429, 432, 435, 457, 460, 464, 548, 549, 552, 614, 628(2), 646, 647, 650, 651, 652, 653, 729, 733, 734, 735, 739, 740, 765(3), 768, 769(2), 803, 808, 809, 889, 893, 894, 900, 902, 903, 966(2), 968(2), 970(2), 1002, 1003, 1005, 1007, 1009(3), 1010, 1011, 1013(2), 1015, 1033, 1037, 1040, 1069(2), 1071, 1079, 1080, 1082, 1115, 1116(2), 1127, 1128, 1129, 1175(3), 1189(2), 1190, 1280, 1281, 1282, 1283(2), 1286, 1297, 1298, 1299, 1314, 1315, 1319, 1324, 1325, 1326, 1442, 1443, 1444, 1455, 1456, 1457, 1485, 1487(2), 1498, 1499, 1501, 1586, 1588(2), 1596, 1598, 1599, 1614(2), 1616, 1622, 1623, 1624, 3154(4), 3155(2), 3160(2), 3161, 3162(3), 3173(2), 3174, 3176, 3177(2), 3178(2), 3179, 3188(2), 3190**
$Co^{2+}(Bpy)_3$	0.82 (0.07)	25, 26, 26, 29, 31, 46, 75, 76, 81, 83, 84, 99, 112(2), 121, 136, 154, 156, 193, 194, 196, 221, 237, 237, 249, 260, 264, 347(2), 351, 406, 407, 417(2), 418(2), 434, 440, 441, 456, 457, 462, 549(2), 552, 628(3), 648(2), 651, 652, 653(2), 732(3), 735, 736, 738, 766(2), 767, 769, 770(2), 806(2), 807, 890(2), 892, 901(2), 904, 968(2), 969(2), 971(2), 1006(2), 1008(3), 1009, 1012(4), 1013, 1018, 1037, 1040(2), 1070(3), 1080(2), 1082, 1116, 1117(2), 1128, 1129(2), 1174, 1175(2), 1189(3), 1281, 1282, 1283, 1284, 1285, 1287, 1298, 1299(2), 1320, 1321(2), 1325(2), 1327, 1443, 1445(2), 1457(2), 1458, 1486, 1488(2), 1502(2), 1503, 1589(3), 1598, 1599, 1600, 1615(2), 1616, 1623, 1625(2), 3155, 3156(3), 3157(2), 3161(3), 3162(2), 3163, 3173(2), 3174, 3177(3), 3178(2), 3179, 3188(2), 3189

Table B.1. (continued) Vibrational Frequencies and Average Vibrational Energies at 298 K.

Species	E_{vib} (eV)[a]	Vibrational frequencies (cm^{-1})[b]
$Ni^{2+}(Bpy)_3$	0.81 (0.07)	27, 28, 29, 31, 32, 50, 80, 83, 84, 86, 91, 100, 119, 120, 127, 143, 163, 166, 200, 201, 223, 240, 242, 246, 252, 271, 272, 351 (2), 354, 409, 410, 418, 419(2), 420, 434, 443(2), 459, 460, 467, 549(2), 552, 629(3), 650(2), 653(4), 731, 732, 733, 736, 737, 739, 767(3), 770(3), 806(2), 807, 890, 891, 892, 901(2), 903, 968, 969(3), 971(2), 1007, 1008(2), 1009(3), 1012(3), 1015(2), 1022, 1037, 1041(2), 1070, 1071(2), 1081(2), 1083, 1117(2), 1118, 1129(2), 1130, 1174, 1175(2), 1188, 1189(2), 1282(2), 1283, 1284, 1285, 1288, 1299, 1300(2), 1300, 1322, 1323(2), 1324, 1325, 1326, 1444, 1445, 1446, 1458(3), 1486, 1489(2), 1503, 1504(2), 1590(3), 1599(2), 1600, 1616(3), 1624, 1626(2), 3158(3), 3159(3), 3164(2), 3165(2), 3166(2), 3173, 3174(2), 3178(3), 3179(3), 3187, 3188(2)
$Cu^{2+}(Bpy)_3$	0.82 (0.07)	20, 23, 28, 32, 33, 48, 66, 71, 77, 78, 82, 93, 93, 99, 114, 135, 142, 160, 161, 198, 206, 208, 239, 251, 254, 257, 278, 344, 347, 358, 407, 408 (2), 413, 415, 420, 428, 440, 443, 460, 471, 473, 548, 552, 555, 623, 624, 633, 648, 651, 652, 654 (2), 657, 728, 734, 737, 738, 744, 745, 766, 767, 768, 770, 772, 773, 804, 813(2), 889, 900(2), 901, 905, 907, 969, 970, 972(2), 980(2), 1000, 1001, 1008, 1009, 1010, 1011, 1013, 1014(2), 1017, 1019, 1026, 1037, 1040(2), 1068, 1069, 1072, 1081, 1082, 1084, 1114, 1115, 1120, 1127, 1129, 1132, 1174(2), 1176, 1187(2), 1190, 1282, 1283, 1284(2), 1285, 1289, 1295(2), 1304, 1321, 1322, 1325(2), 1327, 1328, 1443, 1444, 1447, 1455, 1456, 1460, 1487, 1488, 1490, 1502(2), 1507, 1588(2), 1591, 1599, 1600, 1601, 1611, 1612, 1617, 1623, 1624, 1627, 3135(2), 3158(2), 3159(2), 3160, 3161, 3166(2), 3171(3), 3172, 3175(2), 3177, 3178(2), 3183(2), 3186(2), 3189

Table B.1. (continued) Vibrational Frequencies and Average Vibrational Energies at 298 K.

Species	E_{vib} (eV)[a]	Vibrational frequencies (cm^{-1})[b]
$Zn^{2+}(Bpy)_3$	0.82 (0.07)	25(2), 26, 27, 29, 47, 73, 74, 81, 82(2), 87, 94, 95, 123, 129, 150, 151, 166, 176(2), 211, 222(2), 244, 245, 248, 349(2), 351, 407(2), 412, 415(2), 417, 429, 435, 436, 460(2), 467, 552(2), 555, 627(2), 628, 649(2), 652, 653(2), 654, 737, 739(2), 742(2), 744, 767(3), 771(2), 772, 816(2), 817, 896, 897, 898, 905(2), 907, 972(2), 973(2), 975, 976, 1006(2), 1008, 1010, 1011(2), 1013, 1014(4), 1019, 1038, 1041(2), 1070(3), 1082(2), 1084, 1117(2), 1118, 1128(2), 1130, 1175(3), 1189(2), 1190, 1283(2), 1285, 1286, 1287, 1289, 1297, 1298(2), 1323(2), 1324, 1325, 1327, 1328, 1444, 1445(2), 1457(2), 1458, 1488, 1490(2), 1503, 1504(2), 1591(3), 1601(2), 1602, 1615(3), 1624, 1625(2), 3155(2), 3156(4), 3161(3), 3162(3), 3174(3), 3177(3), 3178(2), 3179, 3189(3)

[a]Uncertainties listed in parentheses are determined as described in the text. [b]Vibrational frequencies scaled by 0.9804 obtained from vibrational analyses of the B3LYP/6-31G* geometry optimized structures. Degeneracies are indicated in parentheses. Vibrational frequencies and average vibrational energies for singlet state $Fe^{2+}(Bpy)_3$ are shown in standard font, while those for quintet state are shown in boldface.

Table B.2. Rotational Constants (in cm^{-1}) of $M^{2+}(Bpy)_x$, where x = 1–3 and the corresponding PSL Transition States for Dissociation of $M^{2+}(Bpy)_3$.

Complex	Energized Molecule		Transition State		
	1-D[a]	2-D[b]	1-D[c]	2-D[c]	2-D[d]
$Fe^{2+}(Bpy)$	0.039	0.015	–	–	–
$Fe^{2+}(Bpy)_2$	0.010	0.005	–	–	–
$Fe^{2+}(Bpy)_3$	0.004	0.003	0.01, 0.098	0.005, 0.018	0.0005
$Co^{2+}(Bpy)$	0.038	0.016	–	–	–
$Co^{2+}(Bpy)_2$	0.010	0.005	–	–	–
$Co^{2+}(Bpy)_3$	0.004	0.004	0.01, 0.098	0.005, 0.018	0.0005
$Ni^{2+}(Bpy)$	0.040	0.016	–	–	–
$Ni^{2+}(Bpy)_2$	0.010	0.005	–	–	–
$Ni^{2+}(Bpy)_3$	0.004	0.004	0.01, 0.098	0.005, 0.018	0.0005
$Cu^{2+}(Bpy)$	0.039	0.016	–	–	–
$Cu^{2+}(Bpy)_2$	0.010	0.005	–	–	–
$Cu^{2+}(Bpy)_3$	0.004	0.003	0.01, 0.098	0.005, 0.018	0.0003
$Zn^{2+}(Bpy)$	0.038	0.015	–	–	–
$Zn^{2+}(Bpy)_2$	0.010	0.005	–	–	–
$Zn^{2+}(Bpy)_3$	0.004	0.004	0.01, 0.098	0.005, 0.018	0.0004

[a]Active external. [b]Inactive external. [c]Rotational constants of the PSL TS treated as free internal rotors. [d]Two-dimensional rotational constant of the PSL TS at threshold, treated variationally and statistically.

Table B.3. Measured and Calculated Sequential and Total Enthalpies of Binding of $M^{2+}(Bpy)_x$ Complexes at 0 K in kJ/mol

		Theory					
		BHandHLYP[c]			M06[d]		
Complex	TCID[a]	D_0	$D_{0,BSSE}$[e]	total[e]	D_0	$D_{0,BSSE}$[e]	total[e]
$Fe^{2+}(Bpy)$	–	929.8	927.1	927.1	975.4	971.9	971.9
$Fe^{2+}(Bpy)_2$	–	535.9	531.8	1458.9	573.9	568.9	1540.8
$Fe^{2+}(Bpy)_3$	248.1 (15.7)	230.4	224.6	1683.5	272.7	264.5	1805.3
$Fe^{2+}(Bpy)_3$	**214.8 (10.4)**	**325.3**	**319.5**	**1778.4**	**303.6**	**295.4**	**1836.2**
$Co^{2+}(Bpy)$	–	1001.3	997.8	997.8	1076.0	1070.8	1070.8
$Co^{2+}(Bpy)_2$	–	553.4	550.1	1547.9	569.8	564.2	1635.0
$Co^{2+}(Bpy)_3$	192.4 (11.2)	218.2	211.7	1759.6	267.0	258.8	1893.8
$Ni^{2+}(Bpy)$	–	1066.1	1062.8	1062.8	1190.4	1186.2	1186.2
$Ni^{2+}(Bpy)_2$	–	524.4	519.7	1582.5	578.1	571.4	1757.6
$Ni^{2+}(Bpy)_3$	205.4(11.9)	276.4	269.5	1852.0	287.3	278.3	2035.9
$Cu^{2+}(Bpy)$	–	1143.0	1140.0	1140.0	1246.9	1243.7	1243.7
$Cu^{2+}(Bpy)_2$	–	544.8	539.3	1679.3	545.5	539.1	1782.8
$Cu^{2+}(Bpy)_3$	150.3 (8.1)	171.8	165.0	1844.3	203.9	195.4	1978.2
$Zn^{2+}(Bpy)$	–	1067.1	1064.0	1064.0	1098.9	1095.6	1095.6
$Zn^{2+}(Bpy)_2$	–	555.5	551.1	1615.1	562.6	557.5	1653.1
$Zn^{2+}(Bpy)_3$	161.3 (7.9)	186.9	180.0	1795.1	229.9	221.7	1874.8
AEU/MAD[f]	11.0 (3.2)		28.1 (20.4)			52.2 (22.5)	
AEU/MAD[g]	**9.9 (1.8)**		**44.3 (39.4)**			**65.1 (13.5)**	

[a]Average values from fits to raw data and data after subtraction of the low-energy feature, Table 4.1. Average values for the singlet state of $Fe^{2+}(Bpy)_3$ complex are shown in standard font, while those of the quintet state of $Fe^{2+}(Bpy)_3$ are shown in boldface. [c]Calculated at the BHandHLYP/6-311+G(2d,2p)//BHandHLYP/6-31G* level of theory including ZPE corrections with frequencies scaled by 0.9472. [d]Calculated at the M06/6-311+G(2d,2p)//M06/6-31G* level of theory including ZPE corrections with frequencies scaled by 0.9940. [e]Also includes BSSE corrections. [f]AEU/MAD values using the singlet state of $Fe^{2+}(Bpy)_3$ in the analysis. [g]AEU/MAD values using the quintet state of $Fe^{2+}(Bpy)_3$ in the analysis.

Table B.4. Geometrical Parameters of the BHandHLYP/6-31G* *cis* and *trans* Conformers of the Neutral Bpy Ligand and Ground-State Structures of the $M^{2+}(Bpy)_x$ Complexes[a]

Complex	M^{2+}–N	∠NCCN	∠NM^{2+}NC	∠NM^{2+}N[b]	∠NM^{2+}N[c]
trans-Bpy	–	180.0	–	–	–
cis-Bpy	–	36.9	–	–	–
$Fe^{2+}(Bpy)$	1.991	0.0	–	85.1	–
$Fe^{2+}(Bpy)_2$	2.068	0.0	83.7	81.1	125.3
$Fe^{2+}(Bpy)_3$	2.036	4.2	64.6	80.1	88.7 (3), 95.8 (6), 174.2 (3)
$Fe^{2+}(Bpy)_3$	**2.208**	**8.7, 10.4 (2)**	**65.6**	**74.8**	**92.5 (3), 96.9 (6), 168.2 (3)**
$Co^{2+}(Bpy)$	1.947	0.0	–	86.9	–
$Co^{2+}(Bpy)_2$	2.036	8.2	84.0	82.3	105.9 (2), 149.4 (2)
$Co^{2+}(Bpy)_3$	2.168	7.5	60.9	75.7	89.3 (3), 97.8 (6), 171.0 (3)
$Ni^{2+}(Bpy)$	1.910	0.0	–	88.6	–
$Ni^{2+}(Bpy)_2$	2.006	5.1	84.9	82.9	105.7 , 148.6
$Ni^{2+}(Bpy)_3$	2.124	8.1	65.5	77.4	90.8 (3), 96.3 (6), 171.0 (3)
$Cu^{2+}(Bpy)$	1.875	0.0	–	89.7	–
$Cu^{2+}(Bpy)_2$	1.981	5.8	54.6	82.8	105.4 (2), 149.2 (2)
$Cu^{2+}(Bpy)_3$	2.068 (4), 2.334 (2)	1.0, 14.7 (2)	64.6	74.9 (2), 79.3	91.7 (3), 95.4 (4), 98.4 (2), 169.4 (3)
$Zn^{2+}(Bpy)$	1.907	0.0	–	92.4	–
$Zn^{2+}(Bpy)_2$	2.011	0.0	83.8	83.1	124.0
$Zn^{2+}(Bpy)_3$	2.177	10.3	64.1	75.7	93.5 (3), 96.0 (6), 168.0 (3)

[a] Average values are given for similar bond distances or angles; degeneracies are listed in parentheses for values that differ sufficiently such that more than one value is needed to describe the bond angle or bond length. Geometrical parameters for the singlet ground-state of $Fe^{2+}(Bpy)_3$ are shown in standard font, while those for quintet excited state are shown in bold. All bond angles (∠) are given in degrees (°) and M^{2+}–N bond lengths in angstroms (Å). [b] intraligand angles. [c] interligand angles.

Table B.5. Geometrical Parameters of the M06/6-31G* *cis* and *trans* Conformers of the Neutral Bpy Ligand and Ground-State Structures of the $M^{2+}(Bpy)_x$ Complexes[a]

Complex	M^{2+}–N	∠NCCN	∠NM^{2+}NC	∠NM^{2+}N[b]	∠NM^{2+}N[c]
trans-Bpy	–	180.0	–	–	–
cis-Bpy	–	35.5	–	–	–
$Fe^{2+}(Bpy)$	1.956	0.0	–	89.3	–
$Fe^{2+}(Bpy)_2$	2.040	0.0	84.0	81.5	125.0
$Fe^{2+}(Bpy)_3$	1.976	0.1, 2.5 (2)	63.6	81.6	88.6 (3), 95.0 (6), 175.3 (3)
$Fe^{2+}(Bpy)_3$	**2.157**	**5.4, 9.6 (2)**	**65.3**	**76.4**	**91.9 (3), 96.3 (6), 169.6 (3)**
$Co^{2+}(Bpy)$	1.927	0.0	–	87.1	–
$Co^{2+}(Bpy)_2$	2.024	6.4	84.0	81.7	104.5 (2), 153.4 (2)
$Co^{2+}(Bpy)_3$	2.125	7.7	63.6	77.3	91.1 (3), 96.1 (6), 170.7 (3)
$Ni^{2+}(Bpy)$	1.897	0.0	–	89.2	–
$Ni^{2+}(Bpy)_2$	1.976	5.0	85.4	84.3	104.8, 147.7
$Ni^{2+}(Bpy)_3$	2.084	6.6	64.9	78.8	90.1 (3), 95.8 (6), 172.4 (3)
$Cu^{2+}(Bpy)$	1.869	0.0	–	89.0	–
$Cu^{2+}(Bpy)_2$	1.958	5.2	56.2	83.7	103.9 (2), 150.5 (2)
$Cu^{2+}(Bpy)_3$	2.024 (4), 2.323 (2)	5.6, 16.0 (2)	60.9	77.7	91.7 (5), 95.2 (2), 100.3 (2), 170.0 (3)
$Zn^{2+}(Bpy)$	1.902	0.0	–	93.2	–
$Zn^{2+}(Bpy)_2$	1.991	3.7	83.6	84.0	115.0 (2), 133.0 (2)
$Zn^{2+}(Bpy)_3$	2.150	10.2	64.4	76.7	93.4 (3), 95.5 (6), 168.7 (3)

[a] Average values are given for similar bond distances or angles; degeneracies are listed in parentheses for values that differ sufficiently such that more than one value is needed to describe the bond angle or bond length. Geometrical parameters for the singlet ground-state of $Fe^{2+}(Bpy)_3$ are shown in standard font, while those for quintet excited state are shown in bold. All bond angles (∠) are given in degrees (°) and M^{2+}–N bond lengths in angstroms (Å). [b] intraligand angles. [c] interligand angles.

Table B.6. Cartesian Coordinates of the B3LYP/6-31G* Optimized Geometries of the *cis* and *trans* Conformers of the Neutral Bpy Ligand.[a]

	cis Bpy				*trans* Bpy		
	x	y	z		x	y	z
C	-0.005871	-0.004549	0.041797	C	0.000000	0.000000	0.000000
C	-0.000909	-0.050210	1.444878	C	0.000000	0.000000	1.394652
C	1.217939	-0.035952	2.118937	C	1.223813	0.000000	2.050435
C	2.394327	0.024024	1.375230	C	2.421400	0.000008	1.270334
C	2.287403	0.072166	-0.016869	C	1.245758	-0.000009	-0.696065
C	-1.290799	-0.020897	-0.720602	C	3.714792	0.000008	1.917644
C	-2.387135	-0.771399	-0.267238	C	4.890433	0.000001	3.884042
C	-3.568624	-0.758409	-1.004845	H	4.878631	-0.000005	4.971626
C	-3.621918	0.000912	-2.171539	C	6.136190	0.000008	3.187978
C	-2.477321	0.709758	-2.544538	C	6.136191	0.000016	1.793325
H	-0.935321	-0.069784	1.997022	C	4.912380	0.000016	1.137541
H	1.245914	-0.061787	3.205121	H	-0.927756	0.000000	-0.563842
H	3.368700	0.038142	1.854530	H	-0.930441	0.000002	1.952999
H	3.183705	0.120721	-0.634113	H	1.257558	-0.000009	-1.783650
H	-2.305888	-1.374211	0.631866	H	7.063948	0.000008	3.751817
H	-4.427435	-1.338674	-0.677764	H	7.066634	0.000022	1.234982
H	-4.519746	0.042628	-2.781043	H	4.832555	0.000022	0.057022
H	-2.478082	1.314500	-3.450624	H	1.303636	0.000000	3.130954
N	1.127798	0.059925	-0.677493	N	2.415156	-0.000002	-0.090399
N	-1.337965	0.707233	-1.849469	N	3.721035	0.000001	3.278376

Table B.6. (continued) Cartesian Coordinates of the B3LYP/6-31G* Optimized Geometries of the Ground State Structures of the $M^{2+}(Bpy)_x$ Complexes.[a]

$Fe^{2+}(Bpy)$				$Co^{2+}(Bpy)$			
	x	y	z		x	y	z
C	-0.746817	0.679828	0.000037	C	0.019943	0.000004	-0.050895
N	-1.380649	-0.540768	0.000315	N	-0.025653	-0.000106	1.320846
C	-1.508742	1.846119	-0.000233	C	1.250106	0.000103	-0.701742
C	0.746817	0.679828	0.000048	C	-1.295632	0.000010	-0.737991
C	-2.732370	-0.617465	0.000349	C	1.113039	-0.000115	2.050906
C	-2.904491	1.767178	-0.000203	C	2.428879	0.000094	0.050549
N	1.380650	-0.540768	0.000163	N	-2.395358	-0.000183	0.083202
C	1.508742	1.846119	-0.000044	C	-1.464367	0.000198	-2.119452
H	-1.033323	2.818949	-0.000480	H	1.303510	0.000179	-1.783929
C	-3.528684	0.518953	0.000102	C	2.362476	-0.000013	1.445234
C	2.732370	-0.617465	0.000177	C	-3.645127	-0.000200	-0.434180
C	2.904491	1.767178	-0.000033	C	-2.755282	0.000181	-2.657024
H	-3.167914	-1.611894	0.000592	H	1.008421	-0.000200	3.131717
H	-3.495466	2.678230	-0.000418	H	3.390689	0.000169	-0.453545
H	1.033323	2.818949	-0.000109	H	-0.606737	0.000365	-2.781609
C	3.528684	0.518954	0.000075	C	-3.861949	-0.000023	-1.805646
H	-4.609051	0.421001	0.000142	H	3.257609	-0.000018	2.058039
H	3.167914	-1.611894	0.000270	H	-4.472365	-0.000360	0.269224
H	3.495466	2.678230	-0.000106	H	-2.891126	0.000328	-3.734399
H	4.609051	0.421002	0.000087	H	-4.876325	-0.000043	-2.190136
Fe^{2+}	0.000000	-1.937180	0.000387	Co^{2+}	-1.855710	-0.000329	1.937389

Table B.6. (continued) Cartesian Coordinates of the B3LYP/6-31G* Optimized Geometries of the Ground State Structures of the $M^{2+}(Bpy)_x$ Complexes.[a]

	$Ni^{2+}(Bpy)$				$Cu^{2+}(Bpy)$		
	x	y	z		x	y	z
C	-0.009004	0.000624	0.020520	C	0.070395	0.080448	-0.172875
N	0.002344	0.000662	1.395059	N	0.051779	-0.223997	1.161054
C	1.194073	0.000687	-0.678653	C	1.285784	0.341606	-0.796763
C	-1.350450	0.000568	-0.606793	C	-1.255278	0.098808	-0.830120
C	1.166791	0.000775	2.081864	C	1.182210	-0.277403	1.891779
C	2.400954	0.000803	0.027647	C	2.468058	0.289731	-0.050067
N	-2.412600	0.000327	0.265728	N	-2.312388	-0.191549	-0.011050
C	-1.585187	0.000769	-1.978339	C	-1.488441	0.380837	-2.172086
H	1.204524	0.000629	-1.762203	H	1.322000	0.584160	-1.852734
C	2.390296	0.000865	1.425249	C	2.419995	-0.022648	1.308962
C	-3.686239	0.000274	-0.187579	C	-3.579229	-0.211091	-0.469141
C	-2.900986	0.000736	-2.451722	C	-2.799133	0.363596	-2.661601
H	1.103656	0.000792	3.165849	H	1.089065	-0.525746	2.945124
H	3.342644	0.000845	-0.513366	H	3.419663	0.493259	-0.532298
H	-0.760333	0.000967	-2.681053	H	-0.664374	0.612967	-2.837096
C	-3.966736	0.000478	-1.547515	C	-3.858590	0.065156	-1.804020
H	3.309705	0.000981	2.001220	H	3.317117	-0.071716	1.917202
H	-4.477649	0.000038	0.555845	H	-4.366709	-0.449832	0.239916
H	-3.089528	0.000917	-3.521267	H	-2.986729	0.582970	-3.708597
H	-4.998207	0.000441	-1.883851	H	-4.886625	0.043420	-2.150238
Ni^{2+}	-1.767771	0.000407	2.033566	Cu^{2+}	-1.705910	-0.525849	1.726070

Table B.6. (continued) Cartesian Coordinates of the B3LYP/6-31G* Optimized Geometries of the Ground State Structures of the $M^{2+}(Bpy)_x$ Complexes.[a]

	Zn^{2+}(Bpy)		
	x	y	z
C	-0.024838	0.000691	0.079397
N	0.039932	0.000695	1.450364
C	1.158206	0.000739	-0.655007
C	-1.385486	0.000629	-0.556888
C	1.225780	0.000757	2.098659
C	2.389588	0.000807	0.008752
N	-2.479151	0.000335	0.272354
C	-1.580343	0.000844	-1.935646
H	1.139722	0.000704	-1.737578
C	2.427455	0.000824	1.403066
C	-3.736946	0.000231	-0.222082
C	-2.879201	0.000735	-2.455114
H	1.194026	0.000763	3.182709
H	3.310549	0.000842	-0.566728
H	-0.737683	0.001114	-2.615518
C	-3.973533	0.000414	-1.590257
H	3.364935	0.000877	1.948980
H	-4.548535	-0.000009	0.497291
H	-3.027996	0.000905	-3.530849
H	-4.993527	0.000312	-1.959724
Zn^{2+}	-1.772656	0.000378	2.044021

Table B.6. (continued) Cartesian Coordinates of the B3LYP/6-31G* Optimized Geometries of the Ground State Structures of the $M^{2+}(Bpy)_x$ Complexes.[a]

$Fe^{2+}(Bpy)_2$				$Fe^{2+}(Bpy)_2$			
	x	y	z		x	y	z
C	-2.776018	-0.525974	-0.525962	H	4.917137	0.735473	-0.735021
N	-1.551648	-0.950078	-0.950232	H	2.483326	3.242791	-3.242713
C	-3.942081	-1.068444	-1.068189	H	4.917130	-0.735530	0.735023
C	-2.776012	0.526007	0.525973	H	2.483294	-3.242819	3.242719
C	-1.471902	-1.901696	-1.901816	H	4.755285	2.478575	-2.478087
C	-3.851866	-2.052861	-2.052574	H	4.755260	-2.478630	2.478088
N	-1.551637	0.950097	0.950243	Fe^{2+}	0.000000	0.000001	0.000005
C	-3.942069	1.068490	1.068201				
H	-4.917138	-0.735473	-0.735016				
C	-2.595591	-2.480130	-2.480056				
C	-1.471879	1.901714	1.901827				
C	-3.851842	2.052906	2.052586				
H	-0.472617	-2.201983	-2.202286				
H	-4.755287	-2.478575	-2.478081				
H	-4.917129	0.735531	0.735028				
C	-2.595561	2.480161	2.480067				
H	-2.483329	-3.242790	-3.242711				
H	-0.472591	2.201990	2.202297				
H	-4.755258	2.478631	2.478094				
H	-2.483291	3.242819	3.242722				
N	1.551647	0.950079	-0.950233				
N	1.551638	-0.950096	0.950241				
C	2.776017	0.525974	-0.525965				
C	1.471900	1.901697	-1.901818				
C	2.776012	-0.526006	0.525970				
C	1.471881	-1.901713	1.901825				
C	3.942080	1.068444	-1.068193				
C	2.595588	2.480131	-2.480058				
C	3.942070	-1.068489	1.068196				
C	2.595563	-2.480160	2.480064				
H	0.472615	2.201985	-2.202286				
H	0.472593	-2.201989	2.202296				
C	3.851864	2.052861	-2.052578				
C	3.851844	-2.052905	2.052582				

Table B.6. (continued) Cartesian Coordinates of the B3LYP/6-31G* Optimized Geometries of the Ground State Structures of the $M^{2+}(Bpy)_x$ Complexes.[a]

$Co^{2+}(Bpy)_2$				$Co^{2+}(Bpy)_2$			
	x	y	z		x	y	z
C	-0.010166	0.230442	-0.050683	H	-4.093634	1.454818	6.384174
N	-0.005720	0.476932	1.289369	H	-3.938073	4.675125	3.534602
C	1.150888	0.392625	-0.806146	H	-3.572286	-0.552553	6.752036
C	-1.311388	-0.210664	-0.620404	H	-1.674542	-4.058497	5.132915
C	1.130302	0.880824	1.889149	H	-4.626965	3.795509	5.788335
C	2.325957	0.811396	-0.180130	H	-2.886834	-2.914408	7.016797
N	-2.339600	-0.314773	0.267546	Co^{2+}	-1.801285	0.168509	2.146518
C	-1.505513	-0.507323	-1.969249				
H	1.151909	0.197763	-1.871563				
C	2.319481	1.060865	1.191319				
C	-3.553959	-0.707773	-0.161747				
C	-2.765912	-0.914229	-2.409564				
H	1.074967	1.062311	2.958202				
H	3.233851	0.939967	-0.761177				
H	-0.691054	-0.425874	-2.678550				
C	-3.810884	-1.017469	-1.492764				
H	3.211622	1.387516	1.714062				
H	-4.335083	-0.772931	0.589568				
H	-2.925123	-1.146924	-3.457859				
H	-4.804118	-1.330063	-1.795499				
N	-2.759252	1.527527	3.281970				
N	-2.100548	-1.015619	3.747193				
C	-3.125514	1.036026	4.498849				
C	-3.051927	2.802529	2.962403				
C	-2.758031	-0.381706	4.758323				
C	-1.729540	-2.301519	3.896272				
C	-3.800547	1.841388	5.415799				
C	-3.722434	3.655031	3.832569				
C	-3.049909	-1.052562	5.945687				
C	-1.991270	-3.024340	5.054959				
H	-2.735957	3.139904	1.979950				
H	-1.209069	-2.755251	3.058351				
C	-4.101763	3.162240	5.080132				
C	-2.663368	-2.385285	6.095652				

Table B.6. (continued) Cartesian Coordinates of the B3LYP/6-31G* Optimized Geometries of the Ground State Structures of the $M^{2+}(Bpy)_x$ Complexes.[a]

$Ni^{2+}(Bpy)_2$				$Ni^{2+}(Bpy)_2$			
	x	y	z		x	y	z
C	-0.012292	0.229705	-0.051738	H	-4.098168	1.483230	6.373815
N	-0.034548	0.468936	1.287759	H	-3.904040	4.657777	3.470303
C	1.158358	0.398110	-0.788351	H	-3.562913	-0.581682	6.751732
C	-1.309150	-0.209946	-0.619538	H	-1.647281	-4.049673	5.063771
C	1.086477	0.873490	1.912471	H	-4.611610	3.822680	5.733523
C	2.320069	0.818038	-0.137195	H	-2.856751	-2.947941	6.972586
N	-2.319171	-0.305567	0.287488	Ni^{2+}	-1.801271	0.168534	2.146522
C	-1.524098	-0.511306	-1.962803				
H	1.175598	0.207504	-1.854841				
C	2.287276	1.060645	1.235589				
C	-3.542639	-0.695864	-0.114284				
C	-2.794855	-0.916059	-2.376648				
H	1.009569	1.049055	2.981259				
H	3.238690	0.953035	-0.699655				
H	-0.719613	-0.435019	-2.684614				
C	-3.823337	-1.011018	-1.439803				
H	3.168968	1.387725	1.775498				
H	-4.309200	-0.754084	0.652553				
H	-2.975437	-1.153729	-3.420369				
H	-4.822762	-1.321715	-1.723495				
N	-2.748264	1.499986	3.277654				
N	-2.103111	-0.989225	3.733185				
C	-3.124941	1.033662	4.499390				
C	-3.028073	2.770089	2.932448				
C	-2.758710	-0.379327	4.757975				
C	-1.720867	-2.273580	3.855447				
C	-3.798445	1.854964	5.401186				
C	-3.697308	3.641167	3.785949				
C	-3.040912	-1.067707	5.936057				
C	-1.971740	-3.016687	5.004346				
H	-2.703710	3.087139	1.945881				
H	-1.201762	-2.707943	3.006386				
C	-4.087375	3.172537	5.040023				
C	-2.642944	-2.400448	6.059905				

Table B.6. (continued) Cartesian Coordinates of the B3LYP/6-31G* Optimized Geometries of the Ground State Structures of the $M^{2+}(Bpy)_x$ Complexes.[a]

	$Cu^{2+}(Bpy)_2$				$Cu^{2+}(Bpy)_2$		
	x	y	z		x	y	z
C	0.000000	0.000000	0.000000	C	-1.945653	-2.044565	6.331102
N	0.000000	0.000000	1.359946	H	-4.258652	1.403382	6.269819
C	1.197542	0.000000	-0.713744	H	-5.041187	4.049966	2.964726
C	-1.345205	0.023065	-0.619540	H	-3.376085	-0.505866	6.797307
C	1.166884	0.008844	2.028141	H	-0.493451	-3.444074	5.533279
C	2.407694	0.002556	-0.018460	H	-5.403445	3.410087	5.369419
N	-2.373584	0.166351	0.258731	H	-2.045091	-2.538447	7.292644
C	-1.586934	-0.110110	-1.986059				
H	1.196509	0.009633	-1.797240				
C	2.395727	0.011083	1.375900				
C	-3.640748	0.171470	-0.191207				
C	-2.902516	-0.097985	-2.451881				
H	1.102780	0.019045	3.111306				
H	3.346898	0.004749	-0.562760				
H	-0.767388	-0.233778	-2.683988				
C	-3.949521	0.041032	-1.541440				
H	3.314675	0.021687	1.951581				
H	-4.418498	0.278572	0.557855				
H	-3.103910	-0.202981	-3.513384				
H	-4.985027	0.046663	-1.863441				
Cu^{2+}	-1.801153	0.168715	2.146555				
N	-3.127700	1.282251	3.090851				
N	-1.703533	-0.774069	3.876659				
C	-3.305884	0.927636	4.391601				
C	-3.740106	2.377195	2.606868				
C	-2.554020	-0.276613	4.814013				
C	-0.990799	-1.882940	4.142405				
C	-4.124871	1.681308	5.231110				
C	-4.568241	3.172728	3.392231				
C	-2.691118	-0.897511	6.054680				
C	-1.082995	-2.550653	5.359413				
H	-3.551352	2.615070	1.565114				
H	-0.337458	-2.237741	3.352014				
C	-4.764878	2.813732	4.725238				

Table B.6. (continued) Cartesian Coordinates of the B3LYP/6-31G* Optimized Geometries of the Ground State Structures of the $M^{2+}(Bpy)_x$ Complexes.[a]

$Zn^{2+}(Bpy)_2$				$Zn^{2+}(Bpy)_2$			
	x	y	z		x	y	z
C	-0.014444	0.231271	-0.038406	H	-4.088715	1.447238	6.375319
N	-0.001925	0.479454	1.298535	H	-3.942269	4.677577	3.538048
C	1.144357	0.391091	-0.799428	H	-3.568466	-0.546200	6.741783
C	-1.317914	-0.209996	-0.609147	H	-1.674524	-4.060358	5.138562
C	1.135409	0.882573	1.894982	H	-4.626977	3.787493	5.789007
C	2.322006	0.809025	-0.178934	H	-2.886972	-2.906379	7.016378
N	-2.349123	-0.316489	0.270869	Zn^{2+}	-1.801279	0.168520	2.146519
C	-1.506253	-0.504799	-1.960123				
H	1.141802	0.195117	-1.864439				
C	2.321765	1.060316	1.192363				
C	-3.561784	-0.709131	-0.161646				
C	-2.764120	-0.911577	-2.406039				
H	1.083895	1.065189	2.963756				
H	3.227631	0.935714	-0.763933				
H	-0.689711	-0.422043	-2.666575				
C	-3.813135	-1.016926	-1.493859				
H	3.216538	1.386509	1.710851				
H	-4.345245	-0.775611	0.586719				
H	-2.918773	-1.142719	-3.455365				
H	-4.804848	-1.329636	-1.801377				
N	-2.758299	1.534338	3.274389				
N	-2.095760	-1.023214	3.742291				
C	-3.120645	1.036344	4.486771				
C	-3.052822	2.809061	2.957974				
C	-2.752099	-0.383521	4.746868				
C	-1.725912	-2.308416	3.894773				
C	-3.796940	1.837146	5.408106				
C	-3.724101	3.656791	3.831728				
C	-3.046260	-1.049333	5.937532				
C	-1.989632	-3.026087	5.055853				
H	-2.738300	3.150002	1.976589				
H	-1.205464	-2.765501	3.059016				
C	-4.101107	3.158109	5.077836				
C	-2.661876	-2.381454	6.093223				

Table B.6. (continued) Cartesian Coordinates of the B3LYP/6-31G* Optimized Geometries of the Ground State Structures of the $M^{2+}(Bpy)_x$ Complexes.[a]

$Fe^{2+}(Bpy)_3$				$Fe^{2+}(Bpy)_3$			
	x	y	z		x	y	z
C	-1.918657	-2.290846	-0.586090	H	-3.781461	0.975313	3.590805
N	-1.536199	-1.103733	-1.118482	H	-1.878159	-0.263616	2.555211
C	-2.216460	-0.608006	-2.166572	H	-1.751693	4.857295	-0.646001
C	-3.302330	-1.259247	-2.743066	H	-0.356933	5.478566	-2.593004
C	-3.706364	-2.476194	-2.196214	H	1.194903	3.758106	-3.576305
C	-3.009963	-2.994813	-1.106574	H	1.268269	1.496028	-2.530218
C	-1.119999	-2.779164	0.569901	C	2.930578	-0.507951	-0.592354
N	-0.238851	-1.895316	1.100359	C	4.092236	-1.050528	-1.154395
C	0.508070	-2.278039	2.149819	C	3.997323	-1.869764	-2.276146
C	0.418570	-3.540481	2.729102	C	2.739144	-2.134928	-2.814806
C	-0.477124	-4.456230	2.180388	C	1.626942	-1.571966	-2.197972
C	-1.251112	-4.072417	1.087290	N	1.707663	-0.776834	-1.115940
H	-1.867573	0.344419	-2.553280	C	2.949569	0.381916	0.596086
H	-3.814952	-0.820485	-3.592174	C	4.133471	0.871619	1.160280
H	-4.554396	-3.015156	-2.607179	C	4.073481	1.696169	2.280549
H	-3.327971	-3.930784	-0.663853	C	2.827453	2.019922	2.815455
H	1.201397	-1.537487	2.536013	C	1.692153	1.507245	2.196873
H	1.040710	-3.795688	3.580119	N	1.739045	0.707136	1.116525
H	-0.570955	-5.456749	2.590944	H	5.064095	-0.849143	-0.720906
H	-1.936593	-4.782541	0.640854	H	4.892630	-2.295228	-2.718562
C	-1.828791	2.368349	0.583832	H	2.617054	-2.766318	-3.688189
C	-2.893477	3.113479	1.102017	H	0.627334	-1.759336	-2.577026
C	-3.609818	2.623256	2.191917	H	5.096123	0.625320	0.729443
C	-3.252203	1.393017	2.741292	H	4.986292	2.080878	2.724515
C	-2.191029	0.700510	2.166760	H	2.732294	2.658057	3.687281
N	-1.491787	1.168528	1.118509	H	0.701260	1.740828	2.573137
C	-1.010524	2.825023	-0.571413	Fe^{2+}	-0.007497	0.002776	0.000229
C	-1.092107	4.121742	-1.090192				
C	-0.301471	4.475587	-2.181477				
C	0.561220	3.526807	-2.726980				
C	0.602030	2.262326	-2.146623				
N	-0.161668	1.908505	-1.099154				
H	-3.176117	4.060030	0.657713				
H	-4.437318	3.194449	2.601202				

Table B.6. (continued) Cartesian Coordinates of the B3LYP/6-31G* Optimized Geometries of the Ground State Structures of the $M^{2+}(Bpy)_x$ Complexes.[a]

$Co^{2+}(Bpy)_3$				$Co^{2+}(Bpy)_3$			
	x	y	z		x	y	z
C	0.169038	0.005081	0.123616	H	-1.322545	5.198095	1.042475
N	0.152075	-0.023178	1.478380	H	-1.915883	2.795843	0.728208
C	1.318753	-0.045866	2.143122	H	-0.338634	2.797288	6.575161
C	2.556198	-0.047162	1.506297	H	-0.197253	0.904290	8.161207
C	2.581201	-0.011338	0.113132	H	-0.675838	-1.421583	7.326701
C	1.375752	0.017308	-0.584452	H	-1.282848	-1.715047	4.926065
C	-1.161054	0.026682	-0.538163	C	-3.528980	-2.286257	2.816664
N	-2.228663	0.148632	0.288268	C	-3.991258	-3.606037	2.775265
C	-3.461876	0.177595	-0.243156	C	-3.132589	-4.621209	2.359387
C	-3.702077	0.094336	-1.611378	C	-1.828895	-4.296017	1.988718
C	-2.609222	-0.037099	-2.466349	C	-1.441961	-2.960367	2.043671
C	-1.326700	-0.073290	-1.923840	N	-2.261442	-1.976319	2.448427
H	1.249707	-0.066158	3.226065	C	-4.373200	-1.143923	3.254237
H	3.470237	-0.071483	2.089634	C	-5.649531	-1.303834	3.804361
H	3.523486	-0.003142	-0.425789	C	-6.380049	-0.179188	4.181693
H	1.384264	0.057122	-1.666850	C	-5.817903	1.084014	4.005414
H	-4.282005	0.274421	0.460847	C	-4.538830	1.166152	3.463267
H	-4.717870	0.127767	-1.990025	N	-3.829865	0.087627	3.091957
H	-2.749549	-0.113201	-3.540096	H	-5.010364	-3.846476	3.052739
H	-0.471497	-0.186964	-2.578837	H	-3.480293	-5.648946	2.323615
C	-0.962262	2.618108	3.867877	H	-1.126821	-5.054472	1.659828
C	-0.596319	3.945533	4.116365	H	-0.439558	-2.658110	1.757608
C	-0.721999	4.893334	3.103265	H	-6.072160	-2.290618	3.949368
C	-1.207297	4.493835	1.859227	H	-7.371556	-0.291228	4.609219
C	-1.540688	3.154424	1.681410	H	-6.351435	1.986217	4.284159
N	-1.427170	2.235175	2.653869	H	-4.057067	2.127258	3.314320
C	-0.867717	1.544756	4.890901	Co^{2+}	-1.792996	0.122127	2.403732
C	-0.532264	1.790053	6.226892				
C	-0.457245	0.725731	7.122488				
C	-0.723394	-0.563594	6.664944				
C	-1.061389	-0.730608	5.325357				
N	-1.131228	0.288951	4.453731				
H	-0.209120	4.243189	5.083165				
H	-0.442006	5.926280	3.285019				

Table B.6. (continued) Cartesian Coordinates of the B3LYP/6-31G* Optimized Geometries of the Ground State Structures of the $M^{2+}(Bpy)_x$ Complexes.[a]

	$Ni^{2+}(Bpy)_3$				$Ni^{2+}(Bpy)_3$		
	x	y	z		x	y	z
C	0.152925	-0.017205	0.179726	H	-1.436506	5.167103	1.012656
N	0.127260	-0.059649	1.533846	H	-2.010004	2.758337	0.710314
C	1.290005	-0.108497	2.203189	H	-0.353974	2.774973	6.532634
C	2.530435	-0.119163	1.571703	H	-0.165862	0.876189	8.109769
C	2.563994	-0.067419	0.179466	H	-0.610727	-1.453240	7.265797
C	1.362309	-0.015027	-0.523258	H	-1.234066	-1.745208	4.870323
C	-1.173537	0.028505	-0.485199	C	-3.492148	-2.250778	2.800722
N	-2.237332	0.176269	0.341285	C	-3.956399	-3.568800	2.740399
C	-3.468519	0.235048	-0.190959	C	-3.091891	-4.582167	2.332041
C	-3.709693	0.152765	-1.559411	C	-1.781028	-4.255309	1.990344
C	-2.620729	-0.007746	-2.414014	C	-1.393364	-2.920322	2.062358
C	-1.339626	-0.071614	-1.870472	N	-2.219395	-1.937914	2.455726
H	1.216554	-0.142447	3.284955	C	-4.337245	-1.110705	3.237119
H	3.440791	-0.163401	2.159622	C	-5.608750	-1.271547	3.797157
H	3.509203	-0.065646	-0.354356	C	-6.340656	-0.146668	4.170854
H	1.374459	0.036857	-1.605099	C	-5.783749	1.116158	3.978587
H	-4.286157	0.354624	0.511651	C	-4.508397	1.198528	3.426710
H	-4.724431	0.210325	-1.938022	N	-3.796736	0.120018	3.062281
H	-2.762687	-0.084311	-3.487498	H	-4.981530	-3.808243	2.995846
H	-0.486004	-0.207619	-2.523425	H	-3.440286	-5.608982	2.280476
C	-0.997955	2.593335	3.830492	H	-1.072693	-5.011756	1.670378
C	-0.644485	3.924617	4.073924	H	-0.385358	-2.617906	1.799153
C	-0.797297	4.870796	3.062868	H	-6.024835	-2.259337	3.954202
C	-1.298752	4.464800	1.827574	H	-7.328386	-0.258296	4.607103
C	-1.620589	3.121457	1.655374	H	-6.318368	2.019445	4.251684
N	-1.477988	2.203869	2.624682	H	-4.033576	2.160483	3.265181
C	-0.877236	1.520266	4.849256	Ni^{2+}	-1.789267	0.127031	2.405987
C	-0.533160	1.765673	6.182541				
C	-0.432082	0.698683	7.072475				
C	-0.680106	-0.592272	6.609856				
C	-1.027204	-0.759092	5.272150				
N	-1.124971	0.263165	4.407252				
H	-0.245360	4.226462	5.034666				
H	-0.526493	5.907012	3.239757				

Table B.6. (continued) Cartesian Coordinates of the B3LYP/6-31G* Optimized Geometries of the Ground State Structures of the $M^{2+}(Bpy)_x$ Complexes.[a]

$Cu^{2+}(Bpy)_3$				$Cu^{2+}(Bpy)_3$			
	x	y	z		x	y	z
C	0.248732	-0.010120	0.360968	H	-0.949930	5.447939	4.189441
N	0.174285	-0.111576	1.712048	H	-1.583180	4.820665	1.834260
C	1.303469	-0.040930	2.439893	H	-1.896881	2.400461	1.300438
C	2.560868	0.126791	1.871394	H	-1.162630	2.130028	7.270154
C	2.648849	0.241804	0.484935	H	-0.851236	0.177391	8.763008
C	1.482800	0.176202	-0.273029	H	-0.575117	-2.104146	7.740512
C	-1.029911	-0.088256	-0.395238	H	-0.647300	-2.303200	5.252914
N	-2.152868	0.089991	0.331439	C	-3.057407	-2.744136	2.801380
C	-3.336024	0.057135	-0.295605	C	-3.326236	-4.114243	2.746832
C	-3.469304	-0.154129	-1.667108	C	-2.316528	-4.996084	2.366663
C	-2.312089	-0.355948	-2.416767	C	-1.058377	-4.487874	2.049714
C	-1.075415	-0.325677	-1.774173	C	-0.862163	-3.111739	2.123799
H	1.177297	-0.125834	3.513832	N	-1.830828	-2.257699	2.489666
H	3.441888	0.172595	2.502192	C	-4.057510	-1.726011	3.198564
H	3.608396	0.388463	-0.001210	C	-5.375975	-2.029919	3.547456
H	1.532057	0.290938	-1.349042	C	-6.245742	-1.000517	3.901742
H	-4.212296	0.211711	0.328817	C	-5.777553	0.311913	3.898638
H	-4.451318	-0.163044	-2.127885	C	-4.451586	0.541137	3.542270
H	-2.367246	-0.537797	-3.485589	N	-3.609473	-0.446343	3.199797
H	-0.169473	-0.501202	-2.342449	H	-4.308116	-4.497156	2.997102
Cu^{2+}	-1.651779	-0.225125	2.646477	H	-2.512730	-6.062713	2.320395
C	-1.175271	2.066328	4.491645	H	-0.242934	-5.137039	1.750039
C	-0.966730	3.401121	4.858290	H	0.098592	-2.671182	1.883766
C	-1.112653	4.411250	3.911280	H	-5.728396	-3.054193	3.544570
C	-1.459190	4.068173	2.605351	H	-7.272404	-1.223568	4.174773
C	-1.636524	2.723051	2.302747	H	-6.419333	1.144205	4.166175
N	-1.503271	1.743474	3.215153	H	-4.042840	1.544876	3.528405
C	-1.034270	0.944822	5.458714				
C	-1.026424	1.142689	6.844603				
C	-0.860827	0.043489	7.685757				
C	-0.712937	-1.222829	7.123232				
C	-0.751214	-1.334035	5.734135				
N	-0.907927	-0.284497	4.916806				
H	-0.671445	3.649591	5.870451				

Table B.6. (continued) Cartesian Coordinates of the B3LYP/6-31G* Optimized Geometries of the Ground State Structures of the $M^{2+}(Bpy)_x$ Complexes.[a]

$Zn^{2+}(Bpy)_3$				$Zn^{2+}(Bpy)_3$			
	x	y	z		x	y	z
C	0.183407	-0.021813	0.112718	H	-1.505890	5.255829	1.114589
N	0.165805	-0.122671	1.461471	H	-2.114197	2.855383	0.805818
C	1.330532	-0.206649	2.123452	H	-0.353448	2.824678	6.581893
C	2.568650	-0.199008	1.487403	H	-0.105791	0.928977	8.152176
C	2.594524	-0.084742	0.098696	H	-0.480204	-1.411256	7.304511
C	1.389901	0.007468	-0.595270	H	-1.096377	-1.713839	4.904975
C	-1.144422	0.059622	-0.554602	C	-3.543888	-2.308031	2.842353
N	-2.209744	0.235908	0.260270	C	-4.015229	-3.624158	2.785653
C	-3.435992	0.318595	-0.279543	C	-3.147015	-4.647650	2.411405
C	-3.670617	0.237331	-1.649154	C	-1.826246	-4.333963	2.096229
C	-2.578499	0.048201	-2.493926	C	-1.433722	-3.000113	2.161721
C	-1.303036	-0.044539	-1.940855	N	-2.262825	-2.009432	2.526273
H	1.259838	-0.284334	3.203767	C	-4.404363	-1.160551	3.240821
H	3.481738	-0.275194	2.067718	C	-5.673394	-1.326151	3.806243
H	3.536931	-0.063082	-0.439714	C	-6.424258	-0.202745	4.146178
H	1.399106	0.114264	-1.673070	C	-5.889022	1.063746	3.918824
H	-4.255086	0.456091	0.419118	C	-4.614417	1.149264	3.366023
H	-4.680790	0.315652	-2.036092	N	-3.887187	0.071846	3.031258
H	-2.714058	-0.031334	-3.568075	H	-5.048497	-3.854794	3.014635
H	-0.449811	-0.210111	-2.587242	H	-3.501295	-5.672670	2.363210
C	-0.981870	2.640454	3.880529	H	-1.116107	-5.098796	1.801224
C	-0.599264	3.964108	4.124019	H	-0.418752	-2.704715	1.915479
C	-0.783865	4.924746	3.131897	H	-6.072553	-2.315062	3.995973
C	-1.342511	4.541354	1.914047	H	-7.409955	-0.318561	4.586054
C	-1.684847	3.203424	1.739970	H	-6.438745	1.965158	4.166930
N	-1.514140	2.273159	2.692506	H	-4.150688	2.112809	3.180024
C	-0.828910	1.558747	4.891266	Zn^{2+}	-1.793302	0.122430	2.404112
C	-0.495843	1.811435	6.226527				
C	-0.363649	0.745317	7.113776				
C	-0.572984	-0.551866	6.649418				
C	-0.914258	-0.723921	5.310980				
N	-1.037870	0.297548	4.448866				
H	-0.149793	4.247822	5.067748				
H	-0.490863	5.954892	3.309192				

[a]Standard Orientation, Å.

APPENDIX C

Table C.1. Vibrational Frequencies and Average Vibrational Energies of Pyr ligand and the $M^{2+}(Pyr)_x$ Complexes at 298 K.[a]

Species	E_{vib} (eV) [b]	Vibrational frequencies (cm^{-1}) [c]
Pyr	0.08 (0.01)	379, 413, 602, 657, 705, 748, 881, 938, 975, 990, 992, 1030, 1065, 1079, 1158, 1229, 1283, 1371, 1458, 1501, 1606, 1611, 3106, 3108, 3129, 3144, 3152
Fe^{2+}(Pyr)	0.13 (0.01)	100, 135, 293, 368, 397, 631, 655, 662, 727, 769, 924, 970, 1006, 1031, 1032, 1060, 1083, 1183, 1215, 1283, 1367, 1456, 1486, 1568, 1589, 3137, 3138, 3164, 3172, 3176
Co^{2+}(Pyr)	0.13 (0.01)	114, 135, 308, 368, 391, 622, 645, 677, 747, 811, 941, 978, 999, 1031(2), 1053, 1084, 1180, 1215, 1284, 1362, 1465, 1475, 1539, 1590, 3142, 3143, 3164, 3175, 3177
Ni^{2+}(Pyr)	0.13 (0.01)	128, 140, 309, 400, 427, 623, 681, 722, 786, 924, 971, 1005, 1034, 1065, 1085, 1096, 1181, 1209, 1291, 1313, 1354, 1447, 1478, 1556, 1572, 3127, 3131, 3154, 3170, 3172
Cu^{2+}(Pyr)	0.13 (0.01)	117, 151, 276, 342, 365, 620, 627, 630, 724, 911, 936, 981, 993, 1009, 1028, 1040, 1086, 1123, 1186, 1311, 1368, 1433, 1444, 1496, 1575, 3162, 3166, 3170, 3175, 3177
Zn^{2+}(Pyr)	0.13 (0.01)	115, 171, 299, 381, 395, 624, 635, 668, 726, 776, 935, 969, 1003, 1021, 1030, 1054, 1084, 1181, 1216, 1287, 1362, 1464, 1477, 1563, 1578, 3158, 3160, 3167, 3174, 3175
$Fe^{2+}(Pyr)_2$	0.30 (0.02)	21, 22, 29, 99, 100, 152(2), 193, 350, 382, 385, 406(2), 641(2), 658, 675, 682(2), 755(2), 856, 857, 945(2), 978, 979, 1009, 1013, 1034, 1035, 1044, 1048, 1069, 1071, 1084, 1085, 1182(2), 1219, 1223, 1295(2), 1371(2), 1465(2), 1495, 1496, 1579(2), 1621(2), 3143(2), 3144(2), 3167(2), 3180(2), 3182, 3183
$Co^{2+}(Pyr)_2$	0.30 (0.02)	15, 16, 23, 96(2), 139(2), 197, 347, 380, 382, 401, 402, 639(2), 662, 673(2), 680, 753(2), 848, 849, 944(2), 978(2), 1009, 1013, 1034(2), 1044, 1048, 1068, 1072, 1084, 1085, 1182(2), 1217, 1220, 1297(2), 1368(2), 1464(2), 1492(2), 1575(2), 1617, 1618, 3145(2), 3146(2), 3167(2), 3180(2), 3183(2)

Table C.1. (continued) Vibrational Frequencies and Average Vibrational Energies of $M^{2+}(Pyr)_x$ Complexes at 298 K.[a]

Species	E_{vib} (eV) [b]	Vibrational frequencies (cm^{-1}) [c]
$Ni^{2+}(Pyr)_2$	0.25 (0.02)	33, 68(2), 126(2), 196, 365, 377, 380, 392(2), 634(2), 657, 674(2), 679, 755(2), 858, 859, 950(2), 981(2), 1001, 1008, 1033(2), 1041, 1045, 1062, 1066, 1083(2), 1180(2), 1221, 1225, 1287(2), 1372(2), 1468(2), 1487, 1488, 1558(2), 1616, 1623, 3161(2), 3163(2), 3169(2), 3180(2), 3183(2)
$Cu^{2+}(Pyr)_2$	0.29 (0.02)	23, 30, 32, 106, 131, 137, 168, 243, 329, 381(2), 403, 410, 628, 629, 656, 664, 672, 676, 751, 752, 820, 822, 943, 945, 978, 979, 1006, 1013, 1029, 1030, 1039, 1040, 1065, 1066, 1085, 1086, 1179(2), 1214, 1220, 1289, 1291, 1364, 1365, 1462, 1463, 1485, 1486, 1555(2), 1590, 1603, 3161(2), 3162(2), 3167(2), 3179(2), 3181, 3182
$Zn^{2+}(Pyr)_2$	0.29 (0.02)	30(3), 115(2), 195(2), 205, 364, 386, 388, 407(2), 641(2), 662, 678(2), 682, 750(2), 859(2), 944(2), 980(2), 1015, 1017, 1037(2), 1045, 1048, 1077, 1085, 1089(2), 1183(2), 1222, 1225, 1302(2), 1372(2), 1472(2), 1498(2), 1582(2), 1626(2), 3158, 3159, 3160(2), 3169(2), 3180(2), 3183(2)
$Fe^{2+}(Pyr)_3$	0.46 (0.04)	10, 25, 26, 30, 34, 36, 100, 103, 108, 132, 149, 178, 193, 290, 291, 386, 389, 390, 414(2), 418, 646(2), 647, 649, 654, 655, 691, 692, 695, 755(3), 869, 870, 872, 943, 944, 946, 976, 977, 978, 1015(2), 1018, 1030(3), 1041, 1042, 1043, 1071, 1072, 1074, 1084, 1085(2), 1178, 1179(2), 1222, 1223, 1227, 1295(2), 1296, 1371(2), 1372, 1464, 1465(2), 1500(2), 1501, 1588(2), 1589, 1627(3), 3140(2), 3140, 3143, 3145, 3149, 3150, 3165, 3166(2), 3177, 3178(2), 3181(2), 3182
$Co^{2+}(Pyr)_3$	0.46 (0.04)	19, 22, 24, 27, 29, 34, 105, 106, 108, 139, 141, 175, 190, 295, 296, 389(2), 390, 412, 417(2), 645, 646(2), 653, 659(2), 689, 691(2), 756(3), 868(2), 869, 944(2), 945, 977(2), 978, 1016(2), 1019, 1030(3), 1043, 1044(2), 1072(2), 1075, 1084, 1085(2), 1178(3), 1220, 1221, 1226, 1297, 1298(2), 1369(2), 1370, 1464(2), 1465, 1499, 1500(2), 1588(3), 1626(2), 1627, 3145, 3146, 3147, 3148(2), 3149, 3166(3), 3178(3), 3181(3)

Table C.1. (continued) Vibrational Frequencies and Average Vibrational Energies of $M^{2+}(Pyr)_x$ Complexes at 298 K.[a]

Species	E_{vib} (eV) [b]	Vibrational frequencies (cm^{-1}) [c]
$Ni^{2+}(Pyr)_3$	0.45 (0.04)	19, 24, 35, 36, 41, 42, 114, 115, 124, 151, 152, 168, 235, 303(2), 389, 390, 393, 416(2), 421, 645(3), 655, 660(2), 688, 689, 690, 755(2), 756, 867(2), 870, 947(2), 948, 979, 980, 981, 1018(2), 1020, 1030(3), 1044(3), 1074(2), 1076, 1086(3), 1178, 1179(2), 1221(2), 1226, 1297, 1298(2), 1370(2), 1371, 1465(3), 1499, 1500, 1501, 1587(3), 1625, 1626(2), 3145(2), 3146, 3163(3), 3168(3), 3179(3), 3182(3)
$Cu^{2+}(Pyr)_3$	0.45 (0.04)	29(2), 35, 40, 42, 46, 117(2), 128, 168, 174, 200, 217, 274, 334, 390, 391, 393, 420, 423, 425, 644, 645(2), 655, 658, 665, 686, 688, 689, 755(2), 756, 861, 866, 867, 946, 947, 949, 980(2), 981, 1018, 1019, 1021, 1029, 1030(2), 1038, 1046, 1047, 1074, 1077, 1079, 1087(2), 1087, 1088, 1178, 1179(2), 1220, 1221, 1225, 1297, 1298, 1300, 1367, 1369, 1370, 1464, 1465, 1466, 1499(2), 1500, 1587(2), 1588, 1620, 1625(2), 3145(2), 3161(2), 3163, 3166, 3167(2), 3171, 3179(3), 3182(3)
$Zn^{2+}(Pyr)_3$	0.45 (0.04)	21, 24, 29, 30, 31, 42, 104, 105, 113, 172, 174, 188, 197, 284, 285, 390, 391, 394, 416, 417(2), 647(3), 653, 657, 658, 693, 695(2), 757, 759(2), 876(2), 879, 951, 953(2), 982(2), 983, 1019(2), 1021, 1032(3), 1045, 1046, 1047, 1077(2), 1081, 1086, 1087(2), 1179(3), 1224, 1225, 1230, 1299(2), 1300, 1374(2), 1375, 1468, 1469(2), 1503, 1504(2), 1590(3), 16313), 3154(2), 3155(3), 3156, 3167(3), 3178(3), 3182(3)
$Fe^{2+}(Pyr)_4$	0.62 (0.05)	23, 26, 27, 30, 35, 36, 42, 50, 56, 106, 112, 114, 137, 141(2), 145, 167, 193, 255(2), 256, 390, 391, 394, 398, 416, 420(2), 426, 641, 642(2), 643, 649, 649(2), 651, 699(2), 701, 703, 755(2), 756(2), 877, 878, 880, 883, 947, 948, 950, 952, 978(2), 979, 981, 1014, 1015(2), 1018, 1025(4), 1038(3), 1039, 1074(3), 1077, 1083(2), 1084, 1088, 1176(4), 1225(2), 1226, 1231, 1292(3), 1294, 1372(2), 1373(2), 1463(3), 1465, 1503(4), 1592(3), 1593, 1628(3), 1629, 3143(2), 3145(2), 3151(3), 3152, 3163, 3164(3), 3175(4), 3179(4)

Table C.1. (continued) Vibrational Frequencies and Average Vibrational Energies of $M^{2+}(Pyr)_x$ Complexes at 298 K.[a]

Species	E_{vib} (eV) [b]	Vibrational frequencies (cm^{-1}) [c]
$Co^{2+}(Pyr)_4$	0.62 (0.05)	22, 27(2), 28, 37, 41(3), 46, 110, 120(2), 138, 153, 161(2), 171, 175, 270(2), 286, 391(2), 392, 395, 420, 423, 424, 426, 644, 645(2), 646, 648, 649(2), 650, 697(3), 698, 755, 756(3), 875, 876(2), 879, 945, 947(3), 977, 978(2), 979, 1017(3), 1020, 1025(4), 1040(4), 1075(3), 1077, 1083, 1084(2), 1085, 1176(4), 1224(2), 1225, 1230, 1292(2), 1293, 1294, 1371, 1372(3), 1463, 1464(2), 1465, 1503(4), 1592, 1593(3), 1629(4), 3146, 3147(2), 3148, 3157(4), 3164(4), 3176(4), 3180(4)
$Ni^{2+}(Pyr)_4$	0.61 (0.05)	21, 22, 29, 31, 41, 42, 46, 48, 59, 117, 126, 127, 142, 148, 154, 167, 171, 180, 254, 275, 292, 390, 392, 393, 399, 421, 425, 426, 429, 641, 642, 645, 646, 649(3), 650, 697(2), 698, 699, 756, 757(2), 758, 874, 876, 878, 881, 946, 948, 951(2), 978, 979, 980, 982, 1015, 1017, 1019, 1021, 1024, 1025(2), 1026, 1038, 1039, 1040, 1041, 1074, 1075, 1076, 1079, 1084, 1084, 1085, 1086, 1175, 1176(3), 1224(2), 1225, 1230, 1292(2), 1293, 1294, 1369, 1370, 1371, 1373, 1463, 1464(3), 1502, 1503(2), 1504, 1592(2), 1593, 1594, 1628(2), 1629(2), 3136, 3147, 3150, 3157, 3159, 3160, 3161, 3163, 3165, 3166, 3167, 3171, 3176(3), 3177, 3180(3), 3183
$Cu^{2+}(Pyr)_4$	0.60 (0.05)	16, 23, 32, 38, 41, 42, 47, 51, 55, 116, 136, 142, 151, 165, 176, 180, 191, 193, 214, 282, 285, 389(2), 393, 397, 426, 430, 434, 440, 639, 644(2), 647, 649, 649, 650(2), 696, 697(2), 698, 758, 760(3), 876(2), 877, 878, 948(2), 953, 954, 981(2), 982(2), 1016, 1018(2), 1023, 1025(4), 1038(2), 1039, 1042, 1075, 1076, 1077, 1080, 1084(2), 1087, 1088, 1175(2), 1176(2), 1224, 1226(2), 1231, 1291, 1293(2), 1295, 1370, 1371, 1373, 1374, 1463, 1464, 1465(2), 1503(2), 1505(2), 1593(2), 1594(2), 1627, 1628(2), 1629, 3141, 3142, 3158(2), 3159(2), 3164(4), 3174(2), 3175(2), 3179(4), 3191(2)

Table C.1. (continued) Vibrational Frequencies and Average Vibrational Energies of $M^{2+}(Pyr)_x$ Complexes at 298 K.[a]

Species	E_{vib} (eV) [b]	Vibrational frequencies (cm^{-1}) [c]
$Zn^{2+}(Pyr)_4$	0.62 (0.05)	23, 26, 27(2), 35, 39(3), 48, 110, 119(2), 137, 156, 167(2), 175, 176, 241, 243, 254, 391(3), 395, 421, 424(2), 426, 644(2), 645(2), 649, 650(2), 651, 700(3), 701, 759(2), 760(2), 882, 883(2), 886, 951, 954(2), 955, 981, 982(2), 984, 1019(3), 1022, 1027(4), 1041(4), 1077(3), 1081, 1084, 1085(2), 1086, 1176(4), 1226(2), 1227, 1233, 1295(3), 1296, 1373, 1374(3), 1466(3), 1467, 1505(4), 1594(3), 1595, 1631, 1632(3), 3149(3), 3150, 3158(4), 3164(4), 3176(4), 3180(4)
$Fe^{2+}(Pyr)_5$	0.79 (0.06)	14, 23, 31, 36, 38, 40(2), 42, 51, 57, 63, 81, 98, 103, 117, 124, 126, 130, 143, 150, 153, 158, 167, 168, 209, 235, 243, 389, 390, 394, 396, 407, 421, 422, 424, 427, 428, 624, 625, 632, 633, 634, 650, 651, 652(2), 653, 700(2), 706(2), 710, 756(2), 757(3), 879, 880, 884, 885, 888, 946, 947, 950, 951, 958, 976, 977, 979(2), 985, 1005, 1008, 1011, 1013, 1016, 1019, 1020, 1021(3), 1035(2), 1036, 1037, 1038, 1074, 1075, 1076(2), 1078, 1080, 1082(2), 1083, 1084, 1172(2), 1173, 1174(2), 1224, 1225, 1226, 1227, 1233, 1286(2), 1289, 1290(2), 1369, 1371(2), 1372, 1373, 1460(2), 1461, 1462(2), 1502, 1503, 1504, 1505(2), 1594, 1595(2), 1596(2), 1626, 1627, 1628, 1629(2), 3149, 3150, 3152, 3153, 3154(2), 3156(3), 3159, 3162(2), 3163(2), 3165, 3171, 3172, 3173(2), 3174, 3176(2), 3178(3)
$Co^{2+}(Pyr)_5$	0.78 (0.06)	14, 18, 34, 36, 41, 42, 43, 44, 56, 61, 67, 79, 104, 115, 125, 133, 136, 143, 158(2), 166, 167, 177, 185, 253, 255, 266, 389, 390, 396, 398, 405, 425, 426, 428, 431, 440, 623, 624, 635, 636, 637, 649, 651, 652, 653(2), 698, 699, 705, 706, 707, 755(2), 756(2), 760, 876, 877, 883(3), 943(2), 949, 950, 956, 974, 975, 979(2), 982, 1006, 1008, 1014, 1016, 1018, 1019, 1020, 1021(2), 1022, 1035, 1036, 1037, 1038, 1039, 1075(3), 1077, 1078, 1081, 1083(2), 1084, 1087, 1172(2), 1174(3), 1223, 1225(2), 1229, 1233, 1286(2), 1289, 1290, 1293, 1366, 1371(2), 1372(2), 1460, 1461(2), 1462, 1463, 1501, 1504, 1505(2), 1506, 1593, 1595, 1596, 1597(2), 1627(2), 1628, 1629(2), 3147, 3148, 3154(2), 3155(2), 3157(2), 3159, 3163(2), 3165(2), 3166, 3170, 3171, 3172, 3173, 3174, 3177(3), 3178(2), 3181

Table C.1. (continued) Vibrational Frequencies and Average Vibrational Energies of $M^{2+}(Pyr)_x$ Complexes at 298 K.[a]

Species	E_{vib} (eV) [b]	Vibrational frequencies (cm^{-1}) [c]
$Ni^{2+}(Pyr)_5$	0.77 (0.06)	17, 26, 39, 40(2), 48, 49, 52, 53, 63, 66, 89, 114, 127, 129, 136, 150(2), 155, 163, 168, 173, 191, 198, 244, 248, 256, 390, 391, 396, 397, 411, 427, 429, 431, 435, 436, 626, 630(2), 634, 636, 650, 652(3), 653, 701, 702, 703, 704, 710, 756(2), 757(2), 758, 880(2), 882(2), 888, 946(2), 952, 953, 960, 977(2), 980, 981, 987, 1008, 1012, 1013, 1015, 1019, 1020(4), 1021, 1036(2), 1037(2), 1038, 1075, 1076(2), 1077, 1079, 1081, 1084(2), 1085, 1086, 1173(4), 1174, 1225(2), 1227, 1228, 1234, 1287(2), 1288, 1290, 1291, 1368, 1370(2), 1371(2), 1461(2), 1462(3), 1503, 1504(2), 1505, 1506, 1594, 1596(3), 1597, 1628(2), 1629(2), 1630, 3144(2), 3156(2), 3158(3), 3162(2), 3164, 3166(2), 3169(2), 3170, 3173(2), 3175(2), 3177, 3178(2), 3180, 3182(2)
$Cu^{2+}(Pyr)_5$	0.77 (0.06)	12(2), 35, 40, 42, 45(2), 49, 53, 59, 66, 84, 113, 122, 123, 129, 130, 139, 149, 157, 173, 174, 198, 207, 221, 247, 250, 389, 390, 395, 398, 404, 421, 429, 432, 440, 441, 621, 628, 634, 637, 640, 650, 651(2), 652, 654, 699, 700, 701, 702, 713, 756, 757(2), 759(2), 879(2), 880(2), 890, 948, 949, 952, 953, 957, 979(2), 980, 981, 985, 1006, 1010, 1016, 1017, 1019, 1021(2), 1022(3), 1034, 1035, 1036(2), 1039, 1076, 1077(2), 1078, 1079, 1081, 1084(2), 1087(2), 1172, 1173(2), 1174(2), 1225, 1226, 1227, 1228, 1235, 1287, 1289, 1290, 1291, 1292, 1369(2), 1370, 1372, 1375, 1460, 1463(3), 1464, 1503, 1504(2), 1505, 1507, 1596(3), 1597(2), 1625, 1627(2), 1629(2), 3146, 3147, 3151(2), 3159(2), 3160(3), 3167(4), 3169, 3172(2), 3174(2), 3175, 3179(4), 3185(2)

Table C.1. (continued) Vibrational Frequencies and Average Vibrational Energies of $M^{2+}(Pyr)_x$ Complexes at 298 K.[a]

Species	E_{vib} (eV) [b]	Vibrational frequencies (cm^{-1}) [c]
$Zn^{2+}(Pyr)_5$	0.79 (0.06)	7, 18, 30, 33, 37, 39, 40, 42, 51, 53, 60, 72, 90, 114(2), 125, 134, 139, 146, 156, 165, 166, 172, 180, 192, 227, 230, 388, 390, 394, 395, 402, 422, 423, 427, 431, 435, 623, 624, 636(2), 637, 651, 652, 653(3), 701(2), 705, 706, 707, 757(2), 759(2), 762, 880, 882, 884, 885, 887, 948, 949, 950, 951, 960, 977, 979, 980(2), 985, 1007, 1009, 1017(2), 1020(2), 1021, 1022(2), 1023, 1035, 1036, 1038, 1039, 1040, 1076, 1077(2), 1078, 1081(2), 1083(2), 1084, 1085, 1172(2), 1174(3), 1225, 1226, 1228, 1229, 1235, 1289(2), 1292, 1293(2), 1370(2), 1372, 1376(2), 1461(2), 1463, 1465(2), 1504, 1505, 1506, 1507(2), 1595, 1597(3), 1598, 1627, 1628, 1631(3), 3146(2), 3150, 3151, 3152, 3153, 3157(2), 3158, 3162(2), 3163, 3164(2), 3168, 3172(2), 3173, 3174, 3176, 3177(2), 3178(2), 3180
$Fe^{2+}(Pyr)_6$	0.96 (0.07)	17, 23, 26, 27, 31, 38, 40, 42, 44, 46, 51, 57, 64, 72, 76, 92, 100, 114, 115, 122, 130, 136, 139, 145, 146, 149, 153, 160, 162, 165, 200, 201, 209, 387, 389, 390, 393, 394, 401, 422, 424(2), 425, 427(2), 616, 619, 620(2), 624(2), 653(4), 654, 655, 701, 703(2), 705, 707, 708, 755, 756, 757(2), 759(2), 883, 884, 885, 886, 887, 889, 949, 951(2), 954, 955, 957, 978, 980(2), 982, 983, 984, 1001, 1002, 1003, 1004, 1006, 1009, 1017(2), 1018(3), 1019, 1033, 1035, 1036, 1037(2), 1038, 1076(2), 1077(3), 1079(2), 1080(2), 1081, 1082, 1083, 1171(4), 1172(2), 1225, 1226, 1227, 1229(2), 1236, 1280(2), 1282, 1283(2), 1284, 1369(2), 1371(3), 1372, 1458, 1459(3), 1460(2), 1501, 1502, 1503, 1504(2), 1505, 1594, 1595(2), 1596(3), 1624, 1625(2), 1626, 1627(2), 3155(4), 3156(2), 3164(4), 3165, 3166, 3170(2), 3171(4), 3179, 3180, 3183(2), 3187, 3188, 3189, 3190(2), 3191(2), 3193

Table C.1. (continued) Vibrational Frequencies and Average Vibrational Energies of $M^{2+}(Pyr)_x$ Complexes at 298 K.[a]

Species	E_{vib} (eV) [b]	Vibrational frequencies (cm^{-1}) [c]
$Co^{2+}(Pyr)_6$	0.92 (0.08)	16, 23, 28, 30, 33, 41, 43, 48, 51, 53, 59, 60, 63, 70, 76, 77, 78, 102, 119, 138, 148, 157, 160, 165, 176, 189, 194, 206, 217, 225, 292, 308, 326, 388, 395, 398, 401, 403, 414, 415, 427, 442, 456, 461, 470, 608, 618, 637, 641(2), 644, 651, 652(2), 654(2), 655, 700, 701, 704, 705, 711, 717, 752, 755, 758, 759, 763, 764, 874(2), 884, 886, 890, 893, 944, 948, 949, 954, 958, 965, 976, 977(2), 987, 990, 993, 996, 1003, 1012, 1016, 1017(2), 1018(2), 1019(2), 1020, 1023, 1032, 1035, 1039(2), 1041, 1043, 1072, 1076(2), 1077, 1078(2), 1080(2), 1087, 1089(2), 1092, 1167, 1171, 1172(2), 1173(2), 1226, 1227, 1229, 1231, 1232, 1238, 1282, 1283, 1285, 1285, 1286, 1287, 1370, 1371, 1372(2), 1379, 1380, 1458(2), 1463(2), 1464, 1466, 1503, 1504, 1506, 1507, 1510, 1512, 1595, 1596(3), 1597, 1600, 1618, 1624, 1632, 1633(2), 1634, 3113, 3115, 3121, 3124, 3151(2), 3152, 3158(2), 3159(2), 3161, 3162, 3167(2), 3169(4), 3174(2), 3175(3), 3189, 3190, 3193, 3194, 3196(2)
$Ni^{2+}(Pyr)_6$	0.94 (0.08)	16, 18, 29, 32, 38, 43, 44, 47, 49, 53, 60, 69, 75, 77, 88, 105, 111, 112, 128, 138, 150, 151, 156(2), 163, 171, 176, 183, 184, 186, 219, 223, 229, 390, 392, 394, 394, 401, 407, 428, 429, 431, 432, 433, 434, 619(2), 622(2), 624, 626, 653(3), 654, 655(2), 702, 703(2), 705, 707(2), 756, 757(2), 758, 759(2), 759, 881, 883, 884, 885, 886, 888, 950, 951, 954, 957, 958(2), 979, 982(2), 983, 985, 986, 1002, 1003, 1004, 1005, 1007, 1011, 1018, 1018(5), 1036, 1037, 1038, 1039, 1040(2), 1077(3), 1078, 1079, 1080, 1082, 1083(2), 1084, 1085(2), 1171(4), 1172(2), 1227, 1230(2), 1231, 1233, 1239, 1279, 1280, 1281(3), 1282, 1369, 1371, 1372, 1373(2), 1374, 1458, 1459(4), 1460, 1502, 1504(2), 1506, 1507, 1508, 1595(3), 1596(2), 1597, 1625, 1626, 1627(2), 1628(2), 3156(6), 3165(2), 3166(4), 3172(6), 3194, 3195, 3197, 3198(2), 3200, 3201, 3203, 3205(2), 3208(2)

Table C.1. (continued) Vibrational Frequencies and Average Vibrational Energies of $M^{2+}(Pyr)_x$ Complexes at 298 K.[a]

Species	E_{vib} (eV) [b]	Vibrational frequencies (cm^{-1}) [c]
$Cu^{2+}(Pyr)_6$	0.94 (0.07)	16, 18, 19, 28, 31, 37, 38, 43, 45, 46, 48, 51, 56, 57, 62, 69, 80, 90, 92, 96, 121, 129(2), 142, 155, 180, 187, 198, 212, 220, 267, 275, 388, 390, 391(2), 400, 404, 414, 415, 428, 435, 441, 445, 607(2), 631, 641, 642, 646, 650, 651(3), 655, 656, 696(2), 701, 702, 713, 715, 751(2), 758(2), 759, 760, 878(2), 882(2), 891, 892, 945, 947, 949, 951, 955, 957, 977, 978, 979(2), 983, 984, 994, 995, 1014(3), 1019(3), 1020(2), 1021, 1025, 1032(2), 1035, 1036, 1037, 1040, 1072, 1073, 1076, 1078(3), 1079, 1082, 1083(2), 1086(2), 1168(2), 1172(2), 1173(2), 1223, 1224, 1226, 1228(2), 1233, 1283, 1284, 1290, 1291, 1293, 1294, 1368(2), 1370(2), 1372, 1373, 1457(2), 1464(3), 1465, 1503(4), 1504, 1505, 1596, 1597(3), 1598, 1599, 1617, 1618, 1630(4), 3117, 3119(2), 3121, 3153(2), 3158(4), 3162, 3163, 3167(2), 3168(2), 3170(2), 3172(2), 3173(2), 3181, 3182, 3184(2), 3187(2), 3189(2)
$Zn^{2+}(Pyr)_6$	0.96 (0.07)	10, 24, 28, 30, 31, 38, 40, 42(2), 49(2), 63, 64, 67, 71, 82, 89, 106, 111, 122, 144, 146, 149, 151, 153, 158, 159, 160, 162, 164, 182, 183, 184, 388, 390, 392, 394, 395, 402, 425(2), 426(3), 427, 619, 620(2), 621, 622, 624, 653, 654(3), 655(2), 703, 704, 705(2), 706, 707, 759(3), 760(2), 761, 885, 887(2), 888, 889, 891, 953, 954, 956, 958, 959, 960, 982, 984(2), 985, 987, 988, 1003(2), 1004, 1005, 1006, 1011, 1019(6), 1034, 1036, 1037(2), 1039(2), 1077(2), 1078(3), 1080, 1081(2), 1082, 1083(2), 1084, 1171(5), 1172, 1225, 1228, 1229, 1230, 1231, 1238, 1282, 1283(3), 1284(2), 1368, 1372, 1373(3), 1374, 1459(3), 1460(2), 1461, 1502, 1504, 1505(2), 1507(2), 1596(3), 1597(3), 1625, 1626(2), 1627(2), 1628, 3155(3), 3156(3), 3165(3), 3166(3), 3171(2), 3172(4), 3190, 3191, 3192(3), 3193, 3194(2), 3195(2), 3196, 3197

[a]The ground spin states of the $Fe^{2+}(Pyr)_x$, $Co^{2+}(Pyr)_x$, $Ni^{2+}(Pyr)_x$, $Cu^{2+}(Pyr)_x$, and $Zn^{2+}(Pyr)_x$ complexes are quintet, quartet, triplet, doublet, and singlet, respectively, for all values of *x*. [b]Uncertainties listed in parentheses are determined as described in the text. [c]Vibrational frequencies scaled by 0.9804 obtained from vibrational analyses of the B3LYP/6-31G* geometry optimized structures. Degeneracies are indicated in parentheses.

Table C.2. Rotational Constants (in cm^{-1}) of $M^{2+}(Pyr)_x$ Complexes and Their Corresponding PSL Transition States for Dissociation.

Complex	Energized Molecule		Transition State	
	1-D[a]	2-D[b]	1-D[c]	2-D[c]
$Fe^{2+}(Pyr)$	0.1935	0.0347	0.2013	0.1382
$Fe^{2+}(Pyr)_2$	0.0974	0.0084	0.1935, 0.2013	0.0347, 0.1382
$Fe^{2+}(Pyr)_3$	0.0100	0.0073	0.0974, 0.2013	0.0084, 0.1382
$Fe^{2+}(Pyr)_4$	0.0057	0.0056	0.0100, 0.2013	0.0073, 0.1382
$Fe^{2+}(Pyr)_5$	0.0048	0.0041	0.0057, 0.2013	0.0056, 0.1382
$Fe^{2+}(Pyr)_6$	0.0034	0.0034	0.0048, 0.2013	0.0041, 0.1382
$Co^{2+}(Pyr)$	0.1915	0.0353	0.2013	0.1382
$Co^{2+}(Pyr)_2$	0.0971	0.0086	0.1915, 0.2013	0.0353, 0.1382
$Co^{2+}(Pyr)_3$	0.0101	0.0075	0.0971, 0.2013	0.0086, 0.1382
$Co^{2+}(Pyr)_4$	0.0061	0.0057	0.0101, 0.2013	0.0075, 0.1382
$Co^{2+}(Pyr)_5$	0.0049	0.0041	0.0061, 0.2013	0.0057, 0.1382
$Co^{2+}(Pyr)_6$	0.0041	0.0029	0.0049, 0.2013	0.0041, 0.1382
$Ni^{2+}(Pyr)$	0.1923	0.0359	0.2013	0.1382
$Ni^{2+}(Pyr)_2$	0.0969	0.0086	0.1923, 0.2013	0.0359, 0.1382
$Ni^{2+}(Pyr)_3$	0.0106	0.0078	0.0816, 0.2013	0.0091, 0.1382
$Ni^{2+}(Pyr)_4$	0.0066	0.0056	0.0106, 0.2013	0.0078, 0.1382
$Ni^{2+}(Pyr)_5$	0.0048	0.0043	0.0066, 0.2013	0.0056, 0.1382
$Ni^{2+}(Pyr)_6$	0.0035	0.0035	0.0048, 0.2013	0.0043, 0.1382

Table C.2. (continued) Rotational Constants (in cm^{-1}) of $M^{2+}(Pyr)_x$ Complexes and Their Corresponding PSL Transition States for Dissociation.

Complex	Energized Molecule		Transition State	
	1-D[a]	2-D[b]	1-D[c]	2-D[c]
$Cu^{2+}(Pyr)$	0.1947	0.0339	0.2013	0.1382
$Cu^{2+}(Pyr)_2$	0.0721	0.0097	0.1946, 0.2013	0.0339, 0.1382
$Cu^{2+}(Pyr)_3$	0.0132	0.0072	0.0713, 0.2013	0.0097, 0.1382
$Cu^{2+}(Pyr)_4$	0.0069	0.0056	0.0132, 0.2013	0.0072, 0.1382
$Cu^{2+}(Pyr)_5$	0.0048	0.0043	0.0069, 0.2013	0.0055, 0.1382
$Cu^{2+}(Pyr)_6$	0.0039	0.0029	0.0048, 0.2013	0.0043, 0.1382
$Zn^{2+}(Pyr)$	0.1920	0.0340	0.2013	0.1382
$Zn^{2+}(Pyr)_2$	0.0973	0.0088	0.1920, 0.2013	0.0340, 0.1382
$Zn^{2+}(Pyr)_3$	0.0103	0.0075	0.0973, 0.2013	0.0088, 0.1382
$Zn^{2+}(Pyr)_4$	0.0060	0.0057	0.0103, 0.2013	0.0075, 0.1382
$Zn^{2+}(Pyr)_5$	0.0049	0.0041	0.0060, 0.2013	0.0057, 0.1382
$Zn^{2+}(Pyr)_6$	0.0034	0.0034	0.0049, 0.2013	0.0041, 0.1382

[a]Active external. [b]Inactive external. [c]Rotational constants of the PSL TS treated as free internal rotors.

Table C.3a. Select Geometrical Parameters of the BHandHLYP/6-31G* Ground-State Structures of the $M^{2+}(Pyr)_x$ Complexes.[a]

Complex	M^{2+}–N	$\angle NM^{2+}N$
$Fe^{2+}(Pyr)$	1.958	–
$Fe^{2+}(Pyr)_2$	1.971	179.7
$Fe^{2+}(Pyr)_3$	2.031	120.0
$Fe^{2+}(Pyr)_4$	2.093	109.0 (2), 110.5 (4)
$Fe^{2+}(Pyr)_5$	2.171 (3), 2.235 (2)	86.5 (3), 90.2 (2), 95.5 (2), 108.9 (2), 169.0
$Fe^{2+}(Pyr)_6$	2.302	89.3 (6), 90.7 (6), 179.3 (3)
$Co^{2+}(Pyr)$	1.873	–
$Co^{2+}(Pyr)_2$	1.920	180.0
$Co^{2+}(Pyr)_3$	1.991	118.5
$Co^{2+}(Pyr)_4$	2.045	105.7 (2), 111.4 (4)
$Co^{2+}(Pyr)_5$	2.110 (3), 2.215 (2)	86.2 (2), 91.3 (2), 93.1 (2), 114.5 (2), 131.0, 173.8
$Co^{2+}(Pyr)_6$	2.270	89.3 (6), 90.7 (6), 179.3 (3)
$Ni^{2+}(Pyr)$	1.868	–
$Ni^{2+}(Pyr)_2$	1.922	180.0
$Ni^{2+}(Pyr)_3$	1.967 (2), 1.975	106.5 (2), 147.1
$Ni^{2+}(Pyr)_4$	2.028	101.1 (2), 108.3 (2), 119.6 (2)
$Ni^{2+}(Pyr)_5$	2.081, 2.127 (4)	86.6 (2), 89.4 (2), 100.8 (4), 158.5 (2)
$Ni^{2+}(Pyr)_6$	2.226	89.9 (2), 90.0 (10), 180.0 (3)
$Cu^{2+}(Pyr)$	1.836	–
$Cu^{2+}(Pyr)_2$	1.896	180.0
$Cu^{2+}(Pyr)_3$	1.925 (2), 1.937	105.8 (2), 148.4
$Cu^{2+}(Pyr)_4$	2.013	94.9, 97.5, 99.1 (2), 137.2 (2)
$Cu^{2+}(Pyr)_5$	2.075 (4), 2.247	86.8 (2), 90.1 (2), 96.4 (2), 104.3 (2), 159.4 (2)
$Cu^{2+}(Pyr)_6$	2.063 (4), 2.815 (2)	89.9, 90.0 (11), 179.9 (3)
$Zn^{2+}(Pyr)$	1.865	–
$Zn^{2+}(Pyr)_2$	1.879	180.0
$Zn^{2+}(Pyr)_3$	1.956	120.0
$Zn^{2+}(Pyr)_4$	2.027	106.1 (2), 111.2 (4)
$Zn^{2+}(Pyr)_5$	2.092 (3), 2.226 (2)	88.1 (3), 92.0 (3), 118.4, 120.8 (2), 177.4
$Zn^{2+}(Pyr)_6$	2.267	89.9 (3), 90.0 (9), 179.9 (3)

Table C.3b. Select Geometrical Parameters of the M06/6-31G* Ground-State Structures of the $M^{2+}(Pyr)_x$ Complexes.[a]

Complex	M^{2+}–N	∠NM^{2+}N
$Fe^{2+}(Pyr)$	1.932	–
$Fe^{2+}(Pyr)_2$	1.947	180.0
$Fe^{2+}(Pyr)_3$	1.995	119.8
$Fe^{2+}(Pyr)_4$	2.045	107.7 (2), 110.4 (4)
$Fe^{2+}(Pyr)_5$	2.107 (3), 2.197 (2)	86.2 (2), 89.9 (2), 94.0 (2), 114.6, 122.7 (2), 179.7
$Fe^{2+}(Pyr)_6$	2.251	88.1 (6), 92.0 (6), 177.0 (3)
$Co^{2+}(Pyr)$	1.892	–
$Co^{2+}(Pyr)_2$	1.901	180.0
$Co^{2+}(Pyr)_3$	1.949	119.9
$Co^{2+}(Pyr)_4$	1.994	106.5 (2), 110.0 (4)
$Co^{2+}(Pyr)_5$	2.057 (3), 2.163 (2)	86.4 (2), 91.9 (4), 118.7 (2), 122.8, 176.8
$Co^{2+}(Pyr)_6$	2.212	88.0 (6), 92.1 (6), 176.7 (3)
$Ni^{2+}(Pyr)$	1.851	–
$Ni^{2+}(Pyr)_2$	1.887	179.7
$Ni^{2+}(Pyr)_3$	1.914, 1.922 (2)	106.5 (2),147.1
$Ni^{2+}(Pyr)_4$	1.981	99.8 (2), 107.3 (2), 122.2 (2)
$Ni^{2+}(Pyr)_5$	2.061 (4), 2.100	88.3 (4), 97.2 (2), 104.0 (2), 158.9 (2)
$Ni^{2+}(Pyr)_6$	2.176	88.3 (6), 91.8 (6), 177.2 (3)
$Cu^{2+}(Pyr)$	1.819	–
$Cu^{2+}(Pyr)_2$	1.848	180.0
$Cu^{2+}(Pyr)_3$	1.893 (2), 1.918	103.3 (2), 153.5
$Cu^{2+}(Pyr)_4$	1.976	93.9, 97.1 (3), 141.3 (2)
$Cu^{2+}(Pyr)_5$	2.044 (4), 2.156	86.3 (2), 92.2 (4), 112.8 (2), 134.4, 174.5
$Cu^{2+}(Pyr)_6$	2.032 (4), 2.409 (2)	85.6 (8), 97.9 (4), 169.7 (3)
$Zn^{2+}(Pyr)$	1.858	–
$Zn^{2+}(Pyr)_2$	1.872	180.0
$Zn^{2+}(Pyr)_3$	1.936	120.0
$Zn^{2+}(Pyr)_4$	2.001	107.2 (2), 110.6 (4)
$Zn^{2+}(Pyr)_5$	2.057 (3), 2.201 (2)	86.2 (2), 90.3 (2), 94.0 (2), 116.6 (2), 126.9, 172.1
$Zn^{2+}(Pyr)_6$	2.226	89.6 (6), 90.4 (6), 179.4 (3)

[a]The spin states of the $Fe^{2+}(Pyr)_x$, $Co^{2+}(Pyr)_x$, $Ni^{2+}(Pyr)_x$, $Cu^{2+}(Pyr)_x$, and $Zn^{2+}(Pyr)_x$ complexes are quintet, quartet, triplet, doublet, singlet, and singlet, respectively, for all values of *x*. Average values are given for similar bond distances or angles; degeneracies are listed in parentheses for values that differ significantly such that more than one value is needed to describe the bond angle or bond distance. Bond angles (∠) are given in degrees (°) and M^{2+}–N bond lengths in angstroms (Å).

Table C.4. Cartesian Coordinates of the B3LYP/6-31G* Optimized Geometries of the Ground State Structures of the $M^{2+}(Pyr)_x$ Complexes.[a]

	$Ca^{2+}(Pyr)$				$Fe^{2+}(Pyr)$		
	x	y	z		x	y	Z
C	-0.002502	0.000000	-0.001624	C	-0.016279	0.000000	-0.009582
C	0.003371	0.000000	1.395762	C	-0.013395	0.000000	1.389407
C	1.221288	0.000000	2.059168	C	1.196712	0.000000	2.065621
C	1.216037	0.000000	-0.685721	C	1.200679	0.000000	-0.699606
C	2.393876	0.000000	0.046456	C	2.386977	0.000000	0.017375
H	1.245252	0.000000	3.147360	H	1.230891	0.000000	3.152514
H	-0.920278	0.000000	1.965062	H	-0.936078	0.000000	1.961775
H	-0.940724	0.000000	-0.548309	H	-0.955759	0.000000	-0.555688
H	1.255578	0.000000	-1.770003	H	1.241567	0.000000	-1.784626
H	3.352334	0.000000	-0.469313	H	3.348358	0.000000	-0.490833
N	2.417222	0.000000	1.407986	N	2.379661	0.000000	1.383087
Ca^{2+}	4.470007	0.000000	2.606067	Fe^{2+}	4.057444	0.000000	2.354958
	$Co^{2+}(Pyr)$				$Ni^{2+}(Pyr)$		
	x	y	z		x	y	z
C	0.031418	0.000000	-0.002604	C	0.032900	0.000000	-0.001808
C	0.013093	0.000000	1.402497	C	0.014031	0.000000	1.397756
C	1.210462	0.000000	2.089036	C	1.215262	0.000000	2.089720
C	1.259749	0.000000	-0.685646	C	1.255717	0.000000	-0.682792
C	2.432345	0.000000	0.042668	C	2.435193	0.000000	0.046391
H	1.243245	0.000000	3.175872	H	1.245003	0.000000	3.177469
H	-0.920590	0.000000	1.956726	H	-0.915862	0.000000	1.959049
H	-0.901784	0.000000	-0.560307	H	-0.901288	0.000000	-0.558869
H	1.304106	0.000000	-1.770482	H	1.308187	0.000000	-1.767528
H	3.404856	0.000000	-0.443816	H	3.406649	0.000000	-0.444456
N	2.406701	0.000000	1.415076	Ni^{2+}	3.982922	0.000000	2.355155
Co^{2+}	3.998807	0.000000	2.364927	N	2.395350	0.000000	1.408349
	$Cu^{2+}(Pyr)$				$Zn^{2+}(Pyr)$		
	x	y	z		x	y	z
C	0.000000	0.000000	0.000000	C	0.036074	0.000000	0.000562
C	0.000000	0.000000	1.389613	C	0.021212	0.000000	1.400318
C	1.223530	0.000000	2.063625	C	1.217931	0.000000	2.096254
C	1.247448	0.000000	-0.679555	C	1.261322	0.000000	-0.676566
C	2.452448	0.000000	0.058563	C	2.442064	0.000000	0.045751
N	2.448528	0.000000	1.398964	H	1.245616	0.000000	3.181005
H	1.258258	0.000000	3.149054	H	-0.907886	0.000000	1.963656
H	-0.922338	0.000000	1.963691	H	-0.896652	0.000000	-0.557673
H	-0.929228	0.000000	-0.564525	H	1.315100	0.000000	-1.761792
H	1.293745	0.000000	-1.765838	H	3.409677	0.000000	-0.445252
H	3.409584	0.000000	-0.453882	N	2.403921	0.000000	1.413570
Cu^{2+}	3.986993	0.000000	2.415357	Zn^{2+}	4.009121	0.000000	2.373724

Table C.4. (continued) Cartesian Coordinates of the B3LYP/6-31G* Optimized Geometries of the Ground State Structures of the Neutral Pyr Ligand and the $M^{2+}(Pyr)_x$ Complexes.[a]

	$Ca^{2+}(Pyr)_2$				$Fe^{2+}(Pyr)_2$		
	x	y	z		x	y	z
C	-0.501183	-0.000060	-0.293242	C	-0.027968	0.000376	-0.017392
C	-0.495751	-0.000267	1.103531	C	-0.031290	-0.008725	1.381816
C	0.719082	0.000163	-0.972915	C	1.192693	0.009101	-0.701326
H	-1.438331	-0.000074	-0.841524	H	-0.964360	0.000645	-0.567623
C	0.722729	-0.000252	1.767312	C	1.177509	-0.008847	2.055670
C	1.894766	0.000182	-0.235984	C	2.369520	0.008582	0.026858
H	-1.419339	-0.000443	1.672577	H	-0.958365	-0.015639	1.945134
H	0.762582	0.000326	-2.056860	H	1.233722	0.016237	-1.785353
N	1.918975	-0.000025	1.122681	N	2.370763	-0.000293	1.392206
H	0.746315	-0.000420	2.855628	H	1.214524	-0.015822	3.141821
H	2.855035	0.000364	-0.748691	H	3.336358	0.015293	-0.469534
C	8.519280	0.000753	4.984562	C	8.149717	0.000619	4.758771
C	7.905791	1.203506	4.626765	C	7.533260	1.208456	4.413894
C	7.907107	-1.202205	4.625201	C	7.544469	-1.207627	4.395930
H	9.456402	0.000909	5.532890	H	9.089374	0.000925	5.303403
C	6.708772	1.160931	3.926314	C	6.336372	1.176581	3.719895
C	6.710032	-1.160030	3.924822	C	6.347265	-1.176564	3.702443
H	8.345298	2.161133	4.884860	H	7.973348	2.163908	4.679008
H	8.347664	-2.159684	4.882048	H	7.993434	-2.162786	4.646838
N	6.099192	0.000349	3.568522	N	5.742601	-0.000184	3.363499
H	6.216355	2.088298	3.639081	H	5.828258	2.094047	3.434858
H	6.218621	-2.087561	3.636400	H	5.847606	-2.094376	3.403895
Ca^{2+}	4.009108	0.000020	2.345559	Fe^{2+}	4.055715	-0.000588	2.379426

Table C.4. (continued) Cartesian Coordinates of the B3LYP/6-31G* Optimized Geometries of the Ground State Structures of the Neutral Pyr Ligand and the $M^{2+}(Pyr)_x$ Complexes.[a]

	$Co^{2+}(Pyr)_2$				$Ni^{2+}(Pyr)_2$		
	x	y	z		x	y	z
C	0.022607	-0.000180	0.003006	C	-0.050174	-0.000079	-0.029229
C	-0.000207	0.000068	1.402827	C	-0.048248	-0.006681	1.372647
C	1.251603	-0.000306	-0.667604	C	1.169894	0.006672	-0.719658
H	-0.906892	-0.000273	-0.559014	H	-0.988912	-0.000188	-0.575764
C	1.198968	0.000183	2.092579	C	1.159823	-0.006449	2.042362
C	2.419296	-0.000183	0.074095	C	2.348723	0.006748	0.000283
H	-0.935072	0.000169	1.953194	H	-0.974109	-0.011986	1.938184
H	1.304766	-0.000494	-1.751139	H	1.204607	0.011863	-1.804023
N	2.397596	0.000058	1.439160	N	2.354354	0.000217	1.370689
H	1.226906	0.000376	3.178960	H	1.203508	-0.011734	3.126792
H	3.394363	-0.000276	-0.405891	H	3.313345	0.012163	-0.497109
C	8.088636	-0.000104	4.764147	C	8.035146	0.001926	4.678382
C	7.477764	1.209726	4.413185	C	7.419992	1.212226	4.329005
C	7.478038	-1.209742	4.412045	C	7.428345	-1.208839	4.316245
H	9.029864	-0.000252	5.306291	H	8.973854	0.002284	5.224970
C	6.279267	1.179578	3.722927	C	6.226723	1.182714	3.633886
C	6.279538	-1.179203	3.721814	C	6.234793	-1.180236	3.621575
H	7.923967	2.164313	4.671147	H	7.862249	2.166970	4.593491
H	7.924450	-2.164472	4.669115	H	7.877207	-2.163243	4.570638
N	5.683728	0.000285	3.378848	N	5.630696	0.001011	3.278329
H	5.771103	2.094822	3.431110	H	5.719575	2.097709	3.344906
H	5.771587	-2.094292	3.429133	H	5.733662	-2.095618	3.323466
Co^{2+}	4.033382	0.000269	2.421251	Ni^{2+}	3.992548	0.000367	2.324471

Table C.4. (continued) Cartesian Coordinates of the B3LYP/6-31G* Optimized Geometries of the Ground State Structures of the Neutral Pyr Ligand and the $M^{2+}(Pyr)_x$ Complexes.[a]

$Cu^{2+}(Pyr)_2$				$Zn^{2+}(Pyr)_2$			
	x	y	z		x	y	z
C	0.074169	-0.268588	0.327691	C	-0.021540	-0.000129	-0.012557
C	0.273664	0.701074	1.319021	C	-0.018555	-0.006546	1.386284
C	1.177087	-0.952131	-0.200840	C	1.196408	0.006484	-0.700572
H	-0.929450	-0.498480	-0.018874	H	-0.960093	-0.000281	-0.558981
C	1.559799	0.954619	1.760588	C	1.190946	-0.006279	2.058216
C	2.441266	-0.657979	0.277454	C	2.377875	0.006603	0.019514
H	-0.557552	1.250313	1.748820	H	-0.943133	-0.011730	1.953877
H	1.058671	-1.707628	-0.970592	H	1.233538	0.011520	-1.784836
N	2.632349	0.300529	1.228961	N	2.377342	0.000263	1.384069
H	1.757043	1.687157	2.536725	H	1.233214	-0.011305	3.142940
H	3.320846	-1.173449	-0.094626	H	3.342051	0.011782	-0.479259
C	7.631368	-0.273227	4.806456	C	8.006513	0.001879	4.661709
C	6.650951	0.677741	5.118667	C	7.391867	1.209050	4.312775
C	7.579371	-0.938951	3.574830	C	7.400264	-1.205703	4.299751
H	8.417985	-0.502631	5.519764	H	8.945036	0.002195	5.208184
C	5.645817	0.931103	4.202750	C	6.196558	1.180789	3.616482
C	6.551404	-0.646300	2.696577	C	6.204683	-1.178247	3.603895
H	6.662030	1.212919	6.062472	H	7.832229	2.164902	4.576331
H	8.322831	-1.679978	3.300134	H	7.847322	-2.161255	4.552915
N	5.610842	0.294826	2.996821	N	5.607707	0.001071	3.264953
H	4.859177	1.649315	4.410649	H	5.690244	2.096772	3.328286
H	6.465543	-1.149382	1.738746	H	5.704583	-2.094570	3.306086
Cu^{2+}	4.350591	0.782942	1.728727	Zn^{2+}	3.992544	0.000552	2.324476

Table C.4. (continued) Cartesian Coordinates of the B3LYP/6-31G* Optimized Geometries of the Ground State Structures of the Neutral Pyr Ligand and the $M^{2+}(Pyr)_x$ Complexes.[a]

	$Ca^{2+}(Pyr)_3$				$Fe^{2+}(Pyr)_3$		
	x	y	z		x	y	z
C	-0.456963	0.011105	-0.239823	C	0.096409	-0.315961	-0.231526
C	-0.443247	-0.040168	1.155367	C	-0.050128	-0.406480	1.155363
C	0.758900	0.058923	-0.924540	C	1.359318	-0.049430	-0.765793
H	-1.397008	0.013711	-0.783072	H	-0.760443	-0.449288	-0.884955
C	0.780652	-0.042588	1.811667	C	1.064954	-0.230718	1.960007
C	1.938791	0.054455	-0.192050	C	2.431408	0.118921	0.097894
H	-1.363549	-0.077384	1.728382	H	-1.014361	-0.608310	1.609275
H	0.795877	0.098539	-2.007949	H	1.514457	0.030081	-1.836341
N	1.969837	0.004245	1.162368	N	2.296273	0.027111	1.446198
H	0.815159	-0.083650	2.898669	H	0.989417	-0.295583	3.041891
H	2.897951	0.092548	-0.704818	H	3.425867	0.336048	-0.281021
C	4.608527	-2.945550	6.719969	C	4.173378	-2.255341	6.762812
C	3.860893	-3.401609	5.632583	C	3.712450	-2.837371	5.578872
C	5.219528	-1.692672	6.639834	C	4.545023	-0.908725	6.758234
H	4.713065	-3.554745	7.612581	H	4.243542	-2.842403	7.673504
C	3.751389	-2.590941	4.510321	C	3.636472	-2.058328	4.434659
C	5.061738	-0.945252	5.480000	C	4.446164	-0.189147	5.576615
H	3.369977	-4.368758	5.650361	H	3.417624	-3.880490	5.539889
H	5.808755	-1.298105	7.460709	H	4.909199	-0.420243	7.655586
N	4.338663	-1.372708	4.415906	N	3.994569	-0.747699	4.424118
H	3.172435	-2.925520	3.651645	H	3.281451	-2.476860	3.496827
H	5.529926	0.033455	5.394984	H	4.734468	0.857211	5.534114
N	5.972744	1.376440	1.619414	N	5.315414	1.593684	2.197663
C	7.254444	0.949608	1.733255	C	6.508348	1.160324	1.714293
C	5.768577	2.592857	1.056812	C	5.127393	2.930869	2.343571
C	8.343924	1.695779	1.303246	C	7.530913	2.030780	1.368092
C	6.801692	3.402192	0.602601	C	6.104509	3.859207	2.017386
H	7.408664	-0.027733	2.186427	H	6.635299	0.086012	1.610341
H	4.736542	2.926995	0.969272	H	4.163471	3.252449	2.729073
C	8.115696	2.946779	0.726714	C	7.328897	3.404732	1.521083
H	9.347966	1.301748	1.418722	H	8.466708	1.636929	0.986262
H	6.577706	4.367905	0.162253	H	5.907470	4.917500	2.150859
H	8.945843	3.555110	0.380899	H	8.112192	4.109171	1.258120
Ca^{2+}	4.094080	0.001454	2.395666	Fe^{2+}	3.859361	0.288030	2.696637

Table C.4. (continued) Cartesian Coordinates of the B3LYP/6-31G* Optimized Geometries of the Ground State Structures of the Neutral Pyr Ligand and the $M^{2+}(Pyr)_x$ Complexes.[a]

	$Co^{2+}(Pyr)_3$				$Ni^{2+}(Pyr)_3$		
	x	y	z		x	y	z
C	-0.043572	0.115569	0.041768	C	0.287098	0.647323	0.075649
C	0.067948	0.387456	1.408013	C	0.294024	0.240335	1.412309
C	1.097920	-0.254684	-0.674273	C	1.497025	0.719466	-0.619953
H	-1.005230	0.189927	-0.456916	H	-0.645913	0.905677	-0.416059
C	1.310967	0.281460	2.012636	C	1.502462	-0.084580	2.010124
C	2.309946	-0.340299	-0.006412	C	2.670149	0.384903	0.039354
H	-0.794971	0.676089	1.998425	H	-0.623910	0.174016	1.986388
H	1.051738	-0.476201	-1.735084	H	1.534736	1.030471	-1.658433
N	2.423446	-0.074362	1.320264	N	2.678255	-0.014258	1.337340
H	1.436776	0.475580	3.073973	H	1.552262	-0.406565	3.044933
H	3.219229	-0.619820	-0.531137	H	3.630753	0.438735	-0.465513
C	4.396899	-2.382256	6.481201	C	3.961849	-3.451995	5.898177
C	4.002490	-3.096924	5.346970	C	3.480268	-3.846949	4.647165
C	4.713242	-1.026737	6.356229	C	4.527668	-2.182299	6.039366
H	4.457845	-2.874266	7.447235	H	3.895723	-4.122744	6.749504
C	3.935069	-2.437585	4.129238	C	3.578332	-2.964499	3.581994
C	4.625986	-0.430846	5.107524	C	4.598868	-1.350778	4.931804
H	3.751361	-4.150661	5.402660	H	3.034699	-4.824195	4.495386
H	5.025103	-0.438657	7.212636	H	4.910320	-1.838373	6.994292
N	4.239066	-1.120083	4.003499	N	4.130932	-1.731330	3.716669
H	3.626644	-2.959275	3.227474	H	3.206429	-3.232826	2.597015
H	4.872215	0.617956	4.968363	H	5.032521	-0.358526	4.997749
N	5.656831	0.909882	1.666855	N	5.694786	0.789389	2.332996
C	6.907050	0.398965	1.526548	C	6.998136	0.438686	2.483706
C	5.450354	2.220248	1.377599	C	5.376152	2.103725	2.229618
C	7.976572	1.172881	1.102884	C	8.012853	1.382473	2.532223
C	6.474153	3.051469	0.950001	C	6.341050	3.098840	2.275136
H	7.038461	-0.651736	1.769530	H	7.215769	-0.622139	2.572151
H	4.436000	2.591875	1.490747	H	4.324403	2.341770	2.110310
C	7.759827	2.521904	0.809530	C	7.681794	2.736194	2.427138
H	8.959204	0.724346	1.004026	H	9.041536	1.059294	2.650331
H	6.265773	4.093072	0.730560	H	6.043952	4.138765	2.192260
H	8.579867	3.150444	0.475629	H	8.456593	3.496009	2.464391
Co^{2+}	4.152199	-0.218483	2.254143	Ni^{2+}	4.335106	-0.582538	2.168369

Table C.4. (continued) Cartesian Coordinates of the B3LYP/6-31G* Optimized Geometries of the Ground State Structures of the Neutral Pyr Ligand and the $M^{2+}(Pyr)_x$ Complexes.[a]

$Cu^{2+}(Pyr)_3$				$Zn^{2+}(Pyr)_3$			
	x	y	z		x	y	z
C	-0.272363	-0.476174	0.254740	C	0.295049	0.484106	-0.161743
C	-0.130081	-0.103540	1.594148	C	0.126529	0.146789	1.183558
C	0.871844	-0.665473	-0.524721	C	1.588952	0.627407	-0.669010
H	-1.259439	-0.620501	-0.174103	H	-0.567579	0.633022	-0.804118
C	1.144328	0.068279	2.113032	C	1.249721	-0.040167	1.974857
C	2.116876	-0.474849	0.055299	C	2.668277	0.434122	0.179678
H	-0.994089	0.052148	2.231207	H	-0.860819	0.027770	1.616576
H	0.804700	-0.958463	-1.566933	H	1.762815	0.886918	-1.707734
N	2.255303	-0.106890	1.355301	N	2.508420	0.102074	1.486362
H	1.298780	0.347045	3.150341	H	1.158360	-0.310489	3.022412
H	3.028949	-0.615558	-0.518145	H	3.687894	0.544449	-0.176525
C	4.424911	-2.231929	5.956960	C	4.095291	-3.689878	5.817184
C	3.850088	-2.791798	4.813921	C	3.486407	-3.863445	4.571741
C	4.872538	-0.909782	5.912450	C	4.695693	-2.463824	6.114614
H	4.522385	-2.816087	6.867028	H	4.102201	-4.496844	6.543623
C	3.734074	-2.015911	3.668821	C	3.492889	-2.811367	3.668600
C	4.739418	-0.192605	4.731500	C	4.672054	-1.456077	5.162455
H	3.491563	-3.815590	4.803905	H	3.011601	-4.800299	4.300857
H	5.322666	-0.434989	6.777752	H	5.177646	-2.288134	7.070320
N	4.175422	-0.736742	3.627599	N	4.077581	-1.619624	3.953008
H	3.279873	-2.409632	2.766171	H	3.025342	-2.906726	2.693480
H	5.088481	0.831127	4.652646	H	5.133572	-0.492315	5.354293
Cu^{2+}	4.002118	0.301368	2.010469	N	5.611921	1.027516	2.489604
N	5.661301	1.233527	1.850795	C	6.875409	0.538657	2.576568
C	6.851976	0.584612	1.833950	C	5.439073	2.359773	2.293348
C	5.636516	2.574008	1.633864	C	7.990833	1.355166	2.467449
C	8.044009	1.248689	1.587072	C	6.510051	3.233596	2.183480
C	6.792213	3.298270	1.383501	H	6.977110	-0.530274	2.737484
H	6.829865	-0.483018	2.026942	H	4.415893	2.716050	2.223954
H	4.666052	3.061626	1.664653	C	7.808963	2.726248	2.269831
C	8.017522	2.627036	1.357785	H	8.982493	0.921388	2.537967
H	8.975356	0.692757	1.575839	H	6.325990	4.291767	2.032093
H	6.729018	4.367830	1.214372	H	8.665182	3.388473	2.184365
H	8.937802	3.170413	1.165746	Zn^{2+}	4.065867	-0.164355	2.643260

Table C.4. (continued) Cartesian Coordinates of the B3LYP/6-31G* Optimized Geometries of the Ground State Structures of the Neutral Pyr Ligand and the $M^{2+}(Pyr)_x$ Complexes.[a]

	$Ca^{2+}(Pyr)_4$				$Ca^{2+}(Pyr)_4$		
	x	y	z		x	y	z
N	-0.206960	-0.204137	-0.355340	H	1.248468	-1.661738	-0.654879
N	-0.254521	-0.129308	3.725048	H	0.191259	-2.629810	-2.677276
N	3.276005	-0.132206	1.764130	H	-1.956417	-1.634003	-3.519550
N	0.871942	3.160598	1.592595	H	-2.944523	0.310563	-2.272307
C	-1.516101	-0.613053	3.650332	H	-1.769745	1.169819	-0.267144
C	0.326580	-0.091947	4.946784	Ca^{2+}	0.921633	0.673331	1.682760
C	1.111025	3.838395	0.445752				
C	0.613541	3.888590	2.703677				
C	-1.362302	0.325890	-0.820102				
C	0.316883	-1.249410	-1.036741				
C	3.588882	-1.389722	2.154609				
C	4.297215	0.681583	1.409090				
C	-2.020418	-0.154522	-1.945894				
C	-0.275156	-1.791249	-2.171347				
C	5.628577	0.283419	1.426773				
C	4.892459	-1.869177	2.201431				
C	1.105245	5.225911	0.367374				
C	0.587991	5.278065	2.713797				
C	-2.225567	-1.061628	4.757953				
C	-0.310759	-0.519604	6.105357				
C	-1.612738	-1.014081	6.011082				
C	-1.467789	-1.234664	-2.636041				
C	5.934103	-1.017441	1.829932				
C	0.839241	5.961954	1.523227				
H	4.031244	1.690898	1.102192				
H	6.405823	0.980160	1.131591				
H	6.963902	-1.360522	1.855247				
H	5.083511	-2.887359	2.523320				
H	2.759343	-2.032040	2.443188				
H	1.311162	3.241406	-0.441678				
H	1.304095	5.715295	-0.580139				
H	0.826826	7.047284	1.496325				
H	0.374435	5.808762	3.635448				
H	0.417736	3.330348	3.616733				
H	-3.234952	-1.440127	4.637190				
H	-2.138960	-1.356785	6.896774				
H	0.205070	-0.466057	7.058177				
H	-1.968684	-0.642048	2.661411				
H	1.343262	0.293117	4.992321				

Table C.4. (continued) Cartesian Coordinates of the B3LYP/6-31G* Optimized Geometries of the Ground State Structures of the Neutral Pyr Ligand and the $M^{2+}(Pyr)_x$ Complexes.[a]

	$Fe^{2+}(Pyr)_4$				$Fe^{2+}(Pyr)_4$		
	x	y	z		x	y	z
N	0.044702	-0.101915	-0.028144	H	1.347744	-1.721063	-0.114595
N	-0.110759	-0.005544	3.348874	H	0.302511	-2.734840	-2.125911
N	2.913176	0.072203	1.744413	H	-1.672673	-1.590516	-3.174275
N	0.866004	2.759831	1.675230	H	-2.506815	0.543987	-2.144485
C	-1.430260	-0.303598	3.291563	H	-1.349813	1.439890	-0.138004
C	0.520553	-0.137720	4.540811	Fe^{2+}	0.926087	0.682311	1.683507
C	0.915454	3.441533	0.504956				
C	0.800621	3.472389	2.824655				
C	-1.016816	0.515488	-0.601687				
C	0.491254	-1.250961	-0.588192				
C	3.244693	-1.123274	2.290269				
C	3.906383	0.831699	1.224840				
C	-1.659414	0.012514	-1.724793				
C	-0.095453	-1.813465	-1.714538				
C	5.236609	0.431512	1.229298				
C	4.550004	-1.594353	2.326903				
C	0.908742	4.828420	0.444930				
C	0.785272	4.861108	2.845912				
C	-2.150902	-0.732256	4.398958				
C	-0.132300	-0.555012	5.692709				
C	-1.493605	-0.859243	5.623599				
C	-1.192035	-1.173974	-2.294379				
C	5.567482	-0.804039	1.787736				
C	0.841953	5.554651	1.636002				
H	3.615334	1.788029	0.800845				
H	5.995103	1.078756	0.802341				
H	6.598320	-1.144394	1.804326				
H	4.762474	-2.560046	2.773023				
H	2.430512	-1.709261	2.707462				
H	0.961405	2.845776	-0.402255				
H	0.952227	5.326792	-0.517590				
H	0.832762	6.640206	1.620761				
H	0.729522	5.384789	3.794157				
H	0.754125	2.901881	3.747330				
H	-3.206447	-0.961063	4.298967				
H	-2.030780	-1.190604	6.506991				
H	0.418508	-0.642274	6.623139				
H	-1.910573	-0.197594	2.323543				
H	1.580489	0.099919	4.557926				

Table C.4. (continued) Cartesian Coordinates of the B3LYP/6-31G* Optimized Geometries of the Ground State Structures of the Neutral Pyr Ligand and the $M^{2+}(Pyr)_x$ Complexes.[a]

	$Co^{2+}(Pyr)_4$				$Co^{2+}(Pyr)_4$		
	x	y	z		x	y	z
N	0.340418	-0.377411	-0.123425	H	1.458795	-2.108416	0.149214
N	-0.026768	0.541122	3.079886	H	0.447815	-3.321452	-1.769609
N	2.883901	-0.414670	2.062541	H	-1.307970	-2.165946	-3.145130
N	1.599619	2.428095	0.834174	H	-1.964778	0.179069	-2.525641
C	-1.339672	0.239394	2.949696	H	-0.855514	1.261974	-0.583521
C	0.443115	0.836289	4.315902	Co^{2+}	1.199870	0.543053	1.466111
C	2.134155	2.660778	-0.388787				
C	1.338006	3.490617	1.630717				
C	-0.601131	0.246147	-0.871864				
C	0.695555	-1.638577	-0.462849				
C	2.819071	-1.560114	2.783236				
C	4.105759	0.078437	1.753340				
C	-1.214914	-0.361965	-1.958482				
C	0.128122	-2.311309	-1.537344				
C	5.283848	-0.548120	2.138863				
C	3.952071	-2.244435	3.201877				
C	2.428688	3.938639	-0.844407				
C	1.602841	4.797993	1.243781				
C	-2.214781	0.230212	4.028208				
C	-0.370474	0.850354	5.440679				
C	-1.725340	0.542798	5.297334				
C	-0.846170	-1.665178	-2.299721				
C	5.209407	-1.731870	2.874482				
C	2.159896	5.029628	-0.014782				
H	4.125304	1.001696	1.183136				
H	6.239181	-0.112295	1.866961				
H	6.113347	-2.244409	3.189026				
H	3.847447	-3.159005	3.775718				
H	1.825362	-1.923543	3.028991				
H	2.320419	1.789783	-1.010427				
H	2.857670	4.072742	-1.831663				
H	2.378418	6.040710	-0.344490				
H	1.373799	5.615955	1.918331				
H	0.901349	3.273491	2.600300				
H	-3.258777	-0.019288	3.872134				
H	-2.385864	0.544565	6.158987				
H	0.053350	1.094849	6.408808				
H	-1.684380	-0.001287	1.949109				
H	1.503442	1.059655	4.391679				

Table C.4. (continued) Cartesian Coordinates of the B3LYP/6-31G* Optimized Geometries of the Ground State Structures of the Neutral Pyr Ligand and the $M^{2+}(Pyr)_x$ Complexes.[a]

	$Ni^{2+}(Pyr)_4$				$Ni^{2+}(Pyr)_4$		
	x	y	z		x	y	z
N	-0.214077	-0.227446	0.033147	H	1.547408	-1.303161	-0.209816
N	-0.182729	-0.266889	3.756310	H	0.884899	-2.313173	-2.380916
N	2.265920	0.288465	1.967814	H	-1.359384	-1.737713	-3.351769
N	-0.276909	2.319272	1.842861	H	-2.843642	-0.155877	-2.082791
C	-1.264644	-1.072860	3.882244	H	-2.033721	0.781688	0.069383
C	0.531108	0.024059	4.868698	Ni^{2+}	0.263880	0.390734	1.895939
C	-0.102830	3.058830	0.721527				
C	-0.817049	2.921581	2.927192				
C	-1.421256	0.085937	-0.496286				
C	0.583379	-1.078233	-0.653675				
C	2.852325	-0.854095	2.394912				
C	3.059756	1.306598	1.569226				
C	-1.867300	-0.436671	-1.702584				
C	0.208254	-1.638302	-1.867834				
C	4.446437	1.218572	1.578295				
C	4.231071	-1.019468	2.426214				
C	-0.451471	4.400857	0.649060				
C	-1.195872	4.258272	2.928625				
C	-1.664812	-1.605447	5.100783				
C	0.191605	-0.468011	6.122242				
C	-0.925115	-1.297963	6.244038				
C	-1.039313	-1.315277	-2.404216				
C	5.046384	0.035216	2.011166				
C	-1.009195	5.015773	1.771918				
H	2.560511	2.211829	1.241055				
H	5.040504	2.065417	1.251886				
H	6.127507	-0.062796	2.027370				
H	4.652571	-1.956712	2.773541				
H	2.188669	-1.648588	2.723658				
H	0.320588	2.545808	-0.135946				
H	-0.289596	4.949151	-0.272836				
H	-1.293572	6.063200	1.744592				
H	-1.628325	4.692319	3.823682				
H	-0.945463	2.305536	3.809949				
H	-2.537675	-2.247643	5.147631				
H	-1.212913	-1.697922	7.211521				
H	0.793962	-0.204044	6.984926				
H	-1.819286	-1.293280	2.973675				
H	1.395542	0.666100	4.734005				

Table C.4. (continued) Cartesian Coordinates of the B3LYP/6-31G* Optimized Geometries of the Ground State Structures of the Neutral Pyr Ligand and the $M^{2+}(Pyr)_x$ Complexes.[a]

$Cu^{2+}(Pyr)_4$				$Cu^{2+}(Pyr)_4$			
	x	y	z		x	y	z
Cu^{2+}	0.020898	-0.052213	-0.030589	H	1.404633	-0.513563	-2.511864
N	0.311052	0.450026	1.888043	H	-0.099481	-1.501322	2.490554
N	1.927852	-0.447437	-0.498824	H	0.145301	-1.030522	4.915261
N	-0.781358	-1.482994	-1.180100	H	0.735684	1.301375	5.645402
N	-1.409825	1.329182	-0.279629	H	1.042525	3.066146	3.883479
C	2.938893	-0.508853	0.396958	H	0.739036	2.445308	1.496479
C	2.235270	-0.544737	-1.814799				
C	-2.518182	1.386643	0.490257				
C	-1.238890	2.270585	-1.236308				
C	0.622839	1.704274	2.280640				
C	0.148218	-0.501398	2.836190				
C	-0.274873	-2.733528	-1.056100				
C	-1.858713	-1.309138	-1.978500				
C	0.787157	2.046010	3.617342				
C	0.289311	-0.234479	4.192562				
C	-2.455842	-2.357516	-2.667240				
C	-0.825011	-3.832167	-1.702141				
C	-3.485659	2.370766	0.328873				
C	-2.158734	3.289341	-1.452950				
C	4.265844	-0.666601	0.017060				
C	3.538199	-0.690414	-2.271065				
C	4.576362	-0.755165	-1.340270				
C	0.616335	1.062378	4.593054				
C	-1.935835	-3.644505	-2.526288				
C	-3.305080	3.341686	-0.657762				
H	-2.243226	-0.300089	-2.060914				
H	-3.314622	-2.161919	-3.300334				
H	-2.384620	-4.483353	-3.049408				
H	-0.384566	-4.813467	-1.561865				
H	0.601924	-2.842933	-0.426726				
H	-2.621520	0.621738	1.253013				
H	-4.361772	2.372736	0.968515				
H	-4.043227	4.124245	-0.804527				
H	-1.975430	4.023188	-2.230501				
H	-0.339527	2.197398	-1.841669				
H	5.038015	-0.716729	0.777197				
H	5.605030	-0.874749	-1.666262				
H	3.729607	-0.755666	-3.336768				
H	2.666151	-0.429361	1.441994				

Table C.4. (continued) Cartesian Coordinates of the B3LYP/6-31G* Optimized Geometries of the Ground State Structures of the Neutral Pyr Ligand and the $M^{2+}(Pyr)_x$ Complexes.[a]

	$Zn^{2+}(Pyr)_4$				$Zn^{2+}(Pyr)_4$		
	x	y	z		x	y	z
N	0.348131	-0.389835	-0.128765	H	1.502976	-2.099909	0.118089
N	-0.034540	0.544167	3.075550	H	0.493835	-3.318636	-1.797683
N	2.889161	-0.412639	2.055094	H	-1.301750	-2.188351	-3.143280
N	1.592393	2.439291	0.842206	H	-1.996942	0.138551	-2.497875
C	-1.349820	0.252960	2.952056	H	-0.883857	1.229321	-0.562799
C	0.443938	0.838710	4.307794	Zn^{2+}	1.199094	0.544568	1.462468
C	2.153624	2.672652	-0.367950				
C	1.306069	3.501085	1.630121				
C	-0.614298	0.220242	-0.860514				
C	0.723803	-1.640643	-0.481668				
C	2.815175	-1.556058	2.777067				
C	4.113942	0.068650	1.741593				
C	-1.229485	-0.391796	-1.944368				
C	0.157002	-2.316772	-1.554184				
C	5.287231	-0.567616	2.125035				
C	3.943038	-2.249709	3.195035				
C	2.451103	3.951488	-0.819468				
C	1.571645	4.809324	1.247123				
C	-2.219737	0.252714	4.034514				
C	-0.363732	0.860562	5.437002				
C	-1.721349	0.563148	5.300893				
C	-0.839324	-1.684712	-2.299893				
C	5.203877	-1.749041	2.863790				
C	2.156552	5.042227	0.001378				
H	4.139983	0.990416	1.169369				
H	6.245718	-0.141356	1.849231				
H	6.103950	-2.269059	3.177216				
H	3.831366	-3.162599	3.770201				
H	1.818870	-1.909872	3.025184				
H	2.357770	1.801980	-0.984223				
H	2.902338	4.085984	-1.796671				
H	2.376867	6.053963	-0.325187				
H	1.322015	5.626923	1.914727				
H	0.849115	3.282941	2.589989				
H	-3.266528	0.011885	3.883871				
H	-2.377555	0.571504	6.165828				
H	0.066800	1.104281	6.402351				
H	-1.700988	0.013515	1.953495				
H	1.506034	1.054306	4.377340				

Table C.4. (continued) Cartesian Coordinates of the B3LYP/6-31G* Optimized Geometries of the Ground State Structures of the Neutral Pyr Ligand and the $M^{2+}(Pyr)_x$ Complexes.[a]

	$Ca^{2+}(Pyr)_5$				$Ca^{2+}(Pyr)_5$		
	x	y	z		x	y	z
N	0.619529	0.373115	-0.472863	C	-4.956677	3.244100	-3.692883
C	0.986508	0.798647	0.756787	H	-3.332273	3.432040	-2.288641
C	1.579024	-0.176262	-1.249497	C	-5.722905	2.340432	-4.429444
C	2.283928	0.691529	1.246099	H	-6.005218	0.238744	-4.878823
H	0.205451	1.249035	1.363956	H	-5.140465	4.312061	-3.744020
C	2.902313	-0.315234	-0.843621	H	-6.525028	2.689784	-5.072457
H	1.266335	-0.516654	-2.232474	N	-1.871863	2.800629	0.013308
C	3.263820	0.124847	0.429914	C	-0.945193	3.765998	-0.176357
H	2.517943	1.048577	2.243506	C	-2.872589	3.063795	0.882306
H	3.629989	-0.760049	-1.514115	C	-0.982752	4.997345	0.469550
H	4.287571	0.029515	0.778854	H	-0.138907	3.534937	-0.868710
N	-1.332197	-1.189724	-3.024107	C	-2.985323	4.264773	1.575016
C	-1.137576	-0.870517	-4.322903	H	-3.608594	2.276190	1.025972
C	-1.241037	-2.494785	-2.685902	C	-2.022964	5.253204	1.364199
C	-0.847012	-1.811889	-5.304845	H	-0.211483	5.734990	0.274523
H	-1.226781	0.181916	-4.582262	H	-3.809861	4.417971	2.263247
C	-0.959784	-3.502559	-3.602521	H	-2.081610	6.202882	1.887273
H	-1.402774	-2.735686	-1.637822	Ca^{2+}	-1.805546	0.572436	-1.235520
C	-0.756578	-3.155696	-4.938922				
H	-0.697808	-1.495034	-6.331662				
H	-0.902357	-4.534474	-3.272601				
H	-0.533608	-3.917018	-5.680277				
N	-3.056370	-0.860850	0.425485				
C	-2.411074	-1.504802	1.423306				
C	-4.397170	-1.013895	0.350913				
C	-3.059810	-2.304008	2.358447				
H	-1.332646	-1.370148	1.468117				
C	-5.125491	-1.792670	1.243741				
H	-4.899827	-0.488744	-0.458226				
C	-4.444670	-2.451719	2.268385				
H	-2.489475	-2.797649	3.138173				
H	-6.201506	-1.878490	1.135279				
H	-4.982511	-3.068047	2.982348				
N	-3.648967	1.438460	-2.769873				
C	-4.397577	0.575795	-3.493196				
C	-3.940431	2.753223	-2.879597				
C	-5.437089	0.978514	-4.324714				
H	-4.142251	-0.476917	-3.402839				

Table C.4. (continued) Cartesian Coordinates of the B3LYP/6-31G* Optimized Geometries of the Ground State Structures of the Neutral Pyr Ligand and the $M^{2+}(Pyr)_x$ Complexes.[a]

	$Fe^{2+}(Pyr)_5$				$Fe^{2+}(Pyr)_5$		
	x	y	z		x	y	z
N	-0.246705	-0.101771	0.389394	C	-5.941022	1.983937	-2.255847
C	-0.367612	-0.636644	1.623990	H	-4.271463	2.502686	-0.997418
C	0.963934	0.387873	0.041876	C	-6.430293	1.049697	-3.168668
C	0.686437	-0.709458	2.528964	H	-5.966837	-0.801765	-4.196174
H	-1.346549	-1.022978	1.887478	H	-6.525437	2.852059	-1.969667
C	2.069945	0.354509	0.883744	H	-7.411626	1.172761	-3.616603
H	1.042526	0.820293	-0.950851	N	-1.706362	2.368295	-0.504372
C	1.932400	-0.206856	2.153805	C	-1.549044	3.287448	-1.482315
H	0.528348	-1.152411	3.506644	C	-1.673068	2.797801	0.776724
H	3.017827	0.760235	0.546192	C	-1.355105	4.639198	-1.223790
H	2.776336	-0.250445	2.835478	H	-1.582010	2.919747	-2.502955
N	-0.943594	-0.295987	-2.750644	C	-1.498642	4.133265	1.119794
C	-1.227550	0.283401	-3.939471	H	-1.781250	2.038686	1.545141
C	0.021097	-1.243726	-2.736417	C	-1.332996	5.074017	0.102213
C	-0.572037	-0.044174	-5.120472	H	-1.226415	5.333200	-2.047513
H	-2.017982	1.026316	-3.935389	H	-1.488121	4.424610	2.164652
C	0.711923	-1.642541	-3.874617	H	-1.187834	6.123899	0.337703
H	0.247932	-1.683860	-1.771309	Fe^{2+}	-1.985594	0.269821	-0.955345
C	0.415423	-1.029514	-5.092382				
H	-0.838295	0.461008	-6.042844				
H	1.470872	-2.414284	-3.802011				
H	0.941524	-1.313314	-5.998694				
N	-3.035037	-1.408397	-0.078556				
C	-2.530077	-2.660942	-0.130700				
C	-4.229125	-1.234455	0.530390				
C	-3.184855	-3.762146	0.407894				
H	-1.567620	-2.774996	-0.619078				
C	-4.940208	-2.279709	1.107868				
H	-4.623789	-0.223426	0.542497				
C	-4.412354	-3.570005	1.043767				
H	-2.737419	-4.747304	0.330500				
H	-5.890709	-2.082500	1.591965				
H	-4.947037	-4.408767	1.478965				
N	-3.890852	0.735627	-2.015973				
C	-4.380136	-0.165039	-2.897010				
C	-4.677388	1.789760	-1.707138				
C	-5.630882	-0.047270	-3.492678				
H	-3.738612	-1.009483	-3.129853				

Table C.4. (continued) Cartesian Coordinates of the B3LYP/6-31G* Optimized Geometries of the Ground State Structures of the Neutral Pyr Ligand and the $M^{2+}(Pyr)_x$ Complexes.[a]

	$Co^{2+}(Pyr)_5$				$Co^{2+}(Pyr)_5$		
	x	y	z		x	y	z
N	0.023200	0.038536	-0.108104	H	-3.473911	3.004190	-2.308128
C	0.083371	0.249530	1.224823	C	-5.995617	1.346187	-3.847770
C	1.182799	-0.238084	-0.740984	H	-6.234644	-0.801916	-3.685685
C	1.263016	0.182505	1.957065	H	-5.425014	3.435068	-3.772804
H	-0.855492	0.477751	1.720009	H	-6.859249	1.497840	-4.488014
C	2.408613	-0.322770	-0.086970	N	-1.578797	2.456676	-0.583525
H	1.122486	-0.398279	-1.811944	C	-0.440752	3.086998	-0.947813
C	2.453400	-0.111030	1.290407	C	-2.472400	3.145505	0.160102
H	1.244990	0.357963	3.027567	C	-0.166183	4.405011	-0.602516
H	3.306164	-0.550799	-0.652228	H	0.269640	2.506323	-1.527386
H	3.392644	-0.171683	1.831621	C	-2.264031	4.458678	0.564493
N	-1.276666	-0.446745	-2.881211	H	-3.381766	2.620213	0.434201
C	-1.273209	0.241363	-4.043934	C	-1.091061	5.105698	0.172605
C	-0.899816	-1.744102	-2.913411	H	0.759174	4.865957	-0.931007
C	-0.885998	-0.324947	-5.252749	H	-3.010840	4.961226	1.169879
H	-1.600649	1.274909	-3.995599	H	-0.901610	6.133557	0.466388
C	-0.520831	-2.390478	-4.083809	Co^{2+}	-1.907592	0.454830	-1.100653
H	-0.903864	-2.272979	-1.965700				
C	-0.506989	-1.667658	-5.277687				
H	-0.890915	0.276868	-6.155229				
H	-0.237682	-3.437247	-4.054250				
H	-0.208441	-2.141448	-6.207793				
N	-2.944319	-0.733465	0.262089				
C	-2.407593	-1.876842	0.746383				
C	-4.179079	-0.387527	0.693082				
C	-3.071837	-2.700949	1.646233				
H	-1.408251	-2.121274	0.404691				
C	-4.899546	-1.145489	1.607539				
H	-4.597735	0.520502	0.274323				
C	-4.340838	-2.328912	2.092031				
H	-2.596490	-3.612111	1.993413				
H	-5.882428	-0.814202	1.925219				
H	-4.882285	-2.947491	2.801237				
N	-3.766434	0.954696	-2.185763				
C	-4.538766	-0.079630	-2.584320				
C	-4.106349	2.183563	-2.628566				
C	-5.651875	0.068646	-3.403520				
H	-4.250015	-1.063482	-2.227262				
C	-5.202866	2.422713	-3.452046				

Table C.4. (continued) Cartesian Coordinates of the B3LYP/6-31G* Optimized Geometries of the Ground State Structures of the Neutral Pyr Ligand and the $M^{2+}(Pyr)_x$ Complexes.[a]

$Ni^{2+}(Pyr)_5$				$Ni^{2+}(Pyr)_5$			
	x	y	z		x	y	z
Ni^{2+}	-0.101199	-0.062065	-0.004443	C	-3.793334	2.044966	-0.857663
N	-0.528043	-0.192204	2.068683	H	-2.837771	0.134130	-1.137315
C	0.435071	-0.617834	2.916728	C	-3.618860	3.344312	-0.378597
C	-1.749140	0.057299	2.589214	H	-2.207078	4.684867	0.572920
C	0.224444	-0.793856	4.278659	H	-4.727250	1.731045	-1.311699
H	1.404455	-0.827486	2.477694	H	-4.419583	4.073886	-0.451311
C	-2.047328	-0.106997	3.938118	N	-0.276775	-0.304944	-2.104208
H	-2.509723	0.398857	1.897035	C	-0.557295	-1.488389	-2.691533
C	-1.042602	-0.535975	4.804349	C	-0.180066	0.780102	-2.905092
H	1.039398	-1.130398	4.910743	C	-0.749584	-1.628909	-4.062239
H	-3.049942	0.102072	4.295714	H	-0.630176	-2.348517	-2.036487
H	-1.241699	-0.668370	5.863396	C	-0.343743	0.723756	-4.283554
N	1.650950	1.020808	0.070459	H	0.030909	1.723649	-2.413551
C	1.952387	1.794982	1.136527	C	-0.636694	-0.504403	-4.878651
C	2.542033	0.983790	-0.945077	H	-0.980556	-2.605306	-4.474692
C	3.121647	2.542131	1.224554	H	-0.246351	1.627972	-4.875037
H	1.230150	1.804434	1.944875	H	-0.775413	-0.581787	-5.952672
C	3.735435	1.697078	-0.932974				
H	2.278289	0.364894	-1.795102				
C	4.035149	2.494564	0.171504				
H	3.307734	3.146333	2.106137				
H	4.412028	1.626134	-1.777997				
H	4.958013	3.064997	0.210607				
N	0.605239	-2.047255	0.151581				
C	1.829753	-2.451196	-0.243261				
C	-0.244925	-2.987696	0.619489				
C	2.243761	-3.778123	-0.187792				
H	2.499083	-1.681035	-0.609981				
C	0.083440	-4.336385	0.694492				
H	-1.218294	-2.638746	0.951658				
C	1.354560	-4.742964	0.285587				
H	3.244539	-4.044011	-0.511254				
H	-0.642952	-5.048161	1.072148				
H	1.645656	-5.787600	0.337732				
N	-1.551662	1.463305	-0.191498				
C	-1.394694	2.720420	0.270555				
C	-2.739002	1.145053	-0.752889				
C	-2.392820	3.686213	0.192042				
H	-0.433313	2.957628	0.712200				

Table C.4. (continued) Cartesian Coordinates of the B3LYP/6-31G* Optimized Geometries of the Ground State Structures of the Neutral Pyr Ligand and the $M^{2+}(Pyr)_x$ Complexes.[a]

$Cu^{2+}(Pyr)_5$				$Cu^{2+}(Pyr)_5$			
	x	y	z		x	y	z
Cu^{2+}	-0.183405	-0.110766	-0.001246	C	-0.831414	-1.577313	-4.031275
N	-0.449532	-0.141413	2.041269	H	-0.828256	-2.328429	-2.012221
C	0.598003	-0.471890	2.828155	C	-0.609535	-0.454166	-4.827292
C	-1.642097	0.072820	2.637042	H	-0.059327	1.642166	-4.782137
C	0.497828	-0.584623	4.209244	H	-1.125374	-2.527579	-4.464136
H	1.540526	-0.653984	2.324311	H	-0.724114	-0.507096	-5.905629
C	-1.827373	-0.031542	4.011508	N	0.405466	-2.087119	0.171022
H	-2.468911	0.333707	1.987704	C	-0.460632	-2.991908	0.676911
C	-0.738330	-0.361499	4.817387	C	1.621892	-2.522347	-0.215673
H	1.374438	-0.846233	4.792290	C	-0.152832	-4.341872	0.799336
H	-2.810327	0.145873	4.434727	H	-1.425808	-2.612118	0.996614
H	-0.850310	-0.445900	5.893992	C	2.012291	-3.853462	-0.114669
N	-1.658525	1.329601	-0.179834	H	2.299825	-1.775635	-0.613736
C	-2.856099	0.986563	-0.702158	C	1.109008	-4.784318	0.398565
C	-1.483407	2.606263	0.217826	H	-0.888935	-5.027305	1.205782
C	-3.907077	1.887163	-0.830624	H	3.006062	-4.148622	-0.434261
H	-2.964432	-0.042338	-1.030237	H	1.382204	-5.831367	0.486789
C	-2.479578	3.571088	0.111887				
H	-0.511963	2.856884	0.629056				
C	-3.717419	3.207287	-0.418428				
H	-4.851191	1.556617	-1.250449				
H	-2.283070	4.585968	0.440890				
H	-4.516637	3.936274	-0.510936				
N	1.765100	1.067539	0.012998				
C	2.069245	1.916883	1.016921				
C	2.669339	0.948510	-0.981948				
C	3.245122	2.659507	1.065407				
H	1.340809	1.995828	1.818213				
C	3.873934	1.644606	-1.012778				
H	2.409359	0.272172	-1.790589				
C	4.170413	2.521264	0.030842				
H	3.427885	3.328576	1.899752				
H	4.560295	1.500810	-1.840678				
H	5.099559	3.082832	0.037740				
N	-0.311920	-0.318782	-2.046694				
C	-0.109935	0.767706	-2.824185				
C	-0.668523	-1.470681	-2.654151				
C	-0.240716	0.740394	-4.207044				
H	0.160259	1.683781	-2.311189				

Table C.4. (continued) Cartesian Coordinates of the B3LYP/6-31G* Optimized Geometries of the Ground State Structures of the Neutral Pyr Ligand and the $M^{2+}(Pyr)_x$ Complexes.[a]

	$Zn^{2+}(Pyr)_5$				$Zn^{2+}(Pyr)_5$		
	x	y	z		x	y	z
N	0.329091	-0.083967	0.184738	H	-3.615758	2.160222	-2.233637
C	0.310983	0.114778	1.519518	C	-5.868929	0.049375	-3.633164
C	1.529513	-0.044069	-0.429806	H	-5.676750	-2.105317	-3.492373
C	1.457527	0.340247	2.273514	H	-5.716564	2.209579	-3.557206
H	-0.663007	0.087150	1.997637	H	-6.787204	0.032254	-4.212247
C	2.725858	0.175093	0.245445	N	-1.439847	2.052564	-0.858635
H	1.526542	-0.197589	-1.503868	C	-0.670858	2.735522	-1.733373
C	2.693079	0.369012	1.626236	C	-2.034941	2.746572	0.135119
H	1.378893	0.488474	3.345353	C	-0.475774	4.109550	-1.653549
H	3.660986	0.191105	-0.304366	H	-0.196983	2.154621	-2.519285
H	3.608315	0.540231	2.184630	C	-1.890272	4.120712	0.287320
N	-0.753411	-1.103660	-2.568459	H	-2.645364	2.175245	0.828386
C	-0.918379	-0.683564	-3.841964	C	-1.096227	4.818406	-0.623881
C	-0.073080	-2.253270	-2.367266	H	0.150873	4.609068	-2.384647
C	-0.413320	-1.376225	-4.935868	H	-2.391284	4.628948	1.104286
H	-1.486173	0.230718	-3.978130	H	-0.963100	5.892073	-0.533050
C	0.449289	-3.013816	-3.406476	Zn^{2+}	-1.592426	-0.040792	-0.967933
H	0.060908	-2.560329	-1.335430				
C	0.280278	-2.567312	-4.717877				
H	-0.567868	-0.988619	-5.937145				
H	0.979480	-3.934471	-3.187416				
H	0.680563	-3.135627	-5.551891				
N	-2.608854	-1.101614	0.524610				
C	-2.059341	-2.189692	1.107274				
C	-3.853200	-0.742041	0.910136				
C	-2.718632	-2.946485	2.068300				
H	-1.052583	-2.446134	0.795722				
C	-4.573387	-1.434713	1.875931				
H	-4.280596	0.121693	0.412696				
C	-3.999911	-2.561966	2.465511				
H	-2.232009	-3.816277	2.496486				
H	-5.565989	-1.096330	2.153276				
H	-4.539690	-3.128608	3.218065				
N	-3.497841	0.094014	-2.138825				
C	-4.080122	-1.070702	-2.495414				
C	-4.100231	1.235986	-2.529060				
C	-5.254951	-1.139399	-3.235248				
H	-3.579620	-1.978521	-2.171565				
C	-5.277550	1.259522	-3.271460				

Table C.4. (continued) Cartesian Coordinates of the B3LYP/6-31G* Optimized Geometries of the Ground State Structures of the Neutral Pyr Ligand and the $M^{2+}(Pyr)_x$ Complexes.[a]

	$Ca^{2+}(Pyr)_6$				$Ca^{2+}(Pyr)_6$		
	x	y	z		x	y	z
N	-0.219987	2.315807	1.169339	H	-1.053161	-3.247774	0.174839
C	0.436166	3.401735	0.705267	C	0.457259	-4.810986	-2.427757
C	-0.992920	2.480813	2.264989	H	1.779952	-3.770684	-3.793465
C	0.349990	4.657503	1.298640	H	-0.899498	-5.492757	-0.881155
H	1.052006	3.248535	-0.176694	H	0.548890	-5.776971	-2.915131
C	-1.137694	3.699646	2.920678	N	-1.612755	-1.041630	1.755496
H	-1.511856	1.596061	2.623188	C	-2.948774	-1.067449	1.555790
C	-0.453044	4.811535	2.429201	C	-1.149404	-1.577627	2.905587
H	0.901751	5.493005	0.880658	C	-3.847282	-1.613278	2.467565
H	-1.773766	3.771195	3.796775	H	-3.302330	-0.632399	0.625371
H	-0.543250	5.777324	2.917227	C	-1.975212	-2.143764	3.872326
N	1.612373	1.042075	-1.757087	H	-0.073020	-1.547224	3.048132
C	1.149443	1.579924	-2.906492	C	-3.352521	-2.163858	3.650288
C	2.948595	1.066111	-1.557811	H	-4.910472	-1.605788	2.250968
C	1.975621	2.146213	-3.872829	H	-1.543883	-2.559032	4.777154
H	0.073033	1.550883	-3.048988	H	-4.025837	-2.598756	4.382846
C	3.847440	1.611838	-2.469293	N	2.031452	-0.578117	1.521230
H	3.302174	0.629627	-0.628085	C	2.482812	0.291295	2.451273
C	3.353003	2.164448	-3.651206	C	2.678335	-1.759172	1.412716
H	1.544440	2.563239	-4.776917	C	3.565651	0.025393	3.284177
H	4.910729	1.602457	-2.253276	H	1.949771	1.235166	2.522511
H	4.026694	2.599047	-4.383591	C	3.769288	-2.108078	2.203303
N	-2.032864	0.577799	-1.521358	H	2.300333	-2.444805	0.660162
C	-2.676454	1.761007	-1.416988	C	4.224171	-1.198459	3.158513
C	-2.488312	-0.294659	-2.446513	H	3.883167	0.764113	4.012754
C	-3.768180	2.109093	-2.206825	H	4.248755	-3.072211	2.070058
H	-2.295084	2.449194	-0.668421	H	5.073411	-1.437581	3.791510
C	-3.572437	-0.029922	-3.278143	Ca^{2+}	-0.000379	0.000219	-0.000398
H	-1.957763	-1.240145	-2.514815				
C	-4.227717	1.196094	-3.156567				
H	-4.244775	3.075121	-2.077071				
H	-3.893331	-0.771147	-4.002684				
H	-5.077576	1.434576	-3.788970				
N	0.220508	-2.314903	-1.169642				
C	0.995860	-2.480026	-2.263470				
C	-0.435980	-3.400927	-0.706171				
C	1.142158	-3.698984	-2.918638				
H	1.514720	-1.594835	-2.620513				
C	-0.347818	-4.656962	-1.298654				

Table C.4. (continued) Cartesian Coordinates of the B3LYP/6-31G* Optimized Geometries of the Ground State Structures of the Neutral Pyr Ligand and the $M^{2+}(Pyr)_x$ Complexes.[a]

	$Fe^{2+}(Pyr)_6$				$Fe^{2+}(Pyr)_6$		
	x	y	z		x	y	z
N	0.043505	-0.021870	-0.012474	H	-2.956378	-1.077233	-4.004219
C	0.029012	-0.131683	1.334290	C	-6.137697	0.088724	-4.020204
C	1.252444	0.054738	-0.612054	H	-6.946331	1.256495	-2.383637
C	1.183556	-0.171979	2.109374	H	-4.984966	-1.088427	-5.427740
H	-0.946587	-0.187819	1.801062	H	-7.044910	0.104105	-4.616582
C	2.454520	0.022556	0.087399	N	-0.672730	-0.524611	-3.134577
H	1.247021	0.147064	-1.691105	C	-0.409346	-1.807872	-3.465800
C	2.424284	-0.094266	1.476991	C	-0.201078	0.427113	-3.969683
H	1.104817	-0.261260	3.187777	C	0.306622	-2.178205	-4.600417
H	3.393117	0.088425	-0.452770	H	-0.796214	-2.565743	-2.796176
H	3.344466	-0.122510	2.052674	C	0.525457	0.147106	-5.123249
N	-3.105469	0.573908	0.687289	H	-0.409839	1.453221	-3.694522
C	-3.527619	-0.371346	1.555498	C	0.787178	-1.182807	-5.450435
C	-3.418987	1.854089	0.984500	H	0.480881	-3.228936	-4.807569
C	-4.252172	-0.088033	2.709581	H	0.876651	0.961126	-5.748822
H	-3.269287	-1.394794	1.312841	H	1.350353	-1.436567	-6.343361
C	-4.137901	2.227784	2.116308	N	-1.548254	2.258162	-1.623255
H	-3.079798	2.605880	0.282509	C	-0.702153	2.996948	-0.872369
C	-4.566250	1.238834	3.000945	C	-2.216061	2.902225	-2.606738
H	-4.560570	-0.896917	3.363724	C	-0.494840	4.359338	-1.067470
H	-4.355148	3.275837	2.294292	H	-0.179609	2.471148	-0.082040
H	-5.129576	1.495135	3.893032	C	-2.070978	4.261061	-2.868424
N	-2.251032	-2.202847	-0.788028	H	-2.886713	2.297160	-3.205837
C	-1.257136	-2.990391	-0.319244	C	-1.191689	5.009386	-2.085427
C	-3.461932	-2.778495	-0.953700	H	0.200102	4.894386	-0.428753
C	-1.428021	-4.335689	-0.008158	H	-2.637301	4.717451	-3.673548
H	-0.289711	-2.517589	-0.195799	H	-1.053707	6.071380	-2.264218
C	-3.719761	-4.116485	-0.669859	Fe^{2+}	-1.888041	0.021670	-1.224957
H	-4.251958	-2.134360	-1.321337				
C	-2.684197	-4.915785	-0.186706				
H	-0.588169	-4.912758	0.364501				
H	-4.715992	-4.516989	-0.825676				
H	-2.851258	-5.963248	0.045144				
N	-3.790582	0.049117	-2.477364				
C	-4.904022	0.684454	-2.049950				
C	-3.855150	-0.568699	-3.677690				
C	-6.085989	0.729176	-2.782200				
H	-4.838212	1.170939	-1.084679				
C	-4.996628	-0.573503	-4.472856				

Table C.4. (continued) Cartesian Coordinates of the B3LYP/6-31G* Optimized Geometries of the Ground State Structures of the Neutral Pyr Ligand and the $M^{2+}(Pyr)_x$ Complexes.[a]

	$Co^{2+}(Pyr)_6$				$Co^{2+}(Pyr)_6$		
	x	y	z		x	y	z
N	0.151219	-0.048992	0.164549	H	-3.237766	-1.862536	-3.085737
C	0.182508	0.468314	1.412274	C	-6.100926	-0.127543	-3.600006
C	1.309626	-0.546670	-0.322456	H	-6.500173	1.756136	-2.605659
C	1.331777	0.508082	2.195723	H	-5.341916	-2.000839	-4.381111
H	-0.753700	0.856676	1.793671	H	-7.036920	-0.156154	-4.149519
C	2.502738	-0.548470	0.393170	N	-0.887155	-1.610360	-2.366392
H	1.271993	-0.951537	-1.326411	C	-0.652045	-2.865317	-1.925550
C	2.519263	-0.009950	1.679895	C	-0.599773	-1.351258	-3.661033
H	1.289299	0.937298	3.191270	C	-0.137715	-3.876314	-2.731038
H	3.398707	-0.964060	-0.055974	H	-0.887505	-3.061281	-0.887286
H	3.433792	0.005080	2.264955	C	-0.081214	-2.301792	-4.534466
N	-2.594045	1.573402	0.317336	H	-0.796675	-0.343435	-4.003485
C	-3.530523	1.320105	1.257697	C	0.156508	-3.593086	-4.064545
C	-2.151729	2.846671	0.222578	H	0.026715	-4.864603	-2.314626
C	-4.046005	2.293323	2.108036	H	0.129140	-2.028272	-5.563114
H	-3.876324	0.296777	1.326809	H	0.559697	-4.358725	-4.720386
C	-2.612213	3.880261	1.032638	N	-0.920136	1.572516	-2.444778
H	-1.398632	3.038135	-0.531164	C	0.337748	2.048391	-2.315427
C	-3.580217	3.603219	1.997179	C	-1.665367	2.094725	-3.443779
H	-4.797793	2.021979	2.841803	C	0.881643	3.023987	-3.145889
H	-2.214312	4.881395	0.903812	H	0.927932	1.635380	-1.507627
H	-3.960949	4.386573	2.645451	C	-1.201864	3.071347	-4.320269
N	-2.590214	-1.651184	0.400311	H	-2.670701	1.707453	-3.545412
C	-1.833043	-2.263402	1.336897	C	0.099390	3.549880	-4.172997
C	-3.879974	-2.044513	0.313603	H	1.900160	3.360740	-2.983183
C	-2.312806	-3.252474	2.190497	H	-1.855092	3.444783	-5.102024
H	-0.799452	-1.947427	1.399967	H	0.492323	4.311720	-4.839344
C	-4.442625	-3.025073	1.125629	Co^{2+}	-1.743447	-0.044917	-1.014842
H	-4.484421	-1.547268	-0.434166				
C	-3.646263	-3.646148	2.086626				
H	-1.647134	-3.701325	2.920348				
H	-5.487152	-3.290990	1.001117				
H	-4.053312	-4.414853	2.736372				
N	-3.675688	-0.052554	-2.176223				
C	-4.595341	0.931264	-2.058700				
C	-3.976159	-1.074207	-3.008062				
C	-5.806183	0.933688	-2.744212				
H	-4.341530	1.747769	-1.394162				
C	-5.162896	-1.150913	-3.730924				

Table C.4. (continued) Cartesian Coordinates of the B3LYP/6-31G* Optimized Geometries of the Ground State Structures of the Neutral Pyr Ligand and the $M^{2+}(Pyr)_x$ Complexes.[a]

	$Ni^{2+}(Pyr)_6$				$Ni^{2+}(Pyr)_6$		
	x	y	z		x	y	z
N	0.269212	-0.002101	0.162812	C	-4.313656	1.050807	-2.065855
C	0.331289	0.491082	1.419325	C	-3.817635	-1.040640	-2.890985
C	1.414550	-0.496623	-0.356170	C	-5.511718	1.094919	-2.771545
C	1.496920	0.510659	2.178543	H	-4.018519	1.884605	-1.442861
H	-0.591736	0.880870	1.827788	C	-4.995126	-1.077965	-3.630783
C	2.622293	-0.518485	0.334057	H	-3.132228	-1.877465	-2.917584
H	1.356543	-0.885832	-1.363970	C	-5.865456	0.010064	-3.573174
C	2.670788	-0.004249	1.629429	H	-6.150169	1.968326	-2.689779
H	1.476748	0.922962	3.181902	H	-5.219297	-1.948772	-4.237890
H	3.505081	-0.931412	-0.142732	H	-6.793113	0.012608	-4.137334
H	3.597416	-0.005009	2.195280	N	-0.758527	-1.593941	-2.355987
N	-2.436903	1.595670	0.406801	C	-0.921204	-2.912093	-2.107126
C	-3.132622	1.275046	1.519837	C	-0.074798	-1.274361	-3.476746
C	-2.273723	2.914089	0.159505	C	-0.429298	-3.920465	-2.930694
C	-3.671121	2.216215	2.392672	H	-1.474315	-3.167967	-1.213709
H	-3.254050	0.220049	1.723834	C	0.450300	-2.216243	-4.356888
C	-2.776883	3.921713	0.977139	H	0.065097	-0.219700	-3.670391
H	-1.722633	3.170861	-0.734853	C	0.272304	-3.571342	-4.083392
C	-3.492867	3.571567	2.120662	H	-0.598871	-4.958995	-2.666124
H	-4.218287	1.883514	3.268543	H	0.989235	-1.884333	-5.238149
H	-2.606300	4.960490	0.714187	H	0.669187	-4.332547	-4.748055
H	-3.898993	4.332201	2.780379	N	-0.784527	1.574052	-2.290364
N	-2.396699	-1.574384	0.348182	C	0.290631	2.311817	-1.934334
C	-1.587829	-2.314315	1.138596	C	-1.340952	1.848758	-3.491468
C	-3.718874	-1.850976	0.401396	C	0.832529	3.314075	-2.733029
C	-2.049009	-3.320168	1.982230	H	0.721749	2.093946	-0.965747
H	-0.529486	-2.095446	1.080126	C	-0.864750	2.833966	-4.350923
C	-4.264342	-2.839768	1.214345	H	-2.194213	1.245969	-3.774825
H	-4.361832	-1.246338	-0.225386	C	0.246051	3.585568	-3.968761
C	-3.415822	-3.593287	2.025059	H	1.697062	3.869274	-2.384514
H	-1.342738	-3.876443	2.589590	H	-1.359542	3.001439	-5.301872
H	-5.336136	-3.008233	1.208497	H	0.643459	4.361652	-4.615756
H	-3.808669	-4.371934	2.671758	Ni^{2+}	-1.599263	0.000695	-0.975689
N	-3.461196	0.003037	-2.110058				

Table C.4. (continued) Cartesian Coordinates of the B3LYP/6-31G* Optimized Geometries of the Ground State Structures of the Neutral Pyr Ligand and the $M^{2+}(Pyr)_x$ Complexes.[a]

$Cu^{2+}(Pyr)_6$				$Cu^{2+}(Pyr)_6$			
	x	y	z		x	y	z
Cu^{2+}	-0.037703	-0.034656	-0.001312	C	-0.001415	1.154091	-4.117751
N	-0.039765	-0.019470	2.027818	H	-0.026273	2.031927	-2.146270
C	1.115238	0.001468	2.725602	C	-0.001501	-0.048378	-4.825224
C	-1.199814	-0.028198	2.717411	H	-0.012925	-2.205224	-4.612873
C	1.151833	0.019678	4.115314	H	0.007286	2.110209	-4.630173
H	2.029060	0.003261	2.143477	H	0.006885	-0.052712	-5.910888
C	-1.246864	-0.022688	4.106814	N	-1.451883	1.415783	-0.007521
H	-2.109616	-0.040047	2.129053	C	-1.163298	2.656067	0.439622
C	-0.050234	0.004413	4.823311	C	-2.700664	1.165885	-0.453941
H	2.107983	0.041231	4.627296	C	-2.102866	3.680753	0.451271
H	-2.206833	-0.035915	4.611892	H	-0.147196	2.817386	0.779036
H	-0.054223	0.013565	5.908971	C	-3.696245	2.136125	-0.464445
N	1.430922	-1.429842	0.005895	H	-2.894401	0.156791	-0.797092
C	2.665079	-1.123282	-0.446474	C	-3.394768	3.419007	-0.006043
C	1.200618	-2.682432	0.451985	H	-1.821210	4.663791	0.813310
C	3.703022	-2.048046	-0.463112	H	-4.687639	1.885249	-0.826354
H	2.810470	-0.104483	-0.785020	H	-4.150746	4.198335	-0.005418
C	2.185170	-3.663960	0.457829	N	-2.213324	-2.252643	0.005934
H	0.195552	-2.890931	0.798346	C	-2.542984	-2.913930	1.131586
C	3.461715	-3.343857	-0.005574	C	-2.869973	-2.604843	-1.115541
H	4.680414	-1.752183	-0.829095	C	-3.504975	-3.920700	1.186510
H	1.949978	-4.659061	0.820095	H	-2.010912	-2.621671	2.034399
H	4.251798	-4.088576	-0.009898	C	-3.850233	-3.594317	-1.162415
N	2.239133	2.272070	-0.005102	H	-2.596520	-2.068232	-2.021598
C	2.613335	2.891485	1.130226	C	-4.175298	-4.269174	0.014074
C	2.854525	2.662319	-1.137154	H	-3.721186	-4.415907	2.127671
C	3.581445	3.892484	1.185148	H	-4.343310	-3.827712	-2.100580
H	2.112397	2.569613	2.040973	H	-4.932401	-5.047438	0.017206
C	3.836205	3.650383	-1.185731				
H	2.545725	2.157833	-2.050499				
C	4.208326	4.281019	0.001332				
H	3.834960	4.353472	2.134381				
H	4.295099	3.916038	-2.132649				
H	4.968445	5.056362	0.003841				
N	-0.023516	-0.036977	-2.029725				
C	-0.017453	-1.197361	-2.718856				
C	-0.017889	1.117919	-2.728000				
C	-0.012191	-1.244950	-4.108207				
H	-0.017080	-2.106950	-2.130077				

Table C.4. (continued) Cartesian Coordinates of the B3LYP/6-31G* Optimized Geometries of the Ground State Structures of the Neutral Pyr Ligand and the $M^{2+}(Pyr)_x$ Complexes.[a]

	$Zn^{2+}(Pyr)_6$				$Zn^{2+}(Pyr)_6$		
	x	y	z		x	y	z
N	0.353501	-0.001034	0.216932	H	-3.020186	-1.667821	-3.263728
C	0.474897	0.683849	1.374654	C	-5.946057	-0.000203	-3.625580
C	1.437858	-0.687664	-0.204172	H	-6.433475	1.741025	-2.431247
C	1.642548	0.709817	2.131431	H	-5.102351	-1.741107	-4.601586
H	-0.402917	1.224963	1.704627	H	-6.872676	-0.001650	-4.191491
C	2.644086	-0.716394	0.489263	N	-0.759873	-1.576977	-2.349863
H	1.329793	-1.228109	-1.136242	C	-0.691658	-2.873135	-1.975794
C	2.753570	-0.003963	1.683143	C	-0.313013	-1.269912	-3.586907
H	1.673039	1.280046	3.053976	C	-0.191195	-3.880319	-2.795039
H	3.477789	-1.287713	0.094652	H	-1.050448	-3.102744	-0.980389
H	3.680155	-0.005051	2.249111	C	0.202356	-2.213674	-4.469944
N	-2.434651	1.581786	0.395695	H	-0.377344	-0.227824	-3.873420
C	-3.335267	1.274682	1.354138	C	0.266707	-3.548237	-4.069897
C	-2.060985	2.875937	0.295172	H	-0.163416	-4.903176	-2.434306
C	-3.880498	2.216381	2.221319	H	0.544383	-1.901798	-5.451211
H	-3.626528	0.234025	1.420137	H	0.663299	-4.309748	-4.734539
C	-2.555934	3.881032	1.120328	N	-0.746724	1.644294	-2.349199
H	-1.336173	3.105897	-0.475657	C	0.529165	2.073042	-2.236813
C	-3.485558	3.548966	2.105688	C	-1.502490	2.222553	-3.307696
H	-4.600447	1.904305	2.970599	C	1.081014	3.061250	-3.046608
H	-2.214484	4.902332	0.988099	H	1.126088	1.603771	-1.465114
H	-3.891373	4.308943	2.766493	C	-1.032383	3.216989	-4.160325
N	-2.437272	-1.642224	0.405085	H	-2.522052	1.868620	-3.392421
C	-1.741179	-2.093561	1.471043	C	0.287016	3.649378	-4.030606
C	-3.647431	-2.200863	0.186151	H	2.114193	3.359553	-2.902513
C	-2.207393	-3.085721	2.328417	H	-1.693430	3.639494	-4.909810
H	-0.771984	-1.640845	1.636954	H	0.685867	4.423484	-4.679102
C	-4.190522	-3.196931	0.992316	Zn^{2+}	-1.593220	0.003093	-0.971481
H	-4.199629	-1.828312	-0.667182				
C	-3.458335	-3.652861	2.087983				
H	-1.595863	-3.403025	3.166618				
H	-5.169674	-3.602434	0.759875				
H	-3.852125	-4.429078	2.737053				
N	-3.545488	0.003671	-2.159340				
C	-4.504250	0.931402	-1.948121				
C	-3.793237	-0.925958	-3.107391				
C	-5.705465	0.966859	-2.649968				
H	-4.292044	1.674663	-1.189861				
C	-4.966113	-0.965310	-3.855417				

Table C.4. (continued) Cartesian Coordinates of the B3LYP/6-31G* Optimized Geometry of the Neutral Pyr Ligand.[a]

	Pyr		
	x	y	z
C	0.033927	0.000000	0.020815
C	0.015623	0.000000	1.415263
C	1.234746	0.000000	2.095911
C	1.267919	0.000000	-0.628917
C	2.428044	0.000000	0.148094
N	2.427456	0.000000	1.487177
H	1.255436	0.000000	3.184999
H	-0.919801	0.000000	1.967283
H	-0.892906	0.000000	-0.546977
H	1.334833	0.000000	-1.713019
H	3.407731	0.000000	-0.328095

[a]Standard Orientation, Å.

Table C.5a. Sequential and Total BDEs of Ground-State $M^{2+}(Pyr)_x$ Complexes at 0 K in kJ/mol.[a]

		BHandHLYP Theory					
		6-31G*//6-31G*			6-311+G(2d,2p)// 6-31G*		
Complex	Spin	D_0	$D_{0,BSSE}$[b]	Total[b]	D_0	$D_{0,BSSE}$[b]	Total[b]
$Fe^{2+}(Pyr)$	5	319.3	317.6	317.6	568.8	567.2	567.2
$Fe^{2+}(Pyr)_2$	5	480.5	478.0	795.6	423.6	421.1	988.3
$Fe^{2+}(Pyr)_3$	5	319.4	317.1	1112.7	304.9	302.5	1290.8
$Fe^{2+}(Pyr)_4$	5	202.3	199.3	1312.0	186.2	183.2	1474.0
$Fe^{2+}(Pyr)_5$	5	100.7	97.1	1409.1	76.4	72.8	1546.8
$Fe^{2+}(Pyr)_6$	5	78.8	75.4	1484.5	52.6	49.3	1596.1
$Co^{2+}(Pyr)$	4	280.7	278.8	278.8	570.3	568.4	568.4
$Co^{2+}(Pyr)_2$	4	457.9	455.5	734.3	433.2	430.8	999.2
$Co^{2+}(Pyr)_3$	4	370.0	367.4	1101.7	356.1	353.6	1352.8
$Co^{2+}(Pyr)_4$	4	234.5	231.3	1333.0	210.1	206.9	1559.7
$Co^{2+}(Pyr)_5$	4	167.4	163.5	1496.5	120.1	116.3	1676.0
$Co^{2+}(Pyr)_6$	4	94.6	92.1	1588.6	84.7	82.3	1758.3
$Ni^{2+}(Pyr)$	3	301.2	299.3	299.3	672.9	670.9	670.9
$Ni^{2+}(Pyr)_2$	3	486.9	484.4	783.7	458.7	456.1	1127.0
$Ni^{2+}(Pyr)_3$	3	311.9	309.1	1092.8	272.8	270.0	1397.0
$Ni^{2+}(Pyr)_4$	3	193.5	190.3	1283.1	169.5	166.3	1563.3
$Ni^{2+}(Pyr)_5$	3	149.8	149.2	1432.3	138.4	137.7	1701.0
$Ni^{2+}(Pyr)_6$	3	70.4	65.7	1498.0	65.8	61.1	1762.1
$Cu^{2+}(Pyr)$	2	262.5	260.3	260.3	751.9	749.7	749.7
$Cu^{2+}(Pyr)_2$	2	508.5	506.0	766.3	426.2	423.7	1173.4
$Cu^{2+}(Pyr)_3$	2	311.3	308.0	1074.3	313.5	310.2	1483.6
$Cu^{2+}(Pyr)_4$	2	196.2	192.3	1266.6	165.8	161.9	1645.5
$Cu^{2+}(Pyr)_5$	2	102.7	98.7	1365.3	90.4	86.5	1732.0
$Cu^{2+}(Pyr)_6$	2	48.2	44.8	1410.1	44.8	41.4	1773.4
$Zn^{2+}(Pyr)$	1	174.1	172.4	172.4	695.9	694.3	694.3
$Zn^{2+}(Pyr)_2$	1	522.5	519.4	691.8	494.7	491.6	1185.9
$Zn^{2+}(Pyr)_3$	1	297.3	294.7	986.5	259.7	257.1	1443.0
$Zn^{2+}(Pyr)_4$	1	210.9	207.3	1193.8	183.6	180.0	1623.0
$Zn^{2+}(Pyr)_5$	1	68.3	64.0	1257.8	56.4	52.1	1675.1
$Zn^{2+}(Pyr)_6$	1	48.8	43.6	1301.4	48.4	43.3	1718.4

[a]Calculated at the BHandHLYP/6-31G* and the BHandHLYP/6-311+G(2d,2p) level of theory using BHandHLYP/6-31G* including ZPE corrections with frequencies scaled by 0.9472. [b]Also includes BSSE corrections.

Table C.5b. Sequential and Total BDEs of Ground-State $M^{2+}(Pyr)_x$ Complexes at 0 K in kJ/mol.[a]

		M06 Theory					
		6-31G*//6-31G*			6-311+G(2d,2p)// 6-31G*		
Complex	Spin	D_0	$D_{0,BSSE}$[b]	Total[b]	D_0	$D_{0,BSSE}$[b]	Total[b]
$Fe^{2+}(Pyr)$	5	370.4	369.6	369.6	603.1	602.4	602.4
$Fe^{2+}(Pyr)_2$	5	481.9	478.8	848.4	428.5	425.4	1027.8
$Fe^{2+}(Pyr)_3$	5	361.2	357.9	1206.3	332.8	329.6	1357.4
$Fe^{2+}(Pyr)_4$	5	237.0	222.9	1429.2	225.4	211.3	1568.7
$Fe^{2+}(Pyr)_5$	5	133.1	127.7	1556.9	115.9	110.5	1679.2
$Fe^{2+}(Pyr)_6$	5	112.1	106.2	1663.1	98.9	93.1	1772.3
$Co^{2+}(Pyr)$	4	398.1	398.0	398.0	693.6	693.6	693.6
$Co^{2+}(Pyr)_2$	4	497.4	494.6	892.6	471.5	468.6	1162.2
$Co^{2+}(Pyr)_3$	4	332.5	329.1	1221.7	311.0	307.7	1469.9
$Co^{2+}(Pyr)_4$	4	237.6	232.8	1454.5	213.9	209.1	1679.0
$Co^{2+}(Pyr)_5$	4	124.9	118.8	1573.3	113.4	107.3	1786.3
$Co^{2+}(Pyr)_6$	4	86.9	84.0	1657.3	91.4	79.6	1865.9
$Ni^{2+}(Pyr)$	3	461.5	452.7	452.7	825.3	816.6	816.6
$Ni^{2+}(Pyr)_2$	3	483.9	480.9	933.6	413.6	410.5	1227.1
$Ni^{2+}(Pyr)_3$	3	332.1	330.9	1264.5	324.7	320.9	1548.0
$Ni^{2+}(Pyr)_4$	3	198.5	193.3	1457.8	177.1	171.9	1719.9
$Ni^{2+}(Pyr)_5$	3	183.7	177.8	1635.6	172.9	166.9	1886.8
$Ni^{2+}(Pyr)_6$	3	102.0	95.9	1731.5	100.5	94.4	1981.2
$Cu^{2+}(Pyr)$	2	401.0	398.7	398.7	909.1	906.9	906.9
$Cu^{2+}(Pyr)_2$	2	461.3	457.9	856.6	402.9	399.5	1306.4
$Cu^{2+}(Pyr)_3$	2	347.8	343.4	1200.0	293.8	289.4	1595.8
$Cu^{2+}(Pyr)_4$	2	215.2	210.2	1410.2	183.4	178.3	1774.1
$Cu^{2+}(Pyr)_5$	2	132.5	127.0	1537.2	119.0	113.5	1887.6
$Cu^{2+}(Pyr)_6$	2	79.7	75.9	1613.1	75.9	72.2	1959.8
$Zn^{2+}(Pyr)$	1	254.2	252.5	252.5	726.2	724.4	724.4
$Zn^{2+}(Pyr)_2$	1	537.1	532.8	785.3	503.1	498.8	1223.2
$Zn^{2+}(Pyr)_3$	1	310.2	305.2	1090.5	270.3	265.3	1488.5
$Zn^{2+}(Pyr)_4$	1	229.4	225.1	1540.7	202.5	198.3	1686.8
$Zn^{2+}(Pyr)_5$	1	99.0	93.2	1633.9	91.1	85.3	1772.1
$Zn^{2+}(Pyr)_6$	1	87.2	80.9	1714.8	81.7	75.4	1847.5

[a]Calculated at the M06/6-31G* and the M06/6-311+G(2d,2p) level of theory using M06/6-31G* including ZPE corrections with frequencies scaled by 0.9940. [b]Also includes BSSE corrections.

Table C.6a. Enthalpies and Free Energies of Binding of $M^{2+}(Pyr)_x$ Complexes at 298 K in kJ/mol.[a]

Complex	ΔH_{298}-ΔH_0[b]	ΔH_{298}[b]	$\sum \Delta H_{298}$[b]	$T\Delta S_{298}$[b]	ΔG_{298}[b]	$\sum \Delta G_{298}$[b]
$Fe^{2+}(Pyr)$	1.4 (1.5)	568.6	568.6	29.3 (3.3)	539.3	539.3
$Fe^{2+}(Pyr)_2$	–1.8 (1.7)	419.3	987.9	42.2 (8.2)	377.1	916.4
$Fe^{2+}(Pyr)_3$	–2.0 (1.7)	300.5	1288.4	43.7 (8.3)	256.8	1173.2
$Fe^{2+}(Pyr)_4$	–2.0 (1.8)	181.2	1469.6	49.2 (8.2)	132.0	1305.2
$Fe^{2+}(Pyr)_5$	–1.2 (2.1)	71.6	1541.1	57.2 (7.5)	14.4	1319.6
$Fe^{2+}(Pyr)_6$	–2.4 (1.7)	46.9	1588.1	49.2 (8.5)	-2.3	1317.3
$Co^{2+}(Pyr)$	1.5 (1.6)	569.9	569.9	31.4 (3.2)	538.5	538.5
$Co^{2+}(Pyr)_2$	–1.5 (1.8)	429.3	999.2	44.6 (7.9)	384.7	923.2
$Co^{2+}(Pyr)_3$	–2.1 (1.7)	351.5	1350.7	44.8 (8.4)	306.7	1229.9
$Co^{2+}(Pyr)_4$	–1.3 (2.5)	205.6	1556.3	52.7 (7.7)	152.9	1382.8
$Co^{2+}(Pyr)_5$	–1.2 (2.3)	115.1	1671.4	54.0 (7.7)	61.1	1443.9
$Co^{2+}(Pyr)_6$	–2.5 (1.8)	79.8	1751.2	50.1 (8.6)	29.7	1473.6
$Ni^{2+}(Pyr)$	1.5 (1.5)	672.4	672.4	31.3 (3.3)	641.1	641.1
$Ni^{2+}(Pyr)_2$	–1.2 (2.0)	454.9	1127.3	46.6 (7.7)	408.3	1049.4
$Ni^{2+}(Pyr)_3$	–0.7 (2.2)	269.3	1396.6	52.2 (7.4)	217.1	1266.5
$Ni^{2+}(Pyr)_4$	–1.7 (1.9)	164.6	1561.2	49.4 (8.1)	115.2	1381.7
$Ni^{2+}(Pyr)_5$	0.9 (2.4)	138.6	1699.8	56.1 (7.3)	82.5	1464.2
$Ni^{2+}(Pyr)_6$	–2.3 (2.1)	58.8	1758.6	48.6 (8.6)	10.2	1474.4
$Cu^{2+}(Pyr)$	1.4 (1.6)	751.1	751.1	31.4 (3.3)	719.7	719.7
$Cu^{2+}(Pyr)_2$	–1.1 (1.9)	422.6	1173.7	46.3 (7.7)	376.3	1096.0
$Cu^{2+}(Pyr)_3$	–1.2 (2.0)	309.0	1482.7	48.5 (7.8)	260.5	1356.5
$Cu^{2+}(Pyr)_4$	–1.4 (2.1)	160.5	1643.2	50.5 (7.8)	110.0	1466.5
$Cu^{2+}(Pyr)_5$	–1.8 (1.7)	84.7	1727.9	51.9 (7.9)	32.8	1499.3
$Cu^{2+}(Pyr)_6$	–6.2 (1.8)	35.2	1763.1	37.8 (9.7)	–2.6	–
$Zn^{2+}(Pyr)$	1.6 (1.6)	695.9	695.9	31.7 (3.2)	664.2	664.2
$Zn^{2+}(Pyr)_2$	–1.4 (1.9)	490.2	1186.1	45.3 (7.9)	444.9	1109.1
$Zn^{2+}(Pyr)_3$	–1.8 (1.8)	255.3	1441.4	45.9 (8.2)	209.4	1318.5
$Zn^{2+}(Pyr)_4$	–1.5 (2.1)	178.5	1619.9	51.9 (7.9)	126.6	1445.1
$Zn^{2+}(Pyr)_5$	–2.3 (1.8)	49.8	1669.7	47.6 (8.4)	2.2	1447.3
$Zn^{2+}(Pyr)_6$	–2.4 (1.9)	40.9	1710.6	49.4 (4.6)	–8.5	–

[a]Uncertainties are listed in parentheses. [b]Values from calculations at the BHandHLYP/6-311+G(2d,2p) level of theory using BHandHLYP/6-31G* optimized geometries with frequencies scaled by 0.9472.

Table C.6b. Enthalpies and Free Energies of Binding of $M^{2+}(Pyr)_x$ Complexes at 298 K in kJ/mol.[a]

Complex	ΔH_{298}-ΔH_0[b]	ΔH_{298}[b]	$\sum \Delta H_{298}$[b]	$T\Delta S_{298}$[b]	ΔG_{298}[b]	$\sum \Delta G_{298}$[b]
$Fe^{2+}(Pyr)$	1.4 (1.6)	603.8	603.8	31.1 (3.3)	572.7	572.7
$Fe^{2+}(Pyr)_2$	–1.8 (1.7)	423.6	1027.4	44.2 (8.2)	379.4	952.1
$Fe^{2+}(Pyr)_3$	1.0 (2.7)	330.6	1358.0	56.7 (6.3)	273.9	1226.0
$Fe^{2+}(Pyr)_4$	–4.1 (1.2)	207.2	1565.2	41.5 (9.7)	165.7	1391.7
$Fe^{2+}(Pyr)_5$	–5.8 (0.8)	104.7	1669.9	40.9 (10.5)	63.8	1455.5
$Fe^{2+}(Pyr)_6$	–5.8 (0.8)	87.3	1757.2	40.9 (10.5)	46.4	1501.9
$Co^{2+}(Pyr)$	1.6 (1.7)	695.2	695.2	32.0 (3.2)	663.2	663.2
$Co^{2+}(Pyr)_2$	–1.1 (1.9)	467.5	1162.7	45.8 (7.7)	421.7	1084.9
$Co^{2+}(Pyr)_3$	–1.5 (1.9)	306.2	1468.9	49.1 (8.0)	257.1	1342.0
$Co^{2+}(Pyr)_4$	–1.3 (2.1)	207.8	1676.7	52.1 (7.8)	155.7	1497.7
$Co^{2+}(Pyr)_5$	–0.6 (2.5)	106.7	1783.4	56.5 (7.3)	50.2	1547.9
$Co^{2+}(Pyr)_6$	–1.9 (2.1)	77.7	1861.1	53.2 (8.2)	24.5	1572.4
$Ni^{2+}(Pyr)$	0.9 (1.5)	817.5	817.5	30.1 (3.7)	787.4	787.4
$Ni^{2+}(Pyr)_2$	–1.4 (2.1)	409.1	1226.6	44.0 (7.8)	365.1	1152.5
$Ni^{2+}(Pyr)_3$	–0.2 (2.1)	320.7	1547.3	53.5 (7.1)	267.2	1419.7
$Ni^{2+}(Pyr)_4$	–0.5 (2.4)	171.4	1718.7	56.0 (7.2)	115.4	1535.1
$Ni^{2+}(Pyr)_5$	–1.5 (2.2)	165.4	1884.1	52.7 (7.9)	112.7	1647.8
$Ni^{2+}(Pyr)_6$	–0.8 (2.4)	93.6	1977.7	55.7 (7.4)	37.9	1685.7
$Cu^{2+}(Pyr)$	1.5 (1.2)	908.4	908.4	31.6 (3.1)	876.8	876.8
$Cu^{2+}(Pyr)_2$	–1.5 (2.3)	398.0	1306.4	45.1 (8.1)	352.9	1229.7
$Cu^{2+}(Pyr)_3$	–0.4 (2.3)	289.0	1595.4	53.3 (7.2)	235.7	1465.4
$Cu^{2+}(Pyr)_4$	–1.0 (2.1)	177.3	1772.7	52.4 (7.6)	124.9	1590.3
$Cu^{2+}(Pyr)_5$	–1.8 (2.0)	111.7	1884.4	50.7 (8.1)	61.0	1651.3
$Cu^{2+}(Pyr)_6$	–1.1 (1.5)	71.1	1955.5	55.6 (7.4)	15.5	1666.8
$Zn^{2+}(Pyr)$	1.6 (1.7)	726.0	726.0	31.8 (3.2)	694.2	694.2
$Zn^{2+}(Pyr)_2$	–1.4 (1.8)	497.4	1223.4	43.8 (7.9)	453.6	1147.8
$Zn^{2+}(Pyr)_3$	–0.5 (2.4)	264.8	1488.2	55.7 (7.2)	209.1	1356.9
$Zn^{2+}(Pyr)_4$	–1.5 (1.5)	196.8	1685.0	50.9 (7.5)	145.9	1502.8
$Zn^{2+}(Pyr)_5$	–1.6 (1.7)	83.7	1768.7	52.1 (7.8)	31.6	1534.4
$Zn^{2+}(Pyr)_6$	–2.2 (1.9)	73.2	1841.9	47.4 (5.4)	25.8	1560.2

[a]Uncertainties are listed in parentheses. [b]Values from calculations at the M06/6-311+G(2d,2p) level of theory using M06/6-31G* optimized geometries with frequencies scaled by 0.9940.

APPENDIX D

PRELIMINARY ENERGY-RESOLVED COLLISION-INDUCED DISSOCIATION STUDIES OF BIS COMPLEXES OF 1,10-PHENANTHROLINE TO THE LATE FIRST-ROW DIVALENT TRANSITION METAL CATIONS: COMPETITION BETWEEN SIMPLE CID AND COULOMB FISSION PROCESSES

D.1 Introduction

Electron transfer (ET) and proton transfer (PT) reactions are ubiquitous in biological, physical, and chemical processes.[1,2] Photosynthesis and respiration are two very important examples of essential life processes driven by ET reactions.[3] PT plays a fundamental role in stabilizing intermediates in enzymatic reactions, protein folding, signaling processing, and in energy lowering of transition states (TSs) in a wide range of molecular biology reactions.[4,5] The main objective behind studying transition metal cation-*N*-donor ligand complexes is to understand their structures and energetics of binding via their fragmentation pathways and the energetics involved in the ET and PT processes that they undergo. The knowledge derived from this study can be applied to applications relevant to DNA and RNA cleavage studies, solar energy conversion, metal analysis, and luminescent materials.[6-10] Positively charged transition metal complexes generally bind to nucleic acids fairly rapidly as a result of ion-pairing interactions.[11] Binding to DNA can also be enhanced by hydrogen-bonding interactions resulting in covalent and/or noncovalent interactions.[12] These interactions interfere with DNA metabolism through intra- and inter-strand DNA cross-linking by the metal cation, resulting in blockage or lack of recognition by replicating enzymes at the metallated sites, and thereby halting DNA synthesis.[13,14] Chromophoric groups of the transition metal complexes can be used to absorb light of suitable wavelength and induce electronic transitions from the ground to an excited state,[15] which is often facilitated by the

ability of the transition metals to vary their oxidation states.[16] Such transitions involving ligand-to-metal and/or metal-to-ligand charge transfer depend on the nature of the metal center and the ligands, and can be utilized in solar energy conversion, the development of luminescent materials, or oxidative cleavage of biomolecules.[17-20]

A detailed description of the energetics and structural changes during the course of an ET and or PT reaction can be obtained by mapping the potential energy surface for the process. The relevant features of the surface, such as TSs, intermediates, and barrier heights give useful insight into the reaction mechanism. Changes in the geometrical parameters such as bond lengths and angles of the complexes in the excited states relative to their positions in the ground state vary depending on the electron density distribution on the metal orbital(s) accepting electron density from the ligand orbital(s) or vice versa. This is essential for understanding the molecular energetics of ET and or PT processes.[21] Knowledge of the energy barrier (activation energy) of the ET and or PT reactions can be useful in interpreting the rates of chemical and biochemical reactions.[22] Tuning of the electron density of the transition metal complex by varying the valence orbital occupation of the metal cation makes it possible to obtain metal complexes with the desired charge transfer properties. Such information is useful to scientists seeking to understand ET/PT mechanisms in small metal complexes. Such mechanistic information can also be utilized to design more efficient chemical processes or for the exploration of techniques designed to confirm a proposed reaction mechanism.[23]

D.2 Rationale of this work

Appendix D is an extension of the work discussed in Chapter 3. In this work, the mechanisms associated with electron transfer Coulomb fission (ETCF), proton transfer

Coulomb fission (PTCF), and simple collision-induced dissociation (CID) pathways of five $M^{2+}(Phen)_2$ complexes are examined by performing electronic structure theory calculations, whereas the kinetic energy dependence of their CID behavior is examined under conditions where useful (preliminary) information can only be determined for the ETCF and simple CID pathways. Severe overlap in several of the product channels, and incomplete acquisition of the relevant experimental data, prevent useful information regarding the PTCF pathway to be elucidated. Because accurate thermochemical modeling of the experimental data is not possible without including all important CID pathways, these limitations prevent absolute energetic information for all pathways to be extracted from this work. Systematic investigation of the influence of electronic structure of the transition metal cation on the energetics of the ETCF, PTCF, and simple CID fragmentation pathways is investigated by varying the metal cation from $Fe^{2+}(d^6)$ to $Co^{2+}(d^7)$ to $Ni^{2+}(d^8)$ to $Cu^{2+}(d^9)$ to $Zn^{2+}(d^{10})$. The energy-resolved CID processes are analyzed using methods developed previously.[24] We derive preliminary second sequential bond dissociation energies (BDEs) and activation energies (AEs) for ETCF of five $M^{2+}(Phen)_2$ complexes and compare these results to values obtained from density functional theory (DFT) calculations performed here. Periodic trends in the energetics of fragmentation of these complexes are examined and compared to those of the analogous $M^{2+}(Phen)_3$ complexes, previously investigated.[25]

D.3 Collision-Induced Dissociation Experiments

D.3.1 Collision-Induced Dissociation Experiments Using GIBMS

Cross sections for CID of five $M^{2+}(Phen)_2$ complexes with Xe, where $M^{2+} = Fe^{2+}$, Co^{2+}, Ni^{2+}, Cu^{2+}, and Zn^{2+} were measured using a guided ion beam mass spectrometer (GIBMS) that has been described in detail in Chapter 2. The $M^{2+}(Phen)_2$ complexes were

generated using an electrospray ionization (ESI) source under conditions similar to those described in Chapter 2. HPLC grade acetonitrile and deionized water were used to prepare solutions containing concentrations of ~0.01 to 0.1 mM $[M(Phen)_2](PF_6)_2$ in a 1:1 (v/v) acetonitrile-water mixture. Thermochemical analyses of the experimental results are explicitly discussed in Chapter 2. The thermochemistry derived from GIBMS studies involves the determination of reaction thresholds, and therefore experiments are generally intentionally performed under low-resolution conditions to minimize discrimination and thereby enhance the sensitivity and accuracy of the threshold determination. However, for GIBMS results to provide accurate energetic information, all product species must be resolved such that the measured product cross sections are not contaminated by overlap with other reaction pathways. In the work performed here, preliminary CID studies of five $M^{2+}(Phen)_2$ complexes were performed under relatively low-resolution conditions, thereby enabling the absolute magnitudes of the CID cross sections to be determined, but which are of limited thermochemical utility because of the severe overlap in several of the product channels, and because several of the products were not collected under variable pressure conditions such that extrapolation to single collision conditions cannot be achieved. Unresolved products of the ETCF and PTCF pathways and products originating from simple CID pathway are collected.

D.3.2 Collision-Induced Dissociation Experiments Using FT-ICR MS

A Fourier transform ion cyclotron resonance mass spectrometer (FT-ICR MS) was also used to investigate the fragmentation pathways for each of the $M^{2+}(Phen)_2$ complexes as described in Chapter 2. The $M^{2+}(Phen)_2$ complexes were generated using an electrospray ionization (ESI) source under conditions similar to those described in Chapter 2. HPLC

grade acetonitrile and deionized water were used to prepare solutions containing concentrations of ~0.1 μM $[M(Phen)_2](PF_6)_2$ in a 1:1 (v/v) acetonitrile-water mixture. High-resolution FT-ICR MS experiments were pursued to definitely establish the CID pathways available to the $M^{2+}(Phen)_2$ complexes, because the initial low-resolution CID studies using the GIBMS showed the production of the $M^+(Phen)$ and $[Phen+H]^+$ product ions. Based on the simple principles of conservation of mass and charge in the CID processes, the complimentary ions, i.e., $Phen^+$ and $[M(Phen-H)]^+$ ions, respectively, must also be produced. Therefore, CID experiments using high-resolution FTICR-MS were performed to confirm the occurrence of both the ETCF and PTCF processes.

D.4 Theoretical Calculations

Theoretical calculations were performed to determine the structures of the $M^{2+}(Phen)_2$ complexes and to map the dissociation pathways observed upon CID of these complexes including all TSs, intermediates, and products, where $M^{2+} = Fe^{2+}$, Co^{2+}, Ni^{2+}, Cu^{2+}, and Zn^{2+} using the Gaussian 09 suite of programs.[26] The details of the theoretical calculations are given in Chapter 2. The vibrational frequencies and rotational constants determined at B3LYP/6-31G* and scaled by 0.9804 are listed in Tables D.1 and D.2 of Appendix D.[27]

D.5 Experimental Results

D.5.1 Cross Sections for Collision-Induced Dissociation

Preliminary energy-resolved CID studies of five $M^{2+}(Phen)_2$ complexes using GIBMS techniques find that simple CID, ETCF, and PTCF pathways occur in parallel and compete with each other. Simple CID involves the loss of an intact neutral Phen ligand, reactions D.1. ETCF results in the production of the $M^+(Phen)$ and $Phen^+$ ions corresponding to reduction of M^{2+} to M^+ and oxidation of the Phen ligand to a radical cation, $Phen^+$,

respectively, reactions D.2. PTCF results in the formation of the $[M(Phen-H)]^+$ and $[Phen+H]^+$ product ions, corresponding to the transfer of a proton from one Phen ligand to the other Phen ligand facilitating charge fission dissociation, reactions D.3.

$$M^{2+}(Phen)_2 + Xe \rightarrow M^{2+}(Phen) + Phen + Xe \quad (D.1)$$

$$M^{2+}(Phen)_2 + Xe \rightarrow M^{+}(Phen) + Phen^{+} + Xe \quad (D.2)$$

$$M^{2+}(Phen)_2 + Xe \rightarrow [M(Phen-H)]^{+} + [Phen+H]^{+} + Xe \quad (D.3)$$

Under low-resolution conditions, the $M^+(Phen)$ and $[M(Phen-H)]^+$ product ions originating from ETCF and PTCF, respectively, and separated by only 1 Da are found to be severely overlapped, particularly on the low mass size. Similarly, severe overlap of the $Phen^+$ and $[Phen+H]^+$ product ions, also separated by only 1 Da also occurs. Severe overlap of these same product ions was first observed for the $M^{2+}(Phen)_3$ complexes discussed in Chapter 3. However, these species represent sequential dissociation products that were not examined for thermochemistry and thus the severe overlap was not problematic and was thus ignored. However in this Chapter, the main objective is to determine accurate thermochemistry for all three of the primary CID pathways, ETCF, PTCF, and simple CID, which requires that the products associated with these process be resolved and their pressure dependence to be examined. Preliminary experimental CID cross sections obtained under low-resolution conditions for the interaction of Xe with five $M^{2+}(Phen)_2$ complexes, where $M^{2+} = Fe^{2+}$, Co^{2+}, Ni^{2+}, Cu^{2+}, and Zn^{2+} are shown in Figure D.1. Only the $M^+(Phen)$, $[Phen+H]^+$, and $M^{2+}(Phen)$ product cross sections representing the ETCF, PTCF, and simple CID pathways, respectively are displayed. This is because the $M^+(Phen)$ and $[M(Phen-H)]^+$ as well as $Phen^+$ and $[Phen+H]^+$ product ions are not cleanly resolved under the relatively low-resolution conditions under which these experiments were carried out. However the species with the

larger m/z is favored over the one with a smaller m/z as indicated by the larger cross section and lower apparent threshold. The M^+(Phen) and $[Phen+H]^+$ products are least contaminated, and thus are expected to provide a more reliable measure of the energy dependence of the ETCF and PTCF pathways than the complementary product ions, $Phen^+$ and $[M(Phen-H)]^+$, respectively. Because the overlapped products are not separated under low-resolution conditions these experiments will need to be repeated under higher-resolution conditions where all of the products of the primary dissociation pathways, ETCF, PTCF and simple CID are resolved in the future. As can be seen in Figure D.1, the M^{2+}(Phen) product cross sections, reactions D.1, exhibit slightly different shapes and decrease in magnitude across the period from ~1.0 $Å^2$ for Fe^{2+} to ~0.06 $Å^2$ for Zn^{2+}. The apparent thresholds for M^{2+}(Phen) vary between ~6 and 10 eV, increase from Fe^{2+} to Co^{2+} to Ni^{2+} to Cu^{2+}, and then decrease for Zn^{2+}. In comparison, the M^+(Phen) product cross sections, reactions D.2, increase in magnitude across the period from ~5.0 $Å^2$ for Co^{2+} to 5.2 $Å^2$ for Fe^{2+} to 5.5 $Å^2$ for Ni^{2+} to ~6.0 $Å^2$ for Cu^{2+}, and then decrease to ~4.0 $Å^2$ for Zn^{2+}. The apparent thresholds for CID reactions D.2 generally follow the reverse trend, and vary from ~2.5 to 8.3 eV. Similarly, the $[Phen+H]^+$ cross sections, reactions D.3, slightly increase in magnitude from ~0.25 $Å^2$ for Fe^{2+} to ~0.4 $Å^2$ for Cu^{2+}, and then decrease to ~0.18 $Å^2$ for Zn^{2+}, whereas the apparent thresholds follow the reverse order, and vary from ~5.0 to 10.0 $Å^2$.

D.5.2 Product Ions in MS Spectra

The MS spectra of five $M^{2+}(Phen)_2$ complexes where M^{2+} = Fe^{2+}, Co^{2+}, Ni^{2+}, Cu^{2+}, and Zn^{2+} obtained using the FTICR-MS are shown in Figure D.2. Four types of product ions are observed in the fragmentation of the $M^{2+}(Phen)_2$ complexes. The M^{2+}(Phen) product ions arise from loss of a neutral Phen ligand, reactions D.1. The M^+(Phen) and $Phen^+$ product

ions arise from ETCF, reactions D.2. The $[M(Phen–H)]^+$ and $[Phen+H]^+$ product ions arise from PTCF, reactions D.3. Dehydrogenation, reactions D.4, results in loss of a hydrogen molecule from the reactant ion. Sequential dissociation through loss of small neutral losses such as HCN, H, CN, CH_2, and CH_3 from either one or both of the complementary ions of the four major pathways is also observed.

$$M^{2+}(Phen)_2 + Ar \rightarrow [M(Phen)_2–H_2]^{2+} + H_2 + Ar \quad (D.4)$$

Therefore, high-resolution FT-ICR MS results not only confirm the presence of $M^+(Phen)$ and $[M(Phen-H)]^+$ as well as the complimentary $Phen^+$ and $[Phen+H]^+$ products that are separated by 1 Da but also shows that these ions are well separated. In addition, these results also indicated that dehydrogenation is also a minor CID pathway for these systems.

D.6 Theoretical Results

Preliminary theoretical studies are performed using the B3LYP, BHandHLYP, and M06 functionals to compliment the experimental studies. The four major pathways observed upon CID of the $M^{2+}(Phen)_2$ complexes include: simple CID (reactions D.1), ETCF (reactions D.2), PTCF (reactions D.3), and dehydrogenation (reactions D.4). Based on the high resolution FT-ICR MS results, the hydrogen loss pathways are minor. However, even a very small contamination of the reactant $M^{2+}(Phen)$ complexes by these products can influence the threshold determinations, particularly if these pathways are lower in energy than the ETCF, PTCF, and simple CID pathways. The mechanisms associated with the dehydrogenation pathway are not modeled theoretically in the present work. Because we have no idea at this point if the hydrogen loss pathways are higher or lower energy pathways, we would like to point out that these pathways will need to be modeled in the future to accurately elucidate the energetics involved in the dissociation of the $M^{2+}(Phen)_2$ complexes.

In the case of the simple CID pathway, where the TSs are assumed to be loose and product-like because the interactions between the M^{2+}(Phen) complex and the departing Phen ligand are largely electrostatic, the molecular parameters of the products are used for data analysis, and therefore no potential energy surfaces need be mapped as the reactant and products are already computed to extract the sequential BDEs. Because the ETCF and PTCF pathways are activated dissociation pathways, the mechanisms of electron and proton transfer are examined to determine molecular parameters for the rate-limiting TSs to allow appropriate thermochemical analysis of the experimentally measured cross sections. For the ETCF pathways, the only plausible mechanisms we've imagined involves the electron hopping from one of the Phen ligands to the M^{2+}(Phen) moiety as they separate, producing the $Phen^{+}$ and M^{+}(Phen) products. The challenge in mapping this mechanism is associated with the density of the electron that is transferred being delocalized over the dissociating complex until the critical M^{+}(Phen)–$Phen^{+}$ distance is achieved and the electron "hops", as such delocalization is harder to describe with a limited number of basis functions. For the PTCF pathways, the mechanisms mapped involve two proton transfers, the first from one of the Phen ligands to the metal center, and the second from the metal center to the other Phen ligand, followed by dissociation to the products. These PTCF pathways exhibit relatively high barriers such that other mechanisms with lower barriers may exist, such as direct insertion of the proton transferred into the M^{2+}–N bond. Therefore, the mechanisms of electron and proton transfer discussed in the following sections are only preliminary, and calculations at higher levels of theory may be needed for to accurately describe the energetics of the ETCF pathways, whereas additional activated dissociation pathways and higher level calculations may need to be considered for the PTCF pathways in the future.

Theoretical structures for the ground-state reactants, TSs, intermediates, and products of the activated dissociation of the $M^{2+}(Phen)_2$ complexes were calculated as described in section D.4. Further details can be found in Chapter 2. The PES landscapes including both optimized structures and the corresponding relative energies of the species involved in the activated dissociation via the ETCF and PTCF pathways of the $M^{2+}(Phen)_2$ complexes are shown in Figures D.3 and D.4, respectively. Important geometrical parameters of the B3LYP/6-31G* optimized geometries of all relevant species, i.e., the $M^{2+}(Phen)_2$ reactants, TSs, intermediates, and products involved in the dissociation of the $M^{2+}(Phen)_2$ complexes via ETCF and PTCF processes are listed in Tables D.3 and D.4 of Appendix D. Cartesian coordinates for each of these structures are listed in Table D.5 of Appendix D. Relative energies for these species are provided in Tables D.6 and D.7 of Appendix D for the ETCF and PTCF pathways, respectively.

D.6.1 Ground State $M^{2+}(Phen)_2$ Complexes

The ground-state structures and structural details of the $M^{2+}(Phen)_2$ complexes have been reported previously.[25] Briefly, the metal cation binds to the lone pairs of the four nitrogen atoms of the two Phen ligands resulting in a distorted tetrahedral coordination geometry around the metal cation as a result of the structural rigidity of the Phen ligand. The individual Phen ligands are planar with ∠NCCN dihedral angles of 0.0°, and are nearly perpendicular to one another, with an $\angle NM^{2+}NC$ angle of ~81.2° in all of the $M^{2+}(Phen)_2$ complexes, except for $Cu^{2+}(Phen)_2$ where the $\angle NM^{2+}NC$ dihedral angle is 49.0°. This difference in geometry arises as a result of Jahn-Teller distortion by which the copper complex is able to minimize Pauli repulsion between the metal cation and Phen ligands by adopting a geometry that is distorted towards square planar.

D.6.2 Activated Dissociation of $M^{2+}(Phen)_2$ via ETCF

For the ETCF process only one TS that connects the reactants and the products was located for all the five $M^{2+}(Phen)_2$ complexes based on the proposed electron hopping mechanism. Figure D.3 shows the activated dissociation of the $M^{2+}(Phen)_2$ complexes along the ETCF pathways. Also shown in the Figures is the energy barrier for simple CID corresponding to loss of the neutral ligand, which occurs at ~500 kJ/mol at B3LYP theory. This large barrier strongly indicates a low accessibility for this reaction. Table D.3 lists important geometrical parameters for these complexes. As can be seen in Figure D.3d, the proposed mechanism for the dissociation of the $Cu^{2+}(Phen)_2$ reactant to form $Cu^{+}(Phen)$ and $Phen^{+}$ products involves ET from one of the Phen ligands to Cu^{2+} resulting in oxidation of the Phen ligand to the $Phen^{+}$ radical cation, and reduction of Cu^{2+} to Cu^{+} accompanied by an increase in the separation between the ionized Phen ligand and the reduced $Cu^{+}(Phen)$ complex via a TS producing an intermediate (Int). The calculated reaction barrier for this TS is 252.0 kJ/mol at the B3LYP level of theory. The structural changes facilitating this dissociation involve major changes in inter- and intra- $\angle NCu^{2+}N$ bond angles as shown in Table D.3b. The $\angle N1Cu^{2+}N10'C$ dihedral angle changes from 49.0° in the reactant to 59.6° in the TS, and finally to 68.7° in the Int during the ETCF process. The Cu^{2+}–N1′ and Cu^{2+}–N10′ bond lengths undergo significant lengthening from 2.607 and 4.824 Å in the TS to 9.904 and 9.020 Å in the Int, respectively. The TS structure shows that the Cu^{2+} cation is interacting with the other Phen ligand through cation π interactions. Lengthening of the Cu^{2+}–N1′ bond distance of the Int leads to smooth dissociation into the $Cu^{+}(Phen)$ and $Phen^{+}$ products as shown in Figure D.3d. The activated dissociation pathway of the $M^{2+}(Phen)_2$ complexes to Fe^{2+}, Co^{2+}, Ni^{2+}, and Zn^{2+} exhibit similar behavior. In comparison to the

$Cu^{2+}(Phen)_2$ complex, the calculated reaction barriers for ETCF of the other $M^{2+}(Phen)_2$ complexes decreases from Fe^{2+} (373.5) to Co^{2+} (292.7) to Ni^{2+} (267.9) to Cu^{2+} (252.0) and increases for Zn^{2+} (331.5) kJ/mol at the B3LYP level of theory. The energy barriers for loss of a neutral Phen ligand lie above 500 kJ/mol at the B3LYP level of theory, which makes simple CID a minor pathway for all of the $M^{2+}(Phen)_2$ complexes. In comparison to B3LYP, the BHandHLYP and M06 levels of theory produce very similar PES landscapes for all of the $M^{2+}(Phen)_2$ complexes. The ETCF barriers are the largest for BHandHLYP, the lowest for M06, whereas B3LYP theory provides barriers that are intermediate between BHandHLYP and M06.

D.6.3 Activated Dissociation of $M^{2+}(Phen)_2$ Complexes to Fe^{2+}, Ni^{2+}, and Cu^{2+} via PTCF

The PESs for PTCF of the $M^{2+}(Phen)_2$ complexes to Fe^{2+}, Ni^{2+}, and Cu^{2+} exhibit three barriers along the reaction coordinate. Figure D.4d shows the activated dissociation of the $Cu^{2+}(Phen)_2$ along the PTCF pathway. The $Fe^{2+}(Phen)_2$ and $Ni^{2+}(Phen)_2$ complexes exhibit highly parallel behavior and are shown in Figures D.4a and D.4c, respectively. Tables D.4, parts a, c, and d list important geometrical parameters for the relevant species. As can be seen in Figure D.4d, the first step along the reaction coordinate of the $Cu^{2+}(Phen)_2$ complex involves PT from C2 of one Phen ligand to the Cu^{2+} cation via TS_1 to produce Int_1. The reaction barrier for this process (TS_1) is 452.8 kJ/mol at the B3LYP level of theory. The Phen ligands twist relative to each other to facilitate the PT as indicated by the major changes in the inter-ligand $\angle N1Cu^{2+}N10'$ and $\angle N1Cu^{2+}N1'$ bond angles from 103.8° and 149.1° in the reactant, to 149.2° and 123.2° in Int_1, respectively. The resulting Int_1 is less stable than the $Cu^{2+}(Phen)_2$ reactant by 387.5 kJ/mol. The second step involves PT from Cu^{2+} to the N10′ atom of the other Phen ligand via TS_2. The reaction barrier for this process (TS_2) is

400.4 kJ/mol (B3LYP). The third step involves the lengthening of the Cu^{2+}–N1′ bond and twisting of the Phen ligands via TS_3 producing an ion-dipole bound complexes of the $[Cu(Phen\text{-}H)]^+$ and $[Phen+H]^+$ Coulomb fission products. The reaction barrier for this process (TS_3) is 311.3 kJ/mol, relatively lower than both TS_1 and TS_2 by 141.5 and 89.1 kJ/mol, respectively. Further lengthening of the Cu^{2+}–N1′ bond of Int_3 leads to smooth dissociation into the $[Cu(Phen\text{-}H)]^+$ and $[Phen+H]^+$ products. The activated dissociation pathway of $M^{2+}(Phen)_2$ complexes to Fe^{2+} and Ni^{2+} exhibit parallel behavior to that of Cu^{2+}. The calculated reaction barriers for PTCF follow the order Ni^{2+}(417.6) < Cu^{2+}(452.8) < Fe^{2+}(471.8) kJ/mol, at the B3LYP level of theory. In comparison to B3LYP theory, BHandHLYP and M06 theories give very parallel shapes for the PES landscapes of Fe^{2+}, Ni^{2+}, and Cu^{2+}, with M06 providing the lowest energy barriers for PTCF, whereas B3LYP is intermediate, and BHandHLYP the most energetic. All three levels of theory agree that TS_1 is the rate-limiting TS for $Cu^{2+}(Phen)_2$ and $Ni^{2+}(Phen)_2$, whereas TS_2 is the rate-limiting TS for $Fe^{2+}(Phen)_2$. Most significantly the PTCF AE is larger than the enthalpy of dissociation for the $M^{2+}(Phen)_2$ complexes to Fe^{2+}, Ni^{2+}, and Cu^{2+} at all the three levels of theory.

D.6.4 Activated Dissociation of $M^{2+}(Phen)_2$ Complexes to Co^{2+} and Zn^{2+} via PTCF

The PESs for PTCF of the $M^{2+}(Phen)_2$ complexes to Co^{2+} and Zn^{2+} exhibit four barriers along the reaction coordinate. Figure D.4 parts b and e shows the activated dissociation of the $Co^{2+}(Phen)_2$ and $Zn^{2+}(Phen)_2$ complexes along the PTCF pathways. As can be seen in the figures, the observed behavior is very similar. Tables D.4, parts b and e list important geometrical parameters of these complexes. As can be seen in Figure D.4e, the first step along the reaction coordinate of the $Zn^{2+}(Phen)_2$ complex involves PT from C2 to N1 of one of the Phen ligands via TS_1 to produce Int_1. The excess proton is stabilized

between C2 and N1 (TS_1) and the reaction barrier for this process is 444.5 kJ/mol at the B3LYP level of theory. The Phen ligands tilt relative to each other as indicated by slight changes in the ∠N1Zn^{2+}N10′C and inter ∠NZn^{2+}N bond angles, whereas the ∠N1CCN10 dihedral angles change from 0.1° to 11.2° to facilitate the PT. The resulting Int_1 is less stable than the $Zn^{2+}(Phen)_2$ reactant by 366.2 kJ/mol at the B3LYP level of theory. The next step involves the migration of the proton from the N1 position to the Zn^{2+} cation with the proton potentially stabilized between N1 and the Zn^{2+} cation (TS_2). During this proton transfer step, the Phen ligands tilt away from each other as indicated by changes in the ∠N1Zn^{2+}N10′C dihedral angles to accommodate the excess proton. The calculated barrier for this process is 430.9 kJ/mol at the B3LYP level of theory. In the third step, the proton migrates from the Zn^{2+} cation to the N10′ position of the other Phen ligand via TS_3 facilitating PT. The Zn^{2+}–H1 bond distance, the ∠N1Zn^{2+}N10′C dihedral angles, and the ∠NZn^{2+}N bond angles of the Int_2, TS_3, and Int_3 species change significantly (see Table D.4e) to facilitate the PT. The barrier for this process (TS_3) is calculated to be 460.7 kJ/mol at the B3LYP level of theory. The fourth step involves the lengthening of the Zn^{2+}–N1′ bond and twisting of the Phen ligands via TS_4 to form an ion-dipole bound complex of the $[Zn(Phen\text{-}H)]^+$ and $[Phen+H]^+$ Coulombic products. The barrier to this reaction process (TS_4) is 384.0 kJ/mol at the B3LYP level of theory, and relatively lower than that for TS_1, TS_2, and TS_3. As the Zn^{2+}–N1′ bond distance increases, Int_4 smoothly dissociates into the $[Zn(Phen\text{-}H)]^+$ and $[Phen+H]^+$ products without a barrier. The PTCF activated dissociation pathway of $Co^{2+}(Phen)_2$ is highly parallel to that of $Zn^{2+}(Phen)_2$. However, the calculated reaction barrier for PTCF of $Co^{2+}(Phen)_2$ is lower than that of $Zn^{2+}(Phen)_2$ by 14.3 kJ/mol at B3LYP theory. The shapes for the PES landscapes of $Co^{2+}(Phen)_2$ and $Zn^{2+}(Phen)_2$ are highly

parallel for all three levels of theory. In both cases, BHandHLYP predicts the largest barrier to PTCF, M06 the lowest, whereas B3LYP is intermediate. All three theories suggest that TS_1 is the rate-limiting TS for $Co^{2+}(Phen)_2$, whereas TS_3 is the rate-limiting step for $Zn^{2+}(Phen)_2$. Most significantly the PTCF AE is larger than the enthalpy of dissociation for both complexes at all the three levels of theory.

D.7 Threshold Analysis

CID of the $M^{2+}(Phen)_2$ complexes displays a variety of pathways including ETCF, PTCF, simple CID, and dehydrogenation. Under low-resolution conditions the overlapping products of the ETCF and PTCF pathways separated by 1 Da (i.e., $M^+(Phen)$ and $[M(Phen\text{-}H)]^+$ as well as $Phen^+$ and $[Phen+H]^+$) are not resolved. Likewise, the reactants and dehydrogenation products ($M^{2+}(Phen)_2$ and $[M(Phen)_2–H_2]^{2+}$ are not resolved under these conditions. Because of the contamination in the measured product ion intensities and computed product cross sections, the ETCF and PTCF product cross sections do not describe the true energy dependence of the data. However, to extract approximate thresholds and relatively accurate cross sectional magnitudes, the $[M(Phen\text{-}H)]^+$ product cross sections of the PTCF pathway are discarded as they are severely contaminated by the $M^+(Phen)$ product of the ETCF pathway, whereas the $M^+(Phen)$ product cross section is measured relatively cleanly such that they more reliable as they are the least contaminated. Because the $Phen^+$ and $[Phen\text{-}H]^+$ product cross sections were only collected under high pressure conditions, the pressure dependence of these product cross sections cannot be established. In addition, these products are severely overlapped in comparison to the $M^+(Phen)$ and $[M(Phen\text{-}H)]^+$ products, and therefore are not included in preliminary threshold analyses performed here. The dehydrogenation products are not considered in threshold analysis either as they were not

collected in the experiments. Without the inclusion of these pathways in the threshold analyses, the threshold determinations are biased. As a result of these limitations in the data, preliminary threshold analyses are performed for the M^+(Phen) and M^{2+}(Phen) product cross sections, which originate from the ETCF and simple CID pathways, respectively, as discussed below. In the future, threshold analyses of the products of the $M^{2+}(Phen)_2$ complexes examined and collected under higher-resolution conditions must be performed to extract accurate thermochemistry for the dissociation of these $M^{2+}(Phen)_2$ complexes.

The model of equation 2.4 was used to independently analyze the thresholds for the M^{2+}(Phen) and M^+(Phen) product cross sections for all five $M^{2+}(Phen)_2$ complexes. The results of these analyses are provided in Table D.8. Fits to the CID cross sections for the $M^{2+}(Phen)_2$ complexes are shown in Figure D.5. In all cases, the experimental cross sections for the M^{2+}(Phen) simple CID product, are accurately reproduced using a loose PSL TS model.[24] Previous work has shown that this model provides the most accurate assessment of the kinetic shifts for CID processes of electrostatically bound ion-molecule complexes.[24,28] The experimental cross sections for the M^+(Phen) ETCF product are modeled using the molecular parameters of the rate-limiting TSs found along the activated dissociation pathways. Table D.8 also lists threshold values, E_0(TS), obtained without including the RRKM lifetime analysis. Comparison of these values with the E_0(PSL) values shows that the kinetic shifts vary from 4.74−5.69 eV for fits to the M^{2+}(Phen) product cross sections (reactions D.1), whereas the kinetic shifts for the E_0(TTS) thresholds vary from 5.68−8.01 eV for fits to the M^+(Phen) product cross sections (reactions D.2).

For all five $M^{2+}(Phen)_2$ complexes, competition between M^{2+}(Phen) and M^+(Phen) occurs and is expected to influence the threshold determinations. Thus, the cross sections for

these products are analyzed using the model of equation 2.5 (using a loose PSL TS for M^{2+}(Phen) and the molecular parameters of the rate-limiting TS for M^{+}(Phen)), and are shown in Figure D.6. The results of these analyses are provided in Table D.9. The (Phen)M^{2+}–Phen BDEs obtained from competitive fits are smaller than the values obtained from independent fits, as expected, and are a consequence of the competition among these reaction channels. The AEs extracted for the ETCF pathways from competitive fitting is affected very little as compared to the thresholds determined from independent fits to this product cross section as this pathway is lower in energy than simple CID. The (Phen)M^{2+}–Phen BDEs obtained from independent fits are larger than the AEs for ETCF obtained from the independent fits. In contrast, the threshold energies extracted from competitive analyses exhibit quite different energetics. The (Phen)Fe^{2+}–Phen BDE is lower than the ETCF AE by 21.6 kJ/mol for the $Fe^{2+}(Phen)_2$ complex. These results are consistent with the fact that the lowest apparent threshold for dissociation of the $Fe^{2+}(Phen)_2$ complex is observed for simple CID. The (Phen)Co^{2+}–Phen BDE is lower by only 3.8 kJ/mol compared to the AE for ETCF of the $Co^{2+}(Phen)_2$ complex. These values do not differ markedly and are consistent with the fact that the ETCF and simple CID pathways exhibit similar apparent thresholds. The (Phen)M^{2+}–Phen BDEs to Ni^{2+} and Cu^{2+} exceed the AEs for ETCF by 36.6 and 123.8 kJ/mol, respectively. These results are consistent with the fact that the ETCF pathways for the complexes to Ni^{2+} and Cu^{2+} exhibit the lowest apparent thresholds among the observed CID pathways. For the Zn^{2+} complex, the (Phen)M^{2+}–Phen BDEs are lower than the ETCF AEs by 35.7 kJ/mol, consistent with the similar apparent thresholds for these two dissociation pathways. The results from competitive fits suggest that the ETCF and simple CID pathways are highly competitive for the complexes to Co^{2+} and Fe^{2+}, moderately

competitive for the complexes to Ni^{2+} and Zn^{2+}, and weak for the complex to Cu^{2+}. Comparison of the results obtained for the competitive and independent analyses allows the competitive shifts to be preliminarily assessed. The competitive shifts for the $(Phen)M^{2+}$–Phen BDEs vary from 1.16 to 0.26 eV in better accord with expectations. In contrast, the threshold for the ETCF pathways is almost unaffected with the thresholds changing by less than 0.1 eV in all cases.

The entropy of activation, $\Delta S^{\ddagger}$ is a measure of the looseness or tightness of the TS and is also a reflection of the complexity of the system. It is largely determined by the molecular parameters used to model the energized molecule and the TS for dissociation but also depends upon the threshold energy. The $\Delta S^{\ddagger}$(PSL) values at 1000 K for reactions D.1 vary from –97.2 to 122.2 J K^{-1} mol^{-1} whereas the $\Delta S^{\ddagger}$(TS) values at 1000 K for reactions D.2 vary from –11.6 to 9.3 J K^{-1} mol^{-1} (see Tables D.8–D.9).

D.8 Discussion

D.8.1 Comparison between Experiment and the Electronic Structure Calculations

Comparison between experimental and theoretical values extracted from dissociation of the $M^{2+}(Phen)_2$ complexes is one way to test the validity of theoretical methods used. However, the challenges encountered in the study of these complexes limit the reliability of such comparisons. The AEs and the BDEs extracted from the ETCF and simple CID pathways, respectively, are only preliminary and most likely represent upper bounds to the true thresholds. In the case of the ETCF pathways, the M^{+}(Phen) products are slightly contaminated by the $[M(Phen\text{-}H)]^{+}$ products, and therefore the approximate AEs extracted could be too low. Furthermore, the PTCF pathway is ignored during the competitive data analyses, and this may also lead to low threshold values for the ETCF and CID pathways.

The AEs derived for ETCF and PTCF pathways from theoretical methods are also preliminary. Theory suggests that the AEs for PTCF are much higher than for the ETCF pathway, whereas experimental data suggest that PTCF is the lowest energy pathway. Therefore, the PESs mapped out for the PTCF pathway are probably not the correct pathways followed in the reactions at low energies, and alternative lower energy pathways must then be available such that these theoretical results likely represent upper bounds to the true AEs for PTCF of the $M^{2+}(Phen)_2$ complexes. The electron and proton transfer processes deal with open shell systems in terms of the reactants, TSs, intermediates and some of the products. Theoretical methods are not as reliable for describing such species as compared to closed shell species.[29-31] To extract highly reliable energetics from theory, calculations using more advanced theories with much larger basis sets may need to be performed. However, these are not easy systems to calculate at higher levels of theory given the size and therefore number of electrons involved and at present is beyond our capabilities of our computational resources. Hence, without more reliable experimental data, the validity of theoretical results cannot be established. Therefore, experimental and theoretical studies involving the $M^{2+}(Phen)_2$ complexes considered thus far are preliminary, and additional experiments performed under higher-resolution conditions are needed. In addition, other mechanisms for the PTCF activated dissociation pathways must be considered in order to accurately determine the energetics of PTCF of the $M^{2+}(Phen)_2$ complexes. Hence, the comparisons discussed below must be handled with caution due to the limitations discussed above.

BDEs for reactions D.1, simple CID, for all five $M^{2+}(Phen)_2$ complexes including independent ZPE and BSSE corrections are listed in Table D.10. Also listed in Table D.10 are the AEs for reactions D.2, ETCF, and corrected for ZPEs. Table D.11 lists the enthalpic

and entropic corrections needed to convert the 0 K reaction enthalpies to enthalpies and free energies at 298 K. The agreement between theory and the TCID experimental values is illustrated in Figure D.7. The trends in the TCID measured and theoretically calculated AEs for ETCF determined at the M06, B3LYP, and BHandHLYP levels of theory are similar across the series of transition metal cations examined, which decrease from Fe^{2+} to Cu^{2+} and then increase for the complex to Zn^{2+}. (see Figure D.7, part a). The measured AEs for ETCF for the $M^{2+}(Phen)_2$ complexes to Ni^{2+} and Cu^{2+} exhibit very good agreement with M06 theory. In contrast, the values calculated for the complexes to Fe^{2+}, Co^{2+}, and Zn^{2+} differ markedly from the measured values. The mean absolute deviation (MAD) between M06 theory and experiment for all the five complexes is 41.6 ± 41.0 kJ/mol, much larger than the absolute experimental uncertainty (AEU), 8.8 ± 0.8 kJ/mol in these values. When Fe^{2+}, Co^{2+}, and Zn^{2+} complexes are not included the MAD reduces to 5.1 ± 2.7 kJ/mol, slightly smaller than the AEU. The measured AEs for ETCF for all of the $M^{2+}(Phen)_2$ complexes disagree with B3LYP theoretical values with the AEs for ETCF computed for the complexes to Fe^{2+} and Zn^{2+} exhibiting the largest deviations from the measured values. The MAD for all the five complexes is 54.3 ± 35.8 kJ/mol, again much larger than the AEU. This suggests that B3LYP theory overestimates the AEs for ETCF. The AEs for ETCF computed using BHandHLYP theory are systematically higher than values obtained using the M06 and B3LYP theories as shown in Figure D.7. The agreement between BHandHLYP theory and the measured AEs for all of the complexes is very poor suggesting that BHandHLYP theory grossly overestimates the AEs for ETCF in all the five complexes. The MAD between BHandHLYP theory and the TCID measured value is 81.7 ± 31.6 kJ/mol, significantly larger than the AEU. Generally, the MADS for $M^{2+}(Phen)_2$ complexes are very large compared to

the AEUs suggesting that all three levels of theories are not able to describe the ETCF AEs effectively for most of the complexes. This poor agreement may be the result of not including the PTCF pathway in the thermochemical analyses, or may be a result of limitations in the level of the theories employed, or both.

The ionization energy of the Phen ligand is calculated to be 8.05, 7.95, and 8.31 eV at the B3LYP, BHandHLYP, and M06 levels of theory, respectively. Compared to the literature value, 8.51 ± 0.02 eV, theory and experimental IEs are in good agreement.[32] This result further suggests that theory might be having a hard time accurately determining the AEs for ETCF of the $M^{2+}(Phen)_2$ systems because of their large size coupled with the presence of unpaired electrons in the shell d orbitals of the metal cations.

The second sequential $(Phen)M^{2+}$–Phen BDEs theoretically determined using M06, BHandHLYP, and B3LYP levels of theory are systematically higher than the TCID measured values for all of the $M^{2+}(Phen)_2$ complexes (see Figure D.7, part b). M06 theory estimates the strongest BDEs for all of the complexes except $Ni^{2+}(Phen)_2$ and $Cu^{2+}(Phen)_2$. The MAD between M06 theory and TCID experimental results is 284.0 ± 61.9 kJ/mol, much larger than the AEU, 52.7 ± 4.2 kJ/mol. B3LYP theory estimates weaker BDEs as compared to those obtained from BHandHLYP and M06 for the $M^{2+}(Phen)_2$ complexes to Fe^{2+}, Co^{2+}, Cu^{2+}, and Zn^{2+}. The MAD between B3LYP theory and TCID experiment is 260.7 ± 60.2 kJ/mol for all the five complexes, significantly higher than the AEU. BHandHLYP theory provides BDEs that are intermediate between those obtained from B3LYP and M06 theories for the Fe^{2+}, Co^{2+}, and Zn^{2+} complexes, but estimates the lowest BDE for Ni^{2+} complex and the highest BDE for the Cu^{2+} complex. The MAD between BHandHLYP theory and the TCID experimental results is 265.5 ± 56.6 kJ/mol, significantly higher than the AEU. The

large difference between the calculated and the measured BDEs indicates that providing an accurate description of the energetics for the dissociation of the $M^{2+}(Phen)_2$ complexes to produce $M^{2+}(Phen)$ and neutral Phen ligand may still be quite challenging at the B3LYP, BHandHLYP, and M06 levels of theory. However, the lack of consideration of the PTCF pathway during competitive data analyses probably contributes significantly to the lower TCID BDEs.

D.8.2 Energetics of the fragmentation processes of the $M^{2+}(Phen)_2$ complexes

D.8.2.1 ETCF Pathway

Only energetics associated with the ETCF and simple CID pathways are included in this discussion for reasons already addressed in the previous sections. Preliminary results illustrate that the AEs for ETCF of the $M^{2+}(Phen)_2$ complexes decrease from Fe^{2+} to Co^{2+} to Ni^{2+} to Cu^{2+}, and increase for Zn^{2+} (see Figure D.7, part a). These results suggest that ETCF is most favorable for the $Cu^{2+}(Phen)_2$ complex in this series. The ETCF process in the $M^{2+}(Phen)_2$ complexes is controlled by a number of factors including the ionization energies (IEs) of the metals and the Phen ligand, the electron configuration of the metal cation, and the ionic radii of the metal cation. The difference between the second IE of the metal and the first IE of the Phen ligand is found to be the critical parameter controlling the ETCF process in this study. As pointed out in previous studies,[33,34] ET from a ligand to a metal upon CID occurs only if IE of the ligand is lower than the second IE of the metal specie. Therefore, ET is energetically accessible to all $M^{2+}(Phen)_2$ complexes as IE (Fe^+) = 16.19, IE (Co^+) = 17.08, IE (Ni^+) = 18.17, IE (Cu^+) = 20.29, IE (Zn^+) = 17.96 eV, and IE (Phen) = 8.51 eV, in better accord with expectations.[32] Because the IE of Phen is lower than the IE of Xe (12.13 eV), ET from the neutral reactant (Xe) is not observed as confirmed by the absence of a signal for

the Xe radical cation at m/z 132.0. In this case, the Phen ligand is the sole source of electrons for the reduction process. The magnitude of the difference between the second IE of the metal specie and the first IE of the Phen ligand varies from complex to complex, i.e., 7.68, 8.57, 9.66, 11.78, and 9.45 eV for $M^{2+}(Phen)_2$ complexes to Fe^{2+}, Co^{2+}, Ni^{2+}, Cu^{2+}, and Zn^{2+}, respectively. A larger difference should result in a lower energy barrier in accordance with the data presented here. The electronic configuration of the metal cation also controls the ETCF process. The Cu^{2+} cation in the $Cu^{2+}(Phen)_2$ complex has an electron configuration of $3d^9$ and favors reduction of Cu^{2+} to Cu^+ ($3d^{10}$) in the $Cu^+(Phen)$ complex, which forms a closed d shell system in the ET process. For Fe^{2+} ($3d^6$), Co^{2+} ($3d^7$), and Ni^{2+} ($3d^8$) cations, their outmost orbitals are neither half nor completely occupied. For Co^{2+} and Ni^{2+} complexes, adoption of an electron into the outermost orbital of these metal cations would lead to ground state electronic configurations of $3d^n$ (n = 8 and 9, respectively). The $3d^n$ configurations of these metal cations provide attractive bonding interactions between the 3d orbitals and the Phen ligand in the ET process. The ground state of Fe^+ is $3d^64s^1$, such that the 4s orbital should be occupied by the incoming electron, which makes ET unfavorable, and hence this complex exhibits a higher energy barrier. The Zn^{2+} metal cation has a valence electronic configuration of $3d^{10}4s^0$ in the $Zn^{2+}(Phen)_2$ complex. The outmost orbital is relatively stable (fully occupied). Because of its full d shell, trapping of an electron in the 3d orbital is not possible. If ET occurs, the incoming electron must occupy the 4s orbital, which lies slightly higher in energy. The corresponding ground state electronic configuration for Zn^{2+} after ET is $3d^{10}4s^1$. Occupation of the 4s orbital results in an increase in Pauli repulsion between the metal cation and the coordinated Phen ligand weakening attractive binding interactions. The ET processes of the $M^{2+}(Phen)_2$ complexes are also correlated with the

ionic radii of the metal cation. The AEs for ETCF of the $M^{2+}(Phen)^2$ complexes decrease slightly from Fe^{2+} to Co^{2+} to Ni^{2+} to Cu^{2+}, and increase for Zn^{2+}. The order coincides with the decreasing order of ionic radii: 0.76, 0.74, 0.73, and 0.72 Å for Fe^{2+}, Co^{2+}, Ni^{2+}, and Cu^{2+}, respectively. The decrease in ionic radii across the series increases the electrostatic bonding allowing for a better approach between the Phen ligand and the metal cation, and thus favoring the ET process. Zn^{2+} with an ionic radius of 0.72 Å deviates from this trend due to an increase in Pauli repulsion between the metal cation and coordinated Phen ligand as its 4s orbital is occupied upon acceptance of the electron from the ligand.

D.8.2.2 Simple CID Pathway

The TCID measured (Phen)M^{2+}–Phen BDEs increase from Fe^{2+} to Co^{2+} to Ni^{2+} to Cu^{2+}, and decrease for Zn^{2+} (see Figure D.7, part b). There is a clear inverse relationship between the ionic size and the BDEs of these metal complexes. This trend reflects the increasing effective charge of the metal cation as the size of the metal cation decreases, increasing the strength of the electrostatic interactions between the metal cation and Phen ligands. It is seen that the trends in the computed BDEs using three different theories and the TCID measured values are not consistent and the possible causes for these are not straightforward to assess. Clearly more reliable experimental and theoretical data is needed to elucidate the energetics associated with fragmentation of the $M^{2+}(Phen)_2$ complexes.

D.8.3 Comparison between the $M^{2+}(Phen)_x$, x = 1–3 complexes

Preliminary CID studies of the $M^{2+}(Phen)_2$ complexes show that three distinctive processes, i.e. ETCF, PTCF, and simple CID occur in parallel and compete with each other as the predominant dissociation processes. In contrast, the $M^{2+}(Phen)_3$ complexes are observed to dissociate by the extrusion of a neutral Phen ligand as the dominant dissociation

pathway.[25] The change in preference for the dissociation process observed in the $M^{2+}(Phen)_3$ complexes is directly linked to the number of ligands attached to the metal cation. The attachment of three Phen ligands to the M^{2+} cation renders neutral ligand loss more favorable than charge transfer reactions because there are sufficient Phen ligands to stabilize the doubly-charged complex, with the result that charge transfer is suppressed and the complex does not break up due to Coulomb explosion. In contrast, when an insufficient number of ligands are bound to the M^{2+} cation, Coulomb fission processes become more likely to occur than loss of a neutral Phen ligand in the dissociation of the $M^{2+}(Phen)_2$ complexes. The threshold dissociation energies of the primary dissociation pathway, simple CID of the $M^{2+}(Phen)_3$ complexes are weakly dependent on the metal cation, whereas those for simple CID of the $M^{2+}(Phen)_2$ complexes are strongly dependent on the metal cation. Apparently, the thresholds for dissociation via simple CID of $M^{2+}(Phen)_2$ (218.8−352.4 kJ/mol) and $M^{2+}(Phen)_3$ (159.6−236.5 kJ/mol) are sufficiently different from each other when comparing analogous complexes and suggest that the $M^{2+}(Phen)_2$ complexes bind more strongly as compared to the $M^{2+}(Phen)_3$ complexes.

Substantial ion intensities of the $M^{2+}(Phen)$ complexes could not be generated by adjusting the ESI conditions. This is not surprising as the $M^{2+}(Phen)$ complexes are expected to be very reactive. The calculated BDEs of the $M^{2+}(Phen)$ exceed 900 kJ/mol, much larger than a typical C−C bond (~400 kJ/mol). These complexes likely undergo spontaneous charge fission dissociation and thus are not expected to be formed other than transiently in the ESI process. Generally, the $M^{2+}(Phen)_x$ complexes become more stable as the number of Phen ligands attached to the metal center increases and completely occupy the first coordination sphere of the metal cation. Therefore, the coordination number of an

$M^{2+}(Phen)_x$ complexes to exist as stable species, $x_{min} = 2$. Furthermore, x_{crit}, which is the maximum number of Phen ligands at which dissociative charge transfer through ET/PT competes with neutral ligand loss, $x_{crit} = 2$ for $M^{2+}(Phen)_x$ complexes in accordance with the energy-dependent definition of critical size.[35]

D.9 Conclusions

The conclusions derived in this Appendix are based on results obtained from preliminary analyses of the CID cross sections for the ETCF and simple CID pathways, and ignoring the PTCF pathway of the $M^{2+}(Phen)_2$ complexes because of severe overlap of the products under the conditions in which the experiments were performed. Investigation into other plausible mechanisms for the activated dissociation via PTCF is expected to provide more information on the correct TSs of the $M^{2+}(Phen)_2$ complexes and eventually lead to AEs that agree much better with experimentally determined values. Furthermore, experimental studies of the $M^{2+}(Phen)_2$ complexes under higher resolution conditions are needed to extract accurate thermochemistry for the ETCF, PTCF, and CID pathways. Based on the analysis of the ETCF and simple CID pathways only, results from competitive analyses provide the correct lowest energy dissociation pathways for all of the $M^{2+}(Phen)_2$ complexes. However, theoretical methods employed i.e., B3LYP, BHandHLYP, and M06 do not predict similar patterns for the $M^{2+}(Phen)_2$ complexes to Fe^{2+}, Co^{2+}, and Zn^{2+}. The measured BDEs exhibit poor agreement with theoretical values derived from all three levels of theory, whereas theory overestimates the AEs for ETCF for most of the $M^{2+}(Phen)_2$ complexes. Because of the limitations in the experimental data evaluation of the strengths and limitations of the theoretical methods employed here is impossible at this point.

Therefore, further experimental and theoretical studies of the $M^{2+}(Phen)_2$ systems are needed to confidently interpret the CID cross sections and provide reliable reaction thermochemistry.

D.10 References

(1) Stubbe, J.; van der Donk, W. A. *Chem. Rev*. **1998**, *98*, 705.

(2) Moser, C. C.; Page, C. C.; Dutton, P. L. *Phil. Trans. Royal. Soc. B*. **2006**, *361*, 1295.

(3) Sun, L.; Hammarstrom, L.; Akermark, B.; Styring, S. *Chem. Soc. Rev*. **2001**, *30*, 36.

(4) Cleland, W. W.; Kreevoy, M. M. *Science*. **1994**, *264*, 1887.

(5) Borgstahl, G. E.; Williams, D. R.; Getzoff, E. D. *Biochemistry*. **1995**, *34*, 6278.

(6) Meyer, T. J. *Acc. Chem. Res*. **1989**, *22*, 163.

(7) Bard, A. J.; Fox, M. A. *Acc. Chem. Res*. **1995**, *28*, 141.

(8) Dandliker, P. J.; Holmlin, R. E.; Barton, J. K. *Science*. **1997**, *257*, 1465.

(9) Balzani, V. Electron Transfer in Chemistry: Principles, Theories, Methods, and Techniques, Wiley-VCH, Weinheim, 2001, pp. 238.

(10) Barton, J. K. Bioinorganic Chemistry, Bertini, I.; Gray, H.; Lippard, S. J.; Valentine, J. S (Ed), University Science Books, Mill Valley, CA, 1994, pp. 455–504.

(11) Emerson, J.; Clarke, M. J.; Ying, W. L.; Sanadi, D. R. *J. Am. Chem. Soc*. **1993**, *115*, 11799.

(12) Grover, N.; Welch, T. W.; Fairley, T. A.; Cory, M.; Thorp, H. H. *Inorg. Chem.* **1994**, *33*, 3544.

(13) Yasbin, R. E.; Mathews, C. R.; Clarke, M. J. *Chem. Biol. Interact*. **1980**, *31*, 355.

(14) Marx, K. A.; Kruger, R.; Clarke, Clarke. *Mol. Cell. Biochem.* **1989**, *86*, 155.

(15) Clarke, M. J.; Bitler, S.; Rennert, D.; Buchbinder, M.; Kelman, A. D. *J. Inorg. Biochem*. **1980**, *12*, 79.

(16) Cheng, C. C.; Goll, J. G.; Neyhart, G. A.; Welch, T. W.; Singh, P.; Thorp, H. H. *J. Am. Chem. Soc.* **1995**, *117*, 2970.

(17) Clarke, M. J. Metal Complexes in Cancer Chemotherapy, Keppler, B. K. (Ed), VCH, Weinheim, 1993, pp. 129−157.

(18) Isied, S. S. (Ed), Electron Transfer Reactions: Inorganic, Organic, Organometallic, and Biological Applications, Advances in Chemistry Series 253, American Chemical Society, Washington DC, pp. 349−397.

(19) Tsushima, M.; Ikeda, N.; Yoshimura, A.; Nozaki, K.; Ohno, T. *Coord. Chem. Rev*. **2000**, *208*, 299.

(20) Baranovski, V. I.; Lubimova, O. O.; Makarov, A. A.; Sizova, O.O. *Chem. Phys. Lett*. **2002**, *361*, 196.

(21) Lincoln, P.; Tuite, E.; Norden, B. *J. Am. Chem. Soc*. **1997**, *119*, 1454.

(22) Olson, E. J. C.; Hu, D.; Hoermann, A.; Barbara, P. F. *J. Phys. Chem. B*. **1997**, *101*, 299.

(23) Meade, T.; Thomas,J.; Kayyem, J. F. *Angew. Chem. Int. Ed. Eng*. **1995**, *34*, 352.

(24) Rodgers, M. T.; Ervin, K.M.; Armentrout, P. B.; *J. Chem. Phys*. **1997**, *106*, 4499.

(25) Nose, H.; Chen, Y.; Rodgers, M. T. *J. Phys. Chem. A*. **2013**, *117*, 4316.

(26) Frisch, M. J.; Trucks, G. W.; Schlegel, H. B.; Scuseria, G. E.; Robb, M. A.; Cheeseman, J. R.; Scalmani, G.; Barone, V.; Mennucci, B.; Petersson, G. A.; Nakatsuji, H.; Caricato, M.; Li, X.; Hratchian, H. P.; Izmaylov, A. F.; Bloino, J.; Zheng, G.; Sonnenberg, J. L.; Hada, M.; Ehara, M.; Toyota, K.; Fukuda, R.; Hasegawa, J.; Ishida, M.; Nakajima, T.; Honda, Y.;

Kitao, O.; Nakai, H.; Vreven, T.; Montgomery, J. A, Jr.; Peralta, J. E.; Ogliaro, F.; Bearpark, M.; Heyd, J. J.; Brothers, E.; Kudin, K. N.; Staroverov, V. N.; Kobayashi, R.; Normand, J.; Raghavachari, K.; Rendell, A.; Burant, J. C.; Iyengar, S. S.; Tomasi, J.; Cossi, M.; Rega, N.; Millam, J. M.; Klene, M.; Knox, J. E.; Cross, J. B.; Bakken, V.; Adamo, C.; Jaramillo, J.; Gomperts, R.; Stratmann, R. E.; Yazyev, O.; Austin, A. J.; Cammi, R.; Pomelli, C.; Ochterski, J. W.; Martin, R. L.; Morokuma, K.; Zakrzewski, V. G.; Voth, G. A.; Salvador, P.; Dannenberg, J. J.; Dapprich, S.; Daniels, A. D.; Farkas, O.; Foresman, J. B.; Ortiz, J. V.; Cioslowski, J.; Fox, D. J. Gaussian, Inc., Wallingford, CT, 2009.

(27) Foresman, J. B.; Frisch, A. E. Exploring Chemistry with Electronic Structure Methods, 2nd ed, Gaussian, Pittsburgh, PA, 1996, pp. 64.

(28) Rodgers, M. T. *J. Phys. Chem. A* **2001**, *105*, 2374.

(29) Jacob, C. R.; Reiher, M. *Int. J. Quantum Chem.* **2012**, *112*, 3661.

(30) Goodpaster, J. D.; Barnes, T. A.; Manby, F. R.; Miler, T. F. *J. Chem. Phys.* **2012**, *137*, 224113.

(31) Schmidt, J. R.; Shenvi, N.; Tully, J. C. *J. Chem. Phys.* **2008**, *129*, 114110.

(32) Sansonetti, J. E.; Martin, W. C.; Young, S. L. *J. Phys. Chem. Ref. Data.* **2005**, *34*, 1559.

(33) Marcus, R. A.; Eyring, H. *Ann. Rev. Phys. Chem*. **1964**, *15*, 155.

(34) Ryden, J.; Oberg, S. *J. Am. Soc. Mass Spectrom*. **2011**, *22*, 2276.

(35) Cooper, T. E.; Armentrout, P. B. *J. Phys. Chem. A*. **2009**, *113*, 13742.

Table D.1a. Vibrational Frequencies and Average Vibrational Energies of $M^{2+}(Phen)_2$ Reactants and Products Involved in the Dissociation of $M^{2+}(Phen)_2$ Complexes through Simple CID Process at 298 K.

Species	E_{vib} (eV)[a]	Vibrational frequencies (cm^{-1}) [b]
$Fe^{2+}(Phen)_2$ Reactant	0.56 (0.06)	18, 26(2), 75(2), 124, 138, 140, 141(2), 232(2), 237(2), 248, 249, 267, 282, 291, 407(2), 425, 435(3), 475(2), 508(2), 510(2), 538, 539, 556, 558, 606, 607, 651(2), 719(2), 724(2), 730, 731, 781(2), 792, 794, 821, 822, 857(2), 869, 871, 904(2), 955(2), 958(2), 984(2), 1005(2), 1009(2), 1033(2), 1070(2), 1099(2), 1111, 1112, 1160(2), 1169(2), 1218, 1220, 1224, 1225, 1232(2), 1267(2), 1331, 1333, 1335(2) 1349, 1351, 1423, 1424, 1426 (2), 1440(2), 1463(2), 1508(2), 1536, 1537, 1594(2), 1603(2), 1613(2), 1638, 1639, 3151(2), 3152(4), 1349, 1351, 1423, 1424, 1426(2), 1440(2), 1463(2), 1508(2), 1536, 1537, 1594(2), 1603(2), 1613(2), 1638, 1639, 3151(2), 3152(4), 3155, 3156(3), 3164(2), 3180 (4)
$Fe^{2+}(Phen)$ Product 1	0.26 (0.03)	71, 137, 142, 229, 239, 244, 280, 293, 399, 424, 437, 467, 500, 507, 522, 558, 598, 658, 701, 724, 729, 762, 784, 819, 858, 873, 904, 958, 962, 991, 1015, 1018, 1023, 1078, 1104, 1105, 1165, 1174, 1214, 1225, 1228, 1261, 1324, 1335, 1342, 1411, 1417, 1440, 1454, 1503, 1529, 1580, 1594, 1600, 1631, 3157, 3158, 3159, 3164 (2), 3169, 3183 (2)
Phen Product 2	0.22 (0.03)	98, 108, 233, 235, 238, 402, 405, 434, 457, 497, 509, 550, 554, 603, 618, 702, 725, 739, 763, 801, 833, 844, 852, 879, 943, 946, 955, 971, 975, 1032, 1044, 1076, 1098, 1144, 1154, 1206, 1215, 1229, 1279, 1309, 1332, 1364, 1400, 1430, 1436, 1465, 1515, 1520, 1572, 1616, 1629, 1639, 3099 (2), 3115, 3123 (2), 3133, 3150 (2)
$Co^{2+}(Phen)_2$ Reactant	0.56 (0.06)	18, 28(2), 77(2), 126, 139, 146(3), 231(2), 248, 251(2), 254, 287(2), 309, 404, 411, 427, 437(2), 438, 477(2), 508(2), 509(2), 539, 540, 557, 559, 604, 608, 651(2), 717(2), 724(2), 733, 735, 780(2), 793, 795, 821, 822, 856(2), 871, 873, 907(2), 953(2), 955(2), 984(2), 1004(2), 1008(2), 1033(2), 1069, 1070, 1099(2), 1113, 1114, 1161(2), 1169(2), 1219, 1220, 1225, 1226, 1233(2), 1267(2), 1335(2), 1337(2), 1350, 1351, 1426(2),1427, 1428, 1440(2), 1464(2), 1508(2), 1537, 1538, 1597(2), 1604(2), 1614(2), 1639(2), 3151(2), 3154(4), 3157(4), 3164(2), 3180(4)

Table D.1a. (continued) Vibrational Frequencies and Average Vibrational Energies of $M^{2+}(Phen)_2$ Reactants and Products Involved in the Dissociation of $M^{2+}(Phen)_2$ Complexes through Simple CID Process at 298 K.

Species	E_{vib} (eV)[a]	Vibrational frequencies (cm^{-1}) [b]
Co^{2+}(Phen) Product 1	0.26 (0.03)	79, 143, 147, 231, 247, 266, 267, 295, 402, 427, 440, 472, 503, 506, 522, 559, 600, 657, 702, 723, 737, 765, 784, 819, 857, 876, 908, 961, 964, 991, 1015, 1018, 1025, 1076, 1101, 1107, 1164, 1173, 1219, 1226, 1228, 1255, 1328, 1335, 1349, 1416, 1423, 1441, 1454, 1500, 1529, 1578, 1588, 1597, 1629, 3157, 3158, 3159, 3164 (2), 3169, 3182 (2)
$Ni^{2+}(Phen)_2$ Reactant	0.55 (0.06)	14, 33(2), 88(2), 135, 146, 147, 166(2), 232(2), 251, 253, 263(2), 284, 294, 326, 408, 411, 429, 439, 445(2), 486(2), 507(2), 516(2), 539, 540, 558, 560, 604, 606, 655(2), 718(2), 723(2), 739(2), 781(2), 795, 798, 823, 824, 856(2), 873(2), 911(2), 953(2), 956(2), 983(2), 1004(2), 1008(2), 1034(2), 1067, 1068, 1097(2), 1114, 1116, 1161(2),1168(2), 1221, 1222, 1227, 1229, 1233(2),1264(2), 1338(2), 1341(2), 1351, 1353, 1426(2), 1435(2), 1441(2), 1466(2), 1506(2), 1537, 1538, 1597(2), 1603(2), 1614(2), 1639(2), 3152(2), 3154(4), 3157(4), 3164(2), 3180(4)
Ni^{2+}(Phen) Product 1	0.26 (0.03)	81, 144, 152, 231, 247, 276, 281, 298, 402, 425, 442, 475, 502, 505 (2), 561, 587, 660, 693, 723, 733, 737, 781, 814, 853, 880, 916, 957, 960, 990, 1014, 1017, 1023, 1073, 1099, 1107, 1166, 1173, 1220, 1227, 1229, 1255, 1323, 1338, 1353, 1417, 1426, 1440, 1456, 1499, 1524, 1574, 1584, 1593, 1630, 3157, 3159 (2), 3165 (2), 3169, 3182 (2)
$Cu^{2+}(Phen)_2$ Reactant	0.55 (0.06)	27, 39(2), 90(2), 140, 141, 145, 159, 168, 196, 233, 238, 251, 261, 273, 281, 299, 318, 409, 415, 430, 435, 440, 445, 480, 488, 507, 508, 511, 513, 539, 543, 560(2), 603, 607, 648, 653, 719, 720, 722, 723, 738, 741, 781, 783, 792, 794, 822, 825, 856, 857, 874, 875, 907, 913, 954, 957, 961, 964, 984(2), 1004, 1005, 1008(2), 1033, 1034, 1067, 1069, 1096, 1098, 1115, 1118, 1160, 1161, 1168(2), 1222, 1223, 1226, 1229, 1233, 1235, 1263, 1266, 1339(2), 1341, 1342, 1350, 1354, 1426(2), 1435(2), 1440, 1442, 1465, 1467, 1507(2), 1537, 1538, 1597(2), 1603, 1604, 1613, 1614, 1639(2), 3153(2), 3156(4), 3160(2), 3162(2), 3165(2), 3180(4)

Table D.1a. (continued) Vibrational Frequencies and Average Vibrational Energies of $M^{2+}(Phen)_2$ Reactants and Products Involved in the Dissociation of $M^{2+}(Phen)_2$ Complexes through Simple CID Process at 298 K.

Species	E_{vib} (eV)[a]	Vibrational frequencies (cm^{-1}) [b]
Cu^{2+}(Phen) Product 1	0.27 (0.03)	72, 142, 146, 215, 227, 267, 271, 273, 300, 425, 432, 444, 478, 497, 504, 510, 562, 656, 681, 721, 727, 745, 759, 799, 834, 880, 915, 948, 950, 973, 1009, 1014, 1020, 1071, 1096, 1116, 1164, 1172, 1223, 1224, 1231, 1257, 1332, 1343, 1351, 1416, 1429, 1437, 1457, 1497, 1518, 1574, 1592, 1595, 1632, 3156, 3158 (2), 3161 (2), 3168, 3180 (2)
$Zn^{2+}(Phen)_2$ Reactant	0.55 (0.06)	24, 27(2), 81(2), 129, 141, 147, 151, 152, 222(2), 233(2), 250, 256, 279, 294, 301, 406, 412, 428, 434, 441(2), 478(2), 509(2), 511(2), 543, 544, 559, 560, 607, 610, 652(2), 724(2), 725(2), 733, 735, 782(2), 804, 806, 829, 831, 859(2), 872, 873, 909(2), 958(2), 961(2), 985(2), 1006(2), 1010(2), 1035(2), 1072, 1073, 1101(2), 1115, 1117, 1162(2), 1169(2), 1220(2), 1227, 1229, 1235(2), 1270(2), 1335(2), 1340(2), 1353, 1355, 1426(2), 1430(2), 1442(2), 1464, 1465, 1509(2), 1538, 1540, 1600(2), 1606(2), 1616(2), 1639(2), 3151(2), 3155(4), 3159(4), 3164(2), 3180(4)
Zn^{2+}(Phen) Product 1	0.26 (0.03)	80, 138, 154, 232, 244, 245, 288, 308, 398, 430, 439, 468, 496, 507, 515, 562, 595, 658, 699, 724, 731, 748, 785, 817, 860, 873, 912, 963, 967, 992, 1017, 1019, 1022, 1081, 1105, 1106, 1167, 1174, 1214, 1225, 1230, 1265, 1333, 1335, 1346, 1411, 1419, 1442, 1453, 1504, 1527, 1583, 1596, 1603, 1630, 3157, 3159, 3160, 3169, 3175 (2), 3185 (2)

[a]Uncertainties listed in parentheses are determined as described in the text. [b]Vibrational frequencies scaled by 0.9804 obtained from vibrational analyses of the B3LYP/6-31G* geometry optimized structures. Degeneracies are indicated in parentheses.

Table D.1b. Vibrational Frequencies and Average Vibrational Energies of $M^{2+}(Phen)_2$ Reactants, Transition States, Intermediates, and Products Involved in the Activated Dissociation of $M^{2+}(Phen)_2$ Complexes through ETCF Process at 298 K.

Species	E_{vib} (eV)[a]	Vibrational frequencies (cm^{-1}) [b]
$Fe^{2+}(Phen)_2$ Reactant	0.56 (0.06)	18, 26(2), 75(2), 124, 138, 140, 141(2), 232(2), 237(2), 248, 249, 267, 282, 291, 407(2), 425, 435(3), 475(2), 508(2), 510(2), 538, 539, 556, 558, 606, 607, 651(2), 719(2), 724(2), 730, 731, 781(2), 792, 794, 821, 822, 857(2), 869, 871, 904(2), 955(2), 958(2), 984(2), 1005(2), 1009(2), 1033(2), 1070(2), 1099(2), 1111, 1112, 1160(2), 1169(2), 1218, 1220, 1224, 1225, 1232(2), 1267(2), 1331, 1333, 1335(2) 1349, 1351, 1423, 1424, 1426 (2), 1440(2), 1463(2), 1508(2), 1536, 1537, 1594(2), 1603(2), 1613(2), 1638, 1639, 3151(2), 3152(4), 1349, 1351, 1423, 1424, 1426(2), 1440(2), 1463(2), 1508(2), 1536, 1537, 1594(2), 1603(2), 1613(2), 1638, 1639, 3151(2), 3152(4), 3155, 3156(3), 3164(2), 3180 (4)
$Fe^{2+}(Phen)_2$ TS	0.55 (0.06)	**-64**, 15, 22, 40, 54, 86, 96, 112, 141, 149, 172, 212, 217, 232, 238, 245, 254, 286, 297, 390, 403(2), 414, 432, 433, 457, 477, 486, 505, 506, 508, 535, 536, 544, 557, 585, 602, 605, 651, 688, 694, 712, 718, 723, 734, 781, 782, 787, 789, 821, 828, 847, 858(2), 870, 873, 904, 950, 952, 968, 974, 976, 986, 989, 1006, 1010(2), 1024, 1030, 1039, 1070, 1073, 1090, 1100, 1114, 1146, 1161, 1162, 1169, 1203, 1219, 1224, 1227, 1233, 1234, 1266(2), 1300, 1326, 1332, 1337, 1345, 1353, 1391, 1420, 1427(2), 1428, 1441, 1450, 1463, 1487, 1500, 1506, 1538, 1552, 1560, 1594, 1602, 1607, 1613, 1616, 1637, 3141, 3145, 3146, 3148(2), 3152, 3153, 3154, 3156, 3157, 3159, 3165, 3170, 3174, 3180, 3181

Table D.1b. (continued) Vibrational Frequencies and Average Vibrational Energies of $M^{2+}(Phen)_2$ Reactants, Transition States, Intermediates, and Products Involved in the Activated Dissociation of $M^{2+}(Phen)_2$ Complexes through ETCF Process at 298 K.

Species	E_{vib} (eV)[a]	Vibrational frequencies (cm^{-1}) [b]
$Fe^{2+}(Phen)_2$ Int	0.60 (0.06)	2, 7, 9, 12, 13, 17, 72, 99, 100, 134, 140, 222, 224, 231, 232, 234, 245, 251, 281, 381, 401, 404, 421, 432, 433, 440, 447, 450, 467, 503, 507, 510, 531(2), 546, 558, 604, 607, 654, 697, 716, 722, 723, 725, 729, 769, 773, 777, 781, 819, 823, 849, 857, 858, 869, 872, 906, 956, 957, 960(2), 962, 985, 989, 993, 1006, 1010, 1025, 1030, 1048, 1073, 1078, 1101, 1102, 1108, 1141, 1152, 1161, 1170, 1204, 1213, 1222, 1231, 1237, 1245, 1261, 1268, 1316, 1328, 1331, 1333, 1337, 1345, 1393, 1416, 1417, 1423, 1440, 1443, 1445, 1459, 1505, 1509(2), 1532, 1533, 1584, 1589, 1593, 1595, 1605, 1613, 1638, 3125, 3128, 3140, 3145, 3146, 3152, 3153, 3155(2), 3160(2), 3165, 3169, 3170, 3181, 3182
$Fe^{+}(Phen)$ Product 1	0.27 (0.03)	60, 119, 137, 191, 212, 232, 247, 266, 407, 424, 432, 472, 500, 507, 539, 556, 605, 648, 721, 723, 729, 778, 796, 823, 855, 866, 899, 959, 962, 978, 1000, 1003, 1034, 1065, 1096, 1110, 1158, 1166, 1219, 1223, 1232, 1267, 1333, 1341, 1354, 1425, 1428, 1439, 1466, 1510, 1537, 1597, 1607, 1618, 1639, 3146, 3149(2), 3152(2), 3160, 3178(2)
$Phen^{+}$ Product 2	0.24 (0.03)	87, 96, 129, 212, 232, 284, 378, 391, 399, 412, 441, 497, 512, 545, 599, 693, 705, 719, 760, 772, 818, 845, 860, 864, 962, 971(2), 998, 1000, 1016, 1044, 1075, 1098, 1138, 1140, 1200, 1235, 1245, 1257, 1321, 1334, 1339, 1400, 1402, 1434, 1444, 1504, 1507, 1536, 1564, 1573, 1602, 3143, 3146(2), 3151, 3152, 3155, 3178(2)
$Co^{2+}(Phen)_2$ Reactant	0.56 (0.06)	18, 28(2), 77(2), 126, 139, 146(3), 231(2), 248, 251(2), 254, 287(2), 309, 404, 411, 427, 437(2), 438, 477(2), 508(2), 509(2), 539, 540, 557, 559, 604, 608, 651(2), 717(2), 724(2), 733, 735, 780(2), 793, 795, 821, 822, 856(2), 871, 873, 907(2), 953(2), 955(2), 984(2), 1004(2), 1008(2), 1033(2), 1069, 1070, 1099(2), 1113, 1114, 1161(2), 1169(2), 1219, 1220, 1225, 1226, 1233(2), 1267(2), 1335(2), 1337(2), 1350, 1351, 1426(2),1427, 1428, 1440(2), 1464(2), 1508(2), 1537, 1538, 1597(2), 1604(2), 1614(2), 1639(2), 3151(2), 3154(4), 3157(4), 3164(2), 3180(4)

Table D.1b. (continued) Vibrational Frequencies and Average Vibrational Energies of $M^{2+}(Phen)_2$ Reactants, Transition States, Intermediates, and Products Involved in the Activated Dissociation of $M^{2+}(Phen)_2$ Complexes through ETCF Process at 298 K.

Species	E_{vib} (eV)[a]	Vibrational frequencies (cm^{-1}) [b]
$Co^{2+}(Phen)_2$ TS	0.55 (0.06)	**-31**, 18, 26, 40, 42, 84, 106, 126, 146, 151, 174, 220, 233, 234, 237, 248, 250, 267, 293, 380, 401, 407, 416, 433, 436, 457, 477, 481, 506, 507, 508, 534, 537, 544, 558, 579, 603, 609, 653, 690, 700, 713, 717, 722, 737, 781, 784, 784, 792, 823, 833, 848, 859(2), 872, 873, 908, 943, 952, 968, 978, 982, 988, 992, 1006, 1010, 1012, 1025, 1030, 1038, 1071, 1073, 1091, 1101, 1113, 1145, 1161(2), 1169, 1204, 1221, 1225, 1227, 1232, 1233, 1266, 1267, 1289, 1328, 1334, 1336, 1347, 1353, 1391, 1424, 1426, 1427, 1429, 1441, 1451, 1463, 1488, 1500, 1506, 1537, 1547, 1558, 1593, 1601, 1603, 1611, 1614, 1637, 3133, 3142, 3144, 3145, 3149, 3152, 3153, 3154, 3156, 3158(2), 3166, 3171, 3174, 3180, 3181
$Co^{2+}(Phen)_2$ Int	0.59 (0.06)	3, 24, 25, 28, 31, 33, 96, 105, 106, 141, 159, 224, 227, 235, 242, 247, 250, 255, 286, 383, 399, 415, 424, 433, 435, 439, 445, 446, 472, 501, 507, 513, 515, 531, 545, 556, 606(2), 648, 695, 711, 720, 721(2), 732, 745, 770, 772, 780, 812, 823, 847, 855, 858, 865, 871, 907, 948, 954, 956, 961, 963, 981, 989, 993, 1002, 1005, 1021, 1022, 1044, 1060, 1076, 1090, 1097, 1104, 1136, 1147, 1153, 1162, 1200, 1203, 1216, 1226, 1234, 1240, 1246, 1248, 1301, 1302, 1307, 1316, 1326, 1336, 1387, 1410, 1413, 1418, 1434, 1438, 1439, 1446, 1495, 1497, 1501, 1516, 1525, 1571, 1573, 1575, 1579, 1584, 1597, 1623, 3124, 3131, 3140, 3146(2), 3151, 3152, 3153(2), 3155, 3156, 3164, 3170, 3171, 3180(2)
$Co^{+}(Phen)$ Product 1	0.26 (0.03)	68, 143(2), 229, 233, 251, 261, 284, 409, 432, 434, 473, 507, 510, 514, 560, 603, 657, 704, 723, 726, 733, 773, 809, 848, 874, 912, 940, 943, 974, 990, 994, 1032, 1068, 1097, 1098, 1156, 1163, 1210, 1221, 1232, 1266, 1319, 1340, 1347, 1421, 1429, 1440, 1445, 1508, 1515, 1594, 1594, 1610, 1642, 3145, 3152(2), 3159(2), 3160, 3177(2)

Table D.1b. (continued) Vibrational Frequencies and Average Vibrational Energies of $M^{2+}(Phen)_2$ Reactants, Transition States, Intermediates, and Products Involved in the Activated Dissociation of $M^{2+}(Phen)_2$ Complexes through ETCF Process at 298 K.

Species	E_{vib} (eV)[a]	Vibrational frequencies (cm^{-1}) [b]
$Ni^{2+}(Phen)_2$ Reactant	0.55 (0.06)	14, 33(2), 88(2), 135, 146, 147, 166(2), 232(2), 251, 253, 263(2), 284, 294, 326, 408, 411, 429, 439, 445(2), 486(2), 507(2), 516(2), 539, 540, 558, 560, 604, 606, 655(2), 718(2), 723(2), 739(2), 781(2), 795, 798, 823, 824, 856(2), 873(2), 911(2), 953(2), 956(2), 983(2), 1004(2), 1008(2), 1034(2), 1067, 1068, 1097(2), 1114, 1116, 1161(2),1168(2), 1221, 1222, 1227, 1229, 1233(2),1264(2), 1338(2), 1341(2), 1351, 1353, 1426(2), 1435(2), 1441(2), 1466(2), 1506(2), 1537, 1538, 1597(2), 1603(2), 1614(2), 1639(2), 3152(2), 3154(4), 3157(4), 3164(2), 3180(4)
$Ni^{2+}(Phen)_2$ TS	0.55 (0.06)	**-51**, 19, 23, 53, 63, 87, 94, 114, 148, 154, 191, 220, 234, 242, 245, 249, 252, 298, 311, 394, 402, 407, 416, 435, 437, 458, 480, 483, 506, 507(2), 533, 535, 545, 560, 576, 602, 609, 654, 681, 696, 711, 718, 722, 741, 780, 781, 784, 786, 821, 822, 848, 858, 861, 873, 874, 910, 945, 954, 969, 978, 981, 987, 991, 1006, 1010(2), 1024, 1030, 1040, 1069, 1073, 1093, 1099, 1116, 1149, 1160, 1162, 1168, 1202, 1222, 1225, 1228, 1234, 1237, 1261, 1265, 1304, 1323, 1338, 1341, 1342, 1355, 1390, 1420, 1427(2), 1434, 1443, 1449, 1463, 1484, 1505, 1507, 1538, 1544, 1563, 1594, 1599, 1600, 1613(2), 1636, 3142, 3146, 3149, 3152, 3153(2), 3155, 3156(2), 3160, 3161, 3165, 3171, 3175, 3179, 3181
$Ni^{2+}(Phen)_2$ Int	0.60 (0.06)	3, 7, 12, 24, 26, 28, 85, 95, 96, 142, 161, 208, 219, 222, 229, 233(2), 252, 285, 355, 401, 408, 409, 418, 427(2), 435, 443, 470, 499, 508, 509, 516, 526, 545, 557, 601, 605, 642, 696, 710, 718, 722(2), 728, 749, 768, 771, 779, 814, 822, 849, 855, 860, 864, 867, 903, 948, 952, 959, 964, 965, 982, 992, 996, 1003, 1006, 1022, 1031, 1049, 1070, 1079, 1097, 1102, 1108, 1139, 1156, 1159, 1168, 1208, 1217, 1222, 1232, 1234, 1245, 1259, 1264, 1321, 1326, 1331, 1337(2), 1347, 1399, 1411, 1424, 1424, 1441(2), 1446, 1459, 1494, 1508, 1509, 1528, 1535, 1585, 1586, 1594, 1598, 1603, 1614, 1637, 3127, 3131, 3142, 3146, 3147, 3151, 3154(2), 3155, 3161, 3162, 3165, 3170, 3171, 3180, 3181

Table D.1b. (continued) Vibrational Frequencies and Average Vibrational Energies of $M^{2+}(Phen)_2$ Reactants, Transition States, Intermediates, and Products Involved in the Activated Dissociation of $M^{2+}(Phen)_2$ Complexes through ETCF Process at 298 K.

Species	E_{vib} (eV)[a]	Vibrational frequencies (cm^{-1}) [b]
$Ni^{+}(Phen)$ Product 1	0.26 (0.03)	73, 135, 147, 230, 247, 262, 267, 289, 404, 431, 443, 471, 494, 506, 508, 562, 596, 646, 701, 720, 723, 737, 773, 806, 849, 882, 911, 938, 942, 974, 992, 995, 1031, 1067, 1093, 1111, 1158, 1165, 1213, 1220, 1231, 1265, 1331, 1338, 1347, 1421, 1428, 1439, 1459, 1510, 1529, 1593, 1604, 1616, 1641, 3146, 3152(2), 3160(2), 3161, 3178(2)
$Cu^{2+}(Phen)_2$ Reactant	0.55 (0.06)	27, 39(2), 90(2), 140, 141, 145, 159, 168, 196, 233, 238, 251, 261, 273, 281, 299, 318, 409, 415, 430, 435, 440, 445, 480, 488, 507, 508, 511, 513, 539, 543, 560(2), 603, 607, 648, 653, 719, 720, 722, 723, 738, 741, 781, 783, 792, 794, 822, 825, 856, 857, 874, 875, 907, 913, 954, 957, 961, 964, 984(2), 1004, 1005, 1008(2), 1033, 1034, 1067, 1069, 1096, 1098, 1115, 1118, 1160, 1161, 1168(2), 1222, 1223, 1226, 1229, 1233, 1235, 1263, 1266, 1339(2), 1341, 1342, 1350, 1354, 1426(2), 1435(2), 1440, 1442, 1465, 1467, 1507(2), 1537, 1538, 1597(2), 1603, 1604, 1613, 1614, 1639(2), 3153(2), 3156(4), 3160(2), 3162(2), 3165(2), 3180(4)
$Cu^{2+}(Phen)_2$ TS	0.55 (0.06)	**-15**, 16, 27, 33, 63, 87, 90, 137, 148, 156, 189, 230, 234, 238, 241, 250, 259, 296, 329, 378, 397, 406, 415, 435, 439, 453, 470, 482, 504, 506, 508, 525, 530, 534, 555, 561, 594, 605, 654, 688, 697, 709, 719, 722, 742, 768, 778, 781, 796, 818, 834, 845, 855, 868, 875, 877, 912, 940, 947, 952, 969, 976, 985, 986, 1005, 1009(2), 1012, 1028, 1030, 1065, 1068, 1091, 1097, 1117, 1139, 1158, 1161, 1168, 1204, 1222, 1228, 1234, 1235, 1241, 1264, 1266, 1306, 1338, 1341, 1342, 1344, 1353, 1393, 1418, 1425, 1432, 1434, 1441, 1446, 1463, 1475, 1502, 1506, 1534, 1535, 1539, 1575, 1594, 1602, 1608, 1612, 1638, 3126, 3140, 3142, 3145, 3152, 3153(2), 3156(2), 3158, 3160, 3163, 3165, 3174, 3180, 3181

Table D.1b. (continued) Vibrational Frequencies and Average Vibrational Energies of $M^{2+}(Phen)_2$ Reactants, Transition States, Intermediates, and Products Involved in the Activated Dissociation of $M^{2+}(Phen)_2$ Complexes through ETCF Process at 298 K.

Species	E_{vib} (eV)[a]	Vibrational frequencies (cm^{-1}) [b]
$Cu^{2+}(Phen)_2$ Int	0.58 (0.06)	3, 4, 9, 26, 27, 32, 86, 92, 93, 135, 159, 185, 194, 214, 222, 233, 237, 247, 284, 317, 392, 401, 406, 408, 420, 428, 437, 440, 469, 495, 507, 511, 521, 522, 545, 559, 602(2), 638, 695, 715, 718, 722(2), 727, 764, 765, 772, 778, 815, 821, 849, 856, 860, 861, 868, 898, 952, 955, 962, 967, 968, 981, 995, 998, 1002, 1005, 1020, 1030, 1049, 1070, 1079, 1096, 1102, 1106, 1136, 1157(2), 1167, 1210, 1214, 1222, 1231, 1232, 1246, 1257, 1266, 1322, 1325, 1327, 1333, 1336, 1348, 1402, 1407, 1423, 1424, 1441(2), 1446, 1458, 1487, 1508, 1508, 1525, 1531, 1582, 1584, 1590, 1599, 1602, 1614, 1637, 3129, 3133, 3143, 3147, 3148, 3150, 3153(2), 3156, 3161(2), 3164, 3171, 3173, 3179(2)
$Cu^{+}(Phen)$ Product 1	0.26 (0.03)	72, 118, 139, 229, 233, 238, 258, 296, 397, 432, 440, 462, 491, 509, 510, 563, 596, 646, 713, 723, 726, 730, 776, 810, 854, 878, 905, 950, 954, 976, 997, 1000, 1029, 1069, 1094, 1108, 1158, 1167, 1205, 1220, 1228, 1271, 1324, 1332, 1351, 1414, 1420, 1440, 1458, 1512, 1528, 1593, 1610, 1618, 1641, 3145, 3151(2), 3160, 3165(2), 3179(2)
$Zn^{2+}(Phen)_2$ Reactant	0.55 (0.06)	24, 27(2), 81(2), 129, 141, 147, 151, 152, 222(2), 233(2), 250, 256, 279, 294, 301, 406, 412, 428, 434, 441(2), 478(2), 509(2), 511(2), 543, 544, 559, 560, 607, 610, 652(2), 724(2), 725(2), 733, 735, 782(2), 804, 806, 829, 831, 859(2), 872, 873, 909(2), 958(2), 961(2), 985(2), 1006(2), 1010(2), 1035(2), 1072, 1073, 1101(2), 1115, 1117, 1162(2), 1169(2), 1220(2), 1227, 1229, 1235(2), 1270(2), 1335(2), 1340(2), 1353, 1355, 1426(2), 1430(2), 1442(2), 1464, 1465, 1509(2), 1538, 1540, 1600(2), 1606(2), 1616(2), 1639(2), 3151(2), 3155(4), 3159(4), 3164(2), 3180(4)

Table D.1b. (continued) Vibrational Frequencies and Average Vibrational Energies of $M^{2+}(Phen)_2$ Reactants, Transition States, Intermediates, and Products Involved in the Activated Dissociation of $M^{2+}(Phen)_2$ Complexes through ETCF Process at 298 K.

Species	E_{vib} (eV)[a]	Vibrational frequencies (cm^{-1}) [b]
$Zn^{2+}(Phen)_2$ TS	0.55 (0.06)	**-48**, 18, 20, 38, 54, 87, 95, 111, 145, 154, 186, 219, 235, 237, 238, 247, 252, 304, 325, 401, 402, 405, 418, 436(2), 462, 477, 490, 508(2), 509, 536, 542, 546, 561, 590, 605, 610, 656, 696, 717, 719, 722, 724, 737, 784, 787, 789, 809, 827, 835, 849, 863, 872, 874, 880, 911, 923, 960, 962, 969, 985, 990, 1002, 1008, 1011, 1012, 1021, 1031, 1035, 1072, 1075, 1094, 1103, 1116, 1142, 1163(2), 1170, 1207, 1220, 1229, 1232, 1234, 1239, 1267, 1269, 1316, 1338, 1340, 1344, 1350, 1353, 1397, 1425, 1426, 1429, 1430, 1442, 1449, 1463, 1486, 1496, 1507, 1537, 1551, 1558, 1597, 1603, 1610, 1614, 1618, 1637, 3081, 3128, 3134, 3137, 3144, 3150, 3154(2), 3156, 3157, 3158, 3165, 3166, 3172, 3182, 3183
$Zn^{2+}(Phen)_2$ Int	0.60 (0.06)	1, 6, 8, 10, 12, 16, 74, 100(2), 136, 138, 216, 222, 226, 233, 234, 236, 247, 293, 362, 401, 404, 422, 428, 432(2), 440, 449, 471, 501, 505, 508, 530, 532, 547, 560, 603, 607, 654, 698, 714, 720, 723, 724, 732, 767, 769, 780, 783, 821, 825, 850, 857, 859, 870, 871, 907, 954, 959, 961, 963, 967, 986, 987, 992, 1010, 1013, 1027, 1030, 1049, 1074, 1078, 1100, 1102, 1110, 1143, 1154, 1162, 1170, 1205, 1219, 1224, 1233, 1239, 1244, 1263, 1267, 1318, 1332, 1336, 1339, 1340, 1351, 1392, 1419, 1422, 1426, 1441, 1443, 1447, 1460, 1508, 1510, 1511, 1530, 1533, 1589, 1594, 1595, 1598, 1604, 1613, 1636, 3123, 3127, 3139, 3144, 3145, 3152, 3153, 3156, 3157, 3166(3), 3168, 3169, 3182, 3183
$Zn^{+}(Phen)$ Product 1	0.27 (0.03)	66, 123, 136, 186, 213, 233, 247, 283, 407, 426, 435, 472, 502, 507, 540, 558, 606, 648, 723, 725, 732, 779(2), 826, 857, 868, 901, 963, 967, 979, 1002, 1005, 1034, 1066, 1096, 1111, 1158, 1166, 1219, 1225, 1233, 1268, 1333, 1344, 1358, 1426, 1429, 1441, 1465, 1511, 1536, 1599, 1609, 1621, 1638, 3147, 3151(2), 3157(2), 3161, 3179(2)

[a]Uncertainties listed in parentheses are determined as described in the text. [b]Vibrational frequencies scaled by 0.9804 obtained from vibrational analyses of the B3LYP/6-31G* geometry optimized structures. Degeneracies are indicated in parentheses.

Table D.1c. Vibrational Frequencies and Average Vibrational Energies of $M^{2+}(Phen)_2$ Reactants, Transition States, Intermediates, and Products Involved in the Activated Dissociation of $M^{2+}(Phen)_2$ Complexes through PTCF Process at 298 K.

Species	E_{vib} (eV)[a]	Vibrational frequencies (cm^{-1}) [b]
$Fe^{2+}(Phen)_2$ Reactant	0.56 (0.06)	18, 26, 26, 75(2), 124, 138, 140, 141(2), 232(2), 237(2), 248, 249, 267, 282, 291, 407(2), 425, 435(3), 475(2), 508(2), 510(2), 538, 539, 556, 558, 606, 607, 651(2), 719(2), 724(2), 730, 731, 781(2), 792, 794, 821, 822, 857(2), 869, 871, 904(2), 955(2), 958(2), 984(2), 1005(2), 1009(2), 1033(2), 1070(2), 1099(2), 1111, 1112, 1160(2), 1169(2), 1218, 1220, 1224, 1225, 1232(2), 1267(2), 1331, 1333, 1335(2) 1349, 1351, 1423, 1424, 1426 (2), 1440(2), 1463(2), 1508(2), 1536, 1537, 1594(2), 1603(2), 1613(2), 1638, 1639, 3151(2), 3152(4), 1349, 1351, 1423, 1424, 1426(2), 1440(2), 1463(2), 1508(2), 1536, 1537, 1594(2), 1603(2), 1613(2), 1638, 1639, 3151(2), 3152(4), 3155, 3156(3), 3164(2), 3180 (4)
$Fe^{2+}(Phen)_2$ TS_1	0.57 (0.06)	**-1348**, 18, 23, 28, 74, 87, 107, 122, 140, 147, 156, 193, 197, 230, 241, 247, 253, 281, 312, 328, 395, 408, 426, 432, 436, 438, 477, 482, 492, 504, 507, 508, 523, 537, 545, 557, 559, 595, 606, 645, 647, 700, 713, 715, 722, 734, 743, 781, 782, 785, 791, 820, 825, 856, 858, 858, 870, 904, 909, 952, 955, 960, 980, 984, 992, 1004, 1007, 1007, 1016, 1032, 1059, 1068, 1097, 1105, 1113, 1119, 1144, 1160, 1164, 1168, 1179, 1214, 1220, 1227, 1228, 1234, 1241, 1265, 1298, 1329, 1333, 1337, 1341, 1351, 1397, 1420, 1427, 1430, 1434, 1440, 1463, 1465, 1486, 1507, 1517, 1537, 1582, 1595, 1598, 1602, 1605, 1614, 1634, 1638, 3145, 3152, 3152, 3153(2), 3155, 3156, 3157, 3159, 3165, 3165, 3177, 3179, 3181, 3190

Table D.1c. Vibrational Frequencies and Average Vibrational Energies of $M^{2+}(Phen)_2$ Reactants, Transition States, Intermediates, and Products Involved in the Activated Dissociation of $M^{2+}(Phen)_2$ Complexes through PTCF Process at 298 K.

Species	E_{vib} (eV)[a]	Vibrational frequencies (cm^{-1}) [b]
$Fe^{2+}(Phen)_2$ Int_1	0.57 (0.06)	20, 23, 34, 70, 82, 128, 134, 150, 152, 162, 204, 230, 238, 245, 253, 267, 278, 287, 315, 320, 409, 414, 426, 436, 437, 440, 480, 486, 507(2), 509, 510, 535, 542, 557, 559, 595, 604, 641, 651, 700, 711, 718, 722, 730, 736, 770, 778, 780, 783, 784, 817, 823, 854, 855, 859, 871, 901, 909, 948, 955, 960, 980, 984, 994, 1003, 1007(2), 1021, 1032, 1068, 1069, 1098, 1099, 1113, 1120, 1150, 1160, 1166, 1168, 1210, 1221, 1225, 1229, 1230, 1233, 1264, 1281, 1328, 1331, 1337, 1339, 1351, 1397, 1417, 1426, 1430, 1430, 1440, 1457, 1464, 1490, 1507, 1522, 1536, 1571, 1587, 1595, 1601, 1607, 1612, 1634, 1638, 1854, 3148, 3152, 3154(2), 3156(2), 3158, 3161, 3163, 3165, 3166, 3179, 3180, 3181, 3185
$Fe^{2+}(Phen)_2$ TS_2	0.56 (0.06)	**-1002**, 16, 27, 29, 74, 78, 115, 133, 143, 149, 150, 205, 223, 231, 238, 246, 259, 276, 281, 292, 406, 414, 421, 427, 432, 445, 476, 478, 504, 506, 507, 514, 539, 544, 552, 557, 595, 609, 628, 638, 702, 703, 715, 719, 722, 724, 771, 781, 782, 785, 813, 822, 846, 852, 858, 860, 887, 896, 897, 931, 956, 959, 979, 984, 993, 995, 1006, 1007, 1019, 1030, 1069, 1072, 1094, 1097, 1107, 1118, 1150, 1155, 1166, 1168, 1209, 1214, 1224, 1228, 1229, 1231, 1260, 1285, 1315, 1326, 1334, 1336, 1353, 1399, 1411, 1416, 1428, 1429, 1435, 1444, 1457, 1463, 1490, 1501, 1523, 1543, 1576, 1580, 1594, 1596, 1608(2), 1633, 1638, 3146, 3150, 3152, 3153, 3155, 3156, 3158, 3161, 3165, 3166, 3171, 3179, 3180, 3182, 3186

Table D.1c. (continued) Vibrational Frequencies and Average Vibrational Energies of $M^{2+}(Phen)_2$ Reactants, Transition States, Intermediates, and Products Involved in the Activated Dissociation of $M^{2+}(Phen)_2$ Complexes through PTCF Process at 298 K.

Species	E_{vib} (eV)[a]	Vibrational frequencies (cm^{-1}) [b]
$Fe^{2+}(Phen)_2$ Int_2	0.57 (0.06)	2, 7, 23, 51, 92, 110, 112, 119, 133, 139, 178, 224, 226, 234, 237, 250, 258, 273, 294, 390, 393, 404, 419, 423, 438, 465, 474, 498, 499, 507, 508, 529, 533, 548, 556, 587, 594, 633, 645, 690, 694, 708, 720, 728, 734, 750, 767, 771, 782, 795, 811, 820, 826, 852, 857, 858, 902, 910, 923, 950, 955, 978, 982, 992, 994, 998, 1004, 1005, 1028, 1067, 1070, 1089, 1103, 1109, 1112, 1152, 1157, 1165, 1169, 1208, 1210, 1222, 1229, 1231, 1236, 1255, 1286, 1310, 1320, 1328, 1341, 1344, 1363, 1400, 1407, 1414, 1428, 1436, 1450, 1454, 1485, 1489, 1510, 1519, 1561, 1572, 1586, 1593, 1603, 1609, 1621, 1633, 1641, 2839, 3146, 3148, 3152, 3153, 3154, 3156, 3157, 3158, 3164, 3168, 3178, 3180, 3181, 3184, 3191
$Fe^{2+}(Phen)_2$ TS_3	0.57 (0.06)	**-18**, 11, 13, 17, 41, 51, 81, 105, 133, 143, 146, 176, 220, 228, 236, 241, 245, 264, 275, 392, 400, 410, 420, 422, 436, 460(2), 493, 500, 501, 504, 528, 540, 551, 558, 593, 602, 621, 660, 702, 710, 715, 716, 720, 734, 767, 778, 786, 802, 823, 828, 852, 853, 856, 866, 883, 896, 908, 955, 965, 979, 980, 982, 998, 1003, 1005, 1006, 1018, 1031, 1048, 1056, 1071, 1093, 1098, 1104, 1154, 1163, 1165, 1171, 1200, 1214, 1222, 1228, 1231, 1235, 1254, 1276, 1289, 1295, 1332, 1336, 1351, 1362, 1384, 1414, 1422, 1424, 1432, 1433, 1464, 1480, 1481, 1495, 1510, 1547, 1561, 1592, 1598, 1603, 1615, 1624, 1629, 1645, 3129, 3140, 3141, 3144, 3148, 3150, 3152, 3154, 3155, 3160, 3163(2), 3172, 3181, 3185, 3381

Table D.1c. (continued) Vibrational Frequencies and Average Vibrational Energies of $M^{2+}(Phen)_2$ Reactants, Transition States, Intermediates, and Products Involved in the Activated Dissociation of $M^{2+}(Phen)_2$ Complexes through PTCF Process at 298 K.

Species	E_{vib} (eV)[a]	Vibrational frequencies (cm^{-1}) [b]
$Fe^{2+}(Phen)_2$ Int_3	0.57 (0.06)	3, 5, 7, 9, 14, 15, 80, 103, 109, 134, 146, 187, 223(2), 231, 237, 245, 246, 302, 385, 398, 410, 420, 427, 432, 461, 472, 492, 497, 498, 504, 533, 535, 551, 556, 589, 600, 620, 646, 701, 702, 710, 714, 720, 738, 770, 774, 784, 800, 815, 827, 834, 851, 854, 864, 885, 891, 905, 952, 953, 962, 968, 976, 981, 999, 1000, 1003, 1005, 1033, 1053, 1053, 1073, 1090, 1105, 1108, 1154, 1161, 1165(2), 1204, 1215, 1219, 1227, 1235, 1238, 1257, 1285, 1296, 1327, 1335, 1336, 1361, 1369, 1387, 1415, 1425, 1426, 1432, 1433, 1466, 1475, 1485, 1495, 1513, 1548, 1562, 1593, 1599, 1604, 1617, 1625, 1630, 1648, 3131, 3132, 3146, 3148, 3150, 3150, 3155, 3156, 3157, 3160, 3164, 3171, 3178, 3185, 3197, 3386
$[Fe(Phen-H)]^+$ Product 1	0.27 (0.03)	86, 112, 123, 145, 227, 234, 242, 256, 390, 422, 432, 468, 491, 499, 534, 556, 593, 653, 705, 708, 741, 778, 787, 827, 858, 863, 906, 953, 973, 978, 998, 1001, 1054, 1092, 1108, 1160, 1164, 1216, 1223, 1238, 1287, 1329, 1354, 1375, 1418, 1430, 1437, 1480, 1495, 1552, 1596, 1605, 1630, 3131, 3145, 3150, 3153, 3159, 3162, 3177
$(Phen+H)^+$ Product 2	0.22 (0.03)	103, 134, 223, 231, 244, 398, 410, 420, 462, 497, 503, 534, 551, 600, 620, 711, 714, 720, 770, 800, 815, 850, 854, 886, 892, 962, 968, 980, 1001, 1004, 1032, 1053, 1073, 1105, 1154, 1165, 1204, 1228, 1236, 1257, 1297, 1336, 1362, 1388, 1426, 1433, 1466, 1484, 1512, 1562, 1599, 1617, 1625, 1648, 3144, 3146, 3150, 3155, 3162, 3172, 3185, 3197, 3377

Table D.1c. (continued) Vibrational Frequencies and Average Vibrational Energies of $M^{2+}(Phen)_2$ Reactants, Transition States, Intermediates, and Products Involved in the Activated Dissociation of $M^{2+}(Phen)_2$ Complexes through PTCF Process at 298 K.

Species	E_{vib} (eV)[a]	Vibrational frequencies (cm^{-1}) [b]
$Co^{2+}(Phen)_2$ Reactant	0.56 (0.06)	18, 28, 28, 77(2), 126, 139, 146(3), 231(2), 248, 251(2), 254, 287(2), 309, 404, 411, 427, 437(2), 438, 477(2), 508(2), 509(2), 539, 540, 557, 559, 604, 608, 651(2), 717(2), 724(2), 733, 735, 780(2), 793, 795, 821, 822, 856(2), 871, 873, 907(2), 953(2), 955(2), 984(2), 1004(2), 1008(2), 1033(2), 1069, 1070, 1099(2), 1113, 1114, 1161(2), 1169(2), 1219, 1220, 1225, 1226, 1233(2), 1267(2), 1335(2), 1337(2), 1350, 1351, 1426(2),1427, 1428, 1440(2), 1464(2), 1508(2), 1537, 1538, 1597(2), 1604(2), 1614(2), 1639(2), 3151(2), 3154(4), 3157(4), 3164(2), 3180(4)
$Co^{2+}(Phen)_2$ TS_1	0.56 (0.06)	**-1588**, 16, 26, 27, 75, 76, 120, 138, 143, 146, 155, 220, 223, 231, 245, 250, 253, 279, 287, 304, 390, 407, 412, 425, 436, 437, 472, 477, 497, 500, 508, 509, 523, 538, 549, 558, 588, 605, 639, 652, 680, 711, 716, 724, 727, 735, 768, 780, 791, 794, 821, 823, 836, 856, 865, 873, 883, 888, 908, 951, 954, 962, 984, 985, 987, 1004, 1008(2), 1024, 1033, 1048, 1071, 1084, 1091, 1099, 1114, 1132, 1161, 1166, 1169, 1186, 1220, 1224, 1226, 1227, 1233(2), 1267, 1273, 1335, 1336, 1340, 1350, 1367, 1420, 1426, 1428, 1430, 1440, 1441, 1464, 1476, 1499, 1508, 1538, 1551, 1594, 1598, 1604, 1606, 1613, 1634, 1639, 2262, 3138, 3151, 3152, 3153, 3154(2), 3156, 3157(2), 3162, 3165(2), 3181(3)
$Co^{2+}(Phen)_2$ Int_1	0.57 (0.06)	15, 26, 27, 73, 76, 101, 129, 144, 150, 159, 191, 226, 231, 241, 246, 252, 265, 287, 295, 371, 407, 414, 424, 435, 436, 466, 476, 493, 503, 508, 509, 522, 537, 547, 559, 600, 605, 629, 653, 678, 694, 715, 717, 724, 734, 746, 771, 780, 792, 793, 820, 836, 851, 855, 873(2), 908, 910, 950, 953, 959, 963, 980, 984, 1001, 1005, 1006, 1009, 1033, 1041, 1072, 1080, 1100, 1101, 1115, 1150, 1162, 1163, 1170, 1202, 1220, 1221, 1226, 1227, 1233, 1257, 1265, 1267, 1334, 1336, 1336, 1349(2), 1369, 1417, 1426, 1428, 1428, 1434, 1441, 1464, 1475, 1487, 1508, 1525, 1538, 1590, 1597, 1598, 1604, 1613, 1632, 1639, 3138, 3151, 3153, 3154(2), 3155, 3157(2), 3158, 3160, 3166(2), 3180, 3181(2), 3338

Table D.1c. (continued) Vibrational Frequencies and Average Vibrational Energies of $M^{2+}(Phen)_2$ Reactants, Transition States, Intermediates, and Products Involved in the Activated Dissociation of $M^{2+}(Phen)_2$ Complexes through PTCF Process at 298 K.

Species	E_{vib} (eV)[a]	Vibrational frequencies (cm^{-1}) [b]
$Co^{2+}(Phen)_2$ TS_2	0.56 (0.06)	**-793**, 20, 24, 28, 59, 77, 92, 134, 142, 144, 152, 176, 234, 235, 241, 248, 253, 276, 288, 304, 407, 412, 418, 431, 435, 439, 475, 479, 504, 507, 507, 510, 538, 545, 555, 559, 592, 607, 629, 651, 699, 711, 720, 723, 726, 735, 780, 781, 785, 793, 808, 822, 825, 857, 860, 867, 873, 901, 907, 956, 958, 960, 981, 983, 994, 1004, 1007, 1008, 1013, 1034, 1068, 1072, 1091, 1097, 1113, 1131, 1153, 1160, 1167, 1168, 1217, 1221, 1226, 1230, 1231, 1233, 1265, 1286, 1332, 1336, 1337, 1338, 1352, 1396, 1411, 1425(2), 1432, 1440, 1455, 1464, 1484, 1507, 1511, 1536, 1557, 1575, 1591, 1595, 1603, 1607, 1614, 1631, 1639, 3147, 3152, 3152, 3152, 3154, 3155, 3156, 3157, 3164(2), 3166, 3179, 3181(2), 3187
$Co^{2+}(Phen)_2$ Int_2	0.56 (0.06)	8, 23, 36, 74, 84, 128, 139, 155, 157, 165, 220, 232, 239, 248, 251, 268, 293, 295, 311, 334, 411, 417, 427, 437(2), 444, 483, 487, 507, 508, 509, 511, 535, 541, 558, 559, 593, 605, 641, 651, 697, 710, 718, 722, 732, 739, 775, 779, 781, 783, 794, 816, 822, 854, 855, 858, 872, 903, 912, 947, 954, 960, 980, 983, 994, 1002, 1006, 1007, 1021, 1033, 1067, 1070, 1096, 1100, 1114, 1120, 1150, 1160, 1167(2), 1210, 1222, 1227, 1229, 1231, 1234, 1263, 1281, 1328, 1335, 1340, 1341, 1353, 1397, 1416, 1426, 1430, 1437, 1441, 1457, 1466, 1490, 1506, 1524, 1536, 1571, 1587, 1595, 1601, 1607, 1613, 1634, 1640, 1937, 3149, 3152, 3154, 3155, 3156, 3157, 3160, 3165(2), 3166(2), 3179, 3180, 3181, 3185

Table D.1c. (continued) Vibrational Frequencies and Average Vibrational Energies of $M^{2+}(Phen)_2$ Reactants, Transition States, Intermediates, and Products Involved in the Activated Dissociation of $M^{2+}(Phen)_2$ Complexes through PTCF Process at 298 K.

Species	E_{vib} (eV)[a]	Vibrational frequencies (cm^{-1}) [b]
$Co^{2+}(Phen)_2$ TS_3	0.56 (0.06)	**-738**, 17, 28, 29, 68, 77, 116, 135, 140, 150, 152, 197, 216, 232, 240, 247, 263, 276, 286, 302, 407, 414, 422, 427, 436, 444, 478, 480, 504, 507, 508, 511, 538, 545, 554, 559, 596, 609, 627, 637, 704, 706, 715, 718, 723, 727, 776, 781, 785, 787, 816, 823, 849, 855, 858, 860, 892, 898, 917, 941, 958, 960, 978, 985, 992, 999, 1005, 1008, 1021, 1032, 1068, 1072, 1095, 1097, 1109, 1117, 1150, 1157, 1165, 1168, 1210, 1215, 1225, 1229, 1230, 1232, 1260, 1286, 1323, 1326, 1337, 1339, 1353, 1399, 1417, 1419, 1429, 1431, 1444, 1448, 1459, 1489, 1492, 1504, 1524, 1559, 1580, 1582, 1592, 1605, 1608, 1613, 1634, 1639, 3146, 3151, 3152, 3153, 3155, 3156, 3159, 3160, 3164, 3166, 3173, 3178, 3180, 3183, 3185
$Co^{2+}(Phen)_2$ Int_3	0.57 (0.06)	18, 19, 23, 58, 72, 104, 118, 121, 145, 154, 166, 187, 230, 239, 243, 247, 258, 277, 293, 396, 405, 413, 427, 430, 439, 464, 482, 504, 505, 506, 508, 532, 540, 550, 557, 593, 599, 630, 634, 702, 705, 716, 718, 722, 728, 774, 775, 781, 784, 812, 819, 838, 850, 856, 857, 886, 894, 898, 949, 952, 965, 976, 987, 989, 1001, 1007, 1011, 1018, 1029, 1065, 1068, 1089, 1095, 1108, 1111, 1148, 1157, 1163, 1172, 1209, 1211, 1220, 1229, 1231, 1235, 1255, 1286, 1305, 1324, 1332, 1336, 1349, 1373, 1399, 1412, 1418, 1431, 1434, 1456, 1461, 1488, 1489, 1516, 1521, 1564, 1580, 1591, 1595, 1607, 1609, 1624, 1635, 1648, 2947, 3144, 3147, 3148, 3150, 3154, 3155, 3158, 3159, 3163, 3168, 3177, 3180, 3183, 3183, 3192

Table D.1c. (continued) Vibrational Frequencies and Average Vibrational Energies of $M^{2+}(Phen)_2$ Reactants, Transition States, Intermediates, and Products Involved in the Activated Dissociation of $M^{2+}(Phen)_2$ Complexes through PTCF Process at 298 K.

Species	E_{vib} (eV)[a]	Vibrational frequencies (cm^{-1}) [b]
$Co^{2+}(Phen)_2$ TS_4	0.57 (0.06)	**-34**, 5, 11, 13, 27, 30, 72, 104, 133, 135, 140, 200, 220, 223, 233, 236, 240, 245, 271, 398, 399, 410, 420, 425, 435, 460, 467, 501, 502, 504, 506, 520, 537, 550, 555, 585, 600, 620, 635, 692, 709, 715, 718, 720, 722, 739, 772, 778, 802, 814, 816, 829, 853, 854, 856, 881, 885, 900, 940, 963, 976, 977, 988, 990, 998, 1004, 1007, 1010, 1033, 1054, 1066, 1074, 1093, 1106, 1108, 1150, 1155, 1164, 1167, 1202, 1205, 1223, 1225, 1226, 1235, 1257, 1278, 1297, 1322, 1329, 1335, 1360, 1386, 1395, 1412, 1422, 1426, 1433, 1453, 1466, 1483, 1486, 1512, 1517, 1562, 1578, 1589, 1600, 1606, 1617, 1624, 1633, 1649, 3066, 3142, 3150(2), 3152, 3153, 3157(2), 3163, 3165, 3168, 3178, 3183, 3185, 3196, 3409
$Co^{2+}(Phen)_2$ Int_4	0.58 (0.06)	2, 4, 4, 5, 11, 11, 58, 103, 118, 133, 134, 154, 218, 223, 229, 231, 240, 245, 267, 397, 398, 408, 410, 420, 436, 461, 471, 497, 498, 503, 504, 519, 535, 551, 553, 580, 600, 620, 631, 691, 710, 714, 715, 720, 724, 742, 771, 776, 800, 807, 814, 815, 851, 854(2), 885, 891, 900, 934, 962, 967, 973, 981, 987, 994, 1000, 1002, 1005, 1033, 1053, 1065, 1073, 1094, 1103, 1105, 1149, 1154, 1162, 1165, 1204, 1207, 1224, 1227(2), 1235, 1257, 1282, 1296, 1320, 1330, 1335, 1361, 1387, 1394, 1415, 1425, 1427, 1433, 1455, 1465, 1482, 1485, 1513, 1516, 1562, 1579, 1585, 1599, 1604, 1617, 1625, 1633, 1648, 3133, 3141, 3147, 3148, 3150, 3152, 3156(2), 3161, 3164, 3170, 3177, 3180, 3185, 3197, 3387
$[Co(Phen\text{-}H)]^+$ Product 1	0.27 (0.03)	63, 127, 132, 197, 207, 228, 239, 272, 397, 414, 437, 467, 497, 504, 517, 553, 581, 632, 691, 717, 724, 737, 776, 810, 816, 854, 901, 934, 972, 987, 993, 999, 1066, 1093, 1105, 1150, 1163, 1204, 1222, 1225, 1279, 1321, 1329, 1395, 1413, 1426, 1453, 1480, 1516, 1580, 1587, 1605, 1633, 3140, 3147, 3152, 3156, 3160, 3177, 3182

Table D.1c. (continued) Vibrational Frequencies and Average Vibrational Energies of $M^{2+}(Phen)_2$ Reactants, Transition States, Intermediates, and Products Involved in the Activated Dissociation of $M^{2+}(Phen)_2$ Complexes through PTCF Process at 298 K.

Species	E_{vib} (eV)[a]	Vibrational frequencies (cm^{-1}) [b]
$Ni^{2+}(Phen)_2$ Reactant	0.55 (0.06)	14, 33(2), 88(2), 135, 146, 147, 166(2), 232(2), 251, 253, 263(2), 284, 294, 326, 408, 411, 429, 439, 445(2), 486(2), 507(2), 516(2), 539, 540, 558, 560, 604, 606, 655(2), 718(2), 723(2), 739(2), 781(2), 795, 798, 823, 824, 856(2), 873(2), 911(2), 953(2), 956(2), 983(2), 1004(2), 1008(2), 1034(2), 1067, 1068, 1097(2), 1114, 1116, 1161(2),1168(2), 1221, 1222, 1227, 1229, 1233(2),1264(2), 1338(2), 1341(2), 1351, 1353, 1426(2), 1435(2), 1441(2), 1466(2), 1506(2), 1537, 1538, 1597(2), 1603(2), 1614(2), 1639(2), 3152(2), 3154(4), 3157(4), 3164(2), 3180(4)
$Ni^{2+}(Phen)_2$ TS_1	0.56 (0.06)	**-1591**, 21, 22, 28, 77, 88, 102, 126, 148, 155, 162, 210, 220, 231, 240, 255, 256, 295, 310, 338, 395, 409, 430, 433, 440, 442, 482, 489, 491, 503, 507, 508, 523, 536, 544, 559, 562, 590, 602, 648, 652, 693, 711, 713, 722, 740, 745, 778, 780, 782, 784, 815, 822, 854, 857, 861, 874, 912, 913, 948, 951, 961, 979, 983, 991, 1002, 1006(2), 1015, 1033, 1059, 1068, 1096, 1106, 1116, 1118, 1141, 1153, 1161, 1164, 1167, 1213, 1222, 1226, 1229, 1235, 1242, 1266, 1300, 1328, 1336, 1340, 1341, 1354, 1397, 1419, 1427, 1434, 1435, 1441, 1463, 1466, 1484, 1507, 1516, 1537, 1584, 1598, 1601, 1603, 1605, 1615, 1634, 1639, 3145, 3152, 3153, 3155(2), 3156, 3158, 3159(2), 3165, 3166, 3178, 3180(2), 3192

Table D.1c. (continued) Vibrational Frequencies and Average Vibrational Energies of $M^{2+}(Phen)_2$ Reactants, Transition States, Intermediates, and Products Involved in the Activated Dissociation of $M^{2+}(Phen)_2$ Complexes through PTCF Process at 298 K.

Species	E_{vib} (eV)[a]	Vibrational frequencies (cm^{-1}) [b]
$Ni^{2+}(Phen)_2$ Int_1	0.56 (0.06)	20, 25, 34, 78, 82, 138, 141, 153, 156, 164, 224, 230, 239, 250, 257, 273, 295, 299, 329, 408, 413, 429, 432, 439, 442, 482, 487, 505, 507(2), 508, 533, 538, 551, 559, 561, 590, 602, 643, 651, 694, 706, 718, 721, 735, 741, 767, 774, 779, 782, 813, 819, 827, 853, 857(2), 874, 906, 914, 945, 949, 954, 980, 984, 994, 1002, 1006, 1006, 1022, 1032, 1067, 1069, 1096, 1102, 1116, 1120, 1151, 1161, 1166, 1167, 1211, 1222, 1227, 1230, 1231, 1235, 1265, 1282, 1329, 1336, 1341, 1342, 1354, 1398, 1418, 1427, 1431, 1435, 1441, 1459, 1465, 1491, 1506, 1525, 1535, 1573, 1592, 1597, 1602, 1608, 1615, 1635, 1639, 2039, 3149, 3152, 3154, 3156(3), 3161(2), 3163, 3165, 3166, 3179, 3180, 3181, 3184
$Ni^{2+}(Phen)_2$ TS_2	0.56 (0.06)	**-853**, 24, 31, 35, 79, 91, 126, 137, 149, 156, 160, 211, 234, 240, 248, 262, 268, 276, 288, 312, 410, 417, 425, 430, 437, 446, 477, 484, 505, 508, 509, 514, 537, 545, 556, 559, 596, 608, 637, 640, 704, 707, 718, 720, 723, 727, 749, 781, 783, 785, 789, 819, 823, 851, 857, 858, 867, 899, 902, 950, 958, 959, 978, 985, 991, 1004, 1006, 1008, 1022, 1031, 1068, 1069, 1097, 1101, 1102, 1119, 1150, 1158, 1166, 1169, 1210, 1217, 1225, 1230, 1231, 1233, 1260, 1286, 1325, 1332, 1338, 1341, 1353, 1400, 1417, 1423, 1430, 1432, 1443, 1457, 1460, 1491, 1503, 1524, 1531, 1580, 1587, 1591, 1594, 1607, 1611, 1634, 1637, 1777, 3147, 3150, 3152, 3154, 3156, 3157, 3159, 3164, 3165, 3167, 3173, 3178, 3180, 3184(2)

Table D.1c. (continued) Vibrational Frequencies and Average Vibrational Energies of $M^{2+}(Phen)_2$ Reactants, Transition States, Intermediates, and Products Involved in the Activated Dissociation of $M^{2+}(Phen)_2$ Complexes through PTCF Process at 298 K.

Species	E_{vib} (eV)[a]	Vibrational frequencies (cm^{-1}) [b]
$Ni^{2+}(Phen)_2$ Int_2	0.56 (0.06)	21, 24, 31, 67, 77, 106, 122, 141, 150, 163, 199, 229, 232, 239, 247, 253, 263, 289, 303, 397, 407, 417, 429, 433, 439, 465, 481, 505, 507, 509, 509, 535, 538, 551, 559, 591, 599, 633, 637, 698, 703, 719, 720, 726, 729, 769, 776, 780, 783, 813, 819, 851, 854, 855, 858, 896, 903, 925, 951, 959, 976, 983, 989(2), 1003, 1007, 1012, 1020, 1029, 1067, 1071, 1093, 1097, 1110, 1115, 1150, 1158, 1165, 1172, 1206, 1210, 1220, 1228, 1230, 1236, 1257, 1283, 1305, 1324, 1332, 1338, 1348, 1374, 1399, 1412, 1417, 1430, 1435, 1457, 1460, 1489, 1491, 1518, 1521, 1567, 1580, 1593, 1594, 1609, 1610, 1624, 1635, 1648, 2930, 3146, 3148, 3151, 3155(2), 3158, 3159, 3163, 3164, 3168, 3177, 3181, 3183, 3184, 3192
$Ni^{2+}(Phen)_2$ TS_3	0.57 (0.06)	**-35**, 6, 8, 11, 26, 31, 73, 104, 137, 139, 144, 223, 234, 235, 240, 245(2), 248, 288, 398, 400, 410, 420, 425, 440, 460, 470, 494, 502, 504, 505, 508, 537, 550, 561, 581, 601, 620, 633, 682, 709, 715, 716, 720, 720, 727, 772, 776, 802, 811, 816, 852, 853(2), 854, 882, 885, 905, 945, 963, 973, 977, 986, 988, 1000, 1007, 1009, 1014, 1033, 1054, 1069, 1074, 1095, 1106, 1110, 1150, 1155, 1165, 1167, 1200, 1205, 1225, 1226(2), 1235, 1257, 1278, 1297, 1322, 1335(2), 1360, 1386, 1397, 1414, 1422, 1427, 1433, 1455, 1466, 1486, 1488, 1512, 1518, 1562, 1580, 1591, 1600, 1608, 1617, 1624, 1634, 1649, 3070, 3146, 3150(2), 3152, 3154, 3157, 3159, 3163, 3165, 3168, 3179, 3183, 3185, 3196, 3409

Table D.1c. (continued) Vibrational Frequencies and Average Vibrational Energies of $M^{2+}(Phen)_2$ Reactants, Transition States, Intermediates, and Products Involved in the Activated Dissociation of $M^{2+}(Phen)_2$ Complexes through PTCF Process at 298 K.

Species	E_{vib} (eV)[a]	Vibrational frequencies (cm^{-1}) [b]
$Ni^{2+}(Phen)_2$ Int_3	0.57 (0.06)	3, 4, 5(2), 6, 9, 71, 102, 133, 137, 140, 223, 231, 232, 234, 241, 244, 254, 288, 398, 398, 410, 420, 424, 441, 461, 471, 493, 498, 503, 504, 508, 535, 551, 560, 580, 600, 620, 633, 681, 710, 714, 716, 719, 720, 729, 771, 775, 800, 810, 815, 846, 851, 853, 854, 885, 891, 905, 942, 962, 967, 971, 981, 983, 997, 1000, 1005, 1012, 1033, 1053, 1069, 1073, 1096, 1105, 1109, 1149, 1154, 1164, 1165, 1201, 1204, 1225, 1227(2), 1235, 1257, 1279, 1297, 1320, 1335, 1335, 1361, 1387, 1397, 1415, 1425, 1428, 1433, 1455, 1466, 1485, 1487, 1513, 1517, 1562, 1579, 1591, 1600, 1608, 1617, 1625, 1634, 1648, 3135, 3145, 3147, 3148, 3150, 3153, 3156, 3160, 3162, 3164, 3170, 3178, 3182, 3185, 3197, 3386
$[Ni(Phen-H)]^+$ Product 1	0.26 (0.03)	71, 137, 141, 233, 235, 241, 254, 288, 399, 424, 442, 471, 491, 502, 508, 560, 580, 632, 681, 714, 719, 729, 775, 809, 846, 852, 906, 943, 970, 982, 995, 1012, 1069, 1095, 1109, 1149, 1164, 1200, 1224, 1227, 1279, 1321, 1336, 1398, 1415, 1428, 1455, 1488, 1518, 1581, 1591, 1609, 1635, 3145, 3147, 3152, 3159, 3161, 3178, 3183
$Cu^{2+}(Phen)_2$ Reactant	0.55 (0.06)	27, 39, 39, 90(2), 140, 141, 145, 159, 168, 196, 233, 238, 251, 261, 273, 281, 299, 318, 409, 415, 430, 435, 440, 445, 480, 488, 507, 508, 511, 513, 539, 543, 560(2), 603, 607, 648, 653, 719, 720, 722, 723, 738, 741, 781, 783, 792, 794, 822, 825, 856, 857, 874, 875, 907, 913, 954, 957, 961, 964, 984(2), 1004, 1005, 1008(2), 1033, 1034, 1067, 1069, 1096, 1098, 1115, 1118, 1160, 1161, 1168(2), 1222, 1223, 1226, 1229, 1233, 1235, 1263, 1266, 1339(2), 1341, 1342, 1350, 1354, 1426(2), 1435(2), 1440, 1442, 1465, 1467, 1507(2), 1537, 1538, 1597(2), 1603, 1604, 1613, 1614, 1639(2), 3153(2), 3156(4), 3160(2), 3162(2), 3165(2), 3180(4)

Table D.1c. (continued) Vibrational Frequencies and Average Vibrational Energies of $M^{2+}(Phen)_2$ Reactants, Transition States, Intermediates, and Products Involved in the Activated Dissociation of $M^{2+}(Phen)_2$ Complexes through PTCF Process at 298 K.

Species	E_{vib} (eV)[a]	Vibrational frequencies (cm^{-1}) [b]
$Cu^{2+}(Phen)_2$ TS_1	0.57 (0.06)	**-1604**, 17, 25, 30, 74, 82, 114, 130, 135, 154, 164, 166, 215, 232, 241, 244, 254, 291, 316, 322, 356, 407, 425, 428, 435, 440, 445, 479, 492, 503, 506, 508, 509, 539, 541, 558, 562, 586, 603, 646, 649, 690, 714, 717, 721, 735, 747, 776, 780, 783, 798, 820, 822, 856, 857, 860, 868, 908, 913, 948, 959, 962, 978, 983, 990, 1003, 1006, 1007, 1013, 1033, 1061, 1068, 1097, 1098, 1114(2), 1136, 1144, 1159, 1164, 1168, 1214, 1221, 1226, 1227, 1235, 1241, 1268, 1301, 1328, 1333, 1336, 1340, 1354, 1397, 1418, 1425, 1430, 1434, 1441, 1463, 1463, 1484, 1508, 1519, 1534, 1580, 1594, 1601, 1603, 1609, 1616, 1637, 1637, 3146, 3148, 3151, 3154, 3155(2), 3157, 3161, 3162, 3164, 3166, 3178, 3179, 3180, 3192
$Cu^{2+}(Phen)_2$ Int_1	0.57 (0.06)	19, 25, 33, 77, 80, 122, 134, 139, 150, 159, 163, 232, 237, 247, 254, 266, 282, 294, 312, 380, 407, 414, 427, 434, 439, 443, 478, 487, 504, 507, 508, 509, 539, 540, 558, 561, 588, 603, 643, 646, 694, 714, 717, 721, 725, 734, 740, 768, 780, 782, 794, 816, 819, 856, 856, 857, 866, 906, 910, 947, 954, 959, 979, 984, 993, 1003, 1006, 1007, 1020, 1032, 1069, 1070, 1098, 1103, 1112, 1120, 1152, 1159, 1166, 1168, 1212, 1221, 1226, 1231, 1232, 1236, 1267, 1283, 1330, 1332, 1341, 1342, 1355, 1400, 1418, 1423, 1431, 1431, 1441, 1460, 1462, 1491, 1507, 1526, 1531, 1574, 1591, 1594, 1602, 1608, 1617, 1635, 1636, 2084, 3149, 3151, 3152, 3154, 3156(2), 3157, 3163, 3164, 3166, 3167, 3178, 3180, 3181, 3185

Table D.1c. (continued) Vibrational Frequencies and Average Vibrational Energies of $M^{2+}(Phen)_2$ Reactants, Transition States, Intermediates, and Products Involved in the Activated Dissociation of $M^{2+}(Phen)_2$ Complexes through PTCF Process at 298 K.

Species	E_{vib} (eV)[a]	Vibrational frequencies (cm^{-1}) [b]
$Cu^{2+}(Phen)_2$ TS_2	0.56 (0.06)	**-463**, 12, 29, 33, 80, 85, 117, 135, 143, 157, 163, 181, 233, 239, 249, 252, 263, 274, 290, 305, 407, 414, 425, 432, 436, 443, 477, 486, 506, 507, 508, 510, 541, 543, 558, 561, 591, 606, 641, 643, 698, 701, 719, 719, 722, 730, 734, 777, 782, 782, 799, 821, 822, 854, 857, 858, 865, 900, 907, 955(2), 960, 979, 985, 992, 1005(2), 1008, 1021, 1032, 1069, 1071, 1097, 1101, 1107, 1120, 1151, 1158, 1166, 1168, 1210, 1222, 1224, 1230, 1232, 1235, 1265, 1285, 1329, 1334, 1340, 1343, 1354, 1402, 1418, 1425, 1430(2), 1441, 1459, 1460, 1492, 1506, 1526, 1529, 1579, 1589, 1596, 1600, 1609, 1615, 1635, 1635, 2050, 3148, 3152, 3153, 3155(2), 3157, 3159, 3160, 3165(2), 3167, 3179, 3180, 3181, 3185
$Cu^{2+}(Phen)_2$ Int_2	0.57 (0.06)	17, 20, 24, 54, 79, 106, 124, 139, 145, 153, 175, 186, 229, 240, 245, 248, 258, 277, 285, 396, 407, 417, 430, 431, 439, 465, 481, 504, 507, 508, 509, 534, 543, 551, 561, 591, 599, 634, 638, 703, 707, 717, 719, 726, 731, 774, 782, 784, 785, 812, 823, 843, 851, 856, 861, 893, 898, 910, 946, 963, 972, 978, 987, 991, 1006, 1007, 1011, 1016, 1031, 1066, 1071, 1093, 1099, 1111, 1114, 1151, 1158, 1164, 1172, 1210, 1210, 1222, 1229, 1230, 1237, 1258, 1286, 1307, 1326, 1333, 1337, 1351, 1376, 1401, 1414, 1418, 1429, 1435, 1458, 1461, 1490, 1491, 1518, 1524, 1569, 1582, 1595, 1609, 1611(2), 1625, 1633, 1649, 3144, 3149, 3150, 3153, 3154, 3155, 3156, 3159, 3160, 3163, 3169, 3177, 3181, 3184(2), 3195

Table D.1c. (continued) Vibrational Frequencies and Average Vibrational Energies of $M^{2+}(Phen)_2$ Reactants, Transition States, Intermediates, and Products Involved in the Activated Dissociation of $M^{2+}(Phen)_2$ Complexes through PTCF Process at 298 K.

Species	E_{vib} (eV)[a]	Vibrational frequencies (cm^{-1}) [b]
$Cu^{2+}(Phen)_2$ TS_3	0.57 (0.06)	**-43**, 9, 14, 20, 33, 46, 83, 108, 133, 136, 146, 216, 226, 231, 235, 240, 244, 250, 279, 398, 398, 409, 421, 428, 440, 456, 467, 499(2), 505, 507, 515, 535, 550, 564, 581, 600, 620, 642, 692, 707, 712, 718, 720, 729, 733, 772, 784, 798, 814, 820, 835, 853(2), 862, 882, 898, 908, 962, 963, 971, 979, 985, 993, 1006, 1007, 1008, 1009, 1033, 1055, 1070, 1076, 1094, 1106, 1113, 1153, 1156, 1166, 1168, 1203, 1204, 1224, 1226, 1227, 1236, 1254, 1280, 1293, 1324, 1335, 1336, 1361, 1385, 1400, 1411, 1420, 1426, 1434, 1458, 1464, 1482, 1487, 1511, 1521, 1563, 1580, 1596, 1610, 1615, 1616, 1621, 1632, 1645, 3141, 3144, 3151, 3152, 3155(2), 3157, 3164, 3165, 3166, 3175, 3181, 3183, 3185, 3198, 3373
$Cu^{2+}(Phen)_2$ Int_3	0.57 (0.06)	4, 5, 6, 7, 8, 9, 75, 103, 132, 134, 135, 223, 229, 231, 235, 240, 245, 245, 281, 397, 398, 410, 420, 426, 441, 461, 466, 495, 498, 504, 507, 509, 535, 551, 565, 581, 600, 620, 642, 691, 710, 714, 718, 720, 726, 731, 770, 780, 799, 815, 816, 835, 851, 854, 859, 885, 890, 899, 955, 961, 967, 974, 981, 988, 1000, 1001, 1005, 1006, 1033, 1053, 1069, 1073, 1095, 1105, 1112, 1153, 1154, 1164, 1165, 1204(2), 1224, 1225, 1227, 1235, 1257, 1282, 1296, 1324, 1335(2), 1361, 1386, 1401, 1412, 1425, 1427, 1433, 1459, 1465, 1485, 1488, 1513, 1523, 1562, 1584, 1599, 1611, 1617, 1621, 1625, 1634, 1648, 3135, 3141, 3148(2), 3150, 3153, 3156, 3162, 3164, 3165, 3171, 3180, 3183, 3185, 3197, 3386
$[Cu(Phen\text{-}H)]^+$ Product 1	0.26 (0.03)	76, 131, 135, 230, 235, 240, 242, 281, 398, 426, 440, 467, 495, 507, 509, 565, 581, 641, 692, 718, 726, 731, 780, 816, 834, 858, 900, 955, 973, 987, 1000, 1007, 1069, 1095, 1111, 1153, 1164, 1205, 1224, 1225, 1282, 1325, 1336, 1402, 1412, 1427, 1459, 1489, 1524, 1585, 1612, 1622, 1635, 3141, 3148, 3152, 3161, 3165, 3179, 3183

Table D.1c. (continued) Vibrational Frequencies and Average Vibrational Energies of $M^{2+}(Phen)_2$ Reactants, Transition States, Intermediates, and Products Involved in the Activated Dissociation of $M^{2+}(Phen)_2$ Complexes through PTCF Process at 298 K.

Species	E_{vib} (eV)[a]	Vibrational frequencies (cm^{-1}) [b]
$Zn^{2+}(Phen)_2$ Reactant	0.55 (0.06)	24, 27(2), 81(2), 129, 141, 147, 151, 152, 222(2), 233(2), 250, 256, 279, 294, 301, 406, 412, 428, 434, 441(2), 478(2), 509(2), 511(2), 543, 544, 559, 560, 607, 610, 652(2), 724(2), 725(2), 733, 735, 782(2), 804, 806, 829, 831, 859(2), 872, 873, 909(2), 958(2), 961(2), 985(2), 1006(2), 1010(2), 1035(2), 1072, 1073, 1101(2), 1115, 1117, 1162(2), 1169(2), 1220(2), 1227, 1229, 1235(2), 1270(2), 1335(2), 1340(2), 1353, 1355, 1426(2), 1430(2), 1442(2), 1464, 1465, 1509(2), 1538, 1540, 1600(2), 1606(2), 1616(2), 1639(2), 3151(2), 3155(4), 3159(4), 3164(2), 3180(4)
$Zn^{2+}(Phen)_2$ TS_1	0.56 (0.06)	**-1596**, 21, 25, 26, 77, 80, 124, 139, 145, 150, 158, 201, 221, 226, 232, 242, 253, 279, 284, 298, 392, 408, 414, 426, 433, 441, 474, 477, 499, 502, 509, 511, 527, 542, 550, 560, 593, 608, 640, 653, 689, 712, 724(2), 728, 734, 779, 782, 794, 803, 829, 833, 843, 859, 868, 873, 884, 894, 911, 956, 960, 966, 985, 987, 991, 1007, 1010(2), 1025, 1035, 1050, 1073, 1086, 1091, 1101, 1117, 1127, 1162, 1167, 1169, 1186, 1220, 1224, 1227, 1228, 1234, 1235, 1270, 1276, 1336, 1340, 1343, 1354, 1369, 1418, 1426, 1429, 1431, 1442, 1444, 1465, 1478, 1501, 1509, 1539, 1553, 1597, 1601, 1606, 1608, 1616, 1633, 1639, 2269, 3137, 3153(2), 3154, 3155, 3156, 3157, 3159, 3160(2), 3165(2), 3181(3)
$Zn^{2+}(Phen)_2$ Int_1	0.57 (0.06)	20, 25, 25, 76, 78, 101, 130, 145, 152, 160, 168, 224, 229, 233, 235, 253, 267, 283, 298, 370, 407, 415, 425, 434, 440, 467, 477, 494, 504, 510(2), 525, 540, 549, 560, 600, 608, 632, 654, 676, 705, 721, 723, 725, 735, 754, 779, 782, 798, 801, 827, 839, 858, 859, 873, 874, 912, 919, 957, 960(2), 966, 980, 986, 999, 1007, 1008, 1011, 1034, 1044, 1075, 1083, 1102, 1105, 1117, 1152, 1163, 1164, 1170, 1202, 1221, 1222, 1228, 1229, 1235, 1259, 1267, 1270, 1337(2), 1339, 1353, 1357, 1372, 1418, 1426, 1429, 1432, 1435, 1442, 1465, 1477, 1488, 1509, 1527, 1539, 1593, 1598, 1600, 1605, 1615, 1632, 1639, 3138, 3153(2), 3155(2), 3156, 3158(2), 3159, 3161, 3166(2), 3181, 3182(2), 3363

Table D.1c. (continued) Vibrational Frequencies and Average Vibrational Energies of $M^{2+}(Phen)_2$ Reactants, Transition States, Intermediates, and Products Involved in the Activated Dissociation of $M^{2+}(Phen)_2$ Complexes through PTCF Process at 298 K.

Species	E_{vib} (eV)[a]	Vibrational frequencies (cm^{-1}) [b]
$Zn^{2+}(Phen)_2$ TS_2	0.57 (0.06)	**-622**, 27, 30, 54, 78, 92, 133, 137, 146, 157, 179, 200, 235, 235, 242, 248, 251, 294, 299, 404, 407, 414, 431, 432, 439, 469, 478, 484, 507, 508, 510, 540, 547, 559, 560, 584, 606, 632, 652, 689, 697, 716, 721, 723, 736, 751, 783, 786, 793, 798, 825, 833, 855, 860, 871, 873, 902, 911, 960, 964, 968, 979, 985, 992, 994,1004, 1007, 1009, 1010, 1034, 1064, 1071, 1093, 1099, 1116, 1116, 1135, 1158, 1161, 1169, 1169, 1214, 1222, 1225, 1228, 1233, 1235, 1266, 1291, 1313, 1337, 1342, 1343, 1354, 1370, 1395, 1424, 1427, 1430, 1431, 1441, 1448, 1464, 1494, 1508, 1537, 1539, 1570, 1597, 1603, 1611, 1616, 1632, 1638, 1804, 3141, 3152, 3153, 3155, 3155, 3156, 3158, 3160, 3165(2), 3167, 3180(3), 3198
$Zn^{2+}(Phen)_2$ Int_2	0.59 (0.06)	11, 19, 27, 43, 76, 81, 120, 134, 138, 142, 163, 193, 213, 233, 238, 244, 253, 262, 289, 386, 392, 412, 421, 425, 432, 440, 453, 462, 479, 486, 509, 514, 519, 543, 548, 558, 564, 565, 598, 610, 649, 663, 677, 708, 724, 726, 732, 760, 766, 781, 786, 805, 816, 829, 858, 859, 870, 890, 906, 953, 956, 960, 967, 983, 985, 988, 1003, 1007, 1012, 1035, 1050, 1069, 1079, 1098, 1114, 1132, 1140, 1160, 1167, 1169, 1207, 1212, 1220, 1227, 1229, 1235, 1271, 1284, 1305, 1331, 1332, 1341, 1355, 1364, 1394, 1419, 1425, 1430, 1437, 1441, 1466, 1480, 1510, 1516, 1537, 1565, 1600, 1607, 1618, 1618, 1627, 1639, 1785, 1998, 3137, 3150, 3152, 3153, 3154, 3155, 3156, 3157, 3161, 3163, 3170, 3178, 3179, 3180, 3224

Table D.1c. (continued) Vibrational Frequencies and Average Vibrational Energies of $M^{2+}(Phen)_2$ Reactants, Transition States, Intermediates, and Products Involved in the Activated Dissociation of $M^{2+}(Phen)_2$ Complexes through PTCF Process at 298 K.

Species	E_{vib} (eV)[a]	Vibrational frequencies (cm^{-1}) [b]
$Zn^{2+}(Phen)_2$ TS_3	0.57 (0.06)	**-1090**, 20, 23, 26, 69, 80, 91, 139, 142, 148, 154, 186, 212, 231, 237, 247, 256, 269, 282, 299, 407, 412, 417, 426, 429, 439, 471, 479, 495, 505, 507, 508, 539, 542, 550, 557, 585, 603, 625, 636, 679, 695, 709, 714, 719, 726, 729, 781, 784, 786, 800, 812, 827, 830, 850, 858, 863, 897, 904, 950, 956, 959, 977, 984, 991, 993, 1002, 1007, 1008, 1028, 1068, 1070, 1092, 1092, 1103, 1114, 1156, 1157, 1167, 1169, 1205, 1215, 1225, 1226, 1231, 1232, 1258, 1273, 1279, 1329, 1336, 1337, 1341, 1349, 1397, 1409, 1414, 1426, 1426, 1439, 1454, 1455, 1488, 1503, 1528, 1531, 1575, 1581, 1587, 1606, 1607, 1621, 1632, 1633, 3136, 3153(2), 3155, 3156, 3158, 3160(2), 3162, 3166(2), 3179, 3181, 3182, 3186
$Zn^{2+}(Phen)_2$ Int_3	0.55 (0.07)	22, 28, 44, 52, 72, 86, 106, 115, 134, 140, 152, 205, 219, 224, 230, 242, 252, 296, 298, 352, 374, 392, 411, 416, 433, 467, 471, 479, 496, 502, 508, 526, 530, 550, 560, 589, 597, 633, 650, 679, 701, 707, 719, 729, 737, 760, 769, 781, 792, 799, 824, 826, 842, 851, 856, 859, 901, 908, 937, 943, 959, 975, 982, 993, 993, 996, 1001, 1006, 1028, 1065, 1071, 1092, 1103, 1110, 1113, 1155, 1159, 1166, 1171, 1212, 1214, 1228, 1229, 1233, 1238, 1259, 1288, 1314, 1335, 1345, 1351, 1353, 1382, 1396, 1408, 1409, 1428, 1435, 1448, 1455, 1488, 1492, 1514, 1529, 1553, 1568, 1574, 1598, 1602, 1609, 1623, 1633, 1637, 3092, 3137, 3147, 3151, 3156(2), 3157, 3158, 3161, 3164, 3169, 3175, 3178, 3181, 3183, 3193

Table D.1c. (continued) Vibrational Frequencies and Average Vibrational Energies of $M^{2+}(Phen)_2$ Reactants, Transition States, Intermediates, and Products Involved in the Activated Dissociation of $M^{2+}(Phen)_2$ Complexes through PTCF Process at 298 K.

Species	E_{vib} (eV)[a]	Vibrational frequencies (cm^{-1}) [b]
$Zn^{2+}(Phen)_2$ TS_4	0.55 (0.07)	**-20**, 9, 16, 18, 43, 54, 74, 104, 138, 144, 157, 208, 220, 232, 237, 244, 245, 270, 307, 396, 400, 410, 422, 423, 429, 460, 470, 483, 500, 502, 504, 519, 541, 551, 560, 593, 602, 621, 656, 698, 709, 710, 716, 720, 725, 750, 778, 786, 802, 824, 832, 843, 853, 856, 870, 883, 903, 909, 960, 965, 970, 981(2), 999, 1004, 1005, 1009, 1025, 1031, 1047, 1057, 1070, 1095, 1098, 1104, 1154, 1165, 1165, 1174, 1199, 1215, 1224, 1228, 1231, 1235, 1254, 1278, 1289, 1308, 1336, 1340, 1354, 1362, 1384, 1408, 1419, 1424, 1432, 1435, 1464, 1480(2), 1500, 1510, 1550, 1561, 1593, 1598, 1607, 1615, 1624, 1632, 1646, 3122, 3131, 3140, 3148, 3148, 3151(2), 3154, 3155, 3163, 3164, 3165, 3172, 3183, 3184, 3383
$Zn^{2+}(Phen)_2$ Int_4	0.57 (0.06)	4, 6, 14, 7, 17, 25, 77, 103, 134, 138, 154, 157, 220, 223, 231, 241, 245, 245, 300, 398, 402, 410, 420, 424, 428, 461, 476, 481, 495, 498, 504, 535, 535, 551, 555, 595, 600, 620, 645, 693, 698, 710, 714, 720, 725, 770, 778, 783, 800, 815, 827, 833, 851, 854, 867, 885, 891, 897, 959(2), 962, 968, 975, 981, 1000, 1001, 1003, 1005, 1033, 1049, 1053, 1073, 1084, 1102, 1105, 1154, 1159, 1165, 1165, 1204, 1214, 1219, 1227, 1235, 1238, 1257, 1280, 1296, 1314, 1327, 1335, 1361, 1368, 1387, 1407, 1423, 1425, 1429, 1433, 1466(2), 1485, 1493, 1513, 1543, 1562, 1589, 1599, 1604, 1617, 1625, 1630, 1648, 3131, 3132, 3147, 3148, 3150, 3151, 3156, 3157, 3158, 3160, 3164, 3171, 3178, 3185, 3197, 3386

Table D.1c. (continued) Vibrational Frequencies and Average Vibrational Energies of $M^{2+}(Phen)_2$ Reactants, Transition States, Intermediates, and Products Involved in the Activated Dissociation of $M^{2+}(Phen)_2$ Complexes through PTCF Process at 298 K.

Species	E_{vib} (eV)[a]	Vibrational frequencies (cm^{-1}) [b]
$[Zn(Phen\text{-}H)]^+$ Product 1	0.26 (0.03)	62, 129, 150, 196, 231, 240, 244, 299, 395, 419, 424, 471, 477, 501, 525, 558, 592, 648, 698, 704, 723, 764, 782, 828, 830, 866, 900, 959, 975, 977, 998, 1003, 1061, 1094, 1101, 1162, 1169, 1218, 1223, 1232, 1280, 1341, 1344, 1398, 1408, 1421, 1442, 1486, 1505, 1554, 1592, 1611, 1633, 3129, 3148, 3151, 3155, 3162, 3166, 3180

[a]Uncertainties listed in parentheses are determined as described in the text. [b]Vibrational frequencies scaled by 0.9804 obtained from vibrational analyses of the B3LYP/6-31G* geometry optimized structures. Degeneracies are indicated in parentheses.

Table D.2a. Rotational Constants (in cm^{-1}) of $M^{2+}(Phen)_2$ Reactants, Products and Their Corresponding PSL Transition States for Dissociation of $M^{2+}(Phen)_2$ Complexes through Simple CID Process.

	Energized Molecule		Transition State		
Complex	1-D[a]	2-D[b]	1-D[c]	2-D[c]	2-D[d]
$Fe^{2+}(Phen)_2$ Reactant	0.0097	0.0034	0.0249, 0.0540	0.0144, 0.0166	0.0002
Fe^{2+}(Phen) Product 1			0.0108	0.0218	
Phen Product 2			0.0540	0.0166	
$Co^{2+}(Phen)_2$ Reactant	0.0097	0.0035	0.0245, 0.0540	0.0144, 0.0166	0.0002
Co^{2+}(Phen) Product 1			0.0108	0.0218	
$Ni^{2+}(Phen)_2$ Reactant	0.0098	0.0035	0.0251, 0.0540	0.0146, 0.0166	0.0002
Ni^{2+}(Phen) Product 1			0.0109	0.0221	
$Cu^{2+}(Phen)_2$ Reactant	0.0098	0.0036	0.0244, 0.0540	0.0145, 0.0166	0.0002
Cu^{2+}(Phen) Product 1			0.0108	0.0218	
$Zn^{2+}(Phen)_2$ Reactant	0.0097	0.0035	0.0244, 0.0540	0.0143, 0.0166	0.0002
Zn^{2+}(Phen) Product 1			0.0107	0.0216	

[a]Active external. [b]Inactive external. [c]Rotational constants of the PSL TS treated as free internal rotors. [d]Two-dimensional rotational constant of the PSL TS at threshold, treated variationally and statistically.

Table D.2b. Rotational Constants (in cm^{-1}) of $M^{2+}(Phen)_2$ Reactants, Transition States, Intermediates, and Products Involved in the Activated Dissociation of $M^{2+}(Phen)_2$ Complexes through ETCF Process.

	Rotational Constants[a]	
Complex	1-D	2-D
$Fe^{2+}(Phen)_2$ Reactant	0.0097	0.0034
$Fe^{2+}(Phen)_2$ TS	0.0087	0.0040
$Fe^{2+}(Phen)_2$ Int	0.0096	0.0009
$Fe(Phen)^+$ Product 1	0.0105	0.0210
$Phen^+$ Product 2	0.0548	0.0164
$Co^{2+}(Phen)_2$ Reactant	0.0097	0.0035
$Co^{2+}(Phen)_2$ TS	0.0097	0.0037
$Co^{2+}(Phen)_2$ Int	0.0097	0.0009
$Co(Phen)^+$ Product 1	0.0108	0.0218
$Ni^{2+}(Phen)_2$ Reactant	0.0097	0.0036
$Ni^{2+}(Phen)_2$ TS	0.0091	0.0040
$Ni^{2+}(Phen)_2$ Int	0.0096	0.0009
$Ni(Phen)^+$ Product 1	0.0110	0.0222
$Cu^{2+}(Phen)_2$ Reactant	0.0098	0.0036
$Cu^{2+}(Phen)_2$ TS	0.0095	0.0034
$Cu^{2+}(Phen)_2$ Int	0.0096	0.0009
$Cu(Phen)^+$ Product 1	0.0108	0.0218
$Zn^{2+}(Phen)_2$ Reactant	0.0097	0.0035
$Zn^{2+}(Phen)_2$ TS	0.0099	0.0033
$Zn^{2+}(Phen)_2$ Int	0.0096	0.0009
$Zn(Phen)^+$ Product 1	0.0104	0.0208

[a]Geometry optimization and frequency calculation were performed at B3LYP/6-31G*. Rotational constants of $M^{2+}(Phen)_2$ reactant and the transition state were employed for thermochemical analysis of experimental data.

Table D.2c. Rotational Constants (in cm^{-1}) of $M^{2+}(Phen)_2$ Reactants, Transition States, Intermediates, and Products Involved in the Activated Dissociation of $M^{2+}(Phen)_2$ Complexes through PTCF Process.

	Rotational constants[a]	
Complex	1-D	2-D
$Fe^{2+}(Phen)_2$ Reactant	0.0097	0.0034
$Fe^{2+}(Phen)_2$ TS_1	0.0098	0.0035
$Fe^{2+}(Phen)_2$ Int_1	0.0096	0.0037
$Fe^{2+}(Phen)_2$ TS_2	0.0097	0.0034
$Fe^{2+}(Phen)_2$ Int_2	0.0095	0.0035
$Fe^{2+}(Phen)_2$ TS_3	0.0109	0.0019
$Fe^{2+}(Phen)_2$ Int_3	0.0116	0.0006
$[Fe(Phen-H)]^+$ Product 1	0.0109	0.0219
$(Phen+H)^+$ Product 2	0.0526	0.0166
$Co^{2+}(Phen)_2$ Reactant	0.0097	0.0035
$Co^{2+}(Phen)_2$ TS_1	0.0097	0.0035
$Co^{2+}(Phen)_2$ Int_1	0.0097	0.0036
$Co^{2+}(Phen)_2$ TS_2	0.0097	0.0034
$Co^{2+}(Phen)_2$ Int_2	0.0096	0.0038
$Co^{2+}(Phen)_2$ TS_3	0.0098	0.0035
$Co^{2+}(Phen)_2$ Int_3	0.0096	0.0031
$Co^{2+}(Phen)_2$ TS_4	0.0113	0.0017
$Co^{2+}(Phen)_2$ Int_4	0.0115	0.0006
$[Co(Phen-H)]^+$ Product 1	0.0109	0.0220
$Ni^{2+}(Phen)_2$ Reactant	0.0097	0.0036
$Ni^{2+}(Phen)_2$ TS_1	0.0098	0.0037
$Ni^{2+}(Phen)_2$ Int_1	0.0097	0.0038
$Ni^{2+}(Phen)_2$ TS_2	0.0098	0.0036
$Ni^{2+}(Phen)_2$ Int_2	0.0096	0.0033
$Ni^{2+}(Phen)_2$ TS_3	0.0112	0.0017
$Ni^{2+}(Phen)_2$ Int_3	0.0115	0.0006
$[Ni(Phen-H)]^+$ Product 1	0.0111	0.0224

Table D.2c. (continued) Rotational Constants (in cm^{-1}) of $M^{2+}(Phen)_2$ Reactants, Transition States, Intermediates, and Products Involved in the Activated Dissociation of $M^{2+}(Phen)_2$ Complexes through PTCF Process.

	Rotational constants[a]	
Complex	1-D	2-D
$Cu^{2+}(Phen)_2$ Reactant	0.0098	0.0036
$Cu^{2+}(Phen)_2$ TS_1	0.0097	0.0036
$Cu^{2+}(Phen)_2$ Int_1	0.0097	0.0037
$Cu^{2+}(Phen)_2$ TS_2	0.0098	0.0036
$Cu^{2+}(Phen)_2$ Int_2	0.0096	0.0033
$Cu^{2+}(Phen)_2$ TS_3	0.0096	0.0026
$Cu^{2+}(Phen)_2$ Int_3	0.0115	0.0006
$[Cu(Phen\text{-}H)]^+$ Product 1	0.0109	0.0220
$Zn^{2+}(Phen)_2$ Reactant	0.0097	0.0035
$Zn^{2+}(Phen)_2$ TS_1	0.0096	0.0035
$Zn^{2+}(Phen)_2$ Int_1	0.0096	0.0036
$Zn^{2+}(Phen)_2$ TS_2	0.0099	0.0033
$Zn^{2+}(Phen)_2$ Int_2	0.0100	0.0032
$Zn^{2+}(Phen)_2$ TS_3	0.0097	0.0034
$Zn^{2+}(Phen)_2$ Int_3	0.0097	0.0035
$Zn^{2+}(Phen)_2$ TS_4	0.0108	0.0018
$Zn^{2+}(Phen)_2$ Int_4	0.0115	0.0006
$[Zn(Phen\text{-}H)]^+$ Product 1	0.0107	0.0214

[a]Geometry optimization and frequency calculation were performed at B3LYP/6-31G*. Rotational constants of $M^{2+}(Phen)_2$ reactant and the rate limiting transition state were employed for thermochemical analysis of experimental data.

Table D.3a. Select B3LYP/6-31G* Geometrical Parameters for the ETCF Activated Dissociation of $Fe^{2+}(Phen)_2$ and $Co^{2+}(Phen)_2$ Complexes[a]

	$Fe^{2+}(Phen)_2$			
	Reactant	TS	Int	Products
Fe^{2+}–N1	2.062	2.057	1.998	2.130
Fe^{2+}–N10	2.062	2.069	1.998	2.130
Fe^{2+}–N1′	2.063	2.264	9.755	–
Fe^{2+}–N10′	2.062	3.979	9.262	–
∠N1Fe^{2+}N10′C	81.2	132.4	94.5	–
∠N1Fe^{2+}N10′	124.2	74.9	143.4	–
∠N1Fe^{2+}N1′	124.1	100.9	141.2	–
∠N1Fe^{2+}N10	83.0	82.2	88.1	79.3
∠N10′Fe^{2+}N1′	83.0	42.4	16.1	–
∠N10′Fe^{2+}N10	124.1	143.9	128.0	–
∠N1′Fe^{2+}N10	124.1	173.6	128.6	–
∠N1CCN10	0.0	0.5	0.0	0.0
∠N1′CCN10′	0.0	7.5	0.0	0.0
	$Co^{2+}(Phen)_2$			
	Reactant	TS	Int	Products
Co^{2+}–N1	2.024	1.990	1.953	1.924
Co^{2+}–N10	2.023	2.028	1.950	1.924
Co^{2+}–N1′	2.024	2.462	9.958	–
Co^{2+}–N10′	2.024	4.230	9.262	–
∠N1Co^{2+}N10′C	81.2	138.5	92.5	–
∠N1Co^{2+}N10′	123.4	74.6	128.6	–
∠N1Co^{2+}N1′	123.4	91.3	128.0	–
∠N1Co^{2+}N10	84.2	84.7	88.8	88.4
∠N10′Co^{2+}N1′	84.1	38.4	16.1	–
∠N10′Co^{2+}N10	123.5	155.7	141.1	–
∠N1′Co^{2+}N10	123.5	157.6	143.4	–
∠N1CCN10	0.0	0.4	0.5	0.0
∠N1′CCN10′	0.0	7.8	0.5	0.0

[a]Bond angles (∠) are given in degrees (°) and bond lengths in angstroms (Å).

Table D.3b. Select B3LYP/6-31G* Geometrical Parameters for the ETCF Activated Dissociation of $Ni^{2+}(Phen)_2$ and $Cu^{2+}(Phen)_2$ Complexes[a]

	$Ni^{2+}(Phen)_2$			
	Reactant	TS	Int	Products
Ni^{2+}–N1	2.003	1.971	1.985	1.872
Ni^{2+}–N10	2.003	1.971	1.986	1.873
Ni^{2+}–N1′	2.003	2.125	9.804	–
Ni^{2+}–N10′	2.003	3.849	9.220	–
∠N1Ni^{2+}N10′C	82.1	132.7	111.7	–
∠N1Ni^{2+}N10′	124.0	75.8	141.4	–
∠N1Ni^{2+}N1′	124.0	97.6	132.2	–
∠N1Ni^{2+}N10	83.2	85.6	94.1	92.5
∠N10′ Ni^{2+}N1′	83.2	44.5	16.3	–
∠N10′ Ni^{2+}N10	124.0	150.0	130.5	–
∠N1′ Ni^{2+}N10	124.0	164.4	133.5	–
∠N1CCN10	0.0	0.8	0.1	0.0
∠N1′CCN10′	0.0	8.3	0.0	0.0
	$Cu^{2+}(Phen)_2$			
	Reactant	TS	Int	Products
Cu^{2+}–N1	1.986	1.937	1.984	1.880
Cu^{2+}–N10	1.985	1.951	1.982	1.881
Cu^{2+}–N1′	1.986	2.607	9.904	–
Cu^{2+}–N10′	1.985	4.824	9.020	–
∠N1Cu^{2+}N10′C	49.0	59.6	68.7	–
∠N1Cu^{2+}N10′	103.8	78.4	130.5	–
∠N1Cu^{2+}N1′	149.2	92.6	133.5	–
∠N1Cu^{2+}N10	84.4	86.9	87.8	96.1
∠N10′Cu^{2+}N1′	84.4	26.4	16.3	–
∠N10′Cu^{2+}N10	149.1	142.9	141.4	–
∠N1′Cu^{2+}N10	103.8	168.2	132.2	–
∠N1CCN10	1.0	0.1	0.1	0.0
∠N1′CCN10′	1.0	5.1	0.0	0.0

[a]Bond angles (∠) are given in degrees (°) and bond lengths in angstroms (Å).

Table D.3c. Select B3LYP/6-31G* Geometrical Parameters for the ETCF Activated Dissociation of $Zn^{2+}(Phen)_2$ Complex[a]

	Reactant	TS	Int	Products
Zn^{2+}–N1	2.024	1.981	1.986	2.056
Zn^{2+}–N10	2.023	1.976	1.985	2.057
Zn^{2+}–N1′	2.023	2.711	9.804	–
Zn^{2+}–N10′	2.024	4.839	9.220	–
∠N1Zn^{2+}N10′C	81.1	145.8	89.2	–
∠N1Zn^{2+}N10′	123.1	66.7	130.5	–
∠N1Zn^{2+}N1′	123.2	91.7	133.5	–
∠N1Zn^{2+}N10	84.6	87.3	87.8	82.7
∠N10′Zn^{2+}N1′	84.6	27.8	16.3	–
∠N10′Zn^{2+}N10	123.2	152.6	139.2	–
∠N1′Zn^{2+}N10	123.2	176.5	125.8	–
∠N1CCN10	0.0	1.1	0.1	0.0
∠N1′CCN10′	0.0	9.7	0.0	0.0

[a]Bond angles (∠) are given in degrees (°) and bond lengths in angstroms (Å).

Table D.4a. Select B3LYP/6-31G* Geometrical Parameters for the PTCF Activated Dissociation of $Fe^{2+}(Phen)_2$ Complex[a]

	Reactant	TS_1	Int_1	TS_2	Int_2	TS_3	Int_3	Products
Fe^{2+}–N1	2.063	1.939	1.983	2.045	2.013	1.906	1.888	1.903
Fe^{2+}–N10	2.063	2.256	2.076	2.098	2.030	2.031	2.116	2.136
Fe^{2+}–N1′	2.061	2.046	2.097	2.068	1.981	6.995	12.14	–
Fe^{2+}–N10′	2.061	2.094	1.986	2.116	3.072	5.795	14.32	–
C1–H1	1.070	1.933	2.885	3.288	3.606	3.218	13.98	–
N10′–H1	4.083	2.504	2.327	1.271	1.042	1.025	1.024	1.025
Fe^{2+}–H1	3.260	1.663	1.527	1.635	2.109	5.251	13.37	–
∠N1Fe^{2+}N10′C	81.2	96.2	57.0	74.5	83.1	142.5	111.6	–
∠N1Fe^{2+}N10′	124.1	139.6	165.1	128.9	105.9	55.2	119.6	–
∠N1Fe^{2+}N1′	124.1	134.8	110.2	128.5	135.1	57.5	118.1	83.7
∠N1Fe^{2+}N10	82.9	76.2	82.5	82.2	82.0	90.2	86.0	–
∠N10′Fe^{2+}N1′	83.0	81.1	82.4	80.2	64.2	22.0	7.0	–
∠N10′Fe^{2+}N10	124.2	121.8	101.1	117.5	127.1	144.5	147.1	–
∠N1′Fe^{2+}N10	124.1	100.1	109.7	125.3	150.2	133.9	142.9	–
∠N1CCN10	0.0	0.3	0.0	0.3	0.5	0.0	0.6	0.0
∠N1′CCN10′	0.0	0.9	0.6	2.8	0.1	0.0	0.1	0.0

[a]Bond angles (∠) are given in degrees (°) and bond lengths in angstroms (Å).

Table D.4b. Select B3LYP/6-31G* Geometrical Parameters for the PTCF Activated Dissociation of $Co^{2+}(Phen)_2$ Complex[a]

	Reactant	TS_1	Int_1	TS_2	Int_2
Co^{2+}–N1	2.023	2.060	2.168	2.428	1.950
Co^{2+}–N10	2.023	2.038	2.034	2.003	2.045
Co^{2+}–N1′	2.025	2.015	2.009	2.043	2.051
Co^{2+}–N10′	2.024	2.021	2.014	1.995	1.963
C1–H1	1.070	1.412	1.999	2.362	2.940
N10′–H1	4.018	3.310	3.211	2.657	2.234
Co^{2+}–H1	3.234	2.477	2.297	1.538	1.483
∠N1Co^{2+}N10′C	81.2	78.2	78.8	76.8	56.7
∠N1Co^{2+}N10′	123.4	122.1	116.4	125.9	164.7
∠N1Co^{2+}N1′	123.4	121.6	125.5	111.4	111.5
∠N1Co^{2+}N10	84.2	83.5	81.6	77.1	84.1
∠N10′Co^{2+}N1′	84.1	84.6	85.1	83.3	82.5
∠N10′Co^{2+}N10	123.5	123.9	127.3	137.3	97.5
∠N1′Co^{2+}N10	123.4	126.3	126.0	124.9	108.6
∠N1CCN10	0.0	4.0	10.6	3.4	0.7
∠N1′CCN10′	0.0	0.1	0.3	0.4	0.4

[a]Bond angles (∠) are given in degrees (°) and bond lengths in angstroms (Å).

Table D.4b. (continued) Select B3LYP/6-31G* Geometrical Parameters for the PTCF Activated Dissociation of $Co^{2+}(Phen)_2$ Complex[a]

	TS_3	Int_3	TS_4	Int_4	Products
Co^{2+}–N1	2.017	2.013	1.936	1.946	1.936
Co^{2+}–N10	2.065	2.030	1.928	1.936	1.922
Co^{2+}–N1′	2.040	1.981	4.947	12.23	–
Co^{2+}–N10′	2.109	3.072	7.057	14.43	–
C1–H1	3.311	3.606	7.353	14.40	–
N10′–H1	1.265	1.042	1.023	1.024	1.025
Co^{2+}–H1	1.574	2.109	6.119	13.47	–
∠N1Co^{2+}N10′C	71.5	71.5	77.5	78.9	–
∠N1Co^{2+}N10′	129.0	105.9	118.6	119.3	–
∠N1Co^{2+}N1′	131.7	135.1	113.5	117.6	–
∠N1Co^{2+}N10	82.4	82.0	90.7	88.4	90.4
∠N10′Co^{2+}N1′	80.6	64.2	16.8	6.8	–
∠N10′Co^{2+}N10	110.8	124.8	148.0	145.7	–
∠N1′Co^{2+}N10	126.6	141.1	141.2	142.1	–
∠N1CCN10	0.3	0.5	0.1	0.3	0.0
∠N1′CCN10′	2.9	0.1	0.2	0.0	0.0

[a]Bond angles (∠) are given in degrees (°) and bond lengths in angstroms (Å).

Table D.4c. Select B3LYP/6-31G* Geometrical Parameters for the PTCF Activated Dissociation of $Ni^{2+}(Phen)_2$ Complex[a]

	Reactant	TS_1	Int_1	TS_2	Int_2	TS_3	Int_3	Products
Ni^{2+}–N1	2.003	1.862	1.939	1.983	1.919	1.875	1.868	1.869
Ni^{2+}–N10	2.003	2.156	2.010	2.023	1.995	1.888	1.888	1.885
Ni^{2+}–N1′	2.003	1.965	1.936	1.999	1.930	4.949	12.37	–
Ni^{2+}–N10′	2.003	2.006	2.018	2.035	2.978	7.061	14.57	–
C1–H1	1.086	1.879	2.798	3.456	3.580	7.431	14.50	–
N10′–H1	3.925	2.672	2.422	1.370	1.043	1.023	1.024	1.025
Ni^{2+}–H1	3.160	1.647	1.435	1.484	2.010	6.124	13.61	–
∠N1Ni^{2+}N10′C	82.1	83.6	88.3	48.6	49.4	71.1	77.6	–
∠N1Ni^{2+}N10′	124.0	117.2	112.7	146.2	110.5	92.8	118.1	–
∠N1Ni^{2+}N1′	124.0	152.4	160.7	107.0	159.2	120.6	116.5	–
∠N1Ni^{2+}N10	83.2	79.8	84.6	84.0	86.4	116.9	92.5	92.7
∠N10′NI^{2+}N1′	83.2	84.1	84.4	83.2	72.1	16.8	6.8	–
∠N10′Ni^{2+}N10	124.0	106.7	103.2	106.4	132.0	143.0	143.5	–
∠N1′Ni^{2+}N10	124.0	112.4	100.5	144.8	113.3	134.7	140.3	–
∠N1CCN10	0.0	1.3	0.2	0.4	0.7	0.1	0.4	0.0
∠N1′CCN10′	0.0	0.2	0.0	3.2	5.2	0.1	0.1	0.0

[a]Bond angles (∠) are given in degrees (°) and bond lengths in angstroms (Å).

Table D.4d. Select B3LYP/6-31G* Geometrical Parameters for the PTCF Activated Dissociation of $Cu^{2+}(Phen)_2$ complex[a]

	Reactant	TS_1	Int_1	TS_2	Int_2	TS_3	Int_3	Products
Cu^{2+}–N1	1.986	1.844	1.928	1.943	1.928	1.868	1.871	1.875
Cu^{2+}–N10	1.985	2.094	1.970	1.989	2.035	1.914	1.899	1.898
Cu^{2+}–N1′	1.986	2.147	2.150	2.050	1.920	3.620	12.24	–
Cu^{2+}–N10′	1.985	1.948	1.961	2.094	2.967	3.648	14.44	–
C1–H1	1.085	1.884	2.781	2.909	3.095	3.393	14.29	–
N10′–H1	3.097	2.608	2.150	1.708	1.032	1.023	1.024	1.025
Cu^{2+}–H1	3.157	1.611	1.421	1.425	2.023	2.656	13.49	–
∠N1Cu^{2+}N10′C	49.1	76.2	66.6	81.5	54.2	63.8	78.9	–
∠N1Cu^{2+}N10′	103.8	152.6	149.2	130.1	97.6	84.4	116.3	–
∠N1Cu^{2+}N1′	149.1	114.9	123.2	136.1	147.4	119.9	114.8	–
∠N1Cu^{2+}N10	84.4	82.0	86.2	86.0	85.6	94.4	94.7	94.6
∠N10′Cu^{2+}N1′	84.4	82.7	82.5	81.7	67.4	44.6	6.8	–
∠N10′Cu^{2+}N10	149.2	110.1	104.3	116.2	135.2	135.2	143.3	–
∠N1′Cu^{2+}N10	103.8	116.0	105.2	107.8	125.8	142.0	140.0	–
∠N1CCN10	0.9	2.4	0.2	0.3	0.5	1.2	0.3	0.0
∠N1′CCN10′	1.0	0.2	0.6	1.8	2.8	0.6	0.0	0.0

[a]Bond angles (∠) are given in degrees (°) and bond lengths in angstroms (Å).

Table D.4e. Select B3LYP/6-31G* Geometrical Parameters for the PTCF Activated Dissociation of $Zn^{2+}(Phen)_2$ Complex[a]

	Reactant	TS_1	Int_1	TS_2	Int_2
Zn^{2+}–N1	2.023	2.067	2.235	3.061	3.027
Zn^{2+}–N10	2.024	2.029	2.004	2.040	2.112
Zn^{2+}–N1′	2.023	2.011	1.997	2.023	2.054
Zn^{2+}–N10′	2.024	2.016	2.004	2.022	2.061
C1–H1	1.070	1.407	1.997	2.469	2.970
N10′–H1	4.020	3.289	3.153	3.260	3.138
Zn^{2+}–H1	3.238	2.492	2.309	1.639	1.561
∠N1Zn^{2+}N10′C	81.1	78.8	77.9	72.0	59.5
∠N1Zn^{2+}N10′	123.2	120.7	113.3	134.9	150.0
∠N1Zn^{2+}N1′	123.2	120.6	119.6	132.9	127.4
∠N1Zn^{2+}N10	84.6	83.8	81.3	70.2	67.7
∠N10′Zn^{2+}N1′	84.6	85.3	86.1	84.6	82.6
∠N10′Zn^{2+}N10	123.1	125.3	130.8	117.7	105.8
∠N1′Zn^{2+}N10	123.2	125.9	128.7	119.3	107.5
∠N1CCN10	0.1	4.2	11.2	0.2	0.5
∠N1′CCN10′	0.0	0.1	0.2	0.1	0.6

[a]Bond angles (∠) are given in degrees (°) and bond lengths in angstroms (Å).

Table D.4e. (continued) Select B3LYP/6-31G* Geometrical Parameters for the PTCF Activated Dissociation of $Zn^{2+}(Phen)_2$ Complex[a]

	TS_3	Int_3	TS_4	Int_4	Products
Zn^{2+}–N1	2.081	1.919	1.926	1.950	1.970
Zn^{2+}–N10	1.995	1.995	1.949	2.121	2.000
Zn^{2+}–N1′	1.994	1.930	7.080	12.11	–
Zn^{2+}–N10′	2.311	2.978	5.815	14.29	–
C1–H1	3.495	3.580	3.216	13.98	–
N10′–H1	1.545	1.043	1.025	1.024	1.025
Zn^{2+}–H1	1.688	2.010	5.309	13.33	–
∠N1Zn^{2+}N10′C	60.0	55.9	80.7	73.01	–
∠N1Zn^{2+}N10′	138.1	111.5	52.5	119.4	–
∠N1Zn^{2+}N1′	121.0	160.6	55.2	117.9	–
∠N1Zn^{2+}N10	85.8	86.4	94.6	84.4	90.9
∠N10′Zn^{2+}N1′	79.7	68.0	21.6	7.0	–
∠N10′Zn^{2+}N10	110.4	125.8	146.3	148.6	–
∠N1′Zn^{2+}N10	128.3	109.9	135.8	144.1	–
∠N1CCN10	1.8	0.7	0.0	0.6	0.0
∠N1′CCN10′	0.7	1.0	0.04	0.1	0.0

[a]Bond angles (∠) are given in degrees (°) and bond lengths in angstroms (Å).

Table D.5. Cartesian Coordinates of the B3LYP/6-31G* Optimized Geometries of the Transition States, Ints, and Products Involved in the Dissociation of $M^{2+}(Phen)_2$ Complexes through ETCF Process.[a]

	Fe(Phen)$_2$ TS				Fe(Phen)$_2$ TS		
	x	y	z		x	y	z
C	-0.070904	0.329023	-0.230743	H	7.168433	2.863980	-3.020368
C	-0.043248	0.338127	1.151583	H	6.465562	-1.878629	-2.300481
C	1.198217	0.309466	1.833672	H	7.440792	0.428739	-2.386603
C	2.365417	0.264576	1.040771	H	4.068497	-2.204525	-3.038257
N	2.321617	0.255096	-0.325169	H	5.711569	4.675475	-3.836889
C	1.137395	0.289350	-0.947194	H	1.051161	4.971716	-5.010475
C	1.324676	0.322585	3.263407	H	0.201774	2.679510	-4.504332
C	3.658653	0.225701	1.666201	Fe	4.206782	0.108227	-1.135871
C	3.754159	0.242125	3.076701				
C	2.551894	0.292125	3.859738				
C	5.051972	0.204182	3.639423				
H	5.170015	0.214636	4.719349				
C	6.159591	0.152246	2.812382				
C	5.975545	0.135923	1.422481				
N	4.763238	0.171777	0.855717				
H	0.421907	0.357162	3.865488				
H	-1.009411	0.351014	-0.773556				
H	-0.967425	0.367871	1.721998				
H	1.159780	0.303398	-2.034023				
H	2.637846	0.302737	4.941901				
H	7.164921	0.121239	3.217575				
H	6.829497	0.090633	0.753525				
C	5.860374	-1.026454	-2.593707				
C	6.398101	0.261423	-2.644250				
C	5.602591	1.356881	-3.071681				
C	4.207863	1.085293	-3.349989				
N	3.708745	-0.186799	-3.324581				
C	4.512827	-1.212483	-3.000339				
C	6.118628	2.679634	-3.226902				
C	3.331943	2.179219	-3.745098				
C	3.912057	3.462070	-3.948407				
C	5.305266	3.680215	-3.677837				
C	3.064643	4.492381	-4.417299				
H	3.468547	5.484127	-4.599868				
C	1.731908	4.212488	-4.639831				
C	1.254329	2.912724	-4.361424				
N	2.020430	1.921671	-3.922426				

Table D.5. (continued) Cartesian Coordinates of the B3LYP/6-31G* Optimized Geometries of the Transition States, Ints, and Products Involved in the Dissociation of $M^{2+}(Phen)_2$ Complexes through ETCF Process.[a]

	$Fe^{2+}(Phen)_2$ Int				$Fe^{2+}(Phen)_2$ Int		
	x	y	z		x	y	z
C	-6.559806	-3.351118	0.840318	H	9.619432	-0.834919	-0.049957
C	-7.857823	-2.892789	0.760400	H	6.495764	-4.357278	-1.097411
C	-8.089316	-1.535715	0.417524	H	8.567032	-3.029179	-0.658623
C	-6.950921	-0.701658	0.169331	H	4.278890	-3.229948	-0.918143
N	-5.694187	-1.159622	0.250677	H	9.371505	1.547555	0.541963
C	-5.517559	-2.442392	0.575759	H	5.576539	4.471463	1.099003
C	-9.397468	-1.000597	0.318261	H	3.631958	2.983053	0.628441
C	-7.170538	0.707800	-0.187401	Fe^{2+}	3.504209	-0.162406	-0.175382
C	-8.514527	1.198106	-0.274060				
C	-9.604427	0.330706	-0.018476				
C	-8.704010	2.561557	-0.619921				
H	-9.711681	2.961441	-0.693305				
C	-7.599746	3.352356	-0.856620				
C	-6.325293	2.764536	-0.742847				
N	-6.107099	1.487164	-0.419846				
H	-10.249475	-1.647191	0.509989				
H	-6.336664	-4.380770	1.098923				
H	-8.701959	-3.548942	0.954275				
H	-4.483180	-2.776297	0.631351				
H	-10.617180	0.718221	-0.088494				
H	-7.697915	4.399120	-1.123858				
H	-5.435233	3.363787	-0.924149				
C	6.444302	-3.307106	-0.832466				
C	7.585895	-2.567928	-0.588841				
C	7.485668	-1.198347	-0.245592				
C	6.189002	-0.635581	-0.165767				
N	5.065547	-1.387201	-0.411238				
C	5.195304	-2.678334	-0.733193				
C	8.635163	-0.381923	0.017312				
C	6.043532	0.762771	0.181844				
C	7.200886	1.538236	0.434318				
C	8.498287	0.933707	0.344025				
C	7.016626	2.900782	0.770622				
H	7.885024	3.522364	0.970042				
C	5.742794	3.430915	0.843440				
C	4.645962	2.598733	0.579766				
N	4.785136	1.308198	0.259474				

Table D.5. (continued) Cartesian Coordinates of the B3LYP/6-31G* Optimized Geometries of the Transition States, Ints, and Products Involved in the Dissociation of $M^{2+}(Phen)_2$ Complexes through ETCF Process.[a]

	Fe^{+}(Phen)				$Phen^{+}$		
	x	y	z		x	y	z
C	0.262443	-3.469120	0.000000	C	-0.021204	-0.000014	-0.007008
C	1.489911	-2.834477	0.000000	C	-0.030312	-0.000089	1.371675
C	1.552754	-1.421071	0.000000	C	1.212676	-0.000073	2.068256
C	0.324693	-0.719409	0.000000	C	2.421488	0.000022	1.288749
N	-0.879923	-1.359407	0.000000	N	2.414291	0.000093	-0.039404
C	-0.907813	-2.691950	0.000000	C	1.225272	0.000075	-0.664116
C	2.783208	-0.681866	0.000000	C	1.287025	-0.000145	3.470935
C	0.324693	0.719409	0.000000	C	3.723488	0.000041	1.988864
C	1.552754	1.421071	0.000000	C	3.739758	-0.000036	3.427123
C	2.783208	0.681866	0.000000	C	2.528604	-0.000127	4.138559
C	1.489911	2.834477	0.000000	C	5.006272	-0.000017	4.079955
H	2.410583	3.411250	0.000000	H	5.051464	-0.000073	5.165491
C	0.262443	3.469120	0.000000	C	6.151388	0.000074	3.312129
C	-0.907813	2.691950	0.000000	C	6.012240	0.000144	1.909941
N	-0.879923	1.359407	0.000000	N	4.835443	0.000128	1.262502
H	3.719165	-1.232252	0.000000	H	0.371124	-0.000217	4.056053
H	0.186431	-4.550789	0.000000	H	-0.940714	-0.000023	-0.582028
H	2.410583	-3.411250	0.000000	H	-0.960818	-0.000160	1.932556
H	-1.889166	-3.157993	0.000000	H	1.268884	0.000136	-1.750802
H	3.719165	1.232252	0.000000	H	2.545524	-0.000185	5.225275
H	0.186431	4.550789	0.000000	H	7.138120	0.000093	3.762136
H	-1.889166	3.157993	0.000000	H	6.894739	0.000217	1.274342
Fe^{2+}	-2.520005	0.000000	0.000000				

Table D.5. (continued) Cartesian Coordinates of the B3LYP/6-31G* Optimized Geometries of the Transition States, Ints, and Products Involved in the Dissociation of $M^{2+}(Phen)_2$ Complexes through ETCF Process.[a]

$Co^{2+}(Phen)_2$ TS				$Co^{2+}(Phen)_2$ TS			
	x	y	z		x	y	z
C	0.081858	0.556046	-0.208685	N	1.957387	1.989382	-4.077587
C	0.053448	0.340646	1.157956	H	7.098588	2.949004	-3.168323
C	1.265454	0.204732	1.877701	H	6.275716	-1.651390	-1.863837
C	2.464730	0.296750	1.138911	H	7.303661	0.610302	-2.213062
N	2.475474	0.515426	-0.213211	H	3.882730	-2.011658	-2.581891
C	1.314972	0.640246	-0.873239	H	5.710224	4.650212	-4.285395
C	1.333203	-0.020705	3.293760	H	1.083110	4.876524	-5.602235
C	3.729232	0.166065	1.804500	H	0.165735	2.702350	-4.786146
C	3.768888	-0.055200	3.199978	Co^{2+}	4.343495	0.545685	-0.897899
C	2.535257	-0.144705	3.928550				
C	5.045540	-0.177372	3.798967				
H	5.123776	-0.347620	4.869035				
C	6.182800	-0.078911	3.018130				
C	6.051540	0.140764	1.638071				
N	4.861831	0.260261	1.041342				
H	0.405892	-0.090484	3.853951				
H	-0.834472	0.658117	-0.779425				
H	-0.893870	0.272663	1.685657				
H	1.373516	0.798413	-1.948115				
H	2.576188	-0.314419	5.000039				
H	7.173034	-0.167853	3.451099				
H	6.929869	0.220959	1.004825				
C	5.695241	-0.832303	-2.276474				
C	6.262595	0.432498	-2.471253				
C	5.501738	1.476519	-3.062398				
C	4.111107	1.188123	-3.355618				
N	3.581458	-0.048607	-3.162418				
C	4.347755	-1.032909	-2.670714				
C	6.051983	2.754761	-3.382642				
C	3.273495	2.236582	-3.917042				
C	3.887355	3.467125	-4.282743				
C	5.275868	3.695721	-4.000420				
C	3.074299	4.439992	-4.909091				
H	3.505100	5.387859	-5.218934				
C	1.738648	4.161612	-5.116015				
C	1.222728	2.926675	-4.663344				

Table D.5. (continued) Cartesian Coordinates of the B3LYP/6-31G* Optimized Geometries of the Transition States, Ints, and Products Involved in the Dissociation of $M^{2+}(Phen)_2$ Complexes through ETCF Process.[a]

$Co^{2+}(Phen)_2$ Int			
	x	y	z
C	-6.354271	2.322388	-2.462376
C	-7.684056	1.999666	-2.257101
C	-8.018861	1.058856	-1.245337
C	-6.950436	0.485613	-0.478169
N	-5.661808	0.805869	-0.689651
C	-5.386001	1.696277	-1.652514
C	-9.358965	0.683069	-0.985634
C	-7.278906	-0.487517	0.578793
C	-8.653915	-0.834744	0.797212
C	-9.668224	-0.241845	0.008866
C	-8.948703	-1.778933	1.818250
H	-9.980870	-2.063511	2.003920
C	-7.911392	-2.315666	2.556371
C	-6.598681	-1.897761	2.261082
N	-6.282220	-1.015828	1.303625
H	-10.156978	1.125835	-1.575531
H	-6.054190	3.035654	-3.222731
H	-8.473490	2.450411	-2.852553
H	-4.331804	1.929597	-1.791940
H	-10.705048	-0.514539	0.186418
H	-8.090670	-3.038005	3.345634
H	-5.761364	-2.299365	2.828491
C	5.758082	2.697652	2.208818
C	7.042355	2.271774	1.901538
C	7.233592	1.171249	1.022922
C	6.075796	0.551118	0.495786
N	4.806906	0.981179	0.801821
C	4.658362	2.029957	1.640000
C	8.526668	0.667111	0.649997
C	6.205041	-0.568318	-0.395957
C	7.489583	-1.045183	-0.750030
C	8.649702	-0.397136	-0.203006
C	7.553231	-2.152603	-1.638426
H	8.521071	-2.547188	-1.935197
C	6.383602	-2.722076	-2.119875
C	5.144548	-2.191681	-1.716854
N	5.050652	-1.139741	-0.874476
H	9.409051	1.149531	1.059420
H	5.586054	3.534547	2.876756
H	7.906301	2.773998	2.328036
H	3.642198	2.344432	1.860207
H	9.631024	-0.770246	-0.480067
H	6.405650	-3.567622	-2.798606
H	4.213132	-2.620680	-2.075285
Co^{2+}	3.533197	-0.161141	-0.138976

$Co^{+}(Phen)$			
	x	y	z
C	-0.005117	0.000000	0.016539
C	0.002586	0.000000	1.400780
C	1.235137	0.000000	2.089703
C	2.414068	0.000000	1.310282
N	2.398780	0.000000	-0.060959
C	1.210718	0.000000	-0.680086
C	1.350763	0.000000	3.521044
C	3.695334	0.000000	1.948415
C	3.783565	0.000000	3.358943
C	2.571518	0.000000	4.129039
C	5.076017	0.000000	3.927594
H	5.190331	0.000000	5.007644
C	6.185450	0.000000	3.099741
C	6.008904	0.000000	1.709643
N	4.798962	0.000000	1.134447
H	0.441374	0.000000	4.114263
H	-0.935998	0.000000	-0.539613
H	-0.928298	0.000000	1.960271
H	1.228822	0.000000	-1.765059
H	2.645961	0.000000	5.212254
H	7.190180	0.000000	3.507616
H	6.863936	0.000000	1.041500
Co^{2+}	4.214026	0.000000	-0.698387

Table D.5. (continued) Cartesian Coordinates of the B3LYP/6-31G* Optimized Geometries of the Transition States, Ints, and Products Involved in the Dissociation of $M^{2+}(Phen)_2$ Complexes through ETCF Process.[a]

$Ni^{2+}(Phen)_2$ TS				$Ni^{2+}(Phen)_2$ TS			
	x	y	z		x	y	z
C	-0.008243	-0.020240	0.001479	H	7.310845	2.694207	-2.922896
C	-0.017586	-0.118144	1.380792	H	6.579007	-1.928219	-1.711815
C	1.206618	-0.115271	2.095073	H	7.587924	0.332387	-2.088709
C	2.387170	-0.016132	1.331096	H	4.140977	-2.273167	-2.259106
N	2.380457	0.084259	-0.029645	H	5.845821	4.450222	-3.840759
C	1.216318	0.083004	-0.684080	H	1.146427	4.730983	-4.840046
C	1.313136	-0.208006	3.524157	H	0.285269	2.514496	-4.083687
C	3.665292	-0.020831	1.975163	Ni^{2+}	4.226537	0.158314	-0.717846
C	3.746589	-0.110510	3.381733				
C	2.531632	-0.202702	4.141820				
C	5.041817	-0.108237	3.951801				
H	5.156120	-0.174980	5.030168				
C	6.155626	-0.023714	3.132557				
C	5.984013	0.054696	1.743722				
N	4.772558	0.058985	1.173147				
H	0.402303	-0.282627	4.110281				
H	-0.932455	-0.021725	-0.565819				
H	-0.956117	-0.197844	1.922197				
H	1.269405	0.182683	-1.764992				
H	2.599350	-0.271924	5.223079				
H	7.158195	-0.020828	3.545694				
H	6.839909	0.113781	1.079065				
C	5.975560	-1.094961	-2.058156				
C	6.528469	0.162295	-2.261441				
C	5.722765	1.227780	-2.747813				
C	4.307782	0.963393	-2.910014				
N	3.787972	-0.290520	-2.748369				
C	4.595858	-1.289204	-2.336255				
C	6.249545	2.510523	-3.059128				
C	3.433057	2.029075	-3.390685				
C	4.023958	3.272857	-3.749197				
C	5.429067	3.484635	-3.566657				
C	3.175595	4.270290	-4.284257				
H	3.588903	5.230081	-4.581027				
C	1.829931	3.998201	-4.424249				
C	1.345567	2.741817	-4.002473				
N	2.113680	1.782665	-3.495537				

Table D.5. (continued) Cartesian Coordinates of the B3LYP/6-31G* Optimized Geometries of the Transition States, Ints, and Products Involved in the Dissociation of $M^{2+}(Phen)_2$ Complexes through ETCF Process.[a]

$Ni^{2+}(Phen)_2$ Int			
	x	y	z
C	-6.189504	2.891288	-1.907375
C	-7.367630	2.416965	-1.360317
C	-7.359215	1.248851	-0.559732
C	-6.113400	0.612368	-0.356638
N	-4.958541	1.098265	-0.906506
C	-4.993581	2.202214	-1.658253
C	-8.539154	0.695909	0.040945
C	-6.045768	-0.581559	0.449504
C	-7.226001	-1.102600	1.027586
C	-8.475196	-0.433464	0.803255
C	-7.101579	-2.277111	1.808857
H	-7.985861	-2.708296	2.269705
C	-5.862975	-2.867442	1.981064
C	-4.739000	-2.288218	1.374297
N	-4.829387	-1.180631	0.632644
H	-9.488507	1.195926	-0.124041
H	-6.171934	3.783143	-2.523895
H	-8.305671	2.934694	-1.540061
H	-4.050165	2.545022	-2.070675
H	-9.372883	-0.845371	1.253806
H	-5.743821	-3.767063	2.574596
H	-3.751354	-2.723317	1.487700
C	6.544483	-2.804027	-1.905893
C	7.844924	-2.464927	-1.597959
C	8.089475	-1.306714	-0.815798
C	6.959685	-0.540238	-0.380705
N	5.699753	-0.881849	-0.686326
C	5.511270	-1.977659	-1.424639
C	9.402109	-0.902077	-0.464535
C	7.191688	0.663599	0.428863
C	8.538756	1.027921	0.754610
C	9.620536	0.233371	0.299280
C	8.740349	2.195098	1.536521
H	9.750771	2.496267	1.799316
C	7.645153	2.924842	1.947174
C	6.366132	2.473359	1.568718
N	6.136210	1.381697	0.835253
H	10.246322	-1.496281	-0.803481
H	6.312849	-3.680459	-2.501873
H	8.682171	-3.065722	-1.942669
H	4.474966	-2.220262	-1.652482
H	10.635215	0.525038	0.556291
H	7.753608	3.823295	2.545418
H	5.482835	3.028535	1.878330
Ni^{2+}	-3.480505	-0.106643	-0.352300

$Ni^{+}(Phen)$			
	x	y	z
C	-0.011355	0.000000	0.015683
C	0.001274	0.000000	1.396508
C	1.238938	0.000000	2.082926
C	2.413736	0.000000	1.301813
N	2.390601	0.000000	-0.070589
C	1.205896	0.000000	-0.686012
C	1.354300	0.000000	3.513712
C	3.702294	0.000000	1.943577
C	3.786684	0.000000	3.351826
C	2.575239	0.000000	4.121798
C	5.080218	0.000000	3.926067
H	5.189260	0.000000	5.006695
C	6.189892	0.000000	3.104203
C	6.016539	0.000000	1.709920
N	4.811576	0.000000	1.135173
H	0.444606	0.000000	4.106475
H	-0.942847	0.000000	-0.539391
H	-0.926895	0.000000	1.960555
H	1.221479	0.000000	-1.770984
H	2.650230	0.000000	5.204982
H	7.194130	0.000000	3.513216
H	6.873089	0.000000	1.043790
Ni^{2+}	4.178138	0.000000	-0.626330

Table D.5. (continued) Cartesian Coordinates of the B3LYP/6-31G* Optimized Geometries of the Transition States, Ints, and Products Involved in the Dissociation of $M^{2+}(Phen)_2$ Complexes through ETCF Process.[a]

$Cu^{2+}(Phen)_2$ TS				$Cu^{2+}(Phen)_2$ TS			
	x	y	z		x	y	z
C	-0.001041	-0.003224	-0.005501	N	1.988654	2.313544	-4.257496
C	0.000242	0.001449	1.377908	H	7.194028	2.862992	-3.435676
C	1.229535	0.004685	2.081170	H	6.053640	-1.607444	-2.019681
C	2.406916	-0.009408	1.305485	H	7.230066	0.574769	-2.410247
N	2.389625	-0.031185	-0.059329	H	3.597199	-1.765170	-2.653098
C	1.219634	-0.018590	-0.703077	H	5.940115	4.645430	-4.586398
C	1.347103	0.024558	3.512618	H	1.332531	5.235182	-5.839095
C	3.689848	0.011347	1.938500	H	0.259020	3.151036	-4.981580
C	3.782126	0.036826	3.346605				
C	2.570813	0.039062	4.118928				
C	5.082669	0.058200	3.904407				
H	5.206737	0.076530	4.983526				
C	6.187283	0.055114	3.071053				
C	6.002929	0.030636	1.679241				
N	4.788632	0.009068	1.123120				
H	0.439835	0.029200	4.108872				
H	-0.929025	0.002123	-0.566514				
H	-0.935554	0.007262	1.929727				
H	1.259489	-0.007756	-1.788523				
H	2.646205	0.053903	5.201834				
H	7.194697	0.070806	3.472035				
H	6.853800	0.026223	1.005817				
Cu^{2+}	4.203267	-0.125484	-0.732846				
C	5.502024	-0.724749	-2.332611				
C	6.165867	0.480038	-2.612419				
C	5.480431	1.545346	-3.238531				
C	4.067991	1.375520	-3.481888				
N	3.430866	0.231475	-3.197183				
C	4.119247	-0.809822	-2.675548				
C	6.131469	2.745585	-3.627187				
C	3.314787	2.460891	-4.095152				
C	4.027997	3.631155	-4.512356				
C	5.425004	3.743505	-4.266621				
C	3.289693	4.655066	-5.159579				
H	3.796206	5.553756	-5.499789				
C	1.936621	4.482003	-5.344217				
C	1.330596	3.295610	-4.863114				

Table D.5. (continued) Cartesian Coordinates of the B3LYP/6-31G* Optimized Geometries of the Transition States, Ints, and Products Involved in the Dissociation of $M^{2+}(Phen)_2$ Complexes through ETCF Process.[a]

$Cu^{2+}(Phen)_2$ Int				$Cu^{2+}(Phen)_2$ Int			
	x	y	z		x	y	z
C	-6.173593	2.891827	-1.905264	H	10.262197	-1.496289	-0.803018
C	-7.351668	2.417610	-1.358005	H	6.328418	-3.680487	-2.500674
C	-7.343197	1.249580	-0.557297	H	8.697837	-3.065787	-1.941839
C	-6.097382	0.613069	-0.354296	H	4.490704	-2.220126	-1.651201
N	-4.942574	1.098860	-0.904363	H	10.651347	0.525157	0.556491
C	-4.977665	2.202731	-1.656223	H	7.770129	3.823742	2.545639
C	-8.523081	0.696749	0.043590	H	5.499238	3.029003	1.878927
C	-6.029694	-0.580776	0.451963	Cu^{2+}	-3.464515	-0.106049	-0.350221
C	-7.209874	-1.101708	1.030252				
C	-8.459071	-0.432546	0.806011				
C	-7.085399	-2.276142	1.811631				
H	-7.969639	-2.707242	2.272639				
C	-5.846797	-2.866504	1.983742				
C	-4.722876	-2.287390	1.376769				
N	-4.813314	-1.179878	0.635011				
H	-9.472435	1.196787	-0.121326				
H	-6.156066	3.783616	-2.521880				
H	-8.289711	2.935358	-1.537683				
H	-4.034288	2.545458	-2.068802				
H	-9.356716	-0.844369	1.256721				
H	-5.727603	-3.766068	2.577353				
H	-3.735233	-2.722518	1.490091				
C	6.560164	-2.804002	-1.904816				
C	7.860659	-2.464922	-1.597085				
C	8.105357	-1.306636	-0.815078				
C	6.975653	-0.540069	-0.379921				
N	5.715669	-0.881661	-0.685344				
C	5.527046	-1.977542	-1.423517				
C	9.418052	-0.902015	-0.464027				
C	7.207809	0.663844	0.429490				
C	8.554934	1.028147	0.755025				
C	9.636623	0.233505	0.299641				
C	8.756675	2.195398	1.536788				
H	9.767142	2.496554	1.799420				
C	7.661560	2.925230	1.947504				
C	6.382472	2.473758	1.569260				
N	6.152412	1.382029	0.835940				

$Cu^{+}(Phen)$			
	x	y	z
C	-0.043459	0.000000	0.023912
C	0.003127	0.000000	1.401899
C	1.254106	0.000000	2.064188
C	2.422311	0.000000	1.267039
N	2.357708	0.000000	-0.107923
C	1.162250	0.000000	-0.696924
C	1.365599	0.000000	3.493700
C	3.724882	0.000000	1.915782
C	3.792500	0.000000	3.328431
C	2.584403	0.000000	4.100723
C	5.074799	0.000000	3.927836
H	5.156894	0.000000	5.010993
C	6.202667	0.000000	3.134784
C	6.051545	0.000000	1.738181
N	4.861190	0.000000	1.138932
H	0.454196	0.000000	4.083852
H	-0.986310	0.000000	-0.511681
H	-0.910825	0.000000	1.988976
H	1.160028	0.000000	-1.781593
H	2.662507	0.000000	5.183698
H	7.198200	0.000000	3.564601
H	6.918581	0.000000	1.086444
Cu^{2+}	4.170122	0.000000	-0.610236

Table D.5. (continued) Cartesian Coordinates of the B3LYP/6-31G* Optimized Geometries of the Transition States, Ints, and Products Involved in the Dissociation of $M^{2+}(Phen)_2$ Complexes through ETCF Process.[a]

$Zn^{2+}(Phen)_2$ TS				$Zn^{2+}(Phen)_2$ TS			
	x	y	z		x	y	z
C	0.161719	0.003755	-0.113719	H	8.880363	4.242296	-3.247492
C	0.216273	0.148192	1.261414	H	11.985130	2.334554	-0.097119
C	1.468750	0.196712	1.919483	H	10.874203	3.807087	-1.791806
C	2.626401	0.098556	1.114610	H	10.800975	0.275398	0.670802
N	2.555249	-0.051335	-0.245787	H	6.667657	3.570229	-4.095104
C	1.356371	-0.094500	-0.839688	H	4.071390	-0.470279	-3.680088
C	1.611888	0.329972	3.341290	H	5.600371	-1.958516	-2.311958
C	3.927306	0.131901	1.729235	Zn^{2+}	4.403671	-0.154099	-0.948958
C	4.038005	0.245271	3.131729				
C	2.845793	0.349653	3.923925				
C	5.345811	0.237070	3.676867				
H	5.477446	0.319844	4.752155				
C	6.441636	0.113417	2.842835				
C	6.250545	0.011263	1.455084				
N	5.024846	0.036456	0.917909				
H	0.715150	0.407338	3.948206				
H	-0.785743	-0.038869	-0.639361				
H	-0.698166	0.221621	1.843434				
H	1.344777	-0.215070	-1.918086				
H	2.943607	0.441495	5.001221				
H	7.450074	0.090563	3.240353				
H	7.091956	-0.095699	0.772679				
C	11.019791	2.076364	-0.519880				
C	10.409410	2.883656	-1.458093				
C	9.157258	2.493907	-1.985893				
C	8.606630	1.265134	-1.529767				
N	9.183002	0.505870	-0.574303				
C	10.353927	0.905891	-0.094570				
C	8.436440	3.303239	-2.928171				
C	7.363138	0.799918	-2.125175				
C	6.644336	1.678670	-3.024368				
C	7.211252	2.932879	-3.404457				
C	5.396407	1.238390	-3.499283				
H	4.809551	1.877570	-4.153377				
C	4.945252	-0.050189	-3.186498				
C	5.793755	-0.885738	-2.392321				
N	6.944842	-0.446706	-1.849699				

Table D.5. (continued) Cartesian Coordinates of the B3LYP/6-31G* Optimized Geometries of the Transition States, Ints, and Products Involved in the Dissociation of $M^{2+}(Phen)_2$ Complexes through ETCF Process.[a]

$Zn^{2+}(Phen)_2$ Int				$Zn^{2+}(Phen)_2$ Int			
	x	y	z		x	y	z
C	-6.157827	2.892361	-1.903177	H	10.277928	-1.496297	-0.802560
C	-7.335851	2.418248	-1.355719	H	6.343846	-3.680515	-2.499489
C	-7.327325	1.250301	-0.554890	H	8.713360	-3.065851	-1.941019
C	-6.081510	0.613761	-0.351981	H	4.506298	-2.219992	-1.649935
N	-4.926752	1.099449	-0.902246	H	10.667331	0.525276	0.556688
C	-4.961895	2.203243	-1.654216	H	7.786497	3.824183	2.545857
C	-8.507155	0.697580	0.046204	H	5.515490	3.029465	1.879517
C	-6.013767	-0.580002	0.454394	Zn^{2+}	-3.448671	-0.105461	-0.348165
C	-7.193895	-1.100827	1.032887				
C	-8.443093	-0.431638	0.808735				
C	-7.069367	-2.275184	1.814373				
H	-7.953566	-2.706201	2.275538				
C	-5.830767	-2.865578	1.986388	$Zn^{+}(Phen)$			
C	-4.706900	-2.286572	1.379212		x	y	z
N	-4.797388	-1.179134	0.637350	C	-0.019850	0.000000	0.022974
H	-9.456510	1.197639	-0.118644	C	-0.000343	0.000000	1.404641
H	-6.140343	3.784085	-2.519889	C	1.236467	0.000000	2.092128
H	-8.273896	2.936014	-1.535332	C	2.411009	0.000000	1.305353
H	-4.018557	2.545889	-2.066951	N	2.375825	0.000000	-0.055963
H	-9.340698	-0.843378	1.259602	C	1.198186	0.000000	-0.677434
H	-5.711533	-3.765084	2.580078	C	1.349648	0.000000	3.523040
H	-3.719260	-2.721727	1.492454	C	3.701121	0.000000	1.947931
C	6.575703	-2.803977	-1.903752	C	3.780773	0.000000	3.359388
C	7.876250	-2.464917	-1.596221	C	2.570433	0.000000	4.131108
C	8.121094	-1.306559	-0.814366	C	5.074725	0.000000	3.932269
C	6.991476	-0.539901	-0.379146	H	5.181471	0.000000	5.013404
N	5.731439	-0.881475	-0.684373	C	6.189239	0.000000	3.115374
C	5.542679	-1.977425	-1.422408	C	6.014352	0.000000	1.721263
C	9.433850	-0.901954	-0.463524	N	4.808837	0.000000	1.155841
C	7.223783	0.664087	0.430110	H	0.439745	0.000000	4.115482
C	8.570963	1.028370	0.755436	H	-0.953779	0.000000	-0.527966
C	9.652563	0.233637	0.299997	H	-0.927460	0.000000	1.970977
C	8.772850	2.195695	1.537051	H	1.222512	0.000000	-1.762970
H	9.783363	2.496838	1.799524	H	2.645739	0.000000	5.214271
C	7.677817	2.925613	1.947830	H	7.191700	0.000000	3.528673
C	6.398663	2.474153	1.569796	H	6.866040	0.000000	1.047731
N	6.168466	1.382356	0.836619	Zn^{2+}	4.280627	0.000000	-0.831902

Table D.5. Cartesian Coordinates of the B3LYP/6-31G* Optimized Geometries of the Transition States, Ints, and Products Involved in the Dissociation of $M^{2+}(Phen)_2$ Complexes through PTCF Process.[a]

$Fe^{2+}(Phen)_2$ TS_1				$Fe^{2+}(Phen)_2$ TS_1			
	x	y	z		x	y	z
C	-0.434033	-0.340165	0.335608	H	6.595896	1.195944	-6.562016
C	-0.192482	-0.141750	1.697782	H	5.102849	4.358083	-3.190659
C	1.126231	0.022320	2.212096	H	6.121469	3.322991	-5.223134
C	2.169053	-0.016791	1.274381	H	3.954725	2.900362	-1.527140
N	1.914744	-0.197519	-0.044369	H	6.382020	-1.248363	-6.782371
C	0.694629	-0.358669	-0.491651	H	4.286055	-4.652773	-4.026524
C	1.504496	0.218342	3.585965	H	3.335883	-3.337750	-2.137163
C	3.541427	0.108683	1.609246	Fe^{2+}	3.326627	-0.269351	-1.371197
C	3.886223	0.295470	2.962337				
C	2.823841	0.349232	3.935529				
C	5.269989	0.406004	3.244793				
H	5.610281	0.549715	4.266420				
C	6.178687	0.325103	2.204197				
C	5.725246	0.134482	0.882194				
N	4.432349	0.026335	0.572611				
H	0.732507	0.259709	4.348046				
H	-1.437032	-0.474094	-0.051959				
H	-1.038180	-0.120312	2.381093				
H	1.838542	-0.609619	-2.029649				
H	3.090693	0.493832	4.978115				
H	7.244570	0.403605	2.388843				
H	6.434578	0.069941	0.062377				
C	5.051488	3.288013	-3.358823				
C	5.613407	2.710980	-4.483152				
C	5.523707	1.311334	-4.672435				
C	4.846335	0.570890	-3.677621				
N	4.302053	1.147221	-2.566629				
C	4.400832	2.471466	-2.419490				
C	6.076493	0.619387	-5.802722				
C	4.708850	-0.850518	-3.814804				
C	5.267493	-1.509954	-4.932849				
C	5.957010	-0.734606	-5.925596				
C	5.107089	-2.914053	-5.001918				
H	5.519468	-3.461935	-5.844505				
C	4.424371	-3.577640	-3.998318				
C	3.891528	-2.843367	-2.927996				
N	4.029219	-1.516041	-2.834326				

Table D.5. (continued) Cartesian Coordinates of the B3LYP/6-31G* Optimized Geometries of the Transition States, Ints, and Products Involved in the Dissociation of $M^{2+}(Phen)_2$ Complexes through PTCF Process.[a]

	$Fe^{2+}(Phen)_2$ Int_1				$Fe^{2+}(Phen)_2$ Int_1		
	x	y	z		x	y	z
C	0.013137	1.162794	0.213781	H	8.114783	2.202163	-5.074804
C	0.137621	1.002296	1.587031	H	5.117850	4.823387	-2.290362
C	1.348738	0.514736	2.149782	H	6.854603	4.120346	-3.941432
C	2.401500	0.200767	1.267558	H	3.879201	3.080667	-1.008351
N	2.268308	0.355400	-0.102685	H	8.481248	-0.220688	-5.327053
C	1.128868	0.810423	-0.543087	H	6.444823	-4.112047	-3.255074
C	1.563580	0.323118	3.556839	H	4.758638	-3.112250	-1.718776
C	3.646889	-0.290054	1.749898	Fe^{2+}	3.893005	-0.192998	-1.097150
C	3.834065	-0.471578	3.138509				
C	2.755795	-0.150864	4.029636				
C	5.094521	-0.967583	3.551834				
H	5.292883	-1.125723	4.608178				
C	6.062806	-1.247026	2.604523				
C	5.783207	-1.034654	1.242856				
N	4.607214	-0.568793	0.816071				
H	0.757605	0.561239	4.243953				
H	-0.895278	1.530788	-0.249283				
H	-0.696804	1.249724	2.238641				
H	2.944239	-0.741407	-2.160904				
H	2.902534	-0.293062	5.095888				
H	7.036592	-1.626416	2.894152				
H	6.529380	-1.245835	0.483368				
C	5.336998	3.774731	-2.458480				
C	6.298260	3.381102	-3.372034				
C	6.558362	2.003954	-3.567493				
C	5.799006	1.092242	-2.800197				
N	4.857709	1.490165	-1.894092				
C	4.635218	2.797395	-1.734238				
C	7.535459	1.495279	-4.488770				
C	6.003922	-0.316694	-2.958320				
C	6.975787	-0.795344	-3.866561				
C	7.738025	0.152912	-4.629469				
C	7.132625	-2.197142	-3.969007				
H	7.863960	-2.608286	-4.659031				
C	6.349653	-3.033600	-3.193336				
C	5.402197	-2.478474	-2.320432				
N	5.234717	-1.156566	-2.201513				

Table D.5. (continued) Cartesian Coordinates of the B3LYP/6-31G* Optimized Geometries of the Transition States, Ints, and Products Involved in the Dissociation of $M^{2+}(Phen)_2$ Complexes through PTCF Process.[a]

$Fe^{2+}(Phen)_2$ TS_2				$Fe^{2+}(Phen)_2$ TS_2			
	x	y	z		x	y	z
C	-0.016595	0.073388	-0.009411	H	8.116035	1.260622	-5.657775
C	-0.016954	0.069389	1.377116	H	5.567502	4.542397	-3.146488
C	1.205726	0.038622	2.102013	H	7.093624	3.434233	-4.785445
C	2.408560	0.016288	1.364900	H	4.357923	3.151917	-1.473693
N	2.398282	0.027380	-0.017537	H	8.292185	-1.193189	-5.518663
C	1.241407	0.051510	-0.614416	H	6.131309	-4.520171	-2.722073
C	1.277517	0.026747	3.535242	H	4.588277	-3.164511	-1.308122
C	3.676282	-0.028593	2.026588	Fe^{2+}	4.295473	0.043864	-0.779449
C	3.714434	-0.041699	3.441484				
C	2.482835	-0.010703	4.176539				
C	4.990343	-0.087930	4.052692				
H	5.067730	-0.097020	5.136274				
C	6.125402	-0.122219	3.265173				
C	5.991488	-0.110782	1.866513				
N	4.806154	-0.065191	1.252243				
H	0.353110	0.046994	4.104105				
H	-0.930826	0.093403	-0.591186				
H	-0.959338	0.088730	1.919035				
H	4.022937	-0.889535	-2.094421				
H	2.526076	-0.020147	5.261306				
H	7.115579	-0.158310	3.705883				
H	6.870955	-0.139645	1.229940				
C	5.698539	3.465881	-3.148432				
C	6.541396	2.848730	-4.055874				
C	6.683004	1.442561	-4.032295				
C	5.933606	0.735533	-3.060765				
N	5.121482	1.353428	-2.150010				
C	5.010902	2.685998	-2.205311				
C	7.538184	0.709812	-4.921903				
C	6.011091	-0.686449	-3.016859				
C	6.863830	-1.394464	-3.891964				
C	7.634587	-0.649829	-4.847362				
C	6.906362	-2.802300	-3.776229				
H	7.552158	-3.378134	-4.432213				
C	6.112184	-3.441307	-2.831096				
C	5.260162	-2.698366	-2.020498				
N	5.211307	-1.340126	-2.093526				

Table D.5. (continued) Cartesian Coordinates of the B3LYP/6-31G* Optimized Geometries of the Transition States, Ints, and Products Involved in the Dissociation of $M^{2+}(Phen)_2$ Complexes through PTCF Process.[a]

	$Fe^{2+}(Phen)_2$ Int_2				$Fe^{2+}(Phen)_2$ Int_2		
	x	y	z		x	y	z
C	2.635908	2.522034	-2.404726	H	-6.170698	-1.424817	-0.620775
C	3.895804	2.248023	-1.891351	H	-2.426164	-3.594761	-2.666400
C	4.065640	1.243006	-0.901769	H	-4.722505	-2.963500	-1.886876
C	2.914892	0.549491	-0.478790	H	-0.500280	-2.217193	-1.967091
N	1.665478	0.822813	-0.992026	H	-6.460242	0.586972	0.780842
C	1.582718	1.756568	-1.894320	H	-3.404701	3.864531	2.574318
C	5.325466	0.890453	-0.308481	H	-1.150250	3.044709	1.767498
C	2.989107	-0.476527	0.505783	Fe^{2+}	0.250856	-0.409283	-0.261287
C	4.238909	-0.802644	1.078401				
C	5.406091	-0.089072	0.641751				
C	4.246184	-1.827854	2.053536				
H	5.179566	-2.119521	2.526564				
C	3.058486	-2.449743	2.392313				
C	1.864686	-2.057553	1.761119				
N	1.815186	-1.094459	0.836433				
H	6.219168	1.417346	-0.628515				
H	2.474335	3.281825	-3.160586				
H	4.759843	2.803025	-2.248492				
H	-1.052937	1.078210	0.471207				
H	6.365114	-0.344773	1.081910				
H	3.031364	-3.239599	3.134965				
H	0.925681	-2.542331	2.011952				
C	-2.587375	-2.743080	-2.014690				
C	-3.849934	-2.391257	-1.585832				
C	-4.011401	-1.256896	-0.757554				
C	-2.849431	-0.530067	-0.378732				
N	-1.592793	-0.902011	-0.793348				
C	-1.494119	-1.969260	-1.606470				
C	-5.310591	-0.836501	-0.316157				
C	-3.042662	0.644574	0.432331				
C	-4.337407	1.051710	0.845983				
C	-5.473453	0.272908	0.456162				
C	-4.448610	2.225251	1.627878				
H	-5.433453	2.547538	1.954158				
C	-3.327282	2.964022	1.976027				
C	-2.076651	2.528257	1.542558				
N	-1.980150	1.412034	0.808792				

Table D.5. (continued) Cartesian Coordinates of the B3LYP/6-31G* Optimized Geometries of the Transition States, Ints, and Products Involved in the Dissociation of $M^{2+}(Phen)_2$ Complexes through PTCF Process.[a]

$Fe^{2+}(Phen)_2$ TS_3				$Fe^{2+}(Phen)_2$ TS_3			
	x	y	z		x	y	z
C	2.056073	-0.579757	-0.389787	H	4.200818	-2.631917	-8.861439
C	1.477727	0.295060	0.504080	H	6.041916	1.611350	-7.393608
C	2.053371	0.504879	1.790642	H	5.287796	-0.318205	-8.791351
C	3.219240	-0.219587	2.078294	H	5.723755	1.527464	-4.920279
N	3.750490	-1.080740	1.131408	H	3.166569	-4.521312	-7.666922
C	3.251961	-1.315983	-0.088118	H	2.222382	-5.354927	-2.971033
C	1.519774	1.389794	2.783442	H	3.106168	-3.234217	-1.841831
C	3.870078	-0.080055	3.351044	Fe^{2+}	5.305809	-1.871372	1.897981
C	3.320545	0.801417	4.315809				
C	2.129641	1.532377	3.998144				
C	3.992706	0.906090	5.556126				
H	3.601354	1.571018	6.321110				
C	5.138427	0.166676	5.792119				
C	5.622234	-0.684125	4.789757				
N	5.013123	-0.808937	3.604101				
H	0.616885	1.947852	2.554270				
H	1.588027	-0.720768	-1.360105				
H	0.571402	0.836793	0.242633				
H	4.052106	-1.587735	-3.193388				
H	1.719122	2.203900	4.745752				
H	5.668260	0.232061	6.735845				
H	6.518384	-1.276074	4.947212				
C	5.579702	0.740409	-6.940944				
C	5.162949	-0.325596	-7.712308				
C	4.563993	-1.440148	-7.078618				
C	4.436424	-1.372516	-5.668957				
N	4.844449	-0.330707	-4.909155				
C	5.399877	0.694077	-5.538895				
C	4.092610	-2.601641	-7.781138				
C	3.831296	-2.483763	-4.995097				
C	3.368344	-3.623050	-5.696087				
C	3.518701	-3.650887	-7.122588				
C	2.784418	-4.661719	-4.937632				
H	2.418570	-5.548604	-5.447622				
C	2.672275	-4.561074	-3.555692				
C	3.145205	-3.417923	-2.912437				
N	3.697441	-2.438636	-3.640764				

Table D.5. (continued) Cartesian Coordinates of the B3LYP/6-31G* Optimized Geometries of the Transition States, Ints, and Products Involved in the Dissociation of $M^{2+}(Phen)_2$ Complexes through PTCF Process.[a]

$Fe^{2+}(Phen)_2$ Int_3				$Fe^{2+}(Phen)_2$ Int_3			
	x	y	z		x	y	z
C	-6.339255	3.370270	0.202909	H	9.921792	-0.528878	3.327095
C	-7.633721	3.105176	0.599274	H	5.150896	-0.775457	2.470733
C	-8.169918	1.779571	0.539265	H	7.385796	-0.775240	3.582247
C	-7.304886	0.792462	0.056427	H	5.005933	-0.382563	0.006734
N	-6.034677	1.134439	-0.317768	H	11.871995	-0.130261	1.876846
C	-5.469172	2.332633	-0.295788	H	12.336185	0.702671	-2.894389
C	-9.491045	1.383584	0.929008	H	9.946431	0.646920	-3.708709
C	-7.692671	-0.576432	-0.057102	Fe^{2+}	-5.077551	-0.330438	-1.027324
C	-9.003518	-0.941137	0.341610				
C	-9.887869	0.076109	0.834290				
C	-9.350974	-2.305798	0.224822				
H	-10.344430	-2.634221	0.517662				
C	-8.426755	-3.215420	-0.259620				
C	-7.151565	-2.768745	-0.637937				
N	-6.783080	-1.487394	-0.546941				
H	-10.177012	2.137075	1.304801				
H	-5.959803	4.386070	0.260350				
H	-8.270776	3.907763	0.964258				
H	8.231894	0.240929	-2.110335				
H	-10.889728	-0.214749	1.134923				
H	-8.670494	-4.267596	-0.355084				
H	-6.414202	-3.464510	-1.025917				
C	6.056677	-0.605891	1.898426				
C	7.292834	-0.605894	2.513279				
C	8.450212	-0.381670	1.731657				
C	8.242331	-0.167962	0.346613				
N	7.033640	-0.167556	-0.258663				
C	5.973028	-0.382719	0.505897				
C	9.785641	-0.362403	2.262465				
C	9.393492	0.063281	-0.477286				
C	10.704293	0.080043	0.053791				
C	10.869149	-0.141776	1.462075				
C	11.767661	0.315398	-0.845524				
H	12.786740	0.334619	-0.469477				
C	11.525429	0.521592	-2.198592				
C	10.213715	0.494949	-2.669641				
N	9.210754	0.271010	-1.809946				

Table D.5. (continued) Cartesian Coordinates of the B3LYP/6-31G* Optimized Geometries of the Transition States, Ints, and Products Involved in the Dissociation of $M^{2+}(Phen)_2$ Complexes through PTCF Process.[a]

	[Fe(Phen-H)]$^+$				[Phen+H]$^+$		
	x	y	z		x	y	z
C	0.068222	0.000000	-0.022007	C	0.114958	-0.000041	-0.074822
C	0.013213	0.000000	1.359053	C	0.065482	-0.000015	1.314322
C	1.206961	0.000000	2.146401	C	1.250353	-0.000010	2.082249
C	2.407407	0.000000	1.430766	C	2.479124	-0.000029	1.381716
N	2.390129	0.000000	0.066169	C	1.353523	-0.000067	-0.714871
C	1.327640	0.000000	-0.712086	C	1.289071	0.000015	3.516660
C	1.287160	0.000000	3.578857	C	3.741892	-0.000026	2.059999
C	3.683850	0.000000	2.066565	C	3.735536	-0.000014	3.476099
C	3.735141	0.000000	3.480992	C	2.482534	0.000011	4.179936
C	2.500457	0.000000	4.214985	C	5.000361	-0.000026	4.110366
C	5.019755	0.000000	4.071072	H	5.062522	-0.000015	5.194874
H	5.116453	0.000000	5.153287	C	6.140957	-0.000051	3.332795
C	6.146049	0.000000	3.266465	C	6.021563	-0.000060	1.923175
C	6.000283	0.000000	1.869629	H	0.351258	0.000035	4.062907
N	4.805593	0.000000	1.271462	H	-0.790490	-0.000047	-0.670053
H	0.368570	0.000000	4.158249	H	-0.895615	0.000004	1.820874
H	-0.851736	0.000000	-0.597834	H	1.472841	-0.000087	-1.791853
H	-0.948451	0.000000	1.867598	H	2.499946	0.000026	5.265968
H	2.547350	0.000000	5.299738	H	7.126707	-0.000066	3.785932
H	7.142282	0.000000	3.694519	H	6.910773	-0.000067	1.297848
H	6.873174	0.000000	1.223894	N	2.472799	-0.000058	0.020762
Fe^{2+}	4.110223	0.000000	-0.747390				

Table D.5. (continued) Cartesian Coordinates of the B3LYP/6-31G* Optimized Geometries of the Transition States, Ints, and Products Involved in the Dissociation of $M^{2+}(Phen)_2$ Complexes through PTCF Process.[a]

$Co^{2+}(Phen)_2$ TS_1				$Co^{2+}(Phen)_2$ TS_1			
	x	y	z		x	y	z
C	-0.020015	0.004072	0.026815	H	6.205375	3.127670	-5.992743
C	-0.013188	0.010099	1.401992	H	4.216603	5.507220	-2.267346
C	1.216271	0.008875	2.141887	H	5.260713	4.924702	-4.461288
C	2.403705	0.026603	1.406394	H	3.781912	3.697723	-0.610938
N	2.377658	0.013183	-0.001971	H	6.742433	0.754448	-6.385607
C	1.175139	0.008803	-0.763137	H	6.200614	-3.256054	-3.717951
C	1.293569	-0.002139	3.570007	H	5.160766	-2.402833	-1.622683
C	3.669813	0.119016	2.044343	Co^{2+}	4.247645	0.532133	-0.692384
C	3.731705	0.085192	3.459870				
C	2.509862	0.012512	4.202464				
C	5.017286	0.150521	4.051952				
H	5.115297	0.117544	5.133463				
C	6.135013	0.264363	3.247253				
C	5.977516	0.337973	1.851463				
N	4.784088	0.272917	1.255883				
H	0.374364	-0.026920	4.147264				
H	-0.965039	-0.022811	-0.507378				
H	-0.949190	-0.001528	1.956398				
H	2.238972	-0.916678	-0.692690				
H	2.561361	-0.011628	5.286841				
H	7.131286	0.316923	3.672174				
H	6.840966	0.462440	1.204597				
C	4.483241	4.483828	-2.506771				
C	5.060817	4.156485	-3.719618				
C	5.393520	2.809818	-4.000273				
C	5.111072	1.851543	-3.000642				
N	4.542012	2.188659	-1.802812				
C	4.236943	3.468704	-1.569808				
C	5.992725	2.382223	-5.232692				
C	5.420868	0.466695	-3.231073				
C	6.011018	0.073644	-4.453877				
C	6.289789	1.068749	-5.450236				
C	6.294118	-1.302356	-4.624467				
H	6.746478	-1.646805	-5.550170				
C	5.993517	-2.196791	-3.613674				
C	5.406741	-1.720872	-2.431391				
N	5.124332	-0.428445	-2.239059				

Table D.5. (continued) Cartesian Coordinates of the B3LYP/6-31G* Optimized Geometries of the Transition States, Ints, and Products Involved in the Dissociation of $M^{2+}(Phen)_2$ Complexes through PTCF Process.[a]

	$Co^{2+}(Phen)_2$ Int_2				$Co^{2+}(Phen)_2$ Int_2		
	x	y	z		x	y	z
C	0.270303	0.032000	-0.221420	H	6.164708	2.225208	-6.123809
C	0.135168	0.187810	1.147438	H	4.434068	4.788335	-2.392170
C	1.275104	0.061143	2.009845	H	5.356664	4.100236	-4.609621
C	2.467671	-0.343433	1.415763	H	4.001110	3.047097	-0.664036
N	2.447676	-0.817382	0.077893	H	6.599730	-0.176966	-6.464557
C	1.369867	-0.668630	-0.797756	H	6.054587	-4.081862	-3.646432
C	1.308741	0.415993	3.397877	H	5.148447	-3.131100	-1.533634
C	3.712837	-0.188053	2.061289	Co^{2+}	4.363226	-0.134490	-0.673429
C	3.733886	0.134118	3.443180				
C	2.489647	0.406047	4.097248				
C	5.006322	0.211912	4.057328				
H	5.081725	0.435374	5.117935				
C	6.148690	0.024351	3.296817				
C	6.035630	-0.189749	1.912936				
N	4.852452	-0.289368	1.294958				
H	0.383234	0.698540	3.890088				
H	-0.563848	0.277048	-0.871969				
H	-0.822771	0.462675	1.583624				
H	2.862678	-1.749886	-0.025888				
H	2.499614	0.651759	5.154733				
H	7.134792	0.080486	3.744349				
H	6.921587	-0.262578	1.289198				
C	4.650651	3.748541	-2.610506				
C	5.161673	3.362577	-3.836263				
C	5.433263	1.996706	-4.088444				
C	5.161830	1.079605	-3.047831				
N	4.651785	1.474447	-1.840033				
C	4.405933	2.772434	-1.633405				
C	5.961193	1.511192	-5.331789				
C	5.418588	-0.320982	-3.245249				
C	5.937232	-0.771554	-4.480300				
C	6.202099	0.181810	-5.520241				
C	6.167687	-2.161086	-4.619096				
H	6.563865	-2.548972	-5.553311				
C	5.887491	-3.013439	-3.567028				
C	5.374982	-2.481845	-2.374264				
N	5.144253	-1.175154	-2.210896				

Table D.5. (continued) Cartesian Coordinates of the B3LYP/6-31G* Optimized Geometries of the Transition States, Ints, and Products Involved in the Dissociation of $M^{2+}(Phen)_2$ Complexes through PTCF Process.[a]

	$Co^{2+}(Phen)_2$ TS_2				$Co^{2+}(Phen)_2$ TS_2		
	x	y	z		x	y	z
C	-0.203157	-0.022788	0.164389	H	6.459912	2.157211	-6.211546
C	-0.132410	0.072272	1.546060	H	4.539590	4.790463	-2.609324
C	1.121879	0.055692	2.218898	H	5.579188	4.075147	-4.765143
C	2.294824	-0.069880	1.440434	H	4.006145	3.073036	-0.885494
N	2.171253	-0.226781	0.077575	H	6.880659	-0.254566	-6.487023
C	1.017318	-0.223724	-0.486451	H	6.094011	-4.099678	-3.623398
C	1.252590	0.172788	3.641737	H	5.088540	-3.080059	-1.582385
C	3.588908	-0.022415	2.041653	Co^{2+}	4.449919	-0.113852	-0.752214
C	3.681868	0.082880	3.452743				
C	2.483626	0.172734	4.233593				
C	4.978991	0.112261	4.018260				
H	5.092809	0.188395	5.095946				
C	6.087709	0.048424	3.195948				
C	5.905139	-0.033476	1.807304				
N	4.695055	-0.064226	1.235488				
H	0.353272	0.261275	4.243149				
H	-1.143409	0.007159	-0.373898				
H	-1.045701	0.159768	2.129446				
H	3.238721	-1.024396	-0.492137				
H	2.573134	0.254764	5.312403				
H	7.093184	0.067483	3.601560				
H	6.761488	-0.073540	1.140604				
C	4.762932	3.747198	-2.803350				
C	5.338909	3.347121	-3.995432				
C	5.615660	1.976758	-4.214426				
C	5.281236	1.080176	-3.175359				
N	4.710533	1.481975	-2.000378				
C	4.460752	2.782930	-1.827993				
C	6.204617	1.461047	-5.418526				
C	5.531529	-0.322350	-3.334764				
C	6.103699	-0.807473	-4.531537				
C	6.437938	0.125008	-5.571280				
C	6.311017	-2.204001	-4.626825				
H	6.748885	-2.622801	-5.528592				
C	5.950816	-3.025951	-3.573545				
C	5.386438	-2.459143	-2.420942				
N	5.186053	-1.141950	-2.296106				

Table D.5. (continued) Cartesian Coordinates of the B3LYP/6-31G* Optimized Geometries of the Transition States, Ints, and Products Involved in the Dissociation of $M^{2+}(Phen)_2$ Complexes through PTCF Process.[a]

$Co^{2+}(Phen)_2$ Int_2				$Co^{2+}(Phen)_2$ Int_2			
	x	y	z		x	y	z
C	-0.063239	0.557971	0.005798	H	8.235964	1.443435	-5.104616
C	0.065017	0.689824	1.381397	H	4.728718	4.186156	-3.116614
C	1.319163	0.466164	2.012721	H	6.679713	3.404357	-4.462647
C	2.409393	0.108534	1.195436	H	3.548862	2.576814	-1.621112
N	2.274523	-0.020868	-0.176682	H	8.838952	-0.929000	-4.848508
C	1.093524	0.194420	-0.681919	H	6.933753	-4.549968	-2.201938
C	1.542641	0.583102	3.426670	H	5.036324	-3.440545	-1.027740
C	3.696420	-0.139376	1.748773	Co^{2+}	3.944478	-0.560479	-1.026312
C	3.892305	-0.016880	3.142269				
C	2.777436	0.352475	3.967023				
C	5.197445	-0.276577	3.626917				
H	5.404817	-0.196049	4.690290				
C	6.198140	-0.631493	2.740061				
C	5.906215	-0.733651	1.368594				
N	4.687861	-0.499282	0.877398				
H	0.708760	0.859223	4.064494				
H	-1.003961	0.716495	-0.509037				
H	-0.799062	0.962754	1.982108				
H	3.184363	-1.433851	-1.953051				
H	2.930432	0.443918	5.037931				
H	7.206265	-0.833252	3.085059				
H	6.674535	-1.013331	0.655272				
C	5.069359	3.158218	-3.058728				
C	6.151563	2.720895	-3.803743				
C	6.568138	1.372290	-3.707466				
C	5.833274	0.542010	-2.834520				
N	4.771615	0.979204	-2.099965				
C	4.400050	2.257280	-2.214209				
C	7.670210	0.804063	-4.433888				
C	6.180239	-0.834658	-2.691340				
C	7.264442	-1.377939	-3.415671				
C	8.004712	-0.512708	-4.292287				
C	7.539725	-2.751601	-3.224821				
H	8.360739	-3.218703	-3.761213				
C	6.751897	-3.492712	-2.360728				
C	5.684502	-2.875297	-1.689358				
N	5.412250	-1.575856	-1.842470				

Table D.5. (continued) Cartesian Coordinates of the B3LYP/6-31G* Optimized Geometries of the Transition States, Ints, and Products Involved in the Dissociation of $M^{2+}(Phen)_2$ Complexes through PTCF Process.[a]

$Co^{2+}(Phen)_2$ TS_3				$Co^{2+}(Phen)_2$ TS_3			
	x	y	z		x	y	z
C	-0.043595	0.110439	0.024959	H	8.128797	1.296515	-5.633310
C	-0.020271	0.046054	1.410307	H	5.470310	4.603828	-3.261113
C	1.216625	-0.005666	2.108858	H	7.043535	3.482654	-4.844807
C	2.400671	0.013314	1.344455	H	4.251411	3.235248	-1.574952
N	2.371757	0.086044	-0.034874	H	8.364800	-1.144229	-5.398587
C	1.202052	0.127018	-0.605567	H	6.240505	-4.411585	-2.490694
C	1.327696	-0.078845	3.538642	H	4.625774	-3.033226	-1.172799
C	3.682049	-0.049853	1.970703	Co^{2+}	4.225953	0.173030	-0.824395
C	3.763056	-0.123514	3.380226				
C	2.550013	-0.134448	4.147174				
C	5.060033	-0.183018	3.944457				
H	5.177287	-0.237915	5.023104				
C	6.166481	-0.170606	3.115371				
C	5.985035	-0.099697	1.722965				
N	4.778968	-0.039996	1.153955				
H	0.418852	-0.090120	4.132323				
H	-0.968547	0.148394	-0.538794				
H	-0.953181	0.034454	1.968552				
H	4.035093	-0.800418	-2.046236				
H	2.620129	-0.189674	5.229184				
H	7.171659	-0.214561	3.520014				
H	6.840883	-0.090324	1.054575				
C	5.620288	3.530131	-3.232789				
C	6.489626	2.905752	-4.109713				
C	6.658217	1.503230	-4.044019				
C	5.903037	0.812220	-3.067531				
N	5.060392	1.435908	-2.191684				
C	4.927163	2.763161	-2.281485				
C	7.548471	0.758899	-4.889664				
C	6.017360	-0.603498	-2.967299				
C	6.909210	-1.322459	-3.792464				
C	7.678494	-0.594494	-4.762131				
C	6.987702	-2.721478	-3.607796				
H	7.663184	-3.309103	-4.222474				
C	6.193094	-3.339881	-2.649648				
C	5.300850	-2.584194	-1.893062				
N	5.220956	-1.237629	-2.034481				

Table D.5. (continued) Cartesian Coordinates of the B3LYP/6-31G* Optimized Geometries of the Transition States, Ints, and Products Involved in the Dissociation of $M^{2+}(Phen)_2$ Complexes through PTCF Process.[a]

$Co^{2+}(Phen)_2$ Int_3				$Co^{2+}(Phen)_2$ Int_3			
	x	y	z		x	y	z
C	0.193753	0.080731	-1.088069	H	6.198003	5.230254	-6.897356
C	0.404752	-0.569726	0.119556	H	4.779932	6.415798	-2.481664
C	1.694315	-0.578387	0.715483	H	5.666871	6.451408	-4.825038
C	2.726831	0.096102	0.034993	H	4.034505	4.270674	-1.512883
N	2.513460	0.742640	-1.163178	H	6.255209	3.133389	-8.199486
C	1.308260	0.709342	-1.652325	H	5.000437	-1.425001	-7.228972
C	2.011761	-1.225651	1.957952	H	4.208606	-1.300203	-4.828338
C	4.050293	0.143800	0.558228	Co^{2+}	4.159498	1.695668	-1.823097
C	4.339540	-0.504275	1.779943				
C	3.280638	-1.190478	2.465518				
C	5.673441	-0.423844	2.244953				
H	5.951854	-0.903690	3.178902				
C	6.610117	0.269910	1.500986				
C	6.222822	0.887016	0.298256				
N	4.974627	0.834286	-0.175321				
H	1.223041	-1.746869	2.491799				
H	-0.778157	0.105665	-1.567112				
H	-0.420621	-1.074659	0.615481				
H	4.261277	0.779904	-3.720484				
H	3.506230	-1.684588	3.405630				
H	7.639979	0.350626	1.831156				
H	6.946189	1.441412	-0.292541				
C	4.860455	5.507824	-3.069179				
C	5.345669	5.524058	-4.359937				
C	5.407207	4.317492	-5.094310				
C	4.981786	3.119821	-4.456688				
N	4.520568	3.110681	-3.161857				
C	4.450678	4.288630	-2.515735				
C	5.874053	4.295030	-6.451148				
C	5.016059	1.909937	-5.237679				
C	5.467323	1.911710	-6.582890				
C	5.905994	3.140390	-7.171963				
C	5.456926	0.687000	-7.290634				
H	5.802282	0.672703	-8.320570				
C	5.011903	-0.483033	-6.692851				
C	4.573105	-0.435278	-5.371095				
N	4.593323	0.727262	-4.706435				

Table D.5. (continued) Cartesian Coordinates of the B3LYP/6-31G* Optimized Geometries of the Transition States, Ints, and Products Involved in the Dissociation of $M^{2+}(Phen)_2$ Complexes through PTCF Process.[a]

$Co^{2+}(Phen)_2$ TS_4				$Co^{2+}(Phen)_2$ TS_4			
	x	y	z		x	y	z
C	0.008693	0.144985	0.013538	H	5.408584	6.246521	-6.861398
C	0.015670	0.130495	1.398505	H	4.458878	4.325429	-2.516754
C	1.239643	0.063353	2.118151	H	4.826015	5.920014	-4.402487
C	2.437299	0.010328	1.375920	H	4.703889	1.878822	-2.917747
N	2.410839	0.025116	-0.011252	H	5.995733	5.271377	-9.045881
C	1.259130	0.089676	-0.612139	H	6.622784	0.704128	-10.580729
C	1.312950	0.044619	3.550499	H	6.191585	-0.654504	-8.496947
C	3.707708	-0.065463	2.039776	Co^{2+}	4.257096	-0.122858	-0.574065
C	3.746828	-0.082354	3.452964				
C	2.517572	-0.024647	4.189406				
C	5.020175	-0.160612	4.067892				
H	5.094146	-0.177078	5.151365				
C	6.153370	-0.217246	3.281480				
C	6.024783	-0.197198	1.882252				
N	4.842939	-0.122157	1.263146				
H	0.389734	0.085234	4.120294				
H	-0.910978	0.194337	-0.557778				
H	-0.922168	0.169580	1.947361				
H	5.642969	0.505642	-6.501148				
H	2.562969	-0.039579	5.274057				
H	7.142169	-0.279906	3.722337				
H	6.904161	-0.244806	1.247621				
C	4.721197	3.966725	-3.506572				
C	4.923827	4.848200	-4.549195				
C	5.263882	4.339680	-5.824449				
C	5.372303	2.930469	-5.937236				
N	5.175800	2.063444	-4.915990				
C	4.859623	2.580514	-3.739062				
C	5.496738	5.169940	-6.973807				
C	5.714092	2.386280	-7.221270				
C	5.941107	3.212353	-8.346635				
C	5.822150	4.633260	-8.185312				
C	6.272366	2.580145	-9.566327				
H	6.452477	3.189082	-10.447837				
C	6.369304	1.196720	-9.649304				
C	6.135293	0.427649	-8.510464				
N	5.821914	1.035430	-7.357437				

Table D.5. (continued) Cartesian Coordinates of the B3LYP/6-31G* Optimized Geometries of the Transition States, Ints, and Products Involved in the Dissociation of $M^{2+}(Phen)_2$ Complexes through PTCF Process.[a]

$Co^{2+}(Phen)_2$ Int_4			
	x	y	z
C	-6.661619	3.494600	-0.066066
C	-7.926395	3.117006	0.356825
C	-8.298091	1.746219	0.393011
C	-7.336857	0.801699	-0.015754
N	-6.081425	1.194916	-0.432263
C	-5.791530	2.463461	-0.443934
C	-9.583909	1.270220	0.817401
C	-7.627811	-0.599656	-0.007690
C	-8.901252	-1.040638	0.416436
C	-9.870643	-0.065447	0.828282
C	-9.139192	-2.435573	0.403328
H	-10.104329	-2.821873	0.717817
C	-8.137448	-3.291391	-0.013628
C	-6.899212	-2.765621	-0.418807
N	-6.635715	-1.454307	-0.423028
H	-10.330475	1.993343	1.131444
H	-6.357485	4.534231	-0.104349
H	-8.645274	3.872938	0.663605
H	8.309837	0.089699	-2.126800
H	-10.847668	-0.411890	1.151228
H	-8.289457	-4.364985	-0.033991
H	-6.101512	-3.424047	-0.748071
C	6.107807	-0.235075	1.944705
C	7.344860	-0.234731	2.558005
C	8.509396	-0.148585	1.759613
C	8.307759	-0.066810	0.359775
N	7.098414	-0.066902	-0.244294
C	6.030988	-0.149353	0.536640
C	9.845816	-0.140417	2.288258
C	9.466203	0.022026	-0.481395
C	10.777897	0.029060	0.047657
C	10.936269	-0.055483	1.471501
C	11.848810	0.119117	-0.868950
H	12.868754	0.126812	-0.494841
C	11.612713	0.197588	-2.236435
C	10.299817	0.187217	-2.704735
N	9.289697	0.101506	-1.828621
H	9.976734	-0.203950	3.364589
H	5.197920	-0.300567	2.531873
H	7.433412	-0.299682	3.638730
H	5.064524	-0.148665	0.036925
H	11.939912	-0.050201	1.884452
H	12.429157	0.266601	-2.945600
H	10.037023	0.245612	-3.754372
Co^{2+}	-5.102375	-0.401721	-0.961461

$[Co(Phen-H)]^+$			
	x	y	z
C	-0.083954	0.000000	0.013284
C	-0.003721	0.000000	1.395222
C	1.258738	0.000000	2.048540
C	2.413868	0.000000	1.241637
N	2.311726	0.000000	-0.139627
C	1.131641	0.000000	-0.684189
C	1.415524	0.000000	3.474267
C	3.721475	0.000000	1.831460
C	3.844224	0.000000	3.239113
C	2.656630	0.000000	4.043598
C	5.153825	0.000000	3.777484
H	5.292911	0.000000	4.854594
C	6.238953	0.000000	2.923889
C	6.027577	0.000000	1.534616
N	4.808488	0.000000	0.986344
H	0.525437	0.000000	4.096030
H	-1.034069	0.000000	-0.508235
H	-0.911473	0.000000	1.993865
H	2.764330	0.000000	5.123999
H	7.254501	0.000000	3.304265
H	6.868600	0.000000	0.848405
Co^{2+}	4.128566	0.000000	-0.811394

Table D.5. (continued) Cartesian Coordinates of the B3LYP/6-31G* Optimized Geometries of the Transition States, Ints, and Products Involved in the Dissociation of $M^{2+}(Phen)_2$ Complexes through PTCF Process.[a]

$Ni^{2+}(Phen)_2$ TS_1				$Ni^{2+}(Phen)_2$ TS_1			
	x	y	z		x	y	z
C	-0.129242	-0.326516	0.035111	H	7.566303	1.689375	-5.902230
C	0.008193	-0.614297	1.382044	H	5.487808	4.916463	-2.729161
C	1.285434	-0.545593	1.986422	H	6.792493	3.925507	-4.599701
C	2.366553	-0.178529	1.156294	H	3.719889	2.227573	-0.719997
N	2.219278	0.104745	-0.169464	H	7.425525	-0.752691	-6.036578
C	1.001549	0.034767	-0.714892	H	5.061319	-4.098964	-3.343495
C	1.544100	-0.821704	3.372508	H	3.953901	-2.715488	-1.599545
C	3.689058	-0.086123	1.693106	Ni^{2+}	3.925137	0.618277	-0.998838
C	3.920591	-0.360462	3.058487				
C	2.806407	-0.732157	3.886132				
C	5.254563	-0.246150	3.515855				
H	5.487145	-0.443722	4.558425				
C	6.252456	0.118693	2.629474				
C	5.926876	0.373313	1.286081				
N	4.678697	0.272543	0.827652				
H	0.711693	-1.104006	4.009736				
H	-1.096743	-0.369343	-0.452773				
H	-0.857338	-0.889713	1.977980				
H	0.917629	0.273976	-1.770609				
H	2.986535	-0.942358	4.935948				
H	7.282989	0.214268	2.953298				
H	6.691701	0.664268	0.572671				
C	5.540647	3.842339	-2.861654				
C	6.267566	3.267617	-3.911030				
C	6.321455	1.856845	-4.112220				
C	5.617142	1.076894	-3.185047				
N	4.949428	1.651402	-2.160785				
C	4.884160	2.947909	-2.006860				
C	6.995142	1.138553	-5.161466				
C	5.494925	-0.333261	-3.247414				
C	6.154981	-1.012153	-4.288692				
C	6.913858	-0.229431	-5.234346				
C	5.991847	-2.419595	-4.315255				
H	6.473076	-3.013207	-5.087385				
C	5.207259	-3.024222	-3.348480				
C	4.576873	-2.245433	-2.354406				
N	4.705559	-0.920154	-2.292138				

Table D.5. (continued) Cartesian Coordinates of the B3LYP/6-31G* Optimized Geometries of the Transition States, Ints, and Products Involved in the Dissociation of $M^{2+}(Phen)_2$ Complexes through PTCF Process.[a]

$Ni^{2+}(Phen)_2$ Int_1				$Ni^{2+}(Phen)_2$ Int_1			
	x	y	z		x	y	z
C	0.035149	-0.341686	-0.033467	H	8.349437	-0.853507	-5.265889
C	0.067570	-0.454812	1.346219	H	7.264181	3.532259	-3.389909
C	1.301852	-0.353788	2.029209	H	8.275666	1.674363	-4.741866
C	2.453627	-0.139011	1.240874	H	3.811756	1.683353	-0.622532
N	2.406057	-0.033136	-0.117050	H	7.499150	-3.119051	-4.822520
C	1.228236	-0.124140	-0.740781	H	4.119008	-4.829626	-1.749556
C	1.454768	-0.448207	3.454744	H	3.330371	-2.766687	-0.592754
C	3.738216	-0.012194	1.854444	Ni^{2+}	4.149704	0.313651	-0.884992
C	3.864323	-0.101473	3.257822				
C	2.681800	-0.327177	4.042608				
C	5.166341	0.045099	3.791481				
H	5.320559	-0.011997	4.865234				
C	6.232896	0.265726	2.938275				
C	6.009530	0.342509	1.551817				
N	4.794642	0.203111	1.023762				
H	0.570191	-0.614849	4.061670				
H	-0.898395	-0.409754	-0.581041				
H	-0.848787	-0.614921	1.907225				
H	1.229497	-0.019275	-1.821193				
H	2.780455	-0.397259	5.121569				
H	7.240875	0.385166	3.320140				
H	6.829537	0.522089	0.863703				
C	6.957001	2.500533	-3.261730				
C	7.507346	1.463290	-4.002190				
C	7.069095	0.125726	-3.802806				
C	6.068480	-0.095079	-2.837601				
N	5.520215	0.942738	-2.104416				
C	5.970318	2.143099	-2.343496				
C	7.577924	-1.011288	-4.518674				
C	5.569796	-1.399481	-2.574763				
C	6.083722	-2.503120	-3.289707				
C	7.104993	-2.270706	-4.271544				
C	5.538536	-3.772016	-2.975879				
H	5.895607	-4.657798	-3.493603				
C	4.553273	-3.870693	-2.010109				
C	4.103064	-2.710779	-1.352813				
N	4.591714	-1.501191	-1.625859				

Table D.5. (continued) Cartesian Coordinates of the B3LYP/6-31G* Optimized Geometries of the Transition States, Ints, and Products Involved in the Dissociation of $M^{2+}(Phen)_2$ Complexes through PTCF Process.[a]

$Ni^{2+}(Phen)_2$ TS_2				$Ni^{2+}(Phen)_2$ TS_2			
	x	y	z		x	y	z
C	0.298510	1.000699	-0.091845	H	7.633507	1.525818	-5.829149
C	0.200735	0.821195	1.279873	H	4.381384	4.343573	-3.560358
C	1.336698	0.420503	2.033515	H	6.085972	3.467000	-5.161431
C	2.544499	0.213982	1.336690	H	3.634443	2.910614	-1.660937
N	2.637534	0.394048	-0.028645	H	8.491536	-0.737612	-5.373327
C	1.555824	0.760504	-0.650036	H	7.427666	-4.058755	-1.980669
C	1.326307	0.218316	3.455306	H	5.593571	-2.962618	-0.676490
C	3.727155	-0.197110	2.021918	Ni^{2+}	4.475679	0.031045	-0.676154
C	3.692335	-0.379687	3.422938				
C	2.457080	-0.163503	4.120997				
C	4.901710	-0.767888	4.047658				
H	4.929805	-0.918198	5.123214				
C	6.039267	-0.948009	3.281700				
C	5.973335	-0.750608	1.891830				
N	4.851507	-0.384926	1.267408				
H	0.399133	0.377051	3.997257				
H	-0.546897	1.302614	-0.699288				
H	-0.749137	0.984616	1.782777				
H	4.311099	-1.057242	-1.672963				
H	2.435682	-0.308877	5.196668				
H	6.980722	-1.238849	3.734599				
H	6.853958	-0.887197	1.271098				
C	4.792869	3.346532	-3.447383				
C	5.735773	2.858354	-4.332742				
C	6.250690	1.552542	-4.149882				
C	5.747482	0.816627	-3.054090				
N	4.831777	1.310406	-2.170913				
C	4.364801	2.543000	-2.374342				
C	7.249394	0.953397	-4.990331				
C	6.222017	-0.507709	-2.820163				
C	7.220311	-1.076775	-3.641364				
C	7.724524	-0.302622	-4.740288				
C	7.659621	-2.381513	-3.320598				
H	8.425629	-2.855682	-3.927530				
C	7.105365	-3.056564	-2.240883				
C	6.093444	-2.453245	-1.493057				
N	5.670482	-1.201879	-1.769268				

Table D.5. (continued) Cartesian Coordinates of the B3LYP/6-31G* Optimized Geometries of the Transition States, Ints, and Products Involved in the Dissociation of $M^{2+}(Phen)_2$ Complexes through PTCF Process.[a]

$Ni^{2+}(Phen)_2$ Int_2				$Ni^{2+}(Phen)_2$ Int_2			
	x	y	z		x	y	z
C	-0.182254	-0.896682	0.013343	H	7.751331	-2.078103	-6.273904
C	-0.051702	-0.297064	1.256415	H	6.842944	1.981255	-3.917200
C	1.226290	0.113702	1.720801	H	7.704843	0.258012	-5.520171
C	2.332729	-0.105658	0.876726	H	5.264980	1.284788	-2.142619
N	2.199271	-0.704119	-0.365125	H	7.006038	-4.422462	-6.057290
C	0.996787	-1.059418	-0.716736	H	3.985345	-6.700811	-3.071725
C	1.453559	0.731887	2.997128	H	3.170693	-4.844151	-1.555614
C	3.647615	0.284412	1.274419	Ni^{2+}	3.889708	-0.753629	-1.271760
C	3.846278	0.876812	2.541921				
C	2.710516	1.094445	3.391507				
C	5.176237	1.215965	2.888143				
H	5.383909	1.673531	3.851237				
C	6.199026	0.955997	1.995458				
C	5.898946	0.368449	0.753077				
N	4.658920	0.045267	0.386783				
H	0.603550	0.904299	3.650099				
H	-1.140456	-1.222208	-0.374760				
H	-0.928239	-0.138595	1.879574				
H	3.972798	-2.662513	-1.895658				
H	2.867598	1.555800	4.361671				
H	7.228436	1.198291	2.235723				
H	6.687232	0.159858	0.035698				
C	6.535472	0.943403	-3.850595				
C	7.006843	-0.006946	-4.731499				
C	6.574941	-1.346319	-4.604145				
C	5.655101	-1.662346	-3.565166				
N	5.195815	-0.706521	-2.691980				
C	5.638927	0.551959	-2.849600				
C	7.050066	-2.364786	-5.496313				
C	5.223119	-3.036175	-3.466125				
C	5.711195	-4.027951	-4.356332				
C	6.640746	-3.657451	-5.379736				
C	5.249919	-5.355826	-4.196501				
H	5.617942	-6.123499	-4.871384				
C	4.342599	-5.685668	-3.201061				
C	3.883563	-4.678031	-2.355455				
N	4.328112	-3.424542	-2.512683				

Table D.5. (continued) Cartesian Coordinates of the B3LYP/6-31G* Optimized Geometries of the Transition States, Ints, and Products Involved in the Dissociation of $M^{2+}(Phen)_2$ Complexes through PTCF Process.[a]

$Ni^{2+}(Phen)_2$ TS_3				$Ni^{2+}(Phen)_2$ TS_3			
	x	y	z		x	y	z
C	-0.101843	-0.127380	0.089773	H	5.626543	6.243834	-6.744383
C	-0.051040	-0.060367	1.471927	H	4.567041	4.277323	-2.445810
C	1.201952	-0.021420	2.141241	H	5.026727	5.893019	-4.293454
C	2.371695	-0.054917	1.356678	H	4.665957	1.832933	-2.904898
N	2.314402	-0.121583	-0.031154	H	6.157099	5.289006	-8.952293
C	1.128414	-0.152097	-0.570299	H	6.521908	0.731313	-10.596053
C	1.332475	0.046265	3.568805	H	6.013194	-0.649715	-8.544734
C	3.665874	-0.025469	1.973935	Ni^{2+}	4.097071	-0.190939	-0.607181
C	3.763477	0.038501	3.381625				
C	2.561564	0.075336	4.163012				
C	5.064599	0.057709	3.940781				
H	5.185869	0.104618	5.019151				
C	6.165300	0.013165	3.108394				
C	5.977060	-0.048948	1.716642				
N	4.767492	-0.066404	1.153638				
H	0.430351	0.071887	4.172226				
H	-1.037958	-0.161196	-0.455430				
H	-0.970056	-0.039366	2.051978				
H	5.531194	0.491987	-6.521326				
H	2.647123	0.124206	5.244204				
H	7.173609	0.022889	3.507200				
H	6.828191	-0.087599	1.044336				
C	4.808452	3.928191	-3.444320				
C	5.062270	4.821122	-4.465681				
C	5.372379	4.324248	-5.753091				
C	5.399072	2.914204	-5.899585				
N	5.151594	2.035750	-4.899311				
C	4.865500	2.542117	-3.710020				
C	5.652831	5.166963	-6.882557				
C	5.709677	2.382121	-7.196541				
C	5.984211	3.220474	-8.302136				
C	5.947037	4.641610	-8.106920				
C	6.279146	2.599591	-9.536876				
H	6.494048	3.218067	-10.403832				
C	6.296795	1.215234	-9.652871				
C	6.018786	0.433898	-8.532449				
N	5.740152	1.030962	-7.364999				

Table D.5. (continued) Cartesian Coordinates of the B3LYP/6-31G* Optimized Geometries of the Transition States, Ints, and Products Involved in the Dissociation of $M^{2+}(Phen)_2$ Complexes through PTCF Process.[a]

$Ni^{2+}(Phen)_2$ Int_3				$Ni^{2+}(Phen)_2$ Int_3			
	x	y	z		x	y	z
C	-6.704629	3.499805	-0.074864	H	10.067804	-0.211945	3.359677
C	-7.960448	3.109144	0.359504	H	5.281870	-0.243253	2.548174
C	-8.305458	1.731678	0.397753	H	7.523899	-0.271417	3.647636
C	-7.336514	0.798840	-0.018316	H	5.139080	-0.091897	0.058665
N	-6.077953	1.195589	-0.450170	H	12.024500	-0.086343	1.869163
C	-5.834643	2.476333	-0.456954	H	12.490154	0.225302	-2.964674
C	-9.582894	1.243383	0.834315	H	10.093261	0.236001	-3.759519
C	-7.620832	-0.607379	-0.005628	Ni^{2+}	-5.175286	-0.367042	-0.932021
C	-8.885794	-1.059030	0.429493				
C	-9.859867	-0.093730	0.850550				
C	-9.112638	-2.456585	0.418071				
H	-10.071541	-2.849201	0.743832				
C	-8.110975	-3.306063	-0.008790				
C	-6.880320	-2.770113	-0.426941				
N	-6.630228	-1.459406	-0.428975				
H	-10.331042	1.961963	1.154715				
H	-6.405584	4.540618	-0.119824				
H	-8.687815	3.854254	0.671226				
H	8.373653	0.104148	-2.121339				
H	-10.830514	-0.448184	1.183694				
H	-8.255802	-4.380529	-0.029616				
H	-6.080071	-3.419176	-0.767514				
C	6.191511	-0.190011	1.959415				
C	7.431014	-0.205758	2.567320				
C	8.592355	-0.136021	1.762840				
C	8.384458	-0.052038	0.363988				
N	7.172892	-0.036730	-0.234788				
C	6.108809	-0.104251	0.551510				
C	9.931687	-0.146584	2.284075				
C	9.539179	0.020654	-0.483265				
C	10.853753	0.009567	0.038356				
C	11.018763	-0.077173	1.461381				
C	11.920264	0.084938	-0.884615				
H	12.942437	0.078720	-0.516592				
C	11.677077	0.167020	-2.250711				
C	10.361432	0.174287	-2.711433				
N	9.355570	0.102357	-1.829413				

$[Ni(Phen-H)]^+$			
	x	y	z
C	-0.018725	0.000000	-0.018995
C	-0.022582	0.000000	1.361498
C	1.207113	0.000000	2.063696
C	2.390261	0.000000	1.293259
N	2.384422	0.000000	-0.080450
C	1.207290	0.000000	-0.707726
C	1.309185	0.000000	3.494111
C	3.663709	0.000000	1.952043
C	3.744502	0.000000	3.357884
C	2.525347	0.000000	4.115118
C	5.036239	0.000000	3.950249
H	5.129834	0.000000	5.033121
C	6.167357	0.000000	3.152455
C	5.951464	0.000000	1.771862
N	4.803258	0.000000	1.156758
H	0.394447	0.000000	4.078960
H	-0.943660	0.000000	-0.584922
H	-0.957505	0.000000	1.914388
H	1.233894	0.000000	-1.792697
H	2.588020	0.000000	5.199022
H	7.169185	0.000000	3.566015
Ni^{2+}	4.193408	0.000000	-0.609996

Table D.5. (continued) Cartesian Coordinates of the B3LYP/6-31G* Optimized Geometries of the Transition States, Ints, and Products Involved in the Dissociation of $M^{2+}(Phen)_2$ Complexes through PTCF Process.[a]

$Cu^{2+}(Phen)_2$ TS_1				$Cu^{2+}(Phen)_2$ TS1			
	x	y	z		x	y	z
C	0.178194	0.706263	-0.062245	H	7.883066	2.041352	-5.440313
C	0.152610	0.621476	1.334355	H	5.458462	4.930064	-2.390414
C	1.324906	0.344723	2.095691	H	6.929661	4.062111	-4.214547
C	2.513484	0.190449	1.367912	H	4.226260	3.310300	-0.949162
N	2.522332	0.344310	0.023471	H	8.016224	-0.406085	-5.693246
C	1.434438	0.559777	-0.663532	H	5.947917	-4.103976	-3.338118
C	1.431631	0.171363	3.520745	H	4.557889	-2.965069	-1.610560
C	3.751450	-0.200009	1.929220	Cu^{2+}	4.077342	-0.037551	-0.891150
C	3.829195	-0.375983	3.323025				
C	2.630676	-0.162861	4.098002				
C	5.090506	-0.776724	3.828888				
H	5.230656	-0.929235	4.895278				
C	6.137260	-0.979815	2.945661				
C	5.945681	-0.798154	1.559528				
N	4.775448	-0.420853	1.045608				
H	0.548182	0.300095	4.138278				
H	-0.721981	0.883888	-0.638636				
H	-0.798102	0.753902	1.845389				
H	2.812386	0.128431	-1.874992				
H	2.687472	-0.293464	5.174486				
H	7.113637	-1.288776	3.302859				
H	6.758109	-0.971744	0.860807				
C	5.569862	3.864853	-2.561037				
C	6.383054	3.381212	-3.568241				
C	6.501829	1.984361	-3.760767				
C	5.763381	1.149959	-2.889140				
N	4.966877	1.635075	-1.898702				
C	4.874514	2.954544	-1.744938				
C	7.320161	1.389315	-4.779328				
C	5.842033	-0.278025	-3.040632				
C	6.654270	-0.839431	-4.054626				
C	7.394323	0.034518	-4.920142				
C	6.687163	-2.249199	-4.154989				
H	7.296292	-2.718518	-4.922422				
C	5.942611	-3.021152	-3.280462				
C	5.159454	-2.388083	-2.305531				
N	5.113749	-1.056380	-2.188740				

Table D.5. (continued) Cartesian Coordinates of the B3LYP/6-31G* Optimized Geometries of the Transition States, Ints, and Products Involved in the Dissociation of $M^{2+}(Phen)_2$ Complexes through PTCF Process.[a]

	$Cu^{2+}(Phen)_2$ Int_1				$Cu^{2+}(Phen)_2$ Int_1		
	x	y	z		x	y	z
C	-0.339473	-0.148549	0.296408	H	7.776030	2.345952	-5.151650
C	-0.143841	-0.156362	1.670365	H	4.582170	4.962229	-2.605304
C	1.170965	-0.140428	2.209724	H	6.390663	4.250737	-4.176537
C	2.248549	-0.119203	1.303838	H	3.415413	3.236995	-1.233061
N	2.044206	-0.115664	-0.064727	H	8.277961	-0.064073	-5.252416
C	0.814218	-0.127225	-0.487607	H	6.410483	-3.939942	-3.016346
C	1.473842	-0.141216	3.614396	H	4.647831	-2.952360	-1.553696
C	3.594269	-0.096132	1.756485	Cu^{2+}	3.733651	-0.089896	-0.992601
C	3.870220	-0.093211	3.140930				
C	2.766977	-0.118759	4.059351				
C	5.235533	-0.063606	3.515447				
H	5.508303	-0.060742	4.566967				
C	6.212068	-0.037258	2.535829				
C	5.839545	-0.042244	1.179009				
N	4.564512	-0.076174	0.794486				
H	0.651922	-0.158897	4.323332				
H	-1.327031	-0.160451	-0.150569				
H	-1.000866	-0.174381	2.338965				
H	3.006074	-0.327894	-2.189036				
H	2.977167	-0.119135	5.124434				
H	7.264715	-0.012124	2.795163				
H	6.588280	-0.020957	0.393664				
C	4.866373	3.919589	-2.696961				
C	5.865904	3.522526	-3.564642				
C	6.204680	2.152049	-3.660180				
C	5.481341	1.252969	-2.841025				
N	4.505773	1.654581	-1.985044				
C	4.205415	2.950026	-1.920832				
C	7.225666	1.644169	-4.532350				
C	5.771239	-0.154616	-2.909820				
C	6.779837	-0.630882	-3.782564				
C	7.503982	0.309817	-4.589282				
C	7.009693	-2.025323	-3.810977				
H	7.772029	-2.430012	-4.470721				
C	6.258201	-2.866292	-3.008673				
C	5.268885	-2.320125	-2.179386				
N	5.046523	-1.002746	-2.127706				

Table D.5. (continued) Cartesian Coordinates of the B3LYP/6-31G* Optimized Geometries of the Transition States, Ints, and Products Involved in the Dissociation of $M^{2+}(Phen)_2$ Complexes through PTCF Process.[a]

	$Cu^{2+}(Phen)_2$ TS_2				$Cu^{2+}(Phen)_2$ TS_2		
	x	y	z		x	y	z
C	-0.064803	-0.419372	0.062997	H	8.432327	1.472948	-5.152782
C	-0.000301	-0.354860	1.447122	H	5.697047	4.636489	-2.692834
C	1.249682	-0.188723	2.102698	H	7.366382	3.602953	-4.239183
C	2.403884	-0.097147	1.299780	H	4.274644	3.162104	-1.274372
N	2.329367	-0.166134	-0.079516	H	8.549485	-0.987812	-5.178033
C	1.153354	-0.317420	-0.610967	H	6.051148	-4.449363	-2.863966
C	1.407706	-0.104917	3.527943	H	4.427435	-3.140539	-1.482587
C	3.692290	0.085038	1.878441	Cu^{2+}	4.102594	0.007169	-0.853635
C	3.821934	0.166828	3.283084				
C	2.641088	0.064557	4.092511				
C	5.129924	0.349014	3.793166				
H	5.286696	0.417030	4.865972				
C	6.197296	0.440540	2.918806				
C	5.969466	0.351533	1.533642				
N	4.752468	0.173047	1.020000				
H	0.524050	-0.177167	4.154392				
H	-1.000232	-0.543131	-0.470460				
H	-0.910996	-0.429595	2.036140				
H	3.647666	-0.527983	-2.092957				
H	2.743855	0.126385	5.171518				
H	7.209190	0.581790	3.282231				
H	6.792262	0.426839	0.829503				
C	5.809691	3.559715	-2.756693				
C	6.730492	2.984496	-3.612137				
C	6.842054	1.575433	-3.672809				
C	5.982181	0.826135	-2.835862				
N	5.089622	1.402304	-1.986141				
C	5.003300	2.732877	-1.954972				
C	7.772830	0.885656	-4.521110				
C	6.036456	-0.608704	-2.873772				
C	6.964472	-1.266733	-3.715406				
C	7.837599	-0.477362	-4.536780				
C	6.964044	-2.680805	-3.698725				
H	7.659777	-3.224605	-4.331511				
C	6.071848	-3.365404	-2.889526				
C	5.165283	-2.642846	-2.103078				
N	5.168241	-1.304888	-2.088813				

Table D.5. (continued) Cartesian Coordinates of the B3LYP/6-31G* Optimized Geometries of the Transition States, Ints, and Products Involved in the Dissociation of $M^{2+}(Phen)_2$ Complexes through PTCF Process.[a]

$Cu^{2+}(Phen)_2$ Int_2				$Cu^{2+}(Phen)_2$ Int_2			
	x	y	z		x	y	z
C	0.500970	-0.673541	-0.156121	H	8.786000	1.040732	-5.083794
C	0.263994	-0.632442	1.209226	H	7.191835	4.195335	-1.855710
C	1.309734	-0.302324	2.113826	H	8.396322	3.070437	-3.744278
C	2.578032	-0.018808	1.570281	H	5.604845	2.881407	-0.492088
N	2.800122	-0.067525	0.208770	H	8.268582	-1.315154	-5.612469
C	1.808273	-0.380237	-0.563354	H	5.148595	-4.525322	-3.817843
C	1.149341	-0.238179	3.539194	H	4.010522	-3.238932	-1.959231
C	3.680052	0.339811	2.407659	Cu^{2+}	4.594779	0.492355	-0.219186
C	3.494383	0.387379	3.808314				
C	2.199170	0.089674	4.350235				
C	4.621060	0.736695	4.591295				
H	4.532581	0.787422	5.672841				
C	5.823885	1.009008	3.968371				
C	5.905111	0.940759	2.565025				
N	4.867777	0.617168	1.793858				
H	0.174633	-0.455694	3.964903				
H	-0.277961	-0.917428	-0.869109				
H	-0.728832	-0.850876	1.594911				
H	4.668551	-1.025634	-1.554239				
H	2.065046	0.132453	5.426825				
H	6.705114	1.277100	4.540837				
H	6.840513	1.155227	2.056540				
C	7.013092	3.153773	-2.099200				
C	7.671872	2.532882	-3.139708				
C	7.393667	1.177310	-3.424990				
C	6.435608	0.503195	-2.617872				
N	5.816601	1.120764	-1.559908				
C	6.108170	2.411569	-1.331245				
C	8.050666	0.493386	-4.502081				
C	6.120029	-0.858403	-2.970022				
C	6.778629	-1.514716	-4.042272				
C	7.766039	-0.804601	-4.797299				
C	6.416152	-2.850814	-4.331232				
H	6.917518	-3.366209	-5.145639				
C	5.433217	-3.502370	-3.600311				
C	4.798045	-2.813429	-2.570459				
N	5.156642	-1.551253	-2.295953				

Table D.5. (continued) Cartesian Coordinates of the B3LYP/6-31G* Optimized Geometries of the Transition States, Ints, and Products Involved in the Dissociation of $M^{2+}(Phen)_2$ Complexes through PTCF Process.[a]

$Cu^{2+}(Phen)_2$ TS_3				$Cu^{2+}(Phen)_2$ TS_3			
	x	y	z		x	y	z
C	0.000000	0.000000	0.000000	N	4.078884	-0.804245	-3.429194
C	0.000000	0.000000	1.389637	H	4.867000	1.220444	-8.251604
C	1.211013	0.000000	2.115491	H	7.255404	4.058256	-5.146425
C	2.424273	0.005313	1.380956	H	6.269422	3.054052	-7.211781
N	2.365413	0.003065	0.017758	H	6.825353	2.974904	-2.944953
C	1.216321	-0.001365	-0.675907	H	3.513009	-0.820728	-7.988686
C	1.273588	-0.007552	3.547646	H	2.192414	-3.494086	-4.159352
C	3.700034	0.005880	2.038394	H	3.263202	-0.001155	-0.472998
C	3.713692	-0.008441	3.457343				
C	2.477800	-0.013611	4.188068				
C	4.981609	-0.018194	4.085758				
H	5.046577	-0.029913	5.169940				
C	6.119057	-0.014190	3.305831				
C	5.988357	0.004353	1.899844				
N	4.818435	0.016388	1.273913				
H	0.345033	-0.010925	4.109384				
H	-0.925223	-0.000993	-0.564232				
H	-0.941728	-0.001607	1.931378				
H	1.300594	-0.010943	-1.755765				
H	2.518671	-0.022680	5.273231				
H	7.107445	-0.023961	3.752861				
H	6.877931	0.008682	1.275509				
Cu^{2+}	5.152468	0.251110	-2.322594				
C	6.639711	3.166879	-5.098691				
C	6.093104	2.609230	-6.236566				
C	5.296025	1.442391	-6.133741				
C	5.098358	0.903754	-4.841386				
N	5.652960	1.464744	-3.715369				
C	6.399846	2.560471	-3.852755				
C	4.701856	0.794803	-7.266592				
C	4.292642	-0.280586	-4.698199				
C	3.723793	-0.906939	-5.825474				
C	3.950323	-0.335895	-7.121412				
C	2.955175	-2.086348	-5.616817				
H	2.516667	-2.592607	-6.473361				
C	2.766784	-2.593384	-4.342463				
C	3.367831	-1.875699	-3.298710				

Table D.5. (continued) Cartesian Coordinates of the B3LYP/6-31G* Optimized Geometries of the Transition States, Ints, and Products Involved in the Dissociation of $M^{2+}(Phen)_2$ Complexes through PTCF Process.[a]

$Cu^{2+}(Phen)_2$ Int_3				$Cu^{2+}(Phen)_2$ Int_3			
	x	y	z		x	y	z
C	-6.539209	3.506238	0.060103	H	9.994653	-0.369814	3.348953
C	-7.803689	3.113231	0.458728	H	5.211074	-0.397939	2.517524
C	-8.176133	1.739352	0.443675	H	7.451301	-0.462949	3.624231
C	-7.219602	0.803149	0.006071	H	5.075843	-0.124743	0.041443
N	-5.960832	1.225682	-0.389728	H	11.956168	-0.159194	1.874181
C	-5.672030	2.482456	-0.353039	H	12.439956	0.382887	-2.936458
C	-9.468189	1.267348	0.849627	H	10.046371	0.417143	-3.740589
C	-7.527255	-0.604421	-0.029830	Cu^{2+}	-5.104768	-0.350733	-0.921262
C	-8.809898	-1.033982	0.382295				
C	-9.770450	-0.063597	0.819893				
C	-9.075490	-2.424137	0.337602				
H	-10.049764	-2.793738	0.644519				
C	-8.096209	-3.294480	-0.095515				
C	-6.847240	-2.782579	-0.489500	$[Cu(Phen-H)]^+$			
N	-6.559490	-1.481669	-0.462780		x	y	z
H	-10.206044	1.990619	1.183064	C	-0.013375	0.000000	-0.040815
H	-6.230350	4.545028	0.063872	C	-0.020899	0.000000	1.341466
H	-8.526769	3.854814	0.789346	C	1.199626	0.000000	2.074376
H	8.320574	0.196310	-2.118262	C	2.405073	0.000000	1.346452
H	-10.751446	-0.410323	1.130038	N	2.382433	0.000000	-0.039138
H	-8.270719	-4.363782	-0.139537	C	1.249296	0.000000	-0.654775
H	-6.061383	-3.445152	-0.836123	C	1.258425	0.000000	3.507149
C	6.123579	-0.309644	1.937479	C	3.675723	0.000000	2.025216
C	7.361255	-0.345966	2.548027	C	3.695759	0.000000	3.439088
C	8.524736	-0.228303	1.751769	C	2.457036	0.000000	4.160589
C	8.321413	-0.078102	0.357663	C	4.962838	0.000000	4.071140
N	7.110938	-0.041583	-0.243396	H	5.020234	0.000000	5.155883
C	6.044712	-0.155763	0.535211	C	6.109962	0.000000	3.304597
C	9.862203	-0.254223	2.277153	C	5.999701	0.000000	1.902751
C	9.479316	0.043168	-0.480626	N	4.826208	0.000000	1.271565
C	10.791976	0.015616	0.045425	H	0.327884	0.000000	4.066464
C	10.951908	-0.137864	1.463253	H	-0.927127	0.000000	-0.623526
C	11.861929	0.141465	-0.868037	H	-0.963835	0.000000	1.882693
H	12.882568	0.124168	-0.496157	H	2.490819	0.000000	5.245776
C	11.624166	0.286227	-2.229774	H	7.093991	0.000000	3.760045
C	10.310437	0.307541	-2.695382	H	6.885724	0.000000	1.276897
N	9.301216	0.187789	-1.822250	Cu^{2+}	4.195558	0.000000	-0.517457

Table D.5. (continued) Cartesian Coordinates of the B3LYP/6-31G* Optimized Geometries of the Transition States, Ints, and Products Involved in the Dissociation of $M^{2+}(Phen)_2$ Complexes through PTCF Process.[a]

$Zn^{2+}(Phen)_2$ TS_1				$Zn^{2+}(Phen)_2$ TS_1			
	x	y	z		x	y	z
C	-0.025697	-0.085441	0.029005	H	6.089774	2.700469	-6.178017
C	-0.010694	-0.017784	1.401913	H	4.227577	5.282028	-2.527544
C	1.222923	0.011806	2.133306	H	5.206012	4.576646	-4.715849
C	2.406667	-0.004495	1.390912	H	3.820547	3.562224	-0.770453
N	2.374023	-0.086298	-0.013506	H	6.593778	0.305141	-6.469649
C	1.162310	-0.125845	-0.771368	H	6.091801	-3.567242	-3.604514
C	1.303996	0.065882	3.560252	H	5.118034	-2.606969	-1.522907
C	3.675058	0.123759	2.022757	Zn^{2+}	4.257506	0.387075	-0.721897
C	3.740076	0.154018	3.438868				
C	2.521210	0.111030	4.188214				
C	5.025671	0.251147	4.025575				
H	5.124251	0.267060	5.107426				
C	6.142684	0.334543	3.216188				
C	5.983005	0.345821	1.819317				
N	4.788461	0.248090	1.231732				
H	0.385947	0.066492	4.139904				
H	-0.974626	-0.132782	-0.497097				
H	-0.943037	-0.003019	1.962370				
H	2.220126	-1.047578	-0.656090				
H	2.576296	0.136114	5.272377				
H	7.138935	0.411752	3.637301				
H	6.844143	0.447671	1.165827				
C	4.476904	4.244783	-2.721652				
C	5.018143	3.849457	-3.930940				
C	5.329439	2.487057	-4.151887				
C	5.063901	1.582504	-3.097967				
N	4.531873	1.988546	-1.906864				
C	4.246074	3.281121	-1.728634				
C	5.890963	1.994496	-5.377609				
C	5.355275	0.182587	-3.269386				
C	5.908742	-0.273171	-4.488444				
C	6.169631	0.669371	-5.539052				
C	6.175669	-1.657842	-4.602204				
H	6.599678	-2.048441	-5.522988				
C	5.896059	-2.502473	-3.543655				
C	5.346640	-1.966802	-2.369589				
N	5.081241	-0.664287	-2.232310				

Table D.5. (continued) Cartesian Coordinates of the B3LYP/6-31G* Optimized Geometries of the Transition States, Ints, and Products Involved in the Dissociation of $M^{2+}(Phen)_2$ Complexes through PTCF Process.[a]

$Zn^{2+}(Phen)_2$ Int_1				$Zn^{2+}(Phen)_2$ Int_1			
	x	y	z		x	y	z
C	0.316518	0.116021	-0.262881	H	5.935271	2.106886	-6.198371
C	0.159126	0.252075	1.104431	H	4.421546	4.744007	-2.428811
C	1.283244	0.094998	1.980888	H	5.205325	4.006387	-4.683408
C	2.482336	-0.315332	1.401111	H	4.120998	3.042823	-0.632642
N	2.475453	-0.770640	0.058707	H	6.378017	-0.298144	-6.510649
C	1.410971	-0.604550	-0.826660	H	6.063643	-4.142203	-3.582220
C	1.290564	0.421338	3.376552	H	5.276765	-3.156312	-1.436670
C	3.714043	-0.186319	2.080740	Zn^{2+}	4.510036	-0.139859	-0.616164
C	3.707219	0.103652	3.470635				
C	2.452830	0.378617	4.103192				
C	4.963323	0.147502	4.119144				
H	5.012531	0.345661	5.186316				
C	6.124261	-0.039091	3.386541				
C	6.044790	-0.215112	1.996784				
N	4.874275	-0.281167	1.348971				
H	0.357138	0.705716	3.852512				
H	-0.501192	0.383878	-0.925464				
H	-0.801846	0.531268	1.530881				
H	2.897371	-1.695894	-0.059845				
H	2.442268	0.599207	5.166140				
H	7.098701	-0.006474	3.860934				
H	6.945085	-0.279764	1.393435				
C	4.632451	3.700576	-2.634950				
C	5.066980	3.287136	-3.881050				
C	5.335218	1.917936	-4.116789				
C	5.138799	1.024228	-3.038930				
N	4.705749	1.448092	-1.813009				
C	4.461598	2.748064	-1.620161				
C	5.789889	1.409197	-5.379464				
C	5.398470	-0.380476	-3.220937				
C	5.846712	-0.852207	-4.476134				
C	6.034990	0.078807	-5.552133				
C	6.087379	-2.241138	-4.599404				
H	6.430395	-2.643758	-5.548303				
C	5.885732	-3.074733	-3.514663				
C	5.440824	-2.524370	-2.304188				
N	5.201941	-1.217275	-2.157135				

Table D.5. (continued) Cartesian Coordinates of the B3LYP/6-31G* Optimized Geometries of the Transition States, Ints, and Products Involved in the Dissociation of $M^{2+}(Phen)_2$ Complexes through PTCF Process.[a]

$Zn^{2+}(Phen)_2$ TS_2				$Zn^{2+}(Phen)_2$ TS_2			
	x	y	z		x	y	z
C	0.189207	-0.913866	0.291872	H	10.674997	1.206610	-3.092689
C	0.165468	-0.549741	1.623361	H	8.036033	4.336136	-0.483956
C	1.356205	-0.198905	2.333154	H	9.824340	3.281946	-1.874931
C	2.604274	-0.225714	1.650620	H	6.061634	2.974062	0.193037
N	2.499477	-0.678459	0.365012	H	10.329617	-1.141149	-3.755042
C	1.489051	-0.996312	-0.260993	H	6.766974	-4.331832	-2.895235
C	1.334793	0.168299	3.714628	H	5.172223	-3.018018	-1.487286
C	3.821639	0.169229	2.298147	Zn^{2+}	5.191074	-0.038303	-0.400070
C	3.750433	0.465981	3.691286				
C	2.493004	0.463411	4.371941				
C	4.954011	0.767034	4.370026				
H	4.924851	0.987091	5.433450				
C	6.146625	0.775044	3.678519				
C	6.121957	0.534842	2.298286				
N	5.008117	0.260631	1.609441				
H	0.382980	0.186985	4.235858				
H	-0.701328	-1.159160	-0.273358				
H	-0.780906	-0.523861	2.158760				
H	3.965285	-1.085899	-0.110668				
H	2.478018	0.711264	5.428740				
H	7.089227	0.986169	4.171260				
H	7.041182	0.585386	1.724795				
C	7.966200	3.299040	-0.792929				
C	8.953071	2.711553	-1.565272				
C	8.823081	1.360135	-1.962256				
C	7.664909	0.671476	-1.534194				
N	6.704714	1.254492	-0.757918				
C	6.851414	2.538415	-0.411327				
C	9.787272	0.670074	-2.772278				
C	7.463026	-0.695715	-1.924680				
C	8.422977	-1.349726	-2.727873				
C	9.595425	-0.630288	-3.139640				
C	8.156485	-2.694902	-3.079997				
H	8.864986	-3.239807	-3.697506				
C	6.995528	-3.303345	-2.638482				
C	6.095115	-2.572672	-1.845849				
N	6.322905	-1.305161	-1.496640				

Table D.5. (continued) Cartesian Coordinates of the B3LYP/6-31G* Optimized Geometries of the Transition States, Ints, and Products Involved in the Dissociation of $M^{2+}(Phen)_2$ Complexes through PTCF Process.[a]

$Zn^{2+}(Phen)_2$ Int_2				$Zn^{2+}(Phen)_2$ Int_2			
	x	y	z		x	y	z
C	-0.868179	-0.417478	0.980410	H	8.506781	0.907046	-5.298064
C	-0.380075	-0.161460	2.264086	H	4.835929	3.746871	-3.914355
C	1.007553	-0.011579	2.573029	H	6.879609	2.835676	-5.027923
C	1.997619	-0.134572	1.539531	H	3.632513	2.335881	-2.248809
N	1.433801	-0.407963	0.311773	H	9.200632	-1.375960	-4.681801
C	0.250283	-0.514221	0.175968	H	7.401694	-4.677258	-1.625205
C	1.441705	0.276121	3.904152	H	5.429457	-3.510500	-0.638055
C	3.394067	0.040414	1.799498	Zn^{2+}	4.044572	-0.666411	-1.196075
C	3.759190	0.339357	3.146301				
C	2.768567	0.443376	4.172157				
C	5.131154	0.539218	3.436229				
H	5.432751	0.769048	4.454118				
C	6.059011	0.446216	2.425132				
C	5.611327	0.141875	1.127794				
N	4.333815	-0.062476	0.806542				
H	0.702068	0.365222	4.692945				
H	-1.906146	-0.534978	0.700894				
H	-1.105941	-0.074120	3.070453				
H	2.626890	-1.275289	-1.433642				
H	3.096591	0.667160	5.182639				
H	7.116936	0.599890	2.607283				
H	6.329075	0.057847	0.318027				
C	5.208700	2.756526	-3.677523				
C	6.338608	2.248865	-4.290927				
C	6.791810	0.950539	-3.961609				
C	6.049098	0.229870	-2.996256				
N	4.934082	0.741139	-2.399298				
C	4.529730	1.966803	-2.736267				
C	7.946337	0.341996	-4.559527				
C	6.459865	-1.101555	-2.630284				
C	7.594698	-1.679824	-3.246920				
C	8.330590	-0.921085	-4.218178				
C	7.936899	-2.998052	-2.865596				
H	8.799103	-3.480816	-3.317017				
C	7.167381	-3.663071	-1.929245				
C	6.058035	-3.010048	-1.368519				
N	5.716241	-1.763687	-1.698834				

Table D.5. (continued) Cartesian Coordinates of the B3LYP/6-31G* Optimized Geometries of the Transition States, Ints, and Products Involved in the Dissociation of $M^{2+}(Phen)_2$ Complexes through PTCF Process.[a]

$Zn^{2+}(Phen)_2$ TS_3				$Zn^{2+}(Phen)_2$ TS_3			
	x	y	z		x	y	z
C	0.065833	0.667211	-0.075141	H	7.602348	1.442140	-5.900200
C	0.011506	0.448889	1.288513	H	5.059626	4.486988	-3.152978
C	1.198091	0.181522	2.030944	H	6.471429	3.475976	-4.953365
C	2.418610	0.104994	1.329578	H	4.255031	3.042462	-1.294212
N	2.403306	0.228972	-0.053737	H	8.148314	-0.957633	-5.729593
C	1.327103	0.483129	-0.678304	H	7.083747	-4.393009	-2.498955
C	1.218843	0.026149	3.457067	H	5.553182	-3.220288	-0.903594
C	3.652969	-0.056880	2.024617	Zn^{2+}	4.392364	0.075104	-0.648590
C	3.644019	-0.198397	3.434914				
C	2.392672	-0.164761	4.130411				
C	4.896788	-0.346765	4.075495				
H	4.937025	-0.454921	5.155781				
C	6.059993	-0.341148	3.326702				
C	5.979475	-0.184110	1.935042				
N	4.812662	-0.046896	1.298064				
H	0.278400	0.071407	3.997452				
H	-0.813682	0.914548	-0.657907				
H	-0.942265	0.494618	1.809968				
H	4.191339	-1.269660	-1.648953				
H	2.393680	-0.279432	5.209900				
H	7.031884	-0.446200	3.795857				
H	6.876228	-0.163865	1.323757				
C	5.321490	3.434880	-3.137464				
C	6.102048	2.871643	-4.129781				
C	6.423914	1.496196	-4.075839				
C	5.923264	0.744382	-2.981354				
N	5.159850	1.321630	-2.002194				
C	4.865946	2.625503	-2.088691				
C	7.227511	0.849202	-5.071628				
C	6.219760	-0.656144	-2.901656				
C	7.031055	-1.268603	-3.891270				
C	7.525855	-0.478240	-4.980355				
C	7.337499	-2.639711	-3.736397				
H	7.956670	-3.136146	-4.477903				
C	6.846607	-3.344868	-2.645738				
C	6.014236	-2.696285	-1.735029				
N	5.718427	-1.385830	-1.852280				

Table D.5. (continued) Cartesian Coordinates of the B3LYP/6-31G* Optimized Geometries of the Transition States, Ints, and Products Involved in the Dissociation of $M^{2+}(Phen)_2$ Complexes through PTCF Process.[a]

$Zn^{2+}(Phen)_2$ Int_3				$Zn^{2+}(Phen)_2$ Int_3			
	x	y	z		x	y	z
C	2.969537	3.077725	-1.636198	H	-5.945644	-1.760849	-0.648901
C	4.156711	2.532600	-1.172221	H	-1.936154	-3.906605	-2.124483
C	4.150244	1.295017	-0.475092	H	-4.321214	-3.325714	-1.618506
C	2.909333	0.655758	-0.284627	H	-0.149230	-2.336591	-1.441745
N	1.724880	1.202207	-0.750060	H	-6.463019	0.359315	0.506791
C	1.812035	2.342574	-1.372795	H	-3.775832	4.015648	2.131392
C	5.330034	0.664725	0.048018	H	-1.422475	3.313239	1.516762
C	2.825176	-0.592737	0.403426	Zn^{2+}	0.255589	0.019424	-0.397606
C	3.999201	-1.184221	0.921863				
C	5.256389	-0.522334	0.720619				
C	3.845802	-2.407722	1.616987				
H	4.716598	-2.904070	2.035793				
C	2.584966	-2.956081	1.758979				
C	1.476705	-2.293838	1.200443				
N	1.582273	-1.146804	0.530030				
H	6.288609	1.153046	-0.097890				
H	2.935189	4.018887	-2.172645				
H	5.097100	3.050989	-1.341628				
H	-1.097575	1.265068	0.413139				
H	6.156253	-0.984107	1.115272				
H	2.435554	-3.888481	2.292294				
H	0.478133	-2.709866	1.296944				
C	-2.198105	-2.983542	-1.619063				
C	-3.509260	-2.660377	-1.340172				
C	-3.799360	-1.444712	-0.680872				
C	-2.715341	-0.590200	-0.334216				
N	-1.413157	-0.925699	-0.614846				
C	-1.186751	-2.094119	-1.238141				
C	-5.150428	-1.078080	-0.365943				
C	-3.042696	0.649737	0.328518				
C	-4.386292	0.988770	0.635296				
C	-5.438677	0.089867	0.270399				
C	-4.633024	2.217223	1.292260				
H	-5.657574	2.486349	1.533292				
C	-3.594865	3.073362	1.627188				
C	-2.292305	2.703823	1.298744				
N	-2.068360	1.537682	0.679432				

Table D.5. (continued) Cartesian Coordinates of the B3LYP/6-31G* Optimized Geometries of the Transition States, Ints, and Products Involved in the Dissociation of $M^{2+}(Phen)_2$ Complexes through PTCF Process.[a]

$Zn^{2+}(Phen)_2$ TS_4				$Zn^{2+}(Phen)_2$ TS_4			
	x	y	z		x	y	z
C	0.078454	0.754847	0.385577	H	6.078903	-0.789271	-8.350045
C	-0.150843	0.447987	1.721891	H	6.939570	3.967973	-8.428034
C	0.895994	-0.011724	2.551377	H	6.811515	1.537621	-8.990903
C	2.179004	-0.145839	1.968906	H	5.962040	4.761869	-6.270162
N	2.346800	0.170025	0.655137	H	4.975175	-2.284090	-6.723221
C	1.361496	0.606577	-0.140123	H	2.857405	-1.639150	-2.472639
C	0.740032	-0.350707	3.936749	H	3.297865	0.050873	0.293310
C	3.309136	-0.607483	2.720279	Zn^{2+}	4.462969	3.024527	-3.948143
C	3.110908	-0.933265	4.085094				
C	1.805057	-0.792331	4.667963				
C	4.246354	-1.388388	4.796516				
H	4.157583	-1.654001	5.846068				
C	5.455055	-1.487968	4.137653				
C	5.531118	-1.133191	2.770721				
N	4.491782	-0.702560	2.070999				
H	-0.240626	-0.250204	4.390807				
H	-0.723405	1.104932	-0.253868				
H	-1.147422	0.559734	2.140056				
H	1.655926	0.810114	-1.167762				
H	1.676201	-1.047486	5.715810				
H	6.345470	-1.833867	4.652043				
H	6.477380	-1.207441	2.240448				
C	6.469994	3.259897	-7.754522				
C	6.395403	1.912304	-8.059810				
C	5.777086	1.006125	-7.165984				
C	5.245734	1.535493	-5.961770				
N	5.335138	2.879578	-5.685135				
C	5.924765	3.713355	-6.547691				
C	5.668620	-0.395400	-7.425546				
C	4.601291	0.660995	-5.012108				
C	4.511887	-0.712025	-5.302234				
C	5.058265	-1.219808	-6.524814				
C	3.864297	-1.540911	-4.343226				
H	3.780109	-2.606769	-4.543653				
C	3.354979	-0.994817	-3.191534				
C	3.452395	0.407739	-2.899287				
N	4.064262	1.144801	-3.817274				

Table D.5. (continued) Cartesian Coordinates of the B3LYP/6-31G* Optimized Geometries of the Transition States, Ints, and Products Involved in the Dissociation of $M^{2+}(Phen)_2$ Complexes through PTCF Process.[a]

$Zn^{2+}(Phen)_2$ Int_4				$Zn^{2+}(Phen)_2$ Int_4			
	x	y	z		x	y	z
C	-6.246844	3.393764	0.146881	H	10.015503	-0.438923	3.345648
C	-7.540923	3.140322	0.552033	H	5.243014	-0.702967	2.503490
C	-8.078463	1.814133	0.527308	H	7.479688	-0.676085	3.611103
C	-7.215133	0.813972	0.068901	H	5.094480	-0.374037	0.030351
N	-5.945203	1.144870	-0.316047	H	11.963758	-0.080009	1.882469
C	-5.378537	2.342675	-0.326075	H	12.421100	0.628308	-2.909509
C	-9.399337	1.429696	0.929281	H	10.029995	0.553780	-3.718344
C	-7.604387	-0.557027	-0.008436	Zn^{2+}	-4.959365	-0.387410	-1.010842
C	-8.914937	-0.909970	0.401675				
C	-9.797542	0.120593	0.869168				
C	-9.263863	-2.276861	0.320907				
H	-10.257158	-2.596594	0.623739				
C	-8.341277	-3.199661	-0.141207				
C	-7.066274	-2.764212	-0.533003				
N	-6.696438	-1.481293	-0.475888				
H	-10.083992	2.193363	1.286462				
H	-5.866345	4.410340	0.177329				
H	-8.176638	3.952740	0.897056				
H	8.317636	0.191110	-2.107269				
H	-10.799192	-0.161377	1.178829				
H	-8.586158	-4.253721	-0.208936				
H	-6.330187	-3.470539	-0.903946				
C	6.148037	-0.549207	1.925547				
C	7.385176	-0.534460	2.538246				
C	8.541512	-0.331742	1.749244				
C	8.331618	-0.153863	0.359448				
N	7.121961	-0.167985	-0.243731				
C	6.062371	-0.362183	0.527827				
C	9.877806	-0.300012	2.277270				
C	9.481676	0.054781	-0.471989				
C	10.793340	0.084038	0.056409				
C	10.960240	-0.101304	1.469716				
C	11.855490	0.294920	-0.850387				
H	12.875186	0.322897	-0.476571				
C	11.611288	0.466152	-2.207970				
C	10.298798	0.428576	-2.676102				
N	9.297003	0.228019	-1.809304				

$[Zn(Phen-H)]^+$			
	x	y	z
C	-0.042425	0.000000	-0.019729
C	-0.016618	0.000000	1.353178
C	1.227563	0.000000	2.049433
C	2.409186	0.000000	1.285464
N	2.309817	0.000000	-0.103773
C	1.183781	0.000000	-0.750142
C	1.315255	0.000000	3.479197
C	3.682439	0.000000	1.952377
C	3.739200	0.000000	3.370408
C	2.521671	0.000000	4.118989
C	5.021521	0.000000	3.967092
H	5.102923	0.000000	5.050502
C	6.158492	0.000000	3.179976
C	6.018215	0.000000	1.785112
N	4.823262	0.000000	1.194536
H	0.391953	0.000000	4.050589
H	-0.983123	0.000000	-0.560223
H	-0.939096	0.000000	1.930035
H	2.574369	0.000000	5.203245
H	7.150010	0.000000	3.618438
H	6.885501	0.000000	1.131724
Zn^{2+}	4.186937	0.000000	-0.702374

[a]Standard Orientation, Å.

Table D.6. Relative Stabilities (in kJ/mol) of the Transition States, Intermediates, and Products Involved in the Activated Dissociation of $M^{2+}(Phen)_2$ Reactant Complexes via ETCF at 0 K.

		B3LYP[a]	BHandHLYP[b]	M06[c]
Complex	Species	D_0[d]	D_0[d]	D_0[d]
$Fe^{2+}(Phen)_2$	Reactant	0.0	0.0	0.0
	TS	373.5	387.5	364.1
	Int	354.7	376.7	341.3
	$Fe^{+}(Phen)$ + $Phen^{+}$ products	343.8	366.3	333.5
$Co^{2+}(Phen)_2$	Reactant	0.0	0.0	0.0
	TS	292.7	354.1	288.2
	Int	274.0	341.3	263.9
	$Co^{+}(Phen)$ + $Phen^{+}$ products	252.1	321.8	249.5
$Ni^{2+}(Phen)_2$	Reactant	0.0	0.0	0.0
	TS	267.9	286.9	239.1
	Int	249.2	275.4	214.9
	$Ni^{+}(Phen)$ + $Phen^{+}$ products	205.6	234.3	186.1
$Cu^{2+}(Phen)_2$	Reactant	0.0	0.0	0.0
	TS	252.0	277.2	237.2
	Int	232.3	265.9	213.2
	$Cu^{+}(Phen)$ + $Phen^{+}$ products	155.7	184.7	145.4
$Zn^{2+}(Phen)_2$	Reactant	0.0	0.0	0.0
	TS	331.5	349.0	325.4
	Int	313.2	336.2	302.0
	$Zn^{+}(Phen)$ + $Phen^{+}$ products	296.5	321.2	290.3

[a] Calculated at the B3LYP/6-311+G(2d,2p)//B3LYP/6-31G* level of theory. [b] Calculated at the BHandHLYP/6-311+G(2d,2p)//B3LYP/6-31G* level of theory. [c] Calculated at the M06/6-311+G(2d,2p)//B3LYP/6-31G* level of theory. [d] Including ZPE corrections scaled by 0.9804.

Table D.7. Relative Stabilities (in kJ/mol) of the Transition States, Intermediates, and Products Involved in the Activated Dissociation of $M^{2+}(Phen)_2$ Reactant Complexes via PTCF at 0 K.

		B3LYP[a]	BHandHLYP[b]	M06[c]
Complex	Species	D_0[d]	D_0[d]	D_0[d]
$Fe^{2+}(Phen)_2$	Reactant	0.0	0.0	0.0
	TS_1	414.4	467.1	406.3
	Int_1	388.7	451.7	380.8
	TS_2	471.8	518.3	446.3
	Int_2	409.1	452.5	403.4
	TS_3	445.3	482.6	415.1
	Int_3	393.9	408.0	390.7
	$[Fe(Phen-H)]^+ + [Phen+H]^+$ products	364.9	367.0	319.5
$Co^{2+}(Phen)_2$	Reactant	0.0	0.0	0.0
	TS_1	446.4	464.6	432.8
	Int_1	367.6	375.4	356.2
	TS_2	439.0	454.1	424.5
	Int_2	380.4	402.3	368.0
	TS_3	432.6	448.6	414.7
	Int_3	362.1	384.1	336.6
	TS_4	419.4	441.5	415.4
	Int_4	355.4	400.4	354.4
	$[Co(Phen-H)]^+ + [Phen+H]^+$ products	268.1	339.2	259.9
$Ni^{2+}(Phen)_2$	Reactant	0.0	0.0	0.0
	TS_1	417.6	457.1	409.7
	Int_1	359.2	439.1	343.9
	TS_2	400.4	454.6	379.6
	Int_2	294.1	370.3	270.1
	TS_3	352.7	412.2	351.4
	Int_3	290.5	348.6	290.2
	$[Ni(Phen-H)]^+ + [Phen+H]^+$ products	199.2	268.9	195.0

Table D.7. (continued) Relative Stabilities (in kJ/mol) of the Transition States, Intermediates, and Products Involved in the Activated Dissociation of $M^{2+}(Phen)_2$ Reactant Complexes via PTCF at 0 K.

		B3LYP[a]	BHandHLYP[b]	M06[c]
Complex	Species	D_0[d]	D_0[d]	D_0[d]
$Cu^{2+}(Phen)_2$	Reactant	0.0	0.0	0.0
	TS_1	452.8	516.8	452.6
	Int_1	387.5	446.6	381.6
	TS_2	400.4	462.5	398.4
	Int_2	221.7	276.7	211.0
	TS_3	311.3	353.1	306.5
	Int_3	215.3	253.7	204.2
	$[Cu(Phen-H)]^+ + [Phen+H]^+$ products	125.2	130.2	122.4
$Zn^{2+}(Phen)_2$	Reactant	0.0	0.0	0.0
	TS_1	444.5	459.4	431.5
	Int_1	366.2	374.2	356.1
	TS_2	430.9	450.4	421.5
	Int_2	381.1	394.7	377.2
	TS_3	460.7	481.1	457.7
	Int_3	359.1	368.4	350.1
	TS_4	384.0	415.2	377.9
	Int_4	375.9	390.2	370.8
	$[Zn(Phen-H)]^+ + [Phen+H]^+$ products	361.3	377.7	346.4

[a] Calculated at the B3LYP/6-311+G(2d,2p)//B3LYP/6-31G* level of theory. [b] Calculated at the BHandHLYP/6-311+G(2d,2p)//B3LYP/6-31G* level of theory. [c] Calculated at the M06/6-311+G(2d,2p)//B3LYP/6-31G* level of theory. [d] Including ZPE corrections scaled by 0.9804.

Table D.8. Fitting Parameters of eq 2.4, Threshold Dissociation Energies at 0 K, and Entropies of Activation at 1000 K of $M^{2+}(Phen)_2$ Complexes Obtained from Independent Analyses of the Simple CID and Primary Activated Dissociation Cross Sections for ETCF Process[a]

Complex	Product	$E_{0,j}$(TS)[c] (eV)	$E_{0,j}$(PSL)[b] (eV)	$E_{0,j}$(TTS)[b] (eV)	Kinetic Shift (eV)
$Fe^{2+}(Phen)_2$	$Fe^{+}(Phen)$	10.80 (0.43)	–	2.79 (0.09)	8.01
	$Fe^{2+}(Phen)$	8.30 (0.11)	3.47 (0.15)	–	4.83
$Co^{2+}(Phen)_2$	$Co^{+}(Phen)$	10.46 (0.25)	–	2.62 (0.11)	7.84
	$Co^{2+}(Phen)$	8.71 (0.18)	3.63 (0.16)	–	5.08
$Ni^{2+}(Phen)_2$	$Ni^{+}(Phen)$	9.71 (0.08)	–	2.43 (0.11)	7.28
	$Ni^{2+}(Phen)$	9.59 (0.79)	3.90 (0.19)	–	5.69
$Cu^{2+}(Phen)_2$	$Cu^{+}(Phen)$	8.02 (0.07)	–	2.34 (0.10)	5.68
	$Cu^{2+}(Phen)$	9.30 (0.12)	3.91 (0.16)	–	5.39
$Zn^{2+}(Phen)_2$	$Zn^{+}(Phen)$	9.94 (0.20)	–	2.63 (0.11)	7.31
	$Zn^{2+}(Phen)$	8.17 (0.38)	3.43 (0.18)	–	4.74

[a]Uncertainties are listed in parentheses. [b]Average values for PSL or TTSs including RRKM analysis. [c]No RRKM analysis.

Table D.8. (continued) Fitting Parameters of eq 2.4, Threshold Dissociation Energies at 0 K, and Entropies of Activation at 1000 K of $M^{2+}(Phen)_2$ Complexes Obtained from Independent Analyses of the Simple CID and Primary Activated Dissociation Cross Sections for ETCF Process[a]

Complex	Product	$\sigma_{0,j}{}^{b}$	n^{b}	$\Delta S^{\ddagger}(TS)^{b}$ (J mol^{-1} K^{-1})
$Fe^{2+}(Phen)_2$	$Fe^{+}(Phen)$	0.4 (0.1)	1.7 (0.1)	−6.9 (0.4)
	$Fe^{2+}(Phen)$	0.1 (0.1)	1.9 (0.1)	94.7 (4.3)
$Co^{2+}(Phen)_2$	$Co^{+}(Phen)$	0.4 (0.1)	1.7 (0.1)	−4.8 (0.6)
	$Co^{2+}(Phen)$	0.1 (0.1)	1.6 (0.1)	97.1 (4.3)
$Ni^{2+}(Phen)_2$	$Ni^{+}(Phen)$	0.8 (0.1)	1.5 (0.1)	−11.6 (0.6)
	$Ni^{2+}(Phen)$	0.1 (0.1)	1.5 (0.1)	97.1 (4.3)
$Cu^{2+}(Phen)_2$	$Cu^{+}(Phen)$	1.3 (0.1)	1.4 (0.1)	9.3 (0.6)
	$Cu^{2+}(Phen)$	0.1 (0.1)	1.3 (0.1)	122.2 (4.2)
$Zn^{2+}(Phen)_2$	$Zn^{+}(Phen)$	0.6 (0.1)	1.6 (0.1)	−3.1 (0.6)
	$Zn^{2+}(Phen)$	0.1 (0.1)	1.8 (0.1)	101.3 (4.2)

[a]Uncertainties are listed in parentheses. [b]Average values for PSL or TTSs including RRKM analysis. [c]No RRKM analysis.

Table D.9. Fitting Parameters of eq 2.5, Threshold Dissociation Energies at 0 K, and Entropies of Activation at 1000 K of $M^{2+}(Phen)_2$ Complexes Obtained from Competitive Analyses of the Simple CID and Activated Dissociation Product Cross Sections for ETCF Process[a]

Complex	Product	$E_{0,j}$(PSL)[c] (eV)	$E_{0,j}$(TTS)[b] (eV)	Competitive Shift (eV)
$Fe^{2+}(Phen)_2$	$Fe^{+}(Phen)$	–	2.77 (0.08)	–0.02
	$Fe^{2+}(Phen)$	2.55 (0.54)	–	–0.92
$Co^{2+}(Phen)_2$	$Co^{+}(Phen)$	–	2.68 (0.09)	0.06
	$Co^{2+}(Phen)$	2.64 (0.62)	–	–0.99
$Ni^{2+}(Phen)_2$	$Ni^{+}(Phen)$	–	2.46 (0.09)	0.03
	$Ni^{2+}(Phen)$	2.84 (0.55)	–	–1.06
$Cu^{2+}(Phen)_2$	$Cu^{+}(Phen)$	–	2.37 (0.10)	0.03
	$Cu^{2+}(Phen)$	3.65 (0.51)	–	–0.26
$Zn^{2+}(Phen)_2$	$Zn^{+}(Phen)$	–	2.64 (0.10)	0.01
	$Zn^{2+}(Phen)$	2.27 (0.51)	–	–1.16

[a]Uncertainties are listed in parentheses. [b]Average values for PSL or TTSs including RRKM analysis. [c]No RRKM analysis.

Table D.9. (continued) Fitting Parameters of eq 2.5, Threshold Dissociation Energies at 0 K, and Entropies of Activation at 1000 K of $M^{2+}(Phen)_2$ Complexes Obtained from Competitive Analyses of the Simple CID and Activated Dissociation Product Cross Sections for ETCF Process[a]

Complex	Product	$\sigma_{0,j}{}^{b}$	n^{b}	$\Delta S^{\ddagger}(TS)^{b}$ (J mol^{-1} K^{-1})
$Fe^{2+}(Phen)_2$	$Fe^{+}(Phen)$	0.4 (0.1)	1.6 (0.1)	−6.9 (0.7)
	$Fe^{2+}(Phen)$	0.4 (0.1)	1.6 (0.1)	−58.9 (43.0)
$Co^{2+}(Phen)_2$	$Co^{+}(Phen)$	0.2 (0.1)	1.4 (0.1)	−4.8 (0.5)
	$Co^{2+}(Phen)$	0.7 (0.2)	1.5 (0.2)	−56.5 (43.0)
$Ni^{2+}(Phen)_2$	$Ni^{+}(Phen)$	1.0 (0.1)	1.4 (0.1)	−11.6 (0.4)
	$Ni^{2+}(Phen)$	1.0 (0.1)	1.4 (0.1)	−56.6 (42.2)
$Cu^{2+}(Phen)_2$	$Cu^{+}(Phen)$	1.3 (0.1)	1.5 (0.1)	9.3 (0.6)
	$Cu^{2+}(Phen)$	1.3 (0.1)	1.5 (0.1)	45.1 (23.3)
$Zn^{2+}(Phen)_2$	$Zn^{+}(Phen)$	0.6 (0.1)	1.7 (0.1)	−3.1 (0.6)
	$Zn^{2+}(Phen)$	0.6 (0.1)	1.7 (0.1)	−97.2 (42.9)

[a] Uncertainties are listed in parentheses. [b] Average values for PSL or TTSs including RRKM analysis. [c] No RRKM analysis.

Table D.10a. Measured and Calculated Reaction Energies of $M^{2+}(Phen)_2$ Complexes at 0 K in kJ/mol

			B3LYP Theory	
Complex	Product	TCID[a]	E_0[b]	$E_{0,BSSE}$[c]
$Fe^{2+}(Phen)_2$	$Fe^+(Phen)$	267.3 (7.7)	373.5	
	$Fe^{2+}(Phen)$	245.7 (52.1)	515.6	511.8
$Co^{2+}(Phen)_2$	$Co^+(Phen)$	258.1 (9.1)	292.7	
	$Co^{2+}(Phen)$	254.3 (59.5)	549.8	545.2
$Ni^{2+}(Phen)_2$	$Ni^+(Phen)$	237.5 (8.4)	267.9	
	$Ni^{2+}(Phen)$	274.1 (53.3)	542.1	537.5
$Cu^{2+}(Phen)_2$	$Cu^+(Phen)$	228.6 (9.5)	252.0	
	$Cu^{2+}(Phen)$	352.4 (49.4)	518.9	514.0
$Zn^{2+}(Phen)_2$	$Zn^+(Phen)$	254.5 (9.5)	331.5	
	$Zn^{2+}(Phen)$	218.8 (49.1)	544.7	540.4
AEU/MAD	ETCF	8.8 (0.8)		54.3 (35.8)
	Simple CID	52.7 (4.2)		260.7 (60.2)

[a]Values obtained from Competitive Analyses of the Simple CID and Activated Dissociation Product Cross Sections for ETCF Process. [b]Calculated at the B3LYP/6-311+G(2d,2p)//B3LYP/6-31G* level of theory including ZPE corrections scaled by 0.9804. [c]Also includes BSSE corrections.

Table D.10b. Measured and Calculated Reaction Energies of $M^{2+}(Phen)_2$ Complexes at 0 K in kJ/mol

			BHandHLYP Theory	
Complex	Product	TCID[a]	E_0[b]	$E_{0,BSSE}$[c]
$Fe^{2+}(Phen)_2$	$Fe^+(Phen)$	267.3 (7.7)	387.5	
	$Fe^{2+}(Phen)$	245.7 (52.1)	523.7	519.7
$Co^{2+}(Phen)_2$	$Co^+(Phen)$	258.1 (9.1)	354.1	
	$Co^{2+}(Phen)$	254.3 (59.5)	557.5	553.1
$Ni^{2+}(Phen)_2$	$Ni^+(Phen)$	237.5 (8.4)	286.9	
	$Ni^{2+}(Phen)$	274.1 (53.3)	512.7	508.1
$Cu^{2+}(Phen)_2$	$Cu^+(Phen)$	228.6 (9.5)	277.2	
	$Cu^{2+}(Phen)$	352.4 (49.4)	545.4	540.0
$Zn^{2+}(Phen)_2$	$Zn^+(Phen)$	254.5 (9.5)	349.0	
	$Zn^{2+}(Phen)$	218.8 (49.1)	556.2	551.9
AEU/MAD	ETCF	8.8 (0.8)		81.7 (31.6)
	Simple CID	52.7 (4.2)		265.5 (56.6)

[a]Values obtained from Competitive Analyses of the Simple CID and Activated Dissociation Product Cross Sections for ETCF Process. [b]Calculated at the BHandHLYP/6-311+G(2d,2p)//BHandHLYP/6-31G* level of theory including ZPE corrections scaled by 0.9804. [c]Also includes BSSE corrections.

Table D.10c. Measured and Calculated Reaction Energies of $M^{2+}(Phen)_2$ Complexes at 0 K in kJ/mol

			M06 Theory	
Complex	Product	TCID[a]	E_0[b]	$E_{0,BSSE}$[c]
$Fe^{2+}(Phen)_2$	$Fe^+(Phen)$	267.3 (7.7)	364.1	
	$Fe^{2+}(Phen)$	245.7 (52.1)	575.4	570.5
$Co^{2+}(Phen)_2$	$Co^+(Phen)$	258.1 (9.1)	288.2	
	$Co^{2+}(Phen)$	254.3 (59.5)	574.2	568.2
$Ni^{2+}(Phen)_2$	$Ni^+(Phen)$	237.5 (8.4)	239.1	
	$Ni^{2+}(Phen)$	274.1 (53.3)	538.3	533.1
$Cu^{2+}(Phen)_2$	$Cu^+(Phen)$	228.6 (9.5)	237.2	
	$Cu^{2+}(Phen)$	352.4 (49.4)	545.5	539.8
$Zn^{2+}(Phen)_2$	$Zn^+(Phen)$	254.5 (9.5)	325.4	
	$Zn^{2+}(Phen)$	218.8 (49.1)	560.7	555.6
AEU/MAD	ETCF	8.8 (0.8)		41.6 (41.0)
	Simple CID	52.7 (4.2)		284 (61.9)

[a]Values obtained from Competitive Analyses of the Simple CID and Activated Dissociation Product Cross Sections for ETCF Process. [b]Calculated at the M06/6-311+G(2d,2p)//M06/6-31G* level of theory including ZPE corrections scaled by 0.9804. [c]Also includes BSSE corrections.

Table D.11. Reaction Enthalpies and Free Energies of $M^{2+}(Phen)_2$ Complexes at 0 and 298 K in kJ/mol[a]

Complex	Product	ΔH_0	ΔH_0[b]	ΔH_{298}[b]	ΔG_{298}[b]
$Fe^{2+}(Phen)_2$	$Fe^{+}(Phen)$	267.3 (7.7)	373.5	375.5	373.2
	$Fe^{2+}(Phen)$	245.7 (52.1)	511.8	510.5	458.9
$Co^{2+}(Phen)_2$	$Co^{+}(Phen)$	258.1 (9.1)	292.7	295.0	293.0
	$Co^{2+}(Phen)$	254.3 (59.5)	545.2	545.0	490.3
$Ni^{2+}(Phen)_2$	$Ni^{+}(Phen)$	237.5 (8.4)	267.9	269.8	266.1
	$Ni^{2+}(Phen)$	274.1 (53.3)	537.5	537.1	483.4
$Cu^{2+}(Phen)_2$	$Cu^{+}(Phen)$	228.6 (9.5)	252.0	254.7	253.4
	$Cu^{2+}(Phen)$	352.4 (49.4)	514.0	514.5	457.6
$Zn^{2+}(Phen)_2$	$Zn^{+}(Phen)$	254.5 (9.5)	331.5	333.4	332.4
	$Zn^{2+}(Phen)$	218.8 (49.1)	540.4	539.4	486.5

[a] Uncertainties are listed in parentheses. Values obtained from competitive analyses of the simple CID and activated dissociation product cross sections for ETCF process. [b] Values from calculations at the B3LYP/6-311+G(2d,2p) level of theory using B3LYP/6-31G* optimized geometries with frequencies scaled by 0.9804.

Table D.11. (continued) Reaction Enthalpies and Free Energies of $M^{2+}(Phen)_2$ Complexes at 298 K in kJ/mol[a]

Complex	Product	ΔH_{298}-ΔH_0[b]	ΔH_{298}	$T\Delta S_{298}$[b]	ΔG_{298}
$Fe^{2+}(Phen)_2$	$Fe^{+}(Phen)$	2.0 (0.1)	269.3 (7.7)	2.3 (0.1)	267.0 (7.7)
	$Fe^{2+}(Phen)$	−1.3 (0.9)	244.4 (52.1)	51.6 (1.6)	192.8 (52.1)
$Co^{2+}(Phen)_2$	$Co^{+}(Phen)$	2.3 (0.1)	260.4 (9.1)	2.0 (0.1)	258.4 (9.1)
	$Co^{2+}(Phen)$	−0.2 (0.9)	254.1 (59.5)	54.7 (1.5)	199.4 (59.5)
$Ni^{2+}(Phen)_2$	$Ni^{+}(Phen)$	1.9 (0.1)	239.4 (8.4)	3.7 (0.1)	235.7 (8.4)
	$Ni^{2+}(Phen)$	−0.4 (0.9)	273.7 (53.3)	53.7 (1.5)	220.0 (53.3)
$Cu^{2+}(Phen)_2$	$Cu^{+}(Phen)$	2.7 (0.1)	231.3 (9.5)	1.3 (0.1)	230.0 (9.5)
	$Cu^{2+}(Phen)$	0.5 (0.8)	352.9 (49.4)	56.9 (1.4)	296.0 (49.4)
$Zn^{2+}(Phen)_2$	$Zn^{+}(Phen)$	1.9 (0.1)	256.4 (9.5)	1.0 (0.1)	255.4 (9.5)
	$Zn^{2+}(Phen)$	−1.0 (0.9)	217.8 (49.1)	52.9 (1.6)	164.9 (49.1)

[a] Uncertainties are listed in parentheses. Values obtained from competitive analyses of the simple CID and activated dissociation product cross sections for ETCF process. [b] Values from calculations at the B3LYP/6-311+G(2d,2p) level of theory using B3LYP/6-31G* optimized geometries with frequencies scaled by 0.9804.

D.12 Figure Captions and Figures

Figure D.1. Cross sections for collision-induced dissociation of the $M^{2+}(Phen)_2$ complexes with Xe as a function of kinetic energy in the center-of-mass frame (lower *x*-axis) and laboratory frame (upper *x*-axis), where M^{2+} = Fe^{2+}, Co^{2+}, Ni^{2+}, Cu^{2+}, and Zn^{2+}, parts a–e, respectively. Data are shown for a Xe pressure of ~0.2 mTorr. Product cross sections for $M^{+}(Phen)$ (red) and $M^{2+}(Phen)$ (green).

Figure D.2. MS spectra of fragmentation of $M^{2+}(Phen)_2$ complexes, where M^{2+} = Fe^{2+}, Co^{2+}, Ni^{2+}, Cu^{2+}, and Zn^{2+}, parts a–e, respectively.

Figure D.3. Potential energy landscape at 0 K for ETCF of the $M^{2+}(Phen)_2$ complexes leading to the transfer of an electron from the Phen ligand to the $M^{2+}(Phen)$ moiety and dissociation, where M^{2+} = Fe^{2+}, Co^{2+}, Ni^{2+}, Cu^{2+}, and Zn^{2+}, parts a–e, respectively. Also shown is the energy barrier for simple CID pathway. Energies are relative to the $M^{2+}(Phen)_2$ reactants, and are taken from theoretical calculations at the B3LYP/6-311+G(2d,2p) (red), BHandHLYP/6-311+G(2d,2p) (blue), and M06/6-311+G(2d,2p) (green) levels of theory using the B3LYP/6-31G* optimized geometries and including ZPE corrections.

Figure D.4. Potential energy landscape at 0 K for PTCF of the $M^{2+}(Phen)_2$ complexes leading to the transfer of a proton from one Phen ligand to the other Phen ligand of the $M^{2+}(Phen)_2$ reactant, where $M^{2+} = Fe^{2+}$, Co^{2+}, Ni^{2+}, Cu^{2+}, and Zn^{2+}, parts a–e, respectively. Energies are relative to the $M^{2+}(Phen)_2$ reactants, and are taken from theoretical calculations at the B3LYP/6-311+G(2d,2p) (red), BHandHLYP/6-311+G(2d,2p) (blue), and M06/6-311+G(2d,2p) (green) levels of theory using the B3LYP/6-31G* optimized geometries and including ZPE corrections.

Figure D.5. Zero-pressure-extrapolated cross sections for collision-induced dissociation of the $M^{2+}(Phen)_2$ complexes, where $M^{2+} = Fe^{2+}$, Co^{2+}, Ni^{2+}, Cu^{2+}, and Zn^{2+} with Xe in the threshold region as a function of kinetic energy in the center-of-mass frame (lower *x*-axis) and laboratory frame (upper *x*-axis). Parts a, c, e, g, and i, show fits for $M^{2+}(Phen)$ product cross sections whereas parts b, d, f, h, and j show fits for $M^{+}(Phen)$ product cross section. Solid lines show the best fits to the data using eq. 2.4 convoluted over the neutral and ion kinetic and internal energy distributions. The dotted lines show the model cross sections in the absence of experimental kinetic energy broadening for reactants with an internal energy corresponding to 0 K.

Figure D.6. Zero-pressure-extrapolated M^+(Phen) and M^{2+}(Phen) product cross sections for collision-induced dissociation of the $M^{2+}(Phen)_2$ complexes, where $M^{2+} = Fe^{2+}$, Co^{2+}, Ni^{2+}, Cu^{2+}, and Zn^{2+}, parts a–e, respectively, with Xe in the threshold region as a function of kinetic energy in the center-of-mass frame (lower *x*-axis) and laboratory frame (upper *x*-axis). Solid lines show the best fits to the data using eq. 2.5 convoluted over the neutral and ion kinetic and internal energy distributions. The dotted lines show the model cross sections in the absence of experimental kinetic energy broadening for reactants with an internal energy corresponding to 0 K.

Figure D.7. Comparison of theoretical and TCID measured ETCF AEs (part a) and (Phen)M^{2+}–Phen BDEs (part b) of the $M^{2+}(Phen)_2$ complexes, where $M^{2+} = Fe^{2+}$, Co^{2+}, Ni^{2+}, Cu^{2+}, and Zn^{2+}, at 0 K in kJ/mol. Values obtained from competitive analyses of the M^+(Phen) and M^{2+}(Phen) product cross sections.

Figure D.1.

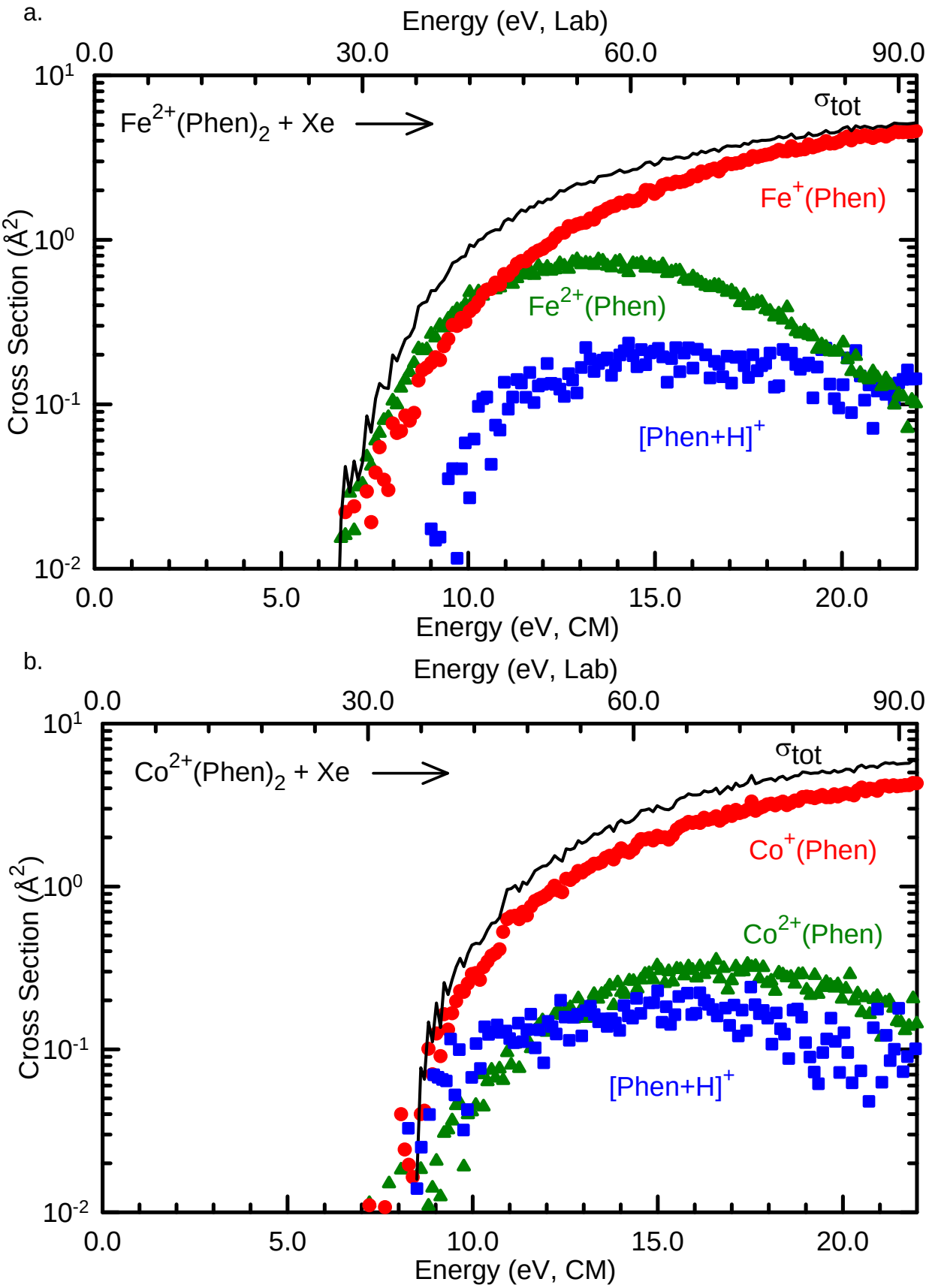
a.
Energy (eV, Lab)
0.0
30.0
60.0
90.0
10^1
10^0
10^{-1}
10^{-2}
Cross Section (Å^2)
$Fe^{2+}(Phen)_2 + Xe$
σ_{tot}
$Fe^+(Phen)$
$Fe^{2+}(Phen)$
$[Phen+H]^+$
0.0
5.0
10.0
15.0
20.0
Energy (eV, CM)
b.
Energy (eV, Lab)
0.0
30.0
60.0
90.0
10^1
10^0
10^{-1}
10^{-2}
Cross Section (Å^2)
$Co^{2+}(Phen)_2 + Xe$
σ_{tot}
$Co^+(Phen)$
$Co^{2+}(Phen)$
$[Phen+H]^+$
0.0
5.0
10.0
15.0
20.0
Energy (eV, CM)

Figure D.1.

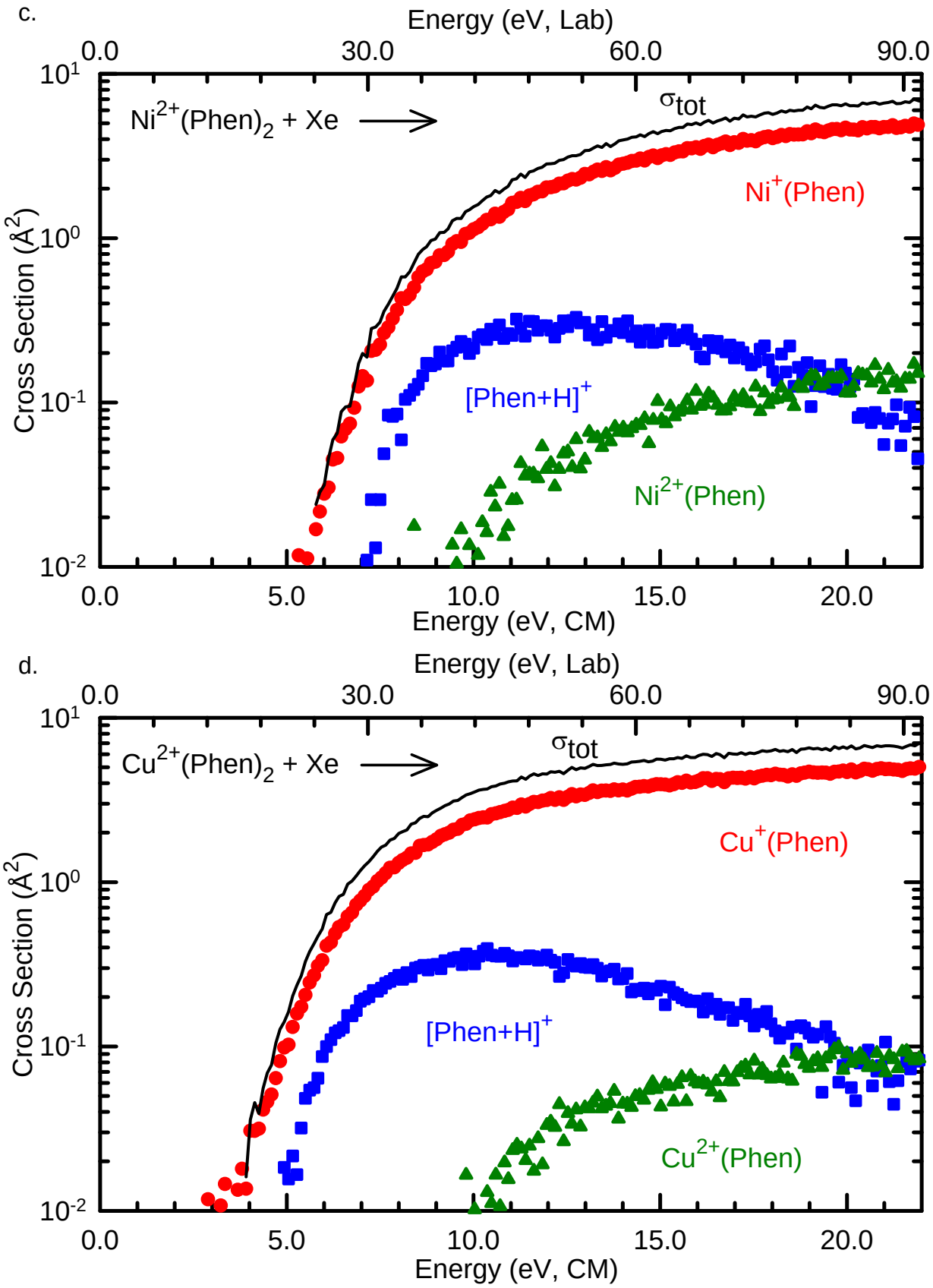
c.
Energy (eV, Lab)
0.0
30.0
60.0
90.0
10^1
10^0
10^{-1}
10^{-2}
Cross Section (Å^2)
$Ni^{2+}(Phen)_2$ + Xe
σ_{tot}
$Ni^+(Phen)$
$[Phen+H]^+$
$Ni^{2+}(Phen)$
0.0
5.0
10.0
15.0
20.0
Energy (eV, CM)
d.
Energy (eV, Lab)
0.0
30.0
60.0
90.0
10^1
10^0
10^{-1}
10^{-2}
Cross Section (Å^2)
$Cu^{2+}(Phen)_2$ + Xe
σ_{tot}
$Cu^+(Phen)$
$[Phen+H]^+$
$Cu^{2+}(Phen)$
0.0
5.0
10.0
15.0
20.0
Energy (eV, CM)

Figure D.1.

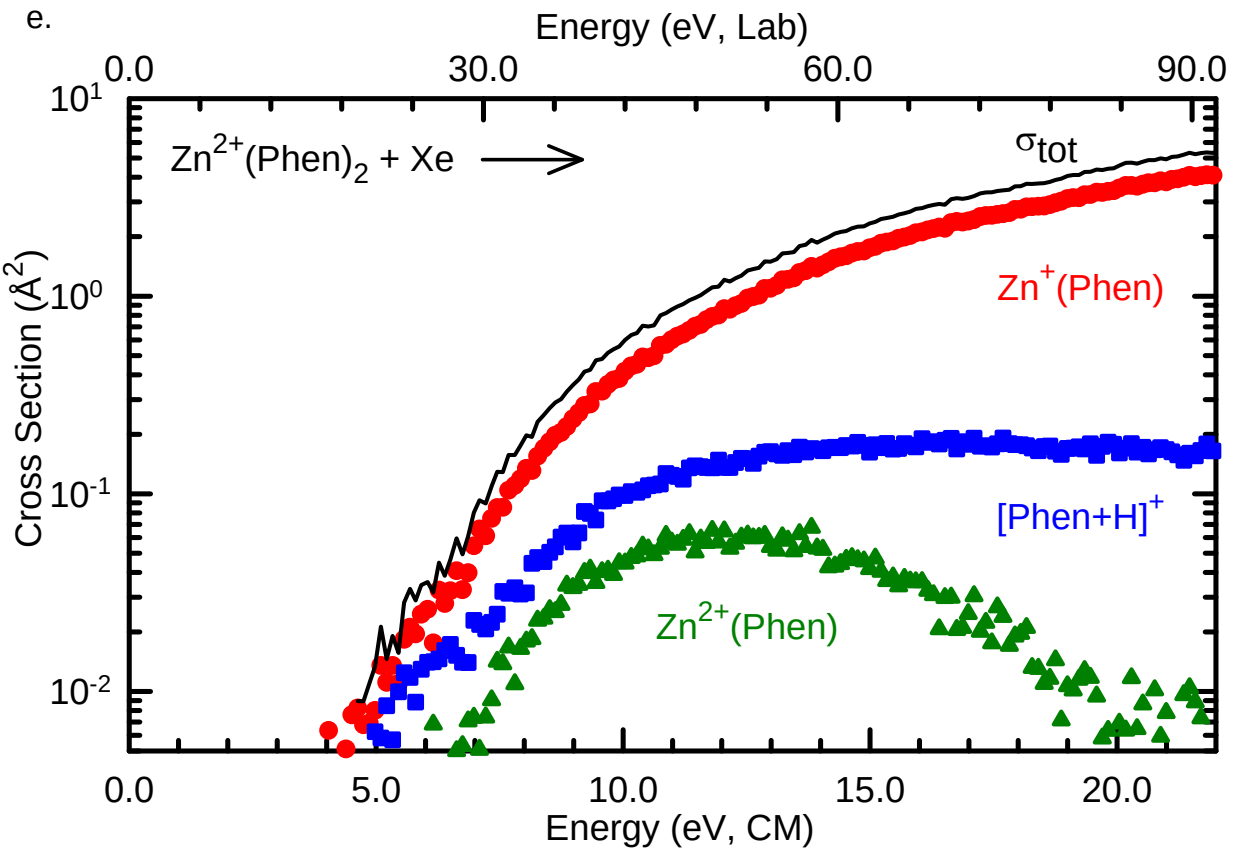
e.
Energy (eV, Lab)
0.0
30.0
60.0
90.0
10^1
10^0
10^{-1}
10^{-2}
Cross Section (Å^2)
$Zn^{2+}(Phen)_2$ + Xe
σ_{tot}
$Zn^+(Phen)$
$[Phen+H]^+$
$Zn^{2+}(Phen)$
0.0
5.0
10.0
15.0
20.0
Energy (eV, CM)

Figure D.2.

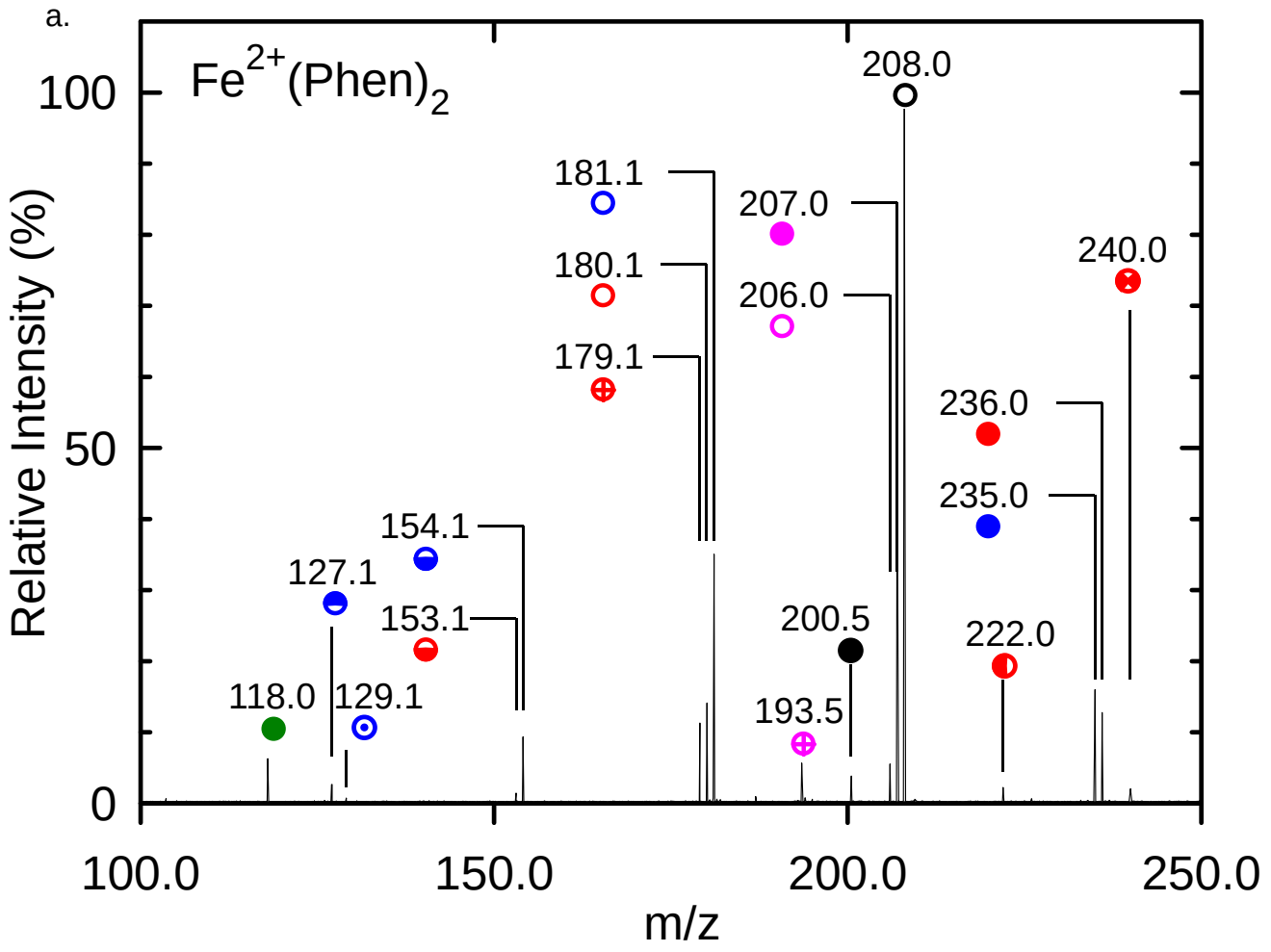
a.
Fe2+(Phen)2
Relative Intensity (%)
100
50
0
100.0
150.0
200.0
250.0
m/z
208.0
181.1
207.0
240.0
180.1
206.0
179.1
236.0
235.0
154.1
127.1
153.1
200.5
222.0
118.0
129.1
193.5

Figure D.2.

a.

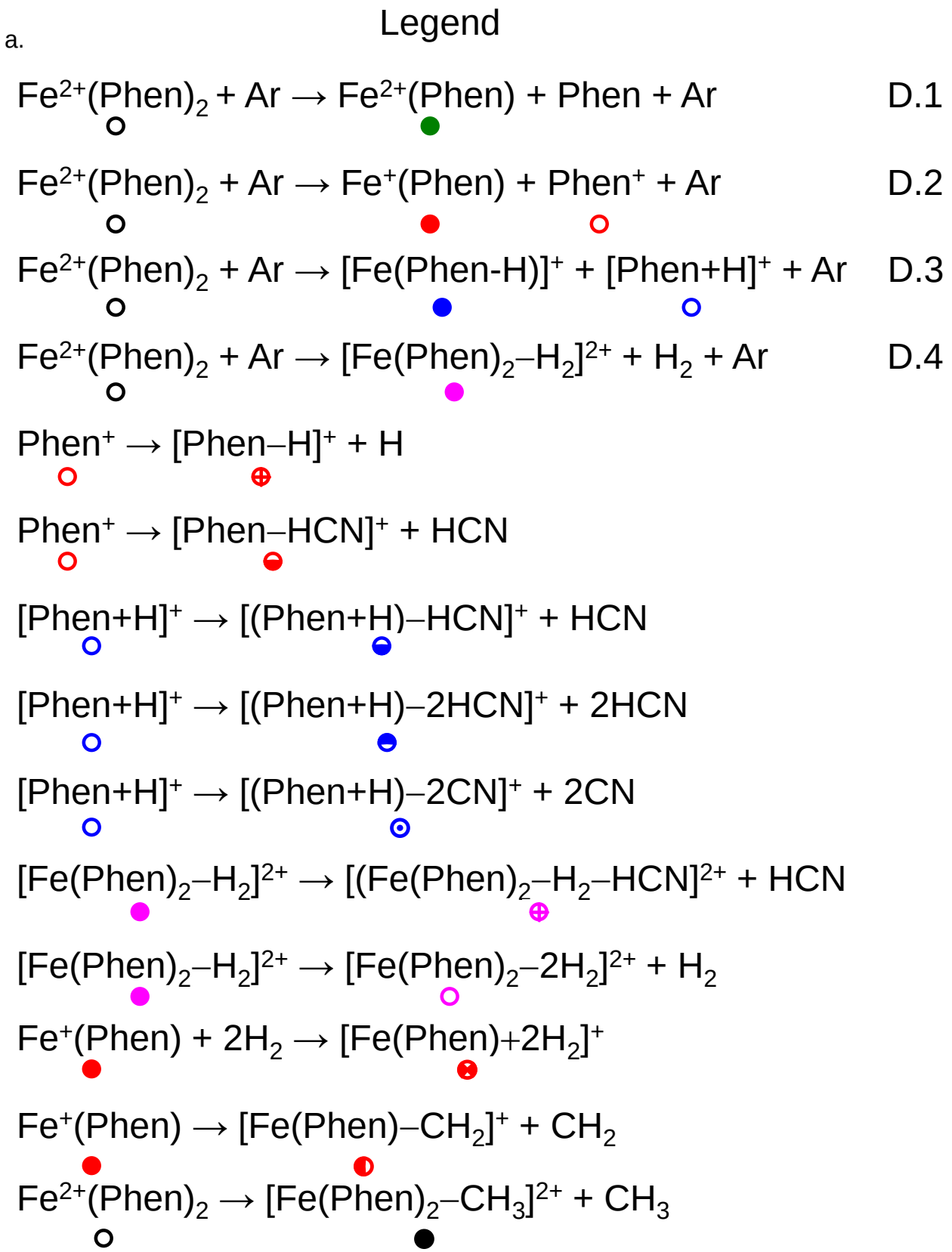
Legend
Fe2+(Phen)2 + Ar → Fe2+(Phen) + Phen + Ar D.1
Fe2+(Phen)2 + Ar → Fe+(Phen) + Phen+ + Ar D.2
Fe2+(Phen)2 + Ar → [Fe(Phen-H)]+ + [Phen+H]+ + Ar D.3
Fe2+(Phen)2 + Ar → [Fe(Phen)2–H2]2+ + H2 + Ar D.4
Phen+ → [Phen–H]+ + H
Phen+ → [Phen–HCN]+ + HCN
[Phen+H]+ → [(Phen+H)–HCN]+ + HCN
[Phen+H]+ → [(Phen+H)–2HCN]+ + 2HCN
[Phen+H]+ → [(Phen+H)–2CN]+ + 2CN
[Fe(Phen)2–H2]2+ → [(Fe(Phen)2–H2–HCN]2+ + HCN
[Fe(Phen)2–H2]2+ → [Fe(Phen)2–2H2]2+ + H2
Fe+(Phen) + 2H2 → [Fe(Phen)+2H2]+
Fe+(Phen) → [Fe(Phen)–CH2]+ + CH2
Fe2+(Phen)2 → [Fe(Phen)2–CH3]2+ + CH3

Figure D.2.

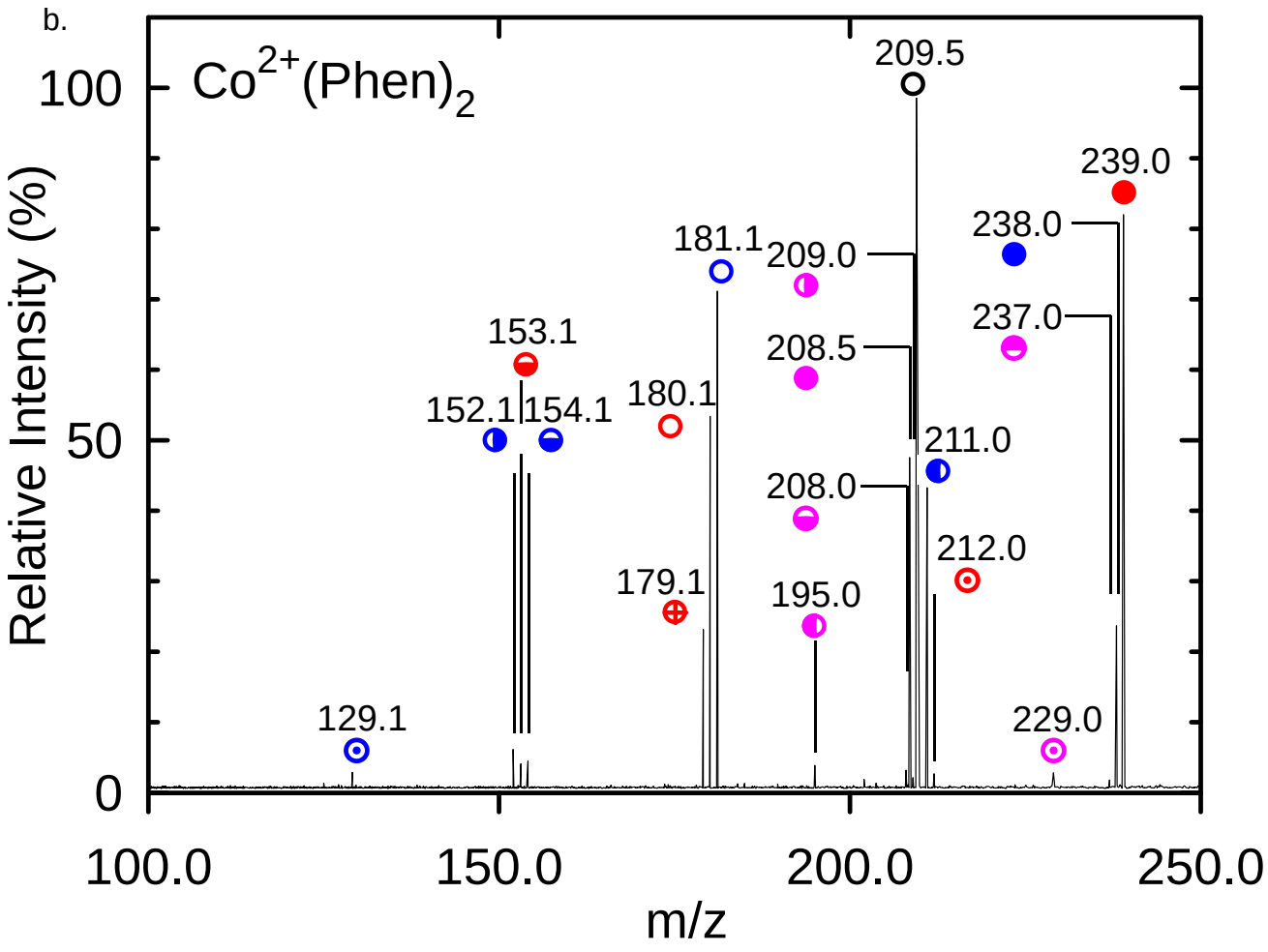
b.
Co2+(Phen)2
Relative Intensity (%)
100
50
0
100.0
150.0
200.0
250.0
m/z
209.5
239.0
238.0
181.1
209.0
237.0
153.1
208.5
152.1
154.1
180.1
211.0
208.0
212.0
179.1
195.0
129.1
229.0

Figure D.2.

b.

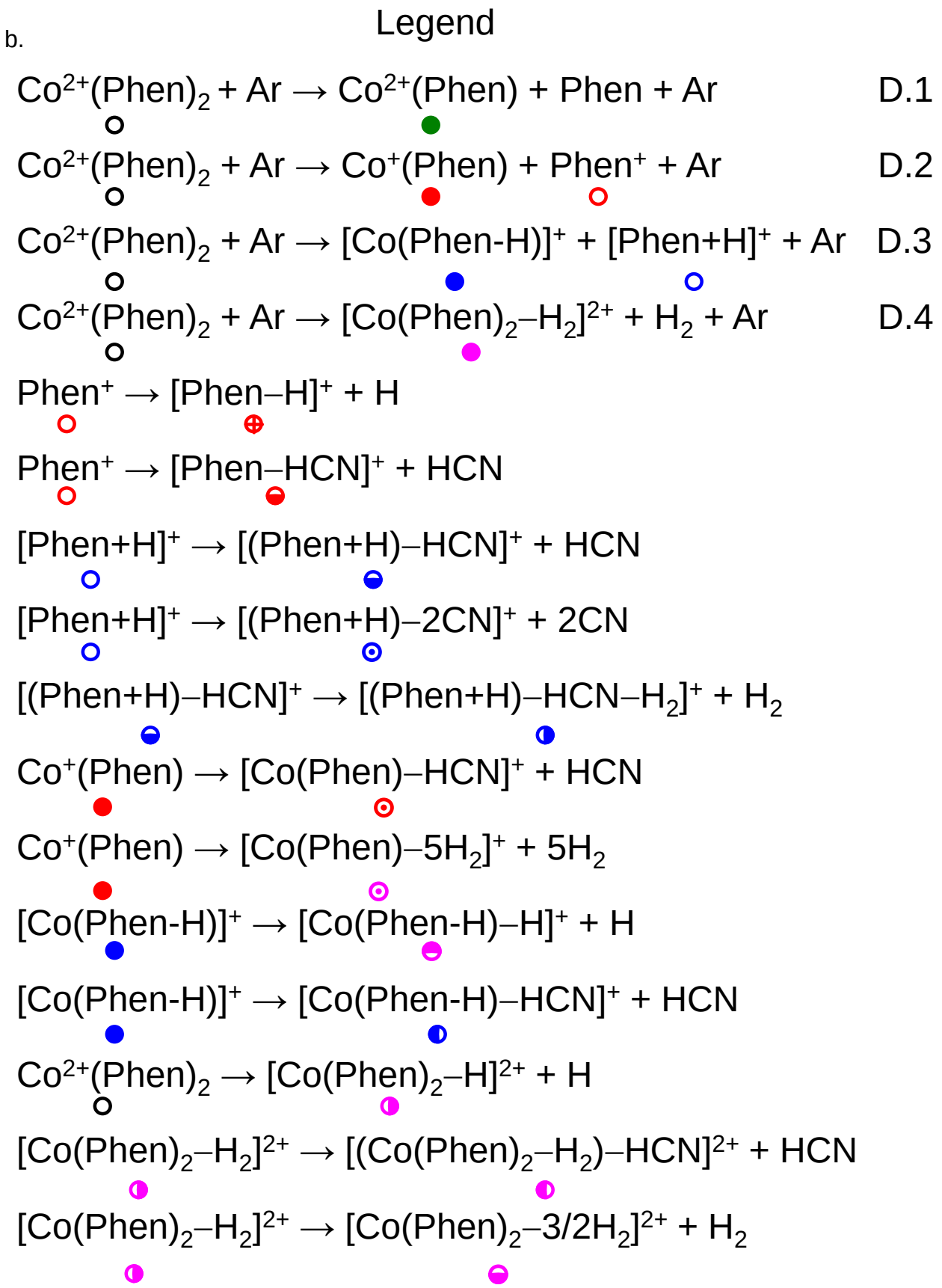
Legend
Co2+(Phen)2 + Ar → Co2+(Phen) + Phen + Ar D.1
Co2+(Phen)2 + Ar → Co+(Phen) + Phen+ + Ar D.2
Co2+(Phen)2 + Ar → [Co(Phen-H)]+ + [Phen+H]+ + Ar D.3
Co2+(Phen)2 + Ar → [Co(Phen)2–H2]2+ + H2 + Ar D.4
Phen+ → [Phen–H]+ + H
Phen+ → [Phen–HCN]+ + HCN
[Phen+H]+ → [(Phen+H)–HCN]+ + HCN
[Phen+H]+ → [(Phen+H)–2CN]+ + 2CN
[(Phen+H)–HCN]+ → [(Phen+H)–HCN–H2]+ + H2
Co+(Phen) → [Co(Phen)–HCN]+ + HCN
Co+(Phen) → [Co(Phen)–5H2]+ + 5H2
[Co(Phen-H)]+ → [Co(Phen-H)–H]+ + H
[Co(Phen-H)]+ → [Co(Phen-H)–HCN]+ + HCN
Co2+(Phen)2 → [Co(Phen)2–H]2+ + H
[Co(Phen)2–H2]2+ → [(Co(Phen)2–H2)–HCN]2+ + HCN
[Co(Phen)2–H2]2+ → [Co(Phen)2–3/2H2]2+ + H2

Figure D.2.

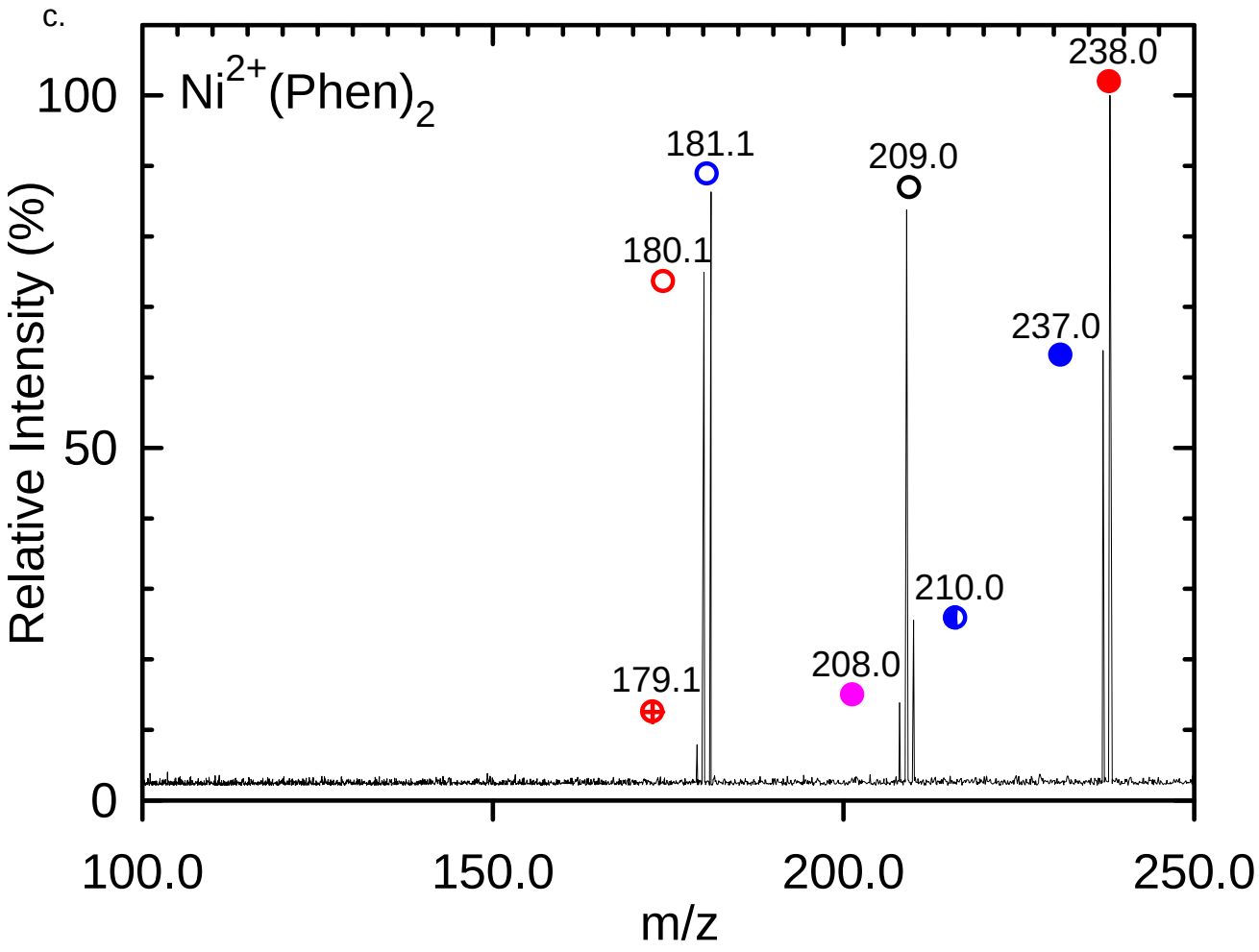

Legend

$Ni^{2+}(Phen)_2 + Ar \rightarrow Ni^{2+}(Phen) + Phen + Ar$ D.1

$Ni^{2+}(Phen)_2 + Ar \rightarrow Ni^{+}(Phen) + Phen^{+} + Ar$ D.2

$Ni^{2+}(Phen)_2 + Ar \rightarrow [Ni(Phen\text{-}H)]^{+} + [Phen+H]^{+} + Ar$ D.3

$Ni^{2+}(Phen)_2 + Ar \rightarrow [Ni(Phen)_2–H_2]^{2+} + H_2 + Ar$ D.4

$Phen^{+} \rightarrow [Phen–H]^{+} + H$

$[Ni(Phen\text{-}H)]^{+} \rightarrow [Ni(Phen\text{-}H)–HCN]^{+} + HCN$

Figure D.2.

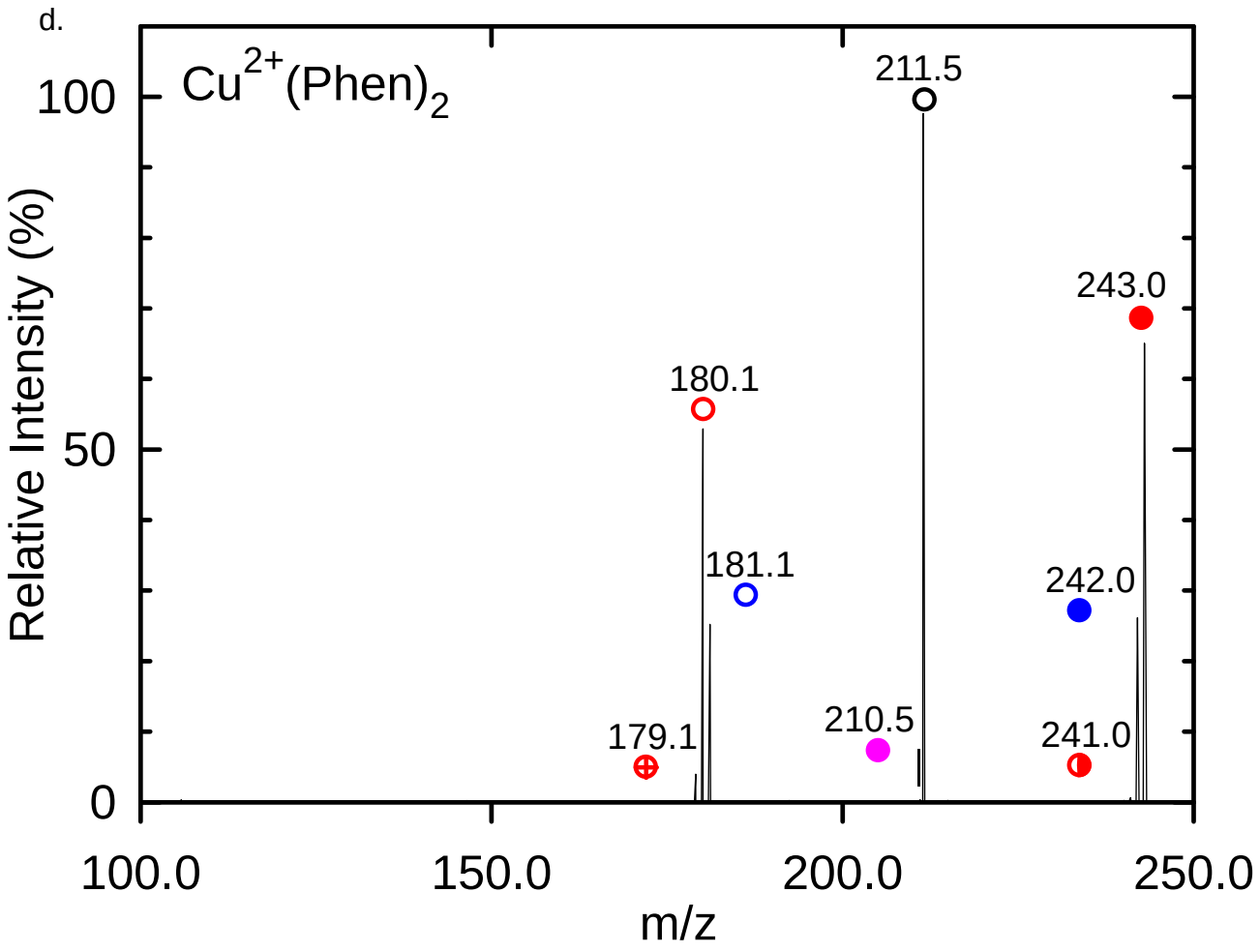

Legend

$Cu^{2+}(Phen)_2 + Ar \rightarrow Cu^{2+}(Phen) + Phen + Ar$ D.1

$Cu^{2+}(Phen)_2 + Ar \rightarrow Cu^{+}(Phen) + Phen^{+} + Ar$ D.2

$Cu^{2+}(Phen)_2 + Ar \rightarrow [Cu(Phen\text{-}H)]^{+} + [Phen+H]^{+} + Ar$ D.3

$Cu^{2+}(Phen)_2 + Ar \rightarrow [Cu(Phen)_2–H_2]^{2+} + H_2 + Ar$ D.4

$Phen^{+} \rightarrow [Phen–H]^{+} + H$

$Cu^{+}(Phen) \rightarrow [Cu(Phen)–H_2]^{+} + H_2$

Figure D.2.

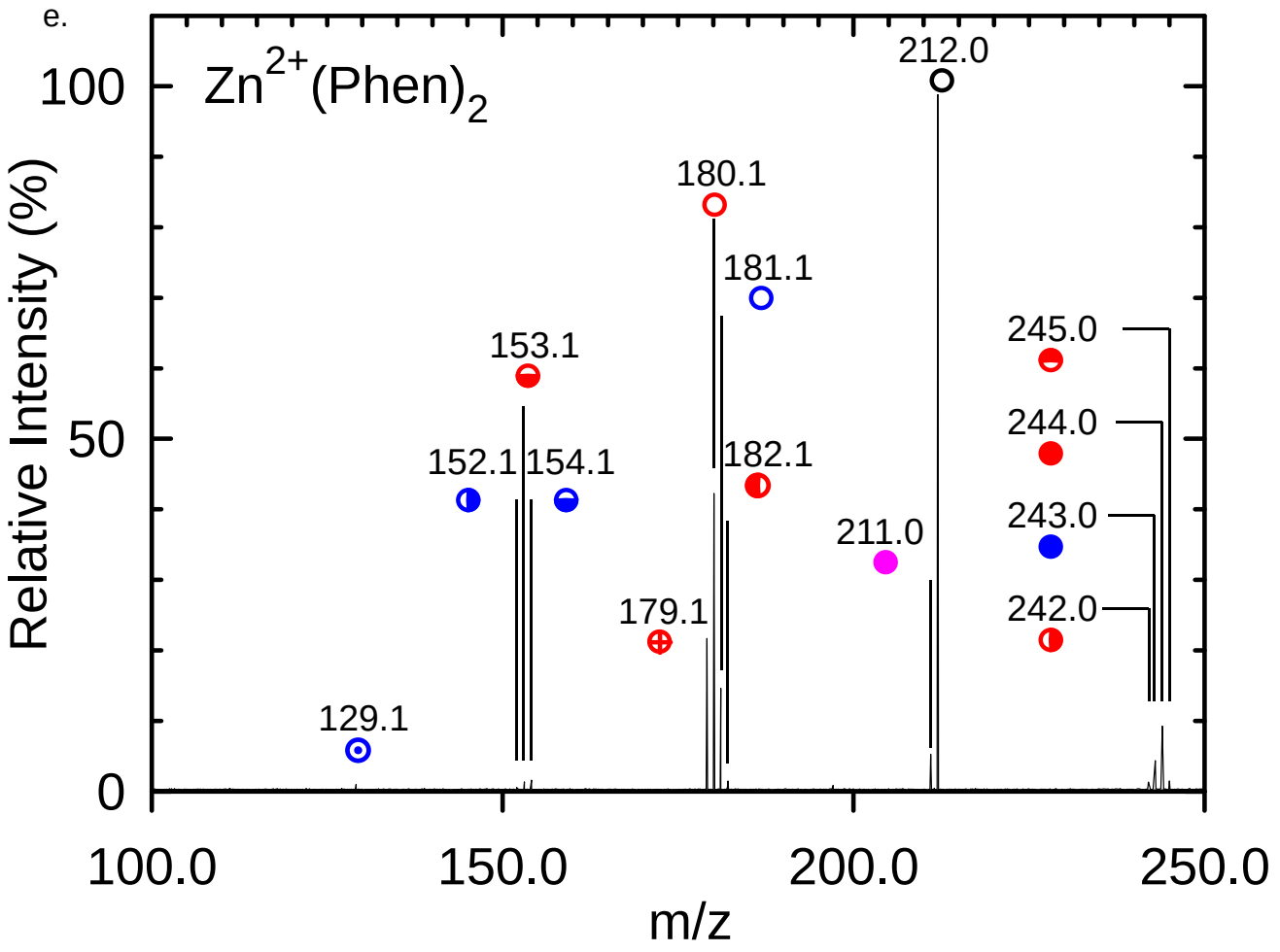
e.
$Zn^{2+}(Phen)_2$
212.0
180.1
181.1
153.1
245.0
244.0
152.1
154.1
182.1
243.0
211.0
179.1
242.0
129.1
Relative Intensity (%)
100
50
0
100.0
150.0
200.0
250.0
m/z

Figure D.2.

e.

Legend

$Zn^{2+}(Phen)_2 + Ar \rightarrow Zn^{2+}(Phen) + Phen + Ar$ D.1

$Zn^{2+}(Phen)_2 + Ar \rightarrow Zn^{+}(Phen) + Phen^{+} + Ar$ D.2

$Zn^{2+}(Phen)_2 + Ar \rightarrow [Zn(Phen\text{-}H)]^{+} + [Phen{+}H]^{+} + Ar$ D.3

$Zn^{2+}(Phen)_2 + Ar \rightarrow [Zn(Phen)_2{-}H_2]^{2+} + H_2 + Ar$ D.4

$Phen^{+} \rightarrow [Phen{-}H]^{+} + H$

$Phen^{+} \rightarrow [Phen{-}HCN]^{+} + HCN$

$Phen^{+} + H_2 \rightarrow [Phen{+}H_2]^{+}$

$[Phen{+}H]^{+} \rightarrow [(Phen{+}H){-}HCN]^{+} + HCN$

$[(Phen{+}H)\text{-}HCN]^{+} \rightarrow [(Phen{+}H){-}HCN\text{-}H_2]^{+} + H_2$

$[Phen{+}H]^{+} \rightarrow [(Phen{+}H){-}2CN]^{+} + 2CN$

$Zn^{+}(Phen) + H \rightarrow [Zn(Phen){+}H]^{+}$

$Zn^{+}(Phen) \rightarrow [Zn(Phen){-}H_2]^{+} + H_2$

Figure D.3.

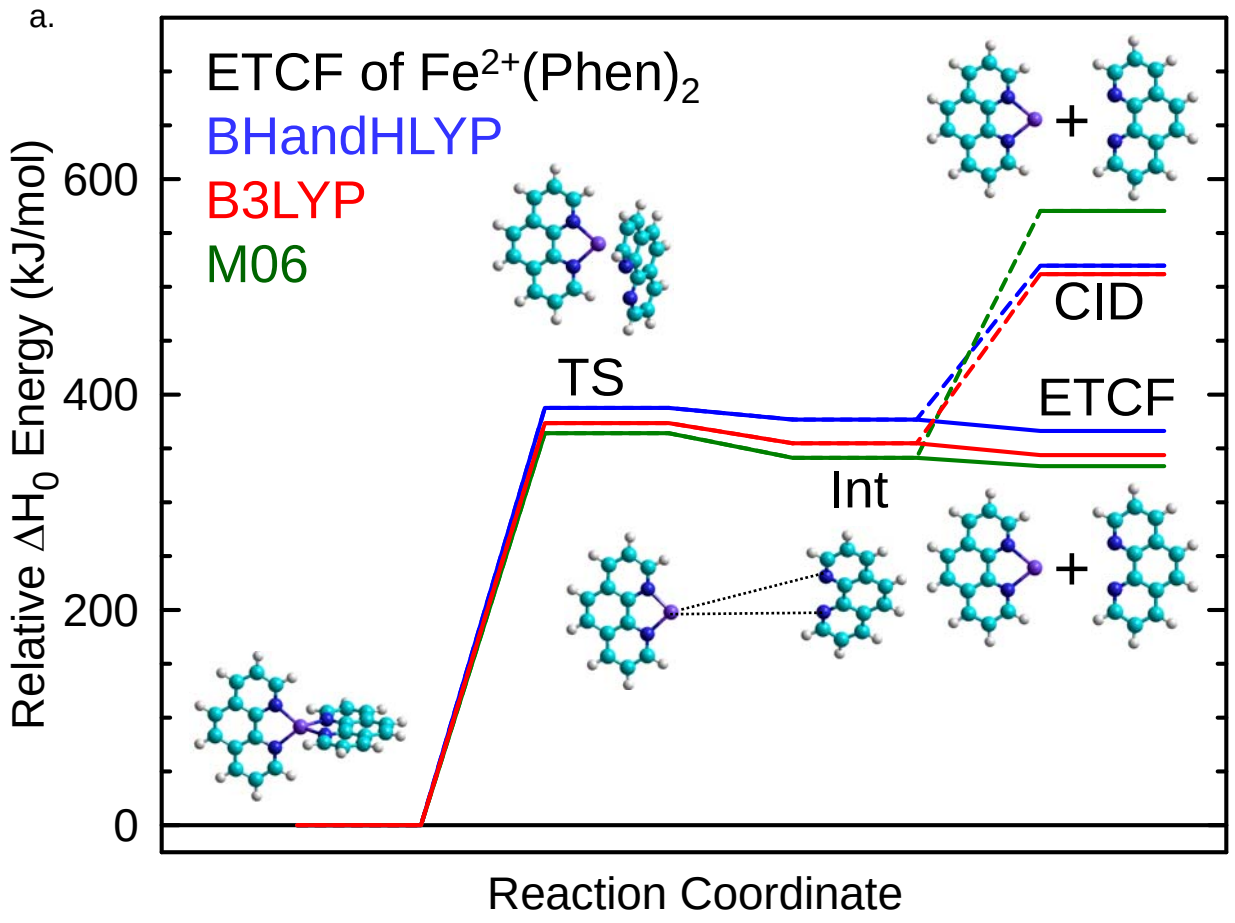
a.
ETCF of $Fe^{2+}(Phen)_2$
BHandHLYP
B3LYP
M06
TS
Int
CID
ETCF
+
+
Relative ΔH_0 Energy (kJ/mol)
0
200
400
600
Reaction Coordinate

Figure D.3.

b.

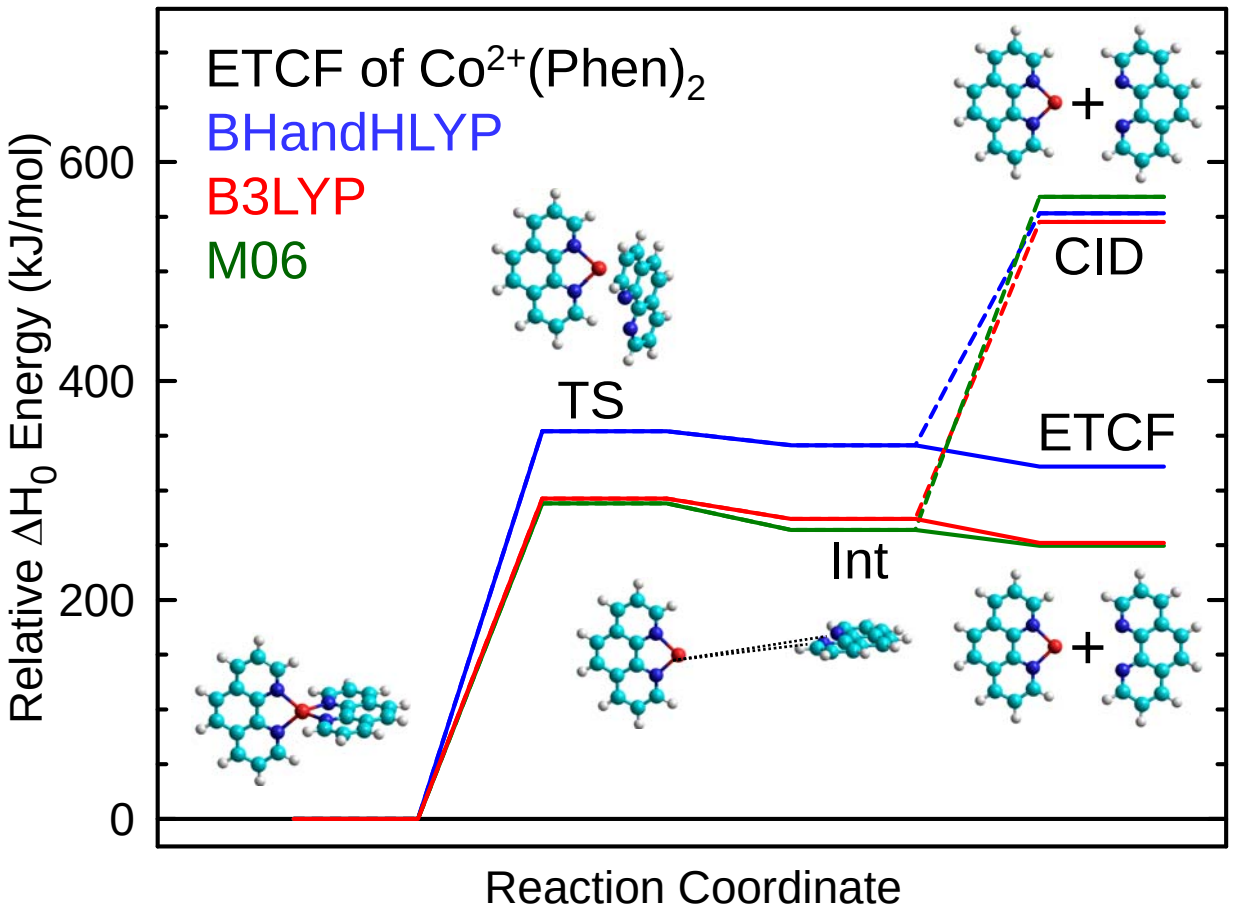
ETCF of Co2+(Phen)2
BHandHLYP
B3LYP
M06
Relative ΔH0 Energy (kJ/mol)
600
400
200
0
TS
CID
ETCF
Int
+
+
Reaction Coordinate

Figure D.3.

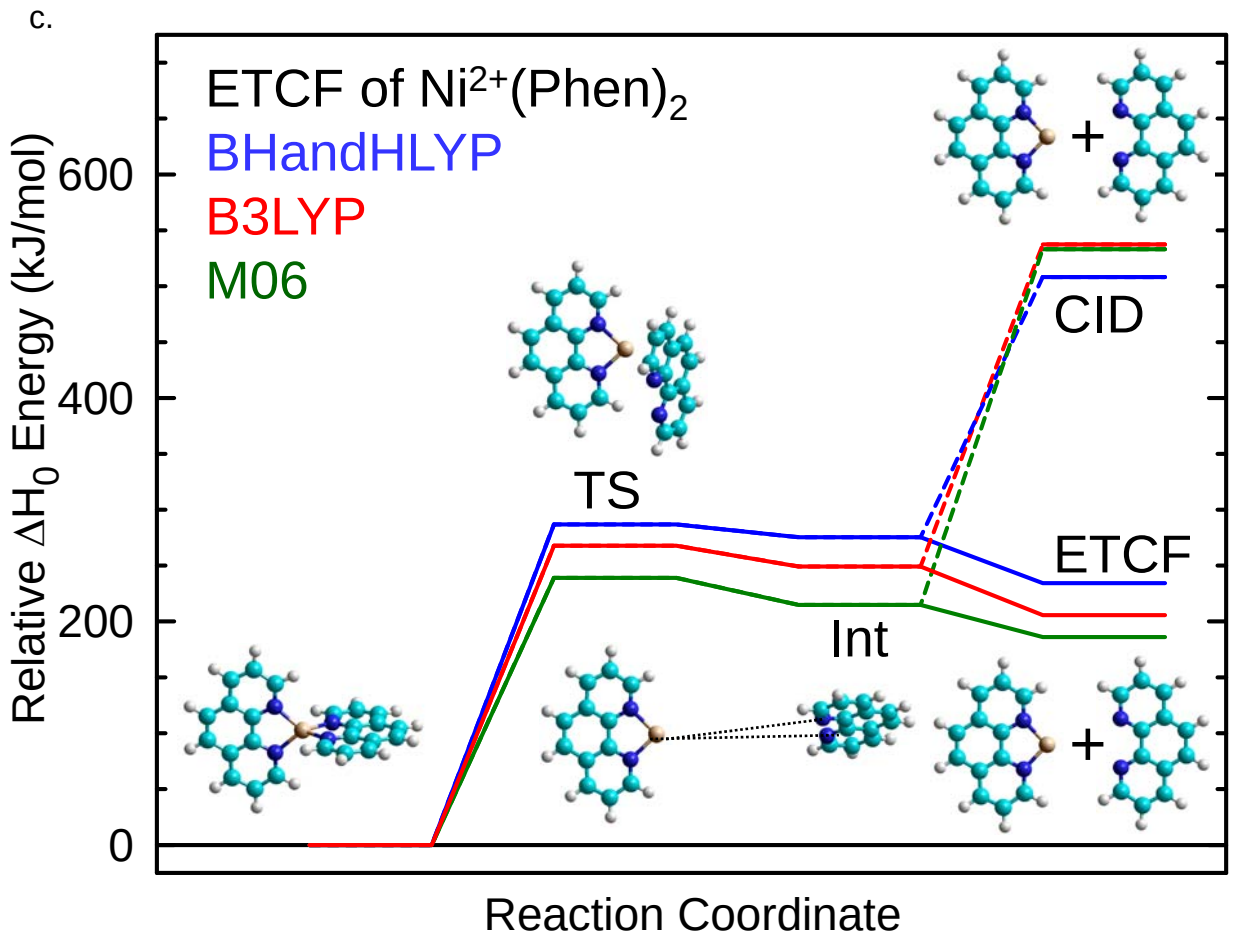
c.
ETCF of Ni2+(Phen)2
BHandHLYP
B3LYP
M06
Relative ΔH0 Energy (kJ/mol)
600
400
200
0
TS
Int
CID
ETCF
+
+
Reaction Coordinate

Figure D.3.

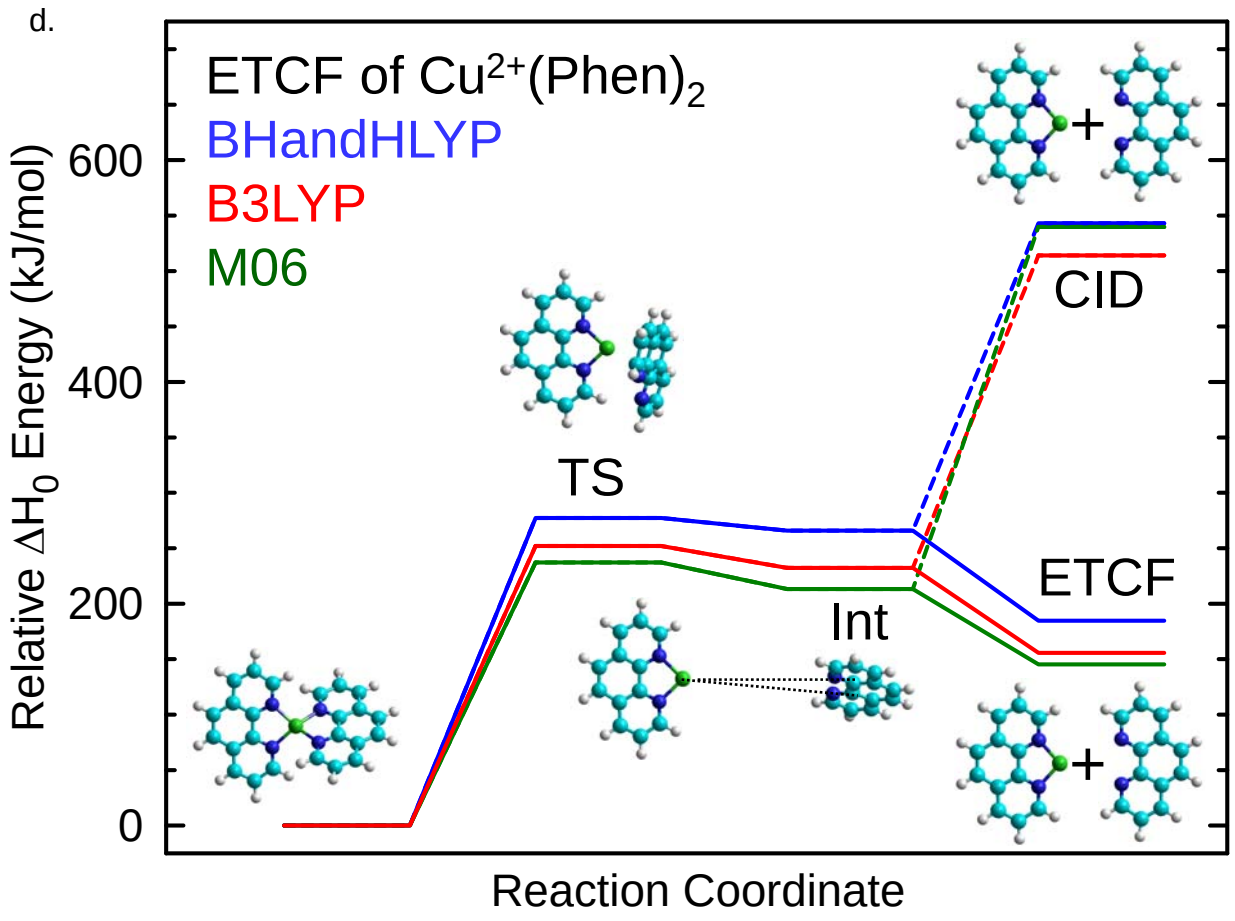
d.
ETCF of Cu2+(Phen)2
BHandHLYP
B3LYP
M06
Relative ΔH0 Energy (kJ/mol)
600
400
200
0
TS
Int
CID
ETCF
+
+
Reaction Coordinate

Figure D.3.

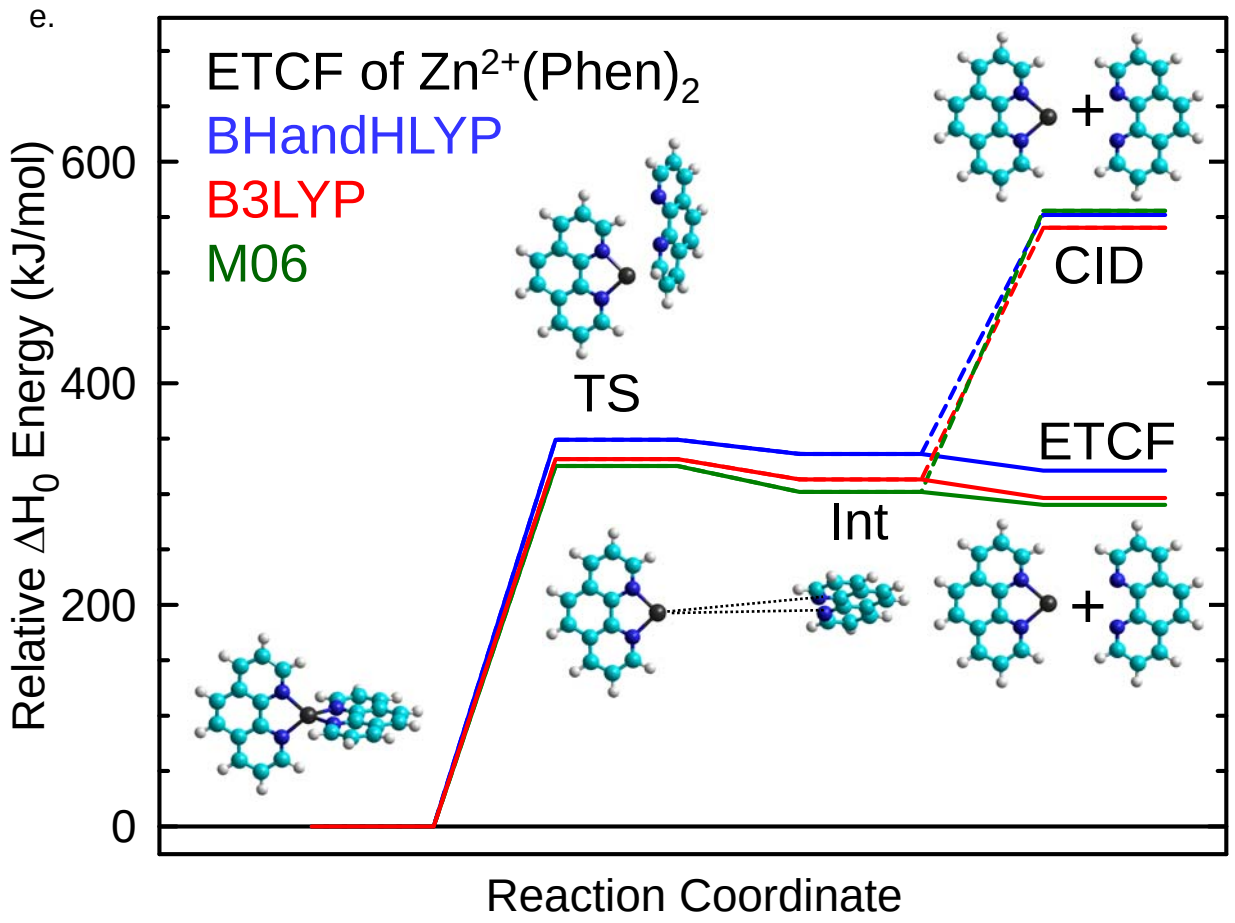
e.
ETCF of Zn2+(Phen)2
BHandHLYP
B3LYP
M06
TS
Int
CID
ETCF
+
+
Relative ΔH0 Energy (kJ/mol)
600
400
200
0
Reaction Coordinate

Figure D.4.

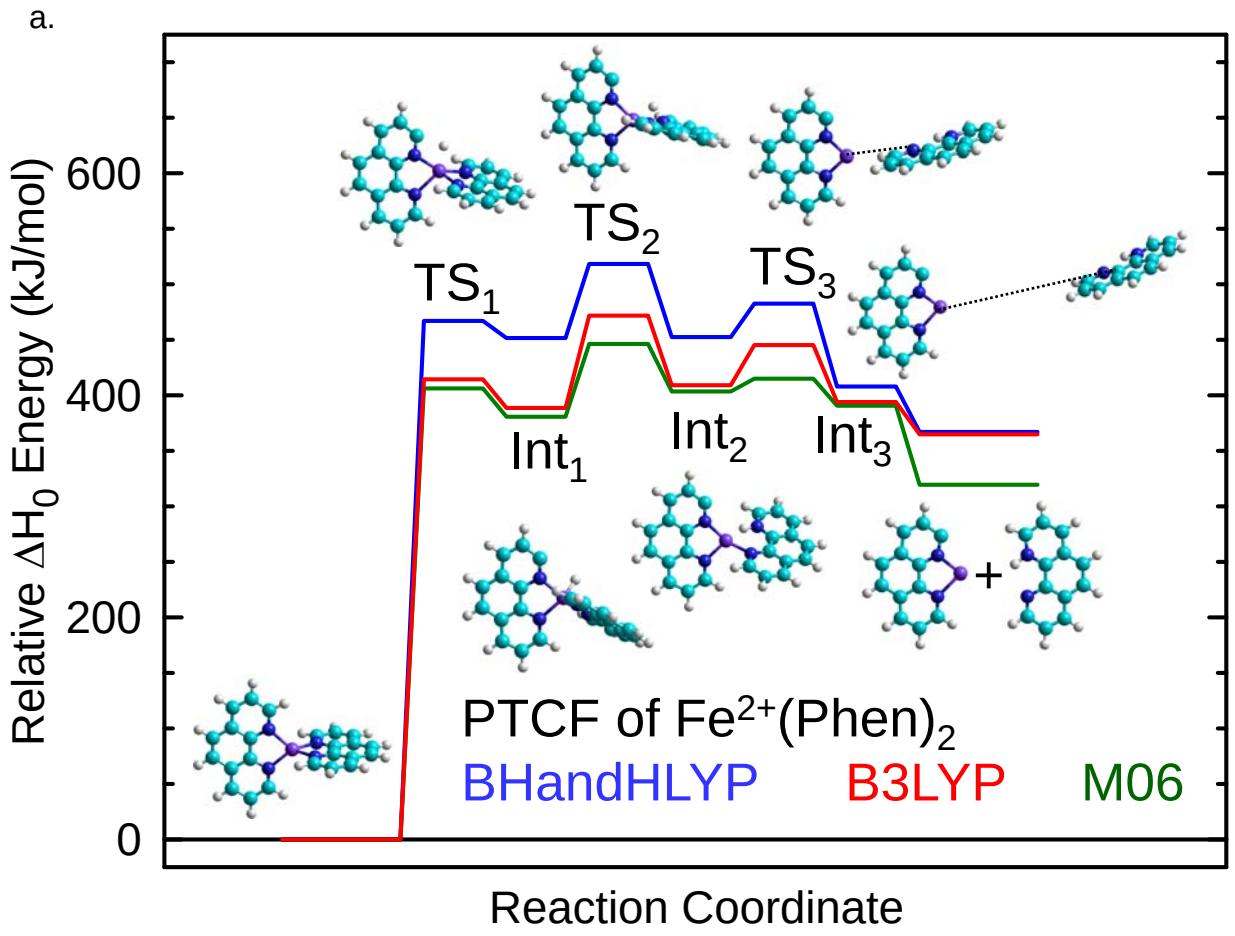
a.
Relative ΔH0 Energy (kJ/mol)
600
400
200
0
TS1
TS2
TS3
Int1
Int2
Int3
+
PTCF of Fe2+(Phen)2
BHandHLYP
B3LYP
M06
Reaction Coordinate

Figure D.4.

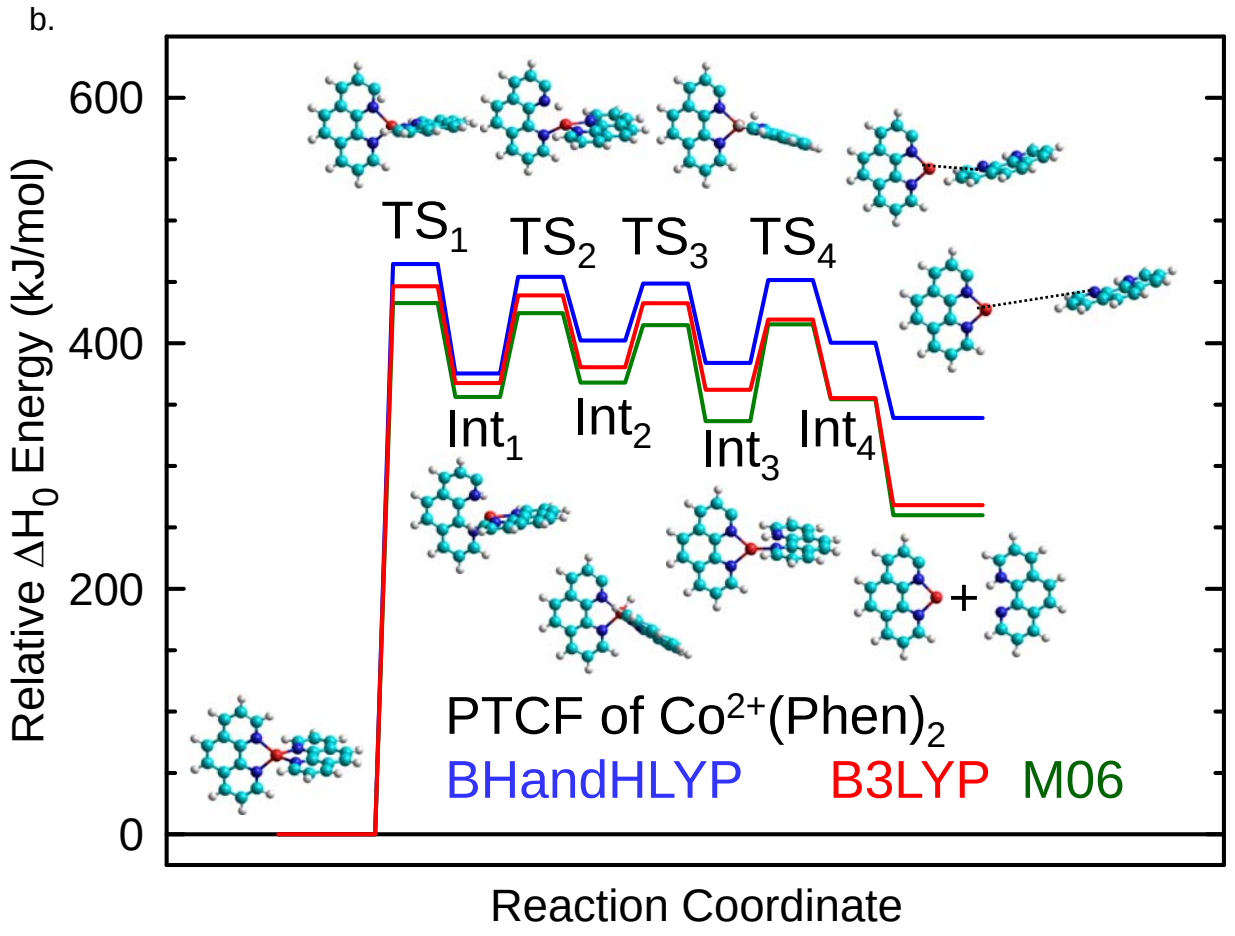
b.
600
400
200
0
Relative ΔH0 Energy (kJ/mol)
TS1
TS2
TS3
TS4
Int1
Int2
Int3
Int4
+
PTCF of Co2+(Phen)2
BHandHLYP
B3LYP
M06
Reaction Coordinate

Figure D.4.

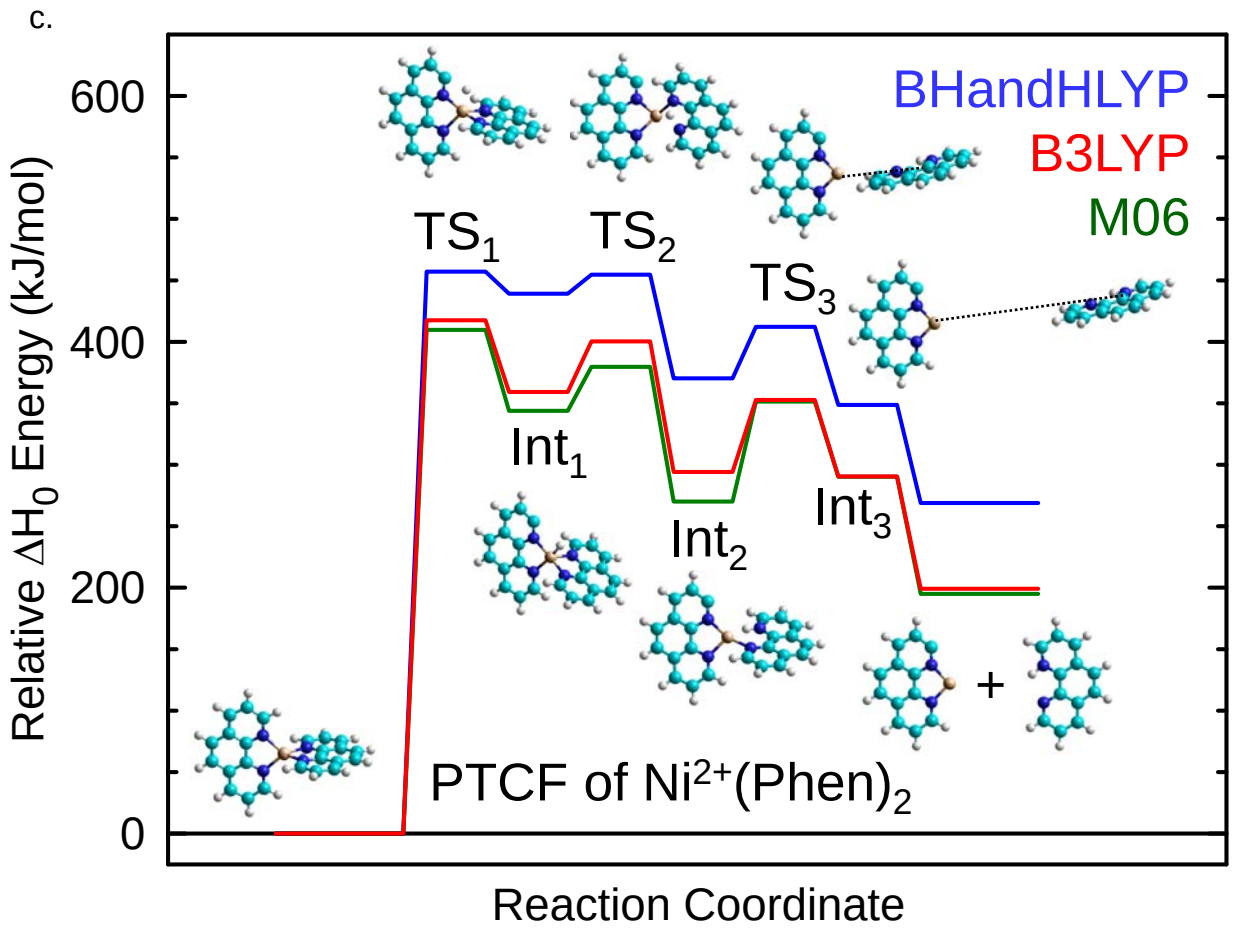
c.
600
400
200
0
Relative ΔH0 Energy (kJ/mol)
BHandHLYP
B3LYP
M06
TS1
TS2
TS3
Int1
Int2
Int3
+
PTCF of Ni2+(Phen)2
Reaction Coordinate

Figure D.4.

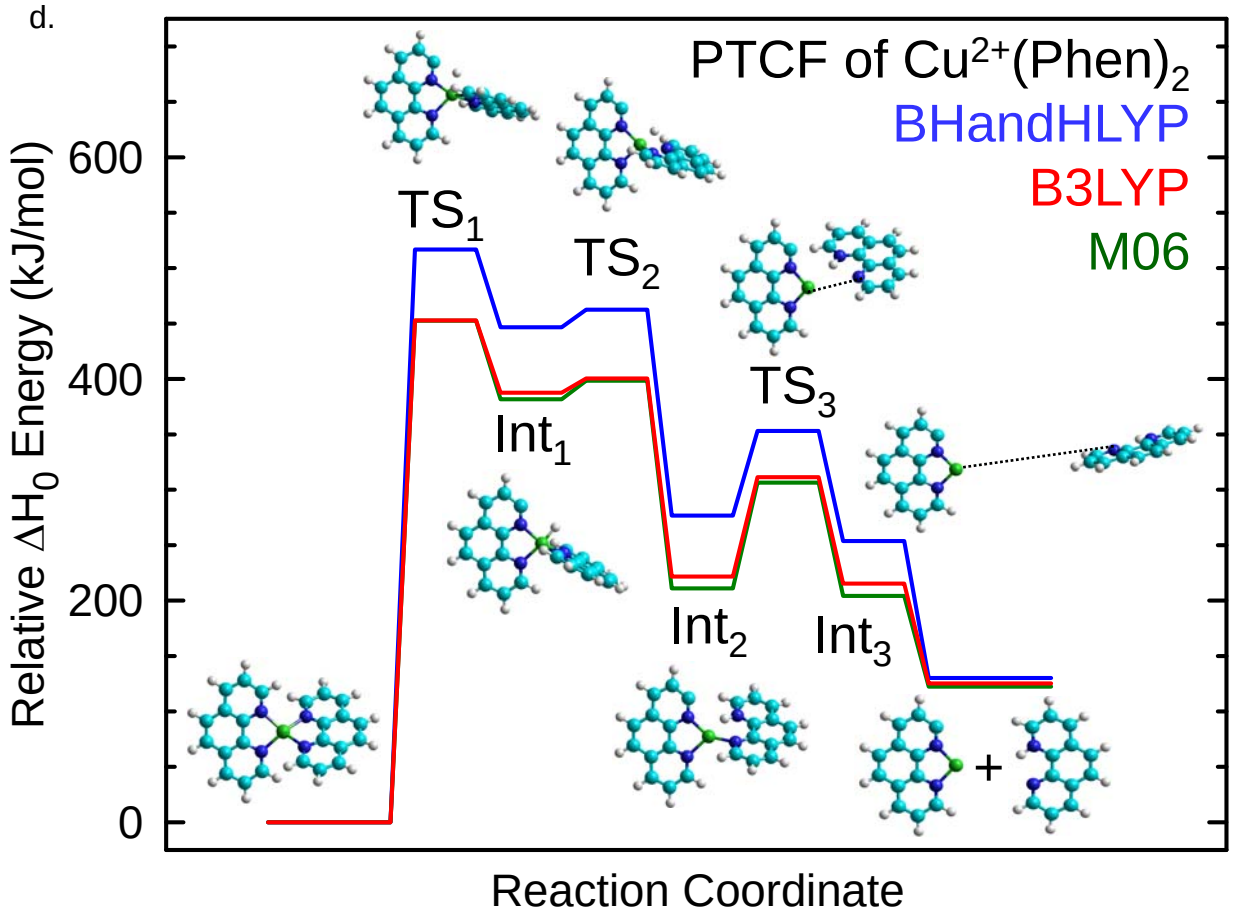
d.
PTCF of Cu2+(Phen)2
BHandHLYP
B3LYP
M06
TS1
TS2
TS3
Int1
Int2
Int3
+
Relative ΔH0 Energy (kJ/mol)
600
400
200
0
Reaction Coordinate

Figure D.4.

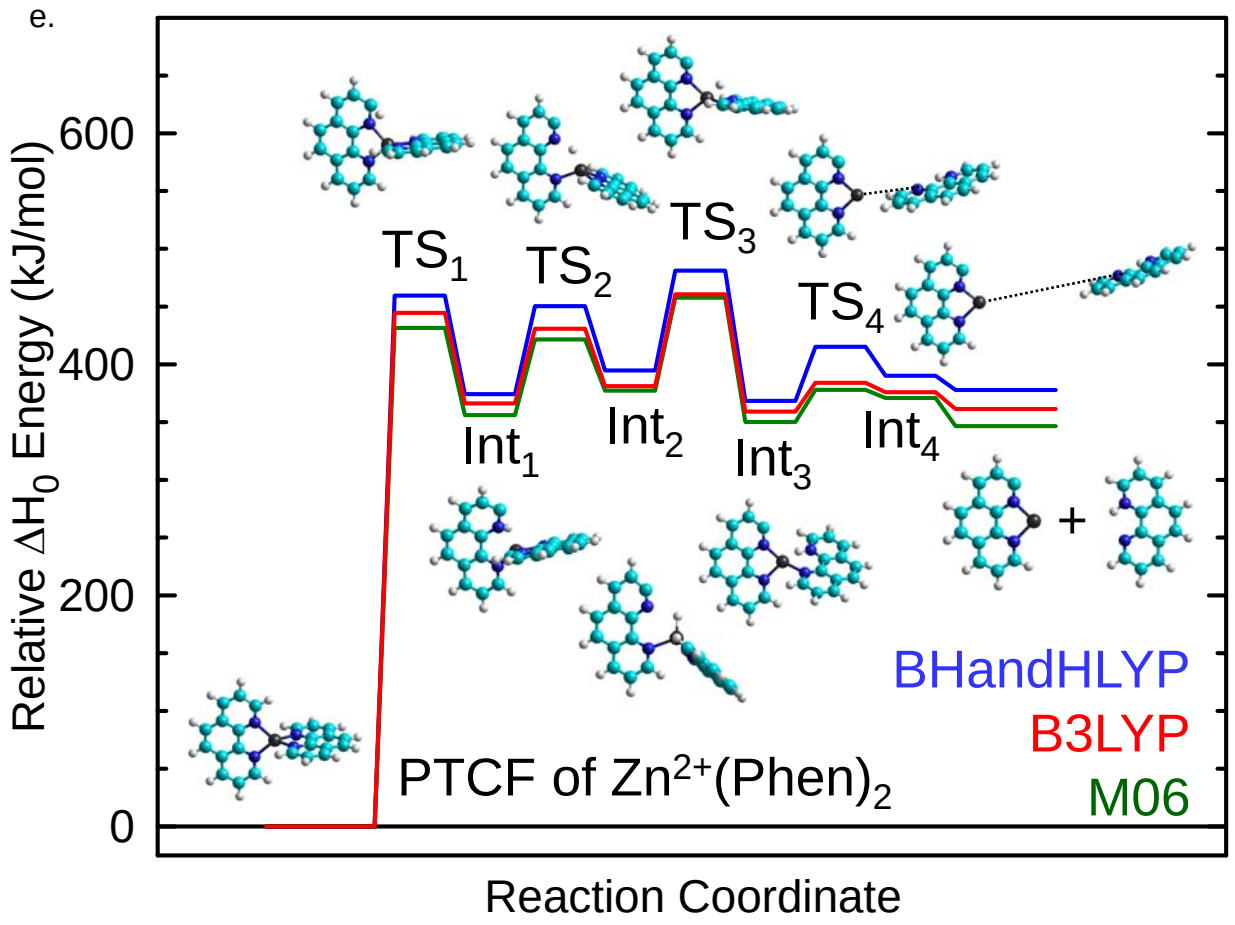
e.
Relative ΔH0 Energy (kJ/mol)
600
400
200
0
TS1
TS2
TS3
TS4
Int1
Int2
Int3
Int4
+
BHandHLYP
B3LYP
M06
PTCF of Zn2+(Phen)2
Reaction Coordinate

Figure D.5.

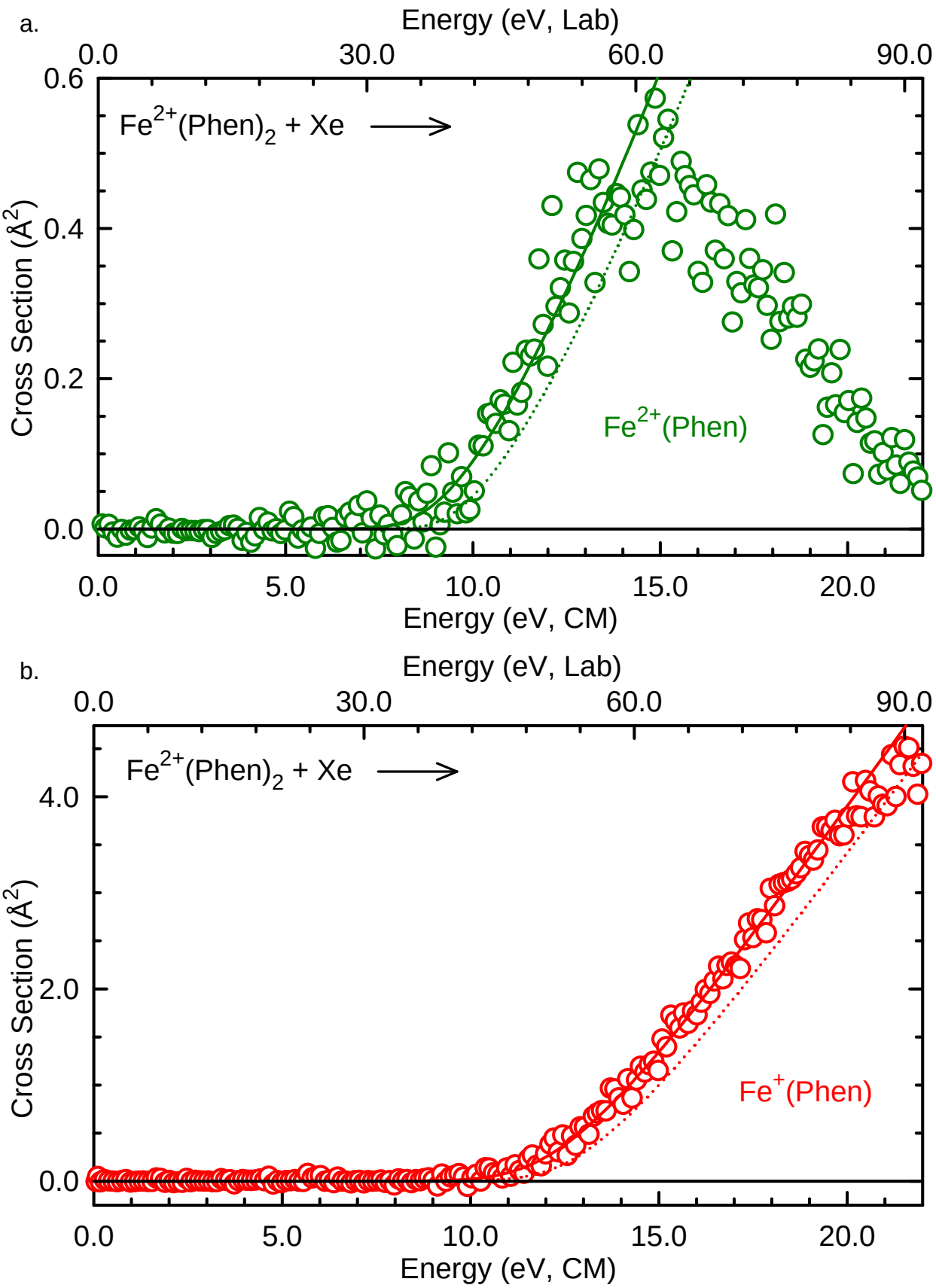
a.
Energy (eV, Lab)
0.0
30.0
60.0
90.0
0.6
0.4
0.2
0.0
Cross Section (Å^2)
Fe^{2+}(Phen)$_2$ + Xe
Fe^{2+}(Phen)
0.0
5.0
10.0
15.0
20.0
Energy (eV, CM)
b.
Energy (eV, Lab)
0.0
30.0
60.0
90.0
4.0
2.0
0.0
Cross Section (Å^2)
Fe^{2+}(Phen)$_2$ + Xe
Fe^{+}(Phen)
0.0
5.0
10.0
15.0
20.0
Energy (eV, CM)

Figure D.5.

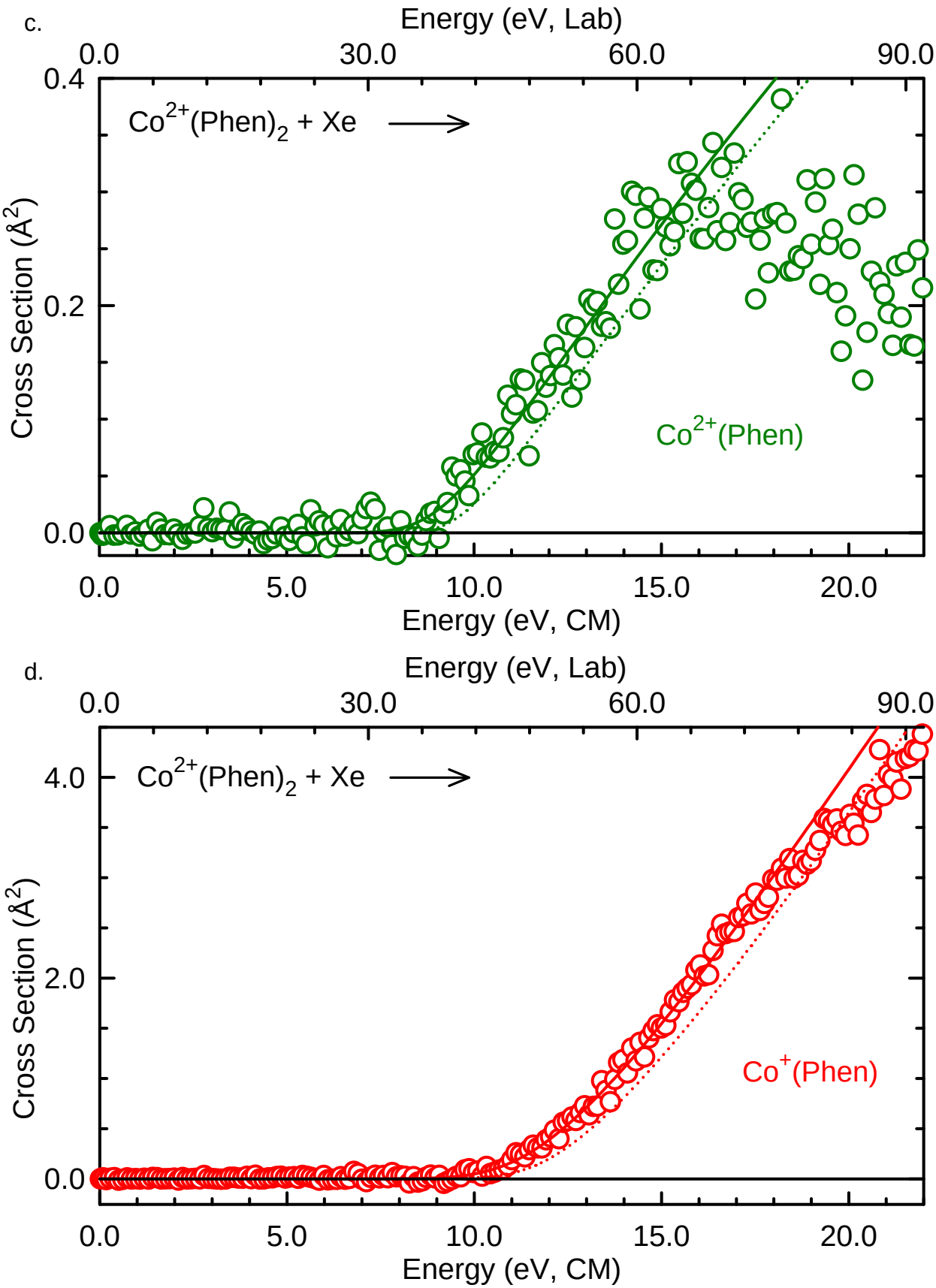
c.
Energy (eV, Lab)
0.0
30.0
60.0
90.0
0.4
0.2
0.0
Cross Section (Å^2)
Co^{2+}(Phen)$_2$ + Xe
Co^{2+}(Phen)
0.0
5.0
10.0
15.0
20.0
Energy (eV, CM)
d.
Energy (eV, Lab)
0.0
30.0
60.0
90.0
4.0
2.0
0.0
Cross Section (Å^2)
Co^{2+}(Phen)$_2$ + Xe
Co^{+}(Phen)
0.0
5.0
10.0
15.0
20.0
Energy (eV, CM)

Figure D.5.

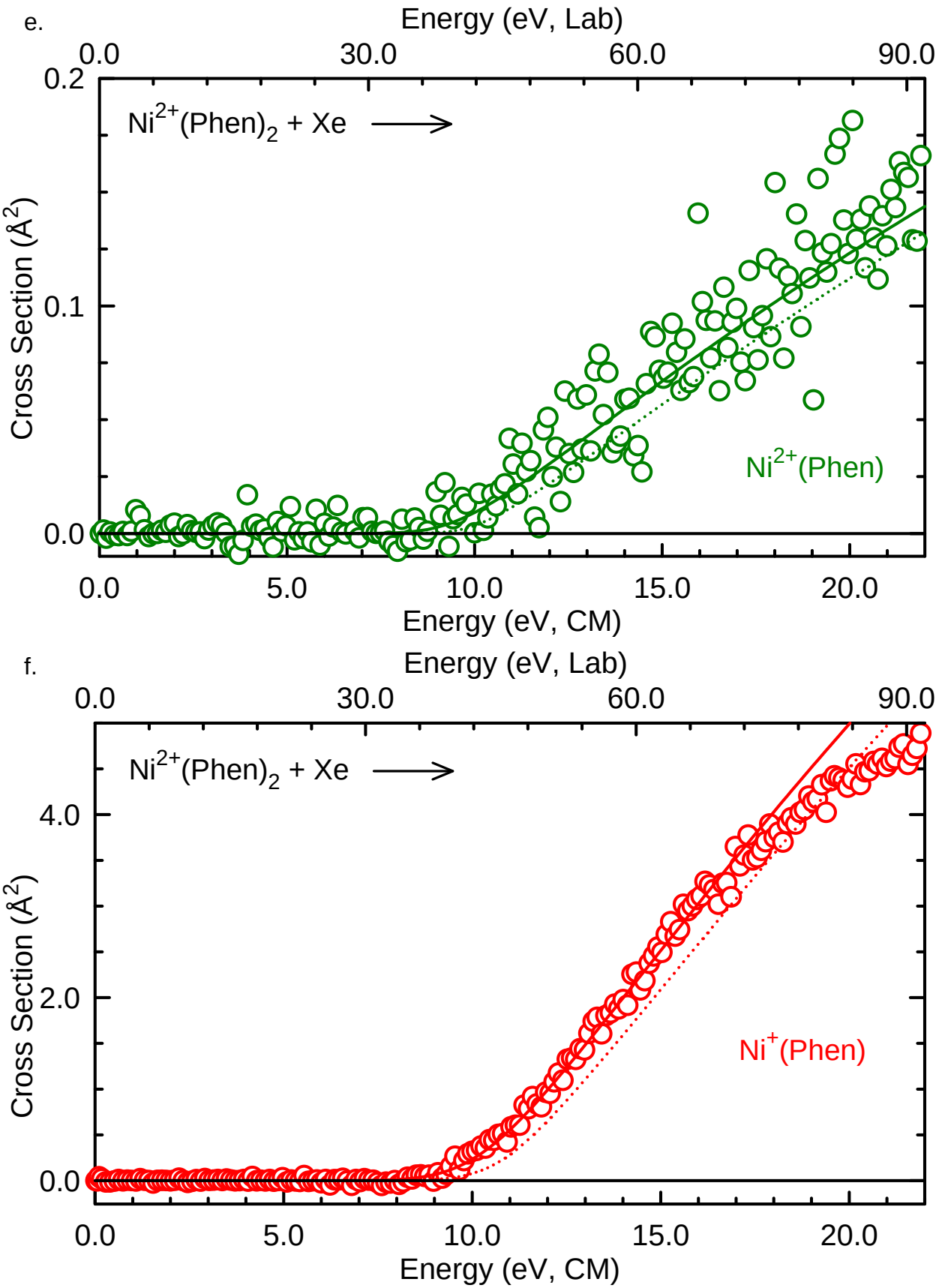
e.
Energy (eV, Lab)
0.0
30.0
60.0
90.0
0.2
0.1
0.0
Cross Section (Å^2)
Ni^{2+}(Phen)$_2$ + Xe ⟶
Ni^{2+}(Phen)
0.0
5.0
10.0
15.0
20.0
Energy (eV, CM)
f.
Energy (eV, Lab)
0.0
30.0
60.0
90.0
4.0
2.0
0.0
Cross Section (Å^2)
Ni^{2+}(Phen)$_2$ + Xe ⟶
Ni^{+}(Phen)
0.0
5.0
10.0
15.0
20.0
Energy (eV, CM)

Figure D.5.

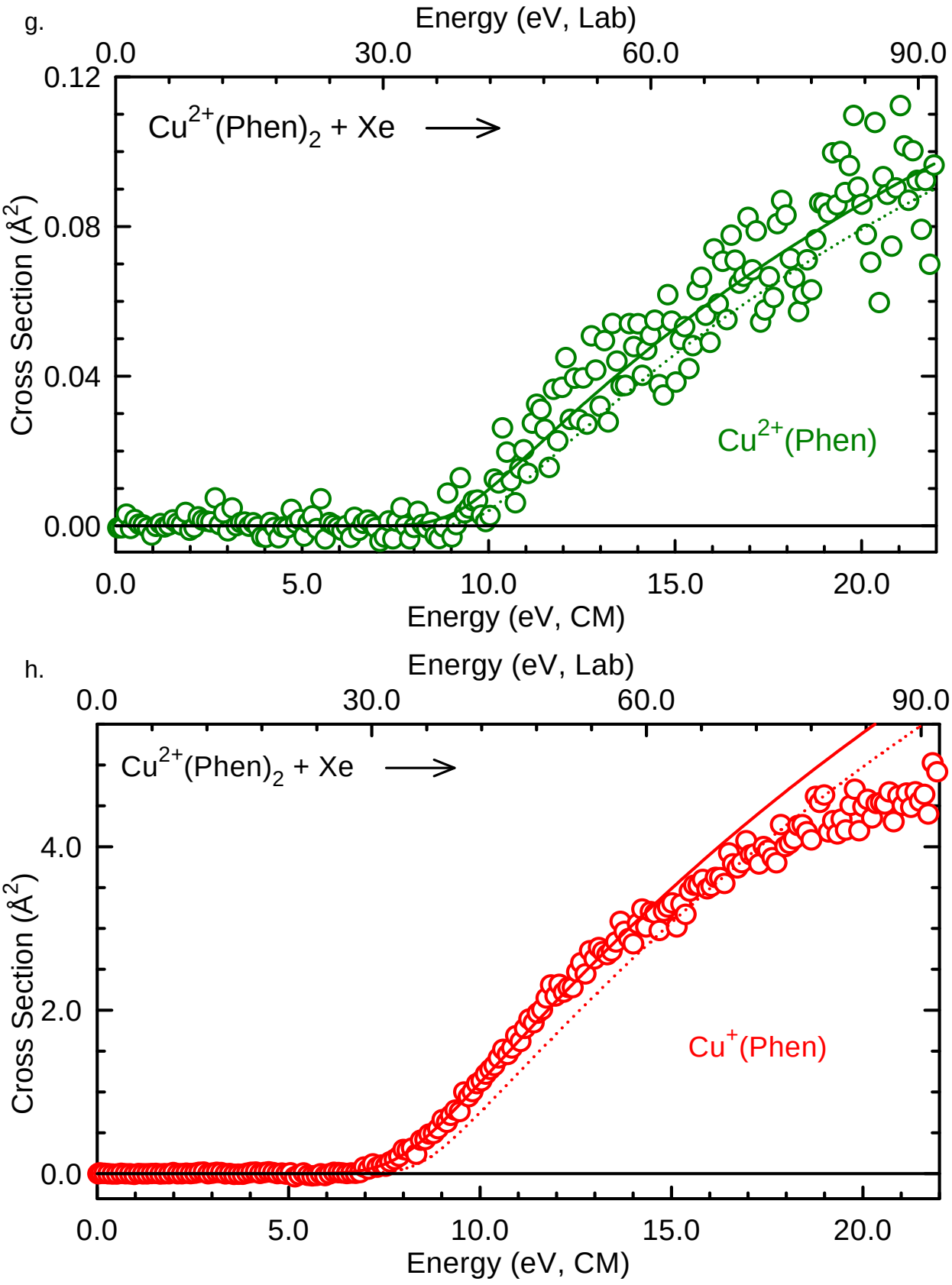
g.
Energy (eV, Lab)
0.0
30.0
60.0
90.0
0.12
0.08
0.04
0.00
Cross Section (Å^2)
$Cu^{2+}(Phen)_2$ + Xe
Cu^{2+}(Phen)
0.0
5.0
10.0
15.0
20.0
Energy (eV, CM)
h.
Energy (eV, Lab)
0.0
30.0
60.0
90.0
$Cu^{2+}(Phen)_2$ + Xe
4.0
2.0
0.0
Cross Section (Å^2)
Cu^{+}(Phen)
0.0
5.0
10.0
15.0
20.0
Energy (eV, CM)

Figure D.5.

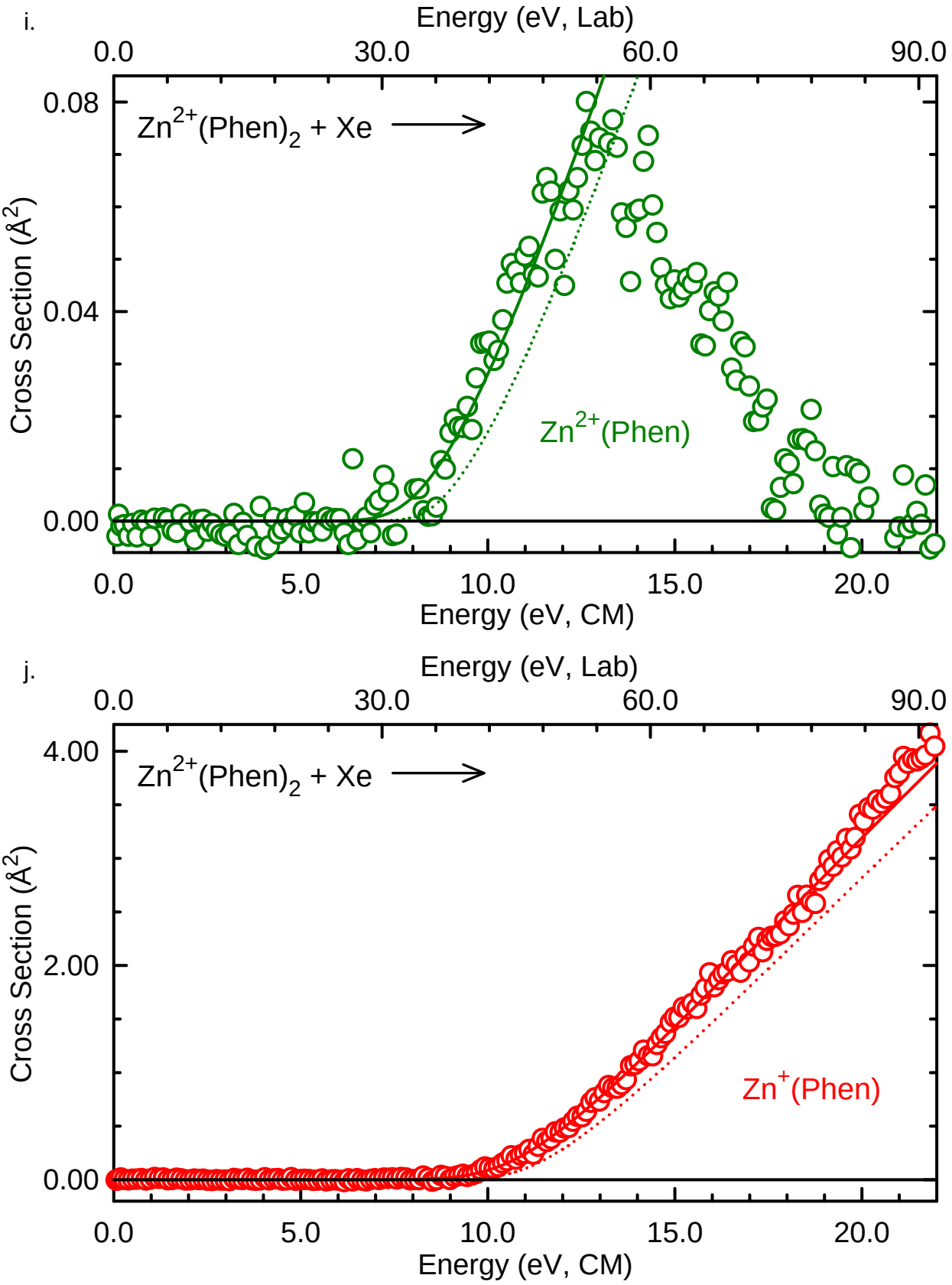
i.
Energy (eV, Lab)
0.0
30.0
60.0
90.0
0.08
0.04
0.00
Cross Section (Å^2)
$Zn^{2+}(Phen)_2$ + Xe
Zn^{2+}(Phen)
0.0
5.0
10.0
15.0
20.0
Energy (eV, CM)
j.
Energy (eV, Lab)
0.0
30.0
60.0
90.0
4.00
2.00
0.00
Cross Section (Å^2)
$Zn^{2+}(Phen)_2$ + Xe
Zn^{+}(Phen)
0.0
5.0
10.0
15.0
20.0
Energy (eV, CM)

Figure D.6.

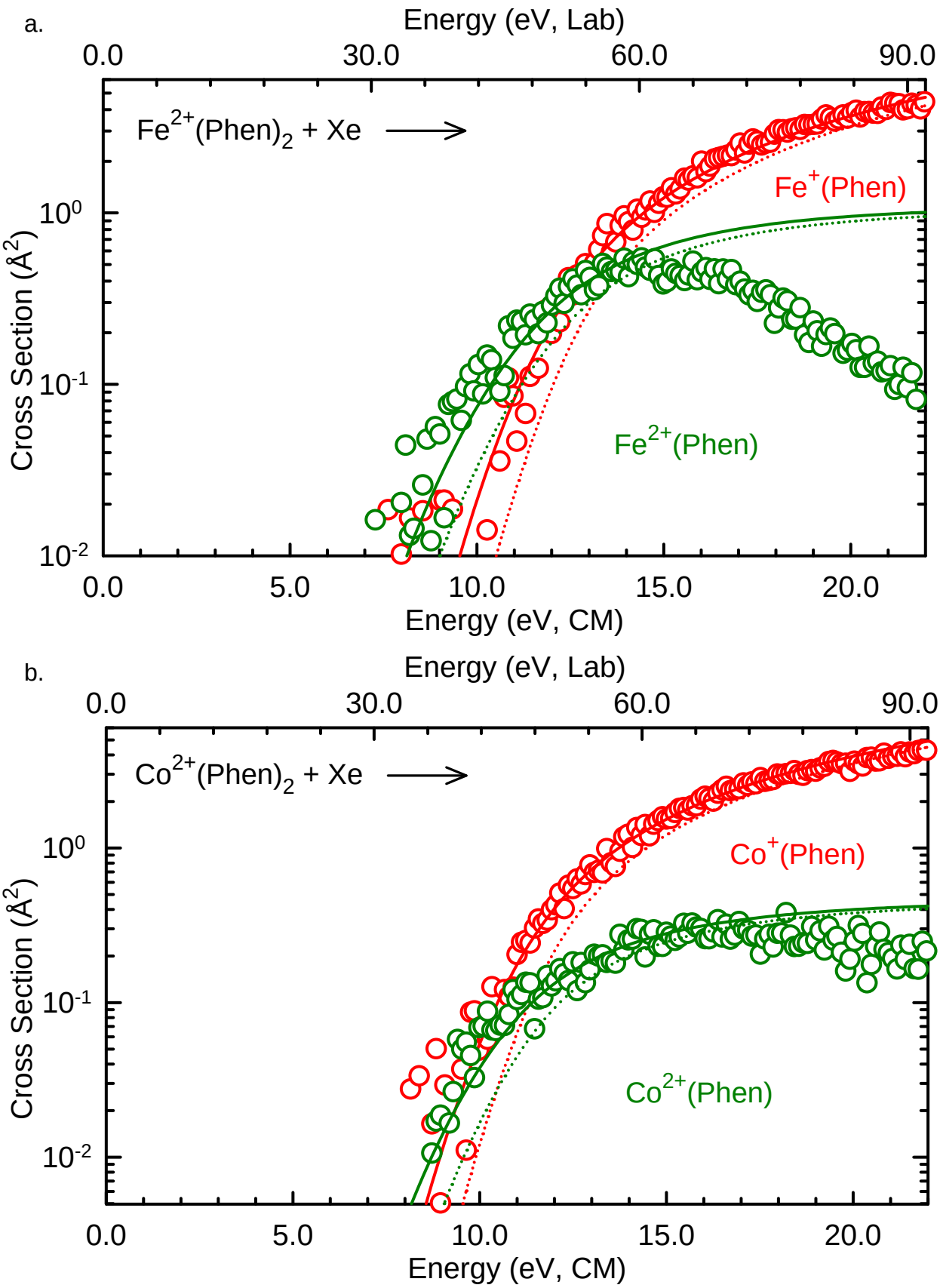
a.
Energy (eV, Lab)
0.0
30.0
60.0
90.0
Fe2+(Phen)2 + Xe
Fe+(Phen)
Fe2+(Phen)
Cross Section (Å2)
10^0
10^-1
10^-2
0.0
5.0
10.0
15.0
20.0
Energy (eV, CM)
b.
Energy (eV, Lab)
0.0
30.0
60.0
90.0
Co2+(Phen)2 + Xe
Co+(Phen)
Co2+(Phen)
Cross Section (Å2)
10^0
10^-1
10^-2
0.0
5.0
10.0
15.0
20.0
Energy (eV, CM)

Figure D.6.

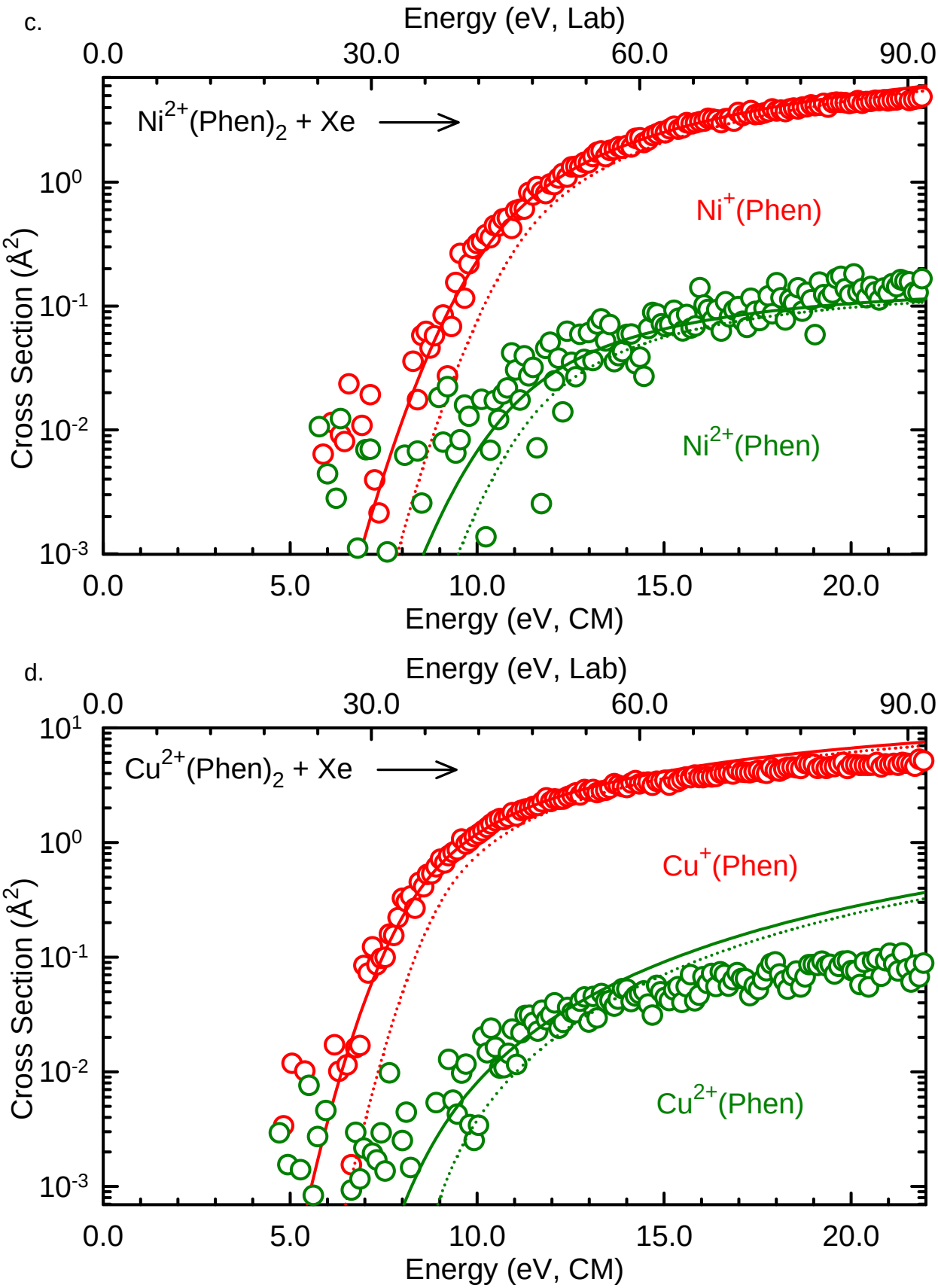
c.
Energy (eV, Lab)
0.0
30.0
60.0
90.0
Ni2+(Phen)2 + Xe
Ni+(Phen)
Ni2+(Phen)
Cross Section (Å2)
10^0
10^-1
10^-2
10^-3
0.0
5.0
10.0
15.0
20.0
Energy (eV, CM)
d.
Energy (eV, Lab)
0.0
30.0
60.0
90.0
Cu2+(Phen)2 + Xe
Cu+(Phen)
Cu2+(Phen)
Cross Section (Å2)
10^1
10^0
10^-1
10^-2
10^-3
0.0
5.0
10.0
15.0
20.0
Energy (eV, CM)

Figure D.6.

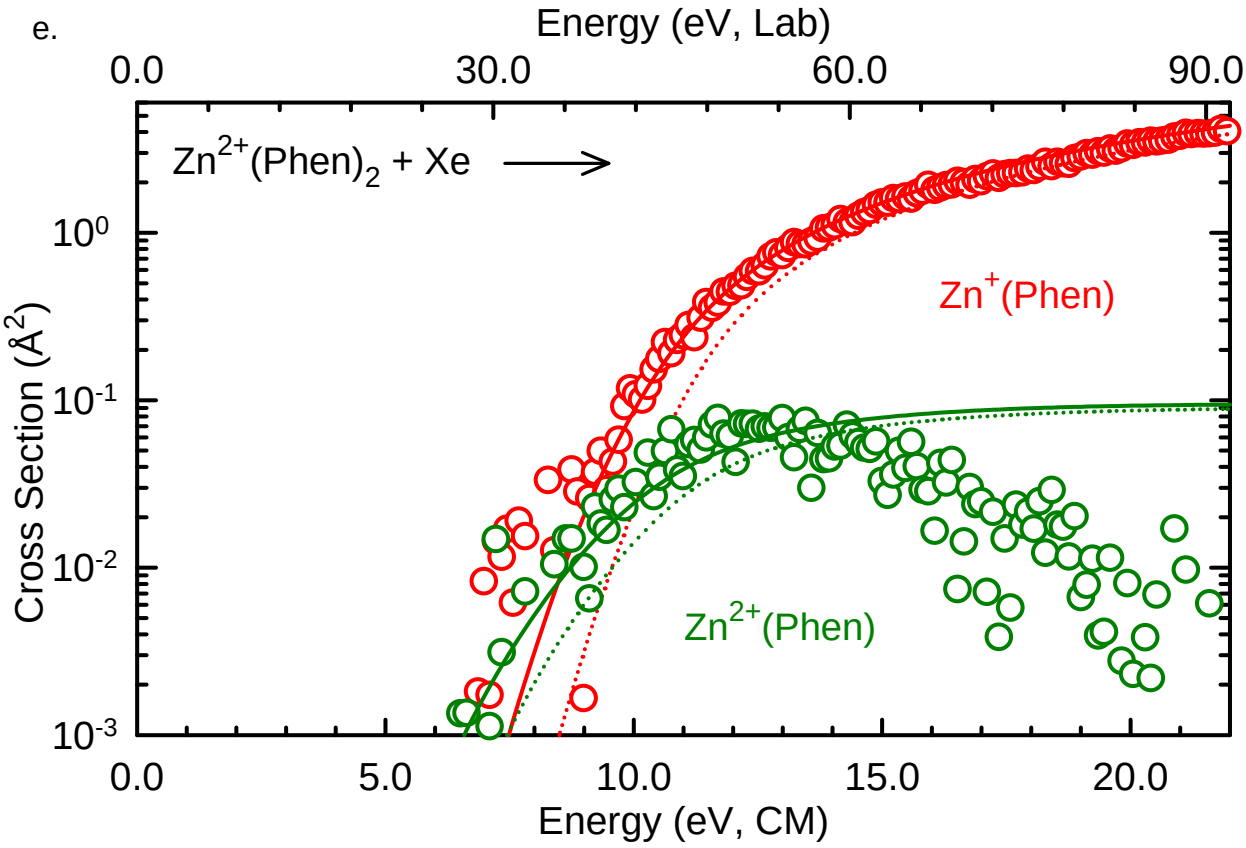
e.
Energy (eV, Lab)
0.0
30.0
60.0
90.0
Zn2+(Phen)2 + Xe
Zn+(Phen)
Zn2+(Phen)
Cross Section (Å2)
10^0
10^-1
10^-2
10^-3
0.0
5.0
10.0
15.0
20.0
Energy (eV, CM)

Figure D.7.

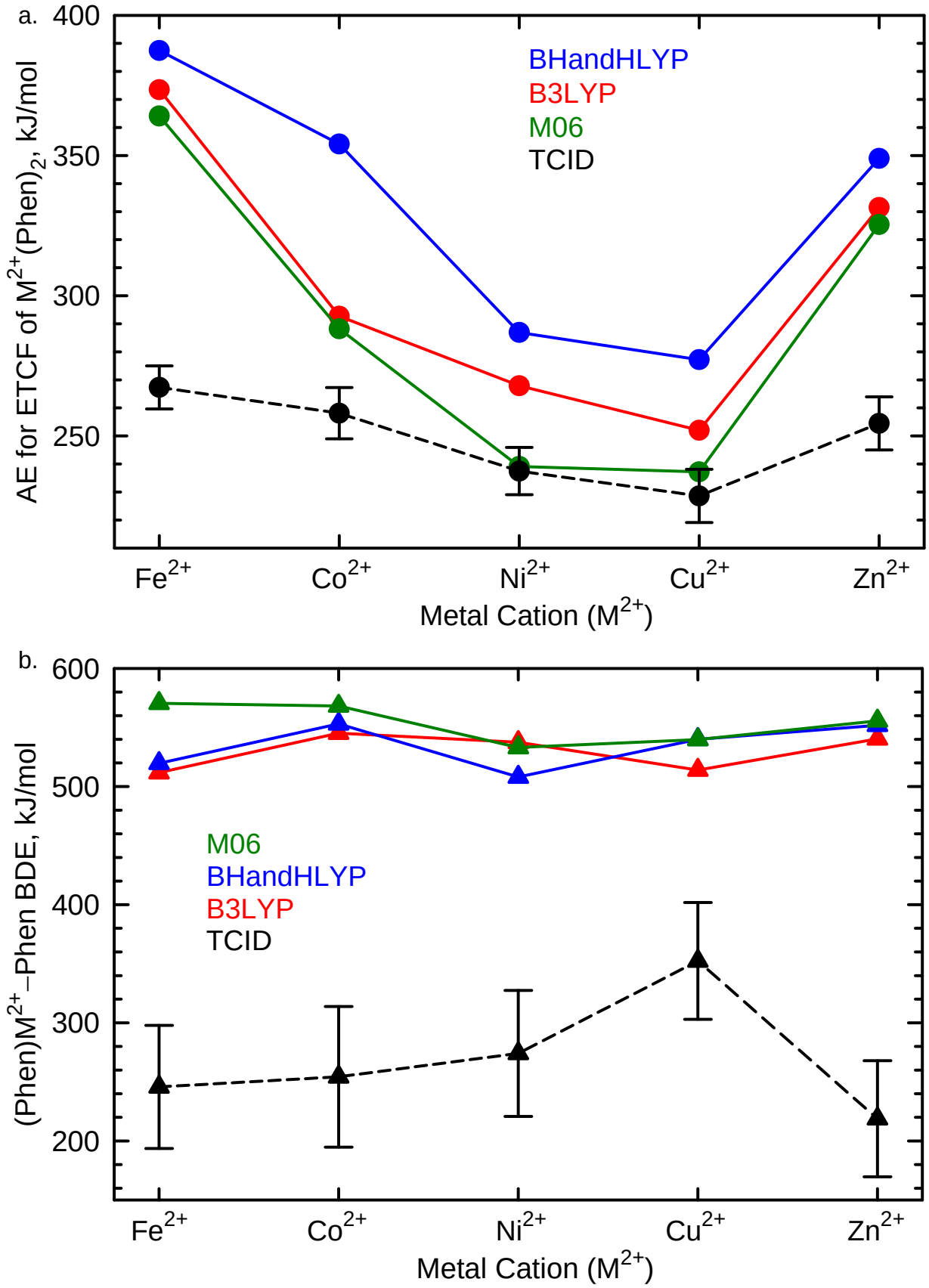
a.
AE for ETCF of $M^{2+}(Phen)_2$, kJ/mol
400
350
300
250
BHandHLYP
B3LYP
M06
TCID
Fe^{2+}
Co^{2+}
Ni^{2+}
Cu^{2+}
Zn^{2+}
Metal Cation (M^{2+})
b.
$(Phen)M^{2+}$–Phen BDE, kJ/mol
600
500
400
300
200
M06
BHandHLYP
B3LYP
TCID
Fe^{2+}
Co^{2+}
Ni^{2+}
Cu^{2+}
Zn^{2+}
Metal Cation (M^{2+})

APPENDIX E

PRELIMINARY ENERGY-RESOLVED COLLISION-INDUCED DISSOCIATION STUDIES OF BIS COMPLEXES of 2,2′-BIPYRIDINE TO THE LATE FIRST-ROW DIVALENT TRANSITION METAL CATIONS: COMPETITION BETWEEN SIMPLE CID AND COULOMB FISSION PROCESSES

E.1 Introduction

Electron transfer (ET) and proton transfer (PT) reactions have received a lot of attention as they are important in a variety of chemical, physical, and biological processes.[1,2] PT plays an important role in chemical interpretation at the molecular level of biological processes such as heredity, mutations, aging, and carcinogenic action.[3] ET is involved in redox reactions within active centers of most proteins such as blue copper proteins and cytochromes.[4,5] The active sites of many metalloproteins exhibit distinctive geometrical features as compared with small protein free inorganic complexes of the same metal cation.[6-8] These distinctive features are a result of the unusual geometric and electronic structures that can be imposed on a metal cation in a protein environment to enable it to carry out electron or proton transfer or other functionalities.[9-12] By studying ET and PT reactions in small inorganic transition metal complexes, knowledge of the geometric changes, electronic changes, and energy states of these compounds during electron or proton transfer is gained. Thus, small inorganic transition metal complexes may serve as model systems for the analysis of the way in which transition metal complexes in proteins and enzymes can undergo conformational changes from their expected ground states in the absence of substrates. Electronic structure theory calculations can be used to determine the changes in the electronic structure of the reduced or oxidized metal complexes associated with the

geometric structure of the ground-state along the ET and PT pathways by performing a potential energy surface (PES) scan for that process. The relevant features of the PES such as intermediates, transition states (TSs) and barrier heights between the reactants and TSs provide insight into the reaction mechanism. For example, the changes in the bond lengths and bond angles of the metal-ligand complexes during such processes can be used to elucidate information regarding the distances involved in charge transfer processes.[13,14] This information can offer insight into the changes in geometrical structure associated with reduction and oxidation processes of small transition metal complexes and its relationship to electronic structure and the specific pathway necessary to achieve efficient ET or PT.[15,16] Furthermore, studying the ET or PT processes of the small transition metal complexes in the gas phase allows us to focus on the properties of the reactants, their transient species and electronic properties that determine their intrinsic reactivity with respect to the reduction and oxidation processes. Such information can be helpful to scientists seeking to understand ET and/or PT mechanisms in small transitional metal complexes involving 2,2′-bipyridine (Bpy) ligands.

E.2 Rationale of this work

Appendix E is an extension of the work discussed in Chapter 4. In this work, the mechanisms associated with electron transfer Coulomb fission (ETCF), proton transfer Coulomb fission (PTCF), and simple collision-induced dissociation (CID) pathways of five $M^{2+}(Bpy)_2$ complexes are examined by performing electronic structure theory calculations, whereas the kinetic energy dependence of their CID behavior is examined under conditions where useful (preliminary) information can only elucidated for the ETCF and simple CID pathways. Severe overlap in several of the product channels, and incomplete acquisition of

the relevant experimental data, prevent useful information regarding the PTCF pathway to be elucidated. Because accurate thermochemical modeling of the experimental data is not possible without including all important CID pathways, these limitations prevent absolute energetic information for all pathways to be extracted from this work. In particular, we examine the influence of the electronic structure of the transition metal cation on the energetics of the ETCF, PTCF, and simple CID fragmentation pathways by systematically varying the metal cation from $Fe^{2+}(d^6)$ to $Co^{2+}(d^7)$ to $Ni^{2+}(d^8)$ to $Cu^{2+}(d^9)$ to $Zn^{2+}(d^{10})$. The energy-resolved CID processes are analyzed explicitly using methods developed previously.[17] We derive preliminary second sequential bond dissociation energies (BDEs) and activation energies (AEs) for ETCF of five $M^{2+}(Bpy)_2$ complexes and compare these results to values obtained from density functional theory calculations performed here. Periodic trends in the energetics of fragmentation of these complexes are examined and compared to those of the analogous $M^{2+}(Phen)_2$ complexes previously investigated (see Chapter 6). Comparisons are also made to the $M^{2+}(Bpy)_3$ and $M^{2+}(Phen)_3$ complexes previously investigated (Chapters 3 and 4).[18,19]

E.3 Collision-Induced Dissociation Experiments

E.3.1 Collision-Induced Dissociation Experiments Using GIBMS

Cross sections for CID of five $M^{2+}(Bpy)_2$ complexes with Xe, where $M^{2+} = Fe^{2+}$, Co^{2+}, Ni^{2+}, Cu^{2+}, and Zn^{2+} were measured using the guided ion beam tandem mass spectrometer (GIBMS) that has been described in detail in Chapter 2. The $M^{2+}(Bpy)_2$ complexes were generated using an electrospray ionization (ESI) source under conditions similar to those described in Chapter 2. The $M^{2+}(Bpy)_2$ complexes are dissolved in a 1:1 (v/v) HPLC grade acetonitrile and deionized water mixture to produce a solution that is

~0.01–0.1 mM concentration in $[M(Bpy)_2](PF_6)_2$. Thermochemical analyses of the experimental results are explicitly discussed in Chapter 2. The thermochemistry derived from GIBMS studies involves the determination of reaction thresholds, and therefore experiments are generally intentionally performed under low-resolution conditions to minimize discrimination and thereby enhance the sensitivity and accuracy of the threshold determination. However, for GIBMS results to provide accurate energetic information, all product species must be resolved such that the measured product cross sections are not contaminated by overlap with other reaction pathways. In the work performed here, preliminary CID studies of five $M^{2+}(Bpy)_2$ complexes were performed under relatively low-resolution conditions, thereby enabling the absolute magnitudes of the CID cross sections to be determined, but which are of limited thermochemical utility because of the severe overlap in several of the product channels, and because several of the products were not collected under variable pressure conditions such that extrapolation to single collision conditions cannot be achieved. Unresolved products of the ETCF and PTCF pathways and products originating from simple CID pathway are collected.

E.3.2 Collision-Induced Dissociation Experiments Using FT-ICR MS

A Fourier transform ion cyclotron resonance mass spectrometer (FT-ICR MS) was also used to investigate the fragmentation pathways for each of the $M^{2+}(Bpy)_2$ complexes as described in Chapter 2. The $M^{2+}(Bpy)_2$ complexes were generated using an ESI source under conditions similar to those described in Chapter 2. HPLC grade acetonitrile and deionized water were used to prepare solutions containing concentrations of ~0.1 μM $[M(Bpy)_2](PF_6)_2$ in a 1:1 (v/v) acetonitrile-water mixture. High-resolution FT-ICR MS experiments were pursued to definitely establish the CID pathways available to the $M^{2+}(Bpy)_2$ complexes,

because the initial low-resolution CID studies using the GIBMS showed the production of the $M^+(Bpy)$ and $[Bpy+H]^+$ product ions. Based on the simple principles of conservation of mass and charge in the CID processes, the complimentary ions, i.e., Bpy^+ and $[M(Bpy-H)]^+$ ions, respectively, must also be produced. Therefore, CID experiments using high-resolution FTICR-MS were performed to confirm the occurrence of both the ETCF and PTCF processes.

E.4 Theoretical Calculations

Theoretical calculations were performed to determine the structures of the $M^{2+}(Bpy)_2$ complexes and to map the dissociation pathways observed upon CID of these complexes including all TSs, intermediates, and products where $M^{2+} = Fe^{2+}$, Co^{2+}, Ni^{2+}, Cu^{2+}, and Zn^{2+} using the Gaussian 09 suite of programs.[20] The details of the theoretical calculations are given in Chapter 2. The vibrational frequencies and rotational constants determined at B3LYP/6-31G* and scaled by 0.9804 are listed in Tables E.1 and E.2 of Appendix E.[21]

E.5 Experimental Results

E.5.1 Cross Sections for Collision-Induced Dissociation

Preliminary energy-resolved CID studies of five $M^{2+}(Bpy)_2$ complexes using GIBMS techniques find that simple CID, ETCF, and PTCF pathways occur in parallel and compete with each other. Simple CID involves the loss of an intact neutral Bpy ligand, reactions E.1. ETCF results in the production of the $M^+(Bpy)$ and Bpy^+ ions corresponding to reduction of M^{2+} to M^+ and oxidation of the Bpy ligand to a radical cation, Bpy^+, respectively, reactions E.2. PTCF results in the formation of the $[M(Bpy-H)]^+$ and $[Bpy+H]^+$ product ions, corresponding to the transfer of a proton from one Bpy ligand to the other Bpy ligand facilitating charge fission dissociation, reactions E.3.

$$M^{2+}(Bpy)_2 + Xe \rightarrow M^{2+}(Bpy) + Bpy + Xe \quad (E.1)$$

$$M^{2+}(Bpy)_2 + Xe \rightarrow M^{+}(Bpy) + Bpy^{+} + Xe \quad (E.2)$$

$$M^{2+}(Bpy)_2 + Xe \rightarrow [M(Bpy\text{-}H)]^{+} + [Bpy+H]^{+} + Xe \quad (E.3)$$

Under low-resolution conditions, the $M^{+}(Bpy)$ and $[M(Bpy\text{-}H)]^{+}$ product ions originating from ETCF and PTCF pathways, respectively, and separated by 1 Da are found to be severely overlapped, particularly on the low m/z side. Similarly, severe overlap of the Bpy^{+} and $[Bpy+H]^{+}$ product ions, also separated by only 1 Da also occurs. Severe overlap of these same product ions was first observed for the $M^{2+}(Bpy)_3$ complexes discussed in Chapter 4. However, these species represent sequential dissociation products that were not examined for thermochemistry and thus the severe overlap was not problematic and thus ignored. Because the main objective of this chapter is to determine accurate thermochemistry for all three of the primary CID pathways, ETCF, PTCF, and simple CID, all of the products associated with these processes must be resolved and their pressure dependence must be examined. Preliminary kinetic energy dependent experimental CID cross sections obtained under low-resolution conditions for the interaction of Xe with five $M^{2+}(Bpy)_2$ complexes are shown in Figure E.1. Only the $M^{+}(Bpy)$, $[Bpy+H]^{+}$, and $M^{2+}(Bpy)$ product cross sections representing the ETCF, PTCF, and simple CID pathways, respectively are displayed. This is because the $M^{+}(Bpy)$ and $[M(Bpy\text{-}H)]^{+}$ as well as Bpy^{+} and $[Bpy+H]^{+}$ product ions are not cleanly resolved under the relatively low-resolution conditions under which these experiments were carried out. However, the species with the larger m/z is favored over the one with a smaller m/z as indicated by the larger cross section and lower apparent threshold. The $M^{+}(Bpy)$ and $[Bpy+H]^{+}$ products are least contaminated, and thus are expected to provide a more reliable measure of the energy dependence of the ETCF and PTCF pathway than the complementary

product ions, $[M(Bpy-H)]^+$ and Bpy^+, respectively. Because the overlapped products are not separated under low-resolution conditions these experiments will need to be repeated under higher-resolution conditions where all of the products of the primary dissociation pathways, ETCF, PTCF, and simple CID are resolved in the future. As can be seen in Figure E.1, the $M^{2+}(Bpy)$ product cross sections, reactions E.1, exhibit slightly different shapes and decrease in magnitude across the period vary from ~2.5 $Å^2$ for Fe^{2+} to 0.1 $Å^2$ for Zn^{2+}. In contrast, the apparent thresholds for $M^{2+}(Bpy)$ vary between ~3–8 eV and increase from Fe^{2+} to Co^{2+} to Ni^{2+} to Cu^{2+}, and then decrease for Zn^{2+}. In comparison, the $M^+(Bpy)$, product cross sections, reactions E.2, have similar shapes and increase in magnitude across the period from Fe^{2+} to Co^{2+} to Ni^{2+} to Cu^{2+} and then decrease for Zn^{2+}. The apparent thresholds for $M^+(Bpy)$ product cross sections generally follow the reverse trend and vary from ~2.0–7.0 eV, whereas the maximum cross section magnitudes vary from ~4 to 7 $Å^2$. Similarly, the $[Bpy+H]^+$ product cross sections, reactions E.3, slightly increase in magnitude from ~0.4 $Å^2$ for Fe^{2+} to ~1.2 $Å^2$ for Cu^{2+}, and then decrease to ~0.5 $Å^2$ for Zn^{2+}, whereas the apparent thresholds follow the reverse order, and vary from ~4.0–7.8 eV. Sequential dissociation through loss of a C_5H_5N moiety at elevated energies is observed for all of the $M^{2+}(Bpy)_2$ complexes.

E.5.2 Product Ions in MS Spectra

The MS spectra of five $M^{2+}(Bpy)_2$ complexes, where M^{2+} = Fe^{2+}, Co^{2+}, Ni^{2+}, Cu^{2+}, and Zn^{2+} obtained using the FTICR-MS are shown in Figure E.2. Four types of product ions are obtained from fragmentation of the $M^{2+}(Bpy)_2$ complexes. The $M^{2+}(Bpy)$ product ions arise from loss of a neutral Bpy ligand, reactions E.1. The $M^+(Bpy)$ and Bpy^+ product ions arise from ETCF, reactions E.2. The $[M(Bpy–H)]^+$ and $[Bpy+H]^+$ product ions arise from

PTCF, reactions E.3. Dehydrogenation, reactions E.4, results in loss of a hydrogen molecule from the reactant ion. Sequential dissociation through neutral loss of small molecules such as HCN, C_2, H, C_5H_5N, CN, C_2H_2, CH_4, CH_3, C_2H_7N, or C_3H_3N from either one or both of the complementary ions of the four major dissociation pathways is also observed.

$$M^{2+}(Bpy)_2 + Ar \rightarrow [M(Bpy)_2\text{–}H_2]^{2+} + H_2 + Ar \qquad (E.4)$$

Therefore, high-resolution FT-ICR MS results not only confirm the presence of $M^+(Bpy)$ and $[M(Bpy\text{-}H)]^+$ as well as the complimentary Bpy^+ and $[Bpy+H]^+$ products that are separated by 1 Da, but also shows that these ions are well separated. In addition, these results also indicate that dehydrogenation is also a minor CID pathway for these systems.

E.6 Theoretical Results

Preliminary theoretical studies are carried out using the B3LYP, BHandHLYP, and M06 levels of theory to support and enhance the experimental studies. The four major pathways observed upon CID of the $M^{2+}(Bpy)_2$ complexes include: simple CID (reactions E.1), ETCF (reactions E.2), PTCF (reactions E.3), and dehydrogenation (reactions E.4). Based on the high resolution FT-ICR MS results, the hydrogen loss pathways are minor. However, even a very small contamination of the reactant $M^{2+}(Bpy)_2$ complexes by these products can influence the threshold determinations, particularly if these pathways are lower in energy than the ETCF, PTCF, and simple CID pathways. The mechanisms associated with the dehydrogenation pathway are not modeled theoretically in the present work. Because we have no idea at this point if the hydrogen loss pathways are higher or lower energy pathways, we would like to point out that these pathways will need to be modeled in the future to accurately elucidate the energetics involved in the dissociation of the $M^{2+}(Bpy)_2$ complexes. In the case of the simple CID pathway, where the TSs are

assumed to be loose and product-like because the interactions between the M^{2+}(Bpy) complex and the departing Bpy ligand are largely electrostatic, the molecular parameters of the products are used for data analysis, and therefore no potential energy surfaces need be mapped as the reactant and products are already computed to extract the sequential BDEs. Because the ETCF and PTCF pathways are activated dissociation pathways, the mechanisms of electron and proton transfer are examined to determine molecular parameters of the rate-limiting TSs in allow appropriate thermochemical analysis of the experimentally measured cross sections. For the ETCF pathway, the only plausible mechanisms we've imagined involves the electron hopping from one of the Bpy ligands to the M^{2+}(Bpy) moiety as they separate, producing the Bpy^{+} and M^{+}(Bpy) products. The challenge in mapping this mechanism is associated with the density of the electron that is transferred being delocalized over the dissociating complex until the critical M^{+}(Bpy)−bpy^{+} distance is achieved and the electron "hops", as such delocalization is harder to describe with a limited number of basis functions. For the PTCF pathways, the mechanisms mapped involve two proton transfers, the first from one of the Bpy ligands to the metal center, and the second from the metal center to the other bpy ligand, followed by dissociation to the products. These PTCF pathways exhibit relatively high barriers such that other mechanisms with lower barriers may exist, such as direct insertion of the proton transferred into the M^{2+}−N bond. Therefore, the mechanisms of electron and proton transfer discussed in the following sections are only preliminary, and calculations at higher levels of theory may be needed for to accurately describe the energetics of the ETCF pathways, whereas additional activated dissociation pathways and higher level calculations may need to be considered for the PTCF pathways in the future.

Theoretical structures for the ground state reactants, TSs, intermediates, and products of the activated dissociation of the $M^{2+}(Bpy)_2$ complexes were calculated as described in section E.4. Further details can be found in Chapter 2. The PES landscapes including both optimized structures and the corresponding relative energies of the species involved in the activated dissociation via ETCF and PTCF of the $M^{2+}(Bpy)_2$ complexes are shown in Figures E.3 and E.4, respectively. Important geometrical parameters of the B3LYP/6-31G* optimized geometries of the $M^{2+}(Bpy)_2$ reactants, TSs, intermediates, and products involved in the dissociation of $M^{2+}(Bpy)_2$ complexes through ETCF and PTCF processes are shown in Tables E.3 and E.4 of Appendix E. Cartesian coordinates for each of these structures are listed in Table E.5 of Appendix E. Relative energies for these species are listed in Tables E.6 and E.7 of Appendix E for ETCF and PTCF, respectively.

E.6.1 Ground State $M^{2+}(Bpy)_2$ Complexes

The ground-state structures and geometrical parameters of the $M^{2+}(Bpy)_2$ complexes have been reported previously.[19] Briefly, the metal cation binds to the lone pairs of the four nitrogen atoms of the two Bpy ligands resulting in distorted tetrahedral coordination geometry around the metal cation. The individual aromatic rings of each Bpy ligands lie in the same plane such that the ∠NCCN dihedral angles are 0.0°, and the two Bpy ligands are almost perpendicular to each other with ∠NM^{2+}NC dihedral angles of ~84.0° in all of the $M^{2+}(Bpy)_2$ complexes, except for $Cu^{2+}(Bpy)_2$ where the ∠NCCN angle is ~55.9°. This difference in the geometry arises as a result of Jahn-Teller distortion by which the copper complex is able to minimize Pauli repulsion between the metal cation and Bpy ligands by adopting a geometry that is distorted toward square planar.

E.6.2 Activated Dissociation of $M^{2+}(Bpy)_2$ via ETCF

For the ETCF processes, two TSs that connect the reactants and the products were located for all five $M^{2+}(Bpy)_2$ complexes based on the proposed electron hopping mechanism. Figure E.3 shows the activated dissociation of the $M^{2+}(Bpy)_2$ complexes along the ETCF pathways. Also shown in the figures is the energy barrier for simple CID corresponding to loss of the neutral Bpy ligand, which occurs at ~500 kJ/mol (B3LYP theory). This large barrier indicates a low accessibility for this reaction. Table E.3 lists important geometrical parameters for these complexes. As can be seen in Figure E.3b, the first step along the reaction coordinate of the proposed mechanism for ETCF of the $Co^{2+}(Bpy)_2$ complex to form $Co^{2+}(Bpy)$ and Bpy^+ products involves rotation of one of the pyridyl moieties about the central C–C bond of one of the Bpy ligands. In the reactant, both Bpy ligands are attached to the Co^{2+} metal center resulting in a *cis* conformation where the two nitrogen atoms of each Bpy ligand are located on the same side of the central C–C bond. Upon lengthening of the Co^{2+}–N2′ bond distance, the C–C central bond of the pyridyl moiety of the Bpy ligand still bound to the Co^{2+} center through N2 rotates via TS_1 to produce Int_1. In this process, the ∠N2CCN2′ dihedral angle increases from 0.1° in the reactant to 94.7° in TS_1 and increases further to 137.6° in Int_1. The calculated reaction barrier for this TS is 155.6 kJ/mol (B3LYP theory). The second step involves electron transfer from one of the Bpy ligands to the metal cation Co^{2+} resulting in oxidation of the Bpy ligand to the Bpy^+ radical cation, and reduction of Co^{2+} to Co^+, which is accompanied by an increase in the separation between the ionized Bpy ligand and the reduced $Co^+(Bpy)$ complex via TS_2 producing Int_2. The calculated reaction barrier of TS_2 is 276.8 kJ/mol (B3LYP theory). The structural changes facilitating this dissociation involve major changes in inter- and intra-

∠NCo^{2+}N bond angles as shown in Table E.3a. The ∠N2″Co^{2+}N2C2 dihedral angle changes significantly from 72.8° in Int_1 to 64.2° in TS_2, and finally to 84.1° in Int_2 during the ETCF process. The Co^{2+}–N2 and Co^{2+}–N2′ bond distances undergo significant lengthening from 2.595 and 4.149 Å in TS_2 to 9.776 and 12.81 Å in Int_2, respectively. In TS_2, the two nitrogen atoms of one Bpy ligand are located on opposite sides of the C–C central bond. The ∠N2CCN2′ dihedral angle changes significantly from 137.6° in Int_1 to 168.7° in TS_2, whereas the ∠N2″CCN2‴ dihedral angle undergoes very little change. The TS_2 structure also shows the Co^{2+} cation interacting with the other Bpy ligand through cation π interactions. The lengthening of the Co^{2+}–N2′ bond distance of Int_2 smoothly dissociates into the Bpy^{+} and Co^{+}(Bpy) products. The activated dissociation pathways of the M^{2+}(Bpy)$_2$ complexes to Fe^{2+}, Ni^{2+}, Cu^{2+}, and Zn^{2+} exhibit similar behavior. The reaction barrier for the central C–C bond rotation process (TS_1) is relatively low in energy as compared to TS_2 for all five M^{2+}(Bpy)$_2$ complexes and is 143.6, 155.6, 155.8, 145.9, and 144.1 kJ/mol (B3LYP theory) for Fe^{2+}, Co^{2+}, Ni^{2+}, Cu^{2+}, and Zn^{2+} complexes, respectively. Hence TS_2 is the rate-limiting TS. The calculated reaction barriers for electron transfer (TS_2) of the M^{2+}(Bpy)$_2$ complexes decrease from Fe^{2+} (354.5) to Co^{2+} (276.8) to Ni^{2+} (254.4) to Cu^{2+} (241.6), and then increase for Zn^{2+} (315.4) kJ/mol. The energy barriers for loss of a neutral Bpy ligand exceed 500 kJ/mol at the B3LYP level of theory, which makes this reaction pathway unfavorable for all five M^{2+}(Bpy)$_2$ complexes. In comparison to B3LYP, BHandHLYP and M06 levels of theory give very similar shapes for the PES landscapes for all of the M^{2+}(Bpy)$_2$ complexes. The ETCF barriers are largest for BHandHLYP theory, the lowest for M06, whereas B3LYP theory provides barriers that are intermediate between BHandHLYP and M06.

E.6.3 Activated Dissociation of $M^{2+}(Bpy)_2$ Complexes to Fe^{2+}, Ni^{2+}, and Cu^{2+} via PTCF

The PES for PTCF of the $M^{2+}(Bpy)_2$ complexes to Fe^{2+}, Ni^{2+}, and Cu^{2+} exhibit three barriers along the reaction coordinate. TSs that connects reactants to products based on the one mechanism considered thus far. The activated dissociation of the Fe^{2+}, Ni^{2+}, and Cu^{2+} complexes along the PTCF pathway are highly parallel and are shown in Figures E.4a, E.4c, and E.4d, respectively. Table E.4 lists important geometrical parameters for the relevant species. As can be seen in Figure E.4d, the first step along the reaction coordinate of the $Cu^{2+}(Bpy)_2$ complex involves PT from C3″ to the Cu^{2+} cation via TS_1 to produce Int_1. The reaction barrier for this process (TS_1) is 437.9 kJ/mol at B3LYP theory. The Bpy ligands twist relative to each other to facilitate the proton transfer as indicated by the major changes in the inter ∠$NCu^{2+}N$ bond angles (see Table E.4d). The resulting Int_1 is less stable than the $Cu^{2+}(Bpy)_2$ reactant by 389.7 kJ/mol. The second step also involves PT from Cu^{2+} to the N2 atom of the other Bpy ligand via TS_2. The reaction barrier for this process is 402.5 kJ/mol. The third step involves the lengthening of the Cu^{2+}–N2′ bond and twisting of the Bpy ligands via TS_3 producing an ion-dipole bound complex of the $[Bpy+H]^+$ and $[Cu(Bpy-H)]^+$ Coulombic fission products. The reaction barrier for this process (TS_3) is 313.3 kJ/mol at B3LYP theory, relatively lower than TS_1 and TS_2 by 124.6 and 89.2 kJ/mol, respectively. Further lengthening of the Cu^{2+}–N2′ bond of Int_3 leads to smooth dissociation into the $[Cu(Bpy-H)]^+$ and $[Bpy+H]^+$ products. The PTCF activated dissociation pathways of the $M^{2+}(Bpy)_2$ complexes to Fe^{2+} and Ni^{2+} exhibit similar behavior to that of Cu^{2+}. The calculated reaction barriers for PTCF follow the order Ni^{2+} (406.7) < Cu^{2+} (437.9) < Fe^{2+} (459.2) kJ/mol, at the B3LYP level of theory. In comparison to B3LYP theory, BHandHLYP and M06 levels of theory give very parallel shapes for the PES landscapes of

Fe^{2+}, Ni^{2+}, and Cu^{2+}, with M06 providing the lowest energy barriers for PTCF, whereas B3LYP is intermediate, and BHandHLYP the most energetic. All three levels of theory agree that TS_1 is the rate-limiting TS for $Cu^{2+}(Bpy)_2$ and $Ni^{2+}(Bpy)_2$, whereas TS_2 is the rate-limiting TS for $Fe^{2+}(Bpy)_2$. Most significantly the PTCF AE is larger than the enthalpy of dissociation for $M^{2+}(Bpy)_2$ complexes to Fe^{2+}, Ni^{2+}, and Cu^{2+} at all the three levels of theory.

E.6.4 Activated Dissociation of $M^{2+}(Bpy)_2$ Complexes to Co^{2+} and Zn^{2+} via PTCF

The PESs for PTCF of the $M^{2+}(Bpy)_2$ complexes to Co^{2+} and Zn^{2+} exhibit four barriers along the reaction coordinate. Figure E.4 parts b and e show the activated dissociation of the $Co^{2+}(Bpy)_2$ and $Zn^{2+}(Bpy)_2$ complexes along the PTCF pathways. As can be seen in the figures, the observed behavior is very parallel. Tables E.4, parts b and e list important geometrical parameters of these complexes. As can be seen in Figure E.4b, the first step along the reaction coordinate of the $Co^{2+}(Bpy)_2$ complex involves PT from C3 to N2 of one of the Bpy ligands via TS_1 to produce Int_1. The excess proton is stabilized between C3 and N2 (TS_1) and the reaction barrier for this process is 441.9 kJ/mol at B3LYP theory. The Bpy ligands tilt relative to each other as indicated by slight changes in the $\angle N2Co^{2+}N2'''C2'''$ and inter $\angle NCo^{2+}N$ bond angles whereas the $\angle N2CCN2'$ dihedral angles change from 0.0° to 18.2° to facilitate PT. The resulting intermediate (Int_1) is less stable than the $Co^{2+}(Bpy)_2$ reactant by 349.5 kJ/mol at the B3LYP level of theory. The next step involves the migration of the proton from the N2 position to the Co^{2+} cation with the proton being potentially stabilized between the N2 and the Co^{2+} cation (TS_2). During this PT step, the Bpy ligands tilt away from each other as indicated by changes in the $\angle NCo^{2+}N$ bond angles to accommodate the excess proton. The calculated barrier for this process is 437.2 kJ/mol (B3LYP). In the third step, the proton migrates from the Co^{2+} cation to the N2″

position of the other Bpy ligand via TS_3 facilitating PT. The Co^{2+}–H3 bond distance, ∠N2Co^{2+}N2‴C2‴ dihedral angles, and ∠NCo^{2+}N bond angles of the Int_2, TS_3, and Int_3 species change significantly (see Table E.4b) to facilitate the PT. The barrier for this process (TS_3) is 437.8 kJ/mol at the B3LYP level of theory. The fourth step involves the lengthening of the Co^{2+}–N2‴ bond and twisting of the Bpy ligands via TS_4 to form an ion-dipole bound complex of the $[Co(Bpy\text{-}H)]^+$ and $[Bpy+H]^+$ Coulombic products. The barrier to this reaction process (TS_4) is 438.9 kJ/mol (B3LYP). As the Co^{2+}–N2‴ bond distance increases, Int_4 smoothly dissociates into the $[Co(Bpy\text{-}H)]^+$ and $[Bpy+H]^+$ products without any barrier. The PTCF activated dissociation pathway of the $Co^{2+}(Bpy)_2$ complex is highly parallel to that of $Zn^{2+}(Bpy)_2$. The calculated reaction barrier for PTCF of $Co^{2+}(Bpy)_2$ is lower than that of $Zn^{2+}(Bpy)_2$ by only 6.8 kJ/mol at B3LYP theory. The shapes of the PES landscapes of $Co^{2+}(Bpy)_2$ and $Zn^{2+}(Bpy)_2$ are highly parallel for all three levels of theory. In both cases, BHandHLYP predicts the barrier to PTCF, M06 the lowest, whereas B3LYP is intermediate. All the three levels of theory find that TS_1 is the rate-limiting TS for both Co^{2+} and Zn^{2+} complexes. Most significantly the PTCF AE is larger than the enthalpy of dissociation for both complexes at all three levels of theory.

E.7 Threshold Analysis

CID of the $M^{2+}(Bpy)_2$ complexes displays a variety of pathways including ETCF, PTCF, simple CID, and dehydrogenation. Under low resolution conditions the overlapping products of the ETCF and PTCF pathways separated by 1 Da (i.e. $M^+(Bpy)$ and $[M(Bpy\text{-}H)]^+$ as well as the Bpy^+ and $[Bpy+H]^+$) are not resolved. Likewise, the reactants and dehydrogenation products ($M^{2+}(Bpy)_2$ and $[M(Bpy)_2–H_2]^{2+}$ are not resolved under these conditions. Because of contamination in the measured product ion intensities and computed

product cross sections, the ETCF and PTCF product cross sections do not describe the true energy dependence of the data. However, to extract approximate thresholds and relatively accurate cross sectional magnitudes, the $[M(Bpy-H)]^+$ product cross sections of the PTCF pathway are discarded as they are severely contaminated by the $M^+(Bpy)$ product of the ETCF pathway, whereas the $M^+(Bpy)$ product cross sections are measured relatively cleanly such that they are more reliable as they are the least contaminated. Because the Bpy^+ and $[Bpy-H]^+$ product cross section were only collected under high pressure conditions, the pressure dependence of these product cross sections cannot be established. In addition, these products are severely overlapped in comparison to the $M^+(Bpy)$ and $[M(Bpy-H)]^+$ products, and therefore are not included in the preliminary threshold analyses performed here. The dehydrogenation products are not considered in the threshold analyses either as they were not collected in the experiments. Without the inclusion of these pathways in the threshold analyses, the threshold determinations are biased. As a result of these limitations in the data, preliminary threshold analyses are performed for the $M^+(Bpy)$ and $M^{2+}(Bpy)$ product cross sections, which originate from the ETCF and simple CID pathways, respectively as discussed below. In the future, threshold analyses of the products of the $M^{2+}(Bpy)_2$ complexes collected and examined under higher-resolution conditions must be performed to extract accurate thermochemistry for the dissociation of these $M^{2+}(Bpy)_2$ complexes.

The model of equation 2.4 was used to independently analyze the thresholds for $M^{2+}(Bpy)$ and $M^+(Bpy)$ product cross sections for all five $M^{2+}(Bpy)_2$ complexes. The results of these analyses are provided in Table E.8. Fits to the CID cross sections for the $M^{2+}(Bpy)_2$ complexes are shown in Figure E.5. In all cases, the experimental cross sections for $M^{2+}(Bpy)$ simple CID are accurately reproduced using a loose PSL TS model.[17] Previous

work has shown that this model provides the most accurate assessment of the kinetic shifts for CID processes of electrostatically bound ion-molecule complexes.[17,22] The experimental cross sections for M^+(Bpy) product, ETCF, are modeled using the molecular parameters of the rate-limiting TSs found along the activated dissociation pathways. Table E.8 also lists threshold values, E_0, obtained without including the RRKM lifetime analysis. Comparison of these values with the E_0(PSL) values shows that the kinetic shifts vary from 3.88−5.04 eV for fits to the M^{2+}(Bpy) product cross sections (reaction E.1), whereas the kinetic shifts for the E_0(TTS) thresholds vary from 5.18−8.08 eV for fits to the M^+(Bpy) product cross sections (reaction E.2).

For all five $M^{2+}(Bpy)_2$ complexes, competition between M^{2+}(Bpy) and M^+(Bpy) occurs and is expected to influence the threshold determinations. Thus, the cross sections for these products are analyzed simultaneously using the model of equation 2.5 (using a loose PSL TS for reaction E.1 and the molecular parameters of the rate-limiting ETCF TS for reaction E.2) and are shown in Figure E.6. The results of these analyses are provided in Table E.9. The (Bpy)M^{2+}−Bpy BDEs obtained from competitive fits are smaller than the values obtained from independent fits, as expected, and are a consequence of the competition among these reaction channels. The AEs extracted for the ETCF pathways from competitive fitting are affected very little as compared to the threshold determined from independent analyses of these product cross sections as these pathways are low in energy than simple CID. The (Bpy)M^{2+}−Bpy BDEs obtained from independent fits are larger than the AEs for ETCF obtained from independent fits. In contrast, the threshold energies extracted from competitive analyses exhibit very different energetics. The (Bpy)M^{2+}−Bpy BDEs are lower than the ETCF AEs by 60.5 and 38.3 kJ/mol for Fe^{2+} and Co^{2+} complexes, respectively,

consistent with simple CID being the lowest energy pathway. For the $M^{2+}(Bpy)_2$ complexes to Ni^{2+} and Cu^{2+}, the $(Bpy)M^{2+}$−Bpy BDEs exceed the AEs for ETCF by 47.4 and 94.2 kJ/mol, respectively, consistent with simple CID being the highest energy pathway for these complexes. The $(Bpy)Zn^{2+}$−Bpy BDE is lower than the AE for ETCF by only 9.6 kJ/mol, consistent with the fact that these two dissociation pathways exhibit very similar apparent thresholds. Comparison of the results obtained for the competitive and independent analyses allow the competitive shifts to be preliminarily assessed. The competitive shifts for the $(Bpy)M^{2+}$−Bpy BDEs vary from −1.22 to −0.51 eV in better accord with expectations. The competitive shifts vary from 0.01 to 0.07 eV for the ETCF AEs. Independent fits to the $M^+(Bpy)$ product cross section led to lower AEs for ETCF for all $M^{2+}(Bpy)_2$ complexes. However, the differences in thresholds between independent and competitive fits are within experimental error.

The entropy of activation, $\Delta S^{\dagger}$ is a measure of the looseness or tightness of the TS and is also a reflection of the complexity of the system. It is largely determined by the molecular parameters used to model the energized molecule and the TS for dissociation but also depends upon the threshold energy. The $\Delta S^{\dagger}$(PSL) values at 1000 K for reaction E.1 vary from −78.0 to 102.0 J K^{-1} mol^{-1} whereas the $\Delta S^{\dagger}$(TS) values at 1000 K for reaction E.2 vary from −3.3 to 12.0 J K^{-1} mol^{-1} (see Tables E.8−E.9).

E.8 Discussion

E.8.1 Comparison between Experiment and Theory

Comparison between experimental and theoretical values extracted from dissociation of the $M^{2+}(Bpy)_2$ complexes is one way to test the validity of theoretical methods used. However, the challenges and limitations encountered in the study of $M^{2+}(Bpy)_2$ complexes

limit the reliability of such comparisons. The AEs and the BDEs extracted from the ETCF and simple CID pathways, respectively, are only preliminary and most likely represent upper bounds to the true thresholds. In the case of the ETCF pathways, the $M^+(Bpy)$ products are slightly contaminated by the $[M(Bpy-H)]^+$ products, and therefore the approximate AEs extracted could be too low. Furthermore, the PTCF pathway is ignored during the competitive data analyses, and this may also lead to low threshold values for the ETCF and CID pathways. The AEs derived for ETCF and PTCF pathways from theoretical methods are also preliminary. Theory suggests that the AEs for PTCF are much higher than for the ETCF pathway, whereas experimental data suggest that PTCF is the lowest energy pathway. Therefore, the PESs mapped out for the PTCF pathway are probably not the correct pathways followed in the reactions at low energies, and alternative lower energy pathways must then be available such that these theoretical results likely represent upper bounds to the true AEs for PTCF of the $M^{2+}(Bpy)_2$ complexes. The electron and proton transfer processes deal with open shell systems in terms of the reactants, TSs, intermediates and some of the products. Theoretical methods are not as reliable for describing such species as compared to closed shell species.[23-25] To extract highly reliable energetics from theory, calculations using more advanced theories with much larger basis sets may need to be performed. However, these are not easy systems to calculate at higher levels of theory given the size and therefore number of electrons involved and at present is beyond the capabilities of our computational resources. Hence, without more reliable experimental data, the validity of theoretical results cannot be established. Therefore, experimental and theoretical studies involving the $M^{2+}(Bpy)_2$ complexes considered thus far are preliminary, and additional experiments performed under higher-resolution conditions are needed. In addition, other mechanisms for the PTCF

activated dissociation pathways must be considered in order to accurately determine the energetics of PTCF of the $M^{2+}(Bpy)_2$ complexes. Hence, the comparisons discussed below must be handled with caution due to the limitations discussed above.

BDEs for reaction E.1, simple CID, for all five $M^{2+}(Bpy)_2$ complexes including independent ZPE and BSSE corrections are listed in Tables E.10. Also listed in Table E.10 are the AEs for reactions E.2, ETCF, and corrected for ZPEs. Table E.11 lists the enthalpic and entropic corrections to convert the 0 K reaction enthalpies and free energies to 298 K. The agreement between the TCID measured values and theoretically determined values is illustrated in Figure E.7. The trends in the TCID measured and theoretically calculated AEs for ETCF AEs determined at the M06, B3LYP, and BHandHLYP levels of theory are similar across the series of transition metal cations examined, which decrease from Fe^{2+} to Cu^{2+} and then increase for the complex to Zn^{2+} (see Figure E.7, part a). The measured AEs for ETCF for the $M^{2+}(Bpy)_2$ complexes to Co^{2+} and Cu^{2+} exhibit good agreement with M06 theory. In contrast, the values calculated for the complexes to Fe^{2+}, Ni^{2+}, and Zn^{2+} differ markedly for the measured AEs. The mean absolute deviation (MAD) between M06 theory and experiment for all the five complexes is 33.6 ± 27.1 kJ/mol, much larger than the absolute experimental uncertainty (AEU), 8.9 ± 1.0 kJ/mol in these values. When Fe^{2+}, Ni^{2+}, and Zn^{2+} complexes are not included the MAD reduces to 7.4 ± 1.8 kJ/mol, slightly lower than the AEU. The measured AEs for ETCF for the Ni^{2+} and Cu^{2+} complexes exhibits good agreement with B3LYP theory whereas the calculated value for Co^{2+} complex lies just outside of experimental error. Again, the ETCF AEs computed for the complexes to Fe^{2+} and Zn^{2+} exhibit the largest deviation from the measured value. The MAD for all the five complexes is 33.7 ± 35.8 kJ/mol, again much larger than the AEU. The Fe^{2+} and Zn^{2+}

complexes are the dominant contributors to this MAD. If these systems are not included the MAD decreases to 7.7 ± 4.8 kJ/mol, much closer to the AEU. The AEs for ETCF computed using BHandHLYP theory are systematically higher than the values obtained using M06 and B3LYP theories by ~29.0 kJ/mol. However, the measured AE for ETCF of $Ni^{2+}(Bpy)_2$ exhibits fairly good agreement with BHandHLYP theory. In contrast, the values calculated for the complexes to Fe^{2+}, Co^{2+}, Cu^{2+}, and Zn^{2+} differ markedly for the measured AEs. The MAD between BHandHLYP theory and the TCID measured value is 62.6 ± 37.2 kJ/mol, significantly larger than the AEU. Generally, the MADS for the $M^{2+}(Bpy)_2$ complexes are very large compared to the AEUs suggesting that all three levels of theories are not able to describe the ETCF AEs effectively for most of the complexes. This poor agreement may be the result of not including the PTCF pathway in the thermochemical analyses, or may be a result of limitations in the level of the theories employed, or both.

The ionization energy of Bpy ligand is calculated to be 8.30, 8.25, and 8.60 eV at B3LYP, BHandHLYP, and M06 levels of theory, respectively. Compared to literature value, 8.35 ± 0.02 eV, theory and experimental IEs are in good agreement.[26] This result suggests that theory might be having a hard time accurately determining the ETCF AEs of the $M^{2+}(Bpy)_2$ systems because of their large size coupled with the presence of open shell d orbitals of the metal cations.

The second sequential $(Bpy)M^{2+}$–Bpy BDEs theoretically determined using M06, BHandHLYP, and B3LYP levels of theory are systematically higher than the TCID measured values in all the $M^{2+}(Bpy)_2$ complexes (see Figure E.7, part b). M06 theory estimates the strongest BDEs for all the $M^{2+}(Bpy)_2$ complexes. The MAD between M06 theory and TCID experiment is 291.3 ± 63.9 kJ/mol, much larger than the AEU, 27.6 ± 3.6

kJ/mol. B3LYP theory estimates the weakest BDEs compared to those obtained from BHandHLYP and M06 for Co^{2+}, Cu^{2+}, and Zn^{2+} complexes. The MAD between B3LYP theory and TCID experiment is 268.0 ± 59.6 kJ/mol for all five complexes, significantly higher than the AEU. BHandHLYP provides BDEs that are intermediate between those obtained from B3LYP and M06 theories for Co^{2+}, Cu^{2+}, and Zn^{2+} complexes but estimates the lowest BDEs for Fe^{2+} and Ni^{2+} complexes. The MAD between BHandHLYP theory and TCID experiment is 270.9 ± 58.6 kJ/mol, significantly higher than the AEU. The large difference between the calculated and the measured BDEs indicates that providing an accurate description of the energetics for the dissociation of the $M^{2+}(Bpy)_2$ complexes to produce $M^{2+}(Bpy)$ and neutral Bpy ligand may still be quite challenging at the B3LYP, BHandHLYP, and M06 levels of theory. However, the lack of consideration of the PTCF pathway during competitive data analyses probably contributes significantly to the lower TCID BDEs.

E.8.2 Energetics of Fragmentation Processes of the $M^{2+}(Bpy)_2$ Complexes

E.8.2.1 ETCF Pathway

Only energetics associated with the ETCF and simple CID pathways are included in this discussion for reasons already discussed in the previous sections. Preliminary results illustrate that the AEs for ETCF of the $M^{2+}(Bpy)_2$ complexes decrease from Fe^{2+} (283.3) to Co^{2+} (263.6) to Ni^{2+} (258.5) to Cu^{2+} (235.8), and increase for Zn^{2+} (241.3) kJ/mol (see Figure E.7, part a). These results suggest that among the systems investigated here, ETCF is most favorable for the $Cu^{2+}(Bpy)_2$ complex. Factors contributing to the electron transfer processes in $M^{2+}(Bpy)_2$ complexes include: the ionization energies of the transition metals

and the Bpy ligand, the ionic radii of the metal cation, and the electronic configuration of the metal cation.

Previous studies have found that electron transfer from a ligand to a metal cation upon CID occurs only if the IE of the ligand is lower than the second IE of the metal cation.[27-29] Because the IE of Bpy (8.35 eV) is lower than the IE of Fe^+ (16.19), Co^+ (17.08), Ni^+ (18.17), Cu^+ (20.29), and Zn^+ (17.96) eV, electron transfer is observed for all of the $M^{2+}(Bpy)_2$ complexes, as expected.[26] The possibility of an electron originating from the neutral reactant is ruled out as the IE of Xe (12.13 eV) is much higher than that of Bpy and is confirmed by the absence of a Xe radical cation at m/z 132.0, indicating that the Bpy ligand is the only source of electrons for the reduction process. The efficiency of the ET process is given by the magnitude of the difference in the respective IEs, i.e., $\Delta IE = IE(M^+) - IE(Bpy)$.[27,28,29] The larger the difference the more efficient the ET process for that complex. This difference increases from Fe^{2+} (7.84) to Co^{2+} (8.73) to Ni^{2+} (9.82) to Cu^{2+} (11.94), and decreases for Zn^{2+} (9.61) eV, and is inversely related to the AEs for ETCF of the $M^{2+}(Bpy)_2$ complexes, as expected. The ET process also becomes more favorable as the size, ionic radii of the metal cation, decreases: Fe^{2+} (0.76), Co^{2+} (0.74), Ni^{2+} (0.73), and Cu^{2+} (0.72) Å, as observed. This is because the decrease in ionic radii increases the electrostatic interactions enabling a closer approach between the Bpy ligand and the metal cation. Zn^{2+} with an ionic radius of 0.72 Å deviates from this trend as its ionic radius is same as Cu^{2+} but the AE for ETCF of $Zn^{2+}(Bpy)_2$ is slightly higher than that of $Cu^{2+}(Bpy)_2$ due to an increase in Pauli repulsion between the Zn^+ cation and the coordinated Bpy ligand as its 4s orbital is occupied in the ET process. The electronic configuration of the metal cation also plays part in the ETCF of the $M^{2+}(Bpy)_2$ complexes. The $Cu^{2+}(Bpy)_2$ complex favors electron transfer more

than the other complexes because the reduction of the Cu^{2+} ($3d^9$) cation in the complex leads to a closed-shell Cu^+ ($3d^{10}$) complex, that is more stable than the analogous open shell Fe^+ ($3d^6\ 4s^1$), Co^+ ($3d^8$), Ni^+ ($3d^9$) and Zn^+ ($3d^{10}\ 4s^1$) counterparts. Compared to Co^{2+} and Ni^{2+} complexes, ET is much less favorable for the complex to Fe^{2+} as in the case for Zn^{2+} complex because of increase in Pauli repulsion between the electrons of these M^+ cations and the coordinated Bpy ligand that prevents attractive binding interactions with the metal 4s electrons.

E.8.2.2 Simple CID Pathway

The second sequential $(Bpy)M^{2+}$–Bpy BDEs of the $M^{2+}(Bpy)_2$ complexes determined experimentally follow the order $Fe^{2+} < Co^{2+} < Ni^{2+} < Cu^{2+} > Zn^{2+}$ as shown in Figure E.7, part b. There is a clear inverse relationship between the ionic radii of the M^{2+} cation and BDEs of these metal complexes, reflecting the increasing effective charge of the metal cation as the size of the metal cation decreases thereby increasing the strength of the electrostatic interactions between the M^{2+} cation and the Bpy ligand. The trend in the TCID measured BDEs is not parallel to the trends observed for B3LYP, BHandHLYP, M06 theoretical methods. Apart from the theoretical methods overestimating the BDEs of $M^{2+}(Bpy)_2$ complexes, differences in the trends are not straightforward to assess.

E.8.3 Comparison between $M^{2+}(Bpy)_x$ and $M^{2+}(Phen)_x$ Complexes

E.8.3.1 Relative Energies of the PES

The activated dissociation of all five $M^{2+}(Bpy)_2$ complexes along the ETCF pathways display two TSs that connect the reactant to the products. In contrast, only one TS is located for all the $M^{2+}(Phen)_2$ complexes (see Appendix D). The first TS located on the PES of the $M^{2+}(Bpy)_2$ complexes involves the rotation of the central C–C bond of a Bpy ligand, while

the other Bpy ligand is still attached to the M^{2+} cation facilitating release of the Bpy^{+} ligand during the ET process. Absence of the rotation of the central C−C bond in the $M^{2+}(Phen)_2$ complexes is due to the rigidness of the Phen ligand. The calculated reaction barrier for ETCF of all of the $M^{2+}(Bpy)_2$ complexes is lower than that of the analogous $M^{2+}(Phen)_2$ complexes by < 20 kJ/mol at the B3LYP theory. BHandHLYP and M06 theories show similar results. The PES for the PTCF processes of all the $M^{2+}(Bpy)_2$ complexes are highly parallel to those of the analogous $M^{2+}(Phen)_2$ complexes. The theoretical reaction barriers for PTCF of all the $M^{2+}(Bpy)_2$ complexes are lower than those of the analogous $M^{2+}(Phen)_2$ complexes by < 15 kJ/mol at the B3LYP theory. BHandHLYP and M06 theories show similar results.

E.8.3.2 Fragmentation Patterns

The CID patterns of the tris-complexes, $M^{2+}(N\text{-}L)_3$ where *N*-*L* = Bpy or Phen, and $M^{2+} = Fe^{2+}$, Co^{2+}, Ni^{2+}, Cu^{2+}, and Zn^{2+} follow a very uniform dissociation pathway in which the principal process is the loss of an intact Bpy or Phen ligand regardless of the electron configuration of the metal cation. In contrast, the CID patterns of the bis-complexes, $M^{2+}(N\text{-}L)_2$ show a much more diverse array of fragmentation pathways including ETCF, PTCF, simple CID, and dehydrogenation that occur in competition. The degree of competition between the four processes in the bis-complexes varies depending on the electronic configuration of the metal cation. The tris-complexes favor simple CID over Coulombic fission processes because the three ligands are sufficient to stabilize the doubly charged complex with the result that charge transfer is suppressed and the complex does not break up due to Coulomb explosion. An insufficient number of ligands in the bis-complexes required to stabilize the (+2) charge leads to Coulomb fission processes being more favorable

in these complexes. The mono-complexes, $M^{2+}(N\text{-}L)$ are not generated in sufficient intensity to enable CID studies. This is likely due to the high electron deficiency in these complexes that makes them too reactive. Chances are high that if generated they will spontaneously undergo charge fission as their BDEs significantly exceed that of a typical C−C bond, > 400 kJ/mol. Therefore, the minimum number of ligands required to stabilize the M^{2+} cations in the $M^{2+}(N\text{-}L)_x$ series of compounds is three. Below this critical number of ligands, the complex dissociates via Coulomb fission processes in competition with simple CID. Thus, $x_{crit} = 2$ for the $M^{2+}(N\text{-}L)_x$ complexes.

E.8.3.3 Energetics of Binding

The $M^{2+}(Bpy)_2$ and $M^{2+}(Phen)_2$ complexes display both similarities and differences in their energy-resolved CID pathways despite the challenges and limitations encountered in this study. The periodic trends in the TCID measured and theoretically determined ETCF AEs obtained from B3LYP, BHandHLYP, and M06 levels of theory are very parallel with a minimum for electron transfer involving the Cu^{2+} complex for both the $M^{2+}(Bpy)_2$ and the $M^{2+}(Phen)_2$ complexes as illustrated in Figure E.7. Although the trends in the AEs for ETCF are very similar, the small difference in the magnitude between the Phen and Bpy complexes is fascinating. Dissociative electron transfer occurs in both $M^{2+}(Bpy)_2$ and $M^{2+}(Phen)_2$ complexes because Bpy (8.35 eV) and Phen (8.51 eV) have IEs that are much lower than IEs of M^+ cations. However, the Bpy ligand has a greater propensity to reduce by ET due to the substantially lower IE of this ligand as compared to that of Phen. Interestingly, the dipole moment and polarizability of Phen (3.31 D and 23.78 $Å^3$, respectively) are greater than those of the Bpy ligand (3.04 D, 19.67 $Å^3$, respectively) which might be taken to imply greater stabilization of cations by Phen versus Bpy. The ions complimentary to $M^+(Bpy)$ and

M^+(Phen) are Bpy^+ and $Phen^+$, respectively. In the $M^{2+}(Phen)_2$ and $M^{2+}(Bpy)_2$ complexes, the Phen and Bpy ligands are complexed to the metal cation in a *cis* orientation. Upon dissociation through electron transfer, the Bpy ligand relaxes to its ground state *trans* conformation producing a more stable free ligand such that less energy (~18.5 kJ/mol) is required for dissociation via ET and is the main source of the difference in the AEs for ETCF between the $M^{2+}(Phen)_2$ and $M^{2+}(Bpy)_2$ complexes.

The second sequential BDEs of the $M^{2+}(Bpy)_2$ and the analogous $M^{2+}(Phen)_2$ complexes determined theoretically and experimentally are nearly uniform. The minor differences in the second sequential BDEs between these complexes are mainly associated with the nature of the ligands. Phen ligands possess two nitrogen donors that are permanently aligned and thus are more preorganized chelators than the Bpy ligands, where the two pyridyl rings of Bpy are free to rotate. Although free Bpy ligand is known to exist in a *trans* planar conformation in solution,[30] it converts to a fixed *cis* planar conformation upon metal complexation. Phen, which is fixed in a planar *cis* conformation, therefore is known to have a greater dipole moment and polarizability than *cis* Bpy. The small differences in the magnitude of the dipole moment and polarizability should lead to slightly enhanced ion-dipole and ion-induced dipole attractions between Phen and the M^{2+} cation resulting in higher BDEs to Phen. However, upon dissociation, the Bpy ligand relaxes to its ground state *trans* conformation producing more stable free ligand such that less energy (~24.5 kJ/mol) is required for dissociation. This difference is reflected in the second sequential BDEs of the $M^{2+}(Bpy)_2$ complexes that closely approach those of the $M^{2+}(Phen)_2$ complexes.

E.9 Conclusions

The CID studies of five $M^{2+}(Bpy)_2$ complexes investigated using GIBMS and FT-ICR MS show that four major pathways exist for these complexes including ETCF, PTCF, simple CID, and dehydrogenation. Theoretically, the energetics associated with these pathways follow the order, AEs for ETCF < AEs for PTCF < BDEs for all five $M^{2+}(Bpy)_2$ complexes. This trend is not consistent with trends in the apparent threshold for these processes for most of the $M^{2+}(Bpy)_2$ complexes. Because of incomplete experimental data and low-resolution conditions under which the experiments were performed, the limitations of the theoretical methods cannot be evaluated at this point. Therefore, experimental studies of $M^{2+}(Bpy)_2$ complexes under higher-resolution conditions are needed. These experimental studies should be accompanied by further investigation into the mechanisms for PTCF and modeling of the dehydrogenation pathways to enable accurate thermochemistry to be extracted for all four major CID pathways of these complexes.

E.10 References

(1) Stubbe, J.; Van der Donk, W. A. *Chem. Rev*. **1998**, *98*, 705.

(2) McEvoy, J. P.; Brudvig, G. W. *Chem. Rev*. **2006**, *106*, 4455.

(3) Lowdin, P.O. *Advan. Quantum Chem*. **1965**, *2*, 213.

(4) Nelson, D. L.; Cox, M. M. Lehninger Principles of Biochemistry, W. H. Freeman and Company, New York, 2008, pp. 711−719.

(5) Armstrong, F. A.; Hill, H. A. O.; Walton, N. J. *Acc. Chem. Res.* **1988**, *21*, 407.

(6) Isied, S. S. (Ed). Electron Transfer Reactions: Inorganic, Organic, Organometallic, and Biological Applications, Advances in Chemistry Series 253, American Chemical Society, Washington, DC, 1995, pp. 317–330.

(7) Solomon, E. I.; Baldwin, M. J.; Lowery, M. D. *Chem. Rev*. **1992**, *92*, 521.

(8) Solomon, E. I.; Lowery, M. D. *Science*. **1993**, *259*, 1575.

(9) Guss, J. M.; Bartunik, H. D.; Freeman, H. C. *Acta. Crystallogr*. **1992**, *B48*, 790.

(10) Guss, J. M.; Harrowell, P. R.; Murata, M.; Norris, V. A.; Freeman, H. C. *J. Mol. Biol*. **1986**, *192*, 361.

(11) Williams, R. J. P. *Eur. J. Biochem.* **1995**, *234*, 363.

(12) Lowery, M. D.; Guckert, J. A.; Gebhard, M. S.; Solomon, E. I. *J. Am. Chem. Soc.* **1993**, *115*, 3012.

(13) Strouse, G. F.; Schoonover, J. R.; Duesing, R.; Boyde, S.; Jones, W. E., Jr.; Meyer, T. J. *Inorg. Chem*. **1995**, *34*, 473.

(14) Baranovski, V. I.; Lubimova, O. O.; Makarov, A. A.; Sizova, O. V. *Chem. Phys. Lett*. **2002**, *361*, 196.

(15) Guo, H.; Wlodawer, A.; Nakayama, T.; Xu, Q.; Guo, H. *Biochemistry*. **2006**, *45*, 9129.

(16) Malmstroem, B. G. *Eur. J. Biochem*. **1994**, *223*, 711.

(17) Rodgers, M. T.; Ervin, K. M.; Armnetrout, P. B. *J. Chem. Phys.* **1997**, *106*, 4499.

(18) Nose, H.; Chen, Y.; Rodgers, M. T. *J. Phys. Chem. A* **2013**, *117*, 4316.

(19) Nose, H.; Rodgers, M. T. *ChemPlusChem*. **2013**, *78*, 1109.

(20) Frisch, M. J.; Trucks, G. W.; Schlegel, H. B.; Scuseria, G. E.; Robb, M. A.; Cheeseman, J. R.; Scalmani, G.; Barone, V.; Mennucci, B.; Petersson, G. A.; Nakatsuji, H.; Caricato, M.;

Li, X.; Hratchian, H. P.; Izmaylov, A. F.; Bloino, J.; Zheng, G.; Sonnenberg, J. L.; Hada, M.; Ehara, M.; Toyota, K.; Fukuda, R.; Hasegawa, J.; Ishida, M.; Nakajima, T.; Honda, Y.; Kitao, O.; Nakai, H.; Vreven, T.; Montgomery, J. A, Jr.; Peralta, J. E.; Ogliaro, F.; Bearpark, M.; Heyd, J. J.; Brothers, E.; Kudin, K. N.; Staroverov, V. N.; Kobayashi, R.; Normand, J.; Raghavachari, K.; Rendell, A.; Burant, J. C.; Iyengar, S. S.; Tomasi, J.; Cossi, M.; Rega, N.; Millam, J. M.; Klene, M.; Knox, J. E.; Cross, J. B.; Bakken, V.; Adamo, C.; Jaramillo, J.; Gomperts, R.; Stratmann, R. E.; Yazyev, O.; Austin, A. J.; Cammi, R.; Pomelli, C.; Ochterski, J. W.; Martin, R. L.; Morokuma, K.; Zakrzewski, V. G.; Voth, G. A.; Salvador, P.; Dannenberg, J. J.; Dapprich, S.; Daniels, A. D.; Farkas, O.; Foresman, J. B.; Ortiz, J. V.; Cioslowski, J.; Fox, D. J. Gaussian, Inc., Wallingford, CT, 2009.

(21) Foresman, J. B.; Frisch, A. E. Exploring Chemistry with Electronic Structure Methods, 2nd ed, Gaussian: Pittsburgh, P. A, 1996, pp. 64.

(22) Rodgers, M. T. *J. Phys. Chem. A* **2001**, *105*, 2374.

(23) Jacob, C. R.; Reiher, M. *Int. J. Quantum Chem.* **2012**, *112*, 3661.

(24) Goodpaster, J. D.; Barnes, T. A.; Manby, F. R.; Miler, T. F. *J. Chem. Phys.* **2012**, *137*, 224113.

(25) Schmidt, J. R.; Shenvi, N.; Tully, J. C. *J. Chem. Phys.* **2008**, *129*, 114110.

(26) Sansonetti, J. E.; Martin, W. C.; Young, S. L. *J. Phys. Chem. Ref. Data.* **2005**, *34*, 1559.

(27) Marcus, R. A.; Eyring, H. *Ann. Rev. Phys. Chem*. **1964**, *15*, 155.

(28) Corongiu, G.; Clementi, E. *J. Chem. Phys*. **1978**, *69*, 4885.

(29) Roithova, J.; Schroder, D. *Phys. Chem. Chem. Phys.* **2007**, *9*, 2341.

(30) McWhinnie, W. R.; Miller, J. D. *Adv. Inorg. Chem. Radiochem.* **1969**, *12*, 135.

Table E.1a. Vibrational Frequencies and Average Vibrational Energies of $M^{2+}(Bpy)_2$ Reactants and Products Involved in the Dissociation of $M^{2+}(Bpy)_2$ Complexes through Simple CID Process at 298 K.

Species	E_{vib} (eV)[a]	Vibrational frequencies (cm^{-1}) [b]
$Fe^{2+}(Bpy)_2$ Reactant	0.53 (0.05)	14, 31(2), 59, 62, 76(2), 127, 134(2), 201, 224, 228, 229, 241(2), 280, 357, 379, 399, 400, 416(2), 437(2), 455(2), 544(2), 645(2), 649(2), 660, 668, 729(2), 736, 737, 761(2), 770(2), 802, 804, 889, 890, 901(2), 967(2), 969(2), 1012(2), 1016(2), 1020(2), 1024(2), 1039(2), 1070(2), 1078(2), 1118(2), 1131(2), 1179(2), 1193, 1194, 1278, 1283(3), 1300, 1302, 1322(2), 1328(2), 1445(2), 1459(2), 1484(2), 1502, 1504, 1586(2), 1593(2), 1612, 1613, 1624(2), 3153(4), 3165(2), 3166(2), 3179(2), 3182(2), 3183(2), 3195(2)
$Fe^{2+}(Bpy)$ Product 1	0.25 (0.02)	56, 76, 139, 205, 227, 250, 280, 380, 390, 407, 428, 446, 531, 641, 661, 674, 711, 723, 750, 772, 786, 887, 899, 972, 975, 1006, 1025(2), 1029, 1036, 1067, 1070, 1119, 1135, 1185, 1199, 1267, 1279, 1301, 1318, 1329, 1441, 1460, 1472, 1499, 1576, 1581, 1599, 1612, 3162(2), 3168, 3169, 3183, 3184, 3186, 3201
Bpy Product 2	0.21 (0.02)	57, 95, 162, 224, 327, 404, 411, 438, 441, 561, 616, 622, 659, 745, 746, 763, 771, 825, 904, 913, 958, 963, 993, 995, 996(2), 1039, 1053, 1075, 1100, 1104, 1158(2), 1268, 1273, 1309, 1314, 1325, 1436, 1462, 1476, 1499, 1585, 1604, 1614, 1615, 3106, 3107, 3130(2), 3151(2), 3180(2)
$Co^{2+}(Bpy)_2$ Reactant	0.52 (0.05)	12, 34(2), 56, 75, 76(2), 128, 140(2), 204, 227(2), 235, 255(2), 322, 360, 380, 391, 408, 417(2), 437(2), 458(2), 543, 545, 646(2), 6492), 662, 669, 727(2), 735, 738, 762(2), 769(2), 802, 804, 890(2), 899(2), 965, 966, 967(2), 1015, 1016(3), 1019(2), 1030(2), 1039(2), 1069, 1070, 1078(2), 1118, 1119, 1131(2), 1178(2), 1192(2), 1278, 1281, 1283(2), 1301(2), 1326(2), 1328(2), 1446(2), 1461(2), 1484(2), 1506(2), 1587(2), 1594(2), 1614(2), 1626(2), 3155(4), 3165(2), 3166(2), 3179(2), 3182(2), 3183(2), 3192(2)
$Co^{2+}(Bpy)$ Product 1	0.24 (0.02)	71, 84, 149, 195, 228, 267, 289, 378, 391, 408, 433, 457, 526, 641, 661, 677, 708, 714, 755, 770, 781, 888, 897, 969, 973, 1012, 1025, 1028, 1031, 1036, 1064, 1070, 1118, 1134, 1184, 1194, 1270, 1280, 1301, 1327, 1329, 1441, 1461, 1472, 1499, 1575, 1580, 1601, 1612, 3159(2), 3168, 3169, 3179, 3183, 3184, 3192

Table E.1a. (continued) Vibrational Frequencies and Average Vibrational Energies of $M^{2+}(Bpy)_2$ Reactants and Products Involved in the Dissociation of $M^{2+}(Bpy)_2$ Complexes through Simple CID Process at 298 K.

Species	E_{vib} (eV)[a]	Vibrational frequencies (cm^{-1}) [b]
$Ni^{2+}(Bpy)_2$ Reactant	0.51 (0.05)	10, 42(2), 76, 78, 85(2), 131, 171(2), 199, 233, 235, 241, 285(2), 339, 362, 380, 400, 407, 422(2), 444(2), 489(2), 544, 545, 648(2), 652(2), 664, 670, 731(2), 739, 740, 765(2), 771(2), 803, 806, 893(2), 899(2), 966(2), 967(2), 1016(2), 1019(4), 1031, 1033, 1039(2), 1067, 1068, 1079(2), 1118(2), 1131(2), 1178(2), 1189(2), 1278, 1283, 1287(2), 1302(2), 1328(2), 1335(2), 1447(2), 1462(2), 1484(2), 1509(2), 1587, 1588, 1594(2), 1614(2), 1625(2), 3154(3), 3155, 3165(2), 3166(2), 3177(2), 3182(2), 3183(2), 3188(2)
$Ni^{2+}(Bpy)$ Product 1	0.24 (0.02)	72, 82, 149, 196, 231, 285, 300, 383, 394, 407, 429, 458, 525, 639, 668, 682, 703, 706, 752, 769, 780, 888, 892, 972, 975, 1013, 1025, 1028, 1030, 1036, 1062, 1068, 1118, 1136, 1184, 1194, 1270, 1280, 1302, 1328, 1331, 1440, 1462, 1471, 1498, 1569, 1575, 1594, 1608, 3161(2), 3167, 3168, 3179, 3183, 3184, 3191
$Cu^{2+}(Bpy)_2$ Reactant	0.52 (0.05)	30, 32, 46, 75, 85, 95, 111, 137, 138, 166, 192, 196, 235, 236, 254, 291, 330, 364, 368, 405, 415, 418, 419, 439, 444, 464, 474, 545, 550, 643, 648(2), 650, 666, 667, 728, 730, 738, 740, 765, 766, 771, 773, 801, 803, 895, 899, 901, 905, 969, 970, 976(2), 1016(2), 1017, 1020(3), 1031, 1036, 1037, 1038, 1067, 1068, 1078, 1080, 1118, 1119, 1130, 1133, 1178(2), 1189(2), 1279, 1284, 1285, 1288, 1303(2), 1327, 1328, 1333, 1334, 1447(2), 1461, 1463, 1484, 1485, 1507, 1508, 1587, 1588, 1593, 1595, 1614(2), 1625(2), 3160(2), 3161, 3162, 3166(2), 3167(2), 3177(2), 3182(2), 3183(2), 3187, 3188
$Cu^{2+}(Bpy)$ Product 1	0.24 (0.02)	71, 79, 141, 193, 232, 274, 301, 382, 391, 405, 427, 460, 525, 637, 663, 683, 689, 695, 750, 754, 774, 861, 883, 965, 969, 1018, 1023, 1025, 1026, 1042, 1063, 1072, 1119, 1132, 1182, 1191, 1269, 1280, 1303, 1325, 1335, 1440, 1459, 1470, 1501, 1578, 1579, 1594, 1602, 3155, 3156, 3166, 3167, 3176, 3182(2), 3186

Table E.1a. (continued) Vibrational Frequencies and Average Vibrational Energies of $M^{2+}(Bpy)_2$ Reactants and Products Involved in the Dissociation of $M^{2+}(Bpy)_2$ Complexes through Simple CID Process at 298 K.

Species	E_{vib} (eV)[a]	Vibrational frequencies (cm^{-1}) [b]
$Zn^{2+}(Bpy)_2$ Reactant	0.52 (0.05)	19, 33(2), 64, 78, 81(2), 130, 146(2), 206, 227(2), 230, 234, 236, 304, 363, 376, 399, 409, 419(2), 441(2), 459, 460, 547, 548, 646(2), 651(2), 664, 668, 735(2), 740, 742, 763(2), 772(2), 812, 814, 894, 895, 904(2), 970(2), 972(2), 1017(2), 1019(2), 1021(2), 1031, 1034, 1041(2), 1070, 1071, 1080(2), 1121, 1122, 1133(2), 1179(2), 1193(2), 1280, 1283, 1287(2), 1302, 1303, 1327, 1328, 1331(2), 1447, 1448, 1462(2), 1488(2), 1505(2), 1588, 1589, 1596(2), 1615(2), 1628(2), 3158(4), 3165(2), 3166(2), 3180(2), 3182(2), 3183(2), 3195(2)
$Zn^{2+}(Bpy)$ Product 1	0.24 (0.02)	56, 84, 152, 207, 229, 267, 288, 384, 388, 410, 433, 447, 529, 641, 664, 676, 708, 712, 750, 775, 783, 887, 905, 976, 979, 1014, 1027, 1028, 1031, 1034, 1067, 1072, 1123, 1136, 1185, 1199, 1255, 1287, 1302, 1325, 1330, 1442, 1463, 1473, 1495, 1579, 1584, 1598, 1613, 3167, 3168, 3176(2), 3185, 3186, 3187, 3203

[a] Uncertainties listed in parentheses are determined as described in the text. [b] Vibrational frequencies scaled by 0.9804 obtained from vibrational analyses of the B3LYP/6-31G* geometry optimized structures. Degeneracies are indicated in parentheses.

Table E.1b. Vibrational Frequencies and Average Vibrational Energies of $M^{2+}(Bpy)_2$ Reactants, Transition States, Intermediates, and Products Involved in the Activated Dissociation of $M^{2+}(Bpy)_2$ Complexes through ETCF Process at 298 K.

Species	E_{vib} (eV)[a]	Vibrational frequencies (cm^{-1}) [b]
$Fe^{2+}(Bpy)_2$ Reactant	0.53 (0.05)	14, 31(2), 59, 62, 76(2), 127, 134(2), 201, 224, 228, 229, 241, 241, 280, 357, 379, 399, 400, 416(2), 437(2), 455(2), 544(2), 645(2), 649(2), 660, 668, 729(2), 736, 737, 761(2), 770(2), 802, 804, 889, 890, 901(2), 967(2), 969(2), 1012(2), 1016(2), 1020(2), 1024(2), 1039(2), 1070(2), 1078(2), 1118(2), 1131(2), 1179(2), 1193, 1194, 1278, 1283(3), 1300, 1302, 1322(2), 1328(2), 1445(2), 1459(2), 1484(2), 1502, 1504, 1586(2), 1593(2), 1612, 1613, 1624(2), 3153(4), 3165(2), 3166(2), 3179(2), 3182(2), 3183(2), 3195(2)
$Fe^{2+}(Bpy)_2$ TS_1	0.52 (0.05)	**-79**, 19, 29, 35, 58, 68, 72, 82, 113, 132, 142, 161, 214, 229, 245, 275, 289, 311, 338, 374, 396, 400, 411, 416, 435, 455, 530, 537, 544, 613, 647, 649, 650, 657, 668, 727, 736, 739, 756, 760, 762, 772, 781, 789, 801, 893, 905, 907, 916, 969, 973, 980, 981, 986, 1013, 1018(2), 1021, 1022, 1023, 1027, 1037, 1038, 1053, 1070, 1075, 1077, 1100, 1118, 1123, 1132, 1172, 1179, 1180, 1194, 1273, 1279, 1282, 1283, 1290, 1300, 1301, 1321, 1323, 1329, 1436, 1445, 1455, 1460, 1466, 1483, 1497, 1504, 1581, 1584, 1585, 1586, 1591, 1611, 1621, 1623, 3141, 3146, 3155, 3157, 3161, 3162, 3165, 3165, 3166, 3174, 3177, 3180, 3182, 3183, 3184, 3195
$Fe^{2+}(Bpy)_2$ Int_1	0.54 (0.05)	16, 27, 30, 61, 64, 77, 83, 101, 129, 138, 150, 186, 209, 229, 241, 260, 279, 340, 366, 371, 400, 411, 416, 417, 436, 455, 501, 543, 543, 611, 646, 649, 650, 655, 666, 728, 736, 737, 759, 760, 765, 771(2), 794, 802, 872, 891, 902, 907, 968, 971, 972, 978, 987, 1012, 1013, 1018, 1018, 1022, 1024, 1025, 1034, 1039, 1052, 1070, 1075, 1078, 1098, 1118, 1119, 1132, 1165, 1178, 1180, 1194, 1262, 1279, 1280, 1283, 1302, 1310, 1312, 1322, 1323, 1330, 1428, 1445, 1460(2), 1468, 1484, 1497, 1503, 1568, 1582, 1585(2), 1592, 1612, 1619, 1623, 3054, 3149, 3150, 3154(2), 3158, 3165(2), 3166, 3176, 3180, 3181, 3182, 3184, 3185, 3195

Table E.1b. (continued) Vibrational Frequencies and Average Vibrational Energies of $M^{2+}(Bpy)_2$ Reactants, Transition States, Intermediates, and Products Involved in the Activated Dissociation of $M^{2+}(Bpy)_2$ Complexes through ETCF Process at 298 K.

Species	E_{vib} (eV)[a]	Vibrational frequencies (cm^{-1}) [b]
$Fe^{2+}(Bpy)_2$ TS_2	0.52 (0.05)	**-56**, 10, 22, 43, 48, 66, 84, 89, 128, 141, 149, 153, 206, 215, 229, 231, 269, 322, 362, 367, 397, 398, 410, 411, 436, 456, 458, 542, 552, 597, 615, 645, 648, 649, 666, 704, 725, 736, 740, 762, 764, 771, 790, 800, 824, 892, 902, 919, 931, 966, 968, 973, 973, 986, 991, 1001, 1012, 1018, 1019, 1022, 1026, 1028, 1038(2), 1065, 1069, 1077, 1086, 1106, 1119, 1132, 1155, 1172, 1180, 1193, 1246, 1257, 1279, 1282, 1283, 1302, 1316, 1327, 1330, 1338, 1415, 1445, 1447, 1454, 1460, 1480, 1482, 1505, 1528, 1557, 1584, 1590, 1591, 1596, 1612, 1623, 3147, 3155, 3157, 3158, 3159, 3162, 3166, 3167, 3170, 3175(2), 3180, 3183, 3184(2), 3194
$Fe^{2+}(Bpy)_2$ Int_2	0.54 (0.05)	4(2), 5, 7, 11, 14, 45, 71, 75, 84, 133, 163, 198, 200, 225, 243, 251, 329, 371, 386, 392, 396, 413, 417, 433, 442, 445, 524, 541, 604, 614, 645, 647, 652, 669, 707, 716, 724, 728, 756, 763, 764, 769, 794, 797, 871, 888, 894, 902, 969, 971, 971, 980, 981, 986, 1005, 1012, 1014, 1017, 1021, 1022, 1025, 1037, 1037, 1057, 1070, 1075, 1096, 1104, 1119, 1131, 1162, 1164, 1180, 1195, 1261, 1268, 1284, 1287, 1298, 1318, 1319, 1325, 1341, 1353, 1431, 1443, 1454, 1456, 1459, 1479, 1490, 1498, 1542, 1558, 1575, 1586, 1590, 1592, 1610, 1622, 3119, 3138, 3155, 3157, 3158, 3159, 3166, 3167, 3169, 3170, 3182, 3183, 3185, 3190, 3193, 3200
$Fe^{+}(Bpy)$ Product 1	0.25 (0.02)	55, 65, 115, 181, 187, 227, 256, 352, 401, 406, 433, 448, 543, 554, 648, 656, 724, 727, 764, 766, 794, 886, 898, 966, 967, 986, 1008, 1012(2), 1018, 1069, 1073, 1115, 1124, 1174, 1188, 1279, 1281, 1301, 1324, 1326, 1445, 1457, 1479, 1502, 1588, 1595, 1616, 1626, 3145, 3145, 3159, 3161, 3174, 3179, 3180, 3187
Bpy^{+} Product 2	0.21 (0.02)	71, 80, 163, 179, 331, 364, 380, 398, 444, 489, 595, 607, 634, 675, 693, 759, 768, 784, 865, 887, 965, 981, 986, 992, 1010, 1014, 1016, 1020, 1038, 1096, 1105, 1163, 1163, 1252, 1309, 1323, 1364, 1377, 1429, 1439, 1450, 1480, 1523, 1540, 1558, 1592, 3144, 3144, 3164(2), 3174, 3175, 3193, 3194

Table E.1b. (continued) Vibrational Frequencies and Average Vibrational Energies of $M^{2+}(Bpy)_2$ Reactants, Transition States, Intermediates, and Products Involved in the Activated Dissociation of $M^{2+}(Bpy)_2$ Complexes through ETCF Process at 298 K.

Species	E_{vib} (eV)[a]	Vibrational frequencies (cm^{-1}) [b]
$Co^{2+}(Bpy)_2$ Reactant	0.52 (0.05)	12, 34(2), 56, 75, 76(2), 128, 140(2), 204, 227(2), 235, 255(2), 322, 360, 380, 391, 408, 417(2), 437(2), 458(2), 543, 545, 646(2), 6492), 662, 669, 727(2), 735, 738, 762(2), 769(2), 802, 804, 890(2), 899(2), 965, 966, 967(2), 1015, 1016(3), 1019(2), 1030(2), 1039(2), 1069, 1070, 1078(2), 1118, 1119, 1131(2), 1178(2), 1192(2), 1278, 1281, 1283(2), 1301(2), 1326(2), 1328(2), 1446(2), 1461(2), 1484(2), 1506(2), 1587(2), 1594(2), 1614(2), 1626(2), 3155(4), 3165(2), 3166(2), 3179(2), 3182(2), 3183(2), 3192(2)
$Co^{2+}(Bpy)_2$ TS_1	0.51 (0.05)	**-88**, 17, 32, 40, 64, 70, 78, 85, 115, 135, 143, 182, 216, 233, 250, 285, 296, 312, 341, 375, 395, 400, 411, 417, 437, 458, 531, 534, 544, 613, 648, 650, 650, 659, 670, 725, 737(2), 754, 761, 762, 772, 784, 787, 802, 893, 904, 908, 918, 967, 973, 979, 981, 986, 1016, 1018, 1021, 1021, 1024, 1024, 1032, 1038, 1039, 1052, 1069, 1075, 1077, 1100, 1119, 1124, 1132, 1173, 1179(2), 1193, 1271, 1280, 1283, 1285, 1290, 1300, 1303, 1322, 1328, 1330, 1437, 1446, 1454, 1462, 1465, 1483, 1496, 1507, 1581, 1585(2), 1586, 1592, 1612, 1620, 1625, 3143, 3147, 3156, 3161, 3162(2), 3166, 3167(2), 3174, 3177, 3180, 3182, 3183, 3184, 3193
$Co^{2+}(Bpy)_2$ Int_1	0.57 (0.05)	14, 26, 33, 59, 71, 75, 84, 103, 129, 142, 156, 206, 217, 232, 250, 266, 298, 344, 367, 373, 401, 413, 416, 421, 436, 457, 501, 541, 543, 611, 648, 649, 649, 657, 668, 725, 732, 737, 756, 761, 765, 771, 776, 791, 801, 882, 891, 901, 907, 967, 970, 972, 979, 988, 1013, 1016, 1017, 1021, 1021, 1024, 1031, 1035, 1039, 1051, 1070, 1074, 1077, 1095, 1120, 1120, 1132, 1166, 1178, 1179, 1193, 1262, 1279, 1280, 1283, 1302, 1310, 1312, 1324, 1326, 1329, 1427, 1446, 1460, 1461, 1467, 1483, 1495, 1506, 1564, 1582, 1586, 1587, 1592, 1613, 1619, 1625, 3072, 3149, 3153, 3155, 3156, 3161, 3166(2), 3167, 3176, 3180, 3181, 3183, 3184, 3185, 3194

Table E.1b. (continued) Vibrational Frequencies and Average Vibrational Energies of $M^{2+}(Bpy)_2$ Reactants, Transition States, Intermediates, and Products Involved in the Activated Dissociation of $M^{2+}(Bpy)_2$ Complexes through ETCF Process at 298 K.

Species	E_{vib} (eV)[a]	Vibrational frequencies (cm^{-1}) [b]
$Co^{2+}(Bpy)_2$ TS_2	0.52 (0.05)	**-61**, 16, 25, 45, 68, 71, 81, 86, 102, 130, 146, 155, 208, 232, 249, 256, 310, 319, 356, 370, 393, 401, 405, 416, 438, 459, 497, 541, 543, 606, 615, 647, 648, 650, 669, 715, 724, 736, 746, 762, 763, 772, 789, 799, 821, 892, 904, 912, 921, 968, 973, 980, 980, 981, 990, 995, 1015, 1018, 1019, 1022, 1027, 1030, 1038, 1043, 1069, 1072, 1077, 1087, 1109, 1119, 1133, 1160, 1173, 1180, 1192, 1250, 1265, 1281, 1284, 1292, 1302, 1312, 1329, 1331, 1332, 1418, 1446, 1454, 1459, 1462, 1483, 1485, 1507, 1537, 1561, 1585, 1590, 1591, 1599, 1612, 1623, 3148, 3152, 3156, 3160(2), 3161, 3166, 3167, 3171, 3175, 3176, 3179, 3183(2), 3184, 3192
$Co^{2+}(Bpy)_2$ Int_2	0.55 (0.05)	5, 15, 22, 26, 28, 43, 49, 62, 73, 87, 120, 163, 193, 197, 224, 252, 288, 329, 380, 381, 389, 393, 406, 415, 431, 443, 454, 520, 524, 600, 612, 644, 646, 660, 681, 697, 702, 712, 713, 757, 760, 766, 768, 776, 800, 872, 886, 894, 901, 963, 966, 974, 975, 981, 982, 1007, 1013, 1014, 1015, 1019, 1024, 1028, 1039, 1041, 1048, 1069, 1079, 1096, 1104, 1121, 1132, 1161, 1163, 1180, 1193, 1258, 1272, 1293, 1297, 1299, 1316, 1325, 1326, 1346, 1362, 1431, 1446, 1448, 1452, 1460, 1482, 1490, 1493, 1530, 1547, 1576, 1590, 1594, 1600, 1613, 1626, 3128, 3139, 3156, 3158, 3163, 3164, 3167, 3169, 3170, 3170, 3178, 3183(2), 3186, 3188, 3191
$Co^{+}(Bpy)$ Product 1	0.24 (0.02)	55, 70, 152, 200, 227, 252, 256, 382, 395, 419, 445, 450, 531, 633, 650, 673, 693, 709, 757, 759, 768, 870, 885, 943, 948, 992, 996, 999, 1032, 1036, 1066, 1069, 1113, 1127, 1172, 1180, 1265, 1277, 1289, 1303, 1320, 1439, 1455, 1472, 1473, 1572, 1581, 1615, 1616, 3151, 3152, 3160, 3162, 3172, 3177, 3179, 3186
$Ni^{2+}(Bpy)_2$ Reactant	0.52 (0.05)	10, 42(2), 76, 78, 85(2), 131, 171(2), 199, 233, 235, 241, 285, 285, 339, 362, 380, 400, 407, 422(2), 444(2), 489(2), 544, 545, 648, 648, 652(2), 664, 670, 731(2), 739, 740, 765(2), 771(2), 803, 806, 893(2), 899(2), 966(2), 967(2), 1016(2), 1019(4), 1031, 1033, 1039(2), 1067, 1068, 1079(2), 1118(2), 1131(2), 1178(2), 1189(2), 1278, 1283, 1287(2), 1302(2), 1328(2), 1335(2), 1447(2), 1462(2), 1484(2), 1509(2), 1587, 1588, 1594(2), 1614(2), 1625(2), 3154(3), 3155, 3165(2), 3166(2), 3177(2), 3182(2), 3183(2), 3188(2)

Table E.1b. (continued) Vibrational Frequencies and Average Vibrational Energies of $M^{2+}(Bpy)_2$ Reactants, Transition States, Intermediates, and Products Involved in the Activated Dissociation of $M^{2+}(Bpy)_2$ Complexes through ETCF Process at 298 K.

Species	E_{vib} (eV)[a]	Vibrational frequencies (cm^{-1}) [b]
$Ni^{2+}(Bpy)_2$ TS_1	0.51 (0.05)	**-86**, 18, 29, 36, 60, 69, 78, 84, 112, 138, 144, 192, 222, 233, 253, 285, 299, 315, 345, 374, 397, 401, 411, 417, 439, 460, 528, 534, 543, 613, 647, 649, 651, 661, 671, 723, 734, 736, 751, 761, 763, 772, 780, 786, 799, 893, 905, 906, 913, 966, 972, 981, 984, 987, 1018, 1019, 1021, 1021, 1023, 1025, 1035, 1037, 1038, 1052, 1067, 1075, 1078, 1101, 1119, 1123, 1132, 1173, 1179, 1179, 1191, 1272, 1280, 1282, 1284, 1292, 1298, 1302, 1322, 1330, 1332, 1436, 1446, 1455, 1462, 1466, 1483, 1495, 1507, 1581, 1583, 1586, 1586, 1592, 1613, 1619, 1625, 3141, 3148, 3156, 3159, 3162, 3163, 3165, 3167, 3168, 3174, 3177, 3178, 3182, 3183(2), 3189
$Ni^{2+}(Bpy)_2$ Int_1	0.53 (0.05)	17, 27, 34, 67, 78, 81(2), 105, 133, 146, 166, 205, 224, 234, 258, 270, 307, 346, 369, 372, 404, 415, 418, 422, 439, 460, 503, 542, 544, 611, 648, 649, 650, 660, 669, 724, 735(2), 758, 763, 766, 771, 779, 797, 799, 894, 897, 902, 908, 967, 973, 973, 979, 991, 1015, 1017, 1019, 1021, 1022, 1024, 1034, 1036, 1038, 1051, 1068, 1075, 1078, 1096, 1119, 1120, 1132, 1167, 1177, 1179, 1191, 1260, 1280, 1281, 1284, 1303, 1310, 1312, 1327, 1330, 1331, 1427, 1447, 1461, 1462, 1467, 1484, 1495, 1507, 1564, 1584, 1586, 1587, 1592, 1613, 1619, 1625, 3045, 3148, 3152, 3156, 3157, 3163, 3166, 3167(2), 3176, 3178, 3181, 3182, 3183, 3184, 3190
$Ni^{2+}(Bpy)_2$ TS_2	0.52 (0.05)	**-89**, 17, 21, 34, 49, 63, 83, 89, 100, 146, 162, 174, 201, 234, 247, 269, 319, 330, 372, 396, 401, 402, 407, 416, 439, 455, 463, 541, 542, 601, 613, 647, 647, 652, 672, 694, 722, 732, 733, 759, 763, 771, 781, 796, 817, 893, 902, 912, 920, 959, 967, 968, 976, 985, 990, 1011, 1017, 1018, 1020, 1022, 1025, 1036, 1038, 1039, 1063, 1067, 1078, 1097, 1107, 1120, 1132, 1166, 1172, 1179, 1191, 1247, 1278, 1280, 1284, 1287, 1303, 1318, 1328, 1334, 1344, 1419, 1446, 1452, 1456, 1463, 1479, 1482, 1508, 1526, 1578, 1584, 1586, 1590, 1591, 1613, 1625, 3147, 3152, 3160, 3161, 3162(2), 3167, 3168, 3172, 3174, 3178, 3179, 3183, 3184, 3188, 3190

Table E.1b. (continued) Vibrational Frequencies and Average Vibrational Energies of $M^{2+}(Bpy)_2$ Reactants, Transition States, Intermediates, and Products Involved in the Activated Dissociation of $M^{2+}(Bpy)_2$ Complexes through ETCF Process at 298 K.

Species	E_{vib} (eV)[a]	Vibrational frequencies (cm^{-1}) [b]
$Ni^{2+}(Bpy)_2$ Int_2	0.54 (0.05)	5(2), 8, 12, 22, 33, 51, 68, 73, 83, 137, 162, 193, 197, 233, 275, 277, 329, 376, 378, 387, 395, 411(2), 430, 443, 452, 513, 526, 600, 611, 642, 647, 657, 674, 696(2), 710, 712, 759, 760, 766, 766, 775, 795, 870, 885, 892, 899, 960, 964, 974, 977, 983, 983, 1009, 1013(2), 1014, 1017, 1024(2), 1039(2), 1047, 1070, 1078, 1096, 1104, 1121, 1132, 1162, 1163, 1179, 1193, 1259, 1270, 1291, 1294, 1300, 1319, 1325, 1326, 1351, 1363, 1430, 1446, 1448, 1451, 1461, 1482, 1488, 1498, 1529, 1544, 1572, 1590, 1594, 1600, 1614, 1626, 3130, 3141, 3157, 3159, 3163, 3164, 3168, 3169, 3171(2), 3177, 3182, 3183, 3187, 3188, 3191
$Ni^{+}(Bpy)$ Product 1	0.23 (0.01)	49, 73, 139, 199, 228, 268, 280, 383, 395, 416, 433, 452, 528, 642, 652, 677, 694, 710, 761, 762, 771, 879, 893, 953, 956, 1000, 1004, 1016, 1038(2), 1068, 1074, 1116, 1128, 1173, 1185, 1268, 1281, 1300, 1317, 1323, 1444, 1459, 1478, 1493, 1585, 1591, 1618, 1626, 3158, 3159, 3163, 3164, 3175, 3180, 3181, 3187
$Cu^{2+}(Bpy)_2$ Reactant	0.52 (0.05)	30, 32, 46, 75, 85, 95, 111, 137, 138, 166, 192, 196, 235, 236, 254, 291, 330, 364, 368, 405, 415, 418, 419, 439, 444, 464, 474, 545, 550, 643, 648(2), 650, 666, 667, 728, 730, 738, 740, 765, 766, 771, 773, 801, 803, 895, 899, 901, 905, 969, 970, 976(2), 1016(2), 1017, 1020(3), 1031, 1036, 1037, 1038, 1067, 1068, 1078, 1080, 1118, 1119, 1130, 1133, 1178(2), 1189(2), 1279, 1284, 1285, 1288, 1303(2), 1327, 1328, 1333, 1334, 1447(2), 1461, 1463, 1484, 1485, 1507, 1508, 1587, 1588, 1593, 1595, 1614(2), 1625(2), 3160(2), 3161, 3162, 3166(2), 3167(2), 3177(2), 3182(2), 3183(2), 3187, 3188
$Cu^{2+}(Bpy)_2$ TS_1	0.51 (0.05)	**-69**, 22, 30, 44, 67, 80, 84, 90, 118, 136, 155, 168, 206, 237, 265, 285, 303, 327, 353, 374, 399, 403, 415, 419, 439, 467, 525, 536, 543, 613, 647, 650, 651, 665, 674, 719, 730, 736, 751, 760, 764, 771, 778, 788, 794, 895, 900, 905, 915, 969, 973, 974, 983, 986, 1018(2), 1021(2), 1023, 1027, 1033, 1040, 1041, 1054, 1066, 1076, 1079, 1104, 1119, 1124, 1132, 1172, 1179, 1179, 1189, 1273, 1281, 1282, 1286, 1295, 1302, 1304, 1321, 1328, 1336, 1436, 1446, 1455, 1463, 1468, 1482, 1497, 1508, 1582, 1585, 1586(2), 1592, 1612, 1620, 1624, 3141, 3144, 3161, 3162, 3163, 3164, 3166, 3167, 3168, 3172, 3177, 3178, 3182, 3183(2), 3187

Table E.1b. (continued) Vibrational Frequencies and Average Vibrational Energies of $M^{2+}(Bpy)_2$ Reactants, Transition States, Intermediates, and Products Involved in the Activated Dissociation of $M^{2+}(Bpy)_2$ Complexes through ETCF Process at 298 K.

Species	E_{vib} (eV)[a]	Vibrational frequencies (cm^{-1}) [b]
$Cu^{2+}(Bpy)_2$ Int_1	0.53 (0.05)	30, 32, 37, 73, 82, 86, 95, 120, 135, 154, 168, 182, 211, 240, 264, 265, 309, 351, 367, 379, 407, 416, 419, 424, 440, 468, 499, 541, 546, 610, 647, 648, 650, 660, 670, 724, 731, 735, 759, 764, 767, 771, 779, 796, 799, 889, 893, 899, 910, 967, 969, 979, 980, 991, 1014, 1017, 1019, 1021, 1023, 1025, 1034, 1036, 1038, 1054, 1068, 1077, 1079, 1100, 1119, 1121, 1133, 1168, 1178, 1179, 1190, 1264, 1280, 1282, 1287, 1304, 1314, 1317, 1327, 1328, 1334, 1429, 1447, 1462(2), 1468, 1483, 1499, 1508, 1563, 1585, 1587, 1588, 1593, 1613, 1621, 1623, 3066, 3148, 3155, 3163, 3165(2), 3167, 3169, 3172, 3173, 3178, 3182, 3183, 3184, 3187, 3188
$Cu^{2+}(Bpy)_2$ TS_2	0.52 (0.05)	**-34**, 10, 27, 45, 53, 77, 80, 86, 106, 154, 158, 179, 210, 233, 239, 253, 310, 327, 372, 378, 399, 400, 414, 416, 438, 448, 465, 539, 540, 600, 613, 647, 648, 650, 672, 697, 717, 727, 732, 762, 764, 768, 788, 791, 833, 889, 895, 915, 926, 964, 968, 971, 975, 987, 989, 1000, 1017(2), 1018, 1020, 1021, 1033, 1035, 1037, 1060, 1069, 1079, 1094, 1106, 1121, 1133, 1163, 1172, 1179, 1191, 1247, 1279, 1284, 1286, 1293, 1305, 1316, 1328, 1335, 1348, 1419, 1446, 1447, 1451, 1463, 1477, 1483, 1508, 1517, 1573, 1579, 1587, 1588, 1592, 1612, 1623, 3143, 3147, 3160(2), 3165, 3166, 3169, 3170, 3172, 3174, 3177, 3179, 3184, 3186, 3190(2)
$Cu^{2+}(Bpy)_2$ Int_2	0.55 (0.05)	4, 5, 9, 11, 12, 14, 15, 73, 74, 78, 133, 160, 189, 198, 222, 247, 260, 328, 372, 381, 384, 392, 406, 415, 432, 443, 449, 506, 531, 598, 610, 639, 646, 653, 677, 690, 701, 705, 720, 759, 759, 766, 767, 779, 789, 868, 887, 890, 902, 963, 966, 974, 980, 983, 986, 1011, 1012, 1013, 1015, 1017, 1019, 1024, 1037(2), 1046, 1069, 1078, 1096, 1104, 1121, 1130, 1162, 1164, 1178, 1192, 1260, 1267, 1289, 1294, 1301, 1323, 1325, 1327, 1356, 1365, 1430, 1446, 1447, 1450, 1461, 1478, 1486, 1494, 1528, 1541, 1566, 1588, 1594, 1599, 1613, 1624, 3132, 3142, 3159, 3161, 3162, 3163, 3167, 3168, 3172(2), 3176, 3181, 3182, 3188, 3189, 3190
$Cu^{+}(Bpy)$ Product 1	0.23 (0.02)	43, 74, 132, 208, 216, 238, 258, 385, 386, 417, 435, 440, 528, 642, 652, 678, 692, 721, 756, 765, 773, 880, 901, 962, 966, 1005, 1010, 1012, 1033, 1036, 1071, 1076, 1119, 1126, 1175, 1191, 1257, 1282, 1296, 1319, 1324, 1443, 1459, 1476, 1488, 1590, 1595, 1613, 1624, 3160, 3161, 3167, 3168, 3178, 3181, 3182, 3196

Table E.1b. (continued) Vibrational Frequencies and Average Vibrational Energies of $M^{2+}(Bpy)_2$ Reactants, Transition States, Intermediates, and Products Involved in the Activated Dissociation of $M^{2+}(Bpy)_2$ Complexes through ETCF Process at 298 K.

Species	E_{vib} (eV)[a]	Vibrational frequencies (cm^{-1}) [b]
$Zn^{2+}(Bpy)_2$ Reactant	0.52 (0.05)	19, 33(2), 64, 78, 81(2), 130, 146(2), 206, 227(2), 230, 234, 236, 304, 363, 376, 399, 409, 419(2), 441(2), 459, 460, 547, 548, 646(2), 651(2), 664, 668, 735(2), 740, 742, 763(2), 772(2), 812, 814, 894, 895, 904(2), 970(2), 972(2), 1017(2), 1019(2), 1021(2), 1031, 1034, 1041(2), 1070, 1071, 1080(2), 1121, 1122, 1133(2), 1179(2), 1193(2), 1280, 1283, 1287(2), 1302, 1303, 1327, 1328, 1331(2), 1447, 1448, 1462(2), 1488(2), 1505(2), 1588, 1589, 1596(2), 1615(2), 1628(2), 3158(4), 3165(2), 3166(2), 3180(2), 3182(2), 3183(2), 3195(2)
$Zn^{2+}(Bpy)_2$ TS_1	0.51 (0.05)	**-78**, 21, 28, 36, 58, 70, 80, 87, 124, 133, 147, 164, 222, 228, 233, 283, 297, 318, 343, 378, 398, 401, 415, 418, 440, 460, 533, 540, 544, 615, 649, 651, 652, 663, 672, 731, 739, 744, 757, 762, 763, 774, 783, 788, 806, 896, 908, 909, 915, 973(2), 981, 983, 987, 1018, 1020(2), 1023, 1025, 1028, 1035, 1040, 1042, 1057, 1070, 1079, 1080, 1102, 1122, 1127, 1133, 1172, 1180, 1181, 1194, 1276, 1279, 1286, 1287, 1294, 1301, 1303, 1319, 1330, 1333, 1439, 1447, 1456, 1463, 1470, 1486, 1503, 1505, 1585, 1587, 1589, 1589, 1594, 1613, 1625, 1627, 3140, 3144, 3160, 3161, 3163(2), 3167, 3168(2), 3172, 3179, 3181, 3183(2), 3184, 3195
$Zn^{2+}(Bpy)_2$ Int_1	0.53 (0.05)	19, 24, 32, 63, 71, 77, 85, 107, 133, 148, 155, 183, 220, 227, 233, 266, 292, 346, 372, 375, 401, 414, 418, 423, 440, 459, 504, 544, 545, 611, 648, 650, 651, 659, 668, 732, 739, 741, 761, 762, 767, 773, 778, 798, 809, 885, 895, 906, 910, 972, 974, 974, 981, 990, 1015, 1019, 1020, 1023, 1024, 1025, 1033, 1038, 1040, 1055, 1071, 1078, 1080, 1100, 1122, 1123, 1134, 1166, 1179, 1180, 1195, 1266, 1280, 1282, 1287, 1304, 1313, 1315, 1323, 1328, 1332, 1430, 1448, 1462, 1462, 1471, 1487, 1499, 1505, 1570, 1584, 1588, 1589, 1595, 1614, 1623, 1627, 3069, 3149, 3155, 3156, 3160, 3162, 3166, 3167(2), 3176, 3181(2), 3183, 3184, 3186, 3196

Table E.1b. (continued) Vibrational Frequencies and Average Vibrational Energies of $M^{2+}(Bpy)_2$ Reactants, Transition States, Intermediates, and Products Involved in the Activated Dissociation of $M^{2+}(Bpy)_2$ Complexes through ETCF Process at 298 K.

Species	E_{vib} (eV)[a]	Vibrational frequencies (cm^{-1}) [b]
$Zn^{2+}(Bpy)_2$ TS_2	0.52 (0.05)	**-75**, 19, 25, 35, 61, 66, 71, 85, 95, 142, 156, 184, 226, 231, 235, 248, 300, 320, 375, 390, 398, 406, 409, 417, 439, 457, 473, 542, 557, 603, 616, 648, 650, 653, 671, 717, 728, 736, 743, 759, 763, 774, 788, 802, 834, 895, 908, 916, 932, 959, 969, 973, 983, 984, 992, 1016, 1018, 1020, 1021, 1022, 1025, 1035, 1041, 1042, 1070, 1073, 1080, 1090, 1108, 1124, 1135, 1168, 1172, 1182, 1196, 1252, 1277, 1284, 1286, 1295, 1305, 1320, 1327, 1334, 1338, 1416, 1448, 1452, 1455, 1462, 1484, 1487, 1505, 1524, 1579, 1587, 1593, 1595, 1598, 1612, 1626, 3111, 3142, 3153, 3159, 3162, 3163, 3165, 3167, 3168, 3172, 3178, 3183, 3184, 3186, 3189, 3198
$Zn^{2+}(Bpy)_2$ Int_2	0.57 (0.05)	4(2), 7, 8, 10, 15, 57, 71, 78, 84, 132, 163, 196, 197, 229, 237, 256, 329, 370, 386, 392, 397, 409, 418, 435, 443, 450, 524, 540, 605, 615, 647, 647, 652, 668, 709, 716, 723, 730, 759, 763, 764, 772, 787, 796, 869, 890, 893, 906, 971, 974, 976, 979, 983, 987, 1006, 1011, 1018, 1020, 1023, 1024, 1027, 1036, 1039, 1058, 1069, 1077, 1097, 1104, 1120, 1133, 1163, 1164, 1180, 1194, 1262, 1272, 1289, 1289, 1301, 1318, 1329, 1329, 1340, 1352, 1431, 1445, 1455, 1457, 1462, 1481, 1491, 1501, 1545, 1562, 1583, 1587, 1594, 1595, 1609, 1622, 3122, 3136, 3154, 3155, 3164, 3165, 3168(2), 3169, 3170, 3182, 3184, 3185, 3190, 3193, 3197
$Zn^{+}(Bpy)$ Product 1	0.25 (0.02)	53, 71, 118, 183, 191, 227, 252, 360, 400, 408, 438, 448, 546, 641, 651, 662, 733, 737, 765, 770, 808, 894, 905, 975, 976, 1012, 1014, 1015, 1025, 1038, 1069, 1078, 1117, 1129, 1175, 1189, 1280, 1290, 1299, 1326, 1332, 1446, 1461, 1485, 1503, 1592, 1600, 1615, 1628, 3157, 3157, 3161, 3162, 3175, 3181, 3182, 3189

[a] Uncertainties listed in parentheses are determined as described in the text. [b] Vibrational frequencies scaled by 0.9804 obtained from vibrational analyses of the B3LYP/6-31G* geometry optimized structures. Degeneracies are indicated in parentheses.

Table E.1c. Vibrational Frequencies and Average Vibrational Energies of $M^{2+}(Bpy)_2$ Reactants, Transition States, Intermediates, and Products Involved in the Activated Dissociation of $M^{2+}(Bpy)_2$ Complexes through PTCF Process at 298 K.

Species	E_{vib} (eV)[a]	Vibrational frequencies (cm^{-1}) [b]
$Fe^{2+}(Bpy)_2$ Reactant	0.53 (0.05)	14, 31(2), 59, 62, 76(2), 127, 134(2), 201, 224, 228, 229, 241(2), 280, 357, 379, 399, 400, 416(2), 437(2), 455(2), 544(2), 645(2), 649(2), 660, 668, 729(2), 736, 737, 761(2), 770(2), 802, 804, 889, 890, 901(2), 967(2), 969(2), 1012(2), 1016(2), 1020(2), 1024(2), 1039(2), 1070(2), 1078(2), 1118(2), 1131(2), 1179(2), 1193, 1194, 1278, 1283(3), 1300, 1302, 1322(2), 1328(2), 1445(2), 1459(2), 1484(2), 1502, 1504, 1586(2), 1593(2), 1612, 1613, 1624(2), 3153(4), 3165(2), 3166(2), 3179(2), 3182(2), 3183(2), 3195(2)
$Fe^{2+}(Bpy)_2$ TS_1	0.53 (0.05)	**-1159**, 18, 25, 34, 72, 75, 79, 99, 120, 122, 145, 193, 197, 210, 227, 238, 273, 325, 362, 385, 391, 404, 413, 415, 436, 438, 460, 472, 496, 543, 551, 638, 639, 641, 649, 662, 677, 699, 725, 738, 739, 757, 764, 770, 773, 799, 801, 890, 900(2), 912, 966, 968, 969, 1004, 1004, 1012, 1013, 1016, 1018, 1019, 1026, 1030, 1037, 1063, 1068, 1078, 1080, 1107, 1117, 1131, 1141, 1176, 1178, 1183, 1191, 1267, 1282(2), 1286, 1301, 1308, 1320, 1328, 1330, 1341, 1423, 1430, 1446, 1460, 1465, 1485, 1486, 1507, 1553, 1586, 1588, 1594, 1602, 1613, 1621, 1624, 3152, 3153, 3154, 3156, 3164, 3165, 3166, 3172, 3176, 3178, 3181, 3182, 3183, 3190, 3193
$Fe^{2+}(Bpy)_2$ Int_1	0.53 (0.05)	20, 31, 40, 71, 80, 84, 95, 129, 133, 156, 194, 209, 232, 235, 242, 277, 315, 334, 359, 376, 406, 411, 419, 429, 440, 443, 462, 469, 541, 551, 640, 645, 646, 648, 660, 668, 697, 719, 734, 738, 758, 764, 770, 773, 781, 795, 797, 888, 897, 898, 907, 964, 968, 972, 995, 1004, 1014(2), 1015, 1019(2), 1028, 1032, 1039, 1069, 1071, 1077, 1078, 1111, 1118, 1133, 1136, 1176, 1179, 1187, 1191, 1258, 1280, 1282, 1295, 1302, 1313, 1326, 1327, 1329, 1418, 1431, 1445, 1461, 1465, 1484, 1494, 1506, 1547, 1585, 1589, 1593, 1597, 1613, 1619, 1624, 1853, 3156, 3158, 3162, 3163, 3166, 3167(2), 3176, 3178, 3182(2), 3183, 3185, 3187, 3190

Table E.1c. (continued) Vibrational Frequencies and Average Vibrational Energies of $M^{2+}(Bpy)_2$ Reactants, Transition States, Intermediates, and Products Involved in the Activated Dissociation of $M^{2+}(Bpy)_2$ Complexes through PTCF Process at 298 K.

Species	E_{vib} (eV)[a]	Vibrational frequencies (cm^{-1}) [b]
$Fe^{2+}(Bpy)_2$ TS_2	0.53 (0.05)	**-1157**, 15, 28, 34, 72, 77, 86, 90, 115, 122, 136, 179, 193, 210, 222, 231, 263, 313, 352, 360, 398, 409, 415, 421, 438, 440, 460, 474, 541, 550, 620, 635, 640, 641, 651, 660, 697, 715, 735, 736, 756, 758, 769, 772, 789, 797, 866, 890, 895, 899, 908, 962, 964, 969, 970, 990, 1003, 1009(2), 1015, 1016, 1017, 1029, 1033, 1061, 1068, 1070, 1078, 1108, 1116, 1133, 1135, 1175, 1179, 1186, 1187, 1259, 1269, 1281, 1288, 1302, 1309, 1320, 1326, 1328, 1391, 1421, 1431, 1441, 1459, 1466, 1482, 1488, 1499, 1554, 1560, 1586, 1589, 1601, 1613, 1621, 1624, 3146, 3154, 3155, 3164(2), 3166, 3170, 3174, 3177, 3180, 3181, 3183, 3184, 3187(2)
$Fe^{2+}(Bpy)_2$ Int_2	0.54 (0.05)	15, 30, 34, 56, 69, 77, 85, 95, 131, 141, 155, 188, 206, 227, 230, 279, 287, 323, 353, 365, 399, 401, 415, 421, 441, 454, 456, 516, 552, 580, 619, 632, 633, 647, 649, 657, 697, 732, 736, 737, 749, 758, 771, 780, 797, 823, 850, 893, 906, 907, 951, 963, 966, 977, 978, 979, 994, 1002, 1009, 1014, 1017, 1020, 1021, 1032, 1052, 1070, 1072, 1079, 1112, 1116, 1135, 1163, 1176, 1178, 1190, 1210, 1245, 1256, 1285, 1293, 1301, 1308, 1322, 1324, 1378, 1418, 1423, 1430, 1454, 1466, 1471, 1491, 1497, 1509, 1553, 1583, 1589, 1601, 1608, 1620, 1621, 3154, 3156(2), 3161, 3165(2), 3172, 3173, 3178, 3182(3), 3187, 3190, 3192, 3366
$Fe^{2+}(Bpy)_2$ TS_3	0.54 (0.05)	**-29**, 2, 10, 12, 26, 35, 51, 77, 78, 98, 125, 156, 163, 204, 214, 222, 229, 332, 358, 391, 394, 409, 416, 434, 435, 439, 444, 545, 550, 610, 630, 635, 640, 646, 658, 695, 721, 733, 737, 751, 765, 766, 770, 793, 809, 882, 892, 906, 908, 933, 967, 968, 981, 994, 997, 999, 1008, 1012, 1014, 1018, 1022, 1026, 1035, 1054, 1069, 1076, 1077, 1104, 1105, 1115, 1129, 1174(2), 1188, 1189, 1239, 1249, 1273, 1291, 1301, 1302, 1320, 1327, 1343, 1376, 1416, 1423, 1451, 1461, 1471, 1486, 1488, 1549, 1551, 1590, 1591, 1599, 1606, 1619, 1623, 1644, 3047, 3152, 3155, 3157, 3164, 3166, 3167, 3175, 3177, 3181, 3186, 3187, 3189, 3193, 3197, 3339

Table E.1c. (continued) Vibrational Frequencies and Average Vibrational Energies of $M^{2+}(Bpy)_2$ Reactants, Transition States, Intermediates, and Products Involved in the Activated Dissociation of $M^{2+}(Bpy)_2$ Complexes through PTCF Process at 298 K.

Species	E_{vib} (eV)[a]	Vibrational frequencies (cm^{-1}) [b]
$Fe^{2+}(Bpy)_2$ Int_3	0.60 (0.05)	4, 23, 33, 37, 45, 67, 79, 101, 135, 138, 139, 142, 195, 220, 214, 226, 313, 321, 355, 359, 373, 390, 397, 412, 416, 418, 433, 508, 518, 575, 604, 623, 639, 657, 659, 660, 667, 672, 686, 707, 716, 720, 731, 737, 741, 775, 809, 824, 825, 827, 842, 895, 901, 904, 913, 915, 950, 950, 953, 969, 981, 985, 987, 1003, 1024, 1031, 1035, 1050, 1059, 1089, 1089, 1104, 1118, 1136, 1146, 1154, 1163, 1191, 1221, 1229, 1266, 1277, 1283, 1295, 1324, 1331, 1341, 1347, 1382, 1399, 1421, 1444, 1448, 1472, 1515, 1527, 1572, 1585, 1590, 1615, 1622, 3288, 3297, 3303, 3305, 3306, 3308(2), 3311, 3313, 3315, 3316, 3319, 3320, 3322, 3324, 3682
$[Fe(Bpy\text{-}H)]^+$ Product 1	0.23 (0.02)	98, 108, 115, 117, 160, 213, 331, 354, 377, 417, 440, 480, 557, 631, 638, 712, 720, 748, 763, 777, 808, 901, 921, 966, 980, 1007, 1008, 1011, 1038, 1061, 1093, 1103, 1136, 1174, 1177, 1247, 1283, 1310, 1361, 1378, 1446, 1461, 1472, 1565, 1588, 1598, 1625, 3143, 3146, 3158, 3163, 3168, 3173, 3179
$[Bpy+H]^+$ Product 2	0.21 (0.02)	69, 96, 162, 228, 334, 392, 404, 431, 436, 541, 610, 637, 646, 721, 736, 764, 766, 806, 883, 900, 941, 976, 988, 996, 1008, 1009, 1018, 1033, 1052, 1074, 1103, 1116, 1173, 1185, 1235, 1274, 1301, 1330, 1343, 1372, 1451, 1471, 1487, 1547, 1598, 1605, 1622, 1648, 3148, 3157, 3165, 3168, 3176, 3186, 3191, 3198, 3290
$Co^{2+}(Bpy)_2$ Reactant	0.52 (0.05)	12, 34(2), 56, 75, 76(2), 128, 140(2), 204, 227(2), 235, 255(2), 322, 360, 380, 391, 408, 417(2), 437(2), 458(2), 543, 545, 646(2), 6492), 662, 669, 727(2), 735, 738, 762(2), 769(2), 802, 804, 890(2), 899(2), 965, 966, 967(2), 1015, 1016(3), 1019(2), 1030(2), 1039(2), 1069, 1070, 1078(2), 1118, 1119, 1131(2), 1178(2), 1192(2), 1278, 1281, 1283(2), 1301(2), 1326(2), 1328(2), 1446(2), 1461(2), 1484(2), 1506(2), 1587(2), 1594(2), 1614(2), 1626(2), 3155(4), 3165(2), 3166(2), 3179(2), 3182(2), 3183(2), 3192(2)

Table E.1c. (continued) Vibrational Frequencies and Average Vibrational Energies of $M^{2+}(Bpy)_2$ Reactants, Transition States, Intermediates, and Products Involved in the Activated Dissociation of $M^{2+}(Bpy)_2$ Complexes through PTCF Process at 298 K.

Species	E_{vib} (eV)[a]	Vibrational frequencies (cm^{-1}) [b]
$Co^{2+}(Bpy)_2$ TS_1	0.53 (0.05)	**-1635**, 11, 31, 34, 67, 75, 76, 92, 117, 135, 146, 176, 215, 230, 234, 252, 256, 312, 347, 369, 382, 388, 400, 416, 418, 437, 457, 469, 529, 543, 619, 621, 647, 649, 654, 666, 667, 726, 736, 740, 755, 762, 769, 774, 802, 814, 833, 889, 899, 903, 945, 954, 964, 966, 971, 989, 1016, 1017, 1020(2), 1021, 1031, 1032, 1039, 1054, 1061, 1070, 1078(2), 1119, 1120, 1132, 1162, 1179, 1182, 1193, 1215, 1272, 1280, 1283, 1297, 1302, 1313, 1326, 1328, 1348, 1437, 1446, 1458, 1461, 1484, 1486, 1507, 1518, 1585, 1587, 1594, 1609, 1614, 1618, 1626, 2277, 3148, 3151, 3154, 3157, 3162, 3165, 3165, 3166, 3167, 3175, 3180, 3182, 3183, 3184, 3194
$Co^{2+}(Bpy)_2$ Int_1	0.54 (0.05)	15, 21, 27, 63, 71, 75, 90, 106, 122, 132, 172, 183, 219, 234, 249, 265, 279, 350, 367, 383, 403, 413, 416, 428, 437, 456, 494, 535, 543, 612, 631, 647, 648, 649, 666, 706, 727, 736, 752, 762, 766, 768, 780, 801, 806, 860, 888, 897, 901, 910, 962, 964, 975, 980, 987, 1009, 1015(2), 1016, 1019, 1024, 1030, 1039, 1054, 1070(2), 1078, 1079, 1119, 1120, 1132, 1177, 1178, 1180, 1193, 1233, 1244, 1279, 1282, 1296, 1301, 1317, 1326, 1327, 1359, 1369, 1446, 1458, 1461, 1472, 1483, 1484, 1506, 1535, 1580, 1587, 1593, 1594, 1614, 1618, 1625, 3151, 3153, 3154, 3156, 3164, 3165(2), 3166, 3171, 3172, 3180, 3181, 3182, 3183, 3194, 3410
$Co^{2+}(Bpy)_2$ TS_2	0.53 (0.05)	**-1030**, 19, 32, 37, 72, 76, 81, 91, 93, 135, 140, 165, 205, 224, 233, 240, 258, 317, 350, 367, 402, 409, 416, 425, 432, 440, 460, 472, 545, 549, 613, 636, 644, 649, 653, 664, 694, 730, 738, 741, 753, 764, 771, 778, 799, 804, 892, 899, 902, 911, 933, 967, 968, 971, 972, 1001, 1014(2), 1015, 1019(2), 1027, 1029, 1039, 1069, 1070, 1072, 1078, 1115, 1118, 1131, 1150, 1178, 1183, 1191, 1193, 1262, 1281, 1285, 1296, 1303, 1313, 1327, 1327, 1330, 1406, 1424, 1445, 1459, 1461, 1481, 1483, 1506, 1541, 1544, 1586, 1587, 1592, 1594, 1615, 1617, 1625, 3152, 3155, 3156, 3162, 3165, 3166, 3167, 3175, 3178, 3181, 3182, 3183, 3184, 3185, 3190

Table E.1c. (continued) Vibrational Frequencies and Average Vibrational Energies of $M^{2+}(Bpy)_2$ Reactants, Transition States, Intermediates, and Products Involved in the Activated Dissociation of $M^{2+}(Bpy)_2$ Complexes through PTCF Process at 298 K.

Species	E_{vib} (eV)[a]	Vibrational frequencies (cm^{-1}) [b]
$Co^{2+}(Bpy)_2$ Int_2	0.53 (0.05)	15, 29, 40, 78, 81, 85, 92, 132, 141, 155, 195, 204, 236, 241, 248, 282, 330, 361, 373, 379, 404, 415, 422, 428, 442, 443, 465, 469, 542, 551, 641, 643, 647, 648, 661, 667, 695, 720, 734, 737, 758, 766, 770, 774, 794, 796, 817, 888, 897, 897, 908, 964, 968, 972, 997, 1004, 1014, 1015, 1016, 1018, 1019, 1029, 1032, 1037, 1067, 1069, 1078, 1079, 1112, 1118, 1132, 1137, 1176, 1178, 1187, 1188, 1258, 1281, 1285, 1297, 1304, 1312, 1327, 1327, 1333, 1419, 1431, 1446, 1461, 1465, 1485, 1495, 1506, 1549, 1585, 1589, 1594, 1598, 1614, 1619, 1624, 1915, 3155, 3157, 3160, 3164, 3165, 3167, 3168, 3176, 3177, 3181, 3182, 3183, 3185, 3187(2)
$Co^{2+}(Bpy)_2$ TS_3	0.52 (0.05)	**-1070**, 19, 32, 41, 73, 82, 87, 93, 125, 131, 151, 189, 202, 227, 233, 247, 273, 319, 356, 367, 402, 415, 419, 420, 442, 449, 461, 473, 542, 553, 625, 640, 643, 644, 654, 662, 698, 720, 737(2), 756, 761, 770, 773, 792, 799, 884, 893, 896, 909, 934, 964, 967, 969, 978, 990, 1003, 1011, 1013, 1016, 1017, 1019, 1030, 1035, 1065, 1069, 1072, 1079, 1110, 1120, 1136, 1139, 1176, 1179, 1187, 1188, 1257, 1272, 1284, 1294, 1307, 1309, 1322, 1326, 1328, 1422, 1427, 1437, 1459, 1465, 1480, 1488, 1491, 1533, 1555, 1568, 1588, 1589, 1603, 1615, 1620, 1631, 3154, 3156, 3157, 3165, 3166, 3168, 3172, 3175, 3177, 3181, 3182, 3185, 3185, 3187, 3188
$Co^{2+}(Bpy)_2$ Int_3	0.54 (0.05)	9, 24, 33, 64, 74, 76, 85, 109, 136, 143, 166, 205, 215, 231, 237, 269, 289, 341, 365, 381, 398, 404, 417, 422, 440, 457, 484, 525, 550, 583, 615, 632, 635, 648, 655, 660, 696, 714, 736, 738, 746, 758, 771, 779, 796, 809, 868, 894, 897, 907, 946, 966, 967, 970, 986, 992, 1002, 1005, 1015, 1017(2), 1018, 1022, 1033, 1052, 1063, 1071, 1078, 1113, 1120, 1135, 1146, 1176, 1178, 1189, 1212, 1253, 1255, 1290, 1293, 1303, 1310, 1317, 1323, 1353, 1414, 1422, 1429, 1441, 1457, 1466, 1473, 1492, 1521, 1552, 1575, 1589, 1599, 1602, 1613, 1621, 3155, 3155, 3158, 3159, 3164, 3166, 3168, 3174, 3178, 3182, 3183, 3184, 3187, 3188, 3189, 3270

Table E.1c. (continued) Vibrational Frequencies and Average Vibrational Energies of $M^{2+}(Bpy)_2$ Reactants, Transition States, Intermediates, and Products Involved in the Activated Dissociation of $M^{2+}(Bpy)_2$ Complexes through PTCF Process at 298 K.

Species	E_{vib} (eV)[a]	Vibrational frequencies (cm^{-1}) [b]
$Co^{2+}(Bpy)_2$ TS_4	0.54 (0.05)	**-15**, 7, 14, 19, 35, 44, 69, 79, 95, 99, 122, 136, 159, 202, 216, 229, 272, 333, 361, 379, 394, 405, 412, 431, 434, 435, 454, 543, 545, 611, 622, 635, 646, 652, 694, 701, 721, 732, 736, 745, 767, 770, 775, 798, 808, 892, 896, 903, 914, 954, 968, 976, 985, 995, 1006, 1007, 1011(3), 1018, 1020, 1033, 1039, 1048, 1059, 1074, 1080, 1097, 1101, 1116, 1129, 1174, 1180, 1185, 1193, 1221, 1260, 1275, 1283, 1300, 1303, 1330, 1331, 1340, 1366, 1370, 1424, 1449, 1458, 1470, 1480, 1486, 1526, 1543, 1583, 1588, 1597, 1604, 1619, 1620, 1644, 3141, 3142, 3154, 3157, 3159, 3164, 3165, 3169(2), 3176, 3178, 3180, 3183, 3191, 3193, 3302
$Co^{2+}(Bpy)_2$ Int_4	0.55 (0.05)	4, 7, 9, 14, 19, 20, 51, 67, 71, 87, 96, 129, 161, 193, 218, 228, 280, 333, 361, 376, 392, 405, 413, 419, 431, 436, 461, 539, 541, 600, 611, 636, 646(2), 680, 688, 720, 727, 736, 749, 764, 766, 769, 791, 806, 883, 891, 900, 905, 939, 956, 965, 976, 985, 995, 999, 1007, 1009, 1011, 1014, 1019, 1032, 1034, 1054, 1061, 1075, 1077, 1102, 1103, 1116, 1131, 1174(2), 1181, 1186, 1237, 1263, 1273, 1296, 1302, 1309, 1329, 1343, 1345, 1374, 1406, 1442, 1451, 1467, 1472, 1486, 1487, 1548, 1558, 1587, 1599, 1607, 1609, 1623, 1625, 1647, 3135, 3139, 3149, 3158, 3159, 3163, 3166, 3169, 3172, 3181(2), 3185, 3186, 3191, 3197, 3307
$[Co(Bpy\text{-}H)]^+$ Product 1	0.23 (0.02)	15, 81, 93, 120, 172, 211, 305, 349, 369, 414, 430, 465, 545, 621, 641, 693, 706, 732, 752, 772, 796, 895, 914, 961, 986, 1001, 1003, 1011, 1039, 1059, 1086, 1101, 1129, 1175, 1181, 1259, 1285, 1305, 1356, 1391, 1434, 1462, 1478, 1556, 1584, 1585, 1627, 3142, 3148, 3159, 3162, 3171, 3172, 3180
$Ni^{2+}(Bpy)_2$ Reactant	0.52 (0.05)	10, 42(2), 76, 78, 85(2), 131, 171(2), 199, 233, 235, 241, 285, 285, 339, 362, 380, 400, 407, 422(2), 444(2), 489(2), 544, 545, 648(2), 652(2), 664, 670, 731(2), 739, 740, 765(2), 771(2), 803, 806, 893(2), 899(2), 966(2), 967(2), 1016(2), 1019(4), 1031, 1033, 1039(2), 1067, 1068, 1079(2), 1118(2), 1131(2), 1178(2), 1189(2), 1278, 1283, 1287(2), 1302(2), 1328(2), 1335(2), 1447(2), 1462(2), 1484(2), 1509(2), 1587, 1588, 1594(2), 1614(2), 1625(2), 3154(3), 3155, 3165(2), 3166(2), 3177(2), 3182(2), 3183(2), 3188(2)

Table E.1c. (continued) Vibrational Frequencies and Average Vibrational Energies of $M^{2+}(Bpy)_2$ Reactants, Transition States, Intermediates, and Products Involved in the Activated Dissociation of $M^{2+}(Bpy)_2$ Complexes through PTCF Process at 298 K.

Species	E_{vib} (eV)[a]	Vibrational frequencies (cm^{-1}) [b]
$Ni^{2+}(Bpy)_2$ TS_1	0.52 (0.05)	**-1408**, 20, 25, 36, 72, 77, 85, 101, 117, 127, 161, 200, 212, 232, 239, 255, 269, 348, 366, 393, 395, 406, 414, 419, 441, 442, 464, 477, 535, 543, 559, 639, 641, 646, 649, 667, 683, 693, 721, 732, 736, 757, 766, 768, 773, 796, 797, 888, 896, 901, 912, 962, 964, 969, 1003, 1004, 1012, 1014, 1017, 1018, 1021, 1030, 1034, 1038, 1060, 1068, 1079, 1083, 1107, 1119, 1132, 1143, 1175, 1178, 1182, 1189, 1264, 1278, 1281, 1285, 1294, 1304, 1309, 1328, 1333, 1341, 1420, 1432, 1447, 1462, 1464, 1483, 1486, 1507, 1551, 1587, 1588, 1595, 1604, 1615, 1621, 1626, 3152, 3156, 3158, 3159, 3164, 3165, 3167, 3171, 3175, 3177, 3182(2), 3183, 3188, 3194
$Ni^{2+}(Bpy)_2$ Int_1	0.52 (0.05)	22, 31, 41, 76, 80, 87, 97, 136, 145, 158, 197, 219, 236, 244, 259, 293, 343, 364, 380, 402, 411, 420, 423, 441, 442, 466, 470, 540, 548, 574, 641, 645, 648(2), 664, 671, 691, 716, 729, 730, 759, 765, 768, 773, 790, 793, 845, 886, 894, 895, 907, 962, 964, 968, 999, 1004, 1014, 1017, 1018, 1020, 1021, 1031, 1035, 1040, 1067, 1070, 1078, 1079, 1113, 1119, 1133, 1138, 1176, 1178, 1186, 1188, 1259, 1280, 1285, 1297, 1304, 1312, 1327, 1328, 1332, 1421, 1432, 1447, 1462, 1466, 1486, 1496, 1506, 1550, 1587, 1591, 1596, 1601, 1614, 1621, 1625, 2039, 3157, 3159, 3160, 3164, 3166, 3167, 3168, 3176, 3177, 3182, 3182, 3183, 3184, 3187(2)
$Ni^{2+}(Bpy)_2$ TS_2	0.52 (0.05)	**-966**, 18, 31, 42, 75, 81, 87, 100, 124, 137, 159, 186, 208, 230, 232, 255, 268, 328, 358, 368, 402, 416, 418, 421, 441, 446, 462, 472, 543, 552, 629, 636, 644, 647, 657, 660, 697, 722, 735, 738, 759, 761, 773, 773, 795, 797, 891, 896, 899, 908, 966, 968, 969, 971, 986, 989, 1002, 1015, 1016(2), 1018, 1024, 1032, 1037, 1064, 1069, 1073, 1078, 1112, 1119, 1135, 1138, 1175, 1179, 1187(2), 1256, 1273, 1287, 1293, 1307, 1310, 1325, 1325, 1328, 1423, 1430, 1439, 1462, 1466, 1480, 1490, 1500, 1553, 1572, 1590, 1591, 1602, 1611, 1619, 1621, 1741, 3155, 3156, 3159, 3165, 3166, 3168, 3175, 3176, 3178, 3181, 3182, 3185, 3186, 3187, 3188

Table E.1c. (continued) Vibrational Frequencies and Average Vibrational Energies of $M^{2+}(Bpy)_2$ Reactants, Transition States, Intermediates, and Products involved in the Activated Dissociation of $M^{2+}(Bpy)_2$ Complexes through PTCF Process at 298 K.

Species	E_{vib} (eV)[a]	Vibrational frequencies (cm^{-1}) [b]
$Ni^{2+}(Bpy)_2$ Int_2	0.53 (0.05)	16, 21, 33, 69, 77, 83, 91, 113, 132, 144, 159, 198, 211, 228, 233, 263, 305, 346, 366, 382, 393, 403, 419, 425, 442, 459, 490, 532, 549, 576, 624, 630, 648, 650, 657, 661, 694, 719, 735, 740, 748, 759, 771, 774, 784, 793, 852, 895, 900, 908, 953, 968, 972, 984, 985, 995, 1000, 1013, 1016, 1017, 1018, 1021, 1033, 1034, 1060, 1070, 1078(2), 1113, 1122, 1134, 1162, 1175, 1179, 1187, 1218, 1252, 1271, 1293, 1293, 1310, 1311, 1322, 1324, 1356, 1422, 1427, 1429, 1456, 1466, 1473, 1489, 1490, 1530, 1550, 1575, 1590, 1600, 1609, 1615, 1621, 3155, 3156, 3158, 3163, 3165, 3166, 3173, 3174, 3176, 3181, 3182, 3183, 3185, 3187, 3196, 3249
$Ni^{2+}(Bpy)_2$ TS_3	0.54 (0.05)	**-34**, 3, 9, 13, 27, 28, 54, 71, 74, 99, 139, 164, 194, 224, 229, 238, 262, 332, 381, 390, 391, 408, 419, 433, 434, 436, 450, 535, 544, 611, 629, 636, 646, 650, 660, 666, 709, 720, 736, 752, 765(2), 766, 772, 808, 881, 886, 902, 905, 933, 959, 981, 987, 988, 992, 994, 1008, 1010, 1012, 1013, 1022, 1033, 1035, 1054, 1068, 1076, 1078, 1104, 1111, 1117, 1129, 1173, 1175, 1186, 1188, 1239, 1242, 1273, 1290, 1300, 1306, 1317, 1326, 1342, 1375, 1417, 1423, 1450, 1463, 1472, 1483, 1488, 1549, 1549, 1588, 1599, 1601, 1606, 1622, 1623, 1644, 3074, 3155, 3156, 3159, 3165, 3167, 3168, 3175(2), 3181, 3184, 3186, 3187, 3193, 3197, 3343
$Ni^{2+}(Bpy)_2$ Int_3	0.55 (0.05)	5, 8, 9, 11, 17, 18, 52, 63, 70, 96, 132, 163, 173, 209, 228, 228, 263, 334, 374, 390, 392, 406, 415, 425, 432, 437, 454, 533, 542, 611, 617, 636, 643, 646, 655, 661, 710, 721, 736, 748, 764, 766, 767, 773, 806, 883, 886, 902, 903, 938, 957, 958, 981, 986, 991, 995, 1008, 1009(2), 1014, 1019, 1033, 1034, 1053, 1068, 1075, 1081, 1103, 1109, 1115, 1130, 1174(2), 1186(2), 1237, 1251, 1274, 1291, 1302(2), 1322, 1329, 1343, 1373, 1407, 1438, 1451, 1466, 1473, 1481, 1488, 1548, 1558, 1589, 1598, 1607, 1610, 1623, 1624, 1646, 3102, 3149, 3158, 3161, 3166, 3166, 3170, 3174, 3181(2), 3182, 3185, 3186, 3192, 3197, 3308
$[Ni(Bpy\text{-}H)]^+$ Product 1	0.25 (0.02)	49, 72, 135, 193, 223, 226, 270, 384, 389, 419, 433, 451, 534, 626, 649, 657, 666, 707, 752, 764, 770, 884, 900, 956, 980, 986, 1004, 1012, 1033, 1068, 1078, 1110, 1128, 1171, 1184, 1243, 1290, 1305, 1318, 1413, 1424, 1463, 1481, 1551, 1588, 1601, 1623, 3153, 3157, 3163, 3174, 3180, 3183, 3186

Table E.1c. (continued) Vibrational Frequencies and Average Vibrational Energies of $M^{2+}(Bpy)_2$ Reactants, Transition States, Intermediates, and Products Involved in the Activated Dissociation of $M^{2+}(Bpy)_2$ Complexes through PTCF Process at 298 K.

Species	E_{vib} (eV)[a]	Vibrational frequencies (cm^{-1}) [b]
$Cu^{2+}(Bpy)_2$ Reactant	0.52 (0.05)	30, 32, 46, 75, 85, 95, 111, 137, 138, 166, 192, 196, 235, 236, 254, 291, 330, 364, 368, 405, 415, 418, 419, 439, 444, 464, 474, 545, 550, 643, 648(2), 650, 666, 667, 728, 730, 738, 740, 765, 766, 771, 773, 801, 803, 895, 899, 901, 905, 969, 970, 976(2), 1016(2), 1017, 1020(3), 1031, 1036, 1037, 1038, 1067, 1068, 1078, 1080, 1118, 1119, 1130, 1133, 1178(2), 1189(2), 1279, 1284, 1285, 1288, 1303(2), 1327, 1328, 1333, 1334, 1447(2), 1461, 1463, 1484, 1485, 1507, 1508, 1587, 1588, 1593, 1595, 1614(2), 1625(2), 3160(2), 3161, 3162, 3166(2), 3167(2), 3177(2), 3182(2), 3183(2), 3187, 3188
$Cu^{2+}(Bpy)_2$ TS_1	0.53 (0.05)	**-1393**, 19, 29, 37, 56, 77, 80, 101, 124, 133, 159, 165, 194, 228, 232, 238, 281, 332, 358, 373, 391, 402, 411, 418, 437, 440, 454, 461, 480, 546, 548, 636, 638, 644, 649, 663, 681, 687, 726, 735, 736, 756, 764, 770, 773, 794, 807, 888, 901(2), 909, 964, 969, 972, 1001, 1004, 1010, 1012, 1014, 1018, 1019, 1028, 1033, 1037, 1060, 1069, 1081, 1084, 1110, 1119, 1132, 1141, 1176, 1178, 1182, 1192, 1256, 1274, 1281, 1287, 1293, 1301, 1310, 1327, 1329, 1338, 1423, 1433, 1445, 1460, 1466, 1484, 1487, 1502, 1545, 1586, 1588, 1598, 1611(2), 1623(2), 3150, 3153, 3161(2), 3164, 3165, 3167, 3171, 3175, 3178, 3181, 3182, 3183, 3193, 3195
$Cu^{2+}(Bpy)_2$ Int_1	0.54 (0.05)	12, 29, 39, 67, 78, 81, 90, 129, 133, 143, 157, 200, 231, 235, 243, 278, 321, 363, 372, 394, 404, 415, 418, 430, 439, 447, 459, 470, 545, 548, 635, 641, 647, 649, 661, 668, 690, 723, 729, 733, 750, 759, 764, 770, 772, 790, 804, 887, 893, 901, 906, 965, 967, 970, 997, 1003, 1013, 1014, 1017, 1018, 1022, 1024, 1034, 1038, 1068, 1069, 1079, 1081, 1115, 1119, 1132, 1137, 1177, 1178, 1186, 1191, 1257, 1280, 1287, 1299, 1301, 1312, 1327, 1328, 1330, 1421, 1433, 1444, 1459, 1467, 1487, 1495, 1499, 1549, 1586, 1590, 1599, 1602, 1609, 1620, 1622, 2089, 3155, 3157, 3163, 3164, 3165, 3167, 3168, 3176, 3178, 3181, 3182, 3183, 3185, 3187, 3192

Table E.1c. (continued) Vibrational Frequencies and Average Vibrational Energies of $M^{2+}(Bpy)_2$ Reactants, Transition States, Intermediates, and Products Involved in the Activated Dissociation of $M^{2+}(Bpy)_2$ Complexes through PTCF Process at 298 K.

Species	E_{vib} (eV)[a]	Vibrational frequencies (cm^{-1}) [b]
$Cu^{2+}(Bpy)_2$ TS_2	0.52 (0.05)	**-464**, 15, 33, 43, 74, 81, 87, 90, 127, 138, 159, 176, 198, 225, 239, 248, 266, 313, 360, 371, 402, 413, 418, 425, 438, 444, 463, 470, 546, 551, 634, 640, 646, 648, 657, 666, 695, 724, 734, 735, 744, 759, 764, 773, 773, 794, 808, 893, 895, 904, 907, 968, 971, 972, 995, 1002(2), 1017(2), 1020(2), 1023, 1035, 1036, 1067, 1070, 1079(2), 1115, 1119, 1132, 1137, 1176, 1178, 1187, 1190, 1256, 1278, 1291, 1297, 1301, 1312, 1326, 1327, 1330, 1423, 1433, 1443, 1460, 1467, 1485, 1493, 1498, 1552, 1584, 1591, 1597, 1604, 1607, 1620, 1622, 2046, 3156, 3160(2), 3164, 3166, 3166, 3169, 3176, 3178, 3182(2), 3183, 3185, 3187, 3191
$Cu^{2+}(Bpy)_2$ Int_2	0.54 (0.05)	15, 25, 28, 55, 69, 78, 84, 100, 136, 142, 158, 175, 194, 210, 228, 256, 285, 343, 363, 393, 400, 404, 423, 428, 441, 464, 475, 537, 553, 621, 634, 642, 643, 652, 663, 694, 713, 738, 741, 756, 761, 764, 775, 791, 799, 852, 897, 899, 907, 911, 971, 972, 975, 979, 1000, 1003, 1014, 1016, 1018, 1022, 1026, 1032, 1038, 1060, 1068, 1080, 1083, 1110, 1111, 1125, 1134, 1175, 1182, 1186, 1191, 1253, 1256, 1281, 1292, 1300, 1306, 1309, 1329, 1337, 1393, 1419, 1440, 1442, 1468, 1473, 1487, 1489, 1553, 1557, 1584, 1591, 1611, 1611, 1624, 1627, 1636, 3152, 3154, 3156, 3163, 3168, 3169, 3173, 3179, 3180, 3183, 3184, 3185(2), 3194, 3196, 3203
$Cu^{2+}(Bpy)_2$ TS_3	0.53 (0.05)	**-54**, 11, 18, 25, 33, 49, 61, 68, 86, 102, 141, 159, 176, 221, 228, 232, 256, 330, 371, 389, 397, 406, 419, 424, 429, 437, 458, 540, 543, 611, 633, 636, 645(2), 669, 679, 719, 723, 734, 751, 764(2), 775, 787, 805, 879, 898, 902, 913, 943, 967, 972, 973, 984, 994, 1001, 1006, 1013, 1015, 1017, 1023, 1032, 1035, 1054, 1068, 1076, 1078, 1104, 1112, 1119, 1133, 1177, 1178, 1188, 1191, 1233, 1247, 1278, 1291, 1301, 1303, 1326, 1329, 1339, 1375, 1412, 1441, 1448, 1465, 1471, 1481, 1487, 1547, 1554, 1589, 1596, 1604, 1610, 1619, 1624, 1642, 3141, 3152, 3163(2), 3168(2), 3174, 3176, 3179, 3182, 3184, 3186(2), 3198, 3200, 3346

Table E.1c. (continued) Vibrational Frequencies and Average Vibrational Energies of $M^{2+}(Bpy)_2$ Reactants, Transition States, Intermediates, and Products Involved in the Activated Dissociation of $M^{2+}(Bpy)_2$ Complexes through PTCF Process at 298 K.

Species	E_{vib} (eV)[a]	Vibrational frequencies (cm^{-1}) [b]
$Cu^{2+}(Bpy)_2$ Int_3	0.54 (0.05)	5(2), 7, 9, 10, 18, 42, 70, 78, 96, 132, 163, 177, 223, 228, 231, 254, 334, 375, 392, 395, 406, 418, 430, 432, 437, 455, 542, 543, 611, 636(2), 645, 646, 671, 677, 719, 721, 736, 752, 764, 767, 771, 783, 806, 883, 891, 902, 906, 938, 966, 971, 981, 986, 995, 996, 1008, 1009, 1012, 1016, 1019, 1034(2), 1053, 1068, 1075, 1081, 1103, 1112, 1115, 1134, 1174, 1175, 1186, 1188, 1237, 1251, 1274, 1290, 1302, 1302, 1327, 1329, 1343, 1373, 1416, 1443, 1451, 1467, 1473, 1482, 1488, 1548, 1562, 1590, 1598, 1607, 1613, 1623, 1627, 1646, 3102, 3149, 3158, 3161, 3166, 3167, 3170, 3174, 3181(2), 3182, 3185(2), 3192, 3197, 3308
$[Cu(Bpy\text{-}H)]^+$ Product 1	0.25 (0.02)	26, 79, 131, 183, 219, 231, 255, 379, 388, 418, 436, 446, 540, 636, 646, 666, 676, 717, 751, 770, 780, 889, 906, 966, 970, 994, 1009, 1014, 1033, 1069, 1079, 1111, 1133, 1174, 1187, 1249, 1290, 1300, 1327, 1413, 1442, 1466, 1481, 1561, 1590, 1614, 1629, 3149, 3161, 3167, 3174, 3181, 3184, 3186
$Zn^{2+}(Bpy)_2$ Reactant	0.52 (0.05)	19, 33(2), 64, 78, 81(2), 130, 146(2), 206, 227(2), 230, 234, 236, 304, 363, 376, 399, 409, 419(2), 441(2), 459, 460, 547, 548, 646(2), 651(2), 664, 668, 735(2), 740, 742, 763(2), 772(2), 812, 814, 894, 895, 904(2), 970(2), 972(2), 1017(2), 1019(2), 1021(2), 1031, 1034, 1041(2), 1070, 1071, 1080(2), 1121, 1122, 1133(2), 1179(2), 1193(2), 1280, 1283, 1287(2), 1302, 1303, 1327, 1328, 1331(2), 1447, 1448, 1462(2), 1488(2), 1505(2), 1588, 1589, 1596(2), 1615(2), 1628(2), 3158(4), 3165(2), 3166(2), 3180(2), 3182(2), 3183(2), 3195(2)
$Zn^{2+}(Bpy)_2$ TS_1	0.53 (0.05)	**-1637**, 17, 30, 33, 69, 78, 80, 95, 122, 140, 152, 176, 209, 225, 227, 234, 252, 295, 349, 370, 381, 386, 402, 418, 421, 441, 459, 473, 532, 546, 618, 628, 647, 651, 656, 668, 679, 734, 740, 747, 758, 763, 772, 777, 811, 817, 848, 894, 904, 907, 947, 954, 969, 971, 975, 993, 1018, 1020, 1022, 1022, 1025, 1034(2), 1041, 1056, 1061, 1071, 1081(2), 1121, 1123, 1133, 1157, 1180, 1183, 1194, 1213, 1275, 1282, 1288, 1301, 1303, 1312, 1328, 1331, 1351, 1440, 1448, 1459, 1462, 1488, 1489, 1506, 1521, 1587, 1589, 1596, 1609, 1616, 1620, 1629, 2287, 3148, 3155, 3158, 3159, 3162, 3164, 3166, 3167(2), 3176, 3181, 3183(2), 3184, 3196

Table E.1c. (continued) Vibrational Frequencies and Average Vibrational Energies of $M^{2+}(Bpy)_2$ Reactants, Transition States, Intermediates, and Products Involved in the Activated Dissociation of $M^{2+}(Bpy)_2$ Complexes through PTCF Process at 298 K.

Species	E_{vib} (eV)[a]	Vibrational frequencies (cm^{-1}) [b]
$Zn^{2+}(Bpy)_2$ Int_1	0.54 (0.05)	20, 29, 32, 67, 76, 77, 86, 117, 132, 146, 151, 186, 214, 231, 236, 260, 281, 345, 352, 374, 391, 402, 417, 422, 440, 459, 474, 529, 544, 600, 635, 649, 650, 654, 669, 702, 732, 739, 753, 754, 762, 771, 780, 803, 808, 853, 893, 904, 907, 930, 968, 969, 971, 974, 998, 1019, 1020, 1021, 1022, 1023, 1024, 1035, 1041, 1048, 1069, 1071, 1074, 1081, 1120, 1123, 1134, 1172, 1180, 1181, 1195, 1238, 1273, 1280, 1287, 1296, 1304, 1315, 1328, 1332, 1350, 1380, 1448, 1457, 1460, 1462, 1484, 1488, 1493, 1506, 1580, 1588, 1595, 1615, 1617, 1620, 1628, 3146, 3156, 3158, 3159, 3161, 3164, 3166, 3167, 3168, 3174, 3182, 3183(2), 3185, 3197, 3390
$Zn^{2+}(Bpy)_2$ TS_2	0.54 (0.05)	**-56**, 15, 22, 40, 55, 68, 82, 86, 113, 120, 154, 179, 199, 210, 234, 258, 266, 296, 325, 365, 386, 404, 421, 422, 443, 446, 454, 486, 515, 547, 551, 612, 639, 643, 648, 651, 656, 664, 734, 737, 742, 750, 764, 772, 778, 794, 813, 895, 897, 902, 905, 910, 970, 972, 976, 982, 1015(2), 1019(2), 1022, 1030, 1032, 1040, 1046, 1070, 1077, 1081, 1110, 1121, 1132, 1142, 1178, 1181, 1188, 1192, 1256, 1281, 1283, 1288, 1291, 1302, 1323, 1328, 1330, 1395, 1444, 1447, 1461, 1462, 1480, 1488, 1504, 1514, 1589, 1592, 1597, 1610, 1616, 1628, 1643, 1931, 3143, 3156, 3156, 3157, 3164, 3165, 3166, 3177, 3179, 3181, 3182, 3183, 3186, 3193, 3216
$Zn^{2+}(Bpy)_2$ Int_2	0.56 (0.05)	12, 21, 23, 27, 64, 71, 79, 84, 115, 130, 156, 179, 193, 202, 234, 250, 262, 319, 361, 382, 390, 404, 420, 430, 443, 448, 459, 481, 496, 539, 548, 600, 634, 639, 642, 647, 652, 662, 729, 737, 742, 748, 765, 767, 772, 791, 813, 882, 895(2), 905, 908, 969, 973(2), 978, 1013, 1015, 1018(2), 1022, 1028, 1031, 1034, 1040, 1070, 1079, 1081, 1110, 1121, 1132, 1142, 1178(2), 1189, 1192, 1237, 1281, 1283, 1288, 1293, 1302, 1324, 1327, 1330, 1389, 1438, 1447, 1452, 1461, 1479, 1489, 1504, 1514, 1589, 1593, 1598, 1609, 1616, 1628, 1740, 1958, 3140, 3154, 3156, 3161, 3164, 3165, 3167, 3177, 3178, 3181(2), 3183, 3188, 3193, 3221

Table E.1c. (continued) Vibrational Frequencies and Average Vibrational Energies of $M^{2+}(Bpy)_2$ Reactants, Transition States, Intermediates, and Products Involved in the Activated Dissociation of $M^{2+}(Bpy)_2$ Complexes through PTCF Process at 298 K.

Species	E_{vib} (eV)[a]	Vibrational frequencies (cm^{-1}) [b]
$Zn^{2+}(Bpy)_2$ TS_3	0.53 (0.05)	**-1120**, 20, 30, 33, 70, 76, 83, 91, 99, 137, 144, 180, 205, 222(2), 242, 246, 288, 351, 364, 400, 411, 413, 425, 436, 439, 459, 466, 542, 543, 610, 622, 636, 642, 658, 661, 679, 696, 727, 739, 743, 749, 757, 771, 777, 800, 810, 889, 898(2), 907, 943, 952, 967, 969, 972, 996, 1008, 1011, 1019(2), 1022, 1031, 1037, 1065, 1067, 1075, 1080, 1109, 1117, 1134(2), 1179, 1180, 1191, 1192, 1235, 1262, 1275, 1288, 1300, 1306, 1308, 1312, 1326, 1328, 1393, 1436, 1447, 1458, 1472, 1480, 1490, 1495, 1544, 1565, 1586, 1587, 1603, 1613, 1619, 1627, 3144, 3160, 3161, 3162, 3166, 3167, 3169, 3174, 3179, 3182(2), 3184, 3186, 3188, 3194
$Zn^{2+}(Bpy)_2$ Int_3	0.55 (0.05)	19, 27, 44(2), 51, 75, 91, 132, 138, 141, 142, 162, 188, 200, 218, 250, 294, 302, 343, 369, 376, 378, 405, 407, 410, 454, 472, 522, 524, 594, 612, 642, 652, 653, 667, 678, 687, 711, 733, 740, 746, 761, 766, 769, 783, 801, 886, 887, 896, 905, 961, 968(2), 980, 1002, 1003, 1010, 1017, 1019, 1020, 1027, 1031, 1045, 1058, 1067, 1079, 1085, 1108, 1113, 1127, 1132, 1176, 1182, 1187, 1190, 1242, 1266, 1294, 1305, 1306, 1317, 1322, 1347, 1357, 1391, 1408, 1442, 1451, 1468, 1479, 1490, 1494, 1542, 1550, 1581, 1594, 1597, 1609, 1612, 1623, 1639, 3142, 3151, 3152, 3165, 3166, 3171(2), 3178, 3180, 3181, 3184, 3185, 3186, 3194, 3197, 3300
$Zn^{2+}(Bpy)_2$ TS_4	0.54 (0.05)	**-17**, 8, 10, 16, 30, 46, 61, 75, 84, 97, 141, 161, 190, 224, 230, 238, 251, 330, 363, 378, 389, 408, 417, 425, 430, 439, 453, 539, 545, 609, 611, 635, 650, 653, 665, 687, 719, 730, 735, 736, 766, 767, 774, 799, 809, 874, 894, 910, 913, 922, 968, 971, 978, 986, 992, 998, 1005, 1008, 1017, 1019, 1022, 1024, 1038, 1057, 1062, 1076, 1083, 1100, 1104, 1115, 1128, 1174, 1182, 1189, 1198, 1241, 1260, 1273, 1296, 1297, 1302, 1322, 1326, 1340, 1378, 1397, 1408, 1447, 1461, 1470, 1483, 1485, 1526, 1550, 1581, 1589, 1594, 1604, 1620, 1624, 1642, 2923, 3141, 3156, 3161, 3164, 3165, 3168, 3172, 3177(2), 3183, 3186, 3193, 3197, 3198, 3375

Table E.1c. (continued) Vibrational Frequencies and Average Vibrational Energies of $M^{2+}(Bpy)_2$ Reactants, Transition States, Intermediates, and Products Involved in the Activated Dissociation of $M^{2+}(Bpy)_2$ Complexes through PTCF Process at 298 K.

Species	E_{vib} (eV)[a]	Vibrational frequencies (cm^{-1}) [b]
$Zn^{2+}(Bpy)_2$ Int_4	0.55 (0.05)	4, 7(2), 10(2), 14, 25, 64, 68, 97, 130, 162, 181, 215, 228, 233, 246, 334, 362, 374, 392, 405, 416, 425, 432, 436, 455, 539, 541, 610, 612, 636, 646, 649, 661, 682, 720, 732, 735, 736, 764, 767, 772, 795, 806, 883, 892, 901, 907, 939, 965, 970, 977, 985, 996, 996, 999, 1008, 1009, 1016, 1019, 1027, 1034, 1053, 1063, 1075, 1086, 1102, 1103, 1116, 1130, 1174, 1179, 1186, 1196, 1237, 1270, 1274, 1297, 1302, 1309, 1329, 1330, 1343, 1373, 1400, 1426, 1451, 1464, 1472, 1487, 1491, 1536, 1548, 1580, 1593, 1599, 1606, 1620, 1623, 1646, 3130, 3136, 3156, 3157, 3163, 3166, 3169, 3173, 3176(2), 3182, 3185, 3192, 3193, 3197, 3308
$[Zn(Bpy\text{-}H)]^+$ Product 1	0.25 (0.02)	8, 61, 131, 187, 226, 228, 247, 365, 368, 416, 426, 449, 536, 612, 652, 663, 681, 730, 732, 771, 793, 890, 910, 969, 970, 988, 1000, 1014, 1024, 1063, 1084, 1102, 1128, 1180, 1197, 1264, 1297, 1304, 1326, 1402, 1416, 1462, 1488, 1531, 1583, 1591, 1623, 3139, 3155, 3162, 3166, 3177, 3182, 3196

[a] Uncertainties listed in parentheses are determined as described in the text. [b] Vibrational frequencies scaled by 0.9804 obtained from vibrational analyses of the B3LYP/6-31G* geometry optimized structures. Degeneracies are indicated in parentheses.

Table E.2a. Rotational Constants (in cm^{-1}) of $M^{2+}(Bpy)_2$ Reactants, Products and Their Corresponding PSL Transition States for Dissociation of $M^{2+}(Bpy)_2$ Complexes through Simple CID Process.

	Energized Molecule		Transition State		
Complex	1-D[a]	2-D[b]	1-D[c]	2-D[c]	2-D[d]
$Fe^{2+}(Bpy)_2$ Reactant	0.0097	0.0034	0.0249, 0.0540	0.0144, 0.0166	0.0002
Fe^{2+}(Bpy) Product 1			0.0386	0.0155	
Bpy Product 2			0.0953	0.0181	
$Co^{2+}(Bpy)_2$ Reactant	0.0097	0.0035	0.0245, 0.0540	0.0144, 0.0166	0.0002
Co^{2+}(Bpy) Product 1			0.0382	0.0156	
$Ni^{2+}(Bpy)_2$ Reactant	0.0098	0.0035	0.0251, 0.0540	0.0146, 0.0166	0.0002
Ni^{2+}(Bpy) Product 1			0.0398	0.0157	
$Cu^{2+}(Bpy)_2$ Reactant	0.0098	0.0036	0.0244, 0.0540	0.0145, 0.0166	0.0002
Cu^{2+}(Bpy) Product 1			0.0388	0.0157	
$Zn^{2+}(Bpy)_2$ Reactant	0.0097	0.0035	0.0244, 0.0540	0.0143, 0.0166	0.0002
Zn^{2+}(Bpy) Product 1			0.0382	0.0154	

[a]Active external. [b]Inactive external. [c]Rotational constants of the PSL TS treated as free internal rotors. [d]Two-dimensional rotational constant of the PSL TS at threshold, treated variationally and statistically.

Table E.2b. Rotational Constants (in cm^{-1}) of $M^{2+}(Bpy)_2$ Reactants, Transition States, Intermediates, and Products Involved in the Activated Dissociation of $M^{2+}(Bpy)_2$ Complexes through ETCF Process.

	Rotational Constants[a]	
Complex	1-D	2-D
$Fe^{2+}(Bpy)_2$ Reactant	0.0096	0.0048
$Fe^{2+}(Bpy)_2$ TS_1	0.0095	0.0053
$Fe^{2+}(Bpy)_2$ Int_1	0.0095	0.0051
$Fe^{2+}(Bpy)_2$ TS_2	0.0106	0.0049
$Fe^{2+}(Bpy)_2$ Int_2	0.0102	0.0013
$Fe(Bpy)^+$ Product 1	0.0348	0.0155
Bpy^+ Product 2	0.0953	0.0181
$Co^{2+}(Bpy)_2$ Reactant	0.0096	0.0050
$Co^{2+}(Bpy)_2$ TS_1	0.0095	0.0054
$Co^{2+}(Bpy)_2$ Int_1	0.0095	0.0053
$Co^{2+}(Bpy)_2$ TS_2	0.0101	0.0054
$Co^{2+}(Bpy)_2$ Int_2	0.0099	0.0010
$Co(Bpy)^+$ Product 1	0.0384	0.0157
$Ni^{2+}(Bpy)_2$ Reactant	0.0097	0.0051
$Ni^{2+}(Bpy)_2$ TS_1	0.0093	0.0056
$Ni^{2+}(Bpy)_2$ Int_1	0.0095	0.0055
$Ni^{2+}(Bpy)_2$ TS_2	0.0099	0.0049
$Ni^{2+}(Bpy)_2$ Int_2	0.0099	0.0010
$Ni(Bpy)^+$ Product 1	0.0399	0.0158
$Cu^{2+}(Bpy)_2$ Reactant	0.0097	0.0052
$Cu^{2+}(Bpy)_2$ TS_1	0.0094	0.0056
$Cu^{2+}(Bpy)_2$ Int_1	0.0096	0.0054
$Cu^{2+}(Bpy)_2$ TS_2	0.0120	0.0047
$Cu^{2+}(Bpy)_2$ Int_2	0.0099	0.0010
$Cu(Bpy)^+$ Product 1	0.0387	0.0156
$Zn^{2+}(Bpy)_2$ Reactant	0.0096	0.0050
$Zn^{2+}(Bpy)_2$ TS_1	0.0095	0.0054
$Zn^{2+}(Bpy)_2$ Int_1	0.0096	0.0052
$Zn^{2+}(Bpy)_2$ TS_2	0.0114	0.0045
$Zn^{2+}(Bpy)_2$ Int_2	0.0104	0.0010
$Zn(Bpy)^+$ Product 1	0.0340	0.0154

[a]Geometry optimization and frequency calculation were performed at B3LYP/6-31G*. Rotational constants of $M^{2+}(Bpy)_2$ reactant and the transition state were employed for thermochemical analysis of experimental data.

Table E.2c. Rotational Constants (in cm^{-1}) of $M^{2+}(Bpy)_2$ Reactants, Transition States, Intermediates, and Products Involved in the Activated Dissociation of $M^{2+}(Bpy)_2$ Complexes through PTCF Process.

	Rotational Constants[a]	
Complex	1-D	2-D
$Fe^{2+}(Bpy)_2$ Reactant	0.0096	0.0048
$Fe^{2+}(Bpy)_2$ TS_1	0.0097	0.0050
$Fe^{2+}(Bpy)_2$ Int_1	0.0097	0.0052
$Fe^{2+}(Bpy)_2$ TS_2	0.0097	0.0048
$Fe^{2+}(Bpy)_2$ Int_2	0.0096	0.0054
$Fe^{2+}(Bpy)_2$ TS_3	0.0122	0.0020
$Fe^{2+}(Bpy)_2$ Int_3	0.0137	0.0007
$[Fe(Bpy\text{-}H)]^+$ Product 1	0.0389	0.0157
$(Bpy+H)^+$ Product 2	0.0968	0.0177
$Co^{2+}(Bpy)_2$ Reactant	0.0096	0.0050
$Co^{2+}(Bpy)_2$ TS_1	0.0096	0.0050
$Co^{2+}(Bpy)_2$ Int_1	0.0100	0.0052
$Co^{2+}(Bpy)_2$ TS_2	0.0097	0.0049
$Co^{2+}(Bpy)_2$ Int_2	0.0099	0.0052
$Co^{2+}(Bpy)_2$ TS_3	0.0097	0.0050
$Co^{2+}(Bpy)_2$ Int_3	0.0095	0.0052
$Co^{2+}(Bpy)_2$ TS_4	0.0123	0.0025
$Co^{2+}(Bpy)_2$ Int_4	0.0137	0.0008
$[Co(Bpy\text{-}H)]^+$ Product 1	0.0388	0.0159
$Ni^{2+}(Bpy)_2$ Reactant	0.0097	0.0051
$Ni^{2+}(Bpy)_2$ TS_1	0.0097	0.0053
$Ni^{2+}(Bpy)_2$ Int_1	0.0099	0.0054
$Ni^{2+}(Bpy)_2$ TS_2	0.0097	0.0051
$Ni^{2+}(Bpy)_2$ Int_2	0.0097	0.0052
$Ni^{2+}(Bpy)_2$ TS_3	0.0124	0.0021
$Ni^{2+}(Bpy)_2$ Int_3	0.0137	0.0008
$[Ni(Bpy\text{-}H)]^+$ Product 1	0.0401	0.0159

Table E.2c. (continued) Rotational Constants (in cm^{-1}) of $M^{2+}(Bpy)_2$ Reactants, Transition States, Intermediates, and Products Involved in the Activated Dissociation of $M^{2+}(Bpy)_2$ Complexes through PTCF Process.

	Rotational Constants[a]	
Complex	1-D	2-D
$Cu^{2+}(Bpy)_2$ Reactant	0.0097	0.0052
$Cu^{2+}(Bpy)_2$ TS_1	0.0096	0.0052
$Cu^{2+}(Bpy)_2$ Int_1	0.0099	0.0052
$Cu^{2+}(Bpy)_2$ TS_2	0.0097	0.0051
$Cu^{2+}(Bpy)_2$ Int_2	0.0094	0.0047
$Cu^{2+}(Bpy)_2$ TS_3	0.0097	0.0037
$Cu^{2+}(Bpy)_2$ Int_3	0.0137	0.0008
$[Cu(Bpy\text{-}H)]^+$ Product 1	0.0391	0.0158
$Zn^{2+}(Bpy)_2$ Reactant	0.0096	0.0050
$Zn^{2+}(Bpy)_2$ TS_1	0.0096	0.0050
$Zn^{2+}(Bpy)_2$ Int_1	0.0098	0.0052
$Zn^{2+}(Bpy)_2$ TS_2	0.0101	0.0044
$Zn^{2+}(Bpy)_2$ Int_2	0.0102	0.0044
$Zn^{2+}(Bpy)_2$ TS_3	0.0096	0.0049
$Zn^{2+}(Bpy)_2$ Int_3	0.0094	0.0047
$Zn^{2+}(Bpy)_2$ TS_4	0.0117	0.0028
$Zn^{2+}(Bpy)_2$ Int_4	0.0137	0.0008
$[Zn(Bpy\text{-}H)]^+$ Product 1	0.0365	0.0155

[a]Geometry optimization and frequency calculation were performed at B3LYP/6-31G*. Rotational constants of $M^{2+}(Bpy)_2$ reactant and the rate limiting transition state were employed for thermochemical analysis of experimental data.

Table E.3a. Select B3LYP/6-31G* Geometrical Parameters for the ETCF Activated Dissociation of $Fe^{2+}(Bpy)_2$ and $Co^{2+}(Bpy)_2$ Complexes.[a]

$Fe^{2+}(Bpy)_2$						
	Reactant	TS_1	Int_1	TS_2	Int_2	Products
Fe^{2+}–N2	2.053	2.021	2.038	2.283	8.032	–
Fe^{2+}–N2′	2.053	2.966	3.726	4.105	11.24	–
Fe^{2+}–N2″	2.053	2.047	2.043	2.048	1.992	2.103
Fe^{2+}–N2‴	2.053	2.027	2.045	2.059	1.991	2.103
∠N2″Fe^{2+}N2C2	83.8	67.1	75.7	41.5	90.3	–
∠N2″Fe^{2+}N2′	124.8	127.2	134.5	96.9	137.3	–
∠N2″Fe^{2+}N2	124.8	147.4	150.0	103.1	138.5	–
∠N2″Fe^{2+}N2‴	81.8	82.8	82.3	80.9	87.4	78.4
∠N2′Fe^{2+}N2	81.8	78.4	67.4	61.2	10.1	–
∠N2′Fe^{2+}N2‴	124.9	135.0	122.3	126.5	134.6	–
∠N2Fe^{2+}N2‴	124.9	91.3	103.2	171.3	133.9	–
∠N2″CCN2‴	0.0	1.8	0.6	1.0	0.2	0.0
∠N2CCN2′	0.0	100.2	137.4	164.1	179.8	180.0
$Co^{2+}(Bpy)_2$						
	Reactant	TS_1	Int_1	TS_2	Int_2	Products
Co^{2+}–N2	2.013	1.979	1.995	2.595	9.776	–
Co^{2+}–N2′	2.013	2.882	3.643	4.149	12.81	–
Co^{2+}–N2″	2.013	2.005	2.007	2.011	1.942	1.901
Co^{2+}–N2‴	2.013	1.995	2.002	1.987	1.942	1.901
∠N2″Co^{2+}N2C2	84.0	73.2	72.8	64.2	84.1	–
∠N2″Co^{2+}N2′	124.1	130.2	129.2	176.1	134.7	–
∠N2″Co^{2+}N2	124.2	143.7	152.1	124.1	136.9	–
∠N2″Co^{2+}N2‴	83.0	83.7	83.7	83.2	87.9	88.9
∠N2′Co^{2+}N2	83.0	79.5	69.5	59.6	10.1	–
∠N2′Co^{2+}N2‴	124.1	128.5	124.7	97.5	137.3	–
∠N2Co^{2+}N2‴	124.1	92.2	102.2	100.5	133.0	–
∠N2″CCN2‴	0.0	1.3	0.5	0.1	4.5	0.0
∠N2CCN2′	0.1	94.7	137.6	168.7	179.2	180.0

[a]Bond angles (∠) are given in degrees (°) and bond lengths in angstroms (Å).

Table E.3b. Select B3LYP/6-31G* Geometrical Parameters for the ETCF Activated Dissociation of $Ni^{2+}(Bpy)_2$ and $Cu^{2+}(Bpy)_2$ Complexes.[a]

$Ni^{2+}(Bpy)_2$						
	Reactant	TS_1	Int_1	TS_2	Int_2	Products
Ni^{2+}–N2	1.987	1.951	1.966	2.073	9.772	–
Ni^{2+}–N2′	1.987	2.929	3.640	4.105	12.80	–
Ni^{2+}–N2″	1.987	1.965	1.974	1.956	1.882	1.862
Ni^{2+}–N2‴	1.987	1.954	1.966	1.948	1.882	1.862
∠N2″Ni^{2+}N2C2	85.2	72.1	63.7	100.6	84.1	–
∠N2″Ni^{2+}N2′	124.6	120.0	114.7	109.5	132.8	–
∠N2″Ni^{2+}N2	124.6	157.7	175.5	131.7	135.1	–
∠N2″Ni^{2+}N2‴	82.2	84.5	84.0	84.8	91.7	91.0
∠N2′Ni^{2+}N2	82.2	80.3	69.8	61.4	10.1	–
∠N2′Ni^{2+}N2‴	124.6	120.3	115.7	165.6	135.4	–
∠N2Ni^{2+}N2‴	124.6	93.1	94.3	110.5	131.1	–
∠N2″CCN2‴	0.0	1.1	1.8	0.3	4.3	0.0
∠N2CCN2′	0.0	100.3	138.7	163.3	179.0	180.0
$Cu^{2+}(Bpy)_2$						
	Reactant	TS_1	Int_1	TS_2	Int_2	Products
Cu^{2+}–N2	1.973	1.913	1.940	2.241	9.523	–
Cu^{2+}–N2′	1.973	3.152	3.839	4.568	12.55	–
Cu^{2+}–N2″	1.973	1.951	1.965	1.948	1.880	1.876
Cu^{2+}–N2‴	1.973	1.928	1.945	1.935	1.881	1.876
∠N2″Cu^{2+}N2C2	55.9	50.5	60.2	25.2	84.1	–
∠N2″Cu^{2+}N2′	105.3	106.7	104.6	168.2	132.4	–
∠N2″Cu^{2+}N2	148.6	108.4	114.1	136.8	134.7	–
∠N2″Cu^{2+}N2‴	83.3	84.8	84.2	85.2	92.7	94.8
∠N2′Cu^{2+}N2	83.3	74.8	64.9	51.2	10.3	–
∠N2′Cu^{2+}N2‴	148.6	162.6	158.1	105.6	134.9	–
∠N2Cu^{2+}N2‴	105.3	114.5	130.3	83.4	130.5	–
∠N2″CCN2‴	5.9	3.9	3.9	1.9	4.7	0.1
∠N2CCN2′	5.8	100.2	140.4	170.1	178.6	180.0

[a]Bond angles (∠) are given in degrees (°) and bond lengths in angstroms (Å).

Table E.3c. Select B3LYP/6-31G* Geometrical Parameters for the ETCF Activated Dissociation of $Zn^{2+}(Bpy)_2$ Complex.[a]

	$Zn^{2+}(Bpy)_2$					
	Reactant	TS_1	Int_1	TS_2	Int_2	Products
Zn^{2+}–N2	2.013	1.948	1.979	2.445	9.413	–
Zn^{2+}–N2′	2.013	3.118	3.781	4.741	12.69	–
Zn^{2+}–N2″	2.013	1.989	2.000	1.975	1.978	2.045
Zn^{2+}–N2‴	2.013	1.979	1.997	1.967	1.978	2.045
∠N2″Zn^{2+}N2C2	83.7	67.5	67.8	51.9	69.4	–
∠N2″Zn^{2+}N2′	123.8	134.6	130.8	141.3	135.0	–
∠N2′Zn^{2+}N2	123.8	140.5	152.9	162.4	139.9	–
∠N2″Zn^{2+}N2‴	83.6	85.2	84.7	86.1	86.7	81.5
∠N2′Zn^{2+}N2	83.6	75.0	66.4	36.9	8.1	–
∠N2′Zn^{2+}N2‴	123.8	133.4	127.4	109.1	138.2	–
∠N2Zn^{2+}N2‴	123.8	86.7	100.2	81.1	133.1	–
∠N2″CCN2‴	0.0	1.0	0.8	0.1	0.1	0.0
∠N2CCN2′	0.0	97.5	138.5	173.3	179.4	180.0

[a]Bond angles (∠) are given in degrees (°) and bond lengths in angstroms (Å).

Table E.4a. Select B3LYP/6-31G* Geometrical Parameters for the PTCF Activated Dissociation of $Fe^{2+}(Bpy)_2$ Complex.[a]

	Reactant	TS_1	Int_1	TS_2	Int_2	TS_3	Int_3	Products
Fe^{2+}–N2	2.053	2.080	1.977	2.064	1.913	5.042	12.26	–
Fe^{2+}–N2′	2.053	2.036	2.081	2.114	2.940	7.133	14.51	–
Fe^{2+}–N2″	2.053	1.939	1.969	2.015	1.924	2.014	1.728	1.843
Fe^{2+}–N2‴	2.053	2.155	2.061	2.112	2.008	2.027	1.746	2.280
C3″–H3″	1.086	1.963	2.816	2.805	2.904	7.839	12.79	–
N2–H3″	3.947	2.483	2.952	1.307	1.030	1.027	1.000	1.030
Fe^{2+}–H3″	3.149	1.614	1.529	1.650	2.081	6.169	13.60	–
∠N2″Fe^{2+}N2′C2′	83.8	76.6	59.1	69.2	68.3	81.4	77.8	–
∠N2″Fe^{2+}N2	124.8	141.1	110.7	123.2	96.0	131.6	87.0	–
∠N2″Fe^{2+}N2′	124.8	137.4	166.2	136.7	143.8	133.6	83.2	–
∠N2″Fe^{2+}N2‴	81.8	76.1	81.0	78.6	83.9	83.8	112.1	83.7
∠N2Fe^{2+}N2′	81.8	80.5	81.1	78.6	67.4	14.9	7.7	–
∠N2Fe^{2+}N2‴	124.9	118.8	110.3	140.9	129.8	139.9	160.7	–
∠N2′Fe^{2+}N2‴	124.9	92.0	102.1	108.5	131.8	142.6	164.1	–
∠N2″CCN2‴	0.1	0.8	0.5	1.1	3.2	0.1	0.4	0.0
∠N2CCN2′	0.0	4.0	2.8	11.5	22.4	0.3	0.0	0.0

[a]Bond angles (∠) are given in degrees (°) and bond lengths in angstroms (Å).

Table E.4b. Select B3LYP/6-31G* Geometrical Parameters for the PTCF Activated Dissociation of $Co^{2+}(Bpy)_2$ Complex.[a]

	Reactant	TS_1	Int_1	TS_2	Int_2
Co^{2+}–N2	2.013	2.052	2.262	2.189	1.943
Co^{2+}–N2′	2.013	2.028	2.191	2.024	2.023
Co^{2+}–N2″	2.013	2.006	2.013	2.026	1.972
Co^{2+}–N2‴	2.013	2.010	2.004	1.999	2.038
C3–H3	1.086	1.419	2.057	2.270	2.788
N2″–H3	3.876	3.359	4.334	2.655	2.665
Co^{2+}–H3	3.119	2.492	2.378	1.554	1.481
∠N2Co^{2+}N2‴C2‴	84.0	94.4	76.1	97.6	66.2
∠N2Co^{2+}N2″	83.0	123.4	139.7	126.1	121.8
∠N2Co^{2+}N2‴	124.1	122.0	128.6	111.6	156.1
∠N2Co^{2+}N2′	124.1	82.1	69.6	78.4	82.4
∠N2″Co^{2+}N2‴	83.0	83.4	83.6	81.9	80.8
∠N2‴Co^{2+}N2′	83.0	123.1	123.2	133.0	106.6
∠N2‴Co^{2+}N2′	124.1	128.6	115.1	130.3	99.7
∠N2CCN2′	0.0	18.2	34.7	11.5	1.6
∠N2″CCN2‴	0.0	0.0	1.7	0.7	2.1

[a]Bond angles (∠) are given in degrees (°) and bond lengths in angstroms (Å).

Table E.4b. (continued) Select B3LYP/6-31G* Geometrical Parameters for the PTCF Activated Dissociation of $Co^{2+}(Bpy)_2$ Complex.[a]

	TS_3	Int_3	TS_4	Int_4	Products
Co^{2+}–N2	1.975	1.924	1.852	1.898	1.839
Co^{2+}–N2′	2.057	2.008	2.005	1.975	2.060
Co^{2+}–N2″	2.017	1.913	6.043	11.83	–
Co^{2+}–N2‴	2.063	2.940	5.421	13.74	–
C3–H3	3.035	2.904	2.993	12.62	–
N2″–H3	1.342	1.030	1.030	1.029	1.030
Co^{2+}–H3	1.575	2.081	4.735	12.73	–
∠N2Co^{2+}N2‴C2‴	73.5	68.3	85.5	109.0	–
∠N2Co^{2+}N2″	127.6	96.0	63.5	105.7	–
∠N2Co^{2+}N2‴	136.8	143.8	68.6	99.9	–
∠N2Co^{2+}N2′	82.1	83.9	85.8	82.1	80.7
∠N2″Co^{2+}N2‴	79.9	67.4	25.5	7.9	–
∠N2‴Co^{2+}N2′	125.5	129.8	149.2	171.1	–
∠N2‴Co^{2+}N2′	110.0	131.8	143.0	170.0	–
∠N2CCN2′	1.0	3.2	3.8	5.3	0.0
∠N2″CCN2‴	8.4	22.4	0.3	0.7	0.0

[a]Bond angles (∠) are given in degrees (°) and bond lengths in angstroms (Å).

Table E.4c. Select B3LYP/6-31G* Geometrical Parameters for the PTCF Activated Dissociation of $Ni^{2+}(Bpy)_2$ Complex.[a]

	Reactant	TS_1	Int_1	TS_2	Int_2	TS_3	Int_3	Products
Ni^{2+}–N2	1.987	1.952	1.926	1.962	1.972	5.117	11.53	–
Ni^{2+}–N2′	1.987	1.989	2.001	2.039	2.142	7.178	13.41	–
Ni^{2+}–N2″	1.987	1.858	1.923	1.962	1.989	1.864	1.867	1.858
Ni^{2+}–N2‴	1.987	2.079	1.992	2.022	1.985	1.883	1.899	1.880
C3″–H3″	1.086	1.895	2.715	2.902	3.219	7.529	12.11	–
N2–H3″	3.796	2.609	2.409	1.329	1.030	1.027	1.029	1.030
Ni^{2+}–H3″	3.062	1.581	1.436	1.506	2.266	6.208	12.40	–
∠N2″Ni^{2+}N2′C2′	85.2	85.6	66.8	62.5	78.5	76.4	123.5	–
∠N2″Ni^{2+}N2	124.6	121.6	114.8	114.1	103.1	123.4	96.9	–
∠N2″Ni^{2+}N2′	124.6	150.8	160.3	152.8	148.1	118.2	90.5	–
∠N2″Ni^{2+}N2‴	82.2	79.2	83.2	82.5	82.7	90.8	91.5	90.7
∠N2Ni^{2+}N2′	82.2	82.7	83.1	81.6	80.5	15.2	8.2	–
∠N2Ni^{2+}N2‴	124.6	105.7	102.8	128.1	124.7	140.2	169.5	–
∠N2′Ni^{2+}N2‴	124.6	111.7	101.5	105.8	121.7	133.2	168.4	–
∠N2″CCN2‴	0.0	2.5	0.8	1.8	0.0	0.4	7.6	0.0
∠N2CCN2′	0.0	0.7	0.2	9.7	27.6	0.5	0.9	0.0

[a]Bond angles (∠) are given in degrees (°) and bond lengths in angstroms (Å).

Table E.4d. Select B3LYP/6-31G* Geometrical Parameters for the PTCF Activated Dissociation of $Cu^{2+}(Bpy)_2$ Complex.[a]

	Reactant	TS_1	Int_1	TS_2	Int_2	TS_3	Int_3	Products
Cu^{2+}–N2	1.973	1.953	1.985	2.107	1.913	3.413	11.53	–
Cu^{2+}–N2′	1.973	2.126	2.102	2.027	2.940	3.594	13.41	–
Cu^{2+}–N2″	1.973	1.840	1.912	1.924	1.924	1.858	1.867	1.863
Cu^{2+}–N2‴	1.973	2.031	1.950	1.973	2.008	1.913	1.899	1.893
C3″–H3″	1.085	1.912	2.711	2.843	2.903	3.291	12.11	–
N2–H3″	3.014	2.600	2.389	1.710	1.030	1.025	1.029	1.030
Cu^{2+}–H3″	3.064	1.550	1.420	1.426	2.081	2.612	12.40	–
∠N2″Cu^{2+}N2′C2′	55.9	81.0	71.9	83.6	68.3	68.4	112.5	–
∠N2″Cu^{2+}N2	105.3	120.0	128.8	139.0	96.0	85.3	96.9	–
∠N2″Cu^{2+}N2′	148.5	150.5	145.5	129.4	143.8	121.4	90.5	–
∠N2″Cu^{2+}N2‴	83.3	81.1	84.8	84.7	83.9	92.0	91.5	92.5
∠N2Cu^{2+}N2′	83.3	81.6	81.4	80.3	67.4	44.6	8.2	–
∠N2Cu^{2+}N2‴	148.6	113.4	105.2	108.0	129.8	135.1	169.5	–
∠N2′Cu^{2+}N2‴	105.3	110.3	104.7	117.0	131.8	142.7	168.4	–
∠N2″CCN2‴	5.9	4.8	0.4	0.3	3.2	8.5	7.6	0.0
∠N2CCN2′	5.8	1.6	2.4	7.5	22.4	3.7	0.9	0.0

[a]Bond angles (∠) are given in degrees (°) and bond lengths in angstroms (Å).

Table E.4e. Select B3LYP/6-31G* Geometrical Parameters for the PTCF Activated Dissociation of $Zn^{2+}(Bpy)_2$ Complex.[a]

	Reactant	TS_1	Int_1	TS_2	Int_2
Zn^{2+}–N2	2.013	2.063	2.242	3.015	3.006
Zn^{2+}–N2′	2.013	2.021	2.011	2.078	2.104
Zn^{2+}–N2″	2.013	2.002	1.992	2.027	2.037
Zn^{2+}–N2‴	2.013	2.005	1.988	2.032	2.046
C3–H3	1.085	1.417	2.026	2.735	2.930
N2″–H3	3.883	3.317	3.321	3.176	3.121
Zn^{2+}–H3	3.130	2.508	2.390	1.594	1.571
∠N2Zn^{2+}N2‴C2‴	83.7	91.6	103.1	99.8	97.4
∠N2Zn^{2+}N2″	123.8	121.0	115.8	152.5	155.7
∠N2Zn^{2+}N2‴	123.8	121.0	122.0	122.3	122.1
∠N2Zn^{2+}N2′	83.6	82.6	78.8	70.2	68.6
∠N2″Zn^{2+}N2‴	83.6	84.3	85.3	82.5	81.8
∠N2″Zn^{2+}N2′	123.8	126.1	129.7	111.8	108.9
∠N2‴Zn^{2+}N2′	123.8	126.9	129.5	116.1	111.3
∠N2CCN2′	0.0	18.9	33.4	30.5	25.2
∠N2″CCN2‴	0.0	0.5	2.3	3.8	5.0

[a]Bond angles (∠) are given in degrees (°) and bond lengths in angstroms (Å).

Table E.4e. (continued) Select B3LYP/6-31G* Geometrical Parameters for the PTCF Activated Dissociation of $Zn^{2+}(Bpy)_2$ Complex.[a]

	TS_3	Int_3	TS_4	Int_4	Products
Zn^{2+}–N2	2.057	1.924	1.957	2.002	1.969
Zn^{2+}–N2′	1.988	2.008	1.993	1.997	1.999
Zn^{2+}–N2″	1.986	1.913	3.732	11.43	–
Zn^{2+}–N2‴	2.250	2.940	5.487	13.32	–
C3–H3	3.519	2.904	4.450	11.98	–
N2″–H3	1.540	1.030	1.025	1.029	1.030
Zn^{2+}–H3	1.702	2.081	4.493	12.31	–
∠N2Zn^{2+}N2‴C2‴	116.8	68.3	46.8	63.2	–
∠N2Zn^{2+}N2″	141.0	96.0	91.5	95.9	–
∠N2Zn^{2+}N2‴	118.4	143.8	105.2	90.1	–
∠N2Zn^{2+}N2′	84.6	83.9	90.4	87.9	89.4
∠N2″Zn^{2+}N2‴	79.4	67.4	25.0	8.2	–
∠N2″Zn^{2+}N2′	109.1	129.8	177.1	174.1	–
∠N2‴Zn^{2+}N2′	132.8	131.8	152.2	169.5	–
∠N2CCN2′	7.3	3.2	7.5	6.1	0.0
∠N2″CCN2‴	5.6	22.4	2.8	0.3	0.0

[a]Bond angles (∠) are given in degrees (°) and bond lengths in angstroms (Å).

Table E.5. Cartesian Coordinates of the B3LYP/6-31G* Optimized Geometries of the Transition States, Ints, and Products Involved in the Dissociation of $M^{2+}(Bpy)_2$ Complexes through ETCF Process.[a]

$Fe^{2+}(Bpy)_2$ TS_1				$Fe^{2+}(Bpy)_2$ TS_1			
	x	y	z		x	y	z
C	-0.357126	-0.422940	0.161864	H	-4.586180	-4.605600	1.985860
N	-0.395578	-0.511562	1.523567	H	-4.803688	2.040517	6.980398
C	0.847542	-0.583144	-0.523436	H	-2.609506	-4.418673	3.524623
C	-1.654654	-0.155907	-0.516885	Fe^{2+}	-2.280949	-0.205581	2.260054
C	0.741347	-0.751399	2.207718				
C	2.020936	-0.828969	0.190842				
N	-2.749474	-0.065188	0.292639				
C	-1.785126	0.004709	-1.896181				
H	0.884083	-0.520248	-1.603896				
C	1.971295	-0.913779	1.581497				
C	-3.964103	0.182975	-0.239356				
C	-3.043161	0.261768	-2.444271				
H	0.653178	-0.810705	3.288252				
H	2.961194	-0.952881	-0.337433				
H	-0.922915	-0.062270	-2.547954				
C	-4.153389	0.353154	-1.605647				
H	2.860941	-1.102639	2.172121				
H	-4.791793	0.237147	0.461315				
H	-3.149455	0.390264	-3.517028				
H	-5.145252	0.553234	-1.995703				
N	-2.790647	0.817154	3.927416				
N	-4.941066	-1.362635	2.877932				
C	-3.753923	0.030556	4.473499				
C	-2.537177	2.032736	4.459655				
C	-3.909635	-1.278405	3.751013				
C	-5.151227	-2.539390	2.275689				
C	-4.505453	0.438452	5.566574				
C	-3.239460	2.497695	5.564161				
C	-3.020368	-2.343266	3.985811				
C	-4.349210	-3.671149	2.484223				
H	-1.763171	2.625191	3.982474				
H	-6.001296	-2.581610	1.599253				
C	-4.237722	1.693488	6.121209				
C	-3.254920	-3.565969	3.336335				
H	-5.276218	-0.207571	5.972460				
H	-3.011677	3.475422	5.974579				
H	-2.223249	-2.245644	4.718373				

Table E.5. (continued) Cartesian Coordinates of the B3LYP/6-31G* Optimized Geometries of the Transition States, Ints, and Products Involved in the Dissociation of $M^{2+}(Bpy)_2$ Complexes through ETCF Process.[a]

$Fe^{2+}(Bpy)_2$ Int_1				$Fe^{2+}(Bpy)_2$ Int_1			
	x	y	z		x	y	z
C	0.086278	0.014905	-0.021118	H	-3.456988	-4.920397	2.484162
N	0.093170	-0.144586	1.334419	H	-5.161403	2.323406	6.252719
C	1.285193	0.066251	-0.733102	H	-1.279125	-3.778605	2.984697
C	-1.251544	0.131712	-0.661854	Fe^{2+}	-1.784795	-0.135028	2.138884
C	1.269852	-0.247985	1.986353				
C	2.498240	-0.044333	-0.052584				
N	-2.324666	0.078990	0.178025				
C	-1.434594	0.282461	-2.036667				
H	1.287120	0.193269	-1.808510				
C	2.494924	-0.203291	1.332849				
C	-3.571212	0.174771	-0.326618				
C	-2.727183	0.384977	-2.552862				
H	1.217973	-0.370052	3.064204				
H	3.433651	-0.004630	-0.602112				
H	-0.587186	0.321329	-2.709765				
C	-3.817407	0.331498	-1.685673				
H	3.416283	-0.290632	1.898027				
H	-4.387629	0.124961	0.387575				
H	-2.875973	0.504341	-3.621559				
H	-4.836647	0.407439	-2.048063				
N	-2.691149	0.905840	3.637773				
N	-4.670255	-1.970344	3.617895				
C	-3.590334	0.088025	4.254311				
C	-2.663067	2.217021	3.963557				
C	-3.515173	-1.334250	3.830022				
C	-4.621884	-3.229266	3.162135				
C	-4.506538	0.568715	5.183865				
C	-3.526367	2.756657	4.909154				
C	-2.248731	-1.936544	3.602456				
C	-3.429572	-3.902323	2.858042				
H	-1.936932	2.833971	3.443396				
H	-5.582131	-3.723694	3.036700				
C	-4.467254	1.923016	5.520161				
C	-2.223980	-3.258766	3.115769				
H	-5.220411	-0.112857	5.632338				
H	-3.468488	3.812460	5.150351				
H	-1.350993	-1.527357	4.075815				

Table E.5. (continued) Cartesian Coordinates of the B3LYP/6-31G* Optimized Geometries of the Transition States, Ints, and Products Involved in the Dissociation of $M^{2+}(Bpy)_2$ Complexes through ETCF Process.[a]

	$Fe^{2+}(Bpy)_2$ TS_2				$Fe^{2+}(Bpy)_2$ TS_2		
	x	y	z		x	y	z
C	-0.071492	0.201879	0.605597	H	-4.762645	-5.329764	5.660382
N	-0.102143	0.766609	1.847471	H	-0.589879	1.680326	5.650084
C	1.068889	0.303070	-0.190262	H	-6.445445	-3.686766	4.784630
C	-1.310410	-0.501918	0.186380	Fe^{2+}	-1.875795	0.464459	2.849390
C	0.979701	1.428694	2.305423				
C	2.185602	0.989224	0.289317				
N	-2.316858	-0.513551	1.104354				
C	-1.478420	-1.115416	-1.053853				
H	1.097875	-0.145600	-1.175617				
C	2.143457	1.564152	1.559289				
C	-3.487337	-1.116710	0.817371				
C	-2.690552	-1.742601	-1.349794				
H	0.901607	1.859310	3.298554				
H	3.076868	1.071627	-0.324998				
H	-0.684356	-1.108624	-1.790459				
C	-3.713486	-1.744582	-0.402148				
H	2.989911	2.105640	1.967026				
H	-4.247174	-1.083816	1.591721				
H	-2.830593	-2.221517	-2.313946				
H	-4.668677	-2.218419	-0.599561				
N	-3.871815	0.475053	3.957143				
N	-2.746972	-2.641079	5.388150				
C	-3.150643	-0.394402	4.725123				
C	-3.502950	1.781158	3.891094				
C	-3.655769	-1.764823	4.914452				
C	-3.156081	-3.883522	5.633663				
C	-1.906946	0.009072	5.285679				
C	-2.339915	2.273239	4.509410				
C	-4.996349	-2.090283	4.668387				
C	-4.479723	-4.307750	5.429796				
H	-4.156973	2.431999	3.316640				
H	-2.406049	-4.572841	6.012671				
C	-1.516093	1.352039	5.186442				
C	-5.411462	-3.395399	4.940619				
H	-1.316155	-0.728878	5.817322				
H	-2.081384	3.325062	4.439834				
H	-5.692025	-1.338891	4.310973				

Table E.5. (continued) Cartesian Coordinates of the B3LYP/6-31G* Optimized Geometries of the Transition States, Ints, and Products Involved in the Dissociation of $M^{2+}(Bpy)_2$ Complexes through ETCF Process.[a]

	$Fe^{2+}(Bpy)_2$ Int_2				$Fe^{2+}(Bpy)_2$ Int_2		
	x	y	z		x	y	z
C	5.653568	-0.722275	-0.280310	H	-8.432708	0.982743	-3.923131
N	4.425565	-1.319081	-0.335409	H	-7.288237	-0.918422	3.957225
C	6.806079	-1.475822	-0.506815	H	-5.927018	0.859449	-3.750239
C	5.691947	0.742616	0.025961	Fe^{2+}	3.023032	0.047118	0.028500
C	4.326771	-2.635192	-0.608135				
C	6.699152	-2.838458	-0.789009				
N	4.495877	1.373613	0.222201				
C	6.883486	1.463524	0.113739				
H	7.786817	-1.019317	-0.467830				
C	5.439831	-3.433032	-0.841627				
C	4.466241	2.692186	0.499153				
C	6.848255	2.828908	0.400961				
H	3.323776	-3.048799	-0.637609				
H	7.595049	-3.425492	-0.965617				
H	7.839672	0.979351	-0.037883				
C	5.620745	3.458745	0.597602				
H	5.316528	-4.488406	-1.057954				
H	3.485462	3.133948	0.643733				
H	7.774671	3.390616	0.469344				
H	5.552910	4.517395	0.822279				
N	-4.956643	-0.255381	0.891817				
N	-8.198223	0.208576	-0.646137				
C	-6.306079	-0.187451	0.773384				
C	-4.463618	-0.555326	2.084758				
C	-6.849944	0.140866	-0.546647				
C	-8.720535	0.502163	-1.826702				
C	-7.182262	-0.420754	1.862442				
C	-5.256274	-0.804877	3.225974				
C	-5.991460	0.371071	-1.650575				
C	-7.943841	0.747041	-2.983261				
H	-3.378888	-0.605516	2.159922				
H	-9.805950	0.549972	-1.878350				
C	-6.642683	-0.733740	3.104404				
C	-6.554679	0.677804	-2.883409				
H	-8.250505	-0.349860	1.698445				
H	-4.784102	-1.046188	4.173027				
H	-4.920545	0.301390	-1.504991				

Table E.5. (continued) Cartesian Coordinates of the B3LYP/6-31G* Optimized Geometries of the Transition States, Ints, and Products Involved in the Dissociation of $M^{2+}(Bpy)_2$ Complexes through ETCF Process.[a]

	Fe^{+}(Bpy)				Bpy^{+}		
	x	y	z		x	y	z
C	-0.741974	0.718116	0.000035	C	0.036897	-0.000150	0.053660
N	-1.328314	-0.508126	0.000273	C	-0.004760	-0.000096	1.447689
C	-1.518949	1.878320	-0.000192	C	1.198918	0.000040	2.139735
C	0.741974	0.718116	0.000041	C	2.419273	0.000127	1.395754
C	-2.668710	-0.606273	0.000301	C	1.302891	-0.000072	-0.604884
C	-2.909234	1.772030	-0.000163	C	3.692752	0.000272	2.081408
N	1.328314	-0.508125	0.000198	C	4.809133	0.000454	4.082046
C	1.518949	1.878320	-0.000095	H	4.764849	0.000493	5.168792
H	-1.054443	2.856947	-0.000397	C	6.075124	0.000543	3.423503
C	-3.499358	0.509405	0.000093	C	6.116784	0.000488	2.029472
C	2.668710	-0.606273	0.000221	C	4.913107	0.000348	1.337426
C	2.909234	1.772030	-0.000071	H	-0.873603	-0.000255	-0.537642
H	-3.076933	-1.613217	0.000499	H	-0.951465	-0.000159	1.977995
H	-3.521515	2.668330	-0.000340	H	1.347171	-0.000113	-1.691630
H	1.054442	2.856947	-0.000211	H	6.985626	0.000649	4.014802
C	3.499358	0.509406	0.000089	H	7.063490	0.000551	1.499170
H	-4.576526	0.385052	0.000127	H	4.865592	0.000297	0.255004
H	3.076933	-1.613217	0.000348	H	1.246431	0.000090	3.222157
H	3.521515	2.668330	-0.000175	N	2.453676	0.000064	0.035441
H	4.576526	0.385053	0.000114	N	3.658347	0.000322	3.441720
Fe^{2+}	0.000000	-2.138087	0.000426				

Table E.5. (continued) Cartesian Coordinates of the B3LYP/6-31G* Optimized Geometries of the Transition States, Ints, and Products Involved in the Dissociation of $M^{2+}(Bpy)_2$ Complexes through ETCF Process.[a]

$Co^{2+}(Bpy)_2$ TS_1				$Co^{2+}(Bpy)_2$ TS_1			
	x	y	z		x	y	z
C	-0.392830	-0.451519	0.178654	H	-4.386825	-4.703866	2.075328
N	-0.455748	-0.605672	1.532640	H	-4.801812	2.088274	6.890305
C	0.812582	-0.630431	-0.498368	H	-2.483023	-4.424931	3.688816
C	-1.672840	-0.097790	-0.491197	Co^{2+}	-2.290007	-0.237017	2.252938
C	0.655771	-0.931318	2.220831				
C	1.962062	-0.967048	0.218764				
N	-2.756907	0.002384	0.328305				
C	-1.801526	0.121803	-1.861464				
H	0.867151	-0.511775	-1.573599				
C	1.886092	-1.121271	1.602383				
C	-3.964852	0.310202	-0.181776				
C	-3.053176	0.446177	-2.389793				
H	0.546351	-1.039253	3.295496				
H	2.904371	-1.106790	-0.301841				
H	-0.944825	0.046066	-2.519960				
C	-4.154502	0.541024	-1.540275				
H	2.756432	-1.382089	2.194328				
H	-4.785897	0.360358	0.526758				
H	-3.161540	0.620996	-3.455739				
H	-5.141378	0.788684	-1.915382				
N	-2.857722	0.853054	3.803995				
N	-4.842493	-1.441634	2.835515				
C	-3.748437	0.035786	4.421365				
C	-2.650055	2.102488	4.270464				
C	-3.850613	-1.306953	3.748051				
C	-5.004576	-2.641376	2.266955				
C	-4.470387	0.444128	5.533202				
C	-3.333235	2.573912	5.384498				
C	-2.954279	-2.344351	4.061425				
C	-4.190329	-3.748409	2.551051				
H	-1.929788	2.712983	3.735741				
H	-5.822028	-2.724485	1.555184				
C	-4.254584	1.737066	6.020712				
C	-3.136140	-3.592449	3.445028				
H	-5.181548	-0.226693	6.002827				
H	-3.147803	3.580449	5.743342				
H	-2.187358	-2.201379	4.818112				

Table E.5. (continued) Cartesian Coordinates of the B3LYP/6-31G* Optimized Geometries of the Transition States, Ints, and Products Involved in the Dissociation of $M^{2+}(Bpy)_2$ Complexes through ETCF Process.[a]

	$Co^{2+}(Bpy)_2$ Int_1				$Co^{2+}(Bpy)_2$ Int_1		
	x	y	z		x	y	z
C	0.084149	0.082302	-0.007088	H	-3.264630	-4.850376	2.619567
N	0.092390	0.004912	1.354530	H	-5.032997	2.510992	6.151526
C	1.280293	0.179743	-0.717154	H	-1.101509	-3.656149	3.055526
C	-1.257545	0.057777	-0.649571	Co^{2+}	-1.759760	-0.084888	2.121764
C	1.264749	0.025716	2.018041				
C	2.492726	0.198897	-0.025549				
N	-2.319620	-0.028765	0.200571				
C	-1.458503	0.115973	-2.027913				
H	1.280120	0.242007	-1.798441				
C	2.488929	0.121429	1.366535				
C	-3.573058	-0.055782	-0.292040				
C	-2.758911	0.088912	-2.535568				
H	1.211088	-0.035369	3.100915				
H	3.427570	0.274823	-0.572170				
H	-0.619344	0.182493	-2.709428				
C	-3.836928	0.001913	-1.655974				
H	3.409320	0.135155	1.939815				
H	-4.377611	-0.125452	0.433742				
H	-2.922906	0.135468	-3.607680				
H	-4.860960	-0.021031	-2.011955				
N	-2.577460	1.008512	3.576464				
N	-4.518009	-1.888145	3.675468				
C	-3.463852	0.208726	4.231797				
C	-2.552406	2.330933	3.846227				
C	-3.370346	-1.225602	3.854282				
C	-4.451819	-3.158669	3.261024				
C	-4.377696	0.718725	5.148003				
C	-3.411911	2.900241	4.777960				
C	-2.095127	-1.812409	3.631305				
C	-3.249861	-3.820575	2.960718				
H	-1.834140	2.928923	3.294408				
H	-5.403777	-3.675766	3.166568				
C	-4.343108	2.085385	5.429252				
C	-2.054168	-3.149910	3.182589				
H	-5.083930	0.051185	5.628553				
H	-3.359106	3.964901	4.977928				
H	-1.201899	-1.376495	4.085048				

Table E.5. (continued) Cartesian Coordinates of the B3LYP/6-31G* Optimized Geometries of the Transition States, Ints, and Products Involved in the Dissociation of $M^{2+}(Bpy)_2$ Complexes through ETCF Process.[a]

	$Co^{2+}(Bpy)_2$ TS_2				$Co^{2+}(Bpy)_2$ TS_2		
	x	y	z		x	y	z
C	-0.601870	-0.539267	0.746380	H	0.045466	-1.528822	7.858424
N	-1.381720	-1.291252	1.574025	H	-5.652976	1.084536	2.689307
C	0.573637	-1.064569	0.213492	H	-1.528127	-3.478184	7.726177
C	-1.098610	0.832581	0.474188	Co^{2+}	-2.960712	-0.305066	2.264477
C	-1.019787	-2.552422	1.882754				
C	0.946399	-2.372452	0.530431				
N	-2.266409	1.168513	1.095321				
C	-0.452527	1.744655	-0.358220				
H	1.199054	-0.472044	-0.443020				
C	0.139259	-3.130511	1.377862				
C	-2.800101	2.391113	0.901969				
C	-1.006873	3.011248	-0.552061				
H	-1.684558	-3.096108	2.546792				
H	1.858836	-2.790664	0.116758				
H	0.472950	1.482382	-0.856221				
C	-2.200915	3.343872	0.087563				
H	0.396064	-4.149627	1.645042				
H	-3.729211	2.603545	1.420791				
H	-0.509096	3.727557	-1.198375				
H	-2.662310	4.316982	-0.039365				
N	-4.115530	-2.417566	3.473519				
N	-1.882978	-0.449122	5.312083				
C	-3.778098	-1.345430	4.229044				
C	-4.936334	-2.237734	2.426853				
C	-2.731640	-1.497817	5.261530				
C	-0.908003	-0.489912	6.225017				
C	-4.334831	-0.053096	3.990463				
C	-5.449100	-0.980080	2.049295				
C	-2.639079	-2.621721	6.084831				
C	-0.750595	-1.555223	7.121484				
H	-5.182685	-3.127497	1.852436				
H	-0.229446	0.358488	6.244888				
C	-5.186790	0.122197	2.882179				
C	-1.626151	-2.637478	7.046491				
H	-4.113640	0.757360	4.676061				
H	-6.083237	-0.887254	1.173438				
H	-3.346385	-3.438654	5.989649				

Table E.5. (continued) Cartesian Coordinates of the B3LYP/6-31G* Optimized Geometries of the Transition States, Ints, and Products Involved in the Dissociation of $M^{2+}(Bpy)_2$ Complexes through ETCF Process.[a]

	$Co^{2+}(Bpy)_2$ Int_2				$Co^{2+}(Bpy)_2$ Int_2		
	x	y	z		x	y	z
C	-6.167972	0.728854	-0.287183	H	8.688031	2.590402	3.403224
N	-4.945564	1.199385	-0.672572	H	8.429253	-2.135914	-3.287994
C	-7.322721	1.441756	-0.605666	H	6.248070	1.991755	3.239921
C	-6.181334	-0.555523	0.477275	Co^{2+}	-3.674104	-0.081293	-0.142099
C	-4.851717	2.348418	-1.359947				
C	-7.224230	2.636950	-1.317877				
N	-4.981522	-1.188166	0.632410				
C	-7.340168	-1.114643	1.013884				
H	-8.299489	1.075594	-0.313675				
C	-5.971489	3.102215	-1.702151				
C	-4.913219	-2.350059	1.301338				
C	-7.268794	-2.322650	1.707155				
H	-3.852716	2.667383	-1.636170				
H	-8.121955	3.193368	-1.567950				
H	-8.297291	-0.618922	0.906282				
C	-6.038831	-2.954583	1.854836				
H	-5.850774	4.026636	-2.256212				
H	-3.930968	-2.801194	1.388812				
H	-8.169090	-2.760006	2.126967				
H	-5.940482	-3.894795	2.386291				
N	5.805794	-0.775486	-0.717129				
N	8.832463	0.684574	0.615571				
C	7.124839	-0.478048	-0.603287				
C	5.443659	-1.544007	-1.726638				
C	7.518570	0.366853	0.523479				
C	9.211273	1.454720	1.618719				
C	8.107830	-0.952468	-1.517936				
C	6.349053	-2.066221	-2.689312				
C	6.547923	0.820696	1.459265				
C	8.315217	1.959229	2.602567				
H	4.382861	-1.774243	-1.800904				
H	10.270570	1.695940	1.670206				
C	7.705410	-1.756927	-2.573535				
C	6.961599	1.625053	2.508796				
H	9.144427	-0.675861	-1.363948				
H	5.979769	-2.693014	-3.494955				
H	5.513024	0.527951	1.326140				

Table E.5. (continued) Cartesian Coordinates of the B3LYP/6-31G* Optimized Geometries of the Transition States, Ints, and Products Involved in the Dissociation of $M^{2+}(Bpy)_2$ Complexes through ETCF Process.[a]

	$Co^{+}(Bpy)$		
	x	y	z
C	-0.014116	0.000895	0.032110
N	-0.014138	0.000887	1.403353
C	1.184219	0.000403	-0.682572
C	-1.352564	0.001445	-0.605326
C	1.171382	0.000397	2.052391
C	2.399539	-0.000103	-0.001551
N	-2.417184	0.001916	0.258903
C	-1.552923	0.001490	-1.986135
H	1.176965	0.000413	-1.765870
C	2.393028	-0.000105	1.393428
C	-3.668259	0.002438	-0.252486
C	-2.847611	0.002026	-2.500504
H	1.122625	0.000410	3.136679
H	3.334126	-0.000488	-0.552841
H	-0.707278	0.001106	-2.663240
C	-3.926570	0.002514	-1.616277
H	3.314417	-0.000489	1.965296
H	-4.479373	0.002804	0.468730
H	-3.008602	0.002063	-3.573563
H	-4.951265	0.002942	-1.971231
Co^{2+}	-1.799087	0.001659	2.056170

Table E.5. (continued) Cartesian Coordinates of the B3LYP/6-31G* Optimized Geometries of the Transition States, Ints, and Products Involved in the Dissociation of $M^{2+}(Bpy)_2$ Complexes through ETCF Process.[a]

$Ni^{2+}(Bpy)_2$ TS_1				$Ni^{2+}(Bpy)_2$ TS_1			
	x	y	z		x	y	z
C	0.430863	-0.075455	0.152348	H	-1.911635	-4.201738	4.252017
N	0.610456	0.419761	1.401631	H	-2.913361	3.882571	6.449033
C	1.502311	-0.377716	-0.675984	H	-2.734483	-3.206912	6.408211
C	-1.024780	-0.244096	-0.190214	Ni^{2+}	-1.199950	0.391533	2.129185
C	1.853518	0.641497	1.873274				
C	2.793814	-0.144168	-0.193873				
N	-1.527077	-1.495777	-0.086982				
C	-1.797843	0.861686	-0.591642				
H	1.331415	-0.780654	-1.668317				
C	2.971373	0.376002	1.091523				
C	-2.805154	-1.682830	-0.439437				
C	-3.137672	0.645089	-0.945319				
H	1.933581	1.033129	2.881903				
H	3.654847	-0.364677	-0.817530				
H	-1.343538	1.843503	-0.697858				
C	-3.643613	-0.650424	-0.883923				
H	3.962646	0.568324	1.487361				
H	-3.174631	-2.702542	-0.366426				
H	-3.755265	1.469437	-1.288935				
H	-4.666360	-0.868153	-1.174462				
N	-1.729162	1.700066	3.496706				
N	-1.702297	-0.935913	3.472218				
C	-2.168755	1.107153	4.642711				
C	-1.702302	3.042575	3.401864				
C	-2.141363	-0.376785	4.633740				
C	-1.623334	-2.273776	3.348141				
C	-2.601579	1.879714	5.718701				
C	-2.120569	3.866658	4.440789				
C	-2.521915	-1.181485	5.705119				
C	-1.986979	-3.128083	4.384468				
H	-1.334353	3.456560	2.468105				
H	-1.268276	-2.646138	2.391985				
C	-2.577982	3.272011	5.616420				
C	-2.442643	-2.570585	5.578482				
H	-2.954424	1.412042	6.630072				
H	-2.085880	4.944323	4.325197				
H	-2.873124	-0.743601	6.631811				

Table E.5. (continued) Cartesian Coordinates of the B3LYP/6-31G* Optimized Geometries of the Transition States, Ints, and Products Involved in the Dissociation of $M^{2+}(Bpy)_2$ Complexes through ETCF Process.[a]

$Ni^{2+}(Bpy)_2$ Int_1				$Ni^{2+}(Bpy)_2$ Int_1			
	x	y	z		x	y	z
C	-0.052547	-0.001303	-0.012852	H	-2.940445	-5.115181	1.330726
N	-0.175275	0.143475	1.333162	H	-3.740518	0.794692	7.292561
C	1.188240	-0.109559	-0.630972	H	-3.792868	-5.302584	3.688538
C	-1.358713	-0.040497	-0.718656	Ni^{2+}	-2.075559	-0.083727	1.784824
C	0.929563	0.217895	2.100462				
C	2.332525	-0.023481	0.164294				
N	-1.504561	-0.927765	-1.709636				
C	-2.412284	0.808148	-0.281455				
H	1.243684	-0.246968	-1.704973				
C	2.202432	0.153407	1.545197				
C	-2.698759	-1.010201	-2.307723				
C	-3.664352	0.693680	-0.921279				
H	0.775594	0.322046	3.169507				
H	3.316979	-0.090299	-0.288608				
H	-2.184847	1.723251	0.275388				
C	-3.818282	-0.251595	-1.926919				
H	3.073638	0.225866	2.187078				
H	-2.765855	-1.713011	-3.134899				
H	-4.477083	1.366015	-0.661389				
H	-4.761031	-0.369522	-2.450850				
N	-2.537783	0.351832	3.653450				
N	-2.619044	-1.904544	2.290658				
C	-3.040238	-0.715515	4.334460				
C	-2.457074	1.554330	4.253938				
C	-3.066199	-1.989369	3.574375				
C	-2.575367	-3.006186	1.518763				
C	-3.480097	-0.574465	5.649596				
C	-2.878080	1.758288	5.563407				
C	-3.497756	-3.207595	4.095729				
C	-2.989839	-4.250141	1.982773				
H	-2.041827	2.366140	3.664076				
H	-2.196460	-2.877360	0.509534				
C	-3.399255	0.674046	6.269097				
C	-3.460489	-4.348422	3.291602				
H	-3.884003	-1.420162	6.193109				
H	-2.798241	2.742676	6.011298				
H	-3.854966	-3.278857	5.116036				

Table E.5. (continued) Cartesian Coordinates of the B3LYP/6-31G* Optimized Geometries of the Transition States, Ints, and Products Involved in the Dissociation of $M^{2+}(Bpy)_2$ Complexes through ETCF Process.[a]

$Ni^{2+}(Bpy)_2$ TS_2				$Ni^{2+}(Bpy)_2$ TS_2			
	x	y	z		x	y	z
C	0.265032	0.246011	0.698393	H	3.359428	-4.654507	3.653846
N	0.073506	1.117194	1.734831	H	-2.205431	-0.159533	8.131405
C	1.574165	-0.161618	0.311705	H	2.505515	-5.012329	5.992150
C	-0.915051	-0.255002	-0.025253	Ni^{2+}	0.536496	-0.434740	3.029368
C	1.170944	1.601690	2.393221				
C	2.672623	0.303251	1.019742				
N	-0.690581	-1.352991	-0.778700				
C	-2.155709	0.398743	0.042754				
H	1.670756	-0.839944	-0.528479				
C	2.473143	1.191378	2.101616				
C	-1.705374	-1.831434	-1.492319				
C	-3.208511	-0.113128	-0.716313				
H	0.971106	2.338758	3.166439				
H	3.677683	-0.000472	0.741394				
H	-2.274879	1.294037	0.642501				
C	-2.983790	-1.245182	-1.496612				
H	3.310336	1.588055	2.667407				
H	-1.500906	-2.714983	-2.091506				
H	-4.179519	0.371861	-0.707968				
H	-3.772544	-1.670687	-2.108664				
N	-0.458825	-0.212161	4.698177				
N	1.295380	-2.004701	3.898538				
C	-0.169280	-1.175156	5.615101				
C	-1.356120	0.748696	4.981971				
C	0.816178	-2.187313	5.162864				
C	2.184416	-2.877404	3.385168				
C	-0.789397	-1.173058	6.862555				
C	-2.009381	0.803061	6.209033				
C	1.243788	-3.266631	5.932778				
C	2.645017	-3.974124	4.103951				
H	-1.546897	1.476342	4.199503				
H	2.526962	-2.683969	2.373935				
C	-1.716614	-0.171967	7.162172				
C	2.167091	-4.168047	5.399572				
H	-0.562067	-1.935426	7.598066				
H	-2.727646	1.591388	6.405630				
H	0.865894	-3.413176	6.937487				

Table E.5. (continued) Cartesian Coordinates of the B3LYP/6-31G* Optimized Geometries of the Transition States, Ints, and Products Involved in the Dissociation of $M^{2+}(Bpy)_2$ Complexes through ETCF Process.[a]

$Ni^{2+}(Bpy)_2$ Int_2				$Ni^{2+}(Bpy)_2$ Int_2			
	x	y	z		x	y	z
C	-6.148827	0.729488	-0.286105	H	8.707500	2.590852	3.403093
N	-4.926427	1.199930	-0.671628	H	8.448082	-2.136179	-3.287595
C	-7.303569	1.442401	-0.604587	H	6.267504	1.992283	3.240020
C	-6.162187	-0.554805	0.478493	Ni^{2+}	-3.654981	-0.080742	-0.141103
C	-4.832581	2.348884	-1.359134				
C	-7.205079	2.637514	-1.316934				
N	-4.962390	-1.187479	0.633616				
C	-7.321008	-1.113821	1.015241				
H	-8.280332	1.076309	-0.312490				
C	-5.952346	3.102688	-1.701344				
C	-4.894087	-2.349302	1.302664				
C	-7.249634	-2.321757	1.708639				
H	-3.833586	2.667780	-1.635459				
H	-8.102800	3.193940	-1.567007				
H	-8.278118	-0.618075	0.907651				
C	-6.019685	-2.953722	1.856304				
H	-5.831632	4.027045	-2.255513				
H	-3.911848	-2.800466	1.390121				
H	-8.149918	-2.759031	2.128559				
H	-5.921337	-3.893879	2.387855				
N	5.824851	-0.775369	-0.716700				
N	8.851667	0.684716	0.615636				
C	7.143915	-0.477971	-0.602979				
C	5.462618	-1.543986	-1.726101				
C	7.537756	0.367037	0.523668				
C	9.230576	1.454956	1.618676				
C	8.126826	-0.952528	-1.517644				
C	6.367925	-2.066340	-2.688780				
C	6.567191	0.821019	1.459471				
C	8.334606	1.959607	2.602530				
H	4.401805	-1.774188	-1.800270				
H	10.289886	1.696139	1.670064				
C	7.724302	-1.757086	-2.573128				
C	6.980969	1.625473	2.508887				
H	9.163444	-0.675946	-1.363756				
H	5.998562	-2.693205	-3.494330				
H	5.532271	0.528300	1.326448				

Table E.5. (continued) Cartesian Coordinates of the B3LYP/6-31G* Optimized Geometries of the Transition States, Ints, and Products Involved in the Dissociation of $M^{2+}(Bpy)_2$ Complexes through ETCF Process.[a]

	$Ni^+(Bpy)$		
	x	y	z
C	-0.017288	0.000684	0.047355
N	-0.012065	0.000629	1.413499
C	1.176661	0.000800	-0.670344
C	-1.365754	0.000617	-0.583180
C	1.164014	0.000691	2.067251
C	2.392318	0.000862	0.014012
N	-2.417527	0.000413	0.288761
C	-1.580500	0.000745	-1.959569
H	1.168810	0.000833	-1.753592
C	2.387833	0.000809	1.406762
C	-3.673172	0.000334	-0.194800
C	-2.885036	0.000662	-2.453900
H	1.109734	0.000646	3.150798
H	3.327074	0.000951	-0.537205
H	-0.744119	0.000916	-2.648061
C	-3.950969	0.000450	-1.557498
H	3.309476	0.000856	1.977911
H	-4.470093	0.000168	0.541367
H	-3.061158	0.000762	-3.524687
H	-4.980182	0.000378	-1.898621
Ni^{2+}	-1.767758	0.000379	2.033948

Table E.5. (continued) Cartesian Coordinates of the B3LYP/6-31G* Optimized Geometries of the Transition States, Ints, and Products Involved in the Dissociation of $M^{2+}(Bpy)_2$ Complexes through ETCF Process.[a]

$Cu^{2+}(Bpy)_2$ TS_1				$Cu^{2+}(Bpy)_2$ TS_1			
	x	y	z		x	y	z
C	-0.498545	-0.555866	0.087424	H	-3.052698	-5.181493	2.892863
N	-0.623840	-0.938311	1.389784	H	-5.792575	1.947795	6.169439
C	0.589482	-0.975266	-0.674453	H	-1.455669	-4.066442	4.476000
C	-1.583670	0.318949	-0.407821	Cu^{2+}	-2.130068	-0.124483	2.276159
C	0.311894	-1.727409	1.949954				
C	1.559366	-1.793032	-0.091966				
N	-2.496617	0.676586	0.535035				
C	-1.715325	0.758277	-1.723318				
H	0.692212	-0.665914	-1.707768				
C	1.421686	-2.175094	1.241942				
C	-3.545719	1.447838	0.204958				
C	-2.800160	1.567316	-2.067805				
H	0.157732	-1.999354	2.987959				
H	2.413236	-2.122925	-0.675538				
H	-0.991861	0.472305	-2.477649				
C	-3.733012	1.916089	-1.092276				
H	2.156103	-2.805619	1.730813				
H	-4.243533	1.686280	0.999860				
H	-2.914485	1.914891	-3.089854				
H	-4.592271	2.536035	-1.323290				
N	-3.217467	0.802509	3.548808				
N	-4.473213	-2.115531	2.967164				
C	-3.951020	-0.115699	4.222139				
C	-3.377241	2.120919	3.798176				
C	-3.624700	-1.526146	3.830537				
C	-4.242403	-3.392820	2.647436				
C	-4.896147	0.261222	5.167316				
C	-4.290480	2.563254	4.744956				
C	-2.501998	-2.172291	4.377381				
C	-3.169801	-4.137355	3.164860				
H	-2.755539	2.806278	3.231267				
H	-4.949458	-3.846084	1.957169				
C	-5.065430	1.622471	5.431598				
C	-2.282910	-3.515976	4.037303				
H	-5.479822	-0.492887	5.683902				
H	-4.393067	3.625503	4.938547				
H	-1.879223	-1.671184	5.114606				

Table E.5. (continued) Cartesian Coordinates of the B3LYP/6-31G* Optimized Geometries of the Transition States, Ints, and Products Involved in the Dissociation of $M^{2+}(Bpy)_2$ Complexes through ETCF Process.[a]

	$Cu^{2+}(Bpy)_2$ Int_1				$Cu^{2+}(Bpy)_2$ Int_1		
	x	y	z		x	y	z
C	0.074193	0.151240	0.005461	H	-0.470895	-4.661839	4.025246
N	0.096725	0.093429	1.365896	H	-6.415393	1.081846	5.294629
C	1.253981	0.310108	-0.719555	H	0.594535	-2.401959	3.914905
C	-1.273696	0.055038	-0.598220	Cu^{2+}	-1.674256	-0.014815	2.163247
C	1.268594	0.198181	2.019512				
C	2.467962	0.415367	-0.039527				
N	-2.295280	0.006228	0.298635				
C	-1.527231	0.004819	-1.967644				
H	1.234595	0.361764	-1.801592				
C	2.477960	0.363427	1.354131				
C	-3.564681	-0.094061	-0.131111				
C	-2.845817	-0.097560	-2.414970				
H	1.229681	0.155160	3.103149				
H	3.392505	0.542003	-0.594147				
H	-0.714468	0.037407	-2.683499				
C	-3.882838	-0.149951	-1.484720				
H	3.399128	0.449846	1.919826				
H	-4.334337	-0.130119	0.632172				
H	-3.056181	-0.138790	-3.479152				
H	-4.919145	-0.232820	-1.793343				
N	-3.219121	0.537439	3.199188				
N	-3.261466	-2.769373	4.315966				
C	-3.613246	-0.396993	4.104170				
C	-3.944411	1.666052	3.046429				
C	-2.708235	-1.564553	4.177892				
C	-2.455261	-3.837547	4.272904				
C	-4.771799	-0.243850	4.860112				
C	-5.089396	1.899915	3.797461				
C	-1.310255	-1.359840	4.026738				
C	-1.069603	-3.757807	4.059791				
H	-3.590597	2.378484	2.308056				
H	-2.936879	-4.801359	4.418603				
C	-5.515060	0.926546	4.708079				
C	-0.485348	-2.500840	3.973910				
H	-5.065051	-1.026865	5.550271				
H	-5.640691	2.824214	3.662698				
H	-0.872641	-0.396298	4.306354				

Table E.5. (continued) Cartesian Coordinates of the B3LYP/6-31G* Optimized Geometries of the Transition States, Ints, and Products Involved in the Dissociation of $M^{2+}(Bpy)_2$ Complexes through ETCF Process.[a]

	$Cu^{2+}(Bpy)_2$ TS_2				$Cu^{2+}(Bpy)_2$ TS_2		
	x	y	z		x	y	z
C	-0.433767	0.470247	0.655560	H	-3.900512	2.190953	4.774996
N	-0.592645	0.253884	1.990116	H	-5.136154	-1.507764	2.876137
C	0.805634	0.847414	0.143506	H	0.860491	0.640911	8.095276
C	-1.650853	0.258091	-0.158732	H	-5.543307	0.944266	3.330766
C	0.450244	0.385996	2.827314				
C	1.888748	0.994525	1.012033				
N	-2.744359	-0.161867	0.537514				
C	-1.718845	0.451797	-1.537046				
H	0.937414	1.019611	-0.917970				
C	1.711820	0.758842	2.374421				
C	-3.899991	-0.398218	-0.109959				
C	-2.918730	0.208229	-2.206731				
H	0.258173	0.188285	3.876358				
H	2.859763	1.285265	0.623373				
H	-0.850747	0.789395	-2.090392				
C	-4.029035	-0.225203	-1.483607				
H	2.531063	0.855475	3.078170				
H	-4.736886	-0.734997	0.490959				
H	-2.981518	0.355240	-3.280448				
H	-4.978850	-0.428378	-1.965923				
Cu^{2+}	-2.381032	-0.328978	2.444179				
N	-1.837211	2.500771	5.988819				
N	-2.321206	-0.813498	4.631333				
C	-1.649052	1.168268	5.865608				
C	-1.066116	3.158677	6.846523				
C	-2.581194	0.489364	4.961620				
C	-3.265766	-1.523036	3.962862				
C	-0.680958	0.452926	6.595231				
C	-0.075572	2.531557	7.628079				
C	-3.746102	1.155937	4.492354				
C	-4.408793	-0.911800	3.418714				
H	-1.236558	4.229238	6.928019				
H	-3.069582	-2.585700	3.836104				
C	0.116397	1.157890	7.497472				
C	-4.644869	0.460151	3.702294				
H	-0.590147	-0.621548	6.480382				
H	0.516611	3.118059	8.323340				

Table E.5. (continued) Cartesian Coordinates of the B3LYP/6-31G* Optimized Geometries of the Transition States, Ints, and Products Involved in the Dissociation of $M^{2+}(Bpy)_2$ Complexes through ETCF Process.[a]

	$Cu^{2+}(Bpy)_2$ Int_2				$Cu^{2+}(Bpy)_2$ Int_2		
	x	y	z		x	y	z
C	-6.129880	0.730114	-0.285042	H	5.551318	0.528645	1.326751
N	-4.907487	1.200467	-0.670697	H	8.726766	2.591296	3.402964
C	-7.284616	1.443038	-0.603523	H	8.466717	-2.136441	-3.287202
C	-6.143239	-0.554097	0.479694	H	6.286736	1.992804	3.240118
C	-4.813643	2.349344	-1.358332				
C	-7.186127	2.638071	-1.316004				
N	-4.943456	-1.186801	0.634804				
C	-7.302045	-1.113011	1.016579				
H	-8.261373	1.077015	-0.311321				
C	-5.933402	3.103155	-1.700548				
C	-4.875153	-2.348555	1.303972				
C	-7.230672	-2.320875	1.710101				
H	-3.814654	2.668172	-1.634758				
H	-8.083843	3.194505	-1.566077				
H	-8.259143	-0.617239	0.909000				
C	-6.000738	-2.952872	1.857753				
H	-5.812689	4.027447	-2.254824				
H	-3.892926	-2.799748	1.391412				
H	-8.130945	-2.758070	2.130129				
H	-5.902391	-3.892977	2.389397				
Cu^{2+}	-3.636056	-0.080197	-0.140120				
N	5.843711	-0.775254	-0.716277				
N	8.870673	0.684856	0.615701				
C	7.162794	-0.477895	-0.602676				
C	5.481380	-1.543964	-1.725572				
C	7.556743	0.367218	0.523855				
C	9.249679	1.455188	1.618633				
C	8.145625	-0.952588	-1.517356				
C	6.386603	-2.066457	-2.688255				
C	6.586258	0.821338	1.459674				
C	8.353794	1.959979	2.602493				
H	4.420554	-1.774133	-1.799645				
H	10.309001	1.696336	1.669925				
C	7.743000	-1.757244	-2.572727				
C	7.000138	1.625888	2.508976				
H	9.182264	-0.676029	-1.363567				
H	6.017162	-2.693394	-3.493713				

Table E.5. (continued) Cartesian Coordinates of the B3LYP/6-31G* Optimized Geometries of the Transition States, Ints, and Products Involved in the Dissociation of $M^{2+}(Bpy)_2$ Complexes through ETCF Process.[a]

	Cu^{+}(Bpy)		
	x	y	z
C	0.034358	0.057406	-0.072650
N	0.067424	-0.220702	1.266121
C	1.215954	0.317915	-0.766249
C	-1.312341	0.068664	-0.744061
C	1.247561	-0.240365	1.907705
C	2.437525	0.295506	-0.092541
N	-2.405113	-0.198707	0.033751
C	-1.466010	0.339533	-2.103526
H	1.201596	0.539113	-1.825759
C	2.458072	0.011907	1.269268
C	-3.628018	-0.197494	-0.522463
C	-2.739493	0.338686	-2.673487
H	1.209065	-0.466629	2.967495
H	3.357601	0.498228	-0.631413
H	-0.608357	0.552294	-2.728742
C	-3.843239	0.065869	-1.871871
H	3.384108	-0.015906	1.832727
H	-4.454290	-0.416128	0.144842
H	-2.860046	0.549497	-3.731342
H	-4.850880	0.054732	-2.272277
Cu^{2+}	-1.722813	-0.496289	1.755894

Table E.5. (continued) Cartesian Coordinates of the B3LYP/6-31G* Optimized Geometries of the Transition States, Ints, and Products Involved in the Dissociation of $M^{2+}(Bpy)_2$ Complexes through ETCF Process.[a]

$Zn^{2+}(Bpy)_2$ Reactant				$Zn^{2+}(Bpy)_2$ Reactant			
	x	y	z		x	y	z
C	-0.119472	0.205543	-0.226008	H	-2.622485	-5.491978	2.816007
N	-0.088542	-0.128308	1.091848	H	-4.127873	1.759007	6.801785
C	1.063636	0.466380	-0.918639	H	-3.645456	-5.030844	5.067406
C	-1.469554	0.269148	-0.852687	Zn^{2+}	-1.930499	-0.450496	1.838078
C	1.090811	-0.208538	1.735646				
C	2.284829	0.382572	-0.249162				
N	-2.519965	-0.014252	-0.036916				
C	-1.681457	0.596328	-2.192676				
H	1.046587	0.732745	-1.968125				
C	2.303110	0.039345	1.101937				
C	-3.774704	0.020311	-0.522943				
C	-2.982931	0.631498	-2.694138				
H	1.052207	-0.479196	2.786139				
H	3.209586	0.583940	-0.780862				
H	-0.849802	0.823197	-2.848071				
C	-4.051278	0.338941	-1.847588				
H	3.231612	-0.036135	1.656947				
H	-4.571722	-0.214944	0.175412				
H	-3.156140	0.885149	-3.735335				
H	-5.076794	0.355654	-2.199565				
N	-2.649093	0.466942	3.479776				
N	-2.463850	-2.126557	2.817755				
C	-3.117171	-0.418510	4.399580				
C	-2.703894	1.787928	3.732344				
C	-3.014616	-1.858567	4.031849				
C	-2.333809	-3.401862	2.407319				
C	-3.655165	0.031345	5.606109				
C	-3.227743	2.298586	4.914506				
C	-3.447250	-2.896639	4.858130				
C	-2.745127	-4.479251	3.183697				
H	-2.315357	2.445469	2.961007				
H	-1.887270	-3.553300	1.429592				
C	-3.710870	1.401047	5.865621				
C	-3.311366	-4.217711	4.430517				
H	-4.029719	-0.668003	6.343185				
H	-3.253459	3.370081	5.079091				
H	-3.886785	-2.690682	5.826144				

Table E.5. (continued) Cartesian Coordinates of the B3LYP/6-31G* Optimized Geometries of the Transition States, Ints, and Products Involved in the Dissociation of $M^{2+}(Bpy)_2$ Complexes through ETCF Process.[a]

$Zn^{2+}(Bpy)_2$ TS_1				$Zn^{2+}(Bpy)_2$ TS_1			
	x	y	z		x	y	z
C	0.019284	0.069058	-0.040830	H	-3.179129	-4.812272	1.878927
N	-0.000588	0.122598	1.320334	H	-4.946250	1.786208	6.610028
C	1.232978	0.045179	-0.727115	H	-1.356372	-4.150456	3.474630
C	-1.309824	0.037366	-0.715622	Zn^{2+}	-1.865860	0.186602	2.007907
C	1.155770	0.156643	2.011121				
C	2.430069	0.078692	-0.009940				
N	-2.394401	0.044087	0.106410				
C	-1.475897	0.003016	-2.099279				
H	1.258434	0.001218	-1.808864				
C	2.395009	0.135952	1.382881				
C	-3.638918	0.007621	-0.407097				
C	-2.765678	-0.025613	-2.634347				
H	1.074087	0.202450	3.092346				
H	3.378457	0.060923	-0.537950				
H	-0.620663	0.000794	-2.763676				
C	-3.866295	-0.025861	-1.778615				
H	3.303593	0.165276	1.974081				
H	-4.454209	-0.004623	0.309183				
H	-2.903779	-0.048798	-3.710910				
H	-4.881447	-0.050107	-2.159165				
N	-2.718763	0.957462	3.580372				
N	-4.267033	-1.701657	2.630548				
C	-3.456103	-0.020918	4.166828				
C	-2.761755	2.221857	4.057097				
C	-3.306090	-1.364042	3.514892				
C	-4.195746	-2.915605	2.072857				
C	-4.271724	0.246336	5.258366				
C	-3.550866	2.550110	5.150416				
C	-2.224833	-2.200806	3.834324				
C	-3.171736	-3.833014	2.346723				
H	-2.155821	2.961464	3.544342				
H	-4.995127	-3.169686	1.381118				
C	-4.317503	1.551111	5.756601				
C	-2.161851	-3.464521	3.230221				
H	-4.857923	-0.549158	5.705028				
H	-3.565902	3.571392	5.514969				
H	-1.493159	-1.901086	4.580059				

Table E.5. (continued) Cartesian Coordinates of the B3LYP/6-31G* Optimized Geometries of the Transition States, Ints, and Products Involved in the Dissociation of $M^{2+}(Bpy)_2$ Complexes through ETCF Process.[a]

$Zn^{2+}(Bpy)_2$ Int_1				$Zn^{2+}(Bpy)_2$ Int_1			
	x	y	z		x	y	z
C	0.077392	0.079462	0.010063	H	-3.591390	-5.055105	1.899902
N	0.059847	-0.045057	1.365827	H	-5.047360	1.788887	6.440357
C	1.287885	0.217135	-0.669804	H	-1.379701	-3.983562	2.403424
C	-1.249194	0.062455	-0.669664	Zn^{2+}	-1.807112	-0.230325	2.058173
C	1.215759	-0.033351	2.057559				
C	2.484191	0.227790	0.048633				
N	-2.333862	-0.092779	0.137294				
C	-1.410005	0.200529	-2.048380				
H	1.311657	0.315616	-1.747918				
C	2.451777	0.101484	1.436902				
C	-3.571688	-0.112770	-0.392183				
C	-2.693438	0.179300	-2.596538				
H	1.138470	-0.133593	3.135784				
H	3.429486	0.334541	-0.474366				
H	-0.553509	0.327033	-2.698802				
C	-3.795612	0.020364	-1.757635				
H	3.359428	0.107037	2.030254				
H	-4.394887	-0.238298	0.304016				
H	-2.826228	0.287855	-3.668488				
H	-4.807819	0.001216	-2.146150				
N	-2.699008	0.610452	3.612045				
N	-4.712932	-2.238900	3.405073				
C	-3.582954	-0.257235	4.174929				
C	-2.633650	1.882052	4.062206				
C	-3.542041	-1.630733	3.612096				
C	-4.701738	-3.442406	2.818509				
C	-4.455822	0.140841	5.182538				
C	-3.455103	2.334731	5.086668				
C	-2.296345	-2.213645	3.262102				
C	-3.533917	-4.082410	2.376980				
H	-1.919520	2.537765	3.574699				
H	-5.671465	-3.919843	2.699740				
C	-4.385371	1.454834	5.647318				
C	-2.310946	-3.474803	2.635561				
H	-5.161900	-0.574228	5.588954				
H	-3.375187	3.361855	5.425463				
H	-1.372634	-1.868150	3.733007				

Table E.5. (continued) Cartesian Coordinates of the B3LYP/6-31G* Optimized Geometries of the Transition States, Ints, and Products Involved in the Dissociation of $M^{2+}(Bpy)_2$ Complexes through ETCF Process.[a]

$Zn^{2+}(Bpy)_2$ TS_2				$Zn^{2+}(Bpy)_2$ TS_2			
	x	y	z		x	y	z
C	-0.485605	-0.280039	0.684198	H	-1.938982	-5.016317	7.125456
N	-0.925394	-0.223259	1.975697	H	-2.453646	2.834114	5.046658
C	0.792734	-0.755189	0.398401	H	-4.125508	-4.930583	5.896018
C	-1.441371	0.172657	-0.367368	Zn^{2+}	-2.746502	0.518175	2.039626
C	-0.129758	-0.643757	2.981375				
C	1.621275	-1.178123	1.439392				
N	-2.663175	0.589724	0.068012				
C	-1.144025	0.175342	-1.729550				
H	1.151441	-0.803335	-0.622021				
C	1.152647	-1.127350	2.750566				
C	-3.592977	1.005333	-0.814667				
C	-2.107426	0.605939	-2.643934				
H	-0.537686	-0.605650	3.986479				
H	2.618729	-1.547233	1.221617				
H	-0.176661	-0.152202	-2.089075				
C	-3.354355	1.026843	-2.183014				
H	1.761850	-1.454850	3.585604				
H	-4.546463	1.322816	-0.405425				
H	-1.881723	0.610019	-3.705828				
H	-4.128190	1.365723	-2.862923				
N	-4.176686	-0.430933	3.780708				
N	-1.790721	-1.823076	6.049976				
C	-3.305143	-0.469647	4.814333				
C	-4.488324	0.779282	3.239730				
C	-2.973585	-1.781333	5.400901				
C	-1.448773	-2.969754	6.638483				
C	-2.705301	0.713000	5.325965				
C	-3.827492	1.973260	3.598738				
C	-3.842262	-2.874746	5.301997				
C	-2.259387	-4.113868	6.615006				
H	-5.318145	0.782953	2.532109				
H	-0.491955	-2.980467	7.154495				
C	-2.928928	1.923859	4.692791				
C	-3.472406	-4.064268	5.931633				
H	-2.057183	0.633509	6.191184				
H	-4.105353	2.916586	3.136171				
H	-4.783255	-2.784805	4.770961				

Table E.5. (continued) Cartesian Coordinates of the B3LYP/6-31G* Optimized Geometries of the Transition States, Ints, and Products Involved in the Dissociation of $M^{2+}(Bpy)_2$ Complexes through ETCF Process.[a]

	$Zn^{2+}(Bpy)_2$ Int_2				$Zn^{2+}(Bpy)_2$ Int_2		
	x	y	z		x	y	z
C	-6.242860	-0.544658	-0.409820	H	5.405505	-3.252369	2.646633
N	-5.044009	-1.139225	-0.663935	H	7.075059	2.684121	-2.794252
C	-7.427375	-1.173347	-0.791560	H	7.889693	-2.930197	2.882626
C	-6.200663	0.778656	0.281283	Zn^{2+}	-3.568726	0.002717	-0.007201
C	-4.989178	-2.333222	-1.282967				
C	-7.373562	-2.412221	-1.433855				
N	-4.967241	1.266574	0.590864				
C	-7.341787	1.508904	0.610865				
H	-8.388648	-0.714401	-0.597048				
C	-6.137290	-3.005141	-1.685376				
C	-4.836367	2.451650	1.215581				
C	-7.209124	2.738788	1.258995				
H	-4.000361	-2.746198	-1.452777				
H	-8.293093	-2.905536	-1.733154				
H	-8.329616	1.135563	0.371444				
C	-5.938482	3.221374	1.568444				
H	-6.056880	-3.965845	-2.181809				
H	-3.823959	2.777134	1.430588				
H	-8.094678	3.310879	1.517832				
H	-5.797019	4.171591	2.071379				
N	9.103239	0.569777	-0.219798				
N	5.803753	-0.787307	0.370915				
C	7.768299	0.399033	-0.360801				
C	9.697760	1.476331	-0.981094				
C	7.142225	-0.615107	0.492917				
C	5.232176	-1.709664	1.132213				
C	6.996396	1.147907	-1.283298				
C	9.010860	2.268755	-1.928607				
C	7.931334	-1.371467	1.394910				
C	5.935818	-2.512769	2.055143				
H	10.770867	1.593076	-0.847227				
H	4.157107	-1.832621	1.015865				
C	7.635242	2.094220	-2.075480				
C	7.312214	-2.332985	2.183958				
H	5.931386	0.962217	-1.348813				
H	9.555778	2.994240	-2.524133				
H	8.996623	-1.182129	1.443833				

Table E.5. (continued) Cartesian Coordinates of the B3LYP/6-31G* Optimized Geometries of the Transition States, Ints, and Products Involved in the Dissociation of $M^{2+}(Bpy)_2$ Complexes through ETCF Process.[a]

	Zn^{+}(Bpy)		
	x	y	z
C	0.046110	0.000000	-0.028274
N	-0.011286	0.000000	1.326367
C	1.276645	0.000000	-0.686366
C	-1.266686	0.000000	-0.733035
C	1.119531	0.000000	2.048103
C	2.452751	0.000000	0.064481
N	-2.364031	0.000000	0.063318
C	-1.398123	0.000000	-2.122289
H	1.330110	0.000000	-1.768193
C	2.378790	0.000000	1.455830
C	-3.590420	0.000000	-0.480389
C	-2.673801	0.000000	-2.687659
H	0.999465	0.000000	3.127070
H	3.415115	0.000000	-0.437676
H	-0.525989	0.000000	-2.764622
C	-3.792588	0.000000	-1.857216
H	3.270266	0.000000	2.072995
H	-4.423370	0.000000	0.215873
H	-2.787025	0.000000	-3.767236
H	-4.799571	0.000000	-2.259219
Zn^{2+}	-1.920297	0.000000	2.059566

[a]Standard Orientation, Å.

Table E.5. Cartesian Coordinates of the B3LYP/6-31G* Optimized Geometries of the Transition States, Ints, and Products Involved in the Dissociation of $M^{2+}(Bpy)_2$ Complexes through PTCF Process.[a]

$Fe^{2+}(Bpy)_2$ TS_1				$Fe^{2+}(Bpy)_2$ TS_1			
	x	y	z		x	y	z
C	-0.004699	-0.235373	0.010966	H	-3.374718	-4.478240	3.531863
N	0.060385	0.013309	1.346855	H	-3.701789	3.436263	6.680619
C	1.150320	-0.529998	-0.713273	H	-4.508792	-3.734257	5.646821
C	-1.365874	-0.179878	-0.576345	Fe^{2+}	-1.718890	0.390899	2.260984
C	1.250690	-0.020009	1.977755				
C	2.382059	-0.562690	-0.058624				
N	-2.367791	0.027713	0.318218				
C	-1.636324	-0.320761	-1.937355				
H	1.098930	-0.737061	-1.775371				
C	2.436447	-0.304702	1.310718				
C	-3.639629	0.102159	-0.116208				
C	-2.957167	-0.248149	-2.382130				
H	1.244051	0.197535	3.041297				
H	3.286707	-0.787561	-0.614891				
H	-0.835591	-0.476867	-2.650180				
C	-3.979431	-0.035400	-1.457987				
H	3.374052	-0.319152	1.855280				
H	-4.400704	0.271943	0.639450				
H	-3.180593	-0.352922	-3.439251				
H	-5.017470	0.029618	-1.764902				
N	-2.459865	1.299257	3.805243				
N	-2.666033	-1.186314	3.383852				
C	-3.154677	0.673295	4.791455				
C	-2.200716	2.590393	3.817512				
C	-3.280612	-0.775513	4.534808				
C	-2.714624	-2.487435	3.054277				
C	-3.615319	1.449959	5.849456				
C	-2.615352	3.447310	4.823363				
C	-3.951492	-1.669860	5.363494				
C	-3.365362	-3.438313	3.839447				
H	-1.240361	1.932549	2.236465				
H	-2.218077	-2.772543	2.131715				
C	-3.343638	2.829436	5.853229				
C	-3.992664	-3.021382	5.011407				
H	-4.174689	1.009217	6.667357				
H	-2.395571	4.508393	4.823972				
H	-4.434395	-1.323386	6.270678				

Table E.5. (continued) Cartesian Coordinates of the B3LYP/6-31G* Optimized Geometries of the Transition States, Ints, and Products Involved in the Dissociation of $M^{2+}(Bpy)_2$ Complexes through PTCF Process.[a]

$Fe^{2+}(Bpy)_2$ Int_1				$Fe^{2+}(Bpy)_2$ Int_1			
	x	y	z		x	y	z
C	-0.098051	-0.234936	-0.042350	H	-1.533146	-5.047714	3.181029
N	0.017387	-0.329777	1.311967	H	-5.473466	1.704269	6.391955
C	1.004942	-0.476846	-0.862224	H	-3.169288	-4.911932	5.084323
C	-1.446963	0.119434	-0.540834	Fe^{2+}	-1.613849	0.099627	2.343905
C	1.204922	-0.646858	1.866534				
C	2.233060	-0.804170	-0.288814				
N	-2.400209	0.242234	0.422013				
C	-1.756402	0.322523	-1.885500				
H	0.912754	-0.412914	-1.939683				
C	2.336858	-0.892402	1.099437				
C	-3.659043	0.563642	0.073334				
C	-3.064326	0.653805	-2.242356				
H	1.239528	-0.687893	2.950311				
H	3.096708	-0.986168	-0.920656				
H	-0.995274	0.233904	-2.651339				
C	-4.035237	0.775412	-1.249022				
H	3.274467	-1.138556	1.585494				
H	-4.378042	0.649696	0.881887				
H	-3.317486	0.816320	-3.285361				
H	-5.061850	1.030369	-1.487782				
N	-2.927364	0.705009	3.679270				
N	-2.089100	-1.723300	3.178870				
C	-3.464920	-0.275678	4.489108				
C	-3.311467	1.946228	3.857474				
C	-2.983270	-1.640493	4.204618				
C	-1.593401	-2.926444	2.837075				
C	-4.385282	0.085401	5.466347				
C	-4.214409	2.413929	4.790787				
C	-3.385014	-2.775083	4.907914				
C	-1.956130	-4.099087	3.492905				
H	-0.832218	1.377401	2.650313				
H	-0.887710	-2.940145	2.013207				
C	-4.758254	1.428472	5.621806				
C	-2.865315	-4.019162	4.546769				
H	-4.820738	-0.666675	6.113774				
H	-4.473825	3.463039	4.875514				
H	-4.090472	-2.699456	5.727127				

Table E.5. (continued) Cartesian Coordinates of the B3LYP/6-31G* Optimized Geometries of the Transition States, Ints, and Products Involved in the Dissociation of $M^{2+}(Bpy)_2$ Complexes through PTCF Process.[a]

	$Fe^{2+}(Bpy)_2$ TS_2				$Fe^{2+}(Bpy)_2$ TS_2		
	x	y	z		x	y	z
C	0.063515	0.192534	0.028588	H	-2.742652	-5.708915	2.885721
N	0.110696	0.185468	1.406575	H	-3.808001	1.399709	7.354459
C	1.232071	0.429985	-0.693337	H	-3.844118	-5.389604	5.123671
C	-1.249043	-0.119677	-0.558996	Fe^{2+}	-1.630830	-0.602372	2.310566
C	1.294114	0.399266	2.060913				
C	2.439932	0.633425	-0.028272				
N	-2.168828	-0.608511	0.318136				
C	-1.550024	0.050405	-1.912704				
H	1.207009	0.422210	-1.776702				
C	2.471887	0.600750	1.372609				
C	-3.386735	-0.954467	-0.142299				
C	-2.815725	-0.302993	-2.376932				
H	1.236148	0.424917	3.144144				
H	3.347797	0.814116	-0.594652				
H	-0.818086	0.465129	-2.595921				
C	-3.749574	-0.820250	-1.478430				
H	3.395392	0.748034	1.921683				
H	-4.084271	-1.350618	0.589324				
H	-3.067595	-0.174107	-3.424771				
H	-4.743343	-1.111412	-1.800765				
N	-2.396024	0.106916	4.034673				
N	-2.354533	-2.373455	3.204873				
C	-2.965277	-0.792583	4.899863				
C	-2.329684	1.377297	4.351339				
C	-2.950484	-2.192089	4.417265				
C	-2.299078	-3.614088	2.687434				
C	-3.478305	-0.328625	6.105912				
C	-2.807739	1.940291	5.523800				
C	-3.496856	-3.262425	5.124752				
C	-2.817611	-4.727984	3.342086				
H	-0.838795	0.819879	2.041344				
H	-1.821497	-3.711905	1.716692				
C	-3.402445	1.038716	6.413183				
C	-3.426949	-4.546257	4.582398				
H	-3.933980	-1.010504	6.814607				
H	-2.729071	3.000073	5.736654				
H	-3.972069	-3.104232	6.085981				

Table E.5. (continued) Cartesian Coordinates of the B3LYP/6-31G* Optimized Geometries of the Transition States, Ints, and Products Involved in the Dissociation of $M^{2+}(Bpy)_2$ Complexes through PTCF Process.[a]

	$Fe^{2+}(Bpy)_2$ Int_2				$Fe^{2+}(Bpy)_2$ Int_2		
	x	y	z		x	y	z
C	2.926365	-0.428733	0.502236	H	-4.915073	2.242648	2.649000
N	1.782036	-1.137124	0.697116	H	-4.667509	-2.998388	-1.903973
C	4.124036	-0.796807	1.114550	H	-1.054416	1.216957	-0.066382
C	2.788145	0.744099	-0.392414	Fe^{2+}	0.244202	-0.383587	-0.351696
C	1.815845	-2.216277	1.496417				
C	4.148607	-1.919748	1.942358				
N	1.510710	0.980784	-0.836526				
C	3.809924	1.588714	-0.811809				
H	5.028307	-0.220976	0.955277				
C	2.974729	-2.644039	2.139582				
C	1.269507	1.984850	-1.628663				
C	3.521349	2.658372	-1.672290				
H	0.879344	-2.750760	1.621206				
H	5.073126	-2.220355	2.425219				
H	4.831394	1.424059	-0.488974				
C	2.212385	2.884287	-2.107491				
H	2.950157	-3.522691	2.774772				
H	4.322808	3.312848	-2.004179				
H	1.955448	3.699945	-2.773304				
N	-1.885041	1.458903	0.492999				
N	-1.505399	-1.064719	-0.716023				
C	-2.885788	0.539715	0.517986				
C	-1.904514	2.629513	1.167524				
C	-2.750067	-0.672553	-0.323718				
C	-1.411020	-2.139691	-1.534124				
C	-3.994823	0.830154	1.316143				
C	-2.997537	2.948169	1.951068				
C	-3.897427	-1.356466	-0.739482				
C	-2.509965	-2.861414	-1.981389				
H	-1.036917	3.267979	1.047954				
H	-0.409903	-2.431716	-1.834543				
C	-4.050529	2.028477	2.028062				
C	-3.781630	-2.466106	-1.573112				
H	-4.804033	0.115403	1.398453				
H	-3.020689	3.886705	2.493026				
H	-4.879540	-1.007258	-0.444264				
H	-2.363456	-3.713129	-2.636750				

Table E.5. (continued) Cartesian Coordinates of the B3LYP/6-31G* Optimized Geometries of the Transition States, Ints, and Products Involved in the Dissociation of $M^{2+}(Bpy)_2$ Complexes through PTCF Process.[a]

	$Fe^{2+}(Bpy)_2$ TS_3				$Fe^{2+}(Bpy)_2$ TS_3		
	x	y	z		x	y	z
C	0.400009	0.148139	-0.580236	H	-7.026644	-0.453337	10.692650
N	0.417473	0.019448	0.777222	H	-3.929983	-4.866798	6.013258
C	1.581295	0.373205	-1.288836	H	-4.588220	0.777335	6.717972
C	-0.928533	0.036014	-1.241825	Fe^{2+}	-1.440611	-0.299308	1.523115
C	1.586665	0.112554	1.435195				
C	2.789838	0.467708	-0.598735				
N	-2.000032	-0.184146	-0.408114				
C	-1.149947	0.136720	-2.612086				
H	1.570660	0.475845	-2.367132				
C	2.797371	0.336112	0.788501				
C	-3.198161	-0.291705	-0.922876				
C	-2.450490	0.015262	-3.121899				
H	1.539468	0.002503	2.513958				
H	3.712693	0.642565	-1.142915				
H	-0.328722	0.308615	-3.297296				
C	-3.530728	-0.207509	-2.264021				
H	3.715880	0.403768	1.360851				
H	-2.617226	0.095204	-4.192608				
H	-4.549038	-0.306835	-2.621197				
N	-5.116756	0.570020	7.573756				
N	-3.957737	-0.992660	5.836192				
C	-5.224370	-0.757531	7.833391				
C	-5.640193	1.543353	8.345205				
C	-4.568539	-1.645259	6.844211				
C	-3.342694	-1.714376	4.900808				
C	-5.925080	-1.136229	8.978223				
C	-6.341166	1.200033	9.487334				
C	-4.584761	-3.038733	6.949982				
C	-3.304389	-3.112228	4.919101				
H	-5.478143	2.563984	8.018904				
H	-2.856268	-1.158254	4.095948				
C	-6.481428	-0.157426	9.801707				
C	-3.937263	-3.782623	5.963194				
H	-6.036452	-2.184190	9.227284				
H	-6.766161	1.974928	10.114555				
H	-5.083525	-3.541421	7.770926				
H	-2.791191	-3.658194	4.134199				

Table E.5. (continued) Cartesian Coordinates of the B3LYP/6-31G* Optimized Geometries of the Transition States, Ints, and Products Involved in the Dissociation of $M^{2+}(Bpy)_2$ Complexes through PTCF Process.[a]

	$Fe^{2+}(Bpy)_2$ Int_3				$Fe^{2+}(Bpy)_2$ Int_3		
	x	y	z		x	y	z
C	-9.216099	-0.364026	-0.164684	H	9.665874	-3.378713	1.107591
N	-8.992370	-1.359573	-1.039851	H	6.171740	4.344663	-1.558786
C	-10.523952	0.032416	0.146320	H	10.867384	-1.238678	0.695898
C	-8.024295	0.347476	0.502374	Fe^{2+}	5.461259	-0.926093	0.097523
C	-10.010208	-2.001051	-1.639516				
C	-11.598945	-0.616232	-0.461455				
N	-6.769920	-0.031386	0.205299				
C	-8.255799	1.385625	1.415047				
H	-10.696249	0.825467	0.843660				
C	-11.338063	-1.645844	-1.365660				
C	-5.705360	0.565637	0.767014				
C	-7.169878	2.024895	2.014849				
H	-9.804732	-2.790153	-2.332335				
H	-12.605264	-0.329251	-0.238154				
H	-9.255808	1.685274	1.649766				
C	-5.878771	1.609251	1.686316				
H	-12.144387	-2.159813	-1.845845				
H	-4.718195	0.242054	0.510695				
H	-7.324477	2.819725	2.714309				
H	-5.029174	2.082906	2.132114				
N	5.368444	0.699897	-0.480349				
N	7.109635	-1.436975	0.359483				
C	6.676434	1.032100	-0.423948				
C	4.346404	1.507227	-0.911147				
C	7.708829	-0.208543	0.071311				
C	7.715644	-2.559781	0.703628				
C	6.989467	2.404870	-0.813668				
C	4.579842	2.874821	-1.330925				
C	9.093266	-0.115685	0.202561				
C	9.117396	-2.503132	0.829330				
H	-8.051885	-1.627780	-1.248544				
H	7.170198	-3.463272	0.879959				
C	5.928771	3.342136	-1.274524				
C	9.803687	-1.279469	0.587347				
H	8.003677	2.743029	-0.769784				
H	3.713621	3.417377	-1.647460				
H	9.604241	0.805693	0.015833				

Table E.5. (continued) Cartesian Coordinates of the B3LYP/6-31G* Optimized Geometries of the Transition States, Ints, and Products Involved in the Dissociation of $M^{2+}(Bpy)_2$ Complexes through PTCF Process.[a]

	[Fe(Bpy-H)]$^+$				[Bpy+H]$^+$		
	x	y	z		x	y	z
C	0.137733	0.000165	-0.175366	C	0.075056	0.000000	-0.094818
N	-0.037780	0.000048	1.193372	C	-0.043387	0.000000	1.301499
C	1.408077	0.000124	-0.741224	C	1.091466	0.000000	2.109600
C	-1.135027	0.000276	-0.947472	C	2.356643	0.000000	1.519653
C	1.053829	-0.000089	1.974216	C	1.342182	0.000000	-0.648466
C	2.530876	-0.000022	0.088827	C	3.673568	0.000000	2.195195
N	-2.131225	0.000621	-0.066190	C	3.824630	0.000000	3.583719
C	-1.533432	-0.000115	-2.277208	C	5.121230	0.000000	4.101710
H	1.515736	0.000219	-1.820868	H	5.279670	0.000000	5.175433
C	2.353583	-0.000127	1.469491	C	6.201462	0.000000	3.223130
C	-3.443875	0.000293	-0.154158	C	5.948300	0.000000	1.845623
C	-2.932719	-0.000194	-2.517263	H	-0.796824	0.000000	-0.738058
H	0.881028	-0.000180	3.046514	H	-1.027288	0.000000	1.760100
H	3.527474	-0.000048	-0.341453	H	1.539700	0.000000	-1.713929
H	-0.834578	-0.000424	-3.107383	H	7.222869	0.000000	3.588350
C	-3.897772	-0.000053	-1.500280	H	6.763132	0.000000	1.126787
H	3.196856	-0.000241	2.151184	N	2.416396	0.000000	0.164228
H	-3.267094	-0.000474	-3.551326	N	4.715072	0.000000	1.342159
H	-4.953202	-0.000258	-1.750664	H	3.382897	0.000000	-0.192636
Fe^{2+}	-2.243293	0.000264	1.773341	H	0.995458	0.000000	3.188268
				H	2.969169	0.000000	4.250171

Table E.5. (continued) Cartesian Coordinates of the B3LYP/6-31G* Optimized Geometries of the Transition States, Ints, and Products Involved in the Dissociation of $M^{2+}(Bpy)_2$ Complexes through PTCF Process.[a]

$Co^{2+}(Bpy)_2$ TS_1				$Co^{2+}(Bpy)_2$ TS_1			
	x	y	z		x	y	z
C	0.026989	0.129312	-0.118353	H	5.707371	2.654241	-4.933797
C	-0.015990	0.392268	1.238718	H	3.014597	-0.355452	4.094339
C	1.164213	0.371767	2.028547	H	1.101277	0.579850	3.091813
C	2.374270	0.109109	1.435648	Co^{2+}	4.242235	0.543045	-0.674305
N	2.407776	-0.040691	0.036510				
C	1.257274	-0.048457	-0.805959				
C	3.693791	0.076382	2.094325				
C	3.869707	-0.154926	3.458266				
C	5.160154	-0.148942	3.990063				
H	5.313391	-0.328687	5.049655				
C	6.245503	0.081359	3.144732				
C	6.003148	0.295778	1.791270				
N	4.760891	0.296399	1.270554				
H	-0.891174	0.081733	-0.696144				
H	-0.963177	0.600228	1.729932				
H	2.288791	-1.002931	-0.608865				
H	7.262989	0.092626	3.519817				
H	6.818708	0.478252	1.098213				
C	4.235059	4.465025	-2.476081				
C	4.832686	4.182123	-3.703177				
C	5.243599	2.877655	-3.980952				
C	5.050451	1.878142	-3.027930				
N	4.464743	2.165821	-1.831982				
C	4.068596	3.425296	-1.568501				
C	5.452746	0.460239	-3.226437				
C	6.065908	-0.014606	-4.385614				
C	6.409048	-1.363915	-4.480066				
H	6.884442	-1.740988	-5.380180				
C	6.136308	-2.215960	-3.410947				
C	5.524091	-1.682326	-2.282840				
N	5.187908	-0.381693	-2.188255				
H	3.902451	5.465510	-2.222766				
H	4.979520	4.965455	-4.440193				
H	3.606348	3.595477	-0.600998				
H	6.388425	-3.270057	-3.444908				
H	5.292959	-2.306460	-1.424729				
H	6.277472	0.650576	-5.213666				

Table E.5. (continued) Cartesian Coordinates of the B3LYP/6-31G* Optimized Geometries of the Transition States, Ints, and Products Involved in the Dissociation of $M^{2+}(Bpy)_2$ Complexes through PTCF Process.[a]

$Co^{2+}(Bpy)_2$ Int_1				$Co^{2+}(Bpy)_2$ Int_1			
	x	y	z		x	y	z
C	0.605102	0.568615	-0.210170	H	5.336387	3.279497	-4.523026
C	0.270115	0.635455	1.147357	H	3.421778	-1.056712	4.226992
C	1.203700	0.203615	2.116430	H	1.128651	0.536894	3.146537
C	2.305455	-0.510008	1.682376	Co^{2+}	3.765420	0.358391	-0.818966
N	2.297602	-0.893584	0.362559				
C	1.676735	-0.229913	-0.664028				
C	3.698373	-0.475716	2.177220				
C	4.129238	-0.723132	3.474878				
C	5.482839	-0.554417	3.778123				
H	5.845749	-0.748496	4.782692				
C	6.358558	-0.143014	2.773990				
C	5.858652	0.089648	1.494128				
N	4.558700	-0.066237	1.178265				
H	0.034256	1.141934	-0.934007				
H	-0.623418	1.163279	1.469319				
H	2.929571	-1.658661	0.123855				
H	7.415514	-0.001409	2.972006				
H	6.515205	0.414406	0.692384				
C	3.448386	4.500619	-1.987278				
C	4.183008	4.486451	-3.171991				
C	4.764814	3.293597	-3.603269				
C	4.602785	2.135026	-2.843592				
N	3.884589	2.161366	-1.686630				
C	3.323613	3.313581	-1.274843				
C	5.179334	0.815869	-3.219723				
C	5.907614	0.598306	-4.389280				
C	6.405662	-0.676102	-4.663486				
H	6.970615	-0.853868	-5.573217				
C	6.167726	-1.711844	-3.761528				
C	5.434565	-1.430720	-2.614522				
N	4.951693	-0.203301	-2.344578				
H	2.980802	5.407180	-1.619338				
H	4.304382	5.392060	-3.758123				
H	2.757533	3.271781	-0.349631				
H	6.535684	-2.716373	-3.938687				
H	5.223518	-2.207387	-1.885656				
H	6.086717	1.404454	-5.089945				

Table E.5. (continued) Cartesian Coordinates of the B3LYP/6-31G* Optimized Geometries of the Transition States, Ints, and Products Involved in the Dissociation of $M^{2+}(Bpy)_2$ Complexes through PTCF Process.[a]

	$Co^{2+}(Bpy)_2$ TS_2				$Co^{2+}(Bpy)_2$ TS_2		
	x	y	z		x	y	z
C	0.251822	0.296429	-0.273663	H	6.194315	2.462454	-4.873407
C	0.104126	0.294159	1.119564	H	6.766001	0.435083	-5.154871
C	1.224853	0.176164	1.955718	H	2.966152	-0.341757	4.119104
C	2.493841	0.025913	1.409774	H	1.099436	0.237091	3.030697
N	2.588519	-0.031554	0.033558				
C	1.534903	0.063504	-0.730039				
C	3.770654	-0.013888	2.141715				
C	3.859138	-0.193832	3.522843				
C	5.114991	-0.193608	4.129498				
H	5.201001	-0.331354	5.202782				
C	6.252628	-0.016977	3.341741				
C	6.093962	0.144926	1.969491				
N	4.884550	0.144555	1.374062				
H	-0.588790	0.422319	-0.946727				
H	-0.885239	0.391220	1.558255				
H	3.596834	-0.822525	-0.385838				
H	7.246258	-0.007385	3.776178				
H	6.952971	0.280916	1.319620				
C	4.578649	4.218573	-2.465589				
C	5.243181	3.963909	-3.664514				
C	5.678198	2.667779	-3.943364				
C	5.441788	1.652824	-3.016478				
N	4.792671	1.908724	-1.848319				
C	4.373096	3.160400	-1.586903				
C	5.856013	0.241581	-3.206123				
C	6.516776	-0.232395	-4.338916				
C	6.857709	-1.582924	-4.420276				
H	7.370855	-1.961509	-5.298783				
C	6.530764	-2.435150	-3.366346				
C	5.871840	-1.902006	-2.264707				
N	5.542350	-0.597547	-2.179152				
H	4.225238	5.212014	-2.212443				
H	5.422686	4.762319	-4.377731				
H	3.858430	3.309983	-0.642616				
H	6.775266	-3.491283	-3.392798				
H	5.591598	-2.525846	-1.422664				
Co^{2+}	4.648315	0.295549	-0.630817				

Table E.5. (continued) Cartesian Coordinates of the B3LYP/6-31G* Optimized Geometries of the Transition States, Ints, and Products Involved in the Dissociation of $M^{2+}(Bpy)_2$ Complexes through PTCF Process.[a]

	$Co^{2+}(Bpy)_2$ Int_2				$Co^{2+}(Bpy)_2$ Int_2		
	x	y	z		x	y	z
C	0.001426	-0.161252	0.055197	H	-1.255848	-4.591540	3.446844
N	0.088897	0.045239	1.395704	H	-4.862188	2.312147	6.738224
C	1.145901	-0.428754	-0.697921	H	-2.679822	-4.369908	5.505521
C	-1.367827	-0.073458	-0.491617	Co^{2+}	-1.602060	0.454795	2.324224
C	1.288099	0.010644	2.006409				
C	2.387297	-0.474466	-0.065591				
N	-2.326245	0.154949	0.443142				
C	-1.696497	-0.206429	-1.840572				
H	1.073986	-0.598383	-1.765707				
C	2.461842	-0.252615	1.310066				
C	-3.613774	0.255752	0.068028				
C	-3.032892	-0.100220	-2.227201				
H	1.297077	0.205767	3.073927				
H	3.284603	-0.676130	-0.642124				
H	-0.929278	-0.382856	-2.585194				
C	-4.010501	0.132751	-1.259422				
H	3.408882	-0.271815	1.838050				
H	-4.336698	0.440471	0.856681				
H	-3.304673	-0.196815	-3.273711				
H	-5.058726	0.220852	-1.522958				
N	-2.720825	1.151129	3.752525				
N	-1.867060	-1.281243	3.329427				
C	-3.117248	0.224404	4.697142				
C	-3.089404	2.401413	3.906557				
C	-2.647075	-1.149514	4.440059				
C	-1.391237	-2.493965	2.996604				
C	-3.890009	0.642617	5.773415				
C	-3.857034	2.921214	4.929826				
C	-2.951239	-2.248705	5.241352				
C	-1.659137	-3.631901	3.750946				
H	-1.052160	1.811281	2.097159				
H	-0.778659	-2.542129	2.102745				
C	-4.260616	1.990380	5.892509				
C	-2.450784	-3.504129	4.891967				
H	-4.209360	-0.066958	6.527826				
H	-4.118715	3.971899	4.983097				
H	-3.569291	-2.137145	6.124589				

Table E.5. (continued) Cartesian Coordinates of the B3LYP/6-31G* Optimized Geometries of the Transition States, Ints, and Products Involved in the Dissociation of $M^{2+}(Bpy)_2$ Complexes through PTCF Process.[a]

$Co^{2+}(Bpy)_2$ TS_3				$Co^{2+}(Bpy)_2$ TS_3			
	x	y	z		x	y	z
C	-0.035839	0.070893	-0.010694	H	-1.391154	-4.904979	3.839335
N	-0.115679	0.112198	1.347316	H	-4.923373	2.256377	6.602334
C	1.188565	0.174442	-0.676273	H	-2.611757	-4.437163	5.987278
C	-1.329601	-0.066474	-0.694143	Co^{2+}	-1.969376	0.000104	2.133315
C	1.018821	0.249911	2.059948				
C	2.356407	0.313332	0.070226				
N	-2.429582	0.049511	0.122463				
C	-1.510907	-0.312032	-2.055144				
H	1.234464	0.159814	-1.758950				
C	2.271052	0.350654	1.462615				
C	-3.691130	-0.047651	-0.388361				
C	-2.796548	-0.435954	-2.576675				
H	0.910829	0.279832	3.139648				
H	3.316552	0.397210	-0.428747				
H	-0.649736	-0.422612	-2.703470				
C	-3.903814	-0.306728	-1.727392				
H	3.155778	0.461280	2.080120				
H	-4.502784	0.097840	0.316132				
H	-2.936430	-0.626982	-3.635815				
H	-4.917646	-0.398110	-2.101357				
N	-2.958103	0.848503	3.617895				
N	-2.119561	-1.649247	3.352466				
C	-3.262642	0.009020	4.665529				
C	-3.347226	2.097533	3.655582				
C	-2.780029	-1.383218	4.515044				
C	-1.636570	-2.886420	3.139471				
C	-3.975391	0.517034	5.745648				
C	-4.057267	2.701765	4.679118				
C	-2.966124	-2.373611	5.479430				
C	-1.793579	-3.921563	4.056084				
H	-2.298703	1.050668	1.006848				
H	-1.109347	-3.042839	2.203510				
C	-4.369579	1.863749	5.753858				
C	-2.470769	-3.657092	5.245646				
H	-4.232975	-0.117134	6.585790				
H	-4.348491	3.745345	4.649035				
H	-3.488069	-2.155715	6.403746				

Table E.5. (continued) Cartesian Coordinates of the B3LYP/6-31G* Optimized Geometries of the Transition States, Ints, and Products Involved in the Dissociation of $M^{2+}(Bpy)_2$ Complexes through PTCF Process.[a]

$Co^{2+}(Bpy)_2$ Int_3				$Co^{2+}(Bpy)_2$ Int_3			
	x	y	z		x	y	z
C	2.925088	-0.426179	0.504499	H	-4.916855	2.245262	2.649439
N	1.780815	-1.134604	0.699599	H	-4.668270	-2.997772	-1.901180
C	4.122747	-0.793860	1.117073	H	-1.055836	1.218818	-0.065145
C	2.786822	0.746243	-0.390681	Co^{2+}	0.242998	-0.381687	-0.349668
C	1.814672	-2.213399	1.499380				
C	4.147366	-1.916432	1.945378				
N	1.509400	0.982605	-0.835008				
C	3.808553	1.590775	-0.810360				
H	5.026974	-0.218007	0.957620				
C	2.973546	-2.640756	2.142830				
C	1.268169	1.986300	-1.627603				
C	3.519945	2.660028	-1.671335				
H	0.878216	-2.747923	1.624328				
H	5.071878	-2.216729	2.428450				
H	4.830011	1.426362	-0.487367				
C	2.210995	2.885623	-2.106744				
H	2.949013	-3.519128	2.778407				
H	4.321367	3.314437	-2.003442				
H	1.954035	3.700963	-2.772936				
N	-1.886538	1.460915	0.494057				
N	-1.506499	-1.063180	-0.713835				
C	-2.887183	0.541624	0.519357				
C	-1.906206	2.631819	1.168067				
C	-2.751245	-0.670998	-0.321802				
C	-1.411919	-2.138501	-1.531456				
C	-3.996324	0.832289	1.317285				
C	-2.999336	2.950695	1.951372				
C	-3.898487	-1.355239	-0.737354				
C	-2.510736	-2.860559	-1.978490				
H	-1.038670	3.270331	1.048297				
H	-0.410742	-2.430531	-1.831667				
C	-4.052230	2.030917	2.028672				
C	-3.782485	-2.465232	-1.570485				
H	-4.805462	0.117484	1.399835				
H	-3.022642	3.889464	2.492919				
H	-4.880668	-1.006027	-0.442367				
H	-2.364069	-3.712544	-2.633463				

Table E.5. (continued) Cartesian Coordinates of the B3LYP/6-31G* Optimized Geometries of the Transition States, Ints, and Products Involved in the Dissociation of $M^{2+}(Bpy)_2$ Complexes through PTCF Process.[a]

$Co^{2+}(Bpy)_2$ TS_4				$Co^{2+}(Bpy)_2$ TS_4			
	x	y	z		x	y	z
C	0.854855	-0.427436	-0.405630	H	-5.477955	6.327865	4.498802
N	1.747299	-0.071219	0.573957	H	-6.754583	0.439911	8.331185
C	1.288120	-1.107647	-1.541937	H	-3.441387	1.992839	3.899789
C	-0.555904	-0.039213	-0.162023	Co^{2+}	0.771001	0.888297	2.039585
C	3.052329	-0.378571	0.430004				
C	2.638856	-1.427973	-1.680093				
N	-0.733710	0.694256	0.977107				
C	-1.674808	-0.338011	-0.918268				
H	0.580005	-1.381986	-2.315556				
C	3.538360	-1.059231	-0.679156				
C	-1.874988	1.145485	1.494748				
C	-2.924511	0.114189	-0.449752				
H	3.715398	-0.068527	1.231532				
H	2.983579	-1.957955	-2.562573				
H	-1.609257	-0.913428	-1.835167				
C	-3.034133	0.825402	0.742532				
H	4.595678	-1.288258	-0.752442				
H	-3.813777	-0.108955	-1.033455				
H	-4.015905	1.138033	1.085308				
N	-3.853829	2.931246	3.996598				
N	-4.271851	0.758369	5.367329				
C	-4.758274	3.048359	5.002155				
C	-3.498195	3.933952	3.169541				
C	-5.000196	1.814108	5.780009				
C	-4.428531	-0.401472	6.004534				
C	-5.354863	4.297460	5.187904				
C	-4.072352	5.181546	3.327185				
C	-5.906031	1.748937	6.841957				
C	-5.311324	-0.566712	7.079042				
H	-2.765794	3.676424	2.412709				
H	-3.829174	-1.234462	5.646444				
C	-5.011629	5.358404	4.352518				
C	-6.059804	0.528364	7.502079				
H	-6.081858	4.439114	5.977860				
H	-3.795674	5.994994	2.666810				
H	-6.481323	2.613190	7.155005				
H	-5.403508	-1.532295	7.564999				

Table E.5. (continued) Cartesian Coordinates of the B3LYP/6-31G* Optimized Geometries of the Transition States, Ints, and Products Involved in the Dissociation of $M^{2+}(Bpy)_2$ Complexes through PTCF Process.[a]

$Co^{2+}(Bpy)_2$ Int_4				$Co^{2+}(Bpy)_2$ Int_4			
	x	y	z		x	y	z
C	-9.157155	-0.261795	-0.038785	H	9.362558	-3.346810	1.283423
N	-8.771381	-1.329710	-0.781238	H	6.526839	4.102081	-1.639768
C	-10.525628	-0.074982	0.159215	H	10.679985	-1.223628	1.022752
C	-8.047309	0.577283	0.470551	Co^{2+}	4.942170	-1.090224	-0.005989
C	-9.617111	-2.217832	-1.339184				
C	-11.431876	-0.972152	-0.403620				
N	-6.823127	0.133424	0.124464				
C	-8.250654	1.728153	1.235234				
H	-10.879001	0.762095	0.748553				
C	-10.979531	-2.058526	-1.163828				
C	-5.759131	0.823931	0.531497				
C	-7.128474	2.443341	1.658108				
H	-9.169758	-3.024456	-1.908012				
H	-12.496559	-0.826370	-0.249518				
H	-9.246360	2.068667	1.497463				
C	-5.862390	1.986589	1.302879				
H	-11.669409	-2.765601	-1.609205				
H	-4.787317	0.435844	0.234228				
H	-7.247927	3.342659	2.253910				
H	-4.965372	2.511710	1.610291				
N	5.451471	0.685831	-0.440522				
N	6.881745	-1.278880	0.315219				
C	6.777923	0.989784	-0.348800				
C	4.539971	1.476729	-0.924520				
C	7.589353	-0.130778	0.152096				
C	7.520254	-2.398068	0.713641				
C	7.181822	2.245497	-0.774558				
C	4.858867	2.767052	-1.365264				
C	8.959894	-0.084039	0.406452				
C	8.885411	-2.424394	0.971702				
H	-7.749116	-1.404490	-0.874452				
H	6.912237	-3.290215	0.828584				
C	6.210892	3.123149	-1.287562				
C	9.613511	-1.242418	0.821131				
H	8.223114	2.547425	-0.733338				
H	4.120130	3.447542	-1.770885				
H	9.504562	0.845805	0.283909				

Table E.5. (continued) Cartesian Coordinates of the B3LYP/6-31G* Optimized Geometries of the Transition States, Ints, and Products Involved in the Dissociation of $M^{2+}(Bpy)_2$ Complexes through PTCF Process.[a]

	$[Co(Bpy-H)]^+$		
	x	y	z
C	0.018848	0.000000	-0.105956
N	0.060144	0.000000	1.245447
C	1.235427	0.000000	-0.767351
C	-1.380860	0.000000	-0.586152
C	1.095759	0.000000	2.053434
C	2.406542	0.000000	0.024861
N	-2.328691	0.000000	0.409269
C	-1.752421	0.000000	-1.928931
H	1.305394	0.000000	-1.850094
C	2.361734	0.000000	1.420057
C	-3.630095	0.000000	0.066937
C	-3.104568	0.000000	-2.268176
H	3.370002	0.000000	-0.478139
H	-0.989198	0.000000	-2.699520
C	-4.062438	0.000000	-1.254772
H	3.278958	0.000000	1.999179
H	-4.344783	0.000000	0.884629
H	-3.404559	0.000000	-3.311408
H	-5.123895	0.000000	-1.475882
Co^{2+}	-1.461890	0.000000	2.278133

Table E.5. (continued) Cartesian Coordinates of the B3LYP/6-31G* Optimized Geometries of the Transition States, Ints, and Products Involved in the Dissociation of $M^{2+}(Bpy)_2$ Complexes through PTCF Process.[a]

$Ni^{2+}(Bpy)_2$ TS_1				$Ni^{2+}(Bpy)_2$ TS_1			
	x	y	z		x	y	z
C	-0.035745	-0.077358	0.064378	H	-2.305560	-5.254333	2.667361
N	0.002978	-0.168805	1.419824	H	-4.648997	1.915000	6.680644
C	1.140467	-0.114807	-0.684130	H	-3.805848	-5.090294	4.675642
C	-1.396091	0.055200	-0.502706	Ni^{2+}	-1.737423	-0.053541	2.296318
C	1.182984	-0.293972	2.054073				
C	2.364536	-0.244634	-0.027703				
N	-2.391865	0.049139	0.420905				
C	-1.682076	0.173941	-1.862714				
H	1.109978	-0.043391	-1.764882				
C	2.389324	-0.337795	1.363986				
C	-3.671097	0.159220	0.026952				
C	-3.011031	0.288750	-2.271409				
H	1.150799	-0.355917	3.137517				
H	3.287202	-0.270984	-0.598926				
H	-0.886076	0.180639	-2.597920				
C	-4.024600	0.279220	-1.313625				
H	3.320808	-0.438067	1.910047				
H	-4.423198	0.150098	0.809541				
H	-3.248813	0.385348	-3.326113				
H	-5.068959	0.365931	-1.592486				
N	-2.801333	0.466443	3.728407				
N	-2.360678	-1.903605	3.010876				
C	-3.416199	-0.417040	4.551594				
C	-2.788811	1.768342	3.911450				
C	-3.179684	-1.806828	4.106028				
C	-2.072131	-3.120134	2.526802				
C	-4.106552	0.108873	5.639513				
C	-3.442837	2.387087	4.963872				
C	-3.710786	-2.935146	4.721620				
C	-2.569951	-4.293507	3.095272				
H	-1.626324	1.517702	2.436598				
H	-1.421776	-3.152811	1.658355				
C	-4.114514	1.503288	5.828509				
C	-3.400895	-4.198105	4.208421				
H	-4.625765	-0.533134	6.342896				
H	-3.437123	3.458990	5.121942				
H	-4.356767	-2.835687	5.587356				

Table E.5. (continued) Cartesian Coordinates of the B3LYP/6-31G* Optimized Geometries of the Transition States, Ints, and Products Involved in the Dissociation of $M^{2+}(Bpy)_2$ Complexes through PTCF Process.[a]

$Ni^{2+}(Bpy)_2$ Int_1				$Ni^{2+}(Bpy)_2$ Int_1			
	x	y	z		x	y	z
C	-0.025660	-0.172065	0.021462	H	-1.521316	-4.846979	2.857605
N	0.025168	-0.067905	1.375614	H	-5.476571	1.795534	6.289143
C	1.143236	-0.371389	-0.714160	H	-3.185023	-4.796169	4.740535
C	-1.382341	-0.053043	-0.554966	Ni^{2+}	-1.667548	0.264245	2.232043
C	1.203357	-0.141371	2.021741				
C	2.365989	-0.452743	-0.048669				
N	-2.365065	0.137727	0.361001				
C	-1.675700	-0.119625	-1.917310				
H	1.106088	-0.457544	-1.793624				
C	2.399574	-0.337445	1.341736				
C	-3.638178	0.272023	-0.039338				
C	-2.999899	0.016697	-2.334483				
H	1.176088	-0.036810	3.101827				
H	3.282106	-0.600551	-0.611859				
H	-0.889289	-0.270301	-2.647510				
C	-3.999456	0.214821	-1.382677				
H	3.331339	-0.390338	1.893974				
H	-4.378771	0.430879	0.737793				
H	-3.244370	-0.028581	-3.391068				
H	-5.039484	0.327809	-1.668397				
N	-2.951583	0.860131	3.534191				
N	-2.091787	-1.530959	2.983339				
C	-3.485490	-0.138052	4.323597				
C	-3.327141	2.099519	3.747152				
C	-2.999779	-1.491337	3.998117				
C	-1.588391	-2.714288	2.596231				
C	-4.396598	0.197897	5.317416				
C	-4.226011	2.541166	4.697998				
C	-3.408285	-2.654684	4.648299				
C	-1.953988	-3.913768	3.201027				
H	-1.346335	1.635381	1.949164				
H	-0.872659	-2.691438	1.781476				
C	-4.767349	1.537159	5.507556				
C	-2.877705	-3.880832	4.244501				
H	-4.824561	-0.570257	5.951078				
H	-4.483303	3.588232	4.810831				
H	-4.128508	-2.613302	5.457179				

Table E.5. (continued) Cartesian Coordinates of the B3LYP/6-31G* Optimized Geometries of the Transition States, Ints, and Products Involved in the Dissociation of $M^{2+}(Bpy)_2$ Complexes through PTCF Process.[a]

$Ni^{2+}(Bpy)_2$ TS_2				$Ni^{2+}(Bpy)_2$ TS_2			
	x	y	z		x	y	z
C	-0.001628	-0.005458	0.002766	H	-0.845595	-4.748697	3.915577
N	-0.003020	0.003940	1.362483	H	-5.413878	1.933729	6.329328
C	1.188031	-0.012379	-0.726716	H	-2.376453	-4.486589	5.892827
C	-1.343706	0.016809	-0.606070	Ni^{2+}	-1.771029	0.060222	2.212136
C	1.171165	0.002484	2.018410				
C	2.402122	-0.012209	-0.040283				
N	-2.368353	0.252817	0.272368				
C	-1.633531	-0.198893	-1.952015				
H	1.175586	-0.004037	-1.810490				
C	2.394898	-0.003342	1.354581				
C	-3.658046	0.313882	-0.150241				
C	-2.956431	-0.160450	-2.391014				
H	1.118603	0.007432	3.102499				
H	3.338506	-0.012620	-0.589103				
H	-0.834104	-0.410403	-2.652412				
C	-3.984521	0.096772	-1.476109				
H	3.317581	0.002369	1.924620				
H	-4.397006	0.544156	0.608719				
H	-3.184233	-0.326399	-3.439198				
H	-5.022753	0.134872	-1.786932				
N	-3.057199	0.757775	3.519055				
N	-1.868323	-1.580441	3.389796				
C	-3.356245	-0.106269	4.548364				
C	-3.589303	1.955063	3.528821				
C	-2.699866	-1.428988	4.456224				
C	-1.228814	-2.749420	3.220759				
C	-4.208022	0.315210	5.563795				
C	-4.448979	2.475262	4.478176				
C	-2.898274	-2.461445	5.372722				
C	-1.381502	-3.822964	4.094276				
H	-2.051896	1.144411	1.205376				
H	-0.574193	-2.818592	2.357708				
C	-4.754015	1.605859	5.530740				
C	-2.231054	-3.673209	5.188892				
H	-4.453249	-0.345297	6.387153				
H	-4.848239	3.480992	4.415730				
H	-3.562935	-2.332195	6.218862				

Table E.5. (continued) Cartesian Coordinates of the B3LYP/6-31G* Optimized Geometries of the Transition States, Ints, and Products Involved in the Dissociation of $M^{2+}(Bpy)_2$ Complexes through PTCF Process.[a]

	$Ni^{2+}(Bpy)_2$ Int_2				$Ni^{2+}(Bpy)_2$ Int_2		
	x	y	z		x	y	z
C	2.888319	0.543544	0.520864	H	-2.948547	-3.514808	2.782740
N	1.887772	1.462941	0.495196	H	-4.319323	3.315733	-2.003848
C	3.997392	0.834310	1.318854	H	-5.071255	-2.212559	2.431273
C	2.752415	-0.669315	-0.319948	Ni^{2+}	-0.241751	-0.380237	-0.347420
C	1.907503	2.634028	1.168907				
C	4.053353	2.033119	2.029929				
N	1.507666	-1.061813	-0.711636				
C	3.899705	-1.353485	-0.735506				
H	4.806424	0.119418	1.401701				
C	3.000565	2.952989	1.952264				
C	1.413115	-2.137410	-1.528903				
C	3.783733	-2.463753	-1.568271				
H	1.040051	3.272604	1.048864				
H	4.917925	2.247527	2.650748				
H	4.881876	-1.003997	-0.440814				
C	2.511970	-2.859425	-1.975904				
H	3.023907	3.891898	2.493567				
H	0.411929	-2.429703	-1.828826				
H	4.669543	-2.996246	-1.898976				
H	2.365327	-3.711644	-2.630580				
N	-1.507813	0.984103	-0.833794				
N	-1.779676	-1.131793	0.702583				
C	-2.785303	0.748321	-0.389330				
C	-1.266403	1.987240	-1.627046				
C	-2.923854	-0.423446	0.506665				
C	-1.813791	-2.210024	1.503112				
C	-3.806857	1.592776	-0.809594				
C	-2.209027	2.886426	-2.106816				
C	-4.121695	-0.790646	1.119176				
C	-2.972863	-2.636880	2.146541				
H	1.057110	1.220921	-0.064068				
H	-0.877386	-2.744477	1.628724				
C	-3.518037	2.661390	-1.671286				
C	-4.146592	-1.912640	1.948256				
H	-4.828347	1.428795	-0.486480				
H	-1.951879	3.701262	-2.773554				
H	-5.025864	-0.214883	0.959070				

Table E.5. (continued) Cartesian Coordinates of the B3LYP/6-31G* Optimized Geometries of the Transition States, Ints, and Products Involved in the Dissociation of $M^{2+}(Bpy)_2$ Complexes through PTCF Process.[a]

$Ni^{2+}(Bpy)_2$ TS_3				$Ni^{2+}(Bpy)_2$ TS_3			
	x	y	z		x	y	z
C	0.531034	-1.195522	-0.464938	H	-6.463858	5.844301	8.326062
N	0.716847	-0.258634	0.512719	H	-4.631772	-0.733132	6.249340
C	1.527684	-2.122357	-0.764662	H	-3.805467	4.653307	4.482829
C	-0.779561	-1.142571	-1.162714	Ni^{2+}	-0.804943	0.847403	0.602996
C	1.880661	-0.234519	1.186721				
C	2.731900	-2.090541	-0.060359				
N	-1.643666	-0.155948	-0.724992				
C	-1.173119	-1.990602	-2.191261				
H	1.377188	-2.863880	-1.540043				
C	2.913873	-1.130752	0.932676				
C	-2.816805	-0.059347	-1.305605				
C	-2.435663	-1.843913	-2.780692				
H	1.978820	0.531560	1.949091				
H	3.514581	-2.806759	-0.289188				
H	-0.508197	-2.767787	-2.548595				
C	-3.304516	-0.845697	-2.333018				
H	3.834987	-1.069477	1.501525				
H	-2.736994	-2.506656	-3.586885				
H	-4.289188	-0.694586	-2.760029				
N	-4.366270	4.960027	5.286254				
N	-3.649816	2.579709	4.487766				
C	-4.810048	3.936343	6.058616				
C	-4.619675	6.262074	5.525374				
C	-4.407898	2.584715	5.601698				
C	-3.246266	1.404487	4.007006				
C	-5.580529	4.258137	7.175657				
C	-5.381223	6.613665	6.625393				
C	-4.785718	1.416982	6.270239				
C	-3.572814	0.182919	4.604172				
H	-4.202501	6.976443	4.825296				
H	-2.634569	1.430621	3.103701				
C	-5.864083	5.594928	7.456170				
C	-4.356191	0.193405	5.755831				
H	-5.956327	3.475066	7.822315				
H	-5.590874	7.657716	6.826681				
H	-5.396998	1.445871	7.165195				
H	-3.221674	-0.749607	4.174837				

Table E.5. (continued) Cartesian Coordinates of the B3LYP/6-31G* Optimized Geometries of the Transition States, Ints, and Products Involved in the Dissociation of $M^{2+}(Bpy)_2$ Complexes through PTCF Process.[a]

$Ni^{2+}(Bpy)_2$ Int_3				$Ni^{2+}(Bpy)_2$ Int_3			
	x	y	z		x	y	z
C	-8.930450	-0.266223	-0.014479	H	9.353288	-3.137938	1.377478
N	-8.543950	-1.363637	-0.712536	H	6.243783	4.135538	-1.529510
C	-10.298623	-0.072160	0.177666	H	10.452328	-0.890936	1.110798
C	-7.819553	0.594357	0.452960	Ni^{2+}	4.850130	-1.167629	-0.070400
C	-9.389251	-2.275355	-1.230775				
C	-11.204568	-0.995485	-0.342703				
N	-6.600161	0.153502	0.090466				
C	-8.018643	1.755887	1.202497				
H	-10.654061	0.792141	0.724693				
C	-10.751733	-2.113052	-1.055545				
C	-5.531409	0.860951	0.459044				
C	-6.894433	2.490261	1.581207				
H	-8.942695	-3.104529	-1.766927				
H	-12.269134	-0.843656	-0.193732				
H	-9.010151	2.087907	1.489832				
C	-5.630724	2.041000	1.204092				
H	-11.440538	-2.841453	-1.466909				
H	-4.562704	0.460037	0.154852				
H	-7.008221	3.399780	2.162470				
H	-4.743816	2.598032	1.482783				
N	5.068324	0.642024	-0.475317				
N	6.704973	-1.362672	0.284373				
C	6.405307	0.950798	-0.373644				
C	4.224769	1.524014	-0.924482				
C	7.289325	-0.139138	0.131940				
C	7.445402	-2.396865	0.722048				
C	6.833374	2.218126	-0.741384				
C	4.555493	2.813495	-1.323931				
C	8.639717	0.048159	0.424000				
C	8.796958	-2.274809	1.029142				
H	-7.522935	-1.431665	-0.821452				
H	6.932235	-3.347215	0.819052				
C	5.905284	3.149471	-1.223204				
C	9.401046	-1.028608	0.878498				
H	7.880840	2.488296	-0.681108				
H	3.821486	3.512956	-1.706887				
H	9.098630	1.022858	0.309166				

Table E.5. (continued) Cartesian Coordinates of the B3LYP/6-31G* Optimized Geometries of the Transition States, Ints, and Products Involved in the Dissociation of $M^{2+}(Bpy)_2$ Complexes through PTCF Process.[a]

	$[Ni(Bpy-H)]^+$		
	x	y	z
C	0.008022	0.000000	0.001721
N	-0.003756	-0.000035	1.368215
C	1.210627	0.000031	-0.702346
C	-1.327913	0.000007	-0.646890
C	1.163716	-0.000038	2.035396
C	2.417496	0.000028	-0.002491
N	-2.402840	-0.000095	0.221226
C	-1.553985	0.000105	-2.018092
H	1.215050	0.000052	-1.785746
C	2.396248	-0.000005	1.390189
C	-3.611978	-0.000096	-0.287413
C	-2.864276	0.000098	-2.514250
H	1.097647	-0.000064	3.118624
H	3.358924	0.000050	-0.542438
H	-0.722359	0.000192	-2.712620
C	-3.945282	-0.000006	-1.630219
H	3.310615	-0.000008	1.972949
H	-3.036634	0.000175	-3.586667
H	-4.975314	-0.000015	-1.967469
Ni^{2+}	-1.784199	-0.000144	1.973201

Table E.5. (continued) Cartesian Coordinates of the B3LYP/6-31G* Optimized Geometries of the Transition States, Ints, and Products Involved in the Dissociation of $M^{2+}(Bpy)_2$ Complexes through PTCF Process.[a]

$Cu^{2+}(Bpy)_2$ TS_1				$Cu^{2+}(Bpy)_2$ TS_1			
	x	y	z		x	y	z
C	-0.114365	-0.093026	0.052403	H	-2.096751	-5.289408	2.885215
N	-0.089270	-0.224214	1.404269	H	-4.648879	1.916462	6.685979
C	1.075807	-0.155205	-0.676462	H	-3.626800	-5.114469	4.869646
C	-1.453364	0.110244	-0.562099	Cu^{2+}	-1.820670	-0.131975	2.303806
C	1.078703	-0.406186	2.051837				
C	2.285669	-0.343533	-0.010793				
N	-2.495592	0.107322	0.302244				
C	-1.650802	0.294838	-1.932326				
H	1.065873	-0.058822	-1.755060				
C	2.291357	-0.472862	1.378540				
C	-3.740280	0.286640	-0.164449				
C	-2.947365	0.478857	-2.413615				
H	1.028050	-0.496271	3.131944				
H	3.213252	-0.387155	-0.573051				
H	-0.816484	0.301742	-2.623164				
C	-4.014312	0.474052	-1.517223				
H	3.211569	-0.618046	1.933553				
H	-4.538948	0.280356	0.571441				
H	-3.116824	0.626365	-3.475590				
H	-5.036543	0.614080	-1.851329				
N	-2.869488	0.442970	3.701991				
N	-2.294383	-1.936620	3.105963				
C	-3.419310	-0.437944	4.575271				
C	-2.879901	1.745195	3.861232				
C	-3.129734	-1.831140	4.187078				
C	-1.949920	-3.155301	2.666019				
C	-4.088528	0.101194	5.671256				
C	-3.495764	2.374410	4.928842				
C	-3.621445	-2.957519	4.838263				
C	-2.405525	-4.325314	3.274268				
H	-1.690010	1.409375	2.403380				
H	-1.287118	-3.190935	1.807431				
C	-4.127120	1.496952	5.829817				
C	-3.253458	-4.223553	4.374514				
H	-4.562037	-0.539109	6.407803				
H	-3.497931	3.449169	5.066356				
H	-4.282574	-2.853429	5.691892				

Table E.5. (continued) Cartesian Coordinates of the B3LYP/6-31G* Optimized Geometries of the Transition States, Ints, and Products Involved in the Dissociation of $M^{2+}(Bpy)_2$ Complexes through PTCF Process.[a]

	$Cu^{2+}(Bpy)_2$ Int_1				$Cu^{2+}(Bpy)_2$ Int_1		
	x	y	z		x	y	z
C	0.014643	-0.101052	0.041003	H	-1.616837	-4.856882	2.823218
N	-0.016838	0.085970	1.383403	H	-4.980719	1.869591	6.699399
C	1.240066	-0.247096	-0.614805	H	-2.992106	-4.767858	4.925023
C	-1.304444	-0.134820	-0.646112	Cu^{2+}	-1.832794	0.207464	2.176577
C	1.124140	0.155979	2.094689				
C	2.425041	-0.184593	0.116213				
N	-2.384223	-0.025584	0.161402				
C	-1.450390	-0.262567	-2.029590				
H	1.276126	-0.406832	-1.685389				
C	2.370282	0.020697	1.495350				
C	-3.616805	-0.030067	-0.369098				
C	-2.732100	-0.272825	-2.579797				
H	1.025427	0.326397	3.161538				
H	3.380207	-0.290588	-0.388607				
H	-0.586612	-0.345188	-2.677987				
C	-3.837212	-0.155742	-1.738321				
H	3.269557	0.081659	2.098373				
H	-4.445553	0.069755	0.325025				
H	-2.861570	-0.366019	-3.653500				
H	-4.849456	-0.156052	-2.127671				
N	-2.874104	0.875559	3.634563				
N	-2.133254	-1.537094	2.993825				
C	-3.301812	-0.110250	4.500835				
C	-3.201898	2.119035	3.879909				
C	-2.883465	-1.472403	4.128803				
C	-1.700243	-2.727270	2.548513				
C	-4.062222	0.249309	5.607238				
C	-3.949971	2.583042	4.944640				
C	-3.204915	-2.625513	4.843173				
C	-1.986215	-3.915427	3.214562				
H	-1.591842	1.547859	1.774875				
H	-1.110628	-2.717549	1.638013				
C	-4.387120	1.594492	5.831951				
C	-2.750070	-3.860824	4.380018				
H	-4.407534	-0.507704	6.301895				
H	-4.176600	3.634669	5.078722				
H	-3.801029	-2.568380	5.746554				

Table E.5. (continued) Cartesian Coordinates of the B3LYP/6-31G* Optimized Geometries of the Transition States, Ints, and Products Involved in the Dissociation of $M^{2+}(Bpy)_2$ Complexes through PTCF Process.[a]

$Cu^{2+}(Bpy)_2$ TS_2				$Cu^{2+}(Bpy)_2$ TS_2			
	x	y	z		x	y	z
C	-0.118367	-0.176308	-0.084335	H	-2.713448	-5.807613	0.622517
N	-0.118712	-0.472228	1.238486	H	-4.251495	-0.844213	7.288835
C	1.093400	-0.096089	-0.774227	H	-3.731688	-6.392198	2.845427
C	-1.452255	0.036912	-0.703260	Cu^{2+}	-2.055921	-0.884228	1.956589
C	1.031338	-0.653141	1.915637				
C	2.290292	-0.300552	-0.088119				
N	-2.514527	-0.245209	0.088105				
C	-1.627284	0.509607	-2.005389				
H	1.109869	0.118034	-1.836001				
C	2.263478	-0.583307	1.279324				
C	-3.760075	-0.066847	-0.384743				
C	-2.920559	0.689394	-2.495880				
H	0.943791	-0.851566	2.978630				
H	3.235712	-0.233870	-0.617435				
H	-0.775412	0.748296	-2.630630				
C	-4.007585	0.395193	-1.674315				
H	3.174814	-0.741277	1.845562				
H	-4.575051	-0.302630	0.291937				
H	-3.073070	1.060502	-3.504471				
H	-5.028620	0.525474	-2.015961				
N	-2.748145	-0.750254	3.746699				
N	-2.573234	-2.783204	2.096139				
C	-3.232724	-1.944915	4.235240				
C	-2.814690	0.315371	4.501830				
C	-3.127772	-3.084768	3.302547				
C	-2.440188	-3.746729	1.169840				
C	-3.775575	-1.978805	5.514949				
C	-3.333071	0.393983	5.780895				
C	-3.552550	-4.380437	3.595226				
C	-2.841657	-5.059854	1.397345				
H	-1.368973	0.361231	2.054034				
H	-2.000751	-3.448680	0.223351				
C	-3.825937	-0.811568	6.289662				
C	-3.406257	-5.378943	2.631600				
H	-4.165491	-2.905134	5.920356				
H	-3.353575	1.320309	6.343454				
H	-3.992362	-4.615370	4.557411				

Table E.5. (continued) Cartesian Coordinates of the B3LYP/6-31G* Optimized Geometries of the Transition States, Ints, and Products Involved in the Dissociation of $M^{2+}(Bpy)_2$ Complexes through PTCF Process.[a]

	$Cu^{2+}(Bpy)_2$ Int_2				$Cu^{2+}(Bpy)_2$ Int_2		
	x	y	z		x	y	z
C	0.094395	0.240335	0.038730	H	-3.207454	-6.174344	1.937415
N	0.074470	0.332198	1.394536	H	-3.704936	0.406778	7.218333
C	1.341359	0.325578	-0.585119	H	-3.796596	-6.131181	4.382066
C	-1.195636	0.098036	-0.676836	Cu^{2+}	-2.498931	-1.033769	1.786858
C	1.168897	0.518166	2.164840				
C	2.493978	0.516517	0.177056				
N	-2.272824	-0.389924	0.000242				
C	-1.295586	0.512754	-2.009153				
H	1.416230	0.223396	-1.660489				
C	2.412477	0.622423	1.570863				
C	-3.455107	-0.454227	-0.656909				
C	-2.517100	0.430678	-2.673086				
H	1.000091	0.578457	3.233732				
H	3.458793	0.577021	-0.317254				
H	-0.435139	0.930084	-2.518185				
C	-3.620161	-0.059645	-1.978144				
H	3.294348	0.774000	2.182771				
H	-4.298662	-0.844333	-0.096557				
H	-2.603457	0.755459	-3.704897				
H	-4.596313	-0.136995	-2.444540				
N	-2.741054	-0.485417	3.614859				
N	-2.882547	-2.867129	2.510863				
C	-3.160713	-1.490162	4.451217				
C	-2.665994	0.738805	4.050124				
C	-3.201355	-2.835729	3.832475				
C	-2.892173	-4.047474	1.869548				
C	-3.508909	-1.170947	5.758948				
C	-2.990087	1.165080	5.330947				
C	-3.532167	-3.997315	4.529690				
C	-3.213511	-5.247116	2.499830				
H	-0.844875	0.227755	1.847578				
H	-2.632332	-4.023459	0.815898				
C	-3.425585	0.158809	6.197894				
C	-3.539896	-5.218142	3.854125				
H	-3.854571	-1.937899	6.442349				
H	-2.915725	2.202050	5.637191				
H	-3.779532	-3.959857	5.584234				

Table E.5. (continued) Cartesian Coordinates of the B3LYP/6-31G* Optimized Geometries of the Transition States, Ints, and Products Involved in the Dissociation of $M^{2+}(Bpy)_2$ Complexes through PTCF Process.[a]

	$Cu^{2+}(Bpy)_2$ TS_3				$Cu^{2+}(Bpy)_2$ TS_3		
	x	y	z		x	y	z
C	0.012866	-0.026928	0.004120	H	-4.241011	-0.962769	7.341416
N	-0.009742	-0.032160	1.370340	H	-6.121919	5.926813	2.897644
C	1.220111	-0.054591	-0.691425	H	-5.707793	0.991636	7.933404
C	-1.312473	0.002117	-0.677583	H	-3.684688	1.776576	2.541205
C	1.151941	-0.071264	2.045673				
C	2.421757	-0.095849	0.017883				
N	-2.411587	0.203926	0.131664				
C	-1.523135	-0.155132	-2.041848				
H	1.234580	-0.036859	-1.774688				
C	2.390072	-0.105198	1.410012				
C	-3.611739	0.239066	-0.367588				
C	-2.827252	-0.114032	-2.560202				
H	1.078125	-0.077017	3.127697				
H	3.366957	-0.118927	-0.515265				
H	-0.690927	-0.330450	-2.713429				
C	-3.919993	0.090881	-1.715349				
H	3.299712	-0.139330	1.999386				
H	-2.984042	-0.249244	-3.626956				
H	-4.938370	0.121543	-2.085277				
Cu^{2+}	-1.848055	0.035078	1.894305				
N	-4.202187	2.659727	2.589424				
N	-3.902199	0.826795	4.501905				
C	-4.822984	2.910515	3.771605				
C	-4.230619	3.489507	1.523825				
C	-4.692376	1.873938	4.818574				
C	-3.762248	-0.152626	5.400153				
C	-5.526713	4.112761	3.881192				
C	-4.920390	4.682979	1.603816				
C	-5.359037	1.970154	6.043894				
C	-4.389661	-0.140086	6.650101				
H	-3.700014	3.155458	0.640636				
H	-3.126157	-0.986730	5.117025				
C	-5.574077	4.994208	2.803711				
C	-5.200665	0.942836	6.975122				
H	-6.032546	4.361894	4.805207				
H	-4.947036	5.352816	0.752253				
H	-5.996200	2.815001	6.277849				

Table E.5. (continued) Cartesian Coordinates of the B3LYP/6-31G* Optimized Geometries of the Transition States, Ints, and Products Involved in the Dissociation of $M^{2+}(Bpy)_2$ Complexes through PTCF Process.[a]

$Cu^{2+}(Bpy)_2$ Int_3				$Cu^{2+}(Bpy)_2$ Int_3			
	x	y	z		x	y	z
C	-8.955434	-0.265145	-0.014351	H	9.329850	-3.126447	1.378744
N	-8.568303	-1.362478	-0.712184	H	6.216403	4.144743	-1.529743
C	-10.323721	-0.071804	0.177713	H	10.427651	-0.878887	1.111667
C	-7.845030	0.596141	0.452958	Cu^{2+}	4.825646	-1.158915	-0.069657
C	-9.413081	-2.274765	-1.230275				
C	-11.229137	-0.995732	-0.342507				
N	-6.625382	0.155893	0.090588				
C	-8.044788	1.757705	1.202265				
H	-10.679656	0.792405	0.724562				
C	-10.775659	-2.113184	-1.055120				
C	-5.557034	0.864006	0.459064				
C	-6.920998	2.492776	1.580870				
H	-8.966048	-3.103794	-1.766253				
H	-12.293791	-0.844465	-0.193600				
H	-9.036490	2.089230	1.489504				
C	-5.657028	2.044143	1.203882				
H	-11.464046	-2.842047	-1.466366				
H	-4.588097	0.463571	0.154980				
H	-7.035309	3.402343	2.161954				
H	-4.770438	2.601721	1.482494				
N	5.042849	0.650781	-0.474916				
N	6.680585	-1.352861	0.285213				
C	6.379657	0.960316	-0.373259				
C	4.198819	1.532216	-0.924277				
C	7.264263	-0.129032	0.132563				
C	7.421574	-2.386558	0.723110				
C	6.807032	2.227810	-0.741229				
C	4.528840	2.821803	-1.323964				
C	8.614542	0.059070	0.424630				
C	8.773052	-2.263694	1.030224				
H	-7.547247	-1.429961	-0.821055				
H	6.908931	-3.337174	0.820281				
C	5.878441	3.158548	-1.223258				
C	9.376453	-1.017187	0.879360				
H	7.854346	2.498573	-0.680972				
H	3.794457	3.520783	-1.707078				
H	9.072918	1.034002	0.309623				

Table E.5. (continued) Cartesian Coordinates of the B3LYP/6-31G* Optimized Geometries of the Transition States, Ints, and Products Involved in the Dissociation of $M^{2+}(Bpy)_2$ Complexes through PTCF Process.[a]

	$[Cu(Bpy-H)]^+$		
	x	y	z
C	0.030778	0.000004	-0.033707
N	-0.009622	0.000015	1.332705
C	1.250522	-0.000005	-0.708850
C	-1.284097	-0.000008	-0.739731
C	1.142688	0.000016	2.024521
C	2.441409	-0.000004	0.017139
N	-2.406026	0.000133	0.059001
C	-1.457664	-0.000141	-2.117620
H	1.280809	-0.000002	-1.791665
C	2.390340	0.000003	1.408496
C	-3.595072	0.000136	-0.459113
C	-2.753323	-0.000130	-2.659619
H	1.051202	0.000022	3.105130
H	3.394283	-0.000009	-0.502537
H	-0.604207	-0.000264	-2.785065
C	-3.868888	0.000014	-1.823554
H	3.291310	0.000002	2.011761
H	-2.881388	-0.000236	-3.738562
H	-4.881818	0.000027	-2.209006
Cu^{2+}	-1.835489	0.000161	1.832855

Table E.5. (continued) Cartesian Coordinates of the B3LYP/6-31G* Optimized Geometries of the Transition States, Ints, and Products Involved in the Dissociation of $M^{2+}(Bpy)_2$ Complexes through PTCF Process.[a]

	$Zn^{2+}(Bpy)_2$ TS_1				$Zn^{2+}(Bpy)_2$ TS_1		
	x	y	z		x	y	z
C	0.060127	0.064261	-0.162239	H	6.186924	0.649569	-5.239718
C	0.000878	0.348720	1.189563	H	5.681041	2.648503	-4.918992
C	1.173661	0.354314	1.989669	H	2.991657	-0.340891	4.080354
C	2.391910	0.097479	1.410695	H	1.098654	0.579691	3.048561
N	2.443340	-0.073147	0.017177				
C	1.296296	-0.113343	-0.840460				
C	3.701787	0.098949	2.092557				
C	3.854833	-0.122382	3.461557				
C	5.132967	-0.084612	4.020029				
H	5.267854	-0.256253	5.083469				
C	6.230757	0.166712	3.196769				
C	6.012210	0.368899	1.837832				
N	4.780630	0.338425	1.293814				
H	-0.852884	-0.003474	-0.746464				
H	-0.953183	0.552967	1.668868				
H	2.341489	-1.043123	-0.617329				
H	7.239422	0.204471	3.593256				
H	6.837126	0.568288	1.161035				
C	4.295062	4.467437	-2.418395				
C	4.859765	4.181507	-3.660442				
C	5.241706	2.872422	-3.954991				
C	5.051999	1.869766	-3.003457				
N	4.499978	2.162048	-1.795362				
C	4.132025	3.425484	-1.513172				
C	5.427926	0.445416	-3.226614				
C	5.995541	-0.022298	-4.412440				
C	6.317942	-1.373952	-4.535310				
H	6.757738	-1.744936	-5.455830				
C	6.070516	-2.236994	-3.468683				
C	5.503627	-1.710863	-2.314155				
N	5.189260	-0.407248	-2.193807				
H	3.985914	5.472007	-2.151915				
H	5.003739	4.966689	-4.396064				
H	3.696611	3.596650	-0.533875				
H	6.307905	-3.293542	-3.524748				
H	5.293251	-2.342572	-1.456632				
Zn^{2+}	4.297495	0.526529	-0.659356				

Table E.5. (continued) Cartesian Coordinates of the B3LYP/6-31G* Optimized Geometries of the Transition States, Ints, and Products Involved in the Dissociation of $M^{2+}(Bpy)_2$ Complexes through PTCF Process.[a]

	$Zn^{2+}(Bpy)_2$ Int_1				$Zn^{2+}(Bpy)_2$ Int_1		
	x	y	z		x	y	z
C	0.438608	0.343930	-0.353208	H	5.470006	1.363097	-5.295984
C	0.243686	0.539877	1.006898	H	4.882478	3.247436	-4.620842
C	1.303028	0.308575	1.922700	H	3.132672	-0.849267	4.102191
C	2.461988	-0.260274	1.463161	H	1.229642	0.653674	2.949134
N	2.489034	-0.657971	0.110936				
C	1.538902	-0.397056	-0.865312				
C	3.773494	-0.288713	2.127141				
C	3.976287	-0.583330	3.474324				
C	5.274109	-0.556834	3.985382				
H	5.452026	-0.786835	5.031415				
C	6.339920	-0.244080	3.137950				
C	6.074240	0.037796	1.804006				
N	4.820440	0.022004	1.301520				
H	-0.324946	0.665815	-1.055310				
H	-0.693132	0.943660	1.382359				
H	3.039980	-1.500249	-0.068101				
H	7.361331	-0.216592	3.501184				
H	6.871988	0.292954	1.113476				
C	3.659975	4.562007	-1.746283				
C	4.081809	4.502026	-3.073868				
C	4.547886	3.293391	-3.592115				
C	4.581842	2.161832	-2.776997				
N	4.163406	2.233748	-1.483462				
C	3.717735	3.402273	-0.983511				
C	5.070606	0.832381	-3.239996				
C	5.491475	0.582381	-4.546066				
C	5.940255	-0.692426	-4.893233				
H	6.266601	-0.894240	-5.908692				
C	5.963789	-1.697430	-3.927502				
C	5.529029	-1.388151	-2.644646				
N	5.093875	-0.159197	-2.307587				
H	3.295269	5.483618	-1.306507				
H	4.053171	5.386162	-3.703101				
H	3.402346	3.397151	0.054764				
H	6.306606	-2.700074	-4.157594				
H	5.527309	-2.138210	-1.859971				
Zn^{2+}	4.299610	0.463171	-0.589830				

Table E.5. (continued) Cartesian Coordinates of the B3LYP/6-31G* Optimized Geometries of the Transition States, Ints, and Products Involved in the Dissociation of $M^{2+}(Bpy)_2$ Complexes through PTCF Process.[a]

$Zn^{2+}(Bpy)_2$ TS_2				$Zn^{2+}(Bpy)_2$ TS_2			
	x	y	z		x	y	z
C	-0.849633	-0.046273	1.255116	H	6.842305	0.856264	-5.197956
C	-0.247577	0.294215	2.478132	H	3.385667	-0.539203	3.823134
C	1.150352	0.349464	2.636405	H	1.553145	0.656379	3.594717
C	2.036750	0.047578	1.587444	Zn^{2+}	3.775655	0.216856	-1.310100
N	1.362570	-0.250685	0.436025				
C	0.158518	-0.284792	0.342110				
C	3.510978	0.029829	1.743805				
C	4.040399	-0.255315	3.007969				
C	5.418221	-0.200440	3.215266				
H	5.832219	-0.418994	4.194626				
C	6.242976	0.133952	2.146037				
C	5.653454	0.367633	0.906790				
N	4.324967	0.315292	0.691538				
H	-1.915030	-0.101493	1.074677				
H	-0.887640	0.531026	3.325545				
H	2.438381	-0.630857	-1.128009				
H	7.319867	0.201011	2.256168				
H	6.267491	0.607140	0.044421				
C	3.583433	4.172427	-3.075921				
C	4.551300	4.057824	-4.072705				
C	5.248046	2.858237	-4.213247				
C	4.964290	1.793248	-3.356146				
N	4.020261	1.916539	-2.386889				
C	3.351165	3.075347	-2.254491				
C	5.646361	0.472544	-3.437470				
C	6.572604	0.143110	-4.428877				
C	7.148107	-1.127308	-4.434617				
H	7.866322	-1.394089	-5.203628				
C	6.785546	-2.047201	-3.451608				
C	5.854423	-1.657275	-2.495501				
N	5.303929	-0.430219	-2.482514				
H	3.018841	5.087344	-2.934857				
H	4.764535	4.890589	-4.735540				
H	2.605496	3.114710	-1.466835				
H	7.205516	-3.046618	-3.426192				
H	5.530217	-2.339858	-1.716091				
H	6.004005	2.765288	-4.983070				

Table E.5. (continued) Cartesian Coordinates of the B3LYP/6-31G* Optimized Geometries of the Transition States, Ints, and Products Involved in the Dissociation of $M^{2+}(Bpy)_2$ Complexes through PTCF Process.[a]

	$Zn^{2+}(Bpy)_2$ Int_2				$Zn^{2+}(Bpy)_2$ Int_2		
	x	y	z		x	y	z
C	-0.086096	-0.267051	-0.146516	H	-4.128965	-3.416946	3.085261
N	-0.075610	0.215428	1.122978	H	-2.130009	2.964113	8.027049
C	1.085750	-0.743083	-0.738707	H	-4.951401	-2.710286	5.361078
C	-1.401840	-0.241594	-0.841881	Zn^{2+}	-1.898453	0.884541	1.739463
C	1.077682	0.238564	1.813060				
C	2.279068	-0.716744	-0.018562				
N	-2.458122	0.161757	-0.091146				
C	-1.570718	-0.585161	-2.184853				
H	1.077681	-1.135380	-1.748102				
C	2.279464	-0.215996	1.282534				
C	-3.679311	0.241605	-0.647778				
C	-2.840723	-0.511055	-2.756253				
H	1.028839	0.641100	2.819925				
H	3.195144	-1.083213	-0.471121				
H	-0.728303	-0.895647	-2.790515				
C	-3.917753	-0.091030	-1.976820				
H	3.186631	-0.175598	1.875132				
H	-4.481134	0.587614	-0.002772				
H	-2.982067	-0.771698	-3.800501				
H	-4.918823	-0.012863	-2.386246				
N	-2.259537	2.377163	4.323691				
N	-2.701243	-0.355460	3.237967				
C	-2.644616	1.291502	5.066179				
C	-1.932637	3.418653	4.831537				
C	-3.100911	0.010329	4.485599				
C	-3.077968	-1.564249	2.782514				
C	-2.561883	1.556450	6.447247				
C	-1.800191	3.885501	6.114297				
C	-3.925429	-0.817322	5.256928				
C	-3.866358	-2.453864	3.509396				
H	-2.308131	2.350041	2.129378				
H	-2.734061	-1.827073	1.787670				
C	-2.166227	2.808794	6.950378				
C	-4.312520	-2.064177	4.767305				
H	-2.788313	0.765772	7.152940				
H	-1.485337	4.867014	6.442443				
H	-4.283593	-0.487837	6.224769				

Table E.5. (continued) Cartesian Coordinates of the B3LYP/6-31G* Optimized Geometries of the Transition States, Ints, and Products Involved in the Dissociation of $M^{2+}(Bpy)_2$ Complexes through PTCF Process.[a]

$Zn^{2+}(Bpy)_2$ TS_3				$Zn^{2+}(Bpy)_2$ TS_3			
	x	y	z		x	y	z
C	0.000273	0.000978	-0.000166	H	-4.702651	-3.691438	3.617783
N	0.000801	0.000145	1.362827	H	-2.090166	3.472394	7.181009
C	1.206663	0.003423	-0.706958	H	-5.506525	-2.531086	5.699635
C	-1.318314	0.006044	-0.668907	Zn^{2+}	-1.738105	0.296336	2.275499
C	1.173593	-0.000129	2.029937				
C	2.415078	-0.009245	-0.013423				
N	-2.417940	0.128171	0.137425				
C	-1.495787	-0.141010	-2.048162				
H	1.213085	0.025423	-1.789522				
C	2.401644	-0.013216	1.381265				
C	-3.672539	0.094476	-0.384799				
C	-2.780179	-0.186501	-2.586068				
H	1.113847	0.001368	3.113417				
H	3.353858	-0.011414	-0.558288				
H	-0.639674	-0.248776	-2.703014				
C	-3.890032	-0.085211	-1.737083				
H	3.319404	-0.024347	1.958728				
H	-4.484217	0.234771	0.321827				
H	-2.915190	-0.300239	-3.656907				
H	-4.903652	-0.132889	-2.120124				
N	-1.794937	1.589881	3.874130				
N	-2.881700	-0.864714	3.413753				
C	-2.634384	1.060037	4.840370				
C	-1.085850	2.629039	4.093187				
C	-3.286555	-0.232948	4.549702				
C	-3.388182	-2.074246	3.100412				
C	-2.739665	1.760212	6.034627				
C	-1.072747	3.357319	5.284374				
C	-4.245729	-0.816207	5.381380				
C	-4.327183	-2.713648	3.898463				
H	-2.402840	1.330859	1.099101				
H	-3.019099	-2.530685	2.187617				
C	-1.981258	2.924124	6.248281				
C	-4.766943	-2.066572	5.054826				
H	-3.381239	1.393201	6.827461				
H	-0.428606	4.215956	5.434257				
H	-4.585479	-0.305208	6.274083				

Table E.5. (continued) Cartesian Coordinates of the B3LYP/6-31G* Optimized Geometries of the Transition States, Ints, and Products Involved in the Dissociation of $M^{2+}(Bpy)_2$ Complexes through PTCF Process.[a]

	$Zn^{2+}(Bpy)_2$ Int_3				$Zn^{2+}(Bpy)_2$ Int_3		
	x	y	z		x	y	z
C	2.921365	-0.418633	0.511091	H	-4.921902	2.252994	2.650857
N	1.777292	-1.127193	0.706865	H	-4.670647	-2.995864	-1.892893
C	4.119016	-0.785105	1.124402	H	-1.059978	1.224289	-0.061582
C	2.782889	0.752575	-0.385645	Zn^{2+}	0.239437	-0.376172	-0.343717
C	1.811344	-2.204935	1.508057				
C	4.143841	-1.906590	1.954174				
N	1.505482	0.987916	-0.830550				
C	3.804418	1.596913	-0.806208				
H	5.023079	-0.209150	0.964394				
C	2.970225	-2.631058	2.152312				
C	1.264069	1.990491	-1.624508				
C	3.515624	2.664939	-1.668640				
H	0.875043	-2.739617	1.633499				
H	5.068349	-2.205942	2.437835				
H	4.825865	1.433276	-0.482782				
C	2.206689	2.889512	-2.104623				
H	2.945855	-3.508612	2.789027				
H	4.316890	3.319192	-2.001431				
H	1.949589	3.703893	-2.771935				
N	-1.890878	1.466840	0.497129				
N	-1.509752	-1.058718	-0.707377				
C	-2.891223	0.547251	0.523421				
C	-1.911074	2.638616	1.169605				
C	-2.754711	-0.666422	-0.316127				
C	-1.414650	-2.135073	-1.523574				
C	-4.000625	0.838588	1.320740				
C	-3.004472	2.958151	1.952266				
C	-3.901643	-1.351570	-0.731040				
C	-2.513140	-2.858064	-1.969906				
H	-1.043725	3.277259	1.049180				
H	-0.413314	-2.427174	-1.823184				
C	-4.057077	2.038125	2.030551				
C	-3.785104	-2.462611	-1.562698				
H	-4.809542	0.123621	1.404055				
H	-3.028203	3.897621	2.492580				
H	-4.883999	-1.002286	-0.436724				
H	-2.366057	-3.710855	-2.623737				

Table E.5. (continued) Cartesian Coordinates of the B3LYP/6-31G* Optimized Geometries of the Transition States, Ints, and Products Involved in the Dissociation of $M^{2+}(Bpy)_2$ Complexes through PTCF Process.[a]

$Zn^{2+}(Bpy)_2$ TS_4				$Zn^{2+}(Bpy)_2$ TS_4			
	x	y	z		x	y	z
C	0.394377	-0.881129	0.062669	H	-6.923282	5.807918	6.374570
N	0.653338	-0.707936	1.389101	H	-4.280213	-0.734843	7.310300
C	1.270049	-1.640421	-0.720524	H	-3.650097	3.612515	3.597607
C	-0.830383	-0.228043	-0.476854	Zn^{2+}	-0.669013	0.619498	2.067664
C	1.737998	-1.268979	1.957439				
C	2.386826	-2.228205	-0.130919				
N	-1.560068	0.642640	0.325839				
C	-1.290776	-0.439710	-1.764686				
H	1.095107	-1.769103	-1.780955				
C	2.628351	-2.046769	1.232873				
C	-2.647369	1.268355	-0.049905				
C	-2.450572	0.216135	-2.214652				
H	1.880638	-1.079746	3.016844				
H	3.066837	-2.820725	-0.735107				
H	-0.773025	-1.120832	-2.428962				
C	-3.136966	1.063072	-1.361324				
H	3.488323	-2.490257	1.722115				
H	-2.799560	0.042900	-3.229569				
H	-4.040320	1.568163	-1.687352				
N	-4.345482	4.116428	4.156356				
N	-3.258575	1.748759	4.506163				
C	-4.788860	3.426654	5.237731				
C	-4.759114	5.354480	3.818874				
C	-4.199828	2.078146	5.415481				
C	-2.701484	0.548378	4.607688				
C	-5.734932	4.045592	6.053776				
C	-5.698177	5.994524	4.608050				
C	-4.595479	1.213505	6.440686				
C	-3.021462	-0.389988	5.589384				
H	-4.322493	5.787580	2.926580				
H	-1.936128	0.325058	3.850766				
C	-6.187293	5.327250	5.737429				
C	-3.992748	-0.041992	6.525885				
H	-6.115373	3.537436	6.931068				
H	-6.037131	6.989889	4.345333				
H	-5.356773	1.497005	7.158381				
H	-2.528517	-1.355811	5.617338				

Table E.5. (continued) Cartesian Coordinates of the B3LYP/6-31G* Optimized Geometries of the Transition States, Ints, and Products Involved in the Dissociation of $M^{2+}(Bpy)_2$ Complexes through PTCF Process.[a]

	$Zn^{2+}(Bpy)_2$ Int_4				$Zn^{2+}(Bpy)_2$ Int_4		
	x	y	z		x	y	z
C	-8.945931	-0.251360	-0.021310	H	9.418164	-3.005725	1.338728
N	-8.564426	-1.322488	-0.761379	H	6.146799	4.115283	-1.650745
C	-10.313455	-0.054583	0.172514	H	10.430964	-0.724651	1.047327
C	-7.830431	0.580244	0.485342	Zn^{2+}	4.731040	-1.235837	0.008853
C	-9.414107	-2.205759	-1.320405				
C	-11.223796	-0.947805	-0.390473				
N	-6.613181	0.135300	0.120232				
C	-8.021986	1.721505	1.267505				
H	-10.664064	0.787830	0.755689				
C	-10.776076	-2.038625	-1.146939				
C	-5.541044	0.818004	0.520110				
C	-6.892447	2.429767	1.680665				
H	-8.970784	-3.015817	-1.887538				
H	-12.287919	-0.794170	-0.240192				
H	-9.012553	2.058394	1.552621				
C	-5.631630	1.975341	1.301938				
H	-11.468777	-2.742943	-1.592287				
H	-4.573838	0.426071	0.211057				
H	-7.001126	3.322381	2.288510				
H	-4.734433	2.505005	1.603102				
N	4.958414	0.674136	-0.547477				
N	6.703797	-1.304418	0.310784				
C	6.303092	0.960538	-0.405669				
C	4.069871	1.527907	-0.955474				
C	7.231814	-0.073707	0.118398				
C	7.470388	-2.326692	0.735609				
C	6.726822	2.215765	-0.814476				
C	4.447400	2.823652	-1.364001				
C	8.584506	0.159626	0.391947				
C	8.822002	-2.164855	1.002475				
H	-7.543061	-1.398240	-0.861717				
H	6.974245	-3.284062	0.861527				
C	5.797915	3.142133	-1.313245				
C	9.380024	-0.894237	0.834558				
H	7.775064	2.484239	-0.764089				
H	3.715129	3.537387	-1.724734				
H	9.015154	1.145257	0.267614				

Table E.5. (continued) Cartesian Coordinates of the B3LYP/6-31G* Optimized Geometries of the Transition States, Ints, and Products Involved in the Dissociation of $M^{2+}(Bpy)_2$ Complexes through PTCF Process.[a]

	$[Zn(Bpy\text{-}H)]^+$		
	x	y	z
C	0.019489	0.000000	-0.000320
N	0.045974	0.000000	1.389441
C	1.237212	0.000000	-0.658408
C	-1.285168	0.000000	-0.715473
C	1.138596	0.000000	2.100913
C	2.437536	0.000000	0.074597
N	-2.405655	0.000000	0.054257
C	-1.403662	0.000000	-2.110113
H	1.276713	0.000000	-1.740660
C	2.397092	0.000000	1.457781
C	-3.628379	0.000000	-0.506360
C	-2.668584	0.000000	-2.691728
H	3.385662	0.000000	-0.457426
H	-0.524720	0.000000	-2.741629
C	-3.806277	0.000000	-1.881669
H	3.307688	0.000000	2.047769
H	-4.471357	0.000000	0.177879
H	-2.764422	0.000000	-3.773041
H	-4.805338	0.000000	-2.302607
Zn^{2+}	-1.835421	0.000000	1.970214

[a]Standard Orientation, Å.

Table E.6. Relative Stabilities of the Transition States, Intermediates, and Products Involved in the Activated Dissociation of $M^{2+}(Bpy)_2$ Reactant Complexes via ETCF at 0 K in kJ/mol.

		B3LYP[a]	BHandHLYP[b]	M06[c]
Complex	Species	D_0[d]	D_0[d]	D_0[d]
$Fe^{2+}(Bpy)_2$	Reactant	0.0	0.0	0.0
	TS_1	143.6	162.4	142.9
	Int_1	132.7	153.2	130.7
	TS_2	354.5	375.0	344.3
	Int_2	335.9	355.5	320.3
	$Fe^{+}(Bpy) + Bpy^{+}$ products	323.9	345.0	312.8
$Co^{2+}(Bpy)_2$	Reactant	0.0	0.0	0.0
	TS_1	155.6	155.8	144.5
	Int_1	141.5	144.5	131.1
	TS_2	276.8	341.2	269.7
	Int_2	257.8	329.2	245.6
	$Co^{+}(Bpy) + Bpy^{+}$ products	234.7	308.5	230.5
$Ni^{2+}(Bpy)_2$	Reactant	0.0	0.0	0.0
	TS_1	155.8	165.5	151.2
	Int_1	144.2	147.4	138.1
	TS_2	254.4	273.0	227.8
	Int_2	236.0	261.6	203.4
	$Ni^{+}(Bpy) + Bpy^{+}$ products	189.0	219.7	174.0
$Cu^{2+}(Bpy)_2$	Reactant	0.0	0.0	0.0
	TS_1	145.9	152.7	145.0
	Int_1	135.4	145.6	130.7
	TS_2	241.6	267.6	227.2
	Int_2	222.9	255.9	203.2
	$Cu^{+}(Bpy) + Bpy^{+}$ products	142.5	171.9	131.4
$Zn^{2+}(Bpy)_2$	Reactant	0.0	0.0	0.0
	TS_1	144.1	165.2	142.8
	Int_1	135.4	157.8	131.2
	TS_2	315.4	338.5	303.0
	Int_2	296.7	326.8	278.9
	$Zn^{+}(Bpy) + Bpy^{+}$ products	280.4	310.8	267.0

[a]Calculated at the B3LYP/6-311+G(2d,2p)//B3LYP/6-31G* level of theory. [b]Calculated at the BHandHLYP/6-311+G(2d,2p)//B3LYP/6-31G* level of theory. [c]Calculated at the M06/6-311+G(2d,2p)//B3LYP/6-31G* level of theory. [d] Including ZPE corrections scaled by 0.9804.

Table E.7. Relative Stabilities of the Transition States, Intermediates, and Products Involved in the Activated Dissociation of $M^{2+}(Bpy)_2$ Reactant Complexes via PTCF at 0 K in kJ/mol.

		B3LYP[a]	BHandHLYP[b]	M06[c]
Complex	Species	D_0[d]	D_0[d]	D_0[d]
$Fe^{2+}(Bpy)_2$	Reactant	0.0	0.0	0.0
	TS_1	409.1	451.6	400.6
	Int_1	373.4	440.5	365.6
	TS_2	459.2	511.1	438.5
	Int_2	388.4	431.8	380.7
	TS_3	428.4	465.9	408.1
	Int_3	365.1	368.8	357.2
	$[Fe(Bpy-H)]^+ + [Bpy+H]^+$ products	328.3	328.1	282.6
$Co^{2+}(Bpy)_2$	Reactant	0.0	0.0	0.0
	TS_1	441.9	457.6	428.4
	Int_1	349.5	373.6	322.4
	TS_2	437.2	455.8	424.4
	Int_2	395.5	417.6	371.7
	TS_3	437.8	456.3	418.2
	Int_3	390.2	411.4	376.2
	TS_4	438.9	457.0	421.2
	Int_4	361.4	400.5	358.3
	$[Co(Bpy-H)]^+ + [Bpy+H]^+$ products	281.2	350.2	274.1
$Ni^{2+}(Bpy)_2$	Reactant	0.0	0.0	0.0
	TS_1	406.7	445.8	395.5
	Int_1	359.3	387.2	355.0
	TS_2	397.9	438.0	385.2
	Int_2	360.1	411.3	356.3
	TS_3	369.1	428.1	367.8
	Int_3	313.7	349.3	289.8
	$[Ni(Bpy-H)]^+ + [Bpy+H]^+$ products	197.9	253.4	192.6

[a]Calculated at the B3LYP/6-311+G(2d,2p)//B3LYP/6-31G* level of theory. [b]Calculated at the BHandHLYP/6-311+G(2d,2p)//B3LYP/6-31G* level of theory. [c]Calculated at the M06/6-311+G(2d,2p)//B3LYP/6-31G* level of theory. [d]Including ZPE corrections scaled by 0.9804.

Table E.7. (continued) Relative Stabilities of the Transition States, Intermediates, and Products Involved in the Activated Dissociation of $M^{2+}(Bpy)_2$ Reactant Complexes via PTCF at 0 K in kJ/mol.

		B3LYP[a]	BHandHLYP[b]	M06[c]
Complex	Species	D_0[d]	D_0[d]	D_0[d]
$Cu^{2+}(Bpy)_2$	Reactant	0.0	0.0	0.0
	TS_1	437.9	506.5	436.3
	Int_1	389.7	448.3	383.5
	TS_2	402.5	464.3	400.2
	Int_2	226.7	283.1	218.6
	TS_3	313.3	356.8	307.7
	Int_3	217.4	256.7	204.3
	$[Cu(Bpy-H)]^+ + [Bpy+H]^+$ products	133.6	160.5	120.8
$Zn^{2+}(Bpy)_2$	Reactant	0.0	0.0	0.0
	TS_1	448.7	466.3	435.6
	Int_1	350.2	358.3	338.3
	TS_2	440.6	457.9	424.7
	Int_2	287.4	307.9	285.7
	TS_3	394.5	412.5	382.9
	Int_3	297.4	353.2	289.4
	TS_4	393.6	412.0	391.6
	Int_4	372.6	387.1	371.6
	$[Zn(Bpy-H)]^+ + [Bpy+H]^+$ products	362.3	374.5	343.3

[a]Calculated at the B3LYP/6-311+G(2d,2p)//B3LYP/6-31G* level of theory. [b]Calculated at the BHandHLYP/6-311+G(2d,2p)//B3LYP/6-31G* level of theory. [c]Calculated at the M06/6-311+G(2d,2p)//B3LYP/6-31G* level of theory. [d] Including ZPE corrections scaled by 0.9804.

Table E.8. Fitting Parameters of eq 2.4, Threshold Dissociation Energies at 0 K, and Entropies of Activation at 1000 K of $M^{2+}(Bpy)_2$ Complexes Obtained from Independent Analyses of the Simple CID and Primary Activated Dissociation Cross Sections for ETCF Process.[a]

Complex	Product	$E_{0,j}(TS)^c$ (eV)	$E_{0,j}(PSL)^b$ (eV)	$E_{0,j}(TTS)^b$ (eV)	Kinetic Shift (eV)
$Fe^{2+}(Bpy)_2$	$Fe^{+}(Bpy)$	10.95 (0.14)	–	2.87 (0.12)	8.08
	$Fe^{2+}(Bpy)$	8.05 (0.06)	3.50 (0.15)	–	4.55
$Co^{2+}(Bpy)_2$	$Co^{+}(Bpy)$	10.22 (0.13)	–	2.69 (0.12)	7.53
	$Co^{2+}(Bpy)$	7.81 (0.20)	3.56 (0.15)	–	4.25
$Ni^{2+}(Bpy)_2$	$Ni^{+}(Bpy)$	9.45 (0.13)	–	2.64 (0.11)	6.81
	$Ni^{2+}(Bpy)$	8.82 (0.36)	3.78 (0.18)	–	5.04
$Cu^{2+}(Bpy)_2$	$Cu^{+}(Bpy)$	7.61 (0.07)	–	2.43 (0.10)	5.18
	$Cu^{2+}(Bpy)$	8.73 (0.21)	3.93 (0.17)	–	4.80
$Zn^{2+}(Bpy)_2$	$Zn^{+}(Bpy)$	8.38 (0.13)	–	2.46 (0.11)	5.92
	$Zn^{2+}(Bpy)$	7.23 (0.22)	3.35 (0.14)	–	3.88

[a]Uncertainties are listed in parentheses. [b]Average values for PSL or TTSs including RRKM analysis. [c] No RRKM analysis.

Table E.8. (continued) Fitting Parameters of eq 2.4, Threshold Dissociation Energies at 0 K, and Entropies of Activation at 1000 K of $M^{2+}(Bpy)_2$ Complexes Obtained from Independent Analyses of the Simple CID and Primary Activated Dissociation Cross Sections for ETCF Process.[a]

Complex	Product	$\sigma_{0,j}{}^{b}$	n^{b}	$\Delta S^{\ddagger}(TS)^{b}$ (J mol^{-1} K^{-1})
$Fe^{2+}(Bpy)_2$	$Fe^{+}(Bpy)$	0.8 (0.1)	1.5 (0.1)	−6.9 (0.8)
	$Fe^{2+}(Bpy)$	0.2 (0.1)	1.7 (0.1)	92.6 (4.3)
$Co^{2+}(Bpy)_2$	$Co^{+}(Bpy)$	0.7 (0.1)	1.8 (0.1)	−12.8 (0.7)
	$Co^{2+}(Bpy)$	0.2 (0.1)	1.5 (0.1)	93.4 (4.3)
$Ni^{2+}(Bpy)_2$	$Ni^{+}(Bpy)$	1.1 (0.1)	1.6 (0.1)	−3.3 (0.7)
	$Ni^{2+}(Bpy)$	0.2 (0.1)	1.2 (0.1)	97.8 (4.3)
$Cu^{2+}(Bpy)_2$	$Cu^{+}(Bpy)$	0.9 (0.1)	1.3 (0.1)	12.0 (0.6)
	$Cu^{2+}(Bpy)$	0.1 (0.1)	1.5 (0.1)	117.5 (4.2)
$Zn^{2+}(Bpy)_2$	$Zn^{+}(Bpy)$	0.4 (0.1)	1.6 (0.1)	−5.4 (0.7)
	$Zn^{2+}(Bpy)$	0.1 (0.1)	1.8 (0.1)	102.0 (4.3)

[a]Uncertainties are listed in parentheses. [b]Average values for PSL or TTSs including RRKM analysis. [c]No RRKM analysis.

Table E.9. Fitting Parameters of eq 2.5, Threshold Dissociation Energies at 0 K, and Entropies of Activation at 1000 K of $M^{2+}(Bpy)_2$ Complexes Obtained from Competitive Analyses of the Simple CID and Activated Dissociation Product Cross Sections for ETCF Process.[a]

Complex	Product	$E_{0,j}(PSL)$[c] (eV)	$E_{0,j}(TTS)$[b] (eV)	Competitive Shift (eV)
$Fe^{2+}(Bpy)_2$	$Fe^{+}(Bpy)$	–	2.94 (0.08)	0.07
	$Fe^{2+}(Bpy)$	2.31 (0.34)	–	−1.19
$Co^{2+}(Bpy)_2$	$Co^{+}(Bpy)$	–	2.73 (0.08)	0.04
	$Co^{2+}(Bpy)$	2.34 (0.27)	–	−1.22
$Ni^{2+}(Bpy)_2$	$Ni^{+}(Bpy)$	–	2.68 (0.10)	0.04
	$Ni^{2+}(Bpy)$	3.17 (0.31)	–	−0.61
$Cu^{2+}(Bpy)_2$	$Cu^{+}(Bpy)$	–	2.44 (0.09)	0.01
	$Cu^{2+}(Bpy)$	3.42 (0.27)	–	−0.51
$Zn^{2+}(Bpy)_2$	$Zn^{+}(Bpy)$	–	2.50 (0.10)	0.04
	$Zn^{2+}(Bpy)$	2.40 (0.24)	–	−0.95

[a]Uncertainties are listed in parentheses. [b]Average values for PSL or TTSs including RRKM analysis. [c]No RRKM analysis.

Table E.9. (continued) Fitting Parameters of eq 2.5, Threshold Dissociation Energies at 0 K, and Entropies of Activation at 1000 K of $M^{2+}(Bpy)_2$ Complexes Obtained from Competitive Analyses of the Simple CID and Activated Dissociation Product Cross Sections for ETCF Process.[a]

Complex	Product	$\sigma_{0,j}{}^{b}$	n^{b}	$\Delta S^{\ddagger}(TS)^{b}$ (J mol^{-1} K^{-1})
$Fe^{2+}(Bpy)_2$	$Fe^{+}(Bpy)$	1.2 (0.5)	1.5 (0.1)	−6.9 (0.7)
	$Fe^{2+}(Bpy)$	1.2 (0.5)	1.5 (0.1)	−78.0 (35.5)
$Co^{2+}(Bpy)_2$	$Co^{+}(Bpy)$	1.1 (0.1)	1.6 (0.1)	−12.8 (0.8)
	$Co^{2+}(Bpy)$	1.1 (0.1)	1.6 (0.1)	−77.1 (37.1)
$Ni^{2+}(Bpy)_2$	$Ni^{+}(Bpy)$	1.5 (0.1)	1.5 (0.1)	−3.3 (0.4)
	$Ni^{2+}(Bpy)$	1.5 (0.1)	1.5 (0.1)	−12.7 (24.7)
$Cu^{2+}(Bpy)_2$	$Cu^{+}(Bpy)$	1.0 (0.1)	1.3 (0.1)	12.1 (0.6)
	$Cu^{2+}(Bpy)$	1.0 (0.1)	1.3 (0.1)	30.7 (25.5)
$Zn^{2+}(Bpy)_2$	$Zn^{+}(Bpy)$	0.4 (0.1)	1.6 (0.1)	−5.4 (0.5)
	$Zn^{2+}(Bpy)$	0.4 (0.1)	1.6 (0.1)	−65.5 (32.3)

[a]Uncertainties are listed in parentheses. [b]Average values for PSL or TTSs including RRKM analysis. [c]No RRKM analysis.

Table E.10a. Measured and Calculated Reaction Energies of $M^{2+}(Bpy)_2$ Complexes at 0 K in kJ/mol.

			B3LYP Theory	
Complex	Product	TCID[a]	E_0[b]	$E_{0,BSSE}$[c]
$Fe^{2+}(Bpy)_2$	$Fe^+(Bpy)$	283.3 (8.2)	354.5	
	$Fe^{2+}(Bpy)$	222.8 (32.4)	530.8	526.6
$Co^{2+}(Bpy)_2$	$Co^+(Bpy)$	263.6 (7.8)	276.8	
	$Co^{2+}(Bpy)$	225.3 (25.9)	546.2	541.7
$Ni^{2+}(Bpy)_2$	$Ni^+(Bpy)$	258.5 (9.8)	254.4	
	$Ni^{2+}(Bpy)$	305.9 (30.2)	539.7	534.1
$Cu^{2+}(Bpy)_2$	$Cu^+(Bpy)$	235.8 (8.7)	241.6	
	$Cu^{2+}(Bpy)$	330.0 (25.8)	517.9	512.5
$Zn^{2+}(Bpy)_2$	$Zn^+(Bpy)$	241.3 (10.1)	315.4	
	$Zn^{2+}(Bpy)$	231.7 (23.6)	545.3	540.9
AEU/MAD	ETCF	8.9 (1.0)		33.7 (35.8)
	Simple CID	27.6 (3.6)		268.0 (59.6)

[a]Values obtained from competitive analyses of the simple CID and activated dissociation product cross sections for ETCF Process. [b]Calculated at the B3LYP/6-311+G(2d,2p)//B3LYP/6-31G* level of theory including ZPE corrections scaled by 0.9804. [c]Also includes BSSE corrections.

Table E.10b. Measured and Calculated Reaction Energies of $M^{2+}(Bpy)_2$ Complexes at 0 K in kJ/mol

			BHandHLYP Theory	
Complex	Product	TCID[a]	E_0[b]	$E_{0,BSSE}$[c]
$Fe^{2+}(Bpy)_2$	$Fe^+(Bpy)$	283.3 (8.2)	375.0	
	$Fe^{2+}(Bpy)$	222.8 (32.4)	520.4	516.3
$Co^{2+}(Bpy)_2$	$Co^+(Bpy)$	263.6 (7.8)	341.2	
	$Co^{2+}(Bpy)$	225.3 (25.9)	553.4	550.1
$Ni^{2+}(Bpy)_2$	$Ni^+(Bpy)$	258.5 (9.8)	273.0	
	$Ni^{2+}(Bpy)$	305.9 (30.2)	518.1	513.3
$Cu^{2+}(Bpy)_2$	$Cu^+(Bpy)$	235.8 (8.7)	267.6	
	$Cu^{2+}(Bpy)$	330.0 (25.8)	544.3	538.8
$Zn^{2+}(Bpy)_2$	$Zn^+(Bpy)$	241.3 (10.1)	338.5	
	$Zn^{2+}(Bpy)$	231.7 (23.6)	556.2	551.8
AEU/MAD	ETCF	8.9 (1.0)		62.6 (37.2)
	Simple CID	27.6 (3.6)		270.9 (58.6)

[a]Values obtained from competitive analyses of the simple CID and activated dissociation product cross sections for ETCF Process. [b]Calculated at the BHandHLYP/6-311+G(2d,2p)//B3LYP/6-31G* level of theory including ZPE corrections scaled by 0.9804. [c]Also includes BSSE corrections.

Table E.10c. Measured and Calculated Reaction Energies of $M^{2+}(Bpy)_2$ Complexes at 0 K in kJ/mol

			M06 Theory	
Complex	Product	TCID[a]	E_0[b]	$E_{0,BSSE}$[c]
$Fe^{2+}(Bpy)_2$	$Fe^+(Bpy)$	283.3 (8.2)	344.3	
	$Fe^{2+}(Bpy)$	222.8 (32.4)	573.4	568.5
$Co^{2+}(Bpy)_2$	$Co^+(Bpy)$	263.6 (7.8)	269.7	
	$Co^{2+}(Bpy)$	225.3 (25.9)	570.6	565.0
$Ni^{2+}(Bpy)_2$	$Ni^+(Bpy)$	258.5 (9.8)	227.8	
	$Ni^{2+}(Bpy)$	305.9 (30.2)	547.3	540.5
$Cu^{2+}(Bpy)_2$	$Cu^+(Bpy)$	235.8 (8.7)	227.2	
	$Cu^{2+}(Bpy)$	330.0 (25.8)	546.7	540.3
$Zn^{2+}(Bpy)_2$	$Zn^+(Bpy)$	241.3 (10.1)	303.0	
	$Zn^{2+}(Bpy)$	231.7 (23.6)	563.2	558.1
AEU/MAD	ETCF	8.9 (1.0)		33.6 (27.1)
	Simple CID	27.6 (3.6)		291.3 (63.9)

[a]Values obtained from competitive analyses of the simple CID and activated dissociation product cross sections for ETCF Process. [b]Calculated at the M06/6-311+G(2d,2p)//B3LYP/6-31G* level of theory including ZPE corrections scaled by 0.9804. [c]Also includes BSSE corrections.

Table E.11. Reaction Enthalpies and Free Energies of $M^{2+}(Bpy)_2$ Complexes at 0 and 298 K in kJ/mol.[a]

Complex	Product	ΔH_0	ΔH_0^b	ΔH_{298}^b	ΔG_{298}^b
$Fe^{2+}(Bpy)_2$	$Fe^{+}(Bpy)$	283.3 (8.2)	354.5	356.4	354.4
	$Fe^{2+}(Bpy)$	222.8 (32.4)	526.6	525.4	474.5
$Co^{2+}(Bpy)_2$	$Co^{+}(Bpy)$	263.6 (7.8)	276.8	278.7	275.2
	$Co^{2+}(Bpy)$	225.3 (25.9)	541.7	541.8	485.7
$Ni^{2+}(Bpy)_2$	$Ni^{+}(Bpy)$	258.5 (9.8)	254.4	257.4	256.7
	$Ni^{2+}(Bpy)$	305.9 (30.2)	534.1	534.2	480.5
$Cu^{2+}(Bpy)_2$	$Cu^{+}(Bpy)$	235.8 (8.7)	241.6	244.3	241.8
	$Cu^{2+}(Bpy)$	330.0 (25.8)	512.5	512.4	455.9
$Zn^{2+}(Bpy)_2$	$Zn^{+}(Bpy)$	241.3 (10.1)	315.4	317.3	315.8
	$Zn^{2+}(Bpy)$	231.7 (23.6)	540.9	540.0	487.1

[a]Uncertainties are listed in parentheses. Values obtained from competitive analyses of the simple CID and activated dissociation product cross sections for ETCF process. [b]Values from calculations at the B3LYP/6-311+G(2d,2p) level of theory using B3LYP/6-31G* optimized geometries with frequencies scaled by 0.9804.

Table E.11. (continued) Reaction Enthalpies and Free Energies of $M^{2+}(Bpy)_2$ Complexes at 298 K in kJ/mol.[a]

Complex	Product	ΔH_{298}-ΔH_0[b]	ΔH_{298}	$T\Delta S_{298}$[b]	ΔG_{298}
$Fe^{2+}(Bpy)_2$	$Fe^{+}(Bpy)$	1.9 (0.1)	285.2 (8.2)	2.1 (0.1)	283.2 (8.2)
	$Fe^{2+}(Bpy)$	−1.2 (0.7)	221.6 (32.4)	50.9 (1.4)	170.7 (32.4)
$Co^{2+}(Bpy)_2$	$Co^{+}(Bpy)$	1.9 (0.1)	265.5 (7.8)	3.5 (0.1)	262.0 (7.8)
	$Co^{2+}(Bpy)$	0.1 (0.7)	225.4 (25.9)	56.1 (1.3)	169.3 (25.9)
$Ni^{2+}(Bpy)_2$	$Ni^{+}(Bpy)$	3.0 (0.2)	261.5 (9.8)	0.7 (0.2)	260.8 (9.8)
	$Ni^{2+}(Bpy)$	0.1 (0.7)	306.0 (30.2)	53.7 (1.3)	252.3 (30.2)
$Cu^{2+}(Bpy)_2$	$Cu^{+}(Bpy)$	2.7 (0.1)	238.5 (8.7)	2.5 (0.1)	236.0 (8.7)
	$Cu^{2+}(Bpy)$	−0.10 (0.6)	329.9 (25.8)	56.5 (1.2)	273.4 (25.8)
$Zn^{2+}(Bpy)_2$	$Zn^{+}(Bpy)$	1.9 (0.1)	243.2 (10.1)	1.5 (0.1)	241.7 (10.1)
	$Zn^{2+}(Bpy)$	−0.9 (0.7)	230.8 (23.6)	52.9 (1.4)	177.9 (23.7)

[a]Uncertainties are listed in parentheses. Values obtained from competitive analyses of the simple CID and activated dissociation product cross sections for ETCF process. [b]Values from calculations at the B3LYP/6-311+G(2d,2p) level of theory using B3LYP/6-31G* optimized geometries with frequencies scaled by 0.9804.

E.12 Figure Captions and Figures

Figure E.1. Cross sections for collision-induced dissociation of the $M^{2+}(Bpy)_2$ complexes with Xe as a function of kinetic energy in the center-of-mass frame (lower *x*-axis) and laboratory frame (upper *x*-axis), where M^{2+} = Fe^{2+}, Co^{2+}, Ni^{2+}, Cu^{2+}, and Zn^{2+}, parts a–e, respectively. Data are shown for a Xe pressure of ~0.2 mTorr. Product cross sections for $M^{+}(Bpy)$ (red), $M^{2+}(Bpy)$ (green), and $[M(Bpy)_2–Pyr]^{2+}$ (black).

Figure E.2. MS spectra of fragmentation of $M^{2+}(Bpy)_2$ complexes, where M^{2+} = Fe^{2+}, Co^{2+}, Ni^{2+}, Cu^{2+}, and Zn^{2+}, parts a–e, respectively.

Figure E.3. Potential energy landscape at 0 K for ETCF of the $M^{2+}(Bpy)_2$ complexes leading to the transfer of an electron from the Bpy ligand to the $M^{2+}(Bpy)$ moiety and dissociation, where M^{2+} = Fe^{2+}, Co^{2+}, Ni^{2+}, Cu^{2+}, and Zn^{2+}, parts a–e, respectively. Also shown is the energy barrier for simple CID pathway. Energies are relative to the $M^{2+}(Bpy)_2$ reactants, and are taken from theoretical calculations at the B3LYP/6-311+G(2d,2p) (red), BHandHLYP/6-311+G(2d,2p) (blue), and M06/6-311+G(2d,2p) (green) levels of theory using the B3LYP/6-31G* optimized geometries and including ZPE corrections.

Figure E.4. Potential energy landscape at 0 K for PTCF of the $M^{2+}(Bpy)_2$ complexes leading to the transfer of a proton from one Bpy ligand to the other Bpy ligand of the $M^{2+}(Bpy)_2$ reactant, where M^{2+} = Fe^{2+}, Co^{2+}, Ni^{2+}, Cu^{2+}, and Zn^{2+}, parts a–e, respectively. Energies are relative to the $M^{2+}(Bpy)_2$ reactants, and are taken from theoretical calculations at the B3LYP/6-311+G(2d,2p) (red), BHandHLYP/6-311+G(2d,2p) (blue), and M06/6-311+G(2d,2p) (green) levels of theory using the B3LYP/6-31G* optimized geometries and including ZPE corrections.

Figure E.5. Zero-pressure-extrapolated cross sections for collision-induced dissociation of the $M^{2+}(Bpy)_2$ complexes, where M^{2+} = Fe^{2+}, Co^{2+}, Ni^{2+}, Cu^{2+}, and Zn^{2+} with Xe in the threshold region as a function of kinetic energy in the center-of-mass frame (lower *x*-axis) and laboratory frame (upper *x*-axis). Parts a, c, e, g, and i, show fits for $M^{2+}(Bpy)$ product cross sections whereas parts b, d, f, h, and j show fits for $M^{+}(Bpy)$ product cross section. Solid lines show the best fits to the data using eq. 2.4 convoluted over the neutral and ion kinetic and internal energy distributions. The dotted lines show the model cross sections in the absence of experimental kinetic energy broadening for reactants with an internal energy corresponding to 0 K.

Figure E.6. Zero-pressure-extrapolated M^+(Bpy) and M^{2+}(Bpy) product cross sections for collision-induced dissociation of the $M^{2+}(Bpy)_2$ complexes, where M^{2+} = Fe^{2+}, Co^{2+}, Ni^{2+}, Cu^{2+}, and Zn^{2+}, parts a–e, respectively, with Xe in the threshold region as a function of kinetic energy in the center-of-mass frame (lower *x*-axis) and laboratory frame (upper *x*-axis). Solid lines show the best fits to the data using eq. 2.5 convoluted over the neutral and ion kinetic and internal energy distributions. The dotted lines show the model cross sections in the absence of experimental kinetic energy broadening for reactants with an internal energy corresponding to 0 K.

Figure E.7. Comparison of theoretical and TCID measured ETCF AEs (part a) and $(N\text{-}L)M^{2+}$–$(N\text{-}L)$ BDEs (part b) of the $M^{2+}(N\text{-}L)_2$ complexes, where M^{2+} = Fe^{2+}, Co^{2+}, Ni^{2+}, Cu^{2+}, and Zn^{2+}, and *N*-*L* = Bpy and Phen at 0 K in kJ/mol. Values obtained from competitive analyses of the $M^+(N\text{-}L)$ and $M^{2+}(N\text{-}L)$ product cross sections.

Figure E.1.

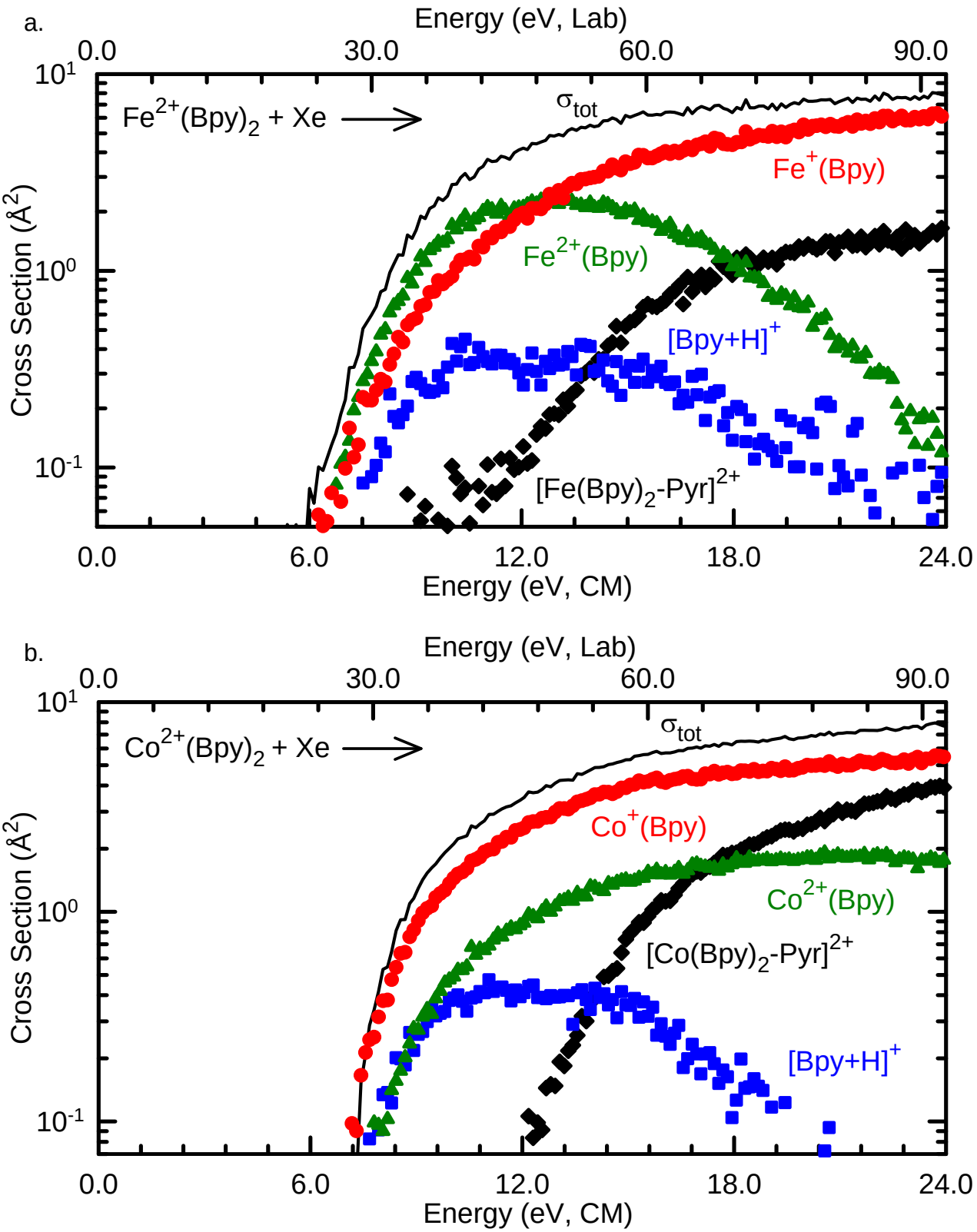
a.
Energy (eV, Lab)
0.0
30.0
60.0
90.0
10^1
10^0
10^{-1}
Cross Section (Å^2)
$Fe^{2+}(Bpy)_2$ + Xe
σ_{tot}
$Fe^+(Bpy)$
$Fe^{2+}(Bpy)$
$[Bpy+H]^+$
$[Fe(Bpy)_2\text{-}Pyr]^{2+}$
0.0
6.0
12.0
18.0
24.0
Energy (eV, CM)
b.
Energy (eV, Lab)
0.0
30.0
60.0
90.0
10^1
10^0
10^{-1}
Cross Section (Å^2)
$Co^{2+}(Bpy)_2$ + Xe
σ_{tot}
$Co^+(Bpy)$
$Co^{2+}(Bpy)$
$[Co(Bpy)_2\text{-}Pyr]^{2+}$
$[Bpy+H]^+$
0.0
6.0
12.0
18.0
24.0
Energy (eV, CM)

Figure E.1.

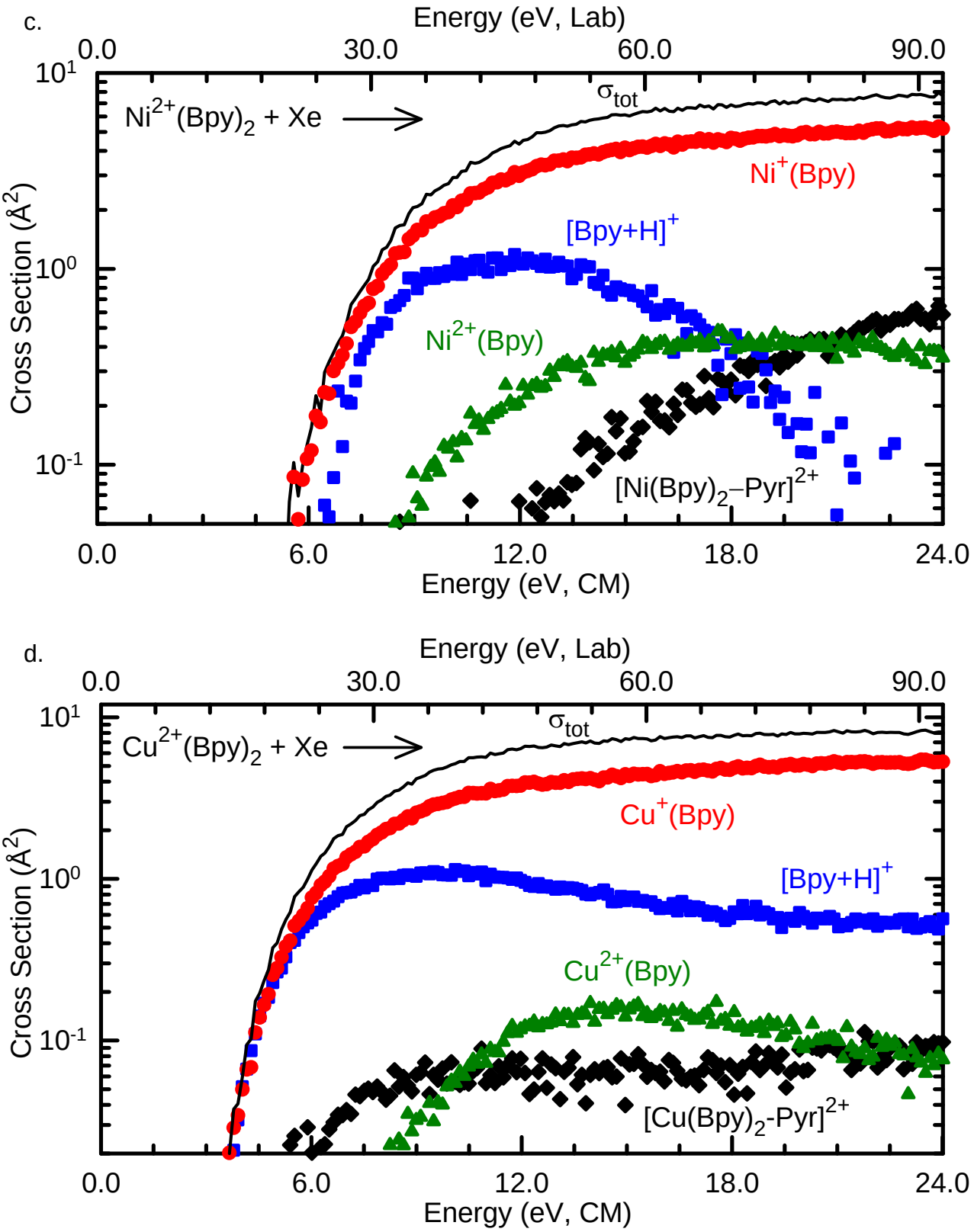
c.
Energy (eV, Lab)
0.0
30.0
60.0
90.0
10^1
10^0
10^{-1}
Cross Section (Å^2)
$Ni^{2+}(Bpy)_2$ + Xe
σ_{tot}
$Ni^+(Bpy)$
$[Bpy+H]^+$
$Ni^{2+}(Bpy)$
$[Ni(Bpy)_2–Pyr]^{2+}$
0.0
6.0
12.0
18.0
24.0
Energy (eV, CM)
d.
Energy (eV, Lab)
0.0
30.0
60.0
90.0
10^1
10^0
10^{-1}
Cross Section (Å^2)
$Cu^{2+}(Bpy)_2$ + Xe
σ_{tot}
$Cu^+(Bpy)$
$[Bpy+H]^+$
$Cu^{2+}(Bpy)$
$[Cu(Bpy)_2$-Pyr$]^{2+}$
0.0
6.0
12.0
18.0
24.0
Energy (eV, CM)

Figure E.1.

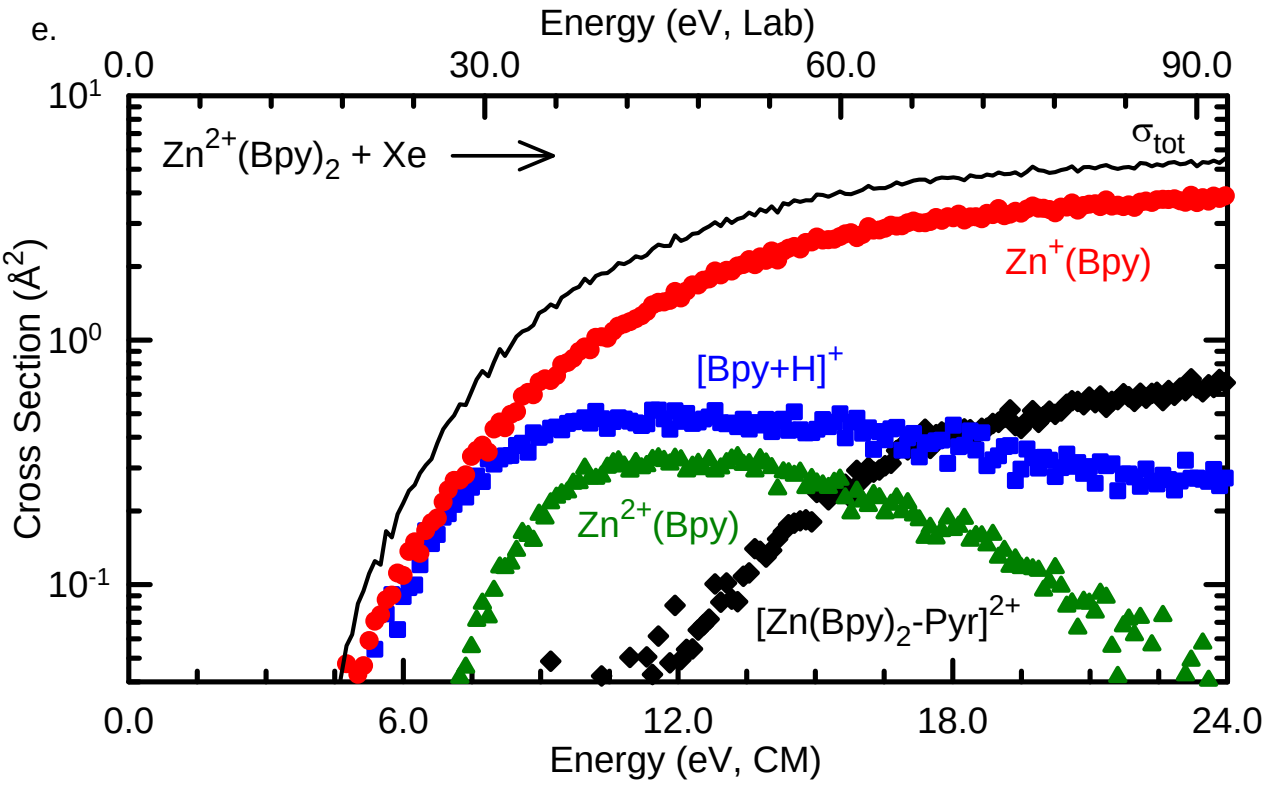
e.
Energy (eV, Lab)
0.0
30.0
60.0
90.0
10^1
10^0
10^{-1}
Cross Section (Å^2)
$Zn^{2+}(Bpy)_2$ + Xe
σ_{tot}
$Zn^+(Bpy)$
$[Bpy+H]^+$
$Zn^{2+}(Bpy)$
$[Zn(Bpy)_2\text{-}Pyr]^{2+}$
0.0
6.0
12.0
18.0
24.0
Energy (eV, CM)

Figure E.2.

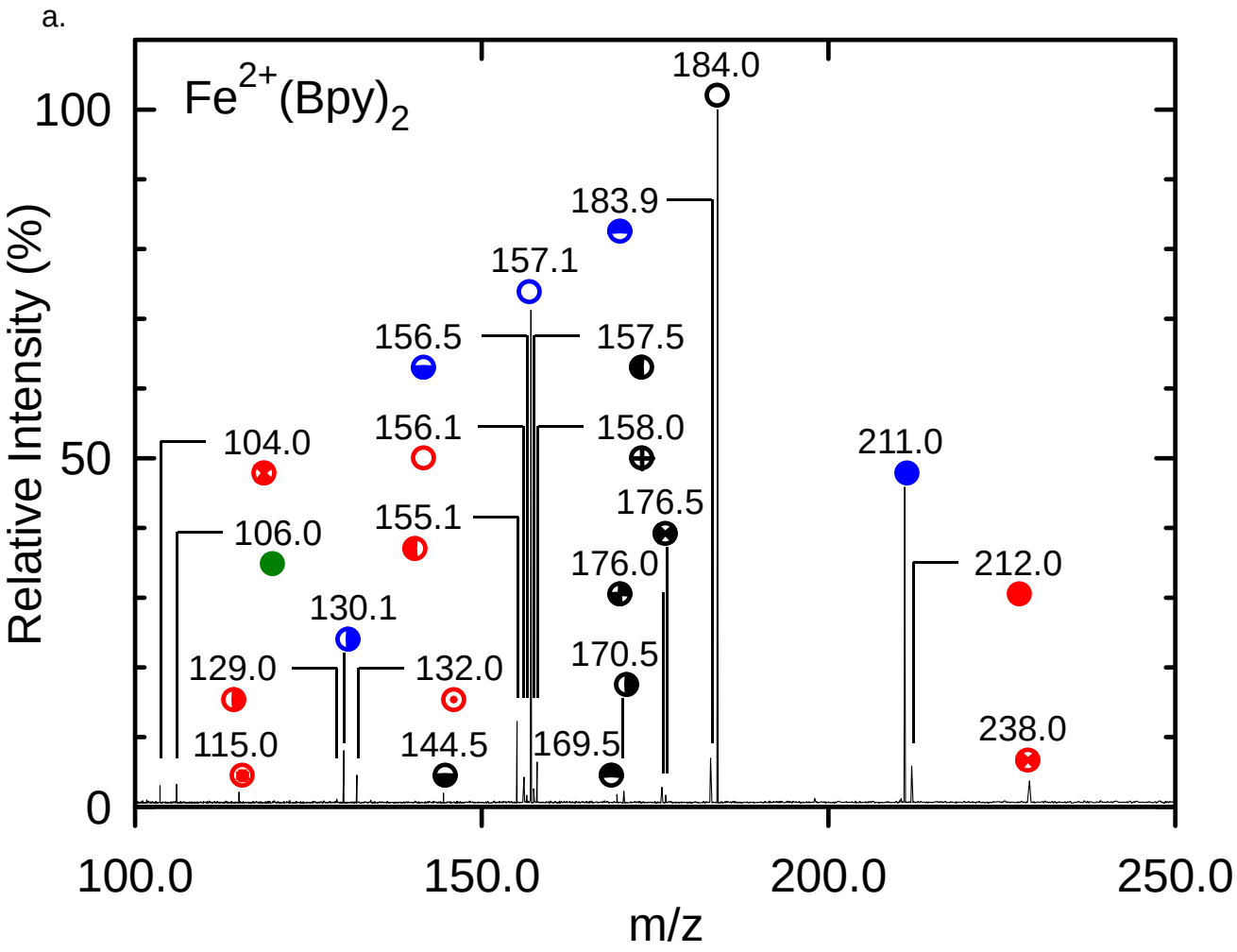

Legend

$Fe^{2+}(Bpy)_2 + Ar \rightarrow Fe^{2+}(Bpy) + Bpy + Ar$ E.1

$Fe^{2+}(Bpy)_2 + Ar \rightarrow Fe^{+}(Bpy) + Bpy^{+} + Ar$ E.2

$Fe^{2+}(Bpy)_2 + Ar \rightarrow [Fe(Bpy\text{-}H)]^{+} + [Bpy+H]^{+} + Ar$ E.3

$Fe^{2+}(Bpy)_2 + Ar \rightarrow [Fe(Bpy)_2\text{–}H_2]^{2+} + H_2 + Ar$ E.4

Figure E.2.

a.

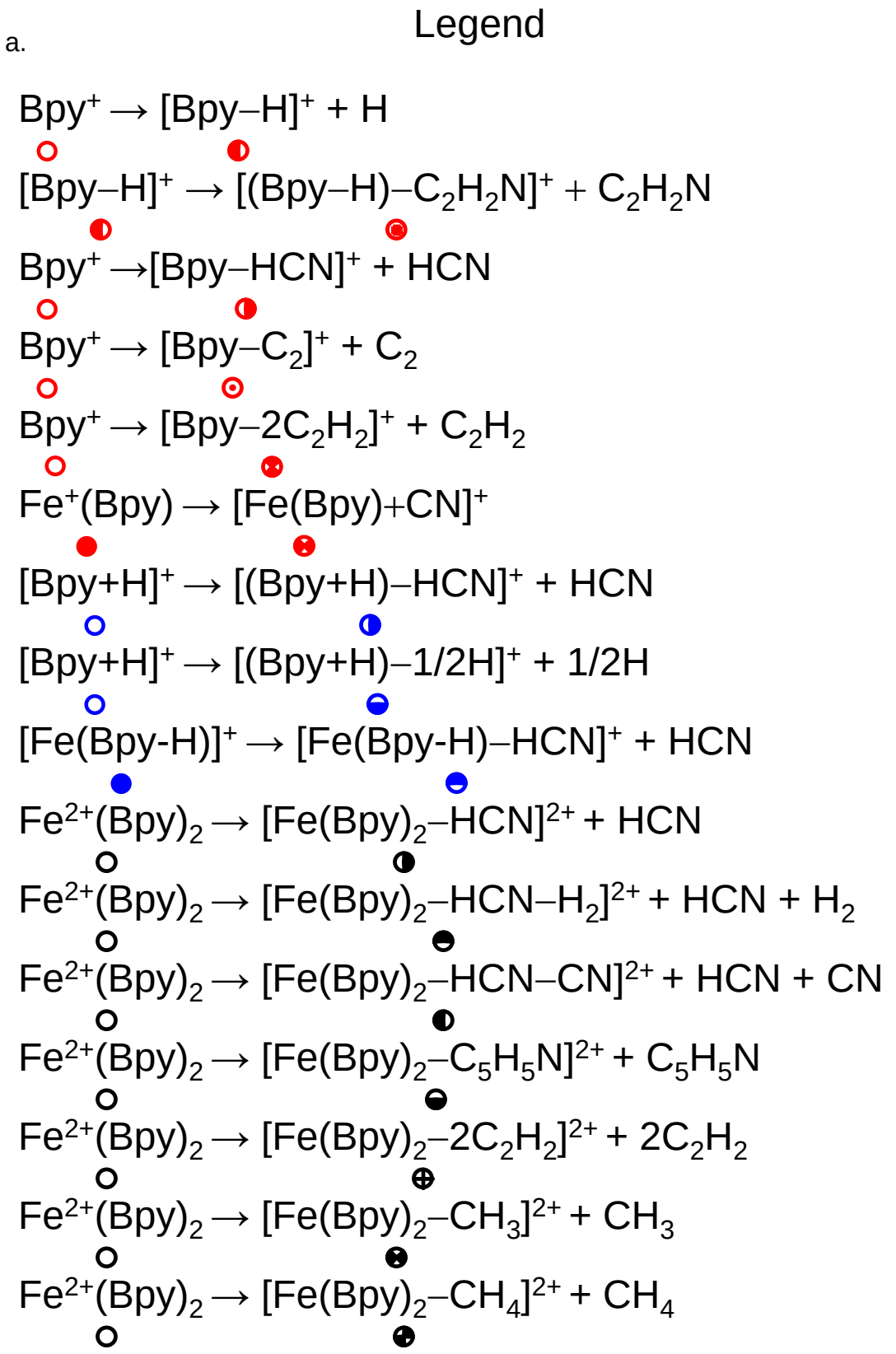
Legend
Bpy+ → [Bpy–H]+ + H
[Bpy–H]+ → [(Bpy–H)–C2H2N]+ + C2H2N
Bpy+ →[Bpy–HCN]+ + HCN
Bpy+ → [Bpy–C2]+ + C2
Bpy+ → [Bpy–2C2H2]+ + C2H2
Fe+(Bpy) → [Fe(Bpy)+CN]+
[Bpy+H]+ → [(Bpy+H)–HCN]+ + HCN
[Bpy+H]+ → [(Bpy+H)–1/2H]+ + 1/2H
[Fe(Bpy-H)]+ → [Fe(Bpy-H)–HCN]+ + HCN
Fe2+(Bpy)2 → [Fe(Bpy)2–HCN]2+ + HCN
Fe2+(Bpy)2 → [Fe(Bpy)2–HCN–H2]2+ + HCN + H2
Fe2+(Bpy)2 → [Fe(Bpy)2–HCN–CN]2+ + HCN + CN
Fe2+(Bpy)2 → [Fe(Bpy)2–C5H5N]2+ + C5H5N
Fe2+(Bpy)2 → [Fe(Bpy)2–2C2H2]2+ + 2C2H2
Fe2+(Bpy)2 → [Fe(Bpy)2–CH3]2+ + CH3
Fe2+(Bpy)2 → [Fe(Bpy)2–CH4]2+ + CH4

Figure E.2.

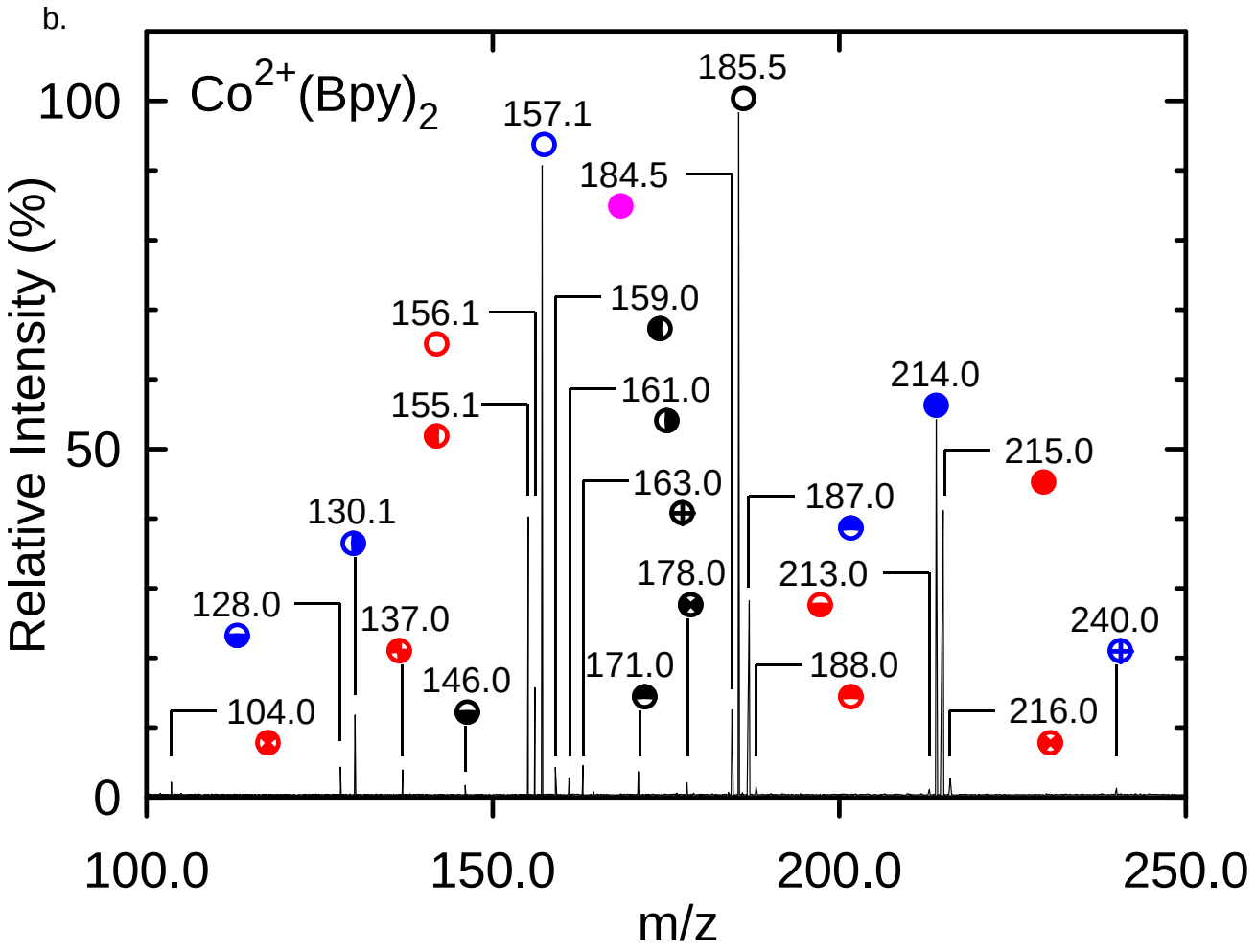

Legend

$Co^{2+}(Bpy)_2 + Ar \rightarrow Co^{2+}(Bpy) + Bpy + Ar$ E.1

$Co^{2+}(Bpy)_2 + Ar \rightarrow Co^{+}(Bpy) + Bpy^{+} + Ar$ E.2

$Co^{2+}(Bpy)_2 + Ar \rightarrow [Co(Bpy\text{-}H)]^{+} + [Bpy+H]^{+} + Ar$ E.3

$Co^{2+}(Bpy)_2 + Ar \rightarrow [Co(Bpy)_2\text{–}H_2]^{2+} + H_2 + Ar$ E.4

Figure E.2.

b.

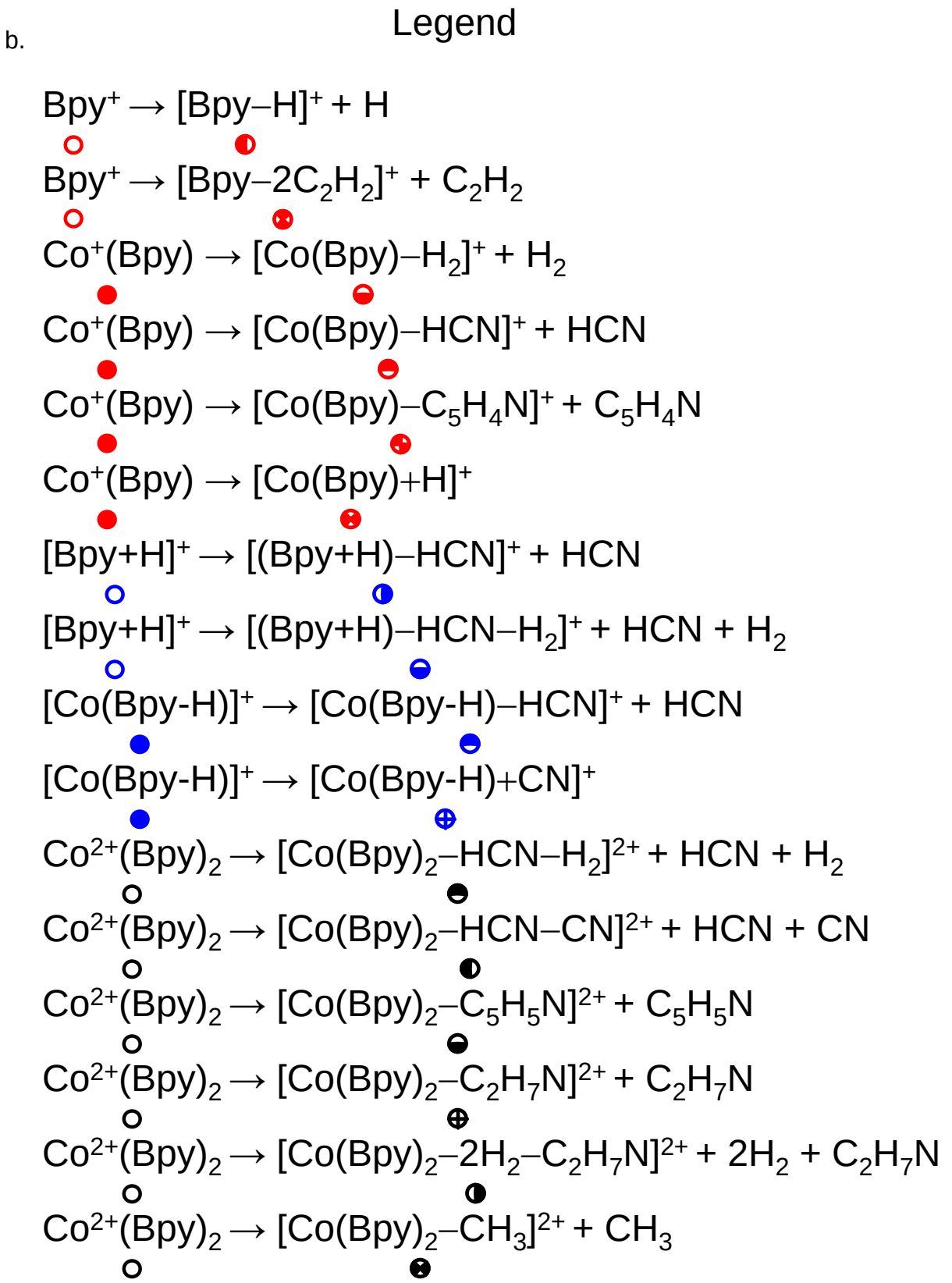
Legend
Bpy+ → [Bpy–H]+ + H
Bpy+ → [Bpy–2C2H2]+ + C2H2
Co+(Bpy) → [Co(Bpy)–H2]+ + H2
Co+(Bpy) → [Co(Bpy)–HCN]+ + HCN
Co+(Bpy) → [Co(Bpy)–C5H4N]+ + C5H4N
Co+(Bpy) → [Co(Bpy)+H]+
[Bpy+H]+ → [(Bpy+H)–HCN]+ + HCN
[Bpy+H]+ → [(Bpy+H)–HCN–H2]+ + HCN + H2
[Co(Bpy-H)]+ → [Co(Bpy-H)–HCN]+ + HCN
[Co(Bpy-H)]+ → [Co(Bpy-H)+CN]+
Co2+(Bpy)2 → [Co(Bpy)2–HCN–H2]2+ + HCN + H2
Co2+(Bpy)2 → [Co(Bpy)2–HCN–CN]2+ + HCN + CN
Co2+(Bpy)2 → [Co(Bpy)2–C5H5N]2+ + C5H5N
Co2+(Bpy)2 → [Co(Bpy)2–C2H7N]2+ + C2H7N
Co2+(Bpy)2 → [Co(Bpy)2–2H2–C2H7N]2+ + 2H2 + C2H7N
Co2+(Bpy)2 → [Co(Bpy)2–CH3]2+ + CH3

Figure E.2.

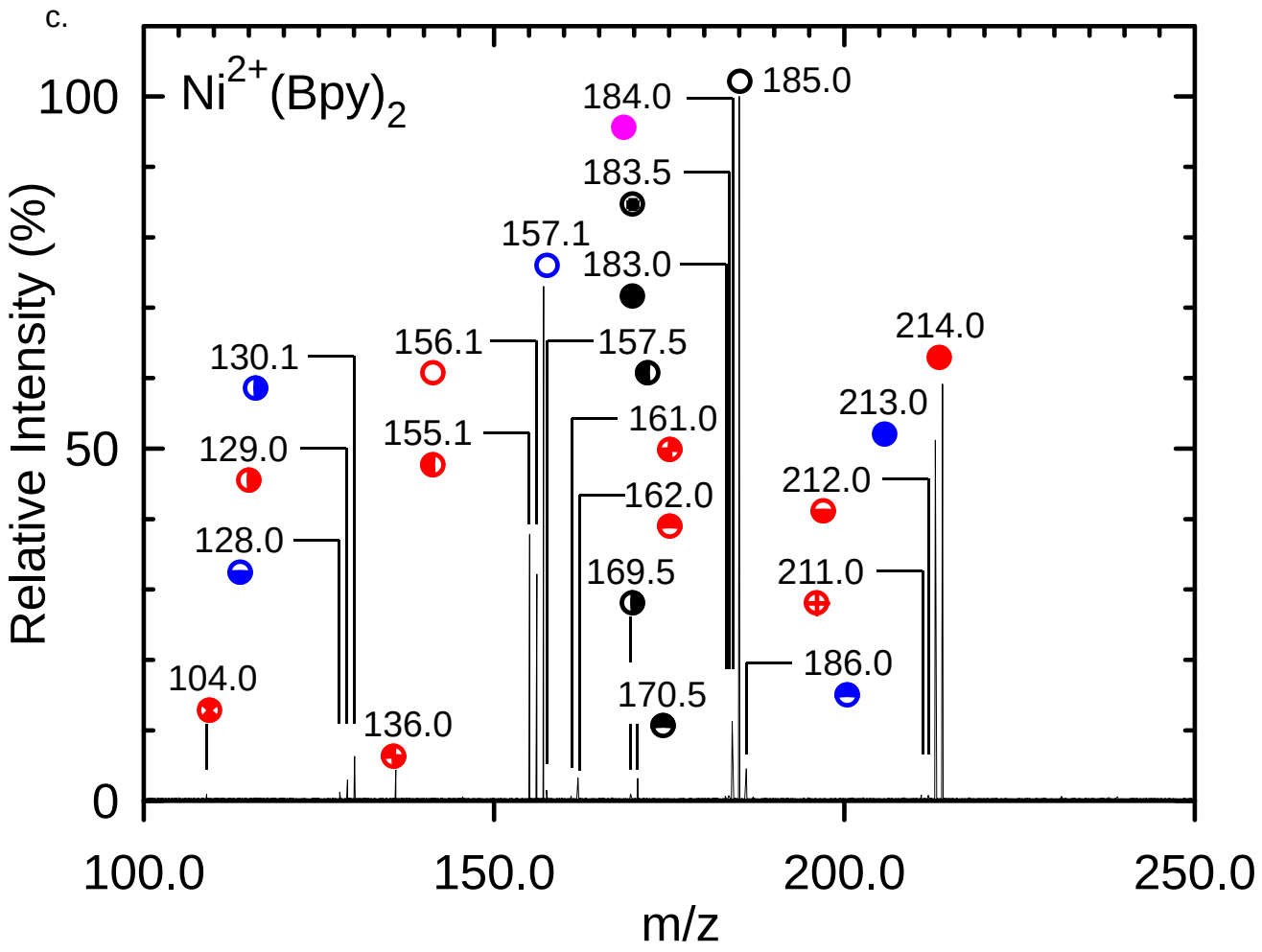

Legend

$Ni^{2+}(Bpy)_2 + Ar \rightarrow Ni^{2+}(Bpy) + Bpy + Ar$ E.1

$Ni^{2+}(Bpy)_2 + Ar \rightarrow Ni^{+}(Bpy) + Bpy^{+} + Ar$ E.2

$Ni^{2+}(Bpy)_2 + Ar \rightarrow [Ni(Bpy\text{-}H)]^{+} + [Bpy+H]^{+} + Ar$ E.3

$Ni^{2+}(Bpy)_2 + Ar \rightarrow [Ni(Bpy)_2\text{–}H_2]^{2+} + H_2 + Ar$ E.4

Figure E.2.

c.

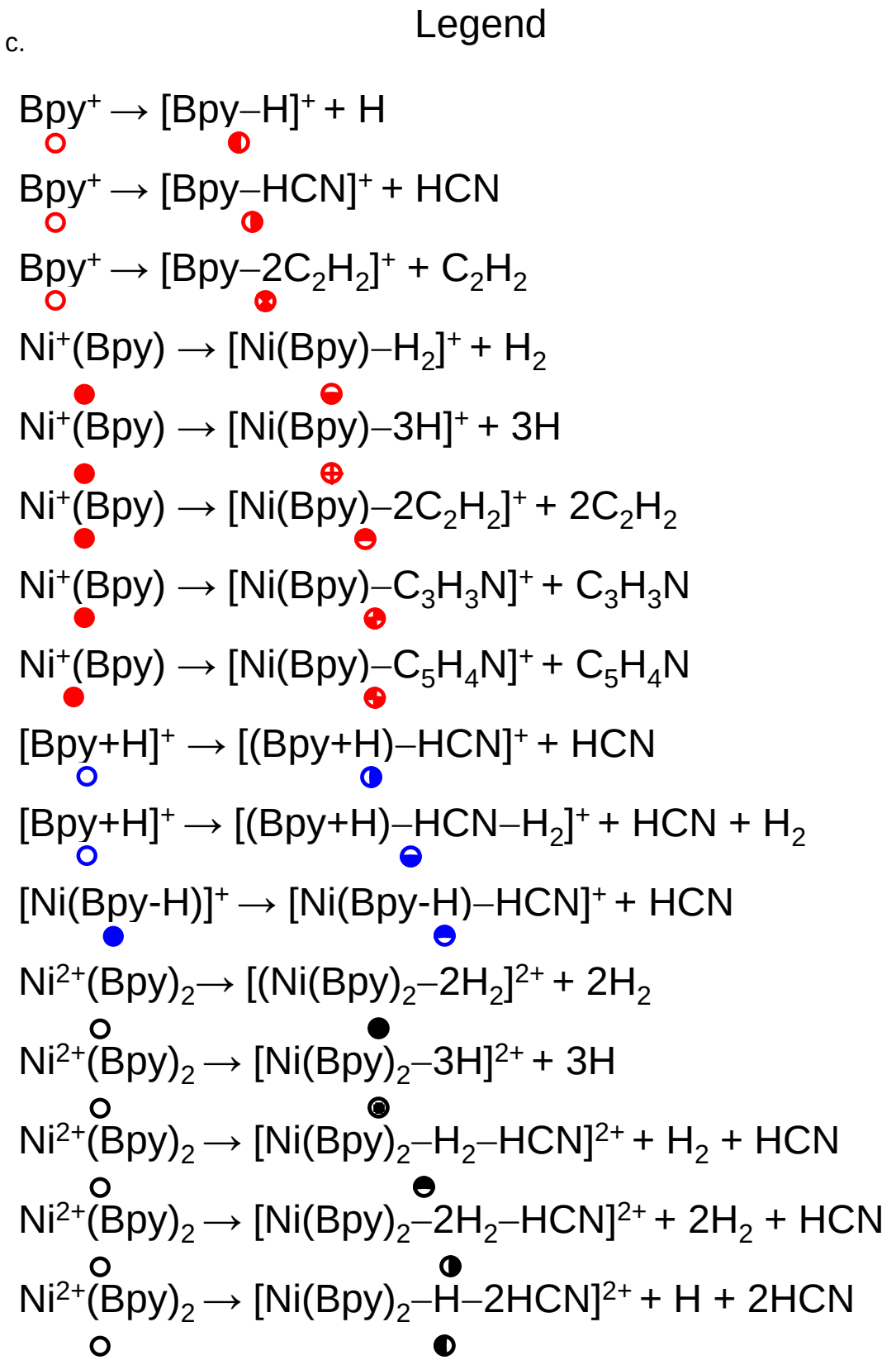
Legend
Bpy+ → [Bpy–H]+ + H
Bpy+ → [Bpy–HCN]+ + HCN
Bpy+ → [Bpy–2C2H2]+ + C2H2
Ni+(Bpy) → [Ni(Bpy)–H2]+ + H2
Ni+(Bpy) → [Ni(Bpy)–3H]+ + 3H
Ni+(Bpy) → [Ni(Bpy)–2C2H2]+ + 2C2H2
Ni+(Bpy) → [Ni(Bpy)–C3H3N]+ + C3H3N
Ni+(Bpy) → [Ni(Bpy)–C5H4N]+ + C5H4N
[Bpy+H]+ → [(Bpy+H)–HCN]+ + HCN
[Bpy+H]+ → [(Bpy+H)–HCN–H2]+ + HCN + H2
[Ni(Bpy-H)]+ → [Ni(Bpy-H)–HCN]+ + HCN
Ni2+(Bpy)2→ [(Ni(Bpy)2–2H2]2+ + 2H2
Ni2+(Bpy)2 → [Ni(Bpy)2–3H]2+ + 3H
Ni2+(Bpy)2 → [Ni(Bpy)2–H2–HCN]2+ + H2 + HCN
Ni2+(Bpy)2 → [Ni(Bpy)2–2H2–HCN]2+ + 2H2 + HCN
Ni2+(Bpy)2 → [Ni(Bpy)2–H–2HCN]2+ + H + 2HCN

Figure E.2.

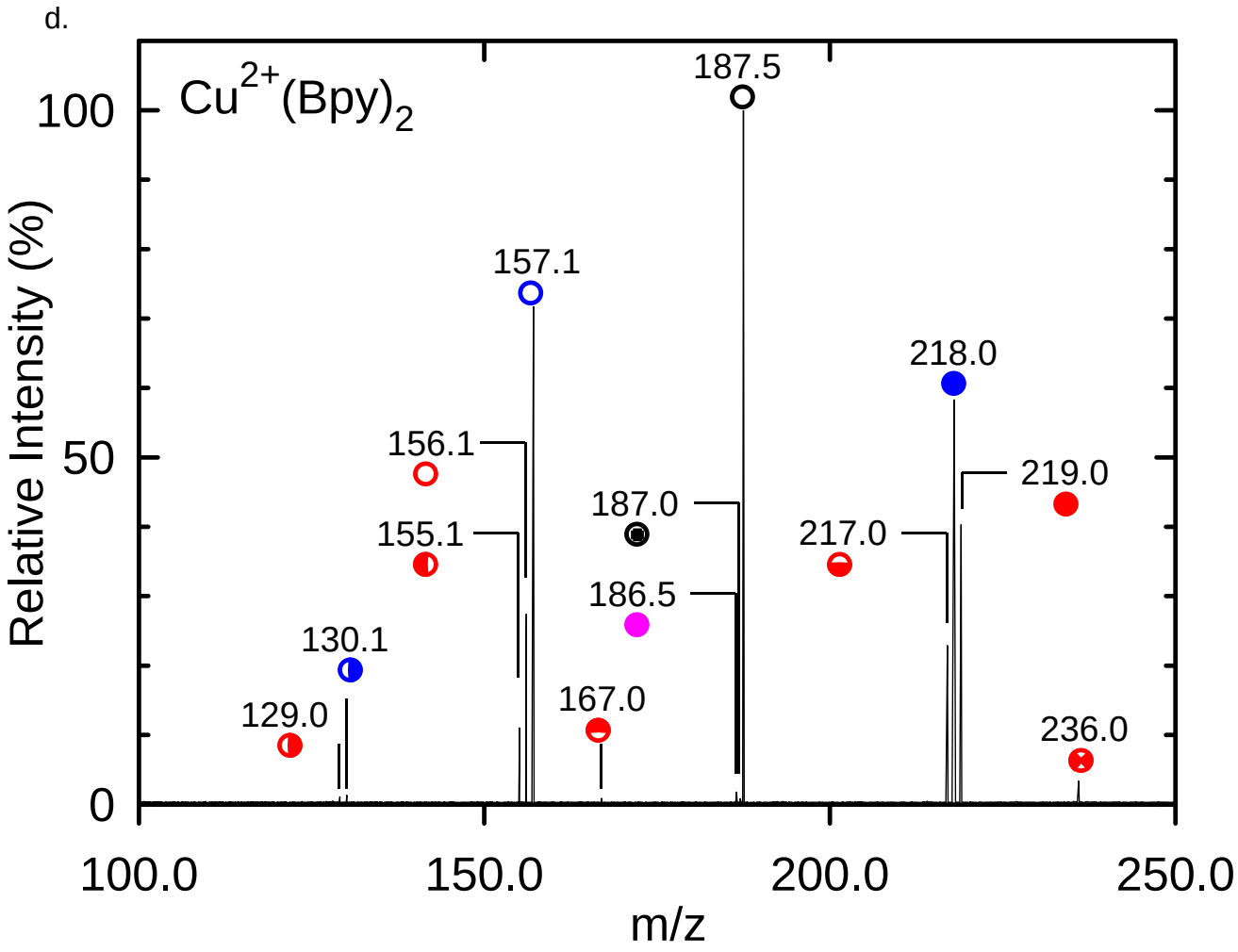
d.
Cu2+(Bpy)2
187.5
157.1
218.0
156.1
219.0
187.0
155.1
217.0
186.5
130.1
167.0
129.0
236.0
Relative Intensity (%)
100
50
0
100.0
150.0
200.0
250.0
m/z

Figure E.2.

d.

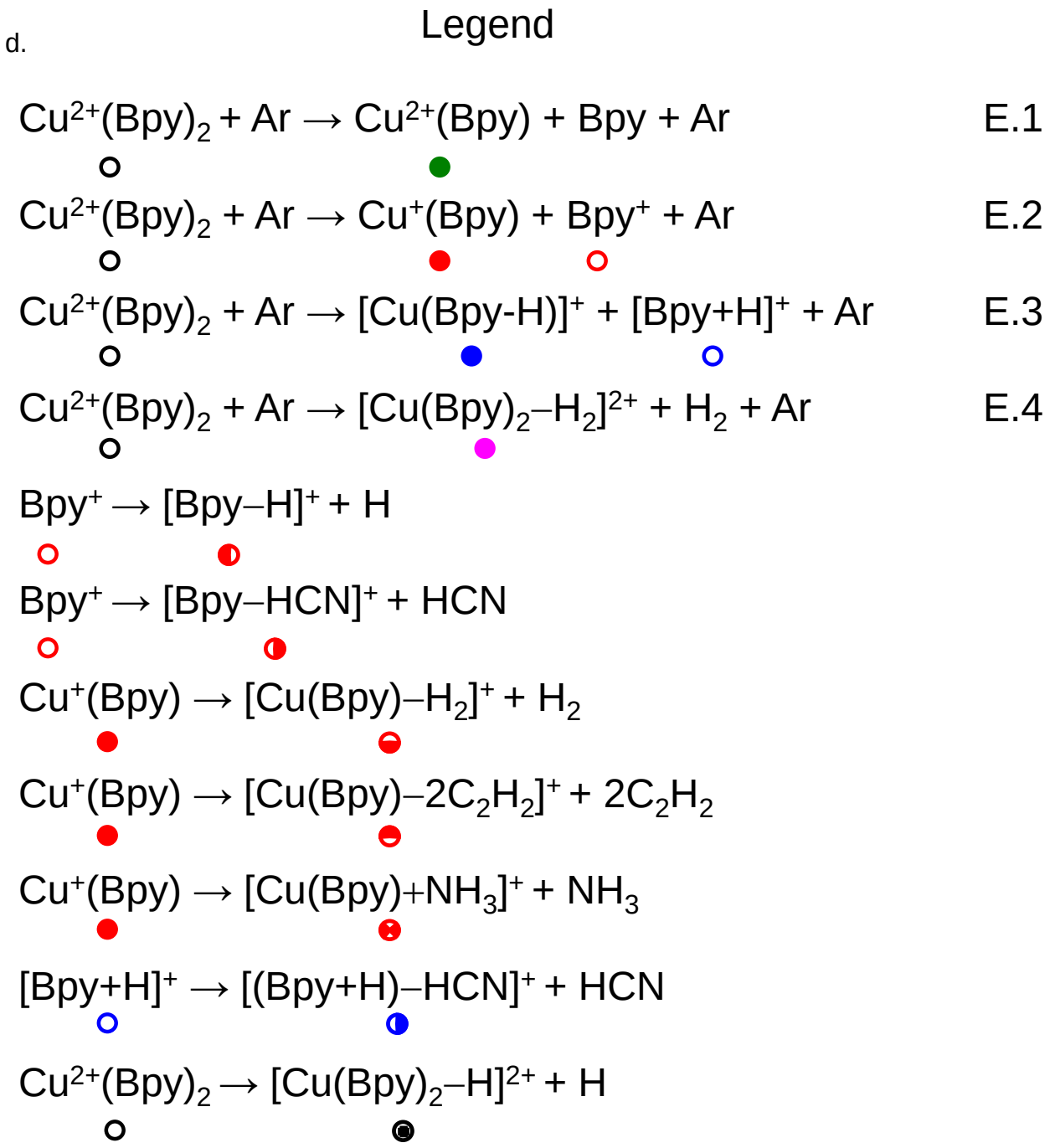
Legend
Cu2+(Bpy)2 + Ar → Cu2+(Bpy) + Bpy + Ar
E.1
Cu2+(Bpy)2 + Ar → Cu+(Bpy) + Bpy+ + Ar
E.2
Cu2+(Bpy)2 + Ar → [Cu(Bpy-H)]+ + [Bpy+H]+ + Ar
E.3
Cu2+(Bpy)2 + Ar → [Cu(Bpy)2–H2]2+ + H2 + Ar
E.4
Bpy+ → [Bpy–H]+ + H
Bpy+ → [Bpy–HCN]+ + HCN
Cu+(Bpy) → [Cu(Bpy)–H2]+ + H2
Cu+(Bpy) → [Cu(Bpy)–2C2H2]+ + 2C2H2
Cu+(Bpy) → [Cu(Bpy)+NH3]+ + NH3
[Bpy+H]+ → [(Bpy+H)–HCN]+ + HCN
Cu2+(Bpy)2 → [Cu(Bpy)2–H]2+ + H

Figure E.2.

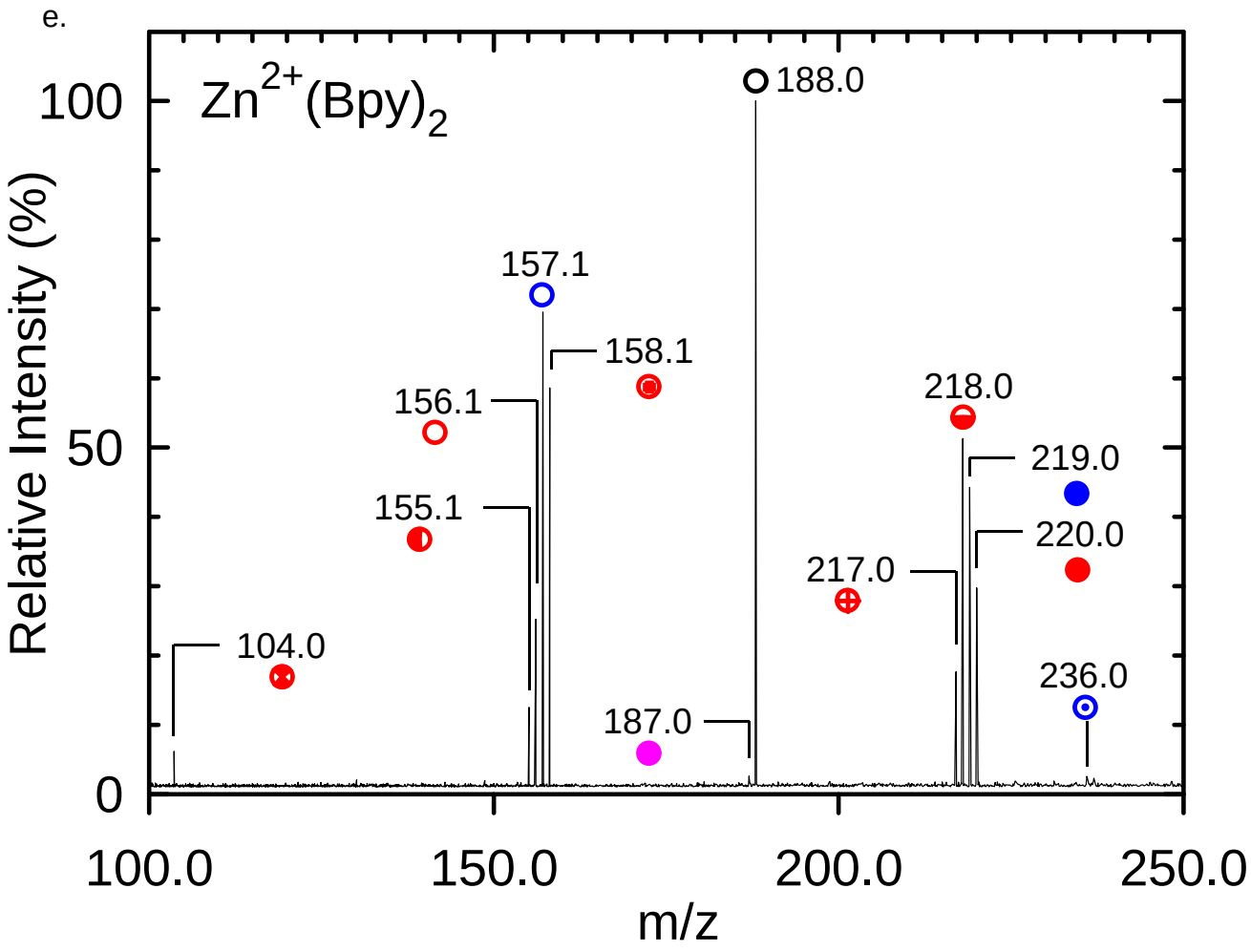
e.
$Zn^{2+}(Bpy)_2$
188.0
157.1
158.1
156.1
218.0
219.0
155.1
220.0
217.0
104.0
236.0
187.0
Relative Intensity (%)
100
50
0
100.0
150.0
200.0
250.0
m/z

Figure E.2.

e.

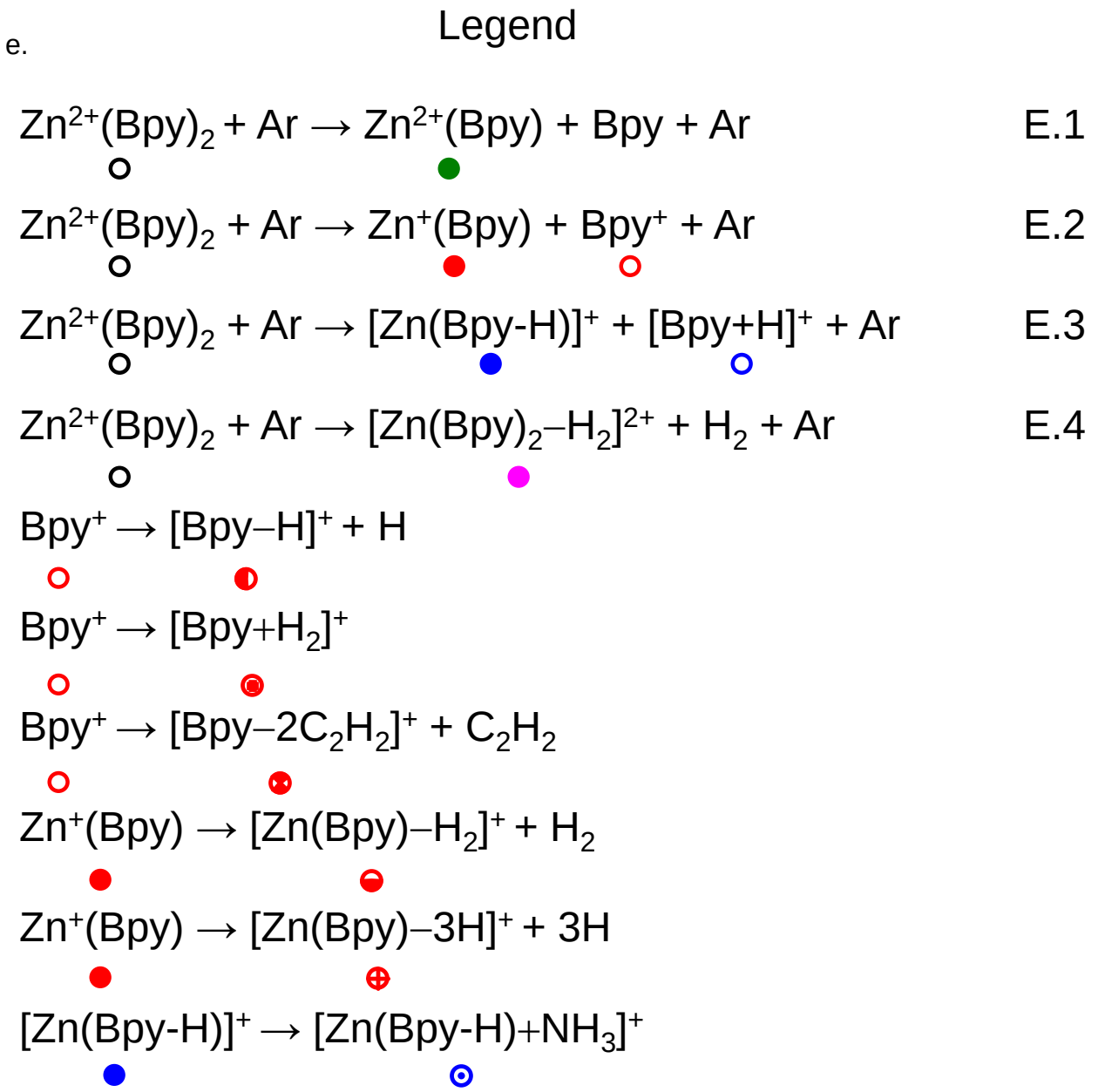
Legend
$Zn^{2+}(Bpy)_2 + Ar \rightarrow Zn^{2+}(Bpy) + Bpy + Ar$ E.1
$Zn^{2+}(Bpy)_2 + Ar \rightarrow Zn^{+}(Bpy) + Bpy^{+} + Ar$ E.2
$Zn^{2+}(Bpy)_2 + Ar \rightarrow [Zn(Bpy\text{-}H)]^{+} + [Bpy{+}H]^{+} + Ar$ E.3
$Zn^{2+}(Bpy)_2 + Ar \rightarrow [Zn(Bpy)_2{-}H_2]^{2+} + H_2 + Ar$ E.4
$Bpy^{+} \rightarrow [Bpy{-}H]^{+} + H$
$Bpy^{+} \rightarrow [Bpy{+}H_2]^{+}$
$Bpy^{+} \rightarrow [Bpy{-}2C_2H_2]^{+} + C_2H_2$
$Zn^{+}(Bpy) \rightarrow [Zn(Bpy){-}H_2]^{+} + H_2$
$Zn^{+}(Bpy) \rightarrow [Zn(Bpy){-}3H]^{+} + 3H$
$[Zn(Bpy\text{-}H)]^{+} \rightarrow [Zn(Bpy\text{-}H){+}NH_3]^{+}$

Figure E.3.

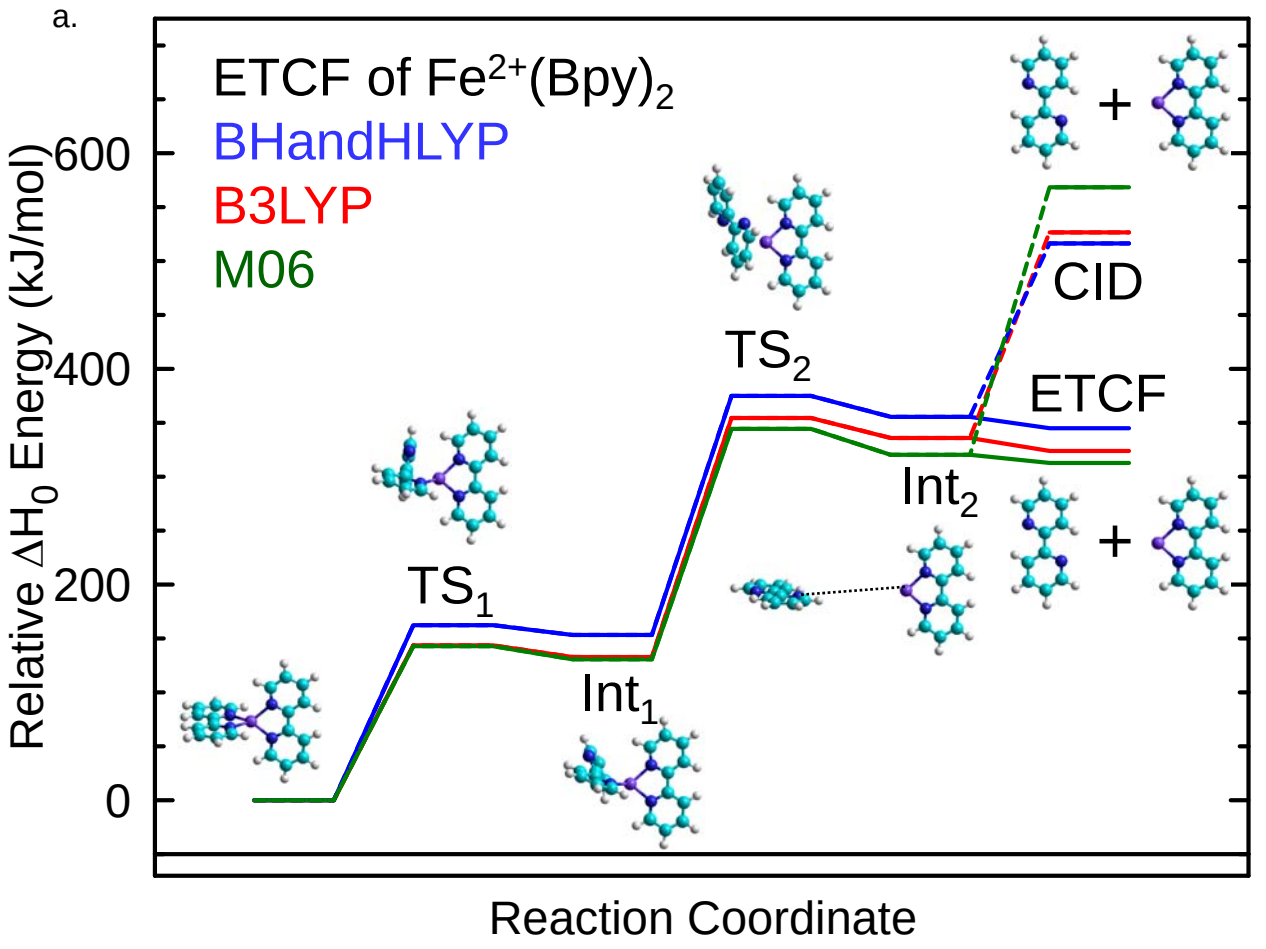
a.
ETCF of Fe2+(Bpy)2
BHandHLYP
B3LYP
M06
Relative ΔH0 Energy (kJ/mol)
600
400
200
0
TS1
Int1
TS2
Int2
CID
ETCF
+
+
Reaction Coordinate

Figure E.3.

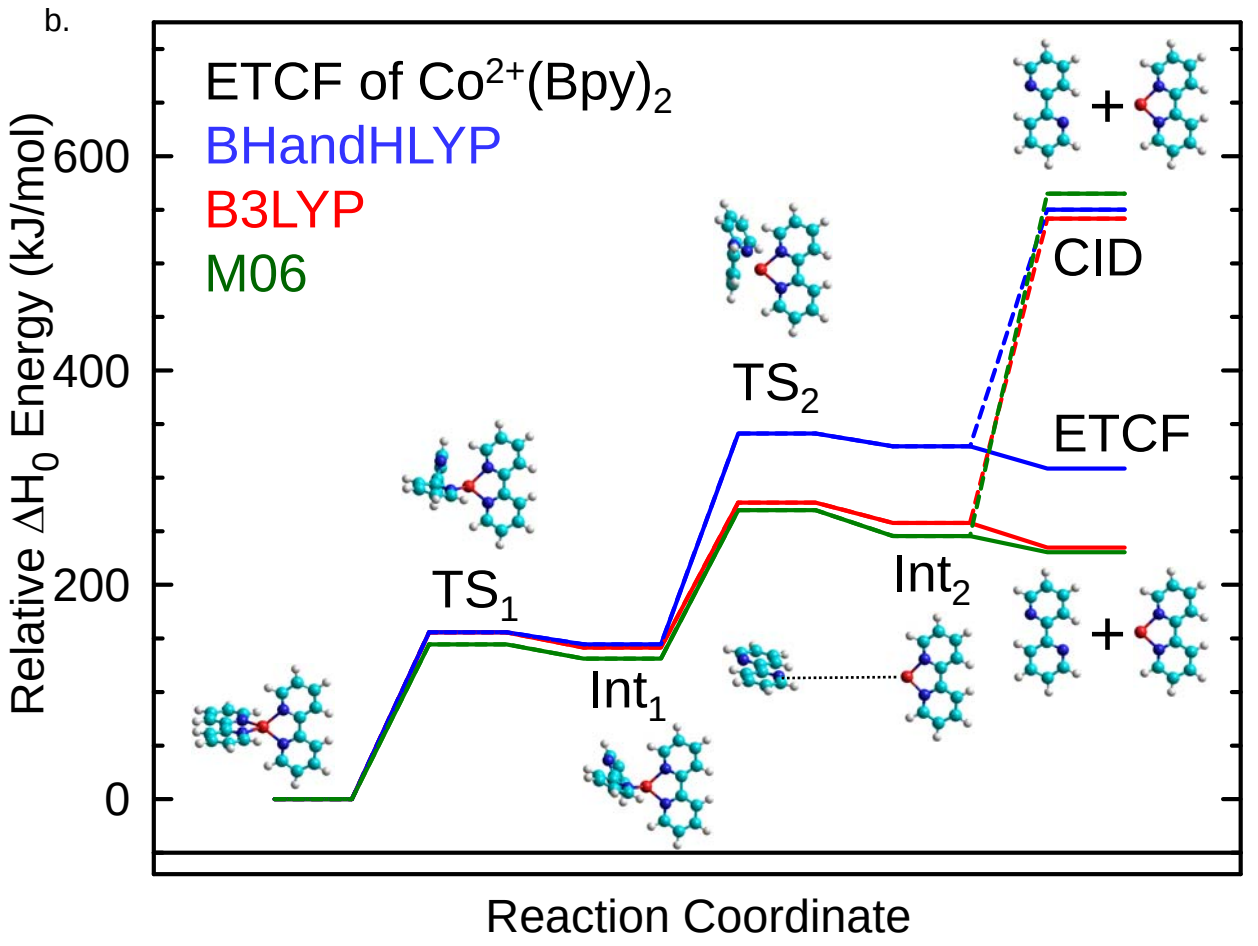
b.
ETCF of $Co^{2+}(Bpy)_2$
BHandHLYP
B3LYP
M06
Relative ΔH_0 Energy (kJ/mol)
600
400
200
0
TS_1
Int_1
TS_2
Int_2
CID
ETCF
+
+
Reaction Coordinate

Figure E.3.

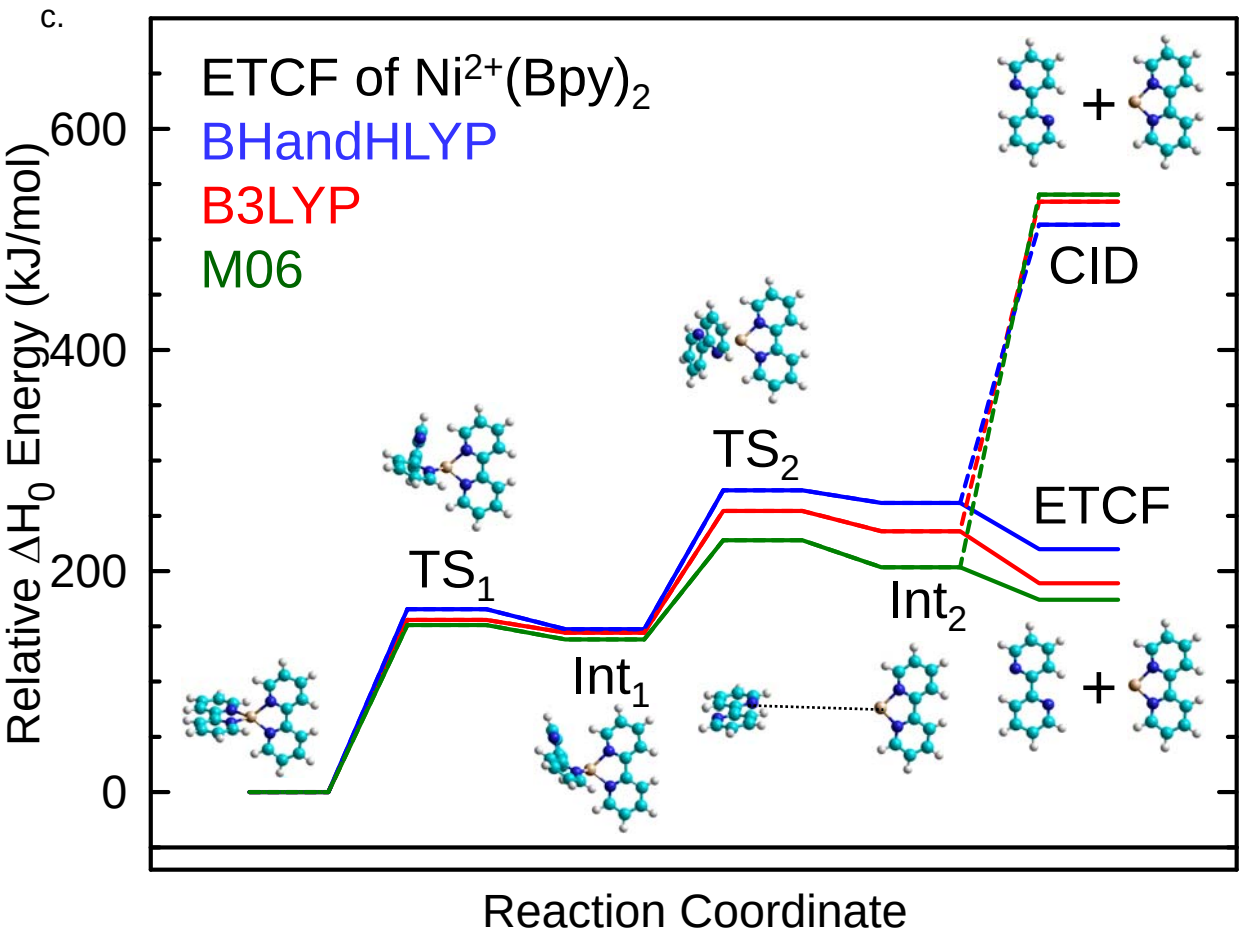
c.
ETCF of Ni2+(Bpy)2
BHandHLYP
B3LYP
M06
Relative ΔH0 Energy (kJ/mol)
600
400
200
0
TS1
Int1
TS2
Int2
CID
ETCF
+
+
Reaction Coordinate

Figure E.3.

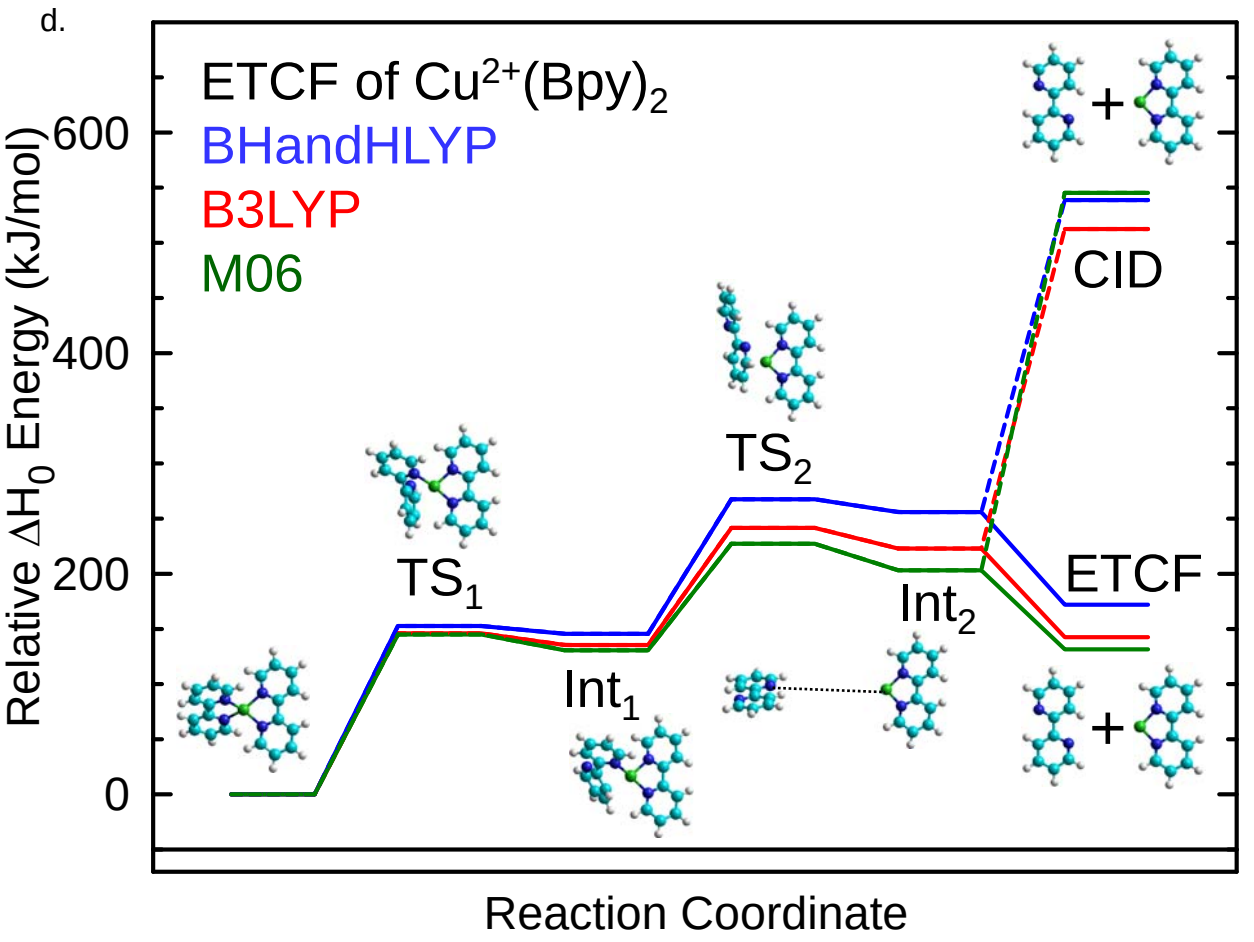
d.
ETCF of Cu2+(Bpy)2
BHandHLYP
B3LYP
M06
Relative ΔH0 Energy (kJ/mol)
600
400
200
0
TS1
TS2
Int1
Int2
CID
ETCF
Reaction Coordinate

Figure E.3.

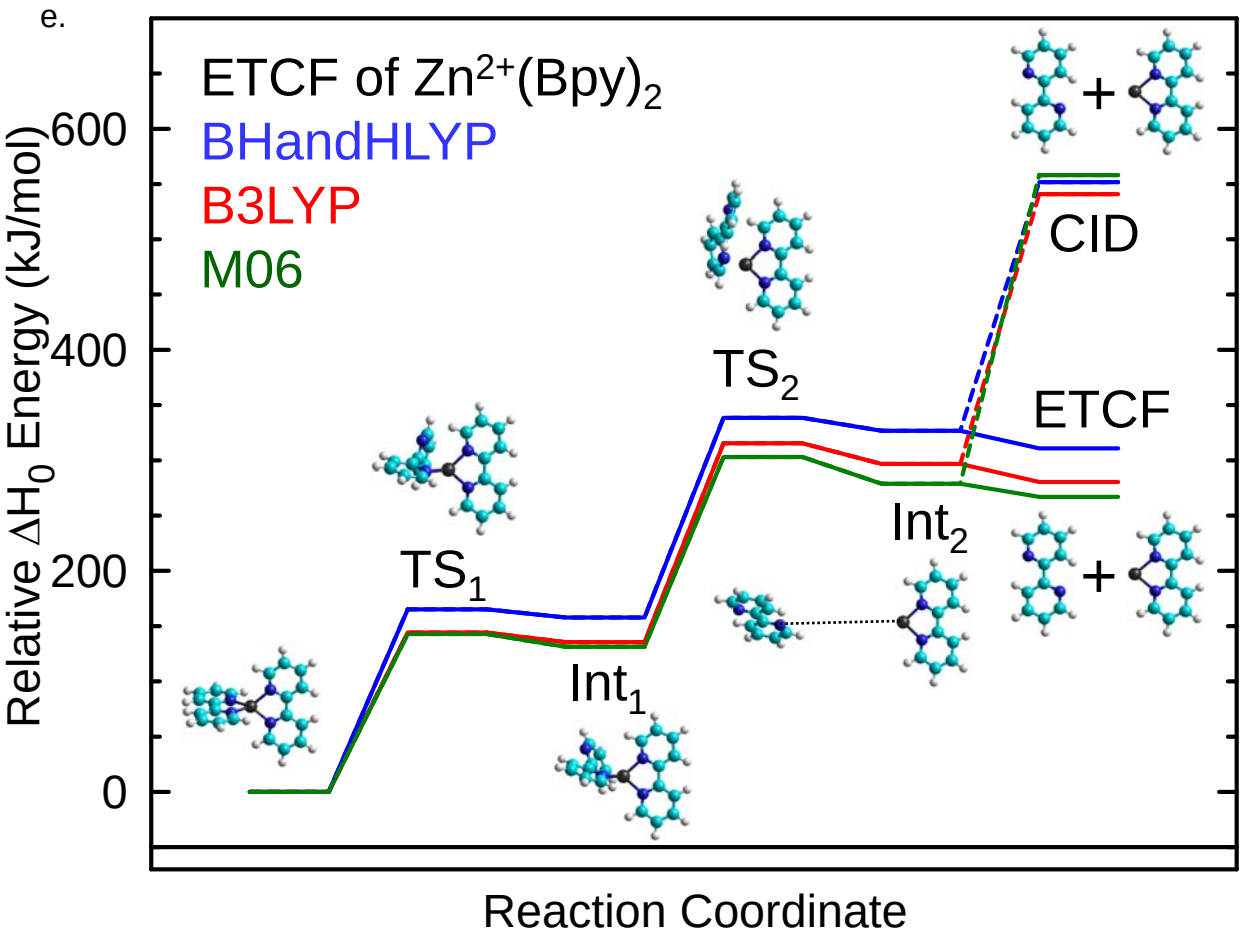
e.
ETCF of Zn2+(Bpy)2
BHandHLYP
B3LYP
M06
Relative ΔH0 Energy (kJ/mol)
600
400
200
0
TS1
Int1
TS2
Int2
CID
ETCF
+
+
Reaction Coordinate

Figure E.4.

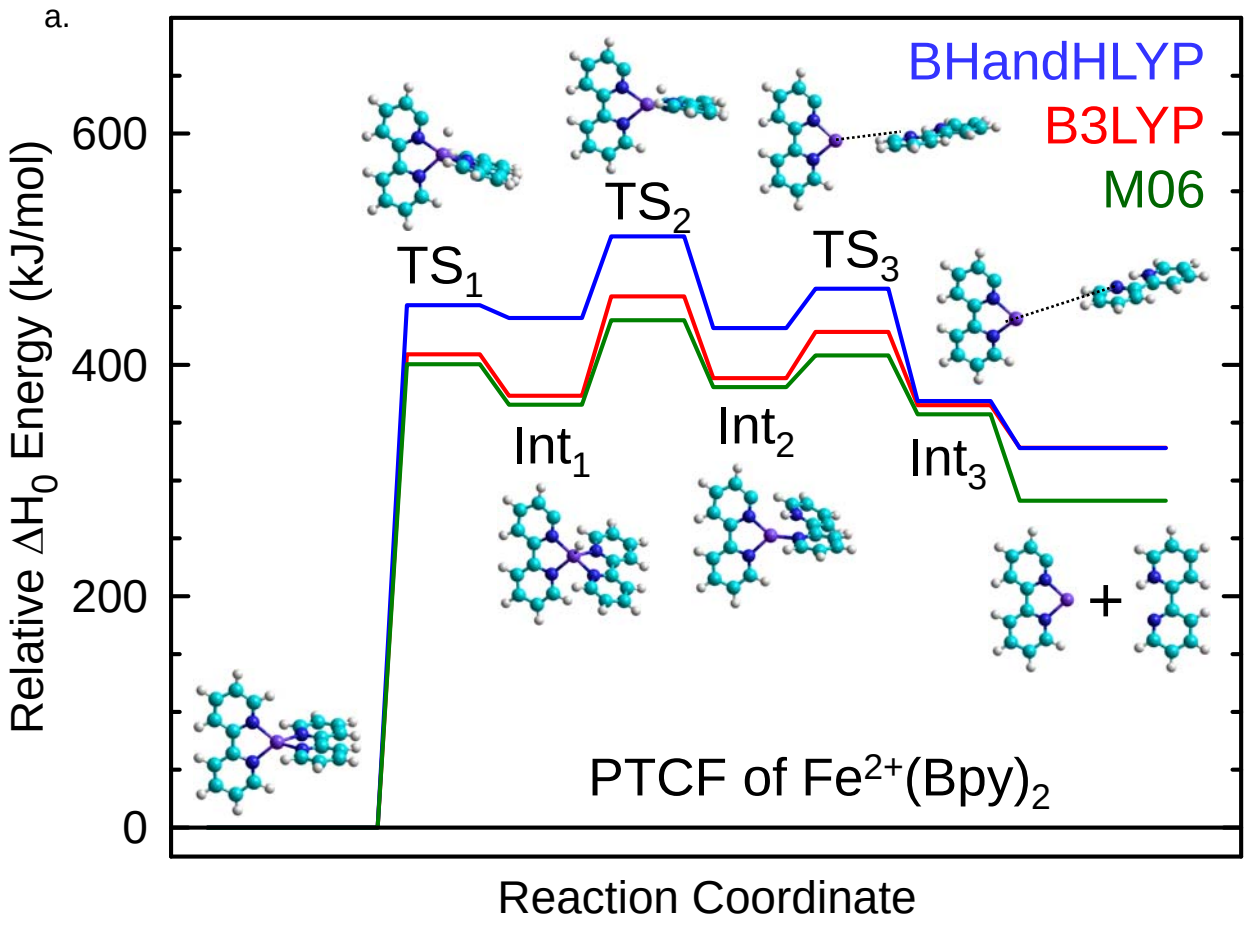
a.
BHandHLYP
B3LYP
M06
TS1
TS2
TS3
Int1
Int2
Int3
+
PTCF of Fe2+(Bpy)2
Relative ΔH0 Energy (kJ/mol)
600
400
200
0
Reaction Coordinate

Figure E.4.

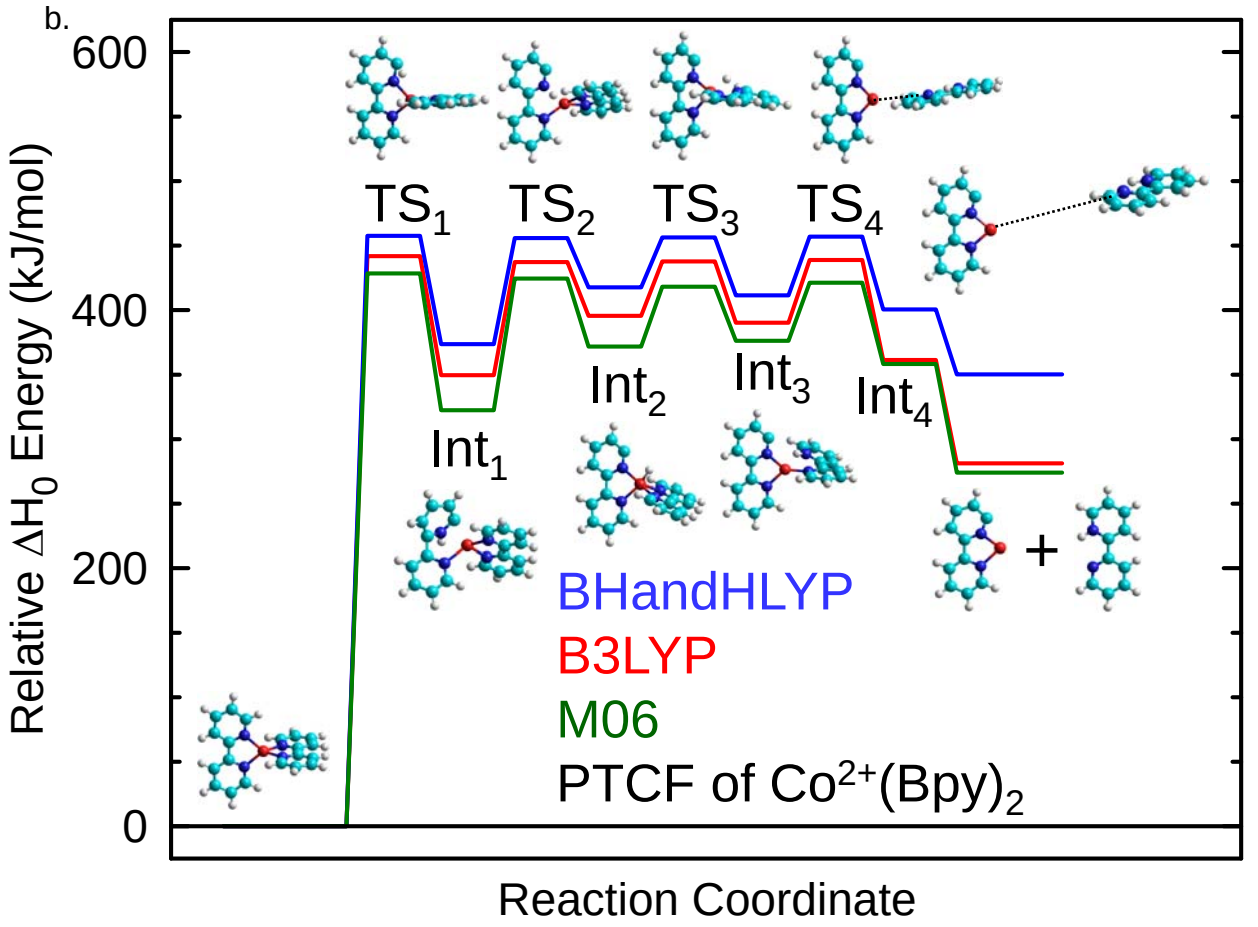
b.
600
400
200
0
Relative ΔH0 Energy (kJ/mol)
TS1
TS2
TS3
TS4
Int1
Int2
Int3
Int4
+
BHandHLYP
B3LYP
M06
PTCF of Co2+(Bpy)2
Reaction Coordinate

Figure E.4.

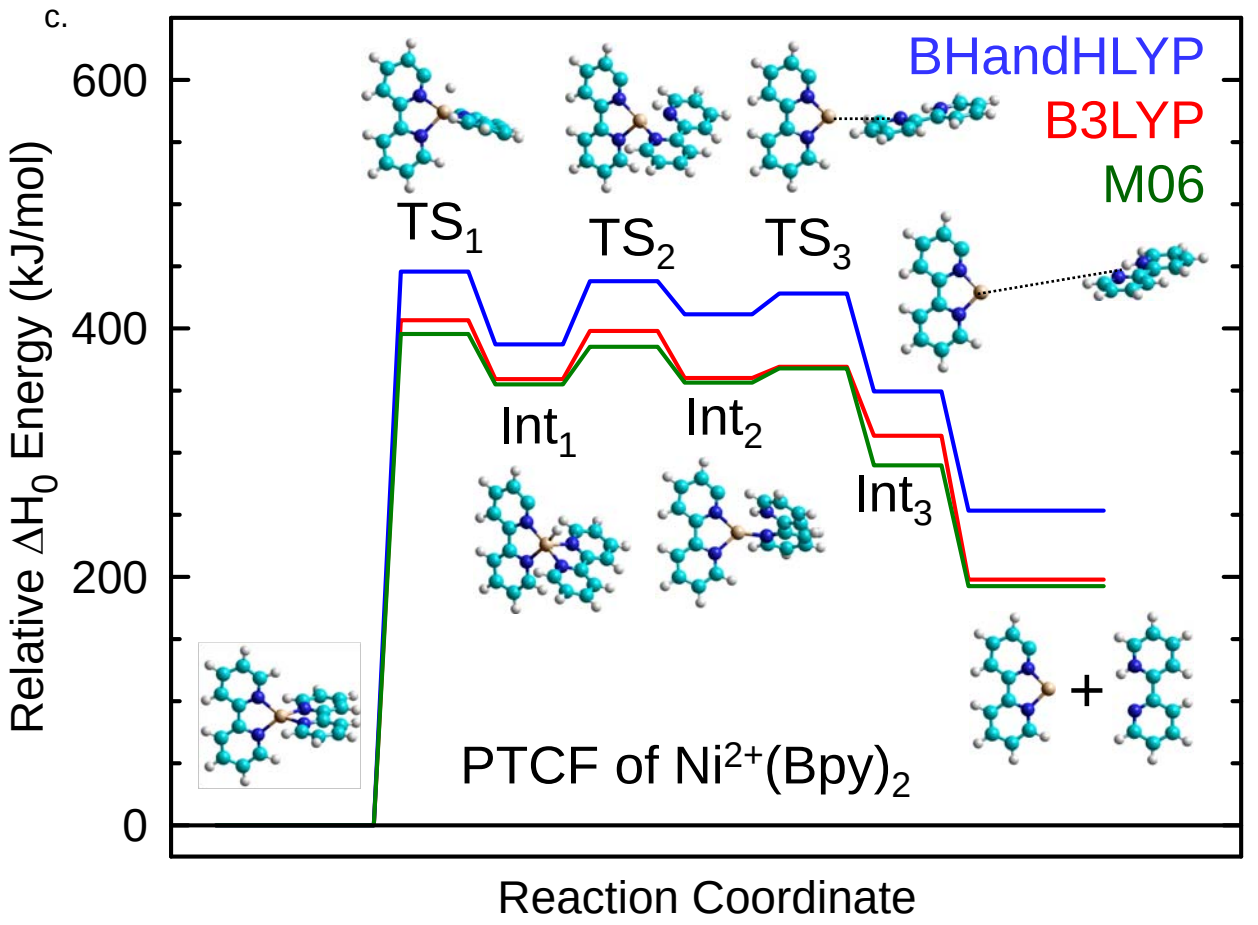
c.
600
400
200
0
Relative ΔH0 Energy (kJ/mol)
BHandHLYP
B3LYP
M06
TS1
TS2
TS3
Int1
Int2
Int3
+
PTCF of Ni2+(Bpy)2
Reaction Coordinate

Figure E.4.

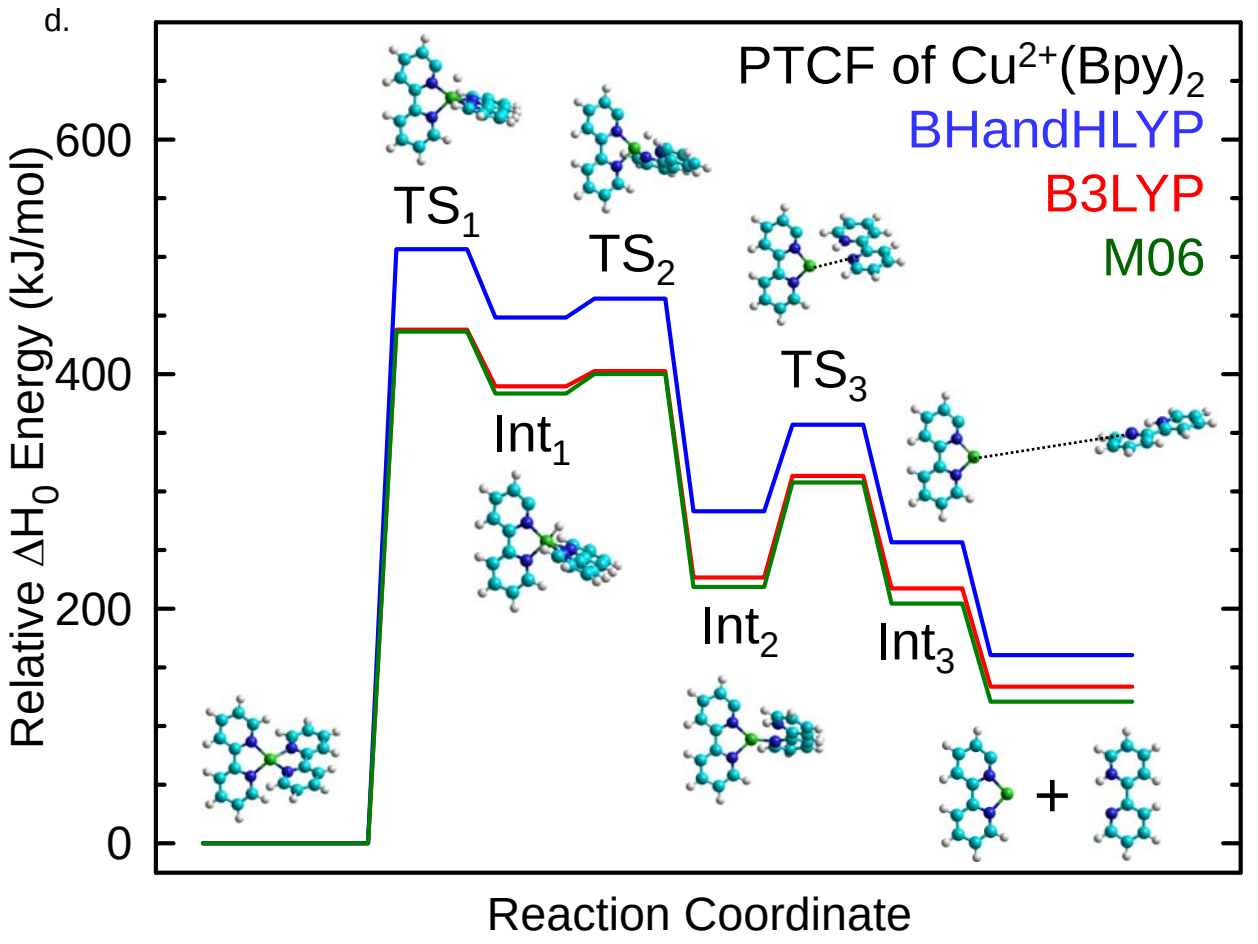
d.
PTCF of $Cu^{2+}(Bpy)_2$
BHandHLYP
B3LYP
M06
TS_1
TS_2
TS_3
Int_1
Int_2
Int_3
+
Relative ΔH_0 Energy (kJ/mol)
0
200
400
600
Reaction Coordinate

Figure E.4.

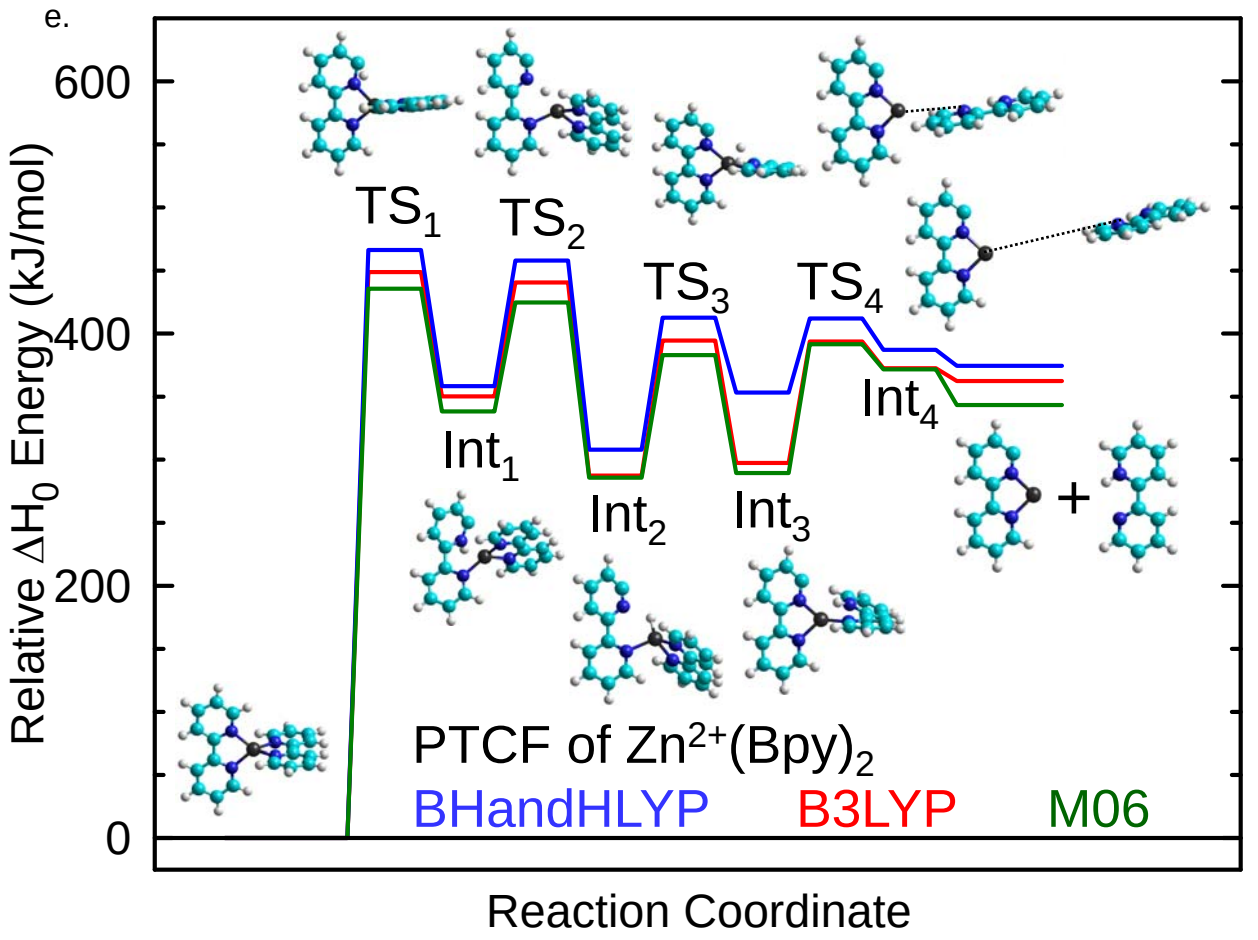
e.
600
400
200
0
Relative ΔH0 Energy (kJ/mol)
TS1
TS2
TS3
TS4
Int1
Int2
Int3
Int4
+
PTCF of Zn2+(Bpy)2
BHandHLYP
B3LYP
M06
Reaction Coordinate

Figure E.5.

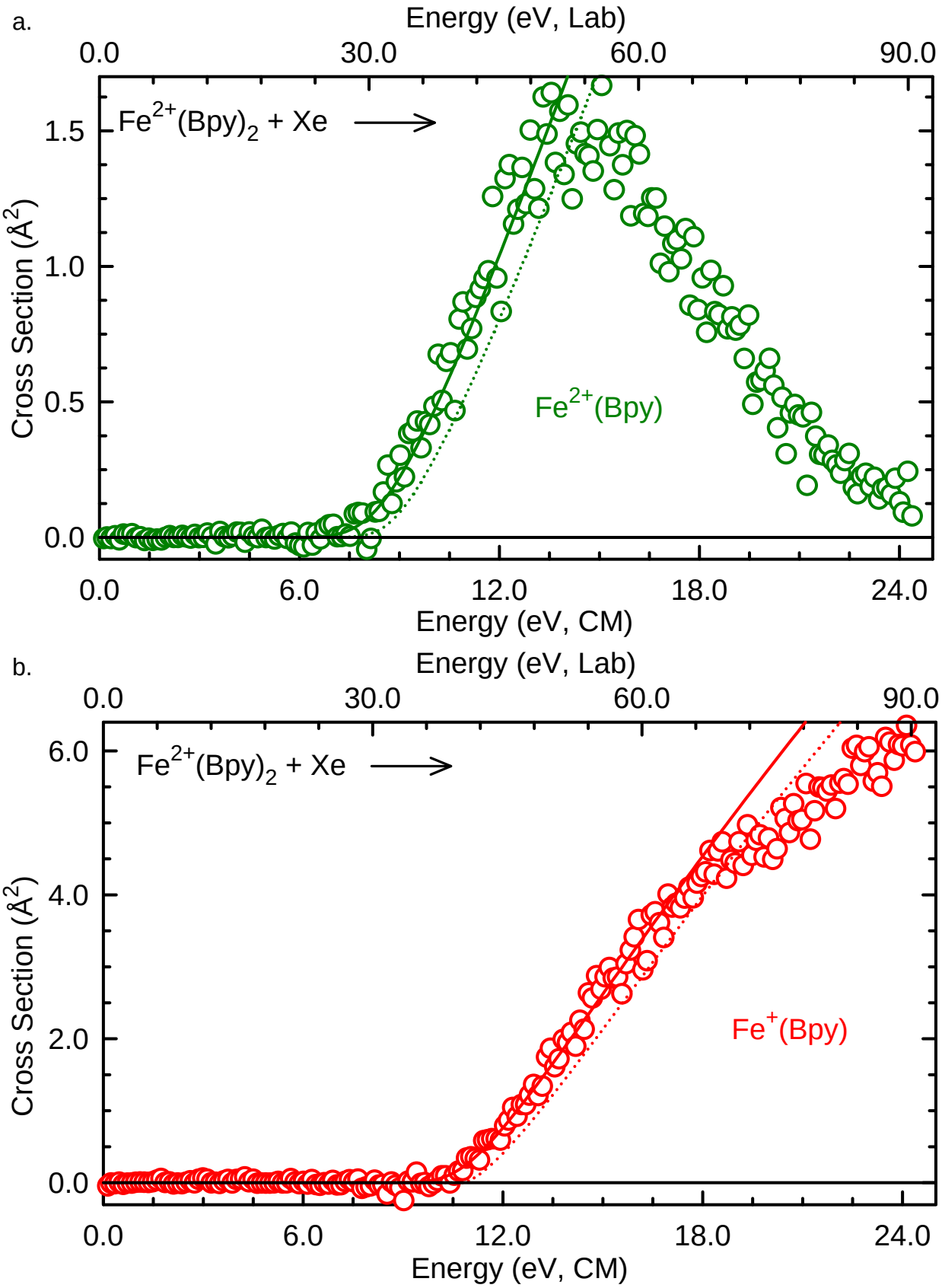
a.
Energy (eV, Lab)
0.0
30.0
60.0
90.0
Fe2+(Bpy)2 + Xe
Fe2+(Bpy)
Cross Section (Å2)
1.5
1.0
0.5
0.0
0.0
6.0
12.0
18.0
24.0
Energy (eV, CM)
b.
Energy (eV, Lab)
0.0
30.0
60.0
90.0
Fe2+(Bpy)2 + Xe
Fe+(Bpy)
Cross Section (Å2)
6.0
4.0
2.0
0.0
0.0
6.0
12.0
18.0
24.0
Energy (eV, CM)

Figure E.5.

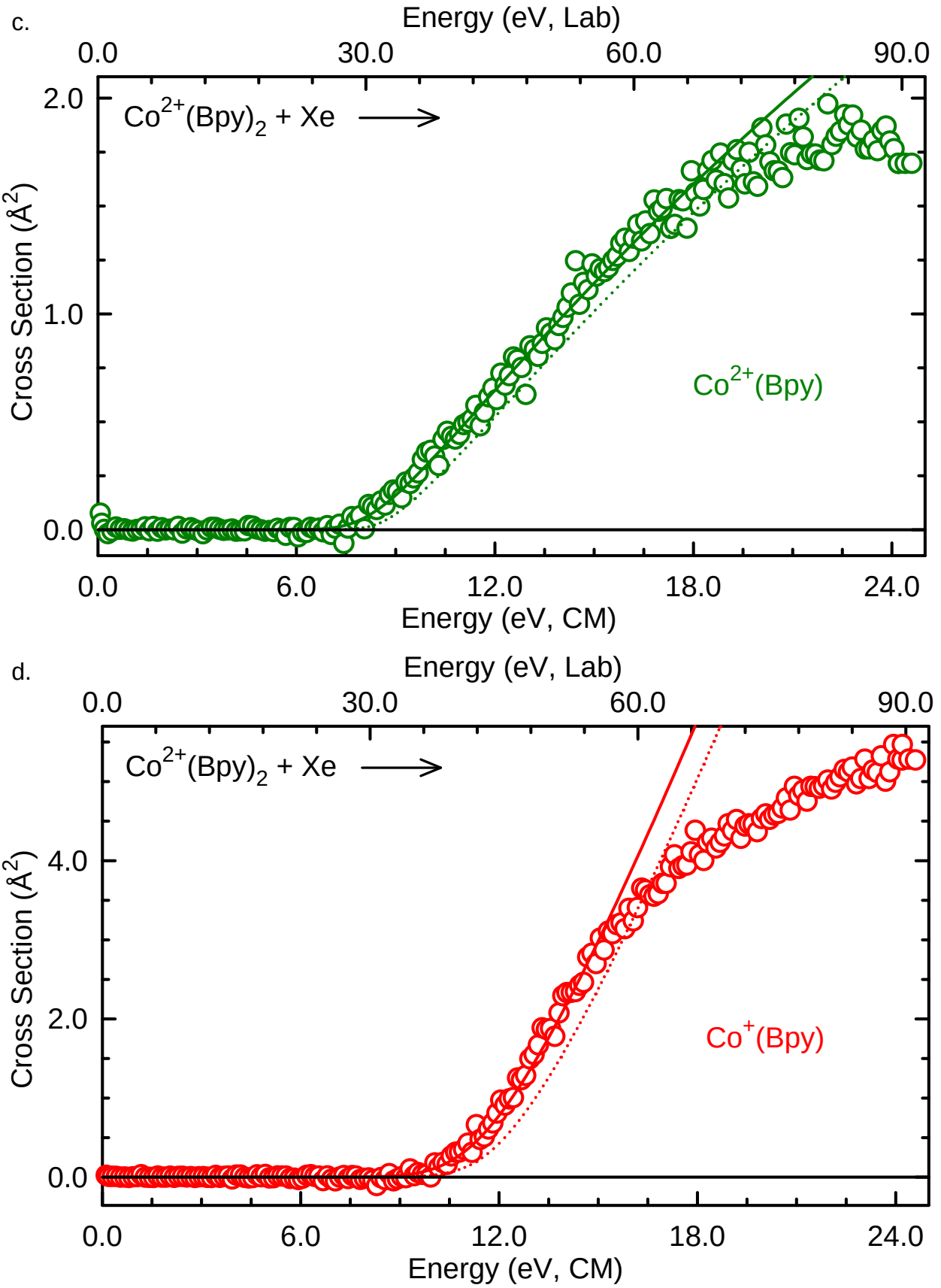
c.
Energy (eV, Lab)
0.0
30.0
60.0
90.0
2.0
1.0
0.0
Cross Section (Å^2)
Co^{2+}(Bpy)$_2$ + Xe
Co^{2+}(Bpy)
0.0
6.0
12.0
18.0
24.0
Energy (eV, CM)
d.
Energy (eV, Lab)
0.0
30.0
60.0
90.0
4.0
2.0
0.0
Cross Section (Å^2)
Co^{2+}(Bpy)$_2$ + Xe
Co^{+}(Bpy)
0.0
6.0
12.0
18.0
24.0
Energy (eV, CM)

Figure E.5.

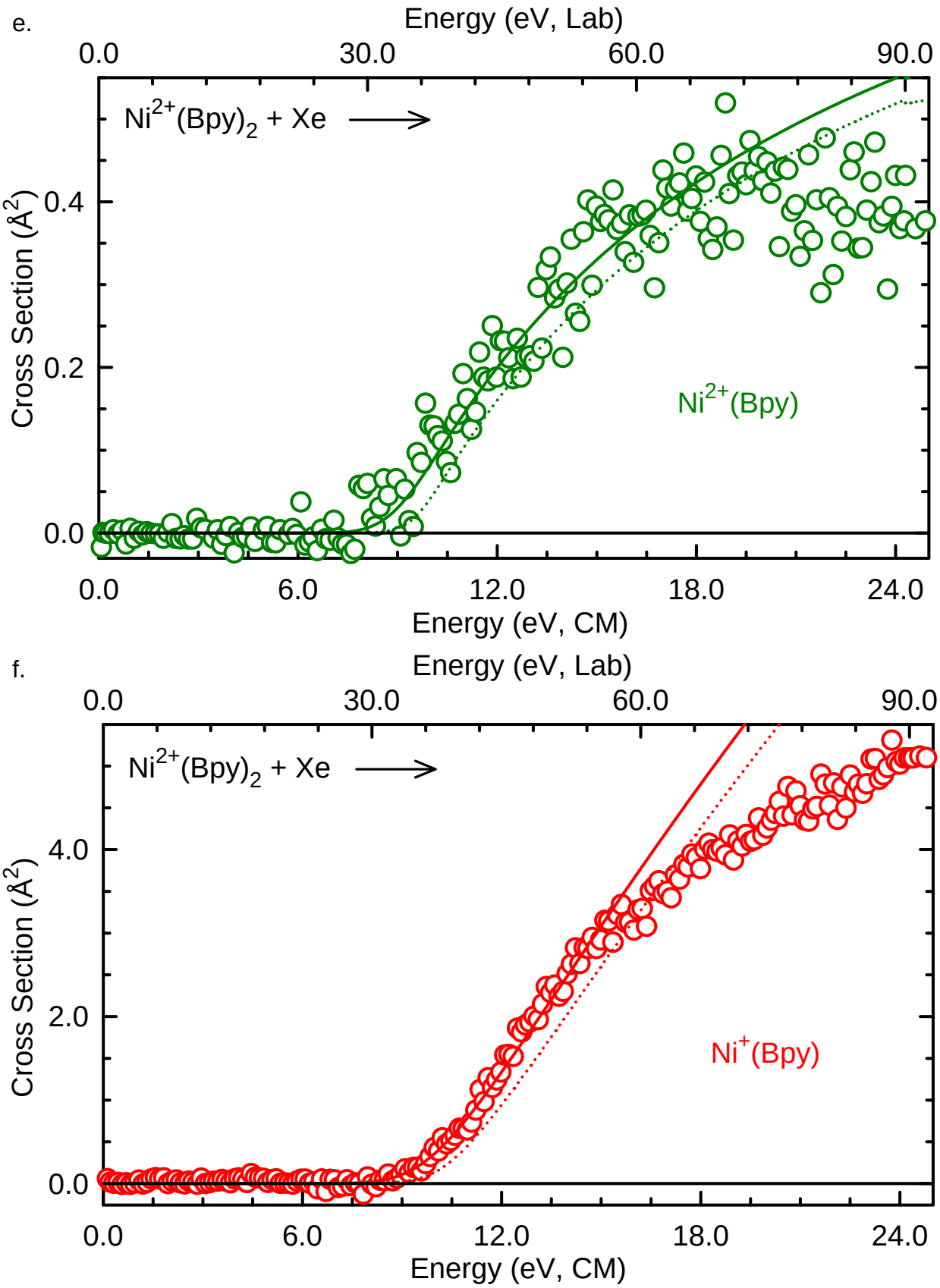
e.
Energy (eV, Lab)
0.0
30.0
60.0
90.0
Ni2+(Bpy)2 + Xe
Cross Section (Å2)
0.4
0.2
0.0
Ni2+(Bpy)
0.0
6.0
12.0
18.0
24.0
Energy (eV, CM)
f.
Energy (eV, Lab)
0.0
30.0
60.0
90.0
Ni2+(Bpy)2 + Xe
Cross Section (Å2)
4.0
2.0
0.0
Ni+(Bpy)
0.0
6.0
12.0
18.0
24.0
Energy (eV, CM)

Figure E.5.

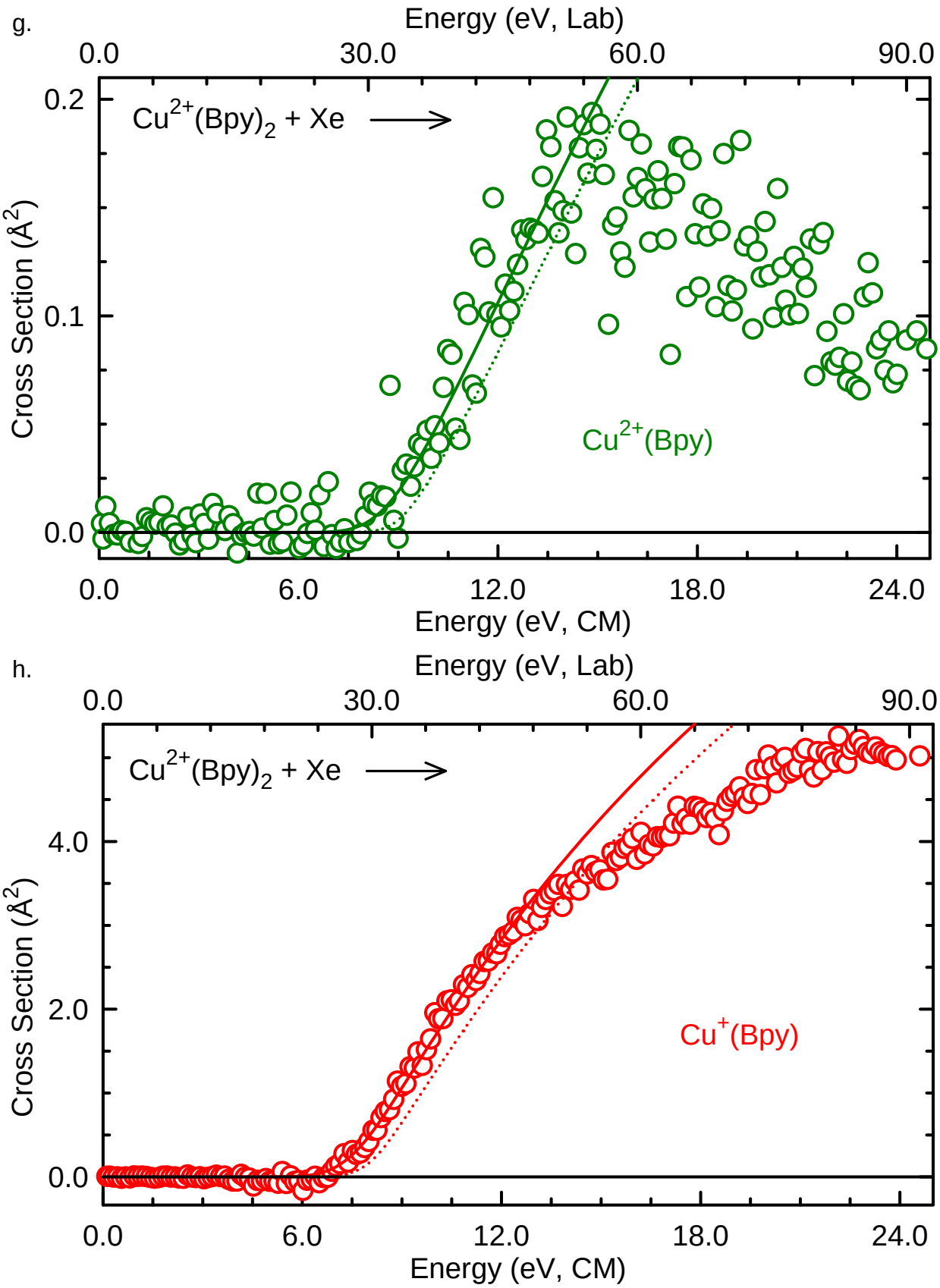
g.
Energy (eV, Lab)
0.0
30.0
60.0
90.0
0.2
0.1
0.0
Cross Section (Å^2)
Cu^{2+}(Bpy)$_2$ + Xe
Cu^{2+}(Bpy)
0.0
6.0
12.0
18.0
24.0
Energy (eV, CM)
h.
Energy (eV, Lab)
0.0
30.0
60.0
90.0
4.0
2.0
0.0
Cross Section (Å^2)
Cu^{2+}(Bpy)$_2$ + Xe
Cu^{+}(Bpy)
0.0
6.0
12.0
18.0
24.0
Energy (eV, CM)

Figure E.5.

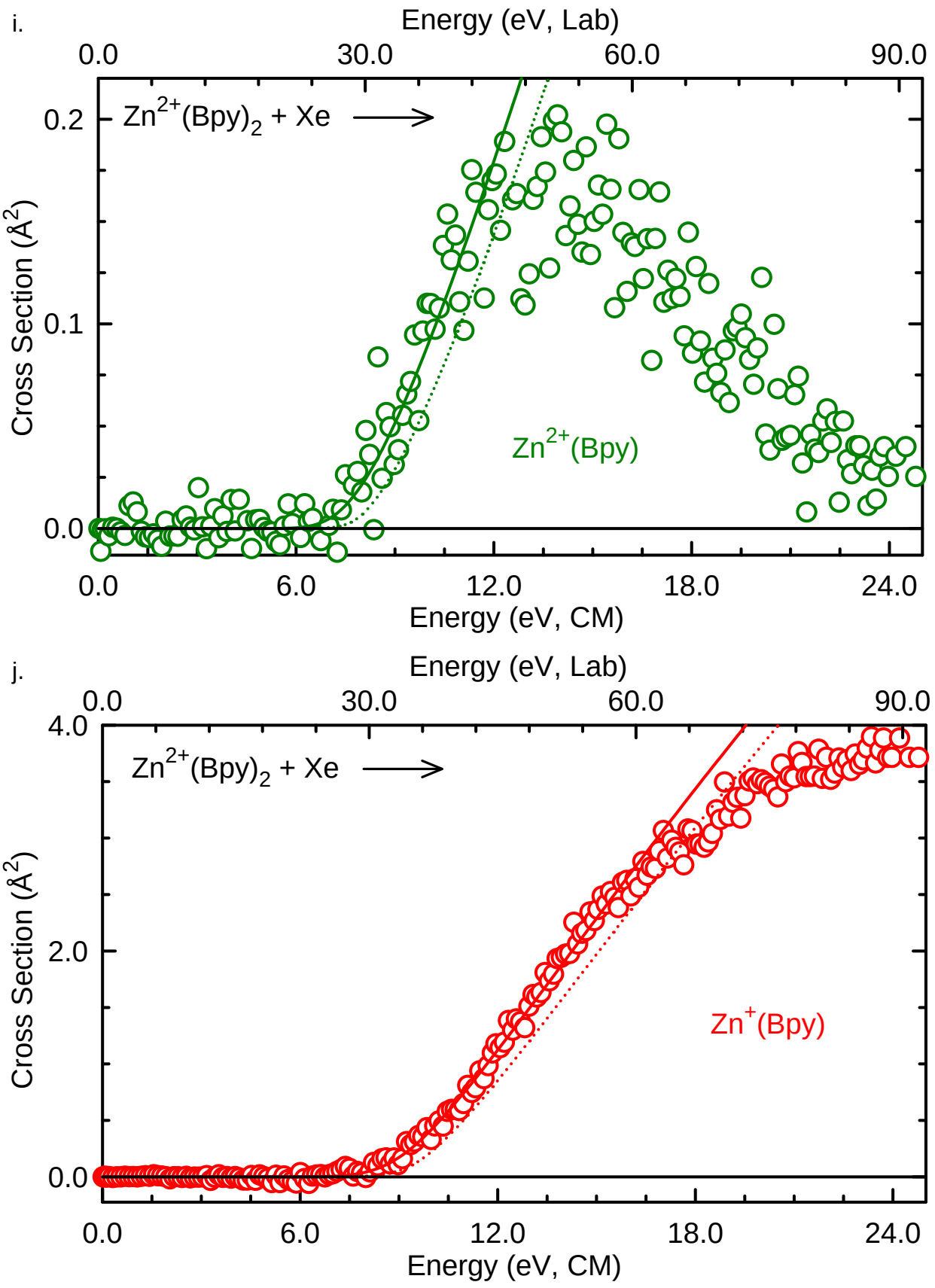
i.
Energy (eV, Lab)
0.0
30.0
60.0
90.0
$Zn^{2+}(Bpy)_2$ + Xe
0.2
0.1
0.0
Cross Section (Å^2)
Zn^{2+}(Bpy)
0.0
6.0
12.0
18.0
24.0
Energy (eV, CM)
j.
Energy (eV, Lab)
0.0
30.0
60.0
90.0
4.0
$Zn^{2+}(Bpy)_2$ + Xe
2.0
0.0
Cross Section (Å^2)
Zn^{+}(Bpy)
0.0
6.0
12.0
18.0
24.0
Energy (eV, CM)

Figure E.6.

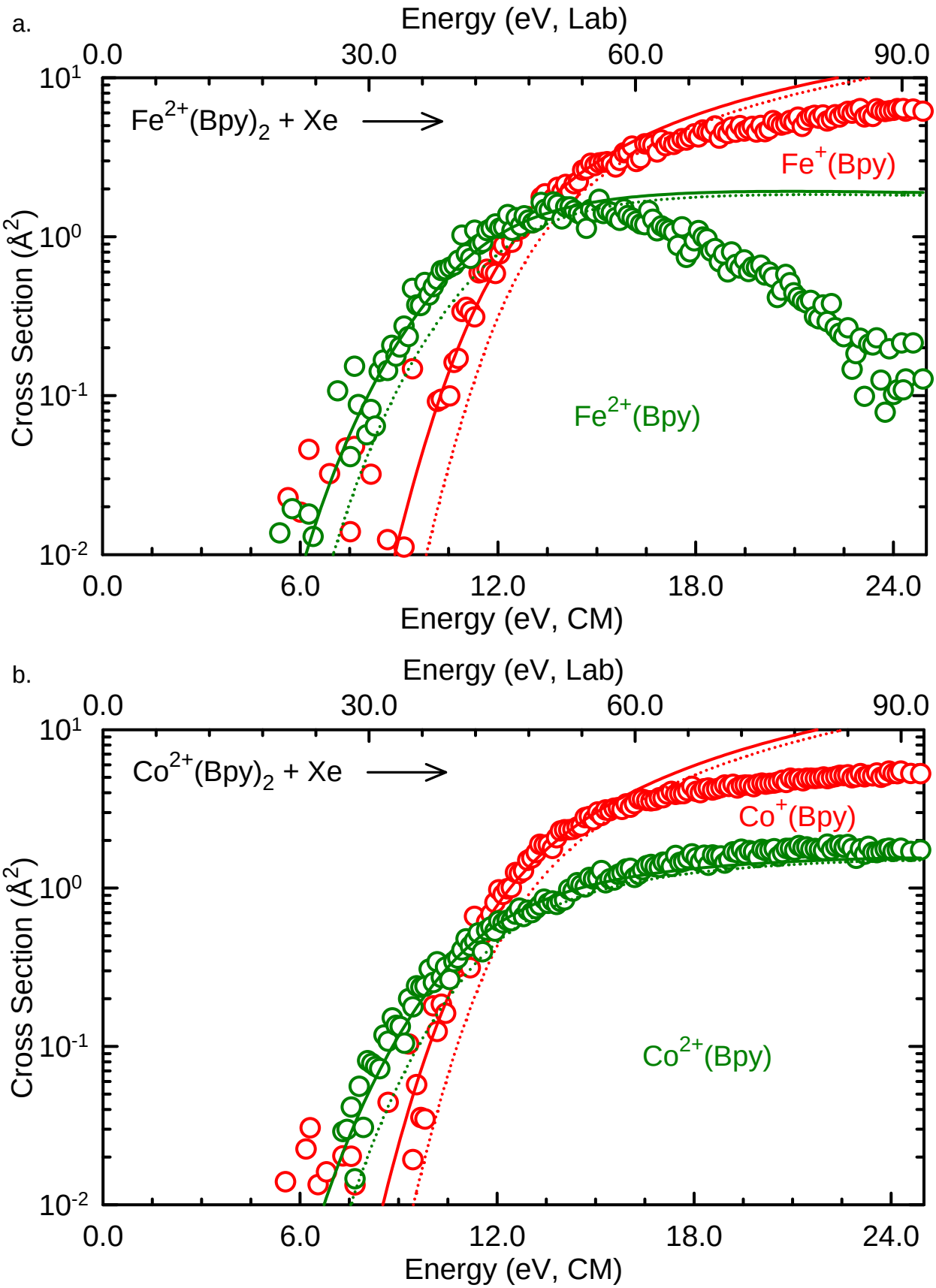
a.
Energy (eV, Lab)
0.0
30.0
60.0
90.0
10^1
10^0
10^{-1}
10^{-2}
Cross Section (Å^2)
$Fe^{2+}(Bpy)_2$ + Xe
$Fe^+(Bpy)$
$Fe^{2+}(Bpy)$
0.0
6.0
12.0
18.0
24.0
Energy (eV, CM)
b.
Energy (eV, Lab)
0.0
30.0
60.0
90.0
10^1
10^0
10^{-1}
10^{-2}
Cross Section (Å^2)
$Co^{2+}(Bpy)_2$ + Xe
$Co^+(Bpy)$
$Co^{2+}(Bpy)$
0.0
6.0
12.0
18.0
24.0
Energy (eV, CM)

Figure E.6.

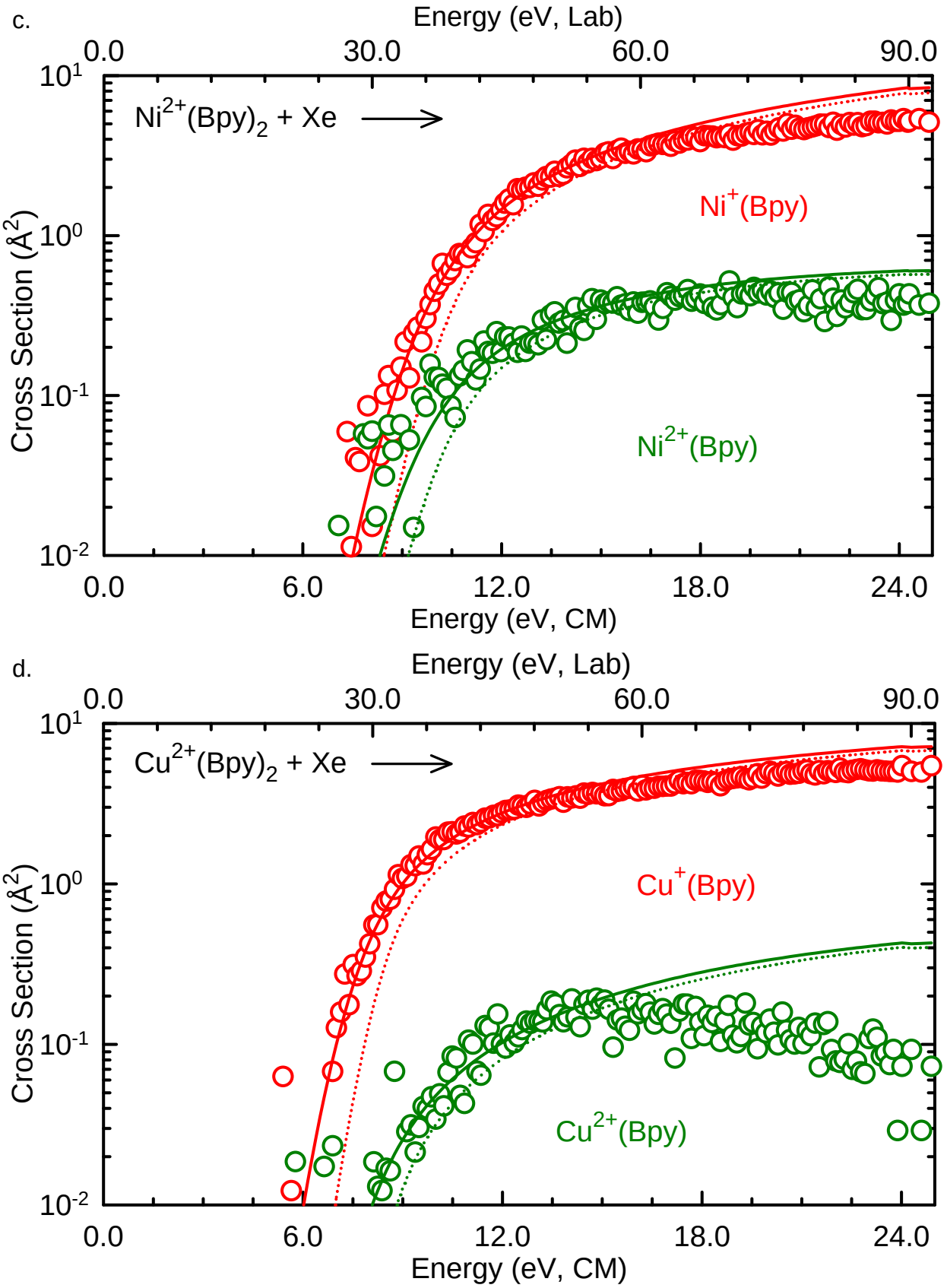
c.
Energy (eV, Lab)
0.0
30.0
60.0
90.0
10^1
10^0
10^{-1}
10^{-2}
Cross Section (Å^2)
$Ni^{2+}(Bpy)_2$ + Xe
$Ni^+(Bpy)$
$Ni^{2+}(Bpy)$
0.0
6.0
12.0
18.0
24.0
Energy (eV, CM)
d.
Energy (eV, Lab)
0.0
30.0
60.0
90.0
10^1
10^0
10^{-1}
10^{-2}
Cross Section (Å^2)
$Cu^{2+}(Bpy)_2$ + Xe
$Cu^+(Bpy)$
$Cu^{2+}(Bpy)$
0.0
6.0
12.0
18.0
24.0
Energy (eV, CM)

Figure E.6.

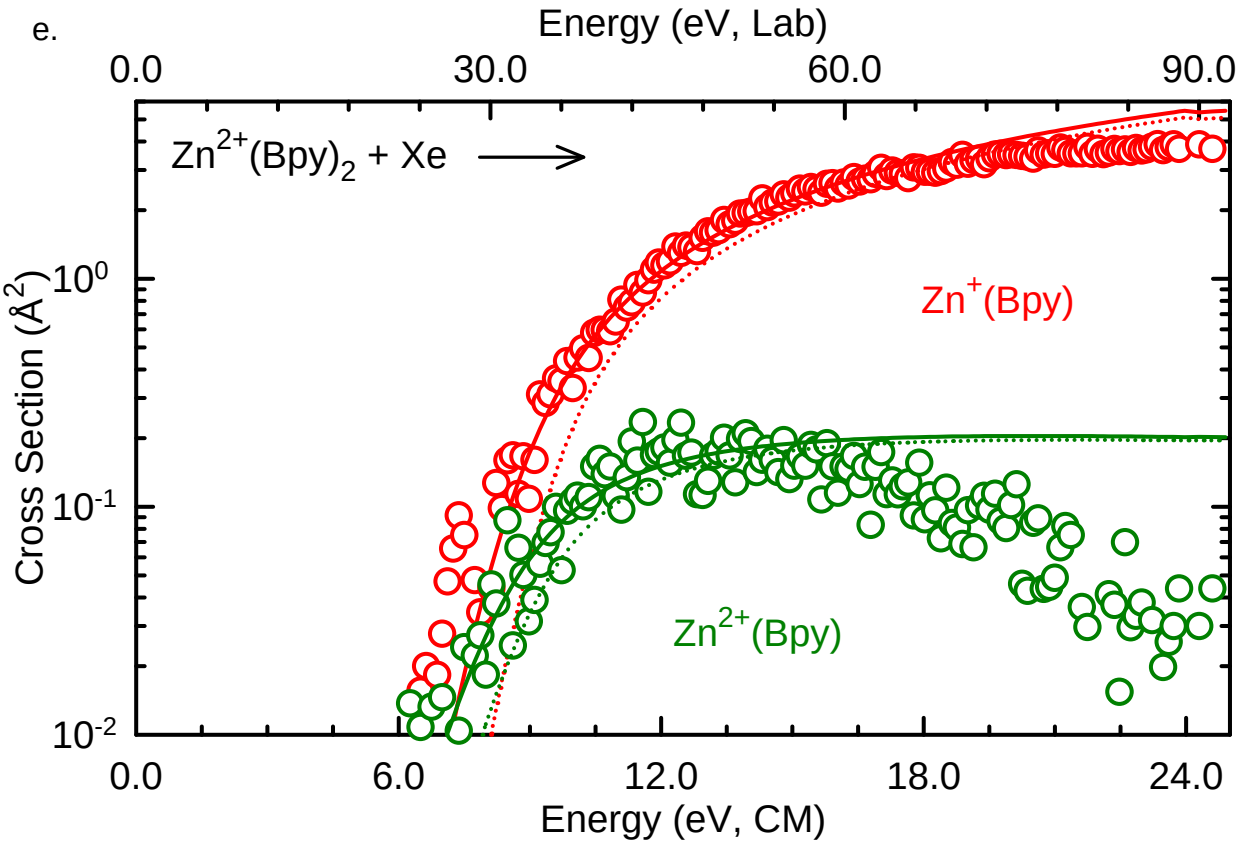
e.
Energy (eV, Lab)
0.0
30.0
60.0
90.0
Zn2+(Bpy)2 + Xe
Zn+(Bpy)
Zn2+(Bpy)
Cross Section (Å2)
10^0
10^-1
10^-2
0.0
6.0
12.0
18.0
24.0
Energy (eV, CM)

Figure E.7.

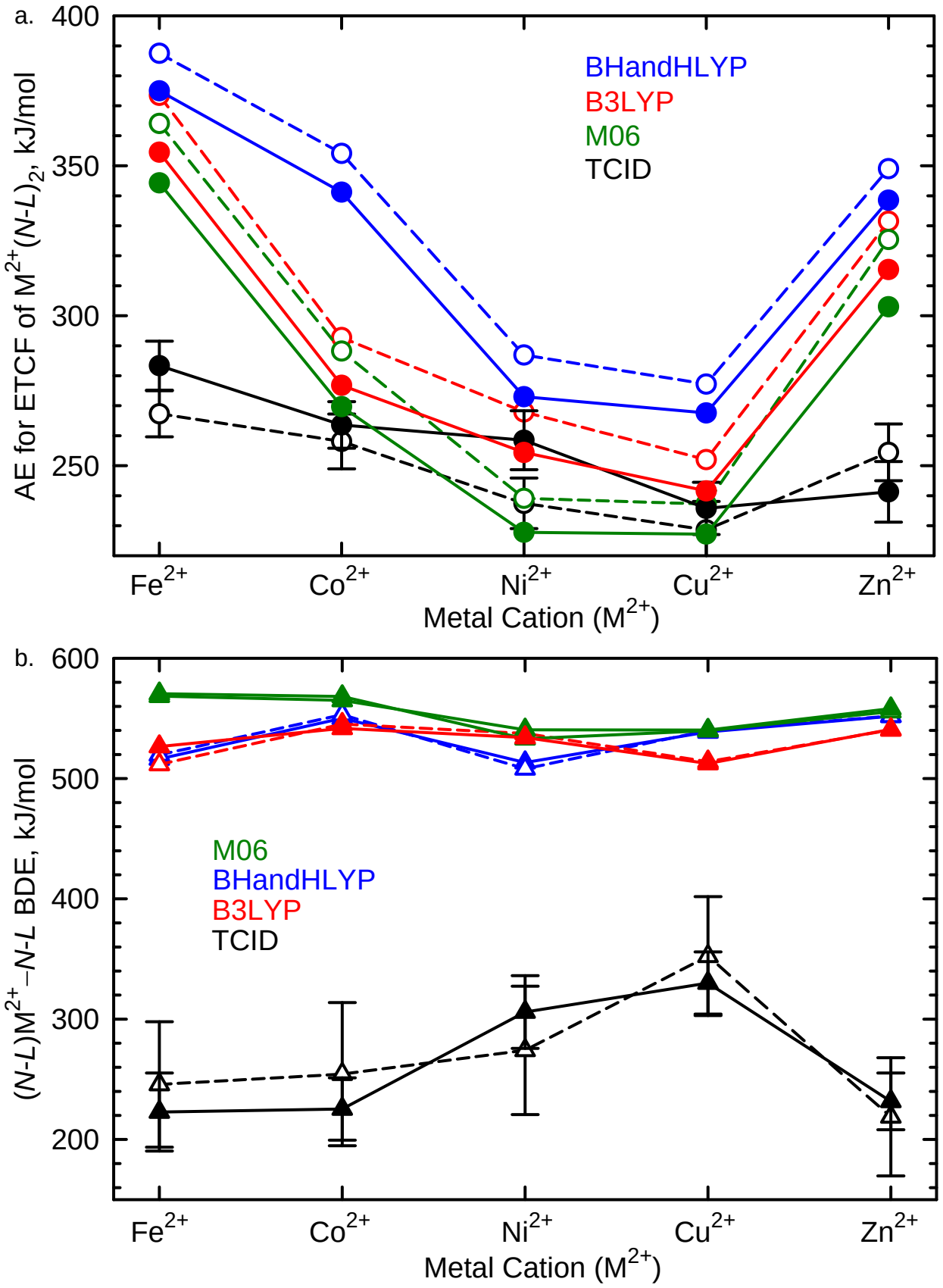
a.
AE for ETCF of $M^{2+}(N\text{-}L)_2$, kJ/mol
400
350
300
250
BHandHLYP
B3LYP
M06
TCID
Fe^{2+}
Co^{2+}
Ni^{2+}
Cu^{2+}
Zn^{2+}
Metal Cation (M^{2+})
b.
$(N\text{-}L)M^{2+}\text{–}N\text{-}L$ BDE, kJ/mol
600
500
400
300
200
M06
BHandHLYP
B3LYP
TCID
Fe^{2+}
Co^{2+}
Ni^{2+}
Cu^{2+}
Zn^{2+}
Metal Cation (M^{2+})

APPENDIX F

PRELIMINARY CONCLUSIONS AND FUTURE DIRECTIONS

F.1 Preliminary Conclusions

Energy-resolved collision-induced dissociation (CID) studies carried out in a custom-built guided ion beam tandem mass spectrometer (GIBMS) have been used to probe the structures, energetics of binding, and fragmentation behavior of a series of transition metal-ligand complexes. These experimental studies are supported and enhanced by complementary electronic structure theory calculations using several theoretical methods including B3LYP, BHandHLYP, and M06 functionals to determine the stable low-energy structures of the transition metal-ligand complexes and the relevant species associated with their CID behavior. These studies probe the effects of the electronic structure of the metal cation on the structures, ligand binding, and fragmentation mechanisms by including the five late first-row transition metals cation in their +2 oxidations states, $Fe^{2+}(d^6)$, $Co^{2+}(d^7)$, $Ni^{2+}(d^8)$, $Cu^{2+}(d^9)$, and $Zn^{2+}(d^{10})$. The *N-L* donor ligands investigated include 2,2'-bipyridine (Bpy) and 1,10-phenanthroline (Phen). The series of inter-related studies carried out in this thesis are designed to probe the influence of the electronic structure of the metal cation and the nature of *N-L* donor ligands on the geometry, binding strength, and fragmentation patterns of the transition metal cation-ligand complexes which are relevant to electron and proton transfer processes.

The kinetic energy dependent cross sections for the interaction of M^{2+} cations with Phen and Bpy ligands are determined by collision-induced dissociation using a guided ion beam tandem mass spectrometer. The M^{2+} cations examined in these studies include: Fe^{2+}, Co^{2+}, Ni^{2+}, Cu^{2+}, and Zn^{2+}. In this work, CID experiments were limited to the $M^{2+}(Bpy)_2$ and

$M^{2+}(Phen)_2$ complexes only. Preliminary CID studies of the $M^{2+}(Phen)_2$ and $M^{2+}(Bpy)_2$ complexes are carried out using GIBMS under low-resolution conditions. Preliminary dissociation studies of these complexes find that simple CID, ETCF, and PTCF pathways occur in parallel and compete with each other. Dehydrogenation reactions likely also occur as minor reaction pathways, but could not be differentiated from the major dissociation pathways under the low-resolution conditions under which these preliminary experiments were performed. These pathways are influenced by the electronic occupation of the metal cation such that simple CID becomes less favored across the period, whereas ETCF and PTCF become more favorable. In comparison to the $M^{2+}(Phen)_3$ and $M^{2+}(Bpy)_3$ complexes, the $M^{2+}(Phen)_2$ and $M^{2+}(Bpy)_2$ complexes bind more strongly. Their BDEs exceed those of a typical C–C bond (> 400 kJ/mol), implying that the binding of the second Phen or Bpy ligand is more covalent in nature. As a result, the CID behavior of the $M^{2+}(Phen)_2$ and $M^{2+}(Bpy)_2$ complexes is much richer and provides an opportunity to probe the metal-to-ligand and ligand-to-metal charge transfer behavior in much greater detail. Under low-resolution conditions in which the CID experiments of $M^{2+}(Phen)_2$ and $M^{2+}(Bpy)_2$ complexes were carried out, severe overlap of the products originating from ETCF and PTCF pathways and separated by 1 Da is observed. To extract accurate thermochemistry for the ETCF, PTCF, and simple CID pathways of these complexes, experimental studies under high-resolution conditions are needed.

The fragmentation mechanisms of $M^{2+}(N\text{-}L)_2$ complexes where M^{2+} = Fe^{2+}, Co^{2+}, Ni^{2+}, Cu^{2+}, and Zn^{2+}, and *N-L* = Bpy and Phen are determined at B3LYP level of theory using the 6-31G* basis set. Activation energies (AEs) and bond dissociation energies (BDEs) are determined at B3LYP, BHandHLYP, and M06 levels of theory with

6-311+G(2d,2p) basis set. The activated dissociation pathways of the $M^{2+}(Phen)_2$ and $M^{2+}(Bpy)_2$ complexes corresponding to ETCF and PTCF are observed as the primary dissociation pathways upon CID of these complexes, therefore their potential energy surfaces are mapped theoretically to determine the rate-limiting TSs, which are needed for accurate thermochemical analysis of the experimental data. Because of the low-resolution conditions under which the experiments were performed and the lack of complete experimental data for these systems, accurate thermochemical results cannot be extracted from this work, and the strengths and limitations of the theoretical methods employed cannot be evaluated. However, the limited experimental results available suggest that the PTCF pathways are low in energy, and most cases appear to be the lowest energy pathway available. In contrast, the theoretical results suggest that PTCF is higher in energy than ETCF, and thus suggest that the PTCF pathways mapped likely do not correspond to the lowest energy PTCF pathways available to these systems such that further investigations into other plausible mechanisms involved in the activated dissociation through PTCF are needed. Furthermore, additional CID experimental studies performed under higher resolution conditions (i.e., where the ETCF and PTCF as well as dehydrogenation pathways can be resolved are needed before reliable thermochemical data can be extracted from these systems.

F.2 Future Directions

Of the two series of $M^{2+}(N\text{-}L)_x$ complexes studied experimentally, i.e., $M^{2+}(N\text{-}L)_2$ and $M^{2+}(N\text{-}L)_3$, the $M^{2+}(N\text{-}L)_3$ project is completed. However, for the studies of the $M^{2+}(N\text{-}L)_2$ complexes there exists a number of projects that should be carried out to enable accurate thermochemical data to be extracted. These projects include:

(1) CID experimental studies under higher resolution conditions. CID studies of $M^{2+}(N\text{-}L)_2$ complexes examined in this thesis were performed under low-resolution conditions. As a result, severe overlap of the $M^+(N\text{-}L)$ and $[M(N\text{-}L)\text{-}H]^+$ as well as $[N\text{-}L]^+$ and $[(N\text{-}L)+H]^+$ product ions originating from the ETCF and PTCF pathways, respectively was observed. Due to severe overlap, accurate thermochemistry of the $M^{2+}(N\text{-}L)_2$ complexes could not be determined. Under high-resolution conditions, all resolved products need to be collected under all pressure conditions to be able to establish the pressure dependence of the product cross sections. All important pathways, i.e., ETCF, PTCF, simple CID, and dehydrogenation need to be analyzed simultaneously for accurate thermochemistry of $M^{2+}(N\text{-}L)_2$ complexes to be determined. FT-ICR experiments show the presence of dehydrogenation as minor pathways. In this thesis, these pathways were not collected. However, CID studies of loss of hydrogen need to be examined in order to extract accurate thresholds of the $M^{2+}(N\text{-}L)_2$ complexes as even a small contamination by a species that exhibits a lower threshold may be sufficient to bias the threshold determinations leading to incorrect thresholds.

(2) Modeling of the activated dissociation pathways. The mechanism of proton transfer in all $M^{2+}(N\text{-}L)_2$ complexes have been examined in this thesis. More plausible mechanisms that are lower in energy than those mapped thus far seem likely. Preliminary CID experimental results for the $M^{2+}(N\text{-}L)_2$ complexes suggest that PTCF is the lowest energy pathway, whereas the theoretical results suggest that the rate-limiting TSs for these pathways are much higher than for the ETCF pathways, suggesting that the PES mapped thus far is not the correct pathway followed in the reactions at lower energies, i.e., near threshold. Therefore, alternative pathways that are lower in energy need to be determined. Based on

FT-ICR results, pathways resulting in loss of hydrogen have been found although they are small. Because our studies involve determining thresholds, these pathways can influence threshold determination if they are lower in energy than the ETCF, PTCF, and simple CID pathways. Theoretical calculations and potential energy surface mapping are needed to model the hydrogen loss activated dissociation pathways of all $M^{2+}(N\text{-}L)_2$ complexes in order to determine whether they are higher or lower energy pathways than ETCF, PTCF, and simple CID.

(3) Theoretical calculations at higher levels of theory using larger basis sets. Theoretical calculations and potential energy surface mapping have been carried out in this thesis. B3LYP, BHandHLYP, and M06 levels of theory using 6-31G* basis set for geometry optimization and zero point energy (ZPE) corrections, and using the 6-311+G(2d,2p) basis set for single point energy calculations and basis set superposition error (BSSE) corrections have been examined. ETCF and PTCF deal with open shell systems in terms of the reactants, TSs, intermediates, and some of the products. While it is known that theoretical methods are not as reliable for describing such species as compared to closed shell species,[1-3] more advanced theories with much larger basis sets are needed to extract highly reliable energetics from theory.

(4) Theoretical and experimental study of the influence of other metal cations, higher oxidation states, and substituted forms of *N*-*L* donor ligands. Such studies will allow assessment of new metals, substituent effects, and further determination of the influence of charge on the geometric structures and binding energies. The strength of metal-ligand interactions is found to depend upon a number of properties of the metals and *N*-*L* donor ligands. Ionic radii, ionization energies, oxidation states, and valence electronic

configuration strongly influence the binding interaction. The nature and number of *N-L* donor atoms available for binding, and the molecular polarizability and dipole moment also influence the binding interaction. Metal-ligand interactions define the structure of transition metal complexes by maintaining the stability of molecular system, and therefore have a profound impact on their physical and chemical properties and hence underlie their functionality. Geometric structures and binding energies of transition metal complexes involving Pyr, Bpy, and Phen have been studied[4-11] and continue to be of interest to our group. Thus, comparison between the results from current and future work via complimentary studies of higher oxidation states, substituted *N-L* donor ligands, and other metal cations that enable the geometric structures and binding energies to be tuned should establish the most favorable complexes for use in electron and proton transfer applications.

F.3 References

(1) Jacob, C. R.; Reiher, M. *Int. J. Quantum Chem.* **2012**, *112*, 3661.

(2) Goodpaster, J. D.; Barnes, T. A.; Manby, F. R.; Miler, T. F. *J. Chem. Phys.* **2012**, *137*, 224113.

(3) Schmidt, J. R.; Shenvi, N.; Tully, J. C. *J. Chem. Phys.* **2008**, *129*, 114110.

(4) Rodgers, M. T.; Stanley, J. R.; Amunugama, R. *J. Am. Chem. Soc*. **2000**, *122*, 10969.

(5) Rannulu, N. S.; Rodgers, M. T. *J. Phys. Chem. A* **2007**, *111*, 3465.

(6) Rannulu, N. S. Doctoral dissertation, Wayne State University. 2008, pp.393.

(7) Rannulu, N. S.; Rodgers, M. T. *J. Phys. Chem. A* **2009**, *113*, 4534.

(8) Rannulu, N. S.; Rodgers, M. T. *J. Phys. Chem. A* **2012**, *116*, 1319.

(9) Nose, H.; Chen, Y.; Rodgers, M. T. *J. Phys. Chem. A* **2013**, 117, 4316.

(10) Nose, H.; Rodgers, M. T. *ChemPlusChem* **2013**, 78, 1109.

(11) Nose, H.; Rodgers, M. T. *J. Phys. Chem. A* **2014**, under review.

ABSTRACT

EXPERIMENTAL AND THEORETICAL STUDIES OF BINDING INTERACTIONS IN DIVALENT TRANSITION METAL CATION-*N*-DONOR LIGAND COMPLEXES: STRUCTURES, SEQUENTIAL BOND DISSOCIATION ENERGIES, MECHANISMS AND ENERGETICS OF COLLISION-INDUCED DISSOCIATION

by

HOLLINESS NOSE

May 2014

Advisor: Prof. M. T. Rodgers

Major: Chemistry (Inorganic)

Degree: Doctor of Philosophy

The dissertation research described here involves a series of experiments that have been designed to probe the influence of the electronic structure of the metal cation, the nature and number of ligands, as well as the effects of chelation and steric interactions on the geometry and binding strength of transition metal cation-ligand complexes. The experimental studies make use of energy-resolved collision-induced dissociation (CID) techniques that are carried out in a custom-built guided ion beam tandem mass spectrometer (GIBMS) to probe the structures, energetics, and fragmentation behavior of the complexes of interest. Electronic structure theory calculations including several density functional theory methods are employed to determine stable low-energy structures of the $M^{2+}(N\text{-L})_x$ complexes and the relevant species associated with their CID behavior. The five late first-row transition metal cations in their 2+ oxidation states, Fe^{2+}, Co^{2+}, Ni^{2+}, Cu^{2+}, and Zn^{2+}, are included in this work. The *N*-donor ligands (*N*-*L*) investigated here include pyridine (Pyr), a monodentate ligand, and two pyridine based bidentate ligands, 2,2′-bipyridine (Bpy), and 1,10-

phenanthroline (Phen). The structures and energetics of these complexes are investigated theoretically, while the CID behavior is investigated experimentally.

In Chapters 3 and 4, we found that the dominant dissociation pathway for all $M^{2+}(Phen)_3$ and $M^{2+}(Bpy)_3$ complexes is loss of an intact Phen and Bpy ligand, respectively. In both cases, the BDEs computed using the M06 theory are found to be the largest, BHandHLYP values are intermediate, whereas B3LYP produced the smallest values. Very good agreement between the B3LYP theoretically calculated and TCID experimentally determined BDEs was found for both $M^{2+}(Phen)_3$ and $M^{2+}(Bpy)_3$ complexes, suggesting that the B3LYP functional is capable of accurately describing the binding in these complexes. The sequential BDEs of $M^{2+}(Phen)_x$ and $M^{2+}(Bpy)_x$ complexes are observed to decrease monotonically with increasing ligation for all five metal cations regardless of which theory is employed. The sd hybridization of the M^{2+} cation plays a major role in enhancing the binding energy of the first Phen and Bpy ligand. The decline in effective charge retained by M^{2+} cation upon binding of Phen and Bpy ligand (s), Pauli repulsion between the valence electrons of the metal cation and those donated by Phen and Bpy ligands, and ligand-ligand repulsive interactions with each successive ligand bound also contribute to the fall off in the strength of binding with increasing ligation. Periodic trends indicate that the binding in all $M^{2+}(Phen)_x$ and $M^{2+}(Bpy)_x$ complexes is dominated by the electronic structure of the metal cation and to a lesser extent by the nature of the ligand. For both Phen and Bpy complexes, the charge of the metal cation is found to be the dominant contributing factor to the differences in the strength of binding between M^{2+} and M^{+} complexes, however the differences in the strength of binding are much smaller for cations of the same charge.

Comparisons between the Phen and Bpy complexes suggest that the flexibility of the Bpy ligand plays a significant role in enhancing its binding interactions with the M^{2+} cations.

Chapter 5 examines the ground-state structures and sequential binding energies of the $M^{2+}(Pyr)_x$ complexes, x = 1−6 by density functional theory methods. Structures of the $Ca^{2+}(Pyr)_x$ complexes are compared to those of the $M^{2+}(Pyr)_x$ complexes to Fe^{2+}, Co^{2+}, Ni^{2+}, Cu^{2+}, and Zn^{2+} to further assess the effects of the d-orbital occupation of the preferred binding geometries. The B3LYP, BHandHLYP, and M06 levels of theory yield very similar geometries for the analogous $M^{2+}(Pyr)_x$ complexes. The overall trends in the sequential BDEs for all five metal cations at all three levels of theory examined are highly parallel, and are determined by a balance of the effects of the valence electronic configuration and hybridization of the metal cation, but are also influenced by ligand-ligand repulsive interactions. Present results for the $M^{2+}(Pyr)_x$ complexes are compared to the analogous complexes to the late first-row monovalent transition metal cations, Co^+, Ni^+, Cu^+, and Zn^+ previously investigated to assess the effect of the charge/oxidation state on the structures and sequential binding energies. Trends in the sequential binding energies of the $M^{2+}(Pyr)_x$ complexes are also compared to the analogous $M^{2+}(water)_x$, $M^{2+}(imidazole)_x$, $M^{2+}(Bpy)_x$, and $M^{2+}(Phen)_x$ complexes.

Preliminary studies covered in Appendices D and E are inter-related and describe the results of mapping the mechanisms and energetics of fragmentation pathways of $M^{2+}(Phen)_2$ and $M^{2+}(Bpy)_2$ complexes, respectively. Four types of reaction pathways are observed in competition in all the $M^{2+}(Phen)_2$ and $M^{2+}(Bpy)_2$ complexes including ETCF, PTCF, simple CID, and dehydrogenation. For all the $M^{2+}(Phen)_2$ and $M^{2+}(Bpy)_2$ complexes, severe overlap of the products separated by 1 Da originating from the ETCF and PTCF pathways is

observed because the experiments were performed under low-resolution conditions. Preliminary data analysis of the cross sections is performed for the ETCF and simple CID pathways, without consideration of the PTCF pathway for all the $M^{2+}(Phen)_2$ and $M^{2+}(Bpy)_2$ complexes. As a result, the activation energies and bond dissociation energies extracted are only approximate. To extract accurate thermochemistry for the ETCF, PTCF, and simple CID pathways of both the $M^{2+}(Phen)_2$ and $M^{2+}(Bpy)_2$ complexes, experimental studies under high-resolution conditions are needed. Only one mechanism is investigated for ETCF and PTCF activated dissociation of each $M^{2+}(Phen)_2$ and $M^{2+}(Bpy)_2$ complexes. Investigation into other plausible mechanisms involved in the PTCF activated dissociation is needed because the current PES is likely not be the lowest energy PTCF pathway. Because of the low-resolution and incomplete experimental data, the strengths and limitations of the theoretical methods employed cannot be evaluated. Therefore, further experimental and theoretical studies of $M^{2+}(Phen)_2$ and $M^{2+}(Bpy)_2$ systems are needed to enable appropriate interpretation of the experimental data and accurate thermochemistry to be extracted.

AUTOBIOGRAPHICAL STATEMENT

HOLLINESS NOSE

EDUCATION

Wayne State University, Doctor of Philosophy in Chemistry, 2014.
Thesis Topic: "Experimental and Theoretical Studies of Binding Interactions in Divalent Transition Metal Cation-*N*-Donor Ligand Complexes: Structures, Sequential Bond Dissociation Energies, Mechanisms and Energetics of Collision-Induced Dissociation."

University of the Ryukyus, Master of Science in Chemistry, Biology and Marine Science, 2005.
Thesis Topic: "Search for Biologically Active Substances from Okinawa Marine Organisms: Isolation and Structures of the Compounds which Inhibit the Cleavage of the Fertilized Sea Urchin Eggs."

University of Nairobi, Bachelor of Science in Chemistry, 2002.
Research Topic: "Radical Scavenging Activities of Flavonoids from the Root Bark of Erythrina Abyssinica."

SELECTED PUBLICATIONS AND PRESENTATIONS

(1) **Holliness Nose, Yu Chen, and M. T. Rodgers**, "Energy-Resolved Collision-Induced Dissociation Studies of 1,10-phenanthroline Complexes of the Late First-Row Divalent Transition Metal Cations: Determination of the Third Sequential Binding Energies" *J. Phys. Chem. A*, **2013**, 117(20), 4316–4330.

(2) **Holliness Nose and M. T. Rodgers**, "Energy-Resolved Collision-Induced Dissociation Studies of 2,2′-bipyridine Complexes of the Late First-Row Divalent Transition Metal Cations: Determination of the Third Sequential Binding Energies" *ChemPlusChem*, **2013**, 78, 1109–1123.

(3) **Holliness Nose and M. T. Rodgers**, "Influence of the d Orbital Occupation on the Structures and Sequential Binding Energies of Pyridine to the Late First-Row Divalent Transition Metal Cations: A DFT Study" *J. Phys. Chem. A*, **2014**, under review.

(4) **Holliness Nose** and M. T. Rodgers, "Energy-Resolved Collision-Induced Dissociation Studies of 1,10-Phenanthroline Complexes of the Late First-Row Divalent Transition Metal Cations: Determination of the Third Sequential Binding Energies" Proceedings of the 61st ASMS Conference on Mass Spectrometry and Allied Topics, Minneapolis Convention Center, Minneapolis, MN, June 9–13, **2013**.